CORA Cork Open Research Archive
Cartlann Taighde Oscailte Chorcaí

Title	Investigations on the factors influencing selectivity in reactions of nucleophiles containing multiple reactive sites
Authors	Sheehy, Kevin J.
Publication date	2023-01-06
Original Citation	Sheehy, K. J. 2023. Investigations on the factors influencing selectivity in reactions of nucleophiles containing multiple reactive sites. PhD Thesis, University College Cork.
Type of publication	Doctoral thesis
Rights	© 2023, Kevin J. Sheehy. - https://creativecommons.org/licenses/by/4.0/
Download date	2026-10-22 22:13:31
Item downloaded from	https://hdl.handle.net/10468/14595

UCC
University College Cork, Ireland
Coláiste na hOllscoile Corcaigh

Ollscoil na hÉireann, Corcaigh

National University of Ireland, Cork



Investigations on the Factors Influencing Selectivity in Reactions of Nucleophiles Containing Multiple Reactive Sites

Thesis presented by

Kevin J. Sheehy, BSc

for the degree of

Doctor of Philosophy

University College Cork

School of Chemistry

Head of School: Prof. Anita Maguire

Supervisor: Dr. Peter Byrne

2023

Table of Contents

Chapter 1: Discussion of the Factors Influencing Selectivity in Reactions of Ambident Nucleophiles

1.0. Detailed Table of Contents 1

1.1. Reactivity of Ambident Nucleophiles 2

1.2. Rationalisation of Selectivity in Reactions of Ambident Reactants 11

1.3. Criticism of the HSAB Theory and Related Concepts as Rationalisations of Ambident Reactivity 38

1.4. Alternative Rationalisations of Selectivity in Reactions of Ambident Reactants 53

1.5. References 72

Chapter 2: N vs. O Selectivity in Reactions of Diazine *N*-Oxides

2.0. Detailed Table of Contents 78

2.1. Selectivity in Reactions of Ambident Nucleophiles - Diazine *N*-Oxides 79

2.2. Spectroscopic Investigations – Reference δ_N Values 83

2.3. Investigations into the Ambident Reactivity of Diazine *N*-Oxides 100

2.4. References 127

Chapter 3: Experimental for Reactions of Diazine *N*-oxides

3.0. Detailed Table of Contents 131

3.1. General Experimental 133

3.2. Preparation of *N*-Oxides 136

3.3. NMR Spectral Data for Starting Compounds **1** – **3**, **18** – **21**, **23** 139

3.4. Synthesis of 4-Methylbenzyl Chloride 143

3.5. Reactions of Diazines and *N*-Oxides with Alkylating Agents 144

3.6. Reactions of Diazine *N*-Oxides with MeI, MeOTf and Benzhydrylium Ions 158

3.7. Control Experiments 177

3.8. Competition Experiment: Pyrazine *N*-Oxide vs Pyrimidine *N*-Oxide 188

3.9. Determination of 2nd Order Rate Constant to Verify Computationally Determined Value of $\Delta G^{\ddagger}$ 189

3.10. Calculations of Thermodynamic and Activation Parameter Values 195

3.11. References 199

Chapter 4: Reactions of Cyclic Enolates with Various Alkylating Agents

4.0. Detailed Table of Contents 201

4.1. Analysis of Ambident Reactivity of Cyclic Enolates with Various Alkylating Agents – the O/C Ratio 202

4.2. Reaction of Cyclic Enolates with "Soft" Alkylating Agents in Various Solvents. 205

4.3. Reactions of Tetramethylammonium Enolates with Substituted Benzyl Bromides 226

4.4. Reactions to Establish the Reversibility or Irreversibility of Alkylations of Cyclic Enolates 232

4.5. References 238

Chapter 5: Experimental for Reactions of Cyclic Enolates

5.0. Detailed Table of Contents 240

5.1. General Experimental 242

5.2. Preparation of Tetramethylammonium and Lithium Enolates 251

5.3. Determination of O/C Ratios in Enolate Ethylation Reactions 255

5.4. Determination of O/C Ratios in Enolate Trideuteromethylations 276

5.5. Determination of O/C Ratios in Enolate Methylation Reactions 287

5.6. Determination of O/C Ratios in Alkylations of Lithium Enolates 289

5.7. Preparation of Benzylated Derivatives of 1,3-Diketones 297

5.8. Determination of O/C Ratios in Enolate Benzylation Reactions 310

5.9. Control Experiments and Crossover Experiments 325

5.10. References 338

Chapter 6: Development of a Novel Model for Rationalising Selectivity in Reactions of Ambident Nucleophiles

6.0. Detailed Table of Contents 340

6.1. Introduction 342

6.2. Basis for Development of a New General Model for Rationalisation of Selectivities in Reactions of Ambident Nucleophiles (Including Enolates) 343

6.3. Construction of Gibbs Energy Profile Diagrams for Reactions of Enolate **1-Me$_4$N** with Ethylating Agents in CD_3CN 366

6.4. Construction of Gibbs Energy Profile Diagrams for Reactions of Enolate **1-Me$_4$N** with Methylating Agents in CD_3CN 395

6.5. Discussion of on O- vs C-Selectivity in Reactions of Enolates and Generation of Approximated Gibbs Energy Profile Diagrams 407

6.6. References 419

Chapter 7: Experimental for Development of Novel Model

7.0. Detailed Table of Contents 421

7.1. General Experimental 422

7.2. Reactions of **1-Me$_4$N** with Various Alkylating Agents in CD_3CN 428

7.3. Determination of $\Delta G^{\ddagger}$ Values for Reactions of DMAP + Various Electrophiles in CD_3CN 447

7.4. Competition Experiments Between Enolate **1-Me$_4$N** and DMAP with Various Electrophiles in CD_3CN at 20 °C 475

7.5. References 506

Chapter 8: Conclusions & Future Work

8.0. Detailed Table of Contents 507

8.1. Conclusions 508

8.2. Future Work 511

8.3. References 514

Parts of this thesis have been published in the following academic journals:

K. J. Sheehy, L. M. Bateman, N. Flosbach, M. Breugst, P. A. Byrne. "Identification of N- or O-Alkylation of Aromatic Nitrogen Heterocycles and *N*-Oxides Using ^{1}H-^{15}N HMBC NMR Spectroscopy" *Eur. J. Org. Chem.* **2020**, *22*, 3270-3281.

K. J. Sheehy, L. M. Bateman, N. Flosbach, M. Breugst, P. A. Byrne. "Competition Between N and O: Use of Diazine *N*-Oxides as a Test Case for the Marcus Theory Rationale for Ambident Reactivity" *Chem. Sci.* **2020**, *11*, 9630-9647.

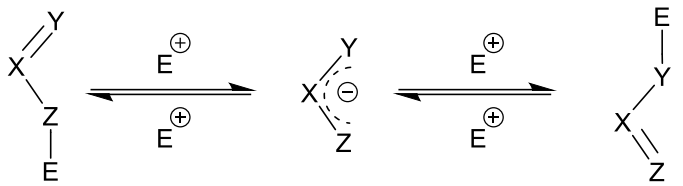
Appendices referred to in the text are available at the following link:
https://tinyurl.com/KSheehyPhDThesisAppendices

Symbols and abbreviations

app. d	apparent doublet (spectra)
app. t	apparent triplet (spectra)
Ar	aryl group
Bn	benzyl group
COSY	Correlation NMR Spectroscopy
d	doublet (spectral)
dd	doublet of doublets (spectral)
DBU	1,8-diazabicyclo[5.4.0]undec-7-ene
DME	dimethoxyethane
DMF	*N*,*N*-dimethylformamide
DMSO	dimethyl sulfoxide
δ	delta (spectral – chemical shift in ppm)
Hz	hertz
HMBC	Heteronuclear multiple bond correlation NMR spectroscopy
HRMS	high resolution mass spectrometry
HSQC	Heteronuclear single quantum correlation spectroscopy
IR	infrared spectroscopy
J	NMR coupling constant

k	rate constant
KHMDS	potassium hexamethyldisilazide (potassium bis(trimethylsilyl)amide)
m	meta
m	multiplet (spectral)
$[M]^+$	mass of molecular ion (mass spectrometry)
m.p	melting point
MHz	megahertz
o	ortho
p	para
PTFE	polytetrafluoroethylene
q	quartet (spectral)
s	singlet (spectral)
t	triplet (spectral)
TS	Transition State
UV	ultraviolet (spectroscopy)

Abstract



A fundamental goal in organic chemistry is to be able to understand and rationalise why chemical processes occur as they do. Naturally, therefore, an understanding of the factors that govern regioselectivity in chemical reactions is of paramount importance – i.e., if a compound contains more than one reactive site, which one is preferred, and why? An ambident chemical species is defined as one whose molecular entities each possess two alternative and strongly interacting reactive centres which may partake in a reaction. These centres are connected in such a way that reaction at either site greatly reduces the favourability of a subsequent attack at the second site. Reliably accounting for the regioselectivity observed in reactions of ambident nucleophiles and electrophiles is a challenge laden with difficulties and potential pitfalls. In this thesis, the concept of hard and soft acids and bases (HSAB), which is commonly applied to organic reactivity in an attempt to rationalise and predict the reactivity of these substrates, is found to be an inadequate and misleading simplification of the myriad factors which determine the outcome of the reactions of ambident nucleophiles. This conclusion is drawn from rigorous examination of reactions of various ambident nucleophiles, such as enolates and diazine *N*-oxides.

The preferred site of alkylation of diazine *N*-oxides by representative hard and soft alkylating agents was established conclusively using the underutilised $^{1}H–^{15}N$ HMBC NMR technique in combination with other NMR spectroscopic methods, giving outcomes which could not be explained in the context of the hard/soft acid/base (HSAB) principle. In lieu of this, a Marcus theory-based approach was used instead to rationalise these results, utilising calculated values of Marcus intrinsic barriers ($\Delta G^{\ddagger}_{int}$) and $\Delta_r G°$ to derive Gibbs energies of activation ($\Delta G^{\ddagger}$) values for the processes of N- and O-methylation. These values, as well as those derived directly from DFT calculations, closely reproduced the observed experimental N- vs. O-alkylation selectivities for methylation reactions of pyrazine *N*-oxides and pyrimidine *N*-oxide, thereby demonstrating the value in alternative approaches to rationalising the outcomes of reactions of ambident nucleophiles.

A novel approach to rationalising ambident reactivity is proposed herein which analyses reactions of enolates in which the Marcus theory-based approach described above has limited use. The first steps towards the construction of this model are taken in this thesis, involving the close examination of alkylation reactions of enolates and the determination of values of $\Delta G^{\ddagger}$ for the competing processes of O- and C-alkylation. This model reveals defining characteristics in the Gibbs energy profile diagrams which describe the reactions of ambident nucleophiles, enabling a greater understanding of the factors which dictate site selectivity in these reactions.

Chapter 1: Discussion of Factors Influencing Selectivity in Reactions of Ambident Nucleophiles

1.1. Reactivity of Ambident Nucleophiles **2**

1.2. Rationalisation of Selectivity in Reactions of Ambident Reactants **11**

1.2.1. Kornblum's Rule: S_N1 vs. S_N2 character of a reaction 11

1.2.2. Choice of Solvent and "Selective Solvation" 12

1.2.3. Nature of the Cation 16

1.2.4. Nature of the Leaving Group – HSAB Theory and the Concepts of Charge- and Orbital-Controlled Reactions 29

1.3. Criticism of the HSAB Theory and Related Concepts as Rationalisations of Ambident Reactivity **38**

1.4. Alternative Rationalisations of Selectivity in Reactions of Ambident Reactants **53**

1.4.1 The Marcus Approach to Ambident Reactivity 53

1.4.2 Distortion/Interaction Model and Activation Strain Model 67

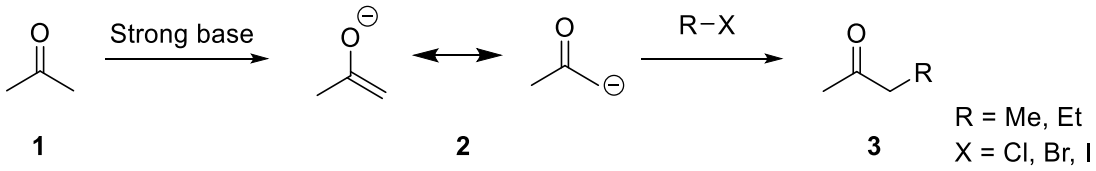
1.5. References **72**

Appendices referred to in the text are available at the following link:
https://tinyurl.com/KSheehyPhDThesisAppendices

1.1. Reactivity of Ambident Nucleophiles

Enolate anions are amongst the most widely used ambident species employed in organic synthesis.[1–8] The delocalised enolate system possesses both oxyanion and carbanion character which confers upon it an ability to react with electrophiles at either the oxygen atom or the carbon atom. The versatility they have is closely linked to their ambident nature – alkylation at carbon is an essential method for carbon-carbon bond formation,[9] while alkylation at oxygen can be used to produce vinyl ethers. A simple reaction of an enolate ion is shown in Scheme 1-1. Ketones, carboxylic acids, esters and carboxamides can all form enolate ions through deprotonation with a strong base. Deprotonation of a ketone (**1**) with a suitable base generates the enolate anion **2** (see Scheme 1-1), allowing the nucleophilic enolate carbon to attack the electrophilic centre on an alkyl halide, resulting in new carbon-carbon bond formation (in product **3**).

Scheme 1-1. Reaction of an enolate anion. The enolate anion is generated in a reaction of a ketone with a suitable base. R can by an alkyl group (methyl, ethyl) or a larger group such as benzyl. Use of a strong base ensures the complete deprotonation of the starting material.

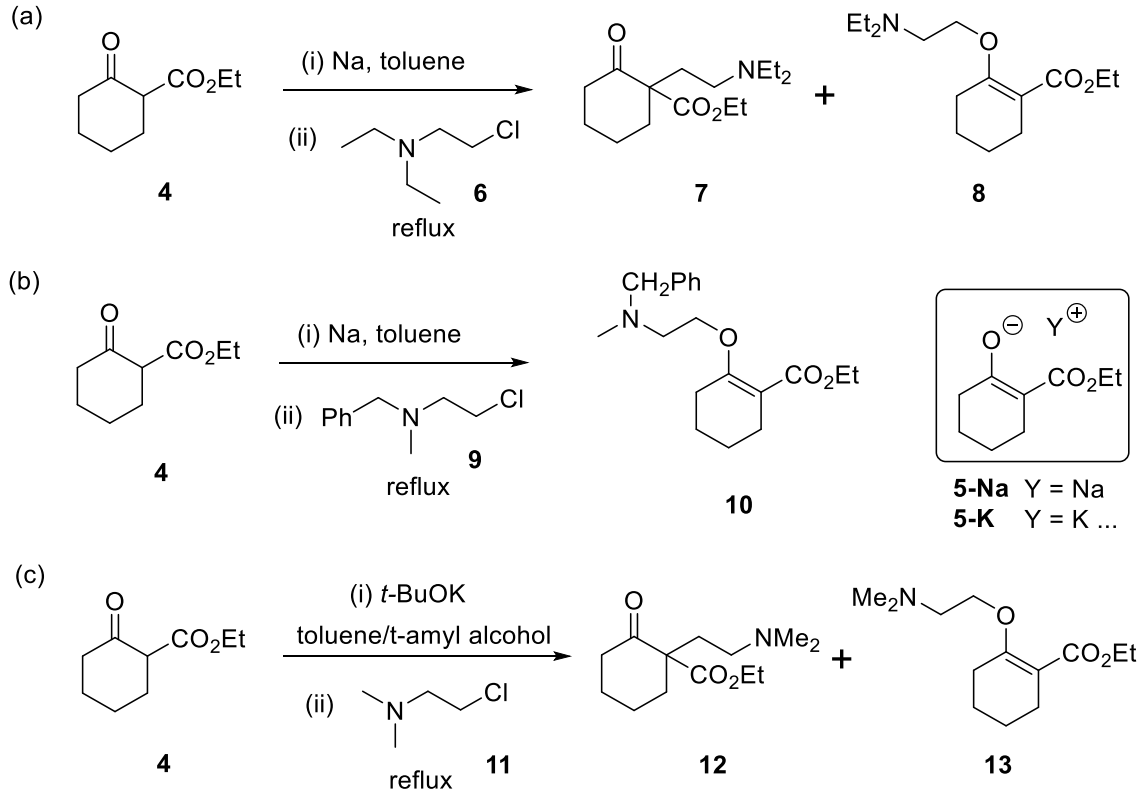


Being one of the common methods for carbon-carbon bond formation, the alkylation of enolates is discussed in depth in many common organic chemistry textbooks[10,11] and synthetic guides,[12] as well as reviews that cover more specific applications of these reactions, such as allylic alkylation,[13,14] asymmetric alkylation[15] and asymmetric transition-metal-catalysed reactions.[16]

Although C-alkylation of the enolate is often the desired outcome in reactions of this type, O-alkylation is possible in many instances. Early research into the products of reactions of these ambident nucleophiles was often hindered by the appearance of unexpected O-alkylation products when using alkyl halide reagents similar to those that gave exclusive C-alkylation when using other enolate substrates. An example is demonstrated in Scheme 1-2, concerning reactions of enolate derivatives of 2-carbethoxycyclohexanone (**3**) with alkyl chlorides. Reactions of the sodium enolate of **4** (**5-Na**, see Scheme 1-2) were reported by Barltrop to exclusively form the C-alkylation product (**7**) in a reaction with diethyl-β-chloroethylamine (**8**),[17] leaving later investigators surprised when a reaction of the same enolate gave exclusive O-alkylation when using methylbenzyl-β-chloroethylamine (**9**).[18] Another study found that alkylation of **5-K** with dimethyl-β-chloroethylamine gave a mixture of O- and C-alkylation products, leading Doering and Rhoads to claim there is "*no uniformity in the behaviour of…* (**4**)" with regard to the site of alkylation.[19] A subsequent re-examination of the original Barltrop reaction (reaction of Scheme 1-2(a)) by Rhoads, Reynolds and Raulins revealed that the actual products of

the alkylation were actually a mixture of C- and O-alkylated derivatives, with the O-alkylated product (**8**) predominating.[20]

Scheme 1-2. (a) Reactions of the sodium enolate of 2-carbethoxycyclohexanone (**5-Na**) with β-chloroethylamines were originally reported to give the C-alkylation product (**7**) exclusively.[17] A later analysis showed that not only was the O-alkylation product (**8**) also forming in the reaction, but it was the major product.[20] **(b)** Another study in the interim reported the exclusive formation of the O-alkylation product when using a similar alkyl chloride (**9**).[18] **(c)** The reaction of the potassium enolate of 2-carbethoxycyclohexanone (**5-K**) with **11** gave a mixture of **12** and **13**.



Another example of confusion arising from the unexpected O-alkylation of enolates is illustrated in Scheme 1-3. The assertation by Kabachnik *et. al.* that the enol of ethyl α-*sec*-butylacetoacetate (**17**) exists entirely in the *trans* configuration[21] was challenged by Rhoads *et. al.* when they deduced that this misconception occurred by the researchers neglecting to predict the formation of the O-alkylation product (**18**) in their reaction of the sodium enolate of ethyl acetoacetate (**15-Na**) with *sec*-butyl iodide (**16**).[22] Their general claim that "*(O-alkylation)'s importance under quite ordinary alkylating conditions has been underestimated*" was later accepted by Kabachnik and co-workers when a reinvestigation of these experiments revealed a small amount of O-alkylation occurred in all reactions of the sodium enolate of ethyl acetoacetate (**15-Na**) with methyl bromide (**19**), ethyl bromide (**22**) and *s*-butyl bromide (**25**).[23]

Scheme 1-3. (a) Rhoads. *et. al.* postulated that by neglecting to predict the formation of **18** in a reaction of **15-Na** and **16**, Kabachnik *et. al.* had misinterpreted data which led them to claim that the enol form of **17** exists almost solely in the *trans*-configuration. By repeating the experiment, Rhoads. *et. al.* proved by Gas-Liquid Partition Chromatography (GLPC) that **18** was forming in varying amounts between 6 and 8%. **(b)** Later reinvestigations by Kabachnik and co-workers revealed that small amounts of O-alkylated products (**18**, **21** and **24**) were formed in reactions of **15-Na** and various alkyl bromides (**19**, **22** and **25**).

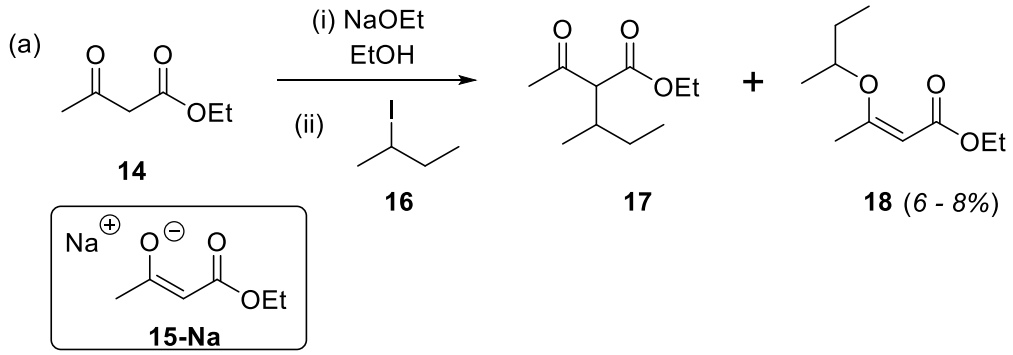
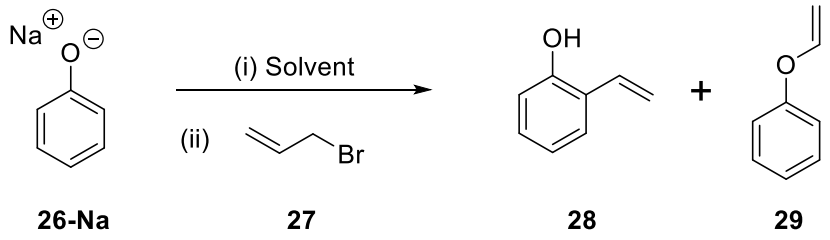


Table 1-1. By swapping the solvent used in the reaction of sodium phenoxide (**26-Na**) with **27**, Claisen *et. al.* successfully altered the course of the reaction of the ambident species to furnish the desired C-alkylation product (**28**).[24]



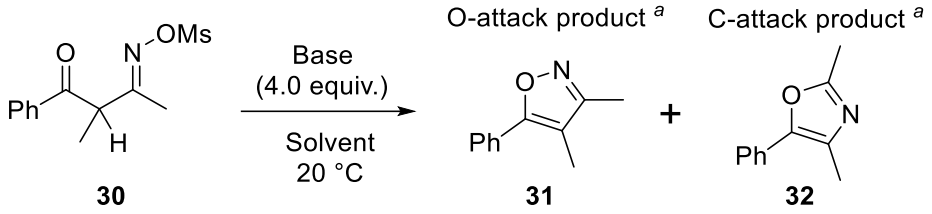
Entry	Solvent	C-allyl product (28)	O-allyl product (29)
1	Acetone	1-3 %	95 %
2	Benzene	60-70 %	30 %

Phenoxides, which are in many respects similar to enolates, have also been the source of unexpected reactivity due to their ambident character. Claisen *et. al.* found that in their attempts to synthesise 2-allylphenol ((**28**), see Table 1-1 above) by allylation of sodium phenoxide (**26-Na**) in acetone, the major product was allyl phenyl ether (**29**), the O-

alkylation product. However, upon switching the solvent from acetone or alcohols to benzene or toluene (in which the phenoxide salt was not soluble), the major product of the reaction became that of the C-alkylation process (**28**).[24]

Even in recent investigations, analysing and understanding the competing modes of O- and C-reactivity of enolates proved necessary to rationalise selectivities in reactions that are more complex than the simple alkylations discussed above. Ning, Otani and Ohwada investigated the various possible mechanisms of intramolecular cyclization of 3-sulfonyloxyimino-2-methyl-1-phenyl-1-butanone (**30**) (see Table 1-2 below), wherein O- or C-attack of an enolate intermediate may result in different cyclic products being formed.[25] The results in Table 1-2 below illustrate these authors investigations into whether or not different counter-ions affect the selectivity of the intramolecular cyclization of the enolate intermediate.

Table 1-2. Ning, Otani and Ohwada investigated the factors that affect the intramolecular cyclization reaction of (**30**) under basic conditions, involving an enolate intermediate. The yields in this table were determined based on ^{1}H NMR signals of the crude products.



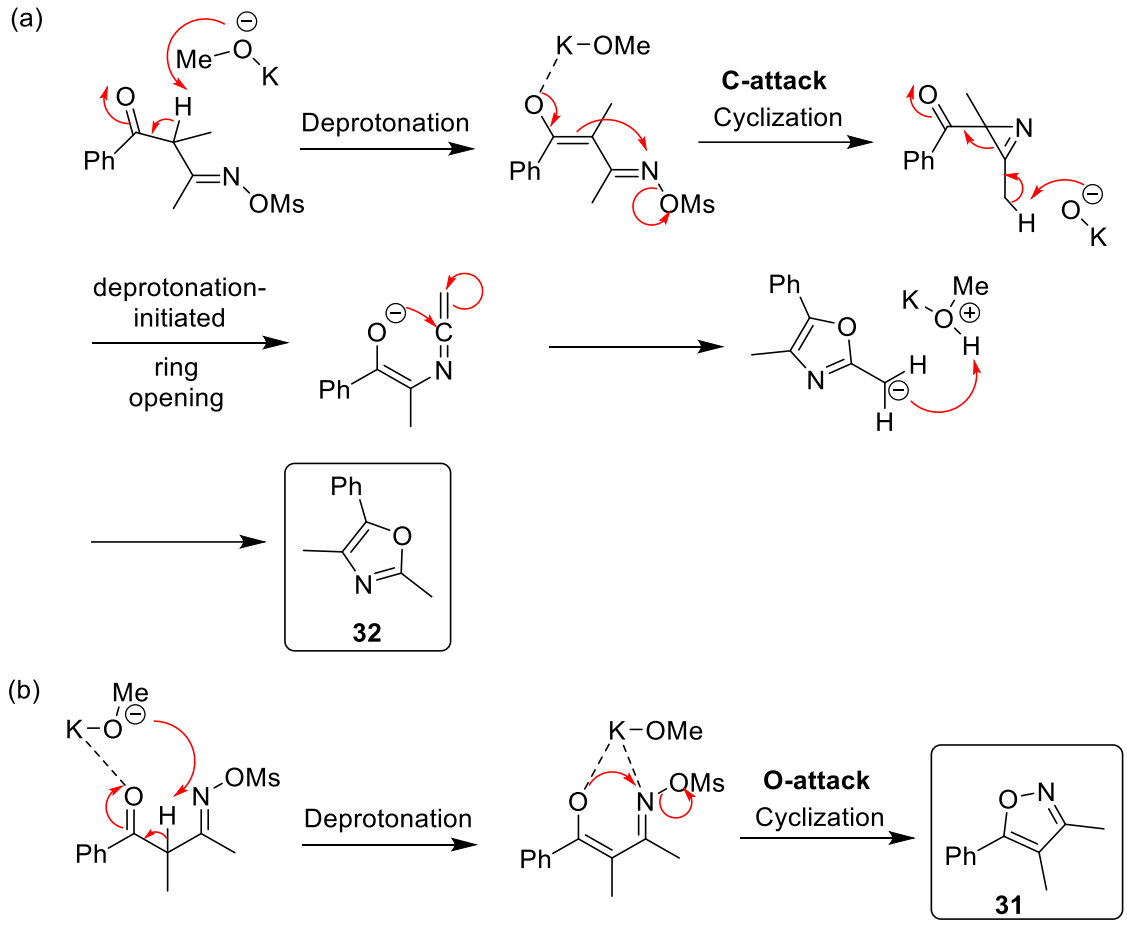
30 **31** **32**

#	Base	Additive	Solvent	Product		O-attack : C-attack Ratio
				31	**32**	
1	*t*-BuOK	None	THF	42%	44%	49:51
2	*t*-BuONa	None	THF	35%	41%	47:53
3	*t*-BuOK	18-crown-6	THF	38%	35%	52:48
4	*t*-BuOK	NEt_3 (10 equiv.)	THF	38%	41%	48:52
5	*t*-BuOK	NEt_3 (10 equiv.)	Toluene	41%	43%	49:51

[a] The mechanisms of formation of each of the products, accounting for how they are formed from an O-attack and C-attack respectively, are proposed below in Figure 1-1.

These experiments revealed that the changing of the counter-ion (from K to Na, compare Table 1-2 entries 1 and 2) resulted in only negligible effects on the ratio of products formed from the O- and C-attack of the enolate. The addition of 18-crown-6 or NEt_3 (in an attempt to affect the aggregation state of the enolate (see Table 1-2 entries 3 – 5)) also did not result in a substantial change in the observed ratio of products, which remained at approximately 50 : 50 in all of the reaction conditions attempted. A mechanism for the formation of **31** and **32** *via* enolate C-attack (see Figure 1-1(a)) and O-attack (see Figure 1-1(b)) was proposed by the authors and validated using computational methods.[25,26]

Figure 1-1. Mechanisms illustrating how **31** and **32** may form from the intramolecular cyclization of an enolate intermediate from the reaction drawn in Table 1-2 above by **(a)** C- and **(b)** O-attack. These transformations were investigated by computational methods by Ning, Otani and Ohwada.[25]



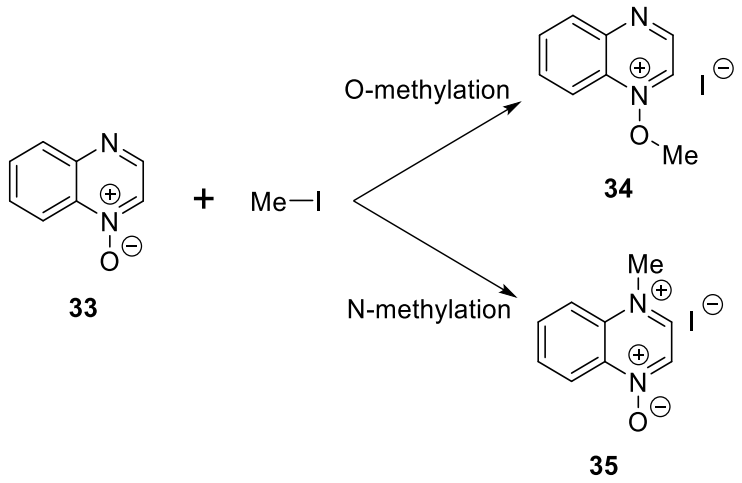
The competing reaction pathways which may occur in the reaction illustrated in Table 1-2 are an excellent example issues which may arise with syntheses utilising ambident species such as enolates. Each of the examples outlined above show that the formation of both C- and O-alkylation products in the reactions of enolates is a common phenomenon which requires careful consideration for the modern synthetic chemist.

Aside from enolates, the ambident reactivity of other nucleophiles engenders similar issues regarding the selectivity of a reaction, and the identification of the major and minor products (see Scheme 1-3 above). Competition between the nitrogen and oxygen nucleophilic sites in compounds such as amide anions, nitrite anions and diazine *N*-oxides have caused notable difficulty for chemists throughout the literature.

Work by Landquist in which quinoxaline *N*-oxides (e.g., **33**, see Scheme 1-4 below) were synthesised and used in reactions with simple alkylating agents highlighted the difficultly in identifying the products of an ambident nucleophile with N and O nucleophilic sites.[27] As can be seen in Scheme 1-4, a reaction of **33** with methyl iodide produced both O- and N-methylated adducts of **33** (**34** and **35**). Landquist was only able to conclude that the

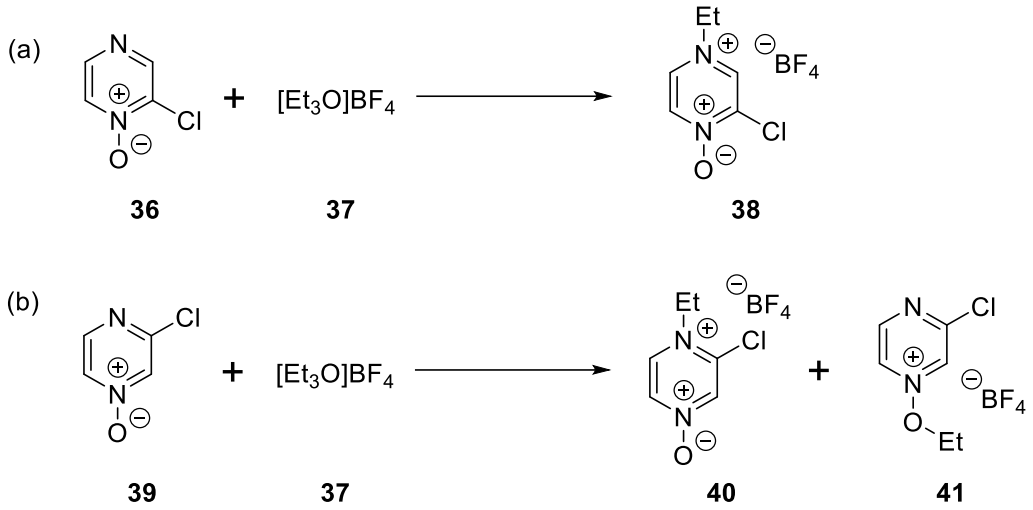
major product was the N-methylated adduct (**35**), as the majority of the products did not decompose to quinoxaline upon addition of a base.

Scheme 1-4. Upon synthesis of quinoxaline N-oxide (**33**) and subsequent reaction with methyl iodide, the N-methylation product (**35**) and O-methylation product (**34**) were produced in unequal yield and could only be differentiated through chemical derivatisation.



Aside from the inherent difficulty in identifying the products of the reaction of an ambident nucleophile such as **33** (in Scheme 1-4 above), the selectivity of reactions of nucleophiles containing reactive nitrogen and oxygen sites is often just as difficult to account for. Cmoch observed that in reactions of substituted pyrazine *N*-oxides, the same alkylating agent could react at both the nitrogen and oxygen atoms in compounds which had near-identical structures.[28] As seen below in Scheme 1-5, the reaction of 2-chloropyrazine (**36**) with $[Et_3O]BF_4$ (**37**) gave only one product, which was determined by Cmoch to be the N-ethylated adduct (**38**) of the starting material. However, the reaction of 3-chloropyrazine (**39**) with $[Et_3O]BF_4$ (**37**) was found to produce each of the products that result from N-ethylation (**40**) and O-ethylation (**41**). The O-ethylation product (**41**) was found to be the major product of the reaction, being present in a 3:1 ratio compared to the N-ethylation product (**40**). The vastly different selectivity between the alkylation reactions of **36** and **39** with the same electrophile perfectly encapsulates the unpredictable nature of reactions of heterocyclic ambident nucleophiles such as **33**.

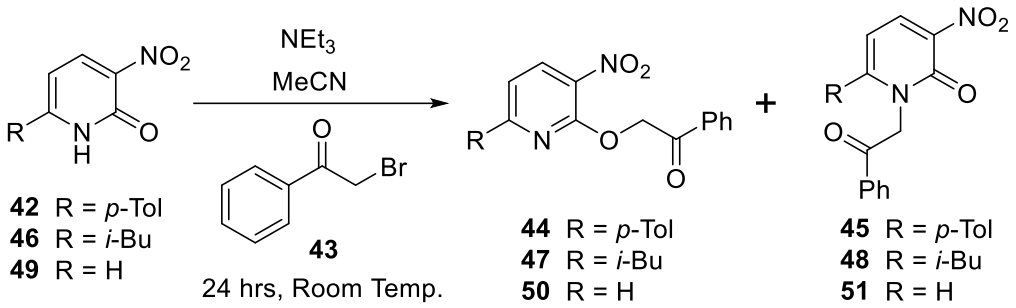
Scheme 1-5. (a) The reaction of 2-chloropyrazine (**36**) with triethyloxonium tetrafluoroborate ($[Et_3O]BF_4$, **37**) gives the N-ethylation product (**38**) exclusively. **(b)** However, when 3-chloropyrazine (**39**) is employed in the same reaction, both the N-ethylation product (**40**) and the O-ethylation product (**41**) are observed in the reaction mixture. The O-alkylation product (**41**) was favoured in a 3:1 ratio over the N-alkylation product (**40**).



Unsurprisingly, a major goal of many synthetic chemists when optimising novel reaction conditions which employ ambident nucleophiles is to quell the formation of one of the products, such that the reaction occurs selectively at one of the nucleophilic sites.

Nishiwaki *et al*. found that the reaction of various nitropyridones (such as **42** below in Table 1-3) gave both O- and N-alkylation products (e.g., **43** and **44** in Table 1-3) in reactions with various electrophiles. They found that the unwanted N-alkylation reaction could be prevented from occurring by substitution of the nitropyridone ring at the 6-position (see Table 1-3, compare entries 1 and 2 to entry 3). When the pyridone was substituted with bulky substituents such as *p*-Tol (Table 1-3 entry 1) or *i*-Bu (Table 1-3 entry 2) the reactions proceeded with alkylation only occurring at the oxygen atom. When there was no bulky substituent (i.e., R = H, see entry 3 in Table 1-3), the N-alkylation product was formed exclusively. The authors here indicate that congestion around the ring nitrogen is successfully able to suppress the reactivity of the nitrogen atom, enabling O-alkyation to predominate.

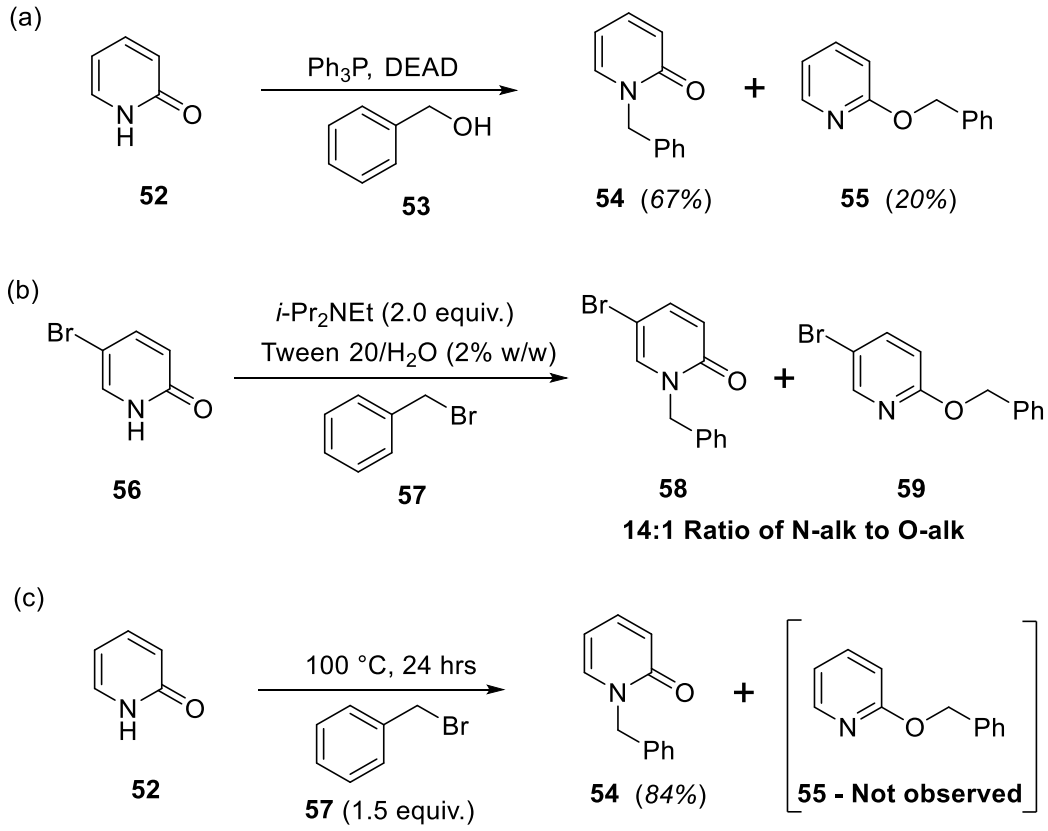
Table 1-3. A selection of results from the work of Nishiwaki *et al*.[29] The alkylation of nitropyridones (**42**, **46** and **49**) with **43** in MeCN resulted in variable alkylation of the N- or O-atom, depending on the substituents on the pyridone ring.



Entry	R	O-alkylation		N-alkylation	
		Product	Yield (%)	Product	Yield (%)
1	*p*-Tol	**44**	94	**45**	0
2	*i*-Bu	**47**	70	**48**	0
3	H	**50**	0	**51**	90

The convenient synthesis of N-substituted-2-pyridones is sought after by chemists of varying disciplines due to the presence of analogous motifs in biologically active molecules and natural products,[30,31] as well as their versatility in organic synthesis.[32,33] As such, there are numerous examples in the literature where the synthesis of these molecules is attempted, wherein the authors must contend with the problem of competing oxygen and nitrogen reactive sites. A small selection of the methodologies which have been employed for the synthesis of N-substituted-2-pyridones is outlined below in Scheme 1-6. The reaction shown in Scheme 1-6(a) is one of many Mitsunobu reactions performed by Comins and Jianhua using a selection of solvents and alcohols.[34] These reactions were found to be more capable of producing O-alkylation products selectively when certain solvent/alcohol combinations were employed. However, some examples, such as the one shown in Scheme 1-6(a), could produce a large amount of the N-alkylated derivative (**54**). Ren and co-workers found that high levels of N-alkylation were observed in reactions of various 2-pyridones (e.g., **56** in Scheme 1-6(b)) which used a surfactant (such as Tween 20) in water in order to improve the solubility of the starting materials.[35] Many reactions with various bases, surfactants and organohalides (such as benzyl bromide, **57**) were carried out, one of which is shown in Scheme 1-6(b). A large preference for the N-alkylated product was observed in these reactions (a 14:1 preference for N-alkylation over O-alkylation was seen in the example drawn in Scheme 1-6(b)).

Scheme 1-6. (a) A Mitsunobu reaction of 2-pyridone (**52**) was found to yield mixtures of O- and N-alkylated products in varying yields.[34] However, these reactions were generally more capable of occurring with O-selectivity. **(b)** Ren and co-workers developed and optimised mild conditions which allowed for the alkylation of 2-pyridones in water, with large preferences for N-alkylation being observed over O-alkylation.[35] **(c)** An entirely regioselective preparation of N-substituted-2-pyridones was developed by Feng *et al*. which uses no base and no catalyst.[36]



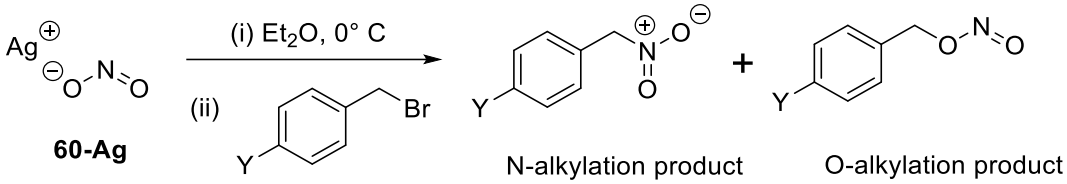
Finally, Feng *et al*. serendipitously discovered conditions which allowed for the selective synthesis of N-substituted-2-pyridones which use no catalyst and no base. The reaction tolerated a wide range of organohalides, with complete N-selectivity being observed in each case. The specific reaction drawn in Scheme 1-6(c) depicts the optimised conditions outlined by the authors which allows for the most convenient synthesis of a large yield of the N-alkylated product (**54** in the case of Scheme 1-6(c)). The reaction was also found to be viable with a variety of other substituted pyridones and pyridone analogues.

1.2. Rationalisation of Selectivity in Reactions of Ambident Reactants

1.2.1. Kornblum's Rule: S_N1 vs. S_N2 character of a reaction

Given the ubiquity of the reactions of ambident nucleophiles in organic syntheses, being able to understand and predict the outcome of reactions of enolates and other ambident nucleophiles is of utmost importance. Pioneering work on understanding the factors that controlled reactions of ambident nucleophiles was done by Kornblum *et. al.* in the 1950s, through study of reactions of the nitrite anion.[37–41] Analysis of these reactions of competing N vs. O alkylation processes led to the so-called *Kornblum rule* which provides a rationale for the behaviour of various alkyl halides reacting with the nitrite anion.

Table 1-4. Kornblum's reactions of silver nitrite with various benzyl bromides which led to his hypothesis on the factors which influence site of addition in reactions of ambident nucleophiles.[39]



60-Ag

N-alkylation product

O-alkylation product

61 Y = NO_2
57 Y = H
66 Y = CH_3
69 Y = OCH_3

62 Y = NO_2
64 Y = H
67 Y = CH_3
70 Y = OCH_3

63 Y = NO_2
65 Y = H
68 Y = CH_3
71 Y = OCH_3

Entry	Y	N-alkylation product % [a, b]	O-alkylation product % [a, b]
1	NO_2	84 (75)	16 (5)
2	H	70 (61)	30 (28)
3	CH_3	52 (45)	48 (37)
4	OCH_3	39 (26)	61 (55)

[a] The yield of nitro compound was determined by titration, and the yield of the nitrite ester was assumed to be the difference between the % of nitro compound and total yield of products.

[b] The isolated yields for each compound are given in parentheses.

Kornblum determined the product ratios of reactions of silver nitrite (**60-Ag**) with a series of benzyl bromides (**57, 61**, **66** and **69**). The product ratios determined are shown in Table 1-4. The series of reactions, from entries 1 – 4, was designed to increase the carbenium ion character of the transition state and observe the effects that had on the rates of the reactions and on and product composition. The reaction involving benzyl bromide **61** (with a *para*-nitro group as an electron withdrawing group to reduce the electron density on the electrophilic carbon) was correctly predicted by Kornblum *et. al.* to have the slowest rate of reaction and the largest proportion of N-benzylation product (nitroalkane **62**) formed (see Table 1-4 entry 1). Of all of the reactions investigated as shown in Table 1-4 entry 4, a *para*-methoxy substituent on the benzyl bromide (compound **69**) produces the opposite effect and should have the highest carbenium character in its transition state.

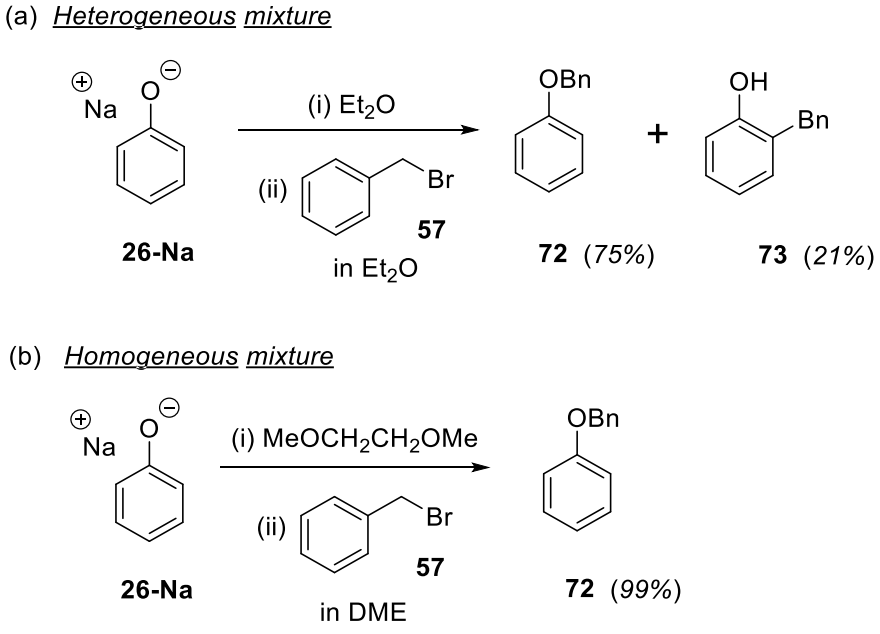
The reaction in Table 1-4 entry 4 gave the highest amount of O-benzylation product (nitrite ester **71**) formation and the fastest rate. The authors took this observation as evidence that a carbenium ion reacts more readily at the oxygen atom of a nitrite ion than at the nitrogen atom. They summarised their rationale for the factors that influence selectivity in reactions of ambident anions as follows: "*The greater the S_N1 character of the transition state the greater is the preference for covalency formation with the atom of higher electronegativity and, conversely, the greater the S_N2 contribution to the transition state the greater the preference for bond formation to the atom of lower electronegativity*".

This method of predicting the behaviour of ambident anions proved popular and was frequently cited to explain the observed reactivity of reactions of enolates,[42–44] pyridone anions and quinolone anions[45] and trinitromethane anions.[46]

1.2.2. Choice of Solvent and "Selective Solvation"

Further development of this idea focused on solubility and solvent choice, both of which Kornblum *et. al.* determined had a profound effect on the selectivity of these reactions.[47–49]

Scheme 1-7. Reactions of sodium phenoxide (**26-Na**) with **57** in two different solvents. **(a)** When Et_2O is used, in which **26-Na** is sparingly soluble, a mixture of both O- and C-alkylation products (**72** and **73**) are observed. **(b)** Using monoglyme (dimethoxyethane) as the solvent, the phenoxide is completely soluble and the homogeneous mixture gives only the O-alkylation product (**72**).



As shown in Scheme 1-7, the group observed that reactions of sodium phenoxide (**26-Na**) with benzyl bromide (**57**) proceeded differently depending on whether the solvent used created a heterogeneous or homogeneous mixture.[47] A similar effect was observed in reactions of **26-Na** with allyl bromide (**27**). The authors suggest that the odd preference for C-alkylation when the mixtures are heterogeneous is not in violation of their

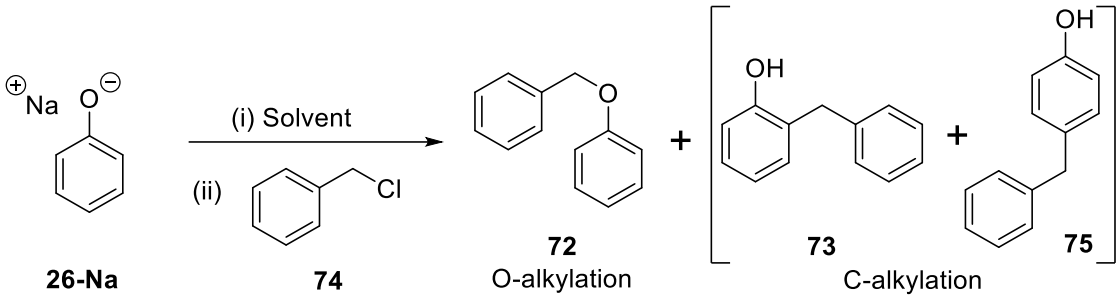
previously stated hypothesis about the nature of ambident reactivity, as the heterogeneous processes cannot be characterised as more S_N1- or S_N2-like. The "overriding factor" of heterogeneous mixtures undergoing C-alkylation was offered as an explanation for Claisen's observation of high levels of C-alkylation product in reactions of sodium phenoxide (**26-Na**) with allyl bromide (**27**) in benzene,[24] as highlighted in section 1.1 (see Table 1-1).

Further investigation into reactions of **26-Na** led Kornblum, Berrigan and Le Noble to introduce "selective solvation" as a factor which could influence the course of the reaction.[48,49] In their study, summarised in Table 1-5 below, they found that in solvents such as DMF and THF, the reaction of sodium phenoxide (**28-Na**) with benzyl chloride (**74**) and allyl bromide (**27**, not shown) produced the O-alkylated ether (**72**) in quantitative yield. However, in other solvents, such as water and 2,2,2-trifluoroethanol (see Table 1-5, entries 5 and 6), a large amount of carbon alkylation (to the *ortho*- and *para*-substituted products (**73** and **75**)) was observed. The authors proposed that in solvents that are unusually effective at forming hydrogen bonds, the oxygen atom of the phenoxide anion was "intensely solvated", leading to a decreased ability for the oxygen to attack the electrophile. The disfavoured carbon alkylation processes thus become favoured in the absence of another pathway.

The possibility that the carbon alkylation was proceeding by a S_N1 process was rejected through the measurement of a second order rate constant and the observation that no solvolysis products (e.g., benzyl alcohol) are formed in the reaction, which would be indicative of carbenium ion formation. The authors acknowledge that the O-alkylation of sodium phenoxide in the solvents in entries 1 – 4 in Table 1-5, as well as in methanol and ethanol,[50] must be second order processes.

Seemingly in contravention of the rule established in reference 39, they conclude that solvent incorporation into the activated complex will result in changes being observed in the preferred reaction pathway. This selective solvation, in combination with potential enhanced solvation of the leaving group of the alkylating agent, were offered as explanations as to why solvent choice could have such a profound influence on the course of a reaction. Evidence for the suggestion that selective solvation could impede the progress of an anion undergoing a substitution reaction was offered in a reference to a study showing that the addition of water slows the reaction of iodide anions with *n*-butyl bromide in acetone.[51]

Table 1-5. In reactions of sodium phenoxide, Kornblum, Berrigan and Le Noble noted that in solvents with a high propensity for hydrogen bond formation, increased amounts of carbon alkylation products (**73** and **75**) are observed.[48]



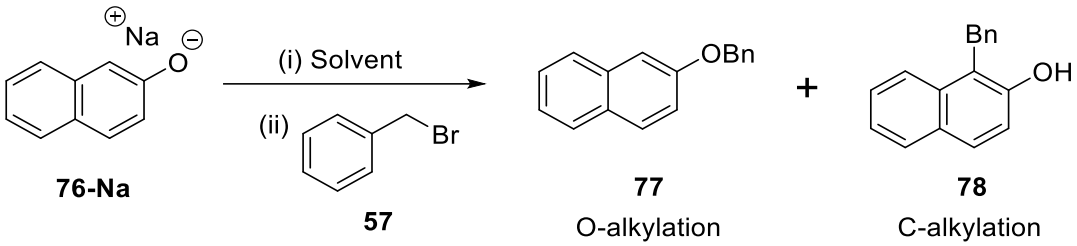
Entry	Solvent	O-alkylation %	C-alkylation %
1	DMF	100 [a]	0
2	Dioxane	100 [a]	0
3	Methanol	100 [a]	0
4	THF	100 [a]	0
5	Water	65 [b]	24[b]
6	2,2,2-Trifluoroethanol	62 [b]	26[b]

[a] The yield of these compounds was determined by gas chromatography.

[b] The yield shown in these examples is the isolated yield.

The effect of solvent choice and solvation on the course of reactions of ambident nucleophiles was further explored by Kornblum, Seltzer and Haberfield, who studied the changes observed in a reaction's product composition in solvents of differing dielectric constants.[52] A reaction between sodium β-naphthoxide (**76-Na**) and benzyl bromide (**57**) was used to demonstrate this effect. The results are shown in Table 1-6. The fact that the use of DMF and DMSO (see Table 1-6, entries 1 and 2) results in quantitative O-alkylation (**77**) whereas using the potent hydrogen bonding solvents 2,2,2-trifluoroethanol and water (see Table 1-6 entries 7 and 8) give large amounts of C-alkylation (**78**) is to be expected from the reactions shown in reference 48. The novelty here is shown within the set of aprotic solvents (Table 1-6, entries 1 – 4), where entries 3 and 4 show a considerable amount of carbon alkylation products (**78**) despite the fact the solvents are not capable of hydrogen bonding. The factor that the authors determine to be relevant here is the dielectric constant – even in aprotic solvents, a low dielectric constant causes a shift towards C-alkylation.

Table 1-6. By altering the solvent used in a reaction of sodium β-naphthoxide (**76-Na**) and **57**, varying levels of carbon alkylation products (**78**) are observed. The authors suggest that a high dielectric constant favours O-alkylation, while protic solvents or those with low dielectric constants favour C-alkylation.



76-Na **57** **77** O-alkylation **78** C-alkylation

Entry [a]	Solvent	Dielectric Constant [b]	O-alkylation %	C-alkylation % [c]
1	DMF	37	97	0
2	Dimethyl sulfoxide	45	95	0
3	DME	7	70	22
4	THF	7	60	36
5	Methanol	33	57	34
6	Ethanol	24	52	28
7	2,2,2-Trifluoroethanol	27	7	85
8	Water	80	10	84

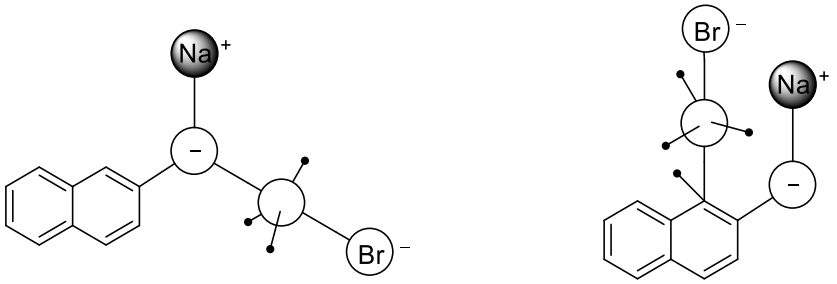
[a] Reactions conducted at room temperature unless otherwise noted.

[b] Values between 20 and 25 °C.

[c] This yield includes any dibenzylated products arising from further benzylation of 1-benzyl-2-naphthol.

The exact reason this effect is produced, according to the authors, is the ability of the solvent to reduce electrostatic interactions between the ions of the ion pair. A simple approximation of the transition states for both alkylation processes was used to help illustrate this hypothesis, shown in Figure 1-2. The distance between the ion pair in the transition state that results in O-alkylation is a factor which disfavours this process, as charge must be transferred from the oxygen atom to the bromine atom for the reaction to proceed. The sodium ion is exerting an attractive force on the bromine atom which makes this less likely to occur. In a solvent with a low dielectric constant, this attractive force is at its greatest, thus disfavouring oxygen alkylation. In contrast, a solvent with a high dielectric constant, such as DMF, will effectively shield a departing bromide anion from the attractive forces of the sodium ion. In the case of the C-alkylation transition state, the close proximity of the sodium and bromine ions means there is but a small removal of charge from the sodium ion. The carbon alkylation is considered to proceed with relative insensitivity to the dielectric constant of the solvent – only O-alkylation is hindered by a solvent with a low dielectric constant.

Figure 1-2. Kornblum, Seltzer and Haberfield presented a simplified geometry for the transition states that result in O- and C -alkylation.[52] Charge must be transferred from the oxygen atom to bromine in order for it to depart – when the two atoms are far apart this must be achieved against the attractive force of the sodium ion. This was suggested to disfavour oxygen alkylation in solvents with low dielectric constants. The sizes of the atoms drawn are not representative.



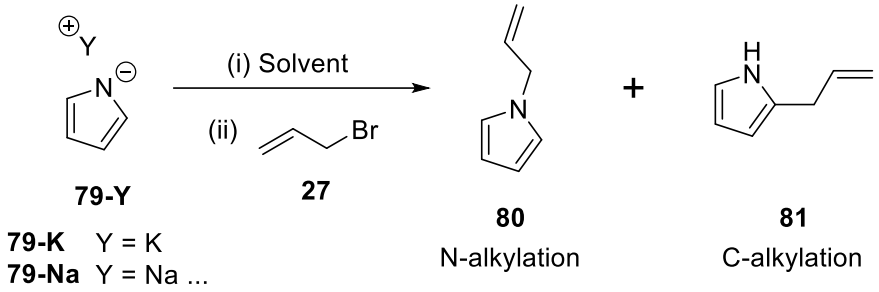
An important contrast is drawn by the authors between entries 1 and 5, and entries 6 and 7 in Table 1-6. Although DMF and methanol have similar dielectric constants, methanol shows a much greater affinity for C-alkylation. Kornblum, Seltzer and Haberfield claim this typifies their concept of "selective solvation" – the ability of methanol to form hydrogen bonds effectively blocks the ability of the oxygen atom to undergo substitution.[52] The same is true of ethanol and 2,2,2-trifluoroethanol, for which the dielectric constants are similar, but the increased ability of 2,2,2-trifluoroethanol to form hydrogen bonds results in a much greater proportion of C-alkylation.

1.2.3. Nature of the Cation

The influence that the cation of the ambident species could have on the course of the reaction was also analysed in this work.[52] The authors point out that the influence that a cation may have, and the solvent chosen for the reaction are inextricably linked – the relationship of the cation and anion in solution is determined by what the solvent has done to the ion pair in the process of solvating the salt. The authors propose that in aprotic solvents with a low dielectric constant, such as THF or diethyl ether, the anion is likely to be a part of an ion aggregate (such as those seen in Figure 1-2) as it reacts. As a result, smaller cations such as Li^+ and Na^+ will serve to hinder O-alkylation processes from occurring more than if K^+ or R_4N^+ were employed. This is due to the closer association that a smaller cation will have with the oxygen atom. In polar solvents (i.e., those with a high dielectric constant) such as DMF or DMSO, powerful solvation of the cation is considered to result in a species which is the closest approximation to a "free" ambident ion. Cation size is again the main consideration here – the implication of this is that cations will be more effectively solvated in the order $Li^+ > Na^+ > K^+ > R_4N^+$. Despite this, Kornblum, Seltzer and Haberfield reiterate that even if the anion were to react as an ion pair, the high dielectric constant means that the electrostatic force that serves to make O-alkylation less favourable is minimised.[52] In the case of protic solvents such as water and alcohols, the authors imply that the nature of the cation will be of relative unimportance. The high dielectric constant will result in a low impedance to O-alkylation if the reactants

react as an ion pair and the "selective solvation" of the oxygen atom by a protic solvent will result in a preference for carbon alkylation regardless.

Table 1-7. In solvents with low dielectric constants such as THF and toluene, the nature of the cation was shown to influence the site of addition allyl bromide (**27**) to a pyrrole anion (**79-Y**).[53] Reactions were carried out at 65 °C under homogeneous conditions.



79-Y

79-K Y = K
79-Na Y = Na ...

27

80
N-alkylation

81
C-alkylation

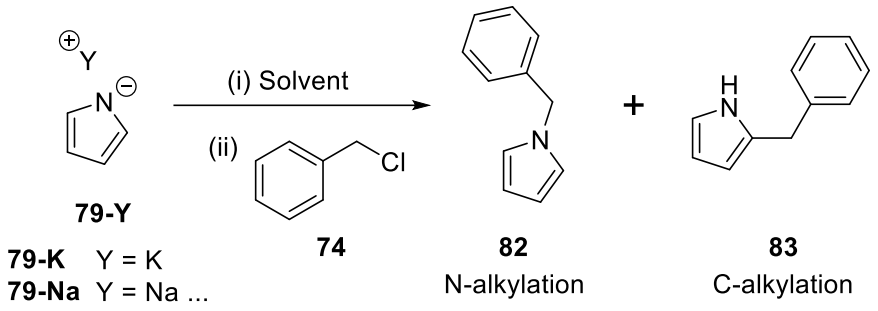
#	Y	Solvent	Yield of N- and C-alkylation (%)	N-alkylation % [a]	C-alkylation % [a]
1	K	THF	54	83.1	16.9
2	Na	THF	50	19.9	80.1
3	K	Toluene	44	84.0	16.0
4	Na	Toluene	42	80.2	19.8
5	Li	Toluene	40	62.3	37.7
6	K	DMSO	47	92.2	7.8
7	Na	DMSO	43	79.1	20.9
8	Li	DMSO	47	56.3	43.7
9	K	DMF	49	91.3	8.7
10	Na	DMF	43	66.6	33.4
11	Li	DMF	49	54.3	45.7

[a] The percentages here are relative percentages of products from a total isolated yield (e.g., the yield of the reaction in entry 1 was 54%, of which 83.1% was a N-alkylated product and 16.9% was a C-alkylated product).

In support of these claims regarding cation influence, the authors offer examples from literature, two of which are represented in Table 1-7, Table 1-8 and Table 1-9. Table 1-7 and Table 1-8 (Table 1-7 above and Table 1-8 below), each representing data from Vanderwerf and co-workers,[53] show the results of reactions of different salts of pyrrole (**79-Y**) with allyl bromide (**27**) and benzyl chloride (**74**) in the non-polar solvents THF and toluene under homogeneous conditions. As can be seen when comparing entries 1 – 2 of Table 1-7 and 1 – 3 of Table 1-8, all of which concern reactions in THF, the relative percentage of N-alkylation (**80** or **81**) increases with the decreasing coordinating ability of the counter ion for each alkyl halide. This trend is also seen in Table 1-7 entries 3 – 6 and Table 1-8 entries 4 – 7 in toluene. In the case of benzyl chloride (**74**) reactions in Table 1-8, the amount of N-alkylation (**82**) increases when changing the cation in the order $Li^+ < Na^+ < K^+ < (CH_3)_3NC_6H_5^+$ (see Table 1-8 entries 4 – 7). Interestingly, the same

study also reports that in reactions of allyl bromide (**27**) in the polar solvents DMSO and DMF, this effect is retained, with increasing N-alkylation (**80**) being observed in the order $Li^+ < Na^+ < K^+$ (see Table 1-7 entries 6 – 11). This is contrary to the expectations of Kornblum, Seltzer and Haberfield,[52] whose rationale would predict that the increased dielectric constant would preclude the cation from making a large impact on the site of addition of the alkylating agent.

Table 1-8. In solvents with low dielectric constants such as THF and toluene, the nature of the cation was shown to influence the site of addition of benzyl chloride (**74**) to a pyrrole anion (**79-Y**).[53] Reactions were done at 65 °C under homogeneous conditions.



#	Y	Solvent	Yield of N- and C-alkylation (%)	N-alkylation % [a]	C-alkylation % [a]
1	K	THF	76	99.7	0.3
2	Na	THF	70	84.3	15.7
3	Li	THF	35	19.2	80.8
4	$(CH_3)_3NC_6H_5$	Toluene	46	99.1	0.9
5	K	Toluene	44	83.2	16.8
6	Na	Toluene	45	58.2	41.8
7	Li	Toluene	40	56.5	43.5
8	K	DMSO	80	100	0
9	Na	DMSO	72	100	0
10	Li	DMSO	56	99.0	1.0
11	Li	DMF	37	98.6	1.4

[a] The percentages here are relative percentages of products from a total isolated yield (e.g., the yield of the reaction in entry 1 was 76%, of which 99.7% was a N-alkylated product and 0.3% was a C-alkylated product).

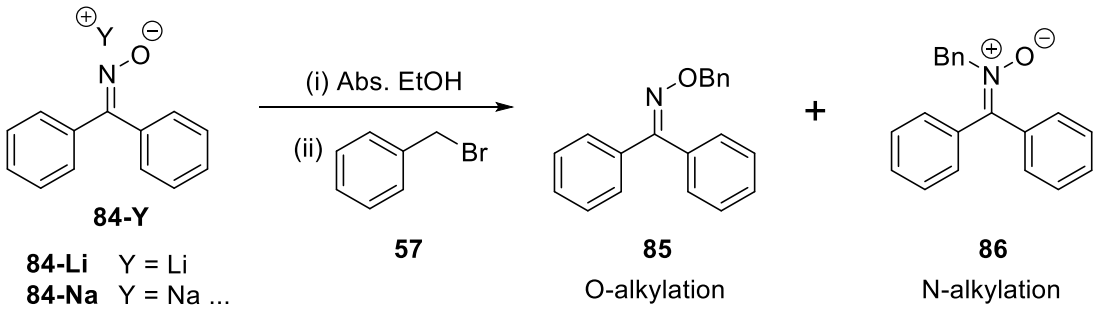
However, when the electrophile was benzyl chloride (**74**), N-alkylation occurred almost exclusively when the reactions took place in DMSO or DMF (see Table 1-8 entries 8 – 11, exclusive N-alkylation was reported in entries 8 and 9).

Vanderwerf and co-workers postulate a similar explanation for the transition states observed in the cases for N-alkylation and C-alkylation as those seen in Figure 1-2. A notable difference, however, is that they suppose that the N-alkylation is most likely produced by a reaction of the "free" pyrrole anion – thus explaining why the cations with

the lowest coordinating ability seem to give the largest proportions of N-alkylated products.

Table 1-9 shows data from Smith and Robertson[54] which demonstrates that in reactions of benzophenone oxime salts (**84-Y**) with benzyl bromide (**57**) in absolute ethanol, altering the cation does not produce a large change in the O- vs N-alkylation ratio (**85** vs. **86**) that is subsequently observed in the products.

Table 1-9. This set of reactions where salts of benzophenone oxime (**84-Y**) react with benzyl bromide (**57**) in absolute ethanol shows there is no significant influence of the cation on the proportion of products formed. Kornblum, Berrigan and Le Noble and used these data to support the claim that in polar protic solvents, the influence of the cation on the course of the reaction is negligible.



84-Y

84-Li Y = Li
84-Na Y = Na ...

57

85
O-alkylation

86
N-alkylation

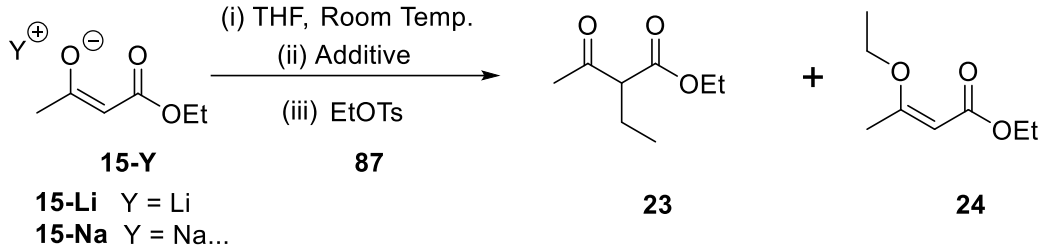
Entry	Y	O-alkylation %	N-alkylation % [a]
1	Li	73	22
2	Na	70	23
3	K	77	20
4	$(CH_3)_4N$	69	23

[a] Note that for the N-alkylation process, there are two possible conformations of the resulting nitrone. Only one is drawn in the scheme above, but both are represented in the values shown in the table.

The authors found it "*difficult to reconcile*" that the product ratio did not change much between reaction of salts of cations with such different field strengths, whereas Kornblum, Seltzer and Haberfield use this finding as an exemplar of the insignificance of the cation in reactions of ambident nucleophiles that take place in polar protic solvents.[52]

The large effect that the cation of an enolate and the reaction solvent can have on the outcome of reactions of ambident nucleophiles is exemplified by a set of experiments conducted by Nee, Leroux and Seyden-Penne.[55] The authors were investigating the effect that a "solid solvent" could have on the reaction of enolates of ethyl acetoacetate (**14**) with ethyl tosylate (**87**). The "solid solvent" in this case was an analogue of the highly polar and aprotic solvent HMPA mounted on a polystyrene-type resin. A selection of their results is shown below in Table 1-10, demonstrating the effects that the addition of both "solid" and liquid HMPA could have on the outcome of a reaction of the metal enolates **15-Y** in THF.

Table 1-10. Ethylations of various metal enolates (**15-Y**) by ethyl tosylate **87** in THF solution at room temperature.[55] Nee, Leroux and Seyden-Penne investigated the effect that the addition of "solid" (resin-bound) HMPA and liquid HMPA could have on the ratio of the products of the reaction (**23** and **24**). All reactions were performed at a concentration of 0.33 mol L^{-1} of the reactants. All reactions proceeded for 24 hours unless otherwise noted.



15-Y **87**

15-Li Y = Li
15-Na Y = Na...

23 **24**

#	Y	Additive	Eq. of Additive	Yield %	C-alkylation %	O-alkylation %
1	Li	None	N/A	< 5	0	0
2	Li	"Solid" HMPA [b]	1	19	34	66
3	Li	HMPA	1	54	41	59
4 [a]	Li	HMPA	2	83	34	66
5	Na	None	N/A	18	> 99	< 1
6	Na	"Solid" HMPA [b]	1	44	62.5	37.5
7	Na	HMPA	1	46	70	30
8	Na	HMPA	4	83	44	56
9	K	None	N/A	62	88	12
10	K	"Solid" HMPA [b]	1	94	31	69
11	K	HMPA	1	50	73	27
12	K	HMPA	4	100	30	70
13	K	HMPA	10	100	14	86

[a] This reaction was allowed to proceed for 74 hours.

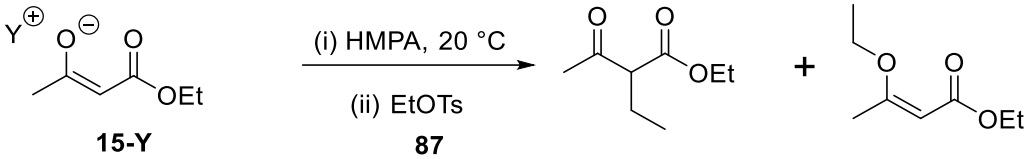
[b] The "solid" HMPA was an analogue of the highly polar and aprotic solvent HMPA mounted on a polystyrene-type resin.

The results show the striking effect that the added HMPA has on the course of the reactions. One obvious observation that can be made when comparing Table 1-10 entries 1 and 2 is that the lithium enolate of ethyl acetoacetate (**15-Li**) will not react with **87** in THF without any added HMPA. In the case of **15-Na** and **15-K**, the addition of enough equivalents of HMPA to the reaction can cause the selectivity to invert from preferential C-alkylation (**23**) to preferential O-alkylation (**24**) (this can be seen when comparing Table 1-10 entries 5 and 8 for **15-Na** and Table 1-10 entries 9 and 10 for **15-K**). Additionally, the presence of HMPA in the reaction mixtures increases the yield over the same timescale when comparing to the reactions in THF alone. These reactions

demonstrate the supposed difference between metal enolate reactions in non-polar aprotic solvents and in polar aprotic solvents as outlined by Kornblum, Berrigan and Le Noble.[49]

A pair of studies by Reutov and co-workers investigating the kinetics of the alkylation of various metal enolates of ethyl acetoacetate (i.e., metal enolates derived from compound **14**, denoted as **15-Y**) revealed some points of note with regard to the role of the cation in the reaction of ambident nucleophiles.[56,57] Relevant data from their reactions of various metal enolates of **15-Y** with ethyl tosylate (EtOTs, **87**) in HMPA are shown below in Table 1-11.

Table 1-11. Ethylations of various metal enolates of **15-Y** by **87** in HMPA solution at 20 °C. The concentration of the enolate is equal to the concentration of **87** in all reactions. The C vs O ratio of the products (k_c / k_o) remains constant in each reaction.



15-Y

15-Li Y = Li
15-Na Y = Na...

87

23

24

+ YOTs

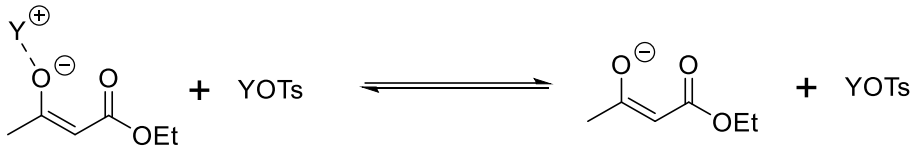
#	Y	[Enolate] × 10^2 (mol L^{-1})	$k_2 \times 10^3$ [a] (L mol^{-1} sec^{-1})	k_c / k_o	#	Y	[Enolate] × 10^2 (mol L^{-1})	$k_2 \times 10^3$ [a] (L mol^{-1} sec^{-1})	k_c / k_o
1	Li	2.00	0.34	0.13	**9**	K	1.06	9.4	0.13
2	Li	4.00	0.23	0.13	**10**	K	2.06	7.7	0.13
3	Li	6.00	0.14	0.13	**11**	K	4.08	6.1	0.13
4	Li	8.00	0.12	0.13	**12**	K	7.28	3.2	0.13
5	Na	2.00	5.7	0.13	**13**	Cs	1.00	12.5	0.13
6	Na	4.00	4.0	0.13	**14**	Cs	1.92	10.8	0.13
7	Na	6.00	3.5	0.13	**15**	Cs	4.01	8.7	0.13
8	Na	8.30	3.0	0.13	**16**	Cs	8.00	6.0	0.13

[a] The rate constants are an average of three or more independent measurements. The potential deviation is ± 5%.

As can be seen in the data above, the C vs, O alkylation ratio (k_c / k_o) observed in each reaction is insensitive to changes in the cation of the enolate or the concentration of the reagents. It is likely that this effect can be attributed not only to the high polarity of the HMPA solvent but also its powerful cation solvating ability – one measurement by Reich and Kulicke suggests that HMPA is approximately 285 times more effective at solvating lithium cations than THF.[58] Reutov and co-workers determined that the rate constant does not depend on the initial ethyl tosylate (**87**) concentration. However, when the initial enolate concentration is changed there is a profound effect on the observed rate constant. Throughout all metal enolate reaction series (Table 1-11 entries 1 – 4, entries 4 – 8 etc.) a decrease in the initial enolate concentration resulted in an increase in the measured rate constant. The authors account for this observation by citing the "common cation effect"

– the salt produced in the reaction when either **23** or **24** is formed (YOTs) is capable of re-forming the metal enolate from the "free" anion. This rationale is predicated on the idea that the uncomplexed "free enolate" (**88** in Scheme 1-8 below) is significantly more reactive than the metal enolate complex. The production of YOTs shifts the equilibrium (shown below in Scheme 1-8) to the left, which reduces the quantity of reactive species present in the mixture.

Scheme 1-8. Reactions of various metal enolates of ethyl acetoacetate (**15-Y**) with ethyl tosylate (**87**) results in the formation of the corresponding alkali metal tosylate (YOTs). The authors argue that the formation of this salt shifts the equilibrium shown below to the left, favouring the non-dissociated species and resulting in an observed reduction in the measured rate constant.

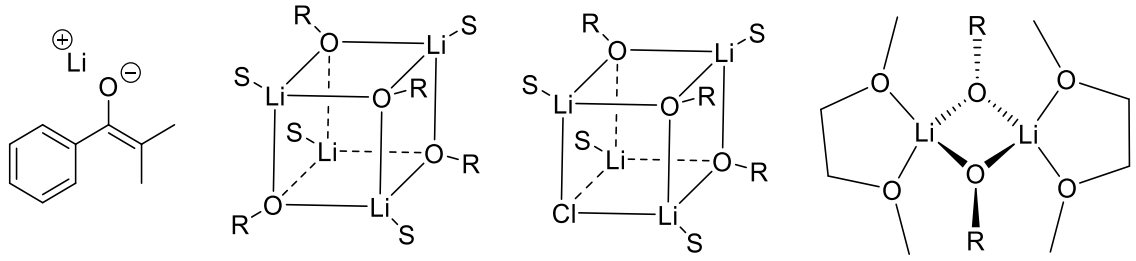


15-Y **88**

The authors tested this hypothesis by adding an equimolar amount of sodium tosylate (NaOTs) to a reaction of **15-Na** with ethyl tosylate (**87**) in HMPA – they observed a reduction in the reaction rate of 1.5 times relative to the same reaction with no NaOTs added. This "common ion effect" has also been demonstrated to have an effect on the rates of solvolysis reactions of aliphatic halides and haloalkanes.[59–61]

In polar aprotic solvents, ion-pair aggregates are believed to be the reactive species in reactions of enolates. A pair of studies by Jackman and Lange[62] and Jackman and Dunne[63] investigated the influence that these aggregates could have on the site of addition in reactions of enolates.

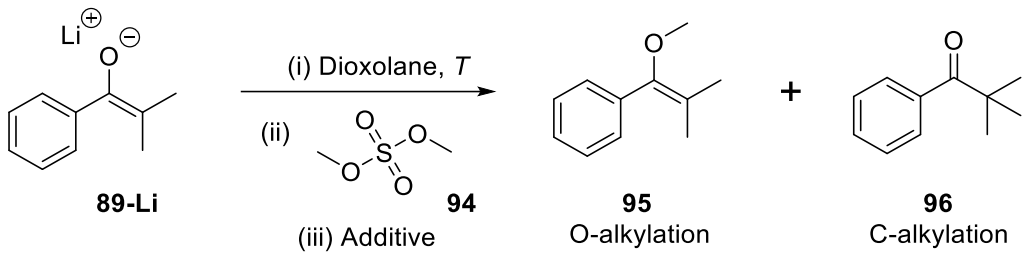
Figure 1-3. Jackman and Lange[62] investigated the conformation and reactivity of the aggregates of lithioisobutyrophenone (**89-Li**) in two polar aprotic solvents – dioxolane and dimethoxyethane (DME). **89-Li** in dioxolane exists as the tetramer **90** which can appear as two different solvates depending on temperature – a lower temperature yields the more highly solvated complex. The addition of lithium chloride (**91**) converts the tetramer **90** to **92** which incorporates the chlorine atom. In DME, the authors suggest that the dimer **93** is the major species seen in solution with approximately 15% of **90** (the tetramer) also present. These species were characterised in separate works by Jackman and Haddon[64] and Jackman and Szeverenyi.[65]



The authors aimed to use these ion-pair aggregates of known conformation to investigate the theory that a lithium cation may "block" the oxygen atom in an enolate reaction taking place in a solvent with a low dielectric constant.[66] To achieve this, a variety of methylating agents were employed, as well as several cation complexing reagents (such as crown ethers and cryptands). Initially, the effect of temperature on the C- vs. O-alkylation ratio of a reaction between **90**-**Li** and dimethyl sulfate (**94**) in the two solvents was determined. A selection of results is shown below in Table 1-12.

The authors prefaced the experiment by proposing that the expected product ratio (C/O ratio) for a reaction between **89-Li** and a given alkylating agent should be characteristic for a certain aggregate species of **89-Li** (see Figure 1-3, **90** or **92**). Although the rate of the reaction should be affected by changes in temperature, the C/O ratio should remain the same as long as the same aggregate species is involved in the reaction. Jackman and Lange found that between 30 °C and 75 °C (Table 1-12 entries 5 – 9) the C/O ratio was relatively insensitive to changes in temperature. However, at temperatures below 30 °C, the amount of C-alkylation (**96**) increases considerably (see Table 1-12 entries 1 – 4). The authors ascribe this observed change in selectivity to the increased presence of the highly solvated tetramer species in low-temperature solutions of dioxolane. This variance in observed selectivity at different temperatures confirms the important role that aggregates play in determining the selectivity of the reaction of ambident nucleophiles. The addition of LiCl (**91**, Table 1-12 entries 10 – 15) to the reaction mixtures did not appear to greatly affect the observed selectivity at any of the chosen temperatures.

Table 1-12. Results (C/O ratios) for reactions between **89-Li** and dimethyl sulfate (**94**) in dioxolane at various temperatures.[66] The effect of LiCl (**91**) addition to the reaction mixture was also investigated. The C/O ratio is essentially constant in the temperature range 30 – 75 °C. At temperatures below 30 °C, considerably more C-alkylation (**96**) is observed. Obtaining a half-life ($t_{1/2}$) for certain low temperature reactions was not feasible as the reaction was prohibitively slow.

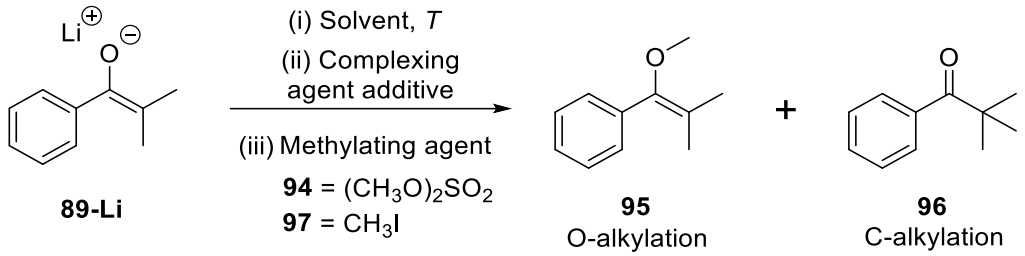


89-Li **94** **95** O-alkylation **96** C-alkylation

#	*T* (°C)	$t_{1/2}$ (mins)	Additive	C/O ratio	#	*T* (°C)	$t_{1/2}$ (mins)	Additive	C/O ratio
1	–20	N/A	None	1.56	**10**	–20	N/A	1.23 eq. LiCl	1.50
2	–10	2000	None	1.27	**11**	–10	N/A	1.23 eq. LiCl	1.08
3	0	720	None	1.22	**12**	2	420	1.23 eq. LiCl	1.04
4	11	170	None	0.96	**13**	11	160	1.23 eq. LiCl	0.92
5	23	80	None	0.89	**14**	25	60	1.23 eq. LiCl	0.92
6	40	14	None	0.89	**15**	50	5	1.23 eq. LiCl	0.82
7	50	8	None	0.79					
8	62	3	None	0.82					
9	73	< 1	None	0.79					

The half-lives of the reactions shown in Table 1-12 are the amounts of time required for the enolate **89-Li** to reach half of its initial concentration in each experiment. The authors propose that these results indicate that the reactivity of the tetramers is unaffected by replacement of $^{-}$OR with $^{-}$Cl in the aggregate structure (see Figure 1-3, **90** and **92**). The authors note that the ^{13}C NMR chemical shifts of all carbon atoms of the enolate anion are not changed when examining a solution of species **92** vs. a low temperature solution of **90** – a fact which supports the theory that the two species have a similar electron distribution.[65] The authors then examined the effect that the addition of a cation complexing agent would have on the C/O ratio observed in the reactions of **89-Li** with various methylating agents (**94** and **97**) in dioxolane and DME. The structures of the complexing agents used are seen below in Chart 1-1. The results of these experiments are shown in part below in Table 1-13. These experiments revealed the substantial effect that complexation of the lithium cation of **89-Li** has on the C vs. O product ratio of the reactions.

Table 1-13. The reaction between **89-Li** and two methylating agents (dimethyl sulfate (**94**) and methyl iodide (**97**)) in dioxolane and DME was examined.[66] When a Li^+ complexing additive was added to the reaction, a profound effect on the C/O ratio was observed. All reactions were carried out at a **89-Li** concentration of 0.162 mol L^{-1} at 23 °C.



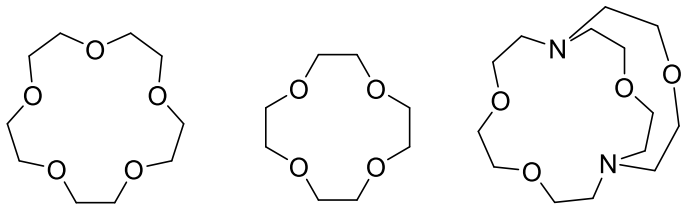
#	Complexing Agent [a]		Methylating Agent	Solvent	C/O Ratio
	Identity	Equivalents			
1	None	N/A	$(CH_3O)_2SO_2$	Dioxolane	0.89
2	15-crown-5 (**98**)	1.00	$(CH_3O)_2SO_2$	Dioxolane	0.39
3	12-crown-4 (**99**)	1.00	$(CH_3O)_2SO_2$	Dioxolane	0.25
4	[2.1.1]-cryptand (**100**)	1.10	$(CH_3O)_2SO_2$	Dioxolane	0.08
5	None	N/A	CH_3I	Dioxolane	> 100
6	15-crown-5 (**98**)	1.00	CH_3I	Dioxolane	49
7	12-crown-4 (**99**)	1.26	CH_3I	Dioxolane	24
8	[2.1.1]-cryptand (**100**)	1.10	CH_3I	Dioxolane	6
9	None	N/A	$(CH_3O)_2SO_2$	DME	1.22
10	15-crown-5 (**98**)	1.00	$(CH_3O)_2SO_2$	DME	0.33
11	12-crown-4 (**99**)	1.26	$(CH_3O)_2SO_2$	DME	0.28
12	[2.1.1]-cryptand (**100**)	1.10	$(CH_3O)_2SO_2$	DME	0.08
13	None	N/A	CH_3I	DME	> 200
14	15-crown-5 (**98**)	1.00	CH_3I	DME	49
15	12-crown-4 (**99**)	1.00	CH_3I	DME	49
16	[2.1.1]-cryptand (**100**)	1.10	CH_3I	DME	8

[a] The structures of the complexing agents are shown below in Chart 1-1.

In all experiments, the addition of a complexing agent (**98**, **99** or **100**) resulted in an increase in the amount of O-alkylation observed (i.e., a decrease in the C/O ratio). In some cases (see Table 1-13 entries 9 and 10), addition of a complexing agent caused the preferred product of the reaction to switch from **96** to **95**. Perhaps the most striking observation can be made when comparing Table 1-13 entries 13 and 16 – the addition of **100** to the reaction mixture in a reaction of **89-Li** with **97** in DME causes the C/O ratio to change from over 200 to 8. The authors propose that the complexing agents must create

new reactive species, unlike any seen in Figure 1-3, upon encapsulation of the lithium cation of **89-Li**.

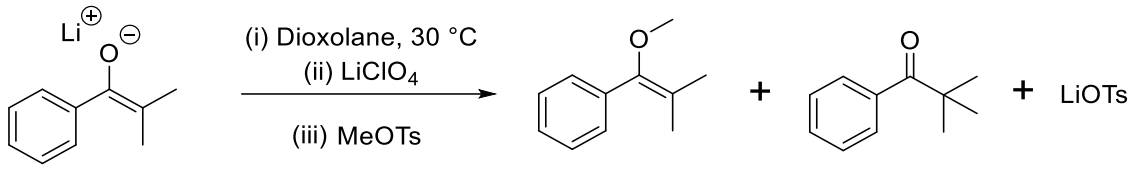
Chart 1-1. Structures of various cation complexing agents employed in the study of Jackman and Lange.[66]



15-crown-5 **98** | 12-crown-4 **99** | [2.1.1]-cryptand **100**

A further nuance of how aggregates may affect the outcomes of reactions of ambident species was revealed in work by Jackman and Dunne.[63] In a reaction between **89-Li** and methyl *p*-toluenesulfonate (**101**, MeOTs) in dioxolane, the salt by-product LiOTs (**102**) forms as the reaction progresses. Jackman and Dunne state that the formation of LiOTs (**102**) during the reaction gives rise to mixed aggregates which react in a different manner to the cubic tetramer which is seen at the start of the reaction.

Table 1-14. The production of LiOTs in a reaction between **89-Li** and methyl *p*-toluenesulfonate (**101**, MeOTs) results in an altered C/O product ratio as the reaction progresses.[63] This effect was demonstrated by the addition of $LiClO_4$ (**103**) to the reaction mixture in varying concentrations, which should incur the formation of similar aggregates as those produced by (**92**) formation.



89-Li | **101** | **95** O-alkylation | **96** C-alkylation | **102**

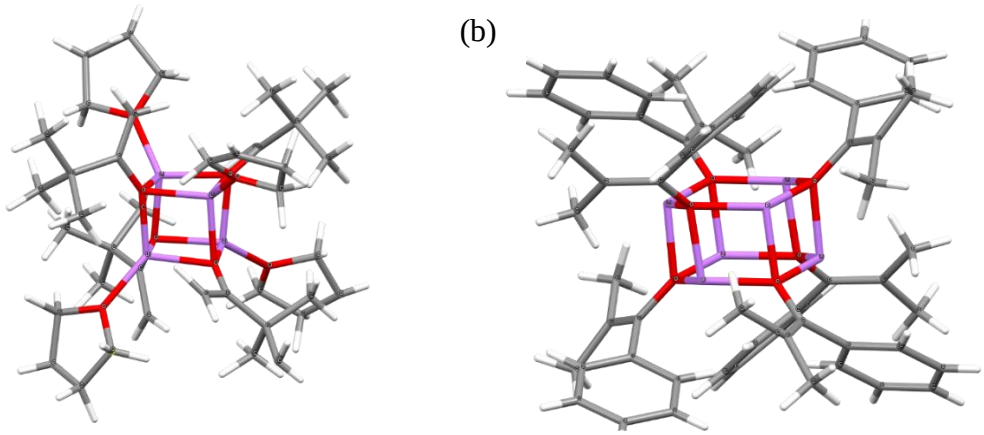
Entry	[$LiClO_4$] (mol L^{-1})	C/O ratio	Entry	[$LiClO_4$] (mol L^{-1})	C/O ratio
1	0	5.69 ± 0.15	**6**	0.11	0.99 ± 0.02
2	0.005	4.67 ± 0.08	**7**	0.22	1.03 ± 0.03
3	0.027	2.10 ± 0.03	**8**	0.33	0.72 ± 0.03
4	0.05	1.88 ± 0.05	**9**	0.43	0.78 ± 0.04
5	0.081	1.27 ± 0.03			

As a result, the C/O ratio is affected as the LiOTs (**102**) concentration increases – meaning the final C/O product ratio is directly changed by the emergence of new ion-pair aggregates as the reaction proceeds. To demonstrates this effect, the authors set up a series of reactions with varying levels of $LiClO_4$ (**103**) added – which should affect aggregates

in a similar way to the presence of LiOTs (**102**). The results are seen in Table 1-14 above. The relative formation of the C-alkylated product (**96**) was highest when no $LiClO_4$ (**103**) was present in the reaction (Table 1-14 entry 1) – a scenario similar to the beginning of a reaction when no LiOTs (**102**) has formed. Increasing concentrations of $LiClO_4$ cause the O-alkylated product (**95**) to form in greater amounts, with **95** eventually becoming the major product of the reaction (Table 1-14 entries 8 and 9). These reactions demonstrate the numerous intricacies that may arise from the nature of the cation and the ion-pair aggregates which may direct the course of reaction of an ambident nucleophile. The structures and reactivities of the mixed aggregates of organometallic compounds (such as lithium enolates) has been detailed in reviews[58,67,68] and computational studies.[69] X-ray crystallography studies have confirmed that lithium enolates are aggregated both in the presence or absence of a solvent.[70,71]

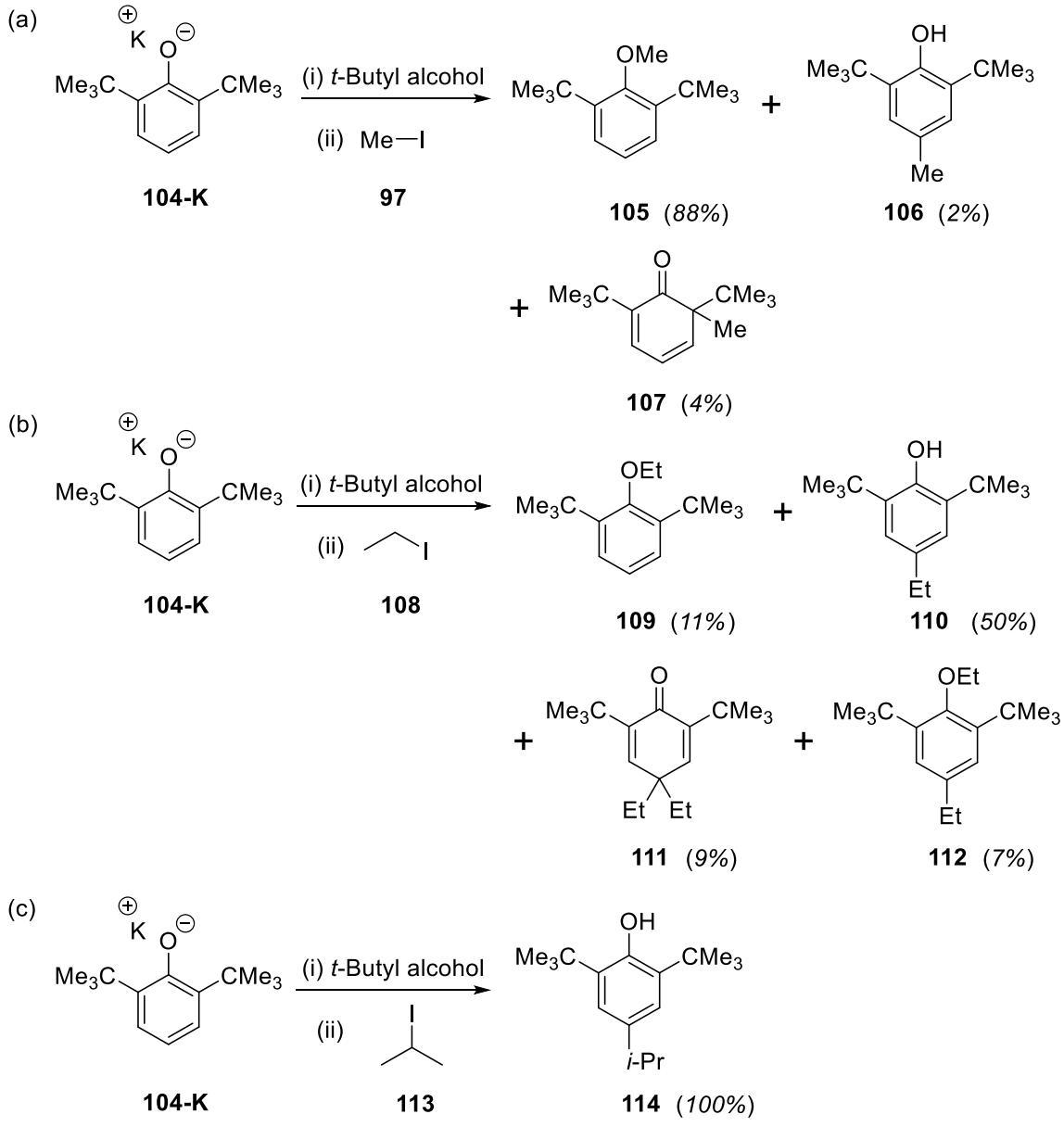
Figure 1-4. (a) X-ray crystal structure showing the cubic tetrameric structure of the aggregate of the lithium enolate of 3,3-dimethyl-2-butanone formed from a THF solution of the enolate.[70] The solvated cubic tetramer shown is of the same type described by Jackman and Szeverenyi[65] (see **90**, Figure 1-3). **(b)** X-Ray crystal structure showing the hexameric structure of the aggregate of lithioisobutyrophenone (**89-Li**) formed in the absence of solvent.[71,72] In each figure, the red vertices are the sites of oxygen atoms and the pink vertices are lithium atoms. The grey vertices are carbon atoms and the white termini of the structure are hydrogen atoms.

(a) (b)



Kornblum and Seltzer produced a short study demonstrating that the steric hindrance could influence the site of addition in reactions of potassium 2,6-di-*t*-butylphenoxide (**104-K**) with methyl, ethyl and isopropyl iodides (**97**, **108** and **113**).[73] They showed that O-alkylation of **104-K** becomes less prevalent as the size of the alkyl group of the electrophile increases (i.e., O-alkylation decreases in the order MeI > EtI > *i*-PrI). These reactions are illustrated below in Scheme 1-9. Reaction (a) demonstrates that with methyl iodide (**97**), the major product of the reaction is the O-alkylation product **105**. Upon switching the electrophile to a bulkier alkyl group like isopropyl iodide (**113**) in reaction (c), only the C-alkylation product (**114**) is formed.

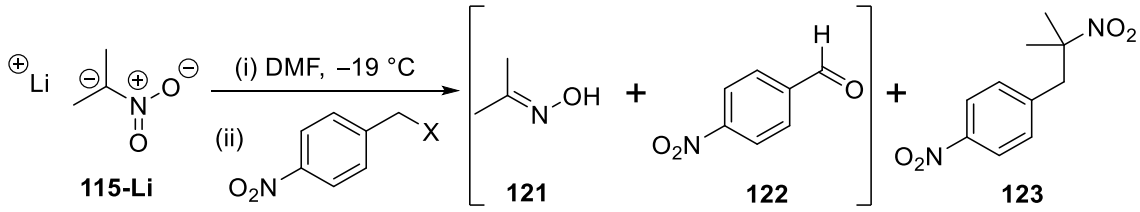
Scheme 1-9. Reactions of potassium 2,6-di-*t*-butylphenoxide (**104-K**) with increasingly bulky alkyl halides. **(a)** With methyl iodide (**97**), the major product is O-alkylation (**105**). **(b)** The use of ethyl iodide (**108**) results in preferential C-alkylation. **(c)** When using isopropyl iodide (**113**), only the C-alkylation product (**114**) is observed. Note the appearance of the di-C-alkylated product (**111**) and the mixed O- and C-alkylation product (**112**) observed in the reaction of **104-K** with **108**. Analogous products are commonly observed in the alkylation of enolates.



1.2.4. Nature of the Leaving Group – HSAB Theory and the Concepts of Charge- and Orbital-controlled Reactions

A separate study by Kornblum, Pink and Yorka (of which details are given in Table 1-15 below) examined the effect the nature of the alkyl halide could have on the site of addition of the lithium salt of 2-nitropropane (**115-Li**).[74] The group was investigating an odd result observed by Hass and Bender,[75] which involved the reactions of nine *para*-substituted benzyl halides with the sodium salt of 2-nitropropane (**115-Na**). Of the halides, which included *para*-methyl, *para*-bromo, *para*-trifluoromethyl and *para*-nitro substituents, only *para*-nitro benzyl chloride (**118**) was observed to give any carbon alkylation at all, with the rest undergoing O-alkylation processes exclusively. Kornblum, Pink and Yorka investigated this phenomenon by synthesising various *para*-nitro benzyl reagents (**61**, **116** – **120**) with different leaving groups and observing their reactions with the **115-Li**. The data returned from this study are shown in Table 1-15 below (note that the mechanism for the formation of the O-alkylation products is shown in Scheme 1-10 below).

Table 1-15. Amounts of O- and C-alkylation products formed in reactions of lithium salt of 2-nitropropane (**115-Li**). The percentage values given are the isolated yields of the compounds.



116 X = $^{+}NMe_3$
117 X = Pentachlorobenzoate ester
118 X = Cl **119** X = OTs
61 X = Br **120** X = I

Entry [b]	X	O-alkylation %	C-alkylation %
1 [c]	$^{+}NMe_3$	0	93
2 [c]	Pentachlorobenzoate ester	0	93
3	Cl	1	95
4	OTs	32	40
5	Br	65	17
6	I	81	7

[a] O-alkylation of the 2-nitropropane anion results in nitronic esters. These are not isolated, but the oxime (**121**) and aldehyde (**122**) shown above to denote O-alkylation must be derived from the decomposition of a nitronic ester.

[b] The reactions were done at –19 °C unless otherwise noted.

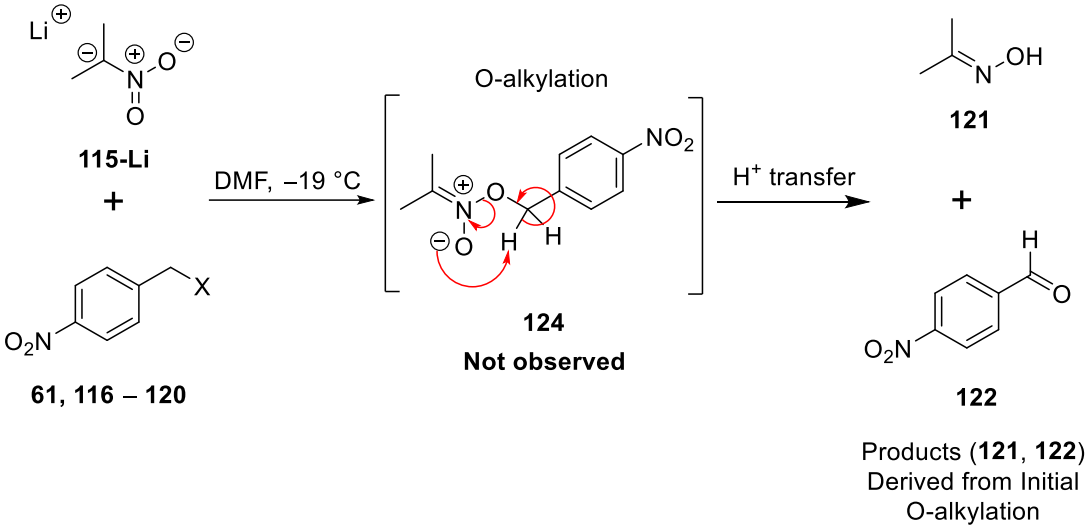
[c] Run at 25 °C

Kornblum, Pink and Yorka observed a complete swap in the preferred site of addition when going from leaving groups such as $^{+}NMe_3$ (**116**) to iodide (**120**). Of particularly stark contrast are Table 1-15 entries 3 and 6 – chloride giving almost entirely C-alkylation

products (**123**) whilst iodide gives mostly O-alkylation (**121** and **122**). This effect was not observed for unsubstituted benzyl halides, in which reactions of **115-Li** with benzyl chloride, benzyl iodide and benzyl tosylate all give between 82% and 84% O-alkylation and ~1% of the C-alkylation product.

Note that the products shown in Table 1-15 as "O-alkylation products" are formed from the decomposition of the nitronic ester (**124**, see below) that is originally formed from the O-benzylation of **115-Li**. A mechanism showing how compounds **121** and **122** in Table 1-15 arise as a result of an initial O-alkylation of **115-Li** is shown below in Scheme 1-10.

Scheme 1-10. Proposed mechanism for the formation of products **121** and **122** from the unstable initial O-alkylation product **124** (nitronic ester).



A follow-up study revealed that the use of trialkyloxonium tetrafluoroborates of the type first prepared by Meerwein[76,77] enabled quantitative conversion to the nitronic ester in reactions of salts of nitroethane and *para*-nitrophenylnitromethane.[78]

Shortly after Kornblum's investigations into ambident reactivity, Ralph G. Pearson introduced his concept of hard and soft acids and bases,[79–83] which attempted to rationalise the stability of metal complexes and the mechanisms of their formation. The theory proposes that certain chemical species are "hard", owing to their small size, low polarizability, high electronegativity and high oxidation state. "Soft" species are those that have large atomic radii, high polarizability, low electronegativity and a low oxidation state. The central supposition of this theory is that "hard" acids preferentially coordinate with "hard" bases, and "soft" acids prefer to coordinate with "soft" bases. The proposed favourability of "hard-hard" and "soft-soft" interactions was thus suggested to provide a prediction of how any two chemical species may interact. The classification of an ion as "hard" or "soft" was originally done using equilibrium constants of the reactions of two Lewis bases competing for a Lewis acid. The foundations of this theory were laid in a previous investigation by Edwards and Pearson[84] into the factors which control the rates of reactions of nucleophiles.

Both Klopman[85] and Salem[86] furthered these ideas by using molecular orbital perturbation theory to formulate equations that describe the energy changes that occur as two chemical species approach each other and begin to interact. Their findings are simplified and summarised in Equation 1.1.

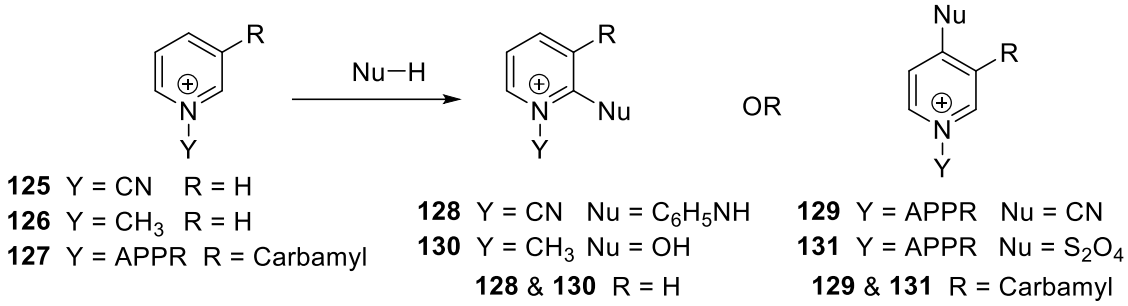
$$E_{\mathrm{i}} = E_{\mathrm{core}} + E_{\mathrm{electrostatic}} + E_{\mathrm{overlap}} \qquad (1.1)$$

Equation 1.1, taken from Isaacs' *Physical Organic Chemistry* 2nd ed.,[87] describes the forces of interaction between a nucleophile and electrophile in the early stages of bond formation. The core term is the electron-electron repulsion energy between the species. The electrostatic term is the attraction as a result of the charge or dipolar character of the species, and the overlap term describes attraction as a result of the interaction of their frontier orbitals. The overlap term will be large if the reacting partners have a symmetry compatible HOMO and LUMO that are similar in energy. Klopman draws parallels with HSAB theory in saying that "hard-hard" interactions are charge-controlled (i.e., the electrostatic term is the largest contributor) whereas "soft-soft" interactions are orbital-controlled (i.e., the overlap term is the largest contributor).

Klopman specifically noted that his theory about chemical reactivity provided a way to link the concepts of HSAB theory with reactions of ambident nucleophiles.[85] An example came in the form of the various sites of addition that could occur on the pyridinium ion, illustrated in Table 1-16. Kosower found that in reactions of various 1-substituted pyridinium rings (**125** – **127**) with various nucleophiles, addition occurred at either the 2- (**128** and **130**) or 4-position (**129** and **131**) of the ring.[88] The products of some of these reactions are shown in Table 1-16. Kosower observed that when the nucleophile was aniline or hydroxide, addition at the 2-position was observed (**128** and **130**) whereas CN^- and $S_2O_4^-$ added to the 4-position (**129** and **131**).

Klopman calculated the perturbation produced by five theoretical nucleophiles of increasing hardness interacting with the 2- and 4-positions of a pyridinium ion. The calculations revealed that the hardest nucleophiles preferentially reacted at the 2-position and the softer nucleophiles preferentially reacted at the 4-position. Subsequently, Klopman used these observations to diagnose that the 2-position was the local "hard" site of the pyridinium ion, and the 4-position was the local "soft" site.

Table 1-16. Sites of addition to pyridinium ions (**125 – 127**) in reactions with various nucleophiles.[88]



125 Y = CN R = H
126 Y = CH_3 R = H
127 Y = APPR R = Carbamyl

128 Y = CN Nu = C_6H_5NH
130 Y = CH_3 Nu = OH
128 & **130** R = H

129 Y = APPR Nu = CN
131 Y = APPR Nu = S_2O_4
129 & **131** R = Carbamyl

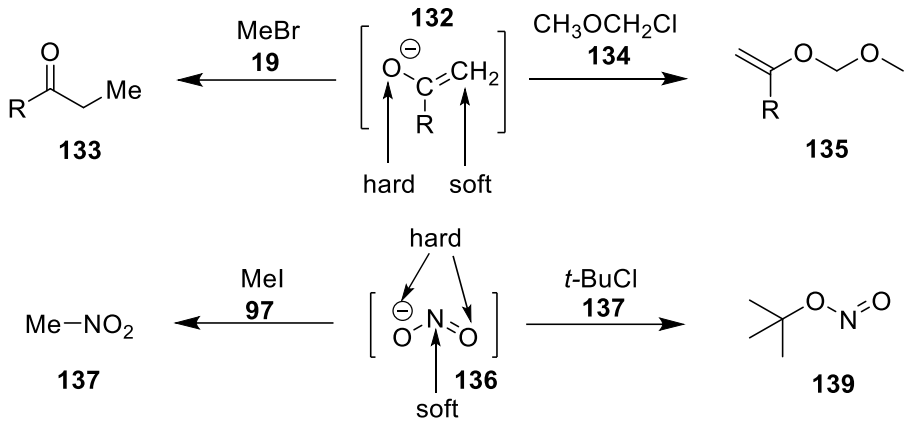
Entry [a]	Y	Nucleophile	Other ring substituents	Site of addition
1	CN	$C_6H_5NH_2$	None	2-position
2	CH_3	OH^-	None	2-position
3	APPR [b]	CN^-	3-Carbamyl	4-position
4	APPR	$S_2O_4^-$	3-Carbamyl	4-position

[a] The counter-ion for each pyridinium compound is not given in the original manuscript.
[b] APPR = Adenosinediphosphate-ribosyl.

Klopman posited that this was a perfect match with the observations of Kosower – the "hard" nucleophiles ^-OH and $C_6H_5NH_2$ (Table 1-16 entries 1 and 2) attached to the 2-position as those reactions are charge controlled, and the soft nucleophiles CN^- and $S_2O_4^-$ (Table 1-16 entries 3 and 4) added to the 4-position due to orbital control. It is noteworthy that Klopman does not acknowledge that there may be an influence on the site of additions by steric interaction with the adduct present at the 3-position in the various reactions performed by Kosower that are drawn in Table 1-16. Klopman noted that this supposition could also be applied to explain the site of addition of other ambident nucleophiles such as enolates and nitrite anions as shown below in Scheme 1-11. For example, the nitrite anion (**136**) shown in is deemed to have "hard" and "soft" local sites which will preferentially react with "hard" and "soft" electrophiles, respectively. Klopman posits that a "soft" electrophile such as MeI (**97**) will react at the "soft" nitrogen atom of the nitrite anion (**136**), and the "hard" electrophile *t*-BuCl (**138**) will preferentially react with the "hard" oxygen site of the anion.

The combination of HSAB theory and Klopman and Salem's theories of charge-controlled and-orbital controlled reactions make up the basis for the vast majority of modern rationalisations of ambident reactivity. The attraction towards this general idea was immediate – for example R. F. Hudson used the theory of hard and soft acids and bases to rationalise selectivities in substitution reactions of organophosphorus compounds.[89]

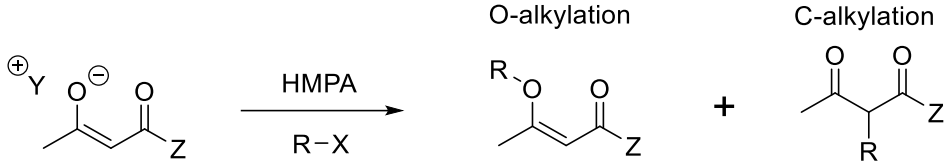
Scheme 1-11. Klopman suggested that the observed selectivity in reactions of ambident anions such as those shown below could be explained through use of his equation which calculates the perturbation energy produced by a nucleophile reacting at each reactive site.



A paper by Kurts *et. al.* cited both Pearson and Klopman in attempt to rationalise the selectivities observed in reactions of sodium acetylacetonate (**140-Na**) and the potassium enolate of ethyl acetoacetate (**15-K**) with alkyl bromides (**19**, **22**, **25**), alkyl iodides (**16**, **98** and **109**) and alkyl tosylates (**88**, **102** and **143**).[90] The results of some of these reactions are shown below in Table 1-17.

The authors note that there seems to be an alkyl group influence on the O vs. C ratio, observed when comparing, for example, Table 1-17 entries 1, 4 and 8, or entries 3, 7 and 11. As the alkyl group increases in size (and consequently, "softness"), the amount of O-alkylation decreases. Note that it is the authors suggestion in this instance that larger alkyl groups are "softer". There appears to be a strong correlation between the "softness" of the alkyl halide employed and the level of C-alkylation observed – all series of reactions shown below (e.g., Table 1-17 entries 1 – 3, 4 – 7, 8 – 11 etc.) demonstrate that the amount of C-alkylation increases as the alkylating agent becomes "softer". The alkylating agents are considered "softer" when the leaving groups have larger atomic radii and are more polarisable (i.e., the trend of alkylating agent "softness" decreases in the order R–I > R–Br > R–Cl > R–OTs). Referencing Klopman,[85] the authors state that the decrease in O-alkylation observed in the alkyl tosylate series (Table 1-17 entries 1, 4 and 8 and entries 12, 15 and 19) must be due to the electron-donating properties of the alkyl group altering the electrostatic interaction (see Equation 1.1 above) between the reactants. Although this is in overall agreement with what was seen in previously established literature (i.e., an increase in C-selectivity upon going from R–OTs to R–I), the magnitude of this effect is reduced, and O-alkylation is preferred for reactions of *s*-BuI (**16**) with each of the enolates **15-K** and **141-Na** (see Table 1-17 entries 8 and 19). The opposite is true for any other reaction of alkyl iodides. The conclusion drawn is that both the softness of the alkyl group and nature of the leaving group will both have an influence on the course of the reaction, though it is not possible to determine which influence is bigger prior to doing the reaction.

Table 1-17. Kurts *et. al.* investigated the effect of the nature of the alkylating agent on the O vs. C ratio observed in reactions of the sodium enolates of acetylacetone (**140-Na**) and the potassium enolate of ethyl acetoacetate (**15-K**).[90] The reactions were run at 20 °C unless otherwise noted.



15-K Z = OEt Y = K
140-Na Z = Me Y = Na

21 Z = OEt R = Me
24 Z = OEt R = Et
18 Z = OEt R = *s*-Bu
144 Z = Me R = Me
146 Z = Me R = Et
148 Z = Me R = *s*-Bu

20 Z = OEt R = Me
23 Z = OEt R = Et
17 Z = OEt R = *s*-Bu
145 Z = Me R = Me
147 Z = Me R = Et
149 Z = Me R = *s*-Bu

R–X = ...

101 = MeOTs **19** = MeBr **97** = MeI
87 = EtOTs **141** = EtCl **22** = EtBr **108** = EtI
142 = *s*-BuOTs **143** = *s*-BuCl **25** = *s*-BuBr **16** = *s*-BuI

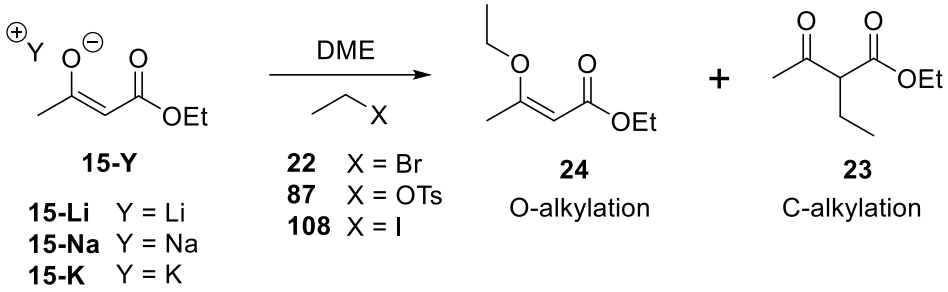
#	Y	Z	R	X	O vs. C Ratio [a]	#	Y	Z	R	X	O vs. C Ratio [a]
1	Na	Me	Me	OTs	97 : 3	**12**	K	OEt	Me	OTs	89 : 11
2	Na	Me	Me	Br	12 : 88	**13**	K	OEt	Me	Br	14 : 86
3	Na	Me	Me	I	3 : 96	**14**	K	OEt	Me	I	5 : 95
4	Na	Me	Et	OTs	90 : 10	**15**	K	OEt	Et	OTs	88 : 12
5	Na	Me	Et	Cl	62 : 37	**16**	K	OEt	Et	Cl	60 : 40
6	Na	Me	Et	Br	42 : 58	**17**	K	OEt	Et	Br	39 : 51
7	Na	Me	Et	I	17 : 83	**18**	K	OEt	Et	I	13 : 87
8 [b]	Na	Me	*s*-Bu	OTs	85 : 15	**19** [d]	K	OEt	*s*-Bu	OTs	86 : 14
9 [c]	Na	Me	s-Bu	Cl	83 : 17	**20** [d]	K	OEt	*s*-Bu	Cl	86 : 14
10 [c]	Na	Me	*s*-Bu	Br	81 : 19	**21** [d]	K	OEt	*s*-Bu	Br	78 : 22
11 [c]	Na	Me	*s*-Bu	I	62 : 38	**22**	K	OEt	*s*-Bu	I	56 : 44

[a] The percentages here are relative percentages of products from a total isolated yield. The value shown for C-alkylation includes any contributions from C,C-dialkylated products.
[b] Run at 60 °C. [c] Run at 50 °C. [d] Run at 40 °C.

A study by Guibé, Sarthou and Bram investigating the reactions of the enolates of ethyl acetoacetate in dimethoxyethane also employed the rationale suggested by Pearson and Klopman to explain the results of their series of ethylations using alkyl halides (**22** and **109**) and ethyl tosylate (**88**).[91] A selection of their results are shown below in Table 1-18. The aim of the authors of this work was to investigate the reactivity of the ion-associated and ion-dissociated forms of the various alkali enolates through measurement of C/O alkylation ratios and rates of alkylation. These results show that the O-selectivity of the reactions of **15-Li**, **15-Na** and **15-K** with ethylating agents increases in the order R—I <

R—Br < R—OTs, with the authors claiming this is solely due to the relative "softness" and "hardness" of these ethylating agents.

Table 1-18. The ethylations of various alkali metal enolates of ethyl acetoacetate (**15-Y**) was studied by Guibé, Sarthou and Bram.[91] The results are given as C/O alkylation ratios (all of which have C/O > 1, meaning all reactions shown below had more C-alkylated products than O-alkylated ones). [a]



15-Y

15-Li Y = Li
15-Na Y = Na
15-K Y = K

22 X = Br
87 X = OTs
108 X = I

24
O-alkylation

23
C-alkylation

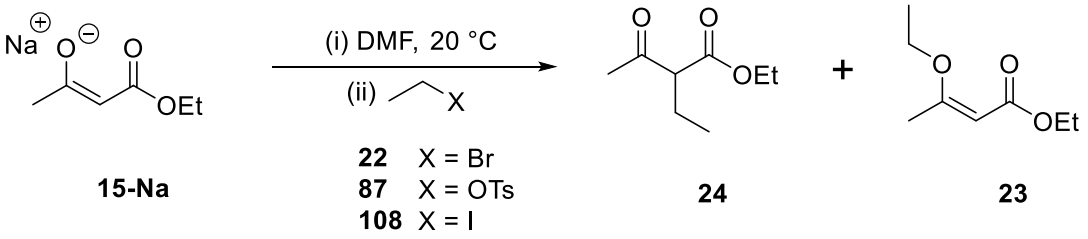
#	X	Y	C/O ratio	#	X	Y	C/O Ratio	#	X	Y	C/O Ratio
1	I	Li	>100	**4**	I	Na	>100	**7**	I	K	>100
2 [b]	Br	Li	70	**5**	Br	Na	60	**8**	Br	K	41
3	OTs	Li	2.08 – 2.32	**6**	OTs	Na	6.0	**9**	OTs	K	4.7

[a] All reactions use an enolate concentration of 0.05 mol L^{-1} and a temperature of 40 °C unless otherwise stated. The concentration of the alkylating agent in each reaction is as follows: EtI (0.1 mol L^{-1}); EtBr (0.3 mol L^{-1}); EtOTs (0.2 mol L^{-1}).

[b] Reaction was done at a temperature of 60 °C and an EtBr concentration of 0.75 mol L^{-1}.

Kurts *et. al.* used HSAB principles to explain the observed rates of reaction of **15-Na** with various alkyl halides and an alkyl tosylate in DMF (see Table 1-19 below).[56] Their results indicate that the rate of O-alkylation (**24**) is relatively insensitive to changes in the leaving group from OTs to Br to I, whereas the C-alkylation reaction (**23**) becomes considerably faster. The authors comment that the anion of **14** (i.e., the "free anion" **88,** see Scheme 1-8) must have a "soft" local site at the C-nucleophilic atom, thus the transition state for C-alkylation (**23**) must be lower when the leaving group is a "softer" base.

Table 1-19. The rate of reactions for ethylations of **15-Na** by various ethylating agents (**22**, **87** and **108**) in DMF solution at 20 °C was measured by Kurts *et. al*.[56] As the ethylating agent becomes "softer", the amount of **24** increases relative to **23** in the final product mixture. [a]



15-Na

22 X = Br
87 X = OTs
108 X = I

24 **23**

#	X	k_c / k_o	k_c (L mol^{-1} sec^{-1})	k_o (L mol^{-1} sec^{-1})
1	OTs	1.87	5.93×10^{-4}	3.17×10^{-4}
2	Br	27	1.35×10^{-2}	5×10^{-4}
3	I	64	0.25	$\sim 4 \times 10^{-3}$

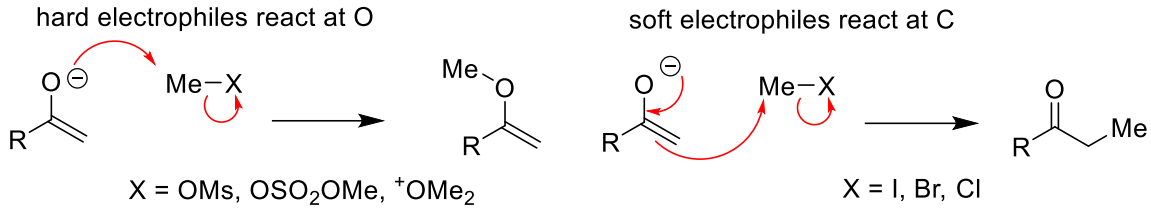
[a] The concentration of the enolate and the ethylating agent is set at 4.20×10^{-2} mol L^{-1} in each reaction.

[b] The rate constants are an average of three or more independent measurements. The potential deviation is ± 5%.

Numerous reviews have detailed the principles of HSAB theory and orbital and charge control as they apply to synthetic organic chemistry[81,92–95] and researchers refer to these theories in discussion about observed selectivity throughout the literature in reactions of enolates,[62,96,97] benzophenone anions,[98] dialkylphenylsulfonium salts,[99] sulfonanilides,[100] thioamides[101] and ring-closing reactions,[102] amongst others (see examples in a review of ambident reactivity by Mayr *et. al*).[103] Mentions of these concepts appear in most major organic chemistry textbooks in the context of site-specific additions to an ambident nucleophile.[10,104,105] In these textbooks, it is given as a rule of thumb to be used by the synthetic chemist to aid in reagent selection to achieve substitution at a specific site or increase the rate of a reaction. Figure 1-5 below is an example of such, taken from a section of *Organic Chemistry 2nd Ed.* by Clayden, Greeves and Warren.[10]

March's Advanced Organic Chemistry 6th Ed. summarises the factors that affect regioselectivity in reactions of ambident nucleophiles as a combination of the pioneering work of Kornblum *et. al.* and Pearson's HSAB theory:[104] "*The principle of hard and soft acids and bases states that hard acids prefer hard bases and soft acids prefer soft bases (…) In an S_N1 mechanism, the nucleophile attacks a carbocation, which is a hard acid. In an S_N2 mechanism, the nucleophile attacks the carbon atom of a molecule, which is a softer acid. The more electronegative atom of an ambident nucleophile is a harder base than the less electronegative atom. We may thus make the statement: As the character of a given reaction changes from S_N1- to S_N2-like, an ambident nucleophile becomes more likely to attack with its less electronegative atom. Therefore, changing from S_N1 to S_N2 conditions should favour C-attack by ^-CN, N-attack by NO_2^-, C-attack by enolate or phenoxide ions, etc*".

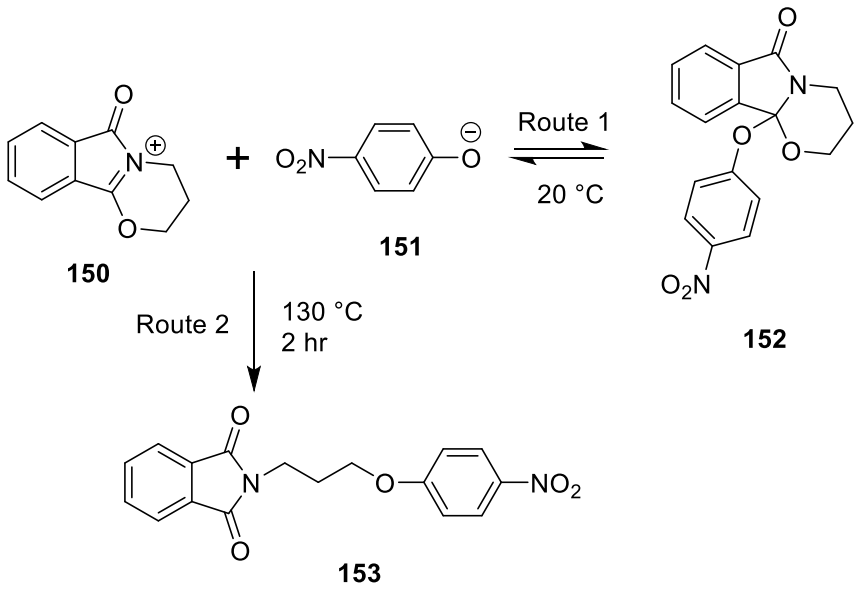
Figure 1-5. An adaption of a figure from *Organic Chemistry 2nd Ed.* by Clayden, Greeves and Warren, page 590. The reaction of enolates is summarised by designating the oxygen atom as the hard site, making it more likely to react with alkyl sulfates and sulfonates, and the carbon atom as the soft site, more likely to react with alkyl halides. The authors also mention that polar aprotic solvents such as DMSO and DMF promote O-alkylation while THF and DME promote C-alkylation.



1.3. Criticism of the HSAB Theory and Related Concepts as Rationalisations of Ambident Reactivity

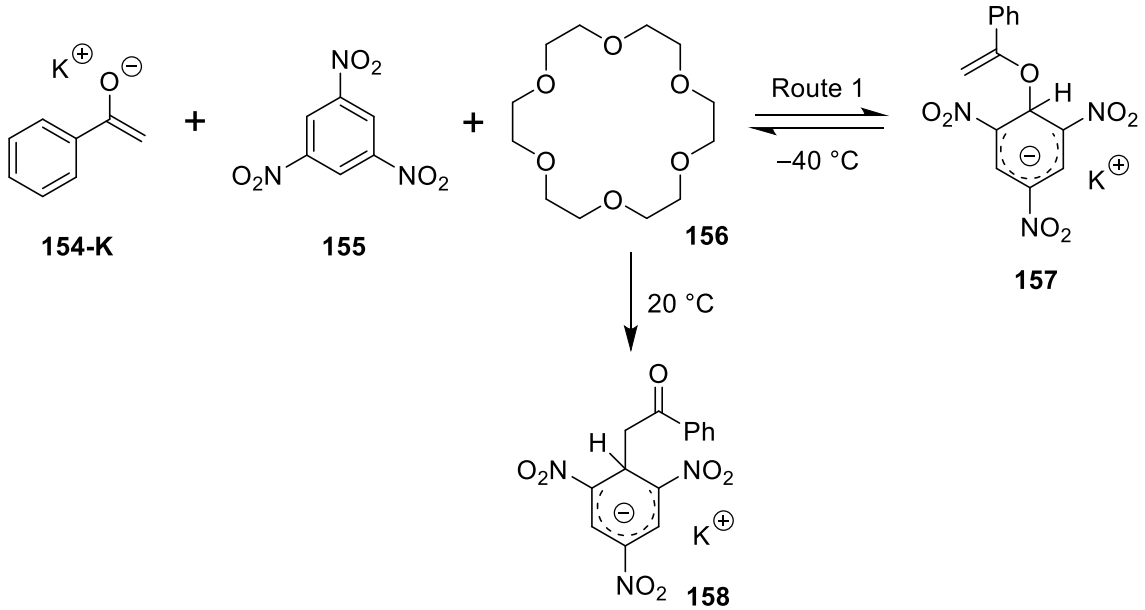
The hard-soft acid-base approach to ambident reactivity has seen frequent usage by chemists across all disciplines since its inception, and remains in contemporary use.[100,106–110] However, its use in rationalising and predicting the outcomes of reactions has not been without criticism. Drago criticised the terminology "hard" and "soft" as relatively non-descript terms which imply a certain "either-or" character to reactions, without acknowledging that "*all Lewis acid-base type interactions are composed of some electrostatic and some covalent properties, i.e., ionic-covalent or hardness-softness are not mutually exclusive properties*".[111] He notes that many authors who wish to affirm their results will cite HSAB theory after knowing the results of the experiment – meaning it offers little use to those who wish to predict the result of a future experiment. Gompper and Wagner also highlight the fact that use of the HSAB concept to describe the outcomes of reactions of ambident species makes no distinction between reactions that occur under kinetic control and those that occur under thermodynamic control, even though different products may be formed under these conditions.[112] A review by Hünig shows numerous examples of reactions of ambident electrophiles and various nucleophiles where the site of addition can change under conditions of kinetic or thermodynamic control,[113] an example of which is shown in Scheme 1-12. At 20 °C, product **152** is formed reversibly from the reaction of **150** and **151**. However, at higher temperatures (120 °C), the product of thermodynamic control is formed through reaction of **151** with a different electrophilic site of **150**.

Scheme 1-12. An adapted scheme from a review of the reactions of ambident electrophiles.[113] This reaction of a phthalimidium ion (**150**) with a *p*-nitrophenoxide ion (**151**) demonstrates that under conditions of kinetic (Route 1) and thermodynamic (Route 2) control, different products (**152** or **153**) may be formed.



An example of an enolate which can form different products under conditions of kinetic or thermodynamic control is seen in the work of Buncel *et. al.*,[114] which has been illustrated below in Scheme 1-13. The reaction of the potassium enolate of acetophenone (**154-K**) with 1,3,5-trinitrobenzene (**155**) in the presence of a crown ether (18-crown-6, **156**) was examined in a 1 : 1 mixture of deuterated acetonitrile and deuterated DME. The reaction was conducted at –50 °C and monitored by NMR spectroscopy. The temperature of the reaction was increased in 5 °C increments every 30 minutes. At –40 °C, the O-alkylation product (**157**) was the main product of the reaction, with a small amount of the C-alkylation product (**158**) present. As the temperature of the sample was increased, the signals of **157** began to decrease in intensity, with a corresponding increase in the intensity of signals associated with **158**. At 20 °C, the signals of **157** had completely disappeared. Evidently, the "hardness" or "softness" of the electrophile is not dictating the reactivity of the ambident species towards **155**.

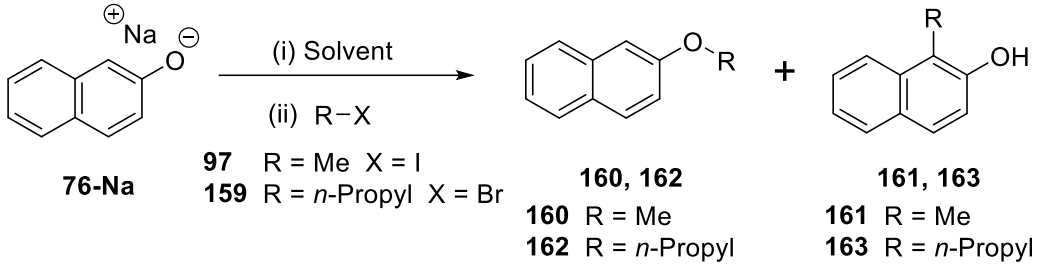
Scheme 1-13. In a reaction of the potassium enolate of acetophenone (**154-K**) with **155** in the presence of 18-crown-6 (**156**) in a 1 : 1 mixture of deuterated acetonitrile (CD_3CN) and deuterated dimethoxyethane (DME-d_{10}), different products are observed at different temperatures.[114] At –40 °C, the dominant product observed in the spectrum was **157**, the O-alkylation product. Upon increase of the temperature to 20 °C, no trace of **157** remained and **158** (the C-alkylation product) was the dominant contributor to the spectrum.



Recent works by the group of Mayr have questioned the ability of HSAB theory to predict the selectivity observed in reactions of the thiocyanate anion,[115] the cyanide ion,[116] the nitrite anion,[117] imide and amide anions,[118] and pyridone anions.[119] A comprehensive review published by Mayr, Breugst and Ofial in 2011 analyses the reactivity of the ambident anions previously specified as well as anilines, enamines, nitronate anions, enolate anions, phenoxides and phenols, sulfinate anions and sulfoxides.[103] The conclusion made in this paper is that the rationalization of ambident reactivity by the HSAB or "charge/orbital control" concepts must be promptly abandoned. This assertion

was driven in part by mass-analysis of literature reports of selectivities for many ambident nucleophiles and electrophiles to find that "the number of cases where the HSAB principle and the concept of charge- and orbital-controlled reactions give correct predictions approximate the number of cases where they fail". Indeed, examples of early research into ambident reactivity often contain observations that are incompatible with modern applications of Kornblum's Rule or HSAB theory. Such an example can be found in a work by Kornblum, Seltzer and Haberfield investigating the effect of the dielectric constant of a solvent on the observed ratio of O- and C-alkylation products.[52]

Table 1-20. Reactions of sodium β-naphthoxide (**76-Na**) with methyl iodide (**97**) and *n*-propyl bromide (**159**) in various solvents as reported by Kornblum, Seltzer and Haberfield.[52] Reactions were conducted at 20 °C unless otherwise noted.



76-Na

97 R = Me X = I
159 R = *n*-Propyl X = Br

160, 162
160 R = Me
162 R = *n*-Propyl

161, 163
161 R = Me
163 R = *n*-Propyl

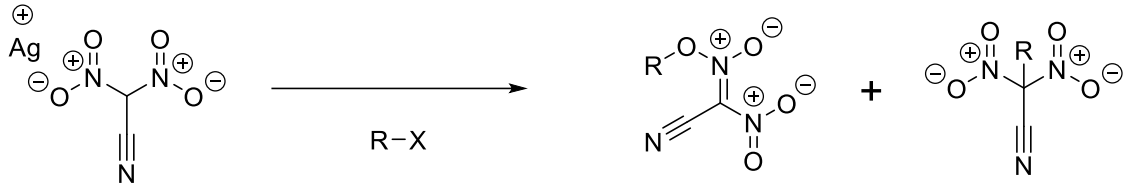
#	Solvent	R	X	O-alkylation %	C-alkylation % [c]
1 [a]	DMF	Me	I	91	3
2 [b]		*n*-propyl	Br	98	0
3 [a]	DMSO	Me	I	90	4
4 [b]		*n*-propyl	Br	95	0
5	DME	Me	I	86	10
6		*n*-propyl	Br	96	0
7	THF	Me	I	80	13
8		*n*-propyl	Br	96	0
9	Ethanol	Me	I	83	12
10		*n*-propyl	Br	95	Trace
11	2,2,2-Trifluoroethanol	Me	I	57	34
12		*n*-propyl	Br	81	10
13	Water	Me	I	66	30
14		*n*-propyl	Br	88	5

[a] Reactions conducted at 30 °C. [b] Reactions conducted at 35 °C.

The data reported by Kornblum, Seltzer and Haberfield was presented in support of their claim that solvents with a low dielectric constant (see Table 1-20 entries 5 – 8 above) or a high hydrogen bonding capacity (Table 1-20 entries 9 – 14 above) will promote C-alkylation (**161** or **163**) in reactions of sodium β-naphthoxide (**76-Na**). However, each entry in Table 1-20 shows preferential O-alkylation (**160** or **162**) with the "soft"

electrophiles methyl iodide (**97**) and *n*-propyl bromide (**159**), which is not the expected result if one attempts to predict the reaction outcome using commonly applied HSAB-derived rationales such as those seen in Figure 1-5. Papers from researchers investigating allylpyrroles,[120] nitroformate salts,[121] isoxazoles (see Table 1-21 below)[122] and enolates[123] noted behaviour in their reactions of ambident species seemingly in violation of Kornblum's proposed rule – usually that purposefully attempting to increase the S_N1 character of a reaction did not result in an increase in substitution on the atom of higher electronegativity.

Table 1-21. The alkylation of silver dinitroacetonitrile (**164-Ag**) was studied by Hammond *et. al.* and an apparent violation of Kornblum's rule was found.[121] Methyl iodide (**97**) was found to alkylate only at the oxygen atom, whereas the use of allyl (**27**) and *t*-butyl bromide (**165**) results in carbon alkylation – despite the fact that the *t*-butyl bromide reaction should have the highest S_N1 character.



164-Ag

97 R = Me X = I
27 R = Allyl X = Br
165 R = *t*-Bu X = Br

166 R = Me
168 R = Allyl
170 R = *t*-Bu

167 R = Me
169 R = Allyl
171 R = *t*-Bu

Entry	R	X	O-alkylation %	C-alkylation %
1 [a]	Me	I	58	0
2 [b]	Allyl	Br	0	35
3 [a]	*t*-Butyl	Br	0	17

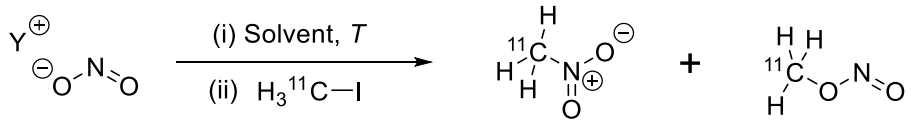
[a] Heterogeneous reaction.

[b] Reaction in acetonitrile solution.

The review of Mayr, Breugst and Ofial even points out that one of the prototypical reactions of ambident nucleophiles which Klopman notes is appropriately interpreted by his theories of charge- and orbital-control does not proceed as written. As seen in Scheme 1-11, Klopman predicted that the product of a reaction between the nitrite anion (**136**) and the "soft" electrophile methyl iodide (**97**) would be nitromethane (**137**), as a result of addition to the "soft" nitrogen atom of the nitrite anion. Results from Schoeps *et. al.*,[124] shown in part below in Table 1-22, demonstrate that this reaction cannot reliably produce nitromethane alone. These authors observed that a significant amount of methyl nitrite (**172-^{11}C**) was being produced in their reactions of nitrite salts (**60-Y**) with ^{11}C-labelled methyl iodide (**97-^{11}C**). In some instances, such as Table 1-22 entries 3 and 4, formation of the O-alkylation product (**172-^{11}C**) was even marginally favoured over C-alkylation. When revisiting the reactions of ambident nucleophiles that prompted Kornblum, Klopman and Pearson to suggest their concise rationalisations for the observed reactivity, one often finds conflicting and contrasting results from other papers. This insight calls

into question the use of Kornblum's rule, HSAB theory and the related theories of charge- and orbital-control as a predictive tool for synthetic chemists to apply for reactions of ambident reactants as is commonly seen in popular organic chemistry textbooks.

Table 1-22. In an attempt to produce ^{11}C-labelled nitromethane (**137-^{11}C**), Schoeps *et. al.*[124] employed ^{11}C-labelled methyl iodide (**97-^{11}C**) in a reaction with two nitrite salts (**60-Na** and **60-Ag**) in various solvents. The authors were pursuing reaction conditions which would optimise the formation of nitromethane (**137**) over the methyl nitrite (**172**). [a]



60-Y **97-^{11}C** **137-^{11}C** **172-^{11}C**

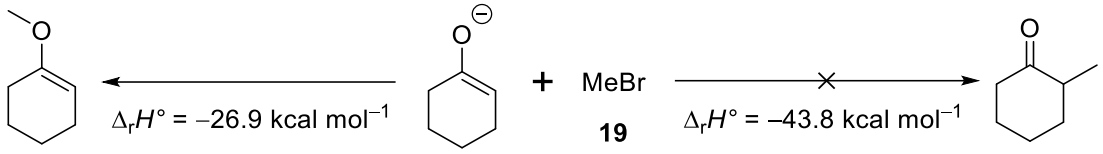
60-Na Y = Na
60-Ag Y = Ag

Entry	Solvent	Y	*T*	N-alkylation %	O-alkylation %
1	DMSO	Na	Room Temp.	54	46
2			100 °C	51	49
3		Ag	Room Temp.	46	54
4			100 °C	49	51
5	DMF	Na	Room Temp.	54	46
6			100 °C	53	47
7		Ag	Room Temp.	54	46
8			100 °C	87	13

[a] 0.5 ml solvent and 100 mg of nitrite salt was used in each reaction. The reaction time was 3 minutes.

The examination of gas-phase reactions of enolates also demonstrates the issues with predicting ambident reactivity using HSAB theory. Jones *et. al.* observed experimentally that in reactions of the enolate of cyclohexanone (**173**) with methyl bromide (**19**), the O-alkylation product (**174**) is formed exclusively (see Scheme 1-14).[125] Reactions in the gas phase are of particular interest to the study of these reactions, as solvent effects and the nature of the cation cannot influence the selectivity observed. These authors note the conflicting factors at play in the reaction shown below – O-alkylation could potentially be expected as the negative charge rests primarily on the oxygen atom and there is no possibility of a counter-ion or "selective solvation" impeding its ability to undergo nucleophilic attack.

Scheme 1-14. The reaction of the anion of cyclohexanone (**173**) with **19** in the gas phase gives exclusive O-alkylation (**174**).[125] This occurs despite the fact that **19** is a "soft" electrophile, and that the C-alkylation process (**175**) is the thermodynamically favoured pathway.

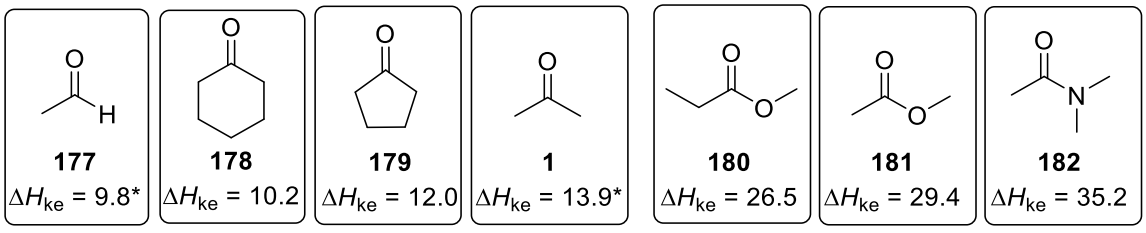


174 **173** **175**

However, as the C-alkylated product (**175**) is thermodynamically favoured, an argument could also be made that this is the expected product under these conditions. Jones *et. al.* conclude that one could reconcile their gas-phase observations with the solution-phase data that exists in the literature by assuming that the alkylation of enolates proceeds under kinetic control in irreversible systems and under thermodynamic control in reversible (or equilibrating) ones.

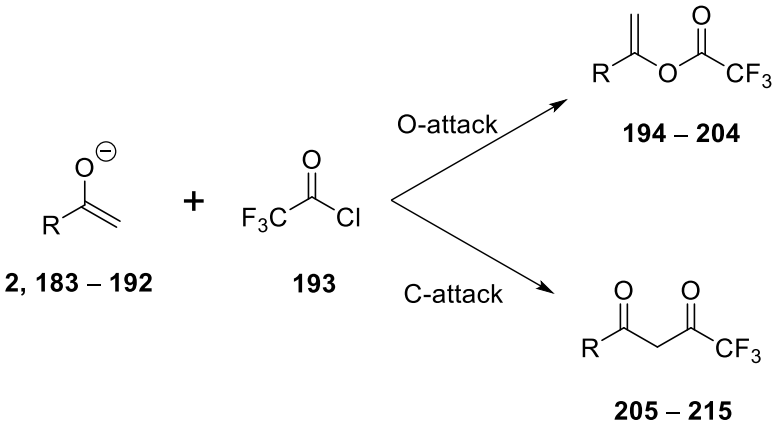
An apparent relationship between the enthalpy difference (ΔH_{ke}) between the keto and enol forms of the ketone from which the enolate is derived and O/C selectivity was noted by Brickhouse and Squires in their own study of gas-phase enolate ion reactions.[126] A selection of enolates and their ΔH_{ke} values are shown in Figure 1-6. Their findings prompted them to suggest that compounds with a lower ΔH_{ke} (between 10 – 15 kcal/mol) will favour O-alkylation whereas higher values of ΔH_{ke} (>20 kcal/mol) will favour C-alkylation. However, they also observed exceptions.

Figure 1-6. Various ketones and the enthalpy difference between their keto and enol forms.[126] Unmarked values are estimated from thermochemical group-equivalents. Values marked with an asterisk (*) are experimentally derived.[127] Values are given in kcal/mol. The authors proposed that the enolates of ketones with a ΔH_{ke} value above ~20 kcal/mol were more likely to favour C-alkylation.



The trend of oxygen attack being favoured in gas-phase reactions of enolates with electrophiles was also seen in the work of Zhong and Brauman.[128] The results of their reactions of various enolates (**2**, **183** – **192**) with CF_3COCl (**193**) are shown in Table 1-23.

Table 1-23. Gas-phase reactions of various enolates (**2**, **183** – **192**) with CF_3COCl (**193**) were examined by Zhong and Brauman.[128] The enolate anions were generated by proton abstraction from the carbonyl precursor by F^- and the O/C ratio was determined by FT-ICR mass spectrometry. [a]

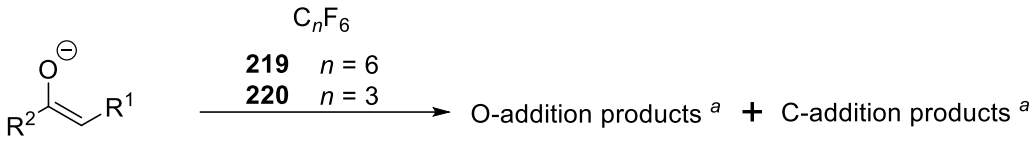


#	R	Enolate	O-acylation Product	C-acylation Product	O/C Ratio	ΔH_{ke} [b]
1	CF_3	**183**	**194**	**205**	7.5	5
2	H	**184**	**195**	**206**	5.9	9.8
3	*m*-$CF_3C_6H_6$	**185**	**196**	**207**	6.9	9.8
4	*m*-FC_6H_4	**186**	**197**	**208**	5.9	10
5	*m*-$CH_3OC_6H_4$	**187**	**198**	**209**	5.8	10.1
6	C_6H_5	**188**	**199**	**210**	6.0	10.3
7	*m*-$CH_3C_6H_4$	**189**	**200**	**211**	6.4	10.3
8	$(CH_3)_3C$	**190**	**201**	**212**	4.1	12.3
9	CH_3	**2**	**202**	**213**	4.0	13.9
10	CH_2=CH	**191**	**203**	**214**	3.3	15
11	F	**192**	**204**	**215**	0.9	28

[a] The products of each reaction (**194** – **215**) were ionized for the purposes of mass spectrometric detection.
[b] The difference in the enthalpies of the starting materials, in kcal/mol.

Most reactions showed a large preference for O-acylation in the competition between the two processes, with preferential C-acylation only being observed when R = F (Table 1-23 entry 11). The results below show a large dependence of the selectivity of the reaction (i.e., the product O/C ratio) on the identity of the R group of the enolate (see Table 1-23 and associated image for the structures of the enolates involved). The authors also note a correlation between the observed ratio and the energy difference (ΔH_{ke}) between the keto and enol forms of the ketone from which the enolate is derived – with a higher ΔH_{ke} more C-acylation is observed.

Table 1-24. Oxygen *vs.* carbon addition in the gas-phase reaction of various enolates (**2**, **184**, **188, 216** – **218**) with hexafluorobenzene (**219**) and hexafluoropropene (**220**).[129] The enolate anions were generated *via* proton abstraction from the parent ketone or aldehyde using generated amide or hydroxide anions. As the enolate ion is changed, preferential O- or C-addition may be observed even when employing the same electrophiles (**219** or **220**). The ratio was determined by FT-ICR mass spectrometry.



216 $R^1 = H$ $R^2 = N(CH_3)_2$
188 $R^1 = H$ $R^2 = C_6H_5$
184 $R^1 = H$ $R^2 = H$
2 $R^1 = H$ $R^2 = CH_3$
217 $R^1 = C_2H_5$ $R^2 = CH_3$
218 $R^1 = C_2H_5$ $R^2 = H$

Entry	R^1	R^2	Electrophile	O- /C-addition ratio
1	H	$N(CH_3)_2$	C_6F_6	1/99
2			C_3F_6	1/99
3	H	C_6H_5	C_6F_6	6/94
4			C_3F_6	6/94
5	H	H	C_6F_6	81/19
6			C_3F_6	94/6
7	H	CH_3	C_6F_6	19/81
8			C_3F_6	84/16
9	C_2H_5	CH_3	C_6F_6	29/71
10			C_3F_6	86/14
11	C_2H_5	H	C_6F_6	84/16
12			C_3F_6	95/5

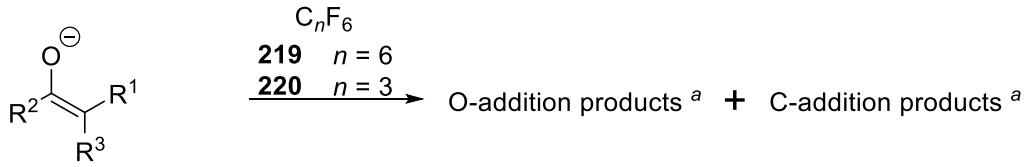
[a] The yield of O-addition and C-addition products in these reactions was determined by the quantity of characteristic ions detected in the experiment, with certain ions indicating O-addition *vs.* C-addition. As such, there are no single structures that can be drawn above which are representative of a product of O- or C-addition.

Freriks, de Koning and Nibbering also investigated the gas-phase ambident reactivity of acyclic[129] and cyclic[130] enolate anions. A selection of results from their study of acyclic enolates is shown in Table 1-24 above.

Here, they found that by varying the enolate employed, they could effect varying levels of O- or C-addition using the same electrophile – a behaviour that cannot be explained simply in the principles of HSAB theory or any other rationalisation of ambident reactivity that has been discussed. In reactions of acyclic enolate anions (**2**, **184**, **188**, **216**

– **218**) with hexafluorobenzene (**219**) and hexafluoropropene (**220**), the ratio of the observed products shows a large variety of O- and C-addition. The authors determine that this means the observed ratio reflects the relative activation energies of the initial addition *via* either the carbon or oxygen nucleophilic pathway. The authors draw particular attention to the results of the enolate anion of acetaldehyde (**184**, Table 1-24 entries 5 and 6) and the enolate anion of acetone (**2**, Table 1-24 entries 7 and 8). They note that the competition of the oxygen and carbon nucleophilic centres cannot be exclusively controlled by the charge distribution between the oxygen and carbon atoms in gas-phase reactions of enolates – if it were, then the reactions of **184** and **2** with **219** or **220** would both result in dominant O-addition. Instead, as can be observed in Table 1-24 entry 7, reaction of **219** with the enolate anion of acetone (**2**) results in preferential C-addition. This is a point of considerable significance considering the large influence that charge density would be expected to have on gas-phase reactions.

Table 1-25. A selection of results from a study of the gas phase reaction of various unsolvated and monosolvated enolate anions (**2**, **184** and **221**) with **219** and **220**.[131] The monohydrated enolate anions were made *in situ* by a reaction with a monohydrated ethoxide.



184 R^1 = H, R^2 = H, R^3 = H
2 R^1 = H, R^2 = CH_3, R^3 = H
221 R^1 = D, R^2 = CD_3, R^3 = D

# [b]	R^1	R^2	R^3	Electrophile	O/C addition ratio (unsolvated anion)	O/C addition ratio (monosolvated anion)
1	H	H	H	C_6F_6	81/19	97/3
2				C_3F_6	94/6	95/5
3	H	CH_3	H	C_6F_6	19/81	35/65
4				C_3F_6	84/16	80/20
5	D	CD_3	D	C_6F_6	22/78	43/57
6				C_3F_6	85/15	84/16

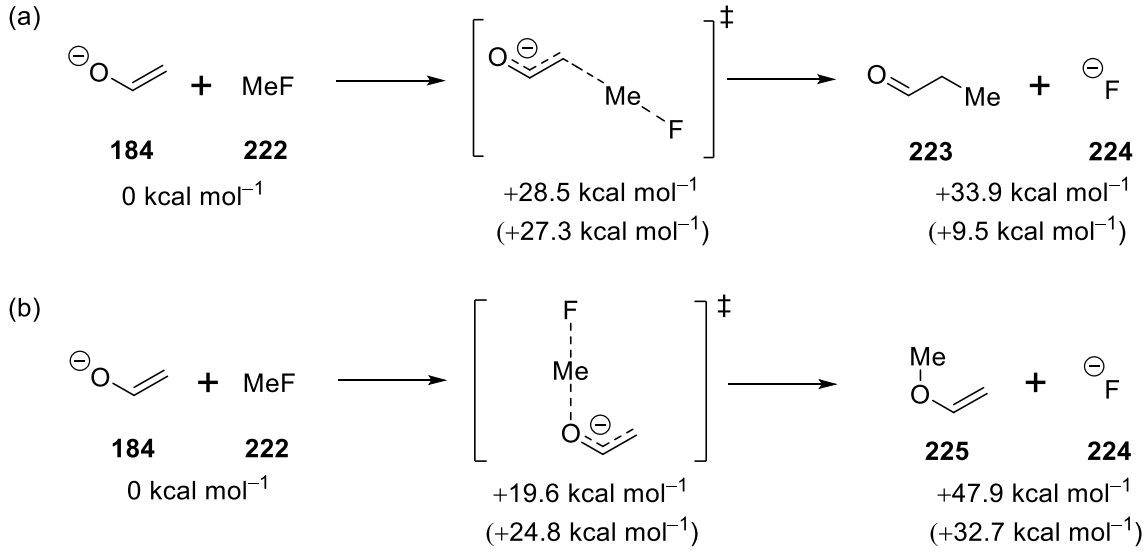
[a] The yield of O-addition and C-addition products in these reactions was determined by the quantity of characteristic ions detected in the experiment, with certain ions indicating O-addition *vs*. C-addition. As such, there are no single structures that can be drawn above which are representative of a product of O- or C-addition.

Gas-phase reactions of monohydrated enolate ions were then conducted by Freriks, de Koning and Nibbering in an attempt to gain insight into the influence that "selective solvation" of the oxygen atom by a solvent molecule may have on the ambident reactivity of the enolate in question.[131] A selection of their observed results is shown in Table 1-25.

Though the authors expected the water molecule in the monohydrated enolate ions to be associated with the oxygen atom and greatly influence the mode of reaction with the perfluorocarbon compounds **219** and **220**, they observed no large influence on the ratio observed. This was attributed to the possibility that the water molecule could have vapourised away from the reaction complex at the point of addition. Alternately, the authors posit that the insensitivity to the presence of a water molecule in the reaction could indicate that there is but a small difference in the entropy of activation between the two addition processes.

Theoretical studies of enolate anion reactions have also contributed evidence that the HSAB treatment of ambident reactivity is inappropriate. A computational study by Houk and Paddon-Row, illustrated in Scheme 1-15, examined the reaction of enolate **184** (the anion derived from acetaldehyde) with methyl fluoride (**222**).[132] Those authors calculated that the activation energy for O-alkylation is lower than that of C-alkylation, despite the fact that C-alkylation is the thermodynamically preferred process.

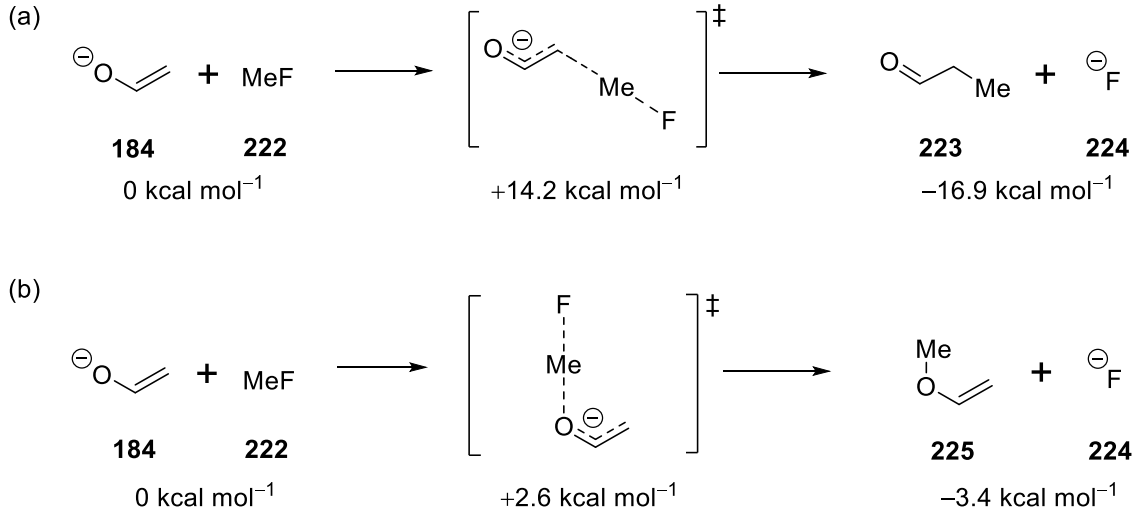
Scheme 1-15. Houk and Paddon-Row[132] calculated the activation energies for the two possible modes of reaction of the anion of acetaldehyde (**184**) with **222** in the gas phase. The structures shown in brackets are transition states. The values shown are relative energies for various stationary points of the reaction. The values are calculated using *ab initio* Hartree-Fock calculations and the 3-21G basis set, whereas the values in parentheses are calculated using the 6-31G* basis set.



These Hartree-Fock calculations show that depending on the basis set used, the activation energy for the O-alkylation process is between 3 – 9 kcal/mol lower than the C-alkylation process. C-alkylation is the thermodynamically preferred process, with **223** being predicted to be 23.2 kcal/mol more favourable than **225** when using the 6-31G* basis set. The authors note that there is a considerable underestimation of the product stabilities (i.e., the positive values associated with the formation of each of **223** and **225** implies they are endothermic processes) which may be attributed to the fact their calculations used a small basis set lacking a diffuse function. Regardless, the relative energies between the two products and between the two transition states were deemed to be reasonable and

thus useful in making qualitative statements about the energy differences seen in the two processes. Using these calculations of the activation energy, along with experimental gas-phase observations made by Jones *et. al.*,[125] Houk and Paddon-Row suggest that "free" enolate ions will always react at the oxygen atom in a kinetically-controlled reaction, regardless of the "hardness" or "softness" of the alkylating agent. They claim that the C-alkylation of metal enolates that is commonly seen in reactions that take place in solution must be due to co-ordination by metal cations or solvent molecules decreasing the reactivity of the oxygen atom relative to the carbon atom. Their generalised prediction about the ambident reactivity of enolates is that "*O-alkylation of enolates is favoured with all electrophiles. Changes in C/O alkylation ratios with the nature of the alkyl halide are probably not related to the "hardness" or "softness" of the alkyl halide but to the ability of the halide to influence the structures of metal enolate aggregates*". A later study by Marcos and Bertran on the exact same system (**184** + **222** in the gas phase) using *ab initio* Hartree-Fock calculations and a basis set that included diffuse functions agreed with the findings of Houk and Paddon-Row regarding the relative preference for O-alkylation over C-alkylation. [133] Additionally, the use of a basis set which was diffuse-augmented resulted in the calculated energies of reaction becoming negative – indicating exothermic processes. The results of their study are shown in Scheme 1-16. It should be noted at this point, however, that the computational results shown in Scheme 1-15 and 1-16 may be outdated in the present day due to the age of the computational methods employed and the basis sets which lack in complexity. However, as is seen below in Table 1-26, analogous results using modern computational methods have been reported in the literature.

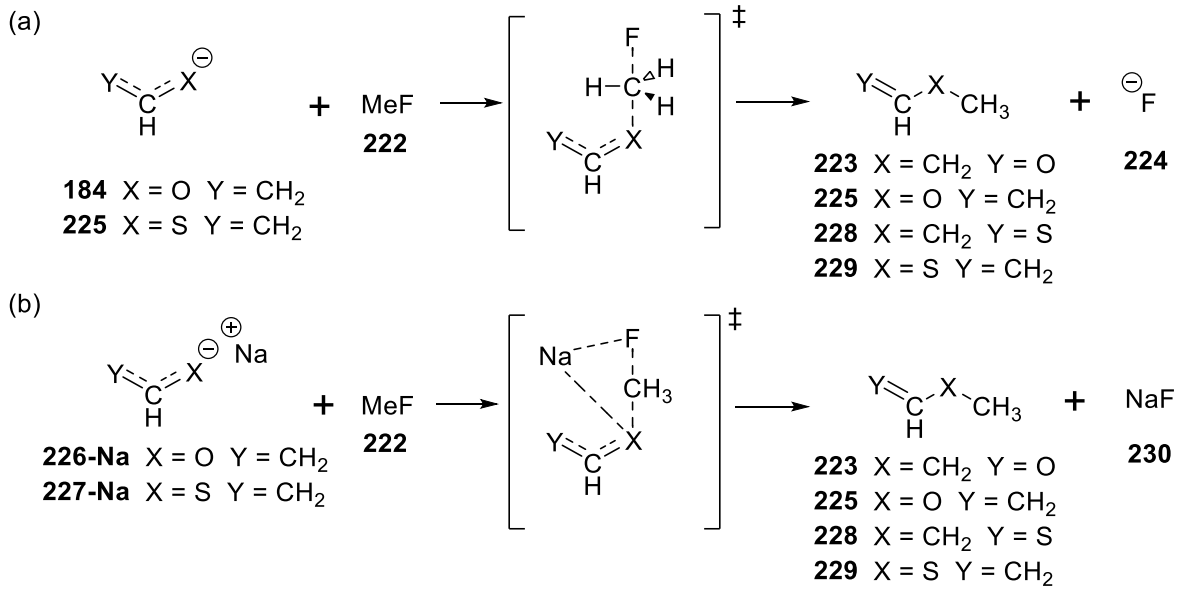
Scheme 1-16. Marcos and Bertran[133] calculated the activation energies for the reaction of **184** with **222** in the gas phase using *ab initio* Hartree-Fock calculations and a different basis set than that used by Houk and Paddon-Row.[132] The structures shown in brackets are transition states. The values shown are relative energies for various stationary points of the reaction. The values shown are calculated using the 3-21+G diffuse-augmented basis set. The key finding of Houk and Paddon-Row, which is that the activation energy of the O-alkylation process is relatively lower than the C-alkylation process, is also demonstrated by their data.



Although the magnitudes of the relative energy differences are not calculated to be the same, the qualitative assumptions made about the ambident reactivity of **184** are identical to those made by Houk and Paddon-Row. A later study by Lee *et. al.* observed the same trends in theoretical reactions of the anion of acetaldehyde (**184**) with **222** in the gas phase and predicted the same effect would be seen with the use of the enolate of thioacetaldehyde (**225**, see structure in Table 1-26 below).[134]

A more recent DFT study (using the M06-2X/6-311+G(d,p) theoretical model as well as the CPCM solvation model) by Burmudžija *et. al.*[135] sought to reinvestigate the theoretical reactions seen in Scheme 1-15 and Scheme 1-16 with modern computational methods. Their calculations attempted to determine the influence that a Na^+ counterion and a solvent (THF) would have on the energy values obtained. A selection of their results are shown below in Table 1-26.

Table 1-26. A DFT study by Burmudžija *et. al.*[135] analysed the reactions of the anion of acetaldehyde (**184**) and the anion of thioacetaldehyde (**225**) with **222** in the gas phase. The authors set to expand on the calculations made by Houk and Paddon-Row[132] and Lee *et. al.*[134] by examining the influence of a Na^+ counterion and a solvent on the energy values obtained. The structures drawn in brackets are approximations of the transition states for the alkylation processes. **(a)** The reaction of the "free" anions with **222**. **(b)** The reaction of the anions with **222** in the presence of a Na^+ counterion.



Entry	Solvent	X	Y	With no counterion		With Na^+ counterion	
				$\Delta G^{\ddagger}$ [a]	$\Delta_r G$ [a]	$\Delta G^{\ddagger}$	$\Delta_r G$
1	None	CH_2	O	107.6	–8.4	135.0	–98.0
2	None	O	CH_2	101.7	65.6	171.9	–24.0
3	None	CH_2	S	151.1	81.1	153.4	–29.2
4	None	S	CH_2	113.9	90.1	157.5	–20.3
5	THF	CH_2	O	107.9	–95.4	89.6	–228.6
6	THF	O	CH_2	102.0	–16.2	132.7	–42.5
7	THF	CH_2	S	148.6	–9.3	137.0	–57.8
8	THF	S	CH_2	114.4	–2.6	132.9	–51.1

[a] The authors state that $\Delta G^{\ddagger}$ indicates the activation free energy and $\Delta_r G$ indicates the reaction free energy.

When there was no counterion factored into the calculation, the authors found that their results were in line with those obtained by the previous groups that had studied this reaction – namely that the O (and S) alkylation processes (Table 1-26 entries 2 and 4) had a lower activation energy than the corresponding C-alkylation processes (Table 1-26 entries 1 and 3). The calculated free energy of reaction for the C-alkylation products was lower than that of the O- or S-alkylation processes (i.e., products **223** and **228** are more thermodynamically favourable than products **225** and **229**).

These trends are also observed even when modifications had been made to account for THF as a solvent (see Table 1-26 entries 4 – 8). However, when the Na^+ counterion is included in the model, the $\Delta G^‡$ and $\Delta_r G$ values are profoundly affected – as can be seen in Table 1-26 entries 1 and 2 and entries 3 and 4, the $\Delta G^‡$ value associated with C-alkylation becomes lower than that of O-alkylation (note that $\Delta G^‡$ and $\Delta_r G$ are the quantities specified by the authors of this paper). When the counterion is accounted for, the C-alkylation process seen in Table 1-26 entry 1 is both kinetically and thermodynamically more favourable than the O-alkylation process seen in entry 2. This trend is observed in all pairs of entries (i.e., Table 1-26 entries 1 + 2, entries 3 + 4, entries 5 + 6) with the exception of entries 7 and 8. Here, the S-alkylation process still has a lower Gibbs free energy of activation ($\Delta G^‡$). The authors note that all calculations which factor in Na^+ as a counterion have much lower Gibbs free energy of reaction (i.e., the reactions are calculated to be more exergonic and exothermic) due to the calculated formation of NaF over F^- – with the former being considerably more stable. These authors claim that these findings confirm the usefulness of the HSAB principle to help examine reactions of ambident systems as the influence of the counterion cannot be ignored in routine solution-phase reactions of enolates. Despite this, it is apparent that the most common depictions of the HSAB treatment of ambident reactivity (see Figure 1-5) make little or no attempt to imply that the solvent and the nature of the counterion are pivotal or decisive factors in reactions of ambident nucleophiles.

It should be highlighted at this point that the principle of hard and soft acids and bases was not originally intended to be used to rationalise the results of the reactions of ambident nucleophiles. The limitations of HSAB theory were frequently commented upon by Pearson[82,136] and disclaimers about the issues associated with indiscriminate application of the HSAB principle to organic reactions have begun to appear in book chapters and other conceptual guides.[137,138] Early reviews of ambident reactivity warned that while the HSAB principle was a useful tool with which to examine the selectivity of a reaction, "*factors such as steric effects, solvent effects, the state of the salt in solution, and certain others frequently play a very considerable and sometimes a decisive role*".[46] Recent works have set about elucidating a physical basis for the "global" hard-soft acid-base theory and assessing the conditions in which it is valid.[139–143] The authors of these works explicitly separate their analysis into discussions about the "global" and "local" HSAB principles – with the "local" HSAB principle referring to reactions of ambident species with discrete "hard" and "soft" sites. The "global" HSAB theory refers specifically to separated species (therefore, it is not relevant to ambident species). Ayers[140] concludes that the "local" HSAB principle is much less robust than its "global" counterpart – saying that exceptions to the principle will be found due to molecule-specific properties that are unrelated to hardness or softness. Another work by Ayers and Cárdenas[143] summarises the uncertainty surrounding this application of the HSAB principle – "*The local HSAB principle, which makes predictions about ambident acids and bases, is on much shakier theoretical ground, so experimental evidence against it is not surprising*". Regardless of this warning, the work of Ayers and Cárdenas quoted above has been referenced in another paper by Wang and Barnes as an explicit

justification of the use of the HSAB principle to rationalise the ambident reactivity observed in their synthesis of glycosides.[144] As the HSAB principle is still frequently cited in modern research as an explanation for the observed selectivity of reactions of ambident species,[100,106–110,145] it behoves chemists to develop and popularise a method of rationalising ambident reactivity that can supersede the HSAB treatment which is currently employed.

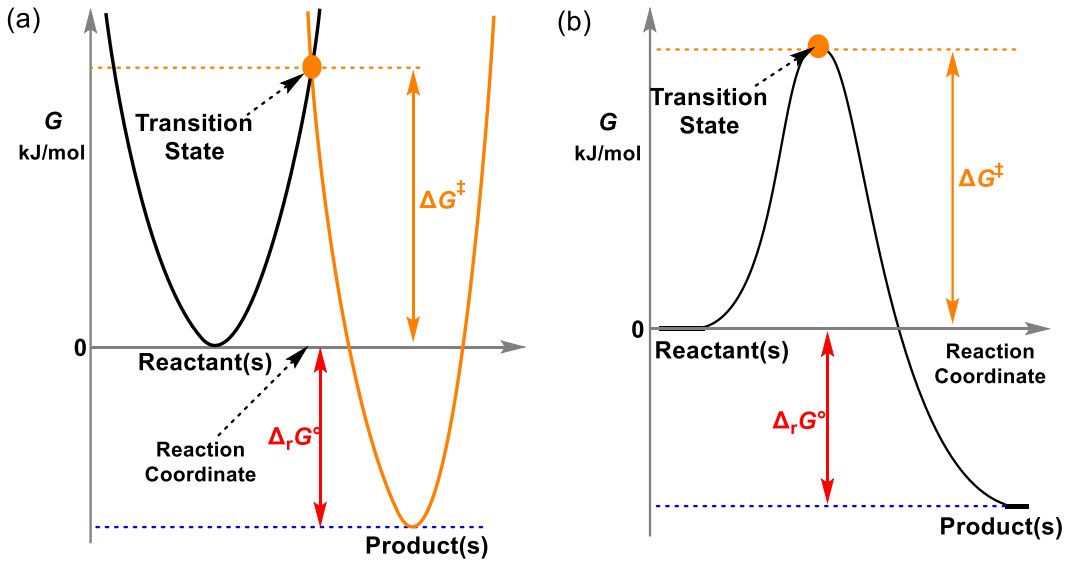
1.4. Alternative Rationalisations of Selectivity in Reactions of Ambident Reactants

1.4.1. The Marcus Approach to Ambident Reactivity

Prominent researchers of ambident reactivity in the modern day, including Mayr and co-workers whose review of ambident reactivity was cited above,[103] have suggested that Marcus theory provides a suitable alternative to HSAB theory in predicting the regioselectivity of kinetically-controlled reactions.

Marcus theory,[146–150] which was proposed by R. A. Marcus in a set of papers beginning in 1956, was developed with the aim of explaining the rates of electron movement from a donor to an acceptor in electron transfer reactions. Although originally developed solely to examine outer-sphere electron transfer processes, expansions and refinements of the theory have also been found to be applicable to other reaction types, such as proton transfers[151] and methyl transfer reactions.[152] In analyses based on Marcus theory, the energy profile for a reaction is represented using two parabolas – one parabola represents the energy associated with reactants and the other parabola represents the energy associated with the products (see Figure 1-7(a) below). The point of high energy where the two parabolas intersect is the transition state and the height of the transition state indicates the size of the activation barrier for the reaction. The lowest point of each parabola indicates the equilibrium position of each potential energy surface (i.e., the energy minima of the reactants and the products, respectively). A comparison between this approach and a standard reaction co-ordinate diagram is shown below in Figure 1-7.

Figure 1-7. (a) A Gibbs energy profile diagram represented using elements found in Marcus theory – mainly the concept of representing the Gibbs energy wells of reactants and products as parabolas. **(b)** A standard Gibbs energy profile diagram (i.e., a section through a Gibbs energy surface). As can be seen by comparing these two representations of Gibbs energy surfaces, they are analogous to one another.



The geometry and intersection point of the parabolas can be used to calculate reaction rates and activation energy for the reaction. The value of the Gibbs free energy of activation ($\Delta G^{\ddagger}$) is the vertical distance along the Gibbs energy axis between the minimum point of the parabola which represents the Gibbs energy well of the reactants (or, the "reactant parabola") and the minimum point of the parabola which represents the Gibbs energy well of the products (or, the "product parabola"). Each parabola comes from the Marcus equation (Equation 1.2) which is itself derived from Marcus' initial equation (Equation 1.3) for the Gibbs free energy of activation ($\Delta G^{\ddagger}$) for an electron transfer reaction.

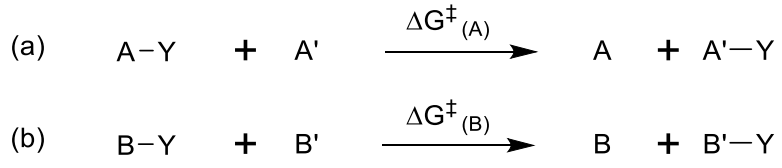
$$\Delta G^{\ddagger} = \Delta G^{\ddagger}_{\text{int}} + \frac{\Delta_{\text{r}}G^{\circ}}{2} + \frac{(\Delta_{\text{r}}G^{\circ})^2}{16\Delta G^{\ddagger}_{\text{int}}} \qquad (1.2)$$

$$\Delta G^{\ddagger} = \frac{(\lambda_o + \Delta_{\text{r}}G^{\circ})^2}{4\lambda_o} \qquad (1.3)$$

Where $\Delta_{\text{r}}G^{\circ}$ is the Gibbs free energy of reaction and λ is the reorganization energy, the energy required to distort the nuclear configuration of the reactant state into the geometry of the product state without the electron transfer occurring. Therefore, the Gibbs free energy of activation ($\Delta G^{\ddagger}$) exhibits a dependence on the standard Gibbs energy of reaction ($\Delta_{\text{r}}G^{\circ}$) and the intrinsic barrier ($\Delta G^{\ddagger}_{\text{int}}$) of a given reaction. The intrinsic barrier ($\Delta G^{\ddagger}_{\text{int}}$) for a reaction is the imaginary Gibbs energy of activation that would exist if the reaction were thermoneutral (i.e., if $\Delta_{\text{r}}G^{\circ}$ were equal to zero) – one can visualise this as arising from alteration of the reaction coordinate such that the Gibbs energy minima of the reactants and products are equal. It enables one to account for the influence that the properties unique to the transition state have on $\Delta G^{\ddagger}$ (independent of the properties of the reactants and products to the Gibbs free energy of activation ($\Delta G^{\ddagger}$) of an identity reaction (i.e., one in which ($\Delta_{\text{r}}G^{\circ}$) is equal to zero). Practically, to access values of $\Delta G^{\ddagger}_{\text{int}}$, one must have access to $\Delta G^{\ddagger}$ values for certain relevant identity reactions, which are discussed below.

An identity reaction is one where the products are chemically identical to the reactants, for example a bimolecular self-exchange reaction of methyl iodide (**97**, CH_3I) with I^-. Examples of two identity reactions are shown in Scheme 1-17.

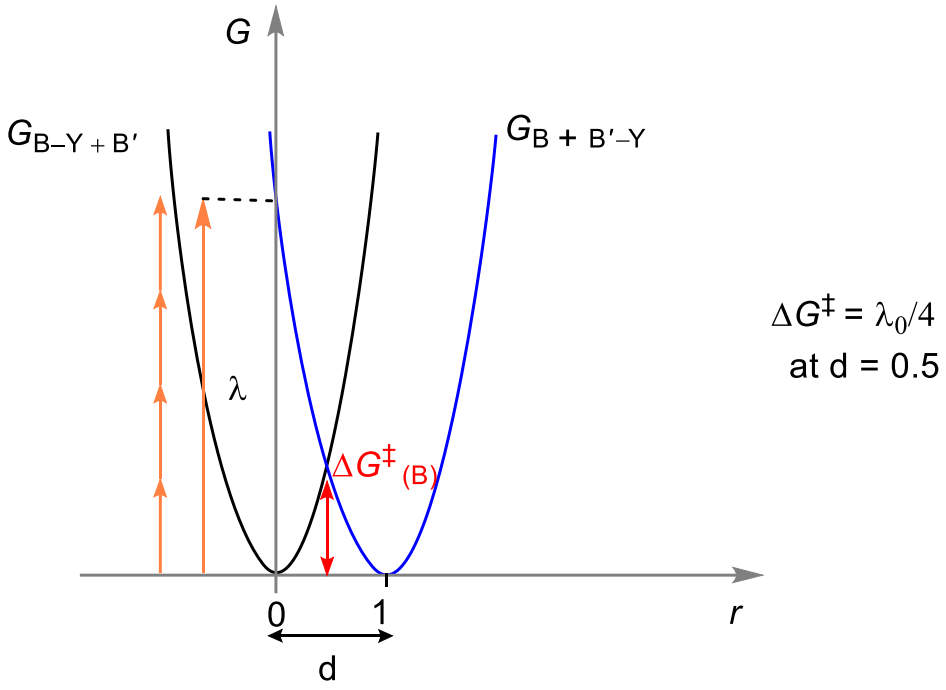
Scheme 1-17. An example of a group transfer identity reaction. **(a)** A has transferred a "Y" group to A′. **(b)** B has transferred a "Y" group to B′. Despite this transfer in each case, the species on the left-hand side of the reaction are identical to the species on the right-hand side.



For two different identity reactions (such as Scheme 1-17(a) and (b) above), the values of the Gibbs free energy of activation ($\Delta G^{\ddagger}_{(A)}$ and $\Delta G^{\ddagger}_{(B)}$) are generally not equal. However, in each of the identity reactions represented in Scheme 1-17, the standard Gibbs energy of reaction ($\Delta_r G°$) is equal to zero. For a reaction where "Y" is transferred from A to B, the intrinsic barrier ($\Delta G^{\ddagger}_{int}$) is calculated as the average of $\Delta G^{\ddagger}_{(A)}$ and $\Delta G^{\ddagger}_{(B)}$ for the identity reactions.

The reaction in Scheme 1-17(b) is represented graphically using parabolas in Figure 1-8.

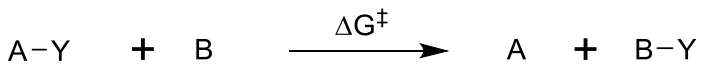
Figure 1-8. Parabolas representing the reactant (black parabola) and product (blue parabola) states for the reaction in Scheme 1-17, where *r* is the reaction co-ordinate. It represents the nuclear co-ordinates of the entire system in the reaction, including solvation shells. In an identity reaction, ($\Delta_r G°$) = 0, thus the Gibbs free energy of activation barrier ($\Delta G^{\ddagger}_{(B)}$) corresponds to the kinetic contribution to the Gibbs free energy of activation.



Marcus calculates the intrinsic barrier of a non-identity reaction as the average of two corresponding identity reactions, in a concept known as the "additivity principle".[153,154] For example, in a bimolecular reaction such as that shown below in Scheme 1-18, the intrinsic barrier would be calculated by Equation 1.4 below:

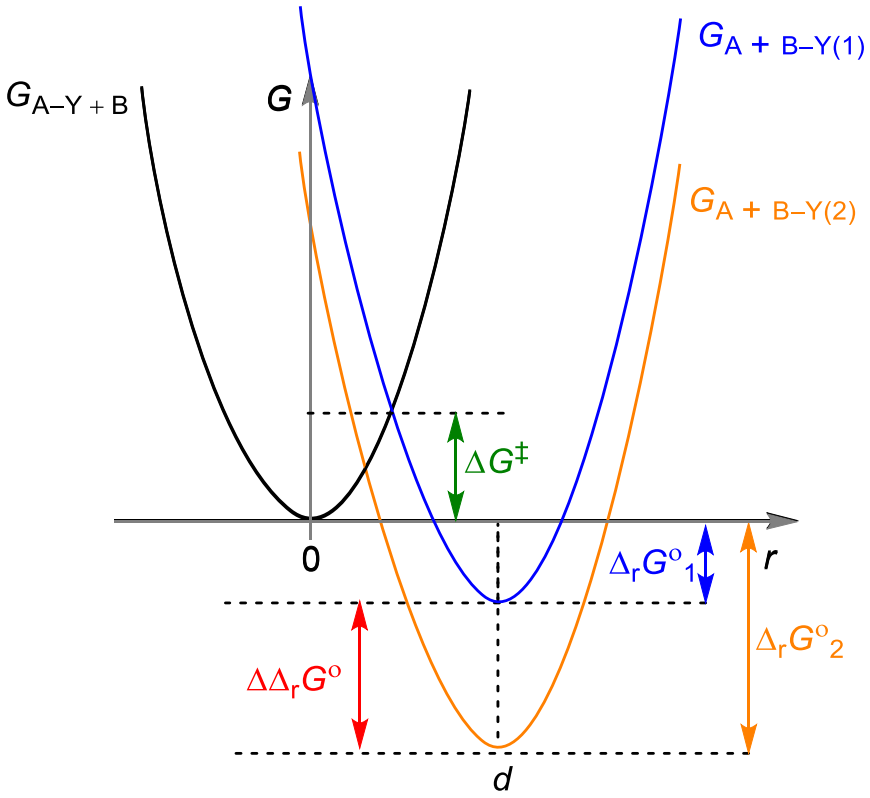
$$\Delta G^{\ddagger}_{int} = \frac{(\Delta G^{\ddagger}_{A} + \Delta G^{\ddagger}_{B})}{2} \qquad (1.4)$$

Scheme 1-18. A non-identity group transfer reaction. The intrinsic barrier ($\Delta G^{\ddagger}_{int}$) for such as reaction would be calculated using the average of the two corresponding identity reactions.



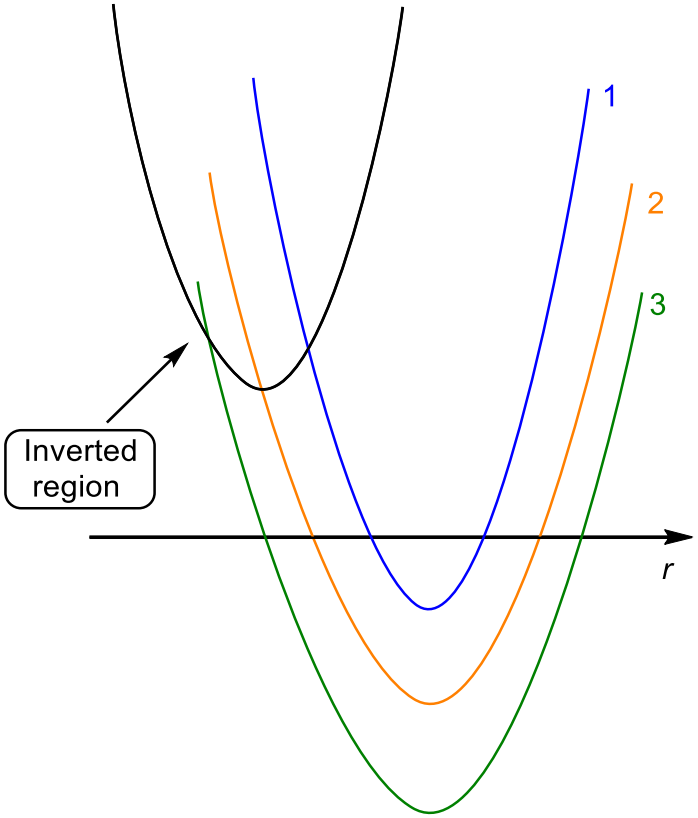
In a bimolecular reaction, the vertical position of the parabola can be adjusted to incorporate thermodynamic parameters (i.e., the scale of $\Delta_r G°$). For exergonic reactions where $\Delta_r G° < 0$, the product parabola is lowered (or, equivalently, the reactant parabola is raised), resulting in a lower activation barrier ($\Delta G^‡$). For endergonic reactions, where $\Delta_r G° > 0$, the product parabola is raised, resulting in an increased activation barrier. An example of this is shown in Figure 1-9.

Figure 1-9. Parabolas representing the reactant (black parabola) and product (blue and orange parabola) states for a bimolecular electron transfer reaction. In an exergonic reaction, the product parabola has its minimum at a lower Gibbs energy than the reactant parabola. This is represented by the lowering of the product parabola relative to the product parabola. In a more exergonic reaction (e.g., $\Delta_r G°_2$, which is more negative than $\Delta_r G°_1$ – compare the orange parabola to the blue parabola), this causes a lowering of the activation barrier ($\Delta G^‡$). (i.e., the point at which the product parabola intersects the reactant parabola is lower down than the intersection point for the less exergonic reaction.) The difference between the standard Gibbs energy of reaction for each of the product parabolas ($\Delta\Delta_r G°$) is shown in the diagram in red.



Note that the above interpretation is in agreement with Hammond's postulate – the increase in exergonicity results in an earlier transition state (i.e., a lower value of $\Delta G^‡$) and a transition state that more closely resembles the reactants than the products.[155] If the product parabola were to be moved upwards rather than downwards, the opposite would be true. In Figure 1-10, increasing the exergonicity of the reaction even further results in an unexpected outcome.

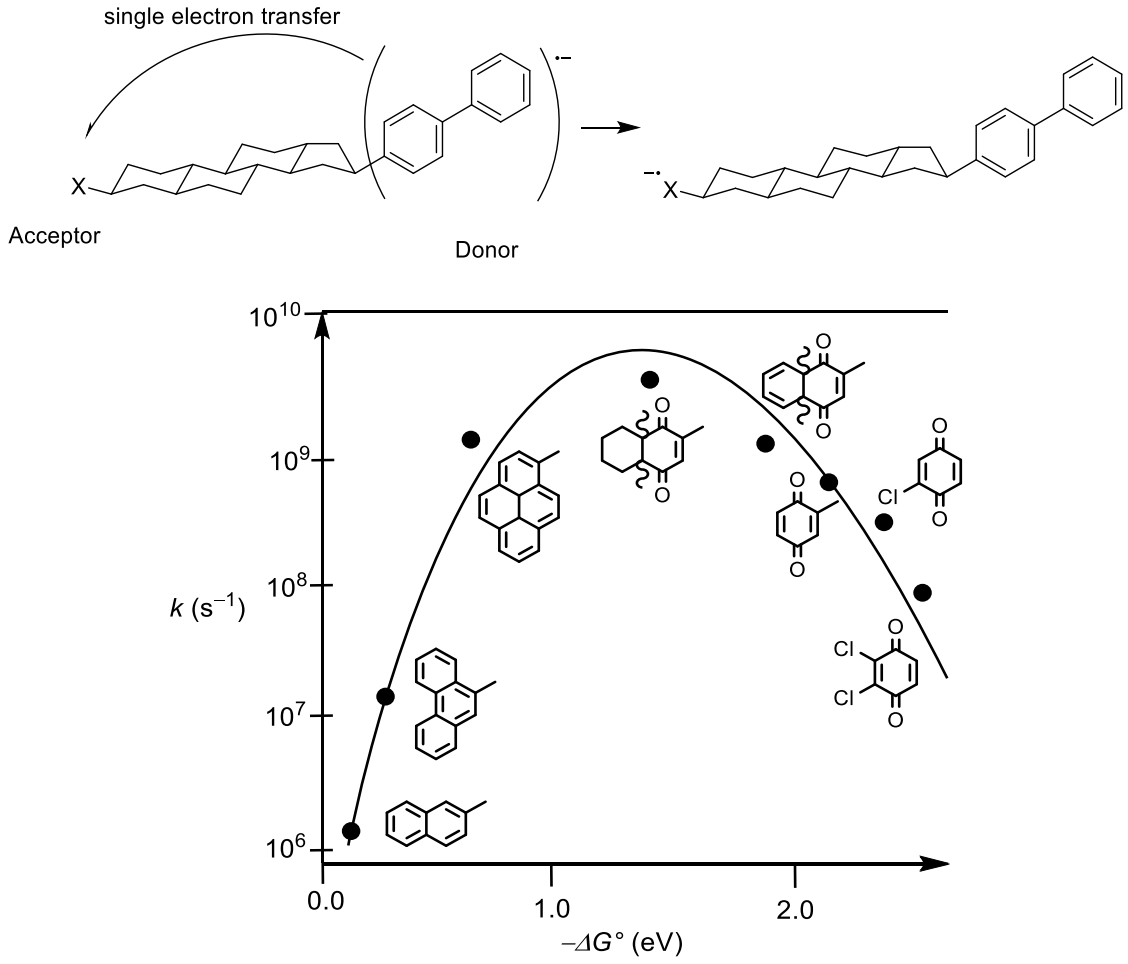
Figure 1-10. With increasingly negative values of $\Delta_rG°$, the "Marcus inverted region" appears. In case "2", the intersection point of the parabolas is at the minimum energy of the reactant parabola, indicating a barrierless reaction. However, in case "3", even though the reaction is more exergonic, the intersection point is no longer at the minimum point of the reactant parabola – indicating the reaction has a barrier.



Parabola 1 in Figure 1-10 (the blue parabola) represents an exergonic reaction (with $\Delta_rG° < 0$), which will have an intrinsic barrier ($\Delta G^{‡}_{int}$) greater than 0 and a rate constant, k_1. Parabola 2 in Figure 1-10 (the orange parabola) represents a reaction in which the product parabola intersects the minimum of the reactant parabola, where $\Delta_rG° = -\lambda$. At this point, the reaction is barrierless, and thus the rate constant for this reaction, k_2 will be greater than that of k_1. Further increasing the exergonicity gives us parabola 3 (the green parabola in Figure 1-10), which lies beyond the lowest point of the reactant parabola and counterintuitively causes the activation barrier ($\Delta G^{‡}$) to be greater than 0 again. This in turn causes the rate constant, k_3, to be lower than k_2, despite its greater $-\Delta_rG°$ value. The observation of this "inverted region", where ever-increasing exergonicity gives rise (beyond a certain point) to a decreasing rate of reaction, seems paradoxical and led to an extensive search for the inverted region in electron transfer reactions. Experiments utilising a series of reactions with increasing exergonicities seemed to yield ever-increasing reaction rates up to the diffusion limit (where k is roughly $10^9 – 10^{10}\ M^{-1}\ s^{-1}$) until Miller, Calcaterra and Closs validated the existence of the inverted region by comparing the rates of intramolecular electron transfer in molecules where the donor-acceptor pair were separated by a rigid steroid structure (see Figure 1-11 below).[156] In these reactions, diffusion control is not a limiting factor as the reaction is intramolecular,

thus the reactive sites of the molecule are in permanent close contact. Previous attempts to find the inverted region in intermolecular reactions were thwarted by the existence of the diffusion limit, which produced a "levelling off" of rate of reaction for reactions with increasingly negative values of $\Delta_r G°$. However, through careful selection of reaction partners, the inverted region can also be observed in bimolecular electron transfer reactions.[157]

Figure 1-11. A graph from the work of Miller, Calcaterra and Closs is reproduced below. By modulating the receptor "X" in various molecules where the donor-acceptor pair were separated by a fixed structure, the Marcus inverted region was observed. Increasing exergonicity ($-\Delta_r G°$, in eV) resulted in a decrease in the rate of reaction observed (k, in s^{-1}).

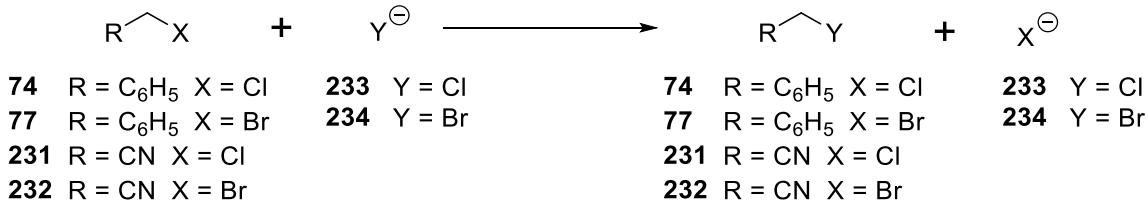


Marcus received a Nobel Prize for his work in 1992 and his theory has been used to explain behaviour in a variety of reaction types such as organometallic reactions,[158] the processes of photosynthesis,[159] and electron transfer between proteins in Cytochrome *c* systems.[160]

Marcus theory has long been proposed as a potential method for interpreting the experimentally observed kinetics of group transfer reactions. Pioneering work in this area was carried out by Brauman and co-workers,[161–164] who investigated the kinetics of S_N2 methyl- and benzyl- transfer reactions in the gas phase. A study by Wladkowski and

Brauman sought to test the so called "additivity principle" seen in Equation 1.4 – the supposition that the intrinsic barrier of a non-identity reaction can be estimated as the average of two corresponding identity reactions.[164] A selection of their results are shown in Table 1-27.

Table 1-27. The observed rates of reaction for two S_N2 systems were studied by Wladkowski and Brauman.[164] The experimental measurements were made with an FT-ICR spectrometer. Cl^- and Br^- ions were generated using electron impact. The activation energy ($\Delta E^{\ddagger}$) and intrinsic barrier ($\Delta E^{\ddagger}_{int}$) for the reactions was determined.



74 R = C_6H_5 X = Cl
77 R = C_6H_5 X = Br
231 R = CN X = Cl
232 R = CN X = Br

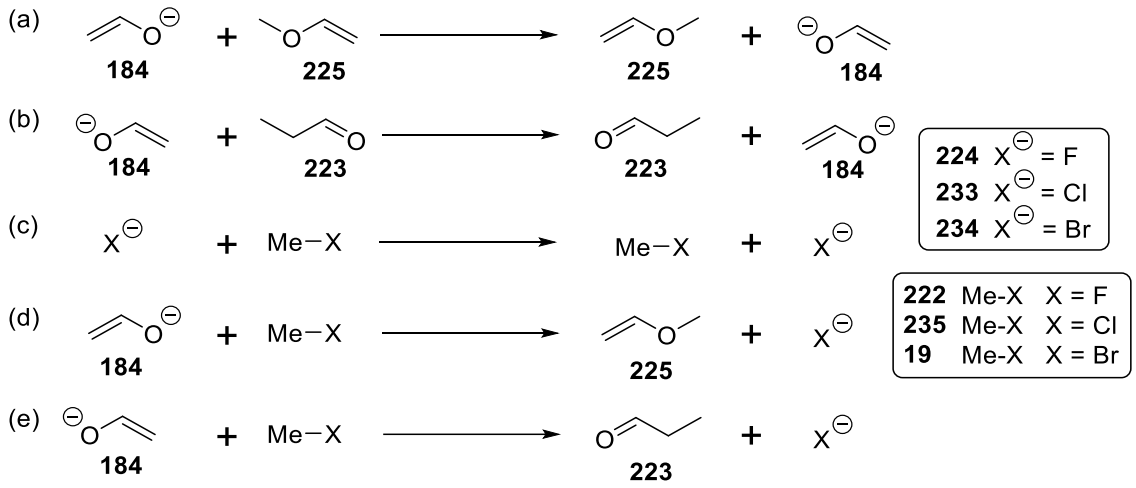
233 Y = Cl
234 Y = Br

Entry	R	X	Y	k_{obs} [a]	$\Delta E^{\ddagger}$ [b]	$\Delta E^{\ddagger}_{int}$ [b]
1	C_6H_5	^{35}Cl	^{37}Cl	0.0068	+0.4	+0.4
2	C_6H_5	^{79}Br	^{81}Br	0.13	–2.5	–2.5
3	C_6H_5	Br	Cl	2.7	–4.5	–0.8
4	CN	^{35}Cl	^{37}Cl	3.3	–5.9	–5.9
5	CN	^{79}Br	^{81}Br	2.6	–7.3	–7.3
6	CN	Br	Cl	12	–9.8	–6.1

[a] Units of 10^{-10} cm^3 s^{-1}. Confidence intervals from the original paper have been omitted here.
[b] Units of kcal mol^{-1} relative to the energy of the reactants.

Wladkowski and Brauman found that it was possible to measure the kinetic properties of identity reactions in which chloride and bromide ions were the nucleophiles employed due to the fact each element has more than one stable and naturally abundant isotope. In the case of the identity reactions (Table 1-27 entries 1 and 2, entries 4 and 5) the activation barrier ($\Delta E^{\ddagger}$) calculated is equal to the intrinsic barrier ($\Delta E^{\ddagger}_{int}$), as the reaction has no thermodynamic component (i.e., $\Delta_r E° = 0$). In the non-identity reactions (Table 1-27 entries 3 and 6) the intrinsic barrier is calculated to be almost exactly the average of the two corresponding identity reactions relevant to that process (see Equation 1.4). In the case of the benzyl bromide substrate (**77**, entry 3), the value of $\Delta E^{\ddagger}_{int}$ calculated (–0.8 kcal mol^{-1}) is within 0.2 kcal mol^{-1} of the mean value obtained by combining Table 1-27 entries 1 and 2. Although the authors note that their method is somewhat limited in only being able to accurately measure $\Delta E^{\ddagger}$ values over a short range (+2 to –8 kcal mol^{-1}), they propose that these results give strong evidence for the applicability of using the "additivity postulate" to estimate the intrinsic barrier of a non-identity reaction when employing Marcus theory to investigate group transfer reactions. Computational results from the group of Schaefer have used high-level theoretical methods to demonstrate that explicitly calculated barriers for S_N2 exchange reactions show good agreement with those calculated using the Marcus equation (Equation 1.2).[165,166]

Table 1-28. Various identity and non-identity reactions of the enolate of acetaldehyde are shown below. In order to calculate the intrinsic barrier for a S_N2 reaction, Equation 1.4 is employed – the intrinsic barrier for is assumed to be the mean of two corresponding identity reactions. Reactions (a) and (b) are the identity reactions for the O- and C-methylation of **184**. Reactions (d) and (e) are non-identity S_N2 reactions for the O- and C-methylations of **184** by an alkyl halide. $\Delta G^{\ddagger}$ values were calculated and compared by Breugst *et al*. using the Marcus equation and by direct calculation using high-level DFT methods. All values given in kJ mol^{-1}.[167]



#	Rxn	X	$\Delta G^{\ddagger}_{int}$	$\Delta_r G°$	$\Delta G^{\ddagger}$ (Marcus Eqn)	$\Delta G^{\ddagger}$ (Direct Calc.)
1	(a)	N/A	+77.0	–19.7 [a]	+77.0	N/A
2	(b)	N/A	+181	–28.8 [a]	+181	N/A
3	(c)	F	+14.7	–38.5 [a]	+14.7	N/A
4	(d)	F	+45.9	+57.0	+78.8	+71.7
5	(e)	F	+97.9	–25.1	+85.8	+89.3
6	(c)	Cl	+31.2	–26.8 [a]	+31.2	N/A
7	(d)	Cl	+54.1	–78.4	+22.0	+16.0
8	(e)	Cl	+106	–160	+41.1	+34.3
9	(c)	Br	+24.7	–22.3 [a]	+24.7	N/A
10	(d)	Br	+50.9	–110	+10.8	+6.9
11	(e)	Br	+103	–92	+29.4	+18.2

[a] Although identity reactions have no $\Delta_r G°$ value with respect to the free reactants, the authors have calculated the $\Delta_r G°$ value with respect to the reactant complexes (see Figure 1-12 below). When filling into the Marcus equation, the authors use the $\Delta G^{\ddagger}_{int}$ value with respect to the free reactants.

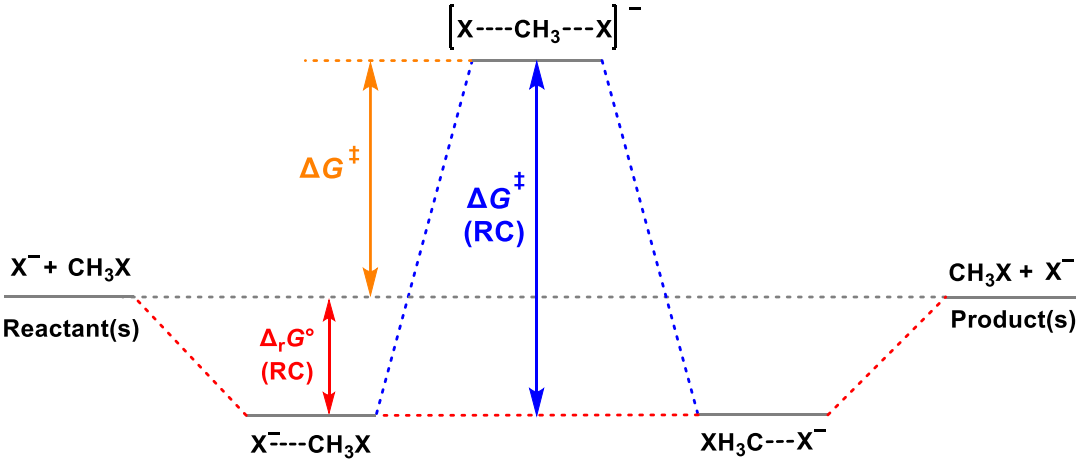
Recent works by Mayr and co-workers have sought to popularise the use of Marcus theory as an alternative method of rationalising the selectivities observed in reactions of ambident nucleophiles and electrophiles. As has been previously mentioned, Mayr and co-workers investigated the ambident reactivity of the thiocyanate anion,[115] the cyanide anion,[116] the nitrite ion,[117] the cyanate anion,[168] nitroalkyl anions,[169] phenylsulfinate ions,[170] imide and amide anions,[118] pyridone anions,[119] and enolate anions.[167]

In each case, they found the use of HSAB theory inadequate in explaining the outcomes of reactions of ambident nucleophiles. In certain cases, these authors demonstrated that using the principles of Marcus theory leads to a more consistent rationalisation of the observed selectivity than any method currently employed for this purpose.[115,119,167,170] An example of such analysis is shown above in Table 1-28, showing reactions of the enolate of acetaldehyde (**184**). In Table 1-28 entries 1 and 2, values for the activation barrier ($\Delta G^{\ddagger}$) were calculated for the identity reaction where a methyl group is transferred from **225** to **184** in an O-methylation identity reaction, and from **223** to **184** in a C-methylation identity reaction. Note that in an identity reaction, the activation barrier ($\Delta G^{\ddagger}$) has the same value as the intrinsic barrier ($\Delta G^{\ddagger}_{int}$) as the reactions have no thermodynamic component with respect to the reactants (i.e., influence from ($\Delta_r G°$)). These reactions are drawn as (a) and (b) respectively in the table shown above. The reaction (c) represents an identity reaction where a methyl group is exchanged between an alkyl halide and a halide anion (see Table 1-28 entries 3, 6 and 9). The authors used the "additivity principle" discussed above to calculate the intrinsic barrier ($\Delta G^{\ddagger}_{int}$) for the bimolecular S_N2 processes of O-alkylation (reaction (d)) and C-alkylation (reaction (e)) as the averages of the activation barriers ($\Delta G^{\ddagger}$) of the corresponding identity reactions. Thus, for the O-alkylation process seen in Table 1-28 entry 4, where **184** reacts with **222**, the $\Delta G^{\ddagger}_{int}$ value is calculated as the average of the two activation barriers of the relevant identity reactions in Table 1-28 entries 1 and 3. This value for the intrinsic barrier is combined with a calculated Gibbs free energy of reaction value ($\Delta_r G°$) to obtain a value for the free energy of activation ($\Delta G^{\ddagger}$) through the use of the Marcus equation (Equation 1.2) (see column "$\Delta G^{\ddagger}$ (Marcus Eqn)" in Table 1-28 above).

The $\Delta G^{\ddagger}$ values calculated in this manner were then compared to $\Delta G^{\ddagger}$ values obtained through direct calculation *via* high-level DFT computations at the G3(+) level of theory (see column "$\Delta G^{\ddagger}$ (Direct Calc.)" in Table 1-28 above). The authors found that the values calculated using the Marcus method agreed with those that were directly calculated within a mean absolute error of 5.1 kJ mol^{-1}. They observed the same trends were consistent through both methods of obtaining $\Delta G^{\ddagger}$ values, namely that the $\Delta G^{\ddagger}$ values for O-alkylation reactions of **184** were lower than the value of the corresponding C-alkylation reaction in all cases (compare Table 1-28 entries 4 and 5, entries 7 and 8, entries 10 and 11). These observations led Breugst *et. al.* to determine that Marcus theory is a suitable method to examine the underlying factors which influence ambident reactivity. The Gibbs free energy of reaction ($\Delta_r G°$) calculated in each case shows a strong preference for C-alkylated product formation over O-alkylated product formation (see Table 1-28 entries 4 and 5). However, the intrinsic barrier for O-alkylation (reaction (d)) is lower in all cases than the intrinsic barrier for C-alkylation (reaction (e)) (see Table 1-28 entries 4 and 5). There is a general intrinsic preference favouring O-alkylation, and a general thermodynamic preference favouring C-alkylation. As both $\Delta G^{\ddagger}_{int}$ and $\Delta_r G°$ values are used in calculating the activation barrier ($\Delta G^{\ddagger}$) *via* the Marcus equation, this results in the value of $\Delta G^{\ddagger}$ having a dependence on the magnitudes of each of the quantities involved.

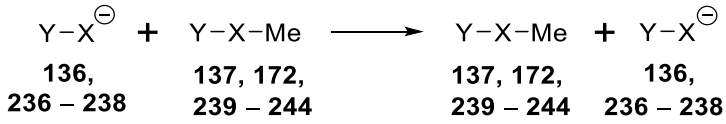
The significance of the reactant complexes, mentioned in Table 1-28 and 1-29, is outlined in Figure 1-12 below.

Figure 1-12. In calculations of gas phase identity S_N2 reactions, a double-well potential with a central inversion barrier is often the outcome. As a result, the activation barrier ($\Delta G^{\ddagger}$) may be determined relative to the reactants (i.e., $\Delta G^{\ddagger}$) or relative to the reactant complexes (i.e., $\Delta G^{\ddagger}$ (RC)). The energy minima of the two reactant complexes arise due to ion-molecule complexes.[166,167]



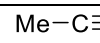
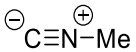
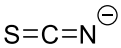
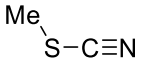
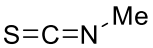
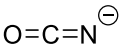
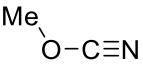
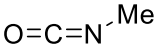
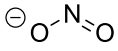
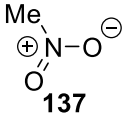
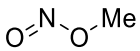
To further analyse this phenomenon, the authors performed an analogous analysis of other ambident nucleophiles, namely CN^- (**236**), SCN^- (**237**), OCN^- (**238**) and NO_2^- (**136**), the results of which are shown in Table 1-29 above. The data show that N-attack is intrinsically favoured in reactions of CN^- (**236**) (i.e., $\Delta G^{\ddagger}_{int}$ for N-alkylation is smaller than $\Delta G^{\ddagger}_{int}$ for C-alkylation), as is S-attack in reactions of SCN^- (**237**) and O-attack in reactions of OCN^- (**238**). The notable outlier is reactions of NO_2^- (**136**), in which $\Delta G^{\ddagger}$ of the identity reaction with respect to the free reactants is almost identical for the processes of N- and O-attack. A difference only appears once the stability of the reactant complexes of NO_2^- (**136**) with $MeNO_2$ (**137**) and MeONO (**172**) is taken into account – once again demonstrating that the intrinsic preference for O-attack over N-attack is maintained.

Table 1-29. Breugst *et al*. calculated $\Delta G^{\ddagger}_{int}$ values for the intrinsic barriers of other ambident nucleophiles (**136, 236** – **238**).[167] The results indicate there is a relationship between the intrinsic barrier and the location of the favoured atom of the ambident nucleophile in the periodic table. The G3(+) level of theory was used. All values given in kJ mol^{-1}.



236 CN^- **237** SCN^- **238** OCN^- **136** ONO^-

239 MeCN **240** CNMe **241** MeSCN **242** SCNMe **243** MeOCN **244** OCNMe **137** $MeNO_2$ **172** MeONO

#	Nucleophile	Nucleophilic atom (X)	Methylation product	$\Delta G^{\ddagger}$	$\Delta_r G°$ (RC) [a]	$\Delta G^{\ddagger}$ (RC) [b]
1	 **236**	C	 **239**	+156	–29.3	+185
2		N	 **240**	+93.8	–32.9	+127
3	 **237**	S	 **241**	+52.2	–36.5	+88.7
4		N	 **242**	+93.7	–25.3	+119
5	 **238**	O	 **243**	+21.6	–40.7	+62.2
6		N	 **244**	+78.4	–23.6	+102
7	 **136**	N	 **137**	+61.4	–35.5	+96.8
8		O	 **172**	+61.1	–19.2	+80.2

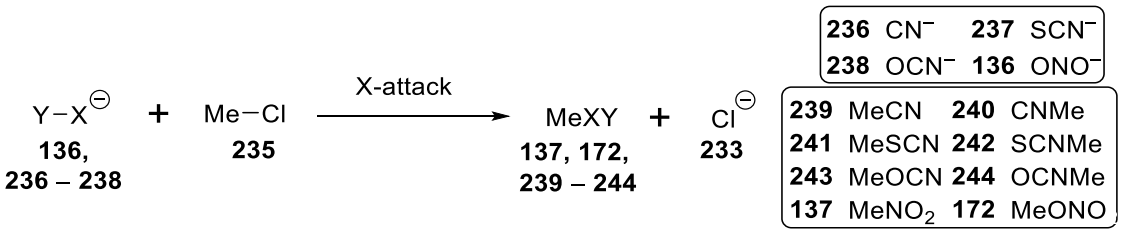
[a] Although identity reactions have no $\Delta_r G°$ value with respect to the free reactants, the authors have calculated the $\Delta_r G°$ value with respect to the reactant complexes.

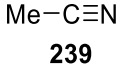
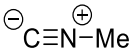
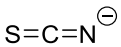
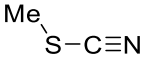
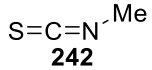
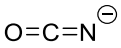
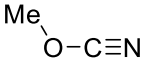
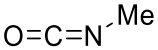
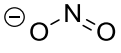
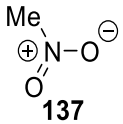
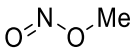
[b] $\Delta G^{\ddagger}$ (RC) is $\Delta G^{\ddagger} - \Delta_r G°$ (RC).

A trend that is observed in these data is that the intrinsic barrier ($\Delta G^{\ddagger}_{int}$) is generally smaller when the attacking atom of a nucleophile is located further to the right in the periodic table. This relationship between the intrinsic barrier and location of an atom in the periodic table had previously been demonstrated by Hoz *et. al.* in their computational investigation of intrinsic barriers in S_N2 identity reactions.[171] The examination of S_N2 reactions of CN^- (**236**), SCN^- (**237**), OCN^- (**238**) and NO_2^- (**136**) led to almost identical observations as those made from the results in Table 1-29. These results are shown in

Table 1-30 below. These values are obtained by combining the values of $\Delta G^{\ddagger}$ of the identity reactions in Table 1-29 above and the $\Delta G^{\ddagger}$ value from the identity reaction of MeCl (**235**) in Table 1-28 (entry 6) through the "additivity principle" (see Equation 1.4).

Table 1-30. The values for the intrinsic barrier ($\Delta G^{\ddagger}_{int}$), the Gibbs free energy of reaction ($\Delta_r G°$) and the Gibbs energy of activation ($\Delta G^{\ddagger}$) for reactions of various ambident nucleophiles (**136, 236** – **238**) with MeCl (**235**) are shown below. These results demonstrate the interplay between kinetic ($\Delta G^{\ddagger}_{int}$) and thermodynamic ($\Delta_r G°$) factors and how they can influence the preferred course of a reaction of an ambident nucleophile. All values given in kJ mol^{-1}.



#	Nucleophile	Nucleophilic atom (X)	Methylation product	$\Delta G^{\ddagger}_{int}$	$\Delta_r G°$ [a]	$\Delta G^{\ddagger}$ [a]
1	 **236**	C	 **239**	+93.6	–131	+39.6
2		N	 **240**	+62.5	–29.8	+48.5
3	 **237**	S	 **241**	+41.7	+87.1	+96.6
4		N	 **242**	+62.5	+71.7	+103
5	 **238**	O	 **243**	+26.4	+119	+119
6		N	 **244**	+54.8	+3.2	+56.4
7	 **136**	N	 **137**	+46.3	–18.1	+37.7
8		O	 **172**	+46.2	–9.2	+41.7

[a] Only Gibbs energies referring to the free reactants are shown here.

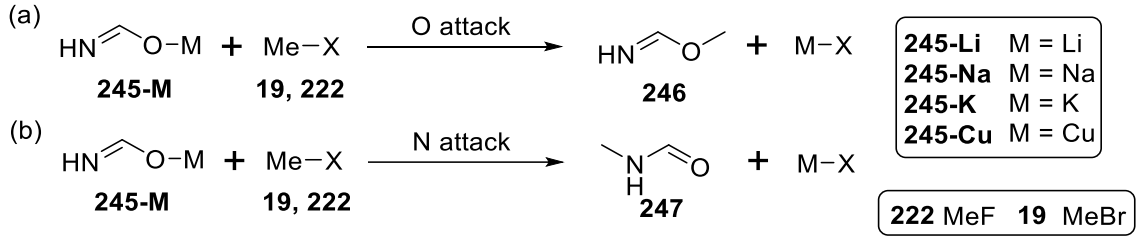
The previously observed trends regarding $\Delta G^{\ddagger}_{int}$ and $\Delta_r G°$ are also borne out in Table 1-30. In each case, the atom further to the right in the periodic table is calculated to have a lower intrinsic barrier than the alternative atom in an S_N2 reaction of an ambident nucleophile (compare the $\Delta G^{\ddagger}_{int}$ values for Table 1-30 entries 1 and 2, 3 and 4 etc.).

However, in each case, the Gibbs free energy of reaction ($\Delta_r G°$) has a larger negative value for the reaction of the atom with the higher intrinsic barrier. A particularly stark example is seen in the reaction of OCN^- (**238**) with MeCl (**235**) (Table 1-30 entries 5 and 6) – the intrinsic barrier for O-attack is 28.4 kJ mol^{-1} lower than the intrinsic barrier for N-attack. However, the Gibbs free energy of reaction of the N-attack process is 115.8 kJ mol^{-1} more favourable than the corresponding O-attack process. This results in the activation barrier ($\Delta G^‡$) for N-attack being 62.6 kJ mol^{-1} lower than the activation barrier for O-attack. The authors point this out as an example where the intrinsic preference for O-attack is overcome by the thermodynamic preference for N-attack. As a consequence, OCN^- (**238**) will generally react at the nitrogen in reactions under kinetic control. An alternate scenario is presented in the reaction of SCN^- (**237**) with MeCl (**235**) (Table 1-30 entries 3 and 4). Here, S-attack is intrinsically preferred over N-attack by 20.8 kJ mol^{-1}. While N-attack is thermodynamically preferred over S-attack, the difference in the thermodynamic preference ($\Delta\Delta G^o$, see Figure 1-9 above) is rather small at just 15.4 kJ mol^{-1}. When the $\Delta G^‡$ values are calculated for each process using the Marcus equation, it is seen that the intrinsic preference for S-attack is not overcome by the thermodynamic preference for N-attack, and thus S-attack will occur preferentially in kinetically controlled methylations of SCN^- (**237**) by MeCl (**235**). When the values for the intrinsic barriers are almost identical for each process, as is seen in Table 1-30 entries 7 and 8 for N- and O-attack of NO_2^-, the process with the lower Gibbs free energy of reaction ($\Delta_r G°$) will have the lower activation barrier (i.e., Table 1-30 entry 7).

Mayr and his co-workers believe that this approach to ambident reactivity is superior to that of the HSAB principle as it adequately differentiates between reactions that are occurring under kinetic and thermodynamic control, which has already been demonstrated in section 1.3 to influence the outcomes of reactions of ambident species. In recent years, this method of rationalising ambident reactivity has been tested by various research groups. Computational work by Wang *et. al.* compared and contrasted the predictive abilities of HSAB theory and Marcus theory with regards to S_N2 reactions of ambident isocyanate nucleophiles (**245-M**, see Table 1-31 below).[172] Notably, this study attempted to calculate the influence that a counterion would have on the values of the Gibbs energy of activation ($\Delta G^‡$) and the intrinsic barrier ($\Delta G^‡_{int}$) of these reactions. A selection of results obtained from reactions where the counterion is taken into account are shown below in Table 1-31.

The $\Delta G^‡$ values of S_N2 reactions (a) and (b) drawn below (see illustration in Table 1-31) were calculated by two methods – direct DFT calculation at the CBS-QB3 level of theory, and a Marcus equation-based calculation. The intrinsic barriers for reactions (a) and (b) were determined by the "additivity principle" discussed above, in a manner analogous to the method in which the barriers for the S_N2 reactions were calculated in Table 1-29 above. Wang *et. al.* determined that the experimental selectivity for the gas-phase reactions shown below was such that predominant N-alkylation was observed when the counterion (M) was Li, Na or K. When the counterion was Cu, predominant O-alkylation was observed. This experimental observation is perfectly aligned with the calculated values of $\Delta G^‡$ shown below.

Table 1-31. Wang *et. al*. tested the Marcus treatment of ambident reactivity by calculating the Gibbs free energy of reaction ($\Delta_r G°$) and the Gibbs energy of activation ($\Delta G^‡$) for various S_N2 reactions of isocyanate salts (**245-M**) with various methyl halides (**19** and **222**).[172] $\Delta G^‡$ values were calculated using the Marcus equation (Equation 1.2) and compared to those obtained *via* direct calculation. The identity reactions that make up the reactions (a) and (b) were utilised to determine the intrinsic barriers for these reactions. The values in parentheses are the $\Delta G^‡$ values calculated when the counterion of the nucleophile was not taken into account. All values given in kJ mol^{-1}.



Entry	Rxn	M	X	$\Delta_r G°$	$\Delta G^‡$ (Direct Calc.)	$\Delta G^‡$ (Marcus Eqn)
1	(a)	Li	F	–0.7	+39.7	+36.2 (+19.8)
2	(b)	Li	F	–21.9	+37.4	+29.1 (+20.6)
3	(a)	Na	F	+7.8	+39.5	+30.7 (+24.3)
4	(b)	Na	F	–13.3	+36.3	+23.9 (+24.3)
5	(a)	K	F	+5.8	+49.5	+38.8 (+23.2)
6	(b)	K	F	–13.8	+45.8	+31.1 (+24.0)
7	(a)	Cu	F	–13.8	+39.5	+35.2 (+13.9)
8	(b)	Cu	F	–22.4	+47.3	+40.1 (+20.4)
9	(a)	Li	Br	–9.7	+30.8	+33.9 (+15.6)
10	(b)	Li	Br	–31.3	+26.7	+27.1 (+16.8)
11	(a)	Na	Br	–9.5	+26.3	+30.0 (+15.7)
12	(b)	Na	Br	–29.6	+24.0	+24.7 (+17.5)
13	(a)	K	Br	–8.1	+27.6	+32.8 (+16.3)
14	(b)	K	Br	–27.4	+22.3	+26.0 (+18.3)
15	(a)	Cu	Br	–23.4	+27.3	+30.1 (+10.1)
16	(b)	Cu	Br	–34.2	+34.6	+34.9 (+16.5)

In the reactions of the various metal enolates of **245-M** with MeF (**222**) in Table 1-31 entries 1– 8, the $\Delta G^‡$ value of O-alkylation is only the lower value when M = Cu (compare Table 1-31 entries 7 and 8). The same trend is observed in the reactions of MeBr (**19**), only in Table 1-31 entry 15, where M = Cu, is the $\Delta G^‡$ value of the O-alkylation process lower than that of the corresponding C-alkylation process (Table 1-31 entry 16). In every case shown below, formation of the C-alkylation products is more thermodynamically favourable than formation of the corresponding O-alkylation products (i.e., more negative $\Delta_r G°$ value, e.g., compare Table 1-31 entries 3 and 4). The authors also performed the

Marcus theory-based calculations with the omission of factors relating to the counterion of the ambident nucleophile. Those $\Delta G^{\ddagger}$ values are shown in parentheses in Table 1-31 above. Interestingly, when the counterion is not accounted for in the calculation, the activation barriers predict the wrong product in almost every instance. In all cases shown below where the effects of the counterion are negated, the $\Delta G^{\ddagger}$ values are much lower than those calculated by any other method and they predict predominant O-alkylation.

The authors believe that the data shown above prove that the Marcus treatment of ambident reactivity is helpful in providing insight into the processes that control ambident reactivity, as the correct selectivity of reactions (a) and (b) above can be predicted and the values of $\Delta G^{\ddagger}$ calculated closely resemble those obtained through direct DFT calculation.

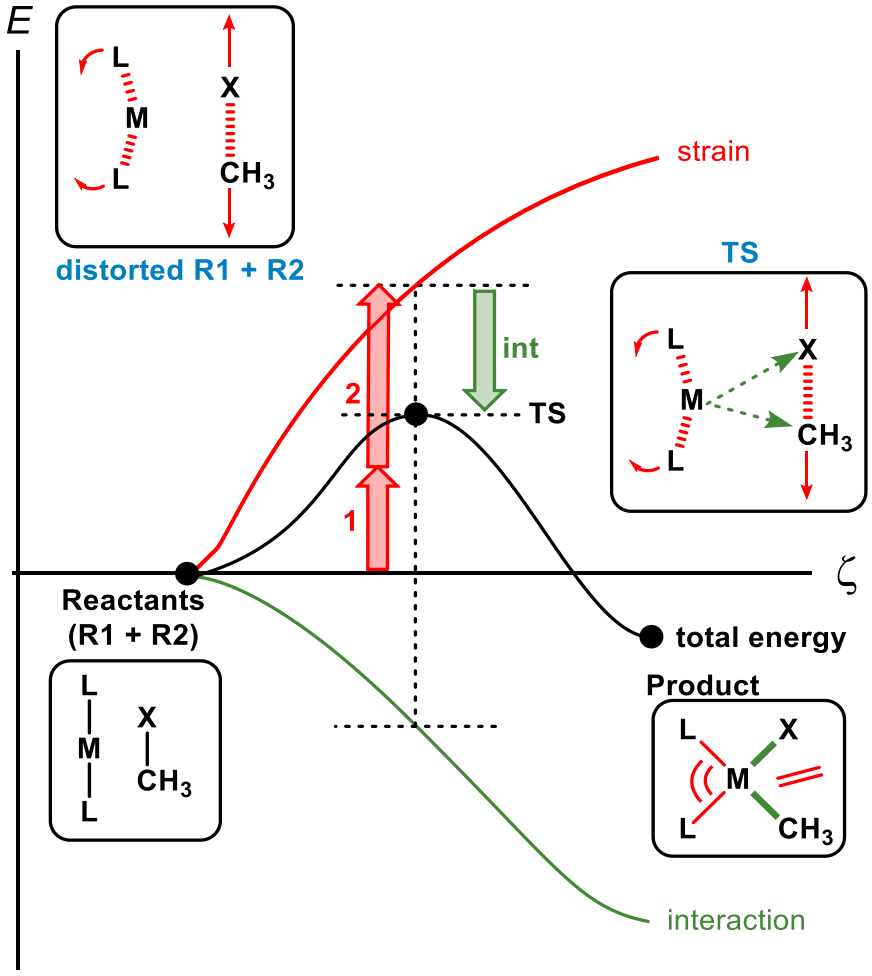
Despite the acknowledgement of many authors that the Marcus treatment of ambident reactivity is an appropriate approach to understanding these reactions,[173–175] there are few instances of research groups testing and expounding upon these foundational concepts. Further research of various reactions of ambident species is needed to determine the robustness of this application of Marcus theory.

1.4.2 Distortion/Interaction Model and Activation Strain Model

The groups of Houk and Bickelhaupt have independently developed a unified model known as either the distortion/interaction model,[176,177] or the activation strain model,[178–180] respectively. This model can be used to analyse the activation barriers which determine reaction rates.[181] This model considers and quantifies (by quantum chemical computational methods) the different energies involved in constructing an activation barrier. In the model, the potential energy surface (which is denoted by (ΔE (ζ)) is considered to be the combination of two contributions along the reaction co-ordinate – the amount of geometrical distortion that the reactants undergo in order to form the transition state, and the energy that results from the interaction of these distorted reactants. The geometrical strain is quantified using the reaction strain parameter ($\Delta E_{strain}(\zeta)$) and is defined as the energy required to distort the reactants from their equilibrium geometries to the geometries in the transition state. It is determined by the physical aspects of the reactants, such as the strengths of bonds which break and the flexibility of bond angles which must become distorted as the potential energy of the reactants traverses the potential energy surface and approaches the transition state. The value of ($\Delta E_{strain}(\zeta)$) is generally positive, meaning it is a destabilising force which gives rise to the activation barrier. The interaction energy ($\Delta E_{int}(\zeta)$) between the reactants arises from the electronic structure of each reactant and how they are oriented as they move towards the transition state. The value of ($\Delta E_{int}(\zeta)$) is generally negative, meaning that it stabilises the reactant complex and is a factor which counteracts the strain term ($\Delta E_{strain}(\zeta)$) and causes the height of the activation barrier to decrease (compared to a case in which only the geometrical strain of the reactants was considered). An example taken from a paper by Bickelhaupt and Houk showing the interplay between the values of ($\Delta E_{strain}(\zeta)$) and

($\Delta E_{int}(\zeta)$ is shown below in Figure 1-13. The strain energy is described by the red curve, and represents unfavourable geometric movements of molecules, such as the stretching of the C—X bond as the reactants approach the transitions state (see examples marked "distorted R1 + R2" in Figure 1-13). The green curve is the stabilising interaction energy, which becomes more negative when favourable interactions arise as the reactants approach the transitions state, such as the interactions between "M" and "CH_3" and "M" and "X" in Figure 1-13.

Figure 1-13. An example of the activation-strain model applied to a metal-mediated C—X bond activation. The potential energy surface (ΔE (ζ)) is defined by the contributions from geometrical strain ($\Delta E_{strain}(\zeta)$) and reactant interactions ($\Delta E_{int}(\zeta)$ as they approach the transition state. Some of the individual contributions that result in increased strain are illustrated below and highlighted in red. An example of an interaction in the reactant complex which stabilises the complex (i.e., contributes to ($\Delta E_{int}(\zeta)$) is highlighted in green below.



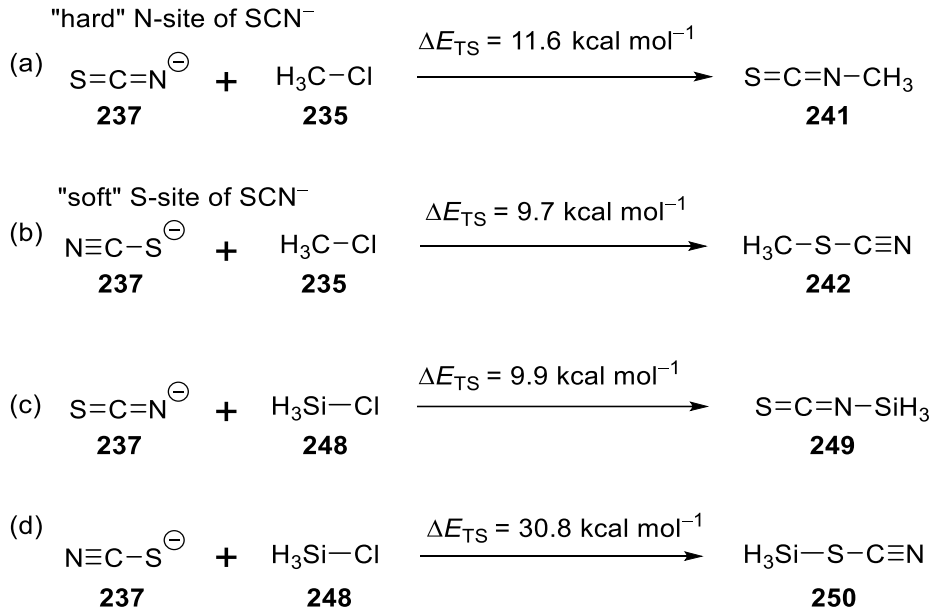
The black curve in Figure 1-13 is the combination of the destabilising strain energy brought about by geometric strain in the transition state, and the stabilising interaction energy. As the influence of the distortion energy and the interaction energy in the transition state combine to determine the activation energy of a reaction in this model, the activation energy may thus be described by Equation 1.5.

$$\Delta E^{\ddagger} = \Delta E^{\ddagger}_{\text{strain}} + \Delta E^{\ddagger}_{\text{int}} \qquad (1.5)$$

The activation-strain model is somewhat similar to Marcus theory in that the reactivity of a given reaction is defined by a combination of thermodynamic contributions and the energy required to distort the reactants towards the geometry of the products at the transition state. In Marcus theory, this reorganisation energy is defined as λ (see discussion in section 1.4.1 above).

This model has been successfully used in a variety of applications, such as rationalising the competition between bimolecular S_N2 nucleophilic substitution and base-induced E2 elimination reactions in reactions of Lewis bases in the gas phase.[182] It has also been used to explain the experimentally-observed Diels-Alder reactivities of cycloalkenones, cycloalkenes and cyclic dienes.[183,184]

Figure 1-14. An example of the gas-phase reactions of the ambident nucleophile SCN^- (**237**) which were investigated by Bickelhaupt and co-workers.[185] Computations at the ZORA-OLYP/TZ2P level of theory revealed that the preferred site of addition on the thiocyanate anion switched from S to N when the electrophile was varied from the "harder" MeCl (**235**) to the "softer" SiH_3Cl (**248**).



The activation strain model has recently been applied by Bickelhaupt and co-workers in an attempt to explain the behaviour of ambident nucleophiles which cannot be accounted for using HSAB theory.[185] In this study, the gas-phase reactivity of three ambident nucleophiles with two electrophiles was assessed using quantum chemical computations. The local "hardness" and "softness" of each of the species was calculated using molecular electrostatic potentials and Fukui functions, which allowed for the identification of the hard and soft sites of ambident nucleophiles such as CN^- (**236**), SCN^- (**237**) and OCN^-

(**238**). One of the key results from their study is illustrated above in Figure 1-14 and discussed below.

For the thiocyanate anion (SCN^-, **237**), the nitrogen atom was calculated by these authors to be the local "hard" site of the anion, and the sulfur atom was calculated to be the local "soft" site. In gas-phase reactions of SCN^- with MeCl (**235**), S-alkylation was calculated to be the favoured process (compare the ΔE_{TS} values in Figure 1-14(a) and (b)). When utilising the HSAB principle as it is commonly applied to ambident reactivity, this is considered to be the expected outcome – the "soft" centre of the SCN^- nucleophile preferentially reacts with the "soft" carbon atom of the electrophile.

However, further calculations were carried out on reactions between SCN^- (**237**) with SiH_3Cl (**248**), an electrophile whose silicon atom should, according to the principles of HSAB theory, be even "softer" than the carbon atom in MeCl (**235**). In this case, the selectivity of the reaction is observed to switch, with the reaction of the "hard" nitrogen atom of the SCN^- (**237**) anion being preferred to the corresponding S-attack reaction (compare the ΔE_{TS} values in Figure 1-14(c) and (d)). This result cannot be rationalised in the context of HSAB theory, as there is no obvious reason why the use of a "softer" electrophile such as SiH_3Cl (**248**) should result in the selectivity of the reaction being altered such that the "hard" nucleophilic site (i.e., the N-atom in SCN^-) is now the preferred site of addition.

Activation strain analyses carried out by Bickelhaupt and co-workers were capable of accounting for the selectivity observed in the instances outlined in Figure 1-14.[185] They found that the observed trends in the activation barriers were mostly associated with energy differences arising from the interaction between the reactants in the transition state ($\Delta E_{int}(\zeta)$, see Equation 1.5) and not differences in the geometrical strain associated with the distortion of the reactant geometry.

The authors determine that the key difference which causes preferential attack of the N-atom of SCN^- (**237**) in a reaction with SiH_3Cl (**248**) was the donor-acceptor orbital interactions which determined the approach of the incoming nucleophile. They determined that the approach of the N-atom of SCN^- is "linear" with respect to the electrophile, whereas the approach of the S-atom is "tilted", due to the magnitudes of the nucleophile-HOMO and electrophile-LUMO orbital interactions. The "linear" attack is favoured in the reaction with SiH_3Cl (**248**), as there are less Pauli repulsion forces (or exclusion-principle repulsion) that destabilise the reactant complex. These results, along with others which may be seen in the paper, serve to demonstrate the potential of tasking models such as the activation strain model with rationalising the experimentally observed behaviours of ambident nucleophiles.

Other computationally derived approaches which may have use in understanding the selectivity of the reactions of ambident nucleophiles include Valence Bond theory as described in the papers of Shaik and co-workers.[186–190] This model seeks to assign a simple quantum mechanical description of a reaction profile by combining molecular orbital and valence bond wave functions. Other emergent methods for elucidating

reaction mechanisms and selectivities using computational methods may be seen in a recent review by Krenske and co-workers.[191]

1.5. References

1. Williard, P. G. In *Comprehensive Organic Synthesis*; Trost, B. M., Fleming, I., Eds.; Pergamon: Oxford, 1991; Vol. 1, pp 1–77.
2. Zhao, Y.; Sakai, N.; Matile, S. *Nat. Commun.* **2014**, *5*, 3911.
3. Doi, R.; Kikushima, K.; Ohashi, M.; Ogoshi, S. *J. Am. Chem. Soc.* **2015**, *137*, 3276–3282.
4. Xu, Z.; Chen, H.; Wang, Z.; Ying, A.; Zhang, L. *J. Am. Chem. Soc.* **2016**, *138*, 5515–5518.
5. Streuff, J.; White, D. E.; Virgil, S. C.; Stoltz, B. M. *Nat. Chem.* **2010**, *2*, 192–196.
6. Minko, Y.; Pasco, M.; Lercher, L.; Botoshansky, M.; Marek, I. *Nature* **2012**, *490*, 522–526.
7. DeMartino, M. P.; Chen, K.; Baran, P. S. *J. Am. Chem. Soc.* **2008**, *130*, 11546–11560.
8. Tomooka, K.; Ezawa, T.; Inoue, H.; Uehara, K.; Igawa, K. *J. Am. Chem. Soc.* **2011**, *133*, 1754–1756.
9. Braun, M. In *Modern Enolate Chemistry: From Preparation to Applications in Asymmetric Synthesis*; John Wiley & Sons, Ltd, 2015.
10. Clayden, J.; Greeves, N.; Warren, S. G. In *Organic Chemistry*; Oxford University Press: New York, 2012; pp 584–613.
11. Klein, D. R. In *Organic Chemistry*; Wiley: New York, 2016; pp 954–1053.
12. Stolz, D.; Kazmaier, U. In *PATAI'S Chemistry of Functional Groups*; John Wiley & Sons, Ltd, 2010.
13. Junk, L.; Kazmaier, U. *ChemistryOpen* **2020**, *9*, 929–952.
14. Braun, M.; Meier, T. *Angew. Chem. Int. Ed.* **2006**, *45*, 6952–6955.
15. Wright, T. B.; Evans, P. A. *Chem. Rev.* **2021**, *121*, 9196–9242.
16. Vargová, D.; Némethová, I.; Plevová, K.; Šebesta, R. *ACS Catal.* **2019**, *9*, 3104–3143.
17. Barltrop, J. A. *J. Chem. Soc. Resumed* **1947**, No. 0, 399–401.
18. Sheehan, J. C.; Mumaw, C. E. *J. Am. Chem. Soc.* **1950**, *72*, 2127–2129.
19. Doering, W. von E.; Rhoads, S. J. *J. Am. Chem. Soc.* **1951**, *73*, 3082–3084.
20. Rhoads, S. J.; Reynolds, R. D.; Raulins, R. *J. Am. Chem. Soc.* **1952**, *74*, 2889–2892.
21. Kabachnik, M. I.; Yoffe, S. T.; Vatsuro, K. V. *Tetrahedron* **1957**, *1*, 317–327.
22. Jane Rhoads, S.; W. Hasbrouck, R.; Pryde, C.; Holder, R. W. *Tetrahedron Lett.* **1963**, *4*, 669–672.
23. Yoffe, S. T.; Vatsuro, K. V.; Kugutcheva, E. E.; Kabachnik, M. I. *Tetrahedron Lett.* **1965**, *6*, 593–600.
24. Kremers, F.; Roth, F.; Tietze, E.; Claisen, L. *Justus Liebigs Ann. Chem.* **1925**, *442*, 210–245.
25. Ning, Y.; Otani, Y.; Ohwada, T. *J. Org. Chem.* **2018**, *83*, 203–219.
26. Ning, Y.; Otani, Y.; Ohwada, T. *J. Org. Chem.* **2017**, *82*, 6313–6326.
27. Landquist, J. K. *J. Chem. Soc. Resumed* **1953**, No. 0, 2816–2821.
28. Cmoch, P. *Magn. Reson. Chem.* **2003**, *41*, 693–698.
29. Nishiwaki, N.; Hisaki, M.; Ono, M.; Ariga, M. *Tetrahedron* **2009**, *65*, 7403–7407.
30. Parlow, J. J.; Kurumbail, R. G.; Stegeman, R. A.; Stevens, A. M.; Stallings, W. C.; South, M. S. *J. Med. Chem.* **2003**, *46*, 4696–4701.
31. Pfefferkorn, J. A.; Lou, J.; Minich, M. L.; Filipski, K. J.; He, M.; Zhou, R.; Ahmed, S.; Benbow, J.; Perez, A.-G.; Tu, M.; Litchfield, J.; Sharma, R.; Metzler, K.; Bourbonais, F.; Huang, C.; Beebe, D. A.; Oates, P. J. *Bioorg. Med. Chem. Lett.* **2009**, *19*, 3247–3252.

32. Torres, M.; Gil, S.; Parra, M. *Curr. Org. Chem. 9*, 1757–1779.
33. Afarinkia, K.; Vinader, V.; Nelson, T. D.; Posner, G. H. *Tetrahedron* **1992**, *48*, 9111–9171.
34. Comins, D. L.; Jianhua, G. *Tetrahedron Lett.* **1994**, *35*, 2819–2822.
35. Hao, X.; Xu, Z.; Lu, H.; Dai, X.; Yang, T.; Lin, X.; Ren, F. *Org. Lett.* **2015**, *17*, 3382–3385.
36. Feng, B.; Li, Y.; Li, H.; Zhang, X.; Xie, H.; Cao, H.; Yu, L.; Xu, Q. *J. Org. Chem.* **2018**, *83*, 6769–6775.
37. Kornblum, N.; Taub, B.; Ungnade, H. E. *J. Am. Chem. Soc.* **1954**, *76*, 3209–3211.
38. Kornblum, N.; Smiley, R. A.; Ungnade, H. E.; White, A. M.; Taub, B.; Herbert, S. A. *J. Am. Chem. Soc.* **1955**, *77*, 5528–5533.
39. Kornblum, N.; Smiley, R. A.; Blackwood, R. K.; Iffland, D. C. *J. Am. Chem. Soc.* **1955**, *77*, 6269–6280.
40. Kornblum, N.; Larson, H. O.; Blackwood, R. K.; Mooberry, D. D.; Oliveto, E. P.; Graham, G. E. *J. Am. Chem. Soc.* **1956**, *78*, 1497–1501.
41. Kornblum, N. In *Organic Reactions*; John Wiley & Sons, Ltd, 2011; pp 101–156.
42. Nakata, H. *Bull. Chem. Soc. Jpn.* **1960**, *33*, 1693–1701.
43. le Noble, W. J.; Puerta, J. E. *Tetrahedron Lett.* **1966**, *7*, 1087–1090.
44. Marshall Beringer, F.; Forgione, P. S.; Yudis, M. D. *Tetrahedron* **1960**, *8*, 49–63.
45. Shen, T. Y.; Lucas, S.; Sarett, L. H. *Tetrahedron Lett.* **1961**, *2*, 43–47.
46. Shevelev, S. A.; Erashko, V. I.; Fainzil'berg, A. A. *Bull. Acad. Sci. USSR Div. Chem. Sci.* **1968**, *17*, 2003–2006.
47. Kornblum, N.; Lurie, A. P. *J. Am. Chem. Soc.* **1959**, *81*, 2705–2715.
48. Kornblum, N.; Berrigan, P. J.; le Noble, W. J. *J. Am. Chem. Soc.* **1960**, *82*, 1257–1258.
49. Kornblum, Nathan.; Berrigan, P. J.; Le Noble, W. J. *J. Am. Chem. Soc.* **1963**, *85*, 1141–1147.
50. Lauer, K.; Shingu, H. *Berichte Dtsch. Chem. Ges. B Ser.* **1936**, *69*, 2731–2742.
51. Cavell, E. a. S. *J. Chem. Soc. Resumed* **1958**, No. 0, 4217–4222.
52. Kornblum, Nathan.; Seltzer, Raymond.; Haberfield, Paul. *J. Am. Chem. Soc.* **1963**, *85*, 1148–1154.
53. Hobbs, C. F.; McMillin, C. K.; Papadopoulos, E. Paul.; VanderWerf, C. A. *J. Am. Chem. Soc.* **1962**, *84*, 43–51.
54. Smith, P. A. S.; Robertson, J. E. *J. Am. Chem. Soc.* **1962**, *84*, 1197–1204.
55. Nee, G.; Leroux, Y.; Seyden-Penne, J. *Tetrahedron* **1981**, *37*, 1541–1545.
56. Kurts, A. L.; Macias, A.; Beletskaya, I. P.; Reutov, O. A. *Tetrahedron* **1971**, *27*, 4759–4767.
57. Kurts, A. L.; Dem'yanov, P. I.; Macias, A.; Beletskaya, I. P.; Reutov, O. A. *Tetrahedron* **1971**, *27*, 4769–4776.
58. Reich, H. J. *Chem. Rev.* **2013**, *113*, 7130–7178.
59. Manege, L. C.; Ueda, T.; Hojo, M.; Fujio, M. *J. Chem. Soc. Perkin Trans. 2* **1998**, No. 9, 1961–1966.
60. Hojo, M.; Ueda, T.; Ueno, E.; Hamasaki, T.; Nakano, T. *Bull. Chem. Soc. Jpn.* **2010**, *83*, 401–414.
61. Hojo, M.; Aoki, S. *Bull. Chem. Soc. Jpn.* **2012**, *85*, 1023–1030.
62. Jackman, L. M.; Lange, B. C. *Tetrahedron* **1977**, *33*, 2737–2769.
63. Jackman, L. M.; Dunne, T. S. *J. Am. Chem. Soc.* **1985**, *107*, 2805–2806.
64. Jackman, L. M.; Haddon, R. C. *J. Am. Chem. Soc.* **1973**, *95*, 3687–3692.
65. Jackman, L. M.; Szeverenyi, N. M. *J. Am. Chem. Soc.* **1977**, *99*, 4954–4962.
66. Jackman, L. M.; Lange, B. C. *J. Am. Chem. Soc.* **1981**, *103*, 4494–4499.

67. Harrison-Marchand, A.; Mongin, F. *Chem. Rev.* **2013**, *113*, 7470–7562.
68. Mongin, F.; Harrison-Marchand, A. *Chem. Rev.* **2013**, *113*, 7563–7727.
69. Pratt, L. M.; Streitwieser, A. *J. Org. Chem.* **2003**, *68*, 2830–2838.
70. Amstutz, R.; Bernd Schweizer, W.; Seebach, D.; Dunitz, J. D. *Helv. Chim. Acta* **1981**, *64*, 2617–2621.
71. Nichols, M. A.; Leposa, C. M.; Hunter, A. D.; Zeller, M. *J. Chem. Crystallogr.* **2007**, *37*, 825–829.
72. Macrae, C. F.; Sovago, I.; Cottrell, S. J.; Galek, P. T. A.; McCabe, P.; Pidcock, E.; Platings, M.; Shields, G. P.; Stevens, J. S.; Towler, M.; Wood, P. A. *J. Appl. Crystallogr.* **2020**, *53*, 226–235.
73. Kornblum, N.; Seltzer, R. *J. Am. Chem. Soc.* **1961**, *83*, 3668–3671.
74. Kornblum, N.; Pink, P.; Yorka, K. V. *J. Am. Chem. Soc.* **1961**, *83*, 2779–2780.
75. Hass, H. B.; Bender, M. L. *J. Am. Chem. Soc.* **1949**, *71*, 1767–1769.
76. Meerwein, H.; Hinz, G.; Hofmann, P.; Kroning, E.; Pfeil, E. *J. Für Prakt. Chem.* **1937**, *147*, 257–285.
77. Meerwein, H.; Battenberg, E.; Gold, H. *J. Für Prakt. Chem.* **1939**, *154*, 83–156.
78. Kornblum, Nathan.; Brown, R. Alan. *J. Am. Chem. Soc.* **1963**, *85*, 1359–1360.
79. Pearson, R. G. *J. Am. Chem. Soc.* **1963**, *85*, 3533–3539.
80. Pearson, R. G. *Science* **1966**.
81. Pearson, R. G.; Songstad, Jon. *J. Am. Chem. Soc.* **1967**, *89*, 1827–1836.
82. Pearson, R. G. *J. Chem. Educ.* **1968**, *45*, 581.
83. Pearson, R. G. *J. Chem. Educ.* **1968**, *45*, 643.
84. Edwards, J. O.; Pearson, R. G. *J. Am. Chem. Soc.* **1962**, *84*, 16–24.
85. Klopman, G. *J. Am. Chem. Soc.* **1968**, *90*, 223–234.
86. Salem, L. *J. Am. Chem. Soc.* **1968**, *90*, 543–552.
87. Isaacs, N. S. In *Physical Organic Chemistry*; Longman Scientific & Technical: Burnt Mill, Harlow, Essex, England, 1995; p 276.
88. Kosower, E. M. *J. Am. Chem. Soc.* **1956**, *78*, 3497–3501.
89. Hudson, R. F. Academic Press: New York, 1965.
90. Kurts, A. L.; Genkina, N. K.; Macias, A.; Beletskaya, L. P.; Reutov, O. A. *Tetrahedron* **1971**, *27*, 4777–4785.
91. Guibé, F.; Sarthou, P.; Bram, G. *Tetrahedron* **1974**, *30*, 3139–3151.
92. Saville, B. *Angew. Chem. Int. Ed. Engl.* **1967**, *6*, 928–939.
93. Ho, T.-L. *Chem. Rev.* **1975**, *75*, 1–20.
94. Geerlings, P.; De Proft, F. *Int. J. Quantum Chem.* **2000**, *80*, 227–235.
95. Hudson, R. F. *Angew. Chem. Int. Ed. Engl.* **1973**, *12*, 36–56.
96. Le Noble, W. J.; Morris, H. F. *J. Org. Chem.* **1969**, *34*, 1969–1973.
97. Singh, J. *J. Org. Chem.* **1980**, *45*, 3368–3369.
98. Murphy, W. S.; Buckley, D. J. *Tetrahedron Lett.* **1969**, *10*, 2975–2978.
99. Umemura, K.; Matsuyama, H.; Kamigata, N. *Bull. Chem. Soc. Jpn.* **1990**, *63*, 2593–2600.
100. Maiti, S.; Mal, P. *J. Org. Chem.* **2018**, *83*, 1340–1347.
101. Samai, S.; Chanda, T.; Ila, H.; Singh, M. S. *Eur. J. Org. Chem.* **2013**, *2013*, 4026–4031.
102. Brown, M. J.; Clarkson, G. J.; Fox, D. J.; Inglis, G. G.; Shipman, M. *Tetrahedron Lett.* **2010**, *51*, 382–384.
103. Mayr, H.; Breugst, M.; Ofial, A. R. *Angew. Chem. Int. Ed.* **2011**, *50*, 6470–6505.
104. March, J. In *Advanced Organic Chemistry*; John Wiley & Sons: Hoboken, 2007; pp 512–518.

105. Anslyn, E. V.; Dougherty, D. A. In *Modern Physical Organic Chemistry*; University Science Books: Sausalito, 2006; pp 288–292.
106. Jiang, J.; Hou, C.; Zhang, S.; Luan, Z.; Zhao, C.; Ke, Z. *J. Org. Chem.* **2015**, *80*, 1661–1671.
107. Ye, X.; Sun, X.; Huang, Z.; Yang, N.; Su, Z.; Hu, C.; Song, Z. *Org. Biomol. Chem.* **2014**, *12*, 3021–3025.
108. Vartanova, A. E.; Levina, I. I.; Ratmanova, N. K.; Andreev, I. A.; Ivanova, O. A.; Trushkov, I. V. *Org. Biomol. Chem.* **2022**, *20*, 7795–7802.
109. Nagaraj, P.; Ramesh, N. G. *Tetrahedron* **2011**, *67*, 9322–9328.
110. Maiti, S.; Alam, T.; Mal, P. *Asian J. Org. Chem.* **2018**, *7*, 715–719.
111. Drago, R. S. *J. Chem. Educ.* **1974**, *51*, 300.
112. Gompper, R.; Wagner, H.-U. *Angew. Chem. Int. Ed. Engl.* **1976**, *15*, 321–333.
113. Hünig, S. *Angew. Chem. Int. Ed. Engl.* **1964**, *3*, 548–560.
114. Buncel, E.; Dust, J. M.; Manderville, R. A. *J. Am. Chem. Soc.* **1996**, *118*, 6072–6073.
115. Loos, R.; Kobayashi, S.; Mayr, H. *J. Am. Chem. Soc.* **2003**, *125*, 14126–14132.
116. Tishkov, A. A.; Mayr, H. *Angew. Chem. Int. Ed.* **2005**, *44*, 142–145.
117. Tishkov, A. A.; Schmidhammer, U.; Roth, S.; Riedle, E.; Mayr, H. *Angew. Chem. Int. Ed.* **2005**, *44*, 4623–4626.
118. Breugst, M.; Tokuyasu, T.; Mayr, H. *J. Org. Chem.* **2010**, *75*, 5250–5258.
119. Breugst, M.; Mayr, H. *J. Am. Chem. Soc.* **2010**, *132*, 15380–15389.
120. Cantor, P. A.; Vanderwerf, C. A. *J. Am. Chem. Soc.* **1958**, *80*, 970–973.
121. Hammond, G. S.; Emmons, W. D.; Parker, C. O.; Graybill, B. M.; Waters, J. H.; Hawthorne, M. F. *Tetrahedron* **1963**, *19*, 177–195.
122. Barbieri, W.; Bernardi, L.; Coda, S.; Colò, V.; Palamidessi, G. *Tetrahedron* **1967**, *23*, 4395–4407.
123. Kurts, A. L.; Beletskaya, I. P. *Bull. Acad. Sci. USSR Div. Chem. Sci.* **1970**, *19*, 781–784.
124. Schoeps, K.-O.; Halidin, C.; Stone-Elander, S.; Långström, B.; Greitz, T. *J. Label. Compd. Radiopharm.* **1988**, *25*, 749–758.
125. Jones, M. E.; Kass, S. R.; Filley, J.; Barkley, R. M.; Ellison, G. B. *J. Am. Chem. Soc.* **1985**, *107*, 109–115.
126. Brickhouse, M. D.; Squires, R. R. *J. Phys. Org. Chem.* **1989**, *2*, 389–409.
127. Holmes, J. L.; Lossing, F. P. *J. Am. Chem. Soc.* **1982**, *104*, 2648–2649.
128. Zhong, M.; Brauman, J. I. *J. Am. Chem. Soc.* **1996**, *118*, 636–641.
129. Freriks, I. L.; De Koning, L. J.; Nibbering, N. M. M. *J. Am. Chem. Soc.* **1991**, *113*, 9119–9124.
130. Freriks, I. L.; de Koning, L. J.; Nibbering, N. M. M. *J. Phys. Org. Chem.* **1992**, *5*, 776–782.
131. Freriks, I. L.; De Koning, L. J.; Nibbering, N. M. M. *J. Org. Chem.* **1992**, *57*, 5976–5979.
132. Houk, K. N.; Paddon-Row, M. N. *J. Am. Chem. Soc.* **1986**, *108*, 2659–2662.
133. Marcos, E. S.; Bertran, J. *J. Chem. Soc. Faraday Trans. 2 Mol. Chem. Phys.* **1989**, *85*, 1531–1538.
134. Lee, I.; Park, H. Y.; Han, I.-S.; Kim, C. K.; Kim, C. K.; Lee, B.-S. *Bull. Korean Chem. Soc.* **1999**, *20*, 559–566.
135. Burmudžija, A.; Marković, S.; Muškinja, J.; Pejović, A.; Tošović, J. *React. Kinet. Mech. Catal.* **2018**, *123*, 201–214.
136. Pearson, R. G. *Inorganica Chim. Acta* **1995**, *240*, 93–98.

137. Uggerud, E. In *Advances in Physical Organic Chemistry*; Williams, I. H., Williams, N. H., Eds.; Academic Press, 2017; Vol. 51, pp 1–57.
138. Grimmel, S. A.; Reiher, M. *CHIMIA* **2021**, *75*, 311–311.
139. Ayers, P. W. *J. Chem. Phys.* **2005**, *122*, 141102.
140. Ayers, P. W. *Faraday Discuss.* **2006**, *135*, 161–190.
141. Ayers, P. W.; Parr, R. G.; Pearson, R. G. *J. Chem. Phys.* **2006**, *124*, 194107.
142. Cárdenas, C.; Ayers, P. W. *Phys. Chem. Chem. Phys.* **2013**, *15*, 13959–13968.
143. Ayers, P. W.; Cárdenas, C. *J. Chem. Phys.* **2013**, *138*, 181106.
144. Wang, Y.-G.; Barnes, E. C. *ACS Omega* **2018**, *3*, 4557–4572.
145. Yaragorla, S.; Pareek, A.; Dada, R. *Tetrahedron Lett.* **2017**, *58*, 4642–4647.
146. Marcus, R. A. *J. Chem. Phys.* **1956**, *24*, 966–978.
147. Marcus, R. A. *J. Chem. Phys.* **1957**, *26*, 867–871.
148. Marcus, R. A. *J. Chem. Phys.* **1957**, *26*, 872–877.
149. Marcus, R. A. *Discuss. Faraday Soc.* **1960**, *29*, 21–31.
150. Marcus, R. A. *J. Phys. Chem.* **1963**, *67*, 853–857.
151. Marcus, R. A. *J. Phys. Chem.* **1968**, *72*, 891–899.
152. Albery, W. J.; Kreevoy, M. M. In *Advances in Physical Organic Chemistry*; Gold, V., Bethell, D., Eds.; Academic Press, 1978; Vol. 16, pp 87–157.
153. Cohen, A. O.; Marcus, R. A. *J. Phys. Chem.* **1968**, *72*, 4249–4256.
154. Marcus, R. A. *J. Am. Chem. Soc.* **1969**, *91*, 7224–7225.
155. Hammond, G. S. *J. Am. Chem. Soc.* **1955**, *77*, 334–338.
156. Miller, J. R.; Calcaterra, L. T.; Closs, G. L. *J. Am. Chem. Soc.* **1984**, *106*, 3047–3049.
157. Thanasekaran, P.; Rajendran, T.; Rajagopal, S.; Srinivasan, C.; Ramaraj, R.; Ramamurthy, P.; Venkatachalapathy, B. *J. Phys. Chem. A* **1997**, *101*, 8195–8199.
158. Hill, R. H. *J. Chem. Soc. Chem. Commun.* **1989**, No. 5, 293–295.
159. Moser, C. C.; Keske, J. M.; Warncke, K.; Farid, R. S.; Dutton, P. L. *Nature* **1992**, *355*, 796–802.
160. Wherland, S.; Pecht, I. *Biochemistry* **1978**, *17*, 2585–2591.
161. Pellerite, M. J.; Brauman, J. I. *J. Am. Chem. Soc.* **1980**, *102*, 5993–5999.
162. Pellerite, M. J.; Brauman, J. I. *J. Am. Chem. Soc.* **1983**, *105*, 2672–2680.
163. Dodd, J. A.; Brauman, J. I. *J. Phys. Chem.* **1986**, *90*, 3559–3562.
164. Wladkowski, B. D.; Brauman, J. I. *J. Phys. Chem.* **1993**, *97*, 13158–13164.
165. Gonzales, J. M.; Pak, C.; Cox, R. S.; Allen, W. D.; Schaefer III, H. F.; Császár, A. G.; Tarczay, G. *Chem. – Eur. J.* **2003**, *9*, 2173–2192.
166. Gonzales, J. M.; Allen, W. D.; Schaefer, H. F. *J. Phys. Chem. A* **2005**, *109*, 10613–10628.
167. Breugst, M.; Zipse, H.; Guthrie, J. P.; Mayr, H. *Angew. Chem. Int. Ed.* **2010**, *49*, 5165–5169.
168. Schaller, H. F.; Schmidhammer, U.; Riedle, E.; Mayr, H. *Chem. – Eur. J.* **2008**, *14*, 3866–3868.
169. Bug, T.; Lemek, T.; Mayr, H. *J. Org. Chem.* **2004**, *69*, 7565–7576.
170. Baidya, M.; Kobayashi, S.; Mayr, H. *J. Am. Chem. Soc.* **2010**, *132*, 4796–4805.
171. Hoz, S.; Basch, H.; Wolk, J. L.; Hoz, T.; Rozental, E. *J. Am. Chem. Soc.* **1999**, *121*, 7724–7725.
172. Wang, Y.-G.; Barnes, E. C.; Kaya, S.; Sharma, V. *J. Comput. Chem.* **2019**, *40*, 2761–2777.
173. Dong, H.; Rahm, M.; Thota, N.; Deng, L.; Brinck, T.; Ramström, O. *Org. Biomol. Chem.* **2012**, *11*, 648–653.

174. Zadeh, F. H.; Fuentealba, P.; Cárdenas, C.; Ayers, P. W. *Phys. Chem. Chem. Phys.* **2014**, *16*, 6019–6026.
175. Seitz, C. G.; Zhang, H.; Mo, Y.; Karty, J. M. *J. Org. Chem.* **2016**, *81*, 3711–3719.
176. Ess, D. H.; Houk, K. N. *J. Am. Chem. Soc.* **2007**, *129*, 10646–10647.
177. Ess, D. H.; Houk, K. N. *J. Am. Chem. Soc.* **2008**, *130*, 10187–10198.
178. Bickelhaupt, F. M. *J. Comput. Chem.* **1999**, *20*, 114–128.
179. Fernández, I.; Bickelhaupt, F. M. *Chem. Soc. Rev.* **2014**, *43*, 4953–4967.
180. Wolters, L. P.; Bickelhaupt, F. M. *WIREs Comput. Mol. Sci.* **2015**, *5*, 324–343.
181. Bickelhaupt, F. M.; Houk, K. N. *Angew. Chem. Int. Ed.* **2017**, *56*, 10070–10086.
182. Vermeeren, P.; Hansen, T.; Jansen, P.; Swart, M.; Hamlin, T. A.; Bickelhaupt, F. M. *Chem. – Eur. J.* **2020**, *26*, 15538–15548.
183. Paton, R. S.; Kim, S.; Ross, A. G.; Danishefsky, S. J.; Houk, K. N. *Angew. Chem. Int. Ed.* **2011**, *50*, 10366–10368.
184. Liu, F.; Paton, R. S.; Kim, S.; Liang, Y.; Houk, K. N. *J. Am. Chem. Soc.* **2013**, *135*, 15642–15649.
185. Bettens, T.; Alonso, M.; De Proft, F.; Hamlin, T. A.; Bickelhaupt, F. M. *Chem. Eur. J.* **2020**, *26*, 3884–3893.
186. Shaik, S. S. *J. Am. Chem. Soc.* **1981**, *103*, 3692–3701.
187. Pross, A.; Shaik, S. S. *Acc. Chem. Res.* **1983**, *16*, 363–370.
188. Shaik, S.; Shurki, A. *Angew. Chem. Int. Ed.* **1999**, *38*, 586–625.
189. Stuyver, T.; De Proft, F.; Geerlings, P.; Shaik, S. *J. Am. Chem. Soc.* **2020**, *142*, 10102–10113.
190. Stuyver, T.; Shaik, S. *J. Am. Chem. Soc.* **2020**, *142*, 20002–20013.
191. Chin, Y. P.; See, N. W.; Jenkins, I. D.; Krenske, E. H. *Org. Biomol. Chem.* **2022**, *20*, 2028–2042.

Chapter 2: N vs. O Selectivity in Reactions of Diazine *N*-Oxides

2.1. Selectivity in Reactions of Ambident Nucleophiles - Diazine *N*-Oxides 79

2.2. Spectroscopic Investigations – Reference δ_N Values 83

2.2.1. Reactions of Diazines and Pyridine *N*-Oxides to Obtain Reference δ_N Values. 85

2.2.2. Investigation of Literature Trends in the δ_N Values of N- and O-alkylated Heterocycles 90

2.2.3. Investigation of ^{1}H-^{13}C HMBC NMR and ^{13}C NMR Spectroscopy Features which Enable Identification of N-alkylation or O-alkylation in Reactions of Heterocycles and Aromatic *N*-Oxides 94

2.2.4. Identification of Characteristic $\Delta(\delta_N)$ Values 98

2.3. Investigations into the Ambident Reactivity of Diazine *N*-Oxides 100

2.3.1 Site of Alkylation of Diazine *N*-Oxides 100

2.3.2 Results of Computational Investigation on the Ambident Reactivity of Diazine *N*-Oxides 110

2.3.3 Activation Barrier Calculations Using Marcus Theory 117

2.3.4 Rationalising the Observed Selectivities in Reactions of Diazine *N*-Oxides ... 122

2.3.5 Reappraisal of Literature Observations on N- vs O-Selectivity in Reactions of Diazine *N*-Oxides 125

2.4. References 127

Appendices referred to in the text are available at the following link:
https://tinyurl.com/KSheehyPhDThesisAppendices

Note: The work described in the following chapter has been published in the following academic journals:

K. J. Sheehy, L. M. Bateman, N. Flosbach, M. Breugst, P. A. Byrne. "Identification of N- or O-Alkylation of Aromatic Nitrogen Heterocycles and *N*-Oxides Using ^{1}H-^{15}N HMBC NMR Spectroscopy" *Eur. J. Org. Chem.* **2020**, *22*, 3270-3281.

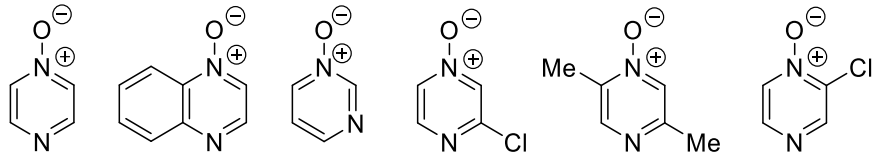
K. J. Sheehy, L. M. Bateman, N. Flosbach, M. Breugst, P. A. Byrne. "Competition Between N and O: Use of Diazine *N*-Oxides as a Test Case for the Marcus Theory Rationale for Ambident Reactivity" *Chem. Sci.* **2020**, *11*, 9630-9647.

2.1. Selectivity in Reactions of Ambident Nucleophiles - Diazine *N*-Oxides

The difficulty inherent in accounting for the selectivities observed in reactions of ambident nucleophiles is exemplified by the fact that the HSAB principle *predicts the incorrect product* in a very large number of cases, as has been reviewed in detail by Mayr and co-workers.[1] The data in Mayr's review article call starkly into question whether the principle adequately explains the observed selectivity in reactions of ambident nucleophiles in which the expected outcome (based on HSAB theory) does match the experimental outcome (see section 1.3). In the present work, the applicability of the Marcus Theory rationale for ambident reactivity (from the work of Mayr and co-workers, as outlined in section 1.4.1) is tested through examination of the reactions of ambident nucleophiles. Additionally, this study will simultaneously probe the deficiencies that are reported to arise when applying the HSAB principle to rationalise ambident reactivity, as is commonly seen throughout the literature (see section 1.2.4). As the applicability of this widely used rationale has come into question, it now behoves physical and synthetic organic chemists to test this Marcus theory-based rationale and other alternatives on their capacity to account for the experimentally observed outcomes of reactions of ambident reactants.

The test substrates chosen for this analysis were diazine *N*-oxides (see Chart 2-1 below), which contain competing N and O nucleophilic sites. Numerous literature examples demonstrate the issues associated with reactions of these nucleophiles which arise from their ambident nature.[2–8]

Chart 2-1. Representative diazine *N*-oxides of the type used in this study. These ambident nucleophiles were using in reactions with representative "hard" and "soft" electrophiles.



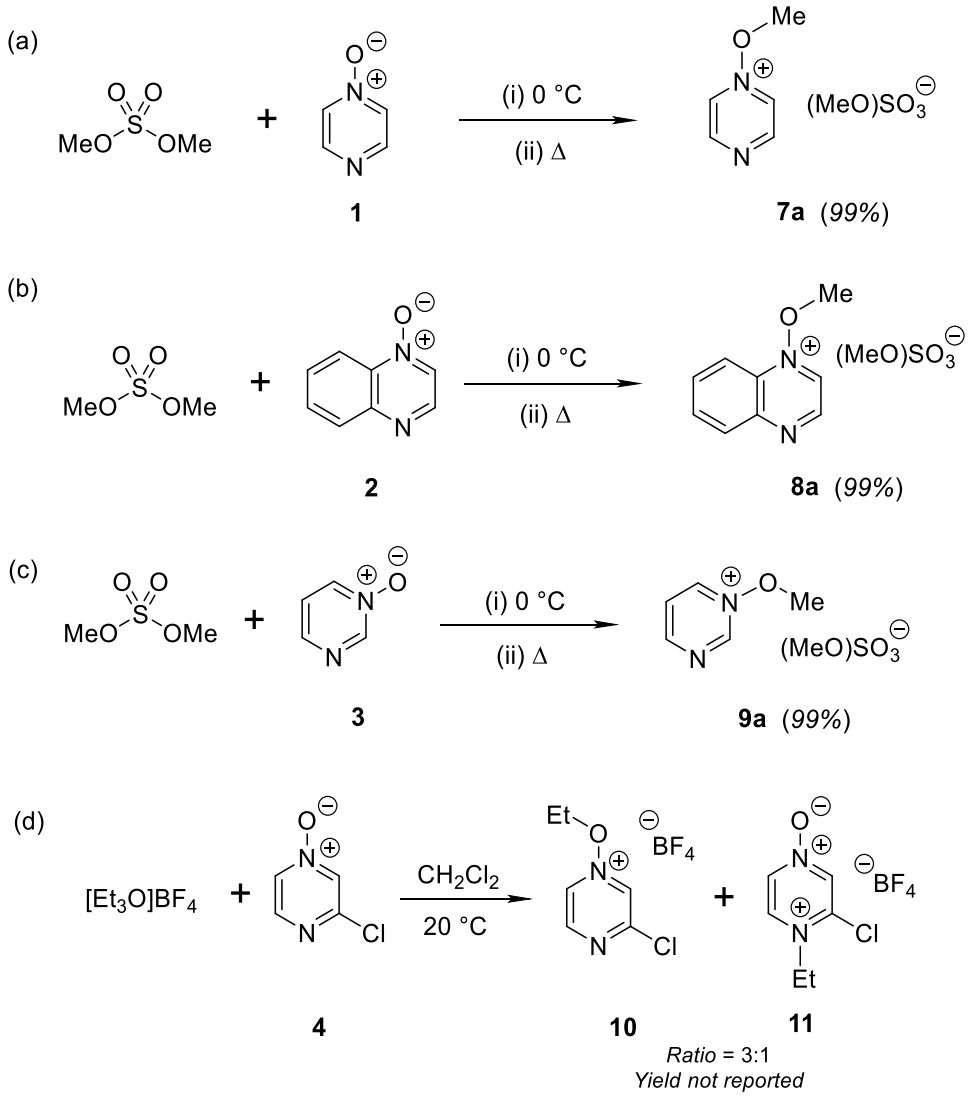
1 **2** **3** **4** **5** **6**

The compounds **1**, **2**, and **3** were chosen as the substrates for reactions with various representative hard and soft electrophiles because, although these reactions show very high site-selectivity (i.e., for N- or O-alkylation), their outcomes are intractable to rationalisation using the HSAB principle, as will be discussed in section 2.3. An additional contributing factor that confounds any attempt to analyse the reactions of these species using the HSAB rationale is that it is not possible to unambiguously identify which nucleophilic site of a diazine *N*-oxide is the hard site, and which is the soft site (see section 2.3.2).[9,10] Compounds **1** – **3** are particularly suitable for this investigation as unlike the reactions of many other ambident nucleophiles containing N and O nucleophilic sites,[6,11–15] reactions of **1** – **3** are not influenced by the presence of a counter-cation, thereby eliminating the need to consider that factor as an influence on the selectivity

observed in a reaction. Additionally, their alkylation products do not undergo secondary reactions (unlike, for example, reactions of amides)[16,17] which may complicate the analysis of the results.

There exist several literature precedents of relevance to the ambident nucleophilicity of diazine *N*-oxides, some of which are illustrated below in Scheme 2-1. Exclusive O-alkylation has been reported to occur in reactions of pyrazine *N*-oxide (**1**), quinoxaline *N*-oxide (**2**) and pyrimidine *N*-oxide (**3**) with "hard" alkylating agent dimethylsulfate ($(Me_2O)_2SO_2$) in a paper by Herzon and co-workers (see Scheme 2-1(a) – (c)).[18] Predominant O-alkylation of the compound **4** was also reported to occur in a reaction with the "hard" electrophile $[Et_3O]BF_4$ in CH_2Cl_2 by Cmoch (see Scheme 2-1(d)).[7]

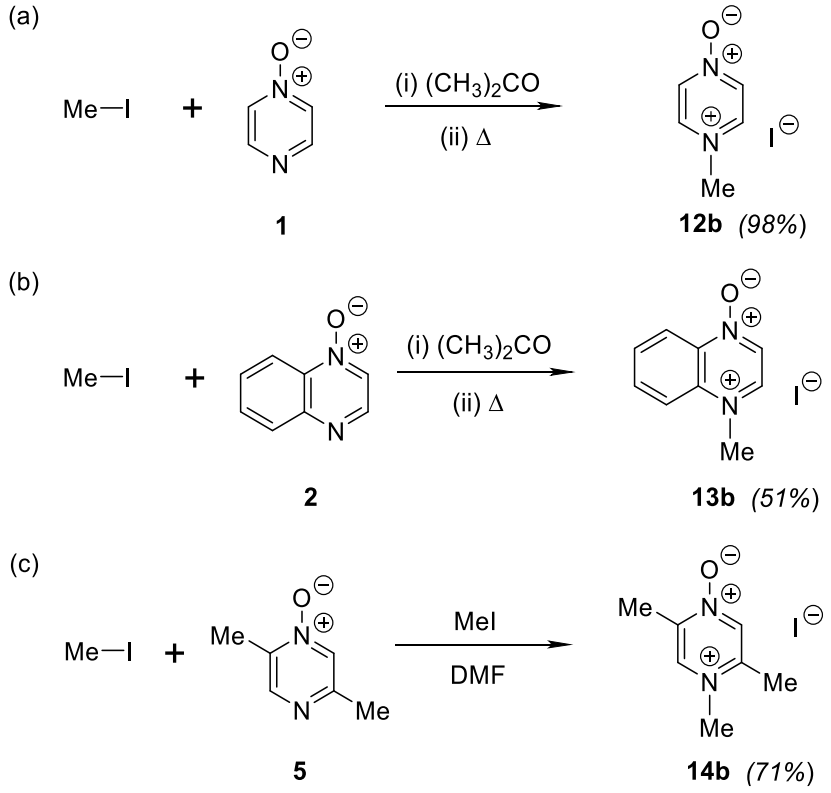
Scheme 2-1. (a), **(b)**, **(c)**, **(d)** Reactions of the diazine *N*-oxides **1** – **4** give predominantly O-alkylation products in reactions with the "hard" alkylating agents $(Me_2O)_2SO_2$ and $[Et_3O]BF_4$.[7,18]



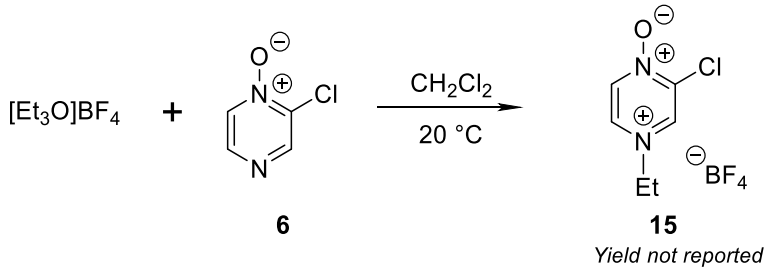
Reactions of compounds **1**, **2** and **5** with the "soft" methylating agent MeI in various solvents (see Scheme 2-2(a) – (c) below) have been reported to give N-methylation

products.[2,3,19] However, a reaction between **6** and the "hard" electrophile $[Et_3O]BF_4$ is reported to give N-ethylation product (**15**) exclusively in CH_2Cl_2 (see Scheme 2-3).[7] This result is in stark contrast with the previous observation that a reaction between compound **4** and $[Et_3O]BF_4$ results in predominant O-alkylation (compare Scheme 2-1(d) with Scheme 2-3. Notwithstanding the ambiguity inherent in assigning the "hard" and "soft" nucleophilic sites in these diazine *N*-oxides, it is apparent that these results cannot all simultaneously be consistent with the HSAB principle.

Scheme 2-2. (a), **(b)**, **(c)** Reactions of the diazine *N*-oxides **1, 2** and **5** give N-alkylation adducts predominantly in reactions with the "soft" alkylating agent MeI.



Scheme 2-3. A reaction of **6** with $[Et_3O]BF_4$ resulted in exclusive N-ethylation, in contrast with what was previously observed in the reaction illustrated in Scheme 2-1(d).



An additional fundamental difficulty exists in the examination of reactions of diazine *N*-oxides: the act of establishing the structure of the product is itself fraught with ambiguity. Consider the alkylation products seen above in Scheme 2-3. The spectral features of the

product of O-alkylation and that of N-alkylation of a particular diazine *N*-oxide are not necessarily readily distinguishable. Most instances in the literature in which product structures have been assigned have been based on the results of chemical derivatisations,[2,3,19] prior to the development of modern spectroscopic methods.

The goal of this study was to establish the N vs. O ratio(s) for the alkylation reactions of **1** – **3** using various representative "hard" and "soft" alkylating agents and use these data to determine conclusively whether "hard/soft" interactions dictate the observed selectivity in the reactions of diazine *N*-oxides. This would enable the subsequent goal of analysing the results using the Marcus theory-based approach proposed by Mayr and co-workers.[1] However, as was described above, difficulty exists in unambiguously identifying and distinguishing the products of a reaction of diazine *N*-oxides using ^{1}H or ^{13}C NMR spectroscopic analysis. In order to unambiguously identify the products of the alkylation reactions of **1** – **3**, a spectroscopic method was developed which would allow unambiguous identification of the site of alkylation in the products of reactions of diazine *N*-oxides.

2.2. Spectroscopic Investigations – Reference δ_N Values

In the course of preliminary studies on the reactions of diazine *N*-oxides, it was established in several cases that standard ^{1}H, ^{13}C and two-dimensional NMR correlation spectra did not allow unambiguous establishment of which Lewis basic site of a given compound had undergone reaction with an alkylating agent. In order to circumvent this problem, alternative means of characterising these compounds spectroscopically were sought. As each of the diazine *N*-oxides of interest (**1** – **3**) contain Lewis basic nitrogen atoms, modern nitrogen NMR spectroscopic techniques were exploited to accomplish this.

To this end, the indirect detection technique of ^{1}H-^{15}N HMBC NMR spectroscopy at natural ^{15}N abundance[20–27] was employed to identify the products of the reactions of compounds **1** – **3** with various electrophiles. This technique exploited the sensitivity of measurement of ^{1}H NMR signals to circumvent the difficulties that are commonly associated with direct detection of ^{15}N NMR resonances. Coupled with cryoprobe technology, this enabled measurement of ^{15}N NMR chemical shifts with relatively short acquisition times (20–30 minutes), and without any requirement for costly ^{15}N-enrichment of analytes. Despite the obvious practicality and utility associated with this method, the problem remained regarding the unambiguous identification of the products of the reactions of the ambident nucleophiles **1** – **3** with various electrophiles. Previous studies have been carried out to establish the manner in which aromatic ^{15}N NMR signals are altered upon N-protonation[20–23,28] and the alterations that occur when aromatic nitrogen atoms co-ordinate to metals.[20–23,29–33] However, data in the literature indicating how aromatic nitrogen NMR signals change upon N-alkylation of azines and diazines or O-alkylation of aromatic *N*-oxides is less readily available. In several instances in publications containing one or more examples of aromatic N-alkylation, statements are made to the effect that N-alkylation of aromatic nitrogen atoms result in large upfield shifts of the δ_N value of the alkylated nitrogen (of the order of 100 ppm).[7,34–38] However, frequently in these instances, no references to other relevant publications were cited, and in some others no experimental data was reported.[35,36] As a result, nitrogen NMR spectral data on aromatic N-heterocycle alkylation reactions is scattered throughout the literature, essentially unconnected in any systematic way to the other relevant pieces of data. Consequently, although important results relating to nitrogen NMR spectroscopic analysis of N-alkylation of aromatic N-heterocycles have been reported in several studies,[28,37–40] the existence of a systematic trend in how δ_N values change upon N-alkylation of diazine *N*-oxides, or any other aromatic heterocycle (which would be of use in a diagnostic sense) has not been definitively established. Furthermore, only two examples exist indicating the effect on δ_N of O-alkylation of *N*-oxides or diazine *N*-oxides.[7,41] As a result, there exists no definitive method of diagnosing the occurrence of N-alkylation of aromatic N-heterocycles or the occurrence of O-alkylation of aromatic *N*-oxides using nitrogen NMR spectroscopy alone.

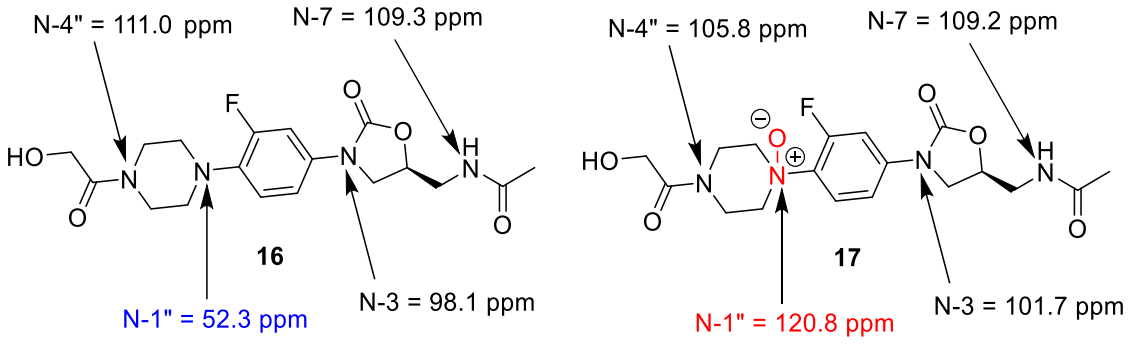
Prompted by this lack of understanding of the effect of N-alkylation of azines and diazines or O-alkylation of aromatic *N*-oxides on the observed ^{15}N NMR shifts, the following goals were set out:

(i) To establish δ_N values for representative aromatic N-heterocycles and *N*-oxides and N- or O-alkylation products derived from these that had not previously been characterised in order to widen the scope of available data, and to hence establish diagnostic changes in δ_N values (i.e., $\Delta(\delta_N)$ values) for these alkylation reactions.

(ii) To gather existing relevant data from the literature and combine it with experimental data in order to establish a systematic basis for understanding the manner in which ^{15}N NMR chemical shifts change during the course of alkylation reactions of N-containing aromatic heterocycles.

As a result of the investigations described in detail below, $\Delta(\delta_N)$ values that are characteristic of N-alkylation reactions of aromatic N-heterocycles and of O-alkylation of aromatic *N*-oxides were established. In tandem with multiple-bond correlation data from two-dimensional NMR spectra (^{1}H-^{15}N HMBC and ^{1}H-^{13}C HMBC NMR spectra) and certain ^{13}C{^{1}H} NMR spectroscopic data, the $\Delta(\delta_N)$ data provided a basis on which to unambiguously diagnose the occurrence of N-alkylation of aromatic N-heterocycles, or O-alkylation of aromatic *N*-oxides. It also enabled distinction between products of N-alkylation and O-alkylation in instances where ambiguity exists, such as in reactions of the ambident nucleophiles **1** – **3**. Long range ^{1}H-^{15}N NMR correlation techniques have been exploited in previous analogous studies to establish the sites of *N*-oxidation of various compounds containing multiple nitrogen environments.[42–44] An example of how this was achieved in the work of Martin and co-workers is seen below in Scheme 2-4.[42]

Scheme 2-4. The site of *N*-oxidation in eperezolid (**16**) was determined unambiguously by observing a systematic large downfield shift of nitrogen resonance values which occurs following oxidation. This method was developed using two-dimensional ^{1}H and ^{15}N NMR spectroscopic techniques. By measuring the ^{15}N NMR signals of **16** and **17** (after the compound has undergone *N*-oxidation), the position which has been oxidised was identified by the significant downfield shift (+68.5 ppm) of the signal associated with that position.



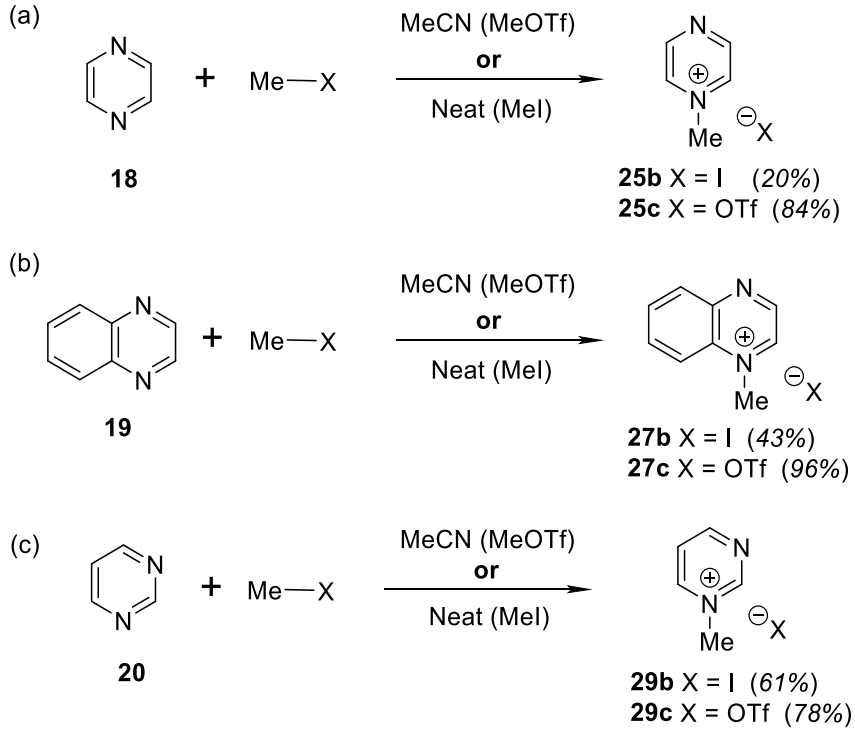
2.2.1. Reactions of Diazines and Pyridine *N*-Oxides to Obtain Reference δ_N Values

To achieve the goals specified above, diazines **18** – **20** and pyridine *N*-oxides **21** – **24** were selected as test substrates for this study (see Schemes 2-5 and 2-6 for the structures of these compounds). These specific compounds were selected on the basis that they should each undergo alkylation reactions with no ambiguity over the site of attachment of the alkyl group in the product. That is, compounds **18** – **20** undergo N-alkylation specifically, while compounds **21** – **23** undergo O-alkylation.

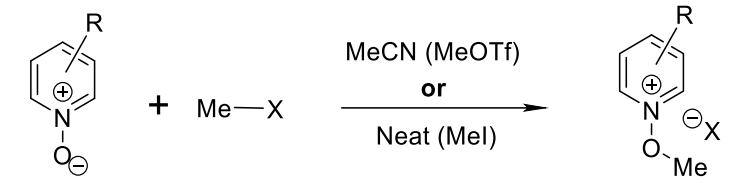
The ^{15}N NMR chemical shifts (δ_N values) of starting compounds **18** – **23** were recorded, as were δ_N values for alkylation adducts derived from **18** – **23**. The compounds were alkylated with MeI, MeOTf and a benzhydryl triflate (**24**, see Scheme 2-7 below for the exact structure of this compound). In each case, the ^{15}N NMR chemical shift values were referenced to liquid ammonia at 0 ppm (equivalent to referencing to nitromethane at 380.2 ppm) as per the convention specified in the work of Willams and Martin.[20]

The alkylation reactions that were conducted are shown below in Schemes 2-5, 2-6 and 2-7, yielding N-alkylation adducts **25** – **30**, and O-alkylation adducts **31** – **35**. The exact details for each of the individual experiments are available in section 3.5 of Chapter 3.

Scheme 2-5. (a), **(b)**, **(c)** MeOTf and MeI were used as methylating agents to effect N-methylation of diazines **18** – **20**. The counter-ion (X^-) for each product is I or OTf throughout. The yields of each reaction are shown in parentheses.



Scheme 2-6. O-methylation of pyridine *N*-oxides **21** – **23**. The counter-ion (X^-) for each product is I or OTf throughout. The yields of each reaction are shown in parentheses.

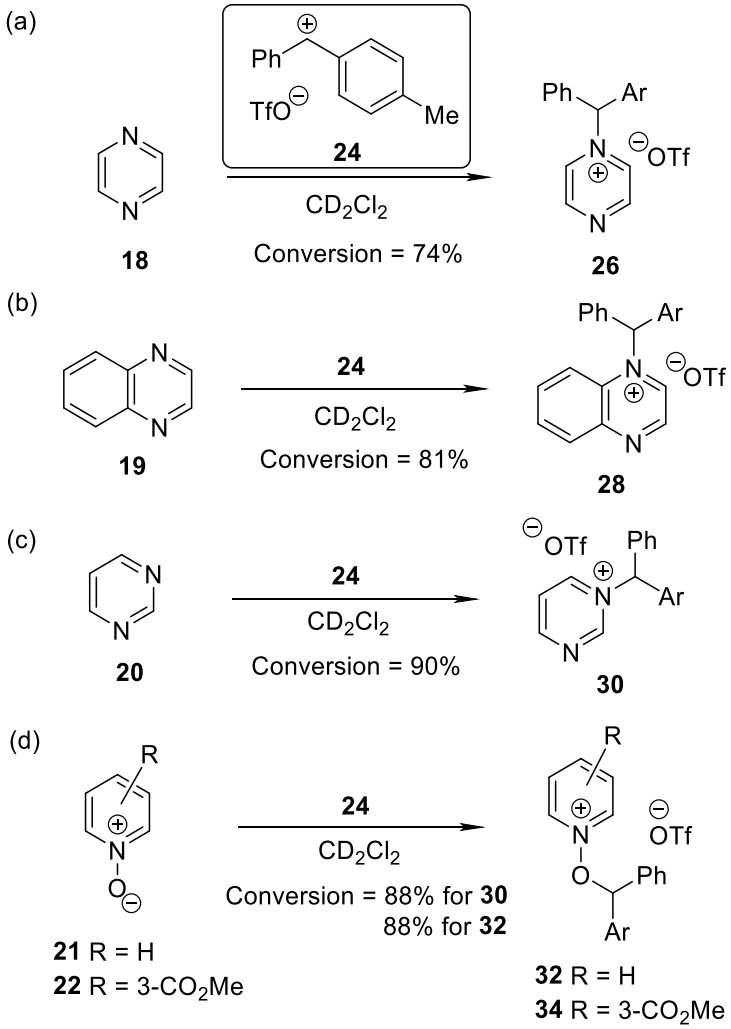


21 R = H
22 R = 3-CO_2Me
23 R = 4-Me

31b R = H, X = I (*59%*),
31c R = H, X = OTf (*78%*)
33 R = 3-CO_2Me, X = OTf (*40%*)
35c R = 4-Me, X = OTf (*84%*) [a]

[a] The reaction which gave the isolated yield of compound **35c** was carried out in $CDCl_3$ solvent. A high level of conversion was seen in the corresponding reaction in MeCN.

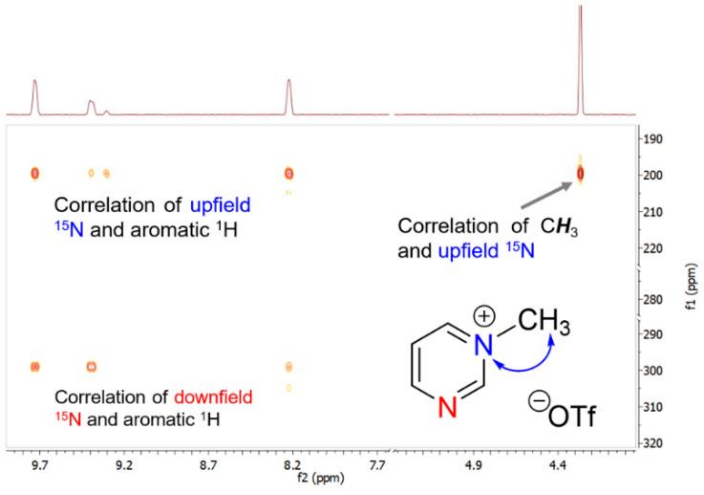
Scheme 2-7. (a), (b), (c), (d) The N- and O-alkylations of the nitrogen heterocycles **18** – **22** were achieved using the benzhydryl triflate **24**, which was generated in solution from the parent benzhydryl chloride and AgOTf. In the structure of each of the products, Ar = *p*-tolyl. As each of the products (**26**, **28**, **30**, **32** and **34**) were hydrolytically unstable, the conversions listed in the scheme were determined from ^{1}H NMR spectra.



As all of the products in Schemes 2-5, 2-6 and 2-7 are hygroscopic and/or hydrolytically unstable, the reactions were conducted under an inert atmosphere of nitrogen gas using Schlenk glassware. The exact details of how this was achieved are described in section 3.1. In the reactions in Scheme 2-7 (employing the benzhydrylium ion **24**), none of the benzhydrylium ions remain in the reaction mixture at the conclusion of the experiment. Compound **24** (and other benzhydrylium ions) are hydrolytically unstable. As such, benzhydrylium ions that do not form N- and O-alkylation adducts are accounted for by benzhydrylium hydrolysis products (such as (bis)benzhydryl) ether and benzhydrol). The hydrolytically unstable benzhydryl adducts (**26**, **28**, **30**, **32** and **34** in Scheme 2-7 above) were not isolated, and instead were characterised by transferring the reaction mixtures directly into an NMR tube under inert atmosphere conditions. The conversions for each of the reactions (a) – (d) in Scheme 2-7 were calculated using the integrations of the signals found in the ^{1}H NMR spectra of these reaction mixtures.

Moisture-stable compounds were isolated – in some instances this was achieved by carrying out separate reactions on larger scale than that used for the ^{1}H-^{15}N HMBC NMR characterisation experiments (details may be found in sections 3.5 and 3.6). Low conversions and yields were observed in some reactions of neat MeI due to the weak Lewis basicities of some of the diazines or *N*-oxides employed. This is perhaps to be expected, considering that the methylation of pyridine *N*-oxide (**21**) by MeI, for example, has been shown to be reversible in MeCN in a paper by Andreev.[45] The δ_N values for each of the N- and O-alkylation adducts (**25** – **35**) and the heterocyclic starting materials (**18** – **23**) were then recorded using ^{1}H-^{15}N HMBC NMR spectroscopy. An example of how δ_N values were extracted from the ^{1}H-^{15}N HMBC NMR spectra is seen below in Figure 2-1.

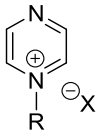
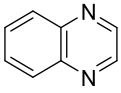
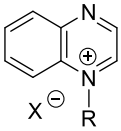
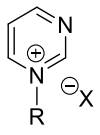
Figure 2-1. ^{1}H-^{15}N HMBC NMR spectrum of **29c** showing the correlation of the N-methyl signal with the upfield ^{15}N signal, enabling the differentiation of the two ^{15}N signals.



Shown in Tables 2-1 and 2-2 below are the δ_N values recorded for starting materials **18** – **23** and for derived N-alkylation adducts **25** – **30** and O-alkylation adducts **31** – **35**. Also shown in Tables 2-1 and 2-2, in the column furthest to the right, are the $\Delta(\delta_N)$ values associated with each of the alkylation reactions. These $\Delta(\delta_N)$ values show the extent to which the chemical shift of a ^{15}N nucleus changes relative to the δ_N value of the starting

material (diazine or pyridine *N*-oxide) upon occurrence of an alkylation reaction. If the δ_N value of an alkylation product is upfield of the δ_N value of the corresponding ^{15}N NMR environment in the starting material, this is represented as a negative value of $\Delta(\delta_N)$. Conversely, a positive value of $\Delta(\delta_N)$ indicate that the chemical shift of the ^{15}N environment in question has moved downfield relative to the corresponding environment in the starting material upon alkylation.

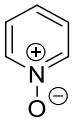
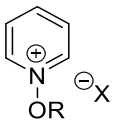
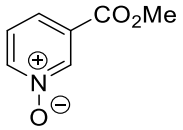
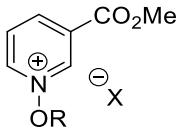
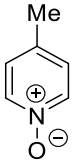
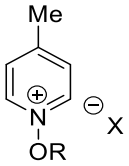
Table 2-1. ^{15}N NMR chemical shift (δ_N) values of starting compounds **18** – **20** and their derived N-alkylation products **25** – **30**, and $\Delta(\delta_N)$ values (change in ^{15}N NMR chemical shift) between starting compounds and products upon N-alkylation. The δ_N values are referenced to liquid ammonia at 0 ppm (equivalent to referencing to nitromethane at 380.2 ppm). Throughout, Ar = *para*-tolyl group.

	#	Compound	R	X	δ_N of compound (ppm) and NMR Solvent		$\Delta(\delta_N)$ (ppm) [a]
	(i)	**18**	–	–	$(CH_3)_2SO$	333.8 [b]	–
	(ii)	**18**	–	–	CH_2Cl_2	333.0	–
	(iii)	**25b**	Me	I	$(CH_3)_2SO$	357.6	+23.8
						221.0	**−112.8**
	(iv)	**25c**	Me	OTf	$(CH_3)_2SO$	357.4	+23.6
						220.7	**−113.1**
25b R = Me, X = I **25c** R = Me, X = OTf **26** R = PhArCH, X = OTf	(v)	**26**	$PhArCH^+$	OTf	CD_2Cl_2	364.4	+31.4
						240.6	**−92.4**
	(vi)	**19**	–	–	$(CD_3)_2SO$	329.9 [b]	–
	(vii)	**19**	–	–	CH_2Cl_2	329.0	–
	(viii)	**27b**	Me	I	$(CH_3)_2SO$	355.5	+25.6
						208.6	**−121.3**
	(ix)	**27c**	Me	OTf	$(CH_3)_2SO$	356.6	+26.7
						208.7	**−121.2**
27b R = Me, X = I **27c** R = Me, X = OTf **28** R = PhArCH, X = OTf	(x)	**28**	$PhArCH^+$	OTf	CD_2Cl_2	363.7	+34.7
						225.3	**−103.7**
	(xi)	**20**	–	–	$(CH_3)_2SO$	295.3 [b]	–
	(xii)	**20**	–	–	CH_2Cl_2	294.4	–
	(xiii)	**29b**	Me	I	$(CH_3)_2SO$	298.7	+3.4
						199.5	**−95.8**
	(xiv)	**29c**	Me	OTf	$(CH_3)_2SO$	299.9	+4.6
						199.4	**−95.9**
29b R = Me, X = I **29c** R = Me, X = OTf **30** R = PhArCH, X = OTf	(xv)	**30**	$PhArCH^+$	OTf	CH_2Cl_2	298.8	+4.4
						218.6	**−75.8**

[a] $\Delta(\delta_N)$ is the change in the δ_N value of the nitrogen atom of the alkylated compound compared to the δ_N value of that nitrogen in the parent compound. The δ_N and $\Delta(\delta_N)$ values associated with the alkylated nitrogen are highlighted in bold in the table in products containing more than one nitrogen NMR environment.

[b] This δ_N value (in $(CD_3)_2SO$ solvent) is reported in the work of Schweng and co-workers.[46]

Table 2-2. ^{15}N NMR chemical shift (δ_N) values of starting compounds **21** – **23** and their derived O-alkylation products **31** – **35**, and $\Delta(\delta_N)$ values (change in ^{15}N chemical shift) between starting compounds and products upon O-alkylation. The δ_N values are referenced to liquid ammonia at 0 ppm (equivalent to referencing to nitromethane at 380.2 ppm). Throughout, Ar = *para*-tolyl group.

	#	Compound	R	X	δ_N of compound (ppm) and NMR Solvent		$\Delta(\delta_N)$ (ppm) [a]
	(i)	**21**	–	–	$(CH_3)_2SO$	295.1 [b]	–
	(ii)	**21**	–	–	CH_2Cl_2	294.0 [b]	–
	(iii)	**31b**	Me	I	$(CH_3)_2SO$	256.8	−38.3
	(iv)	**31c**	Me	OTf	$(CH_3)_2SO$	252.4	−42.7
31b R = Me, X = I **31c** R = Me, X = OTf **32** R = PhArCH, X = OTf	(v)	**31c**	Me	OTf	CH_2Cl_2	251.0	−43.0
	(vi)	**32**	$PhArCH^+$	OTf	CD_2Cl_2	246.0	−48.0
	(vii)	**22**	–	–	$(CD_3)_2SO$	293.2 [c]	–
	(viii)	**22**	–	–	CH_2Cl_2	– [d]	–
	(ix)	**33**	Me	OTf	$(CD_3)_2SO$	247.3	−40.8
33 R = Me, X = OTf **34** R = PhArCH, X = OTf	(x)	**34**	$PhArCH^+$	OTf	CD_2Cl_2	248.3	– [d]
	(xi)	**23**	–	–	$(CD_3)_2SO$	284.3 [e]	–
	(xii)	**35c**	Me	OTf	$(CD_3)_2SO$	247.3	−37.0
35c R = Me, X = OTf							

[a] $\Delta(\delta_N)$ is the change in the δ_N value of the nitrogen atom of the alkylated compound compared to the δ_N value of that nitrogen in the parent compound. The δ_N and $\Delta(\delta_N)$ values associated with the alkylated nitrogen are highlighted in bold in the table in products containing more than one nitrogen NMR environment.

[b] ^{14}N NMR chemical shift values of 85.64 ppm (in $(CH_3)_2SO$) and 85.66 ppm (in CH_2Cl_2), referenced to nitromethane at 0 ppm, were reported by Webb and co-workers.[47] These literature δ_N values equate to 294.6 and 294.5 ppm, respectively, when re-referenced to ammonia at 0 ppm.

[c] The δ_N value given for compound **22** is extracted from a ^1H-^{15}N HMBC NMR spectrum of a reaction of the compound. A comparable value may be seen in the paper of Tsuno and co-workers.[48]

[d] No reference δ_N value for starting compound **22** was obtained in CH_2Cl_2.

[e] A similar δ_N value (285.2 ppm, relative to nitromethane at 380.2 ppm) was determined in $CDCl_3$ solvent in the work of Sanz *et al.*[49]

In Table 2-1, in each instance in which the starting material and/or product contains more than one nitrogen NMR environment (entries (i) – (xv)), the ^{15}N NMR chemical shift of the nitrogen atom of the starting material that undergoes alkylation and that of the alkylated nitrogen atom of the product are highlighted in bold. The $\Delta(\delta_N)$ value associated with the N-alkylation process is also highlighted in each of these instances. In Table 2-2, each of the pyridine *N*-oxides employed (**21** – **23**) contain only one nitrogen environment, and hence there is no potential for ambiguity in instances involving these compounds.

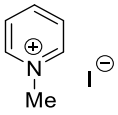
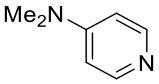
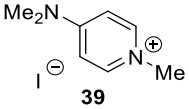
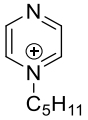
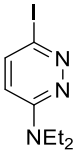
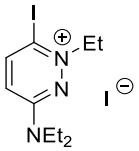
The ^{1}H-^{15}N HMBC NMR spectra of compounds **25** – **30** (N-alkylation adducts of compounds **18** – **20**) indicate that there is a systematic shift upfield of the δ_N value of the alkylated nitrogen environment relative to the δ_N value of the corresponding nitrogen nucleus in the starting material (i.e., the $\Delta(\delta_N)$ value is *negative* – see Table 2-1 entries (i) – (xv)). This is to be expected, as an identical effect (i.e., the upfield shift of the δ_N value of an alkylated nitrogen environment) was previously reported in work by Costisella *et al*.[35] That the upfield signal in each case belongs to the alkylated nitrogen is shown by the existence of a correlation in the ^{1}H-^{15}N HMBC NMR spectrum of the product between the upfield ^{15}N signal and the proton(s) of the methyl or benzhydryl groups (i.e., C*H*Ar$_2$ in the case of a benzhydryl group). The δ_N values of the non-alkylated nitrogen signals move downfield relative to the corresponding δ_N values in the starting materials. The ^{1}H-^{15}N HMBC NMR spectrum of **29c** is shown in Figure 2-1 (a) as an example – in this image, the spectral features described above are clearly visible.

The ^{1}H-^{15}N HMBC NMR spectra of compounds **31** – **35** (O-alkylation adducts) also indicate that there is a systematic shift upfield of the δ_N value of the alkoxypyridinium nitrogen of these compounds relative to the δ_N value of the starting material *N*-oxide nitrogen (see Table 2-2 entries (i)–(xii)). A three-bond coupling interaction is shown to exist for each of these compounds between the alkoxypyridinium nitrogen and the methyl group C*H*$_3$ protons or benzhydryl C*H* proton by correlations in the ^{1}H-^{15}N HMBC NMR spectra of the compounds. Details regarding these coupling interactions may be found alongside the experimental details in section 3.5. The data presented in Tables 2-1 and 2-2 demonstrate that the upfield $\Delta(\delta_N)$ values associated with the alkylated nitrogen atom in N-alkylation reactions are systematically larger than the $\Delta(\delta_N)$ values associated with O-alkylations (e.g., compare Table 2-1 entry (iii) and Table 2-2 (iii) for methylation reactions, and Table 2-2 entry (v) and (vi) for benzhydrylations). This will be discussed further below, after contextualising these results with relevant data found in the literature.

2.2.2. Investigation of Literature Trends in the δ_N Values of N- and O-alkylated Heterocycles

More examples and relevant data were sought in order to strengthen the hypothesis that the trends in the $\Delta(\delta_N)$ values observed in Tables 2-1 and 2-2 were useful in diagnosing the occurrence of N- or O-alkylation in the reaction of nitrogen-containing heterocycles such as azines, diazines and diazine *N*-oxides. A comprehensive literature search was undertaken for examples of these heterocyclic compounds for which nitrogen NMR data of the starting materials and N- and O-alkylated adducts was available. The relevant data which was found is recorded below in Tables 2-3, 2-4 and 2-5.

Table 2-3. Nitrogen (^{14}N or ^{15}N) NMR chemical shift (δ_N) values of starting compounds and derived alkylation products from literature reports, and $\Delta(\delta_N)$ values (change in ^{15}N NMR chemical shift) between starting compounds and products upon N-alkylation. [a] The δ_N values are referenced to liquid ammonia at 0 ppm (equivalent to referencing to nitromethane at 380.2 ppm), and hence in some instances have been re-calculated from the literature values, which are referenced relative to a different standard.

#	Starting Compound	Solvent	δ_N (ppm)	Product	Solvent	δ_N (ppm)	$\Delta(\delta_N)$ (ppm) [a]
(i)	 **36**	$(CH_3)_2SO$	316.2 [b]	 **37b**	$(CH_3)_2SO$	200.3 [c]	−115.9
(ii)	 **38**	$MeNO_2$	**Ring N 275.5** [d]	 **39**	$MeNO_2$	**Ring N 157.9** [d]	−117.6
(iii)	 **18**	H_2O	321.2 [e]	 **40**	D_2O	351.9 [f] **231.4** [f]	+30.7 **−89.8**
(iv)	 **41**	$(CD_3)_2SO$	**403.3** [g] 353.2 [g] 91.9 [g]	 **42**	$(CD_3)_2SO$	**258.0** [g] 300.5 [g] 105.3 [g]	**−145.3** −52.7 +13.4

[a] $\Delta(\delta_N)$ is the change in the δ_N value of the nitrogen atom of the alkylated compound compared to the δ_N value of that nitrogen in the parent compound. The δ_N and $\Delta(\delta_N)$ values associated with the alkylated nitrogen are highlighted in bold in the table in products containing more than one nitrogen NMR environment.

[b] The δ_N value originally reported in the work of Haslinger *et al.*, referenced relative to nitromethane at 0 ppm, was reported as −64.0 ppm.[28] A δ_N value of −63.0 ppm (relative to nitromethane at 0 ppm) has also been reported for this compound in $(CH_3)_2SO$ by Städeli and von Phillipsborn.[50] δ_N values of 275.2 ppm and −57.6 ppm have also been reported for this compound in $(CH_3)_2SO$ relative to external 2 mol L^{-1} $(Me_4{}^{15}N)Cl$ and external 1 mol L^{-1} HNO_3 in D_2O (enriched in ^{15}N), respectively, by Yavari and Roberts.[51] A δ_N value of −62.7 ppm (^{14}N NMR spectroscopy; relative to nitromethane at 0 ppm) has also been reported for this compound in nitromethane by Costisella *et al.*[35]

[c] The δ_N value originally reported in the work of Haslinger *et al.*, referenced relative to nitromethane at 0 ppm, was reported as −179.9 ppm.[28] δ_N values of 159.1 ppm and −173.7 ppm have also been reported for this compound in DMSO relative to external 2 mol L^{-1} $(Me_4{}^{15}N)Cl$ and external 1 mol L^{-1} HNO_3 in D_2O (enriched in ^{15}N), respectively, by Yavari and Roberts.[51] A δ_N value of −179.2 ppm (^{14}N NMR spectroscopy; relative to nitromethane at 0 ppm) has also been reported for this compound in nitromethane by Costisella *et al.*[35]

[d] The δ_N values of these compounds were originally reported in the work of Costisella *et al.*, referenced relative to nitromethane at 0 ppm.[35] The value associated with the starting compound was reported as −104.7 ppm, and the value associated with the product was reported as −222.3 ppm.

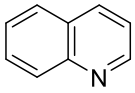
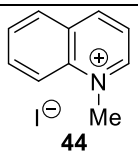
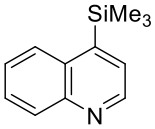
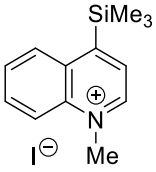
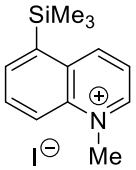
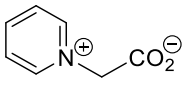
[e] The δ_N value originally reported in the work of Witanowski *et al.*, referenced relative to nitromethane at 0 ppm, was reported as 59.02 ppm.[52]

[f] The δ_N value shown was reported in the work of Kolman *et al.*[53] No information was given on the referencing of the ^{15}N NMR spectrum. Note: The identity of the counter-cation of the pyrazinium ion was not specified.

[g] The δ_N value shown was reported in the work of Katrizky and Dega-Szafran, referenced relative to ammonia at 0 ppm.[54]

Regarding Table 2-3 entry (i), it is worth noting that very similar values of $\Delta(\delta_N)$ (−116.1 ppm in $(CH_3)_2SO$ solvent, −116.5 ppm in $MeNO_2$) can be derived from the data reported by Yavari and Roberts,[51] and Costisella *et al.*, respectively.[35]

Table 2-4. Nitrogen (^{14}N or ^{15}N) NMR chemical shift (δ_N) values of starting compounds and derived alkylation products from literature reports, and $\Delta(\delta_N)$ values (change in ^{15}N NMR chemical shift) between starting compounds and products upon N-alkylation. [a] The δ_N values are referenced to liquid ammonia at 0 ppm (equivalent to referencing to nitromethane at 380.2 ppm), and hence in some instances have been re-calculated from the literature values, which are referenced relative to a different standard.

#	Starting Compound	Solvent	δ_N (ppm)	Product	Solvent	δ_N (ppm)	$\Delta(\delta_N)$ (ppm) [a]
(i)	 **43**	$CDCl_3$	309.1 [b]	 **44**	$(CD_3)_2SO$	188.6 [c]	−120.5
(ii)	 **45**	$CDCl_3$	313.2 [b]	 **46**	$(CD_3)_2SO$	188.8 [c]	−124.4
(iii)	 **47**	$CDCl_3$	310.0 [b]	 **48**	$(CD_3)_2SO$	190.0 [c]	−120.0
(iv)	 **36**	$(CH_3)_2SO$	316.2 [d]	 **49**	$(CD_3)_2SO$	207.3 [e]	−108.9

[a] $\Delta(\delta_N)$ is the change in the δ_N value of the nitrogen atom of the alkylated compound compared to the δ_N value of that nitrogen in the parent compound.

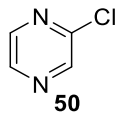
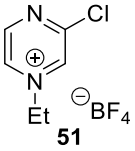
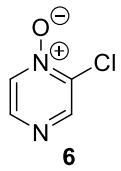
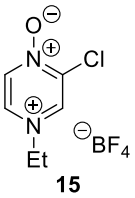
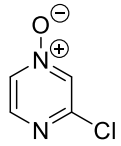
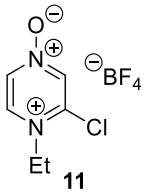
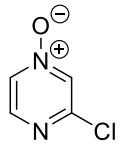
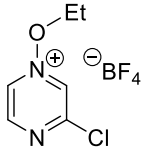
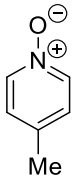
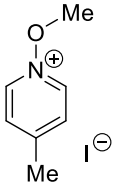
[b] The δ_N values of the quinolines in entries (i) – (iii) originally reported in the work of Lukevics *et al.*,[34] referenced relative to nitromethane at 0 ppm, were reported as −71.1, −67.0 and −70.2 ppm, respectively. Data regarding additional quinolines which follow the trends observed in this Table may also be found in this paper.

[c] The δ_N values of the *N*-methylquinolinium salts in entries (i) – (vii) originally reported in the work of Lukevics *et al.*,[34] referenced relative to nitromethane at 0 ppm, were reported as −191.6, −191.4 and −190.2 ppm, respectively. Data regarding additional *N*-methylquinolinium salts which follow the trends observed in this Table may also be found in this paper.

[d] The δ_N value originally reported in the work of Haslinger *et al.*, referenced relative to nitromethane at 0 ppm, was reported as −64.0 ppm.[28] A δ_N value of −63.0 ppm (relative to nitromethane at 0 ppm) has also been reported for this compound in $(CH_3)_2SO$ by Städeli and von Phillipsborn.[50]

[e] The δ_N value (^{14}N NMR spectroscopy) originally reported in in the work of Szafran *et al.*, referenced relative to nitromethane at 0 ppm, was reported as −172.9 ppm (at 0.1 mol L^{-1} concentration; a slight concentration dependence of δ_N is reported).[55]

Table 2-5. Nitrogen (^{14}N or ^{15}N) NMR chemical shift (δ_N) values of starting compounds and derived alkylation products from literature reports, and $\Delta(\delta_N)$ values (change in ^{15}N NMR chemical shift) between starting compounds and products upon N-alkylation.[a] The δ_N values are referenced to liquid ammonia at 0 ppm (equivalent to referencing to nitromethane at 380.2 ppm), and hence in some instances have been re-calculated from the literature values, which are referenced relative to a different standard.

#	Starting Compound	Solvent	δ_N (ppm)	Product	Solvent	δ_N (ppm)	$\Delta(\delta_N)$ (ppm) [a]
(i)	 **50**	$(CD_3)_2CO$	324.7 [b] **344.5** [b]	 **51**	$(CD_3)_2CO$	345.0 [c] **238.5** [c]	+20.3 **−106.0**
(ii)	 **6**	$(CD_3)_2CO$	305.6 [b] **307.4** [b]	 **15**	$(CD_3)_2CO$	316.7 [c] **201.2** [c]	+11.1 **−106.2**
(iii)	 **4**	$(CD_3)_2CO$	314.4 [b] **295.1** [b]	 **11**	$(CD_3)_2CO$	326.3 [c] **199.1** [c]	+11.9 **−96.0**
(iv)	 **4**	$(CD_3)_2CO$	**314.4** [b] 295.1 [b]	 **10**	$(CD_3)_2CO$	**269.9** [c] 342.9 [c]	**−44.5** +47.8
(v)	 **23**	$CDCl_3$	284.3 [d]	 **35b**	MeOH	245.8 [e]	−38.5

[a] $\Delta(\delta_N)$ is the change in the δ_N value of the nitrogen atom of the alkylated compound compared to the δ_N value of that nitrogen in the parent compound. The δ_N and $\Delta(\delta_N)$ values associated with the alkylated nitrogen are highlighted in bold in the table in products containing more than one nitrogen NMR environment, as are δ_N values of nitrogen atoms of starting materials that undergo N-alkylation.

[b] The δ_N values of the compounds in entries (i) – (iv) originally reported in the work of Cmoch,[7] referenced relative to nitromethane at 0 ppm, were reported as −55.5 and −35.7 ppm for 2-choropyrazine (entry (i)), −74.6 and −72.8 ppm for 2-chloropyrazine *N*-oxide (entry (ii)), and −65.8 and −85.1 ppm for 3-chloropyrazine *N*-oxide (entries (iii) and (iv)).

[c] The δ_N values of the compounds in entries (i) – (iv) originally reported in the work of Cmoch,[7] referenced relative to nitromethane at 0 ppm, were reported as −35.2 and −141.7 ppm (entry (i)), −63.5 and −179.0 ppm (entry (ii)), −53.9 and −181.1 ppm (entry (iii)), and −110.3 and −37.3 ppm (entry (iv)).

[d] The δ_N value originally reported in the work of Dega-Szafran *et al.*,[41] referenced relative to nitromethane at 0 ppm, was reported as −95.9 ppm.

[e] The δ_N value originally reported in the work of Dega-Szafran *et al.*,[41] referenced relative to nitromethane at 0 ppm, was reported as −134.4 ppm.

As in Table 2-1 and 2-2, the δ_N values of the nitrogen atoms of the starting materials or products that are involved in the N- or O-alkylation processes (and the derived $\Delta(\delta_N)$ values) are highlighted in bold in Tables 2-3, 2-4 and 2-5 in instances in which there are more than one nitrogen NMR environments. Across all of the examples from the chemical literature involving N-alkylation of azines, diazines and diazine *N*-oxides for which nitrogen NMR spectral data is available, it is possible to discern that N-alkylation of these compounds results in an upfield shift of the δ_N value of the alkylated nitrogen atom of over 100 ppm (i.e., $\Delta(\delta_N)$ = *ca.* −100 ppm), as indicated in several previous publications on the basis of small numbers of results or without reference to other literature examples.

The compounds involved in these studies were pyridines (3 examples),[28,35,55] quinolines (3 examples shown in Table 2-4, but 4 additional examples may be found in reference 52),[34] pyrazine *N*-oxides (2 examples),[7] and a pyridazine.[54] N-alkylation of purines (which occurs on one of the imidazole nitrogen atoms) has also been reported to result in a large upfield shift in the δ_N value of the alkylated nitrogen ($\Delta(\delta_N)$ = −80 to −90 ppm).[37–40] Two reports from the literature indicate that O-alkylation of azine and diazine *N*-oxides results in much smaller changes in the δ_N values of the *N*-oxide nitrogen nuclei ($\Delta(\delta_N)$ = *ca.* −40 ppm) – see Table 2-5 entries (iv) and (v).[7,41]

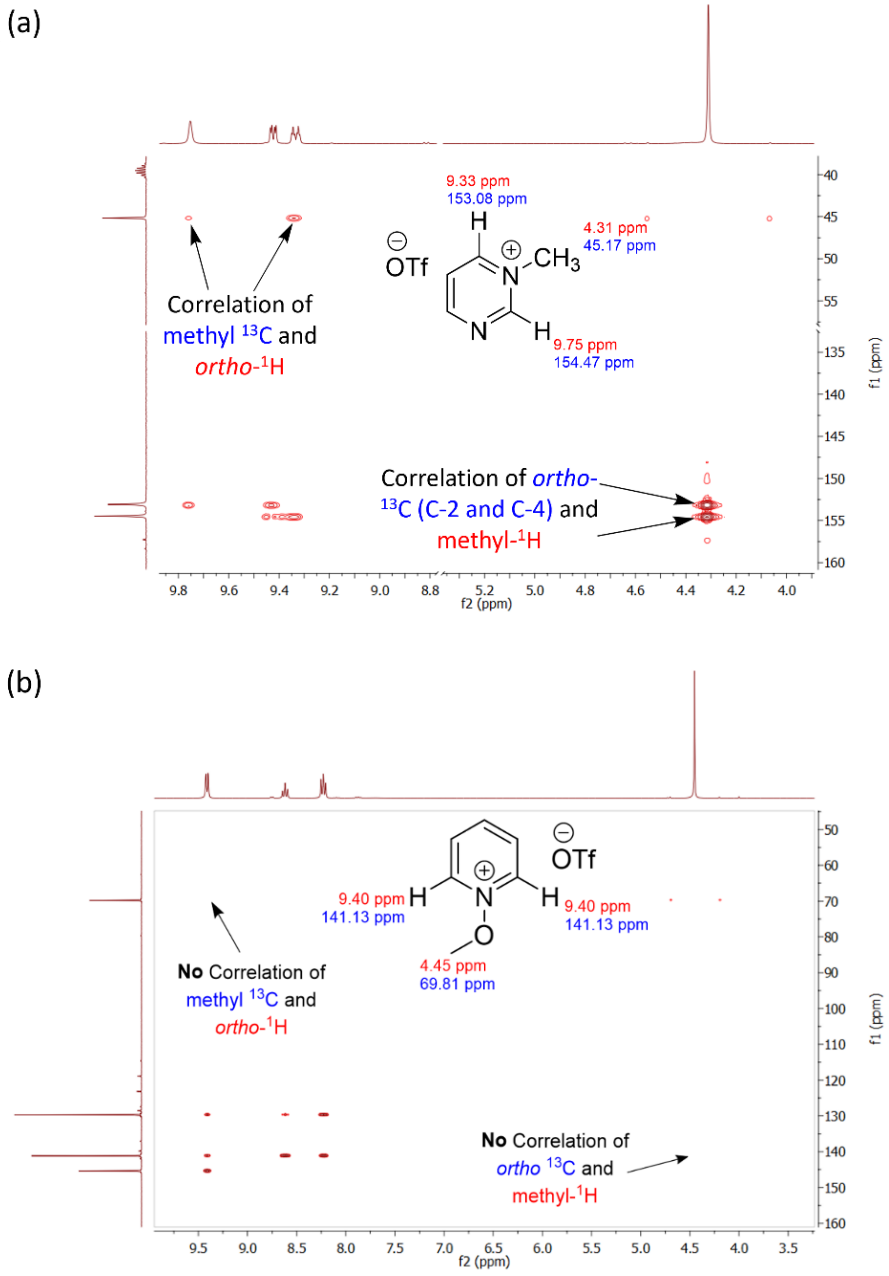
The data in Tables 2-3, 2-4 and 2-5 allows further analysis of the $\Delta(\delta_N)$ values associated with N- and O-alkylation processes. Across all of the adducts of N-alkylation (i.e., those in Tables 2-1 – 2-5; 20 examples in total), the average upfield $\Delta(\delta_N)$ value associated with *N*-alkylation is −109 ppm. The shift upfield in the *N*-oxide nitrogen δ_N value upon O-alkylation is significantly smaller – i.e., the average $\Delta(\delta_N)$ value across the *N*-oxide O-alkylation adducts shown in Tables 2-2 and 2-5 is −42 ppm (8 examples in total). From this data, it can be concluded that there is a characteristic $\Delta(\delta_N)$ value associated with N-alkylation of an azine, diazine or diazine *N*-oxide, distinct from (and significantly larger than) the characteristic $\Delta(\delta_N)$ values associated with O-alkylations of azine *N*-oxides or diazine *N*-oxides.

2.2.3. Investigation of ^{1}H-^{13}C HMBC NMR and ^{13}C NMR Spectroscopy Features which Enable Identification of N-alkylation or O-alkylation in Reactions of Heterocycles and Aromatic *N*-Oxides

Another important observation is that in the ^{1}H-^{13}C HMBC NMR spectra of the N-alkylation adducts **20** – **25** which were described in section 2.2.1, the signals of the N-methyl or N-benzhydryl proton(s) are correlated with the ^{13}C NMR signals of the aromatic carbons directly bound to the alkylated nitrogen. Similarly, the N-methyl or N-benzhydryl Ar_2CH ^{13}C NMR signal is correlated with the ^{1}H NMR signals of the aromatic protons on the *ortho*-positions relative to the quaternised nitrogen. These correlations can be seen in the ^{1}H-^{13}C HMBC spectrum of **29c** shown in Figure 2-2(a) below. The connectivity indicated by the ^{1}H-^{13}C HMBC NMR data for each compound is entirely consistent with the conclusions indicated by the ^{1}H-^{15}N HMBC NMR data.

In contrast, in the ^{1}H-^{13}C HMBC NMR spectra of compounds **31** – **35**, the signals of the O-methyl or O-benzhydryl proton(s) *are not correlated* with the ^{13}C NMR signals of the aromatic carbons directly bound to the *N*-oxide nitrogen (see the example using compound **31c** in Figure 2-2(b) below). Similarly, the O-methyl or O-benzhydryl Ar_2CH ^{13}C NMR signal is not correlated with the ^{1}H NMR signals of the aromatic protons in the *ortho*-positions relative to the alkoxypyridinium group. Hence, the absence of these correlations (in tandem with ^{15}N NMR spectral data) is indicative of O-alkylation.

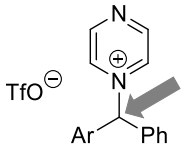
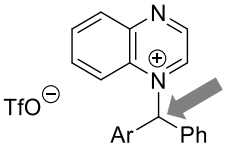
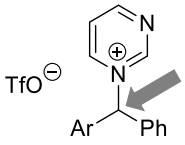
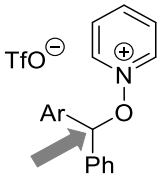
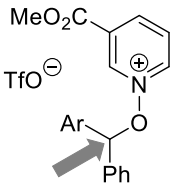
Figure 2-2. (a) ^{1}H-^{13}C HMBC NMR spectrum of **29c** showing correlations between the N-methyl ^{1}H signal and *ortho*-^{13}C signals, and the *ortho*-^{1}H signals and N-methyl group ^{13}C signal. (b) ^{1}H-^{13}C HMBC NMR spectrum of **31c** showing there are no correlations between the N-methyl ^{1}H signal and *ortho*-^{13}C signals, nor any correlation between the *ortho*-^{1}H signals and N-methyl group ^{13}C signal.



Furthermore, a thorough examination of the $^{13}C\{^{1}H\}$ NMR chemical shifts of the N- or O-alkyl group carbon atoms directly bound to the heteroatoms (in the data concerning the compounds synthesised in section 2.2.1 and literature data) revealed that the δ_C values of these carbons can be used to identify N-alkylated aromatic compounds and O-alkylation adducts of aromatic *N*-oxides (alkoxypyridinium ions).

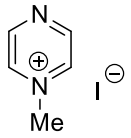
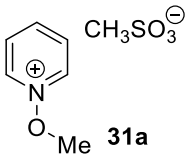
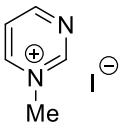
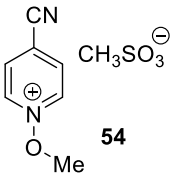
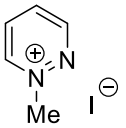
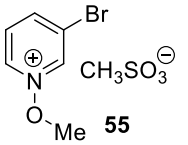
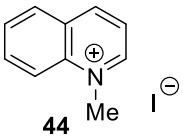
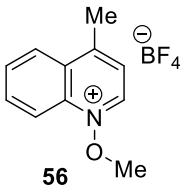
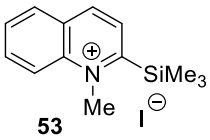
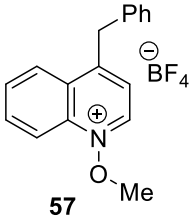
The ^{13}C NMR signals of the *N*-benzhydryl group N*C*H carbons of compounds **26**, **28** and **30** exhibit δ_C values in the range 75 – 80 ppm, as is shown below in Table 2-6 entries (i) – (iii). The δ_C values of the benzhydryl N*C*H carbons in related benzhydrylpyridinium ions found in the literature range from 65 to 76 ppm.[54,56] The δ_C values of the O*C*H benzhydryl group carbon signals of **32** and **34** are substantially higher, at 97.1 and 97.8 ppm, respectively (Table 2-6 entries (iv) and (v))).

Table 2-6. ^{13}C NMR chemical shift (δ_C) values of benzhydryl group Ar_2***C***H carbon nuclei (position indicated by arrow in compounds below) of compounds **26**, **28**, **30**, **32** and **34** in CD_2Cl_2 solvent. Ar = *p*-tolyl throughout.

#	Compound	Compound Number	δ_C (ppm)
(i)		**26**	79.6
(ii)		**28**	75.2
(iii)		**30**	76.6
(iv)		**32**	97.1
(v)		**34**	97.8

Similar trends may be observed when examining the δ_C values of a variety of aromatic N-methylated compounds and alkylation adducts of aromatic *N*-oxides for which ^{13}C NMR spectroscopic data has been reported in the literature. A selection of relevant examples of these δ_C values for compounds that have been N- or O-methylated is shown below in Table 2-7.

Table 2-7. ^{13}C NMR chemical shift (δ_C) values of N^+—CH_3 carbon nuclei (entries (i) to (v) and N^+—OCH_3 carbon nuclei (entries (vi) to (x)) of selected heterocycles which may be found in the literature. Most of the references cited in the table contain multiple examples – only a representative selection has been included here.

#	Compound	Solvent	δ_C (ppm)	#	Product	Solvent	δ_C (ppm)
(i)	 **25b**	CD_3CN	50.32 [a]	(vi)	 **31a**	$(CD_3)_2SO$	69.9 [c]
(ii)	 **29b**	$(CD_3)_2SO$	45.17 [a]	(vii)	 **54**	$(CD_3)_2SO$	70.0 [c]
(iii)	 **52**	$(CD_3)_2SO$	52.07 [a]	(viii)	 **55**	$(CD_3)_2SO$	70.4 [c]
(iv)	 **44**	$(CD_3)_2SO$	45.37 [b]	(ix)	 **56**	$(CD_3)_2SO$	69.5 [c]
(v)	 **53**	$(CD_3)_2SO$	45.77 [b]	(x)	 **57**	CD_3OD	72.9 [c]

[a] This δ_C value was originally reported in the work of Newmark, Tucker and Hardy.[57]

[b] This δ_C value was originally reported in the work of Lukevics *et al.*[34]

[c] This δ_C value was originally reported in the work of Gao *et al.*[58]

Similar systematic trends can be observed when further analysing the literature for N- and O-benzhydrylations[54,56,59–61] and N- and O-ethylations.[62–64] It is clear from this data that for each alkyl group, there is a well-defined characteristic ^{13}C NMR chemical shift range in which one can expect to observe the signal of the *N*-alkyl group N^+—*C* nucleus of an aromatic N-alkylated compound. Similarly, there is a distinct chemical shift range in which the ^{13}C NMR signal of the *O*-alkyl O—*C* nucleus of an alkoxypyridinium ion can be reliably expected to appear. Although in isolation the ^{13}C NMR chemical shift of a single carbon environment is certainly not uniquely diagnostic, it can be used in tandem with $\Delta(\delta_N)$ and ^1H-^{13}C HMBC NMR data to diagnose the occurrence of N- or O-alkylation of aromatic N-heterocycles or *N*-oxides.

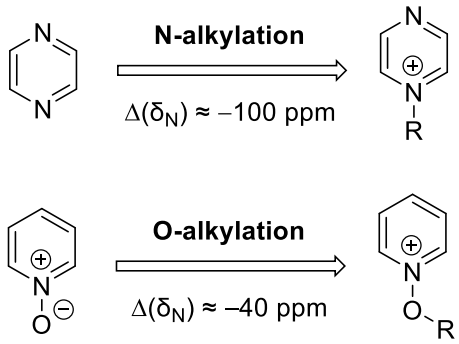
2.2.4. Identification of Characteristic $\Delta(\delta_N)$ Values

Since the starting compounds selected for this study (**7** – **12**) each contain only one Lewis basic site or two equivalent Lewis basic sites, there is no ambiguity over the site of alkylation of these compounds by alkyl electrophiles. Consequently, comparison of the ^{15}N NMR chemical shifts of the alkylation adducts with the chemical shifts of the corresponding nitrogen atoms in the starting materials has enabled diagnostic trends in the magnitudes of the $\Delta(\delta_N)$ values for reactions of these compounds to be associated with N- or O-alkylation (see Tables 2-1 and 2-2). In combination with collected nitrogen NMR spectral data from the literature relating to azine, diazine, or diazine *N*-oxide alkylation (Tables 2–3, 2-4 and 2-5), these results clearly show that N-alkylation reactions of these compounds result in very large upfield shifts in the δ_N values of the alkylated nitrogen atoms ($\Delta(\delta_N)$ values of the order of −100 ppm from starting material to product). Given that a similar phenomenon has also been observed for N-alkylation reactions of purines (with $\Delta(\delta_N)$ values of −80 to −90 ppm for the alkylated nitrogen),[37–40] it is clear that large negative $\Delta(\delta_N)$ values are strongly indicative of N-alkylation of aromatic nitrogen nucleophiles. It has also been established that information from ^{13}C{^{1}H} and ^{1}H-^{13}C HMBC NMR spectra of alkylation adducts can be used to complement the ^{15}N NMR chemical shift data from ^{1}H-^{15}N HMBC NMR spectra. Hence, analysis of products formed in reactions of aromatic N-heterocycles using the ^{1}H-^{15}N HMBC, ^{1}H-^{13}C HMBC and ^{13}C{^{1}H} NMR spectroscopic techniques in tandem provides a definitive means of establishing the occurrence or otherwise of N-alkylation in these reactions.

Similarly, the ^{1}H-^{15}N HMBC NMR spectral data on pyridine *N*-oxides and their O-alkylated derivatives (see Table 2-2) shows that there is a characteristic upfield shift in the δ_N values of aromatic *N*-oxide nitrogen nuclei upon O-alkylation that is of much smaller magnitude ($\Delta(\delta_N)$ = *ca.* −42 ppm) than that observed for the N-alkylations discussed above. This observation aligns closely with the two literature precedents involving O-alkylation of aromatic *N*-oxides in which nitrogen NMR spectral data has been reported Table 2-5 entries (iv) and (v)).[7,41]

^{1}H-^{15}N HMBC NMR spectra of *N*-alkoxypyridinium ions (**20** – **24**) show three-bond coupling interactions between the *N*-oxide nitrogen and alkoxy group protons. ^{1}H-^{13}C HMBC NMR spectra of the O-alkylated adducts show that long-range correlations *are not present* between the O-alkyl protons and carbons and the aromatic carbons and protons.[55] Hence, long-range correlation data obtained from ^{1}H-^{15}N HMBC and ^{1}H-^{13}C HMBC NMR spectra can also be used in tandem with $\Delta(\delta_N)$ values and δ_C values (from ^{13}C NMR spectroscopy) to diagnose the occurrence of O-alkylation of aromatic *N*-oxides. Hence, long-range correlation data obtained from ^{1}H-^{15}N HMBC and ^{1}H-^{13}C HMBC NMR spectra can also be used in tandem with $\Delta(\delta_N)$ values and δ_C values (from ^{13}C NMR spectroscopy) to diagnose the occurrence of O-alkylation of aromatic *N*-oxides.

Figure 2-3. A summary of the findings of the analytical method which was developed in section 2.2. A systematic large upfield shift in the ^{15}N NMR chemical shift is shown to be characteristic of N-alkylation of aromatic N-heterocycles ($\Delta(\delta_N) \approx -100$ ppm). A much smaller systematic change in δ_N is indicative of *N*-oxide O-alkylation (*ca.* −40 ppm).



At this point, the characteristic $\Delta(\delta_N)$ values associated with formation of N-alkylated adducts of aromatic N-heterocycles and O-alkylated adducts of aromatic *N*-oxides (established above) can be compared with some $\Delta(\delta_N)$ values associated with other important chemical transformations of N-heterocycles. In contrast to the large negative $\Delta(\delta_N)$ value associated with N-alkylation of an aromatic N-heterocycle, N-alkylation of aliphatic or alicyclic N-heterocycles (i.e., amines) results a comparatively small downfield shift in δ_N (small positive $\Delta(\delta_N)$). For example, the ^{15}N chemical shift of *N*,*N*-dimethylpiperidinium iodide in $CDCl_3$ is seen to be 8.1 ppm downfield of that of *N*-methylpiperidine in the work of Potmischil *et al.*[65] Similarly, the ^{15}N chemical shift of tetramethylammonium bromide in H_2O is seen to be 5.3 ppm downfield of that of trimethylamine in the work of Vogl, Rehman and Zarras.[66]

N-oxidation of aromatic N-heterocycles results in an upfield shift of δ_N of the oxidised nitrogen of the order of 20 – 30 ppm (i.e., $\Delta(\delta_N) = -20$ to -30 ppm), as can be seen in the work of Sakuma *et al.*[67] and Rao *et al.*[68] In contrast, N-oxidation of aliphatic N-heterocycles (amines) has been reported to result in a large *downfield* shift of the δ_N value of the signal of the nitrogen nucleus involved ($\Delta(\delta_N)$ = *ca.* +68 to +85 ppm), which is demonstrated by the work of Farley *et al.*,[42] Martin *et al.*,[43] and Brough *et al.*[69]

The diagnostic NMR spectroscopic analytical protocols described above are of general utility, and are likely to prove beneficial in other applications in organic chemistry involving aromatic N-heterocycles and *N*-oxides, especially given the analogous effects observed on δ_N values upon N- or O-protonation of aromatic N-heterocycles[20–23,28] and upon complexation of aromatic nitrogen atoms to metals.[20–23,29–33] The diagnostic trends described in this section will allow the unambiguous identification of the structure of products formed in alkylation reactions of aromatic N-heterocycles with ambident nucleophiles (such as compounds **1** – **3** shown in section 2.

2.3. Investigation into the Ambident Reactivity of Diazine *N*-Oxides

With a robust method in hand to distinguish unambiguously between N- and O-alkylation products of alkylation reactions of diazine *N*-oxides, the focus of this project was then shifted to study the alkylations of these compounds.

2.3.1. Site of Alkylation of Diazine *N*-Oxides

Reactions of ambident nucleophiles **1**, **2** and **3** with electrophiles MeI, MeOTf, and benzhydrylium triflates **24** and **58** were carried out using the conditions shown in Scheme 2-8 and Table 2-8. The experimental data for each individual experiment are available in Chapter 3, section 3.6.

Scheme 2-8. (a), **(b)**, **(c)** N- and O-alkylation reactions of the ambident nucleophiles **1** – **3**. Methylation reactions (using MeI or MeOTf) were conducted in $(CD_3)_2SO$, CD_3CN, or MeCN. ^1H-^{15}N HMBC NMR spectra of the adducts were recorded in $(CD_3)_2SO$ solvent. Benzhydrylation reactions were conducted in CD_2Cl_2. See Table 2-8 for details of conversions and yields.

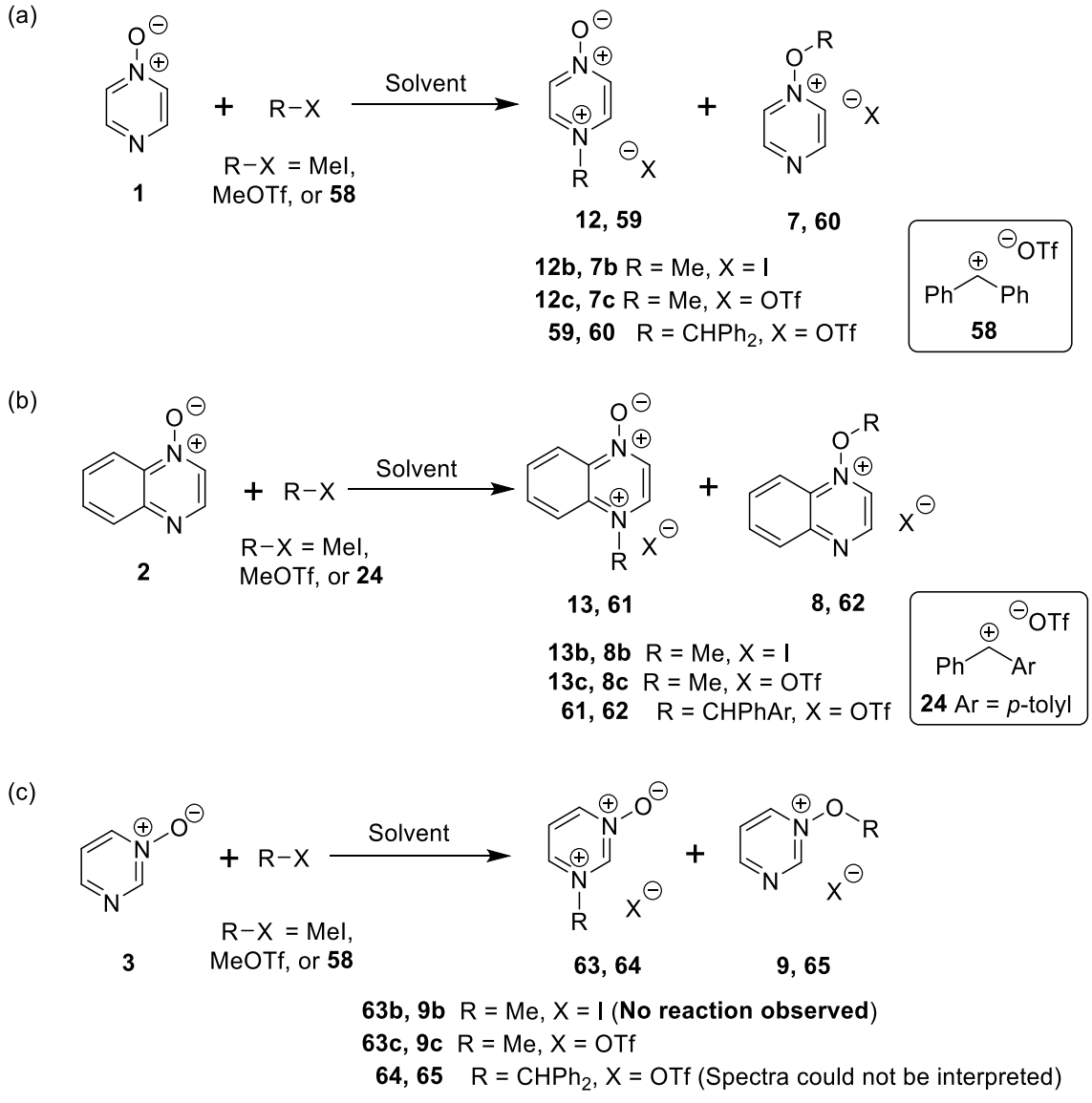
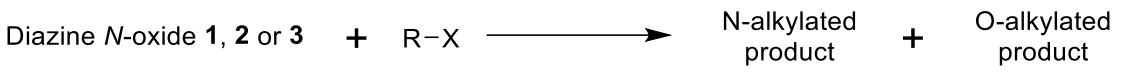
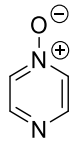
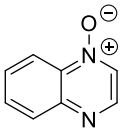
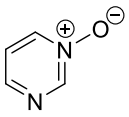


Table 2-8. Alkylation reactions of diazine *N*-oxides **1**, **2** and **3** (as per Scheme 2-5) resulting in formation of N- and O-alkylated products. [a]



Diazine *N*-Oxide	#	Reaction Solvent	R	X	Products		Conversion [b] (Isolated Yield)	N/O Product Ratio
					N-methyl	O-methyl		
 **1**	(i)	CD_3CN or No solvent	Me	I	**12b**	**7b**	24% in CD_3CN (26% with no solvent)	> 99:1
	(ii)	CD_3CN	Me	OTf	**12c**	**7b**	Quantitative (68% yield)	95:5
	(iii)	$(CD_3)_2SO$	Me	OTf	**12c**	**7c**	87%	> 99:1
	(iv)	CD_3CN or CH_2Cl_2	CH_2Ph	OTf	**59**	**60**	Quantitative	> 99:1
 **2**	(v)	No solvent	Me	I	**13b**	**8b**	(Yield = 16%) [c]	> 99:1
	(vi)	CD_3CN	Me	OTf	**13c**	**8c**	Quantitative (57% yield)	89:11
	(vii)	$(CD_3)_2SO$	Me	OTf	**13c**	**8c**	78%	> 99:1
	(viii) [d]	CD_2Cl_2	PhArCH	OTf	**61**	**62**	93%	91:9
 **3**	(ix)	CD_3CN	Me	I	**63b**	**9b**	No products formed	–
	(x)	CD_3CN	Me	OTf	**63c**	**9c**	Quantitative	7:93
	(xi)	$(CD_3)_2SO$	Me	OTf	**63c**	**9c**	76%	7:93
	(xii) [d]	CD_2Cl_2	PhArCH	OTf	**64**	**65**	Spectra could not be interpreted	–

[a] Note that the ^{1}H NMR spectra of the reaction mixtures on their own do not show which product (N vs. O-alkylation) is favoured in each case, only the product ratio.

[b] Conversions represent the combined amount of N- and O-alkylated product formed relative to the amount added of the alkylating agent (always the limiting reagent). These were determined using integrations of appropriate signals in the ^{1}H NMR spectra. For entry (viii), the deviation from quantitative conversion was due to hydrolysis of the alkylating agent. Percentage yields (shown in brackets where applicable) of isolated products were determined from separate reactions run on larger scale using MeCN solvent, or with no solvent (neat reagents) for entries (i) and (v). Products **59**, **61**, **62**, **63c** and **9c** (entries (iv), (viii) and (x), respectively)) decompose upon attempted isolation, and hence no isolated yields could be obtained in these cases.

[c] **2** + MeI were reacted together without solvent. The product was purified prior to NMR spectral characterisation, so the conversion was not determined for this reaction. However, the low isolated yield shown above is indicative of low conversion in this reaction.

[d] In these experiments, Ar = *para*-tolyl.

Note that in some instances shown in Table 2-8 (see entries (i), (ii), (vi), and (x)), MeCN or CD_3CN is used as the reaction solvent, but is not used to acquire all of the NMR spectra recorded. This is due to the fact that these solvents could not be used for ^1H-^{15}N HMBC NMR spectroscopic characterization due to the presence of nitrogen in the solvent. Hence, for the purposes of obtaining ^1H-^{15}N HMBC spectra, the solvent was removed and the residue re-dissolved in $(CD_3)_2SO$ in those cases. CD_2Cl_2 was not a suitable solvent for methylation reactions of diazine *N*-oxides **1** – **3** due to the negligible solubility of the adducts in this solvent. The reaction of **1** with MeI in CD_3CN or MeCN resulted in formation of a single product, albeit with low conversion and yield (i.e., the process of alkylation was completely selective for one site (N or O) – see Table 2-8 entry (i)). No products were observed in the ^1H NMR spectra of the reaction of **2** + MeI in CD_3CN. Product formation was only observed when the reagents were mixed together in the absence of solvent (neat); the data in Table 2-8 entry (v) refer to the reaction run under these conditions. As in the case of **1** + MeI, only a single product was observed by ^1H NMR spectroscopy. Attempted reactions of **3** with MeI in CD_3CN or MeCN did not yield any products, i.e., neither **63b** nor **9b** were observed (see Scheme 2-8(c)).

The reaction of **1** with benzhydrylium triflate **58** in CH_2Cl_2 or CD_3CN also results in the formation of a single product in each case (see Table 2-8 entry (iv)). The ^1H NMR spectrum of the reaction mixture of **2** + **24** in CD_2Cl_2 (see Scheme 2-8(b)) shows formation of two products in a 91:9 ratio. The combined conversion was 93%; the remaining 7% was accounted for by a hydrolysis product (see Table 2-8 entry (viii)). Reaction of **3** with **58** gave ^1H NMR and ^1H-^{15}N HMBC NMR spectra that could not be interpreted, containing broad and unusually shaped signals. As a result, the presence (or absence) of **64** or **65** (see Scheme 2-8(c)) could not be unambiguously determined. This may be ascribed to the very low Lewis basicity of **3**, which may cause the reaction between these reagents to be reversible, and thermodynamically disfavoured.

The reactions of **1** – **3** with MeOTf in CD_3CN yielded mixtures of O- and N-methylation products (see Table 2-8 entries (ii), (vi), and (x)). Addition of MeOTf to $(CD_3)_2SO$ solutions of **1** and **2** resulted in formation of a single product in each case (Table 2-8 entries (iii) and (vii)), while the corresponding reaction of **3** gave two products (Table 2-8 entry (xi)). The rates of these reactions differed greatly depending on the solvent used. Product formation was rapid for reactions in CD_3CN (i.e., the reactions were complete within minutes), but was exceptionally slow in $(CD_3)_2SO$, requiring weeks for high conversions to be obtained. It is highly likely that the active methylating agent in $(CD_3)_2SO$ was the methoxysulfonium salt $[(CD_3)_2S(OMe)]OTf$, and that this electrophile is much less reactive than MeOTf in MeCN. The methylation of $(CH_3)_2SO$ by dimethylsulfate has previously been noted by Forrester et al.[70]

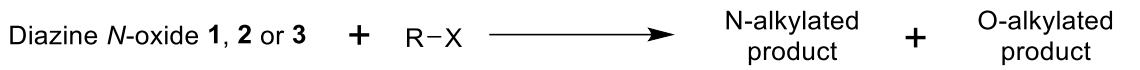
Many of the initial products of the reactions shown in Scheme 2-8 and Table 2-8 do not survive attempts at isolation. Hence, all reactions were conducted on small scale, and the entirety of each reaction mixture was transferred (under an inert atmosphere of nitrogen gas) to an NMR tube for analysis by NMR spectroscopy. In instances in which stable, isolable products were formed, the final (stable) products were isolated from separate

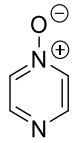
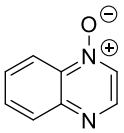
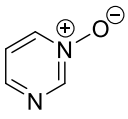
reactions, conducted on larger scale. The adducts of benzhydrylation of **1** and **2** are hydrolytically unstable and could not be isolated. The adduct of **2** + MeI was formed in very low conversion (see Table 2-8 entry (v), and the adduct of **3** + MeOTf became contaminated with multiple decomposition products; hence neither adduct could be isolated in pure form. In fact, decomposition was evident in all of the spectra obtained of this material, regardless of the method employed to synthesise it. The major product remained intact for several days if kept under inert atmosphere (invariably contaminated with decomposition products) but did not survive attempts at isolation. In addition, for the reactions of **1** – **3** with MeOTf in MeCN or CD_3CN solvent, decomposition of the minor product (what was detected in ^{1}H NMR spectra in CD_3CN) occurred upon removal of the MeCN/CD_3CN solvent under vacuum, resulting in the observation of the signals of the major product only in the ^{1}H NMR spectrum of the mixture upon dissolution in $(CD_3)_2SO$.

In all cases shown in Table 2-8, it was impossible to distinguish the site of attachment of the alkyl group unambiguously using standard ^{1}H- or ^{13}C-based one or two-dimensional NMR techniques. That is, the identity of the product(s) in each case could not be reliably assigned as N-alkylated or O-alkylated. In the instances in which mixtures of N- and O-methylation products were obtained, product ratios could be determined using the integrations of signals in ^{1}H NMR spectra, but which product was favoured was not clear. The product ratios determined in this way are shown in Table 2-8.

In order to determine which site (N or O) of each of the ambident nucleophiles **1** – **3** is favoured in the alkylation reactions shown in Scheme 2-8 and Table 2-8, the indirect detection natural abundance ^{1}H-^{15}N HMBC NMR spectroscopic technique described above and in section 2.2 was employed. The ^{15}N NMR chemical shifts of starting compounds **1** – **3** and of the observed alkylation adducts are shown in Table 2-9 below. The $\Delta(\delta_N)$ values associated with these reactions (also shown in Table 2-9) show the extent to which the chemical shifts of the ^{15}N nuclei of the alkylation product(s) differ from the chemical shifts of the corresponding ^{15}N nuclei in the starting materials **1** – **3**. As above, a negative value of $\Delta(\delta_N)$ indicates an upfield shift of the δ_N value of an ^{15}N environment upon alkylation, while a positive value indicates a downfield shift. In several instances (all described above), only one product was formed in the alkylation reactions of **1** – **3**, while in others, the minor product did not survive the process of removal of the MeCN or CD_3CN reaction solvent and replacement with $(CD_3)_2SO$. Hence, in almost all cases, only one product could be characterized using the ^{1}H-^{15}N HMBC NMR technique. In the ^{1}H-^{15}N HMBC spectrum of the reaction of **2** + **58**, no correlations were observed to the small signals of the minor product that was shown to be present by the ^{1}H NMR spectrum. The only instance in which it was possible to determine the δ_N values of both the major and minor alkylation products involved methylation of **3** in $(CD_3)_2SO$ using MeOTf (see Scheme 2-8(c); note that the alkylating agent in this reaction is likely to be methoxysulfonium triflate).

Table 2-9. δ_N and $\Delta(\delta_N)$ values associated with N- and O-alkylation reactions of diazine *N*-oxides **1** – **3** (as are shown in Scheme 2-5). All reactions were carried out in MeCN, which was subsequently removed and replaced with $(CD_3)_2SO$ prior to NMR spectroscopic analysis (except in the instances indicated below). [a]



Diazine *N*-Oxide	#	Products	R−X	δ_N of starting compound (ppm)	N-alkylation		O-alkylation	
					δ_N of product (ppm)	$\Delta(\delta_N)$ (ppm)	δ_N of product (ppm)	$\Delta(\delta_N)$ (ppm)
 **1**	(i)	**12b**, **7b**	MeI	309.3 303.9 [a]	322.3 187.1	+13.0 −116.8	Product (**7b**) not formed	
	(ii)	**12c**, **7c**	MeOTf	309.3 303.9 [a]	322.9 187.8	+13.6 −116.1	Product (**7c**) decomposed during solvent exchange	
	(iii)	**12c**, **7c**	MeOTf	309.3 303.9 [a]	322.9 187.7	+13.6 −116.2	Product (**7c**) not formed	
	(iv) [b]	**59**, **60**	Ph_2CHOTf	311.0 303.5	325.0 201.6	+14.0 −101.9	Product (**60**) not formed	
 **2**	(v)	**13b**, **8b**	MeI	303.2 299.3 [c]	314.4 178.0	+11.2 −121.3	Product (**8b**) not formed	
	(vi)	**13c**, **8c**	MeOTf	303.2 299.3 [c]	314.4 177.6	+11.2 −121.7	Product (**8c**) decomposed during solvent exchange	
	(vii)	**13c**, **8c**	MeOTf	303.2 299.3 [c]	314.4 177.9	+11.2 −121.4	Product (**8c**) not formed	
	(viii)[b,d]	**61**, **62**	PhArCHOTf	302.0 300.3	317.6 190.5	+14.4 −108.8	Signal of **62** not detected in ^1H-^{15}N HMBC	
 **3**	(ix)	**63c**, **9c**	MeOTf	301.3 291.7 [e]	Product (**63c**) decomposed during solvent exchange		303.4 249.4	+2.1 −42.3
	(x)	**63c**, **9c**	MeOTf	301.3 291.7 [e]	293.6 205.2	+1.9 −96.1	303.1 249.1	+1.8 −42.6

[a] Literature δ_N values: 309.33, 303.85 ($(CD_3)_2SO$, referenced to nitromethane at 380 ppm; equivalent to ammonia at 0 ppm) are found in the work of Sakuma *et al*.[67]

[b] These experiments were carried out in CD_2Cl_2, and the reaction mixtures were directly analysed by NMR spectroscopy.

[c] These values were reported in the work of Städeli and Von Philipsborn as δ_N −76.8 and −80.7 ppm (referenced to nitromethane at 0 ppm).[50] Since the ^1H-^{15}N HMBC spectra in this study were referenced to ammonia at 0 ppm, the literature δ_N value has been re-calculated here relative to ammonia at 0 ppm.

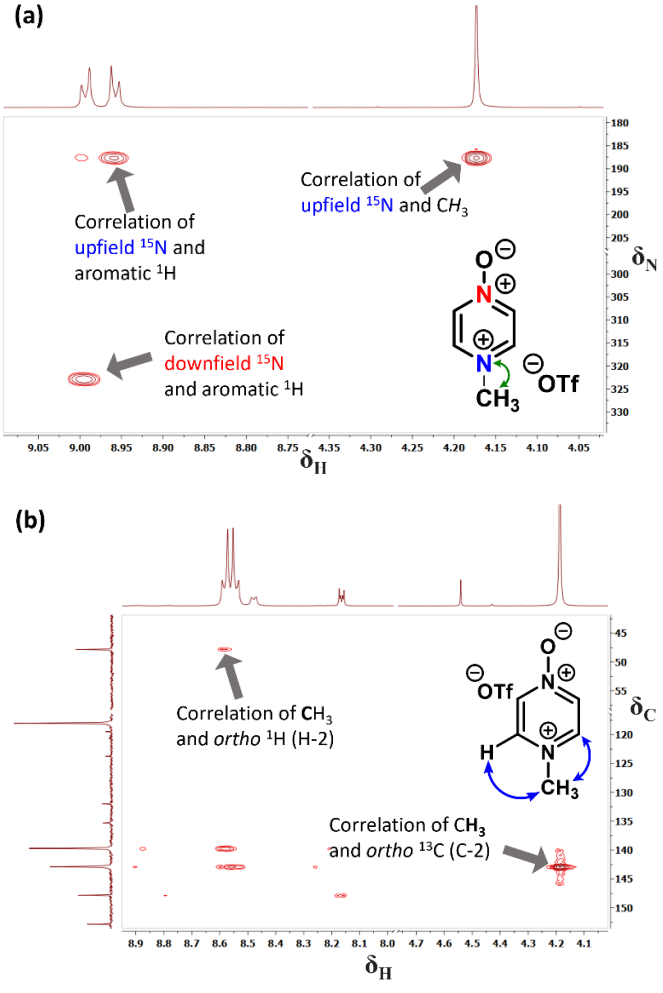
[d] In this experiment, Ar = *para*-tolyl.

[e] The positional assignments for this compound were made with reference to the work of Städeli and Von Philipsborn (which contained this compound referenced to nitromethane at 0 ppm).[50]

The ^1H-^{15}N HMBC NMR spectra of the major or exclusive products formed in the reactions of **1** or **2** with electrophiles MeI, MeOTf, and benzhydrylium **24** and **58** (Scheme 2-8(a) and (b)) all show that the δ_N values of the upfield nitrogen nuclei are shifted upfield

by over 100 ppm relative to the δ_N values of the corresponding nitrogen NMR environments in the starting materials, i.e., $\Delta(\delta_N) > -100$ ppm in each case (see Table 2-9 entries (i), (ii), (iii), (v), (vi) and (vii) for methylations and entries (iv) and (viii) for benzhydrylation reactions). That the upfield signal in the ^{15}N dimension belongs the alkylated nitrogen is confirmed by the existence of a correlation in the ^{1}H-^{15}N HMBC NMR spectrum of this signal with the ^{1}H signal of the N-alkyl proton(s) (for an example, see the spectrum from the reaction of **1** + MeOTf in Figure 2-4(a) below). In the ^{1}H-^{13}C HMBC NMR spectra of each of the major products of the reactions of **1** and **2**, a correlation is shown to exist between the alkyl group (aliphatic) proton(s) and the carbons *ortho* to the upfield nitrogen for all alkylation adducts (see the example in Figure 2-4(b) below). A correlation between the alkyl group aliphatic carbon and the protons *ortho* to the upfield nitrogen is also evident in these spectra. The large upfield $\Delta(\delta_N)$ values and correlation data associated with the alkylation reactions of **1** and **2** are consistent with the preferential (and in some cases exclusive) occurrence of N-alkylation in these reactions.

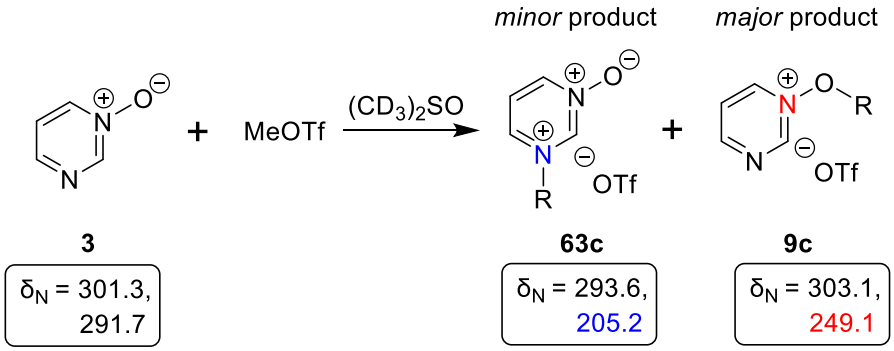
Figure 2-4. (a) Section of the ^{1}H-^{15}N HMBC NMR spectrum of **12c** in $(CD_3)_2SO$ (from reaction of Table 2-9 entry (ii)) showing correlation of N-methyl ^{1}H signal with upfield ^{15}N signal, **(b)** Section of the ^{1}H-^{13}C HMBC NMR spectrum of **12c** in CD_3CN (from reaction of Table 2-9 entry (ii)) showing correlations between the N-methyl ^{1}H signal and *ortho*-^{13}C signals, and the *ortho*-^{1}H signals and N-methyl group ^{13}C signal.



In support of this conclusion, the $^{13}C\{^{1}H\}$ NMR chemical shifts of the methyl group carbon in the major products of the methylation reactions of **1** and **2** are, respectively, 44.1 and 46.6 ppm. These values lie in the middle of the range of δ_C values identified in section 2.2.3 as being characteristic of N-methylation of aromatic N-heterocycles (see Table 2-7 entries (i) – (v) and accompanying discussion). The δ_C values of the minor products of these methylation reactions were, respectively, 68.9 and 70.2 ppm. These values appear in the middle of the δ_C range that is indicative of adducts of O-methylated aromatic *N*-oxides (see Table 2-7 entries (vi) – (x)). The δ_C values of the benzhydryl group aliphatic carbons (Ar_2CH) in the products of the benzhydrylation reactions of **1** and **2** were, respectively, 77.2 and 73.2 ppm. These values are characteristic of N-benzhydrylated products, based on the results which may are shown in Table 2-6 entries (i) – (iii). The above data are all consistent with the conclusion that the major products formed are N-alkylation adducts **12**, **59**, **13** and **61** (see Scheme 2-5 (a) and (b)). These are formed in preference to O-alkylation adducts **7**, **60**, **8** and **62**.

The ^{1}H-^{15}N HMBC NMR spectrum of the reaction mixture produced by adding MeOTf to a $(CD_3)_2SO$ solution of **3** (see Scheme 2-9 below, also Scheme 2-8(c)) showed signals for the major product at δ_N 303.1 and 249.0 ppm (see Table 2-9, entry (x)).

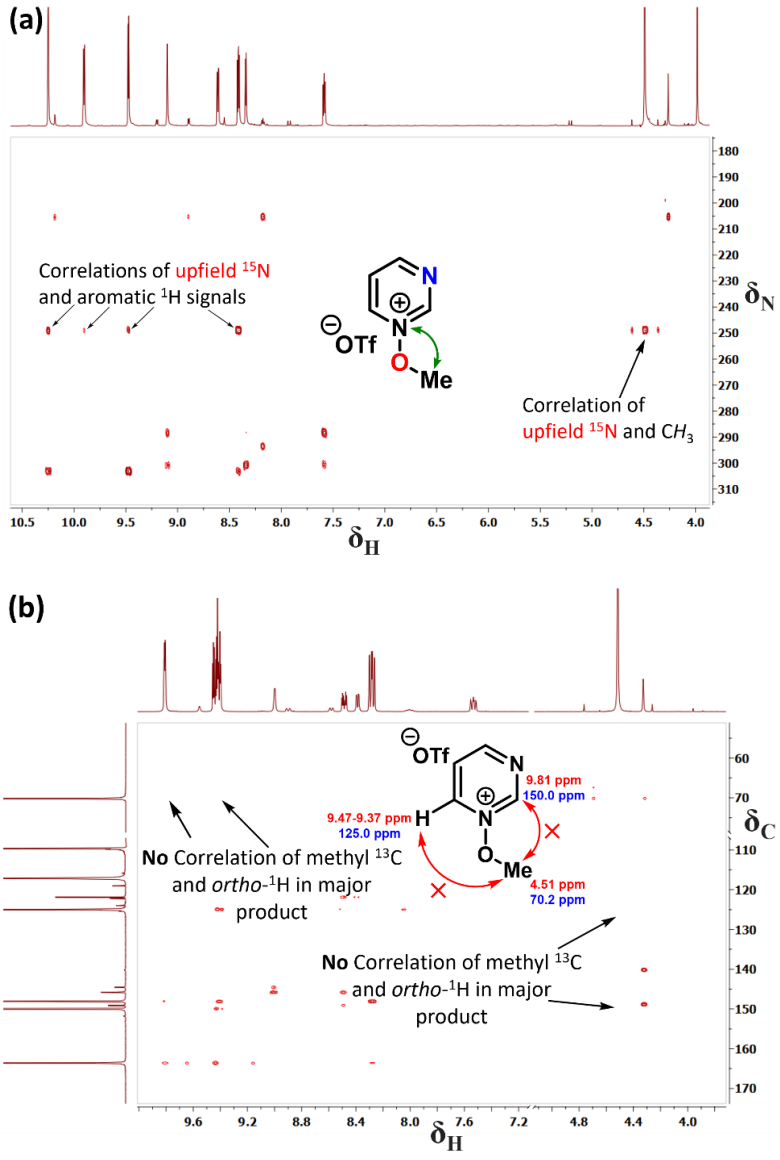
Scheme 2-9. A summary of the ^{1}H-^{15}N HMBC NMR spectral data observed when analysing the products of a reaction of **3** with MeOTf in $(CD_3)_2SO$ solution. In the major product (**9c**), the $\Delta(\delta_N)$ was indicative of *N*-oxide O-alkylation (*ca.* −40 ppm). The nitrogen positions in compound **3** were assigned through reference to data found in a paper by Städeli and Von Philipsborn.[50]



The upfield ^{15}N NMR signal showed a correlation with the methyl group CH_3 protons, indicating that this belongs to the alkylated nitrogen. However, no correlation existed in the ^{1}H-^{13}C HMBC NMR spectrum for the signal of the methyl protons with the signal of the carbons *ortho* to the upfield nitrogen, nor for the signal of the methyl carbon with the signal of the protons *ortho* to upfield nitrogen. The spectra in Figure 2-5 below demonstrate this observation. Based on the δ_N value of the upfield nitrogen signal, the δ_C value of the methyl group carbon of 70.2 ppm (characteristic of a N^+—O—CH_3 ^{13}C NMR signal of a *N*-methoxypyridinium ion as seen in Table 2-7 entries (vi) – (x)), and the features of the ^{1}H-^{13}C HMBC NMR spectrum, the spectral characteristics of the major product are very similar to those of compound **31** (the O-methylated adduct of pyridine *N*-oxide (**21**); see Scheme 2-3(d)), and other aromatic *N*-oxide O-methylation adducts.

Therefore, it may be concluded that the major product of this reaction is O-methylation adduct **9c** (see Scheme 2-9). The upfield signal (δ_N = 249.1 ppm) is assigned to the *N*—OMe nitrogen atom, and hence has a $\Delta(\delta_N)$ value of −42.6 ppm relative to the signal of the *N*-oxide nitrogen atom of **3** (at δ_N = 291.7 ppm; see Table 2-9 entry (x)), while the downfield signal has $\Delta(\delta_N)$ = +1.8 ppm relative to the corresponding signal of **3** (δ_N = 301.3 ppm). The upfield $\Delta(\delta_N)$ value of −42.6 ppm for this reaction is very similar to the $\Delta(\delta_N)$ values observed in formation of methoxypyridinium salts during O-methylation reactions of *N*-oxides (e.g., $\Delta(\delta_N)$ = −42.7 ppm for formation of **31** from **21** + MeOTf; see Table 2-2 entry (iv)).

Figure 2-5. (a) Section of the ^{1}H-^{15}N HMBC NMR spectrum of **9c** in $(CD_3)_2SO$ (from reaction of Table 2-9 entry (x)) showing correlation of O-methyl ^{1}H signal with upfield ^{15}N signal, (b) Section of the ^{1}H-^{13}C HMBC NMR spectrum of **9c** in CD_3CN (from reaction of Table 2-9 entry (x)) showing that there are no correlations between the N-methyl ^{1}H signal and *ortho*-^{13}C signals, and the *ortho*-^{1}H signals and N-methyl group ^{13}C signal.



The $\Delta(\delta_N)$ value associated with formation of the minor product of the reaction of pyrimidine *N*-oxide (**3**) + $[(CD_3)_2S(OMe)]OTf$ in $(CD_3)_2SO$ is considerably larger than the $\Delta(\delta_N)$ value for O-alkylation (see Table 2-9 entry (x); $\Delta(\delta_N) = -96.1$ vs. -42.6 ppm). In addition, the ^1H-^{13}C HMBC NMR spectrum exhibits multiple bond correlations between the N-methyl group and *ortho* aromatic ^1H and ^{13}C signals. The δ_C value of the methyl group carbon of the minor product was 46.6 ppm, which is characteristic of an aromatic N^+—CH_3 carbon (see Table 2-7, entries (i) – (v)). These data are consistent with the minor product being N-methylation adduct **63c** (as seen in Scheme 2-9). The relevant spectral data for the reaction of **3** + MeOTf in CD_3CN (or MeCN) also show that **9c** is the major product formed in this solvent. Although **63c** is formed in the reaction (as shown by ^1H NMR spectral analysis), it does not survive the process of solvent removal and dissolution in $(CD_3)_2SO$ and therefore was not characterised in isolation.

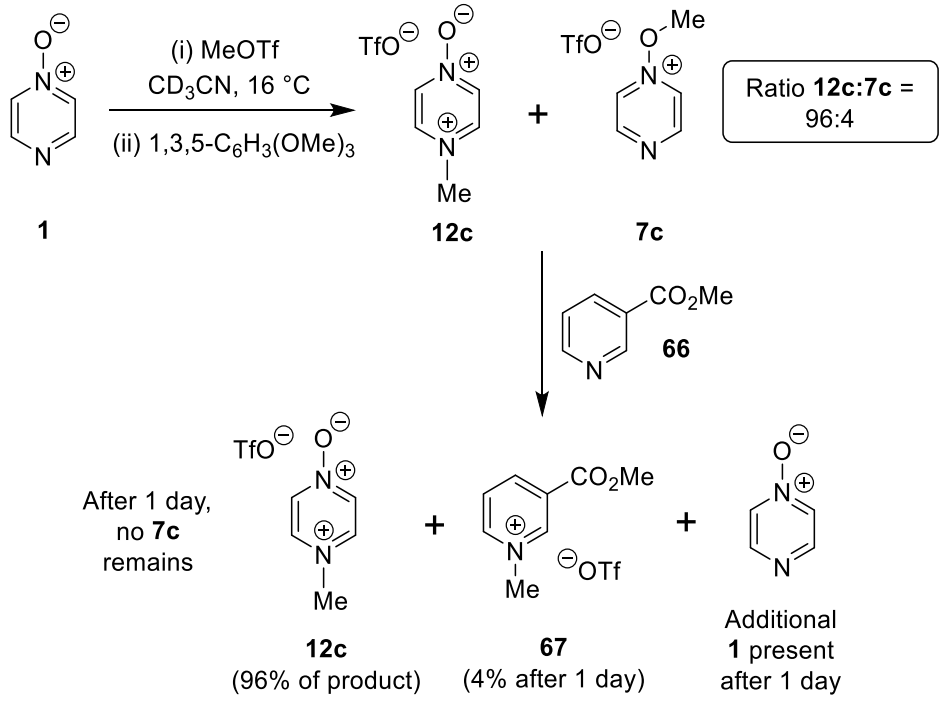
Based on the above data, it is possible to conclude that the N- vs O-methylation ratios in the reactions of **3** with MeOTf (in CD_3CN) and $[(CD_3)_2S(OMe)]OTf$ in $(CD_3)_2SO$ are both 7:93 (in favour of O-methylation; see Table 2-8 entries (x) and (xi)).

The N- vs O-alkylation ratios observed in the reactions of **1** – **3** did not change over time in the absence of perturbation. In order to establish whether or not these reactions occurred under kinetic control, several "crossover experiments" were carried out involving reactions of MeOTf with **1** – **3** (and of MeI with **1**) in CD_3CN followed by addition of a second nucleophile. The method established for investigating the reversibility of these processes involved the addition of a competing nucleophile to a reaction mixture containing the methylation products of a reaction of **1**, **2** or **3**. This competing nucleophile (denoted a "crossover" nucleophile) is included in an attempt to intercept any electrophiles formed as a result of the reverse reaction occurring to the alkylation product which was added. An internal standard (1,3,5-trimethoxybenzene) was added to the reaction mixture to allow the amounts of the products present to be quantified (using the integrations of ^1H NMR spectral signals of the products relative to the integrations of the signals of the internal standard) before and after addition of the second nucleophile, and to enable quantification of the amount of "crossover product" formed. Nucleophiles **18** and **66** (see Schemes 2-10 and 2-11 below) were selected as second nucleophiles because they have been shown in separate studies (carried out in our research group and in the literature)[71] to be considerably stronger Lewis bases than compounds **1** – **3**, and hence are expected to out-compete **1** – **3** for any free alkylating agent present due to their stronger nucleophilicity and the fact that they are present in considerable excess over **1** – **3** under the conditions of the "crossover experiment".

It was observed that the amount of major product formed in the methylation reactions of each of compounds **1** and **2** remained constant with respect to the internal standard during the "crossover experiments" (i.e., the formation of the major product in each case is irreversible (**12b**, **12c**, and **13c** respectively)). For example, the amount of **12c** formed in the reaction of **1** + MeOTf in CD_3CN at 16 °C is invariant at 96% of methylation product throughout the experiment (see the example illustrated in Scheme 2-10 below). In the reactions of **1** and **2** with MeOTf (using **66** or **18** as the second nucleophile), a "crossover

product" is formed at the expense of the minor product (O-methylation adducts **7c** and **8c**) with commensurate production of starting diazine *N*-oxide (**1** or **2**). Although crossover product (**25c** or **67**) is formed from the minor products in these experiments, it is concluded in each case that this is a consequence of the occurrence of an S_N2 reaction between the second nucleophile (**18** or **66**) and the minor product. If this were not the case, then repeated observations of the N/O-methylation ratios over time in alkylation reactions of **1** and **2** should show this ratio changing (to favour the major product), as formation of the major product is irreversible in each case. Consequently, it may be concluded that O-methylation of **1** and **2** are also irreversible processes in CD_3CN solvent at ambient temperatures. Thus, N-methylation of **1** and **2** is observed in each case because they are the kinetically favoured reactions in their respective processes.

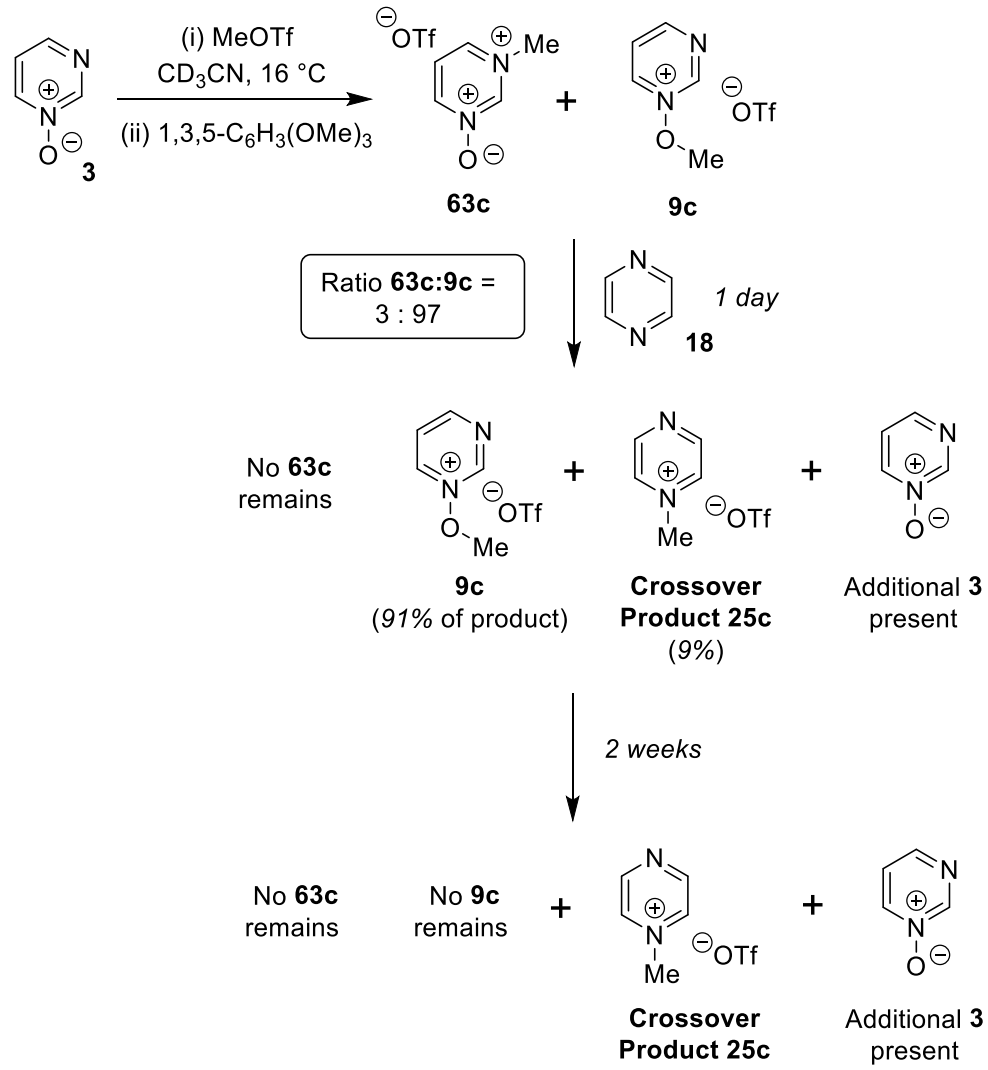
Scheme 2-10. Example of a "crossover experiment" investigating reversibility of reaction of **1** + MeOTf using 1,3,5-trimethoxybenzene as internal standard, and "crossover nucleophile" **66**. The crossover product is compound **67**.



The details of each of the crossover experiments are available in section 3.7. A similar "crossover experiment" involving the reaction of pyrimidine *N*-oxide (**3**) + MeOTf in CD_3CN (with an internal standard added) and pyrazine (**18**) as the 2nd nucleophile also showed formation of "crossover product" **25c**. This reaction is illustrated in Scheme 2-11 below. In ^1H NMR spectra of this reaction mixture recorded early in the reaction, the crossover product (**25c**) was observed to form primarily at the expense of N-methylation product **63c** (minor product of this reaction), but some O-methylation product (**9c**) was also consumed. An amount of **3** formed that was commensurate with the amount of **25c** produced. After two weeks, further crossover product was observed to form at the expense of major product **9c**. It is not clear from these experiments whether formation of **63c** and **9c** from **3** + MeOTf is reversible (i.e., whether **18** reacts with MeOTf formed by reversal

of **63c** and/or **9c** to **3** + MeOTf, or whether crossover product **25c** is formed by direct S_N2 reactions of **18** with **63c** and/or **9c**). A full description of this experiment is available in section 3.7.1.

Scheme 2-11. Example of a "crossover experiment" investigating reversibility of reaction of **3** + MeOTf using 1,3,5-trimethoxybenzene as internal standard, and "crossover nucleophile" **18**. The crossover product is compound **25c**. After a number of days, both of the products of the reaction of **3** with MeOTf were no longer present in solution.

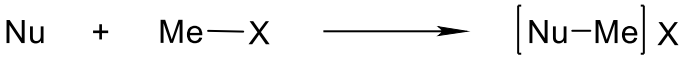


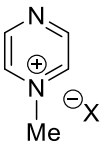
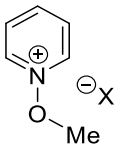
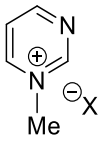
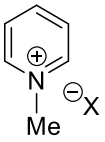
2.3.2. Results from Computational Investigation on the Ambident Reactivity of Diazine *N*-Oxides

The experimental investigation outlined in section 2.3.1 indicates that the ambident nucleophiles pyrazine *N*-oxide (**1**) and quinoxaline *N*-oxide (**2**) (with competing N and O nucleophilic sites) undergo preferential alkylation on nitrogen regardless of the nature of the alkylating agent used, (i.e., independent of whether the electrophile is hard or soft). Ambident nucleophile pyrimidine *N*-oxide (**3**), by contrast, has been shown to undergo preferential O-methylation by MeOTf. In order to be able to understand and rationalise the outcomes of the reactions described above, high level quantum chemical calculations

at the DLPNO-CCSD(T)/def2-TZVPPD/SMD(CH_3CN)//M06-2X-D3/6-311+G(d,p)/SMD(CH_3CN) level of theory were carried out by Prof. Martin Breugst, a collaborator of the Byrne group, at TU Chemnitz, Germany. The aim of this computational investigation was to determine the relative Gibbs energies of the reactants, transition states and products of the reactions of each of compounds **1**, **3**, **18** (pyrazine), and **21** (pyridine *N*-oxide) (structures shown in Chart 2-1, Scheme 2-5 and 2-6) with MeI and MeOTf. The reactions of pyrimidine (**20**) and pyridine (**36**) with MeI and MeOTf were also investigated by Prof. Breugst in the same manner. The computational results can be used to estimate the Gibbs energy of activation ($\Delta G^{\ddagger}$) and standard enthalpy and Gibbs energy of reaction ($\Delta_r H°$ and $\Delta_r G°$, respectively) for each process.

Table 2-10. Calculated $\Delta G^{\ddagger}$, $\Delta_r H°$, $\Delta_r S°$ and $\Delta_r G°$ values for methylation of nucleophiles **7**, **8**, **27**, and **28** by MeI and MeOTf in CH_3CN. Enthalpies, Entropies and Gibbs energy values (in kJ mol^{-1}, or J K^{-1} mol^{-1} in the case of $\Delta_r S°$ values) were calculated by Prof. Martin Breugst at TU Chemnitz, Germany.[a]



#	Nu	X	Product & Number		$\Delta G^{\ddagger}$ (kJ mol^{-1})	$\Delta_r G°$ (kJ mol^{-1})	$\Delta_r S°$ [b] (J K^{-1} mol^{-1})	$\Delta_r H°$ (kJ mol^{-1})
(i)	**18**	I		**25b**	+131	−21	−55	−37
(ii)	**18**	OTf		**25c**	+107	−90	−2	−90
(iii)	**21**	I		**31b**	+123	−7	−55	−24
(iv)	**21**	OTf		**31c**	+97	−75	−2	−76
(v)	**20**	I		**29b**	+130	−23	−55	−39
(vi)	**20**	OTf		**29c**	+106	−91	−2	−91
(vii)	**36**	I		**37b**	+120	−48	−55	−64
(viii)	**36**	OTf		**37c**	+96	−117	−2	−117

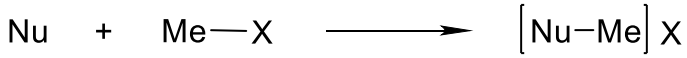
[a] The values shown above were calculated at the DLPNO-CCSD(T)/def2-TZVPPD/SMD(CH3CN)//M06-2X-D3/6-311+G(d,p)/SMD(CH3CN) level of theory, with a confidence interval of ±2 kJ mol^{-1} by Prof. Martin Breugst at TU Chemnitz, Germany.

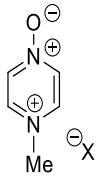
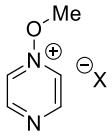
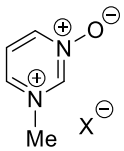
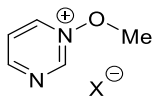
[b] The values of entropies have a confidence interval of ±2 J K^{-1} mol^{-1}.

The accuracy and predictive capability of this computational method have been verified by the agreement of the $\Delta G^{\ddagger}$ values determined experimentally and computationally for the reaction of pyrazine *N*-oxide (**1**) with MeI which is shown below in Scheme 2-13. The results of the computational investigations of the methylation reactions of **18**, **21**, **20** and

36 are presented in Table 2-10 above. Compounds **18**, **20** and **36** undergo N-methylation, and compound **21** undergoes O-methylation. These results provide representative values of $\Delta G^{\ddagger}$, $\Delta_r H°$ and $\Delta_r G°$ for N- and O-methylation reactions in which there is no ambiguity over the site of methylation. Unsurprisingly, the reactions involving MeOTf have systematically smaller calculated $\Delta G^{\ddagger}$ values and are more exergonic than the reactions involving MeI. The values of $\Delta G^{\ddagger}$ and $\Delta_r G°$ for methylation of **18** by MeI are very similar to the corresponding values for **20** (see Table 2-10 entries (i) and (v)). The $\Delta G^{\ddagger}$ and $\Delta_r G°$ values for the reactions of **18** and **20** with MeOTf are also very similar (see Table 2-10 entries (ii) and (vi)). This suggests that the nucleophilicities and Lewis basicities of **18** and **20** are very similar. The reactions involving pyridine (**36**; Table 2-10 entries (vii) and (viii)) are both more kinetically and thermodynamically favourable than the corresponding reactions of **18** and **20** with the two methylating agents. This is consistent with a report by Mayr, Ofial and co-workers indicating greater Lewis basicity of **36** compared to **20** in reactions with benzhydrylium ions.[71]

Table 2-11. Calculated $\Delta G^{\ddagger}$, $\Delta_r H°$, $\Delta_r S°$ and $\Delta_r G°$ values for methylation of nucleophiles **1** and **3** by MeI and MeOTf in CH_3CN. Enthalpies, Entropies and Gibbs energy values (in kJ mol^{-1}, or J K^{-1} mol^{-1} in the case of $\Delta_r S°$ values) were calculated by Prof. Martin Breugst at TU Chemnitz, Germany. [a]



#	Nu	X	Product & Number	$\Delta G^{\ddagger}$ (kJ mol^{-1})	$\Delta_r G°$ (kJ mol^{-1})	$\Delta_r S°$ [b] (J K^{-1} mol^{-1})	$\Delta_r H°$ (kJ mol^{-1})
(i)	**1**	I	 **12b**	+133	−20	−55	−37
(ii)	**1**	OTf	**12c**	+108	−88	−2	−90
(iii)	**1**	I	 **7b**	+140	+31	−55	+14
(iv)	**1**	OTf	**7c**	+115	−38	−2	−38
(v)	**3**	I	 **63b**	+138	+4	−55	−13
(vi)	**3**	OTf	**63c**	+113	−64	−2	−66
(vii)	**3**	I	 **9b**	+127	+38	−55	+3
(viii)	**3**	OTf	**9c**	+103	−48	−2	−49

[a] The values shown above were calculated at the DLPNO-CCSD(T)/def2-TZVPPD/SMD(CH3CN)//M06-2X-D3/6-311+G(d,p)/SMD(CH3CN) level of theory, with a confidence interval of ±2 kJ mol^{-1} by Prof. Martin Breugst at TU Chemnitz, Germany.

[b] The values of entropies have a confidence interval of ±2 J K^{-1} mol^{-1}.

The results of the computational investigations of the methylation reactions of **1** and **3** are presented in Table 2-11 above. The reaction of pyrazine *N*-oxide (**1**) with MeOTf was found computationally to result in kinetically and thermodynamically preferred N-methylation (compare Table 2-11 entries (ii) and (iv)). This calculation indicates that methylation of **1** by MeOTf is an irreversible process at room temperature (regardless of the site of methylation), in agreement with the results of the "crossover experiments" (see Schemes 2-9 and 2-10 above and accompanying discussion). The relative magnitudes of $\Delta G^{\ddagger}$(N) and $\Delta G^{\ddagger}$(O) calculated for this reaction suggest that a small amount of O-methylated product (*ca.* 5 – 7%) should be produced, as is observed experimentally (N/O methylation ratio = 95:5 for reaction at 20 °C; see Table 2-11 entry (ii)). The process of estimating N/O ratios using values of $\Delta G^{\ddagger}$ is described below in section 2.3.3. (see Equation 2.4 and surrounding discussion).

The reaction of **1** with MeI was also found to result in kinetically and thermodynamically preferred N-methylation (compare Table 3 entries (i) and (iii)), which is consistent with the results of the crossover experiments (where the formation of **12b** is found to be irreversible). This reaction has been observed experimentally to be very slow. Only a small amount of conversion had occurred after several days, consistent with the high activation barrier found computationally (shown in Table 2-11) and determined through a kinetic investigation (described below). In contrast to the reaction of **1** with MeOTf (above), O-methylation of **1** by MeI was found computationally to be thermodynamically disfavoured and therefore reversible (see Table 2-11 entry (iii)). No O-methyl adduct (**7b**) was observed experimentally for this reaction, which is consistent with kinetically disfavoured and reversible O-methylation.

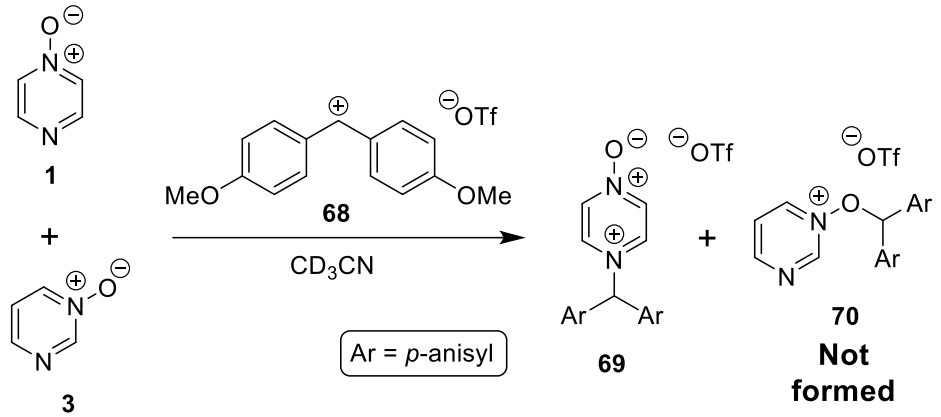
The $\Delta G^{\ddagger}$(N) and $\Delta_r G°$(N) values for N-methylation of **1** (by MeOTf or MeI) are similar to the corresponding values for diazines **18** and **20** (compare Table 2-11 entry (ii) with Table 2-10 entries (ii) and (vi), and Table 2-11 entry (i) with Table 2-10 entries (i) and (v)). In contrast, the $\Delta G^{\ddagger}$(O) and $\Delta_r G°$(O) values for O-methylation of **1** (by MeOTf or MeI) are significantly less favourable than the corresponding reactions of *N*-oxide **21** (compare Table 2-11 entry (iv) with Table 2-10 entry (iv), and Table 2-11 entry (iii) with Table 2-10 entry (iii)). The implication of this is that the oxygen site of **1** is deactivated relative to the oxygen site of **21**, both as a nucleophile and as a Lewis base. Literature precedent demonstrates that the remote deactivation of a Lewis basic nitrogen site is possible.[72]

The calculations performed by Prof. Breugst on the reaction of pyrimidine *N*-oxide (**3**) with MeOTf indicate that, despite the fact that N-methylation (formation of **63c**) is thermodynamically favoured over O-methylation (formation of **9c**), the kinetically preferred process in this reaction is O-methylation (compare Table 2-11 entries (vi) and (viii)). The difference between the calculated values of $\Delta G^{\ddagger}$(N) and $\Delta G^{\ddagger}$(O) suggests that a small amount of N-methylation (*ca.* 1–3%) should occur. These results are in quite close agreement with the experimental observations – O-methylation is indeed favoured, and approximately 7% of the product formed is N-methylation adduct **63c** (in CD_3CN or $(CD_3)_2SO$; see Table 2-8 entries (x) and (xi))). These calculations indicate that both

reactions are essentially irreversible (however, this may not be the case; see the discussion of the "crossover experiment" involving **3** + MeOTf above). The calculations on the reaction of **3** with MeI indicate that both O- and N-methylation (formation of **9b** and **63b**, respectively) are reversible. O-Methylation was found to be kinetically preferred, again despite the fact that this process is less thermodynamically favourable than N-methylation (compare Table 2-11 entries (v) and (vii)). As no product formation was observed experimentally when this reaction was attempted in CD_3CN or MeCN, it is not possible to verify the applicability of these particular computational results.

The calculated Gibbs energies of activation for N- and O-methylation of pyrimidine *N*-oxide **3** (by MeI or MeOTf), while higher than the $\Delta G^{\ddagger}$ values for comparable reactions of similar compounds (e.g., pyrazine *N*-oxide (**1**), pyrazine (**18**), pyridine *N*-oxide (**21**) and pyridine (**36**)), are not especially different to those $\Delta G^{\ddagger}$ values (compare Table 2-11 entry (vi) with Table 2-10 entries (ii) and (vi), Table 2-11 entry (v) with Table 2-10 entries (i) and (v), Table 2-11 entry (viii) with Table 2-10 entry (iv), and Table 2-11entry (vii) with Table 2-10 entry (iii)). However, comparison of the $\Delta_r G°$ values for the same reactions indicates that both O- and N-methylation reactions of pyrimidine *N*-oxide **3** are far less thermodynamically favourable than the corresponding reactions of **1**, **18**, **21** and **36**. This computational observation has been verified experimentally through a thermodynamic "competition experiment" in which product **69** (derived from pyrazine *N*-oxide (**1**) in a reversible reaction) is formed to the complete exclusion of **70** (derived from pyrimidine *N*-oxide (**3**)) when **1**, **3** and benzhydrylium ion **68** are mixed in CD_3CN (see Scheme 2-12 below). It is possible that the O and N nucleophilic/Lewis basic sites of **3** are deactivated in a similar manner to the O site of **1**.

Scheme 2-12. "Competition experiment" between reversible reactions of **1** and **3** with benzhydrylium ion **68**. The product derived from the alkylation of **1** (compound **69**) is formed to the complete exclusion of the product formed by the alkylation of **3** (compound **70**). The experimental data concerning this "competition experiment" is given in section 3.8.

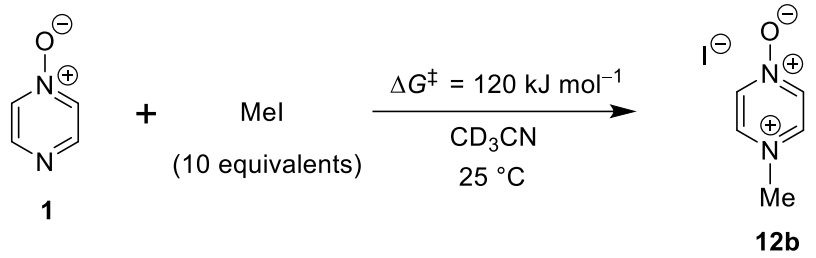


Computationally determined values of $\Delta_r S°$ do not differ greatly from each other across all reactions of MeI with **1**, **3**, **18**, **21**, **20** and **36**, or across all reactions of MeOTf with the same nucleophiles, regardless of whether N- or O-methylation is occurring. Across

all reactions of MeI in Table 3, $\Delta_r S°$ remains constant around -55 ± 2 J $K^{-1}mol^{-1}$, while a value of -2 ± 2 J $K^{-1}mol^{-1}$ was observed across the reactions of MeOTf (using 99% confidence intervals). Therefore, the computational data suggest that enthalpy changes are primarily responsible for dictating the differences between the $\Delta_r G°$ values in the various reactions in Table 2-10 and Table 2-11. However, it is not possible to unambiguously ascribe the differences in $\Delta_r H°$ to specific effects.

In order to verify the applicability of the computational methods discussed above to determine the magnitudes of activation barriers, a kinetic investigation was conducted on the reaction of pyrazine *N*-oxide (**1**) with MeI in CD_3CN at 25 °C. During this experiment, ^{1}H NMR spectroscopy was used to determine the concentrations of the reactants and product (**12b**; see Scheme 2-13 below). The experiment was conducted under pseudo-first order conditions, with MeI present in ten-fold excess over **1**. Using the method described in detail in section 3.9, an approximate $\Delta G^‡$ value for this reaction was determined to be 1.2×10^2 kJ mol^{-1}. This value is within 10% of the $\Delta G^‡$ values predicted for this reaction using the DLPNO-CCSD(T)/def2-TZVPPD/SMD(CH_3CN)//M06-2X-D3/6-311+G(d,p)/SMD] method (133 kJ mol^{-1}, see Table 2-11 entry (i)). This relatively close agreement between computational and experimental results demonstrates that this computational method is capable of modelling kinetic phenomena of this type rather accurately.

Scheme 2-13. The reaction of **1** + MeI in CD_3CN at 25 °C under pseudo-first order conditions (excess MeI) was monitored by ^{1}H NMR spectroscopy to enable determination of an approximate $\Delta G^‡$ value for the reaction at 25 °C.

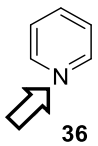
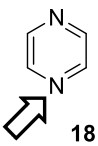
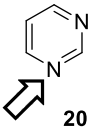
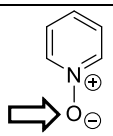
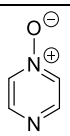
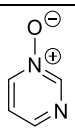


1 **12b**

Further computational data was provided by Prof. Martin Breugst with the goal of enabling attempts to rationalise the behaviour of the ambident nucleophiles **1** – **3** in reactions with methylating agents. As mentioned previously (at the end of section 1.3), recent works have attempted to quantify "global hardness" by ascribing the "hardness" of a given molecule to certain physical molecular properties of that molecule.[73–75] Despite the existence of these methods, the "global" HSAB theory refers specifically to separated species and are not expected to allow quantification of "local hardness" (i.e., they do not have the ability to differentiate between strongly interacting nucleophilic sites such as those in ambident nucleophiles in terms of relative "softness" and "hardness"). Derivation of functions that reliably indicate the "local hardness" and "local softness" of sites in a molecule (such as an ambident nucleophile) has proved a difficult endeavour.[10,76] At present, such approaches cannot be applied without ambiguity. On the basis that oxygen is more electronegative than nitrogen, it may be reasonably anticipated

that the oxygen site of a diazine *N*-oxide such as **1** – **3** should be harder than the nitrogen site. However, although there is a formal negative charge on the *N*-oxide oxygen atoms in these compounds, it is not clear which nucleophilic site in each ambident nucleophile should have the highest negative charge density, thereby potentially complicating the issue. To probe this question, Prof. Breugst calculated the charge distribution for the ambident *N*-oxides with a variety of methods (ChelpG, Merz−Singh−Kollman, natural bond order (NBO), and atoms in molecules (AIM)), the results of which are shown below in Table 2-12. However, through analysis of the results of the charge density calculations in Table 2-12, there was no uniform agreement between methods on which site bears the highest negative charge density in compounds **1** and **3**. The NBO method predicts the oxygen atom of both **1** and **3** to bear the greater negative charge density, and the Merz-Singh-Kollman and ChelpG methods predict the nitrogen atom of both **1** and **3** to bear the greater negative charge. According to the computational data, N-methylation of both **1** and **3** results in a minor shortening of the *N*-oxide N—O bond. The calculated N—O bond lengths of diazine *N*-oxides **1** and **3** and N-methyldiazinium cations **12** and **63** are, respectively, 1.27 Å, 1.29 Å, 1.25 Å and 1.27 Å. These bond lengths (and other details pertaining to the computational analysis) may be found in section 4 of Appendix A. O-methylation of **1** and **3** results in a lengthening of the N—O bond (to 1.36 Å for each of **7** and **9**, the O-methylated cationic derivatives of **1** and **3**). O-methylation of **1** or **3** removes the favourable electrostatic interaction between N and O, and also diminishes the partial resonance of the *N*-oxide with the aromatic system, thereby removing resonance stabilisation effects that may help to stabilise the positive charge in the product. This may contribute to making N-methylation of **1** and **3** more thermodynamically favourable than O-methylation.

Table 2-12. Charge density calculations using different computational methods (NBO,[77] Merz-Singh-Kollman,[78,79] ChelpG,[80] AIM)[81] at the M06-2X-D3/6-311+G(d,p)/SMD(CH_3CN) level of theory. The values shown below were calculated by Prof. Martin Breugst at TU Chemnitz, Germany.

Nu	 **36**	 **18**	 **20**	 **21**	 **1**		 **3**	
Nucleophilic site	N	N	N	O	N	O	N	O
NBO	−0.514	−0.460	−0.528	−0.656	−0.490	−0.589	−0.484	−0.648
Merz-Singh-Kollman	−0.842	−0.564	−0.917	−0.719	−0.732	−0.679	−0.704	−0.300
ChelpG	−0.719	−0.558	−0.921	−0.710	−0.745	−0.700	−0.706	−0.665
AIM	−1.245	−1.215	−1.238	−0.669	−1.205	−0.616	−1.228	−1.215

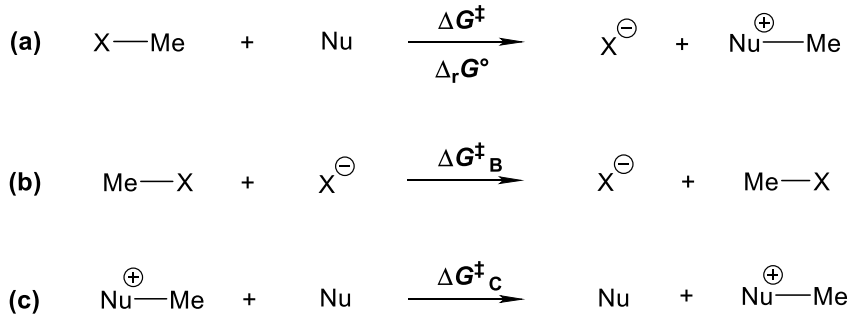
2.3.3. Activation Barrier Calculations Using Marcus Theory

Noting the deficiencies of the HSAB principle, Mayr and co-workers have advanced Marcus theory for rationalising the outcomes of reactions of ambident nucleophiles.[1] The Marcus equation (shown below as Equation 2.1) allows $\Delta G^{\ddagger}$ to be separated out into its contributions from $\Delta_r G°$ (the standard Gibbs energy of reaction) and $\Delta G^{\ddagger}_{int}$, the Marcus intrinsic barrier.

$$\Delta G^{\ddagger} = \Delta G^{\ddagger}_{\text{int}} + \frac{\Delta_r G°}{2} + \frac{(\Delta_r G°)^2}{16\Delta G^{\ddagger}_{\text{int}}} \quad (2.1)$$

A detailed discussion of the principles underlying Marcus theory and how they may be applied to ambident reactivity is available in section 1.4. In reactions of ambident nucleophiles with competing sites of differing nucleophilicity, the different nucleophilic sites have different values of each of $\Delta G^{\ddagger}_{int}$ and $\Delta_r G°$. Mayr and co-workers have suggested that the selectivities in such reactions can be rationalised through an appraisal of the factors that influence the values of the two parameters in the Marcus equation ($\Delta G^{\ddagger}_{int}$ and $\Delta_r G°$).[1] They have employed this approach to qualitatively rationalise the outcomes of reactions of a variety of ambident nucleophiles.[1,82–86] By substituting the $\Delta G^{\ddagger}_{int}$ and $\Delta_r G°$ values provided by Prof. Breugst into the Marcus equation (Equation 2.1 above), values of $\Delta G^{\ddagger}$ for the reactions of interest were calculated. The process by which values of $\Delta G^{\ddagger}$ and the intrinsic barrier ($\Delta G^{\ddagger}_{int}$) were calculated for each of the reactions of compounds **1** and **3** with MeI and MeOTf is described in detail below.

Scheme 2-14. (a) Methyl transfer reaction from MeX to Nu, with Gibbs energy of activation = $\Delta G^{\ddagger}$ and $\Delta_r G° \neq 0$; (b) Methyl transfer identity reaction from MeX to X^-, with Gibbs energy of activation = $\Delta G^{\ddagger}_B$ and $\Delta_r G° = 0$; (c) Methyl transfer identity reaction from Nu^+—Me to Nu, with Gibbs energy of activation = $\Delta G^{\ddagger}_C$ and $\Delta_r G° = 0$.

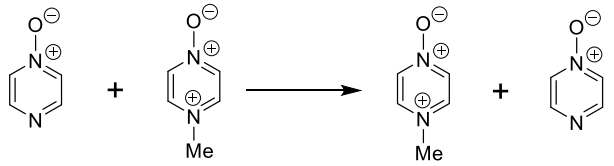
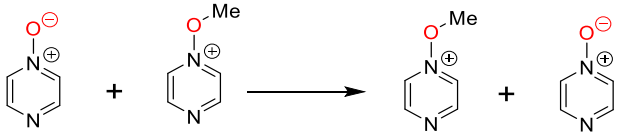
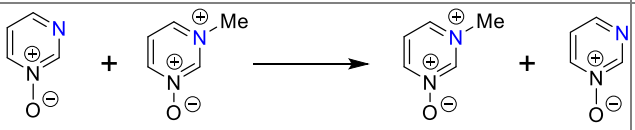
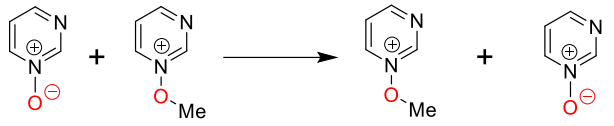
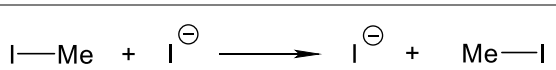
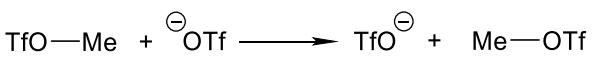


Consider an S_N2 reaction of a nucleophile (Nu) with an alkyl electrophile such as MeX (e.g., X = I, OTf, etc.), with a Gibbs energy of activation $\Delta G^{\ddagger}$ and a standard Gibbs energy of reaction $\Delta_r G°$. Such a reaction can be thought of as a methyl group transfer from X^- to the nucleophile (see Scheme 2-9 (a)). To calculate $\Delta G^{\ddagger}$ using the Marcus equation (see Equation 2.1) the Marcus intrinsic barrier ($\Delta G^{\ddagger}_{int}$) must be determined. In order to access the value of the Marcus intrinsic barrier ($\Delta G^{\ddagger}_{int}$) for the S_N2 reaction of Nu + MeX, the Gibbs energies of activation for the reactions shown in Scheme 2-14 (b) and (c) must be determined. These methyl group transfer reactions are identity reactions since the

products and the reactants are the same (see section 1.4). They are thermoneutral (i.e., $\Delta_r G° = 0$ for each one). The Gibbs energy of activation for methyl transfer from Me—X to X^- is $\Delta G^‡_B$, and the Gibbs energy of activation for methyl transfer from Nu^+—Me to Nu is $\Delta G^‡_C$. Using the Gibbs energies of activation of the identity reactions shown in Scheme 2-14(b) and (c), the intrinsic barrier ($\Delta G^‡_{int}$) for the reaction of the nucleophile (Nu) with MeX (Scheme 2-14(a)) can be calculated using Equation 2.2 (i.e., $\Delta G^‡_{int}$ for the methylation of the nucleophile is taken to be the average of the Gibbs energies of activation of the identity reactions shown in Scheme 2-14(b) and (c)):

$$\Delta G_0^‡ = \frac{1}{2}\left(\Delta G_B^‡ + \Delta G_C^‡\right) \qquad (2.2)$$

Table 2-13. $\Delta G^‡$ values (in kJ mol^{-1}) for methyl transfer identity reactions of **1** and **3** at both the N and O nucleophilic sites, and of iodide and triflate were calculated by Prof. Martin Breugst at TU Chemnitz, Germany, at the DLPNO-CCSD(T)/def2-TZVPPD/SMD(CH3CN)//M06-2X-D3/6-311+G(d,p)/SMD(CH3CN) level of theory.[a]

Reaction	Compound Number	Site of Methylation	$\Delta G^‡$ of Identity Reaction
	**1**	N	176
	**1**	O	142
	**3**	N	167
	**3**	O	125
	Iodide	I	112
	Triflate	O	123

[a] The values shown above were calculated by Prof. Martin Breugst at TU Chemnitz, Germany.

Values of Gibbs energies of activation for methyl group transfer identity reactions of the type shown in Scheme 2-14(b) and (c) were calculated for nucleophiles **1** and **3** and also iodide and triflate (see Table 2-13 above). These calculations were done by Prof. Martin Breugst at the DLPNO-CCSD(T)/def2-TZVPPD/SMD(CH3CN)//M06-2X-D3/6-311+G(d,p)/SMD(CH3CN) level of theory.

Using the $\Delta G^{\ddagger}$ values calculated for the methyl transfer identity reactions (found in Table 2-13), values of the intrinsic barrier ($\Delta G^{\ddagger}_{int}$) were calculated for each of the reactions of compounds **1** and **3** with MeI and MeOTf using Equation 2.2 (see Table 2-14, specifically the "Marcus $\Delta G^{\ddagger}$" column).

Zhu and co-workers have challenged the applicability of Marcus theory in recent years, and have developed an alternative equation to rationalize the outcomes of hydride transfer reactions.[61,87–90] This alternative also incorporates an intrinsic barrier or a proxy thereof. In addition to using the Marcus equation, an adaptation of the equation put forward by Zhu (see Equation 2.3 below) was used to calculate $\Delta G^{\ddagger}$ values for the methylation reactions of nucleophiles **1** and **3**. This adaptation of the Zhu equation is shown in Equation 2.3.

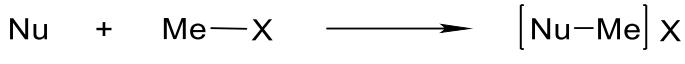
$$\Delta G^{\ddagger} = \frac{1}{2}\left(\Delta G^{\ddagger}_{\mathrm{XMe/X}} + \Delta G^{\ddagger}_{\mathrm{NuMe/Nu}}\right) + \frac{\Delta_r G^{\circ}}{2} \qquad (2.3)$$

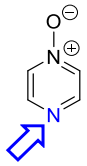
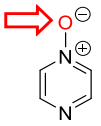
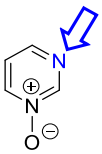
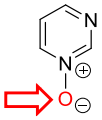
where $\Delta G^{\ddagger}_{\mathrm{XMe/X}} = \Delta G^{\ddagger}_{\mathrm{B}}$ from Scheme 2-14(b), $\Delta G^{\ddagger}_{\mathrm{NuMe/Nu}} = \Delta G^{\ddagger}_{\mathrm{C}}$ from Scheme 2-14(c) (i.e., $\Delta G^{\ddagger}_{\mathrm{XMe/X}}$ and $\Delta G^{\ddagger}_{\mathrm{NuMe/Nu}}$ are the Gibbs energies of activation for the methyl group transfer identity reactions shown in Scheme 2-14(b) and (c), for which $\Delta_r G^{\circ} = 0$), and $\Delta G^{\ddagger}$ and $\Delta_r G^{\circ}$ are, respectively, the Gibbs energy of activation and standard Gibbs energy of reaction for the methyl group transfer reaction shown in Scheme 2-14(a).

The first term in Equation 2.3 (involving the activation barriers for the identity reactions) is identical to the expression for the Marcus intrinsic barrier shown in Equation 2.2, and the second term is identical to the second term of the Marcus equation (Equation 2.1 above). Hence, the Marcus equation and Zhu equation differ only in the exclusion of the quadratic term of the Marcus equation from the latter equation.

Using the $\Delta G^{\ddagger}$ values calculated for the methyl transfer identity reactions (Table 2-13), values of the intrinsic barrier ($\Delta G^{\ddagger}_{int}$) were calculated for each of the reactions of compounds **1** and **3** with MeI and MeOTf using Equation 2.1 (Marcus equation) and Equation 2.3 (Zhu equation). It is noteworthy that, for both ambident nucleophiles **1** and **3**, the intrinsic barrier for methyl transfer to oxygen ($\Delta G^{\ddagger}_{int}$(O)) is lower than that for methylation of nitrogen ($\Delta G^{\ddagger}_{int}$(N)) (e.g., compare Table 2-14 entries (iii) and (i), and entries (vii) and (v)). Hoz and co-workers previously established through computational investigations that the $\Delta G^{\ddagger}_{int}$ values associated with reactions of nucleophiles centred on 2nd row elements depend on the identity of the element at the nucleophilic site, with $\Delta G^{\ddagger}_{int}$ decreasing in the order C > N > O > F (i.e., from left to right across the periodic table).[91] Discussion relevant to these trends in the values of intrinsic barriers may be found in section 1.4.1. The lower intrinsic barriers (or, intrinsic preference) for O-alkylation over N-alkylation observed for **1** and **3** in the values calculated in Table 2-14 are in line with this general trend.

Table 2-14. Values of intrinsic barriers ($\Delta G^{\ddagger}_{int}$) for methylation reactions of nucleophiles **1** and **3**, and derived values of $\Delta G^{\ddagger}$ for methylation reactions of these nucleophiles (Scheme 2-14(a) with Nu = N or O nucleophilic site of **1** or **3**) calculated using Marcus equation (Equation 2.1) and Zhu equation (Equation 2.3) by employing values of $\Delta_r G°$ from Table 2-13. The site of methylation of each nucleophile is indicated by an arrow. [a]



Nu	#	Product Number	X	$\Delta G^{\ddagger}$ for Identity Reactions		$\Delta G^{\ddagger}_{int}$	$\Delta_r G°$	Marcus $\Delta G^{\ddagger}$	Zhu $\Delta G^{\ddagger}$	DFT $\Delta G^{\ddagger}$
				X^- + MeX	Nu + MeNu					
	i	**12c**	OTf	123	176	+149.5	−88	+108.7	+105.5	+108
	ii	**12b**	I	112	176	+144	−20	+134.2	+134	+133
	iii	**7c**	OTf	123	142	+132.5	−38	+114.3	+113.5	+115
	iv	**7b**	I	112	142	+127.0	+31	+143.0	+142.5	+140
	v	**63c**	OTf	123	167	+145.0	−64	+114.8	+113	+113
	vi	**63b**	I	112	167	+139.5	+4	+141.5	+141.5	+138
	vii	**9c**	OTf	123	125	+124.0	−48	+101.2	+100	+103
	viii	**9b**	I	112	125	+118.5	+21	+129.2	+129	+127

[a] The Gibbs energy values have units of kJ mol^{-1}.

The value calculated for $\Delta G^{\ddagger}_{int}$ for each reaction was substituted into the Marcus equation (Equation 2.1) and Zhu equation (Equation 2.3) along with the $\Delta_r G°$ values calculated for the reaction in question (these values are shown in Table 2-11 and in Table 2-14), enabling calculation of a value for $\Delta G^{\ddagger}$ according to the Marcus and Zhu equations for the reaction of Nu + MeX. For ambident nucleophiles **1** and **3**, there are two $\Delta G^{\ddagger}$ values – one for reaction at each of the nucleophilic sites of the ambident nucleophile. Comparison of the $\Delta G^{\ddagger}$ values obtained using the Marcus equation (shown in the "Marcus $\Delta G^{\ddagger}$" column in Table 2-14) with the $\Delta G^{\ddagger}$ values directly calculated as described above (values from Table 2-11, reproduced in the "DFT $\Delta G^{\ddagger}$" column in Table 2-14) shows a close correspondence between the two methods. The $\Delta G^{\ddagger}$ values calculated using the adapted Zhu equation (Equation 2.3) are also very similar to the values calculated using the Marcus equation (see Table 2-14). This is because the quadratic term of Equation 2.1 is very small in all reactions investigated here due to the relatively small $\Delta_r G°$ values of

these reactions. Consequently, there is close agreement between the $\Delta G^{\ddagger}$ values calculated using each of the methods.

For these nucleophiles, the ratios of the products (i.e., N/O ratio) predicted by the DFT calculations, Marcus calculations and Zhu calculations were obtained using Equation 2.4.

$$\frac{k_{\mathrm{N}}}{k_{\mathrm{O}}} = e^{-\left(\frac{\Delta\Delta G^{\ddagger}}{RT}\right)} = e^{-\left(\frac{\Delta G^{\ddagger}(\mathrm{N}) - \Delta G^{\ddagger}(\mathrm{O})}{RT}\right)} \qquad (2.4)$$

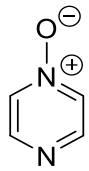
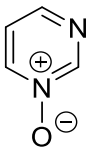
Where k_{N} and $\Delta G^{\ddagger}$(N) are the rate constant (in L mol^{-1} s^{-1}) and Gibbs energy of activation (kJ mol^{-1}), respectively, for N-methylation. Subsequently, k_{O} and $\Delta G^{\ddagger}$(O) are the rate constant (in L mol^{-1} s^{-1}) and Gibbs energy of activation (kJ mol^{-1}), respectively, for O-methylation. R is the universal gas constant, and the temperature, T, was set to 298 K. Using Equation 3.4, the N/O product ratios of reactions of 1 and 3 with MeI and MeOTf could be estimated using the $\Delta G^{\ddagger}$ values produced by the use of each of the computational methods. Using the Marcus equation specifically, and the "Marcus $\Delta G^{\ddagger}$" values from Table 2-14, the product ratio calculated in this manner for methylation of **1** by MeOTf was 90:10 ± 2 (in favour of N-methylation), and for **1** + MeI the ratio was 97:3 ± 2 (O-methylation was also calculated to be reversible, (i.e., $\Delta_{\mathrm{r}}G° > 0$; experimentally no O-methylation is observed)). The product ratio calculated for methylation of **3** by MeOTf was 0.4:99.6 ± 2 (in favour of O-methylation), and for **3** + MeI the ratio was calculated to be 1:99 ± 2 (both O and N-methylation were calculated to be reversible, (i.e., $\Delta_{\mathrm{r}}G° > 0$, and no product formation was observed experimentally)). An example of how these calculations are carried out (using Equation 2.4) is available in section 3.9.1.

Shown in Table 2-15 are the N/O product ratios predicted by the use of the values of $\Delta G^{\ddagger}$ found in Table 2-14 and Equation 2.4. There is close agreement between the $\Delta G^{\ddagger}$ values calculated using Equation 2.1 (Marcus equation), Equation 2.3 (Zhu equation) and those calculated directly at the DLPNO-CCSD(T)/def2-TZVPPD/SMD//M06-2X-D3/6-311+G(d,p)/SMD level of theory (as can be seen by comparison of the values in Table 2-14). Naturally, therefore, the product ratios determined using these three different methods of calculation agree quite closely (see results in Table 2-15). All of these methods of determining the product ratios are close to the true values observed experimentally, as can be seen by comparison of the computationally determined product ratios in Table 2-15 with the experimentally determined product ratios in Table 2-8 above (and reproduced in Table 2-15 for ease of comparison).

The experimentally observed ratio of N- to O-methylation for the reaction of **1** + MeOTf was 95:5 (see Table 2-8, entry (ii)). Direct calculation of the $\Delta G^{\ddagger}$ values at the DLPNO-CCSD(T)/def2-TZVPPD/SMD(CH_3CN)//M06-2X-D3/6-311+G(d,p)/SMD(CH_3CN)] level of theory indicated a N/O ratio of 94:6 for this reaction (Table 2-15 entry (v)), while calculation of the N/O ratio using the Marcus equation gave a ratio of 90:10 (see Table 2-15 entry (i)). Use of the Zhu equation gave a N/O ratio of 96:4 (see Table 2-15 entry (iii)). The experimentally observed ratio of N- to O-methylation for the reaction of **3** + MeOTf was 7:93 (see Table 2-8, entry (x)). The DFT calculations indicated a ratio of 2:98

for this reaction (Table 2-15 entry (xi)), while calculation of the N/O ratio using the Marcus equation gave a ratio of 0.4 : 99.6, (see Table 2-15 entry (vii)) and calculation using the Zhu equation gave a ratio of 0.5 : 99.5 (see Table 2-15 entry (ix)). That the experimental selectivities (in N- vs. O-methylations of **1** and **3** by MeOTf) are reproduced quite closely using the Marcus and Zhu equations and direct computation indicates that these methods are highly useful in understanding the factors that control Gibbs energies of activation in nucleophilic substitution reactions.

Table 2-15. Calculated ratios of N vs O methylation for reactions of nucleophiles **1** and **3** with MeOTf and MeI. The Gibbs energy values have units of kJ mol^{-1}.

Nucleophile (Nu) and Product Number	Entry	Method	Electrophile	$\Delta\Delta G^{\ddagger}$	$\left(\frac{\Delta\Delta G^{\ddagger}}{RT}\right)$	N/O Ratio	
						Calc. [a]	Expt. [b]
 **1**	(i)	Marcus	MeOTf	−5.4	−2.2	90 : 10	95 : 5
	(ii)	Marcus	MeI	−8.8	−3.6	97 : 3	> 99 : 1
	(iii)	Zhu	MeOTf	−8.0	−3.2	96 : 4	95 : 5
	(iv)	Zhu	MeI	−8.5	−3.4	97 : 3	> 99 : 1
	(v)	DFT	MeOTf	−7.0	−2.8	94 : 6	95 : 5
	(vi)	DFT	MeI	−7.0	−2.8	94 : 6	> 99 : 1
 **3**	(vii)	Marcus	MeOTf	+13.6	+5.5	0.4 : 99.6	7 : 93
	(viii)	Marcus	MeI	+12.3	+5.0	0.7 : 99.3	No reaction
	(ix)	Zhu	MeOTf	+13.0	+5.3	0.5 : 99.5	7 : 93
	(x)	Zhu	MeI	+12.5	+5.0	0.6 : 99.4	No reaction
	(xi)	DFT	MeOTf	+10.0	+4.0	1.7 : 98.3	7 : 93
	(xii)	DFT	MeI	+11.0	+4.4	1.2 : 98.8	No reaction

[a] The method by which these values were determined is described above, using the values of given in Table 2-14 in combination with Equation 2.4. A demonstration of how these values were calculated is found in section 3.9.1.

[b] The experimentally measured N/O ratios in this column were originally listed in Table 2-8 in section 2.3.1, and are reproduced here.

2.3.4. Rationalising the Observed Selectivities in Reactions of Diazine *N*-Oxides

The kinetic preference of compound pyrazine *N*-oxide (**1**) for N-methylation by the "soft" electrophile MeI (forming compound **12b**) and by the "hard" electrophile MeOTf (forming compound **12c**) has been demonstrated experimentally and computationally. The alkylation reactions of quinoxaline *N*-oxide (**2**) by MeI, MeOTf and benzhydrylium triflates (**24** or **58**) and of **1** by **24** or **58** are all also almost certainly irreversible, and all yield N-alkylated products preferentially or exclusively. The reaction of pyrimidine *N*-oxide (**3**) + MeOTf gives O-methylated product (**9c**) predominantly, and the

computational investigations detailed in section 2.3.3 indicate that this is due to the kinetic favourability of formation of **9c**. It is evident from these results that each nucleophile exhibits a preferred site of alkylation *which is independent of the nature of the electrophile used* (the nitrogen atom for **1** and **2**, and the oxygen atom for **3**) (i.e., these outcomes cannot be dictated by hard/soft acid/base interactions). A fundamentally different set of factors must dictate the observed selectivities in these reactions. An alternative rationale to account for these observations is described below.

Although the above evidence clearly shows that the HSAB principle does not apply in this set of reactions, and thereby renders unnecessary the identification of which nucleophilic site of each of **1** – **3** is "harder" and which is "softer", it is nonetheless appropriate to discuss the difficulty and ambiguity inherent in attempts at such identifications. The features that are employed to determine whether a reactant is hard or soft are charge (charge density), size, polarizability and electronegativity.[9,75,92–94] For "hard" bases or nucleophiles, the donor atom is typically negatively charged and/or has a local excess of electron density, and is of small size, low polarizability and high electronegativity. For "soft" bases or nucleophiles, the donor atom typically does not bear a formal negative charge and exhibits low negative charge density, and is of large size, high polarizability and low electronegativity. As mentioned previously, there was no agreement between the four computational methods employed in an attempt to determine which site bears the highest negative charge density in compounds **1** and **3** (see Table 2-12). As a result, there is ambiguity over which site of compounds **1** and **3** is the "hard site.

An alternative rationale, based on Marcus theory, is presented below to explain the results of the experimental and computational investigations described in section 2.3. In the following discussion, the intrinsic barriers for alkylation at the oxygen and nitrogen atoms of compounds **1** and **3** are referred to, respectively, as $\Delta G^{\ddagger}_{int}$(O) and $\Delta G^{\ddagger}_{int}$(N). The standard Gibbs energies of reaction for O- and N-alkylation are referred to, respectively, as $\Delta_r G°$(O) and Δ_rG°(N).

Although O-methylation is intrinsically preferred (i.e., the intrinsic barrier for O-alkylation is lower than that of N-alkylation) over N-methylation (for diazine *N*-oxides, and in general (see discussion of the work of Hoz and co-workers in section 2.3.3)[91] in reactions of **1** and **2**, the intrinsic preference for O-alkylation is modest. $\Delta G^{\ddagger}_{int}$(O) is calculated to be only 17 kJ mol^{-1} lower than $\Delta G^{\ddagger}_{int}$(N) for the reactions of **1** with MeI or MeOTf (compare Table 2-13 entry (i) vs. (iii), and entry (ii) vs. (iv)). The $\Delta_r G°$(N) values for these reactions are substantially more favourable than the corresponding $\Delta_r G°$(O) values. Consequently, the very favourable contribution of $\Delta_r G°$(N) to $\Delta G^{\ddagger}$(N) supersedes the favourable contribution of $\Delta G^{\ddagger}_{int}$(O) to $\Delta G^{\ddagger}$(O), such that $\Delta G^{\ddagger}$(N) is much lower than $\Delta G^{\ddagger}$(O) for alkylations of **1** and **2**. That is, the intrinsic favourability of O-alkylation is outweighed by the thermodynamic favourability of N-alkylation, so in these irreversible reactions, N-alkylation is kinetically preferred.

In the reactions of pyrimidine *N*-oxide (**3**) with MeOTf, the value of $\Delta_r G°$(N) is much less favourable with respect to $\Delta_r G°$(O) than is the case for the corresponding reaction of pyrazine *N*-oxide (**1**). $\Delta G^{\ddagger}_{int}$(O) is calculated to be 21 kJ mol^{-1} lower than $\Delta G^{\ddagger}_{int}$(N) for

both MeOTf and MeI (compare Table 2-13 entry (vii) with entry (v), and entry (viii) with entry (vi)), so O-methylation of **3** is intrinsically preferred. Since the thermodynamic favourability of N-methylation of **3** is diminished (relative to the corresponding reactions of **1**), and O-methylation is intrinsically favoured, $\Delta G^{\ddagger}$(O) is lower than $\Delta G^{\ddagger}$(N), and hence O-methylation of **3** is the kinetically dominant reaction. In this case, it seems likely that the free nitrogen Lewis basic site of **3** is deactivated due to an electronic effect. This Lewis basic site is connected through a network of π-bonds to an *N*-oxide group in a *meta* position relative to it, which may act as an electron withdrawing group, thereby diminishing the Lewis basicity (electron donor capacity) of the free nitrogen atom. The reaction of **3** with MeI was calculated to be thermodynamically unfavourable ($\Delta_r G° > 0$ for both O and N), and therefore reversible. This is consistent with the experimental observation that no product was formed in this reaction.

As discussed above, the $\Delta_r G°$ values calculated for N- and O-methylations of **3** by both MeI and MeOTf are much less favourable than the $\Delta_r G°$ values of methylation reactions of other, similar compounds (e.g., **1**, **18**, **20** and **21**; see Table 2-12 and Table 2-13). In the context of this analysis based on the Marcus equation, this information may be used to rationalise the relatively high $\Delta G^{\ddagger}$(O) and $\Delta G^{\ddagger}$(N) values calculated for the methylation reactions of **3**. The less favourable $\Delta_r G°$ values for O- and N-methylations of **3** influence the magnitudes of the $\Delta G^{\ddagger}$ values for these reactions, causing them to be higher than the $\Delta G^{\ddagger}$ values of reactions of similar nucleophiles.

As is described in detail in section 2.3.3, operationally, the value of the intrinsic barrier ($\Delta G^{\ddagger}_{int}$) for a reaction is accessed as the average of two identity reactions. Since there is no leaving group formed in the addition of a nucleophile to carbenium ions such as **24** and **58** (structures in Scheme 2-8 above), only one identity reaction of the required two can be identified to model such processes using Marcus theory. Hence, the straightforward method described in section 2.3.3 for accessing values of intrinsic barriers cannot be employed for reactions involving carbenium ions. Alternative methods for estimating the magnitudes of the intrinsic barriers for such reactions or analogues thereof have been reported, but these do not allow quantitative determinations of the type performed above for reactions involving electrophiles from which leaving groups become cleaved.[95,96] Hence only a qualitative appraisal of the outcomes of the reactions of **1** and **2** with benzhydrylium ions is possible, which is given below.

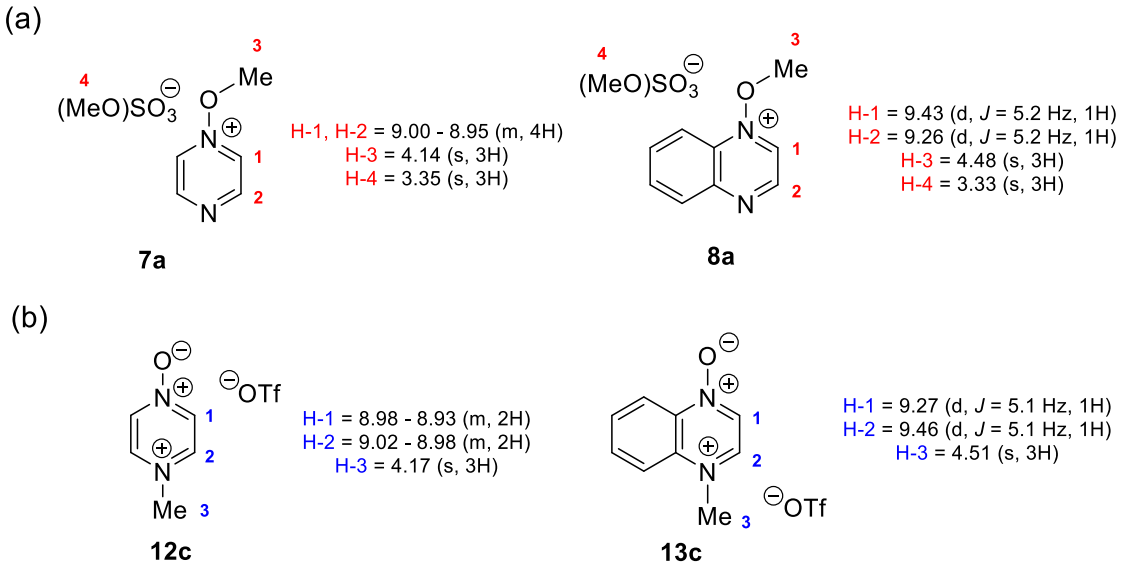
It is proposed that the observation of strongly preferred or exclusive N-benzhydrylation of nucleophiles **1** and **2** in their reactions with benzhydrylium ions (**58** or **24**) arises as a consequence of the same factors that dictate the outcomes of the reactions of these nucleophiles with MeI or MeOTf. That is, in each case, O-benzhydrylation is intrinsically favoured ($\Delta G^{\ddagger}_{int}$(O) is smaller than $\Delta G^{\ddagger}_{int}$(N)) but the influence of $\Delta_r G°$(N) on $\Delta G^{\ddagger}$(N) outweighs the influence of $\Delta G^{\ddagger}_{int}$(O) on $\Delta G^{\ddagger}$(O), and consequently N-benzhydrylation is the kinetically preferred process. As discussed above, it was not possible to determine what occurred in the reaction of **3** + benzhydrylium ion **58** (see Table 2-8 entry (xii)), so further comment on this is not possible.

2.3.5. Reappraisal of Literature Observations on N- vs O-Selectivity in Reactions of Diazine *N*-Oxides

It has been noted that, due to the ambiguity that has up until now been inherent in determining which product is formed predominantly in reactions of ambident nucleophiles containing N and O nucleophilic sites, there exist notable cases in the literature in which the products of such reactions may have been misidentified.[7,18,97,98]

Comparison of the ^{1}H NMR spectrum of N-methylated product **12c** (from reactions of MeOTf with **1**; Scheme 2-8(a)) with the ^{1}H NMR spectra assigned to O-methylation adduct **7a** (see Figure 2-6(a) below) in the work of Herzon and co-workers shows that the signals are essentially identical (see Figure 2-6(a) below).[18] A similar observation can also be made on comparison of the ^{1}H NMR signals of N-methylated product **13c** (from **2** + MeOTf; Scheme 2-8(b)) and those assigned to O-methylated adduct **8a** in the same paper (see Figure 2-6(b) below). A distinct set of signals belonging to the O-methylated adducts **7c** and **8c** have been identified by the reactions in this work that appear at different chemical shifts to the N-methylated adducts **12c** and **13c** (see section 3.6 for details of the ^{1}H NMR signals of these compounds). Furthermore, the ^{13}C NMR chemical shifts reported for the methyl group carbons (either N—*C*H$_3$ or O—*C*H$_3$) of the products are 47.2 and 44.5 ppm, respectively.[18] These δ_C values are indicative of formation of N-methylation products **12a** and **13a**, as demonstrated by the results shown in Table 2-7 and the associated discussion.

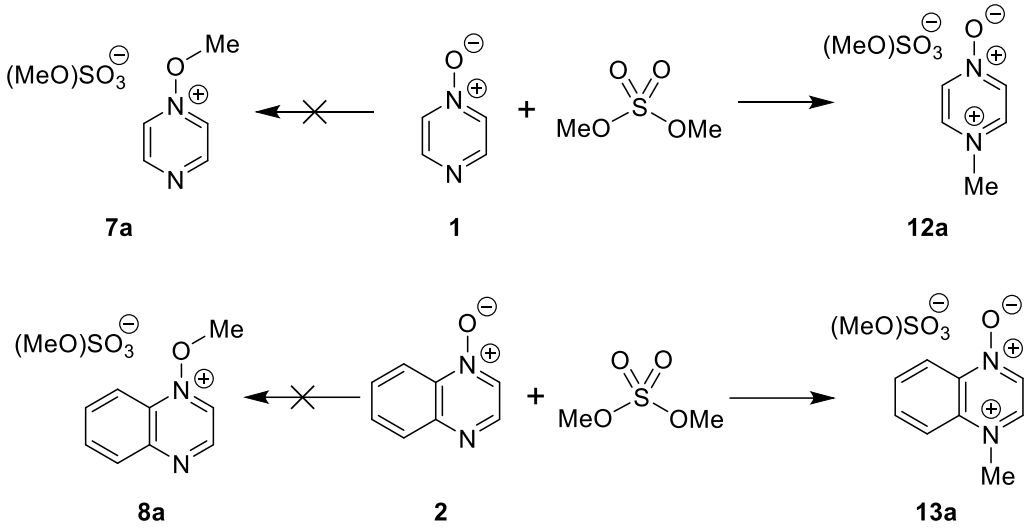
Figure 2-6. (a) ^{1}H NMR signals reported by Herzon and co-workers for compounds **7a** and **8a** in $(CD_3)_2SO$.[18] (b) ^{1}H NMR signals reported in this work for compounds **12c** and **13c** in $(CD_3)_2SO$. The structures of **12c** and **13c** were confirmed in this work using a combination of ^{1}H-^{13}C HMBC and ^{1}H-^{15}N HMBC NMR spectroscopic characterization.



Hence, the data gathered in this chapter indicate that it is highly unlikely that **1** and **2** undergo preferential O-methylation in reactions with dimethylsulfate, a close analogue of MeOTf. The methodology for the hydroheteroarylation of alkenes reported in the paper

of Herzon and co-workers was predicated on the use of *N*-methoxypyridinium salts or other *N*-methoxyheteroarenium salts. That this otherwise highly successful methodology did not work for these compounds can be explained by the fact that N-methylated compounds **12a** and **13a** were almost certainly employed rather than the intended O-methylated compounds **7a** and **8a**. Problems of this type are illustrative of the need for a much more rigorous understanding of the factors that dictate the outcomes in reactions of ambident nucleophiles such as diazine *N*-oxides.

Scheme 2-15. Reactions of compounds **1** and **2** with dimethylsulfate have been reported to give O-methylated products **7a** and **8a**.[18] The data in this chapter indicate that N-methylated adducts **12a** and **13a** are likely to be the major products.



The results outlined in this chapter demonstrate that the predictive capabilities of the HSAB theory as it is commonly applied to ambident reactivity are of questionable utility. It is apparent that the approach of Mayr and co-workers, based around Marcus theory, is able to account for the behaviour of ambident reactants in a manner in which the HSAB principle cannot.[1] This work developed upon the approach of Mayr and co-workers to show that it can be applied to semi-quantitatively rationalise product ratios in reactions of ambident nucleophiles, and demonstrated the utility of ^{1}H-^{15}N HMBC NMR spectroscopy in establishing the site of attachment in reactions of nitrogen-containing compounds. In the cases investigated here, calculation of $\Delta G^{\ddagger}$ values using the equations of Marcus (Equation 2.1) or Zhu (Equation 2.3) yields values that reproduce closely the experimental N/O methylation ratios for reactions of ambident nucleophiles pyrazine *N*-oxide (**1**) and pyrimidine *N*-oxide (**3**). The intrinsic barrier ($\Delta G^{\ddagger}_{int}$) associated with an alkylation reaction of a nucleophile can be considered a property of the compounds involved in the reaction. The interplay between this quantity and the thermodynamic favourability of the reaction (quantified through $\Delta_r G°$) dictates the magnitude of the activation barrier for the reaction ($\Delta G^{\ddagger}$). The close agreement between the reaction selectivities determined experimentally and those calculated using the Marcus and Zhu equations (see Table 2-15 and associated discussion) is demonstrative of the utility of the concept of the intrinsic barrier.

2.4. References

1. Mayr, H.; Breugst, M.; Ofial, A. R. *Angew. Chem. Int. Ed.* **2011**, *50*, 6470–6505.
2. Landquist, J. K. *J. Chem. Soc.* **1953**, No. 0, 2816–2821.
3. Koelsch, C. F.; Gumprecht, W. H. *J. Org. Chem.* **1958**, *23*, 1603–1606.
4. Breugst, M.; Tokuyasu, T.; Mayr, H. *J. Org. Chem.* **2010**, *75*, 5250–5258.
5. Głaszczka, R.; Jaźwiński, J. *J. Mol. Struct.* **2014**, *1061*, 150–159.
6. Breugst, M.; Mayr, H. *J. Am. Chem. Soc.* **2010**, *132*, 15380–15389.
7. Cmoch, P. *Magn. Reson. Chem.* **2003**, *41*, 693–698.
8. Wang, Y.-G.; Barnes, E. C. *ACS Omega* **2018**, *3*, 4557–4572.
9. Cárdenas, C.; Ayers, P. W. *Phys. Chem. Chem. Phys.* **2013**, *15*, 13959–13968.
10. Torrent-Sucarrat, M.; De Proft, F.; Geerlings, P.; Ayers, P. W. *Chem. Eur. J.* **2008**, *14*, 8652–8660.
11. Hopkins, G.; Jonak, J.; Minnemeyer, H.; Tieckelmann, H. *J. Org. Chem.* **1967**, *32*, 4040–4044.
12. Arévalo, A.; Ovando-Segovia, S.; Flores-Alamo, M.; García, J. J. *Organometallics* **2013**, *32*, 2939–2943.
13. Koch, T. H.; Sluski, R. J.; Moseley, R. H. *J. Am. Chem. Soc.* **1973**, *95*, 3957–3963.
14. Tishkov, A. A.; Schmidhammer, U.; Roth, S.; Riedle, E.; Mayr, H. *Angew. Chem. Int. Ed.* **2005**, *44*, 4623–4626.
15. Kornblum, N.; Smiley, R. A.; Blackwood, R. K.; Iffland, D. C. *J. Am. Chem. Soc.* **1955**, *77*, 6269–6280.
16. Bredereck, H.; Gompper, R.; Rempfer, H.; Klemm, K.; Keck, H. *Chem. Ber.* **1959**, *92*, 329–337.
17. Challis, B. C.; Challis, J. In *The Chemistry of Amides*; Zabicky, J., Ed.; Interscience: London, UK, 1970; pp 731–858.
18. Ma, X.; Dang, H.; Rose, J. A.; Rablen, P.; Herzon, S. B. *J. Am. Chem. Soc.* **2017**, *139*, 5998–6007.
19. Ohta, A.; Matsunaga, M.; Iwata, N.; Watanabe, T. *Heterocycles* **1977**, *8*, 351.
20. Martin, G. E.; Williams, A. J. In *Annu. Rev. NMR Spectrosc.*; Webb, G. A., Ed.; Academic Press, 2015; Vol. 84, pp 1–76.
21. Marek, R.; Lycka, A.; Kolehmainen, E.; Sievanen, E.; Tousek, J. *Curr. Org. Chem.* *11*, 1154–1205.
22. Martin, G. E.; Williams, A. J. In *Annu. Rev. NMR Spectrosc.*; Academic Press, 2005; Vol. 55, pp 1–119.
23. Marek, R.; Lycka, A. *Curr. Org. Chem. 6*, 35–66.
24. Köck, M.; Junker, J.; Lindel, T. *Org. Lett.* **1999**, *1*, 2041–2044.
25. Williamson, R. T.; Buevich, A. V.; Martin, G. E. *Tetrahedron Lett.* **2014**, *55*, 3365–3366.
26. Storz, T.; Bartberger, M. D.; Sukits, S.; Wilde, C.; Soukup, T. *Synthesis* **2008**, *2008*, 201–214.
27. Kline, M.; Cheatham, S. *Magn. Reson. Chem.* **2003**, *41*, 307–314.
28. Haslinger, E.; Schlederer, M.; Robien, W.; Wolschann, P. *Monatsh. Chem.* **1984**, *115*, 1345–1351.
29. Pazderski, L. *Magn. Reson. Chem.* **2008**, *46*, S3–S15.
30. Shanahan, R. M.; Hickey, A.; Bateman, L. M.; Light, M. E.; McGlacken, G. P. *J. Org. Chem.* **2020**, *85*, 2585–2596.
31. Kleinmaier, R.; Arenz, S.; Karim, A.; Carlsson, A.-C. C.; Erdélyi, M. *Magn. Reson. Chem.* **2013**, *51*, 46–53.

32. Pazderski, L.; Pawlak, T.; Sitkowski, J.; Kozerski, L.; Szłyk, E. *Magn. Reson. Chem.* **2010**, *48*, 417–426.
33. Pazderski, L. In *Annu. Rev. NMR Spectrosc.*; Webb, G. A., Ed.; Academic Press, 2013; Vol. 80, pp 33–179.
34. Lukevics, E.; Leipiņš, E.; Segal, I.; Fleisher, M. *J. Organomet. Chem.* **1991**, *406*, 283–298.
35. Costisella, B.; Schulz, J.; Teichmann, H.; Donaths, C.; Meisels, M. *Phosphorus, Sulfur Silicon Relat. Elem* **1990**, *53*, 367–371.
36. Lethesh, K. C.; Van Hecke, K.; Van Meervelt, L.; Nockemann, P.; Kirchner, B.; Zahn, S.; Parac-Vogt, T. N.; Dehaen, W.; Binnemans, K. *J. Phys. Chem. B* **2011**, *115*, 8424–8438.
37. Marek, R.; Brus, J.; Toušek, J.; Kovács, L.; Hocková, D. *Magn. Reson. Chem.* **2002**, *40*, 353–360.
38. Hocek, M.; Pohl, R.; Císařová, I. *Eur. J. Org. Chem.* **2005**, *2005*, 3026–3030.
39. Bakkestuen, A. K.; Gundersen, L.-L.; Petersen, D.; Utenova, B. T.; Vik, A. *Org. Biomol. Chem.* **2005**, *3*, 1025–1033.
40. Roggen, H.; Gundersen, L.-L. *Eur. J. Org. Chem.* **2008**, *2008*, 5099–5106.
41. Dega-Szafran, Z.; Szafran, M.; Sitkowski, J.; Stefaniak, L. *J. Phys. Org. Chem.* **1996**, *9*, 746–750.
42. Farley, K. A.; Bowman, P. B.; Brumfield, J. C.; Crow, F. W.; Duholke, W. K.; Guido, J. E.; Robins, R. H.; Sims, S. M.; Smith, R. F.; Thamann, T. J.; Vonderwell, B. S.; Martin, G. E. *Magn. Reson. Chem.* **1998**, *36*, S11–S16.
43. Martin, G. E.; Hadden, C. E.; Blinn, J. R.; Sharaf, M. H. M.; Tackie, A. N.; Schiff Jr, P. L. *Magn. Reson. Chem.* **1999**, *37*, 1–6.
44. Hadden, C. E.; Duholke, W. K.; Guido, J. E.; Robins, R. H.; Martin, G. E.; Sharaf, M. H. M.; Schiff Jr., P. L. *J. Heterocycl. Chem.* **1999**, *36*, 525–531.
45. Andreev, V. P. *Chem. Heterocycl. Compd.* **2010**, *46*, 184–195.
46. Dokalik, A.; Kalchhauser, H.; Mikenda, W.; Schweng, G. *Magn. Reson. Chem.* **1999**, *37*, 895–902.
47. Witanowski, M.; Sicinska, W.; Biernat, S.; Webb, G. A. *J. Magn. Reson.* **1989**, *83*, 351–357.
48. Sawada, M.; Takai, Y.; Yamano, S.; Misumi, S.; Hanafusa, T.; Tsuno, Y. *J. Org. Chem.* **1988**, *53*, 191–194.
49. Sanz, D.; Perona, A.; Claramunt, R. M.; Elguero, J. *Tetrahedron* **2005**, *61*, 145–154.
50. Städeli, W.; Philipsborn, W. V.; Wick, A.; Kompiš, I. *Helv. Chim. Acta.* **1980**, *63*, 504–522.
51. Yavari, I.; Roberts, J. D. *Org. Magn. Reson.* **1979**, *12*, 87–91.
52. Witanowski, M.; Sicinska, W.; Biernat, S.; Webb, G. A. *J. Magn. Reson.* **1991**, *91*, 289–300.
53. Kolman, V.; Babinský, M.; Kulhánek, P.; Marek, R.; Sindelar, V. *New J. Chem.* **2011**, *35*, 2854–2859.
54. Katritzky, A. R.; Dega-Szafran, Z. *Magn. Reson. Chem.* **1989**, *27*, 1090–1093.
55. Szafran, M.; Dega-Szafran, Z.; Katrusiak, A.; Buczak, G.; Głowiak, T.; Sitkowski, J.; Stefaniak, L. *J. Org. Chem.* **1998**, *63*, 2898–2908.
56. Brotzel, F.; Kempf, B.; Singer, T.; Zipse, H.; Mayr, H. *Chem. Eur. J.* **2007**, *13*, 336–345.
57. Newmark, R. A.; Tucker, A.; Hardy, L. C. *Magn. Reson. Chem.* **1996**, *34*, 728–729.
58. Gao, X.; Han, S.; Zheng, M.; Liang, A.; Li, J.; Zou, D.; Wu, Y.; Wu, Y. *J. Org. Chem.* **2019**, *84*, 4040–4049.

59. Bennasar, M.-L.; Roca, T.; Monerris, M.; Juan, C.; Bosch, J. *Tetrahedron* **2002**, *58*, 8099–8106.
60. Bennasar, M.-L.; Roca, T.; Zulaica, E.; Monerris, M. *Tetrahedron* **2004**, *60*, 6785–6789.
61. Huang, W.; Guo, J.; Xiao, Y.; Zhu, M.; Zou, G.; Tang, J. *Tetrahedron* **2005**, *61*, 9783–9790.
62. Kabatc, J.; Kostrzewska, K.; Dobosz, R.; Orzeł, Ł.; Jurek, K. *J. Polym. Sci., Part A: Polym. Chem.* **2017**, *55*, 2840–2850.
63. Shukla, D.; Adiga, S. P.; Ahearn, W. G.; Dinnocenzo, J. P.; Farid, S. *J. Org. Chem.* **2013**, *78*, 1955–1964.
64. Fuentes, A.; Martínez-Palou, R.; Jiménez-Vázquez, H. A.; Delgado, F.; Reyes, A.; Tamariz, J. *Monatsh. Chem.* **2005**, *136*, 177–192.
65. Potmischil, F.; Duddeck, H.; Nicolescu, A.; Deleanu, C. *Magn. Reson. Chem.* **2007**, *45*, 231–235.
66. Vogl, O.; Rehman, A.; Zarras, P. *Monatsh. Chem.* **2000**, *131*, 437–449.
67. Sakuma, C.; Maeda, M.; Tabei, K.; Ohta, A.; Kerim, A.; Kurihara, T. *Magn. Reson. Chem.* **1996**, *34*, 567–570.
68. Someswara Rao, N.; Babu Rao, G.; Murthy, B. N.; Das, M. M.; Prabhakar, T.; Lalitha, M. *Spectrochim. Acta, Part A.* **2002**, *58*, 2737–2757.
69. Brough, P.; Klumpp, C.; Bianco, A.; Campidelli, S.; Prato, M. *J. Org. Chem.* **2006**, *71*, 2014–2020.
70. Forrester, J.; Jones, R. V. H.; Preston, P. N.; Simpson, E. S. C. *J. Chem. Soc., Perkin Trans. 1* **1995**, No. 18, 2289–2291.
71. Mayr, H.; Ammer, J.; Baidya, M.; Maji, B.; Nigst, T. A.; Ofial, A. R.; Singer, T. *J. Am. Chem. Soc.* **2015**, *137*, 2580–2599.
72. Byrne, P. A.; Kobayashi, S.; Breugst, M.; Laub, H.; Mayr, H. *J. Phys. Org. Chem.* **2016**, *29*, 759–767.
73. Ayers, P. W. *Faraday Discuss.* **2006**, *135*, 161–190.
74. Ayers, P. W. *J. Chem. Phys.* **2005**, *122*, 141102.
75. Ayers, P. W.; Parr, R. G.; Pearson, R. G. *J. Chem. Phys.* **2006**, *124*, 194107.
76. Zadeh, F. H.; Fuentealba, P.; Cárdenas, C.; Ayers, P. W. *Phys. Chem. Chem. Phys.* **2014**, *16*, 6019–6026.
77. Glendening, E. D.; Landis, C. R.; Weinhold, F. *J. Comput. Chem.* **2013**, *34*, 1429–1437.
78. Singh, U. C.; Kollman, P. A. *J. Comput. Chem.* **1984**, *5*, 129–145.
79. Besler, B. H.; Merz Jr., K. M.; Kollman, P. A. *J. Comput. Chem.* **1990**, *11*, 431–439.
80. Breneman, C. M.; Wiberg, K. B. *J. Comput. Chem.* **1990**, *11*, 361–373.
81. Bader, R. F. W. *Atoms in Molecules: A Quantum Theory*.; Clarendon Press, 1994: Oxford.
82. Mayer, R. J.; Breugst, M.; Hampel, N.; Ofial, A. R.; Mayr, H. *J. Org. Chem.* **2019**, *84*, 8837–8858.
83. Byrne, P. A.; Karaghiosoff, K.; Mayr, H. *J. Am. Chem. Soc.* **2016**, *138*, 11272–11281.
84. Maji, B.; Mayr, H. *Angew. Chem. Int. Ed.* **2013**, *52*, 11163–11167.
85. Maji, B.; Troshin, K.; Mayr, H. *Angew. Chem. Int. Ed.* **2013**, *52*, 11900–11904.
86. Nigst, T. A.; Ammer, J.; Mayr, H. *Angew. Chem. Int. Ed.* **2012**, *51*, 1353–1356.
87. Zhu, X.-Q.; Yang, J.-D. *J. Phys. Org. Chem.* **2013**, *26*, 271–273.
88. Zhu, X.-Q.; Deng, F.-H.; Yang, J.-D.; Li, X.-T.; Chen, Q.; Lei, N.-P.; Meng, F.-K.; Zhao, X.-P.; Han, S.-H.; Hao, E.-J.; Mu, Y.-Y. *Org. Biomol. Chem.* **2013**, *11*, 6071–6089.

89. Fu, Y.-H.; Shen, G.-B.; Li, Y.; Yuan, L.; Li, J.-L.; Li, L.; Fu, A.-K.; Chen, J.-T.; Chen, B.-L.; Zhu, L.; Zhu, X.-Q. *ChemistrySelect* **2017**, *2*, 904–925.
90. Shen, G.-B.; Xia, K.; Li, X.-T.; Li, J.-L.; Fu, Y.-H.; Yuan, L.; Zhu, X.-Q. *J. Phys. Chem. A* **2016**, *120*, 1779–1799.
91. Hoz, S.; Basch, H.; Wolk, J. L.; Hoz, T.; Rozental, E. *J. Am. Chem. Soc.* **1999**, *121*, 7724–7725.
92. Pearson, R. G. *J. Am. Chem. Soc.* **1963**, *85*, 3533–3539.
93. Pearson, R. G. *Science* **1966**.
94. Parr, R. G.; Pearson, R. G. *J. Am. Chem. Soc.* **1983**, *105*, 7512–7516.
95. Byrne, P. A.; Kobayashi, S.; Würthwein, E.-U.; Ammer, J.; Mayr, H. *J. Am. Chem. Soc.* **2017**, *139*, 1499–1511.
96. Richard, J. P.; Toteva, M. M.; Crugeiras, J. *J. Am. Chem. Soc.* **2000**, *122*, 1664–1674.
97. Demberelnyamba, D.; Shin, B. K.; Lee, H. *Chem. Commun.* **2002**, No. 14, 1538–1539.
98. Yang, J.; Zhang, Q.; Zhu, L.; Zhang, S.; Li, J.; Zhang, X.; Deng, Y. *Chem. Mater.* **2007**, *19*, 2544–2550.

Chapter 3: Experimental for Reactions of Diazine *N*-oxides

Table of Contents

3.1. General Experimental 133

3.2. Preparation of *N*-Oxides 136

3.3. NMR Spectral Data for Starting Compounds 1 – 3, 18 – 21, 23 139

3.3.1. NMR Spectral data for Starting Materials in $(CH_3)_2SO/(CD_3)_2SO$ 139

3.3.2. NMR Spectral data for Starting Materials in CH_2Cl_2 140

3.4. Synthesis of 4-Methylbenzyl Chloride 143

3.5. Reactions of Diazines and *N*-Oxides with Alkylating Agents 144

3.6. Reactions of Diazine *N*-Oxides with MeI, MeOTf and Benzhydrylium Ions 158

3.6.1. Reactions of Pyrazine *N*-Oxide (**1**) 158

3.6.2. Reactions of Quinoxaline *N*-Oxide (**2**) 164

3.6.2. Reactions of Pyrimidine *N*-Oxide (**3**) 170

3.7. Control Experiments 177

3.7.1. Crossover Experiment – Pyrazine *N*-Oxide (**1**) with MeOTf and Methyl Nicotinate (**66**) 177

3.7.2. Crossover Experiment – Quinoxaline *N*-Oxide (**2**) with MeOTf and Pyrazine (**18**) 180

3.7.3. Crossover Experiment – Pyrimidine *N*-Oxide (**3**) with MeOTf and Pyrazine (**18**) 181

3.7.4. Crossover Experiment – 4-Methylpyrazinium-*N*-Oxide Iodide (**12b**) with MeOTf and Methyl Nicotinate (**66**) 186

3.8. Competition Experiment: Pyrazine *N*-Oxide vs Pyrimidine *N*-Oxide 188

3.9. Determination of 2nd Order Rate Constant to Verify Computationally Determined Value of $\Delta G^{\ddagger}$ 189

3.9.1. Example Calculation to Obtain the Product Ratio Predicted by the Marcus Calculations..... 194

3.10. Calculations of Thermodynamic and Activation Parameter Values..... 195

3.11. References 199

Appendices referred to in the text are available at the following link:
https://tinyurl.com/KSheehyPhDThesisAppendices

3.1. General Experimental

Commercial diazines and alkylating agents were obtained from Fluorochem, Sigma-Aldrich and Alfa Aesar.

CH_2Cl_2, $CDCl_3$, Et_2O, CH_3CN (MeCN), CD_3CN, $(CH_3)_2SO$, $(CD_3)_2SO$ and THF were dried over activated 3 Å molecular sieves and stored under an atmosphere of nitrogen in flasks with grease-free J. Young's valves.[1] Molecular sieves (10 weight percent per unit volume of compound to be dried, 20 weight percent was used when drying THF) were activated by flame drying in the storage flask(s) for 5 – 10 minutes (depending on quantity of sieves to be dried).[1] After flame-drying, the storage flask was immediately connected to a Schlenk line, subjected to vacuum (between 2 and 5×10^{-3} mbar), and allowed to stand until the sieves had cooled. The flask was then subjected to several vacuum/refill cycles to establish a nitrogen atmosphere inside,[2] and the solvent/compound to be dried was then added by cannula transfer directly from a Winchester bottle which was sealed using a rubber septum (sized for a B29 ground glass socket joint).

Solvents that were used in relative bulk (MeCN, CH_2Cl_2, Et_2O, THF) were stored in a specialised flask with two J. Young's valves, one of which was modified to facilitate easy access of a needle to the body of the flask through the side-arm of the valve. When accessing the dry solvent, the angled side-arm was sealed with a rubber septum, and the small volume contained between the septum and the sealed tap of the J. Young's valve was flushed with a stream of nitrogen gas for a minimum of five minutes prior to opening the valve. The solvent required several days after commencing drying to reach maximal dryness (analysis by Karl Fischer titration for all but $(CH_3)_2SO$ and $(CD_3)_2SO$) but was dry enough for most purposes after one day. Solvents stored in this manner were found to retain water contents of less than 10 ppm for more than one year.

For all reactions conducted using Schlenk glassware, the Schlenk flask was dried in an oven, then attached to vacuum *via* Schlenk manifold and placed under vacuum ($\leq 5 \times 10^{-3}$ mbar). The flask was then filled with nitrogen gas by the pump and fill technique (three repeats of the following cycle: evacuation to $\leq 5 \times 10^{-3}$ mbar, re-fill with nitrogen gas).[2] Solids and reagents were then introduced to the flasks against a fast nitrogen flow either directly from narrow vials or using a powder funnel.

NMR spectra were recorded on Bruker Avance III 600, Bruker Avance III 500, Bruker Avance I 400 and Bruker Avance III 300 NMR spectrometers. ^1H and ^{13}C NMR chemical shifts were referenced to tetramethylsilane (TMS). ^1H NMR spectra (proton coupled mode, 600 MHz, 400 MHz and 300 MHz respectively) $^{13}C\{^1H\}$ NMR spectra (proton decoupled mode; 150 MHz,100 MHz and 75 MHz, respectively), HSQC NMR spectra, HMBC NMR spectra and COSY NMR spectra were acquired at 300 K on the 300 and 600 MHz instruments and 293 K on the 400 MHz instrument. ^1H NMR spectra on the 500 MHz instrument were recorded at 298 K. ^1H NMR spectra were acquired using a 30° pulse (Bruker zg pulse programme), an acquisition time of 2.65 seconds, and a time domain data size of 32768 or 65536 points. A relaxation delay of 5 seconds

was used in most instances; exceptions to this are noted where applicable below. Signal assignments in the ^{1}H and ^{13}C NMR spectra were made with reference to information contained in the two-dimensional NMR spectra. ^{1}H-^{15}N HMBC NMR spectra were recorded at 300 K on a Bruker Avance III 600 NMR spectrometer [600 MHz (^{1}H), 60.8 MHz (^{15}N)], equipped with Bruker BBFO cryoprobe (coil temperature 16 K) and referenced externally to ammonia, the value of which was uncorrected. ^{1}H-^{15}N HMBC NMR spectra were acquired using the Bruker hmbcqpndqf pulse program (2D H-1/X correlation *via* heteronuclear zero and double quantum coherence optimised on long range couplings), with 4 scans and spectral widths of 600–650 ppm. All ^{1}H-^{15}N HMBC NMR spectra (which can be seen in Appendix A) were processed (post-acquisition) by application of t1 noise reduction. All spectra were run at University College Cork. Spectra recorded in non-deuterated solvents were acquired using the Bruker NOESY presat (noesygppr) solvent suppression pulse sequence, using presaturation during the mixing time and relaxation delay. Chemical shifts (δ) are expressed as parts per million (ppm), positive shift being downfield from TMS; coupling constants (*J*) are expressed in Hertz (Hz). Splitting patterns in ^{1}H-NMR spectra are designated as: s (singlet), bs (broad singlet), d (doublet), dd (doublet of doublets), ddd (doublet of doublets of doublets), t (triplet), td (triplet of doublets), q (quartet), quin (quintet) and m (multiplet). Infrared spectra were measured using a FTIR UATR2 spectrometer. The samples were dissolved in acetonitrile which was placed over the crystal of the spectrometer using a dropper. After the evaporation of the acetonitrile had occurred, pressure was applied to the sample on the crystal and a spectrum was recorded. Data are represented as follows: frequency of absorption (cm^{-1}), intensity of absorption (s = strong, m = medium, w = weak, br = broad). High resolution (precise) mass spectra (HRMS) were recorded on a Waters LCT Premier TOF LC–MS instrument using electrospray ionization in positive ionization mode (ESI+) using 50 % acetonitrile/water containing 0.1 % formic acid as eluent. Samples were made up at a concentration of approximately 1 mg ml^{-1}.

General Procedures

General Procedure A: Removal of Solvent while Maintaining an Inert Atmosphere

The following procedure was used to remove the solvent and volatile reagents from a Schlenk flask containing a completed reaction mixture while maintaining an inert atmosphere. A Schlenk manifold connected to a rotary vane vacuum pump *via* a liquid nitrogen cold trap (and a nitrogen supply) was connected to a second vacuum trap, which was also attached to the closed reaction flask (containing a solution in a volatile solvent under nitrogen atmosphere). The trap and tubing connecting it to the Schlenk manifold and reaction flask were placed under vacuum ($\leq 5 \times 10^{-3}$ mbar). The vacuum trap was then filled with nitrogen gas by the pump and fill technique (see description above, and reference 2). The trap was then placed under vacuum and then cooled with liquid N_2. At this point, the tap on the Schlenk flask was opened and volatile solvent was removed and collected in the trap. After approximately 30 minutes, the entirety of

the trap and the Schlenk flask were re-filled with nitrogen gas through the Schlenk manifold and the tap of the Schlenk flask was closed. The trap was removed and the flask was re-attached directly to the Schlenk manifold. This procedure was repeated when removing excess Et_2O after conducting an Et_2O wash in some experiments (see below).

Procedure B: Preparation of Samples for NMR Spectroscopy Under Inert Atmosphere

The following procedure was used to transfer the products of the alkylation reactions (dissolved in an appropriate solvent) into NMR tubes while maintaining an inert atmosphere over the products. The products were formed in an N_2-filled Schlenk flask using inert atmosphere techniques. The appropriate solvent (specified for individual reactions below) was introduced to the Schlenk flask by syringe and *ca.* 10 mg of the product was dissolved. An empty NMR tube was placed in a long Schlenk tube. The long Schlenk tube, containing the NMR tube, was evacuated and re-filled with nitrogen ≥ 3 times, creating an inert atmosphere inside the flask. The solution to be examined (in dry $(CH_3)_2SO$, $(CD_3)_2SO$ or CH_2Cl_2) was drawn into a syringe through a needle. The reaction mixture was transferred into the NMR tube under nitrogen. The NMR tube was then sealed by a rubber septum cap. After fitting the rubber septum to the NMR tube, the seal was secured by wrapping the external edge of the septum where it contacted the surface of the NMR tube with PTFE tape. The outside of the PTFE tape and rubber septum were then wrapped with a layer of Parafilm to further secure the nitrogen atmosphere inside the NMR tube. The NMR tube was then transferred to the NMR spectrometer and NMR spectra were recorded.

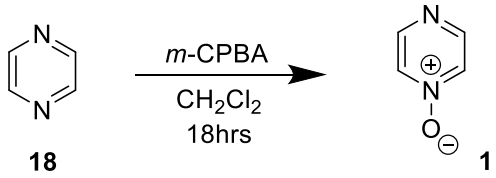
Procedure C: Preparation of Benzhydryl Adducts of Heterocycles and *N*-Oxides

The following procedure was used to synthesise the benzhydryl adducts of the heterocycles discussed in Chapter 2. The appropriate benzhydryl chloride (1 equivalent) was weighed into a reaction vessel and transferred into a glove box containing a nitrogen atmosphere. Dry CD_2Cl_2 (0.85 ml) was added, followed by the heterocycle or *N*-oxide (1 equivalent). AgOTf (1.1 – 1.2 equivalents) was then added, causing the immediate precipitation of AgCl. The reaction vessel was sealed, agitated (15 minutes for 4-methylbenzhydryl chloride, 60 minutes for benzhydryl chloride), and then filtered (removing AgCl) through a syringe filter into an NMR tube. The NMR tube was sealed using a rubber septum. After fitting the rubber septum to the NMR tube, the seal was secured by wrapping the external edge of the septum where it contacted the surface of the NMR tube with PTFE tape. Finally, the NMR tube was placed in a long Schlenk flask and removed from the glove box. The outside of the PTFE tape and rubber septum were then wrapped with a layer of Parafilm to further secure the nitrogen atmosphere inside the NMR tube and the sample was brought to the NMR spectrometer. All products underwent relatively rapid decomposition (hydrolysis) on exposure to moisture, and hence were only characterized by inert atmosphere NMR spectroscopy.

3.2. Preparation of *N*-Oxides

Preparation of *N*-oxides was achieved using a modification of established literature procedures.[3,4] It is recommend the use of a slight excess of diazine (relative to the amount of 3-chloroperbenzoic acid) in order to remove the need to use quenching agents (e.g. Ph_3P, Na_2SO_3) in these reactions.

(i) Preparation of Pyrazine *N*-Oxide (1) [4]

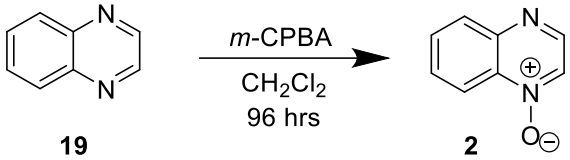


18 **1**

Pyrazine (**18**) (1.12 g, 14.0 mmol) was dissolved in CH_2Cl_2 (70 ml). 3-Chloroperbenzoic acid (3.08 g, 13.8 mmol) was added in one portion, and the solution was stirred for 18 hrs, turning a cloudy white colour (due to precipitated 3-chlorobenzoic acid). The reaction mixture was washed twice with saturated sodium sulfite solution (*ca.* 40 ml each) and once with a solution of brine (*ca.* 40 ml). The recovered organic phase was dried over Na_2SO_4, and the drying agent was removed by filtration. The solvent was then removed under reduced pressure. The residue was purified by column chromatography using 100% EtOAc, yielding a colourless, needle-like solid (**1**). (0.56 g, 5.8 mmol, 42%). This material was immediately transferred to a glove box upon isolation.

^{1}H NMR (300 MHz, $CDCl_3$) δ 8.52 – 8.44 (m, 2H), 8.15 – 8.08 (m, 2H).[5]

(ii) Preparation of Quinoxaline *N*-oxide (2)

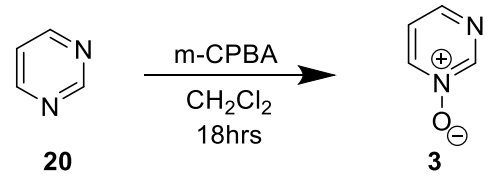


19 **2**

Quinoxaline (**19**) (1.70 g, 13.1 mmol) was dissolved in 100 ml CH_2Cl_2. 3-Chloroperbenzoic acid (2.39 g, 13.8 mmol) was added in one portion, and the solution was stirred for 4 days. Precipitated 3-chlorobenzoic acid appeared in the reaction mixture after a few hours. The reaction mixture was washed twice with saturated sodium sulfite solution (*ca.* 40 ml each) and once with a solution of brine (*ca.* 40 ml). The recovered organic phase was dried over Na_2SO_4, and the drying agent was removed by filtration. The solvent was then removed under reduced pressure. The residue was purified by column chromatography in silica using 70:30 ethyl acetate/cyclohexane, yielding light tan-coloured solid (**2**). (1.27 g, 8.68 mmol, 66% yield). This material was immediately transferred to a glove box upon isolation.

^{1}H NMR (300 MHz, $CDCl_3$) δ 8.68 (d, J = 3.6 Hz, 1H), 8.59 (dd, J = 8.6, 1.4 Hz, 1H), 8.35 (d, J = 3.6 Hz, 1H), 8.19 – 8.11 (m, 1H), 7.88 – 7.72 (m, 2H).[6]

(iii) Preparation of Pyrimidine *N*-oxide (3)

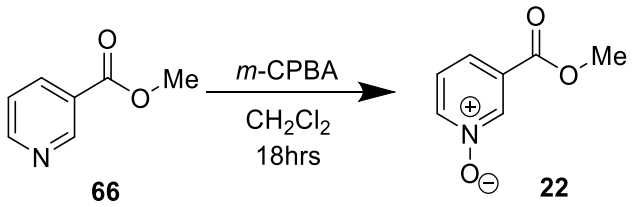


Pyrimidine (**20**) (1.74 g, 21.7 mmol) was dissolved in CH_2Cl_2 (110 ml). 3-Chloroperbenzoic acid (5.62 g, 32.6 mmol) was added in one portion, and the solution was stirred for 48 hrs, turning a cloudy white colour (due to precipitated 3-chlorobenzoic acid). PPh_3 (3.90 g, 14.9 mmol) was added, and the solution was stirred for 3 hours. The solvent was removed under reduced pressure. The residue was purified by column chromatography using 90 : 10 EtOAc/Cyclohexane, yielding a white crystalline solid (**3**). (0.993 g, 10.3 mmol, 48%). The product is very hygroscopic and hence was transferred to a glove box immediately after isolation.

^{1}H NMR (300 MHz, $CDCl_3$) δ 9.01 (m (fine splitting not resolved), 1H), 8.42 – 8.35 (m, 1H), 8.25 (dd, *J* = 4.7, 1.4 Hz, 1H), 7.35 – 7.28 (m, 1H).[7]

PPh_3 should not be used for quenching purposes, as it was difficult to find chromatographic conditions allowing the product to be separated from triphenylphosphine oxide quench product, and significant loss of product occurred due to co-elution with Ph_3PO.

(iv) Preparation of Methyl Nicotinate *N*-oxide (22)



Methyl nicotinate (**66**) (2.09 g, 15.3 mmol) was dissolved in CH_2Cl_2 (70 ml). 3-Chloroperbenzoic acid (2.59 g, 15.0 mmol) was added in one portion and the solution was stirred for 18 hrs. The mixture was filtered through a Büchner funnel to remove any precipitated 3-chlorobenzoic acid. The organic solvent was washed once with a saturated sodium sulphite solution and once with a solution of brine. The solvent was then removed under reduced pressure. The residue was purified by column chromatography using mixtures of EtOAc and cyclohexane, with progressively smaller amounts of cyclohexane being employed. The column fractions containing pure **22** were combined, and the solvent was removed under vacuum, yielding **22** as a pale yellow solid (0.7166 g, 32%). Many eluted fractions contained both *N*-oxide **22** and 3-chlorobenzoic acid, which led to the low isolated yield. The pure *N*-oxide produced was stored under nitrogen gas in a glove box due to its hygroscopic properties.

^{1}H NMR (300 MHz, $CDCl_3$, 27 °C) δ 8.80 – 8.75 (m, 1H), 8.34 (app. ddd, app. *J* = 6.5, 1.8, 1.1 Hz, 1H), 7.88 – 7.83 (m, 1H), 7.37 (app. dd, app. *J* = 7.7, 6.7 Hz, 1H), 3.97 (s, 3H).[8]

Note: The 3-chloroperbenzoic acid used is a solid consisting of ≤77% *m*-CPBA.

3.3. NMR Spectral Data for Starting Compounds 1 – 3, 18 – 21, 23

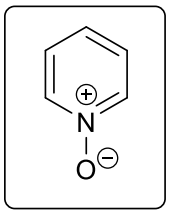
Observation of ^{15}N NMR Chemical Shifts Using the ^{1}H-^{15}N HMBC NMR Spectroscopic Technique

^{15}N NMR chemical shifts values were measured using ^{1}H-^{15}N HMBC NMR spectroscopy. These values were compared with extant ^{14}N and ^{15}N values found in the literature (see below and Chapter 2).

Note: The spectra were recorded using non-deuterated solvents, with the signals of the solvent suppressed during acquisition, as described in the General Experimental section above.

3.3.1. NMR Spectral Data for Starting Materials in $(CH_3)_2SO$/$(CD_3)_2SO$

Pyridine *N*-Oxide (21)

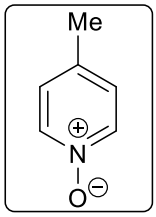


Pyridine *N*-oxide (**21**) (0.052 g) was dissolved in dry DMSO (0.65 ml) in a N_2-filled Schlenk flask and placed in an NMR tube by syringe under nitrogen, which was then sealed with a rubber septum cap. After fitting the rubber septum to the NMR tube, the seal was secured by wrapping the external edge of the septum where it contacted the surface of the NMR tube with PTFE tape. The product was analysed by ^{1}H and ^{1}H-^{15}N HMBC NMR spectroscopy.

^{1}H NMR (600 MHz, $(CH_3)_2SO$) δ 8.19 (app. d, app. *J* = 6.0 Hz, 2H), 7.37 (app. t, app. *J* = 7.1 Hz, 2H), 7.29 (app. t, app. *J* = 7.6 Hz, 1H).[9]

^{15}N NMR (60.8 MHz, $(CH_3)_2SO$): δ 295.1.[10]

4-Methylpyridine *N*-Oxide (23)

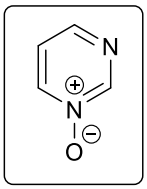


4-Methylpyridine- *N*-oxide (**23**) (0.052 g, 0.48 mmol) was dissolved in dry DMSO-d_6 (0.65 ml) in a N_2-filled Schlenk flask and placed in an NMR tube by syringe under nitrogen, which was then sealed with a rubber septum cap. After fitting the rubber septum to the NMR tube, the seal was secured by wrapping the external edge of the septum where it contacted the surface of the NMR tube with PTFE tape. The product was analysed by ^{1}H and ^{1}H-^{15}N HMBC NMR spectroscopy.

^{1}H NMR (600 MHz, $(CD_3)_2SO$) δ 8.09 (app. d, app. *J* = 6.9 Hz, 2H), 7.23 (app. d, app. *J* = 6.5 Hz, 2H), 2.27 (s, 3H).[9]

^{15}N NMR (60.8 MHz, $(CD_3)_2SO$): δ 284.3.[11]

Pyrimidine *N*-Oxide (3)



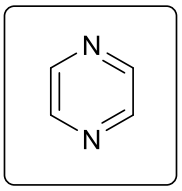
Pyrimidine *N*-oxide (0.047 g) was dissolved in DMSO (0.65 ml) and placed in an NMR tube by syringe under nitrogen, which was then sealed with a rubber septum cap. After fitting the rubber septum to the NMR tube, the seal was secured by wrapping the external edge of the septum where it contacted the surface of the NMR tube with PTFE tape. ^{1}H NMR and ^{1}H-^{15}N HMBC NMR spectra were recorded on this sample.

^{1}H NMR (600 MHz, DMSO) δ 9.04 (s, 1H), 8.58–8.52 (m, 1H), 8.25 (dd, *J* = 4.7, 1.0 Hz, 1H), 7.55 – 7.49 (m, 1H).

^{15}N NMR (60.8 MHz, DMSO): δ 301.3, 291.7.

3.3.2. NMR Spectral Data for Starting Materials in CH_2Cl_2

Pyrazine (18)



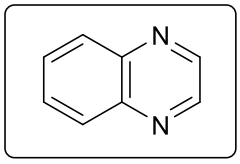
Pyrazine (**18**) (0.063 g) was dissolved in dry CH_2Cl_2 (0.65 ml) in a N_2-filled Schlenk flask and placed in an NMR tube by syringe under nitrogen, which was then sealed with a rubber septum cap. After fitting the rubber septum to the NMR tube, the seal was secured by wrapping the external edge of the septum where it contacted the surface of the NMR tube with PTFE tape. The product was analysed by ^{1}H and ^{1}H-^{15}N HMBC NMR spectroscopy.

^{1}H NMR (600 MHz, CH_2Cl_2) δ 8.54 (s, 4H).

^{15}N NMR (60.8 MHz, CH_2Cl_2): δ 333.0

Quinoxaline (19)

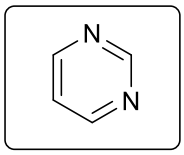
Quinoxaline (**19**) (0.052 g) was dissolved in dry CH_2Cl_2 (0.65 ml) in a N_2-filled Schlenk flask and placed in an NMR tube by syringe under nitrogen, which was then sealed with a rubber septum cap. After fitting the rubber septum to the NMR tube, the seal was secured by wrapping the external edge of the septum where it contacted the surface of the NMR tube with PTFE tape. The product was analysed by ^{1}H and ^{1}H-^{15}N HMBC NMR spectroscopy.



^{1}H NMR (600 MHz, CH_2Cl_2) δ 8.81 (s, 2H), 8.09 (dt, *J* = 6.6, 3.3 Hz, 2H), 7.80 – 7.73 (m, 2H).

^{15}N NMR (60.8 MHz, CH_2Cl_2): δ 329.0

Pyrimidine (20)

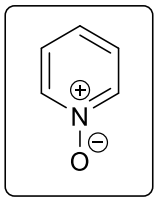


Pyrimidine (**20**) (0.045 g) was dissolved in dry CH_2Cl_2 (0.65 ml) in a N_2-filled Schlenk flask and placed in an NMR tube by syringe under nitrogen, which was then sealed with a rubber septum cap. After fitting the rubber septum to the NMR tube, the seal was secured by wrapping the external edge of the septum where it contacted the surface of the NMR tube with PTFE tape. The product was analysed by ^{1}H and ^{1}H-^{15}N HMBC NMR spectroscopy.

^{1}H NMR (600 MHz, CH_2Cl_2) δ 9.15 (s, 1H), 8.69 (d, *J* = 4.9 Hz, 2H), 7.29 (app. td, app. *J* = 4.9, 1.4 Hz, 1H).

^{15}N NMR (60.8 MHz, CH_2Cl_2): δ 294.4

Pyridine *N*-Oxide (21)

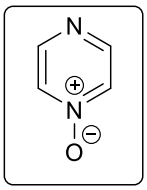


Pyridine *N*-oxide (**21**) (0.096 g) was dissolved in dry CH_2Cl_2 (0.65 ml) in a N_2-filled Schlenk flask and placed in an NMR tube by syringe under nitrogen, which was then sealed with a rubber septum cap. After fitting the rubber septum to the NMR tube, the seal was secured by wrapping the external edge of the septum where it contacted the surface of the NMR tube with PTFE tape. The product was analysed by ^{1}H and ^{1}H-^{15}N HMBC NMR spectroscopy.

^{1}H NMR (600 MHz, CH_2Cl_2) δ 8.13 – 8.06 (m, 1H), 7.25 – 7.15 (m, 2H).

^{15}N NMR (60.8 MHz, CH_2Cl_2): δ 294.0.[10]

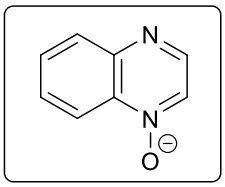
Pyrazine *N*-Oxide (1)



Pyrazine *N*-oxide (**1**) (0.080 g) was dissolved in CH_2Cl_2 (0.65 ml) and placed in an NMR tube by syringe under nitrogen, which was then sealed with a rubber septum cap. After fitting the rubber septum to the NMR tube, the seal was secured by wrapping the external edge of the septum where it contacted the surface of the NMR tube with PTFE tape. ^{1}H NMR and ^{1}H-^{15}N HMBC NMR spectra were recorded on this sample.

^{1}H NMR (600 MHz, CH_2Cl_2) δ 8.40 (app. d, app. *J* = 4.3 Hz, 2H), 8.08 – 8.03 (m, 2H).

^{15}N NMR (60.8 MHz, CH_2Cl_2): δ 311, 303.5



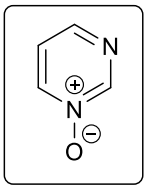
Quinoxaline *N*-Oxide (2)

Quinoxaline *N*-oxide (**2**) (0.055 g) was dissolved in CH_2Cl_2 (0.65 ml) and placed in an NMR tube by syringe under nitrogen, which was then sealed with a rubber septum cap. After fitting the rubber septum to the NMR tube, the seal was secured by wrapping the external edge of the septum where it contacted the surface of the NMR tube with PTFE tape. ^{1}H NMR and ^{1}H-^{15}N HMBC NMR spectra were recorded on this sample.

^{1}H NMR (600 MHz, CH_2Cl_2) δ 8.62 (d, *J* = 3.5 Hz, 1H), 8.50 (app. d, app. *J* = 8.6 Hz, 1H), 8.31 (d, *J* = 3.5 Hz, 1H), 8.09 (app. d, app. *J* = 8.4 Hz, 1H), 7.82 – 7.77 (m, 1H), 7.74 – 7.69 (m, 1H).

^{15}N NMR (60.8 MHz, CH_2Cl_2): δ 302, 300.3.

Pyrimidine *N*-Oxide (3)

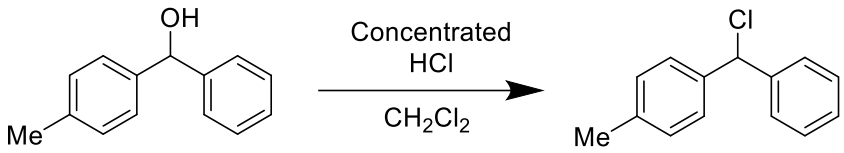


Pyrimidine *N*-oxide (**3**) (0.047 g) was dissolved in CH_2Cl_2 (0.65 ml) and placed in an NMR tube by syringe under nitrogen, which was then sealed by a rubber septum cap and wrapped with PTFE tape. The product was analysed by ^{1}H and ^{1}H-^{15}N HMBC NMR.

^{1}H NMR (600 MHz, CH_2Cl_2) δ 8.90 (s, 1H), 8.32 (app. d, app. *J* = 6.6 Hz, 1H), 8.16 (app. d, app. *J* = 4.6 Hz, 1H), 7.30 – 7.24 (m, 1H).

^{15}N NMR (60.8 MHz, CH_2Cl_2): δ 299.6, 291.4.

3.4. Synthesis of 4-Methylbenzhyldryl Chloride



4-methylbenzhydrol (1.00 g, 5.04 mmol) was dissolved in dichloromethane (16 ml), and the resulting solution was cooled in an ice bath for 10 minutes. Over approximately 20 minutes, concentrated aqueous HCl (37%; 5 ml) was added dropwise from a Pasteur pipette into the solution of 4-methylbenzhydrol at 0 °C. The reaction was stirred at 0 °C for 1.5 hours, and then placed in a refrigerator overnight. The reaction was then transferred into a pre-chilled separating funnel (cooled in freezer in advance), and the dichloromethane phase was separated from the aqueous phase. The aqueous phase was extracted twice with cold dichloromethane (pre-chilled in an ice bath; *ca.* 5 ml per extraction), and the dichloromethane phases were combined and then dried over anhydrous $CaCl_2$. The $CaCl_2$ was removed by filtration. The dichloromethane phases were kept cold at all points by immersing the vessel(s) containing them in an ice bath.

Next, the solvent was removed from the filtrate under vacuum, giving a colourless oil (1.05 g, 4.85 mmol, 96%). The flask containing the product was maintained at room temperature during solvent removal, and a relatively high vacuum was used to remove the solvent as quickly as possible. A sample was removed and dissolved in $CDCl_3$, and a ^{1}H NMR spectrum was obtained.

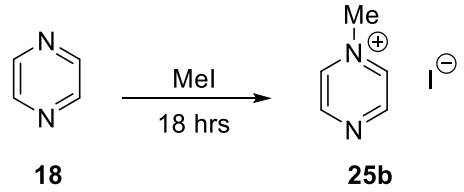
^{1}H NMR (300 MHz, $CDCl_3$) δ 7.46 – 7.26 (m, overlaps with C*H*Cl_3 signal, contains 7H of tolyl and phenyl groups), 7.15 (app. d, app. *J* = 7.9 Hz, 2H), 6.11 (s, 1H, Ar_2CH), 2.34 (s, 3H, CH_3).[12]

An attempt was made to crystallise the product by triturating with *n*-pentane, and hence small signals of this solvent are present in the ^{1}H NMR spectrum recorded of the product.

The product was stored in a freezer, and remains stable at −18 °C for at least one year.

3.5. Reactions of Diazines and *N*-Oxides with Alkylating Agents

Preparation of *N*-Methylpyrazinium Iodide (25b)



18 **25b**

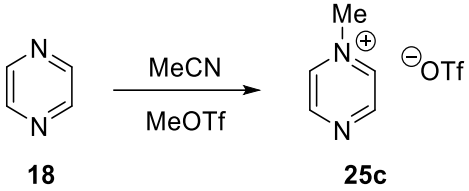
Pyrazine (**18**) (0.089 g, 1.11 mmol) was placed in a N_2-filled Schlenk flask. Methyl iodide (0.21 ml, 0.48g, 3.38 mmol) was added by syringe to the flask, which was wrapped in aluminium foil to protect the contents from light. The MeI was removed under vacuum by Procedure A after stirring of the reaction mixture for 18 hours, and the yellow solid product (**25b**) was washed by addition of dry Et_2O, which was removed by cannula filtration (under inert atmosphere). Three aliquots of dry Et_2O (0.5 ml each) were used in this manner to wash the product (yield = 0.049 g, 20%). A sample of **25b** in dry $(CH_3)_2SO$ was then prepared for ^1H and ^1H-^{15}N HMBC NMR spectroscopic characterisation by Procedure B. Note: An initial attempt to dissolve the product in CH_2Cl_2 was unsuccessful, and a residual amount of this solvent can be seen in the ^1H NMR spectrum.

^{1}H NMR (600 MHz, $(CH_3)_2SO$) δ 9.49 (app. s, 2H), 9.11 (d, *J* = 3.0 Hz, 2H), 4.37 (s, 3H).[13]

^{15}N NMR (60.8 MHz, $(CH_3)_2SO$): δ 357.6, 221.0

Copies of the NMR spectra are shown in section 1 of Appendix A.

Preparations of *N*-Methylpyrazinium Triflate (25c)



18 **25c**

(a) Pyrazine (**18**) (0.142 g, 1.77 mmol) was dissolved in dry MeCN (5 ml) in a N_2-filled Schlenk flask which was wrapped in aluminium foil to protect the product from light. Methyl triflate (0.295 g, 1.79 mmol) was subsequently added dropwise. After *ca.* 18 hours, the MeCN was removed under vacuum by Procedure A and the solid product (**25c**) was washed by addition of dry Et_2O, which was removed by cannula filtration (under inert atmosphere). Three aliquots of dry Et_2O (0.5 ml each) were used in this manner to wash the product (yield = 0.372 g, 86%; product contained *ca.* 2% of **18**, therefore yield = 86% × 0.98 = 84%). A sample of **25c** in dry $(CD_3)_2SO$ was then prepared for ^1H NMR spectroscopic characterisation using Procedure B.

^{1}H NMR (400 MHz, $(CD_3)_2SO$) δ 9.50 (app. s, 2H), 9.13 (app. s, 2H), 4.42 (s, 3H).[13]

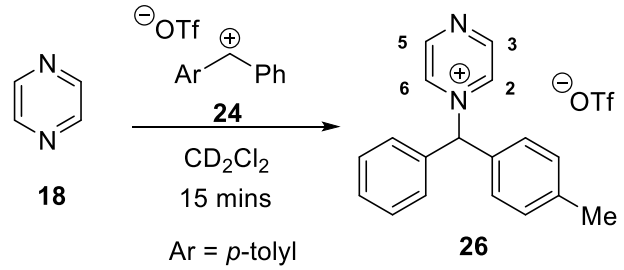
(b) Pyrazine (**18**) (0.142 g, 1.77 mmol) was dissolved in dry MeCN (5 ml) in a N_2-filled Schlenk flask which was wrapped in aluminium foil to protect the product from light. Methyl triflate (0.167 g, 1.02 mmol) was subsequently added dropwise. After *ca.* 30 minutes, the MeCN was removed under vacuum by Procedure A. The solid product (**25c**) was washed with dry Et_2O (3 × 0.4 ml portions) as described above. The product was analysed by ^{1}H and ^{1}H-^{15}N HMBC NMR spectroscopy using Procedure B in $(CH_3)_2SO$.

^{1}H NMR (600 MHz, $(CH_3)_2SO$) δ 9.47 (app. s, 2H), 9.10 (d, J = 3.2 Hz, 2H), 4.38 (s, 3H).[13]

^{15}N NMR (60.8 MHz, $(CH_3)_2SO$): δ 357.4, 220.7

Copies of the NMR spectra are shown in section 1 of Appendix A.

Preparation of 26



Pyrazine (**18**) (0.016 g, 0.20 mmol), 4-methylbenzhydryl chloride (0.041 g, 0.19 mmol) and silver triflate (0.054 g, 0.21 mmol) were combined by the process described in Procedure C to produce **24** in CD_2Cl_2. This product decomposes by hydrolysis if exposed to the ambient atmosphere. Consequently, the product was not isolated. Instead, the reaction mixture (in CD_2Cl_2) was analysed directly by NMR spectroscopy using Procedure B. The signals in the NMR spectra of the reaction mixture assigned to **26** are reported below.

^{1}H NMR (600 MHz, CD_2Cl_2) δ 9.42 (s, 2H, H-3 & H-5), 8.83 (s, 2H, H-2 & H-6), 7.67 (s, 1H, PhTolC*H*), 7.54 – 7.09 (m, 9H, Phenyl H-2, H-3, H-4, H-5 & H-6. Tolyl H-2, H-3, H-5 & H-6), 2.38 (s, 3H, CH_3).

The peak assigned to the starting material **18** is seen at 8.57 ppm. 4H of this compound integrates for 1.75 with respect to 1H of **26**; i.e., 1H of **18** = 0.44 with respect to 1H of **26**.

Peaks assigned to hydrolysis products are seen at 6.14ppm and 5.37ppm. The aromatic protons of these products also contribute to the integration of the multiplet at 7.54 – 7.09 ppm.

^{13}C NMR (150 MHz, CD_2Cl_2) δ 151.7 (C-3 & C-5), 141.6 (Tolyl C-4), 136.4 (C-2 & C-5), 134.2 (Phenyl C-1), 130.9 (Tolyl C-3 & C-5), 130.2 (Phenyl C-3 & C-5), 129.6 (Tolyl C-2 & C-6), 129.5 (Tolyl C-1), 129.3 (Phenyl C-2 & C-6), 79.6 (PhTol*C*H), 21.3 (*C*H_3).

A ^{13}C NMR signal assigned to the *C*$F_3SO_3^-$ ion is present at δ 121.1 (q, *J* = 321 Hz).

^{15}N NMR (60.8 MHz, CD_2Cl_2): δ 364.4, 240.6.

A peak assigned to the starting material **1** appears at 332.0 ppm.

Conversion Calculation (based on consumption of 4-methylbenzhydrylium ion):

2H of Compound **26** corresponds to 2.00, therefore 1H = 1.00.

For the hydrolysis product at 6.14 ppm, 1H = 0.27

For the bis(benzhydryl) ether hydrolysis product signal at 5.37 ppm ($Ar_2CH)_2O$), 2H = 0.09.

$$\text{Conversion} = \frac{1.00}{1.00 + 0.27 + 0.09} \times 100 = 74\%$$

Copies of the NMR spectra are shown in section 1 of Appendix A.

Preparation of *N*-Methylquinoxalinium Iodide (27b)



19 **27b**

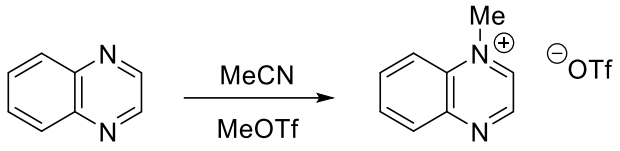
Quinoxaline (**19**) (0.131 g, 1.01 mmol) was placed in a N_2-filled Schlenk flask which was wrapped in aluminium foil to protect the product from light. Methyl iodide (0.19 ml, 0.43 g, 3.03 mmol) was added by syringe to the flask. The MeI was removed under vacuum by Procedure A after stirring of the reaction mixture for 18 hours, and the orange oil product (**27b**) was washed by addition of dry Et_2O, which was removed by cannula filtration (under inert atmosphere). Three aliquots of dry Et_2O (0.5 ml each) were used in this manner to wash the product (yield = 0.117 g, 43%). A sample of **27b** in dry $(CH_3)_2SO$ was then prepared for ^{1}H and ^{1}H-^{15}N HMBC NMR spectroscopic characterisation using Procedure B. Note: An initial attempt to dissolve the product in CH_2Cl_2 was unsuccessful, and a residual amount of this solvent can be seen in the spectrum.

^{1}H NMR (600 MHz, $(CH_3)_2SO$) δ 9.68 (app. d, app. *J* = 2.8 Hz, 1H), 9.58 (app. d, app. *J* = 2.6 Hz, 1H), 8.59 (app. d, app. *J* = 8.7 Hz, 1H), 8.51 (app. d, app. *J* = 8.4 Hz, 1H), 8.36 – 8.30 (m, 1H), 8.27 (t, *J* = 7.7 Hz, 1H), 4.69 (s, 3H).[14]

^{15}N NMR (60.8 MHz, $(CH_3)_2SO$): δ 355.5, 208.6

Copies of the NMR spectra are shown in section 1 of Appendix A.

Preparation of *N*-Methylquinoxalinium Triflate (27c)



19 **27c**

(a) Quinoxaline (**19**) (0.242 g, 1.86 mmol) was dissolved in dry MeCN (5 ml) in a N_2-filled Schlenk flask which was wrapped in aluminium foil to protect the product from light. Methyl triflate (0.304 g, 1.85 mmol) was subsequently added dropwise. After *ca.* 18 hours, the MeCN was removed under vacuum by Procedure A and the solid product (**27c**) was washed by addition of dry Et_2O, which was removed by cannula filtration (under inert atmosphere). Three aliquots of dry Et_2O (0.5 ml each) were used in this manner to wash the product (yield = 0.537 g, 98%; product contained *ca*. 2% (**19**), therefore yield = 98% × 0.98= 96%). A sample of **27c** in dry $(CD_3)_2SO$ was then prepared for ^1H NMR spectroscopic characterisation using Procedure B.

^{1}H NMR (400 MHz, $(CD_3)_2SO$) δ 9.71 (app. d, app. *J* = 2.8 Hz, 1H), 9.61 (app. d, app. *J* = 2.6 Hz, 1H), 8.64 (app. d, app. *J* = 8.7 Hz, 1H), 8.53 (app. d, app. *J* = 8.4 Hz, 1H), 8.39 – 8.33 (m, 1H), 8.29 (app. t, app. *J* = 7.4 Hz, 1H), 4.77 (s, 3H).[14]

Copies of the NMR spectra are shown section 1 of in Appendix A.

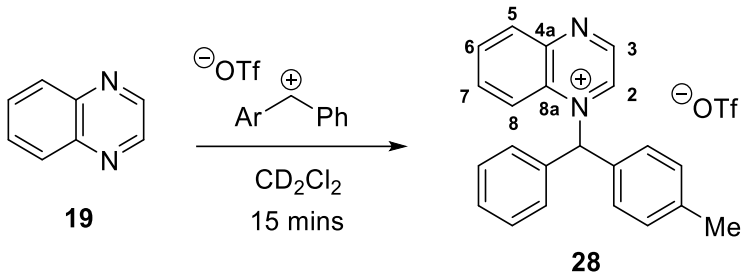
(b) Quinoxaline (**19**) (0.096 g, 0.74 mmol) was dissolved in dry MeCN (5 ml) in a N_2-filled Schlenk flask which was wrapped in aluminium foil to protect the product from light. Methyl triflate (0.087 g, 0.53 mmol) was subsequently added dropwise. After *ca.* 30 minutes, the MeCN was removed under vacuum by Procedure A and the solid product (**27c**) was washed with dry Et_2O (3 × 0.4 ml portions) as described above. The product was analysed by ^1H and ^1H-^{15}N HMBC NMR spectroscopy by Procedure B in DMSO.

^{1}H NMR (600 MHz, $(CH_3)_2SO$) δ 9.68 (app. d, app. *J* = 2.8 Hz, 1H), 9.57 (app. d, app. *J* = 2.5 Hz, 1H), 8.60 (app. d, app. *J* = 8.7 Hz, 1H), 8.51 (app. d, app. *J* = 8.4 Hz, 1H), 8.33 (app. t, app. *J* = 7.3 Hz, 1H), 8.26 (app. t, app. *J* = 7.7 Hz, 1H), 4.72 (s, 3H).[14]

^{15}N NMR (60.8 MHz, $(CH_3)_2SO$): δ 356.6, 208.7.

Copies of the NMR spectra are shown in section 1 of in Appendix A.

Preparation of 28



Quinoxaline (**19**) (0.019 g, 0.015 mmol), 4-methylbenzhydryl chloride (0.030 g, 0.14 mmol) and silver triflate (0.045 g, 0.18 mmol) were combined by the process described in Procedure C to produce **24** in CD_2Cl_2. This product decomposes by hydrolysis if exposed to the ambient atmosphere. Consequently, the product was not isolated. Instead, the reaction mixture (in CD_2Cl_2) was analysed directly by NMR spectroscopy using Procedure B. The signals in the NMR spectra of the reaction mixture assigned to **28** are reported below.

^{1}H NMR (600 MHz, CD_2Cl_2) δ 9.60 (d, *J* = 3.0 Hz, 1H, H-4), 8.74 (d, *J* = 3.0 Hz, 1H, H-2), 8.60 – 8.55 (m, 1H, H-5), 8.55 – 8.50 (m, 1H, H-8), 8.21 – 8.11 (m, 3H, C*H*PhTol, H-6 & H-7), 7.49 – 7.44 (m, 3H, Phenyl H-3, H-4 & H-5), 7.39 – 7.11 (m, 6H, Phenyl H-2 & H-6, Tolyl H-2, H-3, H-5 & H-6), 2.37 (s, 3H, C*H*$_3$).

Signals assigned to the starting material **19** are seen at 8.87 ppm, within the multiplet at 8.21 – 8.11 ppm and 7.83 ppm. 2H of this compound corresponds to an integration of ~0.40 relative to 1H of **28**.

The multiplet at 8.21-8.11 ppm contains 1H each of C*H*PhTol, H-6 & H-7. Also included is 1H of the starting material **19**.

Signals assigned to hydrolysis products are seen at 6.14 ppm and 5.37 ppm. The aromatic protons of these products also contribute to the integration of the multiplet at 7.39 – 7.11 ppm.

^{13}C NMR (150 MHz, CD_2Cl_2) δ 147.7 (C-3), 147.4 (C-4a), 141.4 (Tolyl C-4), 137.7 (C-2), 137.3 (C-7), 134.4 (C-6), 134.4 (Phenyl C-1), 132.6 (C-8), 131.1 (Tolyl C-3 & C-5), 130.9 (C-8a), 130.6 (Phenyl C-4), 130.3 (Phenyl C-3 & C-5), 129.6 (Tolyl C-2 & C-6), 129.5 (Tolyl C-1), 129.2 (Phenyl C-2 & C-6), 120.4 (C-5), 75.2 (*C*HPhTol), 21.3 (*C*H$_3$).

A ^{13}C NMR signal assigned to the *C*$F_3SO_3^-$ ion is seen at 121.1 (q, *J* = 321 Hz).

^{15}N NMR (60.8 MHz, CD_2Cl_2): δ 363.7, 225.3

A peak assigned to the starting material **19** may also be seen at 324.0 ppm.

<u>Conversion Calculation</u> (based on consumption of 4-methylbenzhydrylium ion):

1H of Compound **28** corresponds to 1.00.

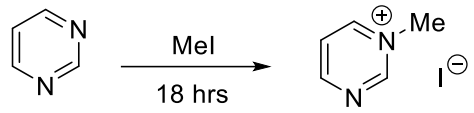
For the benzhydrol hydrolysis product at 6.14 ppm, 1H = 0.12

For the bis(benzhydryl) ether hydrolysis product signal at 5.37 ppm ($Ar_2CH)_2O$), 2H = 0.11.

$$\text{Conversion} = \frac{1.00}{1.00 + \ 0.12 + 0.11} \times \ 100 = 81\%$$

Copies of the NMR spectra are shown in section 1 of Appendix A.

Preparation of *N*-Methylpyrimidinium Iodide (29b)



20 **29b**

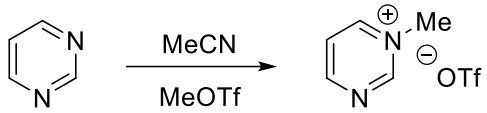
Pyrimidine (**20**) (0.089 g, 1.11 mmol) was placed in a N_2-filled Schlenk flask which was wrapped in aluminium foil to protect the product from light. Methyl iodide (0.21 ml, 0.48g, 3.38 mmol) was added by syringe to the flask. The MeI was removed under vacuum by Procedure A after stirring of the reaction mixture for 18 hours, and the yellow solid product (**29b**) was washed by addition of dry Et_2O, which was removed by cannula filtration (under inert atmosphere). Three aliquots of dry Et_2O (0.5 ml each) were used in this manner to wash the product (yield = 0.150 g, 61%). A sample of **29b** in dry $(CH_3)_2SO$ was then prepared for ^1H and ^1H-^{15}N HMBC NMR spectroscopic characterisation using Procedure B.

^{1}H NMR (600 MHz, $(CH_3)_2SO$) δ 9.77 (s, 1H), 9.41 (app. dd, app. *J* = 4.9, 1.7 Hz, 1H), 9.35 (app. d, app. *J* = 6.3 Hz, 1H), 8.26 (app. t, app. *J* = 5.6 Hz, 1H), 4.26 (s, 3H).[13]

^{15}N NMR (60.8 MHz, $(CH_3)_2SO$): δ 298.7, 199.5

Copies of the NMR spectra are shown in section 1 of Appendix A.

Preparation of *N*-Methylpyrimidinium Triflate (29c)



20 **29c**

(a) Pyrimidine (**20**) (0.138 g, 1.72 mmol) was dissolved in dry MeCN (5 ml) in an inert N_2-filled Schlenk flask which was wrapped in aluminium foil to protect the product from light. Methyl triflate (0.282 g, 1.73 mmol) was subsequently added dropwise. After *ca.* 18 hours, the MeCN was removed under vacuum by Procedure A and the solid product (**29c**) was washed by addition of dry Et_2O, which was removed by cannula filtration (under inert atmosphere). Three aliquots of dry Et_2O (0.5 ml each) were used in this manner to wash the product (yield = 0.337 g, 80%. Product contained *ca*. 2% (**20**), therefore yield = 80% × 0.98= 78%). A sample of

29c in dry $(CD_3)_2SO$ was then prepared for ^1H NMR spectroscopic characterisation using Procedure B.

^{1}H NMR (400 MHz, $(CD_3)_2SO$) δ 9.76 (s, 1H), 9.43 (d, *J* = 4.9 Hz, 1H), 9.34 (d, *J* = 5.7 Hz, 1H), 8.25 (t, *J* = 5.5 Hz, 1H), 4.31 (app. d, *J* = 1.9 Hz, 3H).[13]

It is not clear whether the apparent small splitting of the signal at δ 4.31 is an artefact particular to the acquisition of this spectrum, or whether it is a consequence of ^1H-^{15}N coupling. The corresponding signal in other spectra of the same compound does appear as a singlet (see below).

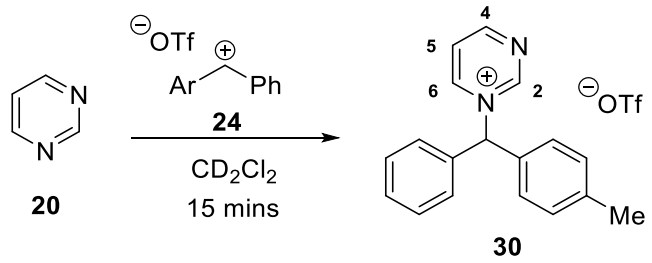
(b) Pyrimidine (**20**) (0.111 g, 1.38 mmol) was dissolved in dry MeCN (5 ml) in a N_2-filled Schlenk flask which was wrapped in aluminium foil to protect the product from light. Methyl triflate (0.159 g, 0.97 mmol) was subsequently added dropwise. After *ca.* 30 minutes, the MeCN was removed under vacuum by Procedure A and the solid product (**29c**) was washed with dry Et_2O (3 × 0.5 ml portions) as described above. The product was analysed by ^1H and ^1H-^{15}N HMBC NMR spectroscopy by Procedure B in $(CH_3)_2SO$.

^{1}H NMR (600 MHz, $(CH_3)_2SO$) δ 9.73 (s, 1H), 9.39 (dd, *J* = 4.9, 1.6 Hz, 1H), 9.30 (app. d, app. *J* = 6.3 Hz, 1H), 8.22 (app. t, app. *J* = 5.5 Hz, 1H), 4.27 (s, 3H).[13]

^{15}N NMR (60.8 MHz, $(CH_3)_2SO$): δ 299.9, 199.4.

Copies of the NMR spectra are shown in section 1 of Appendix A.

Preparation of 30



Pyrimidine (**20**) (0.009 g, 0.11 mmol), 4-methylbenzhydryl chloride (0.024 g, 0.11 mmol) and silver triflate (0.028 g, 0.11 mmol) were combined by the process described in Procedure C to produce **24** in CD_2Cl_2. This product decomposes by hydrolysis if exposed to the ambient atmosphere. Consequently, the product was not isolated. Instead, the reaction mixture (in CD_2Cl_2) was analysed directly by NMR spectroscopy using Procedure B. The signals in the NMR spectra of the reaction mixture assigned to **30** are reported below.

^{1}H NMR (600 MHz, CD_2Cl_2) δ 9.54 (s, 1H, H-2), 9.41 (app. d, app. *J* = 3.5 Hz, 1H, H-4), 9.06 (app. dd, app. *J* = 4.7, 1.7 Hz, 1H, H-6), 8.18 (app. t, app. *J* = 5.6 Hz, 1H, H-5), 7.60 (s, 1H, C*H*PhTol), 7.49 – 7.44 (m, 3H, Phenyl H-3, H-4 & H-5), 7.38 – 7.10 (m, 6H, Phenyl H-2 & H-6. Tolyl H-2, H-3, H-5 & H-6), 2.37 (s, 3H, CH_3).

A peak assigned to a hydrolysis product is seen at 5.36 ppm. The aromatic protons of this product also contribute to the integration of the multiplet at 7.38 – 7.10 ppm.

^{13}C NMR (150 MHz, CD_2Cl_2) δ 165.7 (C-4), 153.7 (C-2), 151.9 (C-6), 141.4 (Tolyl C-4), 134.5 (Phenyl C-1), 131.0 (Tolyl C-1), 130.9 (Tolyl C-3 & C-5), 130.6 (Phenyl C-4), 130.2 (Phenyl C-3 & C-5), 129.5 (Tolyl C-2 & C-6), 129.2 (Phenyl C-2 & C-6), 124.7 (C-5), 76.6 (*C*HPhTol), 21.3 (*C*H$_3$).

A ^{13}C NMR signal assigned to the *C*F$_3$SO$_3^-$ ion is seen at δ 120.9 (q, *J* = 320 Hz).

^{15}N NMR (60.8 MHz, CD_2Cl_2): δ 298.8, 218.6

Conversion Calculation (based on consumption of 4-methylbenzhydrylium ion):

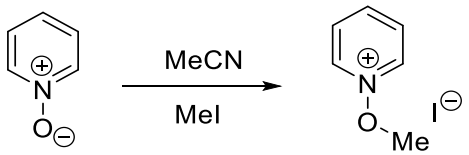
1H of Compound **30** corresponds to 1.00.

For the bis(benzhydryl) ether hydrolysis product signal at 5.36 ppm (Ar$_2$C*H*)$_2$O), 2H = 0.11.

$$\text{Conversion} = \frac{1.00}{1.00 + 0.11} \times 100 = 90\%$$

Copies of the NMR spectra are shown in section 1 of Appendix A.

Preparation of *N*-Methoxypyridinium Iodide (31b)



21 **31b**

(a) Pyridine *N*-oxide (**21**) (0.485 g, 5.1 mmol) was added to a N_2-filled Schlenk flask. Methyl iodide (6.84 g, 48.2 mmol) was subsequently added dropwise *via* syringe. The MeI was removed under vacuum by Procedure A after stirring of the reaction mixture for 40 hours, and the resulting yellow solid product (**31b**) was washed by addition of dry THF, which was removed by cannula filtration (under inert atmosphere). Three aliquots of dry THF (3 ml each) were used in this manner to wash the product (yield = 0.665 g, 59%). A sample of **31b** in dry $(CD_3)_2SO$ was then prepared for ^{1}H NMR spectroscopic characterisation using Procedure B.

^{1}H NMR (300 MHz, $(CD_3)_2SO$) δ 9.51 – 9.46 (m, 2H), 8.68 – 8.58 (m, 1H), 8.31 – 8.23 (m, 2H), 4.45 (s, 3H).[10]

A copy of the ^{1}H NMR spectrum is shown in section 1 of Appendix A.

(b) Pyridine *N*-oxide (**21**) (0.056 g, 0.59 mmol) was dissolved in dry MeCN (5 ml) in a N_2-filled Schlenk flask. Methyl iodide (0.25 g, 1.76 mmol) was subsequently added dropwise *via* syringe. The MeI was removed under vacuum by Procedure A after stirring of the reaction mixture for 18 hours, and the yellow solid product (**31b** was analysed by ^{1}H and ^{1}H – ^{15}N HMBC NMR spectroscopy using Procedure B in DMSO. Note: The reaction did not go to completion and hence the

^{1}H and ^{1}H – ^{15}N HMBC NMR spectra contain significant amounts of the starting material (**21**).

^{1}H NMR (600 MHz, $(CH_3)_2SO$)

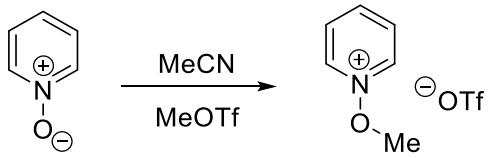
Signals assigned to **31b**: δ 9.46 (app. d, app. *J* = 6.1 Hz, 2H), 8.61 (app. t, app. *J* = 7.7 Hz, 1H), 8.24 (app. t, app. *J* = 7.3 Hz, 2H), 4.42 (s, 3H).[10]

Signals assigned to **21**: δ 8.17 (app. d, app. *J* = 6.1 Hz, 2H), 7.38 (app. t, app. *J* = 7.0 Hz, 2H), 7.30 (app. t, app. *J* = 7.6 Hz, 1H).

^{15}N NMR (60.8 MHz, $(CH_3)_2SO$): δ 256.8 (Also appearing: 295.1, ^{15}N signal of **21**).

Copies of the NMR spectra are shown in section 1 of Appendix A.

Preparations of *N*-Methoxypyridinium Triflate (31c)



21 **31c**

(a) Pyridine *N*-oxide (**21**) (0.220 g, 2.31 mmol) was dissolved in dry MeCN (5 ml) in a N_2-filled Schlenk flask. Methyl triflate (0.384 g, 2.34 mmol) was subsequently added dropwise. After *ca.* 18 hours, the MeCN was removed under vacuum by Procedure A and the solid product (**31c**) was washed by addition of dry Et_2O. The supernatant ether solution was removed by cannula filtration (under inert atmosphere). Three aliquots of dry Et_2O (0.5 ml each) were used in this manner to wash the product (yield = 0.469 g, 78%). A sample of **31c** in dry $(CD_3)_2SO$ was then prepared for ^{1}H and ^{1}H-^{15}N HMBC NMR spectroscopic characterisation using Procedure B.

^{1}H NMR (300 MHz, $(CD_3)_2SO$) δ 9.40 (app. d, app. *J* = 6.3 Hz, 2H), 8.61 (app. t, app. *J* = 7.8 Hz, 1H), 8.22 (app. t, app. *J* = 7.3 Hz, 2H), 4.45 (s, 3H).[15]

A copy of the ^{1}H NMR spectrum is shown in section 1 of Appendix A.

(b) Pyridine *N*-oxide (**21**) (0.064 g, 0.67 mmol) was dissolved in dry MeCN (5 ml) in a N_2-filled Schlenk flask. Methyl triflate (0.111 g, 0.67 mmol) was subsequently added dropwise. After *ca.* 20 minutes, the MeCN was removed under vacuum by Procedure A and the solid product (**31c**) was analysed by ^{1}H and ^{1}H-^{15}N HMBC NMR spectroscopy by Procedure B in $(CH_3)_2SO$. Quantitative conversion to the product was observed.

^{1}H NMR (600 MHz, $(CH_3)_2SO$) δ 9.41 (app. d, app. *J* = 6.3 Hz, 2H), 8.59 (app. t, app. *J* = 7.7 Hz, 1H), 8.21 (app. t, app. *J* = 7.2 Hz, 2H), 4.41 (s, 3H).[15]

^{15}N NMR (60.8 MHz, $(CH_3)_2SO$): δ 252.4

Copies of the NMR spectra are shown in section 1 of Appendix A.

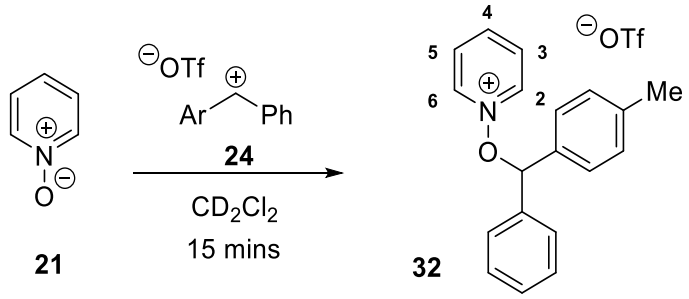
(c) Pyridine *N*-oxide (**21**) (0.0237 g, 0.25 mmol) was dissolved in dry CH_2Cl_2 (0.8 ml) in an inert N_2-filled Schlenk flask. Methyl triflate (0.040 g, 0.24 mmol) was subsequently added dropwise. After *ca.* 30 minutes, the product **31c** was analysed directly by ^{1}H and ^{1}H-^{15}N HMBC NMR spectroscopy by Procedure A in CH_2Cl_2. Quantitative conversion to the product was observed based on the ^{1}H NMR spectrum (based on consumption of MeOTf, i.e., the excess of **21** used remains).

^{1}H NMR (600 MHz, CH_2Cl_2) δ 9.18 (app. d, app. *J* = 6.7 Hz, 2H), 8.57 (app. td, app. *J* = 7.8, 0.8 Hz, 1H), 8.17 (app. t, app. *J* = 7.2 Hz, 2H), 4.47 (s, 3H).[15]

^{15}N NMR (60.8 MHz, CH_2Cl_2): δ 251.0.

Copies of the NMR spectra are shown in section 1 of Appendix A.

Preparation of 32



Pyridine *N*-oxide (**21**) (0.015 g, 0.16 mmol), 4-methylbenzhydryl chloride (0.031 g, 0.14 mmol) and silver triflate (0.048 g, 0.19 mmol) were combined by the process described in Procedure C to produce **24** in CD_2Cl_2. This product decomposes by hydrolysis if exposed to the ambient atmosphere. Consequently, the product was not isolated. Instead, the reaction mixture (in CD_2Cl_2) was analysed directly by NMR spectroscopy using Procedure B. The signals in the NMR spectra of the reaction mixture assigned to **32** are reported below.

^{1}H NMR (600 MHz, CD_2Cl_2) δ 8.93 (app. d, app. *J* = 6.1 Hz, 2H, H-3 & H-5), 8.36 (app. t, app. *J* = 7.8 Hz, 1H, H-4), 7.97 (app. t, app. *J* = 7.3 Hz, 2H, H-2 & H-6), 7.50 (app. dd, *J* = 6.4, 3.0 Hz, 2H, Phenyl H-2 & H-6), 7.44 – 7.10 (m, 7H, Phenyl H-3, H-4 & H-5, Tolyl H-2, H-3, H-5 & H-6), 6.91 (s, 1H, C*H*PhTol), 2.33 (s, 3H, CH_3).

A signal of the starting material **21** appears at δ 8.17 ppm (2H of **21**). This signal integrates for 0.30 relative to 1H of **32**, and hence 1H of **21** = 0.15 relative to 1H of **32**. Other signals are obscured.

^{13}C NMR (150 MHz, CD_2Cl_2) δ 145.4 (C-4), 142.3 (C-3 & C-5), 140.9 (Tolyl C-4), 135.2 (Phenyl C-1), 131.8 (Tolyl C-1), 130.3 (Tolyl C-3 & C-5), 130.2 (Phenyl C-4), 129.7 (C-2 & C-6), 129.5 (Phenyl C-3 & C-5), 128.8 (Phenyl C-2 & C-6), 128.5 (Phenyl C-2 & C-6), 97.1 (*C*HPhTol), 21.3 (*C*H_3).

A ^{13}C NMR signal assigned to the $CF_3SO_3^-$ ion is seen at δ 121.3 (q, J = 321 Hz).

^{15}N NMR (60.8 MHz, CD_2Cl_2): δ 246.0

Conversion Calculation (based on consumption of 4-methylbenzhydrylium ion):

2H of Compound **32** corresponds to 2.00, therefore 1H = 1.00.

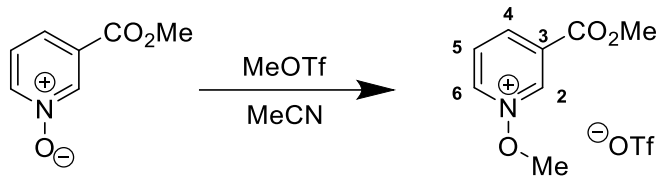
For the benzhydrol hydrolysis product at 6.14 ppm, 1H = 0.04

For the bis(benzhydryl) ether hydrolysis product signal at 5.36 ppm ($Ar_2CH)_2O$), 2H = 0.09.

$$\text{Conversion} = \frac{1.00}{1.00 + 0.04 + 0.09} \times 100 = 88\%$$

Copies of the NMR spectra are shown in section 1 of Appendix A.

Preparation of *N*-Methoxy-3-(methoxycarbonyl)pyridinium Triflate (33)



22 **33**

Methyl Nicotinate *N*-oxide (**22**) (0.054 g, 0.35 mmol) was dissolved in dry MeCN (5 ml) in an inert N_2-filled Schlenk flask. Methyl triflate (0.069 g, 0.42 mmol) was subsequently added dropwise. After *ca.* 48 hours, the MeCN was removed under vacuum by Procedure A and the yellow solid product (**33**) was washed by addition of dry Et_2O. The supernatant ether solution was removed by cannula filtration (under inert atmosphere). Three aliquots of dry Et_2O (3 ml each) were used in this manner to wash the product (yield = 0.045 g, 40%; product contains a small quantity of starting material **22**). A sample of **33** in dry $(CD_3)_2SO$ was then prepared for ^1H and ^1H-^{15}N HMBC NMR spectroscopic characterisation using Procedure B.

^1H NMR (300 MHz, $(CD_3)_2SO$) δ 9.98 (app. t, app. J = 1.6 Hz, 1H, H-2), 9.65 (app. ddd, app. J = 6.6, 2.0, 1.1 Hz, 1H, H-6), 9.03 – 8.96 (m, 1H, H-4), 8.40 – 8.33 (m, 1H, H-5), 4.49 (s, 3H, $COOCH_3$), 4.00 (s, 3H, $NOCH_3$).

^{13}C NMR (75 MHz, $(CD_3)_2SO$) δ 160.0 ($COOCH_3$), 143.0 (C-4), 142.7 (C-6), 140.9 (C-2), 129.8 (C-3), 128.0 (C-3), 68.5 ($NOCH_3$), 52.1 ($COOCH_3$).

^{15}N NMR (60.8 MHz, $(CD_3)_2SO$): δ 252.4

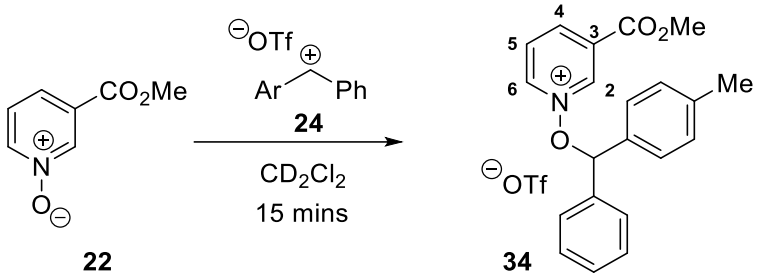
IR (ATR-FTIR), cm^{-1}: 3078 (w), 1740 (s), 1441 (w), 1256 (s), 1156 (s), 1029 (s), 637 (s).

Several attempts at recording HRMS data (by electrospray ionisation in positive mode) for this compound proved unsuccessful, which is ascribed to decomposition of the compound under the different experimental conditions employed.

Copies of the NMR spectra are shown in section 1 of Appendix A.

Preparation of 34

Methyl Nicotinate *N*-oxide (**22**) (0.0188 g, 0.12 mmol), 4-methylbenzhydryl chloride (0.0266 g, 0.12 mmol) and silver triflate (0.039 g, 0.15 mmol) were combined by the process described in Procedure C to produce **24** in CD_2Cl_2. This product decomposes by hydrolysis if exposed to the ambient atmosphere. Consequently, the product was not isolated. Instead, the reaction mixture (in CD_2Cl_2) was analysed directly by NMR spectroscopy using Procedure B. The signals in the NMR spectra of the reaction mixture assigned to **34** are reported below.



^{1}H NMR (600 MHz, CD_2Cl_2) δ 9.30 – 9.27 (m, 1H, H-6), 9.05 (t, *J* = 1.7 Hz, H-2 overlaps with signal of **22**), 8.84 (app. d, app. *J* = 8.0 Hz, 1H, H-4), 8.23 – 8.16 (m, 1H, H-5), 7.54 – 7.50 (m, 2H, Phenyl H-2 & H-6), 7.45 – 7.20 (m, 7H, Phenyl H-3, H-4 & H-5, Tolyl H-2, H-3, H-5 & H-6), 6.95 (s, 1H, C*H*PhTol), 3.99 (s, 3.3H, overlapping signals of CO_2CH_3 of **22** and **34**), 2.34 (s, contains 3.3H, overlapping signals of Tolyl CH_3 of **22** and **34**).

Signals of the bis(benzhydryl) ether hydrolysis product appear at δ 7.32 (4H), 7.14 (4H), and 5.37 (2H). The integration of 1H of this hydrolysis product = 0.07 relative to 1H of **34**. Aromatic protons of this product also contribute to the integration of the multiplet at 7.27 – 7.19 ppm.

Small signals of **22** appear at δ 9.03 (overlaps with signal of **34**), 8.74, 8.32, 7.73 (1H each), each integrating for 0.10 relative to 1H of **34**.

^{13}C NMR (150 MHz, CD_2Cl_2) δ 160.9 (*C*OOCH$_3$), 145.8 (C-6), 145.3 (C-4), 142.7 (C-2), 141.2 (Tolyl C-4), 135.1 (Phenyl C-1), 132.0 (C-3), 131.7 (Tolyl C-1), 130.4 (C-5), 130.3 (Phenyl C-4), 130.3 (Tolyl C-3 & C-5), 129.5 (Phenyl C-3 & C-5), 128.8 (Tolyl C-2 & C-6, 128.5 (C-2 & C-6), 97.8 (*C*HPhTol), 54.4 (COO*C*H$_3$), 21.3 (*C*H$_3$).

A ^{13}C NMR signal assigned to the *C*F$_3$SO$_3^-$ ion is seen at δ 121.0 (q, *J* = 320 Hz).

^{15}N NMR (60.8 MHz, $(CH_3)_2SO$): δ 248.3

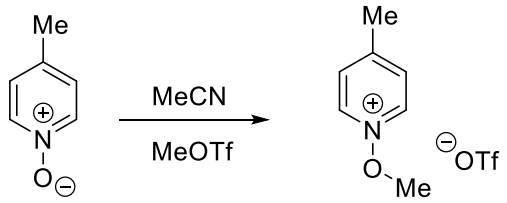
Conversion Calculation (based on consumption of 4-methylbenzhydrylium ion):

1H of Compound **34** corresponds to 1.00.

For the bis(benzhydryl) ether hydrolysis product signal at 5.37ppm (Ar$_2$C*H*)$_2$O), 2H = 0.14.

$$\text{Conversion} = \frac{1.00}{1.00 + 0.14} \times 100 = 88\%$$

Preparation of *N*-Methoxy-4-methylpyridinium Triflate (35c)



23 **35c**

(a) 4-Methylpyridine-*N*-oxide (**23**) (0.251 g, 2.30 mmol) was dissolved in dry MeCN (10 ml) in an inert N_2-filled Schlenk flask. Methyl triflate (0.495 g, 2.53 mmol) was subsequently added dropwise. The MeCN was removed under vacuum after 72 hours by Procedure A and the solid product (**35c**) was washed by addition of dry THF. The supernatant THF solution was removed by cannula filtration (under inert atmosphere). Three aliquots of dry THF (3 ml each) were used in this manner to wash the product. A sample of **35c** in dry $(CD_3)_2SO$ was then prepared for ^1H and ^1H-^{15}N HMBC NMR spectroscopic characterisation using Procedure B. The conversion was observed to be 93% from the integrations in the ^1H NMR spectrum.

^{1}H NMR (600 MHz, $(CD_3)_2SO$)

Signals assigned to **35c**: δ 9.30 (app. d, app. *J* = 7.0 Hz, 2H), 8.08 (app. d, app. *J* = 6.7 Hz, 2H), 4.39 (s, 3H), 2.63 (s, 3H).[16]

Signals assigned to **23**: δ 8.14 (d, *J* = 6.8 Hz, 2H), 7.28 (d, *J* = 6.5 Hz, 2H), 2.30 (s, 3H).

^{15}N NMR (60.8 MHz, $(CD_3)_2SO$): δ 247.3.[17]

Copies of the NMR spectra are shown in section 1 of Appendix A.

(b) 4-Methylpyridine-*N*-oxide (**23**) (0.059 g, 0.54 mmol) was dissolved in $CDCl_3$ (0.6 ml) in an inert atmosphere glove box. Methyl triflate (0.089 g, 0.54 mmol) was added to this solution dropwise (over *ca.* 3 minutes) while agitating the solution. The formation of a small amount of precipitate or emulsion was noted (i.e., the product **35c** has only limited solubility in $CDCl_3$). A portion of this solution (0.2 ml) was transferred to an NMR tube, and further $CDCl_3$ (0.5 ml) was added. The NMR tube was sealed with a rubber septum. ^1H NMR spectroscopic analysis indicated conversion of 92% (i.e., there remained 8% of starting material **23**). The solution in the NMR tube was re-combined with the reaction mixture (open to ambient atmosphere), and the solvent was removed under vacuum, giving a colourless oil. This oil was washed with five portions of diethyl ether (*ca.* 2 ml each). Each portion of ether was decanted off carefully. After the fourth wash, the oil solidified, giving a white solid. This solid was dissolved in the minimum

possible amount of boiling $CHCl_3$, and a small number of drops of boiling diethyl ether was added, causing an oil to separate from the solution. The solution was decanted off from the oil, and further ether (*ca.* 2 ml) was added to the remaining oil, causing is to form a white solid almost instantly. The ether was decanted off, and three further ether washes (2 ml each) of the solid were carried out. The white solid (**35c**) was then dried under vacuum (0.125 g, 84% yield). ^{1}H NMR spectroscopic analysis of this solid in $(CD_3)_2SO$ showed it to be product **35c**.

^{1}H NMR (300 MHz, $(CD_3)_2SO$) δ 9.35 – 9.25 (m, 2H), 8.09 (app. d, app. *J* = 6.7 Hz, 2H), 4.39 (s, 3H), 2.64 (s, 3H).[16]

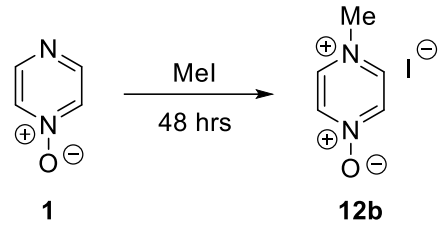
A copy of the ^{1}H NMR spectrum is shown in section 1 of Appendix A.

3.6. Reactions of Diazine *N*-Oxides with MeI, MeOTf and Benzhydrylium Ions

3.6.1. Reactions of Pyrazine *N*-Oxide (1)

Preparation of *N*-Methylpyrazinium *N*-Oxide Iodide (12b)

(a) Experiment Showing Isolated Yield of 12b (Solvent-Free Reaction) – Contains ^{15}N NMR Data

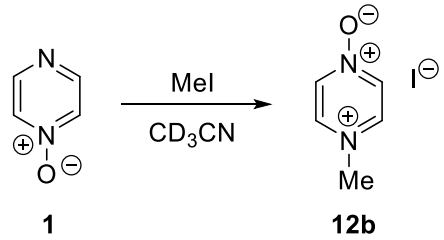


Pyrazine *N*-oxide (**1**) (0.041 g, 0.43 mmol) was placed in a N_2-filled Schlenk flask. Methyl iodide (0.53 ml, 1.2 g, 8.5 mmol) was added by syringe to the flask. The flask was wrapped in foil and left in the dark for 48 hours, after which time the methyl iodide was removed under vacuum using General Procedure A. The resulting yellow solid (**12b**) was washed by addition of dry Et_2O. The supernatant ether solution was removed by cannula filtration (under inert atmosphere). Three aliquots of dry Et_2O (0.5 ml each) were used in this manner to wash the product, (yield = 0.026 g, 0.11 mmol, 26%) A sample of **12b** in dry $(CD_3)_2SO$ was then prepared for ^{1}H and ^{1}H-^{15}N HMBC NMR spectroscopic characterization by Procedure B.

^{1}H NMR (600 MHz, $(CD_3)_2SO$) δ 9.05 – 9.01 (m, 2H), 9.00 – 8.97 (m, 2H), 4.18 (s, 3H, C*H*$_3$).[18]

^{15}N NMR (60.8 MHz, $(CD_3)_2SO$): δ 322.3 (*N*—O), 187.1 (N^+—Me).

(b) Experiment in CD_3CN Showing Low Conversion to 12b



In a glove box, pyrazine *N*-oxide (**1**) (0.019 g, 0.20 mmol) was dissolved in CD_3CN (0.65 ml). Methyl iodide (0.033 g, 0.23 mmol) was added dropwise by syringe to the solution of **1**. The reaction vessel was agitated throughout addition of MeI. After completion of addition of MeI, the entire reaction mixture was transferred to an NMR tube. The NMR tube was sealed with a rubber septum, and the seal was secured by wrapping with PTFE tape and then Parafilm. The NMR tube was take to the NMR spectrometer. A ^{1}H NMR spectrum recorded approximately 20 minutes after mixing of the reactants showed no conversion to **12b** (i.e., only signals of **1** and MeI were

observed). After four days, a second ^{1}H NMR spectrum was obtained. This showed low conversion to **12b**. No signals of **7b** were observed.

^{1}H NMR (300 MHz, CD_3CN)

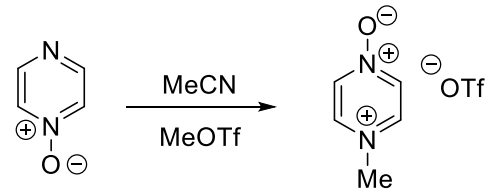
Assigned to **12b**: δ 8.74 – 8.66 (m, 2H), 8.61 – 8.51 (m, 2H), 4.20 (s, 3H, NC*H*$_3$).[18]

Assigned to **1**: δ 8.46 – 8.38 (m, 2H), 8.13 – 8.06 (m, 2H).

Relative to 1H of **12b**, 1H of **1** integrates for 3.1H. Therefore, the conversion to **12b** was 24%. A signal of H_2O is present in the second spectrum since due to ingress of moisture into the NMR tube.

Preparations of 12c and 7c

(a) Experiment Showing Isolated Yield of 12c

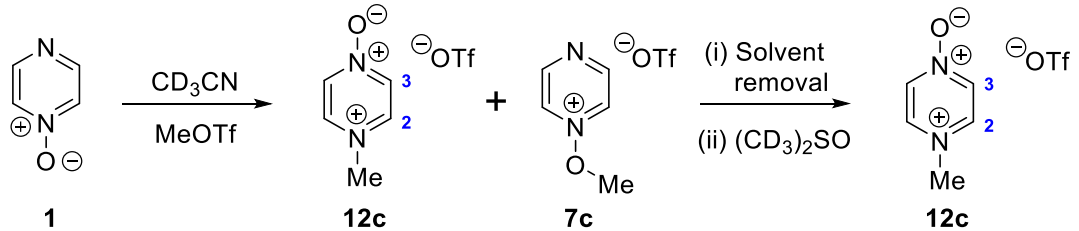


1 **12c**

Pyrazine *N*-oxide (**1**) (0.166 g, 1.73 mmol) was dissolved in CH_3CN (5.0 ml) in a N_2-filled Schlenk flask. Methyl triflate (0.318 g, 1.94 mmol) was then added dropwise. After 96 hours, the CH_3CN was removed under vacuum using General Procedure A. The solid product (**12c**) was washed by addition of dry Et_2O. The supernatant ether solution was removed by cannula filtration (under inert atmosphere). Three aliquots of dry Et_2O (3 ml each) were used in this manner to wash the product (yield = 0.305 g, 1.17 mmol, 68%) A sample of **12c** in dry $(CD_3)_2SO$ was prepared using General Procedure B for ^{1}H NMR spectroscopic characterization.

^{1}H NMR (300 MHz, $(CD_3)_2SO$) δ 9.03 – 8.96 (m, 4H), 4.16 (s, 3H, C*H*$_3$).[18]

(b) Experiment Showing N- vs O-Alkylation Product Ratio (12c vs 7c) – Contains ^{15}N NMR Data



1 **12c** **7c** **12c**

Pyrazine *N*-oxide (**1**) (0.031 g, 0.32 mmol) was dissolved in CD_3CN (0.65 ml) in a N_2-filled Schlenk flask. Methyl triflate (0.050 g, 0.030 mmol) was subsequently added dropwise. The reaction mixture was transferred to an NMR tube and analyzed by NMR spectroscopy using General Procedure B.

Note: Insufficient concentrations of **1** and **7c** in the spectra meant that unambiguous assignments of ^{1}H and ^{13}C NMR signals to specific sites in the structures of these compounds was not possible.

^{1}H NMR (300 MHz, CD_3CN)

Signals assigned to **12c**: δ 8.64 – 8.50 (m, 4H, H-2 and H-3), 4.19 (s, 3H, NC*H*$_3$).

Signals assigned to **7c**: δ 9.48 (dd, *J* = 3.3, 1.6 Hz, 2H), 9.13 (dd, *J* = 3.3, 1.6 Hz, 2H), 4.54 (s, 3H, OC*H*$_3$). Relative to 1H of **12b**, 1H of **7c** integrates for 0.05H.

Signals assigned to the starting material **1**: δ 8.48 (app. d, app. *J* = 4.8 Hz, 1H), 8.16 (app. dd, app. *J* = 3.6, 1.5 Hz, 1H). Relative to 1H of **12c**, 1H of **1** integrates for *ca.* 0.15H.

The signal at δ 8.64 – 8.50 ppm contains 4H of **12c** and 2H of the starting material **1**. The integration of this signal is slightly low with respect to the other signals of **1** and **12c**; this is likely to be due to a slow relaxation rate of one of the contributing protons.

^{13}C{^{1}H} NMR (75 MHz, CD_3CN)

Assigned to **12c**: δ 143.1 (C-2), 139.9 (C-3), 48.1 (N*C*H$_3$)

Assigned to **7c**: δ 153.1, 132.2, 69.1 (O*C*H$_3$)

Assigned to **1**: δ 148.1, 135.6.

Quantitative product formation can be concluded in this experiment on the basis of complete consumption of MeOTf (no signal of MeOTf present in the ^{1}H NMR spectrum). Ratio of N-alkylation and O-alkylation Products (from ^{1}H NMR spectrum):

4H of Compound **12b** = 4.00 – Therefore 1H = 1.00

2H of compound **7c** = 0.10 – Therefore 1H = 0.05

$$\text{Ratio} = \frac{1.00}{1.00 + 0.05} \times 100 = 95\%\ \text{N alkylation}$$

The CD_3CN was removed using General Procedure A and the product mixture was re-dissolved in $(CD_3)_2SO$ to record a ^{1}H-^{15}N HMBC NMR spectrum. Product **7c** did not survive the solvent removal process.

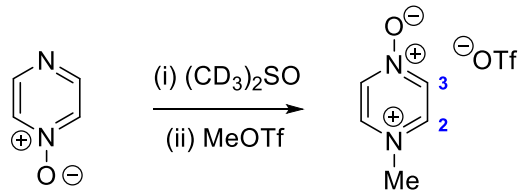
^{1}H NMR (600 MHz, $(CD_3)_2SO$)

Signals assigned to **12c**: δ 9.02 – 8.99 (m, 2H), 8.99 – 8.96 (m, 2H), 4.17 (s, 3H, C*H*$_3$).

Signals assigned to **1**: δ 8.55 – 8.53 (m, 2H), 8.33 – 8.31 (m, 2H). Relative to 1H of **12c**, 1H of **1** integrates for 0.15H.

^{15}N NMR of **12c** (60.8 MHz, $(CD_3)_2SO$): δ 322.9 (*N*—O), 187.8 (*N*$^{+}$—Me).

(c) Experiment Showing Exclusive Formation of 12c in $(CD_3)_2SO$ – Contains ^{15}N and ^{13}C NMR Data



1 **12c**

Pyrazine *N*-oxide (**1**) (0.050 g, 0.52 mmol) was dissolved in $(CD_3)_2SO$ (0.65 ml) in a vial inside an inert atmosphere glove box. Methyl triflate (0.084 g, 0.51 mmol) was subsequently added dropwise. The reaction mixture was transferred to an NMR tube by syringe. The NMR tube was sealed using a rubber septum. After fitting the rubber septum to the NMR tube, the seal was secured by wrapping the external edge of the septum where it contacted the surface of the NMR tube with PTFE tape. Finally, the NMR tube was placed in a long Schlenk flask and removed from the glove box. The outside of the PTFE tape and rubber septum were then wrapped with a layer of Parafilm to further secure the nitrogen atmosphere inside the NMR tube and the sample was brought to the NMR spectrometer. The methoxydimethylsulfonium salt derived from $(CD_3)_2SO$ is likely to be the primary methylating agent in the reaction of **1** + MeOTf in $(CD_3)_2SO$.[10] As a consequence, the methylation of **1** is relatively slow. After 4 weeks the reaction mixture was subjected to ^1H and ^1H-^{15}N HMBC NMR spectroscopic characterization.

^{1}H NMR (600 MHz, $(CD_3)_2SO$)

Signals assigned to **12c**: δ 9.02 – 8.98 (m, 2H), 8.98 – 8.93 (m, 2H), 4.17 (s, 3H, C*H*$_3$).

Signals assigned to **1**: δ 8.55 – 8.51 (m, 2H), 8.34 – 8.30 (m, 2H). Relative to 1H of **12c**, 1H of **1** integrates for 0.23H.

A signal assigned to the methoxydimethylsulfonium salt of $(CD_3)_2SO$ is present at 3.98 ppm. Relative to 1H of **12c**, 1H of the salt integrates for 0.15H.

^{13}C{^{1}H} NMR (150 MHz, $(CD_3)_2SO$)

Signals assigned to **12c**: 142.7 (C-2), 138.7 (C-3), 120.7 (q, *J* = 322 Hz, triflate *C*F$_3$), 46.8.

Signals assigned to **1**: δ 148.2, 134.2.

Signals assigned to methoxydimethylsulfonium salt of $(CD_3)_2SO$: 62.2.

^{15}N NMR of **12c** (60.8 MHz, $(CD_3)_2SO$)

Signals assigned to **12c**: δ 322.9 (*N*—O), 187.7 (*N*$^+$—Me).

Signals assigned to **1**: δ 310.8, 303.7.

Conversion Calculation (based on consumption of the methoxydimethylsulfonium salt as the limiting reagent):

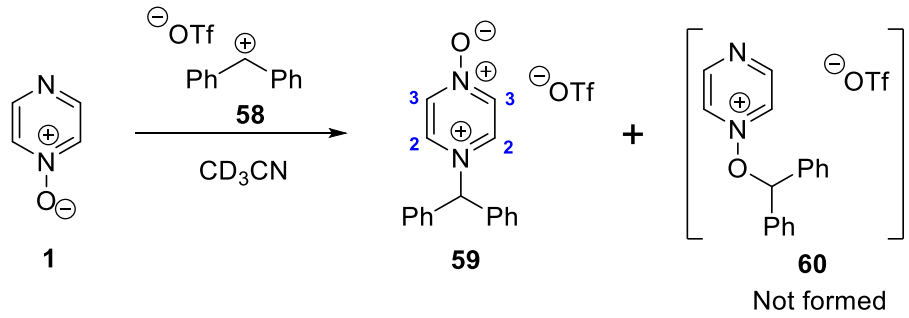
4H of Compound **12c** corresponds to 4.00, therefore 1H = 1.00

For the methoxydimethylsulfonium salt at 3.98 ppm, 3H = 0.46, therefore 1H = 0.15.

$$\text{Conversion} = \frac{1.00}{1.00 + 0.15} \times 100 = 87\%$$

Preparation of 14

(a) Experiment in CD_3CN – Quantitative Conversion to 14 – Contains ^{13}C NMR data



The products of this reaction decompose upon exposure to moisture, and could not be isolated. The products were characterized by recording NMR spectra of the reaction mixture under inert atmosphere.

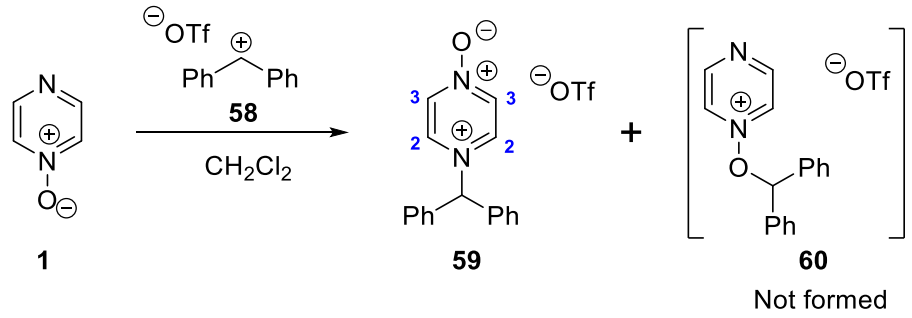
Pyrazine *N*-oxide (**1**) (0.016 g, 0.17 mmol), benzhydryl chloride (0.035 g, 0.17 mmol) and silver triflate (0.054 g, 0.21 mmol) were combined by the process described in General Procedure C to produce **58** in CD_3CN. NMR spectroscopic characterization of the product in CD_3CN was carried out. Quantitative conversion to **59** (based on consumption of the benzhydrylium ion) was observed.

^{1}H NMR (600 MHz, CD_3CN) δ 8.50 (app. s, [a] 4H, H-2, H-3), 7.54 – 7.49 (m, 6H, Phenyl H-3, H-4 & H-5), 7.36 – 7.31 (m, 4H, Phenyl H-2 & H-6), 7.24 (s, 1H, C*H*Ph_2).

^{13}C{^{1}H} NMR (150 MHz, CD_3CN) δ 141.31 (C-3), 140.77 (C-2), 135.30 (Phenyl C-1), 131.05 (Phenyl C-4), 130.54 (Phenyl C-3 & C-5), 129.94 (Phenyl C-2 & C-6), 77.21 (*C*HPh_2).

[a] Apparent singlet (app. s) in ^{1}H NMR spectrum appeared as two barely separated multiplets in other spectra of this compound.

(b) Experiment Showing Exclusive Formation of 59 in CH_2Cl_2 – Contains ^{15}N NMR Data



1 **59** **60**

Not formed

The products of this reaction decompose upon exposure to moisture, and could not be isolated. The products were characterized by recording NMR spectra of the reaction mixture under inert atmosphere.

Pyrazine *N*-oxide (**1**) (0.037 g, 0.39 mmol), benzhydryl chloride (0.077 g, 0.38 mmol) and silver triflate (0.113 g, 0.440 mmol) were combined by the process described in General Procedure C to produce **58** in CH_2Cl_2. The reaction mixture in CH_2Cl_2 was subjected to ^1H and ^1H-^{15}N HMBC NMR spectroscopic characterization using the solvent suppression protocol referred to in the General Experimental. No hydrolysis product can be definitively identified from the ^1H NMR spectrum, although a small amount of material not attributable to **59** is present. Conversion to **59** is estimated to be a minimum of 94% (based on integration of excess **1** relative to **59**).

^1H NMR (600 MHz, CH_2Cl_2)

Assigned to **14**: δ 8.56 – 8.49 (m, 4H, H-2, H-3), 7.52 – 7.48 (m, 6H), 7.35 – 7.31 (m, 4H), 7.29 (s, 1H, Ph_2CH).

Assigned to **1**: δ 8.68 (app. d, app. *J* = 5.4 Hz, 2H), 8.48 (app. d, app. *J* = 5.5 Hz, 2H). Integration relative to 1H of **59** is 0.13H.

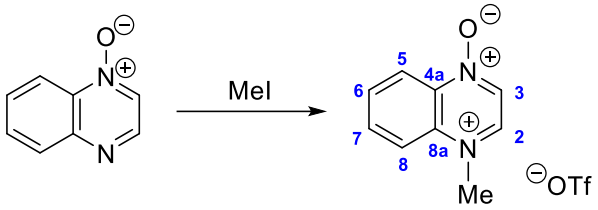
^{15}N NMR (60.8 MHz, CH_2Cl_2): δ 325.0 (*N*—O of **59**), 201.6 (N^+—Me of **59**).

The ^1H and ^1H-^{15}N HMBC NMR spectra are shown in Appendix A.

3.6.2. Reactions of Quinoxaline *N*-Oxide (2)

Preparation of *N*-Methylquinoxalinium *N*-Oxide Iodide (13b)

(a) Experiment Showing Formation of 13b in Low Yield

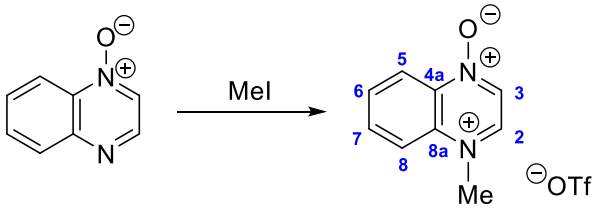


2 **13b**

Quinoxaline *N*-oxide (**2**) (0.023 g, 0.16 mmol) was placed in a N_2-filled Schlenk flask. Methyl iodide (0.684 g, 4.82 mmol) was subsequently added dropwise *via* syringe. The flask was wrapped in foil and left in the dark for 48 hours, before the methyl iodide was removed under vacuum using General Procedure A. The flask was then opened and the red solid product (**13b**) was washed by addition of Et_2O. The supernatant ether solution was removed by cannula filtration. Three aliquots of dry Et_2O (3 ml each) were used in this manner to wash the product in very low yield (2 mg, 0.007 mmol, 4% yield). The recovered product (**13b**) was dissolved in $(CD_3)_2SO$ for ^1H NMR spectroscopic characterization. Some signals from residual Et_2O are present in the ^1H NMR spectrum.

^{1}H NMR (600 MHz, $(CD_3)_2SO$) δ 9.46 (d, *J* = 5.2 Hz, 1H, H-2), 9.28 (d, *J* = 5.2 Hz, 1H, H-3), 8.61 (dd, *J* = 8.7, 1.2 Hz, 1H, H-8), 8.55 – 8.51 (m (app. dd, signal resolution renders *J* values ambiguous), 1H, H-5), 8.34 (m, 1H, H-6), 8.21 – 8.15 (m, 1H, H-7), 4.49 (s, 3H, NC*H*$_3$).

(b) Experiment Showing Formation of 13b in Low Yield – Contains ^{15}N NMR Data



2 **13b**

Quinoxaline *N*-oxide (**2**) (0.044 g, 0.30 mmol) was placed in a N_2-filled Schlenk flask. Methyl iodide (0.129 g, 0.91 mmol) was subsequently added dropwise *via* syringe. The MeI was removed under vacuum using General Procedure A after 18 hours and the solid product (**13b**) was washed by addition of dry Et_2O. The supernatant ether solution was removed by cannula filtration (under inert atmosphere). Three aliquots of dry Et_2O (0.4 ml each) were used in this manner to wash the product (yield = 0.014 g, 0.049 mmol, 16%). A sample of **13b** in dry $(CH_3)_2SO$ was then prepared for ^1H and ^1H-^{15}N HMBC NMR spectroscopic characterization using General Procedure B. Note:

An initial attempt to dissolve the product in CH_2Cl_2 was unsuccessful, and a residual amount of this solvent can be seen in the spectrum.

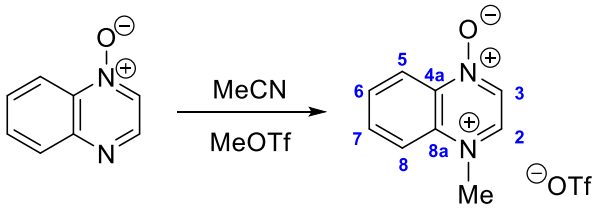
^{1}H NMR (600 MHz, $(CH_3)_2SO$) δ 9.42 (d, *J* = 5.2 Hz, 1H, H-2), 9.25 (d, *J* = 5.2 Hz, 1H, H-3), 8.59 – 8.56 (m (app. dd, *J* values ambiguous), 1H, H-8), 8.51 – 8.48 (m (app. dd, *J* values ambiguous), 1H, H-5), 8.34 – 8.29 (m, 1H, H-6), 8.16 – 8.12 (m, 1H, H-7), 4.46 (s, 3H, NC*H*$_3$).

^{15}N NMR (60.8 MHz, $(CH_3)_2SO$): δ 314.7 (*N*—O), 178.3 (N^+—Me).

Note: This spectrum was recorded in non-deuterated solvent (using the solvent suppression protocol specified in the General Experimental above). Due to a combination of this and the low conversion to product that occurred in this reaction, the product signals are very small. However, the spectral details match well to the ^{1}H NMR spectrum obtained from another repetition of the same experiment, described in part (a), immediately above.

Preparations of 13c and 8c

(a) Experiment Showing Isolated Yield of 13c



2 **13c**

Quinoxaline *N*-oxide (**2**) (0.323 g, 2.21 mmol) was dissolved in CH_3CN (10 ml) in a N_2-filled Schlenk flask. Methyl triflate (0.399 g, 2.43 mmol) was subsequently added dropwise. After 5 hours, the CH_3CN was removed under vacuum using General Procedure A, giving black crystals. The solid product (**13c**) was washed by addition of dry Et_2O. The supernatant ether solution was removed by cannula filtration (under inert atmosphere). Three aliquots of dry Et_2O (3 ml each) were used in this manner to wash the product (yield = 0.389 g, 1.25 mmol, 57%). A sample of **13c** in dry $(CD_3)_2SO$ was then prepared for ^{1}H and ^{1}H-^{13}C HMBC NMR spectroscopic characterization using General Procedure B.

^{1}H NMR (300 MHz, $(CD_3)_2SO$) δ 9.45 (d, *J* = 5.2 Hz, 1H, H-2), 9.27 (d, *J* = 5.2 Hz, 1H, H-3), 8.61 (dd, *J* = 8.7, 1.2 Hz, 1H, H-8), 8.55 – 8.49 (m (app. dd, signal resolution renders *J* values ambiguous), 1H, H-5), 8.39 – 8.30 (m, 1H, H-6), 8.17 (m, 1H, H-7), 4.49 (s, 3H, C*H*$_3$).

^{13}C{^{1}H} NMR (75 MHz, $(CD_3)_2SO$) δ 144.5 (C-2), 140.0 (C-4a), 136.5 (C-6), 135.9 (C-8a), 133.2 (C-7), 133.0 (C-3), 121.1 (C-5), 120.0 (C-8), 44.2 (*C*H$_3$)

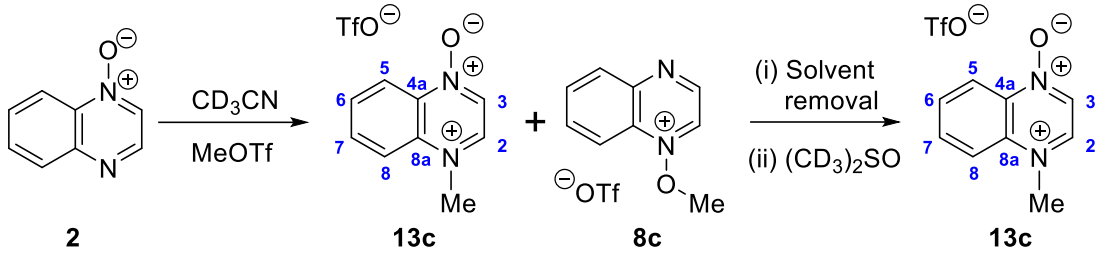
IR (ATR-FTIR), cm^{-1}: 3115 (w), 3092 (w), 1629 (m), 1536 (m), 1408 (m), 1256 (s), 1029 (s), 638 (m).

HRMS-ESI$^+$ (*m/z*): calculated for $[M]^+ = C_9H_9N_2O$ 161.0709; found 161.07069.

(b) Experiment Showing N- vs O-Alkylation Product Ratio (13c vs 8c) – Contains ^{13}C & ^{15}N NMR Data

Quinoxaline *N*-oxide (**2**) (0.047 g, 0.32 mmol) was dissolved in CD_3CN (0.65 ml) in a N_2-filled Schlenk flask. Methyl triflate (0.045 g, 0.27 mmol) was subsequently added dropwise. The reaction mixture was transferred to an NMR tube and analyzed by NMR spectroscopy using General Procedure B.

Note: Insufficient concentrations of **2** and minor product **8c** in the following spectra meant that unambiguous assignment of hydrogen and carbon NMR signals to specific sites in the structures of these compounds was not possible.



^{1}H NMR (400 MHz, CD_3CN)

Assigned to **13c**: δ 8.98 (app. d, app. *J* = 5.1 Hz, 1H, H-2), 8.79 (app. d, app. *J* = 5.2 Hz, 1H, H-3), 8.62 – 8.55 (m, 1H, H-5), 8.48 – 8.23 (m, 2H, H-5 and H-7), 8.16 – 8.06 (m, 1H, H-8), 4.47 (s, 3H, NCH_3).

Assigned to **8c**: δ 9.63 (app. d, app. *J* = 3.4 Hz, 1H), 9.56 (app. d, app. *J* = 3.2 Hz, 1H), 8.62 – 8.55 (m, 1H), 8.48 – 8.23 (m, 2H), 8.16 – 8.06 (m, 1H), 4.69 (s, 3H, OCH_3). Relative to 1H of **13c**, 1H of **8c** integrates for 0.12H.

Assigned to **2**: δ 8.69 (d, *J* = 3.6 Hz, 1H), 8.48 – 8.23 (m, 2H), 8.16 – 8.06 (m, 1H), 7.94 – 7.87 (m, 1H), 7.84 – 7.78 (m, 1H). Relative to 1H of **13c**, 1H of **2** integrates for approximately 0.33H.

The signal between 8.62 and 8.55 ppm contains a 1H signal from **13c** and a 1H signal from **8c**.

The signal between 8.48 and 8.23 ppm contains a 2H signal from **13c**, a 2H signal from **8c** and a 2H signal from **2**.

The signal between 8.16 and 8.06 ppm contains a 1H signal from **13c**, a 1H signal from **8c** and a 1H signal from **2**.

$^{13}C\{^1H\}$ NMR (100 MHz, CD_3CN)

Assigned to **13c**: δ 143.2 (C-2), 140.2 (C-4a), 136.3 (C-6), 135.5 (C-8a), 132.9 (C-7), 132.1 (C-3), 120.1 (C-5), 119.7 (C-8), 44.1 (*C*H_3)

Assigned to **8c**: δ 147.2, 144.7, 140.2, 136.8, 134.7, 131.7, 129.4, 119.1, 116.3, 68.9.

Ratio of N-alkylation and O-alkylation Products (from integrations in ^{1}H NMR spectrum):

3H of Compound **13c** = 3.00 – Therefore 1H = 1.00

3H of compound **8c** = 0.36 – Therefore 1H = 0.12

$$\text{Ratio} = \frac{1.00}{1.00 + 0.12} \times 100 = 89\%\ \text{N alkylation}$$

The CD_3CN was removed using General Procedure A and the product mixture was re-dissolved in $(CD_3)_2SO$ to allow a ^{1}H-^{15}N HMBC NMR spectrum to be recorded. Product **8c** did not survive the solvent removal process.

^{1}H NMR (600 MHz, $(CD_3)_2SO$)

Assigned to **13c**: δ 9.46 (d, *J* = 5.1 Hz, 1H, H-2), 9.29 (d, *J* = 5.1 Hz, 1H, H-3), 8.60 (app. d,* app. *J* = 8.6 Hz, 1H, overlaps partially with signal of **2**, H-8), 8.53 (app. d, [a] app. *J* = 8.8 Hz, 1H, H-5), 8.37 – 8.32 (m, 1H, H-6), 8.20–8.16 (m, overlaps with signal of **2**, 1H, H-7), 4.50 (s, 3H, NCH_3).

Assigned to **2**: δ 8.78 (d, *J* = 3.5 Hz, 1H), 8.63 (d, *J* = 3.5 Hz, 1H, overlaps partially with signal of **13c**), 8.46 – 8.42 (m (app. d, app. *J* = 8.5 Hz), 1H), 8.16 – 8.11 (m, overlaps with signal of **13c**, 1H), 7.96 – 7.92 (m, 1H), 7.88 – 7.84 (m, 1H). Relative to 1H of **13c**, 1H of **2** integrates for 0.26H.

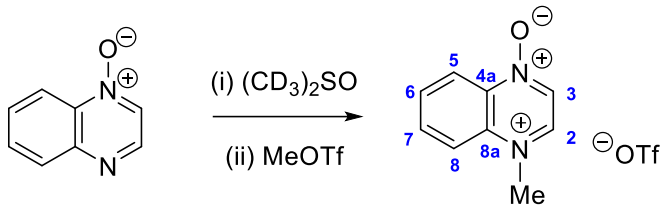
The region between 8.64 and 8.45 ppm contains two 1H signals from **13c** and a 1H signal from **2**.

The region between 8.20 and 8.11 ppm contains a 1H signal from **13c** and a 1H signal from **2**.

^{15}N NMR (60.8 MHz, $(CD_3)_2SO$): δ 314.4 (*N*—O), 178.0 (N^+—Me).

[a] See NMR spectra in experiments described above – these signals are not doublets; signal resolution in this particular spectrum is too low to observe the fine structure of these signals.

(c) Experiment Showing Exclusive Formation of 13c in $(CD_3)_2SO$ – Contains ^{15}N NMR Data



2 **13c**

Quinoxaline *N*-oxide (**2**) (0.057 g, 0.39 mmol) was dissolved in $(CD_3)_2SO$ (0.8 ml) in a vial inside an inert atmosphere glove box. Methyl triflate (0.050 g, 0.31 mmol) was subsequently added dropwise. The reaction mixture was transferred to an NMR tube by syringe. The NMR tube was sealed using a rubber septum. After fitting the rubber septum to the NMR tube, the seal was secured by wrapping the external edge of the septum where it contacted the surface of the NMR tube with PTFE tape. Finally, the NMR tube was placed in a long Schlenk flask and removed from the glove box. The outside of the PTFE tape and rubber septum were then wrapped with a layer of Parafilm to further secure the nitrogen atmosphere inside the NMR tube and the sample was brought to the NMR spectrometer. $(CH_3)_2SO$ is known to react with methylating agents (e.g., dimethyl sulfate) to give methoxydimethylsulfonium salt.[19] The resulting methoxysulfonium salt acts as the primary methylating agent in the reaction of **2** + MeOTf in $(CD_3)_2SO$. As a consequence, the methylation of **2** is relatively slow. After 4 weeks the reaction mixture was subjected to ^1H and ^1H-^{15}N HMBC NMR spectroscopic characterization.

^{1}H NMR (600 MHz, $(CD_3)_2SO$)

Assigned to **13c**: δ 9.46 (d, *J* = 5.1 Hz, 1H, H-2), 9.27 (d, *J* = 5.1 Hz, 1H, H-3), 8.58 (dd, *J* = 8.7, 1.1 Hz, 1H, H-8), 8.54 – 8.50 (m (app. dd, signal resolution renders *J* values ambiguous), 1H, H-5), 8.34 – 8.30 (m, 1H, H-6), 8.18 – 8.14 (m, 1H, overlaps partially with signal of **2**, H-7), 4.51 (s, 3H, C*H*$_3$).

Assigned to **2**: δ 8.78 (d, *J* = 3.6 Hz, 1H), 8.62 (d, *J* = 3.6 Hz, 1H), 8.42 (dd, *J* = 8.6, 1.2 Hz, 1H), 8.14 – 8.10 (1H, overlaps partially with signal of **13c**), 7.95 – 7.89 (m, 1H), 7.87 – 7.81 (m, 1H). Relative to 1H of **13c**, 1H of **2** integrates for approximately 0.78H.

The region between 8.17 and 8.10 ppm contains a 1H signal from **13c** and a 1H signal from **2**.

A signal assigned to the methoxydimethylsulfonium salt of $(CD_3)_2SO$ is present at 3.99 ppm. Relative to 1H of **13c**, 1H of the salt integrates for 0.28H.

^{15}N NMR (60.8 MHz, $(CD_3)_2SO$)

Assigned to **13c**: δ 314.4 (*N*—O), 177.9 (N^+—Me).

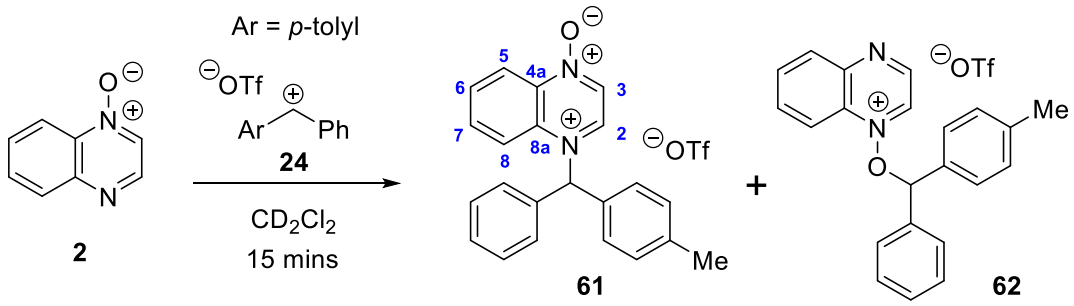
Assigned to **2**: δ 302.3, 299.7.

Conversion Calculation (based on consumption of the methoxydimethylsulfonium salt as the limiting reagent):

For the methoxydimethylsulfonium salt at 3.99 ppm, 3H = 0.84 relative to 1H of **13c**, therefore 1H = 0.28.

$$\text{Conversion} = \frac{1.00}{1.00 + 0.28} \times 100 = 78\%$$

Preparation of 61 and 62



The products of this reaction decompose upon exposure to moisture, and could not be isolated. Consequently, the products were characterized by recording NMR spectra of the reaction mixture under inert atmosphere.

Quinoxaline *N*-oxide (**2**) (0.026 g, 0.18 mmol), 4-methylbenzhydryl chloride (**24**) (0.038 g, 0.18 mmol) and silver triflate (0.044 g, 0.17 mmol) were combined by the process described in Procedure C to produce **61** (major product) + **62** (minor product) in CD_2Cl_2. The reaction mixture in CD_2Cl_2 was then prepared for ^{1}H and ^{1}H-^{15}N HMBC NMR spectroscopic characterization using General Procedure B.

^{1}H NMR (600 MHz, CD_2Cl_2)

Signals assigned to **61**: δ 8.75 (d, *J* = 5.5 Hz, 1H, H-3), 8.60 (app. dd, app. *J* = 8.7, 1.1 Hz, 1H, H-8), 8.53 (d, *J* = 5.5 Hz, 1H, H-2), 8.42 (app. d, app. *J* = 8.9 Hz, 1H, H-5), 8.10 (m, 1H, H-7), 8.02 – 7.97 (m, 1H, H-6), 7.81 (s, 1H, C*H*PhTol), 7.51 – 7.46 (m, 3H, Phenyl H-3, H-4 & H-5), 7.39 – 7.22 (m, 6H, Phenyl H-2 & H-6, Tolyl H-2, H-3, H-5 & H-6), 2.37 (s, 3H, CH_3).

Signals assigned to **62**: δ 8.83 (app. d, app. *J* = 3.6 Hz, 1H), 8.28 (app. d, app. *J* = 8.4 Hz, 1H) and 7.87 (m, 1H). Relative to 1H of **61**, 1H of **62** integrates for 0.10H.

A peak assigned to a hydrolysis product is present at 5.38 ppm. The signals of the aromatic protons of this product also contribute to the integration of the multiplet at 7.39 – 7.22 ppm. Relative to 1H of **61**, 2H of the hydrolysis product integrates for 0.08H.

$^{13}C\{^1H\}$ NMR (150 MHz, CD_2Cl_2)

Signals assigned to **61**: δ 141.4 (Tolyl C-4), 141.2 (C-4a), 140.7 (C-2), 137.5 (C-7), 135.6 (C-8a), 134.8 (Phenyl C-1), 133.5 (C-6), 133.1 (C-3), 130.8 (Tolyl C-3 & C-5), 130.2 (Phenyl C-4), 130.1 (Phenyl C-3 & C-5), 129.5 (Tolyl C-2 & C-6), 129.2 (Phenyl C-2 & C-6), 121.4 (C-5), 121.1 (C-8), 73.2 (*C*HPhTol), 21.3 (*C*H_3).

A ^{13}C NMR signal assigned to the *C*$F_3SO_3^-$ ion is present at δ 120.72 (q, *J* = 320 Hz).

Note: Low concentration of minor product **62** in the $^{13}C\{^1H\}$ NMR spectrum meant that assignment of the very small signals present in the spectrum to this compound could not be done unambiguously.

^{15}N NMR (60.8 MHz, CD_2Cl_2)

Signals assigned to **61**: δ 317.6 (*N*—O), 190.5 (N^+—Me).

No correlations were observed to the ^1H NMR signals of the minor product, **62**.

Ratio of N-alkylation and O-alkylation Products:

1H of compound **61** = 1.00

1H of compound **62** = 0.10

$$\text{Ratio} = \frac{1.00}{1.00 + 0.10} \times 100 = 91\%\ \text{N alkylation}$$

Conversion Calculation (based on consumption of the benzhydrylium ion as the limiting reagent):

1H of Compound **61** corresponds to 1.00.

For the hydrolysis product at 5.38ppm, 2H = 0.08. Therefore, since two equivalents of benzhydrylium ion are consumed in hydrolysis (formation of bis(benzhydryl) ether), the conversion was:

$$\text{Conversion} = \frac{1.00}{1.00 + 0.08} \times 100 = 93\%$$

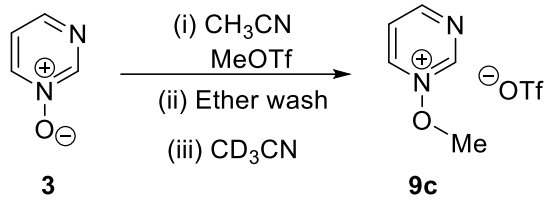
3.6.3. Reactions of Pyrimidine *N*-Oxide (3)

Preparations of 9c and 63c

Removing the solvent from reaction mixtures containing **9c** and/or **63c** causes decomposition of **63c**. Formation of some quantity of degradation products was observed in all instances of reactions of **3** with MeOTf (see below), regardless of whether CD_3CN, MeCN or $(CD_3)_2SO$ were used as solvent *even if the solvent was not*

removed. Taking steps to protect the reaction mixture from light also did not prevent the formation of these degradation products. It is not clear whether the degradation products observed directly in reaction mixtures by ^{1}H NMR spectroscopy (reactions in CD_3CN or $(CD_3)_2SO$ – see below) are derived from decomposition of **63c** or **9c** or both, or if some separate process leads to the formation of the decomposition products observed in the reaction mixtures. Although **9c** survives solvent removal, attempts to isolate it from the decomposition products through crystallization under inert atmosphere (in a Schlenk flask) were unsuccessful, resulting only in formation of further decomposition product(s). Since neither **63c** nor **9c** could be isolated, it was necessary to characterize these products in the reaction mixtures in which they formed by NMR spectroscopy under inert atmosphere. A high-resolution mass spectrum of **9c** (sample maintained under inert atmosphere) was also obtained by subjecting a reaction mixture known (from NMR spectroscopic analysis) to contain only a small amount of decomposition product to electrospray ionization mass spectrometric analysis (see below). This compound (with dimethylsulfate counter-ion rather than triflate) has been characterized previously.[15]

(a) Experiment Showing Approximate Isolated Yield of 9c



3 **9c**

Pure samples of compounds **9c** and/or **63c** could not be obtained from this reaction for the reasons given at the start of section 3.6.3 (above).

Pyrimidine *N*-oxide (**3**) (0.195 g, 2.03 mmol) was dispensed into a Schenk flask and sealed in a glove box. The flask was removed from the glove box and attached to a Schlenk line, and the solid was then dissolved in dry CH_3CN (3 ml). Methyl triflate (0.342 g, 2.08 mmol) was subsequently added dropwise. The flask was wrapped with aluminium foil and the reaction mixture was stirred for 24 hours.

All operations and manipulations of the product were carried out under inert atmosphere – i.e., the product was kept in a Schlenk flask under an atmosphere of N_2 throughout. Dry Et_2O (3 ml) was then added to the reaction mixture, which caused the separation of a yellow oil from the reaction mixture. The supernatant (CH_3CN/Et_2O) was carefully removed by cannula. Two further aliquots of dry Et_2O (3 ml each) were then used to wash the yellow oil. In each case, the Et_2O supernatant was removed by cannula, as above. The product was dried by passing a stream of N_2 gas over the oil to avoid exposing the product to vacuum (for the reasons given at the beginning of section 3.6.3). The oil obtained contained small amounts of decomposition products seen in all experiments involving reaction of **3** with MeOTf (see below). The amount of decomposition product present (based on ^{1}H NMR spectroscopic analysis of this material) is sufficiently small to quote an approximate isolated yield for **9c** of 404 mg (1.55 mmol, 77% yield) from this experiment. All attempts to purify this material further (to obtain completely pure **9c**) resulted in decomposition of the product. A

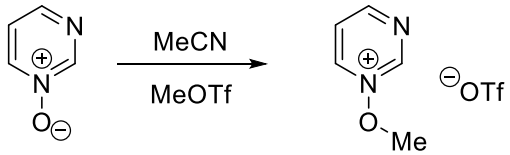
small sample of the product was dissolved in dry CD_3CN and analyzed by NMR spectroscopy using General Procedure B. A separate sample of **9c** was prepared in dry MeCN (approximately 1 mg ml^{-1}) and transferred to a mass spectrometry vial contained in a Schlenk flask under an atmosphere of nitrogen. The sample was maintained under inert atmosphere until directly prior to recording the mass spectrum.

^{1}H NMR (300 MHz, CD_3CN) Signals assigned to **9c**: δ 9.77 (dd, *J* = 2.3, 0.8 Hz, 1H), 9.43 – 9.34 (m, 2H), 8.23 (ddd, *J* = 6.8, 4.9, 0.9 Hz, 1H), 4.47 (s, 3H).

HRMS-ESI$^+$ (*m/z*): Calculated for $[M]^+ = C_5H_7N_2O$ 111.0553; found 111.0550 (44%). Calculated for $[M + H + OTf]^+ = C_6H_8N_2O_4SF_3$ 261.0157; found 261.0150 (100%). The second peak is postulated to belong to the dicationic N-protonated adduct of **9c** associated with triflate to give an entity with a single net positive charge.

Note: The ^{1}H signal at δ 9.77 in compound **9c** has an extremely long relaxation time. A 30° pulse and a relaxation delay of 60 seconds were used during acquisition of the spectrum shown in section 2 of Appendix A, leading to a set of internally consistent integrations for the ^{1}H NMR signals of **9c**.

(b) Reaction in MeCN – After Solvent Removal Only 9c is Observed – Contains ^{15}N NMR Data



3 **9c**

Pure samples of compounds **9c** and/or **63c** could not be obtained from this reaction for the reasons given at the start of section 3.6.3.

Pyrimidine *N*-oxide (**3**) (0.046 g, 0.48 mmol) was dissolved in CH_3CN (5 ml) in a N_2-filled Schlenk flask. Methyl triflate (0.057 g, 0.35 mmol) was subsequently added dropwise. After *ca.* 20 minutes, the CH_3CN was removed under vacuum using General Procedure A and the solid product (**9c**) was washed by addition of dry Et_2O, which was removed by cannula filtration (under inert atmosphere). Three aliquots of dry Et_2O (2 ml each) were used in this manner to wash the product. A sample of the crude product in dry $(CH_3)_2SO$ was then prepared for ^{1}H and ^{1}H-^{15}N HMBC NMR spectroscopic characterization using General Procedure B.

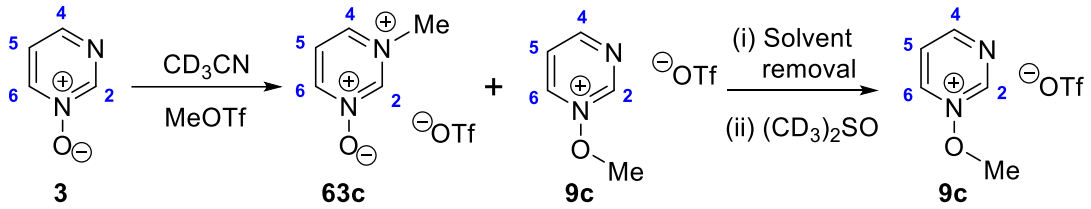
^{1}H NMR (600 MHz, $(CH_3)_2SO$)

Signals assigned to **9c**: δ 10.21 (app. d, app. *J* = 1.8 Hz, 1H), 9.90 – 9.83 (m, 1H), 9.44 (dd, *J* = 4.8, 1.5 Hz, 1H), 8.40 – 8.36 (m, 1H), 4.45 (s, 3H).[15]

Signals assigned to **3**: δ 9.07 (s, 1H, H-2), 8.61 – 8.56 (m, 1H, H-6), 8.33 – 8.29 (m, 1H, H-4), 7.58 – 7.52 (m, 1H, H-5).[11] Relative to 1H of **9c**, 1H of **3** integrates for approximately 0.71H.

$$\text{Conversion} = \frac{1.00}{1.00 + 0.71} \times 100 = 58\%$$

(c) Experiment Showing N- vs O-Alkylation Product Ratio (63c vs 9c) in CD_3CN – Contains ^{15}N and ^{13}C NMR Data



Pure samples of compounds **9c** and/or **63c** could not be obtained from this reaction for the reasons given at the start of section 3.6.3.

Pyrimidine *N*-oxide (**3**) (0.045 g, 0.47 mmol) was dissolved in CD_3CN (0.65 ml) in a N_2-filled Schlenk flask. Methyl triflate (0.067 g, 0.41 mmol) was then added dropwise. The reaction mixture was transferred to an NMR tube and analyzed by NMR spectroscopy using General Procedure B.

^{1}H NMR (400 MHz, CD_3CN)

Signals assigned to **9c**: δ 9.81 (app. d, app. *J* = 1.5 Hz, 1H, H-2), 9.47 – 9.37 (m, 2H, H-4 and H-6), 8.31 – 8.24 (m, 1H, H-5), 4.51 (s, 3H, OC*H*$_3$).

Signals assigned to **63c**: δ 9.56 (s, 1H, H-2), 8.90 (app. d, app. *J* = 6.8 Hz, 1H), 8.58 (app. d, app. *J* = 6.0 Hz, 1H), 8.01 (app. t, app. *J* = 6.0 Hz, 1H), 4.32 (s, 3H, NC*H*$_3$). Relative to 1H of **9c**, 1H of **63c** integrates for 0.08H.

Signals assigned to starting material **3**: δ 8.98 (s, 1H, H-2), 8.50 – 8.42 (m, 1H, H-6), 8.39 – 8.33 (m, 1H, H-4), 7.55 – 7.46 (m, 1H, H-5).[15] Relative to 1H of **9c**, 1H of **3** integrates for 0.30H.

^{13}C{^{1}H} NMR (100 MHz, CD_3CN)

Signals assigned to **9c**: δ 163.6 (C-6), 150.0 (C-2), 148.1 (C-4), 125.0 (C-5), 70.2 (O*C*H$_3$).

Signals assigned to **63c**: δ 151.8, 149.1, 140.2, 124.0, 46.6 (N*C*H$_3$).

Signals assigned to starting material **3**: δ 149.1 (C-2), 145.8 (C-4), 144.5 (C-6), 121.9 (C-5).

A quartet from *C*$F_3SO_3^-$ is present at δ 120.6 (partially overlaps with other signals; *J* = *ca.* 320 Hz).

Ratio of N-alkylation and O-alkylation Products (from integrations in ^{1}H NMR spectrum):

2H of Compound **9c** = 2.00 – Therefore 1H = 1.00

1H of Compound **63c** = 0.08 – Therefore 1H = 0.08

$$\text{Ratio} = \frac{1.00}{1.00 + 0.08} \times 100 = 93\%\ \text{O alkylation}$$

The CD_3CN was removed and the product mixture was re-dissolved in $(CD_3)_2SO$ to allow a ^1H-^{15}N HMBC NMR spectrum to be measured. Product **63c** did not survive the solvent removal process.

^{1}H NMR (600 MHz, $(CD_3)_2SO$)

Signals assigned to **9c**: δ 10.24 (dd, *J* = 2.2, 0.8 Hz, 1H, H-2), 9.89 (ddd, *J* = 6.8, 2.2, 1.6 Hz, 1H, H-6), 9.46 (dd, *J* = 4.8, 1.6 Hz, 1H, H-4), 8.40 (app. ddd, *J* = 6.8, 4.8, 0.8 Hz, 1H, H-5), 4.48 (s, 3H).

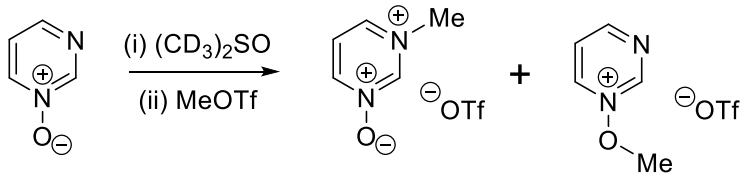
Signals assigned to starting material **3**: δ 9.15 – 9.11 (m, 1H, H-2), 8.64 (ddd, *J* = 6.6, 2.0, 1.5 Hz, 1H, H-6), 8.38 (dd, *J* = 4.8, 1.5 Hz, 1H, H-4), 7.61 (ddd, *J* = 6.6, 4.8, 0.9 Hz, 1H, H-5).[11] Relative to 1H of **9c**, 1H of **3** integrates for approximately 1.80H.

^{15}N NMR (60.8 MHz, $(CD_3)_2SO$)

Signals assigned to **9c**: δ 303.4 (free *N*), 249.4 (*N*$^+$—OMe)

Signals assigned to **3**: δ 300.9, 285.8.

(d) Experiment Showing N- vs O-Alkylation Product Ratio (63c vs 9c) in $(CD_3)_2SO$ – Contains ^{15}N and ^{13}C NMR Data



3 **63c** **9c**

Pyrimidine *N*-oxide (**3**) (0.050 g, 0.52 mmol) was dissolved in $(CD_3)_2SO$ (0.8 ml) in a vial inside an inert atmosphere glove box. Methyl triflate (0.087 g, 0.53 mmol) was subsequently added dropwise. The reaction mixture was transferred to an NMR tube by syringe. The NMR tube was sealed using a rubber septum. After fitting the rubber septum to the NMR tube, the seal was secured by wrapping the external edge of the septum where it contacted the surface of the NMR tube with PTFE tape. Finally, the NMR tube was placed in a long Schlenk flask and removed from the glove box. The outside of the PTFE tape and rubber septum were then wrapped with a layer of Parafilm to further secure the nitrogen atmosphere inside the NMR tube and the sample was brought to the NMR spectrometer. ^{1}H NMR spectra were run periodically over the course of four weeks. Very slow consumption of **3** and growth of **63c** and **9c** was observed from these spectra. The integration of the ^{1}H NMR signal of the methylating agent (likely to be (methoxy)sulfonium triflate)[19] at δ 3.98 ppm also diminished during this time. After four weeks, ^{1}H, ^{13}C{^{1}H}, COSY, ^{1}H-^{13}C HSQC, ^{1}H-^{13}C HMBC and ^{1}H-^{15}N HMBC NMR spectra of the reaction mixture were recorded.

^{1}H NMR (600 MHz, $(CD_3)_2SO$)

Signals assigned to **9c**: δ 10.24 (dd, *J* = 2.2, 0.8 Hz, 1H, H-2, overlaps with signal of **21b**), 9.90 (ddd, *J* = 6.8, 2.2, 1.6 Hz, 1H, H-6), 9.47 (dd, *J* = 4.9, 1.6 Hz, 1H, H-4), 8.41 (ddd, *J* = 6.8, 4.9, 0.8 Hz, 1H, H-5, partially overlaps with signal of **3**), 4.48 (s, 3H, OCH_3).

Signals assigned to **63c**: δ 10.18 (s, 1H, overlaps with signal of **9c**), 9.21 – 9.17 (m, 1H), 8.89 (app. d, app. *J* = 6.1 Hz, 1H), 8.17 (app. t, app. *J* = 6.5 Hz, 1H), 4.26 (s, 3H, NCH_3). Relative to 1H of **9c**, 1H of **63c** integrates for 0.07H.

Signals assigned to **3**: δ 9.09 (m, 1H, H-2), 8.60 (ddd, *J* = 6.6, 2.0, 1.5 Hz, 1H, H-6), 8.33 (dd, *J* = 4.8, 1.5 Hz, 1H, H-4, partially overlaps with signal of **9c**), 7.58 (ddd, *J* = 6.6, 4.8, 1.0 Hz, 1H, H-5).[11] Relative to 1H of **9c**, 1H of **3** integrates for 0.61H.

A signal assigned to the methoxydimethylsulfonium salt of $(CD_3)_2SO$ is present at 3.98 ppm. Relative to 1H of **9c**, 1H of the salt integrates for approximately 0.33H.

Note: The singlet at δ 10.24 ppm has an extremely slow relaxation rate. A 30° pulse and a relaxation delay of 60 seconds were used during acquisition of the spectra above, leading to a set of internally consistent integrations for the ^{1}H NMR signals of **9c**. Use of a 90° pulse and a 60 second relaxation delay gave an integration of the signal at 10.24 ppm of 84% relative to the other 1H signals of **9c**.

^{13}C{^{1}H} NMR (151 MHz, $(CD_3)_2SO$)

Signals assigned to **9c**: δ 163.7 (C-6), 151.2 (C-2), 149.0 (C-4), 125.1 (C-5), 70.4 (O*C*H_3).

No signals in this ^{13}C NMR spectrum could be assigned to the small amount of **63c** present.

Signals assigned to **3**: δ 149.8 (C-2), 145.3 (C-4 or C-6), 145.2 (C-4 or C-6), 122.6 (C-5).

A signal at δ 121.1 (q, *J* = 322 Hz) is assigned to triflate ion ($^-$OSO_2*C*F_3). Small signal derived from decomposition products are also present (see spectra in section 2 of Appendix A and comment at start of section 3.6.3).

^{15}N NMR (60.8 MHz, $(CD_3)_2SO$)

Signals assigned to **9c**: δ 303.1 (free *N*), 249.0 (*N*$^+$—OMe)

Signals assigned to **63c**: δ 293.6 (*N*—O), 205.2 (*N*$^+$—Me)

Signals assigned to **3**: 300.7, 288.4.

<u>Conversion Calculation</u> (based on consumption of the methoxydimethylsulfonium salt as the limiting reagent):

3H of Compound **9c** corresponds to 3.00, therefore 1H = 1.00. 3H of compound **63c** corresponds to 0.21, therefore 1H = 0.07.

For the methoxydimethylsulfonium salt at 3.98 ppm, 3H = 1.00, therefore 1H = 0.33.

$$\text{Conversion} = \frac{1.00 + 0.07}{1.00 + 0.07 + 0.33} \times 100 = 76\%$$

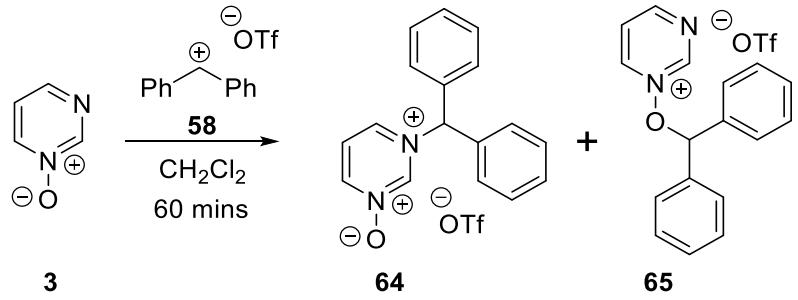
Ratio of N-alkylation and O-alkylation Products (using integrations from ^{1}H NMR spectrum):

1H of Compound **9c** = 1.00

1H of Compound **63c** = 0.07

$$\text{Ratio} = \frac{1.00}{1.00 + 0.07} \times 100 = 93\%\ \text{O alkylation}$$

Attempted Preparation of 64 and 65



3 **64** **65**

No evidence for product formation

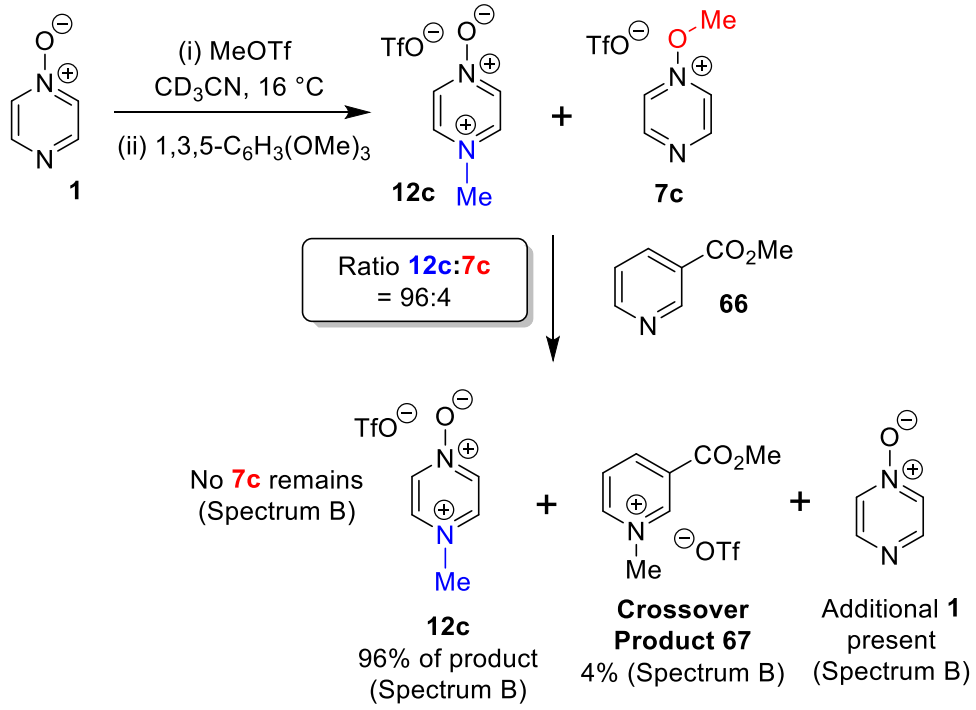
Pyrimidine *N*-oxide (**3**) (0.044 g, 0.46 mmol), benzhydryl chloride (0.093 g, 0.46 mmol) and silver triflate (0.132 g, 0.514 mmol) were combined by the process described in Procedure C in an attempt to produce **22** or **24** in CH_2Cl_2. The reaction mixture was analyzed by NMR spectroscopy using General Procedure B. As can be seen in the spectra in section 2 of Appendix A, the appearances of the signals are highly unusual, and none of these signals could be definitively assigned to any particular species. The identities of the entities formed in this process are not clear.

3.7. Control Experiments

General Procedure D: Crossover Experiments

The following procedure was used to establish whether reactions of diazine *N*-oxides occurred under kinetic control. In a glove box containing a nitrogen atmosphere, the appropriate diazine *N*-oxide (1 equivalent) was weighed into a vial. Dry CD_3CN (usually 0.65 ml) was added. An internal standard, 1,3,5-trimethoxybenzene was subsequently added (approx. 15 mol% relative to the diazine *N*-oxide). The mixture was then transferred into an NMR tube. The NMR tube was sealed using a rubber septum. After fitting the rubber septum to the NMR tube, the seal was secured by wrapping the external edge of the septum where it contacted the surface of the NMR tube with PTFE tape. Finally, the NMR tube was placed in a long Schlenk flask and removed from the glove box and the sample was brought to the NMR spectrometer. A ^1H NMR spectrum was measured and the tube was removed from the spectrometer. A solution of the crossover nucleophile in CD_3CN (amounts specified below) was then injected through the septum cap. The outside of the PTFE tape and rubber septum were then wrapped with a layer of Parafilm to further secure the nitrogen atmosphere inside the NMR tube. A second ^1H NMR spectrum was recorded immediately, and an additional spectrum was obtained after allowing the reaction mixture to stand (in the NMR tube) for two days or more.

3.7.1. Crossover Experiment – Pyrazine *N*-Oxide (1) with MeOTf and Methyl Nicotinate (66)



The following reagents were combined in the process described in General Procedure D. Pyrazine *N*-oxide (**1**) (0.018 g, 0.19 mmol) was dissolved in CD_3CN (0.65 ml) in a vial in a glove box. Methyl triflate (0.024 g, 0.15 mmol) was subsequently added dropwise. To this mixture was added 1,3,5-trimethoxybenzene (0.003 g, 0.02 mmol). The reaction mixture was transferred to an NMR tube and analyzed by NMR

spectroscopy in CD_3CN (Spectrum A). The tube was removed from the spectrometer and methyl nicotinate (**66**) (0.032 g, 0.23 mmol) in CD_3CN (0.15 ml) was injected into the tube through the septum by syringe. The mixture was agitated and a second ^1H NMR spectrum was recorded. No change was observed in the ratio of **12c** and **7c** in this spectrum. An additional ^1H NMR spectrum was recorded after 1 day (Spectrum B).

^{1}H NMR (300 MHz, CD_3CN, 15 second relaxation delay) Spectrum A:

Signals assigned to **12c**: δ 8.55 – 8.49 (m, 4H), 4.15 (s, 3H).

Signals assigned to **7c**: δ 9.45 (dd, *J* = 3.3, 1.6 Hz, 2H), 9.08 (dd, *J* = 3.3, 1.6 Hz, 2H), 4.51 (s, 3H). Relative to 1H of **12c**, 1H of **7c** integrates for 0.04H.

Signals assigned to starting material **1**: δ 8.47 – 8.40 (m, 2H), 8.13 (app. dd, app. *J* = 3.6, 1.5 Hz, 2H). Relative to 1H of **12c**, 1H of **1** integrates for approximately 0.28H.

Signals assigned to internal standard **1,3,5-trimethoxybenzene**: δ 6.09 (s, 3H), 3.74 (s, 9H). Relative to 1H of **12c**, 1H of **1,3,5-trimethoxybenzene** integrates for 0.14H.

Ratio of N-alkylation and O-alkylation Products:

3H of Compound **12c** = 3.00 – Therefore 1H = 1.00

2H of Compound **7c** = 0.08 – Therefore 1H = 0.04

$$\text{Ratio} = \frac{1.00}{1.00 + 0.04} \times 100 = 96\%\ \text{N alkylation}$$

Ratio of major product to internal standard:

3H of Compound **12c** = 3.00 – Therefore 1H = 1.00

3H of internal standard = 0.43 – Therefore 1H = 0.143

$$\text{Ratio} = \frac{1.00}{1.00 + 0.143} \times 100 = 87 : 13$$

^{1}H NMR (300 MHz, CD_3CN, 15 second relaxation delay) Spectrum B:

Signals assigned to **12c**: δ 8.57 – 8.49 (m, 4H), 4.16 (s, 3H).

No signals assigned to **7c**

Signals assigned to starting material **1**: δ 8.46 – 8.38 (m, 2H), 8.08 (app. dd, app. *J* = 3.5, 1.5 Hz, 2H). Relative to 1H of **13b**, 1H of **1** integrates for approximately 0.39H.

Signals assigned to internal standard **1,3,5-trimethoxybenzene**: δ 6.08 (s, 1H), 3.73 (s, 1H). Relative to 1H of **12c**, 1H of **1,3,5-trimethoxybenzene** integrates for approximately 0.15H.

Signals assigned to **66**: δ 9.14 – 9.10 (m, 1H), 8.76 (app. dd, app. *J* = 4.9, 1.7 Hz, 1H), 8.30 – 8.25 (m, 1H), 7.47 (app. ddd, app. *J* = 8.0, 4.9, 0.9 Hz, 1H), 3.90 (s, 3H). Relative to 1H of **12c**, 1H of **66** integrates for 1.57H.

Signals assigned to **crossover product 67**: δ 9.22 (s, 1H), 8.92 (app. d, app. *J* = 8.1 Hz, 1H), 4.39 (s, 3H), 4.00 (s, 3H). Relative to 1H of **12c**, 1H of **67** integrates for 0.04H.[20]

Note: The singlets at 4.39 ppm and 4.16 ppm are overlapping with a minor side product, altering their integration values.

Ratio of **12c** to **crossover product 67**:

4H of Compound **12c** = 4.00 – Therefore 1H = 1.00

1H of **67** = 0.04 – Therefore 1H = 0.04

$$\text{Ratio} = \frac{1.00}{1.00 + 0.04} \times 100 = 96 : 4$$

Ratio of major product to internal standard:

4H of Compound **12c** = 4.00 – Therefore 1H = 1.00

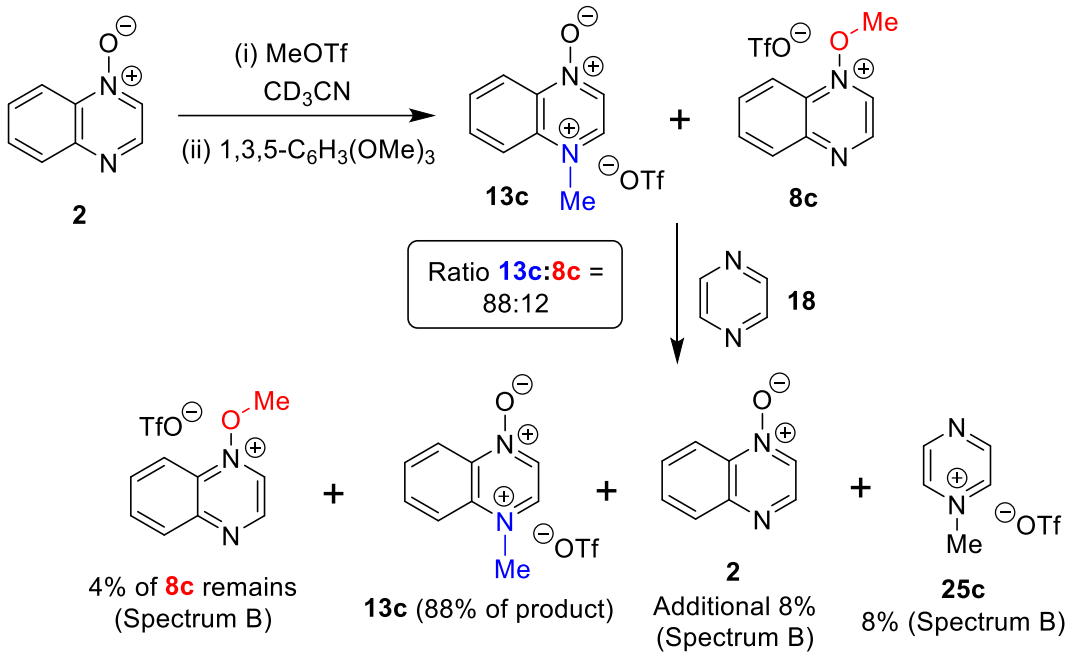
3H of internal standard = 0.45 – Therefore 1H = 0.15

$$\text{Ratio} = \frac{1.00}{1.00 + 0.15} \times 100 = 87 : 13$$

That the relative ratio of N-methylation product (**12c**) and the internal standard (1,3,5-trimethoxybenzene) remains constant after addition of 2nd nucleophile (**66**) demonstrates that the formation of **12c** from **1** + MeOTf is irreversible under the reaction conditions employed.

It can be concluded that formation of crossover product (**67**) derived from O-methylation product **7c** occurs by S_N2 reaction of **7c** + 2nd nucleophile **66**, and that **7c** does not undergo reversal to **1** + MeOTf in CD_3CN at *ca.* 20 °C (i.e., **7c** is formed irreversibly). If this were not the case, then a mixture of **12c** + **7c** should eventually convert entirely to **12c**, since **12c** is formed irreversibly. The ratio of **12c** to **7c** remains invariant with time unless a second nucleophile is added to the reaction mixture.

3.7.2. Crossover Experiment – Quinoxaline *N*-Oxide (2) with MeOTf and Pyrazine (18)



The following reagents were combined in the process described in General Procedure D. Quinoxaline *N*-oxide (**2**) (0.018 g, 0.12 mmol) was dissolved in CD_3CN (0.65 ml) in a vial in a glove box. Methyl triflate (0.019 g, 0.12 mmol) was subsequently added dropwise. To this mixture was added 1,3,5-trimethoxybenzene (5 mg, 0.03 mmol). The reaction mixture was transferred to an NMR tube and analyzed by NMR spectroscopy in CD_3CN (Spectrum A). The tube was removed from the spectrometer and a solution of **7** (8 mg, 0.010 mmol) in CD_3CN (0.20 ml) was injected into the tube through the rubber septum by syringe. The mixture was agitated and a second ^1H NMR spectrum was recorded. No change was observed in the ratio of **13c** and **8c** in this spectrum. After 1 day, and additional ^1H NMR spectrum was recorded (Spectrum B).

^1H NMR (300 MHz, CD_3CN, 15 second relaxation delay) Spectrum A:

Signals assigned to **13c**: δ 8.92 (d, *J* = 5.3 Hz, 1H), 8.75 (d, *J* = 5.3 Hz, 1H), 8.62 – 8.55 (m, overlaps with 1H of **8c**, contains 1H of **13c**), 4.43 (s, 3H).

Signals assigned to **8c**: δ 9.60 (d, *J* = 3.4 Hz, 1H), 9.49 (d, *J* = 3.4 Hz, 1H), 8.56 – 8.52 (overlaps with 1H of **13c**, contains 1H of **8c**), 4.65 (s, 3H). Relative to 1H of **13c**, 1H of **8c** integrates for 0.13H.

Signals assigned to starting material **2**: δ 8.67 (app. d, app. *J* = 3.6 Hz, 1H), 8.46 (app. dd, app. *J* = 8.6, 1.4 Hz, 1H), 8.38 – 8.23 (m, 1H), 7.92–7.84 (m, 1H), 7.83 – 7.75 (m, 1H). Relative to 1H of **13c**, 1H of **2** integrates for approximately 0.38H.

Signals assigned to internal standard **1,3,5-trimethoxybenzene**: δ 6.06 (s, 3H), 3.73 (s, 9H). Relative to 1H of **13c**, 1H of **1,3,5-trimethoxybenzene** integrates for 0.33H.

The section of the spectrum at 8.62 – 8.53 ppm contains 1H each of **13c** and **8c**. The section at 8.38 – 8.23 ppm contains a 2H signal from **13c**, a 2H signal from **8c** and a

1H signal from **2**. The section at 8.15 – 8.07 ppm contains a 1H signal from **13c,** a 1H signal from **8c** and a 1H signal from **2**.

Ratio of N-alkylation and O-alkylation Products:

1H of Compound **13c** = 1.00

1H of Compound **8c** = 0.13

$$\text{Ratio} = \frac{1.00}{1.00 + 0.13} \times 100 = 88\%\ \text{N alkylation}$$

Ratio of major product to internal standard:

1H of Compound **13c** = 1.00

3H of internal standard = 1.00 – Therefore 1H = 0.33

$$\text{Ratio} = \frac{1.00}{1.00 + 0.33} \times 100 = 75 : 25$$

^{1}H NMR (300 MHz, CD_3CN, 15 second relaxation delay) Spectrum B:

Signals assigned to **13c**: δ 8.91 (d, *J* = 5.3 Hz, 1H), 8.76 (d, *J* = 5.3 Hz, overlaps with signal of **25c**, contains 1H of **8c**), 4.43 (s, 3H).

Signals assigned to **8c**: δ 9.61 (d, *J* = 3.4 Hz, 1H), 9.49 (d, *J* = 3.4 Hz, 1H), 8.58 (app. d, app. *J* = 7.3 Hz, 1H), 4.65 (s, 3H). Relative to 1H of **13c**, 1H of **8c** integrates for 0.05H.

Signals assigned to starting material **2**: δ 8.66 (app. d, app. *J* = 3.6 Hz, 1H), 8.46 (app. dd, app. *J* = 8.6, 1.4 Hz, 1H), 7.91–7.83 (m, 1H), 7.82 – 7.74 (m, 1H). Relative to 1H of **13c**, 1H of **2** integrates for approximately 0.55H.

Signals assigned to internal standard **1,3,5-trimethoxybenzene**: δ 6.06 (s, 3H), 3.73 (s, 9H). Relative to 1H of **13c**, 1H of **1,3,5-trimethoxybenzene** integrates for approximately 0.33H.

Signals assigned to **18**: δ 8.57 (s, overlaps with 1H signal of **13c**, contains 4H of **18** (relative integration = 4.05 – 1.00 = 3.05)). Relative to 1H of **13c**, 1H of **18** integrates for (3.05/4) = 0.76H.

Signals assigned to **crossover product 25c**: δ 9.41 – 9.35 (m, 2H), 8.77 – 8.73 (m, 2H, overlaps with signal of **13c**), 4.39 (s, 3H). Relative to 1H of **13c**, 1H of **25c** integrates for approximately 0.07H.

The section of the spectrum between 8.38 and 8.23 ppm contains a 2H signal from **13c**, a 2H signal from **8c** and a 1H signal from **2**. The section at 8.15 – 8.07 ppm contains a 1H signal from **13c,** a 1H signal from **8c** and a 1H signal from **2**. The signal between 8.77 and 8.71 ppm contains a 1H signal from **13c** and a 1H signal from **8c**.

Ratio of **13c** to **crossover product 25c**:

1H of Compound **13c** = 1.00

2H of crossover product = 0.14 – Therefore 1H = 0.07

$$\text{Ratio} = \frac{1.00}{1.00 + 0.07} \times 100 = 93 : 7$$

Ratio of major product to internal standard:

1H of Compound **13c** = 1.02

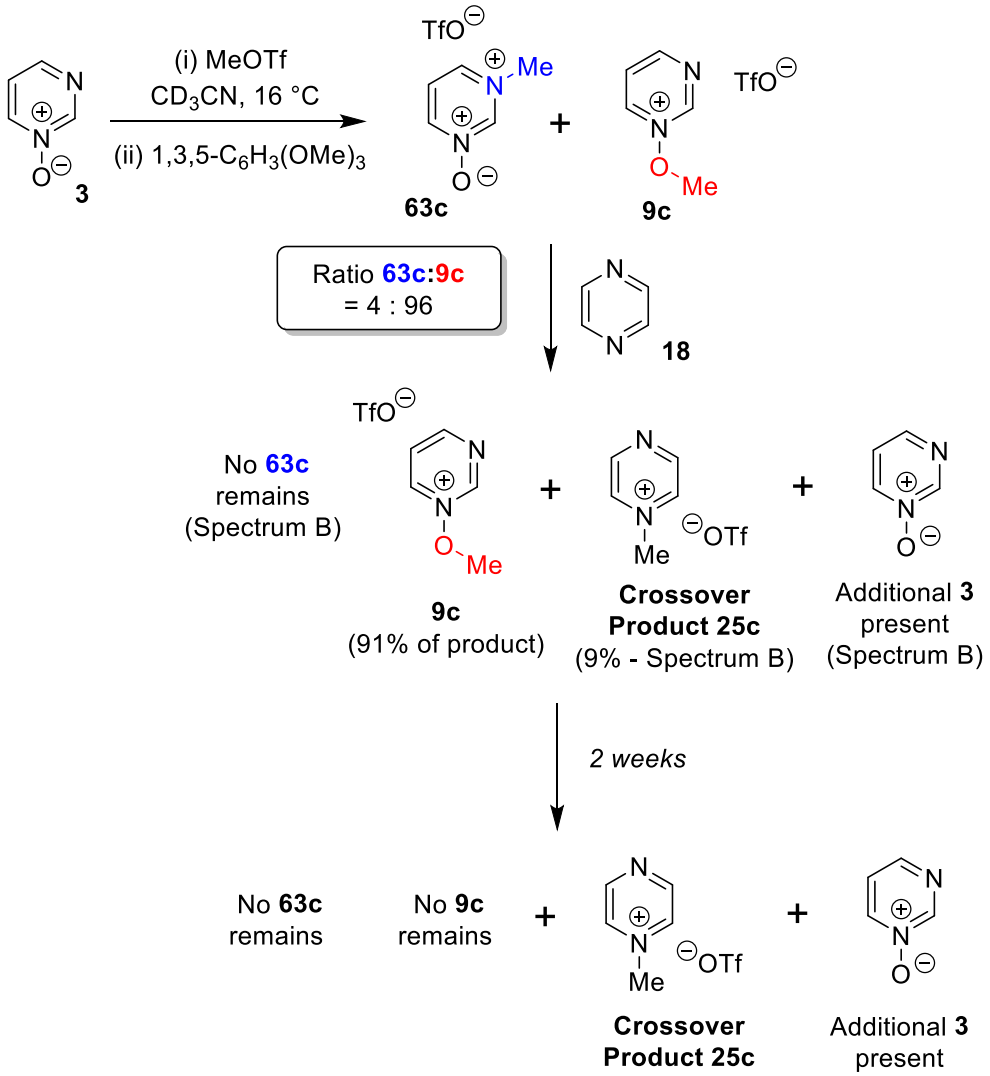
3H of internal standard = 1.00 – Therefore 1H = 0.33

$$\text{Ratio} = \frac{1.02}{1.02 + 0.33} \times 100 = 76 : 24$$

That the relative ratio of N-methylation product (**13c**) and the internal standard (1,3,5-trimethoxybenzene) remains constant after addition of 2nd nucleophile (**18**) demonstrates that the formation of **13c** from **2** + MeOTf is irreversible under the reaction conditions employed.

It can be concluded that formation of crossover product (**25c**) derived from O-methylation product **8c** occurs by S_N2 reaction of **8c** + 2nd nucleophile **18**, and that **8c** does not undergo reversal to **2** + MeOTf in CD_3CN at *ca.* 20 °C (i.e., **8c** is formed irreversibly). If this were not the case, then a mixture of **13c** + **8c** should eventually convert entirely to **13c**, since **13c** is formed irreversibly. The ratio of **13c** to **8c** remains invariant with time unless a second nucleophile is added to the reaction mixture.

3.7.3. Crossover Experiment – Pyrimidine *N*-Oxide (3) with MeOTf and Pyrazine (18)



The following reagents were combined in the process described in General Procedure D. Pyrimidine *N*-oxide (**3**) (0.014 g, 0.15 mmol) was dissolved in CD_3CN (0.65 ml) in a vial in a glove box. Methyl triflate (0.021 g, 0.13 mmol) was subsequently added dropwise. To this mixture was added 1,3,5-trimethoxybenzene (4 mg, 0.02 mmol). The reaction mixture was transferred to an NMR tube and analyzed by NMR spectroscopy in CD_3CN (Spectrum A). The tube was removed from the spectrometer and a 1.33 mol L^{-1} solution of **7** in CD_3CN (0.25 ml, 0.33 mmol) was injected into the tube through the rubber septum by syringe. The mixture was agitated and a second ^1H NMR spectrum was recorded – no change was observed in the ratio of **63c** and **9c** in this spectrum. After 1 day, the mixture was re-analyzed by ^1H NMR spectroscopy (Spectrum B). In spectrum B, only signals of **9c**, starting material **3**, crossover product **25c**, **18** and **1,3,5-trimethoxybenzene** were observed. After two weeks, the mixture was analyzed again by ^1H NMR spectroscopy (Spectrum C). This showed that **9c** remained, and substantial formation of crossover product **25c** along with starting

material **3** and a variety of decomposition products (the latter of which have been observed in all other experiments involving formation of **63c** and **9c** – see above).

^{1}H NMR (300 MHz, CD_3CN, 20 second relaxation delay) Spectrum A:

Signals assigned to **9c**: δ 9.50 – 9.36 (m, 1H), 8.98 – 8.85 (m, 1H), 8.53 (app. d, app. *J* = 6.0 Hz, 1H), 8.13 (s, 1H), 4.30 (s, 3H).

Signals assigned to **63c**: δ 9.78 – 9.77 (m, 1H), 9.43 – 9.36 (m, 2H), 8.33 – 8.17 (m, 1H), 4.51 (s, 3H). Relative to 1H of **9c**, 1H of **63c** integrates for 0.03H.

Signals assigned to starting material **3**: δ 8.95 (s, 1H), 8.41 (m, 1H), 8.34 – 8.23 (m, 1H), 7.51 – 7.43 (m, 1H). Relative to 1H of **9c**, 1H of **3** integrates for 0.31H.

Signals assigned to internal standard **1,3,5-trimethoxybenzene**: δ 6.11 (s, 3H), 3.76 (s, 9H). Relative to 1H of **9c**, 1H of **1,3,5-trimethoxybenzene** integrates for 0.18H.

The section of the spectrum between 9.50 and 9.36 ppm contains a 1H signal from **9c** and a 2H signal from **63c**. The section between 8.98 and 8.85 ppm contains a 1H signal from **63c** and a 1H signal from **3**. The section between 8.41 and 8.23 ppm contains a 1H signal from **9c** and two 1H signals from **3**.

Ratio of N-alkylation and O-alkylation Products:

3H of Compound **9c** = 3.00 – Therefore 1H = 1.00

1H of Compound **63c** = 0.03

$$\text{Ratio} = \frac{1.00}{1.00 + 0.03} \times 100 = 97\%\ \text{O alkylation}$$

Ratio of major product to internal standard:

3H of Compound **9c** = 3.00 – Therefore 1H = 1.00

3H of internal standard = 0.54 – Therefore 1H = 0.18

$$\text{Ratio} = \frac{1.00}{1.00 + 0.18} \times 100 = 85 : 15$$

^{1}H NMR (300 MHz, CD_3CN, 20 second relaxation delay) Spectrum B:

No signals assigned to **63c**.

Signals assigned to **9c**: δ 9.78 (app. dd, app. *J* = 2.2, 0.7 Hz, 1H), 9.43 – 9.37 (m, 2H), 8.31 – 8.25 (m, 1H), 4.51 (s, 3H).

Signals assigned to starting material **3**: δ 8.93 (s, 1H), 8.42 – 8.36 (m, 1H), 8.31 – 8.25 (m, 1H), 7.48 – 7.40 (m, 1H). Relative to 1H of **9c**, 1H of **3** integrates for 0.43H.

Signals assigned to internal standard **1,3,5-trimethoxybenzene**: δ 6.11 (s, 3H), 3.76 (s, 9H). Relative to 1H of **9c**, 1H of **1,3,5-trimethoxybenzene** integrates for 0.18H.

Signals assigned to **18**: δ 8.60 (s, 4H). Relative to 1H of **9c**, 1H of **7** integrates for (11.32/4) = 2.83H.

Signals assigned to **crossover product 25c**: δ 9.43 – 9.37 (m, 2H), 8.76 (d, *J* = 3.1 Hz, 2H), 4.42 (s, 3H). Relative to 1H of **9c**, 1H of **25c** integrates for 0.10H.

The signal between 8.31 and 8.25 ppm contains a 1H signal from **9c** and a 1H signals from **3**.

Ratio of **9c** to **crossover product 25c**:

1H of Compound **9c** = 1.00

2H of crossover product = 0.20 – Therefore 1H = 0.10

$$\text{Ratio} = \frac{1.00}{1.00 + 0.10} \times 100 = 91 : 9$$

Ratio of major product to internal standard:

1H of Compound **9c** = 1.00

3H of internal standard = 0.54 – Therefore 1H = 0.18

$$\text{Ratio} = \frac{1.00}{1.00 + 0.18} \times 100 = 85 : 15$$

^{1}H NMR (400 MHz, CD_3CN, 20 second relaxation delay) Spectrum C: Relative integrations are given relative to 1H of crossover product **25c** since no baseline-separated signals of the internal standard are available.

No signals characteristic of **9c** are present.

Signals assigned to starting material **3**: δ 9.02 (s, 1H), 8.52 – 8.46 (m, 1H), 8.44 – 8.36 (m, 1H), 7.57 – 7.49 (m, 1H). Relative to 1H of **25c**, 1H of **3** integrates for 1.45H.

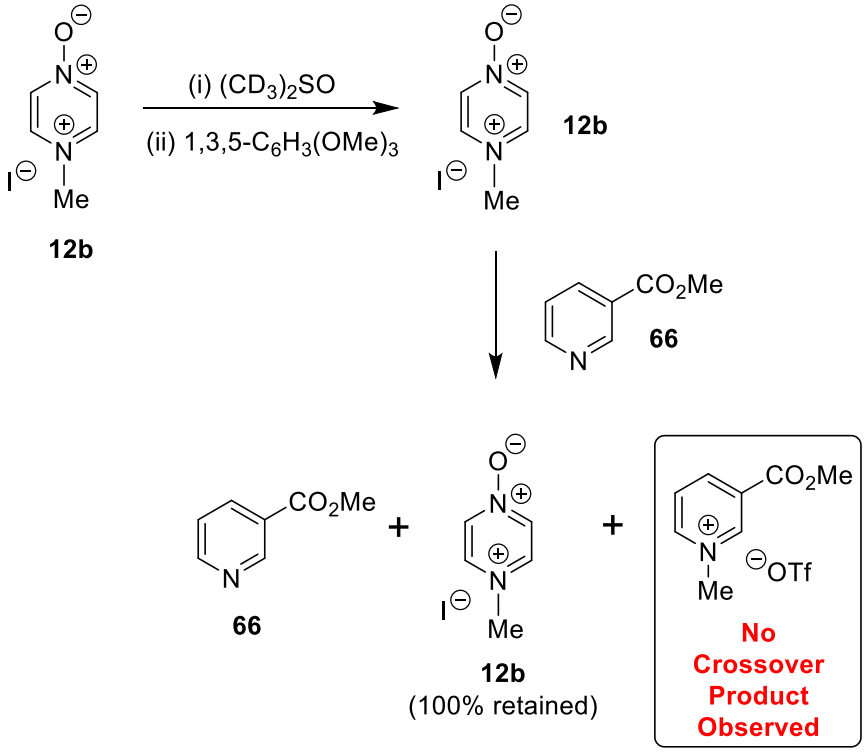
Signals assigned to **18**: δ 8.61 (s, 4H). Relative to 1H of **25c**, 1H of **18** integrates for 3.02H.

Signals assigned to **crossover product 25c**: δ 9.43 – 9.35 (m, 2H), 8.75 – 8.70 (m, 2H), 4.38 (s, 3H).

The signals of the internal standard (1,3,5-trimethoxybenzene) are obscured by signals of decomposition products (see ^{1}H NMR spectrum below). The relative proportion of (**18** + **25c**) to **3** is similar to the relative proportion of (**18** + **25c**) to (**3** + **9c**) in spectrum B (above), but reflects the occurrence of some decomposition of **9c** that was independent of the process of formation of crossover product **25c** by methylation of **18**.

Formation of crossover product (**25c**) derived from both N-methylation and O-methylation products (**63c** and **9c**) may indicate that **63c** and **9c** form reversibly from **3** + MeOTf, or instead that **63c** and **9c** each undergo S_N2 reactions with 2nd nucleophile **18**.

3.7.4. Crossover Experiment – 4-Methylpyrazinium-*N*-Oxide Iodide (12b) with MeOTf and Methyl Nicotinate (66)



The following reagents were combined in the process described in General Procedure D. **12b** (0.031 g, 0.13 mmol) was dissolved in $(CD_3)_2SO$ (0.7 ml) in a vial. To this solution was added 1,3,5-trimethoxybenzene (3 mg, 0.02 mmol). The mixture was transferred to an NMR tube and analyzed by NMR spectroscopy in $(CD_3)_2SO$ (Spectrum A). The tube was removed from the spectrometer and a solution of methyl nicotinate (**66**) (0.026 g, 0.19 mmol) in $(CD_3)_2SO$ (0.15 ml) was injected into the tube through the septum by syringe. The mixture was agitated and re-analyzed by NMR spectroscopy immediately, and again after one day (Spectrum B).

^{1}H NMR (300 MHz, $(CD_3)_2SO$, 10 second relaxation delay) Spectrum A:

Signals assigned to **12b**: δ 8.92 (dd, *J* = 13.3, 5.7 Hz, 4H), 4.16 (s, 3H).

Signals assigned to internal standard **1,3,5-trimethoxybenzene**: δ 6.06 (s, 3H), 3.68 (s, 9H). Relative to 1H of **12b**, 1H of **1,3,5-trimethoxybenzene** integrates for 0.18H.

Note: A singlet belonging to a small amount of an unknown contaminant is present at 8.22 ppm.

The singlet at 3.68 ppm could not be accurately integrated due to its proximity to the H_2O signal.

Ratio of major product to internal standard:

4H of Compound **12b** = 4.00 – Therefore 1H = 1.00

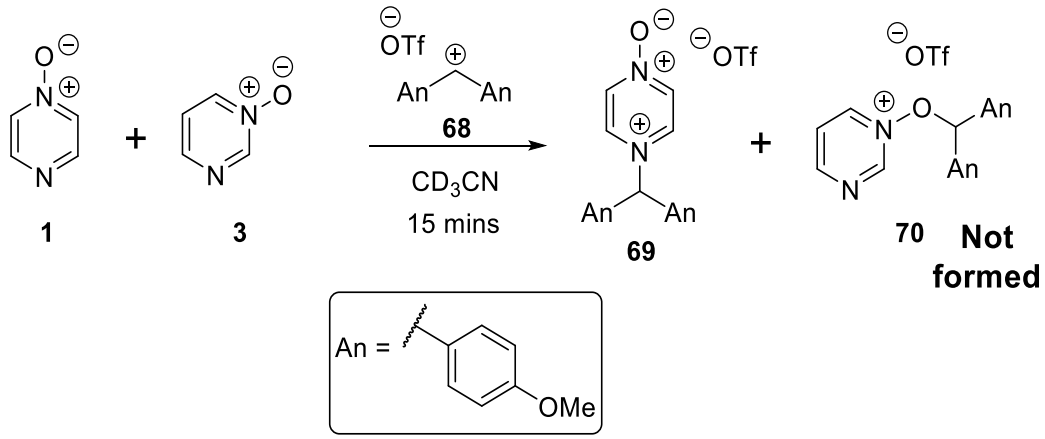
3H of internal standard = 0.55 – Therefore 1H = 0.18

$$\text{Ratio} = \frac{1.00}{1.00 + 0.18} \times 100 = 85 : 15$$

This experiment shows that **12b** is formed irreversibly from **1** + MeI.

As no change in the amount of **12b** present was observed, and no crossover product was formed, it can be concluded that **12b** is formed irreversibly.

3.8. Competition Experiment: Pyrazine *N*-Oxide vs Pyrimidine *N*-Oxide



Under an atmosphere of nitrogen in a glove box, bis(methoxy)benzhydryl chloride (0.009 g, 0.03 mmol) was dissolved in dry CD_3CN (0.85 ml). Pyrazine *N*-oxide **1** (6 mg, 0.06 mmol) was then added, followed by pyrimidine *N*-oxide **3** (0.005 g, 0.05 mmol), and then AgOTf (0.013 g, 0.05 mmol), causing the immediate precipitation of AgCl. The reaction vessel was sealed, agitated for 1 – 2 minutes, and filtered (removing AgCl) through a syringe filter into an NMR tube. The NMR tube was then sealed using a rubber septum. The seal was then wrapped with PTFE tape and Parafilm. Finally, the NMR tube was placed in a long Schlenk flask, which was sealed and then removed from the glove box. The sample was brought to the NMR spectrometer inside the long NMR Schlenk flask to protect it from potential ingress of moisture. The sample was removed from this Schlenk flask directly before loading it into the NMR spectrometer.

^{1}H NMR (400 MHz, CD_3CN) – Integrations are given relative to 1H of **69**.

Signals assigned to **69**: δ 8.52–8.46 (m, overlaps with signal of **1** at δ 8.46–8.41, contains 4H of **69** (4 × pyrazinium H)), 7.30–7.20 (m, contains 4H of **69** (anisyl protons), overlaps with signal of hydrolysis product), 7.11 – 7.00 (m, 5H, contains Ar_2CH and anisyl protons), 3.84(s, 6H, OCH_3).

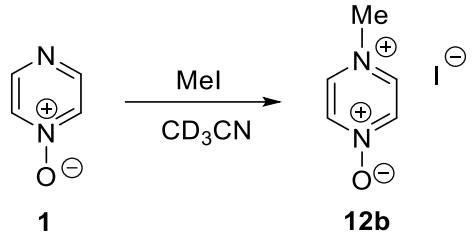
Signals assigned to **1**: δ 8.46–8.41 (m, 2H), 8.15–8.08 (m, 2H). 1H of **1** integrates for 0.70 relative to 1H of **69**.

Signals assigned to **3**: δ 8.92 (s, 1H), 8.41–8.32 (app. d, app. J = 6.3 Hz, 1H), 8.29 – 8.21 (m, 1H), 7.46 – 7.39 (m, 1H). 1H of **3** integrates for 1.58 relative to 1H of **69**.

Small signals arising from the presence of hydrolysis product (bis(4-methoxy)benzhydryl ether) are also present in the ^{1}H NMR spectrum (see section 3 in Appendix A).

No signals attributable to compound **70** are present, i.e., **69** is the only product formed.

3.9. Determination of 2nd Order Rate Constant to Verify Computationally Determined Value of $\Delta G^{\ddagger}$



1 **12b**

Pyrazine *N*-oxide (**1**) (0.010 g, 0.10 mmol) was dissolved in dry CD_3CN (0.20 ml) in a glove box under nitrogen atmosphere. This solution was taken up in a syringe and the syringe was placed in a long Schlenk flask inside the glove box, and the Schlenk flask was sealed. Methyl iodide (0.147 g, 1.04 mmol, 10 equivalents) was dissolved in 0.65 ml dry CD_3CN in the glove box. This solution was placed in an NMR tube, which was sealed using a rubber septum. The seal was then wrapped with PTFE tape and Parafilm. Finally, the NMR tube was placed in a long Schlenk flask, which was then sealed inside the glove box. Both Schlenk flasks were removed from the glove box and brought to the NMR spectrometer.

The Schlenk tubes were placed in the NMR spectrometer room for 20 minutes to allow them to equilibrate to the controlled room temperature of 25 °C. The NMR tube containing the MeI solution was removed from the Schlenk flask and placed in the NMR spectrometer. The probe of the spectrometer was also kept at 25 °C. After obtaining the first ^{1}H NMR spectrum and the correct shim for this sample, the NMR tube was ejected. The pyrazine *N*-oxide solution (0.18 ml, containing 0.090 mmol pyrazine *N*-oxide) in its syringe was removed from its Schlenk flask and added to the NMR tube by injection through the rubber septum. The septum was re-wrapped with parafilm after removal of the syringe. The NMR tube was inverted and then rapidly returned to the spectrometer to obtain NMR spectra of the ongoing reaction at certain intervals.

Each spectrum was obtained using 4 scans, a 5 second relaxation delay and a 30° pulse. The time ascribed to each spectrum was when the spectrum measurement ended. In the obtained spectra, the C*H*D_2CN signal at δ 1.968 was set at a constant integral value throughout and the other signals are given relative to this value.

The following signals were observed in the spectra after addition.

^{1}H NMR (500 MHz, CD_3CN, 298.15 K)

Assigned to **1**: δ 8.49 – 8.38 (m, 2H), 8.14 – 8.06 (m, 2H).

Assigned to MeI: δ 2.20 (s, 3H).

Assigned to **12b**: δ 8.65 – 8.59 (m, 2H), 8.57 – 8.52 (m, 2H), 4.19 (s, 3H, NCH_3).

Note: ^{13}C satellite peaks of the 2H signal of **1** at δ 8.10 appear at δ 8.30 – 8.28 and 7.92 – 7.90. These signals were included in the integration value for that signal. The aromatic signals of **12b** showed a variable chemical shift, moving downfield as the

reaction progressed. The signal also initially appeared as a singlet, before splitting into two doublets as it moved downfield.

The consumption of pyrazine *N*-oxide (**1**) was monitored by observing the decrease in the integration value at 8.10 ppm relative to the signal of C*H*D$_2$CN. The integration value was assigned a concentration value ([**1**]$_t$) relative to the concentration of (**1**) at t = 0.

At t = 0,

$$[\mathbf{1}]_{t=0} = \frac{\left(\frac{0.090\ \text{g}}{96.089\ \text{g mol}^{-1}}\right)}{0.83\ \text{ml}} = 0.113\ \text{mmol/ml}$$

At t = 713 seconds, the integration value of the signal at 8.10 ppm was 99.7% of its value at t = 0, giving:

$$[\mathbf{1}]_{t=713\ \text{s}} = (0.113\ \text{mmol/ml}) \times\ 0.997\ = 0.1127\ \text{mmol/ml}$$

This procedure was continued at various time points in order to monitor the consumption of pyrazine *N*-oxide. After 25 hours, conversion was approximately 28%. An approximate value of the 2nd order rate constant was derived based on data recorded for the reaction up to this level of conversion.

For each ^{1}H NMR spectrum (time t), the integrations of **1** and **12b** at time t (I(**1**) and I(**12b**), respectively) relative to the integration of the residual C*H*D$_2$CN were established (the integration of C*H*D$_2$CN in each spectrum was set equal to an arbitrary value of 15.2). The integration of **12b** was scaled (multiplied by 2/3) to take account of the additional protons contributing to the signal used for the integration.

The total amount of **1** and **12b** present always equals the initial amount of **1** added, i.e.

$$(n(\mathbf{1}) + n(\mathbf{12b})) = n(\mathbf{1})_{t=0}$$

where:

$n(\mathbf{1}) =$ amount of **1** (mmol) at time t

$n(\mathbf{12b}) =$ amount of **12b** (mmol) at time t

$$n(\mathbf{1})_{t=0} = \text{inital amount of } \mathbf{1} \text{ added (mmol)}$$

Hence, the quantity (I(**1**) + I(**12b**)) – the sum of the integrations of the signals of **1** and **12b** (scaled appropriately) – was used to represent the initial amount of **1** added. The consumption of **1** at time t was then established as follows:

$$\text{Consumption of } \mathbf{1} \text{ at time } t = \frac{I(\mathbf{1})}{(I(\mathbf{1}) + I(\mathbf{12b}))} = \frac{[\mathbf{1}]_t}{[\mathbf{1}]_0}$$

See column 4 of Table 3-1 below for the quantities calculated in this manner. The value of [**1**]$_t$/[[**1**]$_0$ at time t is multiplied by [**1**]$_0$ (the initial concentration of **1**) to give [**1**]$_t$ (the concentration of **1** at time t).

Table 3-1. Recorded integration values (*I*) and calculated concentrations of **1** and **12b** at various time points. Note that the integration values of **12b** shown here were scaled to take into account the additional protons contributing to the signal used for the integration.

Time (seconds)	*I*(**1**)	*I*(**12b**)	$[\mathbf{1}]_t$ / $[\mathbf{1}]_0$	$[\mathbf{1}]_t$ (mmol/ml)
0	25.00	0	1	0.1130
713	24.89	0.07	0.997	0.1127
1080	24.87	0.09	0.996	0.1126
1248	24.81	0.13	0.995	0.1124
1620	24.77	0.15	0.994	0.1123
1740	24.76	0.17	0.993	0.1122
2160	24.74	0.19	0.992	0.1121
2460	24.68	0.21	0.991	0.1120
3060	24.63	0.25	0.990	0.1119
3720	24.53	0.31	0.987	0.1116
5460	24.32	0.45	0.982	0.1109
7500	24.03	0.64	0.974	0.1101
8100	23.97	0.69	0.972	0.1098
11760	23.51	0.99	0.959	0.1084
22560	22.48	1.68	0.930	0.1051
29760	21.58	2.29	0.904	0.1022
36960	20.83	2.79	0.882	0.0997
54960	19.00	4.00	0.826	0.0933
72960	16.96	5.36	0.760	0.0859
90960	15.71	6.17	0.718	0.0811

The first-order rate constant k_{obs} at a given nucleophile concentration was obtained by least-squares fitting of the single-exponential function $[\mathbf{1}]_t = [\mathbf{1}]_0 e^{-k_{obs}t} + C$ to the decay curve formed by plotting the values of ($[\mathbf{1}]_t$) versus time (see Figure 3-1 below), where $[\mathbf{1}]_0$ and $[\mathbf{1}]_t$ are the concentrations of (**1**) at time 0 and time *t*, respectively, and C is a constant. An approximate value for the second-order rate constant *k* were obtained by dividing k_{obs} by the concentration of the electrophile (which was in excess).

The graph of ($[\mathbf{1}]_t$) versus time is shown below in Figure 3-1.

For the 2nd order reaction of **1** with MeI (and rate constant *k*):

$$\text{Rate} = k[\mathbf{1}][\text{MeI}]$$

By including ≥ 10 equivalents of MeI, the approximation can be made that:

$$[\text{MeI}]_t = [\text{MeI}]_0$$

Thus, for this pseudo-1st order reaction:

$$\text{Rate} = k_{\text{obs}}[\mathbf{1}]$$

where $k_{\text{obs}} = k[\text{MeI}]_0$

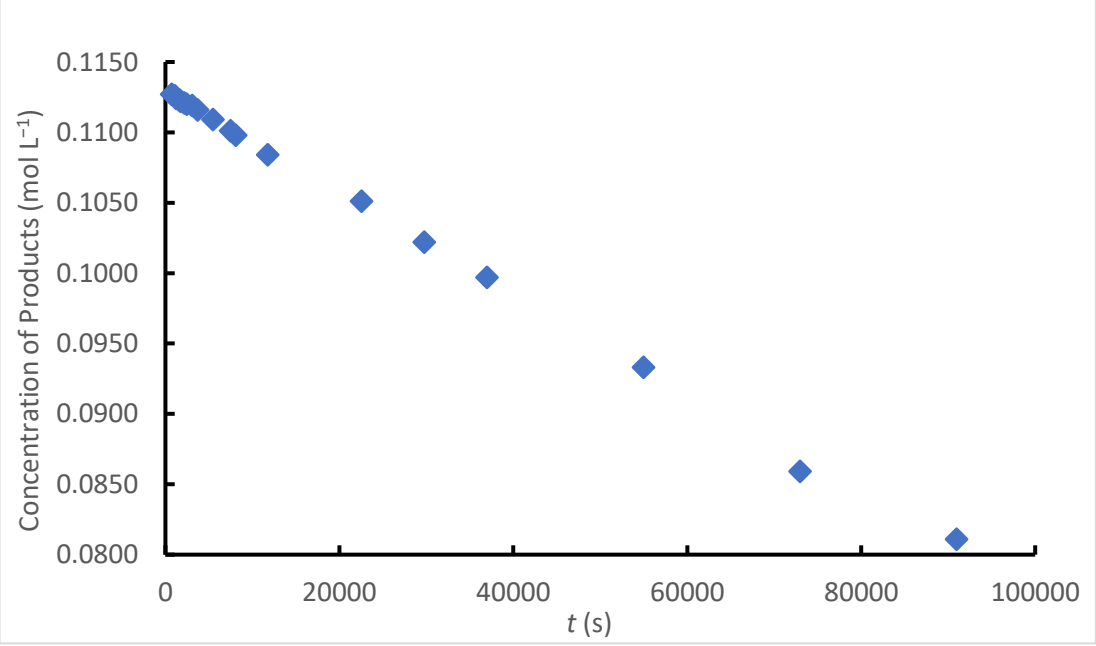


Figure 3-1: The plot of ($[\mathbf{1}]_t$) versus time for the reaction of **1** + MeI in CD_3CN at 25 °C.

The least squares fitting of the plot of the values of $[\mathbf{1}]_t$ shown in Table 3-1 versus time (see plot in Figure 3-1) to the function $[\mathbf{1}]_t = [\mathbf{1}]_0 e^{-k_{obs}t} + C$ gives a value of the pseudo-1st order rate constant of $k_{obs} = 8.04 \times 10^{-7}$ s^{-1}. The coefficient of determination (R^2) value is 0.9991. Hence, since $[MeI]_0 = 1.25$ mol L^{-1},

$$k = \frac{8.04 \times 10^{-7}\ \text{s}^{-1}}{1.25\ \text{mol L}^{-1}}$$

$$= 6.43 \times 10^{-7}\ \text{L mol}^{-1}\ \text{s}^{-1}$$

An identical value of the second order rate constant is also determined by monitoring the growth in the concentration of product **12b**.

This value of k may be related to $\Delta G^{\ddagger}$ by the Eyring equation:

$$k = \boldsymbol{\kappa} \frac{k_B T}{h} \times \frac{RT}{p^{\circ}}\ e^{-\frac{\Delta G^{\ddagger}}{RT}}$$

as seen in Atkins' Physical Chemistry, 9th ed. Section 22.4 pg. 848.[21] The transmission coefficient κ is taken to equal 1.

This equation can be rearranged to:

$$RT \ln\left(\left(\frac{1}{k}\right)\left(\frac{k_B T}{h}\right)\left(\frac{RT}{p^{\circ}}\right)\right) = \Delta G^{\ddagger}$$

giving:

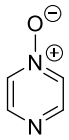
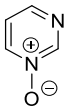
$$\Delta G^{\ddagger} = 1.2 \times 10^{2}\ \text{kJ mol}^{-1}$$

where:

$$R = 8.314\ \text{J K}^{-1}\text{mol}^{-1} \quad T = 298.15\ \text{K}$$
$$p^{\circ} = 10^{5}\ \text{N m}^{-2} \quad k_B = 1.38 \times 10^{-23}\ \text{J K}^{-1} \quad h = 6.63 \times 10^{-34}\ \text{J s}$$

3.9.1. Example Calculation to Obtain the Product Ratio Predicted by the Marcus Calculations

Table 3-2. Values of activation barriers ($\Delta G^{\ddagger}$) for methylation reactions of nucleophiles **1** and **3** with MeOTf, with calculations of the terms used in equation 2.4. The Gibbs energy values have units of kJ mol^{-1}.

Nucleophile (Nu) and Product Number		Entry	Site of Methylation	Marcus $\Delta G^{\ddagger}$	$\Delta\Delta G^{\ddagger}$	$\left(\frac{\Delta\Delta G^{\ddagger}}{RT}\right)$
	**1**	(i)	N	+108.7	−5.44	−2.20
		(ii)	O	+114.3		
	**3**	(iii)	N	+114.8	+13.6	+5.49
		(iv)	O	+101.2		

In the case of **1** + MeOTf:

$$\frac{k_N}{k_O} = e^{-(-2.20)} = 9.03$$

$$\frac{k_N}{k_O} = \frac{9.03}{1 + 9.03} = 90.0\%\ \text{N Methylation}$$

3.10. Calculations of Thermodynamic and Activation Parameter Values

Note: All quantum chemical computations shown here in section 3.10 and in section 5 of Appendix A (which were used to analyse the reactivity of the compounds discussed in Chapter 2) were performed by Prof. Martin Breugst at TU Chemnitz, Germany.

Details on Computational Methodology

The conformational space for each structure was explored with the OPLS-2005 force field[22] and a modified Monte Carlo search algorithm implemented in Macromodel.[23] An energy cut-off of 84 kJ mol^{-1} was employed for the conformational analysis, and structures with heavy-atom root-mean-square deviations (RMSD) up to 0.5 Å after the force field optimizations where considered to be the same conformer. All remaining structures were subsequently optimized with the dispersion-corrected M06-2X functional[24] with Grimme's dispersion correction D3 (zero-damping),[25] the triple-ζ basis set 6-311+G(d,p), and SMD solvation model[26] for acetonitrile. An ultrafine grid was used throughout this study for the numerical integration of the density. Vibrational analysis verified that each structure was a minimum or a transition state and for the latter, following the intrinsic reaction coordinates (IRC) confirmed that all transition states connected the corresponding reactants and products on the potential energy surface. Thermal corrections were obtained from unscaled harmonic vibrational frequencies at the same level of theory for a standard state of 1 mol L^{-1} and 298.15 K. Entropic contributions to free energies were obtained from partition functions evaluated with Grimme's quasi-harmonic approximation.[27] This method employs the free-rotor approximation for all frequencies below 100 cm^{-1}, the rigid-rotor-harmonic-oscillator (RRHO) approximation for all frequencies above 100 cm^{-1}, and a damping function to interpolate between the two expressions. Similar results were obtained from partition functions evaluated with Cramer's and Truhlar's quasiharmonic approximation.[28] This method uses the same approximations as the usual harmonic oscillator approximation, except that all vibrational frequencies lower than 100 cm^{-1} are set equal to 100 cm^{-1}. Electronic energies were subsequently obtained from single point calculations of the M06-2X-D3 geometries employing Neese's domain-based local pair-natural orbital (DLPNO) approach to the CCSD(T) method [DLPNO-CCSD(T)] with the default normalPNO settings,[29–31] the triple-ζ def2-TZVPPD [32,33] in combination with the corresponding auxiliary basis set[34] and the SMD continuum model for acetonitrile.[26] All density functional theory calculations were performed with Gaussian 16,[35] while the DLPNO-CCSD(T) calculations were performed with ORCA 4.[36,37]

Table 3-3: Activation Enthalpies ($\Delta H^{\ddagger}$, in kJ mol^{-1}), Activation Entropies ($\Delta S^{\ddagger}$, in J K^{-1} mol^{-1}), and Gibbs Energies of Activation ($\Delta G^{\ddagger}$, in kJ mol^{-1}) for Identity Methyl Transfer Reactions.

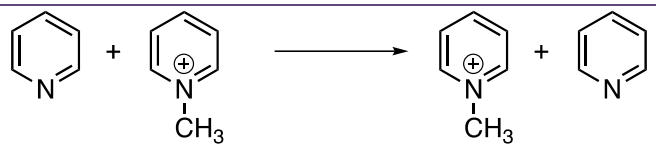
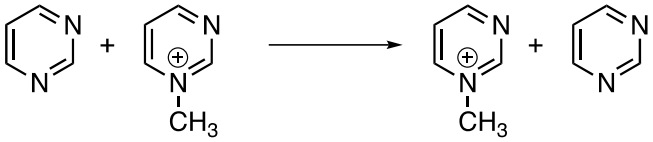
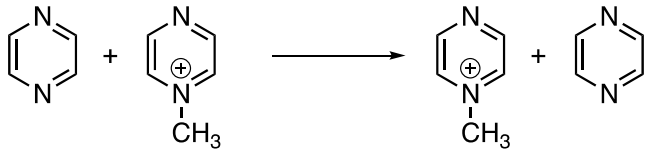
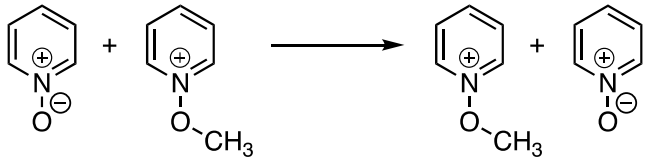
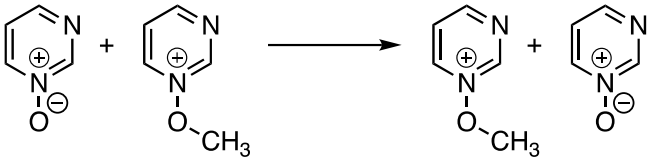
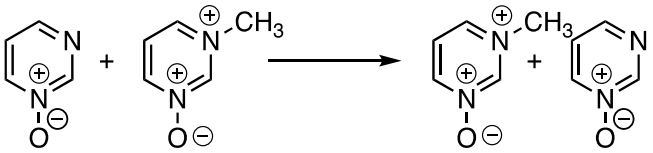
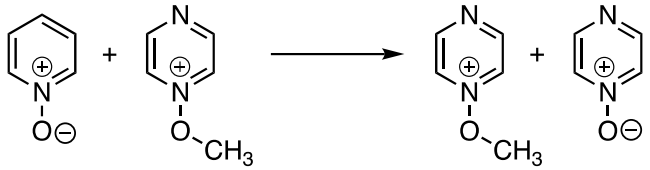
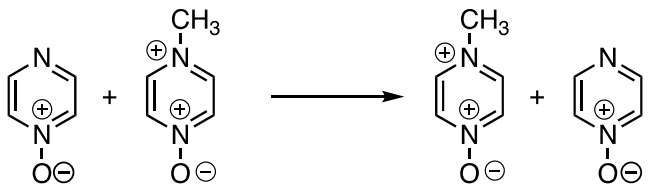
Reaction	$\Delta H^{\ddagger}$	$\Delta S^{\ddagger}$	$\Delta G^{\ddagger}$
	+127	–161	+175
	+123	–171	+175
	+121	–168	+171
	+87	–179	+141
	+73	–175	+125
	+117	–169	+167
	+88	–181	+142
	+125	–171	+176

Table 3-4: Values of Activation Parameters ($\Delta H^{\ddagger}$ (kJ mol^{-1}), $\Delta S^{\ddagger}$ (J K^{-1} mol^{-1})), $\Delta G^{\ddagger}$ (kJ mol^{-1})), and Thermodynamic Parameters ($\Delta_r H°$ (kJ mol^{-1}), $\Delta_r S°$ (J K^{-1} mol^{-1})), $\Delta_r G°$ (kJ mol^{-1})) for Methylation Reactions Using MeI.

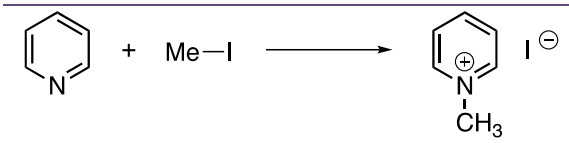
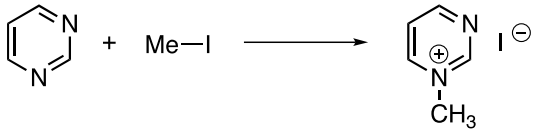
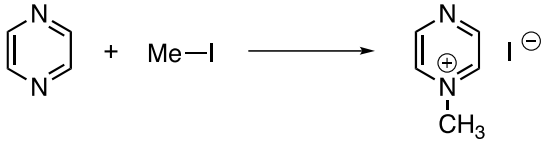
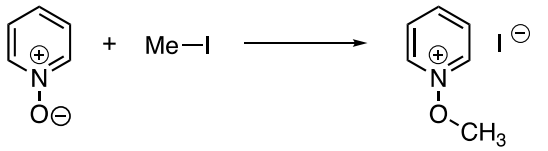
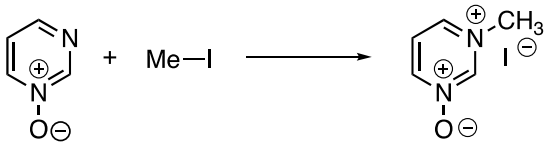
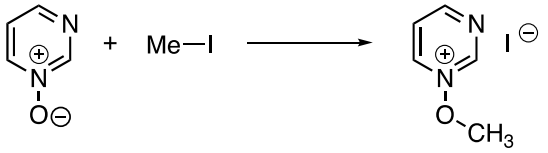
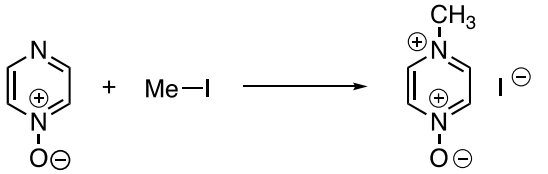
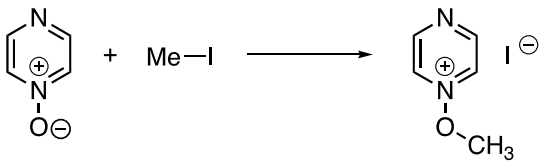
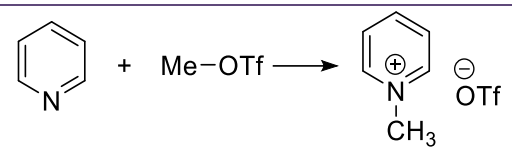
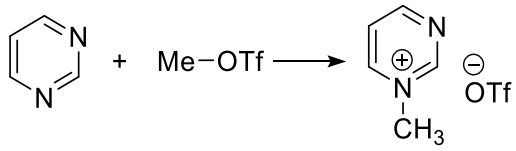
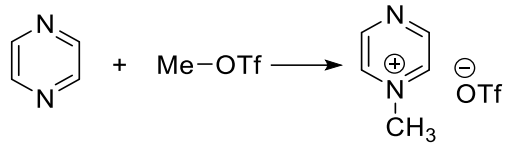
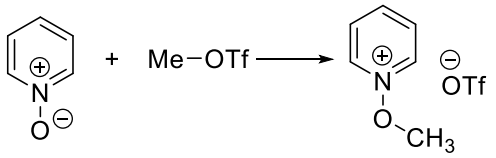
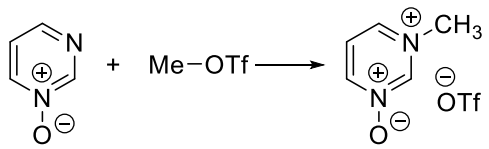
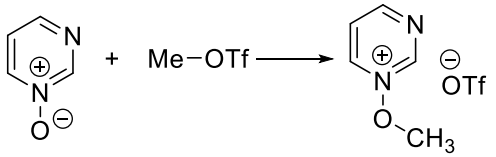
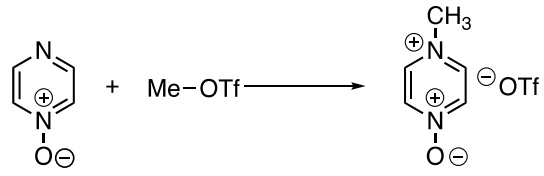
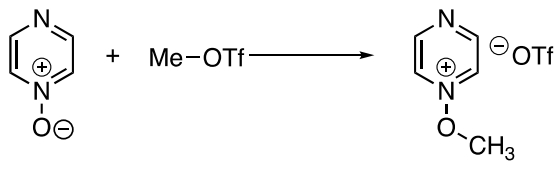
Reaction	$\Delta H^{\ddagger}$	$\Delta S^{\ddagger}$	$\Delta G^{\ddagger}$	$\Delta_r H°$	$\Delta_r S°$	$\Delta_r G°$
	+75	–150	+120	–64	–53	–48
	+84	–154	+130	–39	–52	–23
	+84	–156	+131	–37	–53	–21
	+75	–161	+123	–24	–56	–7
	+92	–154	+138	–13	–58	+4
	+80	–158	+127	+3	–59	+21
	+86	–158	+133	–37	–58	–20
	+92	–161	+140	+14	–55	+31

Table 3-5: Values of Activation Parameters ($\Delta H^{\ddagger}$ (kJ mol^{-1}), $\Delta S^{\ddagger}$ (J K^{-1} mol^{-1})), $\Delta G^{\ddagger}$ (kJ mol^{-1})), and Thermodynamic Parameters ($\Delta_r H°$ (kJ mol^{-1}), $\Delta_r S°$ (J K^{-1} mol^{-1})), $\Delta_r G°$ (kJ mol^{-1})) for Methylation Reactions Using MeOTf.

Reaction	$\Delta H^{\ddagger}$	$\Delta S^{\ddagger}$	$\Delta G^{\ddagger}$	$\Delta_r H°$	$\Delta_r S°$	$\Delta_r G°$
	+47	–164	+96	–117	+1	–117
	+56	–171	+107	–91	+1	–91
	+55	–174	+107	–90	0	–90
	+44	–181	+97	–76	–3	–75
	+62	–173	+113	–66	–5	–64
	+51	–172	+103	–49	–6	–48
	+56	–174	+108	–90	–5	–88
	+61	–180	+115	–38	–2	–38

3.11. References

1. Williams, D. B. G.; Lawton, M. *J. Org. Chem.* **2010**, *75*, 8351–8354.
2. Shriver, D. F.; Drezdon, M. A. *The Manipulation of Air-Sensitive Compounds*, 2nd Edition.; John Wiley & Sons: New York; 1986.
3. Kokatla, H. P.; Thomson, P. F.; Bae, S.; Doddi, V. R.; Lakshman, M. K. *J. Org. Chem.* **2011**, *76*, 7842–7848.
4. Leclerc, J.-P.; Fagnou, K. *Angew. Chem. Int. Ed.* **2006**, *45*, 7781–7786.
5. Głaszczka, R.; Jaźwiński, J. *J. Mol. Struct.* **2014**, *1061*, 150–159.
6. Freire Franco, M. S.; de Paula, M. H.; Glowacka, P. C.; Fumagalli, F.; Clososki, G. C.; da Silva Emery, F. *Tetrahedron Lett.* **2018**, *59*, 2562–2566.
7. Larionov, O. V.; Stephens, D.; Mfuh, A. M.; Arman, H. D.; Naumova, A. S.; Chavez, G.; Skenderi, B. *Org. Biomol. Chem.* **2014**, *12*, 3026–3036.
8. Vasta, J. D.; Raines, R. T. *Bioorgan. Med. Chem.* **2015**, *23*, 3081–3090.
9. Andreev, V. P. *Chem. Heterocycl. Compd.* **2010**, *46*, 184–195.
10. Witanowski, M.; Sicinska, W.; Biernat, S.; Webb, G. A. *J. Magn. Reson.* **1989**, *83*, 351–357.
11. Sanz, D.; Perona, A.; Claramunt, R. M.; Elguero, J. *Tetrahedron* **2005**, *61*, 145–154.
12. Denegri, B.; Streiter, A.; Jurić, S.; Ofial, A. R.; Kronja, O.; Mayr, H. *Chem. Eur. J.* **2006**, *12*, 5415–5415.
13. Newmark, R. A.; Tucker, A.; Hardy, L. C. *Magn. Reson. Chem.* **1996**, *34*, 728–729.
14. Leblanc, N.; Sproules, S.; Pasquier, C.; Auban-Senzier, P.; Raffy, H.; Powell, A. K. *Chem. Commun.* **2015**, *51*, 12740–12743.
15. Ma, X.; Dang, H.; Rose, J. A.; Rablen, P.; Herzon, S. B. *J. Am. Chem. Soc.* **2017**, *139*, 5998–6007.
16. Gao, X.; Han, S.; Zheng, M.; Liang, A.; Li, J.; Zou, D.; Wu, Y.; Wu, Y. *J. Org. Chem.* **2019**, *84*, 4040–4049.
17. Dega-Szafran, Z.; Szafran, M.; Sitkowski, J.; Stefaniak, L. *J. Phys. Org. Chem.* **1996**, *9*, 746–750.
18. V. Jovanovic, M. *Heterocycles* **1985**, *23*, 2299.
19. Forrester, J.; Jones, R. V. H.; Preston, P. N.; Simpson, E. S. C. *J. Chem. Soc., Perkin Trans. 1* **1995**, No. 18, 2289–2291.
20. King, J. A.; Bryant, G. L. *Synth. Commun.* **1994**, *24*, 1923–1935.
21. Atkins, P. W.; De Paula, J. *Physical Chemistry*, 9th Edition.; Oxford University Press: Oxford, 2010.
22. Banks, J. L.; Beard, H. S.; Cao, Y.; Cho, A. E.; Damm, W.; Farid, R.; Felts, A. K.; Halgren, T. A.; Mainz, D. T.; Maple, J. R.; Murphy, R.; Philipp, D. M.; Repasky, M. P.; Zhang, L. Y.; Berne, B. J.; Friesner, R. A.; Gallicchio, E.; Levy, R. M. *J. Comput. Chem.* **2005**, *26*, 1752.
23. Schrödinger Release 2018-3, Macromodel. Schrödinger, LLC: New York, NY, 2018.
24. Zhao, Y.; Truhlar, D. G. *Theor. Chem. Acc.* **2008**, *120*, 215–241.
25. Grimme, S.; Antony, J.; Ehrlich, S.; Krieg, H. *J. Chem. Phys.* **2010**, *132*, 154104.
26. Marenich, A. V.; Cramer, C. J.; Truhlar, D. G. *J. Phys. Chem. B* **2009**, *113*, 6378–6396.
27. Grimme, S. *Chem. Eur. J.* **2012**, *18*, 9955–9964.
28. Ribeiro, R. F.; Marenich, A. V.; Cramer, C. J.; Truhlar, D. G. *J. Phys. Chem. B* **2011**, *115*, 14556–14562.
29. Riplinger, C.; Sandhoefer, B.; Hansen, A.; Neese, F. *J. Chem. Phys.* **2013**, *139*, 134101.

30. Riplinger, C.; Neese, F. *J. Chem. Phys.* **2013**, *138*, 034106.
31. Liakos, D. G.; Neese, F. *J. Chem. Theory Comput.* **2015**, *11*, 4054–4063.
32. Weigend, F.; Ahlrichs, R. *Phys. Chem. Chem. Phys.* **2005**, *7*, 3297–3305.
33. Rappoport, D.; Furche, F. *J. Chem. Phys.* **2010**, *133*, 134105.
34. Hellweg, A.; Hättig, C.; Höfener, S.; Klopper, W. *Theor. Chem. Acc.* **2007**, *117*, 587–597.
35. Gaussian 16, Revision B.01, Frisch, M. J.; Trucks, G. W.; Schlegel, H. B.; Scuseria, G. E.; Robb, M. A.; Cheeseman, J. R.; Scalmani, G.; Barone, V.; Petersson, G. A.; Nakatsuji, H.; Li, X.; Caricato, M.; Marenich, A. V.; Bloino, J.; Janesko, B. G.; Gomperts, R.; Mennucci, B.; Hratchian, H. P.; Ortiz, J. V.; Izmaylov, A. F.; Sonnenberg, J. L.; Williams-Young, D.; Ding, F.; Lipparini, F.; Egidi, F.; Goings, J.; Peng, B.; Petrone, A.; Henderson, T.; Ranasinghe, D.; Zakrzewski, V. G.; Gao, J.; Rega, N.; Zheng, G.; Liang, W.; Hada, M.; Ehara, M.; Toyota, K.; Fukuda, R.; Hasegawa, J.; Ishida, M.; Nakajima, T.; Honda, Y.; Kitao, O.; Nakai, H.; Vreven, T.; Throssell, K.; Montgomery, J. A., Jr.; Peralta, J. E.; Ogliaro, F.; Bearpark, M. J.; Heyd, J. J.; Brothers, E. N.; Kudin, K. N.; Staroverov, V. N.; Keith, T. A.; Kobayashi, R.; Normand, J.; Raghavachari, K.; Rendell, A. P.; Burant, J. C.; Iyengar, S. S.; Tomasi, J.; Cossi, M.; Millam, J. M.; Klene, M.; Adamo, C.; Cammi, R.; Ochterski, J. W.; Martin, R. L.; Morokuma, K.; Farkas, O.; Foresman, J. B.; Fox, D. J. Gaussian, Inc., Wallingford CT, 2016.
36. Neese, F. *Wiley Interdiscip. Rev. Comput. Mol. Sci.* **2012**, *2*, 73–78.
37. Neese, F. *Wiley Interdiscip. Rev. Comput. Mol. Sci.* **2018**, *8*, e1327.

Chapter 4: Reactions of Cyclic Enolates with Various Alkylating Agents

4.1. Analysis of Ambident Reactivity of Cyclic Enolates with Various Alkylating Agents – the O/C Ratio 202

4.2. Reaction of Cyclic Enolates with "Soft" Alkylating Agents in Various Solvents 205

4.2.1. Reactions of cyclic enolates with EtI and EtBr in $CDCl_3$ 206

4.2.2. Reactions of cyclic enolates with EtI and EtBr in $(CD_3)_2SO$ 208

4.2.3. Reactions of cyclic enolates with EtI in THF 210

4.2.4. Reactions of Deuterated Methyl Iodide with Cyclic Enolates in Various Solvents 212

4.2.5. Reactions of cyclic enolates with CD_3I in CH_2Cl_2 and THF 214

4.2.6. Reactions of cyclic enolates with MeI in $CDCl_3$ 217

4.2.7. Reactions of Lithium Enolates **3-Li** and **12-Li** 217

4.2.8. Discussion of Selectivity Observed in Reactions of Cyclic Enolates with Representative "Soft" Electrophiles 222

4.3. Reactions of Tetramethylammonium Enolates with Substituted Benzyl Bromides 226

4.3.1. Reactions of **3-Me_4N** and **12-Me_4N** with Substituted Benzyl Bromides in THF 228

4.4. Reactions to Establish the Reversibility or Irreversibility of Alkylations of Cyclic Enolates 232

4.5. References 238

Appendices referred to in the text are available at the following link:
https://tinyurl.com/KSheehyPhDThesisAppendices

4.1. Analysis of Ambident Reactivity of Cyclic Enolates with Various Electrophiles – the O/C Ratio

Undertaking a systematic analysis of the factors which influence the reactivity of ambident nucleophiles requires a robust procedure which allows a reaction mixture to be analysed with a minimal amount of manipulation. Common features of synthetic procedures, such as aqueous work-ups or column chromatography may lead to incorrect assumptions being made about the selectivity of a reaction (for example, if one of the product of a reaction was water soluble and thus not isolable after an aqueous work-up). To ensure that the selectivity of the reaction is reflective of the kinetic preference for the products, a procedure was devised which involves carrying out the reaction of the ambident nucleophile in a deuterated solvent and directly observing the formation of the products by NMR spectroscopy. To quantify the selectivity of the enolate in question, the amount of O-alkylation products formed was directly compared to the amount of C-alkylation products formed in a given reaction – an approach which may also be seen in many of the literature studies of enolates seen in Chapter 1. The calculation of an O/C ratio for an enolate substrate allows the kinetic preference for O-alkylation to be determined when factors such as reaction solvent, counter-ion and electrophile are altered.

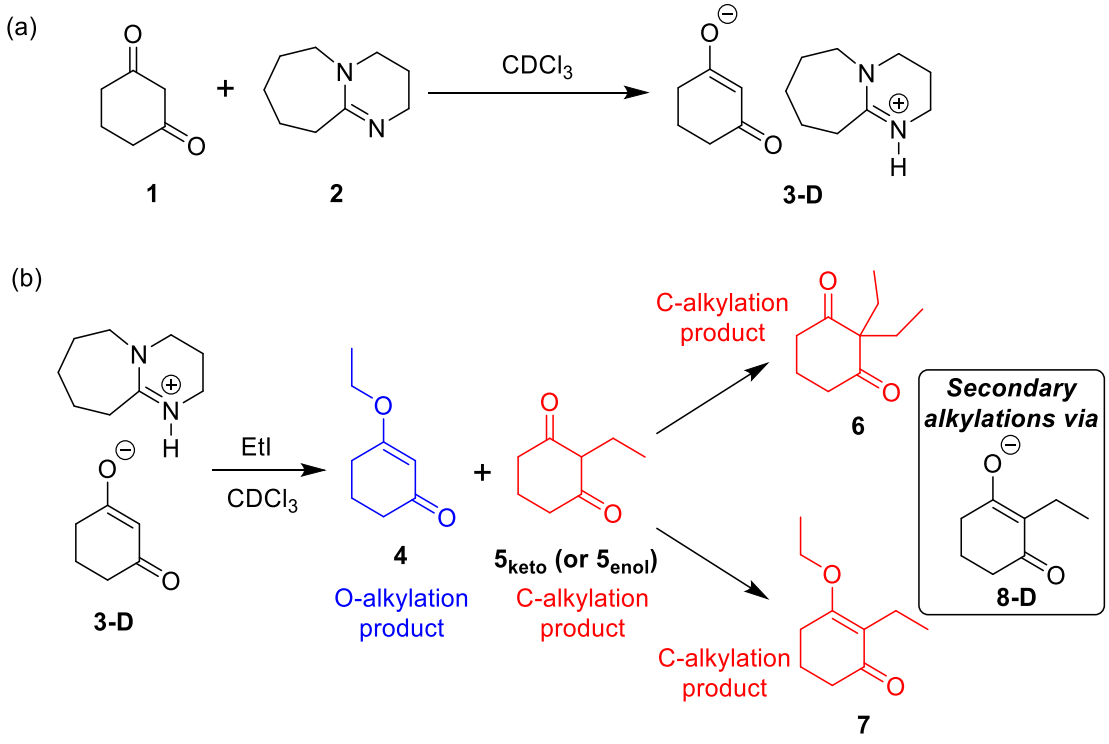
Great care was taken in this study to ensure that the O/C ratios measured by NMR spectroscopy are reflective of the kinetic preferences for the processes of O-alkylation or C-alkylation in a given reaction. All reactions in this study were performed using Schlenk equipment under an inert atmosphere of nitrogen gas. Dry solvents were used for all reactions and NMR studies. Other reagents to be used in these reactions, such as bases and electrophiles, were kept under an atmosphere of inert gas in flasks fitted with J. Young's valves prior to their use. All precautions were undertaken with the aim of allowing direct NMR spectroscopic measurement of the reaction mixture while minimising the number of external factors which may influence the selectivity of the reaction. In instances where the reaction mixture had to be manipulated prior to analysis (for example, a reaction in THF which requires the THF to be removed prior to NMR spectroscopic analysis), test reactions were completed which ensured that the manipulation required did not cause a change in the O/C ratio observed. A detailed description of the precautions taken in these reactions may be found in section 5.1 of Chapter 5.

Experiments have been carried out which establish that the alkylation reactions of these enolates was irreversible, although certain apparent exceptions existed. The irreversibility of these reactions was determined through the use of crossover experiments, which are discussed in section 4.3.

An example of a typical reaction of an ambident nucleophile as described in this chapter is shown below in Scheme 4-1. 1,3-Cyclohexanedione (**1**) is dissolved in a dry deuterated solvent ($CDCl_3$ in this case) before being deprotonated using 1,8-diazabicyclo[5.4.0]undec-7-ene (DBU, **2**) to form an enolate, **3-D**. A limiting amount of

an electrophile (EtI in this case) is added directly to the enolate solution and the mixture is allowed to react. At regular intervals, the reaction mixture is examined by ^{1}H NMR spectroscopy to observe the proportions of the various products (**4**, **5**, **6** and **7**) being formed. Of the 4 possible products of each reaction, only the O-mono-methylation product was considered as the "O" portion of the ratio, i.e., to obtain the O/C ratio, the integrations of the signals of the O-mono-alkylated product (product **4** in Scheme 4-1) was compared to the sum of the integrations of the 3 other products (**5**, **6** and **7**). As can be seen in Scheme 4-1, this is explained by the fact that products **6** and **7** are formed from enolate **8-D**, which is derived from the initial C-alkylation product (**5**) (this is deprotonated by the starting enolate **3-D)**. The integrations of the signals of each of the reaction products (i.e., **4**, **5**, **6** and **7** in Scheme 4-1) in the final ^{1}H NMR spectrum taken for a given reaction are used in the calculation of the O/C ratio. The relative integration of each compound is proportional to its relative concentration (in mol L^{-1}) and hence the relative integrations can be used to determine the relative proportions of O- and C-alkylation products formed in the reaction. A detailed explanation of the method for obtaining the O/C ratio from a reaction mixture is available in section 5.1 of Chapter 5.

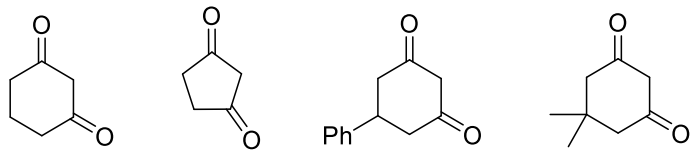
Scheme 4-1. (a) Deprotonation of 1,3-diketone (**1**) by DBU (**2**) to form the DBU-derived enolate of **1**, **3-D**. **(b)** After the enolate is formed *in situ*, a limiting amount of an electrophile is added directly to the reaction mixture. The formation of products **4**, **5**, **6** and **7** was subsequently monitored by periodic NMR spectroscopic analysis of the reaction mixture. Note that the C-mono-alkylated product (**5**) may exist as tautomers in the reaction mixture, which are designated $\mathbf{5_{keto}}$ and $\mathbf{5_{enol}}$.



Reactions described in this chapter involve enolates of the cyclic 1,3-diketones shown in Chart 4-1 below with various electrophiles and in various solvents.

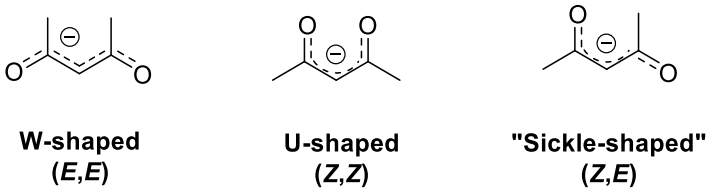
It is important to note that as each of the 1,3-diketones in Chart 4-1 is deprotonated to form a cyclic enolate, the anions are constrained to the W-shaped conformation.

Chart 4-1. 1,3-Diketones used in this study to probe the factors which influence the reactivity of ambident anions. The 1,3-diketones may be deprotonated with a variety of organic and inorganic bases to produce ambident enolate species.



The U-shaped and asymmetric "sickle-shaped" conformations, as shown in Chart 4-2, are not possible for the enolates derived from these compounds. While the HSAB treatment of ambident reactivity makes no provisions for effects of this type, previous literature studies have highlighted the difference in the kinetics of alkylations of enolates which exist in these distinct conformations.[1–3]

Chart 4-2. The various conformations which the enolates of 1,3-diketones may assume. As the enolates in this chapter are all derived from cyclic 1,3-diketones, only the W-shaped arrangement is possible.

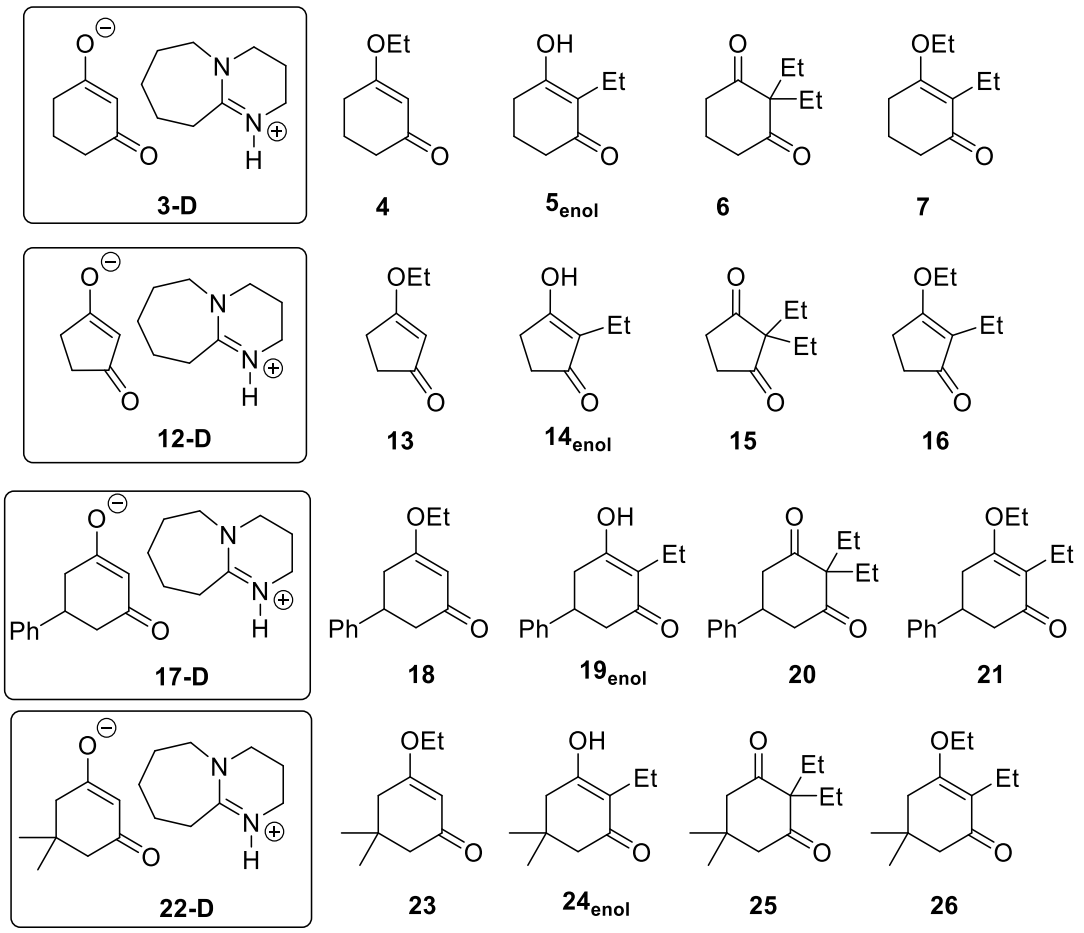


With a consistent and reproducible method for the alkylation and subsequent analysis of these ambident reactions in hand, the product ratios observed in reactions of these enolates with various halogenated electrophiles will be detailed and their agreement or disagreement with the HSAB theory as it is commonly applied will be noted. Given the ubiquity of enolates as reactive entities in organic synthesis, the goal of this investigation was to elucidate the factors which control the product distribution in reactions of this type.

4.2. Reactions of Cyclic Enolates with "Soft" Electrophiles in Various Solvents

Initial work on the reactions of ambident anions considered the effect that changing the solvent would have on the selectivity observed. As discussed in section 1.2.2 and section 1.2.3, the effect that the solvent chosen for the reaction may have is inextricably linked to the nature of the cation of the enolate, as the relationship of the cation and anion in solution is determined by the ability of the solvent to separate the ion pair. As some of the physical properties of solvents (such as dielectric constant, hydrogen bonding capability etc.) are believed to influence the outcomes of ambident reactions occurring in that solvent, it is important to use a set of solvents with differing characteristics to probe the reactivity of the ambident anions. Noting the previously observed variance between the selectivity of ambident species in heterogeneous and homogeneous reaction mixtures,[4,5] the cation chosen for this study must create an enolate that is entirely soluble in a variety of solvents of differing physical properties. DBU (**2**) was chosen as the base used to effect the deprotonation of the cyclic 1,3-diketones in this study (see **1** and **9** – **11** in Chart 4-1). It was chosen for this purpose due to its very high pK_aH value in organic solvents,[6] thereby making it likely to ensure irreversible deprotonation of 1,3-diones. Additionally, DBU (**2**) is easy to store and handle when compared to other bases with similar pK_aH values. Finally, the use of DBU (**2**) gave enolate salts that were soluble in organic solvents, which facilitated spectroscopic observations of the reaction mixture directly by ^{1}H NMR spectroscopy (provided the reaction solvent was deuterated). Although the use of DBU (**2**) as the base imparts the undesirable consequence of numerous ^{1}H NMR peaks which may obscure and overlap important product signals, the swiftness of enolate generation and the fact that the DBU enolate salts consistently gave homogeneous solutions represented a suitable compromise. One consequence of using DBU-derived enolates was an inability to unambiguously assign the signals of products of reactions of the chosen cyclic enolates with methylating agents in ^{1}H NMR spectra of reaction mixtures – overlap between key diagnostic signals of the methylated products and signals of DBU derivatives rendered unambiguous assignment and quantification of all products impossible. Ethylation products of these enolates, obtained through reaction with ethylating agents such as EtI and EtBr, were not found to suffer from the same issue. As there are 4 possible products of each of the reactions discussed below, the relevant enolates (**3-D**, **12-D**, **17-D** and **22-D**) and the products of their reactions with EtI are shown below in Chart 4-3.

Chart 4-3. The enolates and their ethylation products to be discussed in Table 4-1 and Table 4-2. [a]



4.2.1. Reactions of Cyclic Enolates with EtI and EtBr in $CDCl_3$

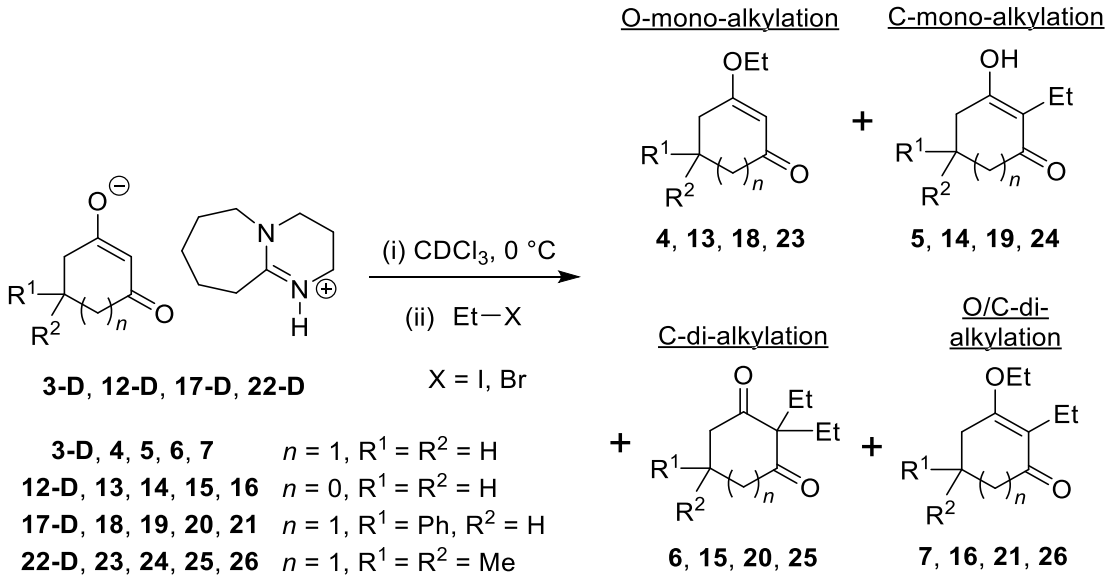
Shown in Table 4-1 are the O/C ratios derived from the reaction of enolates **3-D**, **12-D**, **17-D** and **22-D** with EtI and EtBr in $CDCl_3$. Each reaction was performed at 0 °C in a deliberate attempt to slow the rate of the reaction, thereby allowing the O/C ratio to be measured at differing levels of conversion by NMR spectroscopy.

O-ethylation is preferred in reactions of all enolates examined (i.e., of **3-D**, **12-D**, **17-D** and **22-D**) with EtI or EtBr in $CDCl_3$. In each experiment, the enol form of the C-mono-alkylated product was the only one observed (i.e., $\mathbf{5_{enol}}$, $\mathbf{14_{enol}}$, $\mathbf{19_{enol}}$ and $\mathbf{24_{enol}}$). The reaction of EtI with the enolate derived from 1,3-cyclohexanedione, **3-D**, was seen to produce the lowest amount of O-alkylation products (see Table 4-1 entry (i)). The use of EtBr as the electrophile in place of EtI (Table 4-1 entries (v) – (viii)) resulted in an increase in the amount of O-alkylation products formed compared to the corresponding reactions of EtI, except in the case of enolate **12-D**, where there was a slight decrease (compare Table 4-1 entry (ii) to entry (vi)). The O/C ratio remained constant at all

[a] The mono-C ethylation products ($\mathbf{5_{enol}}$, $\mathbf{14_{enol}}$, $\mathbf{19_{enol}}$ and $\mathbf{24_{enol}}$) are drawn in their enol form in Chart 4-3 above. Keto-enol tautomerism occurs rapidly for these species, so it is likely that both forms are present in solution to varying degrees.

observed levels of conversion in each individual experiment. When maintained at 0 °C, the reactions did not easily go to completion – the reactions in entry (ii) and (iv) showed that the enolate (or its parent enol) and EtI remained unreacted in solution after over 10 days. This demonstrates that the O/C ratio is likely to be an accurate representation of the kinetic ratio of products in this instance, as the ratio does not appear to trend towards the formation of the most thermodynamically stable product over time. The O/C ratios given in Table 4-1, as well as in all tables in this section, was determined by analysing the data from the final NMR spectrum recorded for a given reaction.

Table 4-1. O/C ratios of the products of the reactions of enolates **3-D**, **12-D**, **17-D** and **22-D** with EtI and EtBr in $CDCl_3$. [a]



3-D, **4**, **5**, **6**, **7** — *n* = 1, $R^1 = R^2 = H$
12-D, **13**, **14**, **15**, **16** — *n* = 0, $R^1 = R^2 = H$
17-D, **18**, **19**, **20**, **21** — *n* = 1, R^1 = Ph, $R^2 = H$
22-D, **23**, **24**, **25**, **26** — *n* = 1, $R^1 = R^2$ = Me

#	Enolate	*n*	R^1	R^2	O-Ethylation Product	C-Ethylation Products	O/C Ratio [a,b]
	Reactions of EtI						
(i)	**3-D**	1	H	H	**4**	**5, 6, 7**	84:16
(ii)	**12-D**	0	H	H	**13**	**14, 15, 16**	97:3
(iii)	**17-D**	1	Ph	H	**18**	**19, 20, 21**	93:7
(iv)	**22-D**	1	Me	Me	**23**	**24, 25, 26**	91:9
	Reactions of EtBr						
(v)	**3-D**	1	H	H	**4**	**5, 6, 7**	94:6
(vi)	**12-D**	0	H	H	**13**	**14, 15, 16**	96:4
(vii)	**17-D**	1	Ph	H	**18**	**19, 20, 21**	96:4
(viii)	**22-D**	1	Me	Me	**23**	**24, 25, 26**	93:7

[a] The O/C ratio was determined by direct analysis of the reaction mixture by ^{1}H NMR spectroscopy.

[b] The percentage of C-alkylation is the combined proportion of C-mono-alkylation product, C-di-alkylation product and mixed O/C-di-alkylation product in the reaction mixture. In any given reaction, some products drawn here may not be formed. See chapter 5 section 5.3 for details on the individual reactions.

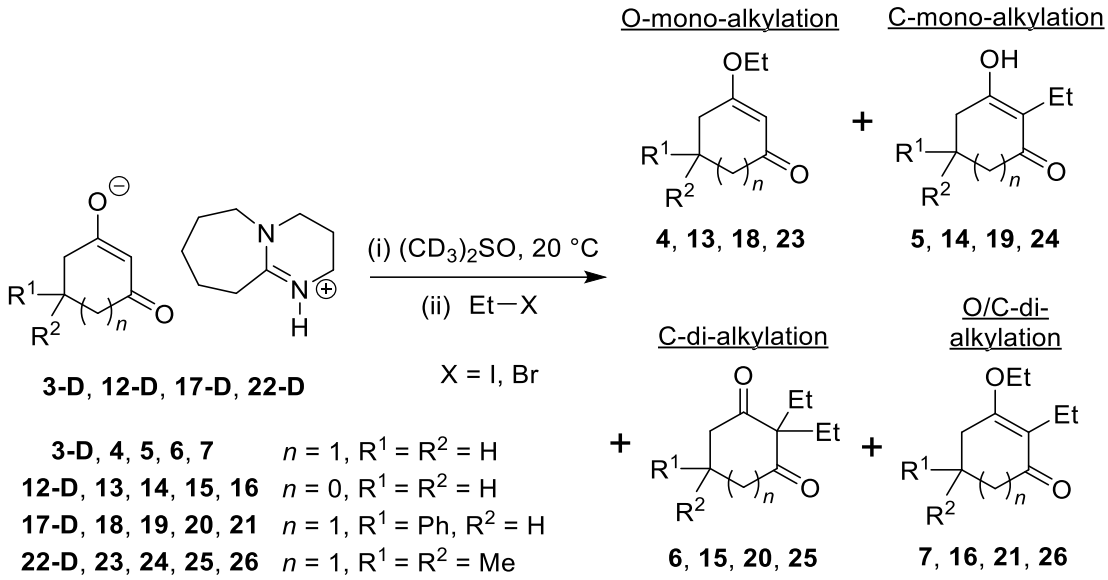
4.2.2. Reactions of Cyclic Enolates with EtI and EtBr in $(CD_3)_2SO$

Although the O-selectivity was extremely high in all cases listed in Table 4-1, the discussion in section 1.2.2 predicts that switching to a solvent with a higher dielectric constant, like deuterated dimethyl sulfoxide $(CD_3)_2SO$, should result in an increased proportion of O-alkylation due to an increased capability for the solvent to reduce electrostatic interaction between the ions of the enolate species.[7,8]

The O/C ratios obtained from reactions of enolates **3-D**, **12-D**, **17-D** and **22-D** with EtI and EtBr in $(CD_3)_2SO$ are shown below in Table 4-2. O-ethylation was once again favoured in all reactions of the enolates in question with EtI and EtBr in $(CD_3)_2SO$. These reactions were performed at 20 °C, just above the melting point of $(CD_3)_2SO$ (19 °C) to assist in the measurement of multiple NMR spectra before the reaction goes to completion.

The reactions were notably faster than the analogous reactions in $CDCl_3$ (the results of which are shown in Table 4-1 above), with the reactions in Table 4-2 entry (i) and (ii) proceeding to full conversion in a maximum of 2 days. The point of full conversion was noted by observing the complete consumption of EtI (or EtBr) in the spectrum, as well as observing that identical spectra were recorded one day apart from each other. The O/C ratio in each ease was lower compared to the corresponding reaction in $CDCl_3$, except in the case of the reaction of enolate **17-D**, in which the O/C ratio remained the same (compare Table 4-1 entry (iii) with Table 4-2 entry (iii)). The reactions of enolate **3-D** and **22-D** with EtI (Table 4-2 entries (i) and (iv)) show only a moderate preference for O-alkylation in $(CD_3)_2SO$. When the electrophile was EtBr, enolate **3-D** and **22-D** showed a noticeably increased amount of O-alkylation compared to the reactions of EtI (compare Table 4-2 entries (v) and (viii) to entries (i) and (iv)). In both series of ethylation reactions, the enolates **3-D** and **22-D** produced the lowest amount of O-alkylation products. A notable difference between entries (i) and (ii) in Table 4-2 compared to entries (i) and (ii) in Table 4-1 is seen in the number of unique alkylation products which were formed. The mixed O/C-di-alkylation products in these reactions (i.e., compound **7** in Table 4-2 entry (i) and compound **16** in entry (ii)) were formed in very low amounts in the reactions in $(CD_3)_2SO$, though products of this type were not seen in any of the reactions presented in Table 4-1.

Table 4-2. O/C ratios of the products of the reactions of enolates **1-D**, **7-D**, **8-D** and **9-D** with EtI and EtBr in $(CD_3)_2SO$. [a]



3-D, **4**, **5**, **6**, **7** $n = 1$, $R^1 = R^2 = H$
12-D, **13**, **14**, **15**, **16** $n = 0$, $R^1 = R^2 = H$
17-D, **18**, **19**, **20**, **21** $n = 1$, $R^1 = Ph$, $R^2 = H$
22-D, **23**, **24**, **25**, **26** $n = 1$, $R^1 = R^2 = Me$

#	Enolate	*n*	R^1	R^2	O-Ethylation Product	C-Ethylation Products	O/C Ratio [a,b]
	Reactions of EtI						
(i)	**3-D**	1	H	H	**4**	**5, 6, 7**	67:33
(ii)	**12-D**	0	H	H	**13**	**14, 15, 16**	91:9
(iii)	**17-D**	1	Ph	H	**18**	**19, 20, 21**	93:7
(iv)	**22-D**	1	Me	Me	**23**	**24, 25, 26**	66:34
	Reactions of EtBr						
(v)	**3-D**	1	H	H	**4**	**5, 6, 7**	88:12
(vi)	**12-D**	0	H	H	**13**	**14, 15, 16**	93:7
(vii)	**17-D**	1	Ph	H	**18**	**19, 20, 21**	93:7
(viii)	**22-D**	1	Me	Me	**23**	**24, 25, 26**	85:15

[a] The O/C ratio was determined by direct analysis of the reaction mixture by ^1H NMR spectroscopy.

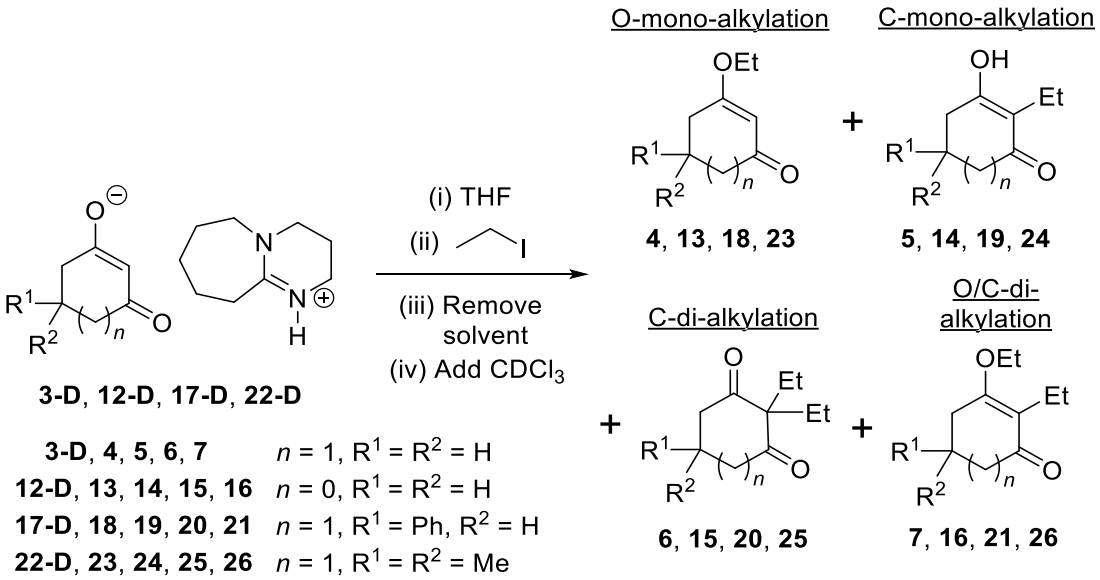
[b] The percentage of C-alkylation is the combined proportion of C-mono-alkylation product, C-di-alkylation product and mixed O/C-di-alkylation product in the reaction mixture. In any given reaction, some products drawn here may not be formed. See chapter 5 section 5.3 for details on the individual reactions.

4.2.3. Reactions of Cyclic Enolates with EtI in THF

THF, being a polar aprotic solvent with a low dielectric constant, was deemed sufficiently distinct from $CDCl_3$ and $(CD_3)_2SO$ to be used to test the degree to which O-alkylation seemed to be preferred in all reactions of EtI with enolates **3-D**, **12-D**, **17-D** and **22-D**. To enable analysis of enolate alkylation reactions using THF (i.e., non-deuterated) as the solvent, it was necessary to apply a vacuum to the reaction mixture to remove the solvent. The remaining material could then be re-dissolved in $CDCl_3$ to enable direct comparison of the NMR spectra recorded with the spectra in section 4.2.1 above. The process of solvent removal by vacuum could, in principle, bring about a change in the O/C ratio, particularly if any of the products of a given reaction (i.e., compounds **4** – **7**, **13** – **16**, **18** – **21**, **23** – **26** in Chart 4-3) are volatile at the vacuum pressure applied. For this reason, the reaction mixtures from entries (i) – (iv) in Table 4-1 were subjected to the vacuum conditions needed to remove THF from a reaction mixture (i.e., a lower vacuum pressure than would be needed to adequately remove $CDCl_3$). The residual material was then re-dissolved in $CDCl_3$ and re-analysed by ^{1}H NMR spectroscopy – in each case, the O/C ratio accurately reflected what was observed before the reaction mixture was subjected to the vacuum pressures. It was established that no material loss (other than solvent removal) resulted from this process, and hence it was deemed feasible to access accurate O/C ratios of the reactions of enolates **3-D**, **12-D**, **17-D** and **22-D** with EtI in THF by removing the THF after the reaction had finished and re-dissolving the crude products in $CDCl_3$. The O/C ratios (measured in $CDCl_3$) obtained from reactions of enolates **3-D**, **12-D**, **17-D** and **22-D** with EtI in THF are shown below in Table 4-3. As the reactions in THF could not be analysed over the course of the reaction by NMR spectroscopy, the reactions were simply allowed to stir at 20 °C overnight before the THF was removed.

The O/C ratios seen in the reactions in THF indicate that O-alkylation by EtI is extremely favourable in the case of each enolate studied (see Table 4-3 entries (i) – (iv)). Each enolate shows greater than 90% O-selectivity in reactions with EtI. Each of the reactions displayed a greater degree of O-selectivity than their counterparts in Table 4-1 and Table 4-2. The enolate derived from 1,3-cyclohexanedione, **3-D**, displays the highest degree of O-selectivity in the reaction with EtI in THF compared to the corresponding reactions in $CDCl_3$ and $(CD_3)_2SO$ (compare entry (i) in Table 4-3 with entry (i) in Table 4-1 and entry (i) in Table 4-2).

Table 4-3. O/C ratios of the products of the reactions of enolates **3-D**, **12-D**, **17-D** and **22-D** with EtI in THF at 20 °C. At the conclusion of the reaction, the THF was removed *in vacuo* and the crude products were re-dissolved in $CDCl_3$ for ^1H NMR analysis. [a]



#	Enolate	*n*	R^1	R^2	O-Ethylation Product	C-Ethylation Products	O/C Ratio [a,b]
	Reactions of EtI						
(i)	**3-D**	1	H	H	**4**	**5, 6, 7**	94:6
(ii)	**12-D**	0	H	H	**13**	**14, 15, 16**	97:3
(iii)	**17-D**	1	Ph	H	**18**	**19, 20, 21**	95:5
(iv)	**22-D**	1	Me	Me	**23**	**24, 25, 26**	96:4

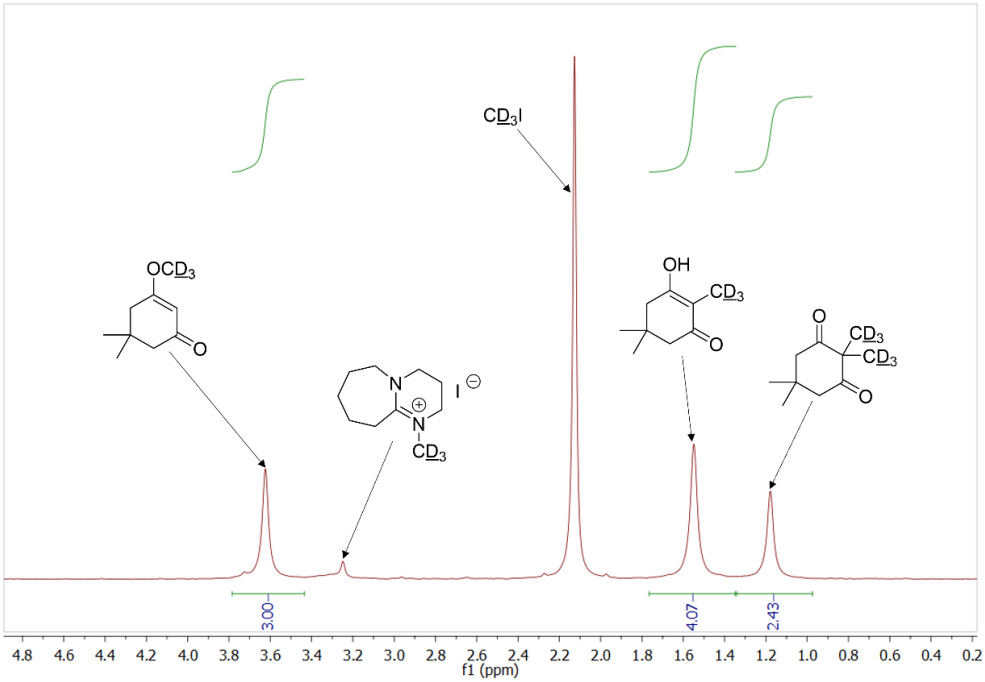
[a] The O/C ratio was determined by direct analysis of the reaction mixture by ^1H NMR spectroscopy.

[b] The percentage of C-alkylation is the combined proportion of C-mono-alkylation product, C-di-alkylation product and mixed O/C-di-alkylation product in the reaction mixture. In any given reaction, some products drawn here may not be formed. See chapter 5 section 5.3 for details on the individual reactions.

4.2.4. Reactions of Deuterated Methyl Iodide with Cyclic Enolates in Various Solvents

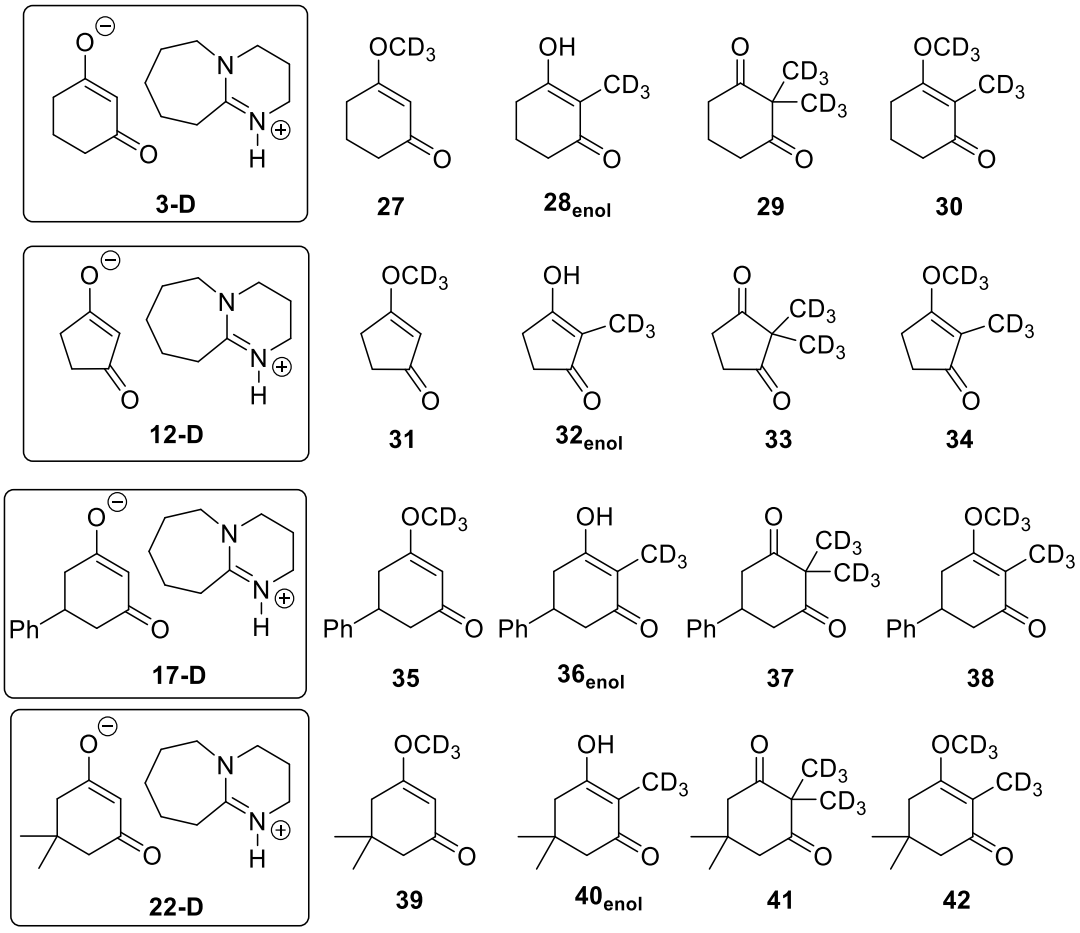
Direct measurement of O/C ratios in reactions of enolates in deuterated solvents by NMR spectroscopy forces a balance to be struck between the solubility of the enolate and the ability to clearly identify and quantify the products seen in a reaction mixture. Alkali metal enolates are expected to have limited solubility in organic solvents, and organic bases such as Et(*i*Pr)$_2$N and DBU (**2**) have a large number of discrete ^{1}H NMR signals which may overlap with important product signals in the spectrum of the reaction mixture. Although the use of DBU (**2**) as a base enabled the measurements of O/C ratios for ethylations of cyclic enolates in $CDCl_3$ and $(CD_3)_2SO$, it was found not to be possible to measure accurate product ratios for the corresponding methylation reactions under these conditions because regions of the ^{1}H NMR spectra of the reaction mixtures that could contain key diagnostic signals indicating the presence of one or more of the enolate methylation products would be obscured by the signals of the base or its conjugate acid. In order to further explore the reactivity of the archetypal soft electrophile, methyl iodide, reactions of deuterated methyl iodide (CD_3I) with various cyclic enolates were carried out in non-deuterated solvents. Analysis of these reaction mixtures by ^{2}H NMR spectroscopy allowed the O/C ratio to be measured directly, as only the signals of the deuterated products appeared in the spectrum. A labelled example of a ^{2}H NMR spectrum obtained from one of these reactions is shown in Figure 4-1 below. As demonstrated by this example, the use of ^{2}H NMR spectroscopy and a deuterated electrophile give spectra that render the process of calculating an O/C ratio comparatively easy.

Figure 4-1. ^{2}H NMR spectrum obtained from a reaction of enolate **22-D** with CD_3I in CH_2Cl_2. The only signals in the spectrum come from deuterated compounds, and hence the relative quantity of O-and C-alkylation products can be easily compared.



The spectrum is only populated with signals of compounds that incorporate deuterium, meaning all of the signals derived from the trideuteromethylation products (i.e., compounds **39** – **42** in Chart 4-4) may be easily measured. The only extraneous signals in the ^{2}H NMR spectrum belong to the unreacted CD_3I and a small amount of trideuteromethylated DBU formed by the nucleophilic attack of DBU (**2**) on CD_3I. [a]

Chart 4-4. The enolates and their trideuteromethylation products to be discussed in this section. Note that the suffix "-D" found in the naming convention of the enolates (e.g., **3-D**, **12-D**) does not relate to deuterium (^{2}H) but rather to the diazabicyclo[5.4.0]undecenium counter-cation of the enolate. [b]



A list of the potential trideuteromethylated products that could form from a reaction of CD_3I with each enolate is shown above in Chart 4-4. Each of the alkylation products observed in Figure 4-1 (i.e., compounds **39** – **42** in Chart 4-4) may be identified in the spectrum by analogy of the chemical shifts of their non-deuterated counterparts in $CDCl_3$ (e.g., the trideuteromethoxy- ^{2}H NMR signal of compound **39** appears at δ 3.62 ppm in

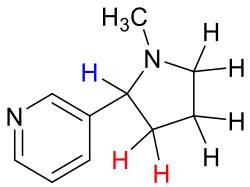
[a] This signal was proven to be derived from this species by analysing the ^{2}H NMR spectrum obtained from a separately conducted reaction of DBU (**2**) + CD_3I in CH_2Cl_2. This may be seen in section 5.4 in the experimental chapter.

[b] The mono-C ethylation products (**28enol**, **32enol**, **36enol** and **40enol**) are drawn in their enol form in Chart 4-4 above. Keto-enol tautomerism occurs rapidly for these species, so it is likely that both forms are present in solution.

CH_2Cl_2, and the methoxy- ^1H NMR signal of the corresponding non-deuterated compound appears at δ 3.68 ppm in $CDCl_3$).[9]

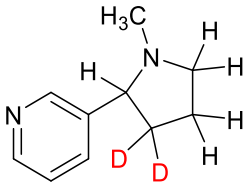
The chemical shift of a deuterium signal is expected to be essentially the same as the analogous ^1H chemical shift in a non-deuterated compound.[10] This is exemplified in a study by Pitner *et al*., where ^1H and ^2H NMR spectroscopic analysis was carried out on nicotine and nicotine which had undergone varying levels of deuteration (see Figure 4-2).[11] In the resulting ^1H and ^2H NMR spectra, the ^1H and ^2H chemical shifts associated with the pyrrolidine signals were found to be essentially identical.

Figure 4-2. ^1H and ^2H NMR spectroscopic analysis of nicotine (**43**) and various deuterium-substituted nicotine analogues (e.g., **44** and **45**) in a study by Pitner et al. reveals that the chemical shifts of the pyrrolidine signals are almost identical in ^1H and ^2H NMR spectroscopy.[11] More examples showing that the ^1H and ^2H NMR signals of these compounds are similar may be found in the original paper.



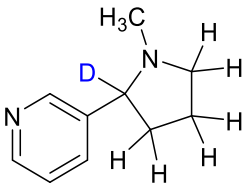
43

^1H NMR δ =
3.08 ppm,
2.19 ppm,
1.72 ppm



44

^2H NMR δ =
2.21 ppm,
1.73 ppm



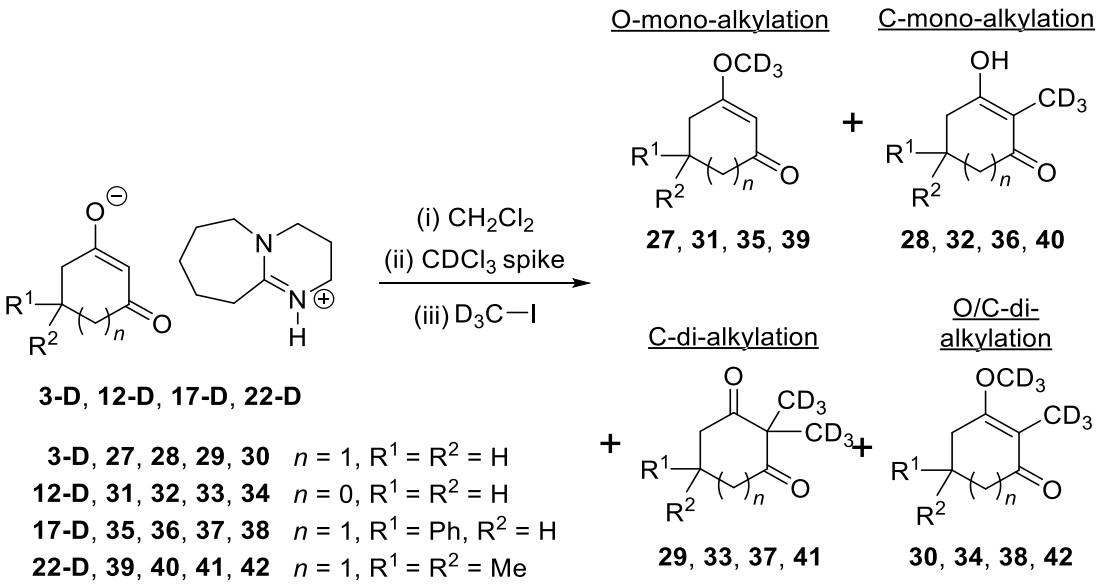
45

^2H NMR δ =
3.07 ppm

4.2.5. Reactions of Cyclic Enolates with CD_3I in CH_2Cl_2 and THF

Shown in Table 4-4 are the O/C ratios derived from the reaction of enolates **3-D**, **12-D**, **17-D** and **22-D** with CD_3I in CH_2Cl_2. As the NMR spectrometer requires a deuterium lock signal in order to limit magnetic field drift, a small amount of $CDCl_3$ was added to each reaction mixture prior to ^2H NMR spectroscopic analysis. As was the case in section 4.2.1, ^2H NMR spectra were recorded at multiple timepoints in order to monitor the progress of the reaction and to ensure the O/C ratio remained constant at varying levels of conversion. A reasonably high level of O-alkylation is seen in the reaction of each enolate with CD_3I, although only enolate **12-D** shows preferential O-alkylation (Table 4-4 entry (ii).

Table 4-4. O/C ratios of the products of the reactions of enolates **3-D**, **12-D**, **17-D** and **22-D** with CD_3I in CH_2Cl_2. A small amount of $CDCl_3$ was added to each reaction mixture to act as the lock signal for the spectrometer. [a]



#	Enolate	*n*	R^1	R^2	O-Ethylation Product	C-Ethylation Products	O/C Ratio [a,b]
	Reactions of CD_3I						
(i)	**3-D**	1	H	H	**27**	**28, 29, 30**	35:65
(ii)	**12-D**	0	H	H	**31**	**32, 33, 34**	78:22
(iii)	**17-D**	1	Ph	H	**35**	**36, 37, 38**	44:56
(iv)	**22-D**	1	Me	Me	**39**	**40, 41, 42**	36:64

[a] The O/C ratio was determined by direct analysis of the reaction mixture by ^2H NMR spectroscopy.

[b] The percentage of C-alkylation is the combined proportion of C-mono-alkylation product, C-di-alkylation product and mixed O/C-di-alkylation product in the reaction mixture. In any given reaction, some products drawn here may not be formed. See chapter 5 section 5.3 for details on the individual reactions.

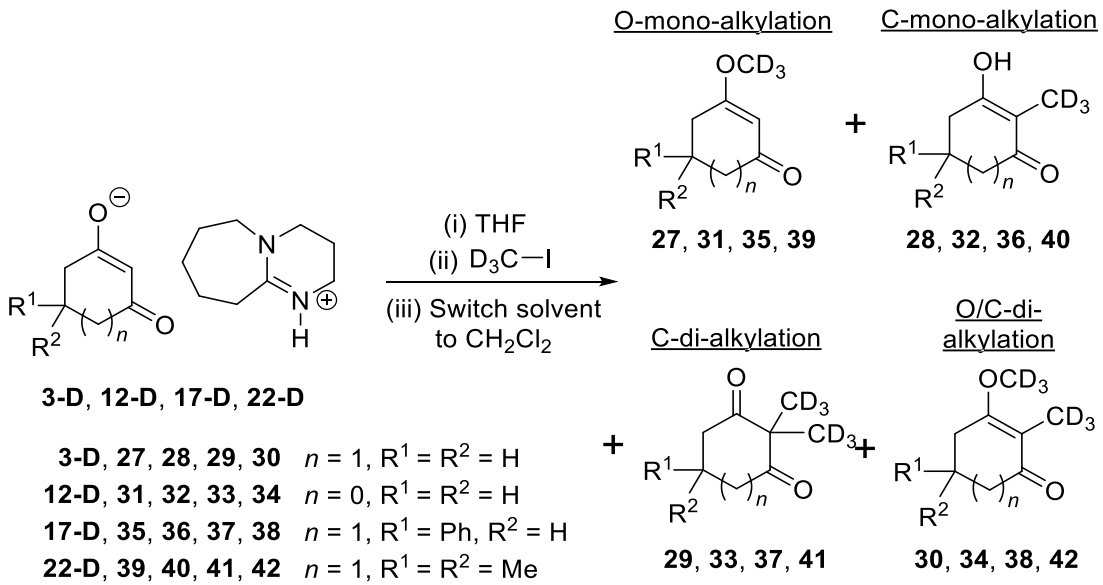
C-trideuteromethylation of enolates **3-D**, **17-D** and **22-D** (Table 4-4 entries (i), (iii) and (iv)) was slightly favoured, although not to the extent that would be expected with the quintessential soft electrophile MeI. [a]

Noting the increase in O-selectivity when reactions of **3-D**, **12-D**, **17-D** and **22-D** were carried out in THF (see section 4.2.3, Table 4-3), the trideuteromethylation reactions were repeated using THF as the solvent. As was the case with the reactions in Table 4-3, the THF was removed *in vacuo* after a set amount of time had passed, at which point the residue was redissolved in CH_2Cl_2. CH_2Cl_2 was chosen as the NMR solvent again so that the product signals should have a similar chemical shift when comparing between the two

[a] Examples of reactions from the literature where MeI gives extremely high levels of C-methylation are discussed in section 1.2, with specific examples being seen in Table 1-17 from the work of Kurts *et al.*[12] Other examples which demonstrate a high degree of C-selectivity in reactions of MeI with enolates are found in the work of Jackman and Lange,[13] and in the work of Rathke and Lindert.[14]

sets of reactions. The reactions in THF were all found to undergo preferential O-trideuteromethylation (Table 4-5, entries (i) – (iv)). Enolates **3-D**, **12-D** and **17-D** showed a large preference for O-alkylation (Table 4-5 entries (i) – (iii)), whereas enolate **22-D** displayed only a moderate preference for the O-alkylation process (Table 4-5, entry (iv)).

Table 4-5. O/C ratios of the products of the reactions of enolates **3-D**, **12-D**, **17-D** and **22-D** with CD_3I in THF. At the conclusion of the reaction, the THF was removed *in vacuo* and the crude reaction products were re-dissolved in CH_2Cl_2 for ^2H NMR analysis. A small amount of $CDCl_3$ was added to each reaction mixture after the dissolution in CH_2Cl_2 to act as the lock signal for the spectrometer. [a]



#	Enolate	*n*	R^1	R^2	O-Ethylation Product	C-Ethylation Products	O/C Ratio [a,b]
	Reactions of CD_3I						
(i)	**3-D**	1	H	H	**27**	**28, 29, 30**	81:19
(ii)	**12-D**	0	H	H	**31**	**32, 33, 34**	84:16
(iii)	**17-D**	1	Ph	H	**35**	**36, 37, 38**	80:20
(iv)	**22-D**	1	Me	Me	**39**	**40, 41, 42**	63:37

[a] The O/C ratio was determined by direct analysis of the reaction mixture by ^2H NMR spectroscopy.

[b] The percentage of C-alkylation is the combined proportion of C-mono-alkylation product, C-di-alkylation product and mixed O/C-di-alkylation product in the reaction mixture. In any given reaction, some products drawn here may not be formed. See chapter 5 section 5.3 for details on the individual reactions.

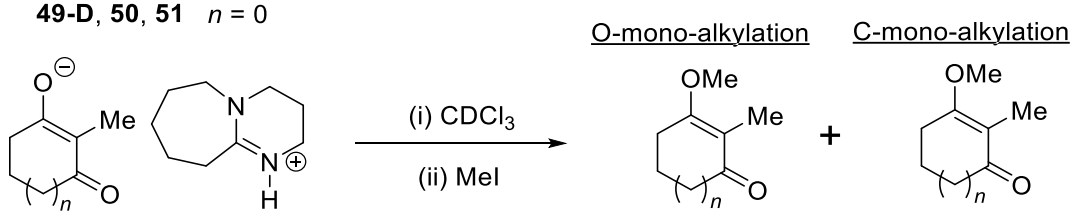
These results show that, as already demonstrated in section 4.2.1, solvent choice can play a decisive role in determining the site of addition of an ambident nucleophile. The fact that a soft electrophile such as CD_3I can furnish a majority of O-alkylation products solely due to the use of THF as a solvent represents a significant failure of the predictive capabilities of the HSAB treatment of selectivity in reactions of ambident nucleophiles.

4.2.6. Reactions of Cyclic Enolates with MeI in $CDCl_3$

As mentioned in the section above, accurate product ratios could not be measured for the methylation reactions of each of the enolates employed in this study when using DBU (**2**) as the base. Regions of the ^{1}H NMR spectra of the reaction which contained key diagnostic signals indicating the presence of one or more of the enolate methylation products were obscured, resulting in O/C ratios that were unreliable or even impossible to measure by ^{1}H NMR spectroscopy. However, determination of O/C ratios was found to be possible by analysis of NMR spectra of reaction mixtures involving enolates **46-D** and **49-D**, each of which bear a methyl substituent at the 2-position (see Table 4-6). In using enolates derived from 2-methylated 1,3-diketones, there were only two possible products of each reaction, making it less likely that the signals of the products would be obscured in the ^{1}H NMR spectra of the reaction mixtures. The O/C ratios derived from the reaction of enolates **46-D** and **49-D** with MeI in $CDCl_3$ are shown in Table 4-6.

Table 4-6. O/C ratios of the products of the reactions of enolates **46-D** and **49-D** with MeI in $CDCl_3$. [a]

46-D, **47**, **48** n = 1
49-D, **50**, **51** n = 0



46-D, **49-D** **47**, **50** **48**, **51**

#	Enolate	*n*	O-Ethylation Product	C-Ethylation Product	O/C Ratio [a]
(i)	**46-D**	1	**47**	**48**	6:94
(ii)	**49-D**	0	**50**	**51**	39:61

[a] The O/C ratio was determined by direct analysis of the reaction mixture by ^{1}H NMR spectroscopy.

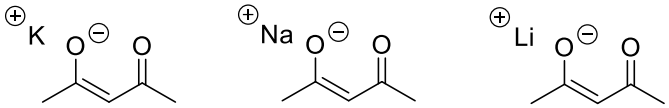
C-methylation of enolates **46-D** and **49-D** by MeI in $CDCl_3$ was favoured in both of the reactions studied. The methylation of enolate **46-D** (Table 4-6 entry (i)) was highly C-selective, whereas the reaction of **49-D** (entry (ii)) showed only a slight preference for C-methylation over O-methylation.

4.2.7. Reactions of Lithium Enolates 3-Li and 12-Li

As is apparent from literature precedent laid out in section 1.2.3 and 1.2.4, the cation of an enolate is one of the variables deemed most likely to influence the reactivity of an ambident anion. In particular, cation size is considered the principal determinant – a smaller cation such as Li^+ or Na^+ should result in more tightly associated ion pairs and form more complex ion aggregates. This notion is supported by the work of Harrelson

and co-workers, in which the thermodynamic properties of ionisation and ion-pairing constants were determined for a variety of enolate salts (shown in Chart 4-5 below).[15] In the example of enolates of acetylacetone (**52-K**, **52-Na** and **52-Li** below), the association constants of the enolate with its counter-cation were found to increase in the order $K^+ < Na^+ < Li^+$.

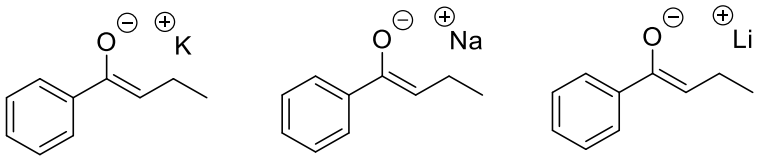
Chart 4-5. The enolates studied by Harrelson and co-workers.[15] The association constant of the enolates was found to increase when the size of the counter cation decreased (i.e., in the order $K^+ < Na^+ < Li^+$).



52-K **52-Na** **52-Li**

This phenomenon has also been demonstrated to affect the rate of reactions of enolates, as is the case in the work of Zook and Gumby where the rates of reaction of various metal enolates of butyrophenone (**53-Na**, **53-K** and **53-Li**) with halogenated electrophiles in Et_2O were determined.[16]

Chart 4-6. The rates of reaction of various metal enolates of butyrophenone (**53-Na**, **53-K** and **53-Li**) with halogenated electrophiles in Et_2O at 30°C were determined by Zook and Gumby.[16]



53-K **53-Na** **53-Li**

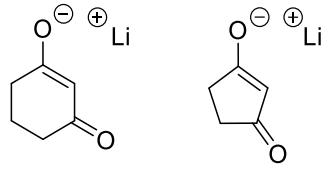
In that study, the rate of ethylation of the enolates of butyrophenone by EtrBr increased more than 6000-fold as the enolate counter-ion was varied from K^+ to Li^+. A similar effect was noted between the reactions of **53-Na** and **53-Li** in reactions with MeI, with the reaction of **53-Na** and MeI proceeding 60 times faster than the corresponding reaction of **53-Li**. The reaction of **53-K** with MeI occurred too quickly to be measured conveniently.

These forces serve to hinder O-alkylation processes for Li^+ enolates from occurring more than if K^+ or R_4N^+ were the counter-ion for a particular enolate species instead. There are numerous literature studies that state the use of tetrabutylammonium (Bu_4N^+) and tetramethylammonium (Me_4N^+) as counter-ions gives rise to less ionic salts and anions which are "freer".[17,18] The large, DBU-derived amidinium cation constituents of each of the enolate salts **3-D**, **12-D**, **17-D** and **22-D** may thus lend themselves to favouring O-alkylation, given their large steric bulk. As the HSAB treatment of ambident reactivity focuses so heavily on the nature of the leaving group of the electrophile in predicting the outcome of a reaction of an ambident nucleophile, the observation that the amidinium cation may aid O-alkylation processes is not factored in if rationalising the selectivities in reactions of ambident nucleophiles using the HSAB principle. Hence, there is no

context in which the overwhelming preference for O-alkylation using EtI and EtBr in the reactions described in the sections above can be accounted for using the HSAB principle.

A body of work by Jackman and co-workers (see section 1.2.3) specifically highlights the blocking effect of a lithium cation on the oxygen nucleophilic site of an enolate species, preventing it from taking part in a reaction with an electrophile in the solvents dioxolane and dimethoxyethane.[13,19–22] A pair of lithium enolates (**3-Li** and **12-Li**, see Chart 4-7 below) were synthesised in order to probe the reactivity of these cyclic enolates when the counter-ion is purported to hinder the process of O-alkylation.

Chart 4-7. The lithium enolates synthesised to assess the reactivity of enolates with a small, tightly bound counter-ion.

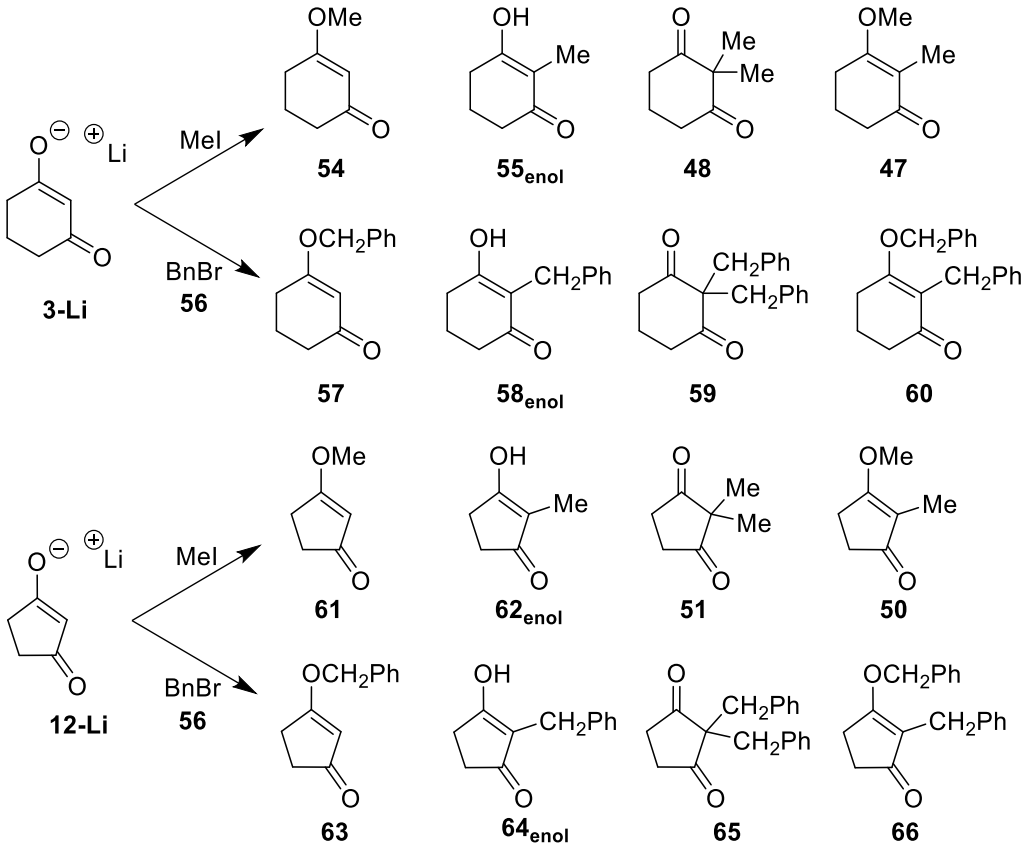


3-Li **12-Li**

The use of lithium enolates presented new benefits and drawbacks with regard to the possible scope of ambident reactions. Lithium enolates were not chosen as the initial substrate for study as it was believed they would not be soluble in many organic solvents, thus limiting the capacity to investigate solvent characteristics on the selectivity of reactions. This assumption was proven correct upon the synthesis and analysis of the lithium enolates **3-Li** and **12-Li**, as they were completely insoluble in $CDCl_3$ and THF. Enolates **3-Li** and **12-Li** were found to be soluble in $(CD_3)_2SO$, however, and thus O/C ratios could still be obtained by examining reactions in this solvent.

With no bulky organic cation (as was the case with **3-D** and **12-D**), the ^1H NMR spectra obtained from a reaction of **3-Li** or **12-Li** were less densely populated with signals. This allowed the scope of possible electrophiles to be extended past the sole use of ethylating agents. Methylations and benzylation reactions could be effectively analysed under these conditions, using MeI and benzyl bromide (**56**) as electrophiles respectively. The possible products of these reactions are shown below in Scheme 4-2.

Scheme 4-2. The possible products resulting from the methylation and benzylation of enolates **3-Li** and **12-Li** with MeI and benzyl bromide (BnBr, **56**) in $(CD_3)_2SO$. [a]

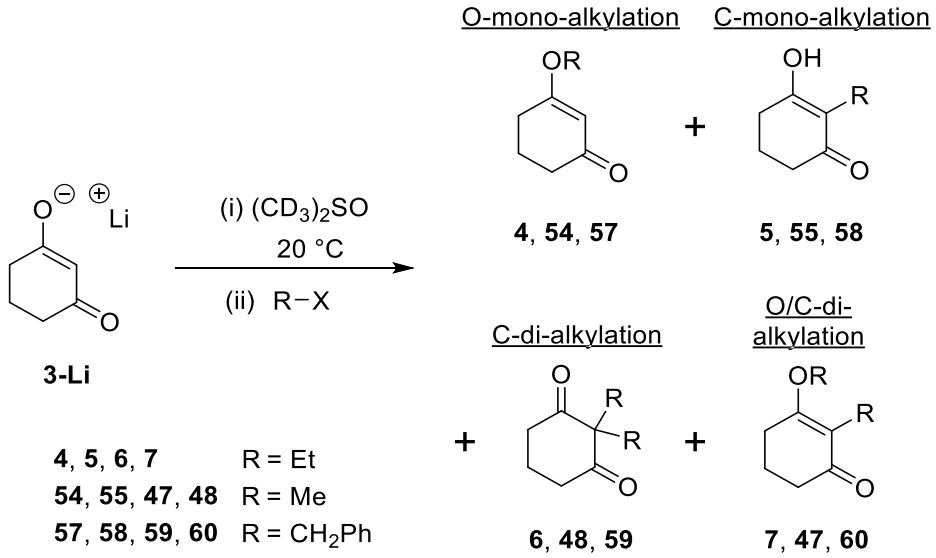


The O/C ratios derived from the reactions of enolate **3-Li** with a variety of electrophiles in $(CD_3)_2SO$ are shown in Table 4-8.

The reactions of both of the ethylating agents employed (EtI and EtBr) showed a reasonably high degree of O-selectivity (Table 4-7 entries (i) and (ii)). These results show reasonable analogy with the reactions of **3-D** with EtI and EtBr in the same solvent (see Table 4-2 entry (i) and entry (v)) – the reaction involving EtBr was slightly more O-selective than the reaction involving EtI. With these ethylating agents, there does not appear to be a notable difference in the observed O/C ratio between using enolate **3-D** or **3-Li** in $(CD_3)_2SO$. The reaction with MeI (Table 4-7 entry (iii)) demonstrated a preference for C-alkylation, with 75% of the products observed in the reaction mixture being derived from C-alkylation processes. When comparing to the data from Table 4-4 entry (i), where enolate **3-D** also underwent preferential C-alkylation in a reaction with CD_3I, it cannot be unambiguously determined that the Li^+ counter-ion is the principal driver of this preferential C-alkylation. The reaction of benzyl bromide (**56**) with **3-Li** (Table 4-7 entry (iv)) also displayed preferential C-alkylation.

[a] The mono-C methylation products (**55**$_{enol}$ and **58**$_{enol}$) and mono-C benzylation products (**62**$_{enol}$ and **64**$_{enol}$) are drawn in their enol form in Scheme 4-2 above. Keto-enol tautomerism occurs rapidly for these species, so it is likely that both forms are present in solution.

Table 4-7. O/C ratios of the products of the reactions of enolate **3-Li** with various electrophiles in $(CD_3)_2SO$ at 20 °C. [a]



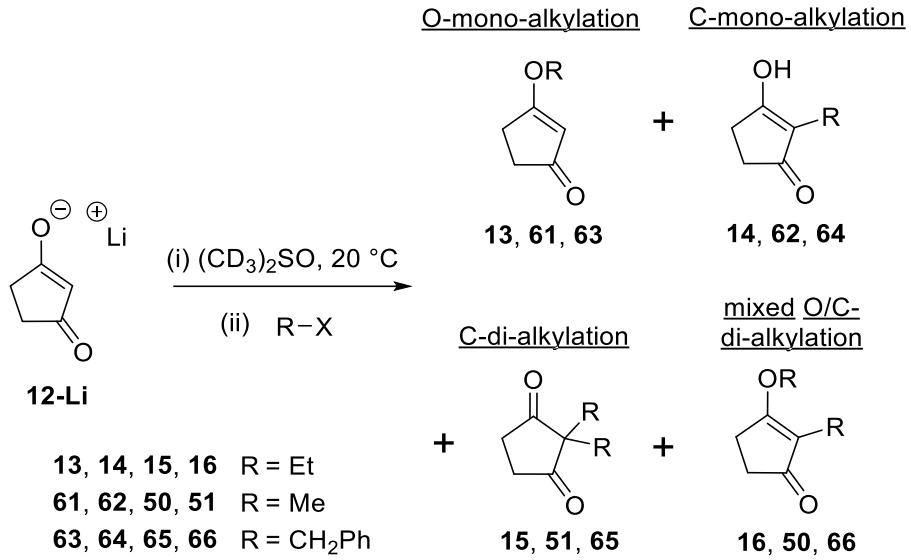
Entry	R–X	O-alkylation %	C-alkylation % [b]
(i)	EtI	71	29
(ii)	EtBr	86	14
(iii)	MeI	25	75
(iv)	BnBr	30	70

[a] The O/C ratio was determined by direct analysis of the reaction mixture by ^{1}H NMR spectroscopy.

[b] The percentage of C-alkylation is the combined proportion of C-mono-alkylation product, C-di-alkylation product and mixed O/C-di-alkylation product in the reaction mixture. In any given reaction, some products drawn here may not be formed. See chapter 5 section 5.3 for details on the individual reactions.

A further set of reactions were carried out under the same conditions, employing **12-Li** as the enolate substrate in place of **3-Li**. The O/C ratios measured from the ^{1}H NMR spectra of these reaction mixtures are shown in Table 4-8 below. Despite the presence of the lithium counter-cation, all of the electrophiles employed in reactions with **12-Li** displayed at least a moderate preference for O-alkylation (Table 4-8 entries (i) – (iv)), while the reaction with EtBr (entry (ii)) displayed an extremely high level of O-selectivity. MeI and BnBr (**56**), which undergo preferential C-alkylation in a comparable reaction with **3-Li**, undergo preferential O-alkylation when **12-Li** is the enolate employed (compare entries (iii) and (iv) in Table 4-8 with entries (iii) and (iv) in Table 4-8). Despite this crucial difference in the selectivity observed between the two enolates (**3-Li** and **12-Li**), a trend may be observed regarding the reactivity of the four electrophiles. In both Table 4-7 and Table 4-8, the level of O-alkylation observed increases in the order MeI < BnBr < EtI < EtBr.

Table 4-8. O/C ratios of the products of the reactions of enolate **12-Li** with various electrophiles in $(CD_3)_2SO$ at 20 °C. [a]



Entry	R–X	O-alkylation %	C-alkylation % [b]
(i)	EtI	75	25
(ii)	EtBr	97	3
(iii)	MeI	63	37
(iv)	BnBr	64	36

[a] The O/C ratio was determined by direct analysis of the reaction mixture by ^{1}H NMR spectroscopy.

[b] The percentage of C-alkylation is the combined proportion of C-mono-alkylation product, C-di-alkylation product and mixed O/C-di-alkylation product in the reaction mixture. In any given reaction, some products drawn here may not be formed. See chapter 5 section 5.3 for details on the individual reactions.

4.2.8. Discussion of Selectivity Observed in Reactions of Cyclic Enolates with Representative "Soft" Electrophiles

Neither EtI nor EtBr furnished preferential C-alkylation with any of the enolates in any of the solvents studied despite being typical "soft" reagents as defined by the conventions of the HSAB principle.[23–26] As outlined in section 1.2.4, in the context of the HSAB treatment of ambident reactivity, the nature of the leaving group of an electrophile is commonly considered to be the most important consideration when predicting the regioselectivity of reactions of that electrophile. In this context, it is therefore surprising that O-ethylation is the preferred process in every reaction of EtI or EtBr with each of the enolates employed in each of the chosen solvents in Tables 4-1, 4-2 and 4-3.

None of the provisions related to solvent discussed in section 1.2.2 or section 1.2.3 account adequately for the high degree of O-selectivity observed in reactions of ambident anions with EtI and EtBr as described in the sections above. When comparing the reactivity of the enolates in each of the solvents, it is observed that the solvent with the highest dielectric constant ($(CD_3)_2SO$) gives the lowest amount of O-alkylation out of any solvent in reactions with EtI and EtBr (compare Table 4-2 entries (i) – (viii) to the

corresponding reactions in Table 4-1 (entries (i) – (viii))). This is unexpected when literature precedent is considered – the higher dielectric constant of $(CD_3)_2SO$ compared to $CDCl_3$ would be expected to facilitate the O-alkylation process due to the ability of $(CD_3)_2SO$ to shield the departing anion from the attractive forces of the counter-cation of the enolate.[7] When EtI was used as an electrophile (Table 4-1 entries (i) – (iv) and Table 4-2 entries (i) – (iv)), the reactions that took place in $(CD_3)_2SO$ displayed selectivity for O-alkylation products lower than or equal to the observed O-selectivity in the corresponding reactions in $CDCl_3$. When EtBr is used as the electrophile (Table 4-1 entries (v) – (viii) and Table 4-2 entries (v) – (viii)), the same pattern is observed. The use of THF as a solvent (see Table 4-3) resulted in over 90 % O-alkylation by EtI in all cases studied. Compiling of all reactions in Tables 4-1 to 4-3, it is apparent that even with "soft" electrophiles such as EtI and EtBr, the enolates **3-D**, **12-D**, **17-D** and **22-D** heavily favour O-ethylation processes in a multitude of reaction conditions – an outcome that is opposite to what would be expected if the HSAB principle were dictating the selectivity in such reactions.

In reactions of CD_3I with enolates **3-D**, **12-D**, **17-D** and **22-D** in CH_2Cl_2, preferential C-methylation was observed in three of the four reactions examined (see Table 4-4, entries (i) – (iv)). A modest preference for C-methylation was also observed in the reaction of **49-D** with MeI in $CDCl_3$ (Table 4-6, entry (ii)), while C-methylation of **46-D** with MeI under the same conditions was strongly favoured (Table 4-6, entry (i)).

Changing the reaction solvent to THF (Table 4-5) results in preferential O-alkylation of each enolate in reactions with CD_3I. This is a remarkable outcome in the context of the applicability of the HSAB principle in rationalising O/C selectivity in reactions of enolates, as predominant methylation of the "hard" O-site of the enolate occurs even with the archetypal "soft" electrophile, CD_3I (a proxy for CH_3I). Observation of predominant O-methylation of **12-D** in CH_2Cl_2 (Table 4-4, entry (ii)) and of a modest preference for C-methylation of enolates **3-D**, **7-D** and **22-D** in CH_2Cl_2 (see Table 4-4 entries (i), (iii) and (iv)) and of enolate **49-D** in $CDCl_3$ (Table 4-6, entry (ii)) represented an unconvincing adherence to the expectations laid out in the HSAB treatment of selectivity in reactions of ambident nucleophiles, with only the reaction of **46-D** with MeI in $CDCl_3$ exhibiting the anticipated high level of C-selectivity (Table 4-6, entry (i)). However, the switch to predominant O-selectivity that results when the reactions take place in THF fundamentally undermines the applications of the principle to the reactions of enolates in general. Pearson and Songstad did note the sensitivity of nucleophilic reactivity parameters to the solvent, though not in the fashion that is demonstrated here.[25] They state that the reactivity order for halide anions may be inverted upon switching from a polar protic solvent, such as methanol, to a polar aprotic solvent, such as DMF. Given the similar dielectric constants of the aprotic solvents CH_2Cl_2 and THF,[27] this does not adequately explain the inversion in O- vs C-alkylation selectivity observed between Tables 4-4 and 4-5.

The use of lithium as a counter-ion for certain cyclic enolates (**3-Li** and **12-Li**, see Chart 4-7) did not result in a systematic "blocking" effect that hindered the process of O-

alkylation, which may have been expected based on the ion association and aggregation considerations discussed at the beginning of section 4.2.7. Of the eight reactions carried out involving "soft" electrophiles and the Li^+ enolates (see Tables 4-7 and 4-8), only two (see Table 4-7 entries (iii) and (iv)) resulted in preferential C-alkylation of the enolate. A possible explanation for this observation is the choice of solvent for the reaction – the formation of lithium ion-pair aggregates should be most prevalent in solvents with a low dielectric constant. With a dielectric constant of approximately 47 at 20 °C,[27] the powerful cation solvating ability of $(CD_3)_2SO$ could minimise the "blocking" capability of the lithium cation.[28] However, instances where the use of smaller cations as counter-ions can effectively depress the O/C ratio of a reaction has been previously observed in DMF[29] and DMSO.[30] This indicates that the use of a lithium counter-ion in the reactions outlined in Table 4-7 and Table 4-8 may still influence the O/C ratio to a considerable degree, despite the powerful cation solvating ability of DMSO. Unfortunately, the lithium enolates **3-Li** and **12-Li** were found not to be soluble in any of the less polar solvents trialled ($CDCl_3$, THF, CH_3CN), which prevented a direct comparison being made between solvents with low and high dielectric constant.

Although it proved not to be possible to test the effect of the lithium counter-ion on O/C ratios in weakly polar or non-polar solvents, important observations can be made regarding the applicability of HSAB theory to the reactions in question using the data described in Tables 4-7 and 4-8. Most notably, it is revealed that the same electrophile can demonstrate a preference for O-alkylation in a reaction with one ambident nucleophile, while undergoing preferential C-alkylation with another very similar ambident nucleophile. This inconsistency may be noted through the comparison of entries (iii) and (iv) in Table 4-7 with entries (iii) and (iv) in Table 4-8. The use of MeI and BnBr (**56**) results in predominant C-alkylation when **3-Li** is the nucleophile, and predominant O-alkylation when **12-Li** is employed. This result calls into question the "symbiotic effect" upon which the HSAB treatment of ambident reactivity is founded – that a "soft" electrophile will preferentially react with the "soft" site of an ambident nucleophile, and a "hard" electrophile will preferentially react at the "hard" site. The notion that a "soft" electrophile such as MeI or BnBr (**56**) could react at the carbon nucleophilic site of one enolate and at the oxygen nucleophilic site of another, very similar enolate under the same reaction conditions (i.e., that the outcome depends on the exact structure of the enolate) undermines the applicability of the HSAB principle in rationalising selectivities in reactions of enolates as ambident nucleophiles.

The predictive capabilities of HSAB theory as it applied to ambident reactivity are cast even further into doubt when the reactions of ethylating agents shown in Table 4-7 are contrasted with the reactions of MeI and BnBr (**56**). The reactions of EtI and EtBr with 1,3-cyclohexanedione-derived lithium enolate **3-Li** (Table 4-7 entries (i) and (ii)) are moderately O-selective, while the reactions of MeI and BnBr (**56**) with **3-Li** (Table 4-7 entries (iii) and (iv)) are moderately C-selective. Given that EtI and MeI (and EtBr and BnBr (**56**)) share the same "soft" counter-cation (iodide or bromide), there is inadequate explanation as to why each alkyl halide would tend towards separate modes of reaction. The iodide cation is the qualitative factor which decides the "softness" of the electrophile

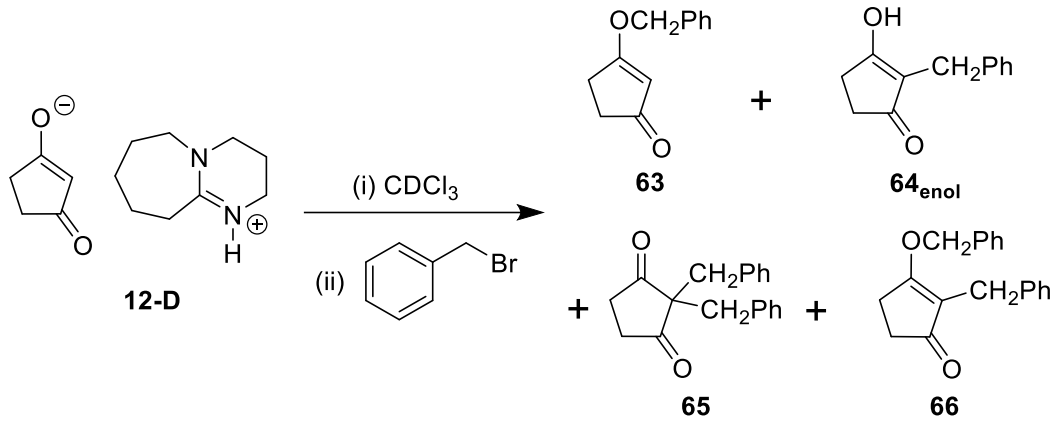
– the alkyl group should merely modulate the reactivity. As explained in section 1.2.4., the size (and consequently, "softness") of an alkyl group of an electrophile may influence the selectivity observed in a reaction with an ambident nucleophile. It is noted in several literature works that in reactions of enolate anions with alkyl halides, the O/C ratio tends to increase in line with the size of the alkyl group of the alkylating agent (i.e., in the order Me < Et < *i*-Pr < *sec*-Bu).[12,31,32] This effect was proposed to be steric in origin – the oxygen atom of an enolate may be approached from almost any direction, while the carbon atom can only be approached perpendicular to the plane of its three σ bonds. Larger (and in particular, highly-branched), alkylating agents are crowded near the site of the leaving group, purportedly resulting in a preference to react at the oxygen atom.[32] Although those expectations are indeed realised when comparing the reactions of MeI and EtI with **3-Li** and **12-Li** (i.e., there is indeed more O-alkylation when EtI is used instead of MeI, see Table 4-7 entries (i) and (iii) and Table 4-8 entries (i) and (iii)), there is no precedent to suggest that one should expect a complete swap in O vs C selectivity upon changing from a methyl halide to an ethyl halide (as occurs in Table 4-7 entries (i) and (iii)).

As MeI is a quintessential "soft" reagent in the context of organic synthesis, it is considered an ideal reagent to use when trying to effect the C-alkylation of enolates such as **3-Li** and **12-Li**. The inability of MeI to react preferentially at the carbon atom of **12-Li** (see Table 4-8 entry (iii)) leaves few remaining options to a chemist using HSAB theory to direct reagent choice in these reaction conditions if C-alkylation is desired. The failure of the HSAB theory in this case could be attributed to particular electronic attributes of **12-Li** or, potentially, of all enolates derived from 1,3-cyclopentanedione (**9**).

4.3. Reactions of Tetramethylammonium Enolates with Substituted Benzyl Bromides

To further investigate the reactivity of cyclic enolates with "soft" electrophiles, additional enolates of the 1,3-diketones discussed above (i.e., **1** and **9**) were prepared for use in reactions with a series of benzyl bromides bearing electron withdrawing or donating substituents at the *para*-position. Performing these reactions under the same conditions as described in section 4.2 allows for direct measurement and determination of the O vs C ratios for each electrophile. As discussed in sections 4.2.1 and 4.2.3, the use of DBU (**2**) as the base in enolate generation created difficulties in the analysis of NMR spectra due to the large number of ^{1}H NMR signals created by the diazabicyclo[5.4.0]undecanium ion. Benzylation reactions of enolates **3-D** and **12-D** using BnBr (**56**) (see Scheme 4-3 below) were attempted in $CDCl_3$. However, the placement of the ^{1}H NMR signals derived from DBU (**2**) meant that an O/C ratio could not be measured. An example of one such experiment may be seen in section 5.9.

Scheme 4-3. The reaction of enolate **12-D** with BnBr (**56**) in $CDCl_3$ did produce products **63** – **66**, however the signals of the C-alkylation products **64$_{enol}$/64$_{keto}$**, **65** and **66** were fully or partially obscured by the signals derived from DBU (**2**) in the ^{1}H NMR spectrum. As a result, no O/C ratio could be extracted from the information given in the ^{1}H NMR spectrum. The same was true when using the enolate derived from 1,3-cyclohexanedione, **3-D**.

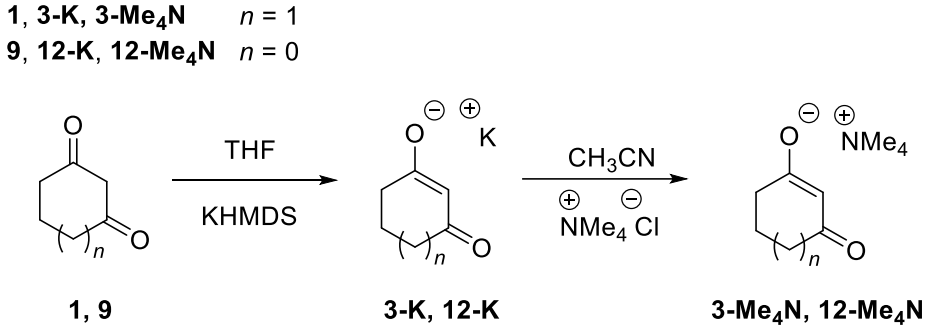


In order to circumvent this issue, new enolates derived from 1,3-cyclohexanedione (**1**) and 1,3-cyclopentanedione (**9**) were synthesised and isolated. The counter-ion chosen for the enolates in this study was the tetramethylammonium cation (Me_4N^+). Salts of this cation are expected to be reasonably soluble in a number of organic solvents, and contribute only one signal to a ^{1}H NMR spectrum of a reaction mixture. The procedure by which the tetramethylammonium enolates **3-Me$_4$N** and **12-Me$_4$N** were synthesised is outlined in Scheme 4-4 below.

Using the tetramethylammonium enolates **3-Me$_4$N** and **12-Me$_4$N** enabled an unobstructed view of critical portions of the ^{1}H NMR spectra obtained from benzylation reactions of these enolates. This enabled unambiguous determination of O/C ratios for reactions of

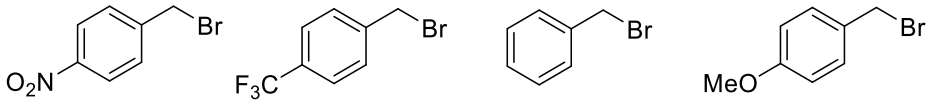
the enolates of interest with benzyl bromides (which are also considered to be soft electrophiles).[25,33] The substituted benzyl bromides chosen to probe the reactivity of **3-Me$_4$N** and **12-Me$_4$N** are shown below in Chart 4-8.

Scheme 4-4. Enolates **3-Me$_4$N** and **12-Me$_4$N** were synthesised by the initial formation of the potassium enolates of **1** and **9** using KHMDS, followed by a salt metathesis reaction using [NMe$_4$]Cl in CH_3CN.



4-Nitrobenzyl bromide (**67**) and 4-(trifluoromethyl)benzyl bromide (**68**) were chosen as they each contain a *para*-electron-withdrawing group, and 4-methoxybenzyl bromide (**69**) was included to examine the effect of an electron-withdrawing substituent. Benzyl bromide (**56**) was included to act as a reference to which the reactions of these substituted benzyl bromides with **3-Me$_4$N** and **12-Me$_4$N** could be compared.

Chart 4-8. The benzyl bromides used in reactions with **3-Me$_4$N** and **12-Me$_4$N**.



67 **68** **56** **69**

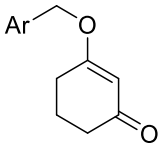
In section 4.2, in which methylation and ethylation reactions are primarily considered, the vast majority of the products of those reactions are identified and characterised in the literature, allowing parallel assignments to be made in the ^{1}H NMR spectra of the reaction mixtures in those sections.

As many of the products of these enolate benzylation reactions had not previously been reported in the literature, authentic samples of these compounds were synthesised and isolated (by methods described in Chapter 5, section 5.8) to aid with signal assignments in the ^{1}H NMR spectra of enolate reaction mixtures similar to the one illustrated in Scheme 4-3 above.

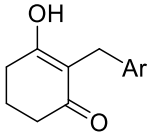
Shown in Chart 4-9 are all of the possible products of reactions of **3-Me$_4$N** and **12-Me$_4$N** with the substituted benzyl bromides (**67**, **68** and **69**, see Chart 4-8). Of the 24 possible products of these reactions, 16 were isolated in a pure form and fully characterised. Of the 8 products which could not be isolated, 3 were found in the literature (compounds **71**, **87** and **91**).[34,35] Where compounds could not be isolated and no literature data existed, ^{1}H

NMR assignments were possible through a combination of ^{13}C and 2D NMR spectroscopic techniques, as well as by comparison to analogous compounds for which characterisation data was available (see section 5.9 for details).

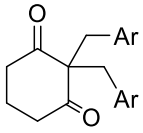
Chart 4-9. The possible products resulting from the benzylation of enolates **3-D** and **12-D** with the substituted benzyl bromides **67**, **68** and **69**. [a] The 8 compounds coloured in red could not be isolated and characterised.



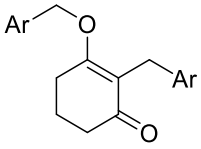
70 Ar = *p*(NO$_2$)C$_6$H$_4$
74 Ar = *p*(CF$_3$)C$_6$H$_4$
78 Ar = *p*(MeO)C$_6$H$_4$



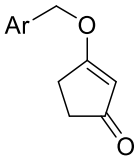
71 Ar = *p*(NO$_2$)C$_6$H$_4$
75 Ar = *p*(CF$_3$)C$_6$H$_4$
79 Ar = *p*(MeO)C$_6$H$_4$



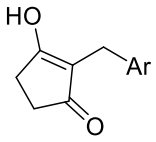
72 Ar = *p*(NO$_2$)C$_6$H$_4$
76 Ar = *p*(CF$_3$)C$_6$H$_4$
80 Ar = *p*(MeO)C$_6$H$_4$



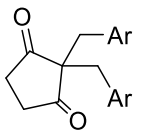
73 Ar = *p*(NO$_2$)C$_6$H$_4$
77 Ar = *p*(CF$_3$)C$_6$H$_4$
81 Ar = *p*(MeO)C$_6$H$_4$



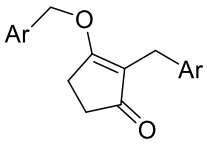
82 Ar = *p*(NO$_2$)C$_6$H$_4$
86 Ar = *p*(CF$_3$)C$_6$H$_4$
90 Ar = *p*(MeO)C$_6$H$_4$



83 Ar = *p*(NO$_2$)C$_6$H$_4$
87 Ar = *p*(CF$_3$)C$_6$H$_4$
91 Ar = *p*(MeO)C$_6$H$_4$



84 Ar = *p*(NO$_2$)C$_6$H$_4$
88 Ar = *p*(CF$_3$)C$_6$H$_4$
92 Ar = *p*(MeO)C$_6$H$_4$



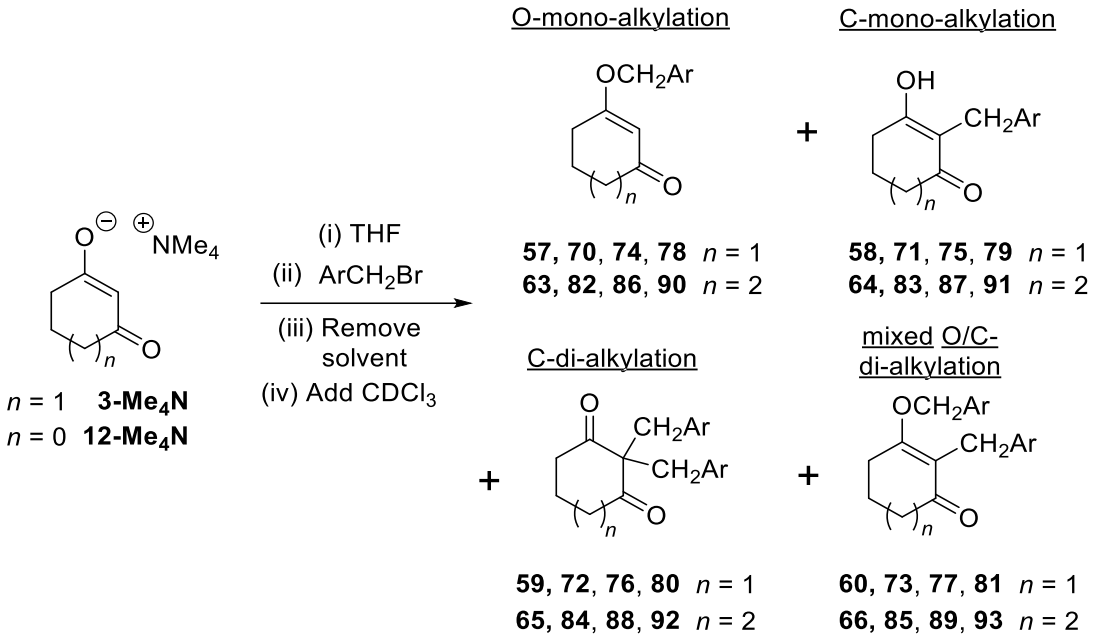
85 Ar = *p*(NO$_2$)C$_6$H$_4$
89 Ar = *p*(CF$_3$)C$_6$H$_4$
93 Ar = *p*(MeO)C$_6$H$_4$

4.3.1. Reactions of 3-Me$_4$N and 12-Me$_4$N with Substituted Benzyl Bromides in THF

With the necessary preparations and ^1H NMR data in place, O/C ratios for reactions of **3-Me$_4$N** and **12-Me$_4$N** with benzyl bromide (**56**) and the substituted benzyl bromides (**67**, **68** and **69**) could be measured. As in section 4.2.3, the reactions were carried out in dry THF and upon conclusion of the reaction, the THF was removed *in vacuo*. The O/C ratios extracted from the ^1H NMR spectra of the crude reaction mixtures in $CDCl_3$ are shown in Table 4-9.

[a] The mono-C benzylation products (**71**, **75**, **79**, **83**, **87** and **91**) are drawn in their enol form in Chart 4-9 above. Keto forms of these products are also possible.

Table 4-9. O/C ratios of the products of the reactions of enolates **3-Me$_4$N** and **12-Me$_4$N** with benzyl bromide (**56**) and the substituted benzyl bromides (**67**, **68** and **69**) in THF. At the conclusion of the reaction, the THF was removed *in vacuo* and the crude reaction products were re-dissolved in $CDCl_3$ for ^{1}H NMR analysis. [a]



Entry	Enolate	Ar	O-alkylation %	C-alkylation % [b]
(i)	**3-Me$_4$N**	*p*-(NO_2)C_6H_4	71	29
(ii)		*p*-(CF_3)C_6H_4	63	37
(iii)		C_6H_5	51	49
(iv)		*p*-(CH_3O)C_6H_4	43	57
(v)	**12-Me$_4$N**	*p*-(NO_2)C_6H_4	80	20
(vi)		*p*-(CF_3)C_6H_4	84	16
(vii)		C_6H_5	61	39
(viii)		*p*-(CH_3O)C_6H_4	50	50

[a] The O/C ratio was determined by direct analysis of the crude reaction mixture by ^{2}H NMR spectroscopy in CH_2Cl_2.

[b] The % of C-alkylation is the combined proportion of C-mono-alkylation product, C-di-alkylation product and mixed O/C-di-alkylation product in the reaction mixture. In any given reaction, some products drawn here may not be formed. See chapter 5 section 5.9 for details on the individual reactions.

The O/C ratios obtained from the set of reactions of **3-Me$_4$N** (Table 4-9, entries (i) – (iv)) and **12-Me$_4$N** (Table 4-9, entries (v) – (viii)) show a reasonably high level of O-alkylation in all cases. Only one reaction in Table 4-9 shows a preference for C-alkylation (the reaction of **3-Me$_4$N** with 4-methoxybenzyl bromide (Table 4-9 entry (iv)). In both sets of reactions, the benzyl bromides which contained an electron withdrawing group gave the largest amounts of O-alkylation products (see Table 4-9, entries (i), (ii), (v) and (vi). In both cases where 4-methoxybenzyl bromide is employed (Table 4-9, entries (iv) and

(viii)), the lowest amount of O-alkylation for that enolate is recorded. It has been previously mentioned (in section 1.2.1) that the amount of S_N1 character in the transition of a reaction may lead to a greater preference for bond formation with the atom of greater electronegativity in the reactions of ambident nucleophiles (i.e., *Kornblum's rule*).[36] The possibility exists when effecting reactions of benzyl bromides that an S_N1 reaction may be in operation instead of or alongside an S_N2 mechanism. However, under the conditions employed in this work (20 °C, $CDCl_3$), significant precedent exists demonstrating that nucleophilic substitutions of benzyl bromides do occur exclusively through S_N2 mechanisms (see descriptions below).

The measured rate of reaction between potassium *p*-nitrobenzoate and benzyl bromide (**56**) in $CHCl_3$ has been reported to be dependent on the concentration of the nucleophile, indicating that in $CHCl_3$ the S_N1 reaction pathway is insignificant.[37] In reactions of substituted pyridines with 4-methoxybenzyl bromide (**69**) in CH_3CN, a similar effect has been observed – as the concentration of the nucleophile increases, the rate of reaction also increases.[38] If an S_N1 process contributed meaningfully to the completion of these reactions, the rate of the reactions would be independent of the concentration of the nucleophile. Another study by Tsuno and co-workers specifically investigates concurrent S_N1 and S_N2 processes in reactions of pyridines with various benzyl bromides in CH_3CN.[39] In the case of benzyl bromides with substituents that are less electron-donating than 4-methylbenzyl bromide, the reactions were first order with regard to pyridine concentration. However, with strongly electron donating substituents (e.g., 4-methoxybenzyl bromide (**69**)), these authors noted varying levels of apparent competition by S_N1 processes. By applying equation 4.1 shown below, the authors investigated the influences of independent S_N1 and S_N2 processes on the rate of reaction. In the case of a reaction of pyridine with 4-methoxybenzyl bromide (**69**) in CH_3CN, a negligible contribution of the S_N1 process to the overall rate constant for the reaction (> 4 %) was measured.

$$k_{\text{obs}} = k_1 + k_2[\text{Nu}] \qquad (4.1)$$

Furthermore, of the benzyl bromides employed in Table 4-9, the most likely reagent to undergo carbocation formation and hence an S_N1 reaction is benzyl bromide **69** (4-methoxybenzyl bromide). If competition of S_N1 mechanisms and S_N2 mechanisms were important in some or all of the reactions shown in Table 4-9, then the reactions of this species should exhibit the highest O-selectivity as they are most likely to involve carbocation formation. In fact, as may be seen in Table 4-9 entries (iv) and (viii), these reactions exhibit the lowest O-selectivity.

Taken together with the preferential O-alkylation reactions of the cyclic enolates discussed above in sections 4.2 by various alkyl halides, this set of observations fundamentally undermines the applicability of the HSAB principle in rationalising the outcomes of reactions of enolates in general. The case of these cyclic enolates may be considered an expansion of the plethora of literature examples demonstrating the

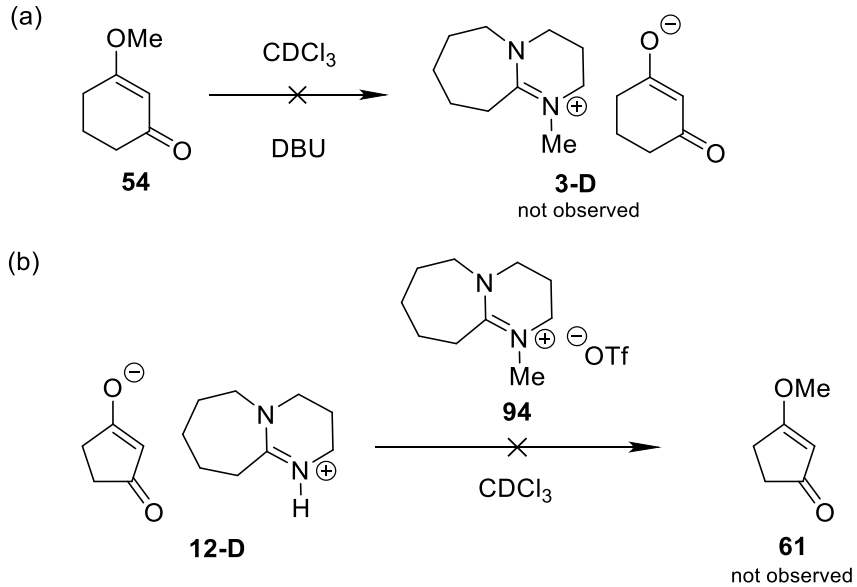
inadequate predictive capabilities of the HSAB treatment of ambident reactivity as outlined in section 1.3. If the HSAB treatment of ambident reactivity cannot account for the reactivity observed in reactions of these cyclic enolates, can it truly be considered capable of predicting the outcome of the reaction of any enolate? As the results in this section undermine the applicability of the HSAB principle with regards to ambident reactivity, a new method of rationalising the selectivity of reactions of ambident nucleophiles is needed. A novel model which attempts to rationalise the behaviour of ambident reactants is described in Chapter 6 below.

4.4. Reactions to Establish the Reversibility or Irreversibility of Alkylations of Cyclic Enolates

An important consideration that must be made to ensure that the O/C ratios measured by NMR spectroscopy in section 4.2 are reflective of the kinetic preferences for the processes of O-alkylation or C-alkylation in a given reaction is that the reactions occur under kinetic control. The observation that the O/C ratios remain consistent at differing levels of conversion (see section 4.2.1) and that they do not change even after a considerable amount of time has passed since the end of the reaction indicate that the O/C ratio is reflective of the kinetic ratio of products. However, in order to unequivocally establish whether the reactions are occurring under kinetic control, the irreversibility of O- and C-alkylation product formation must be demonstrated. To achieve this, a series of experiments were devised which probe whether or not some of the alkylation processes found in reactions in section 4.2 are reversible.

In order to perform the experiments, authentic samples of O-mono-alkylation products discussed in section 4.2 were independently synthesised as shown in section 5.7 of Chapter 5.

Scheme 4-5. (a) A control experiment to probe the reversibility of formation of 3-methoxycyclohex-2-en-1-one (**54**) when DBU (**2**) is present in $CDCl_3$. **(b)** A crossover experiment to investigate the potential for a methylated DBU-derived salt, (**94**), to act as an electrophile in a reaction mixture where **12-D** is present.

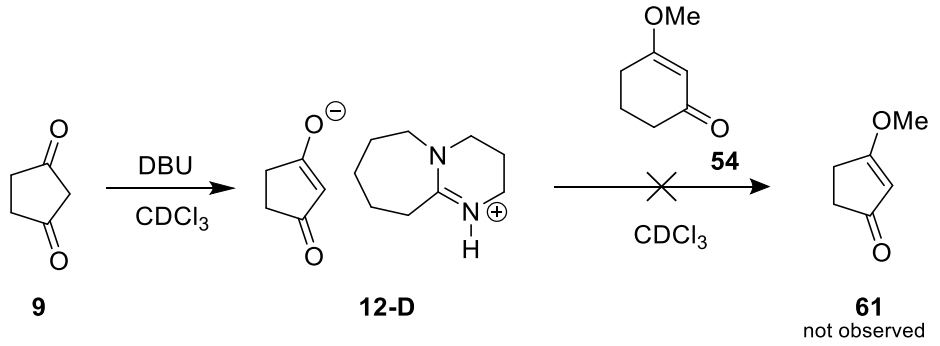


In the experiment represented in Scheme 4-5(a), the effect of the presence of DBU (**2**) on the reversibility of formation of 3-methoxycyclohex-2-en-1-one (**54**) in $CDCl_3$ was investigated. Although DBU (**2**) is considered a non-nucleophilic base, it has been observed in this study that in the presence of an electrophile such as CD_3I or MeOTf, methylation of the basic nitrogen atom is possible. However, in this specific experiment, no signals were observed in the ^1H NMR spectrum of the reaction mixture that were consistent with formation of amidinium enolate salt (**3-D**) – only ^1H NMR signals of the

starting materials were observed. In the experiment represented in Scheme 4-5(b), the potential for the *N*-methyl amidinium salt (**94**) to act as an electrophile to methylate an enolate (**12-D** in this instance) was investigated. DBU (**2**) and MeOTf were first reacted with each other to produce amidinium salt (**94**), and then a solution of the enolate **12-D** in $CDCl_3$ was introduced to the mixture. No signals were observed that indicated **61**, or any of the expected methylation products which could arise from enolate **12-D**, were formed. This experiment reaffirms that the high O/C ratios observed in the alkylation reactions in section 4.2 were solely due to the reaction between the alkyl halide and the enolate in question, as any alkylated DBU species which may potentially form do not appear to be capable of transferring alkyl groups to enolate species in solution.

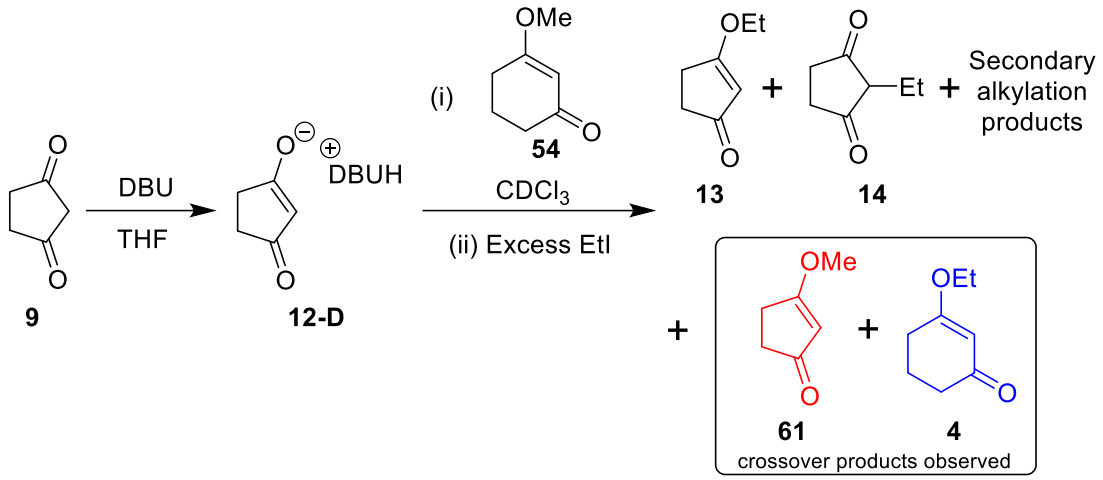
The experiment illustrated in Scheme 4-6 was devised to establish whether or not 3-methoxycyclohex-2-en-1-one (**54**) may act as an alkylating agent in similar conditions to those that would be present in when this product would form in a reaction mixture. In these mixtures, reaction products (such as **54**) would be formed whilst reactive enolate species (such as **12-D**) would still be present. This situation represents a possible scenario in which the product (**54**) may alkylate another nucleophile, thus giving rise to two alkylating species in the solution with differing selectivities. In this instance, no signals were observed in the ^{1}H NMR spectra which indicated that **61** or any of the other possible methylation products of **12-D** had formed.

Scheme 4-6. A control experiment to probe the ability of 3-methoxycyclohex-2-en-1-one (**54**) to act as an alkylating agent when another similar enolate (**12-D**) is present in $CDCl_3$.



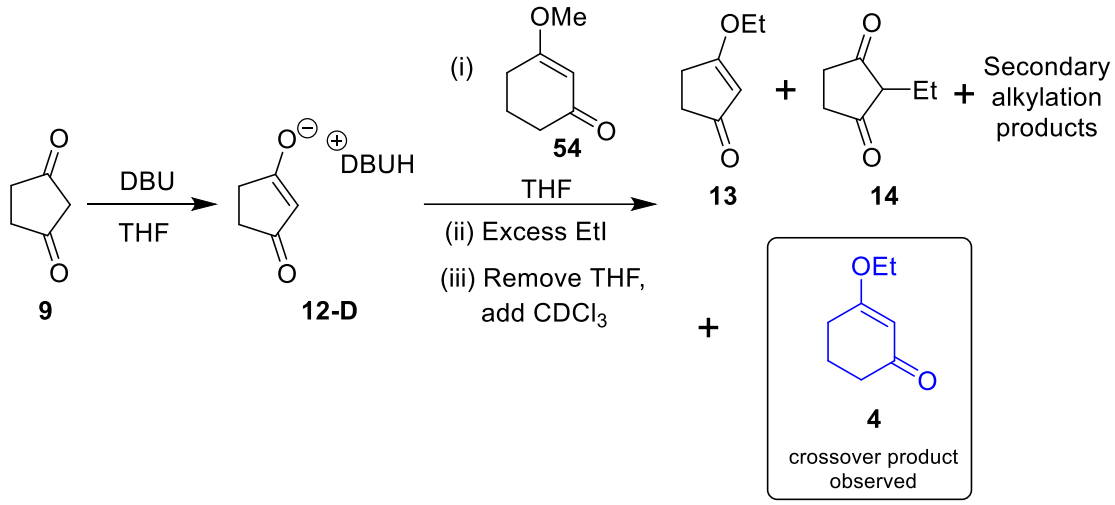
The reaction in Scheme 4-7 below is similar to the one presented in Scheme 4-6, except for the fact that excess EtI was added to the reaction mixture after the enolate (**12-D**) and enone (**54**) were mixed together in the solution. With this addition, the ^{1}H NMR spectrum of the resulting reaction mixture showed not only the signals of the expected O-mono-ethylation product resulting from the ethylation of **12-D**, but also signals indicating the presence of small amounts of the crossover products **61** and **4**. The presence of 3-ethoxycyclohex-2-en-1-one (**4**) in the reaction mixture proved that the formation of **54** must be reversible (at least to a small extent) under these conditions, otherwise the ethylated derivative could not form. Additionally, the signals of 3-methoxycyclopent-2-en-1-one (**61**) indicate that the enolate **12-D** has "intercepted" a reactive methyl species (potentially MeI) after compound **54** decomposed.

Scheme 4-7. A crossover experiment to probe the reversibility of formation of 3-methoxycyclohex-2-en-1-one (**54**) when another enolate (**12-D**) and EtI are present in $CDCl_3$. In this experiment, signals of crossover products, which indicated that the formation of the enone (**54**) was reversible, were observed in the ^1H NMR spectra of the reaction mixture.



In order to verify the identity of the two purported crossover products observed in the ^1H NMR spectrum of the reaction mixture, authentic samples of the compounds in question (**61** and **4**) were added to the reaction mixture and spectra were recorded before and after the addition of these products. When the signals of the crossover products grew in size upon the addition of **61** or **4**, their identities were confirmed.

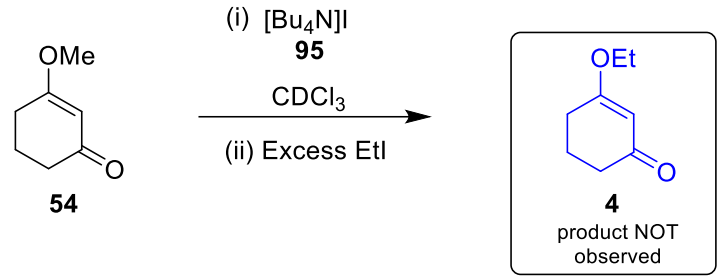
Scheme 4-8. A crossover experiment to probe the reversibility of formation of 3-methoxycyclohex-2-en-1-one (**54**) when another enolate (**12-D**) and EtI are present in THF. In this experiment, signals of a crossover product indicated that the formation of the enone (**54**) was at least partially reversible under these reaction conditions.



A similar experiment to the one shown above in Scheme 4-7 was performed, with the difference being that THF was used as the solvent instead of $CDCl_3$ (see Scheme 4-8). One of the crossover products, **4**, was observed to have formed in this reaction, although no ^1H NMR signals consistent with the formation of **61** were observed. The experiments

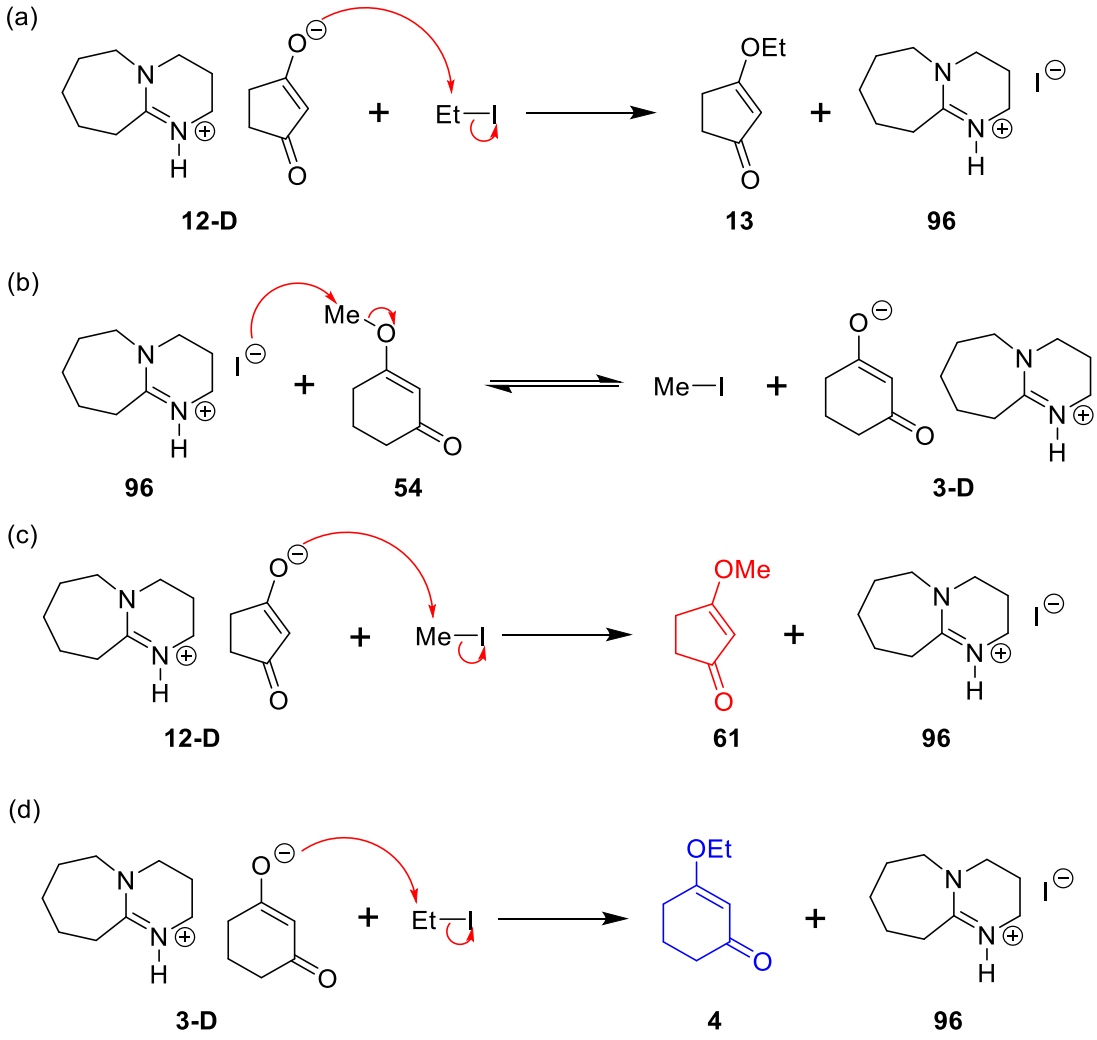
shown in Scheme 4-7 and Scheme 4-8 demonstrate that under certain conditions, the formation of 3-methoxycyclohex-2-en-1-one (**54**) appears to be reversible. It is unlikely that the source of this reversible reaction is a nucleophilic attack by an enolate on the methoxy group of the product – were that the case, relevant products (such as **61** in Scheme 4-7) would be observed in reactions of the type shown in Scheme 4-6. The addition of the electrophile, EtI, seems to be the key element which enables the reversible formation of 3-methoxycyclohex-2-en-1-one (**54**).

Scheme 4-9. A crossover experiment to probe the reversibility of formation of 3-methoxycyclohex-2-en-1-one (**54**) when another enolate (**3-D**), [Bu_4N]I (**95**) and EtI are present in THF.



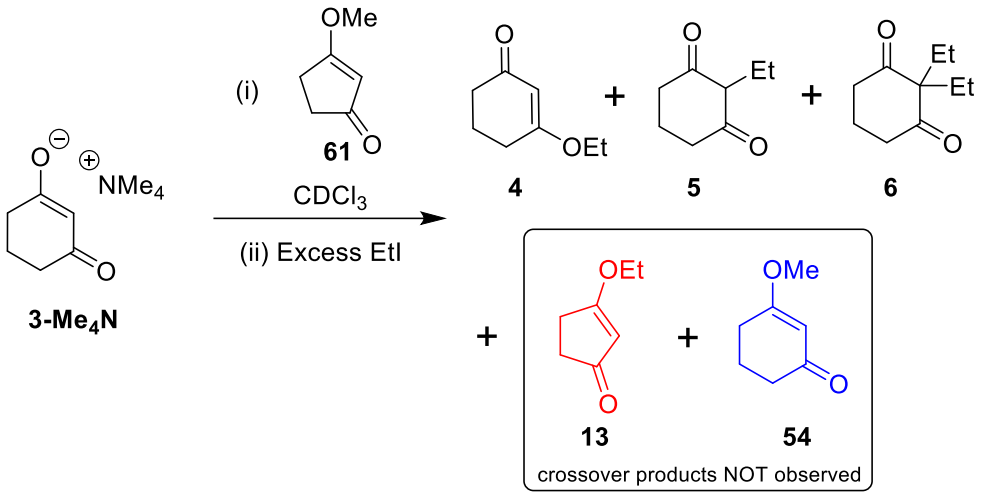
To further analyse the phenomena which led to the formation of the crossover products seen in Schemes 4-7 and 4-8 above, a control experiment was devised in which an iodide salt ([Bu_4N]I, (**95**), see Scheme 4-9) was added to a mixture of an enone and alkylating agent. In this experiment, the addition of the iodide salt did not appear to be capable of inducing the reversible formation of **54**, thereby preventing the formation of any ethylation products such as **4** by reaction of the enolate with EtI. The ammonium iodide salt used in this experiment ([Bu_4N]I, (**95**)) is not the same as the iodide salt which would occur in a reaction mixture such as that seen in Scheme 4-7 (i.e., the iodide salt derived from DBU), and this may be the key distinction which enables the formation of crossover products that was seen in that experiment. Using a combination of the findings of the control experiments discussed in this section, an estimation may be made which enables the process by which crossover products are formed in the experiments illustrated in Schemes 4-7 and 4-8. An illustrated example of this hypothetical process is shown below in Scheme 4-10. Upon the reaction of an enolate with the electrophile (EtI), an amidinium iodide salt (**96**) is generated (see Scheme 4-10(a)). It is possible that the iodide anion of salt **96** engages in nucleophilic attack on the methyl group of enone (**54**), resulting in the formation of 1,3-cyclohexanedione-derived enolate **3-D** and MeI (see Scheme 4-10(b)). The newly generated MeI may then react with the initially added enolate (**12-D**) to give methylated crossover product **61** (see Scheme 4-10(c)), and the newly generated enolate (**3-D**) may react with EtI to give the ethylated crossover product (**4**) (see Scheme 4-10(d)).

Scheme 4-10. An outline of a potential pathway which leads to the formation of crossover products. (a) Iodide salts are formed in tandem with ethylation products in the reaction mixture. (b) The formation of enone **54** may be reversible in the presence of iodide salts, leading to the formation of the enolate (**3-D**) and a reactive methyl species, such as MeI. (c) The newly formed methylating agent may react with enolate **12-D**, giving rise to the "crossover product" **61**. (d) The newly formed enolate (**3-D**) may react with the EtI which is present in the reaction mixture, giving rise to the crossover product **4**.



To establish whether or not this reversibility of formation could be seen with other enone products, the reaction depicted in Scheme 4-11 was carried out. Here, 3-methoxycyclopent-2-en-1-one (**61**) was the compound tested in a reaction with the tetramethylammonium enolate of 1,3-cyclohexanedione (**3-Me$_4$N**). The details of the synthesis of this particular enolate may be found in Chapter 5, section 5.2 below. In contrast to the experiments shown in Scheme 4-7 and 4-8, no crossover products were observed in this reaction when excess EtI was included in the reaction mixture. Only signals of the expected products of the ethylation of **3-Me$_4$N** (i.e., **4**, **5** and **6**) were observed in the ^{1}H NMR spectrum of the reaction mixture.

Scheme 4-11. A crossover experiment to probe the reversibility of formation of 3-methoxycyclopent-2-en-1-one (**61**) when another enolate (**3-Me$_4$N**) and EtI are present in $CDCl_3$.



This suggests that while the formation of 3-methoxycyclohex-2-en-1-one (**54**) may be reversible under the reaction conditions of the type found in section 4.2, the formation of 3-methoxycyclopent-2-en-1-one (**61**) was irreversible under the same reaction conditions.

The control experiments and crossover experiments detailed above seem to indicate that there exists a possibility that certain ammonium or amidinium iodide salts may act as nucleophiles and reversibly attack one of the mono-O-alkylation products tested (compound **54**). This suggests that the O-methylation of enolate **3-D** may be partially (and slowly) reversible in the presence of certain iodide salts. This would mean that the relatively high O-selectivity which was observed in the reactions of this enolate in section 4.2 may actually be a lower bound to the true kinetic preference for O-methylation in reactions of this enolate. No crossover products were observed for reactions of the enolate derived from 1,3-cyclopentanedione (i.e., enolate **12-D**) and thus the high O-selectivities observed in reactions of that enolate in section 4.2 are likely to be truly reflective of the kinetic preference for O-methylation in these reactions. Despite demonstrating here that the formation of one of the products (**54**) is reversible under certain conditions, it is unlikely that reversal of product formation is happening on an appreciable scale in any of the reactions shown in section 4.2. This appears to be case most notably due to the fact that the O/C ratios remain constant at varying levels of conversion, and also do not change when the reactions are re-analysed by ^{1}H NMR spectroscopy after a considerable amount of time has passed. Were any of the products forming reversibly, the O/C ratios should change over time, resulting in an increase in the proportion of the thermodynamically favoured products. As such, it is likely that the O/C ratios measured in section 4.2 are an accurate reflection of the kinetic ratio of the products.

4.5. References

1. Bram, G. *J. Mol. Catal.* **1981**, *10*, 223–229.
2. Rhoads, S. J.; Holder, R. W. *Tetrahedron* **1969**, *25*, 5443–5450.
3. Arnett, E. M.; Maroldo, S. G.; Schriver, G. W.; Schilling, S. L.; Troughton, E. B. *J. Am. Chem. Soc.* **1985**, *107*, 2091–2099.
4. Kornblum, N.; Lurie, A. P. *J. Am. Chem. Soc.* **1959**, *81*, 2705–2715.
5. Kremers, F.; Roth, F.; Tietze, E.; Claisen, L. *Justus Liebigs Ann. Chem.* **1925**, *442*, 210–245.
6. Kaljurand, I.; Kütt, A.; Sooväli, L.; Rodima, T.; Mäemets, V.; Leito, I.; Koppel, I. A. *J. Org. Chem.* **2005**, *70*, 1019–1028.
7. Kornblum, Nathan.; Seltzer, Raymond.; Haberfield, Paul. *J. Am. Chem. Soc.* **1963**, *85*, 1148–1154.
8. Hobbs, C. F.; McMillin, C. K.; Papadopoulos, E. Paul.; VanderWerf, C. A. *J. Am. Chem. Soc.* **1962**, *84*, 43–51.
9. Brasca, M. G.; Amboldi, N.; Ballinari, D.; Cameron, A.; Casale, E.; Cervi, G.; Colombo, M.; Colotta, F.; Croci, V.; D'Alessio, R.; Fiorentini, F.; Isacchi, A.; Mercurio, C.; Moretti, W.; Panzeri, A.; Pastori, W.; Pevarello, P.; Quartieri, F.; Roletto, F.; Traquandi, G.; Vianello, P.; Vulpetti, A.; Ciomei, M. *J. Med. Chem.* **2009**, *52*, 5152–5163.
10. Mantsch, H. H.; Saitô, H.; Smith, I. C. P. *Prog. Nucl. Magn. Reson. Spectrosc.* **1977**, *11*, 211–272.
11. Pitner, T. P.; Edwards, W. B. I.; Bassfield, R. L.; Whidby, J. F. *J. Am. Chem. Soc.* **1978**, *100*, 246–251.
12. Kurts, A. L.; Genkina, N. K.; Macias, A.; Beletskaya, L. P.; Reutov, O. A. *Tetrahedron* **1971**, *27*, 4777–4785.
13. Jackman, L. M.; Lange, B. C. *J. Am. Chem. Soc.* **1981**, *103*, 4494–4499.
14. Rathke, M. W.; Lindert, A. *Synth. Commun.* **1978**, *8*, 9–14.
15. Arnett, E. M.; Maroldo, S. G.; Schilling, S. L.; Harrelson, J. A. *J. Am. Chem. Soc.* **1984**, *106*, 6759–6767.
16. Zook, H. D.; Gumby, W. L. *J. Am. Chem. Soc.* **1960**, *82*, 1386–1389.
17. Winstein, S.; Savedoff, L. G.; Smith, S.; Stevens, I. D. R.; Gall, J. S. *Tetrahedron Lett.* **1960**, *1*, 24–30.
18. Miller, B.; Margulies, H.; Drabb, T.; Wayne, R. *Tetrahedron Lett.* **1970**, *11*, 3805–3808.
19. Jackman, L. M.; Haddon, R. C. *J. Am. Chem. Soc.* **1973**, *95*, 3687–3692.
20. Jackman, L. M.; Szeverenyi, N. M. *J. Am. Chem. Soc.* **1977**, *99*, 4954–4962.
21. Jackman, L. M.; Lange, B. C. *Tetrahedron* **1977**, *33*, 2737–2769.
22. Jackman, L. M.; Dunne, T. S. *J. Am. Chem. Soc.* **1985**, *107*, 2805–2806.
23. Kurts, A. L.; Macias, A.; Beletskaya, I. P.; Reutov, O. A. *Tetrahedron* **1971**, *27*, 4759–4767.
24. Ho, T.-L. *Chem. Rev.* **1975**, *75*, 1–20.
25. Pearson, R. G.; Songstad, Jon. *J. Am. Chem. Soc.* **1967**, *89*, 1827–1836.
26. Klopman, G. *J. Am. Chem. Soc.* **1968**, *90*, 223–234.
27. "Permittivity (Dielectric Constant) of Liquids." In *CRC Handbook of Chemistry and Physics, Internet Version 2005*; Lide, D. R., Ed.; CRC Press, Boca Raton, FL, 2005.
28. Nee, G.; Leroux, Y.; Seyden-Penne, J. *Tetrahedron* **1981**, *37*, 1541–1545.
29. Brieger, G.; Pelletier, W. M. *Tetrahedron Lett.* **1965**, *6*, 3555–3558.
30. le Noble, W. J.; Puerta, J. E. *Tetrahedron Lett.* **1966**, *7*, 1087–1090.

31. Yoffe, S. T.; Vatsuro, K. V.; Kugutcheva, E. E.; Kabachnik, M. I. *Tetrahedron Lett.* **1965**, *6*, 593–600.
32. Le Noble, W. J.; Morris, H. F. *J. Org. Chem.* **1969**, *34*, 1969–1973.
33. Jefcoate, C. R.; Ghisla, S.; Hemmerich, P. *J. Chem. Soc. C* **1971**, No. 0, 1689–1694.
34. Ramachary, D. B.; Kishor, M. *J. Org. Chem.* **2007**, *72*, 5056–5068.
35. Kennedy, J. W. J.; Vietrich, S.; Weinmann, H.; Brittain, D. E. A. *J. Org. Chem.* **2008**, *73*, 5151–5154.
36. Kornblum, N.; Smiley, R. A.; Blackwood, R. K.; Iffland, D. C. *J. Am. Chem. Soc.* **1955**, *77*, 6269–6280.
37. Wong, K.-H. *J. Chem. Soc., Chem. Commun.* **1978**, No. 7, 282–283.
38. Duk-Young, C.; Sung-Hong, K.; Myung-Ho, L.; Soo-Dong, Y.; Mizue, F.; Yuho, T. *J. Korean Chem. Soc.* **1995**, *39*, 643–649.
39. Yoh, S.-D.; Cheong, D.-Y.; Lee, C.-H.; Kim, S.-H.; Park, J.-H.; Fujio, M.; Tsuno, Y. *J. Phys. Org. Chem.* **2001**, *14*, 123–130.

Chapter 5: Experimental for Reactions of Cyclic Enolates

5.1. General Experimental..... 242

5.2. Preparation of Tetramethylammonium and Lithium Enolates..... 251

5.3. Determination of O/C Ratios in Enolate Ethylation Reactions 255

5.3.1. Reactions of 1,3-Cyclohexanedione-derived Enolate **3-D** with EtI..... 255

5.3.2. Reactions of 1,3-Cyclohexanedione-derived Enolate **3-D** with EtBr..... 259

5.3.3. Reactions of 1,3-Cyclopentanedione-derived Enolate **12-D** with EtI 261

5.3.4. Reactions of 1,3-Cyclopentanedione-derived Enolate **12-D** with EtBr . 264

5.3.5. Reactions of 5-Phenylcyclohexan-1,3-dione-derived Enolate **17-D** with EtI..... 266

5.3.6. Reactions of 5-Phenylcyclohexan-1,3-dione-derived Enolate **17-D** with EtBr..... 269

5.3.7. Reactions of 5,5-Dimethylcyclohexan-1,3-dione-derived Enolate **22-D** with EtI..... 271

5.3.8. Reactions of 5,5-Dimethylcyclohexan-1,3-dione-derived Enolate **22-D** with EtBr..... 274

5.4. Determination of O/C Ratios in Enolate Trideuteromethylations 276

5.4.1. Reactions of **3-D** with Deuterated Methyl Iodide..... 279

5.4.2. Reactions of **12-D** with Deuterated Methyl Iodide..... 281

5.4.3. Reactions of **17-D** with Deuterated Methyl Iodide..... 283

5.4.4. Reactions of **22-D** with Deuterated Methyl Iodide..... 285

5.5. Determination of O/C Ratios in Enolate Methylation Reactions..... 287

5.5.1. Reactions of **46-D** with Methyl Iodide 287

5.5.2. Reactions of **49-D** with Methyl Iodide 288

5.6. Determination of O/C Ratios in Alkylations of Lithium Enolates..... 289

5.6.1. Reactions of the 1,3-Cyclohexanedione-Derived Enolate **3-Li** 289

5.6.2. Reactions of the 1,3-Cyclopentanedione-Derived Enolate **12-Li** 293

5.7. Preparation of Benzylated Derivatives of 1,3-Diketones **297**

5.8. Determination of O/C Ratios in Enolate Benzylation Reactions **310**

5.8.1. Reactions of 1,3-Cyclohexanedione-Derived Enolate **3-Me_4N** 312

5.8.2. Reactions of 1,3-Cyclopentanedione-Derived Enolate **12-Me_4N** 319

5.9. Control Experiments and Crossover Experiments **325**

5.10. References **338**

Appendices referred to in the text are available at the following link:
https://tinyurl.com/KSheehyPhDThesisAppendices

5.1. General Experimental

Commercial diazines and alkylating agents were obtained from Fluorochem, Sigma-Aldrich and Alfa Aesar.

CH_2Cl_2, $CDCl_3$, CH_3CN, CD_3CN, $(CH_3)_2SO$, $(CD_3)_2SO$ and THF were dried over activated 3 Å molecular sieves and stored under an atmosphere of nitrogen in flasks with grease-free J. Young's valves.[1] CH_3CN was dried over activated 4 Å molecular sieves and stored in the same fashion. Molecular sieves (10 weight percent per unit volume of compound to be dried, 20 weight percent was used when drying THF) were activated by flame drying in the storage flask(s) for 5 – 10 minutes (depending on quantity of sieves to be dried).[1] After flame-drying, the storage flask was immediately connected to a Schlenk line, subjected to vacuum (between 2 and 5×10^{-3} mbar), and allowed to stand until the sieves had cooled. The flask was then subjected to several vacuum/refill cycles to establish a nitrogen atmosphere inside, and the solvent/compound to be dried was then added by cannula transfer directly from a Winchester bottle which was sealed using a rubber septum (sized for a B29 ground glass socket joint).

Solvents that were used in relative bulk (CH_3CN, CH_2Cl_2, THF) were stored in a specialised flask with two J. Young's valves, one of which was modified to facilitate easy access of a needle to the body of the flask through the side-arm of the valve. When accessing the dry solvent, the angled side-arm was sealed with a rubber septum, and the small volume contained between the septum and the sealed J. Young's valve was flushed with a stream of nitrogen gas for a minimum of five minutes prior to opening the valve. The solvent required several days after commencing drying to reach maximal dryness (<10 ppm H_2O according to analysis by Karl Fischer titration), but was dry enough for most purposes after one day. CH_3CN and THF stored in this manner was found to retain water contents of less than 10 ppm for more than one year.

For all reactions conducted using Schlenk glassware, the Schlenk flask was dried in an oven, then attached to vacuum *via* Schlenk manifold and placed under vacuum ($\leq 5 \times 10^{-3}$ mbar). The flask was then filled with nitrogen gas by the pump and fill technique (three repeats of the following cycle: evacuation to $\leq 5 \times 10^{-3}$ mbar, re-fill with nitrogen gas).[1] Solids and reagents were then introduced to the flasks against a fast nitrogen flow either directly from narrow vials or using a powder funnel.

NMR spectra were recorded on Bruker Avance III 600, Bruker Avance I 400 and Bruker Avance III 300 NMR spectrometers, in proton coupled mode using tetramethysilane (TMS) as the internal chemical shift reference standard. Proton NMR spectra (proton coupled mode, 600 MHz, 400 MHz and 300 MHz respectively) and ^{13}C NMR spectra (proton decoupled mode; 150 MHz, 100 MHz and 75 MHz, respectively) were acquired at 300 K on the 300 MHz instrument and 293 K on the 400 MHz and 600 MHz instruments. All spectra were run at University College Cork. Proton spectra acquired in regular non-deuterated solvents were acquired using the Bruker NOESY presat (noesygppr) water suppression pulse sequence. Chemical shifts (δ) are expressed as parts per million (ppm), positive shift being downfield from TMS;

coupling constants (*J*) are expressed in Hertz (Hz). Splitting patterns in ^{1}H-NMR spectra are designated as: s (singlet), bs (broad singlet), d (doublet), dd (doublet of doublets), ddd (doublet of doublets of doublets), t (triplet), td (triplet of doublets), q (quartet), quin (quintet) and m (multiplet). Infrared spectra were measured using a FTIR UATR2 spectrometer. The samples were dissolved in acetonitrile which was placed over the crystal of the spectrometer using a dropper. After the evaporation of the acetonitrile had occurred, pressure was applied to the sample on the crystal and a spectrum was recorded. Data are represented as follows: frequency of absorption (cm^{-1}), intensity of absorption (s = strong, m = medium, w = weak, br = broad). High resolution (precise) mass spectra (HRMS) were recorded on a Waters LCT Premier Tof LC–MS instrument in electrospray ionization (ESI) mode using 50 % acetonitrile/water containing 0.1 % formic acid as eluent. Samples were made up at a concentration of approximately 1 mg ml^{-1}.

General Procedures

General Procedure for the Alkylation of Enolates in $CDCl_3$

The following procedure (Procedure A) was used to establish the ratios of products formed by a reaction of an enolate and an electrophile in $CDCl_3$:

1,3-dione (1.0 equivalent) was added to a Schlenk flask containing an inert atmosphere of nitrogen gas. Dry $CDCl_3$ (0.7 ml) was added to form a cloudy suspension or a transparent solution, dependent on dione solubility. Dry 1,8-diazabicyclo[5.4.0]undec-7-ene (**2**) (DBU, 0.98 equivalents) was added neat to the solution, forming a transparent solution of the enolate (pale yellow or pink depending on the dione). The solution was stirred for approximately 15 minutes.

An empty NMR tube was placed in a long Schlenk tube. The long Schlenk tube, containing the NMR tube, was evacuated and re-filled with nitrogen ≥ 3 times, creating an inert atmosphere inside the flask. The dione solution was added to the NMR tube under inert atmosphere by syringe. The NMR tube was sealed with a rubber septum cap. After fitting the rubber septum to the NMR tube, the seal was secured by wrapping the external edge of the septum where it contacted the surface of the NMR tube with PTFE tape. The sealed NMR tube was removed from the long Schlenk tube and the section containing the enolate solution was immersed in in an ice/water bath (0 °C) for 15 minutes. A ~0.2 mol L^{-1} solution of the appropriate alkylating agent in $CDCl_3$ (0.15 ml, 1.05 equivalents) was added dropwise through the septum cap over the course of approximately 1 minute. The resultant solution was mixed by shaking (in an ice bath) before the outside of the PTFE tape and rubber septum were wrapped with a layer of Parafilm to further secure the nitrogen atmosphere inside the NMR tube. The NMR tube was kept cold by partial immersion in the ice bath until immediately before it was inserted into the NMR spectrometer (internal temperature 20 °C or 27 °C, depending on the spectrometer used). From the start of sample addition to sample ejection from the spectrometer took 5 – 10 minutes, after which the sample was immediately returned to an ice bath. The sample was then brought to be stored a refrigerator. Further ^{1}H NMR spectra were recorded at regular intervals in a similar manner over the course of

a week. In each case, a detailed description is given for the final NMR spectrum recorded.

Note: Identical signals of the reactants and products are seen in all spectra taken of the reaction mixtures. The observed ratio of O-alkylated products to C-alkylated products remained constant at all measured levels of conversion.

General Procedure for the Alkylation of Enolates in $(CD_3)_2SO$

The following procedure (Procedure B) was used to establish the ratios of products formed by a reaction of an enolate and an electrophile in $(CD_3)_2SO$:

1,3-dione (1.0 equivalent) was added to a Schlenk flask containing an inert atmosphere of nitrogen gas. Dry $(CD_3)_2SO$ (0.7 ml) was added to form a transparent solution. Dry 1,8-diazabicyclo[5.4.0]undec-7-ene (**2**) (DBU, 0.98 equivalents) was added neat to the solution, forming a transparent solution of the enolate (pale yellow or pink depending on the dione). The solution was stirred for approximately 15 minutes.

An empty NMR tube was placed in a long Schlenk tube. The long Schlenk tube, containing the NMR tube, was evacuated and re-filled with nitrogen ≥ 3 times, creating an inert atmosphere inside the flask. The dione solution was added to the NMR tube under inert atmosphere by syringe. The NMR tube was sealed with a rubber septum cap. After fitting the rubber septum to the NMR tube, the seal was secured by wrapping the external edge of the septum where it contacted the surface of the NMR tube with PTFE tape. After keeping the solution(s) in the room containing the NMR spectrometer, air-conditioned to 20 °C, for 10 minutes, a ~0.2 mol L^{-1} solution of the appropriate alkylating agent in $(CD_3)_2SO$ (0.15 ml, 1.05 equivalents) was added dropwise through the septum cap over the course of approximately 1 minute. The resultant solution was mixed by shaking before the outside of the PTFE tape and rubber septum were wrapped with a layer of Parafilm to further secure the nitrogen atmosphere inside the NMR tube. The tube was then inserted into the NMR spectrometer. The tube was kept in a temperature-controlled room at 20 °C throughout the experiment. ^{1}H NMR spectra were recorded at regular intervals over the course of a week.

General Procedure for the Alkylation of Enolates in THF

The following procedure (Procedure C) was used to establish the ratios of products formed by a reaction of an enolate and an electrophile in THF.

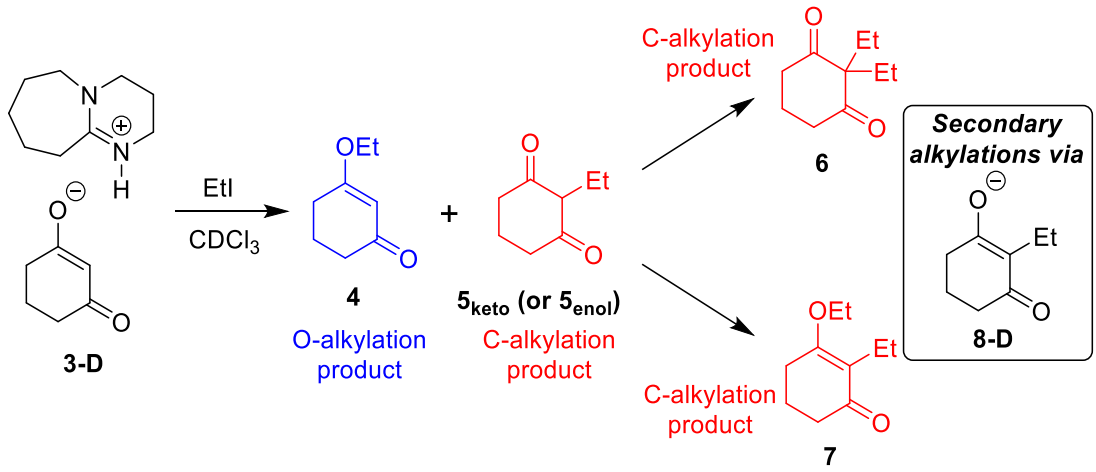
1,3-dione (1.0 equivalent) was added to a Schlenk flask containing an inert atmosphere of nitrogen gas. Dry THF (0.7 ml) was added to form a transparent solution. Dry 1,8-diazabicyclo[5.4.0]undec-7-ene (**2**) (DBU, 0.98 equivalents) was added neat to the solution, forming a transparent solution of the enolate (pale yellow or pink depending on the dione). The solution was stirred for approximately 15 minutes.

To a separate Schlenk flask containing an inert atmosphere of nitrogen gas was added dry THF (0.3 ml). 1.05 equivalents of the appropriate alkylating agent was added to

the THF and the flask was swirled, giving a transparent solution. The contents of this flask were taken up in a syringe (which had been flushed three times with nitrogen gas) and added to the flask containing the enolate solution dropwise over the course of 1 minute. The solution was stirred for approximately 18 hours. The side-arm of the reaction flask was connected with rubber tubing to a vacuum trap, which was itself connected to a Schlenk manifold. The trap was placed under vacuum ($\leq 5 \times 10^{-3}$ mbar). The vacuum trap and the tubing connecting it to the reaction flask and the Schlenk manifold were then filled with nitrogen gas by the pump and fill technique.[2] The trap was then placed under vacuum and then cooled with liquid N_2. At this point the stopcock on the Schlenk flask was opened and volatile reagents and solvent were removed and collected in the trap. After approximately 30 minutes, the entirety of the trap and the Schlenk flask were re-filled with nitrogen gas through the Schlenk manifold and the stopcock of the Schlenk flask was closed. The trap was removed and the flask was re-attached directly to the Schlenk manifold, using the pump and fill technique to establish a nitrogen atmosphere in the tubing used for the attachment.[2] The Schlenk flask containing the reaction mixture was then opened and the contents of the flask were dissolved in dry $CDCl_3$ (0.7 ml). The NMR tube was then transferred to the NMR spectrometer and a ^1H NMR spectrum was recorded.

Assignment of O vs C Ratios

For each reaction of an enolate with an alkylating agent, the selectivity between O-alkylation and C-alkylation of the enolate (the O/C ratio) was determined by comparing the integrations of various signals seen in the ^{1}H NMR spectra of the crude product mixtures. The signals employed for comparison were required to be adequately baseline separated to ensure accurate integration values. Integrations were only used for the purpose of the ratio calculation if they were associated with signals that could be unambiguously attributed to one of the 4 possible alkylation products. The assignments were made in conjunction with reference to literature NMR values of various alkylation products. Of the 4 possible products of each reaction, only the O-mono-methylation product was considered as the "O" portion of the ratio, i.e., to obtain the O/C ratio, the integrations of the signals of the O-mono-alkylated product (product **4** in Scheme 5-1) was compared to the sum of the integrations of the 3 other products (**5**, **6** and **7**). The reason for this is that the two secondary alkylation products, **6** and **7** (Scheme 5-1), are produced by the alkylation of enolate **8-D**, which is formed by the deprotonation of the C-mono-alkylation product **5**. The starting enolate, **3-D**, can deprotonate the C-mono-alkylation product ($\mathbf{5}_{keto}$ or $\mathbf{5}_{enol}$), resulting in enolate **8-D**. This is explained by Scheme 5-1, which shows that the C-di-alkylated product **6** and the O/C mixed di-alkylation product **7** are formed from an initial C-alkylation product.



Scheme 5-1: Alkylation of **3-D** (the enolate produced by a reaction of 1,3-cyclohexanedione (**1**) with DBU (**2**)). Di-alkylation products **6** and **7** are derived from the C-mono-alkylation product **5**.

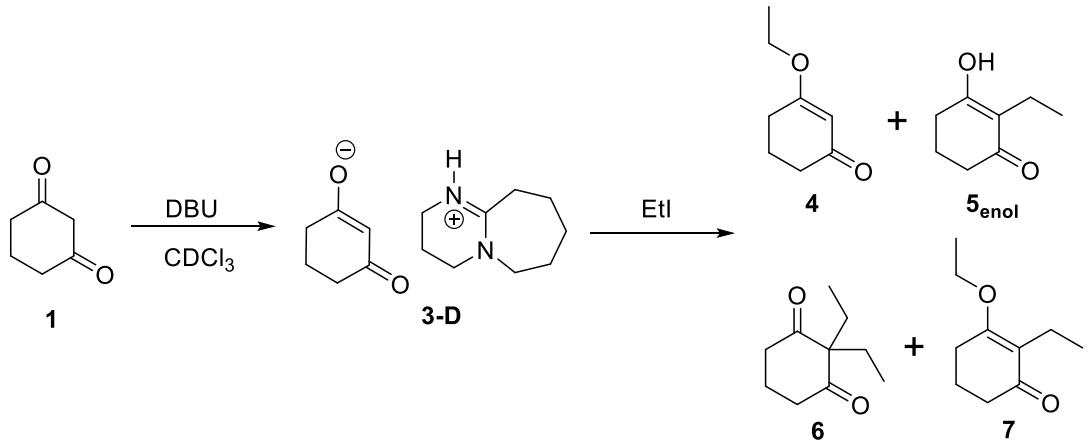
The percentages of O-alkylation and C-alkylation, respectively, are given by equations 5.1 and 5.2 shown below:

$$\text{Percentage of O-alkylation} = \frac{[\mathbf{4}]}{[\mathbf{4}]+[\mathbf{5}]+[\mathbf{6}]+[\mathbf{7}]} \times 100 \qquad (5.1)$$

$$\text{Percentage of C-alkylation} = \frac{[\mathbf{5}]+[\mathbf{6}]+[\mathbf{7}]}{[\mathbf{4}]+[\mathbf{5}]+[\mathbf{6}]+[\mathbf{7}]} \times 100 \qquad (5.2)$$

where [**Y**] is the concentration in mol L^{-1} of compound **Y** (i.e., where **Y** = compound **4**, **5**, **6** or **7**). In the calculations of the O/C ratios, the integrations of compounds **4** – **7** are substituted directly in place of the molar concentrations in the above equation, since the NMR spectra were recorded in a manner that ensures that the integrations of the NMR signals of the compounds are directly proportional to their respective concentrations.

An example of an O vs C ratio assignment for a crude product mixture from the reaction in Scheme 5-1 is shown in Figure 5-1. The spectrum was produced from a reaction using Procedure A above with 1,3-cyclohexanedione (**1**), DBU (**2**) and ethyl iodide in $CDCl_3$.



Scheme 5-2: Reaction of enolate **3-D** (the enolate produced by a reaction of 1,3-cyclohexanedione (**1**) with DBU (**2**)) and ethyl iodide in $CDCl_3$.

Possible products of the reaction include the O-ethylation product (**4**) and three compounds derived from initial C-ethylation - (**5**), (**6**) and (**7**) (see Scheme 5-1 above). The section of the crude ^{1}H NMR spectrum showing the relevant signals is shown in Figure 5-1 below. The spectrum shows signals associated with the tertiary amidinium ion derived from DBU (**2**) marked with a red **X**, seen at 3.53 ppm, 3.32 ppm, 2.80 ppm, 2.00 ppm, 1.66 ppm. Comparisons of the chemical shifts and relative integrations of the signals present with those of values reported in the literature allow the signals at 5.32 ppm (s, 1H), 3.92 ppm (q, J = 7.0 Hz, 1H), 2.42 (t, J = 6.3 Hz, 2H) and 1.37 ppm (t, J = 7.0 Hz, 3H) to be assigned to O-ethylation product (**4**).[3] Another 2H triplet signal associated with this product should be visible at approximately 2.32 ppm, along with a multiplet integrating for 2H at 2.05 – 1.93 ppm. However, these signals are partially obscured by other products. The signal at 0.90 ppm (t, J = 7.4 Hz, 3H) is assigned to C-mono-ethylation product (**5**)[4] and the signals at 2.68 – 2.58 (m, 4H) and 0.75 ppm (t, J = 7.4 Hz, 6H) are assigned to C-di-ethylation product (**6**). No other distinctive signals can be observed for either of these products, as they are obscured by the signals of the tertiary amidinium ion derived from DBU. No distinctive NMR signals of (**7**), which would form *via* initial C-alkylation (see above), can be seen in the spectrum of the reaction mixture.

Note that the C-mono-alkylation product drawn in Scheme 5-1 is the enol form of the product (**5**$_{\mathbf{enol}}$). In many instances, the keto and enol forms of the C-mono-alkylation

product can be observed in the spectra. When this occurs, the signals of each isomer are denominated $\mathbf{5}_{\mathbf{enol}}$ and $\mathbf{5}_{\mathbf{keto}}$. The contribution of both isomers of the product are included in the calculation of the O/C ratio.

Based on the ^{1}H NMR spectral data given above, the integrations of 1H of each of compounds **4**, **5**, **6** and **7** relative to 1H of compound **4** are as follows:

$$I_{\mathbf{4}} = 1.00; \quad I_{\mathbf{5}} = \frac{0.50}{3} = 0.16; \quad I_{\mathbf{6}} = \frac{0.21}{6} = 0.035; \quad I_{\mathbf{7}} = 0.00$$

where $I_{\mathbf{X}}$ is the integration of 1H of compound **X** (**X** = **4**, **5**, **6** or **7**) relative to 1H of compound **4**.

Note that the integration value of the peak associated with compound ($\mathbf{5}_{\mathbf{enol}}$) is divided by 3 as it represents a 3H signal, whereas the integration value of 1.00 from compound (**4**) represents a 1H signal. The integration value of the peak associated with compound (**6**) is divided by 6 as it represents a 6H signal. This allows the O vs C ratio to be assigned as 84:16.

The relative integration of each compound is proportional to its relative concentration (mol L^{-1}), i.e., $[\mathbf{X}] \propto I_{\mathbf{X}}$, and hence the relative integrations can be used to determine the relative proportions of O- and C-alkylation products formed in the reaction. Hence the percentage of O-alkylation is given by:

$$\text{Percentage of O-alkylation} = \frac{I_{\mathbf{4}}}{I_{\mathbf{4}} + I_{\mathbf{5}} + I_{\mathbf{6}} + I_{\mathbf{7}}} \times 100$$

$$= \frac{1.00}{1.00 + 0.16 + 0.035 + 0.00} \times 100 = 84\%$$

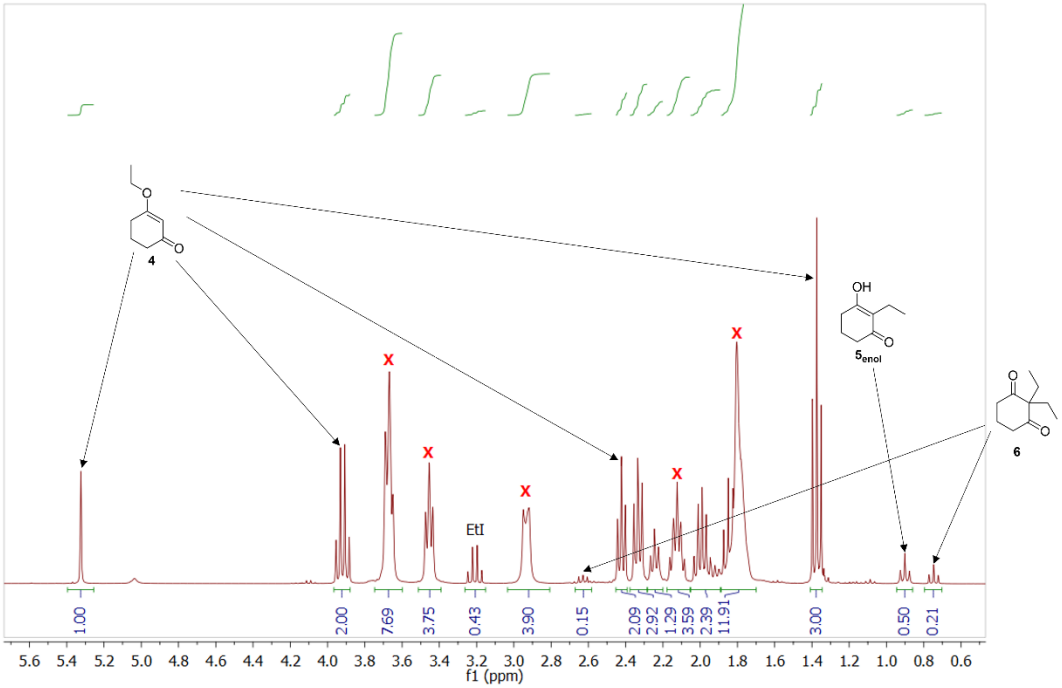


Figure 5-1: ^{1}H NMR spectrum of the crude product of the reaction between **3-D** and ethyl iodide in $CDCl_3$. [a]

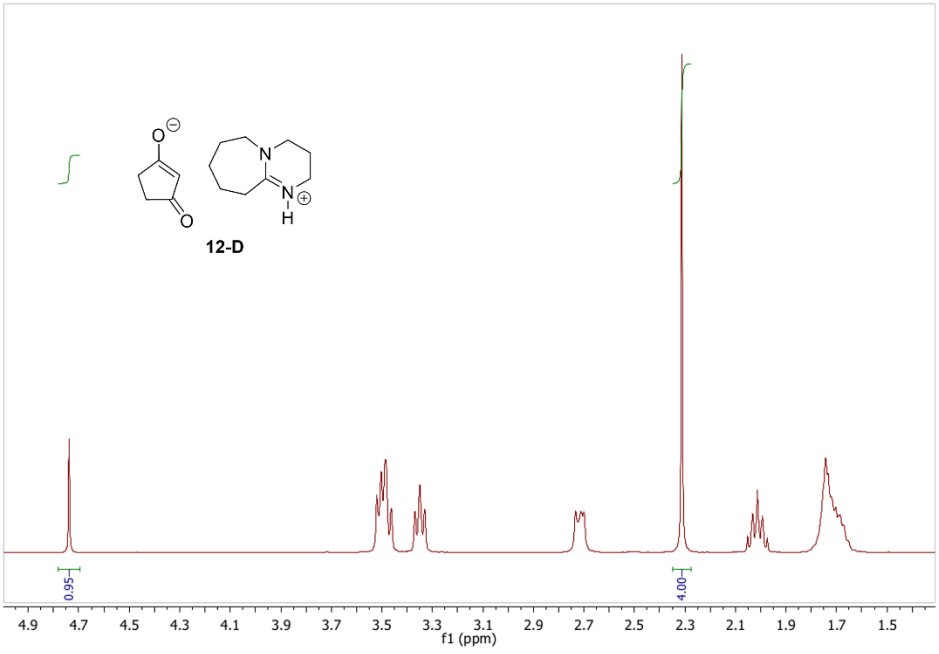


Figure 5-2: ^{1}H NMR spectrum showing the product of a reaction between DBU (**2**) and a different 1,3-diketone, 1,3-cyclopentanedione (**9**) to produce the amidinium ion derived from **9**, **12-D**. The non-integrated peaks coincide with those marked by a red "X" in Figure 5-1.

It should be noted that the signals of the starting material may appear in spectra of reactions of this type. These signals are a composite of the starting enolate and the enol which exist in an equilibrium. This happens as the reaction proceeds because the starting enolate (**3-D** in Figure 5-1 above) may deprotonate the C-mono-alkylation

[a] Signals marked with a red "X" are associated with the amidinium ion derived from DBU, seen at 3.53 ppm, 3.32 ppm, 2.80 ppm, 2.00 ppm and 1.66 ppm.

product, resulting in the formation of the enol of the starting material. Evidence consistent with this is shown in Figure 5-3 below, where the starting material signals from a reaction of the amidinium enolate of dimedone (**22-D**) with ethyl iodide appear at 4.54 ppm and 1.85 ppm. As the reaction progresses, the starting enolate peak at 4.54 ppm both decreases in intensity and moves downfield as the products form. The spectrum at the bottom is the earliest measured timepoint, showing large, broad peaks of the starting enolate (**22-D**) with little conversion. Each spectrum in Figure 5-3 shows an increase in reaction time, with products beginning to form. In the final spectrum, the peak of the starting enolate at 4.54 ppm as disappeared and a large, broad signal has appeared downfield in the ~4.8 ppm region.

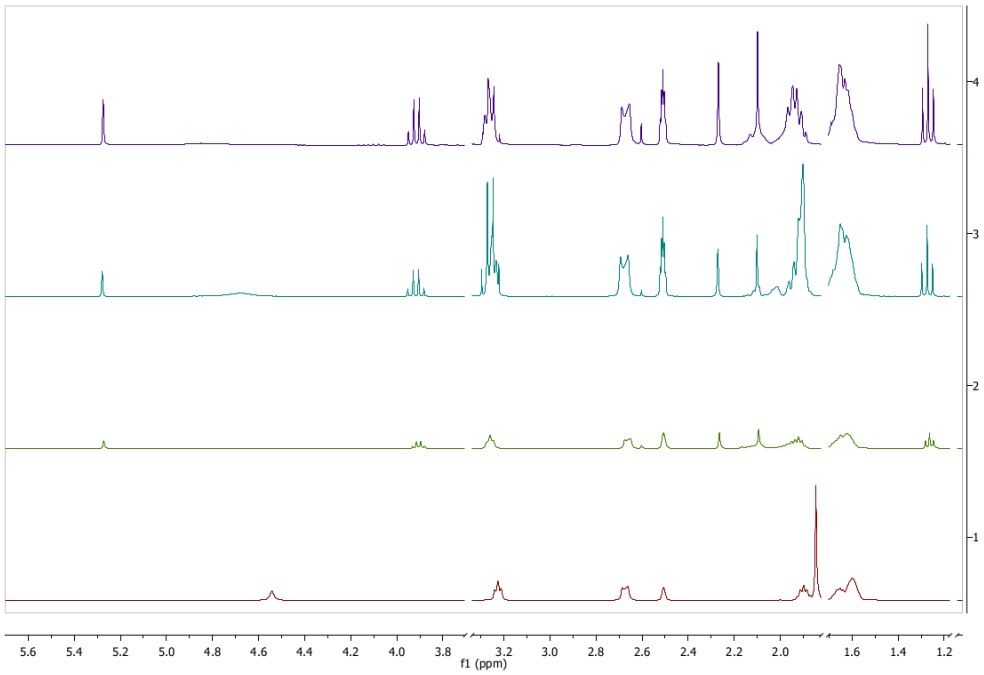
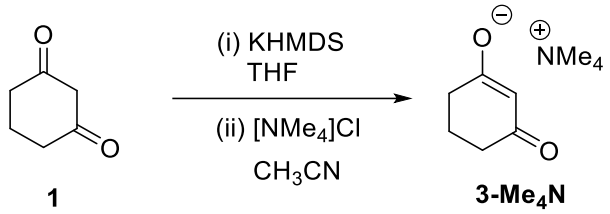


Figure 5-3: Stacked spectra from a reaction between the amidinium enolate of dimedone (**22-D**) and ethyl iodide. The starting enolate signals appear at 4.54 ppm and 1.85 ppm. As the reaction progresses, the peaks get smaller and may shift slightly; a common feature seen in many spectra of these reactions.

5.2. Preparation of Tetramethylammonium and Lithium Enolates

(i) Synthesis of 3-Me_4N



1 **3-Me_4N**

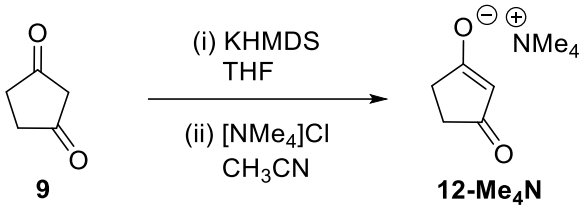
Note: All operations in the following procedure were conducted under an atmosphere of nitrogen gas.

1,3-cyclohexanedione (**1**) (0.94 g, 8.4 mmol) was dissolved in THF (15 ml). KHMDS (1.75 g, 8.8 mmol) was dissolved in THF (10 ml) in a Schlenk flask with a cone-shaped ground glass joint. The dione solution was added to the KHMDS solution dropwise at room temp over *ca.* 1 hr. The dione flask was washed out with separate 3 ml and 2 ml portions of THF. The washings were transferred to the reaction mixture. A white solid in contact with a pale yellow liquid resulted. This was stirred overnight, then the cone Schlenk flask was fitted with the Schlenk filtration apparatus, and mixture was filtered. The residual solid in the Schlenk flask with a cone-shaped ground glass joint was rinsed with THF into the filter stick and onto the frit. The solid was washed with three portions of THF (3 × 3 ml). The solvent was pushed through the frit using nitrogen pressure. The flask containing the filtrate was removed, and an empty Schlenk flask (with nitrogen atmosphere *via* connection to Schlenk manifold) was fitted. The solid in the filter stick was dried under vacuum before being sealed and transferred into a glove box containing a nitrogen atmosphere. The solid potassium enolate (1.02 g, 6.7 mmol) was transferred from the Schlenk filtration apparatus into a Schlenk flask with a cone-shaped ground glass joint, and tetramethylammonium chloride (0.79 g, 7.2 mmol) was then added. The Schlenk flask with a cone-shaped ground glass joint was sealed using a ground glass socket joint fitted with a stopcock. The ground glass joint was secured with a Keck clamp. This flask was removed from the glove box and fitted to nitrogen supply *via* the second stopcock. The side arm of the Schlenk flask was fitted with a rubber septum, and the space between the septum and the closed stopcock was flushed with nitrogen using a syringe and needle fitted to a nitrogen flush line. The stopcock was then opened. Dry CH_3CN (15 ml) was added, and the mixture was stirred for three days. Neither solid appeared to dissolve, but after stirring overnight, the appearance of the mixture had changed, and the solid present was much finer (KCl). This mixture was filtered through a Schlenk filtration apparatus as above to remove undissolved KCl and unreacted potassium enolate. The solids were collected on the frit of the Schlenk filtration apparatus and washed twice with CH_3CN (2 × 3 ml). The combined filtrate was concentrated under vacuum using a 2nd trap between the reaction mixture and the Schlenk line, yielding a slightly pink/orange solid (0.8 g). The ^{1}H NMR spectrum showed the presence of the Me_4N^+ enolate of 1,3-cyclohexanedione (**3-Me_4N**).

^{1}H NMR (300 MHz, $CDCl_3$) δ 4.88 (s, 1H), 3.37 (s, 12H), 2.18 (t, J = 6.1 Hz, 4H), 1.96 – 1.82 (m, 2H).

Note: The product was extremely hygroscopic and was stored in a glove box.

(ii) Synthesis of 12-Me_4N



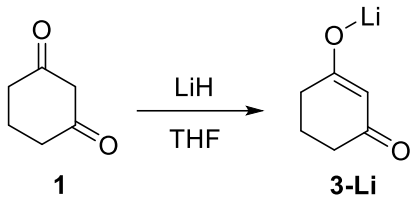
Note: All operations in the following procedure were conducted under an atmosphere of nitrogen gas.

1,3-cyclopentanedione (**9**) (0.49 g, 5.0 mmol) was dissolved in THF (20 ml). KHMDS (1.04 g, 5.2 mmol) was dissolved in THF (10 ml) in a Schlenk flask with a cone-shaped ground glass joint. The dione solution was added to the KHMDS solution dropwise at room temp over *ca.* 1 hr. The dione flask was washed out with separate 3 ml and 2 ml portions of THF. The washings were transferred to the reaction mixture. A white solid in contact with a pale yellow liquid resulted. This was stirred overnight, then the Schlenk flask with a cone-shaped ground glass joint was fitted with a Schlenk filtration apparatus, and mixture was filtered. The residual solid in the Schlenk flask with a cone-shaped ground glass joint was rinsed with THF into the filter stick and onto the frit. The solid was washed with three portions of THF (3 × 3 ml). The solvent was pushed through the frit using nitrogen pressure. The flask containing the filtrate was removed, and an empty Schlenk flask (with nitrogen atmosphere *via* connection to Schlenk manifold) was fitted. The solid in the Schlenk filtration apparatus was dried under vacuum before being sealed and transferred into a glove box containing a nitrogen atmosphere. The solid potassium enolate (0.6 g, 4.4 mmol) was transferred from the Schlenk filtration apparatus into a Schlenk flask with a cone-shaped ground glass joint, and tetramethylammonium chloride (0.46 g, 4.2 mmol) was also added. The Schlenk flask with a cone-shaped ground glass joint was sealed using a ground glass socket joint fitted with a stopcock. The ground glass joint was secured with a Keck clamp. This flask was removed from the glove box and fitted to nitrogen supply *via* the second stopcock. The side arm of the Schlenk flask was fitted with a rubber septum, and the space between the septum and the closed stopcock was flushed with nitrogen, and then the stopcock was opened. Dry CH_3CN (15 ml) was added, and the mixture was stirred for 3 days. Neither solid appeared to dissolve, but after stirring for a week, the appearance of the mixture had changed, and the solid present was much finer (KCl). This mixture was filtered through a Schlenk filtration apparatus as above to remove undissolved KCl and unreacted potassium enolate. The solids were collected on the frit of the Schlenk filtration apparatus and washed twice with CH_3CN (2 × 3 ml). The combined filtrate was concentrated under vacuum using a 2nd trap between the reaction mixture and the Schlenk line, yielding a yellow/orange solid (0.55 g). The ^{1}H NMR spectrum showed the presence of the Me_4N^+ enolate of 1,3-cyclopentanedione (**12-Me_4N**).

^{1}H NMR (300 MHz, $CDCl_3$) δ 4.65 (s, 1H), 3.40 (s, 12H), 2.29 (s, 4H).

Note: The product was extremely hygroscopic and was stored in a glove box.

(iii) Synthesis of 3-Li



1 **3-Li**

Note: All operations in the following procedure were conducted under an atmosphere of nitrogen gas.

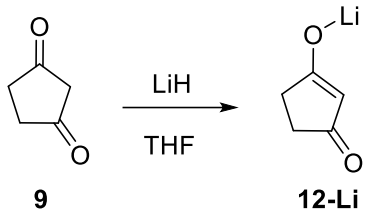
In a glove box under an inert atmosphere of nitrogen gas, a suspension of LiH (0.021 g, 2.64 mmol) in dry THF (5 ml) was prepared in a Schlenk flask. The solution was stirred and solid 1,3-cyclohexanedione (**1**) (0.285 g, 2.54 mmol) was added portion wise through a powder funnel. After addition, the solution was stirred vigorously for 20 minutes. The Schlenk flask was sealed using a glass stopper and subsequently removed from the glove box, where the solution was allowed to stir overnight at room temperature (~ 18 hours). After stirring overnight, a fine white/grey solid had formed in the reaction flask. The side-arm of the reaction flask was connected with rubber tubing to a vacuum trap, which was itself connected to a Schlenk manifold. The trap was placed under vacuum ($\leq 5 \times 10^{-3}$ mbar). The vacuum trap and the tubing connecting it to the reaction flask and the Schlenk manifold were then filled with nitrogen gas by the pump and fill technique.[2] The trap was then placed under vacuum and then cooled with liquid N_2. At this point the stopcock on the Schlenk flask was opened and the solvent was removed and collected in the trap. After approximately 30 minutes, the entirety of the trap and the Schlenk flask were re-filled with nitrogen gas through the Schlenk manifold and the stopcock of the Schlenk flask was closed. The trap was removed and the flask was re-attached directly to the Schlenk manifold, using the pump and fill technique to establish a nitrogen atmosphere in the tubing used for the attachment. The flask was then evacuated before being immediately transferred to the glove box. In the glove box, the white/grey solid (**3-Li**) in the flask was collected using a spatula and weighed, before being transferred to a screw-cap vessel and stored. (Yield = 0.078 g, 0.66 mmol, 26 %).

^{1}H NMR (300 MHz, $(CD_3)_2SO$) δ 4.75 (br. s, 1H), 2.02 (t, *J* = 6.3 Hz, 4H), 1.81 – 1.66 (m, 2H).

Note: The product was extremely hygroscopic and was stored in a glove box.

Note: Residual THF remained in this material after the solvent removal process. Hence, all reactions employing this compound in Section 5.6.1 feature a THF signal at ~3.60 ppm, which is labelled in the relevant spectra.

(iv) Synthesis of 12-Li



9 **12-Li**

In a glove box under an inert atmosphere of nitrogen gas, a suspension of LiH (0.025 g, 3.14 mmol) in dry THF (3.2 ml) was prepared in a Schlenk flask. The solution was stirred and solid 1,3-cyclopentanedione (**9**) (0.297 g, 3.03 mmol) was added portion wise through a powder funnel. After addition, the solution was stirred vigorously for 20 minutes. The Schlenk flask was sealed using a glass stopper and subsequently removed from the glove box, where the solution was allowed to stir overnight at room temperature (~ 18 hours). After stirring overnight, a fine white/grey solid had formed in the reaction flask. The side-arm of the reaction flask was connected with rubber tubing to a vacuum trap, which was itself connected to a Schlenk manifold. The trap was placed under vacuum ($\leq 5 \times 10^{-3}$ mbar). The vacuum trap and the tubing connecting it to the reaction flask and the Schlenk manifold were then filled with nitrogen gas by the pump and fill technique.[2] The trap was then placed under vacuum and then cooled with liquid N_2. At this point the stopcock on the Schlenk flask was opened and the solvent was removed and collected in the trap. After approximately 30 minutes, the entirety of the trap and the Schlenk flask were re-filled with nitrogen gas through the Schlenk manifold and the stopcock of the Schlenk flask was closed. The trap was removed and the flask was re-attached directly to the Schlenk manifold, using the pump and fill technique to establish a nitrogen atmosphere in the tubing used for the attachment. The flask was then evacuated before being immediately transferred to the glove box. In the glove box, the white/grey solid in the flask was collected using a spatula and weighed, before being transferred to a screw-cap vessel and stored. (Yield = 0.290 g, 2.79 mmol, 92%).

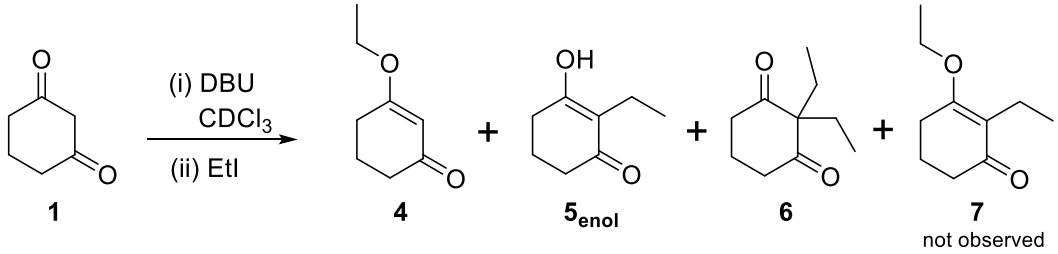
^{1}H NMR (300 MHz, $(CD_3)_2SO$) δ 4.53 (s, 1H), 2.10 (s, 4H).

Note: The product was extremely hygroscopic and was stored in a glove box.

5.3. Determination of O/C Ratios in Enolate Ethylation Reactions

5.3.1. Reactions of 1,3-Cyclohexanedione-Derived Enolate 3-D with EtI

(i) Reaction of Enolate 3-D with Ethyl Iodide in $CDCl_3$



From 1,3-cyclohexanedione (**1**) (0.0313 g, 0.279 mmol), DBU (**2**) (0.0416 g, 0.273 mmol) and ethyl iodide (0.457 g, 0.293 mmol) in $CDCl_3$ by procedure A at 0 °C.

After the product ratio was observed by ^{1}H NMR spectroscopy, the reaction mixture was added to a 100 ml round bottom flask and the solvent was removed under vacuum. The resulting yellow oil was redissolved in $CDCl_3$ and another spectrum was measured. The two spectra measured showed agreement in the calculated O vs C ratio. This indicates that the removal of solvent does not cause an alteration to the O vs C ratio in experiments of this type. On the basis of this knowledge, later experiments were carried out using THF as the solvent which would be subsequently removed from the reaction mixture before measuring the O vs C ratio.

^{1}H NMR (300 MHz, $CDCl_3$) of crude mixture of alkylation products (the underlined integrations are expressed relative to 1H of compound **4**): [a,b]

Assigned to **4**: δ 5.32 (s, 1H, C=C<u>H</u>), 3.92 (q, *J* = 7.0 Hz, 2H, OC<u>H</u>$_2$CH$_3$), 2.42 (t, *J* = 6.3 Hz, 2H, C<u>H</u>$_2$C=C), 1.37 (t, *J* = 7.0 Hz, 3H, OCH$_2$C<u>H</u>$_3$). [3]

Assigned to **5$_{enol}$**: δ 0.90 (t, *J* = 7.4 Hz, 0.41H, C-CH$_2$C<u>H</u>$_3$ (3H of compound **5$_{enol}$**)). [4]

Assigned to **6**: δ 2.68 – 2.58 (m, 0.15H, C<u>H</u>$_2$C=O (4H of compound **6**)), 0.75 (t, *J* = 7.4 Hz, 0.17H, C-CH$_2$C<u>H</u>$_3$ (6H of compound **6**)). [c]

Based on the ^{1}H NMR spectral data given above, the integrations of 1H of each of compounds **4**, **5$_{enol}$**, and **6** relative to 1H of compound **4** are as follows:

$$I_{\mathbf{4}} = 1.00; \quad I_{\mathbf{5}} = \frac{0.50}{3} = 0.16; \quad I_{\mathbf{6}} = \frac{0.21}{6} = 0.035$$

[a] The relevant ^{1}H NMR spectra are shown in Figure B1 and Figure B2 in Appendix B.

[b] Signals of **4 - 6** that are overlapping with other signals: δ 2.36 – 2.30 (m, contains 2H of **4** and 4H of **5$_{enol}$**), 2.04 – 1.89 (m, contains 2H of **4**, 4H of **5$_{enol}$** and 2H of **6**), 1.87 – 1.71 (m, contains 4H of **6**, EtI signal and signals of DBU and derivatives).

[c] No literature data is available for this compound, which was formed in very low quantities (*ca*. 3%). Assignments of NMR signals were made by analogy with analogue 2-ethyl-2-methyl-cyclohexan-1,3-dione in $CDCl_3$: δ 2.77-2.58 (4H, m), 2.10-1.97 (1H, m), 1.92-1.77 (3H, m), 1.21 (3H, s), <u>0.80</u> (3H, t, *J* = 7.5 Hz).[5]

where $I_{\mathbf{X}}$ is the integration of 1H of compound **X** (**X** = **4**, **5**$_{\mathbf{enol}}$ or **6**) relative to 1H of compound **4**. Since $I_{\mathbf{X}} \propto [\mathbf{X}]$ (concentration of **X** in mol L^{-1}), the percentage of O-alkylation is given by:

$$\text{Percentage of O-alkylation} = \frac{I_{\mathbf{4}}}{I_{\mathbf{4}} + I_{\mathbf{5}} + I_{\mathbf{6}}} \times 100$$

$$= \frac{1.00}{1.00 + 0.16 + 0.035} \times 100 = 84\%$$

Integrations give an O vs C ratio of 84:16

After the $CDCl_3$ was removed and the sample was redissolved in $CDCl_3$, a ^1H NMR spectrum was taken and the integrations of **4**, **5**$_{\mathbf{enol}}$ and **6** relative to 1H of **4** were measured again.

$$I_{\mathbf{4}} = 1.00; \quad I_{\mathbf{5}} = \frac{0.50}{3} = 0.16; \quad I_{\mathbf{6}} = \frac{0.21}{6} = 0.035$$

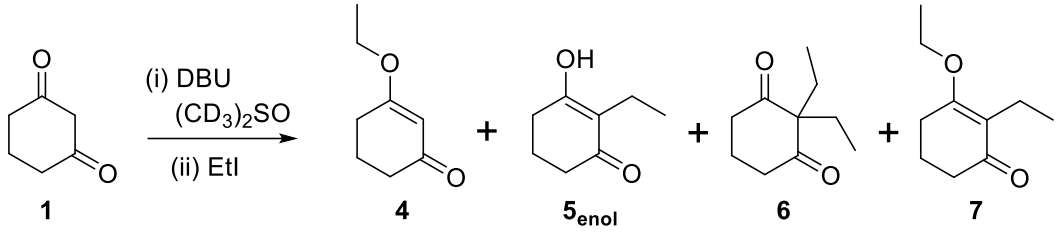
where $I_{\mathbf{X}}$ is the integration of 1H of compound **X** (**X** = **4**, **5**$_{\mathbf{enol}}$ or **6**) relative to 1H of compound **4**. Since $I_{\mathbf{X}} \propto [\mathbf{X}]$ (concentration of **X** in mol L^{-1}), the percentage of O-alkylation is given by:

$$\text{Percentage of O-alkylation} = \frac{I_{\mathbf{4}}}{I_{\mathbf{4}} + I_{\mathbf{5}} + I_{\mathbf{6}}} \times 100$$

$$= \frac{1.00}{1.00 + 0.16 + 0.035} \times 100 = 84\%$$

Integrations give an O vs C ratio of 84:16. As indicated above, this result shows that the O/C ratio is unchanged when the mixture of products is subjected to vacuum.

(ii) Reaction of Enolate 3-D with EtI in $(CD_3)_2SO$



From 1,3-cyclohexanedione (**1**) (0.026 g, 0.23 mmol), DBU (**2**) (0.033 g, 0.22 mmol) and ethyl iodide (0.040 g, 0.26 mmol) in $(CD_3)_2SO$ by procedure B at 20 °C.

^{1}H NMR (400 MHz, $(CD_3)_2SO$) of crude mixture of alkylation products (the underlined integrations are expressed relative to 1H of compound **4**): [a,b]

Assigned to **4**: δ 5.26 (s, 1H, C=C<u>H</u>), 3.90 (q, *J* = 7.0 Hz, 2H, OC<u>H</u>$_2$CH$_3$), 2.37 (t, *J* = 6.2 Hz, 2H, C<u>H</u>$_2$C=C). [3]

Assigned to **5$_{enol}$**: δ 0.81 (t, *J* = 7.4 Hz, 1.16H, C-CH$_2$C<u>H</u>$_3$ (3H of compound **5$_{enol}$**)). [4]

Assigned to **6**: δ 0.63 (t, *J* = 7.4 Hz, 0.37H, C-CH$_2$C<u>H</u>$_3$ (6H of compound **6**)). [c]

Assigned to **7**: δ 4.10 (q, *J* = 7.0 Hz, 0.10H, OC<u>H</u>$_2$CH$_3$ (2H of compound **7**)). [d]

Based on the ^{1}H NMR spectral data given above, the integrations of 1H of each of compounds **4**, **5$_{enol}$**, **6** and **7** relative to 1H of compound **4** are as follows:

$$I_{\mathbf{4}} = 1.00; \quad I_{\mathbf{5}} = \frac{1.16}{3} = 0.386; \quad I_{\mathbf{6}} = \frac{0.37}{6} = 0.062; \quad I_{\mathbf{7}} = \frac{0.10}{2} = 0.05$$

where $I_{\mathbf{X}}$ is the integration of 1H of compound **X** (**X** = **4**, **5$_{enol}$**, **6**, or **7**) relative to 1H of compound **4**. Since $I_{\mathbf{X}} \propto [\mathbf{X}]$ (concentration of **X** in mol L^{-1}), the percentage of O-alkylation is given by:

$$\text{Percentage of O-alkylation} = \frac{I_{\mathbf{4}}}{I_{\mathbf{4}} + I_{\mathbf{5}} + I_{\mathbf{6}} + I_{\mathbf{7}}} \times 100$$

[a] The relevant ^{1}H NMR spectra are shown in Figure B5 and Figure B6 in Appendix B.

[b] Signals of **4 - 7** that are overlapping with other signals: δ 2.71 – 2.56 (m, contains 4H of **6** and signals of DBU and derivatives), 2.31 – 2.07 (m, contains 2H of **4**, 4H of **5$_{enol}$**, 4H of **7** and signals of DBU and derivatives), 1.99 – 1.76 (m, contains 2H of **4**, 4H of **5$_{enol}$**, 2H of **6**, 4H of **7** and signals of DBU and derivatives), 1.73 – 1.53 (m, contains 4H of **6** and signals of DBU and derivatives), 1.32 – 1.21 (m, contains 3H of **4** and 3H of **7**).

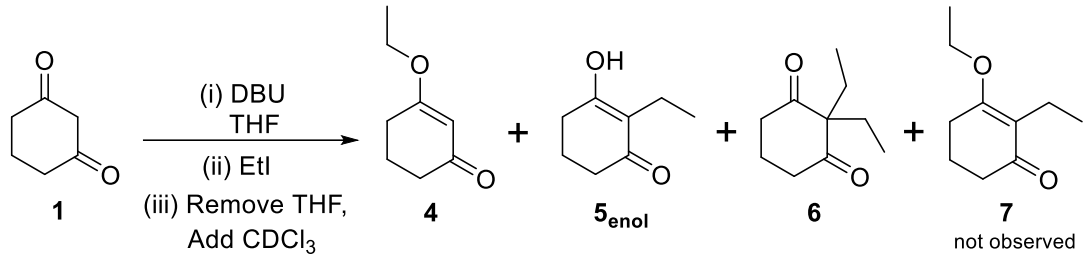
[c] No literature data is available for this compound, which was formed in very low quantities (*ca*. 4%). Assignments of NMR signals were made by analogy with analogue 2-ethyl-2-methyl-cyclohexan-1,3-dione in $CDCl_3$: δ 2.77-2.58 (4H, m), 2.10-1.97 (1H, m), 1.92-1.77 (3H, m), 1.21 (3H, s), <u>0.80</u> (3H, t, *J* = 7.5 Hz).[5] Assignment of this signal was assisted by analysis of COSY NMR spectra, HSQC NMR spectra and HMBC NMR spectra of the crude reaction mixture.

[d] No literature data is available for this compound, which was formed in very low quantities (*ca*. 3%). Assignments of NMR signals were made by analogy with analogue 3-ethoxy-2-methylcyclohex-2-en-1-one in $CDCl_3$: δ <u>4.05</u> (q, *J* = 7.0 Hz, 2H), 2.55 – 2.52 (m, 2H), 2.35 – 2.30 (m, 2H), 1.96 (quint., *J* = 6.3 Hz, 2H), 1.69 (t, <u>*J*</u> = 1.6 Hz, 3H), 1.34 (t, *J* = 7.0 Hz, 3H).[6] Assignment of this signal was assisted by analysis of ^{1}H – ^{1}H COSY NMR spectra, ^{1}H – ^{13}C HSQC NMR spectra and ^{1}H – ^{13}C HMBC NMR spectra of the crude reaction mixture.

$$= \frac{1.00}{1.00 + 0.386 + 0.062 + 0.05} \times \ 100 = 67\%$$

Integrations give an O vs C ratio of 67:33

(iii) Reaction of Enolate 3-D with EtI in THF



From 1,3-cyclohexanedione (**1**) (0.025 g, 0.22 mmol), DBU (**2**) (0.032 g, 0.21 mmol) and ethyl iodide (0.048 g, 0.30 mmol) in THF by procedure C.

^{1}H NMR (400 MHz, $CDCl_3$) of crude mixture of alkylation products (the underlined integrations are expressed relative to 1H of compound **4**): [a,b]

Assigned to **4**: δ 5.33 (1H, C=C<u>H</u>), 3.91 (2H, OC<u>H</u>$_2$CH$_3$), 1.36 (3H, OCH$_2$C<u>H</u>$_3$). [a 3]

Assigned to **5$_{enol}$**: δ 0.97 – 0.88 (0.18H, C-CH$_2$C<u>H</u>$_3$ (3H of compound **5$_{enol}$**)). [a 4]

Assigned to **6**: δ 0.78 – 0.71 (0.02H, C-CH$_2$C<u>H</u>$_3$ (6H of compound **6**)). [a,c]

Based on the ^{1}H NMR spectral data given above, the integrations of 1H of each of compounds **4**, **5$_{enol}$**, and **6** relative to 1H of compound **4** are as follows:

$$I_4 \ = 1.00; \quad I_5 = \frac{0.18}{3} \ = 0.06; \quad I_6 = \ \frac{0.02}{6} \ = 0.003$$

where I_X is the integration of 1H of compound **X** (**X** = **4**, **5$_{enol}$** or **6**) relative to 1H of compound **4**. Since $I_X \propto [\mathbf{X}]$ (concentration of **X** in mol L^{-1}), the percentage of O-alkylation is given by:

$$\text{Percentage of O-alkylation} = \frac{I_4}{I_4 + I_5 + I_6} \times \ 100$$

$$= \frac{1.00}{1.00 + 0.06 + 0.003} \times \ 100 = 94\%$$

Integrations give an O vs C ratio of 94:6

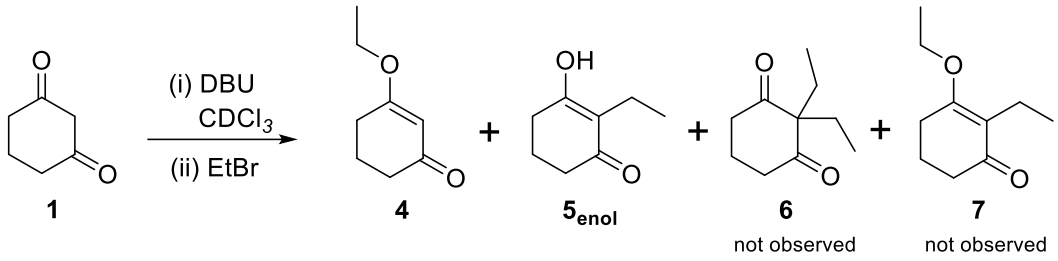
[a] The relevant ^{1}H NMR spectra are shown in Figure B7 and Figure B8 in Appendix B. The signals in the spectra are poorly resolved and hence the multiplicities of each signal are not reported for this reaction.

[b] Signals of **4 - 6** that are overlapping with other signals: δ 2.43 – 2.30 (m, contains 4H of **5** and 4H of **5$_{enol}$**), 2.03 – 1.93 (m, contains 2H of **4**, 4H of **5$_{enol}$** and 2H of **6**), 1.87 – 1.70 (m, contains 4H of **6** and signals of DBU and derivatives).

[c] No literature data is available for this compound, which was formed in very low quantities (*ca.* < 1%). Assignments of NMR signals were made by analogy with analogue 2-ethyl-2-methyl-cyclohexan-1,3-dione in $CDCl_3$: δ 2.77-2.58 (4H, m), 2.10-1.97 (1H, m), 1.92-1.77 (3H, m), 1.21 (3H, s), 0.80 (3H, t, *J* = 7.5 Hz).[5] Assignment of this signal was assisted by analysis of ^{1}H – ^{1}H COSY NMR spectra, ^{1}H – ^{13}C HSQC NMR spectra and ^{1}H – ^{13}C HMBC NMR spectra of the crude reaction mixture.

5.3.2. Reactions of the 1,3-Cyclohexanedione-Derived Enolate 3-D with EtBr

(i) Reaction of Enolate 3-D with EtBr in $CDCl_3$



From 1,3-cyclohexanedione (**1**) (0.0273 g, 0.243 mmol), DBU (**2**) (0.0368 g, 0.241 mmol) and ethyl bromide (0.0293 g, 0.269 mmol) in $CDCl_3$ by procedure A at 0 °C.

^{1}H NMR (300 MHz, $CDCl_3$) of crude mixture of alkylation products (the underlined integrations are expressed relative to 1H of compound **4**): [a,b]

Assigned to **4**: δ 5.34 (s, 1H, C=C<u>H</u>), 3.91 (q, *J* = 7.0 Hz, 2H, OC<u>H</u>$_2$CH$_3$), 2.42 (t, *J* = 6.3 Hz, 2H, C<u>H</u>$_2$C=C), 1.37 (t, *J* = 7.0 Hz, 3H, OCH$_2$C<u>H</u>$_3$). [3]

Assigned to **5$_{enol}$**: δ 0.92 (t, *J* = 7.4 Hz, 0.19H, C-CH$_2$C<u>H</u>$_3$ (3H of compound **5$_{enol}$**)). [4]

Based on the ^{1}H NMR spectral data given above, the integrations of 1H of each of compounds **4** and **5$_{enol}$** relative to 1H of compound **4** are as follows:

$$I_{\mathbf{4}} = 1.00; \quad I_{\mathbf{5}} = \frac{0.19}{3} = 0.063$$

where $I_{\mathbf{X}}$ is the integration of 1H of compound **X** (**X** = **4** or **5$_{enol}$**) relative to 1H of compound **4**. Since $I_{\mathbf{X}} \propto [\mathbf{X}]$ (concentration of **X** in mol L^{-1}), the percentage of O-alkylation is given by:

$$\text{Percentage of O-alkylation} = \frac{I_{\mathbf{4}}}{I_{\mathbf{4}} + I_{\mathbf{5}}} \times 100$$

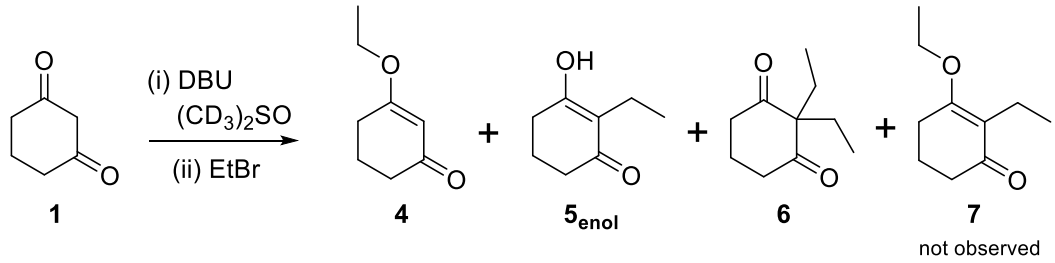
$$= \frac{1.00}{1.00 + 0.063} \times 100 = 94\%$$

Integrations give an <u>O vs C</u> ratio of 94:6

[a] The relevant ^{1}H NMR spectra are shown in Figure B9 and Figure B10 in Appendix B.

[b] Signals of **4 - 5** that are overlapping with other signals: δ 2.37 – 2.31 (m, contains 2H of **4** and 4H of **5$_{enol}$**), 2.03 – 1.94 (m, contains 2H of **4** and 4H of **5$_{enol}$**).

(ii) Reaction of Enolate 3-D with EtBr in $(CD_3)_2SO$



From 1,3-cyclohexanedione (**1**) (0.0244 g, 0.217 mmol), DBU (**2**) (0.032 g, 0.210 mmol) and ethyl bromide (0.0238 g, 0.218 mmol) in $(CD_3)_2SO$ by procedure B at 20 °C.

^{1}H NMR (400 MHz, $(CD_3)_2SO$) of crude mixture of alkylation products (the underlined integrations are expressed relative to 1H of compound **4**): [a,b]

Assigned to **4**: δ 5.27 (s, 1H, C=C<u>H</u>), 3.90 (q, *J* = 7.0 Hz, 2H, OC<u>H</u>$_2$CH$_3$), 2.37 (t, *J* = 6.1 Hz, 2H, C<u>H</u>$_2$C=C), 1.27 (t, *J* = 7.0 Hz, 3H, OCH$_2$C<u>H</u>$_3$). [3]

Assigned to **5enol**: δ 0.78 (t, *J* = 7.3 Hz, 0.40H, C-CH$_2$C<u>H</u>$_3$ (3H of compound **5enol**). [4]

Assigned to **6**: δ 0.64 (t, *J* = 7.3 Hz, 0.02H, C-CH$_2$C<u>H</u>$_3$ (6H of compound **6**)). [c]

Based on the ^{1}H NMR spectral data given above, the integrations of 1H of each of compounds **4**, **5enol**, and **6** relative to 1H of compound **4** are as follows:

$$I_{\mathbf{4}} = 1.00; \quad I_{\mathbf{5}} = \frac{0.40}{3} = 0.13; \quad I_{\mathbf{6}} = \frac{0.02}{6} = 0.003$$

where $I_{\mathbf{X}}$ is the integration of 1H of compound **X** (**X** = **4**, **5enol** or **6**) relative to 1H of compound **4**. Since $I_{\mathbf{X}} \propto [\mathbf{X}]$ (concentration of **X** in mol L^{-1}), the percentage of O-alkylation is given by:

$$\text{Percentage of O-alkylation} = \frac{I_{\mathbf{4}}}{I_{\mathbf{4}} + I_{\mathbf{5}} + I_{\mathbf{6}}} \times 100$$

$$= \frac{1.00}{1.00 + 0.13 + 0.003} \times 100 = 88\%$$

Integrations give an <u>O vs C</u> ratio of 88:12

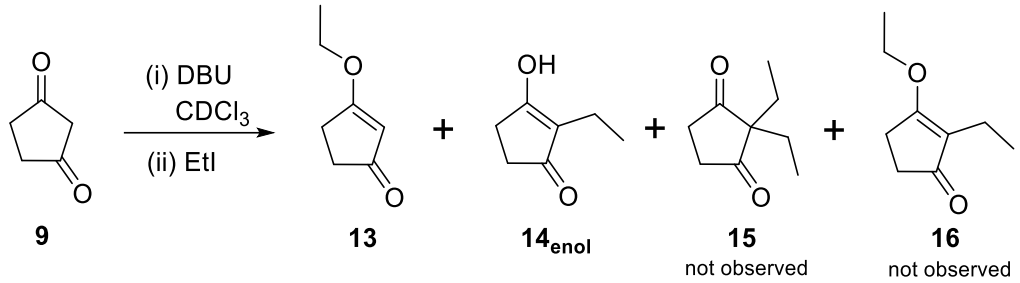
[a] The relevant ^{1}H NMR spectra are shown in Figure B11 and Figure B12 in Appendix B.

[b] Signals of **4 - 6** that are overlapping with other signals: δ 2.75 – 2.61 (m, contains 4H of **6** and signals of DBU and derivatives), 2.24 – 2.06 (m, contains 2H of **4** and 4H of **5enol**), 1.95 – 1.82 (m, contains 2H of **4**, 4H of **5enol**, 2H of **6** and signals of DBU and derivatives), 1.78 – 1.55 (m, contains 4H of **6** and signals of DBU and derivatives).

[c] No literature data is available for this compound, which was formed in very low quantities (*ca.* > 1%). Assignments of NMR signals were made by analogy with analogue 2-ethyl-2-methyl-cyclohexan-1,3-dione in $CDCl_3$: δ 2.77-2.58 (4H, m), 2.10-1.97 (1H, m), 1.92-1.77 (3H, m), 1.21 (3H, s), <u>0.80</u> (3H, t, *J* = 7.5 Hz).[5] Assignment of this signal was assisted by analysis of ^{1}H – ^{1}H COSY NMR spectra, ^{1}H – ^{13}C HSQC NMR spectra and ^{1}H – ^{13}C HMBC NMR spectra of the crude reaction mixture.

5.3.3. Reactions of the 1,3-Cyclopentanedione-Derived Enolate 12-D with EtI

(i) Reaction of Enolate 12-D with EtI in $CDCl_3$



From 1,3-cyclopentanedione (**9**) (0.025 g, 0.25 mmol), DBU (**2**) (0.039 g, 0.26 mmol) and ethyl iodide (0.040 g, 0.26 mmol) in $CDCl_3$ by procedure A at 0 °C.

^{1}H NMR (300 MHz, $CDCl_3$) of crude mixture of alkylation products (the underlined integrations are expressed relative to 1H of compound **13**): [a,b]

Assigned to **13**: δ 5.29 (t, *J* = 1.1 Hz, 1H, C=C<u>H</u>), 4.07 (q, *J* = 7.1 Hz, 2H, OC<u>H</u>$_2$CH$_3$), 2.67 – 2.59 (m, 2H, C<u>H</u>$_2$C=O), 1.42 (t, *J* = 7.1 Hz, 3H, OCH$_2$C<u>H</u>$_3$). [7]

Assigned to **14$_{enol}$**: δ 0.98 (t, *J* = 7.5 Hz, 0.08H, C-CH$_2$C<u>H</u>$_3$ (3H of compound **14$_{enol}$**)).[8]

Based on the ^{1}H NMR spectral data given above, the integrations of 1H of each of compounds **13** and **14$_{enol}$** relative to 1H of compound **13** are as follows:

$$I_{\mathbf{13}} = 1.00; \quad I_{\mathbf{14}} = \frac{0.08}{3} = 0.026$$

where $I_{\mathbf{X}}$ is the integration of 1H of compound **X** (**X** = **13** or **14$_{enol}$**) relative to 1H of compound **13**. Since $I_{\mathbf{X}} \propto [\mathbf{X}]$ (concentration of **X** in mol L^{-1}), the percentage of O-alkylation is given by:

$$\text{Percentage of O-alkylation} = \frac{I_{\mathbf{13}}}{I_{\mathbf{13}} + I_{\mathbf{14}}} \times 100$$

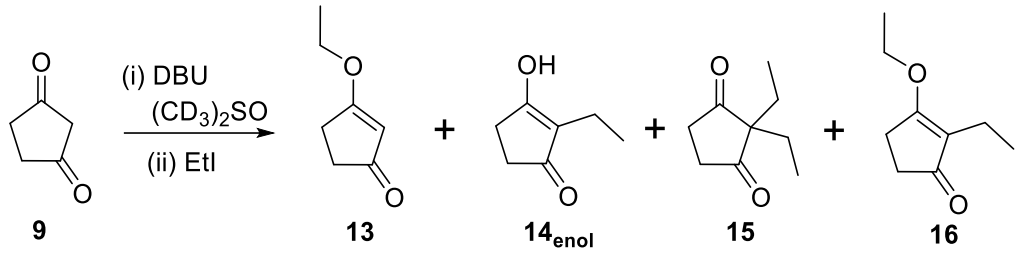
$$= \frac{1.00}{1.00 + 0.026} \times 100 = 97\%$$

Integrations give an <u>O vs C</u> ratio of 97:3

[a] The relevant ^{1}H NMR spectra are shown in Figure B13 and Figure B14 in Appendix B.

[b] Signals of **13 - 14** that are overlapping with other signals: δ 2.47 – 2.40 (m, contains 2H of **13**, 4H of **14$_{enol}$** and signal of starting enolate), 2.17 – 2.07 (m, contains 2H of **14$_{enol}$** and signals of DBU and derivatives).

(ii) Reaction of Enolate 12-D with EtI in $(CD_3)_2SO$



From 1,3-cyclopentanedione (**9**) (0.023 g, 0.24 mmol), DBU (**2**) (0.035 g, 0.23 mmol) and ethyl iodide (0.040 g, 0.25 mmol) in $(CD_3)_2SO$ by procedure B at 20 °C.

^{1}H NMR (400 MHz, $(CD_3)_2SO$) of crude mixture of alkylation products (the underlined integrations are expressed relative to 1H of compound **13**): [a,b]

Assigned to **13**: δ 5.35 (s, 1H, C=C<u>H</u>), 4.07 (q, *J* = 7.0 Hz, 2H, OC<u>H</u>$_2$CH$_3$), 2.32 – 2.25 (m, 2H, C<u>H</u>$_2$C=C). [7]

Assigned to **14$_{enol}$**: δ 0.94 – 0.78 (m, approx. 0.29H, C-CH$_2$C<u>H</u>$_3$ (3H of compound **14$_{enol}$**). [8]

Assigned to **15**: δ 0.66 (t, *J* = 7.5 Hz, 0.04H, C-CH$_2$C<u>H</u>$_3$ (6H of compound **15**)). [9]

Assigned to **16**: δ 4.24 (q, *J* = 7.0 Hz, 0.07H, OC<u>H</u>$_2$CH$_3$ (2H of compound **16**)). [c]

The signal used to obtain the integration of **14$_{enol}$** at 0.94 – 0.78 ppm overlaps with a 2H signal of **16**. The integration value of this set of overlapping signals is 0.29 relative to 1H of **13**. The 2H signal of **16** at 4.24 ppm has a value of 0.07 relative to 1H of **13**. Thus, by subtracting the value associated with 3H of **16** from the integration value of the signal at 0.94 – 0.78 ppm, the approximate integration value of 3H of **14$_{enol}$** can be established. (0.29 – 0.11) = 0.18. Therefore 0.18 is the contribution of 3H of **14$_{enol}$** to the signal at 0.94 – 0.78 ppm. This indicates that 1H of **14$_{enol}$** equals 0.06 integration units relative to 1H of **13**.

Based on the ^{1}H NMR spectral data given above, the integrations of 1H of each of compounds **13**, **14$_{enol}$**, **15** and **16** relative to 1H of compound **13** are as follows:

$$I_{\mathbf{13}} = 1.00; \quad I_{\mathbf{14}} = 0.06; \quad I_{\mathbf{15}} = \frac{0.04}{6} = 0.006; \quad I_{\mathbf{16}} = \frac{0.07}{2} = 0.035$$

where $I_{\mathbf{X}}$ is the integration of 1H of compound **X** (**X** = **13**, **14$_{enol}$**, **15** or **16**) relative to 1H of compound **13**. Since $I_{\mathbf{X}} \propto [\mathbf{X}]$ (concentration of **X** in mol L^{-1}), the percentage of O-alkylation is given by:

[a] The relevant ^{1}H NMR spectra are shown in Figure B15 and Figure B16 in Appendix B.

[b] Signals of **13 - 16** that are overlapping with other signals: δ 2.76 – 2.60 (m, contains 4H of **15** and signals of DBU and derivatives), 2.58 – 2.53 (m, contains 2H of **13**, 4H of **14$_{enol}$** and signal of (CD$_2$<u>H</u>)(CD$_3$)SO), 2.15 – 2.00 (m, contains 2H of **14$_{enol}$**), 1.78 – 1.55 (m, contains 4H of **15** and signals of DBU and derivatives), 1.35 – 1.24 (m, contains 3H of **13** and 3H of **16**). 0.94 – 0.78 (m, contains 3H of **14$_{enol}$** and 3H of **16**).

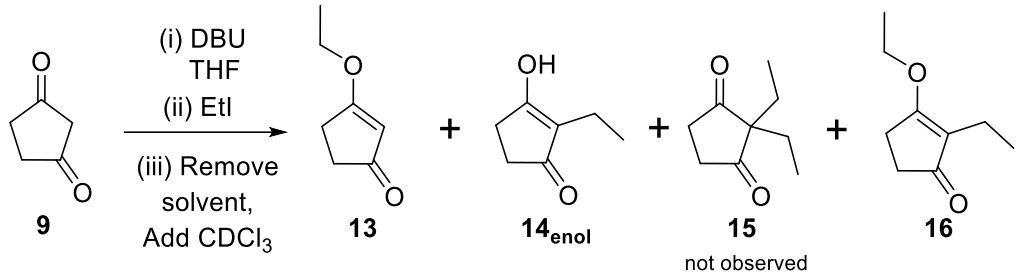
[c] No literature data is available for this compound, which was formed in very low quantities (*ca*. 3%). Assignments of NMR signals were made by analogy with analogue 3-ethoxy-2-methyl-2-cyclopenten-1-one in CCl_4: δ <u>4.22</u> (2H, q, *J* = 6.5 Hz), 1.50 (3H, br s) and 1.32 (3H, d, *J* = 6.5 Hz).[10] Assignment of this signal was assisted by analysis of ^{1}H – ^{1}H COSY NMR spectra, ^{1}H – ^{13}C HSQC NMR spectra and ^{1}H – ^{13}C HMBC NMR spectra of the crude reaction mixture.

$$\text{Percentage of O-alkylation} = \frac{I_{13}}{I_{13} + I_{14} + I_{15} + I_{16}} \times 100$$

$$= \frac{1.00}{1.00 + 0.06 + 0.006 + 0.035} \times 100 = 91\%$$

Integrations give an O vs C ratio of 91:9

(iii) Reaction of Enolate 12-D with EtI in THF



From 1,3-cyclopentanedione (**9**) (0.023 g, 0.24 mmol), DBU (**2**) (0.035 g, 0.23 mmol) and ethyl iodide (0.040 g, 0.25 mmol) in THF by procedure C.

^{1}H NMR (300 MHz, $CDCl_3$) of crude mixture of alkylation products (the underlined integrations are expressed relative to 1H of compound **13**): [a,b]

Assigned to **13**: δ 5.30 (t, *J* = 1.1 Hz, 1H, C=C<u>H</u>), 4.08 (q, *J* = 7.1 Hz, 2H, OC<u>H</u>$_2$CH$_3$), 2.66 – 2.61 (m, 2H, C<u>H</u>$_2$C=O). [7]

Assigned to **14$_{enol}$**: δ 0.98 (t, *J* = 7.5 Hz, 0.04H, C-CH$_2$C<u>H</u>$_3$ (3H of compound **14$_{enol}$**)).[8]

Assigned to **16**: δ 4.25 (m, 0.03H, OC<u>H</u>$_2$CH$_3$ (2H of compound **16**)). [c]

Based on the ^{1}H NMR spectral data given above, the integrations of 1H of each of compounds **13**, **14$_{enol}$**, and **16** relative to 1H of compound **13** are as follows:

$$I_{13} = 1.00; \quad I_{14} = \frac{0.04}{3} = 0.013; \quad I_{16} = \frac{0.03}{2} = 0.015$$

where $I_{\mathbf{X}}$ is the integration of 1H of compound **X** (**X** = **13**, **14$_{enol}$** or **16**) relative to 1H of compound **13**. Since $I_{\mathbf{X}} \propto [\mathbf{X}]$ (concentration of **X** in mol L^{-1}), the percentage of O-alkylation is given by:

$$\text{Percentage of O-alkylation} = \frac{I_{13}}{I_{13} + I_{14} + I_{16}} \times 100$$

$$= \frac{1.00}{1.00 + 0.013 + 0.015} \times 100 = 97\%$$

Integrations give an O vs C ratio of 97:3

---

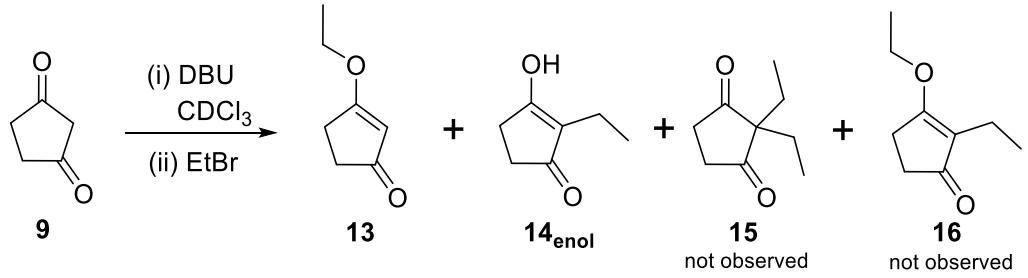
[a] The relevant ^{1}H NMR spectra are shown in Figure B17 and Figure B18 in Appendix B.

[b] Signals of **13 - 16** that are overlapping with other signals: δ 2.47 – 2.40 (m, contains 2H of **13** and 4H of **14$_{enol}$**), 2.18 – 2.07 (m, contains 2H of **14$_{enol}$** and signals of DBU and derivatives), 1.46 – 1.38 (m, contains 3H of **13** and 3H of **16**).

[c] No literature data is available for this compound, which was formed in very low quantities (*ca*. 1%). Assignments of NMR signals were made by analogy with analogue 3-ethoxy-2-methyl-2-cyclopenten-1-one in CCl_4: δ <u>4.22</u> (2H, q, *J* = 6.5 Hz), 1.50 (3H, br s) and 1.32 (3H, d, *J* = 6.5 Hz).[10] Assignment of this signal was assisted by analysis of COSY NMR spectra, HSQC NMR spectra and HMBC NMR spectra of the crude reaction mixture.

5.3.4. Reactions of the 1,3-Cyclopentanedione-Derived Enolate 12-D with EtBr

(i) Reaction of Enolate 12-D with EtBr in $CDCl_3$



From 1,3-cyclopentanedione (**9**) (0.0268 g, 0.273 mmol), DBU (**2**) (0.0411 g, 0.270 mmol) and ethyl bromide (0.0336 g, 0.308 mmol) in $CDCl_3$ by procedure A at 0 °C.

^{1}H NMR (300 MHz, $CDCl_3$) of crude mixture of alkylation products (the underlined integrations are expressed relative to 1H of compound **13**): [a,b]

Assigned to **13**: δ 5.28 (app. d, app. *J* = 1.0 Hz, 0.40H, C=C<u>H</u>), 4.07 (q, *J* = 7.1 Hz, 2H, OC<u>H</u>$_2$CH$_3$), 2.67 – 2.59 (m, 2H, C<u>H</u>$_2$C=O), 2.46 – 2.39 (m, 2H, C<u>H</u>$_2$C=C), 1.42 (t, *J* = 7.1 Hz, 3H, OCH$_2$C<u>H</u>$_3$). [7]

Assigned to **14$_{enol}$**: δ 1.04 – 0.92 (m, 0.14H, C-CH$_2$C<u>H</u>$_3$ (3H of compound **14$_{enol}$**)). [8]

Based on the ^{1}H NMR spectral data given above, the integrations of 1H of each of compounds **13** and **14$_{enol}$** relative to 1H of compound **13** are as follows:

$$I_{\mathbf{13}} = \frac{2.00}{2} = 1.00; \quad I_{\mathbf{14}} = \frac{0.14}{3} = 0.046$$

where $I_{\mathbf{X}}$ is the integration of 1H of compound **X** (**X** = **13** or **14$_{enol}$**) relative to 1H of compound **13**. Since $I_{\mathbf{X}} \propto [\mathbf{X}]$ (concentration of **X** in mol L^{-1}), the percentage of O-alkylation is given by:

$$\text{Percentage of O-alkylation} = \frac{I_{\mathbf{13}}}{I_{\mathbf{13}} + I_{\mathbf{14}}} \times 100$$

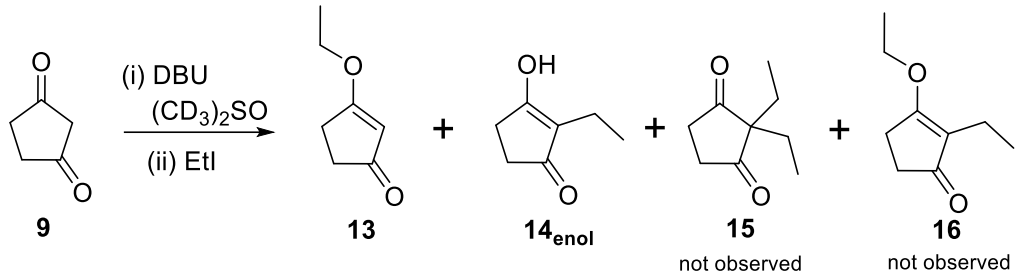
$$= \frac{1.00}{1.00 + 0.046} \times 100 = 96\%$$

Integrations give an <u>O vs C</u> ratio of 96:4

[a] The relevant ^{1}H NMR spectra are shown in Figure B19 and Figure B20 in Appendix B.

[b] Signals of **13 - 14** that are overlapping with other signals: δ 2.46 – 2.39 (m, contains 2H of **13** and 4H of **14$_{enol}$**), 2.12 – 2.02 (m, contains 2H of **14$_{enol}$** and signals of DBU and derivatives).

(ii) Reaction of Enolate 12-D with EtBr in $(CD_3)_2SO$



From 1,3-cyclopentanedione (**9**) (0.0274 g, 0.279 mmol), DBU (**2**) (0.0418 g, 0.274 mmol) and ethyl bromide (0.0335 g, 0.307 mmol) in $(CD_3)_2SO$ by procedure B at 20 °C.

^{1}H NMR (400 MHz, $(CD_3)_2SO$) of crude mixture of alkylation products (the underlined integrations are expressed relative to 1H of compound **13**): [a,b]

Assigned to **13**: δ 5.36 (s, 1H, C=C<u>H</u>), 4.07 (q, *J* = 7.0 Hz, 2H, OC<u>H</u>$_2$CH$_3$), 2.32 – 2.25 (m, 2H, C<u>H</u>$_2$C=C), 1.30 (t, *J* = 7.0, Hz, 3H, OCH$_2$C<u>H</u>$_3$). [11]

Assigned to **14$_{enol}$**: 0.79 (t, *J* = 7.4 Hz, 0.06H, C-CH$_2$C<u>H</u>$_3$ (3H of compound **14$_{enol}$**). [8]

Based on the ^{1}H NMR spectral data given above, the integrations of 1H of each of compounds **13** and **14$_{enol}$** relative to 1H of compound **13** are as follows:

$$I_{\mathbf{13}} = 1.00; \quad I_{\mathbf{14}} = \frac{0.06}{3} = 0.02$$

where $I_{\mathbf{X}}$ is the integration of 1H of compound **X** (**X** = **13** or **14$_{enol}$**) relative to 1H of compound **13**. Since $I_{\mathbf{X}} \propto [\mathbf{X}]$ (concentration of **X** in mol L^{-1}), the percentage of O-alkylation is given by:

$$\text{Percentage of O-alkylation} = \frac{I_{\mathbf{13}}}{I_{\mathbf{13}} + I_{\mathbf{14}}} \times 100$$

$$= \frac{1.00}{1.00 + 0.02} \times 100 = 98\%$$

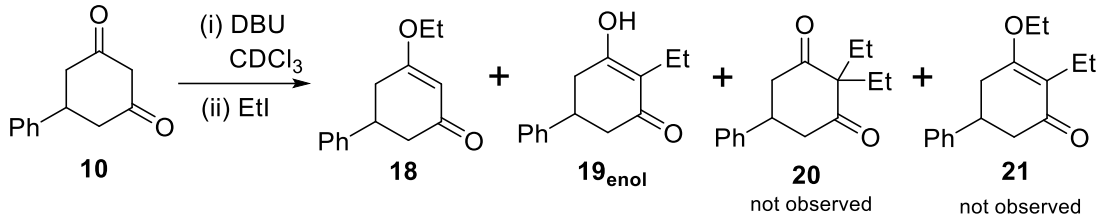
Integrations give an <u>O vs C</u> ratio of 98:2

[a] The relevant ^{1}H NMR spectra are shown in Figure B21 and Figure B22 in Appendix B.

[b] Signals of **13 - 14** that are overlapping with other signals: δ 2.59 – 2.53 (m, contains 2H of **13**, 4H of **14$_{enol}$** and signal of (CD$_2$<u>H</u>)(CD$_3$)SO), 1.94 – 1.85 (m, contains 2H of **14$_{enol}$** and signals of DBU and derivatives).

5.3.5. Reactions of the 5-Phenylcyclohexan-1,3-dione-Derived Enolate 17-D with EtI

(i) Reaction of Enolate 17-D with EtI in $CDCl_3$



From 5-phenylcyclohexan-1,3-dione (**10**) (0.028 g, 0.15 mmol), DBU (**2**) (0.023 g, 0.15 mmol) and ethyl iodide (0.023 g, 0.15 mmol) in $CDCl_3$ by procedure A at 0 °C.

^{1}H NMR (300 MHz, $CDCl_3$) of crude mixture of alkylation products (the underlined integrations are expressed relative to 1H of compound **18**): [a,b]

Assigned to **18**: δ 5.43 (s, 0.38H, C=C<u>H</u>), 4.01 – 3.89 (m, 2H, OC<u>H</u>$_2$CH$_3$), 1.38 (t, *J* = 7.0 Hz, 3H, OCH$_2$C<u>H</u>$_3$). [12]

Assigned to **19$_{enol}$**: δ 0.96 (t, *J* = 7.3 Hz, 0.24H, C-CH$_2$C<u>H</u>$_3$ (3H of compound **19$_{enol}$**)). [13]

Based on the ^{1}H NMR spectral data given above, the integrations of 1H of each of compounds **18** and **19$_{enol}$** relative to 1H of compound **18** are as follows:

$$I_{\mathbf{18}} = \frac{2.00}{2} = 1.00; \quad I_{\mathbf{19}} = \frac{0.24}{3} = 0.08$$

where $I_{\mathbf{X}}$ is the integration of 1H of compound **X** (**X** = **18** or **19$_{enol}$**) relative to 1H of compound **18**. Since $I_{\mathbf{X}} \propto [\mathbf{X}]$ (concentration of **X** in mol L^{-1}), the percentage of O-alkylation is given by:

$$\text{Percentage of O-alkylation} = \frac{I_{\mathbf{18}}}{I_{\mathbf{18}} + I_{\mathbf{19}}} \times 100$$

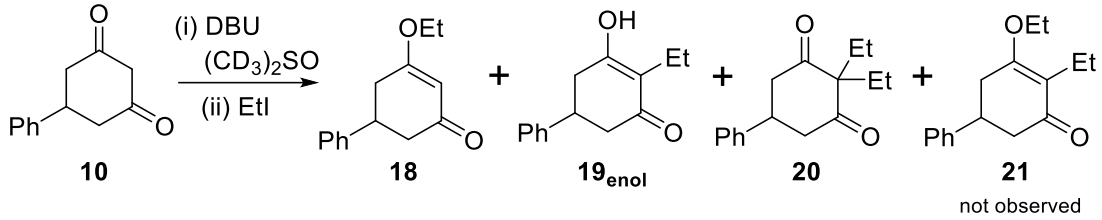
$$= \frac{1.00}{1.00 + 0.08} \times 100 = 93\%$$

Integrations give an <u>O vs C</u> ratio of 93:7

[a] The relevant ^{1}H NMR spectra are shown in Figure B23 and Figure B24 in Appendix B.

[b] Signals of **18 - 19** that are overlapping with other signals: δ 7.38 – 7.14 (m, contains 5H of **18**, 5H of **19$_{enol}$** and $CHCl_3$ signal), 3.41 – 3.29 (m, contains 1H of **18**, 1H of **19$_{enol}$** and signals of DBU and derivatives), 2.70 – 2.42 (m, contains 4H of **18** and 6H of **19$_{enol}$**).

(ii) Reaction of Enolate 17-D with EtI in $(CD_3)_2SO$



From 5-phenylcyclohexan-1,3-dione (**10**) (0.025 g, 0.13 mmol), DBU (**2**) (0.019 g, 0.13 mmol) and ethyl iodide (0.022 g, 0.14 mmol) in $(CD_3)_2SO$ by procedure B at 20 °C.

^{1}H NMR (400 MHz, $(CD_3)_2SO$) of crude mixture of alkylation products (the underlined integrations are expressed relative to 1H of compound **18**): [a,b]

Assigned to **18**: δ 5.39 (s, 1H, C=C<u>H</u>), 4.00 – 3.91 (m, 2H, OC<u>H</u>$_2$CH$_3$). [12]

Assigned to **19$_{enol}$**: δ 0.87 (t, *J* = 7.4 Hz, 0.04H, C-CH$_2$C<u>H</u>$_3$ (3H of compound **19$_{enol}$**)). [13]

Assigned to **20**: δ 0.71 – 0.63 (m, 0.39H, contains δ 0.69 (t, *J* = 7.3 Hz) and 0.65 (t, *J* = 7.5 Hz), 2 × diastereotopic C-CH$_2$C<u>H</u>$_3$ (6H of compound **20**)). [c]

Based on the ^{1}H NMR spectral data given above, the integrations of 1H of each of compounds **18**, **19$_{enol}$**, and **20** relative to 1H of compound **18** are as follows:

$$I_{\mathbf{18}} = 1.00; \quad I_{\mathbf{19}} = \frac{0.04}{3} = 0.013; \quad I_{\mathbf{20}} = \frac{0.39}{6} = 0.065$$

where $I_{\mathbf{X}}$ is the integration of 1H of compound **X** (**X** = **18**, **19$_{enol}$** or **20**) relative to 1H of compound **18**. Since $I_{\mathbf{X}} \propto [\mathbf{X}]$ (concentration of **X** in mol L^{-1}), the percentage of O-alkylation is given by:

$$\text{Percentage of O-alkylation} = \frac{I_{\mathbf{18}}}{I_{\mathbf{18}} + I_{\mathbf{19}} + I_{\mathbf{20}}} \times 100$$

$$= \frac{1.00}{1.00 + 0.013 + 0.065} \times 100 = 93\%$$

Integrations give an <u>O vs C</u> ratio of 93:7

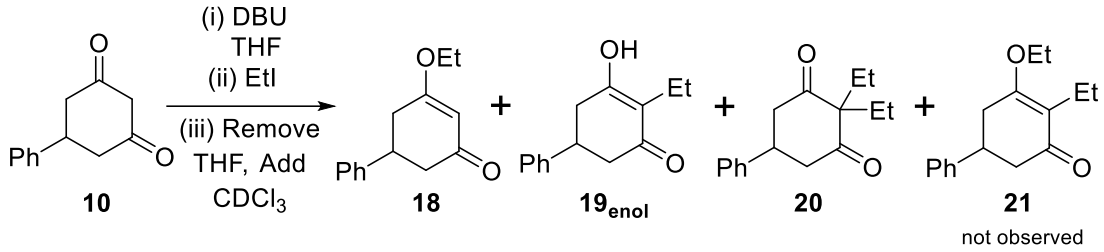
---

[a] The relevant ^{1}H NMR spectra are shown in Figure B25 and Figure B26 in Appendix B.

[b] Signals of **18 - 20** that are overlapping with other signals: δ 7.42 – 7.13 (m, contains 5H of **18**, 5H of **19$_{enol}$** and 10H of **20**), 3.40 – 3.20 (m, contains 1H of **18**, 1H of **19$_{enol}$**, 1H of **20** and signals of DBU and derivatives), 2.79 – 2.31 (m, contains 4H of **18**, 6H of **19$_{enol}$**, 4H of **20**, signals of DBU and derivatives and signal of (CD$_2$<u>H</u>)(CD$_3$)SO), 1.82 – 1.54 (m, contains 4H of **20** and signals of DBU and derivatives).

[c] No literature data is available for this compound, which was formed in very low quantities (*ca*. 6%). Assignments of NMR signals were made by analogy with analogue *cis*-2-ethyl-2-methyl-5-phenylcyclohexan-1,3-dione in $CDCl_3$: δ 7.44-7.33 (m, 2H), 7.32-7.19 (m, 3H), 3.17-2.96 (m, 3H), 2.90-2.67 (m, 2H), 1.93 (q, *J* = 7.4 Hz, 2H), 1.25 (s, 3H), <u>0.85</u> (t, *J* = 7.5 Hz, 3H).[14] Assignment of this signal was assisted by analysis of ^{1}H – ^{1}H COSY NMR spectra, ^{1}H – ^{13}C HSQC NMR spectra and ^{1}H – ^{13}C HMBC NMR spectra of the crude reaction mixture.

(iii) Reaction of Enolate 17-D with EI in THF



From 5-phenylcyclohexan-1,3-dione (**10**) (0.025 g, 0.13 mmol), DBU (**2**) (0.019 g, 0.13 mmol) and ethyl iodide (0.022 g, 0.14 mmol) in THF by procedure C.

^{1}H NMR (400 MHz, $CDCl_3$) of crude mixture of alkylation products (the underlined integrations are expressed relative to 1H of compound **18**): [a,b]

Assigned to **18**: δ 5.43 (s, 1H, C=C<u>H</u>), 4.03 – 3.87 (m, 2H, $OC\underline{H}_2CH_3$), 1.38 (t, *J* = 7.0 Hz, 3H, $OCH_2C\underline{H}_3$). [12]

Assigned to **19$_{keto}$** + **19$_{enol}$**: δ 0.98 – 0.92 (m, 0.13H, contains 2 × t (*J* = 7.4 Hz for each) C-$CH_2C\underline{H}_3$ of each of **19$_{keto}$** and **19$_{enol}$** (3H of each of compound **19$_{keto}$** and compound **19$_{enol}$**)). [13]

Assigned to **20**: δ 0.80 (m, 0.05H, contains δ 0.80 (t, *J* = 7.3 Hz) and 0.79 (t, *J* = 7.5 Hz), 2 × diastereotopic C-$CH_2C\underline{H}_3$ (6H of compound **20**)). [c]

Based on the ^{1}H NMR spectral data given above, the integrations of 1H of each of compounds **18**, **19**, and **20** relative to 1H of compound **18** are as follows:

$$I_{\mathbf{18}} = 1.00; \quad I_{\mathbf{19}} = \frac{0.13}{3} = 0.043; \quad I_{\mathbf{20}} = \frac{0.05}{6} = 0.0083$$

where $I_{\mathbf{X}}$ is the integration of 1H of compound **X** (**X** = **18**, **19** or **20**) relative to 1H of compound **18**. Since $I_{\mathbf{X}} \propto [\mathbf{X}]$ (concentration of **X** in mol L^{-1}), the percentage of O-alkylation is given by:

$$\text{Percentage of O-alkylation} = \frac{I_{\mathbf{18}}}{I_{\mathbf{18}} + I_{\mathbf{19}} + I_{\mathbf{20}}} \times 100$$

$$= \frac{1.00}{1.00 + 0.043 + 0.0083} \times 100 = 95\%$$

Integrations give an <u>O vs C</u> ratio of 95:5

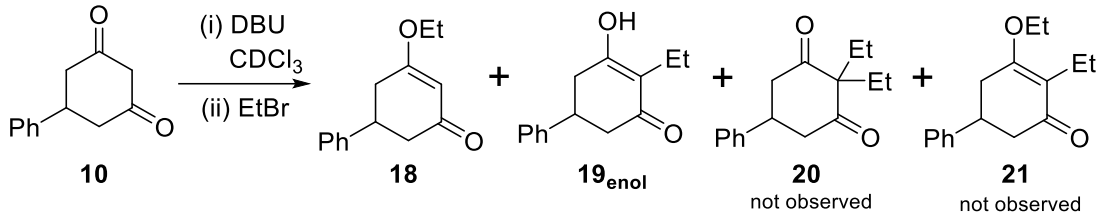
[a] The relevant ^{1}H NMR spectra are shown in Figure B27 and Figure B28 in Appendix B.

[b] Signals of **18 - 20** that are overlapping with other signals: δ 7.40 – 7.19 (m, contains 5H of **18**, 5H of **19$_{enol}$** and 10H of **20**), 3.43 – 3.28 (m, contains 1H of **18**, 1H of **19$_{enol}$** and 1H of **20**), 2.75 – 2.49 (m, contains 4H of **18**, 4H of **19$_{enol}$** and 4H of **20**), 1.91 – 1.69 (m, contains 4H of **20** and signals of DBU and derivatives).

[c] No literature data is available for this compound, which was formed in very low quantities (*ca.* < 1%). Assignments of NMR signals were made by analogy with analogue *cis*-2-ethyl-2-methyl-5-phenylcyclohexan-1,3-dione in $CDCl_3$: δ 7.44-7.33 (m, 2H), 7.32-7.19 (m, 3H), 3.17-2.96 (m, 3H), 2.90-2.67 (m, 2H), 1.93 (q, *J* = 7.4 Hz, 2H), 1.25 (s, 3H), <u>0.85</u> (t, *J* = 7.5 Hz, 3H).[14]

5.3.6. Reactions of the 5-Phenylcyclohexan-1,3-dione-Derived Enolate 17-D with EtBr

(i) Reaction of Enolate 17-D with EtBr in $CDCl_3$



From 5-phenylcyclohexan-1,3-dione (**10**) (0.028 g, 0.15 mmol), DBU (**2**) (0.023 g, 0.15 mmol) and ethyl bromide (0.023 g, 0.15 mmol) in $CDCl_3$ by procedure A at 0 °C.

^{1}H NMR (300 MHz, $CDCl_3$) of crude mixture of alkylation products (the underlined integrations are expressed relative to 1H of compound **18**): [a,b]

Assigned to **18**: δ 5.43 (s, 1H, C=C<u>H</u>), 4.05 – 3.82 (m, 2H, OC<u>H</u>$_2$CH$_3$), 1.38 (t, *J* = 7.0 Hz, 3H, OCH$_2$C<u>H</u>$_3$). [12]

Assigned to **19$_{enol}$**: δ 0.97 (t, *J* = 7.3 Hz, 0.13H, C-CH$_2$C<u>H</u>$_3$ (3H of compound **19$_{enol}$**)). [13]

Based on the ^{1}H NMR spectral data given above, the integrations of 1H of each of compounds **18** and **19$_{enol}$** relative to 1H of compound **18** are as follows:

$$I_{\mathbf{18}} = 1.00; \quad I_{\mathbf{19}} = \frac{0.13}{3} = 0.043$$

where $I_{\mathbf{X}}$ is the integration of 1H of compound **X** (**X** = **18** or **19$_{enol}$**) relative to 1H of compound **18**. Since $I_{\mathbf{X}} \propto [\mathbf{X}]$ (concentration of **X** in mol L^{-1}), the percentage of O-alkylation is given by:

$$\text{Percentage of O-alkylation} = \frac{I_{\mathbf{18}}}{I_{\mathbf{18}} + I_{\mathbf{19}}} \times 100$$

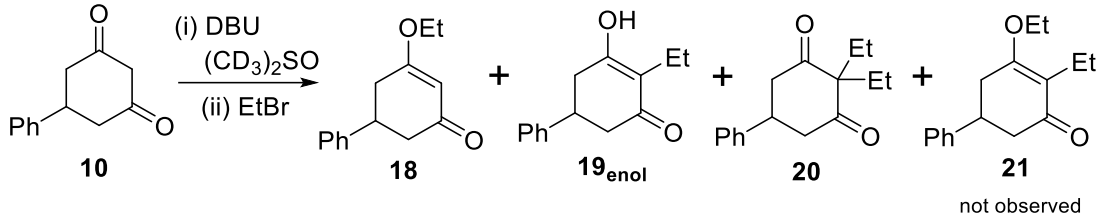
$$= \frac{1.00}{1.00 + 0.043} \times 100 = 96\%$$

Integrations give an <u>O vs C</u> ratio of 96:4

[a] The relevant ^{1}H NMR spectra are shown in Figure B29 and Figure B30 in Appendix B.

[b] Signals of **18 - 19** that are overlapping with other signals: δ 7.40 – 7.15 (m, contains 5H of **18** and 5H of **19$_{enol}$**), 3.46 – 3.27 (m, contains 1H of **18**, 1H of **19$_{enol}$** and signals of DBU and derivatives), 2.71 – 2.45 (m, contains 4H of **18** and 6H of **19$_{enol}$**).

(ii) Reaction of Enolate 17-D with EtBr in $(CD_3)_2SO$



From 5-phenylcyclohexan-1,3-dione (**10**) (0.0292 g, 0.155 mmol), DBU (**2**) (0.0215 g, 0.141 mmol) and ethyl bromide (0.0202 g, 0.185 mmol) in $(CD_3)_2SO$ by procedure B at 20 °C.

^{1}H NMR (400 MHz, $(CD_3)_2SO$) of crude mixture of alkylation products (the underlined integrations are expressed relative to 1H of compound **18**): [a,b]

Assigned to **18**: δ 5.39 (s, 1H, C=C<u>H</u>), 4.02 – 3.88 (m, 2H, OC<u>H</u>$_2$CH$_3$), 1.28 (t, *J* = 7.0 Hz, 3H, OCH$_2$C<u>H</u>$_3$). [12]

Assigned to **19$_{enol}$**: δ 0.80 (t, *J* = 7.3 Hz, 0.37H, C-CH$_2$C<u>H</u>$_3$ (3H of compound **19$_{enol}$**)). [13]

Based on the ^{1}H NMR spectral data given above, the integrations of 1H of each of compounds **18** and **19$_{enol}$** relative to 1H of compound **18** are as follows:

$$I_{\mathbf{18}} = 1.00; \quad I_{\mathbf{19}} = \frac{0.24}{3} = 0.08$$

where $I_{\mathbf{X}}$ is the integration of 1H of compound **X** (**X** = **18** or **19$_{enol}$**) relative to 1H of compound **18**. Since $I_{\mathbf{X}} \propto [\mathbf{X}]$ (concentration of **X** in mol L^{-1}), the percentage of O-alkylation is given by:

$$\text{Percentage of O-alkylation} = \frac{I_{\mathbf{18}}}{I_{\mathbf{18}} + I_{\mathbf{19}}} \times 100$$

$$= \frac{1.00}{1.00 + 0.08} \times 100 = 93\%$$

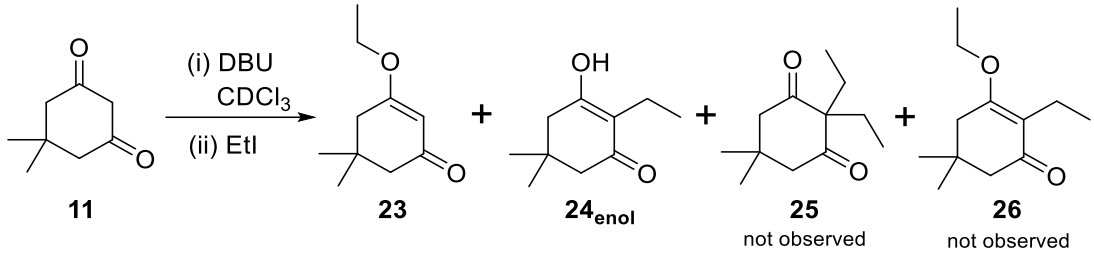
Integrations give an <u>O vs C</u> ratio of 93:7

[a] The relevant ^{1}H NMR spectra are shown in Figure B31 and Figure B32 in Appendix B.

[b] Signals of **18 - 19** that are overlapping with other signals: δ 7.39 – 7.13 (m, contains 5H of **18** and 5H of **19$_{enol}$**), 3.38 – 3.19 (m, contains 1H of **18**, 1H of **19$_{enol}$** and signals of DBU and derivatives), 2.80 – 2.22 (m, contains 4H of **18**, 6H of **19$_{enol}$**, signals of DBU and derivatives and signal of (CD$_2$<u>H</u>)(CD$_3$)SO).

5.3.7. Reactions of the 5,5-Dimethylcyclohexan-1,3-dione-Derived Enolate 22-D with EtI

(i) Reaction of Enolate 22-D with EtI in $CDCl_3$



From 5,5-dimethylcyclohexan-1,3-dione (**11**) (0.030 g, 0.21 mmol), DBU (**2**) (0.030 g, 0.20 mmol) and ethyl iodide (0.034 g, 0.22 mmol) in $CDCl_3$ by procedure A at 0 °C.

^{1}H NMR (300 MHz, $CDCl_3$) of crude mixture of alkylation products (the underlined integrations are expressed relative to 1H of compound **23**): [a,b]

Assigned to **23**: δ 5.33 (s, 1H, C=C<u>H</u>), 3.91 (q, *J* = 7.0 Hz, 2H, OC<u>H</u>$_2$CH$_3$), 2.28 (s, 2H, C<u>H</u>$_2$C=C), 1.37 (t, *J* = 7.0 Hz, 3H, OCH$_2$C<u>H</u>$_3$). [15]

Assigned to **24$_{enol}$**: δ 0.93 (t, *J* = 7.4 Hz, 0.28H, C-CH$_2$C<u>H</u>$_3$ (3H of compound **24$_{enol}$**)). [16]

Based on the ^{1}H NMR spectral data given above, the integrations of 1H of each of compounds **23** and **24$_{enol}$** relative to 1H of compound **23** are as follows:

$$I_{23} = 1.00; \quad I_{24} = \frac{0.28}{3} = 0.093$$

where $I_{\mathbf{X}}$ is the integration of 1H of compound **X** (**X** = **23** or **24$_{enol}$**) relative to 1H of compound **23**. Since $I_{\mathbf{X}} \propto [\mathbf{X}]$ (concentration of **X** in mol L^{-1}), the percentage of O-alkylation is given by:

$$\text{Percentage of O-alkylation} = \frac{I_{23}}{I_{23} + I_{24}} \times 100$$

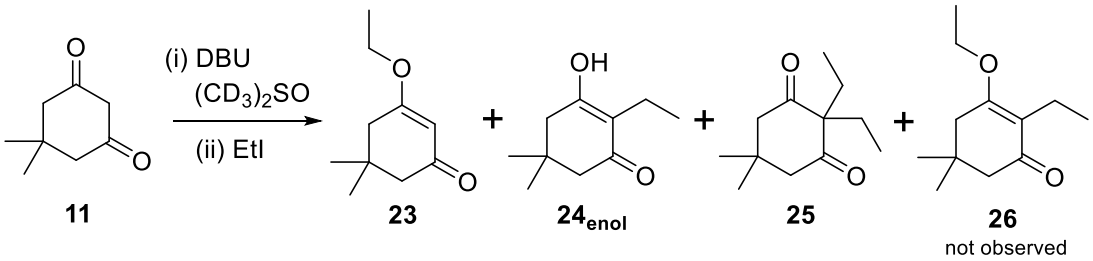
$$= \frac{1.00}{1.00 + 0.093} \times 100 = 91\%$$

Integrations give an <u>O vs C</u> ratio of 91:9

[a] The relevant ^{1}H NMR spectra are shown in Figure B33 and Figure B34 in Appendix B.

[b] Signals of **23 - 24** that are overlapping with other signals: δ 2.24 – 2.13 (m, contains 2H of **23** and 4H of **24$_{enol}$**), 1.11 – 1.00 (m, contains 6H of **23** and 6H of **24$_{enol}$** and 6H of starting enolate).

(ii) Reaction of Enolate 22-D with EtI in $(CD_3)_2SO$



From 5,5-dimethylcyclohexan-1,3-dione (**11**) (0.027 g, 0.19 mmol), DBU (**2**) (0.029 g, 0.19 mmol) and ethyl iodide (0.032 g, 0.21 mmol) in $(CD_3)_2SO$ by procedure B at 20 °C.

^{1}H NMR (400 MHz, $(CD_3)_2SO$) of crude mixture of alkylation products (the underlined integrations are expressed relative to 1H of compound **23**): [a,b]

Assigned to **23**: δ 5.27 (s, 1H, C=C<u>H</u>), 3.91 (q, *J* = 7.0 Hz, 2H, OC<u>H</u>$_2$CH$_3$), 2.26 (s, 2H, C<u>H</u>$_2$C=C), 1.26 (t, *J* = 7.0 Hz, 3H, OCH$_2$C<u>H</u>$_3$). [11]

Assigned to **24$_{enol}$**: δ 0.83 – 0.76 (m, 1.26H, C-CH$_2$C<u>H</u>$_3$ (3H of compound **24$_{enol}$**)). [17]

Assigned to **25**: δ 0.65 (t, *J* = 7.3 Hz, 0.56H, C-CH$_2$C<u>H</u>$_3$ (6H of compound **25**)). [c]

Based on the ^{1}H NMR spectral data given above, the integrations of 1H of each of compounds **23**, **24$_{enol}$**, and **25** relative to 1H of compound **23** are as follows:

$$I_{\mathbf{23}} = 1.00; \quad I_{\mathbf{24}} = \frac{1.26}{3} = 0.42; \quad I_{\mathbf{25}} = \frac{0.56}{6} = 0.093$$

where $I_{\mathbf{X}}$ is the integration of 1H of compound **X** (**X** = **23**, **24$_{enol}$** or **25**) relative to 1H of compound **23**. Since $I_{\mathbf{X}} \propto [\mathbf{X}]$ (concentration of **X** in mol L^{-1}), the percentage of O-alkylation is given by:

$$\text{Percentage of O-alkylation} = \frac{I_{\mathbf{23}}}{I_{\mathbf{23}} + I_{\mathbf{24}} + I_{\mathbf{25}}} \times 100$$

$$= \frac{1.00}{1.00 + 0.42 + 0.093} \times 100 = 66\%$$

Integrations give an <u>O vs C</u> ratio of 66:34

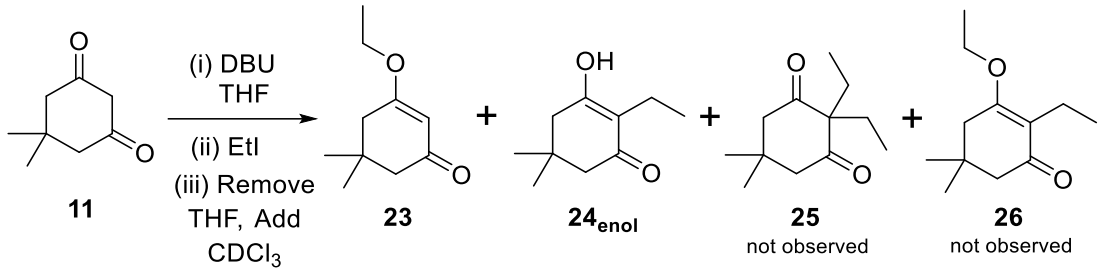
---

[a] The relevant ^{1}H NMR spectra are shown in Figure B35 and Figure B36 in Appendix B.

[b] Signals of **23 - 25** that are overlapping with other signals: δ 2.73 – 2.55 (m, contains 4H of **25** and signals of DBU and derivatives), 2.19 – 2.04 (m, contains 2H of **23** and 2H of **24$_{enol}$**), 1.73 – 1.56 (m, contains 4H of **25** and signals of DBU and derivatives) 1.02 – 0.86 (m, contains 6H of **23**, 6H of **24$_{enol}$** and 6H of **25**).

[c] No literature data is available for this compound, which was formed in very low quantities (*ca.* 6%). Assignments of NMR signals were made using evidence from ^{13}C and 2D NMR spectra of the reaction mixture. There is a correlation in the ^{1}H – ^{1}H COSY NMR spectrum between the signal at 0.65 ppm and another signal at δ 1.69 ppm. The signal at 1.69 ppm has a negative phase in the HSQC spectrum, indicating it is a CH$_2$ moiety. There is a correlation in the ^{1}H – ^{13}C HMBC NMR spectrum between the carbon associated with the ^{1}H signal at 0.65 ppm (9.36 ppm) and the ^{1}H signal at 1.69 ppm. In in the ^{1}H – ^{13}C HMBC NMR spectrum, the ^{1}H signals at δ 1.69 ppm and 0.65 both correlate to the signal of a quaternary carbon at 68.94 ppm in the ^{13}C spectrum. These observations combined make it likely that these signals are the C-CH$_2$C<u>H</u>$_3$ group of a C-di-ethylation product.

(iii) Reaction of Enolate 22-D with EtI in THF



From 5,5-dimethylcyclohexan-1,3-dione (**11**) (0.027 g, 0.19 mmol), DBU (**2**) (0.028 g, 0.18 mmol) and ethyl iodide (0.040 g, 0.26 mmol) in THF by procedure C.

^{1}H NMR (300 MHz, $CDCl_3$) of crude mixture of alkylation products (the underlined integrations are expressed relative to 1H of compound **23**): [a,b]

Assigned to **23**: δ 5.33 (s, 1H, C=C<u>H</u>), 3.92 (q, *J* = 7.0 Hz, 2H, OC<u>H</u>$_2$CH$_3$), 2.20 (s, 2H, C<u>H</u>$_2$C=O), 1.37 (t, *J* = 7.0 Hz, 3H, OCH$_2$C<u>H</u>$_3$). [15]

Assigned to **24_{enol}**: δ 0.93 (t, *J* = 7.4 Hz, 0.14H, C-CH$_2$C<u>H</u>$_3$ (3H of compound **24_{enol}**)). [16]

Based on the ^{1}H NMR spectral data given above, the integrations of 1H of each of compounds **23** and **24_{enol}** relative to 1H of compound **23** are as follows:

$$I_{\mathbf{23}} = 1.00; \quad I_{\mathbf{24}} = \frac{0.14}{3} = 0.046$$

where $I_{\mathbf{X}}$ is the integration of 1H of compound **X** (**X** = **23** or **24_{enol}**) relative to 1H of compound **23**. Since $I_{\mathbf{X}} \propto [\mathbf{X}]$ (concentration of **X** in mol L^{-1}), the percentage of O-alkylation is given by:

$$\text{Percentage of O-alkylation} = \frac{I_{\mathbf{23}}}{I_{\mathbf{23}} + I_{\mathbf{24}}} \times 100$$

$$= \frac{1.00}{1.00 + 0.046} \times 100 = 96\%$$

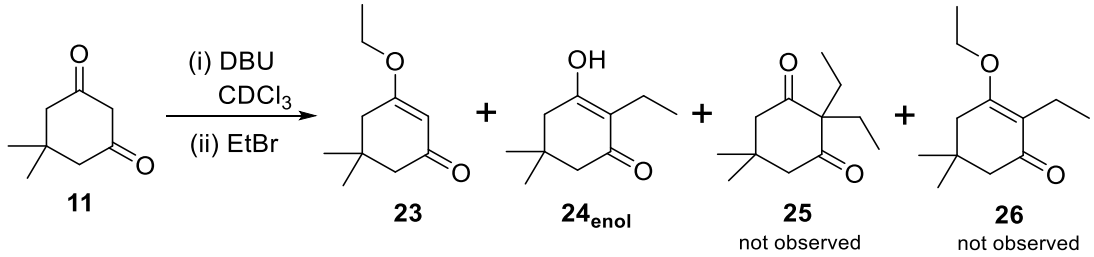
Integrations give an <u>O vs C</u> ratio of 96:4

[a] The relevant ^{1}H NMR spectra are shown in Figure B37 and Figure B38 in Appendix B.

[b] Signals of **23 - 24** that are overlapping with other signals: δ 2.32 – 2.24 (m, contains 2H of **23** and 6H of **24_{enol}**), 1.10 – 1.05 (m, contains 6H of **23** and 6H of **24_{enol}**).

5.3.8. Reactions of the 5,5-Dimethylcyclohexan-1,3-dione-Derived Enolate 22-D with EtBr

(i) Reaction of Enolate 22-D with EtBr in $CDCl_3$



From 5,5-dimethylcyclohexan-1,3-dione (**11**) (0.0283 g, 0.202 mmol), DBU (**2**) (0.0308 g, 0.202 mmol) and ethyl bromide (0.0293 g, 0.269 mmol) in $CDCl_3$ by procedure A at 0 °C.

^{1}H NMR (300 MHz, $CDCl_3$) of crude mixture of alkylation products (the underlined integrations are expressed relative to 1H of compound **23**): [a,b]

Assigned to **23**: δ 5.33 (s, 1H, C=C<u>H</u>), 3.91 (q, *J* = 7.0 Hz, 2H, OC<u>H</u>$_2$CH$_3$), 2.21 (s, 2H, C<u>H</u>$_2$C=O), 1.37 (t, *J* = 7.0 Hz, 3H, OCH$_2$C<u>H</u>$_3$). [15]

Assigned to **24$_{enol}$**: δ 0.93 (t, *J* = 7.4 Hz, 0.21H, C-CH$_2$C<u>H</u>$_3$ (3H of compound **24$_{enol}$**)). [16]

Based on the ^{1}H NMR spectral data given above, the integrations of 1H of each of compounds **23** and **24$_{enol}$** relative to 1H of compound **23** are as follows:

$$I_{\mathbf{23}} = 1.00; \quad I_{\mathbf{24}} = \frac{0.21}{3} = 0.07$$

where $I_{\mathbf{X}}$ is the integration of 1H of compound **X** (**X** = **23** or **24$_{enol}$**) relative to 1H of compound **23**. Since $I_{\mathbf{X}} \propto [\mathbf{X}]$ (concentration of **X** in mol L^{-1}), the percentage of O-alkylation is given by:

$$\text{Percentage of O-alkylation} = \frac{I_{\mathbf{23}}}{I_{\mathbf{23}} + I_{\mathbf{24}}} \times 100$$

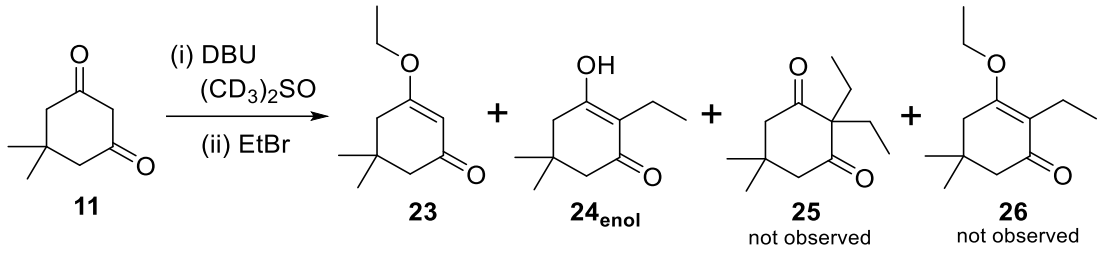
$$= \frac{1.00}{1.00 + 0.07} \times 100 = 93\%$$

Integrations give an <u>O vs C</u> ratio of 93:7

[a] The relevant ^{1}H NMR spectra are shown in Figure B39 and Figure B40 in Appendix B.

[b] Signals of **23 - 24** that are overlapping with other signals: δ 2.32 – 2.24 (m, contains 2H of **23** and 6H of **24$_{enol}$**), 1.10 – 1.01 (m, contains 6H of **32** and 6H of **24$_{enol}$**).

(ii) Reaction of Enolate 22-D with EtBr in $(CD_3)_2SO$



From 5,5-dimethylcyclohexan-1,3-dione (**11**) (0.0329 g, 0.235 mmol), DBU (**2**) (0.0357 g, 0.235 mmol) and ethyl bromide (0.0278 g, 0.255 mmol) in $(CD_3)_2SO$ by procedure B at 20 °C.

^{1}H NMR (400 MHz, $(CD_3)_2SO$) of crude mixture of alkylation products (the underlined integrations are expressed relative to 1H of compound **23**): [a,b]

Assigned to **23**: δ 5.27 (s, 1H, C=C<u>H</u>), 3.91 (q, *J* = 7.0 Hz, 2H, OC<u>H</u>$_2$CH$_3$), 2.26 (s, 2H, C<u>H</u>$_2$C=C), 1.26 (t, *J* = 7.0 Hz, 3H, OCH$_2$C<u>H</u>$_3$). [11]

Assigned to **24$_{enol}$**: δ 0.78 – 0.71 (m, 0.55H, C-CH$_2$C<u>H</u>$_3$ (3H of compound **24$_{enol}$**)). [17]

Based on the ^{1}H NMR spectral data given above, the integrations of 1H of each of compounds **23** and **24$_{enol}$** relative to 1H of compound **23** are as follows:

$$I_{\mathbf{23}} = 1.00; \quad I_{\mathbf{24}} = \frac{0.55}{3} = 0.183$$

where $I_{\mathbf{X}}$ is the integration of 1H of compound **X** (**X** = **23** or **24$_{enol}$**) relative to 1H of compound **23**. Since $I_{\mathbf{X}} \propto [\mathbf{X}]$ (concentration of **X** in mol L^{-1}), the percentage of O-alkylation is given by:

$$\text{Percentage of O-alkylation} = \frac{I_{\mathbf{23}}}{I_{\mathbf{23}} + I_{\mathbf{24}}} \times 100$$

$$= \frac{1.00}{1.00 + 0.183} \times 100 = 85\%$$

Integrations give an <u>O vs C</u> ratio of 85:15

[a] The relevant ^{1}H NMR spectra are shown in Figure B41 and Figure B42 in Appendix B.

[b] Signals of **23 - 24** that are overlapping with other signals: δ 2.12 – 2.02 (m, contains 4H of **23** and 6H of **24$_{enol}$**), 1.00 – 0.88 (m, contains 6H of **23**, 6H of **24$_{enol}$** and enolate signal).

5.4. Determination of O/C Ratios in Enolate Trideuteromethylations

General procedure for the Trideuteromethylation of enolates in CH_2Cl_2

The following procedure (Procedure D) was used to establish the ratios of products formed by a reaction of an enolate and CD_3I in CH_2Cl_2:

The 1,3-dione was added to a Schlenk flask containing an inert atmosphere of nitrogen gas. Dry CH_2Cl_2 (0.7 ml) was added to form a transparent solution**.** Dry 1,8-diazabicyclo[5.4.0]undec-7-ene (**2**) (DBU, ~1 equivalent) was added neat to the solution, forming a transparent solution of the enolate (pale yellow or pink depending on the dione). Dry $CDCl_3$ (1 equivalent) was added to the solution to serve as a reference for ^2H NMR spectroscopy. The solution was stirred for approximately 15 minutes.

An empty NMR tube was placed in a long Schlenk tube. The long Schlenk tube, containing the NMR tube, was evacuated and re-filled with nitrogen ≥ 3 times, creating an inert atmosphere inside the flask. The enolate solution was added to the NMR tube under inert atmosphere by syringe. The NMR tube was sealed with a rubber septum cap. After fitting the rubber septum to the NMR tube, the seal was secured by wrapping the external edge of the septum where it contacted the surface of the NMR tube with PTFE tape. Neat CD_3I (~1 equivalent) was added dropwise through the septum cap over the course of approximately 1 minute. The resultant solution was mixed by shaking before the external part of the septum and PTFE tape were then covered with a layer of Parafilm. The NMR tube was then transferred to the NMR spectrometer and ^2H NMR spectra were recorded.

Note: The signals of the trideuteromethylated compounds in the ^2H NMR spectra were compared to the ^1H NMR signals of their methylated counterparts as found in the literature. All spectra produced by this procedure contain a peak associated with trideuteromethylated DBU at ~3.21 ppm.

General procedure for the Trideuteromethylation of enolates in THF

The following procedure (Procedure E) was used to establish the ratios of products formed by a reaction of an enolate and CD_3I in THF:

The 1,3-dione was added to a Schlenk flask containing an inert atmosphere of nitrogen gas. Dry THF (0.7 ml) was added to form a transparent solution**.** Dry 1,8-diazabicyclo[5.4.0]undec-7-ene (**2**) (DBU, ~1 equivalent) was added neat to the solution, forming a transparent solution of the enolate (pale yellow or pink depending on the dione). The solution was stirred for approximately 15 minutes.

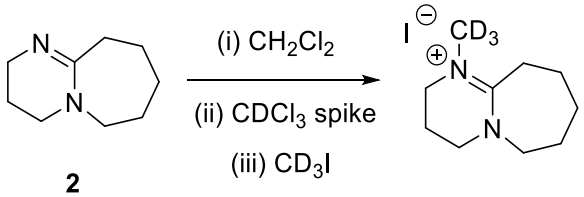
To a separate Schlenk flask containing an inert atmosphere of nitrogen gas was added dry THF (0.3 ml). 1.05 equivalents of CD_3I was added to the THF and the flask was swirled. The contents of this flask were taken up in a syringe (which had been flushed three times with nitrogen gas) and added to the flask containing the enolate solution dropwise over the course of 1 minute. The resultant solution was stirred for approximately 18 hours. The side-arm of the reaction flask was connected with rubber

tubing to a vacuum trap, which was itself connected to a Schlenk manifold. The trap was placed under vacuum ($\leq 5 \times 10^{-3}$ mbar). The vacuum trap and the tubing connecting it to the reaction flask and the Schlenk manifold were then filled with nitrogen gas by the pump and fill technique.[2] The trap was then placed under vacuum and then cooled with liquid N_2. At this point the stopcock on the Schlenk flask was opened and volatile reagents and solvent were removed and collected in the trap. After approximately 30 minutes, the entirety of the trap and the Schlenk flask were re-filled with nitrogen gas through the Schlenk manifold and the stopcock of the Schlenk flask was closed. The trap was removed and the flask was re-attached directly to the Schlenk manifold, using the pump and fill technique to establish a nitrogen atmosphere in the tubing used for the attachment. Dry CH_2Cl_2 (0.7 ml) was added to the flask by syringe to dissolve the crude reaction mixture. Dry $CDCl_3$ (1 equivalent) was added to the solution to serve as a reference for ^2H NMR spectroscopy.

An empty NMR tube was placed in a long Schlenk tube. The long Schlenk tube, containing the NMR tube, was evacuated and re-filled with nitrogen ≥ 3 times, creating an inert atmosphere inside the flask. The reaction mixture was added to the NMR tube under inert atmosphere by syringe. The NMR tube was sealed with a rubber septum cap. After fitting the rubber septum to the NMR tube, the seal was secured by wrapping the external edge of the septum where it contacted the surface of the NMR tube with PTFE tape. The outside of the PTFE tape and rubber septum were then wrapped with a layer of Parafilm to further secure the nitrogen atmosphere inside the NMR tube. The NMR tube was then transferred to the NMR spectrometer and ^2H NMR spectra were recorded.

Note: The signals of the trideuteromethylated compounds in the ^2H NMR spectra were compared to the ^1H NMR signals of their methylated counterparts as found in the literature.

All spectra produced by these procedures (procedure D and E) contain a peak associated with trideuteromethylated DBU at ~3.21 ppm. This peak was proven to belong to the compound that results from the trideuteromethylation of DBU (**2**) by the reaction shown below between DBU and CD_3I in CH_2Cl_2.



2

Dry CH_2Cl_2 (0.7 ml) was added to a Schlenk flask containing an inert atmosphere of nitrogen gas**.** Dry 1,8-diazabicyclo[5.4.0]undec-7-ene (**2**) (0.098 g, 0.64 mmol) was added neat to the solution, forming a transparent. Dry $CDCl_3$ (0.050 g, 0.42 mmol) was added to the solution to serve as a reference for ^2H NMR spectroscopy. The solution was stirred for approximately 15 minutes.

An empty NMR tube was placed in a long Schlenk tube. The long Schlenk tube, containing the NMR tube, was evacuated and re-filled with nitrogen ≥ 3 times, creating

an inert atmosphere inside the flask. The enolate solution was added to the NMR tube under inert atmosphere by syringe. The NMR tube was sealed with a rubber septum cap. After fitting the rubber septum to the NMR tube, the seal was secured by wrapping the external edge of the septum where it contacted the surface of the NMR tube with PTFE tape. Neat CD_3I 0.163 g, 1.12 mmol) was added dropwise through the septum cap over the course of approximately 1 minute. The resultant solution was mixed by shaking before the outside of the PTFE tape and rubber septum were wrapped with a layer of Parafilm to further secure the nitrogen atmosphere inside the NMR tube. The NMR tube was then transferred to the NMR spectrometer and ^2H NMR spectra were recorded.

^2H NMR (75.8 MHz, CH_2Cl_2) of crude reaction mixture:

Assigned to **trideuteromethylated DBU product**: δ 3.21 (s, 3D, N-CD_3)

The signal of CD_3I may also be seen at δ 2.09.

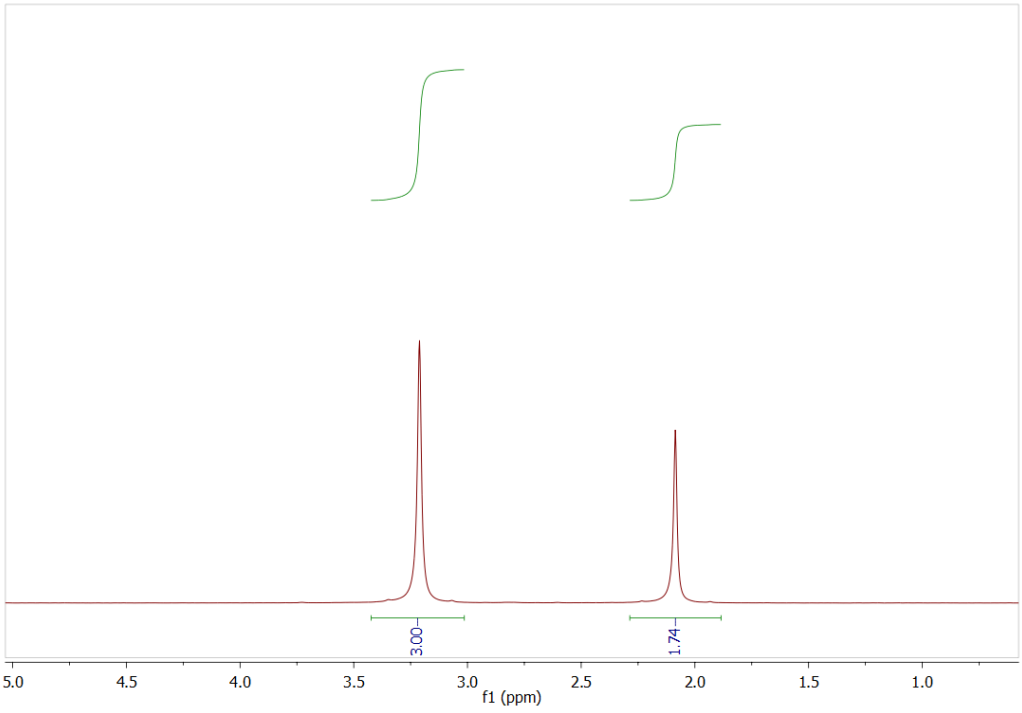
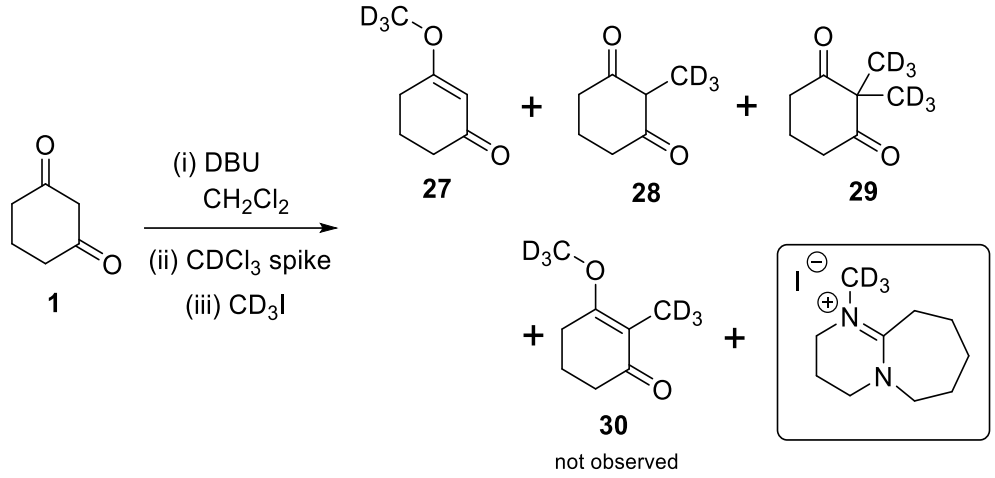


Figure 5-4: ^2H NMR spectrum of the crude product of the reaction between DBU (**2**) and CD_3I in CH_2Cl_2. This signal, at approximately δ 3.21 ppm, may be seen in many of the spectra obtained from the crude reaction mixtures of the experiments below.

5.4.1. Reactions of 3-D with Deuterated Methyl Iodide

(i) Reaction of Enolate 3-D with Deuterated Methyl Iodide (CD_3I) in CH_2Cl_2



From 1,3-cyclohexanedione (**1**) (0.045 g, 0.40 mmol), DBU (**2**) (0.055 g, 0.36 mmol) and deuterated methyl iodide (CD_3I) (0.070 g, 0.48 mmol), $CDCl_3$ (0.056 g) in dry CH_2Cl_2 (0.7 ml) by procedure D.

^2H NMR (75.8 MHz, CH_2Cl_2) of crude mixture of alkylation products (the underlined integrations are expressed relative to 1D [a] of O-trideuteromethylated compound **27**): [b]

Assigned to **27**: δ 3.60 (s, 3D, $OC\underline{D}_3$ (3D of compound **27**)). [18]

Assigned to **28**: δ 1.52 (s, 4.93D, $C\text{-}C\underline{D}_3$ (3D of compound **28**)). [19]

Assigned to **29**: δ 1.17 (s, 1.06D, $C\text{-}C\underline{D}_3$ (6D of compound **29**)). [20]

Based on the ^2H NMR spectral data given above, the integrations of 1D of each of compounds **27**, **28**, and **29** relative to 1D of compound **27** are as follows:

$$I_{\mathbf{27}} = \frac{3.00}{3} = 1.00; \quad I_{\mathbf{28}} = \frac{4.93}{3} = 1.64 \quad I_{\mathbf{29}} = \frac{1.06}{6} = 0.176$$

where $I_{\mathbf{X}}$ is the integration of 1D of compound **X** (**X** = **27**, **28** or **29**) relative to 1D of compound **27**. Since $I_{\mathbf{X}} \propto [\mathbf{X}]$ (concentration of **X** in mol L^{-1}), the percentage of O-alkylation is given by:

$$\text{Percentage of O-alkylation} = \frac{I_{\mathbf{27}}}{I_{\mathbf{27}} + I_{\mathbf{28}} + I_{\mathbf{29}}} \times 100$$

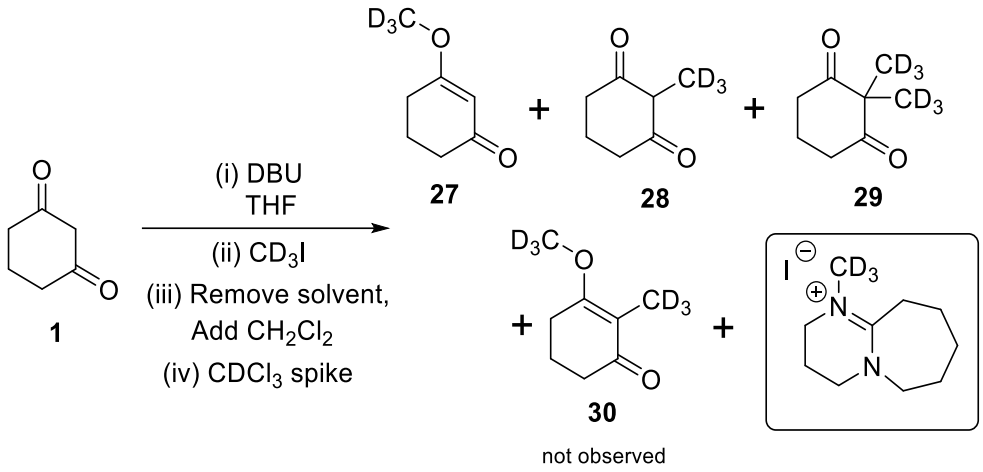
$$= \frac{1.00}{1.00 + 1.64 + 0.176} \times 100 = 35\%$$

Integrations give an O vs C ratio of 35:65

[a] "D" in this context, and in all reactions in section 5.4, refers to deuterium.

[b] The relevant ^2H NMR spectra are shown in Figure B43 and Figure B44 in Appendix B. The literature references given on this page contain ^1H NMR spectral data for the non-deuterated analogues of these products.

(ii) Reaction of Enolate 3-D with Deuterated Methyl Iodide (CD_3I) in THF



From 1,3-cyclohexanedione (**1**) (0.029 g, 0.259 mmol), DBU (**2**) (0.038 g, 0.250 mmol) and deuterated methyl iodide (CD_3I) (0.040 g, 0.276 mmol), $CDCl_3$ (0.068 g) in dry THF (0.7 ml). After stirring for 18 hours, the reaction solvent (THF) was removed under vacuum and the reaction mixture was dissolved in dry CH_2Cl_2 (0.7 ml), as per procedure E.

^{2}H NMR (75.8 MHz, CH_2Cl_2) of crude mixture of alkylation products (the underlined integrations are expressed relative to 1D of O-trideuteromethylated compound **27**): [a]

Assigned to **27**: δ 3.58 (s, 3D, O-CD_3 (3D of compound **27**)). [18]

Assigned to **28**: δ 1.50 (s, 0.18D, C-CD_3 (3D of compound **28**)). [19]

Assigned to **29**: δ 1.15 (s, 0.93D, C-CD_3 (6D of compound **29**)). [20]

Assigned to **30**: δ 3.85 (s, 0.07D, O-CD_3 (3D of compound **30**)). [21]

Based on the ^{2}H NMR spectral data given above, the integrations of 1D of each of compounds **27**, **28**, **29** and **30** relative to 1D of compound **27** are as follows:

$$I_{\mathbf{27}} = \frac{3.00}{3} = 1.00; \quad I_{\mathbf{28}} = \frac{0.18}{3} = 0.06; \quad I_{\mathbf{29}} = \frac{0.93}{6} = 0.16; \quad I_{\mathbf{30}} = \frac{0.07}{3} = 0.023$$

where $I_{\mathbf{X}}$ is the integration of 1D of compound **X** (**X** = **27**, **28**, **29**, or **30**) relative to 1D of compound **27**. Since $I_{\mathbf{X}} \propto [\mathbf{X}]$ (concentration of **X** in mol L^{-1}), the percentage of O-alkylation is given by:

$$\text{Percentage of O-alkylation} = \frac{I_{\mathbf{27}}}{I_{\mathbf{27}} + I_{\mathbf{28}} + I_{\mathbf{29}} + I_{\mathbf{30}}} \times 100$$

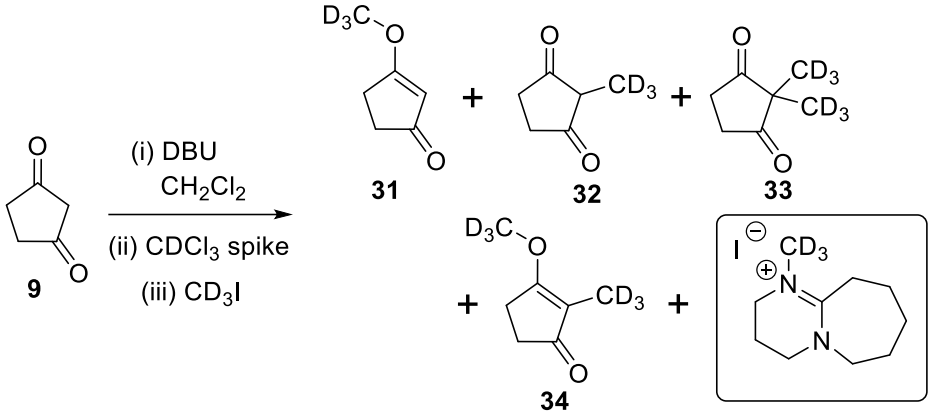
$$= \frac{1.00}{1.00 + 0.06 + 0.16 + 0.023} \times 100 = 81\%$$

Integrations give an O vs C ratio of 81:19

[a] The relevant ^{2}H NMR spectra are shown in Figure B45 and Figure B46 in Appendix B. The literature references given on this page contain ^{1}H NMR spectral data for the non-deuterated analogues of these products.

5.4.2. Reactions of Enolate 12-D with Deuterated Methyl Iodide

(i) Reaction of Enolate 12-D with Deuterated Methyl Iodide (CD_3I) in CH_2Cl_2



From 1,3-cyclopentanedione (**9**) (0.055 g, 0.56 mmol), DBU (**2**) (0.085 g, 0.56 mmol) and deuterated methyl iodide (CD_3I) (0.080 g, 0.55 mmol), $CDCl_3$ (0.052 g) in dry CH_2Cl_2 (0.7 ml) by procedure D.

^{2}H NMR (75.8 MHz, CH_2Cl_2) of crude mixture of alkylation products (the underlined integrations are expressed relative to 1D of O-trideuteromethylated compound **31**): [a]

Assigned to **31**: δ 3.75 (s, 3D, $OC\underline{D}_3$ (3D of compound **31**). [22]

Assigned to **32**: δ 1.37 (s, 0.71D, $C\text{-}C\underline{D}_3$ (3D of compound **32**)). [19]

Assigned to **33**: δ 1.00 (s, 0.17D, $C\text{-}C\underline{D}_3$ (6D of compound **33**). [23]

Assigned to **34**: δ 3.86 (s, 0.04D, $OC\underline{D}_3$ (3D of compound **34**)), 1.45 (s, 0.04D (3D of compound **34**)). [24]

Based on the ^{2}H NMR spectral data given above, the integrations of 1D of each of compounds **31**, **32**, **33** and **34** relative to 1D of compound **31** are as follows:

$$I_{\mathbf{31}} = \frac{3.00}{3} = 1.00; \quad I_{\mathbf{32}} = \frac{0.71}{3} = 0.24; \quad I_{\mathbf{33}} = \frac{0.17}{6} = 0.028; \quad I_{\mathbf{34}} = \frac{0.04}{3} = 0.013$$

where $I_{\mathbf{X}}$ is the integration of 1D of compound **X** (**X** = **31**, **32**, **33**, or **34**) relative to 1D of compound **31**. Since $I_{\mathbf{X}} \propto [\mathbf{X}]$ (concentration of **X** in mol L^{-1}), the percentage of O-alkylation is given by:

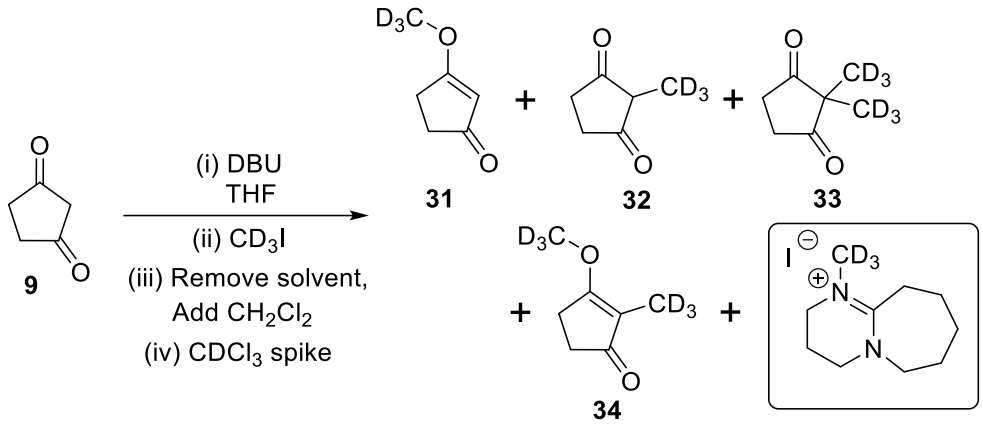
$$\text{Percentage of O-alkylation} = \frac{I_{\mathbf{31}}}{I_{\mathbf{31}} + I_{\mathbf{32}} + I_{\mathbf{33}} + I_{\mathbf{34}}} \times 100$$

$$= \frac{1.00}{1.00 + 0.24 + 0.028 + 0.013} \times 100 = 78\%$$

Integrations give an O vs C ratio of 78:22

[a] The relevant ^{2}H NMR spectra are shown in Figure B47 and Figure B48 in Appendix B. The literature references given on this page contain ^{1}H NMR spectral data for the non-deuterated analogues of these products.

(ii) Reaction of Enolate 12-D with Deuterated Methyl Iodide (CD_3I) in THF



From 1,3-cyclopentanedione (**9**) (0.030 g, 0.306 mmol), DBU (**2**) (0.046 g, 0.302 mmol) and deuterated methyl iodide (CD_3I) (0.060 g, 0.414 mmol), $CDCl_3$ (0.027 g) in dry THF (0.7 ml). After stirring for 18 hours, the reaction solvent (THF) was removed under vacuum and the reaction mixture was dissolved in dry CH_2Cl_2 (0.7 ml), as per procedure E.

^{2}H NMR (75.8 MHz, CH_2Cl_2) of crude mixture of alkylation products (the underlined integrations are expressed relative to 1D of O-trideuteromethylated compound **31**): [a]

Assigned to **31**: δ 3.74 (s, 3D, $OC\underline{D}_3$ (3D of compound **31**). [22]

Assigned to **32**: δ 1.47 (s, 0.50D, $C\text{-}C\underline{D}_3$ (3D of compound **32**)). [19]

Assigned to **33**: δ 0.99 (s, 0.09D, $C\text{-}C\underline{D}_3$ (6D of compound **33**). [23]

Assigned to **34**: δ 3.86 (s, 0.04D, $OC\underline{D}_3$ (3D of compound **34**)). [24]

Based on the ^{2}H NMR spectral data given above, the integrations of 1D of each of compounds **31**, **32**, **33** and **34** relative to 1D of compound **31** are as follows:

$$I_{\mathbf{31}} = \frac{3.00}{3} = 1.00; \quad I_{\mathbf{32}} = \frac{0.50}{3} = 0.16; \quad I_{\mathbf{33}} = \frac{0.09}{6} = 0.015; \quad I_{\mathbf{34}} = \frac{0.03}{3} = 0.01$$

where $I_{\mathbf{X}}$ is the integration of 1D of compound **X** (**X** = **31**, **32**, **33** or **34**) relative to 1D of compound **31**. Since $I_{\mathbf{X}} \propto [\mathbf{X}]$ (concentration of **X** in mol L^{-1}), the percentage of O-alkylation is given by:

$$\text{Percentage of O-alkylation} = \frac{I_{\mathbf{31}}}{I_{\mathbf{31}} + I_{\mathbf{32}} + I_{\mathbf{33}} + I_{\mathbf{34}}} \times 100$$

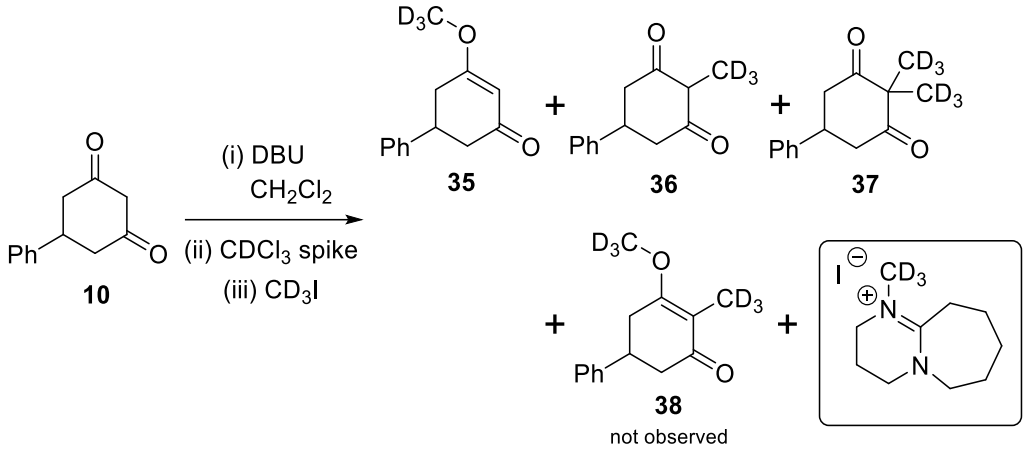
$$= \frac{1.00}{1.00 + 0.16 + 0.015 + 0.01} \times 100 = 84\%$$

Integrations give an O vs C ratio of 84:16

[a] The relevant ^{2}H NMR spectra are shown in Figure B49 and Figure B50 in Appendix B. The literature references given on this page contain ^{1}H NMR spectral data for the non-deuterated analogues of these products.

5.4.3. Reactions of Enolate 17-D with Deuterated Methyl Iodide

(i) Reaction of Enolate 17-D with Deuterated Methyl Iodide (CD_3I) in CH_2Cl_2



From 5-phenylcyclohexan-1,3-dione (**10**) (0.050 g, 0.27 mmol), DBU (**2**) (0.038 g, 0.25 mmol) and deuterated methyl iodide (CD_3I) (0.038 g, 0.26 mmol), $CDCl_3$ (0.0414 g) in dry CH_2Cl_2 (0.7 ml) by procedure D.

^2H NMR (75.8 MHz, CH_2Cl_2) of crude mixture of alkylation products (the underlined integrations are expressed relative to 1D of O-trideuteromethylated compound **35**): [a]

Assigned to **35**: δ 3.48 (s, 3D, $OC\underline{D}_3$ (3D of compound **35**)). [25]

Assigned to **36**: δ 1.40 (s, 3.29D, $C\text{-}C\underline{D}_3$ (3D of compound **36**)). [26]

Assigned to **37**: δ 1.19 – 0.98.162**37** [25]

Based on the ^2H NMR spectral data given above, the integrations of 1D of each of compounds **35**, **36**, and **37** relative to 1D of compound **35** are as follows:

$$I_{\mathbf{35}} = \frac{3.00}{3} = 1.00; \quad I_{\mathbf{36}} = \frac{3.29}{3} = 1.10 \quad I_{37} = \frac{1.02}{6} = 0.17$$

where $I_{\mathbf{X}}$ is the integration of 1D of compound **X** (**X** = **35**, **36** or **37**) relative to 1D of compound **35**. Since $I_{\mathbf{X}} \propto [\mathbf{X}]$ (concentration of **X** in mol L^{-1}), the percentage of O-alkylation is given by:

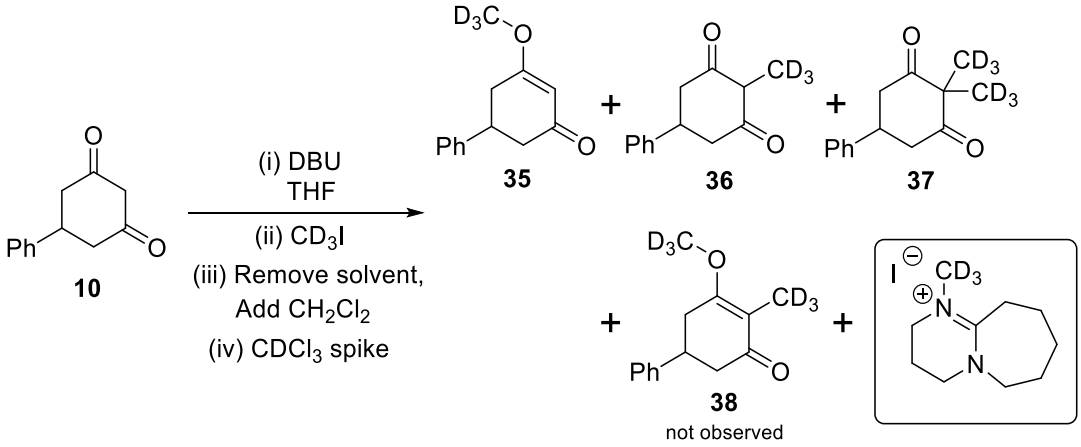
$$\text{Percentage of O-alkylation} = \frac{I_{\mathbf{35}}}{I_{\mathbf{35}} + I_{\mathbf{36}} + I_{\mathbf{37}}} \times 100$$

$$= \frac{1.00}{1.00 + 1.10 + 0.17} \times 100 = 44\%$$

Integrations give an O vs C ratio of 44:56

[a] The relevant ^2H NMR spectra are shown in Figure B51 and Figure B52 in Appendix B. The literature references given on this page contain ^1H NMR spectral data for the non-deuterated analogues of these products.

(ii) Reaction of Enolate 17-D with Deuterated Methyl Iodide (CD_3I) in THF



From 5-phenylcyclohexan-1,3-dione (**10**) (0.050 g, 0.27 mmol), DBU (**2**) (0.038 g, 0.25 mmol) and deuterated methyl iodide (CD_3I) (0.038 g, 0.26 mmol), $CDCl_3$ (0.0414 g) in dry THF (0.7 ml). After stirring for 18 hours, the reaction solvent (THF) was removed under vacuum and the reaction mixture was dissolved in dry CH_2Cl_2 (0.7 ml), as per procedure E.

^{2}H NMR (75.8 MHz, CH_2Cl_2) of crude mixture of alkylation products (the underlined integrations are expressed relative to 1D of O-trideuteromethylated compound **35**): [a]

Assigned to **35**: δ 3.50 (s, 3D, $OC\underline{D}_3$ (3D of compound **35**)). [25]

Assigned to $\mathbf{36}_{\mathbf{keto}}$ and $\mathbf{36}_{\mathbf{enol}}$: δ 1.53 – 1.34 (4641 0.56D, (2 × s, C-$C\underline{D}_3$ of each of $\mathbf{36}_{\mathbf{keto}}$ and $\mathbf{36}_{\mathbf{enol}}$ (3D of each of compound $\mathbf{36}_{\mathbf{keto}}$ and compound $\mathbf{36}_{\mathbf{enol}}$)). [26]

Assigned to **37**: δ 1.21 – 1.00 (1606 0.56D, (2 × C-$C\underline{D}_3$ (6D of compound **37**)). [25]

Based on the ^{2}H NMR spectral data given above, the integrations of 1D of each of compounds **35**, **36**, **and 37** relative to 1D of compound **35** are as follows:

$$I_{\mathbf{35}} = \frac{3.00}{3} = 1.00; \quad I_{\mathbf{36}} = \frac{0.47}{3} = 0.16; \quad I_{\mathbf{37}} = \frac{0.56}{6} = 0.093$$

where $I_{\mathbf{X}}$ is the integration of 1D of compound **X** (**X** = **35**, **36** or **37**) relative to 1D of compound **35**. Since $I_{\mathbf{X}} \propto [\mathbf{X}]$ (concentration of **X** in mol L^{-1}), the percentage of O-alkylation is given by:

$$\text{Percentage of O-alkylation} = \frac{I_{\mathbf{35}}}{I_{\mathbf{35}} + I_{\mathbf{36}} + I_{\mathbf{37}}} \times 100$$

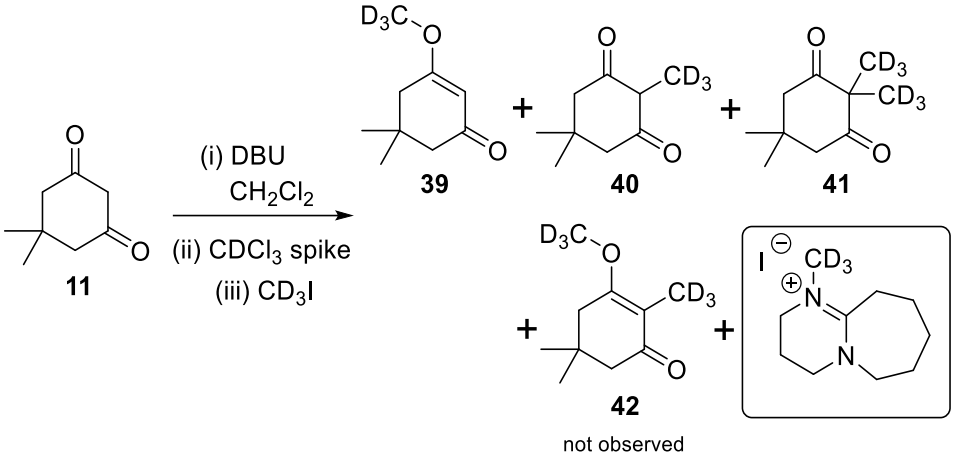
$$= \frac{1.00}{1.00 + 0.16 + 0.093} \times 100 = 80\%$$

Integrations give an O vs C ratio of 80:20

[a] The relevant ^{2}H NMR spectra are shown in Figure B53 and Figure B54 in Appendix B. The literature references given on this page contain ^{1}H NMR spectral data for the non-deuterated analogues of these products.

5.4.4. Reactions of the Enolate 22-D with Deuterated Methyl Iodide

(i) Reaction of Enolate 22-D with Deuterated Methyl Iodide (CD_3I) in CH_2Cl_2



From 5,5-dimethylcyclohexan-1,3-dione (**11**) (0.052 g, 0.37 mmol), DBU (**2**) (0.056 g, 0.37 mmol) and deuterated methyl iodide (CD_3I) (0.054 g, 0.37 mmol), $CDCl_3$ (0.043 g) in dry CH_2Cl_2 (0.7 ml) by procedure D.

^2H NMR (75.8 MHz, CH_2Cl_2) of crude mixture of alkylation products (the underlined integrations are expressed relative to 1D of O-trideuteromethylated compound **39**): [a]

Assigned to **39**: δ 3.63 (s, <u>3D</u>, O<u>C</u>D_3 (3D of compound **39**)). [27]

Assigned to **40**: δ 1.53 (s, <u>4.07D</u>, C-<u>C</u>D_3 (3D of compound **40**)). [28]

Assigned to **41**: δ 1.18 (s, <u>2.43D</u>, C-<u>C</u>D_3 (6D of compound **41**)). [29]

Based on the ^2H NMR spectral data given above, the integrations of 1D of each of compounds **39**, **40**, **and 41** relative to 1D of compound **39** are as follows:

$$I_{\mathbf{39}} = \frac{3.00}{3} = 1.00; \quad I_{\mathbf{40}} = \frac{4.07}{3} = 1.36; \quad I_{\mathbf{41}} = \frac{2.43}{6} = 0.405$$

where $I_{\mathbf{X}}$ is the integration of 1D of compound **X** (**X** = **39**, **40** or **41**) relative to 1D of compound **39**. Since $I_{\mathbf{X}} \propto [\mathbf{X}]$ (concentration of **X** in mol L^{-1}), the percentage of O-alkylation is given by:

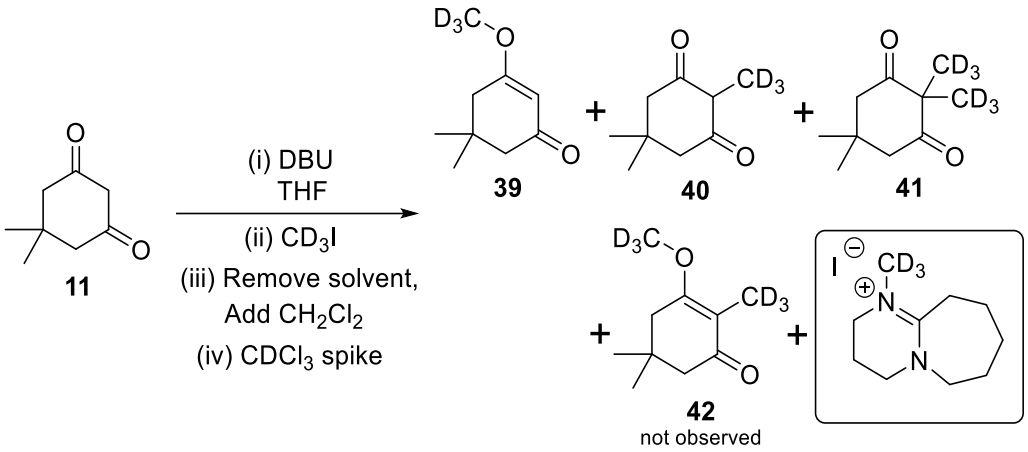
$$\text{Percentage of O-alkylation} = \frac{I_{\mathbf{39}}}{I_{\mathbf{39}} + I_{\mathbf{40}} + I_{\mathbf{41}}} \times 100$$

$$= \frac{1.00}{1.00 + 1.36 + 0.405} \times 100 = 36\%$$

Integrations give an <u>O vs C</u> ratio of 36:64

[a] The relevant ^2H NMR spectra are shown in Figure B55 and Figure B56 in Appendix B. The literature references given on this page contain ^1H NMR spectral data for the non-deuterated analogues of these products.

(ii) Reaction of Enolate 22-D with Deuterated Methyl Iodide (CD_3I) in THF



From 5,5-dimethylcyclohexan-1,3-dione (**11**) (0.029 g, 0.154 mmol), DBU (**2**) (0.0234 g, 0.153 mmol) and deuterated methyl iodide (CD_3I) (0.024 g, 0.166 mmol), $CDCl_3$ (0.028 g) in dry THF (0.7 ml). After stirring for 18 hours, the reaction solvent (THF) was removed under vacuum and the reaction mixture was dissolved in dry CH_2Cl_2 (0.7 ml), as per procedure E.

^2H NMR (75.8 MHz, CH_2Cl_2) of crude mixture of alkylation products (the underlined integrations are expressed relative to 1D of O-trideuteromethylated compound **39**): [a]

Assigned to **39**: δ 3.65 (s, 3D, $OC\underline{D}_3$ (3D of compound **39**)). [27]

Assigned to **40**: δ 1.54 (s, 1.30D, $C\text{-}C\underline{D}_3$ (3D of compound **40**)). [28]

Assigned to **41**: δ 1.20 (s, 0.50D, $C\text{-}C\underline{D}_3$ (6D of compound **41**)). [29]

Assigned to **42**: δ 3.90 (s, 0.18D, $OC\underline{D}_3$ (3D of compound **42**)).

Based on the ^2H NMR spectral data given above, the integrations of 1D of each of compounds **39**, **40**, **41** and **42** relative to 1D of compound **39** are as follows:

$$I_{39} = \frac{3.00}{3} = 1.00;\ I_{40} = \frac{1.30}{3} = 0.433;\ I_{41} = \frac{0.50}{6} = 0.083;\ I_{42} = \frac{0.18}{3} = 0.06$$

where $I_{\mathbf{X}}$ is the integration of 1D of compound **X** (**X** = **39**, **40**, **41** or **42**) relative to 1D of compound **39**. Since $I_{\mathbf{X}} \propto [\mathbf{X}]$ (concentration of **X** in mol L^{-1}), the percentage of O-alkylation is given by:

$$\text{Percentage of O-alkylation} = \frac{I_{39}}{I_{39} + I_{40} + I_{41} + I_{42}} \times 100$$

$$= \frac{1.00}{1.00 + 0.433 + 0.083 + 0.06} \times 100 = 63\%$$

Integrations give an O vs C ratio of 63:37

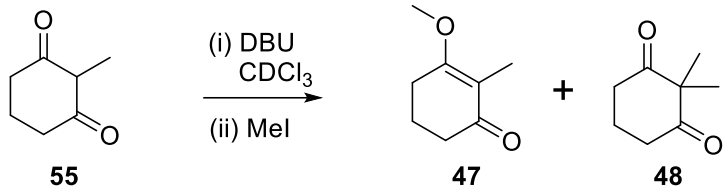
[a] The relevant ^2H NMR spectra are shown in Figure B57 and Figure B58 in Appendix B. The literature references given on this page contain ^1H NMR spectral data for the non-deuterated analogues of these products.

5.5. Determination of O/C Ratios in Enolate Methylation Reactions

5.5.1. Reaction of Enolate 46-D with Methyl Iodide

(i) Reaction of the 46-D with Methyl Iodide in $CDCl_3$

From 2-methyl-1,3-cyclohexanedione (**55**) (0.022 g, 0.17 mmol), DBU (**2**) (0.026 g, 0.17 mmol) and methyl iodide (0.024 g, 0.17 mmol) in $CDCl_3$ by procedure A at 0 °C.



55 **47** **48**

^{1}H NMR (300 MHz, $CDCl_3$) of crude mixture of alkylation products (the underlined integrations are expressed relative to 1H of compound **48**): [a,b]

Assigned to **47**: δ 3.75 (s, 0.18H, OCH_3 (3H of compound **47**)), 2.54 – 2.46 (m, 0.12H, $CH_2C{=}O$ (2H of compound **47**)). [21]

Assigned to **48**: δ 2.63 (t, *J* = 7.0 Hz, 4H, $CH_2C{=}O$) 1.23 (s, 6H, $C\text{-}CH_3$). [20]

Based on the ^{1}H NMR spectral data given above, the integrations of 1H of each of compounds **47** and **48** relative to 1H of compound **48** are as follows:

$$I_{47} = \frac{0.18}{3} = 0.06; \quad I_{48} = \frac{6.00}{6} = 1.00$$

where $I_{\mathbf{X}}$ is the integration of 1H of compound **X** (**X** = **47** or **48**) relative to 1H of compound **48**. Since $I_{\mathbf{X}} \propto [\mathbf{X}]$ (concentration of **X** in mol L^{-1}), the percentage of O-alkylation is given by:

$$\text{Percentage of O-alkylation} = \frac{I_{47}}{I_{47} + I_{48}} \times 100$$

$$= \frac{0.06}{0.06 + 1.00} \times 100 = 6\%$$

Integrations give an O vs C ratio of 6:94

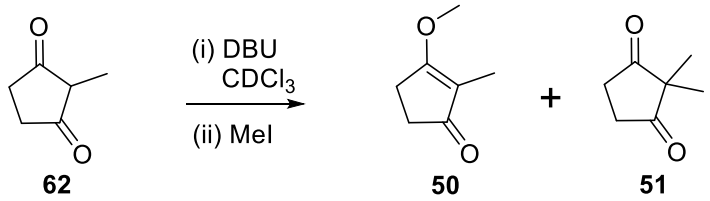
[a] The relevant ^{1}H NMR spectra are shown in Figure B59 and Figure B60 in Appendix B.

[b] Signals of **47 - 48** that are overlapping with other signals: δ 1.94 – 1.75 (m, contains 2H of **47** and 2H of **48**).

5.5.2. Reaction of Enolate 49-D with Methyl Iodide

(i) Reaction of Enolate 49-D with Methyl Iodide in $CDCl_3$

From 2-methyl-1,3-cyclopentanedione (**62**) (0.032 g, 0.28 mmol), DBU (**2**) (0.043 g, 0.28 mmol) and methyl iodide (0.040 g, 0.28 mmol) in $CDCl_3$ by procedure A at 0 °C.



^{1}H NMR (300 MHz, $CDCl_3$) of crude mixture of alkylation products (the underlined integrations are expressed relative to 1H of compound **50**): [a]

Assigned to **50**: δ 3.99 (s, 3H, OCH_3), 2.72 – 2.67 (m, 2H, $CH_2C{=}C$), 2.47 – 2.43 (m, 2H, $CH_2C{=}O$), 1.62 (t, J = 1.5 Hz, 3H, $C\text{-}CH_3$). [24]

Assigned to **51**: δ 2.84 (s, 5.59H, $CH_2C{=}C$ (4H of compound **51**)), 1.15 (s, 9.24H, $C\text{-}CH_3$ (6H of compound **51**)). [23]

Based on the ^{1}H NMR spectral data given above, the integrations of 1H of each of compounds **50** and **51** relative to 1H of compound **50** are as follows:

$$I_{\mathbf{50}} = \frac{3.00}{3} = 1.00; \quad I_{\mathbf{51}} = \frac{9.24}{6} = 1.54$$

where $I_{\mathbf{X}}$ is the integration of 1H of compound **X** (**X** = **50** or **51**) relative to 1H of compound **50**. Since $I_{\mathbf{X}} \propto [\mathbf{X}]$ (concentration of **X** in mol L^{-1}), the percentage of O-alkylation is given by:

$$\text{Percentage of O-alkylation} = \frac{I_{\mathbf{50}}}{I_{\mathbf{50}} + I_{\mathbf{51}}} \times 100$$

$$= \frac{1.00}{1.00 + 1.54} \times 100 = 39\%$$

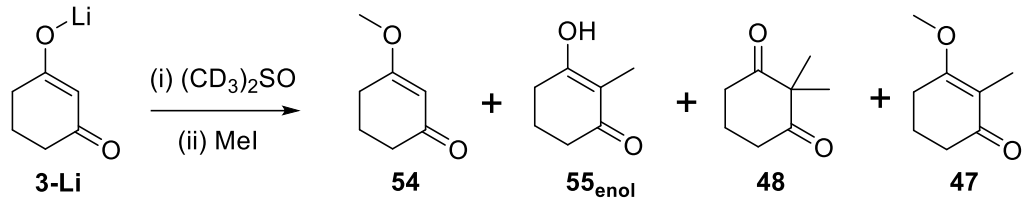
Integrations give an O vs C ratio of 39:61

[a] The relevant ^{1}H NMR spectra are shown in Figure B61 and Figure B62 in Appendix B.

5.6. Determination of O/C Ratios in Alkylations of Lithium Enolates

5.6.1. Reactions of the 1,3-Cyclohexanedione-Derived Enolate 3-Li

(i) Reaction of Enolate 3-Li with Methyl Iodide in $(CD_3)_2SO$



From the lithium enolate of 1,3-cyclohexanedione (**3-Li**) (0.015 g, 0.127 mmol) and methyl iodide (0.0234 g, 0.165 mmol) in $(CD_3)_2SO$ by procedure B at 20 °C.

^{1}H NMR (400 MHz, $(CD_3)_2SO$) of crude mixture of alkylation products (the underlined integrations are expressed relative to 1H of compound **54**): [a,b]

Assigned to **54**: δ 5.29 (s, 1H, C=C<u>H</u>), 3.66 (s, 3H, OC<u>H</u>$_3$), 2.37 (t, *J* = 6.2 Hz, 2H, C<u>H</u>$_2$C=O). [18]

Assigned to **55$_{enol}$**: δ 1.51 (s, 7.42H, C-C<u>H</u>$_3$ (3H of compound **55$_{enol}$**)). [30]

Assigned to **48**: δ 2.65 (t, *J* = 6.8 Hz, 1.77H, C<u>H</u>$_2$C=O (4H of compound **48**)), 1.17 (s, 2.64H, C-C<u>H</u>$_3$ (6H of compound **48**)). [20]

Based on the ^{1}H NMR spectral data given above, the integrations of 1H of each of compounds **54**, **55** and **48** relative to 1H of compound **54** are as follows:

$$I_{\mathbf{54}} = 1.00; \quad I_{\mathbf{55}} = \frac{7.51}{3} = 2.50; \quad I_{\mathbf{48}} = \frac{2.64}{6} = 0.44$$

where $I_{\mathbf{X}}$ is the integration of 1H of compound **X** (**X** = **54**, **55** or **48**) relative to 1H of compound **54**. Since $I_{\mathbf{X}} \propto [\mathbf{X}]$ (concentration of **X** in mol L^{-1}), the percentage of O-alkylation is given by:

$$\text{Percentage of O-alkylation} = \frac{I_{\mathbf{54}}}{I_{\mathbf{54}} + I_{\mathbf{55}} + I_{\mathbf{48}}} \times 100$$

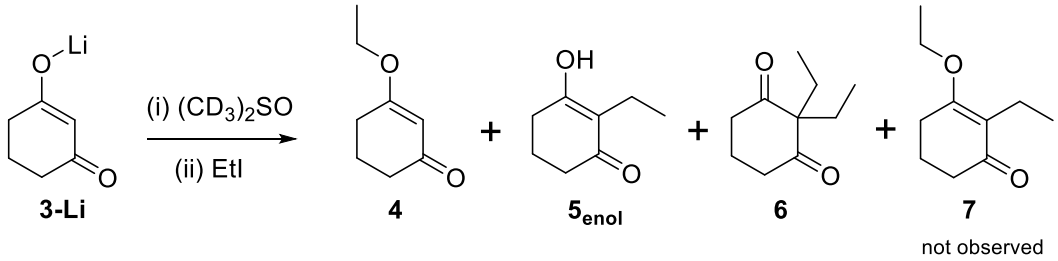
$$= \frac{1.00}{1.00 + 2.50 + 0.44} \times 100 = 25\%$$

Integrations give an <u>O vs C</u> ratio of 25:75

[a] The relevant ^{1}H NMR spectra are shown in Figure B63 and Figure B64 in Appendix B.

[b] Signals of **54**, **55** and **48** that are overlapping with other signals: δ 2.27 – 2.15 (m, contains 2H of **54** and 4H of **55$_{enol}$**), 1.90 – 1.80 (m, contains 2H of **54**, 2H of **55$_{enol}$**, 2H of **48** and THF signal).

(ii) Reaction of Enolate 3-Li with Ethyl Iodide in $(CD_3)_2SO$



From the lithium enolate of 1,3-cyclohexanedione (**3-Li**) (0.015 g, 0.127 mmol) and ethyl iodide (0.0197 g, 0.127 mmol) in $(CD_3)_2SO$ by procedure B at 20 °C.

^{1}H NMR (400 MHz, $(CD_3)_2SO$) of crude mixture of alkylation products (the underlined integrations are expressed relative to 1H of compound **4**): [a,b]

Assigned to **4**: δ 5.26 (s, 1H, C=C<u>H</u>), 3.90 (q, *J* = 7.0 Hz, 2H, OC<u>H</u>$_2$CH$_3$), 2.36 (t, *J* = 6.2 Hz, 2H, C<u>H</u>$_2$C=C), 1.26 (t, *J* = 7.0 Hz, 3H, OCH$_2$C<u>H</u>$_3$). [3]

Assigned to **5$_{enol}$**: δ 0.80 (t, *J* = 7.4 Hz, 1.16H, C-CH$_2$C<u>H</u>$_3$ (3H of compound **5$_{enol}$**)). [4]

Assigned to **6**: δ 2.64 – 2.57 (m, 0.13H, C<u>H</u>$_2$C=O (4H of compound **6**)), 0.63 (t, *J* = 7.4 Hz, 0.17H, C-CH$_2$C<u>H</u>$_3$ (6H of compound **6**)). [c]

Based on the ^{1}H NMR spectral data given above, the integrations of 1H of each of compounds **4**, **5$_{enol}$** and **6** relative to 1H of compound **4** are as follows:

$$I_{\mathbf{4}} = 1.00; \quad I_{\mathbf{5}} = \frac{1.16}{3} = 0.386; \quad I_{\mathbf{6}} = \frac{0.17}{6} = 0.028$$

where $I_{\mathbf{X}}$ is the integration of 1H of compound **X** (**X** = **4**, **5$_{enol}$** or **6**) relative to 1H of compound **4**. Since $I_{\mathbf{X}} \propto [\mathbf{X}]$ (concentration of **X** in mol L^{-1}), the percentage of O-alkylation is given by:

$$\text{Percentage of O-alkylation} = \frac{I_{\mathbf{4}}}{I_{\mathbf{4}} + I_{\mathbf{5}} + I_{\mathbf{6}}} \times 100$$

$$= \frac{1.00}{1.00 + 0.386 + 0.028} \times 100 = 71\%$$

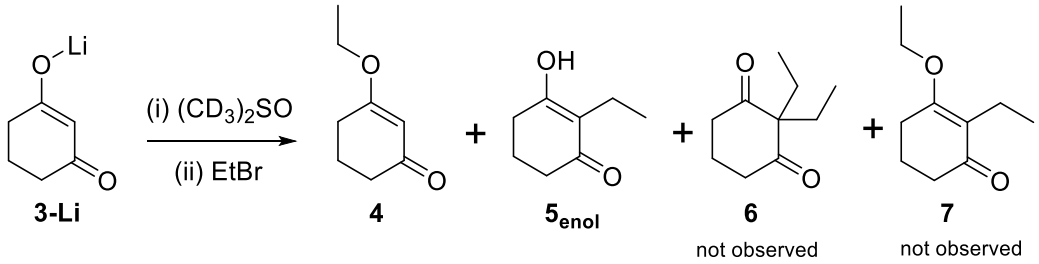
Integrations give an <u>O vs C</u> ratio of 71:29

[a] The relevant ^{1}H NMR spectra are shown in Figure B65 and Figure B66 in Appendix B.

[b] Signals of **4 – 6** that are overlapping with other signals: δ 2.29 – 2.06 (m, contains 2H of **4**, 6H of **5$_{enol}$** and 2H of **6**), 1.93 – 1.62 (m, contains 2H of **4**, 2H of **5$_{enol}$**, 2H of **6** and THF signal).

[c] No literature data is available for this compound, which was formed in very low quantities (*ca*. 2 %). Assignments of NMR signals were made by analogy with analogue 2-ethyl-2-methyl-cyclohexan-1,3-dione in $CDCl_3$: δ 2.77-2.58 (4H, m), 2.10-1.97 (1H, m), 1.92-1.77 (3H, m), 1.21 (3H, s), <u>0.80</u> (3H, t, *J* = 7.5 Hz).[5]

(iii) Reaction of Enolate 3-Li with Ethyl Bromide in $(CD_3)_2SO$



From the lithium enolate of 1,3-cyclohexanedione (**3-Li**) (0.015 g, 0.127 mmol) and ethyl bromide (0.0189 g, 0.173 mmol) in $(CD_3)_2SO$ by procedure B at 20 °C.

^{1}H NMR (400 MHz, $(CD_3)_2SO$) of crude mixture of alkylation products (the underlined integrations are expressed relative to 1H of compound **4**): [a,b]

Assigned to **4**: δ 5.27 (s, 1H, C=C<u>H</u>), 3.90 (q, *J* = 7.0 Hz, 2H, OC<u>H</u>$_2$CH$_3$), 2.36 (t, *J* = 6.2 Hz, 2H, C<u>H</u>$_2$C=C), 1.26 (t, *J* = 7.0 Hz, 3H, OCH$_2$C<u>H</u>$_3$). [3]

Assigned to **5$_{enol}$**: δ 0.80 (t, *J* = 7.3 Hz, 0.50H, C-CH$_2$C<u>H</u>$_3$ (3H of compound **5$_{enol}$**)). [4]

Based on the ^{1}H NMR spectral data given above, the integrations of 1H of each of compounds **4** and **5$_{enol}$** relative to 1H of compound **4** are as follows:

$$I_{\mathbf{4}} = 1.00; \quad I_{\mathbf{5}} = \frac{0.50}{3} = 0.166$$

where $I_{\mathbf{X}}$ is the integration of 1H of compound **X** (**X** = **4** or **5$_{enol}$**) relative to 1H of compound **4**. Since $I_{\mathbf{X}} \propto [\mathbf{X}]$ (concentration of **X** in mol L^{-1}), the percentage of O-alkylation is given by:

$$\text{Percentage of O-alkylation} = \frac{I_{\mathbf{4}}}{I_{\mathbf{4}} + I_{\mathbf{5}}} \times 100$$

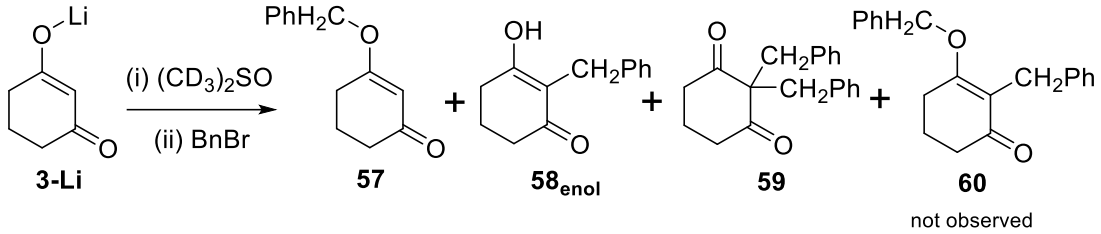
$$= \frac{1.00}{1.00 + 0.166} \times 100 = 86\%$$

Integrations give an <u>O vs C</u> ratio of 86:14

[a] The relevant ^{1}H NMR spectra are shown in Figure B67 and Figure B68 in Appendix B.

[b] Signals of **4 – 5** that are overlapping with other signals: δ 2.22 – 2.16 (m, contains 2H of **4** and 4H of **5$_{enol}$**), 2.19 – 1.96 (m, contains 2H of **5$_{enol}$**), 1.90 – 1.80 (m, contains 2H of **4**), 1.80 – 1.70 (m, contains 2H of **5$_{enol}$** and THF signal).

(iv) Reaction of Enolate 3-Li with Benzyl Bromide (56) in $(CD_3)_2SO$



From the lithium enolate of 1,3-cyclohexanedione (**3-Li**) (0.018 g, 0.152 mmol) and benzyl bromide (**56**) (0.028 g, 0.163 mmol) in $(CD_3)_2SO$ by procedure B at 20 °C.

^{1}H NMR (400 MHz, $(CD_3)_2SO$) of crude mixture of alkylation products (the underlined integrations are expressed relative to 1H of compound **57**): [a,b]

Assigned to **57**: δ 5.42 (s, 1H, C=C<u>H</u>), 2.42 (t, *J* = 6.2 Hz, 2H, C<u>H</u>$_2$C=O). [31]

Assigned to **58$_{enol}$**: δ 3.44 (s, 4.10H, C-C<u>H</u>$_2$Ph (2H of compound **58$_{enol}$**)). [30]

Assigned to **59**: δ 3.10 (s, 1.00H, C-C<u>H</u>$_2$Ph (4H of compound **59**)), 1.03 – 0.88 (m, 0.51H, CH$_2$C<u>H</u>$_2$CH$_2$ (2H of compound **59**)). [32]

Based on the ^{1}H NMR spectral data given above, the integrations of 1H of each of compounds **57**, **58$_{enol}$** and **59** relative to 1H of compound **57** are as follows:

$$I_{\mathbf{57}} = 1.00; \quad I_{\mathbf{58}} = \frac{4.10}{2} = 2.05; \quad I_{\mathbf{59}} = \frac{0.51}{2} = 0.255$$

where $I_{\mathbf{X}}$ is the integration of 1H of compound **X** (**X** = **57**, **58$_{enol}$** or **59**) relative to 1H of compound **57**. Since $I_{\mathbf{X}} \propto [\mathbf{X}]$ (concentration of **X** in mol L^{-1}), the percentage of O-alkylation is given by:

$$\text{Percentage of O-alkylation} = \frac{I_{\mathbf{57}}}{I_{\mathbf{57}} + I_{\mathbf{58}} + I_{\mathbf{59}}} \times 100$$

$$= \frac{1.00}{1.00 + 2.05 + 0.255} \times 100 = 30\%$$

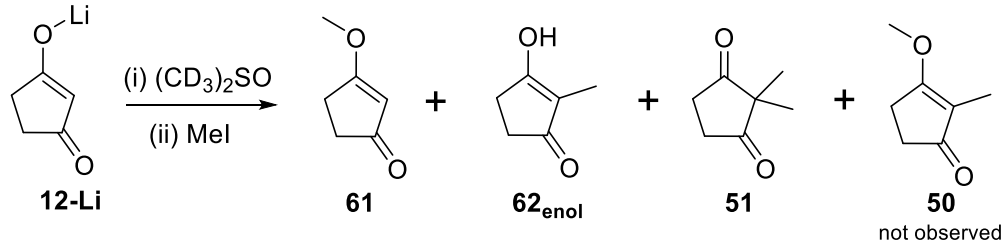
Integrations give an <u>O vs C</u> ratio of 30:70

[a] The relevant ^{1}H NMR spectra are shown in Figure B69 and Figure B70 in Appendix B.

[b] Signals of **57 - 59** that are overlapping with other signals: δ 7.45 – 6.88 (m, contains 5H of **57**, 5H of **58$_{enol}$** and 10H of **59**), 4.96 (broad s, contains 2H of **57** & signal of enol of starting material). 2.29 – 2.17 (m, contains 2H of **57** and 4H of **58$_{enol}$**), 1.92 – 1.68 (m, contains 2H of **57**, 2H of **58$_{enol}$**, 2H of **59** and THF signal).

5.6.2. Reactions of the 1,3-Cyclopentanedione-Derived Enolate 12-Li

(i) Reaction of Enolate 12-Li with Methyl Iodide in $(CD_3)_2SO$



From the lithium enolate of 1,3-cyclopentanedione (**12-Li**) (0.018 g, 0.173 mmol) and methyl iodide (0.026 g, 0.183 mmol) in $(CD_3)_2SO$ by procedure B at 20 °C.

^{1}H NMR (300 MHz, $(CD_3)_2SO$) of crude mixture of alkylation products (the underlined integrations are expressed relative to 1H of compound **61**): [a,b]

Assigned to **61**: δ 5.36 (s, 1H, C=C<u>H</u>), 3.81 (s, 3H, OC<u>H</u>$_3$), 2.59 – 2.53 (m, 2H, C<u>H</u>$_2$C=O). [22]

Assigned to **62$_{enol}$**: δ 1.44 (s, 1.56H, C-C<u>H</u>$_3$ (3H of compound **62$_{enol}$**)). [33]

Assigned to **51**: δ 2.74 (s, 0.22H, C<u>H</u>$_2$C=O (4H of compound **51**), 0.99 (s, 0.37H, C-C<u>H</u>$_3$ (6H of compound **51**). [33]

Based on the ^{1}H NMR spectral data given above, the integrations of 1H of each of compounds **61**, **62$_{enol}$** and **51** relative to 1H of compound **61** are as follows:

$$I_{\mathbf{61}} = 1.00; \quad I_{\mathbf{62}} = \frac{1.56}{3} = 0.52; \quad I_{\mathbf{51}} = \frac{0.37}{6} = 0.0616$$

where $I_{\mathbf{X}}$ is the integration of 1H of compound **X** (**X** = **61**, **62$_{enol}$** or **51**) relative to 1H of compound **61**. Since $I_{\mathbf{X}} \propto [\mathbf{X}]$ (concentration of **X** in mol L^{-1}), the percentage of O-alkylation is given by:

$$\text{Percentage of O-alkylation} = \frac{I_{\mathbf{61}}}{I_{\mathbf{61}} + I_{\mathbf{62}} + I_{\mathbf{51}}} \times 100$$

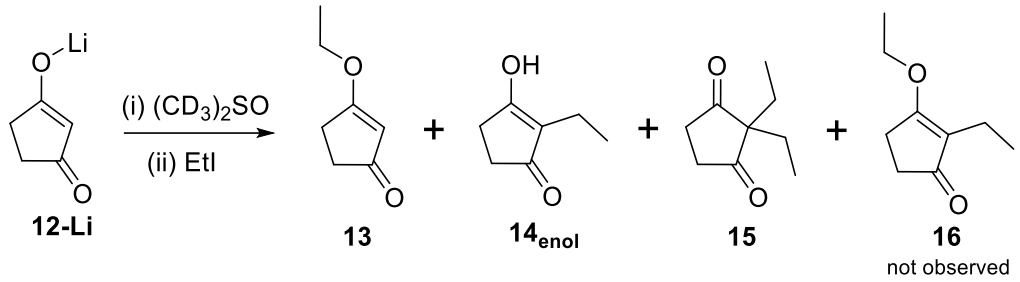
$$= \frac{1.00}{1.00 + 0.52 + 0.0616} \times 100 = 63\%$$

Integrations give an <u>O vs C</u> ratio of 63:37

[a] The relevant ^{1}H NMR spectra are shown in Figure B71 and Figure B72 in Appendix B.

[b] Signals of **51**, **61** and **62** that are overlapping with other signals: δ 2.38 – 2.27 (m, contains 2H of **61** and 4H of **62$_{enol}$**).

(ii) Reaction of the Enolate 12-Li with Ethyl Iodide in $(CD_3)_2SO$



From the lithium enolate of 1,3-cyclopentanedione (**12-Li**) (0.029 g, 0.279 mmol) and ethyl iodide (0.0446 g, 0.286 mmol) in $(CD_3)_2SO$ by procedure B at 20 °C.

^{1}H NMR (300 MHz, $(CD_3)_2SO$) of crude mixture of alkylation products (the underlined integrations are expressed relative to 1H of compound **13**): [a,b]

Assigned to **13**: δ 5.34 (s, 1H, C=C<u>H</u>), 4.06 (q, *J* = 7.0 Hz, 2H, OC<u>H</u>$_2$CH$_3$), 1.30 (q, *J* = 7.0 Hz, 3H, OCH$_2$C<u>H</u>$_3$). [11]

Assigned to **14$_{enol}$**: δ 1.04 (t, *J* = 7.0 Hz, 0.87H, C-CH$_2$C<u>H</u>$_3$ (3H of compound **14$_{enol}$**)). [8]

Assigned to **15**: δ 0.86 (t, *J* = 7.4 Hz, 0.23H, C-CH$_2$C<u>H</u>$_3$ (6H of compound **15**)). [9]

Based on the ^{1}H NMR spectral data given above, the integrations of 1H of each of compounds **13**, **14$_{enol}$** and **15** relative to 1H of compound **13** are as follows:

$$I_{\mathbf{13}} = 1.00 \quad I_{\mathbf{14}} = \frac{0.87}{3} = 0.29 \quad I_{\mathbf{15}} = \frac{0.23}{6} = 0.0383$$

where $I_{\mathbf{X}}$ is the integration of 1H of compound **X** (**X** = **13**, **14$_{enol}$** or **15**) relative to 1H of compound **13**. Since $I_{\mathbf{X}} \propto [\mathbf{X}]$ (concentration of **X** in mol L^{-1}), the percentage of O-alkylation is given by:

$$\text{Percentage of O-alkylation} = \frac{I_{\mathbf{13}}}{I_{\mathbf{13}} + I_{\mathbf{14}} + I_{\mathbf{15}}} \times 100$$

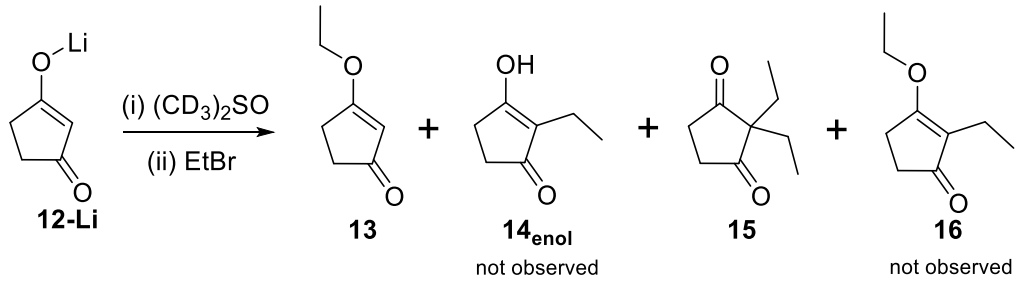
$$= \frac{1.00}{1.00 + 0.29 + 0.0383} \times 100 = 75\%$$

Integrations give an <u>O vs C</u> ratio of 75:25

[a] The relevant ^{1}H NMR spectra are shown in Figure B73 and Figure B74 in Appendix B.

[b] Signals of **13 - 15** that are overlapping with other signals: δ 2.60 – 2.52 (m, contains 2H of **13**), 2.31 – 2.25 (m, contains 2H of **13**).

(iii) Reaction of Enolate 12-Li with Ethyl Bromide in $(CD_3)_2SO$



From the lithium enolate of 1,3-cyclopentanedione (**12-Li**) (0.022 g, 0.211 mmol) and ethyl bromide (0.024 g, 0.221 mmol) in $(CD_3)_2SO$ by procedure B at 20 °C.

^{1}H NMR (300 MHz, $CDCl_3$) of crude mixture of alkylation products (the underlined integrations are expressed relative to 1H of compound **13**): [a,b]

Assigned to **13**: δ 5.35 (s, 1H, C=C<u>H</u>), 4.06 (q, *J* = 7.0 Hz, 2H, OC<u>H</u>$_2$CH$_3$), 2.30 – 2.26 (m, 2H, C<u>H</u>$_2$C=C), 1.30 (t, *J* = 7.0 Hz, 3H, OCH$_2$C<u>H</u>$_3$). [11]

Assigned to **15**: δ 0.89 – 0.81 (m, 0.17H, C-CH$_2$C<u>H</u>$_3$ (6H of compound **15**)). [9]

Based on the ^{1}H NMR spectral data given above, the integrations of 1H of each of compounds **13** and **15** relative to 1H of compound **13** are as follows:

$$I_{\mathbf{13}} = \ 1.00; \quad I_{\mathbf{15}} = \frac{0.17}{6} \ = 0.0283$$

where $I_{\mathbf{X}}$ is the integration of 1H of compound **X** (**X** = **13** or **15**) relative to 1H of compound **13**. Since $I_{\mathbf{X}} \propto [\mathbf{X}]$ (concentration of **X** in mol L^{-1}), the percentage of O-alkylation is given by:

$$\text{Percentage of O-alkylation} = \frac{I_{\mathbf{13}}}{I_{\mathbf{13}} + I_{\mathbf{15}}} \times \ 100$$

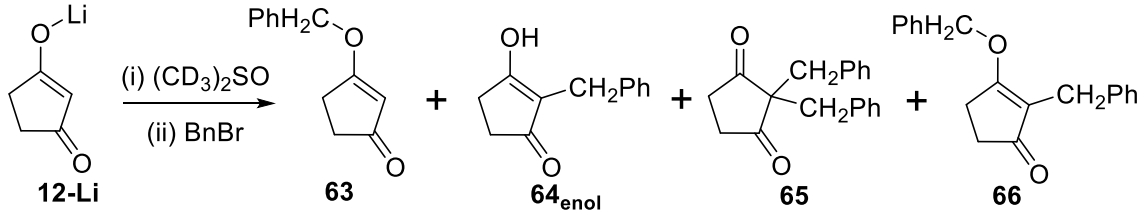
$$= \frac{1.00}{1.00 + 0.0283} \times \ 100 = 97\%$$

Integrations give an <u>O vs C</u> ratio of 97:3

[a] The relevant ^{1}H NMR spectra are shown in Figure B75 and Figure B76 in Appendix B.

[b] Signals of **13 - 15** that are overlapping with other signals: δ 2.59 – 2.46 (m, contains 2H of **13** & signal of (CD$_2$<u>H</u>)(CD$_3$)SO).

(iv) Reaction of Enolate 12-Li with Benzyl Bromide (56) in $(CD_3)_2SO$



From the lithium enolate of 1,3-cyclopentanedione (**12-Li**) (0.017 g, 0.163 mmol) and benzyl bromide (0.0297 g, 0.174 mmol) in $(CD_3)_2SO$ by procedure B at 20 °C.

^{1}H NMR (300 MHz, $CDCl_3$) of crude mixture of alkylation products (the underlined integrations are expressed relative to 1H of compound **63**): [a,b]

Assigned to **63**: δ 5.49 (s, 1H, C=CH). [34]

Assigned to **64$_{enol}$**: δ 3.31 (s, 1.00H, C-CH_2Ph (2H of compound **64$_{enol}$**)). [35]

Assigned to **65**: δ 2.96 (s, 0.19H, C-CH_2Ph (4H of compound **65**)), 2.01 (s, 0.18H, CH_2C=O (4H of compound **65**)). [c]

Assigned to **66**: δ 5.34 (s, 0.05H, O-CH_2Ph (2H of compound **66**)), 3.67 (s, 0.04H, C-CH_2Ph (2H of compound **66**)). [34]

Based on the ^{1}H NMR spectral data given above, the integrations of 1H of each of compounds **63**, **64$_{enol}$**, **65** and **66** relative to 1H of compound **63** are as follows:

$$I_{\mathbf{63}} = 1.00; \quad I_{\mathbf{64}} = \frac{1.00}{2} = 0.5; \quad I_{\mathbf{65}} = \frac{0.19}{4} = 0.048; \quad I_{\mathbf{66}} = \frac{0.05}{2} = 0.025$$

where $I_{\mathbf{X}}$ is the integration of 1H of compound **X** (**X** = **63**, **64$_{enol}$**, **65** or **66**) relative to 1H of compound **63**. Since $I_{\mathbf{X}} \propto [\mathbf{X}]$ (concentration of **X** in mol L^{-1}), the percentage of O-alkylation is given by:

$$\text{Percentage of O-alkylation} = \frac{I_{\mathbf{63}}}{I_{\mathbf{63}} + I_{\mathbf{64}} + I_{\mathbf{65}} + I_{\mathbf{66}}} \times 100$$

$$= \frac{1.00}{1.00 + 0.5 + 0.048 + 0.025} \times 100 = 64\%$$

Integrations give an O vs C ratio of 64:36

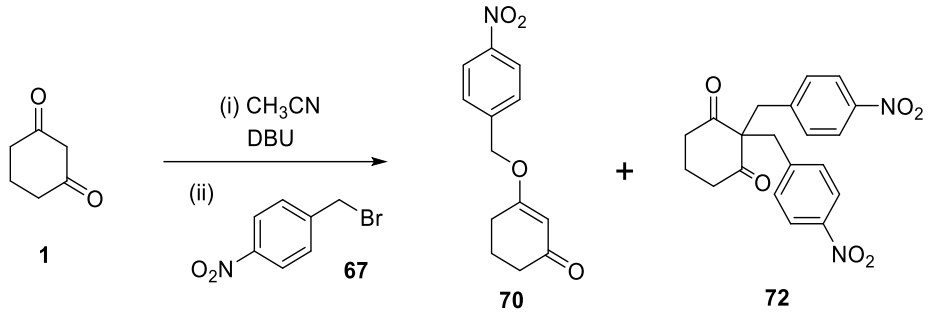
[a] The relevant ^{1}H NMR spectra are shown in Figure B77 and Figure B78 in Appendix B.

[b] Signals of **63 - 66** that are overlapping with other signals: δ 7.96 – 6.92 (m, contains 5H of **63**, 5H of **64**, 10H of **65** and 10H of **66**), 5.14 – 5.09 (m, contains 2H of **63** & signal of starting enolate), 2.62 – 2.58 (m, contains 2H of **63** and 2H of **66**) 2.43 – 2.25 (m, contains 2H of **63**, 4H of **64** and 2H of **63**).

[c] No literature data is available for this compound, which was formed in very low quantities (*ca*. 3 %). Assignments of NMR signals were made by analogy with analogue 2,2-dimethylcyclopentan-1,3-dione in $CDCl_3$: δ 2.80 (s, 4H), 1.15 (s, 4H). [23]

5.7. Preparation of Benzylated Derivatives of 1,3-Diketones

(i) Reaction of 1,3-Cyclohexanedione, DBU and 4-Nitrobenzyl Bromide



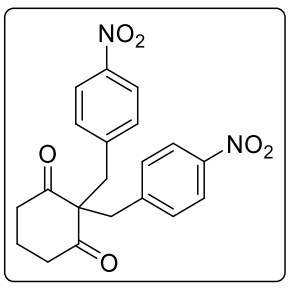
1,3-Cyclohexanedione (**1**) (0.503 g, 4.49 mmol) was dissolved in CH_3CN (15 ml) in a Schlenk flask containing an inert atmosphere of nitrogen gas. 1,8-Diazabicyclo[5.4.0]undec-7-ene (**2**) (0.72 ml, 0.73 g, 4.8 mmol) was subsequently added dropwise, causing the solution to turn yellow. After 10 minutes, 4-nitrobenzyl bromide (**67**) (4.84 g, 22.4 mmol) was quickly added to the Schlenk flask by powder funnel, causing the solution to turn a pale orange colour. The solution was stirred for 2 weeks. The CH_3CN was removed by vacuum, leaving a yellow solid mass. This was dissolved in 20 ml CH_2Cl_2 and triethylamine (3.11 ml, 2.26 g, 22.3 mmol) was added to react with the excess 4-nitrobenzyl bromide (**67**). The solution was transferred to a separatory funnel. The organic phase was washed 3 times with 20 ml portions of deionised water. The phases were separated and the combined aqueous phases were washed twice more with fresh portions of CH_2Cl_2 (20 ml). The combined organic phases were dried over $MgSO_4$, filtered, and concentrated under vacuum to give a yellow oil (crude product, 0.560 g). The residue was purified by column chromatography on silica using 90:10 cyclohexane / EtOAc, yielding (**72**) as colourless crystals (0.04 g, 2%). Compound **70** persistently co-eluted with other contaminants, meaning it could not be isolated from this reaction mixture despite it forming in the reaction.

Note: The yield quoted above is for the product **72** in its pure form. Co-elution of the products is primarily responsible for the low quoted yield.

A sample of **72** in $CDCl_3$ was then prepared for ^1H NMR spectroscopic characterisation.

Spectral data for pure compound **72**: [a]

^{1}H NMR (300 MHz, $CDCl_3$)



δ 8.14 – 8.08 (m, 4H, Aryl H-3), 7.22 – 7.17 (m, 4H, Aryl H-2), 3.34 (s, 4H, C-CH_2), 2.01 – 1.94 (m, 4H, $COCH_2$), 1.05 – 0.92 (m, 2H, $CH_2CH_2CH_2$).

^{13}C NMR (75 MHz, $CDCl_3$) δ 211.3 (C=O), 147.3 (CNO_2), 143.4 (Aryl C-1), 131.0 (Aryl C-2), 123.8 (Aryl C-3), 70.1 (C-CH_2), 44.3 (C-CH_2), 41.3 ($COCH_2$), 14.8 ($CH_2CH_2CH_2$).

[a] The relevant ^1H and ^{13}C NMR spectra are shown in Figure B79, Figure B80 and Figure B81 in Appendix B.

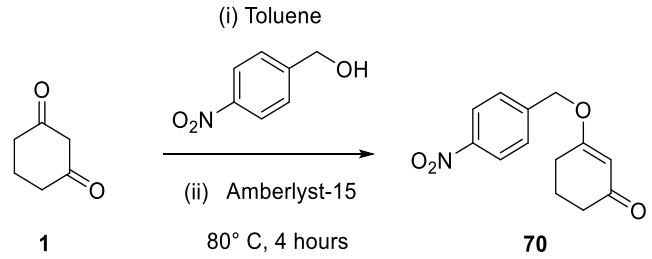
IR (ATR-FTIR), cm^{-1}: 3076 (w), 2924 (m), 1719 (m), 1694 (s), 1605 (m), 1515 (s), 1346 (s), 858 (m).

HRMS-ESI$^+$ (*m*/*z*): $[M + H]^+$ calculated for $C_{20}H_{18}N_2O_6$, 383.12376; found, 383.12315

MP 231 – 232 °C

(ii) Preparation of 3-((4-Nitrobenzyl)oxy)cyclohex-2-en-1-one (70) using Amberlyst-15

70 was prepared using Amberlyst-15 by an established literature procedure. [36]

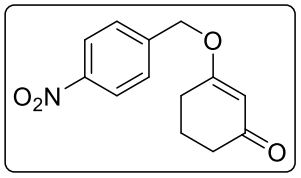


1,3-Cyclohexanedione (**1**) (0.280 g, 2.50 mmol) was dissolved in toluene (7 ml) in a round-bottomed flask and stirred. 4-Nitrobenzyl alcohol (0.387 g, 2.53 mmol) was added to the solution. The solution was heated to 80 °C over the course of 5 minutes. Amberlyst-15 (0.250 g) was added to the solution by powder funnel. The flask was sealed using a greased stopper and allowed to stir for 4 hours. The solution was filtered and the toluene was removed by vacuum. The yellow residue was purified by column chromatography on silica using 70:30 cyclohexane / EtOAc, yielding (**70**) as fine white crystals (0.165 g, 27%).

A sample of **70** in $CDCl_3$ was then prepared for ^{1}H NMR spectroscopic characterisation.

Spectral data for pure compound **70**: [a]

^{1}H NMR (300 MHz, $CDCl_3$)



δ 8.25 – 8.20 (m, 2H, Aryl H-3), 7.55 – 7.50 (m, 2H, Aryl H-2), 5.42 (s, 1H, C=CH), 4.99 (s, 2H, OCH_2), 2.50 (t, *J* = 6.3 Hz, 2H, CH_2C=C), 2.38 – 2.33 (m, 2H, CH_2C=O), 2.07 – 1.97 (m, 2H, $CH_2CH_2CH_2$).

^{13}C NMR (75 MHz, $CDCl_3$) δ 199.5 (C=O), 176.9 (C=CH), 147.9 (CNO_2), 142.3 (Aryl C-1), 128.0 (Aryl C-2), 123.9 (Aryl C-3), 103.8 (C=CH), 68.8 (OCH_2), 36.7 (CH_2C=O), 28.9 (CH_2C=C), 21.1 ($CH_2CH_2CH_2$).

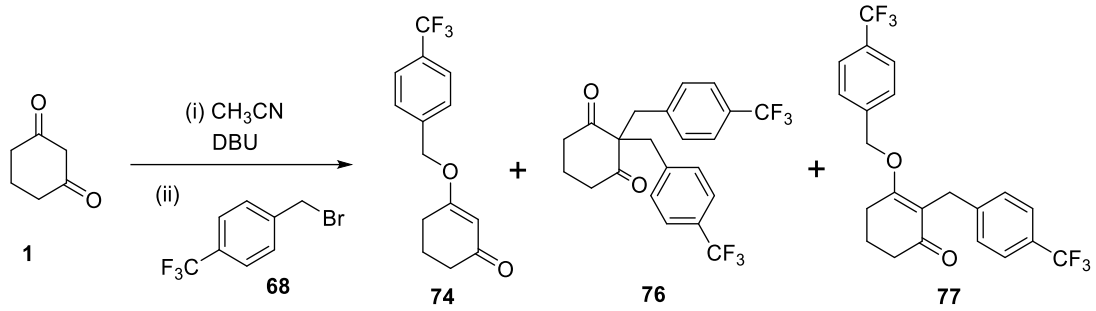
IR (ATR-FTIR), cm^{-1}: 2949 (m), 1645 (m), 1596 (s), 1517 (s), 1343 (s), 1223 (m), 1177 (s), 737 (s).

HRMS-ESI$^-$ (*m*/*z*): $[M - H]^-$ calculated for $C_{13}H_{13}NO_4$, 246.07718; found, 246.07746

[a] The relevant ^{1}H and ^{13}C NMR spectra are shown in Figure 82, Figure 83 and Figure 84 in Appendix B.

MP 87 – 88 °C

(iii) Reaction of 1,3-Cyclohexanedione, DBU and 4-(Trifluoromethyl)benzyl Bromide



1,3-Cyclohexanedione (**1**) (0.502 g, 4.48 mmol) was dissolved in CH_3CN (15 ml) in a Schlenk flask containing an inert atmosphere of nitrogen gas. 1,8-Diazabicyclo[5.4.0]undec-7-ene (**2**) (0.72 ml, 0.73 g, 4.8 mmol) was subsequently added dropwise, causing the solution to turn yellow. After 10 minutes, 4-(trifluoromethyl)benzyl bromide (**68**) (4.84 g, 22.4 mmol) was quickly added to the Schlenk flask by powder funnel, causing the solution to turn a pale orange colour. The solution was stirred for 2 weeks. The CH_3CN was removed by vacuum, leaving a yellow solid mass. This was dissolved in 20 ml CH_2Cl_2 and triethylamine (3.11 ml, 2.26 g, 22.3 mmol) was added to react with the excess 4-(trifluoromethyl)benzyl bromide (**68**). The solution was transferred to a separatory funnel. The organic phase was washed 3 times with 20 ml portions of deionised water. The phases were separated and the aqueous layer was washed twice more with portions of CH_2Cl_2 (20 ml each). The combined organic phases were dried over $MgSO_4$, filtered, and concentrated under vacuum to give a yellow oil (crude product, 0.985 g). The residue was purified by column chromatography on silica using 95 : 5 dichloromethane : MeOH, yielding (**74**) as colourless crystals (0.267 g, 22%), (**76**) as colourless crystals (0.143 g, 7%) and (**77**) as colourless crystals (0.009 g, < 1%).

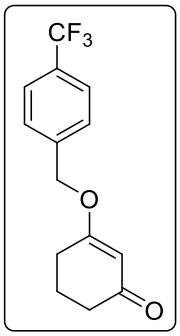
Note: The yields quoted above are for the products **74**, **76** and **77** in their pure form. Co-elution of the products is primarily responsible for the low quoted yields.

Samples of **74, 76** and **77** in $CDCl_3$ were then prepared for ^1H NMR spectroscopic characterisation.

Spectral data for pure compound **74**: [a]

[a] The relevant ^1H, ^{19}F and ^{13}C NMR spectra are shown in Figure B85, Figure B86, Figure B87 and Figure B88 in Appendix B.

^{1}H NMR (300 MHz, $CDCl_3$)



δ 7.68 – 7.58 (m, 2H, Aryl H-3), 7.52 – 7.40 (m, 2H, Aryl H-2), 5.45 (s, 1H, C=CH), 4.95 (s, 2H, OCH_2), 2.49 (t, *J* = 6.3 Hz, 2H, CH_2C=C), 2.37 (m, 2H, CH_2CO), 2.01 (m, 2H, $CH_2CH_2CH_2$).

^{13}C NMR (75 MHz, $CDCl_3$): δ 200.0 (C=O), 177.4 (C=CH), 139.1 (Aryl C-1), 130.8 (q, *J* = 32.6 Hz, C-CF_3), 127.9 (Aryl C-2), 125.8 (q, *J* = 3.7 Hz, Aryl C-3), 124.0 (q, *J* = 272.2 Hz, C-CF_3), 103.7 (C=CH), 69.5 (OCH_2), 36.8 (CH_2C=O), 29.1 (CH_2C=C), 21.3 ($CH_2CH_2CH_2$).

^{19}F NMR (282 MHz, $CDCl_3$) δ −62.7.

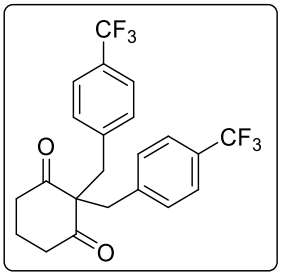
IR (ATR-FTIR), cm^{-1}: 2926 (w), 1731 (w), 1652 (m), 1604 (s), 1322 (s), 1224 (m), 1163 (s), 1110 (s), 1065 (s), 825 (s).

HRMS-ESI$^-$ (*m*/*z*): $[M - H]^-$ calculated for $C_{14}H_{13}F_3O_2$, 269.07949; found, 269.07886

MP 62 – 64 °C

Spectral data for pure compound **76**: [a]

^{1}H NMR (300 MHz, $CDCl_3$)



δ 7.53 – 7.47 (m, 4H, Aryl H-3), 7.17 – 7.11 (m, 4H, Aryl H-2), 3.30 (s, 4H, C-CH_2), 1.91 (t, *J* = 6.6 Hz, 4H, CH_2C=O), 0.96 – 0.85 (m, 2H, $CH_2CH_2CH_2$).

^{13}C NMR (75 MHz, $CDCl_3$): δ 212.0 (C=O), 140.2 (C-CH_2), 130.5 – 128.8 (m, C-CF_3), 130.4 (Aryl C-2), 125.5 (q, *J* = 3.5 Hz, Aryl C-3), 124.0 (q, *J* = 272.2 Hz, C-CF_3), 70.3 (C-CH_2), 44.6 (C-CH_2), 41.4 (CH_2C=O), 14.7 ($CH_2CH_2CH_2$).

^{19}F NMR (282 MHz, $CDCl_3$) δ −62.6.

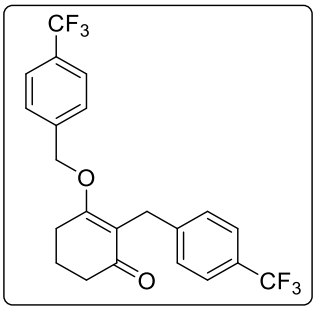
IR (ATR-FTIR), cm^{-1}: 2964 (w), 1719 (m), 1693 (s), 1322 (s), 1161 (s), 1117 (s), 1066 (s), 828 (m).

HRMS-ESI$^-$ (*m*/*z*): $[M - H]^-$ calculated for $C_{22}H_{18}F_6O_2$, 427.11382; found, 427.11208

MP 156 – 157 °C

Spectral data for pure compound **77**: [b]

[a] The relevant ^{1}H, ^{19}F and ^{13}C NMR spectra are shown in Figure B89, Figure B90, Figure B91 and Figure B92 in Appendix B.
[b] The relevant ^{1}H, ^{19}F and ^{13}C NMR spectra are shown in Figure B93, Figure B94, Figure B95 and Figure B96 in Appendix B.



^{1}H NMR (600 MHz, $CDCl_3$)

δ 7.62 – 7.58 (m, 2H, O-Benzyl H-3), 7.45 – 7.42 (m, 2H, C-Benzyl H-3), 7.30 – 7.25 (m, overlaps with $CHCl_3$ signal, 4H, O-Benzyl H-2 and C-Benzyl H-2), 5.13 (s, 2H, OCH_2), 3.72 (s, 2H, C=C-CH_2), 2.61 (t, *J* = 6.2 Hz, 2H, CH_2C=C), 2.41 – 2.38 (m, 2H, CH_2C=O), 2.03 – 1.98 (m, 2H, $CH_2CH_2CH_2$).

^{13}C NMR (151 MHz, $CDCl_3$): δ 197.9 (C=O), 171.5 (CH_2C=C), 145.8 (C-Benzyl Aryl C-1), 140.0 (O-Benzyl Aryl C-1), 130.9 (q, *J* = 32.6 Hz, O-Benzyl C-CF_3), 129.1 (C-Benzyl Aryl C-2), 128.0 (q, *J* = 32.1 Hz, C-Benzyl C-CF_3), 127.2 (O-Benzyl Aryl C-2), 125.9 (q, *J* = 3.7 Hz, O-Benzyl Aryl C-3), 125.1 (q, *J* = 3.8 Hz, C-Benzyl Aryl C-3), 124.6 (q, *J* = 271.7 Hz, C-Benzyl C-CF_3), 124.0 (q, *J* = 272.2 Hz, O-Benzyl C-CF_3), 119.5 (C=C-CH_2), 68.9 (OCH_2), 36.4 (CH_2C=O), 28.1 (C=C-CH_2), 25.7 (CH_2C=C), 21.0 ($CH_2CH_2CH_2$).

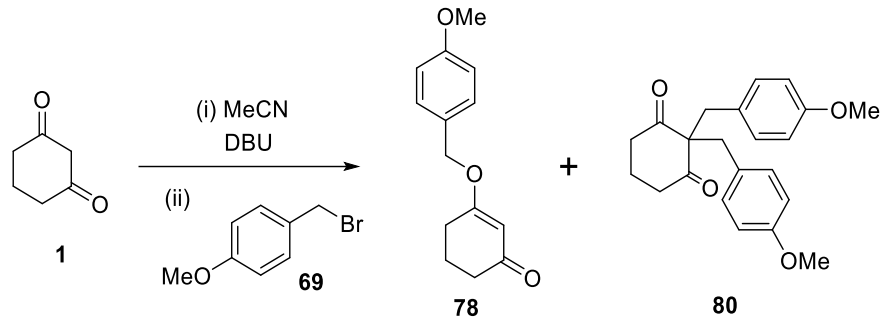
^{19}F NMR (565 MHz, $CDCl_3$) δ −62.3, −62.7.

IR (ATR-FTIR), cm^{-1}: 2924 (w), 1694 (w), 1616 (m), 1325 (s), 1163 (m), 1110 (s), 1067 (s), 1019 (m), 823 (w).

HRMS-ESI$^+$ (*m*/*z*): $[M + H]^+$ calculated for $C_{22}H_{18}F_6O_2$, 429.12838; found, 429.12805

MP 163 – 165 °C

(iv) Reaction of 1,3-Cyclohexanedione, DBU and 4-Methoxybenzyl Bromide

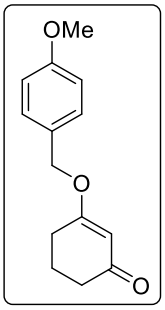


1,3-Cyclohexanedione (**1**) (0.239 g, 2.13 mmol) was dissolved in CH_3CN (8 ml) in a Schlenk flask containing an inert atmosphere of nitrogen gas. 1,8-Diazabicyclo[5.4.0]undec-7-ene (**2**) (0.32 ml, 0.32 g, 2.1 mmol) was subsequently added dropwise, causing the solution to turn yellow. After 10 minutes, 4-methoxybenzyl bromide (**69**) (0.453 g, 2.25 mmol) was added to the Schlenk flask dropwise by syringe. The solution was stirred for 10 days. The CH_3CN was removed by vacuum, leaving a yellow oil. This was dissolved in CH_2Cl_2 (30 ml). The solution was transferred to a separatory funnel. The organic phase was washed 3 times with 20 ml portions of deionised water. The phases were separated and the aqueous layer was washed twice more with portions of CH_2Cl_2 (20 ml each). The combined organic phases were dried over $MgSO_4$, filtered, and concentrated under vacuum to give a yellow oil (crude product, 0.487 g). The residue was purified by column chromatography on silica using 90:10 cyclohexane / EtOAc, incrementally rising to

50:50 as the elution progressed. This purification yielded (**78**) as colourless crystals (0.130 g, 26%), (**80**) as colourless crystals (0.04 g, 5%).

Note: The yields quoted above are for the products **78** and **80** in their pure form. Co-elution of the products is primarily responsible for the low quoted yields.

Spectral data for pure compound **78**: [a]



^{1}H NMR (300 MHz, $CDCl_3$)

δ 7.32 – 7.27 (m, 2H, Aryl H-2), 6.94 – 6.88 (m, 2H, Aryl H-3), 5.48 (s, 1H, C=CH), 4.82 (s, 2H, OCH_2), 3.82 (s, 3H, C-OCH_3), 2.45 (t, *J* = 6.3 Hz, 2H, CH_2C=C), 2.39 – 2.32 (m, 2H, CH_2C=O), 2.05 – 1.94 (m, 2H, $CH_2CH_2CH_2$).

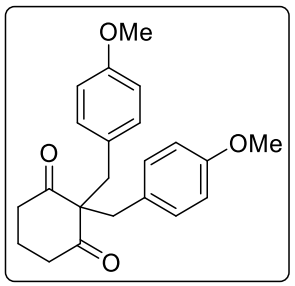
^{13}C NMR (75 MHz, $CDCl_3$) δ 200.0 (C=O), 177.8 (C=CH), 160.1 (C-OCH_3), 129.9 (Aryl C-2), 127.2 (Aryl C-1), 114.3 (Aryl C-3), 103.5 (C=CH), 70.5 (OCH_2), 55.5 (C-OCH_3), 36.9 (CH_2C=O), 29.3 (CH_2C=C), 21.4 ($CH_2CH_2CH_2$).

IR (ATR-FTIR), cm^{-1}: 2946 (m), 1648 (s), 1599 (s), 1514 (s), 1370 (s), 1244 (s), 1172 (s), 822 (s).

HRMS-ESI$^+$ (*m*/*z*): $[M + H]^+$ calculated for $C_{14}H_{16}O_3$, 233.11722; found, 233.11695

MP 59 – 60 °C

Spectral data for pure compound **80**: [b]



^{1}H NMR (300 MHz, $CDCl_3$)

δ 6.96 – 6.89 (m, 4H, Aryl H-2), 6.77 – 6.71 (m, 4H, Aryl H-3), 3.75 (s, 6H, C-OCH_3), 3.16 (s, 4H, C-CH_2), 1.88 (t, *J* = 6.6 Hz, 4H, CH_2C=O), 0.96 – 0.85 (m, 2H, $CH_2CH_2CH_2$).

^{13}C NMR (75 MHz, $CDCl_3$) δ 213.6 (C=O), 158.7 (C-OCH_3), 131.1 (Aryl C-2), 128.6 (Aryl C-1), 114.0 (Aryl C-3), 71.2 (C-CH_2), 55.3 (C-OCH_3), 44.3 (C-CH_2), 41.7 (CH_2C=O), 14.9 ($CH_2CH_2CH_2$).

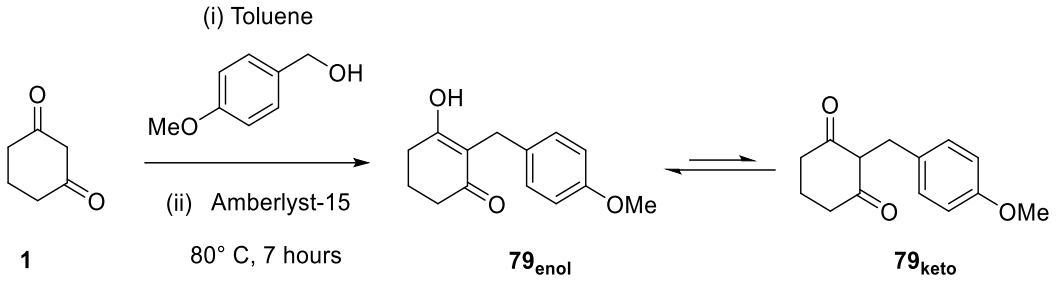
IR (ATR-FTIR), cm^{-1}: 2957 (m), 1718 (m), 1692 (s), 1610 (s), 1512 (s), 1239 (s), 1180 (s), 1032 (s), 816 (s).

HRMS-ESI$^+$ (*m*/*z*): $[M + H]^+$ calculated for $C_{22}H_{24}O_4$, 353.17474; found, 353.17426

MP 127 – 128 °C

[a] The relevant ^{1}H and ^{13}C NMR spectra are shown in Figure B97, Figure B98 and Figure B99 in Appendix B.
[b] The relevant ^{1}H and ^{13}C NMR spectra are shown in Figure B100, Figure B101 and Figure B102 in Appendix B.

(v) Preparation of 3-Hydroxy-2-(4-methoxybenzyl)cyclohex-2-en-1-one (79) using Amberlyst-15

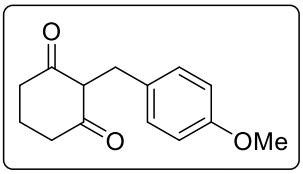


1,3-Cyclohexanedione (**1**) (0.282 g, 2.52 mmol) was dissolved in toluene (4 ml) in a round-bottomed flask and stirred. 4-Methoxybenzyl alcohol (0.349 g, 2.53 mmol) was added to the solution. The solution was heated to 80 °C over the course of 5 minutes. Amberlyst-15 (0.252 g) was added to the solution by powder funnel. The flask was sealed using a greased stopper and allowed to stir for 7 hours. The solution was filtered while hot, removing the Amberlyst-15 from the solution. The yellow solution was allowed to cool. After 10 minutes, white crystals began crashing out of the yellow solution. The solution was left undisturbed overnight, yielding a large amount of white crystals suspended in the solution after 18 hours. The mixture was filtered and the crystals were collected on filter paper and washed 5 times with portions of toluene (2 ml). The product was allowed to air dry in the fumehood for 1 hour before being collected, yielding (**79**) as fine white crystals (0.130 g, 22%).

A sample of **79** in $CDCl_3$ was then prepared for ^1H NMR spectroscopic characterisation.

Note: The product **79** exists in solution as an equilibrium mixture of tautomers **79$_{enol}$** and **79$_{keto}$** (favouring the enol form). ^1H and ^{13}C NMR signals of the keto and enol forms are given below.

^1H NMR (400 MHz, $CDCl_3$) [a]



Assigned to enol tautomer **79$_{enol}$**: δ 7.17 – 7.11 (m, 2H, Aryl H-2), 6.78 – 6.74 (m, 2H, Aryl H-3), 3.75 (s, 3H, OCH_3), 3.59 (s, 2H, $CH_2C{=}C$), 2.42 (t, *J* = 6.5 Hz, 4H, $CH_2C{=}O$), 1.96 – 1.87 (m, 2H, $CH_2CH_2CH_2$). [37]

Assigned to keto tautomer **79$_{keto}$**: δ 7.17 – 7.11 (m, 2H), 6.84 – 6.79 (m, 2H), 3.77 (s, 3H), 3.69 (t, *J* = 5.7 Hz, 1H), 3.14 (d, *J* = 5.7 Hz, 2H), 2.77 – 2.47 (m, 4H), 1.98 – 1.88 (m, 1H), 1.83 – 1.66 (m, 1H).

^{13}C NMR (101 MHz, $CDCl_3$)

Assigned to enol tautomer **79$_{enol}$**: δ 187.4 (C=O), 157.9 (C-OCH_3), 133.0 (Aryl C-1), 129.6 (Aryl C-2), 116.0 ($CH_2C{=}C{-}C{=}O$), 113.9 (Aryl C-3), 55.4 (C-OCH_3), 32.9 ($CH_2C{=}O$), 26.8 ($CH_2C{=}C$), 20.8 ($CH_2CH_2CH_2$).

[a] The relevant ^1H and ^{13}C NMR spectra are shown in Figure B103, Figure B104 and Figure B105 in Appendix B.

Assigned to keto tautomer **79$_{keto}$**: δ 204.4, 158.2, 132.15, 130.3, 114.3, 70.1, 55.3, 40.1, 27.5, 17.1.

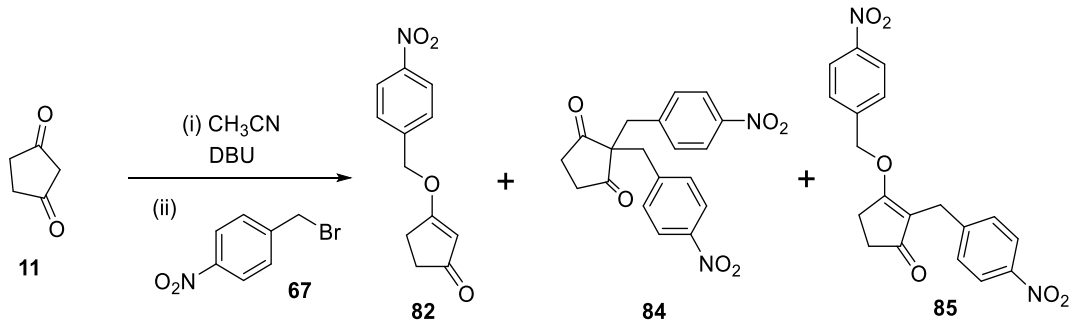
Note: Although HSQC and HMBC NMR spectra of a sample of this compound were recorded, it was not possible to assign the signals of the keto tautomer in the ^{1}H and ^{13}C NMR spectra to specific positions in **79** due to the low concentration of the keto isomer and the presence of signals of diastereotopic protons.

IR (ATR-FTIR), cm^{-1}: 2933 (m), 1706 (m), 1581 (s), 1509 (s), 1370 (s), 1241 (s), 1005 (s), 816 (m).

HRMS-ESI^{+} (*m*/*z*): $[M - H]^{+}$ calculated for $C_{14}H_{16}O_3$, 233.11722; found, 233.11678

MP 146 – 147 °C (lit. 144 – 146 °C). [37]

(vi) Reaction of 1,3-Cyclopentanedione, DBU and 4-Nitrobenzyl Bromide

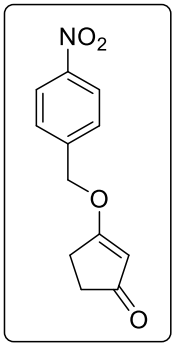


1,3-Cyclopentanedione (**9**) (0.301 g, 3.07 mmol) was dissolved in CH_3CN (15 ml) in a nitrogen-filled Schlenk flask. 1,8-Diazabicyclo[5.4.0]undec-7-ene (**2**) (0.48 ml, 0.489 g, 3.21 mmol) was subsequently added dropwise, causing the solution to turn dark brown. After 10 minutes, 4-nitrobenzyl bromide (**67**) (3.13 g, 14.5 mmol) was quickly added to the Schlenk flask by powder funnel, causing the solution to turn a pale orange colour. The solution was stirred for 2 weeks. The CH_3CN was removed by vacuum, leaving a yellow oil. This was dissolved in CH_2Cl_2 (30 ml) and triethylamine (2.09 ml, 1.52 g, 15.0 mmol) was added to react with the excess 4-nitrobenzyl bromide (**67**). The solution was transferred to a separatory funnel. The organic phase was washed 3 times with 20 ml portions of deionised water. The phases were separated and the aqueous layer was washed twice more with fresh portions of CH_2Cl_2 (20 ml each). The combined organic phases were dried over $MgSO_4$, filtered, and concentrated under vacuum to give a brown oil (crude product, 1.28 g). The residue was purified by column chromatography on silica ausing 100% CH_2Cl_2, switching to 98:2 CH_2Cl_2 / MeOH after 40 fractions, yielding (**82**) as colourless crystals (0.306 g, 43%), (**84**) as colourless crystals (0.083 g, 7%) and (**85**) as colourless crystals (0.040 g, 4%).

Samples of **82**, **84**, and **85** in $CDCl_3$ was then prepared for ^{1}H NMR spectroscopic characterisation.

Note: **84** is sparingly soluble in $CDCl_3$, as well as DMSO-d_6.

Spectral data for pure compound **82**: [a]



^{1}H NMR (300 MHz, $CDCl_3$)

δ 8.26 – 8.17 (m, 2H, Aryl H-3), 7.57 – 7.52 (m, 2H, Aryl H-2), 5.36 (t, *J* = 1.1 Hz, 1H, C=CH), 5.11 (s, 2H, OCH_2), 2.71 – 2.65 (m, 2H, CH_2C=C), 2.47 – 2.42 (m, 2H, CH_2C=O).

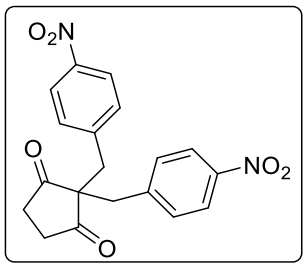
^{13}C NMR (75 MHz, $CDCl_3$): δ 205.5 (C=O), 189.2 (C=CH), 148.0 (C-NO_2), 141.8 (Aryl C-1), 128.1 (Aryl C-3), 124.0 (Aryl C-2), 105.9 (C=CH), 72.0 (OCH_2), 34.2 (CH_2C=O), 28.5 (CH_2C=C).

IR (ATR-FTIR), cm^{-1}: 3072 (w), 2924 (w), 1698 (m), 1677 (s), 1590 (s), 1517 (s), 1434 (m), 1328 (s), 1224 (s), 1185 (s), 843 (s).

HRMS-ESI$^-$ (*m*/*z*): $[M - H]^-$ calculated for $C_{12}H_{11}NO_4$, 232.06153; found, 232.06162

MP 140 – 141 °C

Spectral data for pure compound **84**: [b]



^{1}H NMR (300 MHz, $CDCl_3$)

δ 8.14 – 8.08 (m, 4H, Aryl H-3), 7.25 – 7.20 (m, 4H, Aryl H-2), 3.19 (s, 4H, C-CH_2), 1.95 (s, 4H, CH_2C=O).

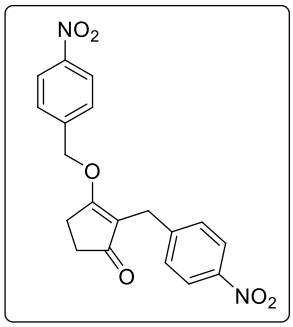
^{13}C NMR (75 MHz, $CDCl_3$): δ 216.0 (C=O), 147.4 (C-NO_2), 142.3 (Aryl C-1), 130.9 (Aryl C-2), 123.9 (Aryl C-3), 64.0 (C-CH_2), 41.7 (C-CH_2), 36.7 (CH_2C=O).

IR (ATR-FTIR), cm^{-1}: 3079 (w), 2922 (w), 1728 (m), 1605 (w), 1517 (s), 1347 (s), 858 (s).

HRMS-ESI$^-$ (*m*/*z*): $[M - H]^-$ calculated for $C_{19}H_{16}N_2O_6$, 367.09356; found, 367.09338

MP > 265 °C (no melting point observed up to 265 °C)

Spectral data for pure compound **85**: [c]



^{1}H NMR (300 MHz, $CDCl_3$)

δ 8.28 – 8.21 (m, 2H, O-Benzyl H-3), 8.10 – 8.04 (m, 2H, C-Benzyl H-3), 7.48 – 7.35 (m, 4H, O-Benzyl H-2 & C-Benzyl H-2), 5.32 (s, 2H, OCH_2), 3.60 (s, 2H, C=C-CH_2), 2.78 – 2.72 (m, 2H, CH_2C=C), 2.54 – 2.49 (m, 2H, CH_2C=O).

^{13}C NMR (75 MHz, $CDCl_3$): δ 203.4 (C=O), 183.5 (C=C-CH_2), 148.1 (O-Benzyl C-NO_2), 147.5 (C-Benzyl Aryl C-1), 146.5 (C-Benzyl C-NO_2), 142.4 (O-Benzyl Aryl C-1), 129.4 (C-Benzyl Aryl C-2), 127.4 (O-Benzyl Aryl C-2),

[a] The relevant ^{1}H and ^{13}C NMR spectra are shown in Figure B106, Figure B107 and Figure B108 in Appendix B.
[b] The relevant ^{1}H and ^{13}C NMR spectra are shown in Figure B109, Figure B110 and Figure B111 in Appendix B.
[c] The relevant ^{1}H and ^{13}C NMR spectra are shown in Figure B112, Figure B113 and Figure B114 in Appendix B.

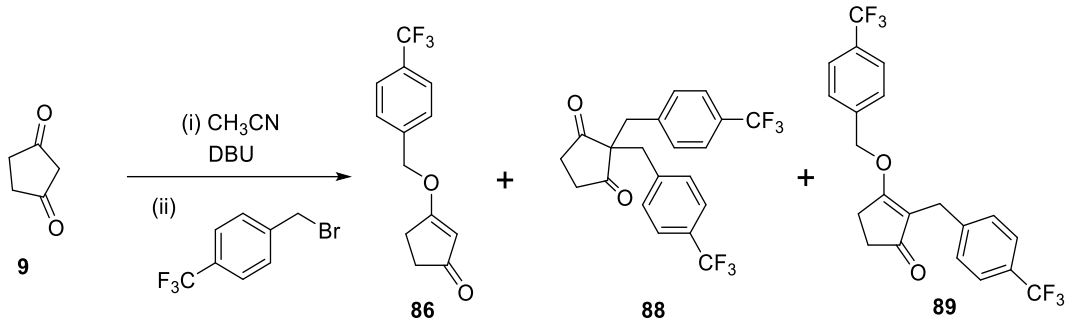
124.2 (O-Benzyl Aryl C-3), 123.6 (C-Benzyl Aryl C-3), 119.8 (C=C-CH_2), 69.7 (OCH_2), 33.6 (CH_2C=O), 27.4 (C=C-CH_2), 25.1 (CH_2C=C).

IR (ATR-FTIR), cm^{-1}: 2924 (w), 1688 (m), 1626 (s), 1604 (m), 1514 (s), 1340 (s), 1109 (m), 847 (m), 725 (m).

HRMS-ESI$^-$ (*m*/*z*): $[M - H]^-$ calculated for $C_{19}H_{16}N_2O_6$, 367.09356; found, 367.09325

MP 137 – 138 °C

(vii) Reaction of 1,3-Cyclopentanedione, DBU and 4-(Trifluoromethyl)benzyl Bromide

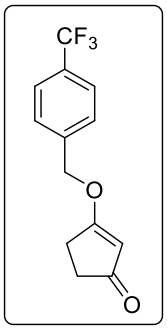


1,3-Cyclopentanedione (**9**) (0.304 g, 3.10 mmol) was dissolved in CH_3CN (15 ml) in a nitrogen-filled Schlenk flask. 1,8-Diazabicyclo[5.4.0]undec-7-ene (**2**) (0.48 ml, 0.49 g, 3.2 mmol) was subsequently added dropwise, causing the solution to turn dark brown. After 10 minutes, 4-(trifluoromethyl)benzyl bromide (**68**) (3.70 g, 15.5 mmol) was quickly added to the Schlenk flask by powder funnel, causing the solution to turn a pale orange colour. The solution was stirred for 2 weeks. The CH_3CN was removed by vacuum, leaving a yellow oil. This was dissolved in CH_2Cl_2 (30 ml) and triethylamine (2.10 ml, 1.52 g, 15.0 mmol) was added to react with the excess 4-(trifluoromethyl)benzyl bromide (**68**). The solution was transferred to a separatory funnel. The organic phase was washed 3 times with 20 ml portions of deionised water. The phases were separated and the aqueous layer was washed twice more with portions of CH_2Cl_2 (20 ml each). The combined organic phases were dried over $MgSO_4$, filtered, and concentrated under vacuum to give a brown oil (crude product, 1.0 g). The residue was purified by column chromatography on silica using 90:10 cyclohexane / EtOAc, 50:50 cyclohexane / EtOAc and 100% EtOAc as the eluent. The process yielded (**86**) as colourless crystals (0.243 g, 31%) and (**88**) as colourless crystals (0.055 g, 4%).

A further purification by column chromatography on silica using 98:2 CH_2Cl_2 / MeOH allowed the separation of compound **89** from a mixture of compounds (**86** + **89**). **89** was obtained as colourless crystals (0.029 g, 2%).

Note: The yields quoted above are for the products **86**, **88** and **89** in their pure form. Co-elution of the products is primarily responsible for the low quoted yields.

Samples of **86**, **88 and 89** in $CDCl_3$ were then prepared for ^1H NMR spectroscopic characterisation.



Spectral data for pure compound **86**: [a]

^{1}H NMR (300 MHz, $CDCl_3$)

δ 7.69 – 7.63 (m, 2H, Aryl H-3), 7.53 – 7.47 (m, 2H, Aryl H-2), 5.38 (t, *J* = 1.1 Hz, 1H, C=CH), 5.08 (s, 2H, OCH_2), 2.72 – 2.66 (m, 2H, CH_2C=C), 2.49 – 2.44 (m, 2H, CH_2C=O).

^{13}C NMR (75 MHz, $CDCl_3$): δ 205.6 (C=O), 189.3 (C=CH), 138.5 (Aryl C-1), 130.9 (q, *J* = 32.7 Hz, C-CF_3), 123.9 (app. q, app. *J* = 271.7 Hz, extends over a range 129.5 – 118.3; hence overlaps with several other signals, C-CF_3), 127.8 (Aryl C-2), 125.8 (q, *J* = 3.3 Hz, Aryl C-3), 105.7 (C=CH), 72.5 (OCH_2), 34.1 (CH_2C=O), 28.5 (CH_2C=C).

^{19}F NMR (282 MHz, $CDCl_3$) δ –62.8.

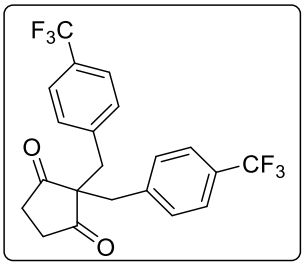
IR (ATR-FTIR), cm^{-1}: 2930 (w), 1704 (m), 1679 (m), 1584 (s), 1321 (s), 1164 (s), 1112 (s), 1066 (s), 1010 (m), 826 (s).

HRMS-ESI$^-$ (*m*/*z*): $[M - H]^-$ calculated for $C_{13}H_{11}F_3O_2$, 255.06384; found, 255.06370

MP 86 – 87 °C

Spectral data for pure compound **88**: [b]

^{1}H NMR (300 MHz, $CDCl_3$)



δ 7.53 – 7.46 (m, 4H, Aryl H-3), 7.20 – 7.14 (m, 4H, Aryl H-2), 3.14 (s, 4H, C-CH_2), 1.87 (s, 4H, CH_2C=O).

^{13}C NMR (75 MHz, $CDCl_3$): δ 216.8 (C=O), 139.2 (Aryl C-1), 130.3 (Aryl C-2), 129.7 (q, *J* = 32.2 Hz, C-CF_3), 125.6 (q, *J* = 3.3 Hz, Aryl C-3), 123.9 (q, *J* = 272.5 Hz, C-CF_3), 64.3 (C-CH_2), 42.0 (C-CH_2), 36.8 (CH_2C=O).

^{19}F NMR (282 MHz, $CDCl_3$) δ –62.7.

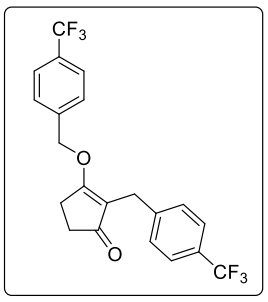
IR (ATR-FTIR), cm^{-1}: 2926 (w), 1725 (s), 1422 (m), 1322 (s), 1167 (s), 1118 (s), 1067 (s), 1019 (s), 907 (s), 730 (s).

HRMS-ESI$^-$ (*m*/*z*): $[M - H]^-$ calculated for $C_{21}H_{16}F_6O_2$, 413.09817; found, 413.09955

MP 120 – 121 °C

[a] The relevant ^{1}H and ^{13}C NMR spectra are shown in Figure B115, Figure B116, Figure B117 and Figure B118 in Appendix B.
[b] The relevant ^{1}H and ^{13}C NMR spectra are shown in Figure B119, Figure B120, Figure B121 and Figure B122 in Appendix B.

Spectral data for pure compound **89**: [a]



^{1}H NMR (600 MHz, $CDCl_3$)

δ 7.64 – 7.61 (m, 2H, O-Benzyl H-3), 7.51 – 7.47 (m, 2H, C-Benzyl H-3), 7.37 – 7.29 (m, 4H, O-Benzyl H-2 & C-Benzyl H-2), 5.25 (s, 2H, OCH_2), 3.56 (s, 2H, C=C-CH_2), 2.72 – 2.68 (m, 2H, CH_2C=C), 2.52 – 2.48 (m, 2H, CH_2C=O).

^{13}C NMR (151 MHz, $CDCl_3$): δ 203.7 (C=O), 183.7 (C=C-CH_2), 144.0 (C-Benzyl Aryl C-1), 139.4 (O-Benzyl Aryl C-1), 130.9 (q, *J* = 32.6 Hz, O-Benzyl C-CF_3), 129.0 (C-Benzyl Aryl C-2), 128.3 (q, *J* = 32.3 Hz, C-Benzyl C-CF_3), 127.2 – 121.5 (m, C-Benzyl C-CF_3), 126.9 (O-Benzyl Aryl C-2), 125.9 (q, *J* = 4.0 Hz, O-Benzyl Aryl C-3), 125.2 (q, *J* = 4.0 Hz, C-Benzyl Aryl C-3), 123.8 (q, *J* = 272.5 Hz, O-Benzyl C-CF_3), 120.4 (C=C-CH_2), 70.0 (OCH_2), 33.6 (CH_2C=O), 27.3 (C=C-CH_2), 25.0 (CH_2C=C).

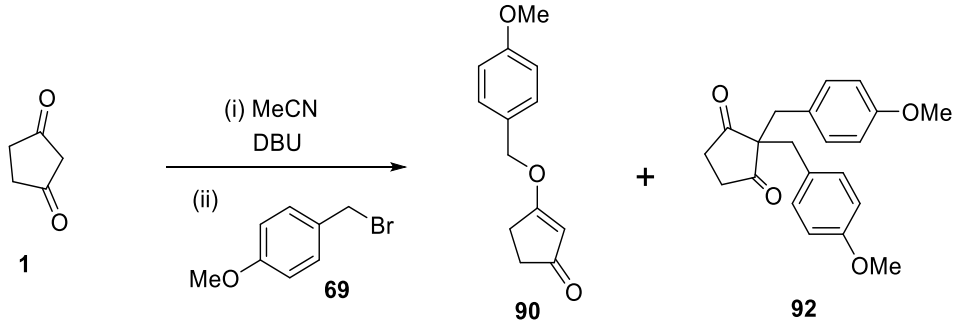
^{19}F NMR (565 MHz, $CDCl_3$) δ –62.3, –62.7.

IR (ATR-FTIR), cm^{-1}: 2927 (w), 1691 (m), 1630 (s), 1355 (m), 1323 (s), 1162 (m), 1110 (s), 1066 (s), 824 (m).

HRMS-ESI$^-$ (*m*/*z*): $[M - H]^-$ calculated for $C_{21}H_{16}F_6O_2$, 413.09817; found, 413.09800

MP 86 – 87 °C

(viii) Reaction of 1,3-Cyclopentanedione, DBU and 4-Methoxybenzyl Bromide



1,3-Cyclopentanedione (**9**) (0.210 g, 2.14 mmol) was dissolved in CH_3CN (8 ml) in a nitrogen-filled Schlenk flask. 1,8-Diazabicyclo[5.4.0]undec-7-ene (**2**) (0.32 ml, 0.33 g, 2.2 mmol) was subsequently added dropwise, causing the solution to turn dark brown. After 20 minutes, 4-methoxybenzyl bromide (**69**) (0.450 g, 2.24 mmol) was added to the Schlenk flask dropwise by syringe. The solution was stirred for 10 days. The CH_3CN was removed by vacuum, leaving a brown oil. This was dissolved in CH_2Cl_2 (30 ml) and the solution was transferred to a separatory funnel. The organic phase was washed 3 times with 20 ml portions of deionised water. The phases were separated and the aqueous layer was washed twice more with portions of CH_2Cl_2 (20 ml each). The combined organic phases were dried over $MgSO_4$, filtered, and concentrated under vacuum to give a brown oil (crude product, 0.448 g). The residue was purified by column chromatography on silica using 90:10 cyclohexane : EtOAc,

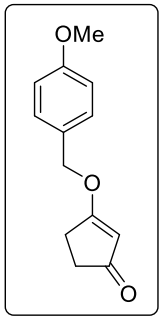
[a] The relevant ^{1}H and ^{13}C NMR spectra are shown in Figure B123, Figure B124, Figure B125 and Figure B126 in Appendix B.

rising to 20 : 80, yielding (**90**) as colourless crystals (0.189 g, 40%), (**92**) as colourless crystals (0.038 g, 5%).

Note: The yields quoted above are for the products **90** and **92** in their pure form. Co-elution of the products is primarily responsible for the low quoted yields.

Samples of **90** and **92** in $CDCl_3$ were then prepared for ^1H NMR spectroscopic characterisation.

Spectral data for pure compound **90**: [a]



^{1}H NMR (300 MHz, $CDCl_3$)

δ 7.33 – 7.27 (m, 2H, Aryl H-2), 6.95 – 6.88 (m, 2H, Aryl H-3), 5.40 (t, *J* = 1.1 Hz, 1H, C=CH), 4.94 (s, 2H, OCH_2), 3.81 (s, 3H, OCH_3), 2.65 – 2.60 (m, 2H, CH_2C=C), 2.47 – 2.40 (m, 2H, CH_2C=O).

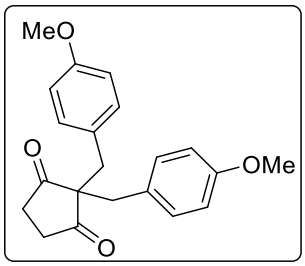
^{13}C NMR (75 MHz, $CDCl_3$): δ 206.0 (C=O), 189.9 (C=CH), 160.2 (C-OCH_3), 129.9 (Aryl C-2), 126.7 (Aryl C-1), 114.3 (Aryl C-3), 105.4 (C=CH), 73.7 (OCH_2), 55.4 (OCH_3), 34.1 (CH_2C=O), 28.8 (CH_2C=C).

IR (ATR-FTIR), cm^{-1}: 3090 (w), 2937 (w), 1693 (s), 1677 (s), 1587 (s), 1517 (s), 1345 (s), 1245 (s), 1177 (s), 1032 (s), 840 (s).

HRMS-ESI$^-$ (*m*/*z*): $[M - H]^-$ calculated for $C_{13}H_{14}O_3$, 217.08702; found, 217.08642

MP 82 – 83 °C

Spectral data for pure compound **92**: [b]



^{1}H NMR (300 MHz, $CDCl_3$)

δ 7.02 – 6.87 (m, 4H, Aryl H-2), 6.78 – 6.63 (m, 4H, Aryl H-3), 3.73 (s, 6H, OCH_3), 3.01 (s, 4H, C-CH_2), 1.80 (s, 4H, CH_2C=O).

^{13}C NMR (75 MHz, $CDCl_3$): δ 218.7 (C=O), 158.7 (C-OCH_3), 131.0 (Aryl C-2), 127.6 (Aryl C-1), 114.0 (Aryl C-3), 65.4 (C-CH_2), 55.3 (OCH_3), 41.8 (C-CH_2), 37.0 (CH_2C=O).

IR (ATR-FTIR), cm^{-1}: 2918 (w), 1721 (s), 1609 (s), 1510 (s), 1461 (m), 1302 (s), 1245 (s), 1179 (s), 1032 (s), 824 (s).

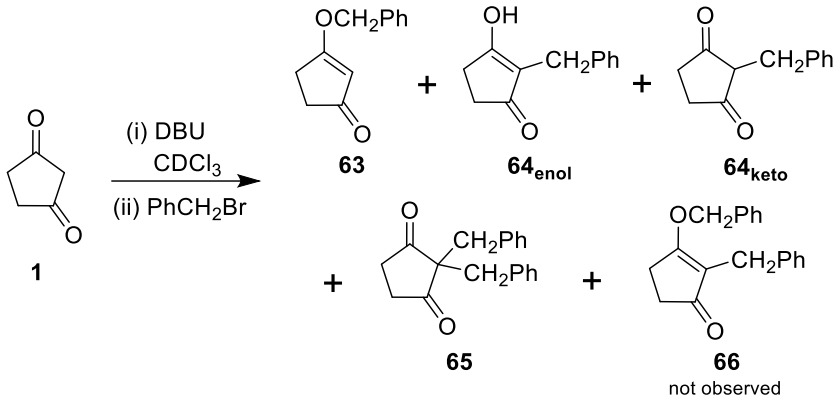
HRMS-ESI$^-$ (*m*/*z*): $[M - H]^-$ calculated for $C_{21}H_{22}O_4$, 339.15909; found, 339.15850

MP 119 – 120 °C

[a] The relevant ^1H and ^{13}C NMR spectra are shown in Figure B127, Figure B128 and Figure B129 in Appendix B.
[b] The relevant ^1H and ^{13}C NMR spectra are shown in Figure B130, Figure B131 and Figure B132 in Appendix B.

5.8. Determination of O/C Ratios in Enolate Benzylation Reactions

(i) Reaction of Enolate 12-D with Benzyl Bromide in $CDCl_3$



From 1,3-cyclohexanedione (**1**) (0.0234 g, 0.239 mmol), DBU (**2**) (0.0368 g, 0.242 mmol) and benzyl bromide (**56**) (0.0388 g, 0.227 mmol) in $CDCl_3$ by procedure A (see page 243 above) at 0 °C.

^{1}H NMR (300 MHz, $CDCl_3$) of crude mixture of alkylation products (the underlined integrations are expressed relative to 1H of compound **63**): [a,b]

Assigned to **63**: δ 5.40 (t, *J* = 1.1 Hz, 1H, C=C<u>H</u>), 5.04 (s, 2H, O-C<u>H</u>$_2$Ph), 2.69 – 2.65 (m, 2H).

Assigned to **64**: All signals overlap with others.

Assigned to **65**: δ 3.09 (s, 0.38H, C-C<u>H</u>$_2$Ph (4H of compound **65**)).

As can be seen in Figure 5-5 below, signals of **64** appear to be present, but cannot be accurately integrated due to overlapping signals of DBU and its derivatives, particularly in the region of the spectrum between 3.61 – 3.52. As a result, no O/C ratio can be measured for a reaction between this enolate and benzyl bromide in $CDCl_3$. Identical issues appeared when attempting to use other DBU derived enolates in reactions with benzyl bromide (**56**).

[a] The relevant ^{1}H NMR spectra are shown in Figure B133 and Figure B134 in Appendix B.

[b] Signals of **63 – 65** that are overlapping with other signals: δ 7.45 – 7.30 (m, contains 5H of **63** and $CDCl_3$ signal), 7.28 – 7.00 (m, contains 5H of **64** and 5H of **65**), 3.61 – 3.52 (m, contains 2H of **64** and signals of DBU and derivatives), 1.85 – 1.64 (m, contains 4H of **65** and signals of DBU and derivatives).

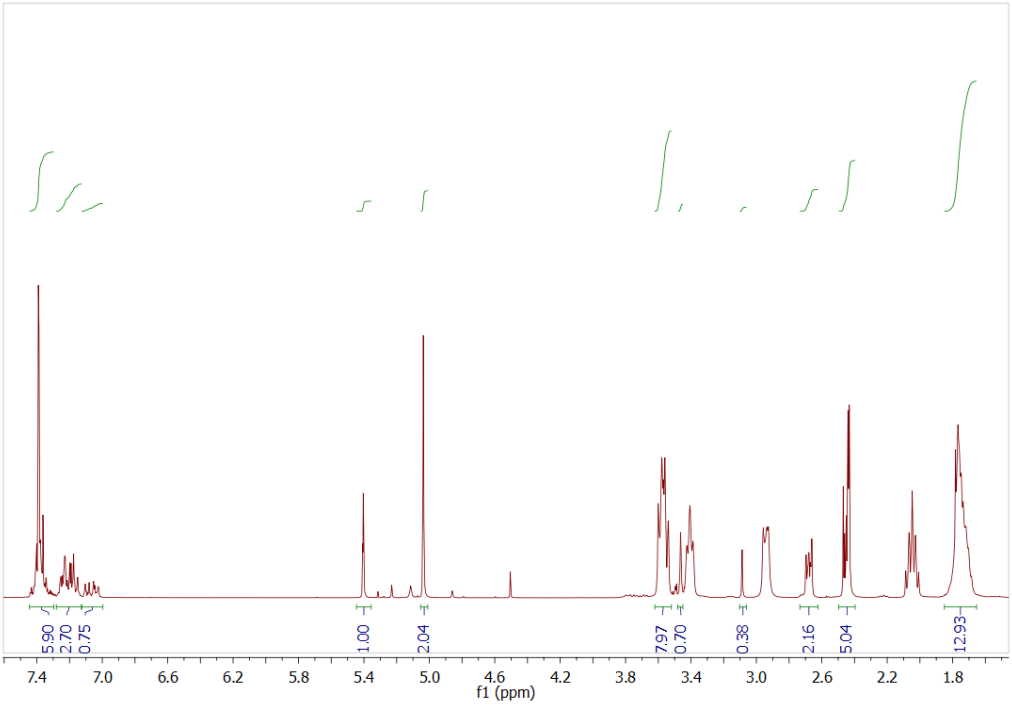


Figure 5-5: ^{1}H NMR spectrum of crude reaction mixture obtained from the reaction of 12-D with benzyl bromide in $CDCl_3$. No O/C ratio could be measured for this reaction.

General Procedure for the Alkylation of Tetramethylammonium Enolates in THF

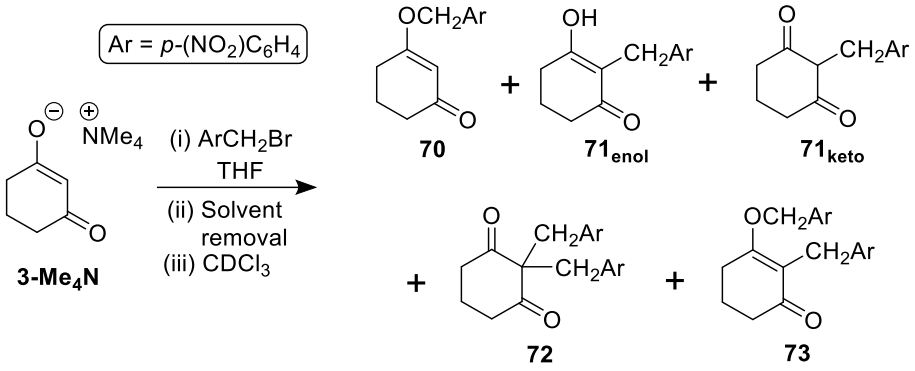
The following procedure (Procedure F) was used to establish the ratios of products formed by a reaction of an enolate and an electrophile in THF.

The tetramethylammonium enolate derived from a 1,3-dione (1.0 equivalent) was added to a Schlenk flask containing an inert atmosphere of nitrogen gas. Dry THF (0.7 ml) was added to form a transparent solution. This mixture was stirred for 15 minutes. To a separate Schlenk flask containing an inert atmosphere of nitrogen gas was added dry THF (0.3 ml). 1.05 equivalents of the appropriate alkylating agent was added to the THF and the flask was swirled, giving a transparent solution. The contents of this flask were taken up in a syringe (which had been flushed three times with nitrogen gas) and added to the flask containing the enolate solution dropwise over the course of 1 minute. The solution was stirred for approximately 18 hours. The side-arm of the reaction flask was connected with rubber tubing to a vacuum trap, which was itself connected to a Schlenk manifold. The trap was placed under vacuum ($\leq 5 \times 10^{-3}$ mbar). The vacuum trap and the tubing connecting it to the reaction flask and the Schlenk manifold were then filled with nitrogen gas by the pump and fill technique.[2] The trap was then placed under vacuum and then cooled with liquid N_2. At this point the stopcock on the Schlenk flask was opened and volatile reagents and solvent were removed and collected in the trap. After approximately 30 minutes, the entirety of the trap and the Schlenk flask were re-filled with nitrogen gas through the Schlenk manifold and the stopcock of the Schlenk flask was closed. The trap was removed and

the flask was re-attached directly to the Schlenk manifold, using the pump and fill technique to establish a nitrogen atmosphere in the tubing used for the attachment. The Schlenk flask containing the reaction mixture was then opened and the contents of the flask were dissolved in dry $CDCl_3$ (0.7 ml). The $CDCl_3$ sample was filtered to remove any insoluble Me_4N^+ salts ([NMe_4]Br or [NMe_4]I) and the filtrate was added to an NMR tube. The NMR tube was then transferred to the NMR spectrometer and a ^1H NMR spectrum was recorded.

5.8.1. Reactions of 1,3-Cyclohexanedione-Derived Enolate 3-Me_4N

(i) Reaction of Enolate of 3-Me_4N with 4-Nitrobenzyl Bromide in THF



The Me_4N^+ enolate of cyclohexan-1,3-dione (**3-Me_4N**) (0.012 g, 0.065 mmol) and 4-nitrobenzyl bromide (**67**) (0.0149 g, 0.069 mmol) were combined in dry THF (1 ml) in the manner described in Procedure F. The THF was removed under vacuum. The reaction mixture was dissolved in $CDCl_3$, and the resulting mixture was transferred to an NMR tube.

^1H NMR (600 MHz, $CDCl_3$) of crude mixture of alkylation products (the underlined integrations are expressed relative to 1H of compound **70**: [a,b]

Assigned to **70**: δ 5.45 (s, 1H, C=C<u>H</u>), 5.01 (s, 2H, O-C<u>H</u>$_2$Ph).

Assigned to **71$_{enol}$**: δ 3.77 (s, 0.15H, C-C<u>H</u>$_2$Ph (2H of compound **71$_{enol}$**)).

Assigned to **71$_{keto}$**: δ 3.61 (t, *J* = 6.6 Hz, 0.04H, C<u>H</u>-CH$_2$Ph (1H of compound **71$_{keto}$**)).

Assigned to **72** : δ 8.14 – 8.09 (m, 0.84H, Aryl H-3 (4H of compound **72**)), 7.21 – 7.18 (m, 0.83H, Aryl H-2 (4H of compound **72**)), 3.35 (s, 0.81H, C-C<u>H</u>$_2$Ph (4H of compound **72**)), 1.00 – 0.95 (m, 0.42H, CH$_2$C<u>H</u>$_2$CH$_2$ (2H of compound **72**)).

Assigned to **73**: δ 5.20 (s, 0.16H, O-C<u>H</u>$_2$Ph (2H of compound **73**)), 3.73 (s, 0.16H, C-C<u>H</u>$_2$Ph (2H of compound **73**)).

---

[a] Full characterisation data for the products **70** and **72** seen in this experiment are given in section 5.8. ^1H NMR data in $CDCl_3$ for the products **71$_{keto}$ and 71$_{enol}$** seen in this experiment are found in the literature.[16] The relevant ^1H NMR spectra are shown in Figure B135 and Figure B136 in Appendix B.

[b] Signals of **70** – **73** that are overlapping with other signals: δ 8.28 – 8.25 (m, contains 2H of **70**), 7.59 – 7.51 (m, contains 2H of **70**), 2.55 – 2.50 (m, contains 2H of **70**), 2.40 – 2.37 (m, contains 2H of **70**), 2.07 – 2.01 (m, contains 2H of **70**), 2.00 – 1.95 (m, contains 4H of **72**).

Based on the ^{1}H NMR spectral data given above, the integrations of 1H of each of compounds **70**, **71$_{enol}$**, **71$_{keto}$**, **72** and **73** relative to 1H of compound **70** are as follows:

$$I_{\mathbf{70}} = 1.00;\ \ I_{\mathbf{71e}} = \frac{0.15}{2} = 0.075;\ \ I_{\mathbf{71k}} = \ 0.04;\ \ I_{\mathbf{72}} = \ \frac{0.42}{2} = 0.21;$$

$$I_{\mathbf{73}} = \ \frac{0.16}{2} = 0.08$$

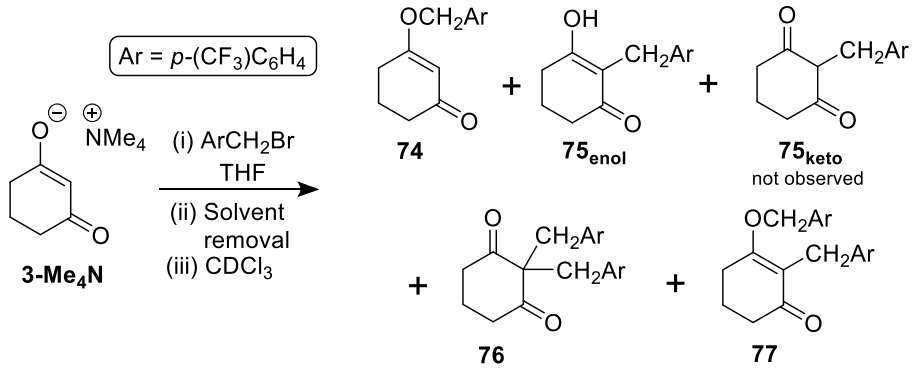
where $I_{\mathbf{X}}$ is the integration of 1H of compound **X** (**X** = **70**, **71$_{enol}$**, **71$_{keto}$**, **72** or **73**) relative to 1H of compound **70**. Since $I_{\mathbf{X}} \propto [\mathbf{X}]$ (concentration of **X** in mol L^{-1}), the percentage of O-alkylation is given by:

$$\text{Percentage of O-alkylation} = \frac{I_{\mathbf{70}}}{I_{\mathbf{70}} + I_{\mathbf{71e}} + I_{\mathbf{71k}} + I_{\mathbf{72}} + I_{\mathbf{73}}} \times \ 100$$

$$= \frac{1.00}{1.00 + 0.075 + 0.04 + 0.21 + 0.08} \times \ 100 = 71\%$$

Integrations give an <u>O vs C</u> ratio of 71:29.

(ii) Reaction of Enolate 3-Me$_4$N with 4-(Trifluoromethyl)benzyl Bromide in THF



The Me_4N^+ enolate of cyclohexan-1,3-dione (0.012 g, 0.065 mmol) and 4-(trifluoromethyl)benzyl bromide (**68**) (0.0166 g, 0.069 mmol) were combined in dry THF (1 ml) in the manner described in Procedure F. The THF was removed under vacuum. The reaction mixture was dissolved in $CDCl_3$, and the resulting mixture was transferred to an NMR tube.

^{1}H NMR (300 MHz, $CDCl_3$) of crude mixture of alkylation products (the underlined integrations are expressed relative to 1H of compound **74**: [a,b]

Assigned to **74**: δ 5.46 (s, <u>1H</u>, C=C<u>H</u>), 4.95 (s, <u>2H</u>, O-C<u>H</u>$_2$Ph).

---

[a] Full characterisation data for the products **74**, **76** and **77** seen in this experiment are given in section 5.8. The relevant ^{1}H NMR spectra are shown in Figure B137 and Figure B138 in Appendix B.

[b] Signals of **74** – **77** that are overlapping with other signals: δ 7.69 – 7.56 (m, contains 2H of **74** and 2H of **77**), 7.50 – 7.43 (m, contains 2H of **74** and 2H of **77**), 7.37 – 7.29 (m, contains 2H of **77**), 7.14 (app. d, app. *J* = 8.0 Hz, contains 2H of **76**), 3.30 (s, contains 2H of **76**), 2.69 – 2.57 (m, contains 2H of **77**), 2.53 – 2.42 (m, contains 2H of **74**), 2.40 – 2.34 (m, contains 2H of **74** and 2H of **77**), 2.07 – 1.97 (m, contains 2H of **74** and 2H of **77**), 1.94 – 1.88 (m, contains 2H of **76**).

Assigned to **75$_{enol}$**: δ 3.69 (s, approx. 0.56H, C-CH_2Ph (contains 2H of compound **75$_{enol}$** and 2H of **77**)).

Assigned to **76**: δ 0.96 – 0.84 (m, 0.59H, $CH_2CH_2CH_2$ (2H of compound **76**)).

Assigned to **77**: δ 5.14 (s, 0.02H, O-CH_2Ph (2H of compound **77**)).

The signal used to obtain the integration of **75$_{enol}$** at 3.69 ppm overlaps with a 2H signal of **77**. The integration value of this set of overlapping signals is 0.58 relative to 1H of **74**. The 2H signal of D at 5.14 ppm has a value of 0.02 relative to 1H of **74**. Thus, by subtracting the value associated with 2H of **77** from the integration value of the signal at 3.69 ppm, the approximate integration value of 2H of **75$_{enol}$** can be established. (0.58 – 0.02) = 0.56. Therefore 0.56 is the contribution of 2H of **75$_{enol}$** to the signal at 3.69 ppm. This indicates that 1H of **75$_{enol}$** equals 0.28 integration units relative to 1H of **74**.

Based on the ^{1}H NMR spectral data given above, the integrations of 1H of each of compounds **74**, **75$_{enol}$**, **76** and **77** relative to 1H of compound **74** are as follows:

$$I_{\mathbf{74}} = 1.00; \quad I_{\mathbf{75}} = 0.28; \quad I_{\mathbf{76}} = \frac{0.59}{2} = 0.295; \quad I_{\mathbf{77}} = \frac{0.02}{2} = 0.01$$

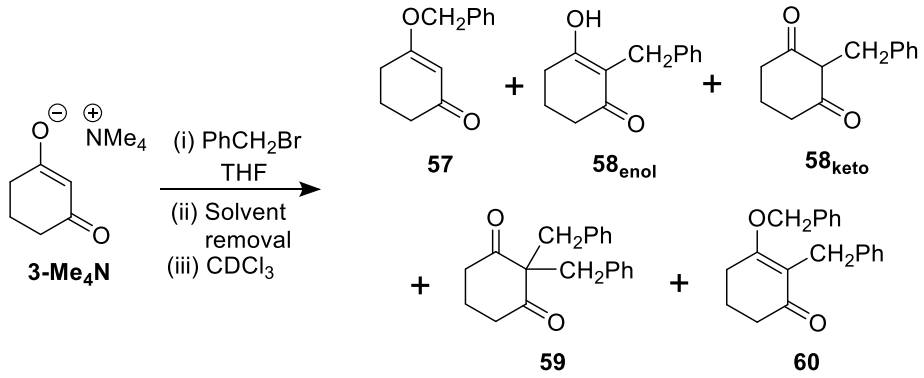
where $I_{\mathbf{X}}$ is the integration of 1H of compound **X** (**X** = **74**, **75$_{enol}$**, **76**, or **77**) relative to 1H of compound **74**. Since $I_{\mathbf{X}} \propto [\mathbf{X}]$ (concentration of **X** in mol L^{-1}), the percentage of O-alkylation is given by:

$$\text{Percentage of O-alkylation} = \frac{I_{\mathbf{74}}}{I_{\mathbf{74}} + I_{\mathbf{75}} + I_{\mathbf{76}} + I_{\mathbf{77}}} \times 100$$

$$= \frac{1.00}{1.00 + 0.28 + 0.295 + 0.01} \times 100 = 63\%$$

Integrations give an O vs C ratio of 63:37.

(iii) Reaction of Enolate 3-Me$_4$N with Benzyl Bromide in THF



The Me_4N^+ enolate of cyclohexan-1,3-dione (**3-Me$_4$N**) (0.025 g, 0.13 mmol) and benzyl bromide (**56**) (0.033 g, 0.19 mmol) were combined in dry THF (0.75 ml) in the manner described in Procedure F. The THF was removed under vacuum. The reaction

mixture was dissolved in dry $CDCl_3$ (0.7 ml), and the resulting mixture was transferred to an NMR tube.

^{1}H NMR (300 MHz, $CDCl_3$) of crude mixture of alkylation products (the underlined integrations are expressed relative to 1H of compound **57**): [a,b]

Assigned to **57**: δ 5.48 (s, 1H, C=C<u>H</u>), 4.89 (s, 2H, O-C<u>H</u>$_2$Ph). [31]

Assigned to **58$_{enol}$**: δ 3.65 (s, approx. 1.08H, C-C<u>H</u>$_2$Ph (2H of compound **58$_{enol}$**)). [38]

Assigned to **58$_{keto}$**: δ 3.59 (t, *J* = 6.6 Hz, 0.05H, C<u>H</u>-CH$_2$Ph (1H of compound **58$_{keto}$**)). [38]

Assigned to **59**: δ 3.24 (s, 1.20H, C-C<u>H</u>$_2$Ph (4H of compound **59**)), 0.88 – 0.75 (m, 0.64H, CH$_2$C<u>H</u>$_2$CH$_2$ (2H of compound **59**)). [32]

Assigned to **60**: δ 5.09 (s, 0.11H, O-C<u>H</u>$_2$Ph (2H of compound **60**)). [34]

The signal used to obtain the integration of **58$_{enol}$** at 3.65 ppm overlaps with a 2H signal of **60**. The integration value of this set of overlapping signals is 1.19 relative to 1H of **57**. The 2H signal of D at 5.09 ppm has a value of 0.11 relative to 1H of **57**. Thus, by subtracting the value associated with 2H of **60** from the integration value of the signal at 3.65 ppm, the approximate integration value of 2H of **58$_{enol}$** can be established. (1.19 – 0.11) = 1.08. Therefore 1.08 is the contribution of 2H of **58$_{enol}$** to the signal at 3.65 ppm. This indicates that 1H of **58$_{enol}$** equals 0.54 integration units relative to 1H of **57**.

Based on the ^{1}H NMR spectral data given above, the integrations of 1H of each of compounds **57**, **58$_{enol}$**, **58$_{keto}$**, **59** and **60** relative to 1H of compound **57** are as follows:

$$I_{\mathbf{57}} = 1.00; \quad I_{\mathbf{58e}} = 0.54; \quad I_{\mathbf{58k}} = 0.05; \quad I_{\mathbf{59}} = \frac{0.64}{2} = 0.32 \quad I_{\mathbf{60}} = \frac{0.11}{2} = 0.055$$

where $I_{\mathbf{X}}$ is the integration of 1H of compound **X** (**X** = **57**, **58$_{enol}$**, **58$_{keto}$**, **59** or **60**) relative to 1H of compound **57**. Since $I_{\mathbf{X}} \propto [\mathbf{X}]$ (concentration of **X** in mol L^{-1}), the percentage of O-alkylation is given by:

$$\text{Percentage of O-alkylation} = \frac{I_{\mathbf{57}}}{I_{\mathbf{57}} + I_{\mathbf{58e}} + I_{\mathbf{58k}} + I_{\mathbf{59}} + I_{\mathbf{60}}} \times 100$$

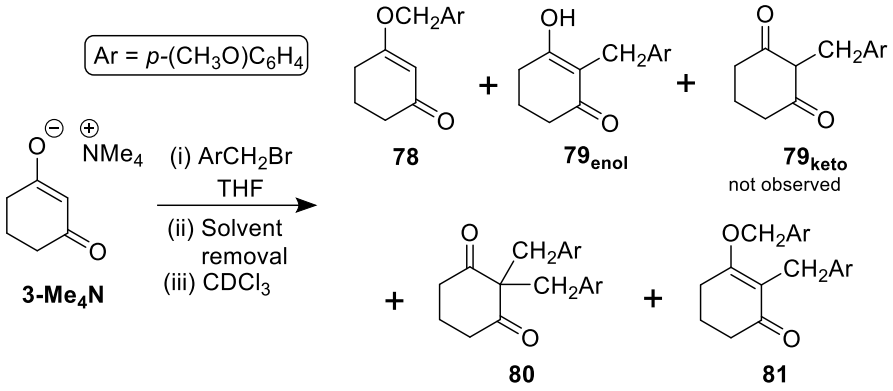
$$= \frac{1.00}{1.00 + 0.54 + 0.05 + 0.32 + 0.055} \times 100 = 51\%$$

Integrations give an <u>O vs C</u> ratio of 51:49.

[a] The relevant ^{1}H NMR spectra are shown in Figure B139 and Figure B140 in Appendix B.

[b] Signals of **57** – **60** that are overlapping with other signals: δ 7.42 – 7.30 (m, contains 2H of **57** and 2H of **60**), 7.23 – 7.14 (m, contains 2H of **59** and 2H of **60**), 7.05 – 6.95 (m, contains 1H of **60**), 2.63 – 2.55 (m, contains 2H of **60**), 2.51 – 2.40 (m, contains 2H of **57**), 2.37 (m, contains 2H of **57** and 2H of **60**), 2.06 – 1.89 (m, contains 2H of **A** and 2H of **60**), 1.88 – 1.81 (m, contains 4H of **59**).

(iv) Reaction of Enolate 3-Me$_4$N with 4-Methoxybenzyl Bromide in THF



The Me_4N^+ enolate of cyclohexan-1,3-dione (**3-Me$_4$N**) (0.0305 g, 0.165 mmol) and 4-methoxybenzyl bromide (**69**) (0.0348 g, 0.173 mmol) were combined in dry THF (1 ml) in the manner described in Procedure F. The THF was removed under vacuum. The reaction mixture was dissolved in $CDCl_3$, and the resulting mixture was transferred to an NMR tube.

^{1}H NMR (600 MHz, $CDCl_3$) of crude mixture of alkylation products (the underlined integrations are expressed relative to 1H of compound **78**): [a,b]

Assigned to **78**: δ 5.48 (s, 1H, C=C<u>H</u>), 4.81 (s, 2H, O-C<u>H$_2$</u>Ph).

Assigned to **79$_{enol}$**: δ 3.58 (s, approx. 0.89H, C-C<u>H$_2$</u>Ph (2H of compound **79$_{enol}$**)).

Assigned to **80**: δ 3.15 (s, approx. 2.87H (partially overlaps with another signal), C-C<u>H$_2$</u>Ph (4H of compound **80**)), 0.91 – 0.86 (m, 1.55H, $CH_2C\underline{H_2}CH_2$ (2H of compound **80**)).

Assigned to **81**: δ 5.01 (s, 0.16H, O-C<u>H$_2$</u>Ph (2H of compound **81**)), 3.55 (s, 0.17H, C-C<u>H$_2$</u>Ph (2H of compound **81**)).

The signal used to obtain the integration of **79$_{enol}$** at 3.58 ppm overlaps with a 2H signal of **81**. The integration value of this set of overlapping signals is 1.05 relative to 1H of **78**. The 2H signal of D at 5.01 ppm has a value of 0.16 relative to 1H of **78**. Thus, by subtracting the value associated with 2H of **81** from the integration value of the signal at 3.58 ppm, the approximate integration value of 2H of **79$_{enol}$** can be established. (1.05 – 0.16) = 0.89. Therefore 0.89 is the contribution of 2H of **79$_{enol}$** to the signal at 3.58 ppm. This indicates that 1H of **79$_{enol}$** equals 0.445 integration units relative to 1H of **78**.

Based on the ^{1}H NMR spectral data given above, the integrations of 1H of each of compounds **78**, **79$_{enol}$**, **80** and **81** relative to 1H of compound **78** are as follows:

---

[a] Full characterisation data for the product **78**, **79$_{enol}$** and **80** seen in this experiment are given in section 5.8. The relevant ^{1}H NMR spectra are shown in Figure B141 and Figure B142 in Appendix B.

[b] Signals of **78** – **81** that are overlapping with other signals: δ 7.30 – 7.25 (m, contains 2H of **78** and $CHCl_3$ signal), 7.18 – 7.14 (m, contains 2H of **79$_{enol}$**), 6.94 – 6.86 (m, contains 2H of **78** and 2H of **80**), 6.82 – 6.78 (m, contains 2H of **79$_{enol}$**), 6.77 – 6.70 (m, contains 2H of **80**), 3.81 (s, contains 3H of **78**), 3.76 (s, contains 3H of **79$_{enol}$**), 3.74 (s, contains 3H of **80**), 3.58 (s, contains 2H of **79$_{enol}$** and 2H of **81**), 2.46 – 2.41 (m, contains 2H of **78** and 2H of **79$_{enol}$**), 2.38 – 2.33 (m, contains 2H of **A**), 2.09 – 1.95 (m, contains 2H of **A** and 2H of **79$_{enol}$**), 1.87 (t, J = 6.6 Hz, contains 4H of **80**).

$$I_{78} = 1.00; \quad I_{79} = 0.445; \quad I_{80} = \frac{1.55}{2} = 0.775; \quad I_{81} = \frac{0.16}{2} = 0.08$$

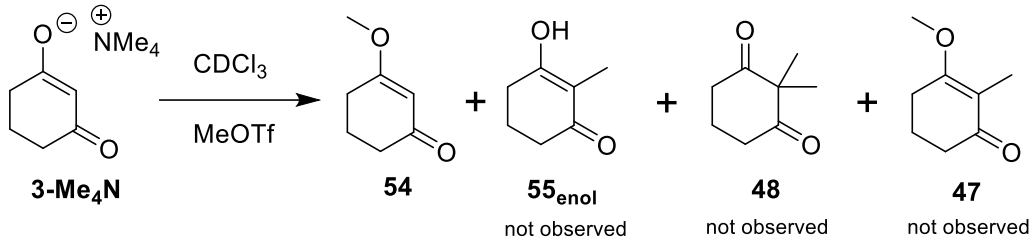
where $I_{\mathbf{X}}$ is the integration of 1H of compound **X** (**X** = **78**, **79**$_{\mathbf{enol}}$, **80** or **81**) relative to 1H of compound **78**. Since $I_{\mathbf{X}} \propto [\mathbf{X}]$ (concentration of **X** in mol L^{-1}), the percentage of O-alkylation is given by:

$$\text{Percentage of O-alkylation} = \frac{I_{78}}{I_{78} + I_{79} + I_{80} + I_{81}} \times 100$$

$$= \frac{1.00}{1.00 + 0.445 + 0.775 + 0.08} \times 100 = 43\%$$

Integrations give an O vs C ratio of 43:57

(v) Reaction of Enolate 3-Me$_4$N with Methyl Triflate in CDCl$_3$



3-Me$_4$N **54** **55$_{enol}$** not observed **48** not observed **47** not observed

The Me_4N^+ enolate of cyclohexan-1,3-dione (**3-Me$_4$N**) (0.0362 g, 0.196 mmol) was added to a Schlenk flask containing an inert atmosphere of nitrogen gas. Dry $CDCl_3$ (0.7 ml) was added to form a transparent pink solution. The solution was stirred for approximately 15 minutes. Methyl triflate (0.0321 g, 0.196 mmol) was added dropwise over the course of 1 minute. The solution was allowed to stir overnight.

An empty NMR tube was placed in a long Schlenk tube. The long Schlenk tube, containing the NMR tube, was evacuated and re-filled with nitrogen ≥ 3 times, creating an inert atmosphere inside the flask. The reaction mixture was added to the NMR tube under inert atmosphere by syringe. The NMR tube was sealed with a rubber septum cap. After fitting the rubber septum to the NMR tube, the seal was secured by wrapping the external edge of the septum where it contacted the surface of the NMR tube with PTFE tape. The outside of the PTFE tape and rubber septum were then wrapped with a layer of Parafilm to further secure the nitrogen atmosphere inside the NMR tube. The NMR tube was then transferred to the NMR spectrometer and ^{1}H NMR spectra were recorded.

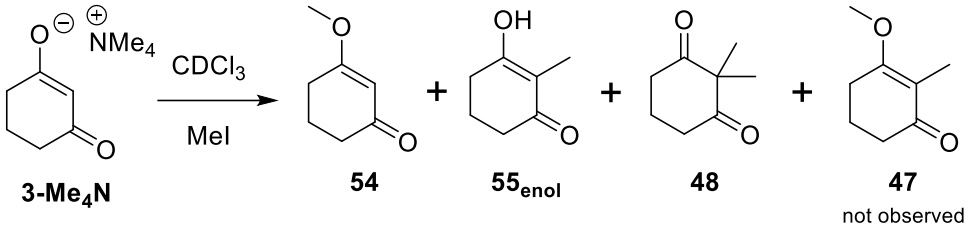
^{1}H NMR (300 MHz, $CDCl_3$) of crude reaction mixture: [a]

Assigned to **54**: δ 5.37 (s, 1H, C=C<u>H</u>), 3.70 (s, 3H, OC<u>H</u>$_3$), 2.45 – 2.30 (m, 4H, C<u>H</u>$_2$C=C, C<u>H</u>$_2$C=O), 2.06 – 1.91 (m, 2H, CH$_2$C<u>H</u>$_2$CH$_2$). [18]

The ^{1}H NMR spectrum shows 100% O-alkylation.

[a] The relevant ^{1}H NMR spectra are shown in Figure B143 and Figure B144 in Appendix B.

(vi) Reaction of Enolate 3-Me_4N with Methyl Iodide in $CDCl_3$



The Me_4N^+ enolate of cyclohexan-1,3-dione (0.020 g, 0.108 mmol) was added to to a Schlenk flask containing an inert atmosphere of nitrogen gas. Dry $CDCl_3$ (0.7 ml) was added to form a transparent pink solution. The solution was stirred for approximately 15 minutes. Methyl iodide (0.0154 g, 0.108 mmol) was added dropwise over the course of 1 minute. The solution was allowed to stir overnight.

An empty NMR tube was placed in a long Schlenk tube. The long Schlenk tube, containing the NMR tube, was evacuated and re-filled with nitrogen ≥ 3 times, creating an inert atmosphere inside the flask. The reaction mixture was added to the NMR tube under inert atmosphere by syringe. The NMR tube was sealed with a rubber septum cap. After fitting the rubber septum to the NMR tube, the seal was secured by wrapping the external edge of the septum where it contacted the surface of the NMR tube with PTFE tape. The outside of the PTFE tape and rubber septum were then wrapped with a layer of Parafilm to further secure the nitrogen atmosphere inside the NMR tube. The NMR tube was then transferred to the NMR spectrometer and ^{1}H NMR spectra were recorded.

^{1}H NMR (300 MHz, $CDCl_3$) of crude reaction mixture (the underlined integrations are expressed relative to 1H of compound **54**): [a,b]

Assigned to **54**: δ 5.36 (s, 1H, C=C<u>H</u>), 3.70 (s, 3H, OC<u>H</u>$_3$). [18]

Assigned to **55$_{enol}$**: δ 1.66 (s, 6.10H, C-C<u>H</u>$_3$ (3H of compound **55$_{enol}$**)). [19]

Assigned to **48**: δ 2.72 – 2.65 (m, 3.07H, C<u>H</u>$_2$C=O (4H of compound **48**)), 1.31 (s, 4.72H, C-C<u>H</u>$_3$ (6H of compound **48**)). [20]

Based on the ^{1}H NMR spectral data given above, the integrations of 1H of each of compounds **54**, **55$_{enol}$** and **48** relative to 1H of compound **54** are as follows:

$$I_{\mathbf{54}} = \frac{3.00}{3} = 1.00 \quad I_{\mathbf{55}} = \frac{6.10}{3} = 2.03 \quad I_{\mathbf{48}} = \frac{4.72}{6} = 0.786$$

where $I_{\mathbf{X}}$ is the integration of 1H of compound **X** (**X** = **54**, **55$_{enol}$** or **48**) relative to 1H of compound **54**. Since $I_{\mathbf{X}} \propto [\mathbf{X}]$ (concentration of **X** in mol L^{-1}), the percentage of O-alkylation is given by:

$$\text{Percentage of O-alkylation} = \frac{I_{\mathbf{54}}}{I_{\mathbf{54}} + I_{\mathbf{55}} + I_{\mathbf{48}}} \times 100$$

[a] The relevant ^{1}H NMR spectra are shown in Figure B145 and Figure B146 in Appendix B.

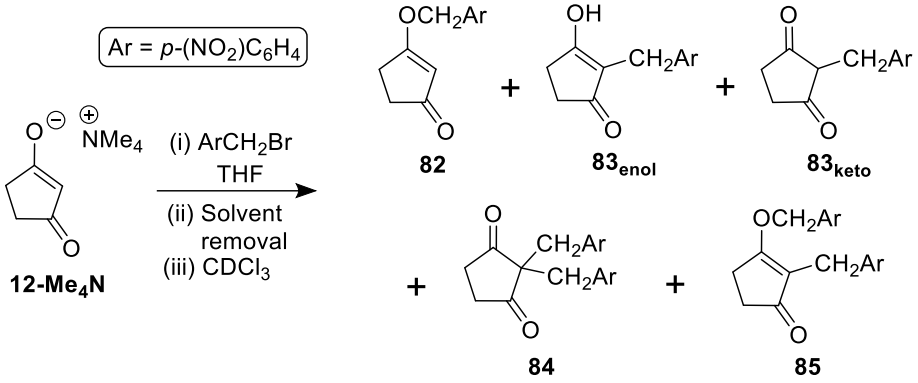
[b] Signals of **48**, **54** and **55** that are overlapping with other signals: δ 2.45 – 2.22 (m, contains 4H of **54** and 4H of **55$_{enol}$**), 2.03 – 1.81 (m, contains 2H of **54**, 2H of **55$_{enol}$** and 2H of **48**).

$$= \frac{1.00}{1.00 + 2.03 + 0.786} \times \ 100 = 26\%$$

Integrations give an O vs C ratio of 26:74

5.8.2. Reactions of 1,3-Cyclopentanedione-Derived Enolate 12-Me_4N

(i) Reaction of Enolate 12-Me_4N with 4-Nitrobenzyl Bromide in THF



The Me_4N^+ enolate of cyclopentan-1,3-dione (**12-Me_4N**) (0.0128 g, 0.075 mmol) and 4-nitrobenzyl bromide (**67**) (0.017 g, 0.079 mmol) were combined in dry THF (1 ml) in the manner described in Procedure F. The THF was removed under vacuum. The reaction mixture was dissolved in $CDCl_3$, and the resulting mixture was transferred to an NMR tube.

^{1}H NMR (300 MHz, $CDCl_3$) of crude mixture of alkylation products (the underlined integrations are expressed relative to 1H of compound **82**): [a,b]

Assigned to **82**: δ 5.40 (t, *J* = 1.1 Hz, 1H, C=C<u>H</u>), 5.13 (s, 2H, O-C<u>H</u>$_2$Ph).

Assigned to **83$_{enol}$**: δ 3.62 – 3.58 (m, approx. 0.16H, C-C<u>H</u>$_2$Ph (2H of compound **83$_{enol}$**)).

Assigned to **83$_{keto}$**: δ 3.67 (t, *J* = 6.2 Hz, 0.03H, C<u>H</u>-CH$_2$Ph (1H of compound **83$_{keto}$**)).

Assigned to **84**: δ 3.18 (s, 0.17H, C-C<u>H</u>$_2$Ph (4H of compound **84**)), 1.95 (s, 0.17H, C<u>H</u>$_2$C=O (4H of compound **84**)).

Assigned to **85**: δ 5.32 (s, 0.19H, O-C<u>H</u>$_2$Ph (2H of compound **85**)), 3.60 (s, 0.19H, C-C<u>H</u>$_2$Ph (2H of compound **85**)).

The signal used to obtain the integration of **83$_{enol}$** at 3.60 ppm overlaps with a 2H signal of **85**. The integration value of this set of overlapping signals is 0.35 relative to 1H of **82**. The 2H signal of D at 5.32 ppm has a value of 0.19 relative to 1H of **82**. Thus, by

---

[a] The relevant ^{1}H NMR spectra are shown in Figure B147 and Figure B148 in Appendix B.

[b] Signals of **82** – **85** that are overlapping with other signals: δ 8.30 – 8.17 (m, contains 2H of **82**, 2H of **85** and 2H of 4-nitrobenzyl bromide),[39] 8.14 – 8.04 (m, contains 2H of **84** and 2H of **85**), 7.59 – 7.53 (m, contains 2H of **82** and 2H of 4-nitrobenzyl bromide),[39] 7.48 – 7.35 (m, contains 4H of **85**), 7.25 – 7.19 (m, contains 2H of **84** and $CHCl_3$ signal), 4.51 (s, 2H of 4-nitrobenzyl bromide),[39] 3.62 – 3.58 (m, contains 2H of **83** and 2H of **85**), 2.77 – 2.69 (m, contains 2H of **82** and 2H of **85**), 2.56 – 2.45 (m, contains 2H of **82** and 2H of **85**).

subtracting the value associated with 2H of **85** from the integration value of the signal at 3.60 ppm, the approximate integration value of 2H of **83enol** can be established. (0.35 – 0.19) = 0.16. Therefore 0.16 is the contribution of 2H of **83enol** to the signal at 3.60 ppm. This indicates that 1H of **83enol** equals 0.08 integration units relative to 1H of **82**. Based on the ^{1}H NMR spectral data given above, the integrations of 1H of each of compounds **82**, **83enol**, **83keto**, **84** and **85** relative to 1H of compound **82** are as follows:

$$I_{\mathbf{82}} = 1.00;\quad I_{\mathbf{83e}} = 0.08;\quad I_{\mathbf{83k}} = 0.03;\quad I_{\mathbf{84}} = \frac{0.17}{4} = 0.043;\quad I_{\mathbf{85}} = \frac{0.19}{2} = 0.095$$

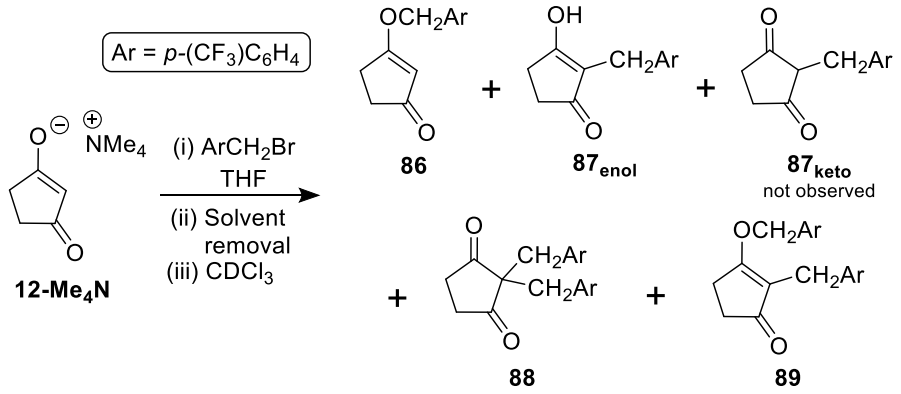
where $I_{\mathbf{X}}$ is the integration of 1H of compound **X** (**X** = **82**, **83enol**, **83keto**, **84** or **85**) relative to 1H of compound **82**. Since $I_{\mathbf{X}} \propto [\mathbf{X}]$ (concentration of **X** in mol L^{-1}), the percentage of O-alkylation is given by:

$$\text{Percentage of O-alkylation} = \frac{I_{\mathbf{82}}}{I_{\mathbf{82}} + I_{\mathbf{83e}} + I_{\mathbf{83k}} + I_{\mathbf{84}} + I_{\mathbf{85}}} \times 100$$

$$= \frac{1.00}{1.00 + 0.08 + 0.03 + 0.043 + 0.095} \times 100 = 80\%$$

Integrations give an <u>O vs C</u> ratio of 80:20

(ii) Reaction of enolate 12-Me$_4$N with 4-(Trifluoromethyl)benzyl Bromide



The Me_4N^+ enolate of cyclopentan-1,3-dione (**12-Me$_4$N**) (0.0128 g, 0.075 mmol) and 4-(trifluoromethyl)benzyl bromide (**68**) (0.019 g, 0.079 mmol) were combined in dry THF (1 ml) in the manner described in Procedure F. The THF was removed under vacuum. The reaction mixture was dissolved in $CDCl_3$, and the resulting mixture was transferred to an NMR tube.

^{1}H NMR (300 MHz, $CDCl_3$) of crude mixture of alkylation products (the underlined integrations are expressed relative to 1H of compound **86**): [a,b]

[a] Full characterisation data for the products **86**, **88** and **89** seen in this experiment are given in section 5.8. ^{1}H NMR data in CD_3OD for the product **87** seen in this experiment may be found in the literature.[40] The relevant ^{1}H NMR spectra are shown in Figure B149 and Figure B150 in Appendix B.

[b] Signals of **86** – **89** that are overlapping with other signals: δ 7.71 – 7.58 (m, contains 2H of **86** and 2H of **89**), 7.55 – 7.45 (m, contains 2H of **86**, 4H of **C** and 2H of **89**), 7.41 – 7.29 (m, contains 4H of **89**),

Assigned to **86**: δ 5.40 (t, *J* = 1.1 Hz, 1H, C=CH), 5.09 (s, 2H, O-CH$_2$Ph).

Assigned to **87$_{enol}$**: δ 3.59 – 3.53 (m, approx. 0.12H, C-CH$_2$Ph (2H of compound **87$_{enol}$**)). [40]

Assigned to **88**: δ 7.17 (d, *J* = 8.0 Hz, 0.19H, Aryl H-2 (4H of compound **88**)), 3.14 (s, 0.18H, C-CH$_2$Ph (4H of compound **88**)), 1.87 (s, 0.18H, CH$_2$C=O (4H of compound **88**)).

Assigned to **89**: δ 5.26 (s, 0.16H, O-CH$_2$Ph (2H of compound **89**)).

The signal used to obtain the integration of **87$_{enol}$** at 3.56 ppm overlaps with a 2H signal of **89**. The integration value of this set of overlapping signals is 0.28 relative to 1H of **86**. The 2H signal of D at 5.26 ppm has a value of 0.16 relative to 1H of **86**. Thus, by subtracting the value associated with 2H of **89** from the integration value of the signal at 3.56 ppm, the approximate integration value of 2H of **87$_{enol}$** can be established. (0.28 – 0.16) = 0.12. Therefore 0.12 is the contribution of 2H of **87$_{enol}$** to the signal at 3.56 ppm. This indicates that 1H of **87$_{enol}$** equals 0.06 integration units relative to 1H of **86**.

Based on the ^{1}H NMR spectral data given above, the integrations of 1H of each of compounds **86**, **87$_{enol}$**, **88** and **89** relative to 1H of compound **86** are as follows:

$$I_{\mathbf{86}} = 1.00; \quad I_{\mathbf{87}} = 0.06; \quad I_{\mathbf{88}} = \frac{0.18}{4} = 0.045; \quad I_{\mathbf{89}} = \frac{0.16}{2} = 0.08$$

where $I_{\mathbf{X}}$ is the integration of 1H of compound **X** (**X** = **86**, **87$_{enol}$**, **88 or 89**) relative to 1H of compound **86**. Since $I_{\mathbf{X}} \propto [\mathbf{X}]$ (concentration of **X** in mol L^{-1}), the percentage of O-alkylation is given by:

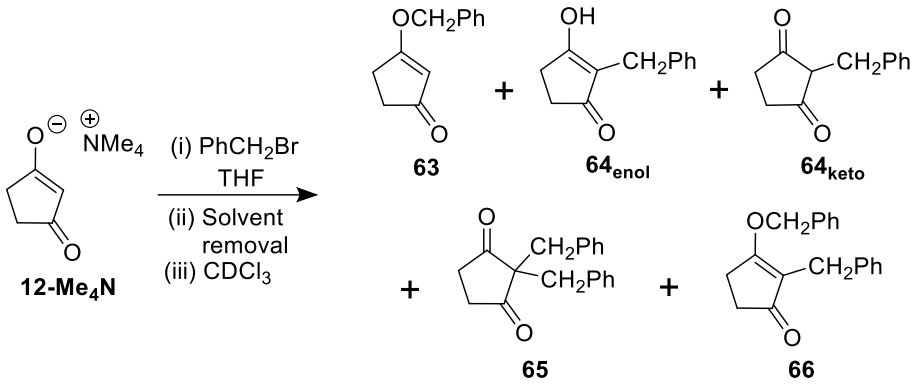
$$\text{Percentage of O-alkylation} = \frac{I_{\mathbf{86}}}{I_{\mathbf{86}} + I_{\mathbf{87}} + I_{\mathbf{88}} + I_{\mathbf{89}}} \times 100$$

$$= \frac{1.00}{1.00 + 0.06 + 0.045 + 0.08} \times 100 = 84\%$$

Integrations give an O vs C ratio of 84:16

3.59 – 3.53 (m, contains 2H of **87** and 2H of **89**), 2.74 – 2.67 (m, contains 2H of **86** and 2H of **89**), 2.53 – 2.46 (m, contains 2H of **86** and 2H of **89**).

(iii) Reaction of Enolate 12-Me_4N with Benzyl Bromide in THF



The Me_4N^+ enolate of cyclopentan-1,3-dione (**12-Me_4N**) (0.0117 g, 0.068 mmol) and benzyl bromide (**56**) (0.0119 g, 0.070 mmol) were combined in dry THF (1 ml) in the manner described in Procedure F. The THF was removed under vacuum. The reaction mixture was dissolved in $CDCl_3$, and the resulting mixture was transferred to an NMR tube.

^{1}H NMR (300 MHz, $CDCl_3$) of crude mixture of alkylation products (the underlined integrations are expressed relative to 1H of compound **63**): [a,b]

Assigned to **63**: δ 5.41 (t, *J* = 1.1 Hz, 1H, C=C<u>H</u>), 5.03 (s, 2H, O-C<u>H</u>$_2$Ph).

Assigned to **64$_{enol}$**: δ 3.52 – 3.45 (m, approx. 0.64H, C-C<u>H</u>$_2$Ph (2H of compound **64$_{enol}$**)).

Assigned to **64$_{keto}$**: δ 3.55 (t, *J* = 6.2 Hz, 0.16H, C<u>H</u>-CH$_2$Ph (1H of compound **64$_{keto}$**)).

Assigned to **65**: δ 3.09 (s, 0.39H, C-C<u>H</u>$_2$Ph (4H of compound **65**)), 1.78 (s, 0.39H, C<u>H</u>$_2$C=O (4H of compound **65**)).

Assigned to **66**: δ 5.21 (s, 0.14H, O-C<u>H</u>$_2$Ph (2H of compound **66**)).

The signal used to obtain the integration of **64$_{enol}$** at 3.48 ppm overlaps with a 2H signal of **66**. The integration value of this set of overlapping signals is 0.78 relative to 1H of **63**. The 2H signal of D at 5.21 ppm has a value of 0.14 relative to 1H of **63**. Thus, by subtracting the value associated with 2H of **66** from the integration value of the signal at 3.48 ppm, the approximate integration value of 2H of **64$_{enol}$** can be established. (0.78 – 0.14) = 0.64. Therefore 0.64 is the contribution of 2H of **64$_{enol}$** to the signal at 3.48 ppm. This indicates that 1H of **64$_{enol}$** equals 0.32 integration units relative to 1H of **63**.

Based on the ^{1}H NMR spectral data given above, the integrations of 1H of each of compounds **63**, **64$_{enol}$**, **64$_{keto}$**, **65** and **66** relative to 1H of compound **63** are as follows:

$$I_{\mathbf{63}} = 1.00; \quad I_{\mathbf{64e}} = 0.32; \quad I_{\mathbf{64k}} = 0.16; \quad I_{\mathbf{65}} = \frac{0.39}{4} = 0.0975; \quad I_{\mathbf{66}} = \frac{0.14}{2} = 0.07$$

[a] The relevant ^{1}H NMR spectra are shown in Figure B151 and Figure B152 in Appendix B.

[b] Signals of **63 – 66** that are overlapping with other signals: δ 7.45 – 7.32 (m, contains 5H of **63** and 3H of **66**), 7.26 – 7.00 (m, contains 7H of **66**), 3.52 – 3.45 (m, contains 2H of **64** and 2H of **66**), 2.69 – 2.65 (m, contains 2H of **63** and 2H of **66**), 2.50 – 2.41 (m, contains 2H of **63** and 2H of **66**).

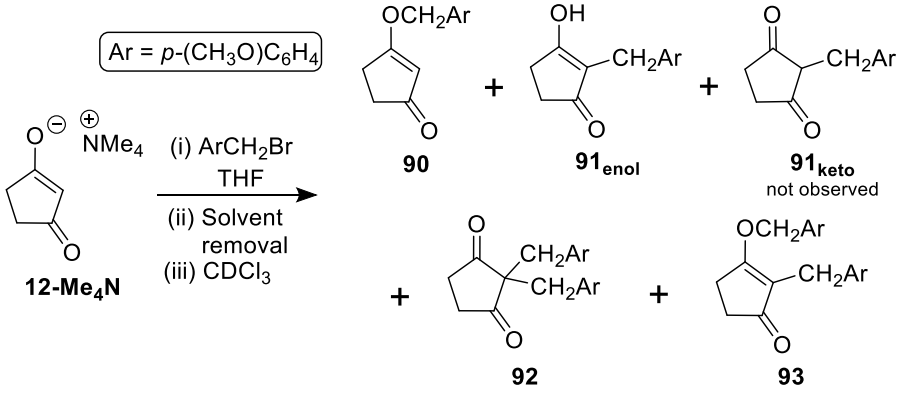
where $I_{\mathbf{X}}$ is the integration of 1H of compound **X** (**X** = **63**, **64**$_{\mathbf{enol}}$, **64**$_{\mathbf{keto}}$, **65** or **66**) relative to 1H of compound **63**. Since $I_{\mathbf{X}} \propto [\mathbf{X}]$ (concentration of **X** in mol L^{-1}), the percentage of O-alkylation is given by:

$$\text{Percentage of O-alkylation} = \frac{I_{63}}{I_{63} + I_{64e} + I_{64k} + I_{65} + I_{66}} \times 100$$

$$= \frac{1.00}{1.00 + 0.32 + 0.16 + 0.0975 + 0.07} \times 100 = 61\%$$

Integrations give an O vs C ratio of 61:39

(iv) Reaction of Enolate 12-Me$_4$N with 4-Methoxybenzyl Bromide in THF



The Me_4N^+ enolate of cyclopentan-1,3-dione (**12-Me$_4$N**) (0.0117 g, 0.068 mmol) and 4-methoxybenzyl bromide (**69**) (0.0119 g, 0.070 mmol) were combined in dry THF (1 ml) in the manner described in Procedure F. The THF was removed under vacuum. The reaction mixture was dissolved in $CDCl_3$, and the resulting mixture was transferred to an NMR tube.

^{1}H NMR (600 MHz, $CDCl_3$) of crude mixture of alkylation products (the underlined integrations are expressed relative to 1H of compound **90**): [a,b]

Assigned to **90**: δ 5.41 (s, 1H, C=C<u>H</u>), 4.94 (s, 2H, O-C<u>H</u>$_2$Ph), 2.66 – 2.62 (m, 2H, C<u>H</u>$_2$C=C).

Assigned to **91**$_{\mathbf{enol}}$: δ 3.43 – 3.39 (m, approx. 1.29H, C-C<u>H</u>$_2$Ph (2H of compound **91**$_{\mathbf{enol}}$)). [40]

Assigned to **92**: δ 3.01 (s, 1.06H, C-C<u>H</u>$_2$Ph (4H of compound **92**)), 1.80 (s, 1.07H, C<u>H</u>$_2$C=O (4H of compound **92**)).

[a] Full characterisation data for the products **90** and **92** seen in this experiment are given in section 5.8. ^{1}H NMR data in $CDCl_3$ for the product **91** seen in this experiment may be found in the literature.[40] The relevant ^{1}H NMR spectra are shown in Figure B153 and Figure B154 in Appendix B.

[b] Signals of **90 – 93** that are overlapping with other signals: δ 7.32 – 7.27 (m, contains 2H of **90**), 6.97 – 6.85 (m, contains 2H of **90** and 4H of **92**), 6.77 – 6.70 (m, contains 4H of **92**), 3.81 (s, contains 3H of **90**), 3.73 (s, contains 3H of **92**), 3.43 – 3.39 (m, contains 2H of **91** and 2H of **93**), 2.49 – 2.42 (m, contains 2H of **90**).

Assigned to **93**: δ 5.14 (s, 0.21H, O-CH_2Ph (2H of compound **93**)).

The signal used to obtain the integration of **91**$_{enol}$ at 3.41 ppm overlaps with a 2H signal of **93**. The integration value of this set of overlapping signals is 1.50 relative to 1H of **90**. The 2H signal of **93** at 5.14 ppm has a value of 0.21 relative to 1H of **90**. Thus, by subtracting the value associated with 2H of **93** from the integration value of the signal at 3.41 ppm, the approximate integration value of 2H of **91**$_{enol}$ can be established. (1.50 – 0.21) = 1.29. Therefore 1.29 is the contribution of 2H of **91**$_{enol}$ to the signal at 3.41 ppm. This indicates that 1H of **91**$_{enol}$ equals 0.645 integration units relative to 1H of **90**.

Based on the ^{1}H NMR spectral data given above, the integrations of 1H of each of compounds **90**, **91**$_{enol}$, **92** and **93** relative to 1H of compound **90** are as follows:

$$I_{\mathbf{90}} = 1.00; \quad I_{\mathbf{91}} = 0.645; \quad I_{\mathbf{92}} = \frac{1.07}{4} = 0.268; \quad I_{\mathbf{93}} = \frac{0.21}{2} = 0.105$$

where $I_{\mathbf{X}}$ is the integration of 1H of compound **X** (**X** = **90**, **91**$_{enol}$, **92** or **93**) relative to 1H of compound **90**. Since $I_{\mathbf{X}} \propto [\mathbf{X}]$ (concentration of **X** in mol L^{-1}), the percentage of O-alkylation is given by:

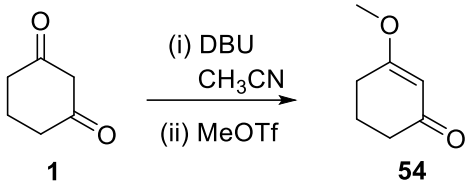
$$\text{Percentage of O-alkylation} = \frac{I_{\mathbf{90}}}{I_{\mathbf{90}} + I_{\mathbf{91}} + I_{\mathbf{92}} + I_{\mathbf{93}}} \times 100$$

$$= \frac{1.00}{1.00 + 0.645 + 0.268 + 0.105} \times 100 = 50\%$$

Integrations give an O vs C ratio of 50:50

5.9. Control Experiments and Crossover Experiments

(i) Synthesis of 3-Methoxycyclohex-2-en-1-one

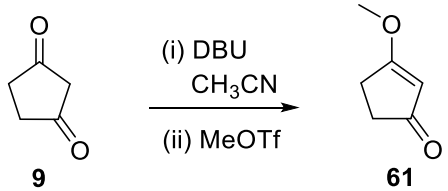


1 **54**

To a Schlenk flask containing an inert atmosphere of nitrogen gas was added 1,3-cyclohexanedione (**1**) (0.153 g, 1.37 mmol). Dry CH_3CN (5 ml) was added which dissolved the dione. Dry DBU (**2**) (0.231 g, 1.52 mmol) was added by syringe and the contents of the flask were stirred for 20 minutes. Methyl triflate (0.267 g, 1.63 mmol) was added by syringe and the mixture was stirred for 16 hours. The reaction mixture was dissolved in DCM (30 ml) and washed with 3 × 20 ml portions of deionised H_2O. The combined aqueous phases were extracted with 2 × 20 ml portions of DCM. The combined organic phases were dried over anhydrous $MgSO_4$ and concentrated to give (**54**) as a yellow oil (0.120 g, 0.951 mmol, 69%). A sample of **54** in $CDCl_3$ was prepared for ^{1}H NMR spectroscopic analysis.

^{1}H NMR (300 MHz, $CDCl_3$) [a] δ 5.37 (s, 1H, C=C<u>H</u>), 3.69 (s, 3H, OC<u>H</u>$_3$), 2.45 – 2.31 (m, 4H, C<u>H</u>$_2$C=C, C<u>H</u>$_2$C=O), 2.04 – 1.91 (m, 2H, CH_2C<u>H</u>$_2CH_2$). [18]

(ii) Synthesis of 3-Methoxycyclopent-2-en-1-one



9 **61**

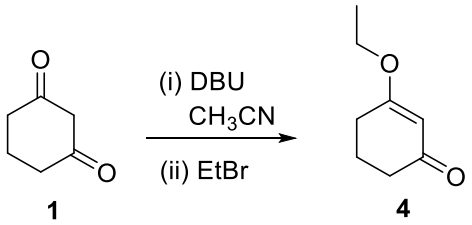
To a Schlenk flask containing an inert atmosphere of nitrogen gas was added 1,3-cyclopentanedione (**9**) (0.102 g, 1.04 mmol). Dry CH_3CN (5 ml) was added which dissolved the dione. Dry DBU (**2**) (0.160 g, 1.05 mmol) was added by syringe and the contents of the flask were stirred for 10 minutes. Methyl triflate (0.180 g, 1.10 mmol) was added dropwise by syringe and the mixture was stirred for 16 hours. The reaction mixture was dissolved in DCM (30 ml) and washed with 3 × 20 ml portions of deionised H_2O. The combined aqueous phases were extracted with 2 × 20 ml portions of DCM. The combined organic phases were dried over anhydrous $MgSO_4$ and concentrated to give (**61**) as a yellow oil (0.104 g, 0.927 mmol, 89%). A sample of **61** in $CDCl_3$ was prepared for ^{1}H NMR spectroscopic analysis.

^{1}H NMR (300 MHz, $CDCl_3$) [b] δ 5.33 (t, *J* = 1.1 Hz, 1H, C=C<u>H</u>), 3.85 (s, 3H, OC<u>H</u>$_3$), 2.65 – 2.58 (m, 2H, C<u>H</u>$_2$C=C), 2.48 – 2.44 (m, 2H, C<u>H</u>$_2$C=O). [22]

[a] The relevant ^{1}H NMR spectra are shown in Figure B155 and Figure B156 in Appendix B.

[b] The relevant ^{1}H NMR spectra are shown in Figure B157 and Figure B158 in Appendix B.

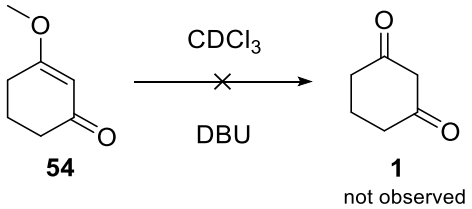
(iii) Synthesis of 3-Ethoxycyclohex-2-en-1-one for Use in "Spike" Experiments.



To a Schlenk flask containing an inert atmosphere of nitrogen gas was added 1,3-cyclohexanedione (**1**) (0.501 g, 4.47 mmol). Dry CH_3CN (15 ml) was added. Dry DBU (**2**) (0.815 g, 5.35 mmol) was added by syringe and the contents of the flask were stirred for 10 mins. Ethyl bromide (0.583 g, 5.35 mmol) was added dropwise by syringe and the mixture was stirred for 16 hours. The reaction mixture was dissolved in DCM (30 ml) and washed with 3 × 20 ml portions of deionised H_2O. The combined aqueous phases were extracted with 2 × 20 ml portions of DCM. The combined organic phases were dried over anhydrous $MgSO_4$ and concentrated to give (**4**) as a yellow oil (0.384 g, 2.74 mmol, 61%). A sample of **4** in $CDCl_3$ was prepared for ^{1}H NMR spectroscopic analysis. The sample of 3-ethoxycyclohex-2-en-1-one was used without further purification in "spike" experiments to assist in verifying signal assignments in reactions in which formation of this product was suspected (see below).

^{1}H NMR (300 MHz, $CDCl_3$, 27 °C) [a] δ 5.35 (s, 1H, C=C<u>H</u>), 3.90 (q, *J* = 7.0 Hz, 2H, OC<u>H</u>$_2$CH), 2.44 – 2.32 (m, 4H, C<u>H</u>$_2$C=C, C<u>H</u>$_2$C=O), 2.05 – 1.93 (m, 2H, CH$_2$C<u>H</u>$_2$CH$_2$), 1.36 (t, *J* = 7.0 Hz, 3H, OCH$_2$C<u>H</u>$_3$). [3]

(iv) Control Experiment to Examine the Reversibility of Formation of 3-Methoxycyclohex-2-en-1-one in $CDCl_3$



3-Methoxycyclohex-2-en-1-one (**54**) (0.120 g, 0.951 mmol) was dissolved in dry $CDCl_3$ (2 ml) in a Schlenk flask containing an inert atmosphere of nitrogen gas to create a 0.476 mol L^{-1} solution of **54**. An aliquot of this solution (0.5 ml, 0.238 mmol) was added to a separate Schlenk flask containing an inert atmosphere of nitrogen gas. Dry DBU (**2**) (0.039 g, 0.26 mmol) was added to the flask by syringe. The mixture was stirred for 1 hour, at which point an extra portion of dry $CDCl_3$ (0.2 ml) was added.

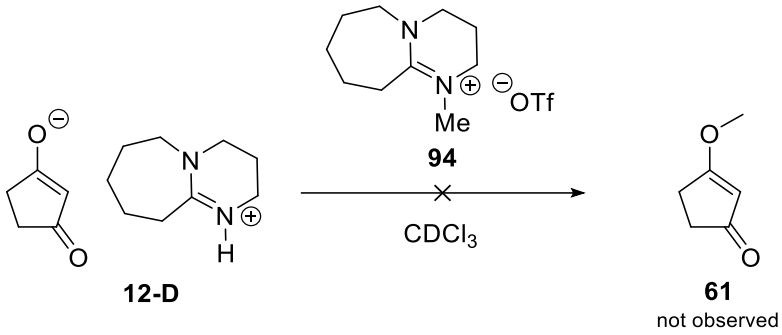
[a] The relevant ^{1}H NMR spectra are shown in Figure B159 and Figure B160 in Appendix B.

An empty NMR tube was placed in a long Schlenk tube. The long Schlenk tube, containing the NMR tube, was evacuated and re-filled with nitrogen ≥ 3 times, creating an inert atmosphere inside the flask. The reaction mixture was added to the NMR tube under inert atmosphere by syringe. The NMR tube was sealed with a rubber septum cap. After fitting the rubber septum to the NMR tube, the seal was secured by wrapping the external edge of the septum where it contacted the surface of the NMR tube with PTFE tape. The outside of the PTFE tape and rubber septum were then wrapped with a layer of Parafilm to further secure the nitrogen atmosphere inside the NMR tube. The NMR tube was then transferred to the NMR spectrometer and ^{1}H NMR spectra were recorded.

Only signals of the starting material (**54**) were observed in the ^{1}H NMR spectra recorded, i.e., no unexpected products were formed.

^{1}H NMR (300 MHz, $CDCl_3$) [a,b] δ 5.37 (s, 1H, C=C<u>H</u>), 3.70 (s, 3H, OC<u>H</u>$_3$), 2.04 – 1.95 (m, 2H, $CH_2C\underline{H}_2CH_2$). [18]

(v) Control Experiment to Determine the Potential of 94 to Act as an Electrophile in $CDCl_3$



1,3-Cyclopentanedione (**9**) (0.032 g, 0.33 mmol) was dissolved in dry $CDCl_3$ (0.6 ml) in a Schlenk flask containing an inert atmosphere of nitrogen gas. Dry DBU (**2**) (0.058 g, 0.38 mmol) was added to the flask by syringe. The mixture was stirred for 10 minutes.

Dry $CDCl_3$ (0.3 ml) was added to a separate Schlenk flask containing an inert atmosphere of nitrogen gas. Dry DBU (**2**) (0.049 g, 0.32 mmol) was added to the flask by syringe, followed by MeOTf (0.050 g, 0.030 mmol). The mixture was stirred for 10 minutes. The contents of this flask were drawn into a syringe and added to the flask containing the enolate (**12-D**) dropwise. The mixture was allowed to stir for 2 hours.

---

[a] The relevant ^{1}H NMR spectra are shown in Figure B161 and Figure B162 in Appendix B.

[b] Signals of **54** that are overlapping with other signals: δ 2.45 – 2.32 (m, contains 4H of **54** and 2H of DBU (**2**) or DBU derivatives).

An empty NMR tube was placed in a long Schlenk tube. The long Schlenk tube, containing the NMR tube, was evacuated and re-filled with nitrogen ≥ 3 times, creating an inert atmosphere inside the flask. The reaction mixture was added to the NMR tube under inert atmosphere by syringe. The NMR tube was sealed with a rubber septum cap. After fitting the rubber septum to the NMR tube, the seal was secured by wrapping the external edge of the septum where it contacted the surface of the NMR tube with PTFE tape. The outside of the PTFE tape and rubber septum were then wrapped with a layer of Parafilm to further secure the nitrogen atmosphere inside the NMR tube. The NMR tube was then transferred to the NMR spectrometer and ^{1}H NMR spectra were recorded.

Only signals of the enolate (**12-D**) and methylated DBU (**94**) were observed in the NMR spectra recorded, i.e., no enolate methylation products were formed.

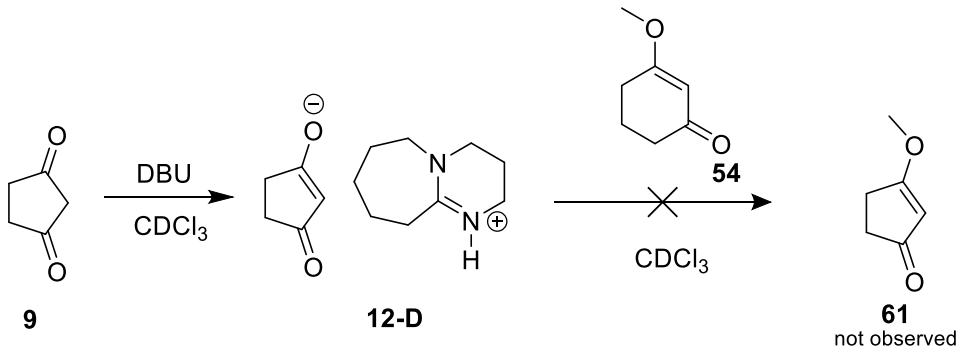
^{1}H NMR (300 MHz, $CDCl_3$) of crude mixture: [a,b]

Assigned to **12-D**: δ 4.75 (s, 1H), 2.82 – 2.72 (m, 2H), 2.33 (s, 4H), 2.13 – 2.02 (m, 2H).

Assigned to **94**: δ 3.74 – 3.66 (m, 2H), 2.22 – 2.13 (m, 2H).

No signals associated with **61** were observed.

(vi) Experiment to Analyse Potential of 3-Methoxycyclohex-2-en-1-one (54) to act as an Electrophile in Reaction with Enolate 12-D in $CDCl_3$



To a Schlenk flask containing an inert atmosphere of nitrogen gas was added 1,3-cyclopentanedione (**9**) (0.0239 g, 0.234 mmol). Dry $CDCl_3$ (0.35 ml) was added which dissolved the dione. Dry DBU (**2**) (0.0345 g, 0.227 mmol) was added by syringe and the contents of the flask were stirred for 10 minutes. An aliquot of a 0.476 mol L^{-1} solution of **54** in $CDCl_3$ (0.5 ml, 0.238 mmol) was added to the flask and the mixture was stirred. The solution was stirred for 20 minutes.

An empty NMR tube was placed in a long Schlenk tube. The long Schlenk tube, containing the NMR tube, was evacuated and re-filled with nitrogen ≥ 3 times, creating

[a] The relevant ^{1}H NMR spectra are shown in Figure B163 and Figure B164 in Appendix B.

[b] Signals of **12-D** and **94** that are overlapping with other signals: δ 2.65 – 2.52 (m, contains 4H of **12-D** and 4H of **94**), 3.48 – 3.31 (m, contains 2H of **12-D** and 5H of **94**), 1.89 – 1.62 (m, contains 6H of **12-D** and 6H of **94**).

an inert atmosphere inside the flask. The reaction mixture was added to the NMR tube under inert atmosphere by syringe. The NMR tube was sealed with a rubber septum cap. After fitting the rubber septum to the NMR tube, the seal was secured by wrapping the external edge of the septum where it contacted the surface of the NMR tube with PTFE tape. The outside of the PTFE tape and rubber septum were then wrapped with a layer of Parafilm to further secure the nitrogen atmosphere inside the NMR tube. The NMR tube was then transferred to the NMR spectrometer and ^{1}H NMR spectra were recorded.

Only signals of the starting material (**54**) were observed in the NMR spectra recorded, i.e., no unexpected products were formed.

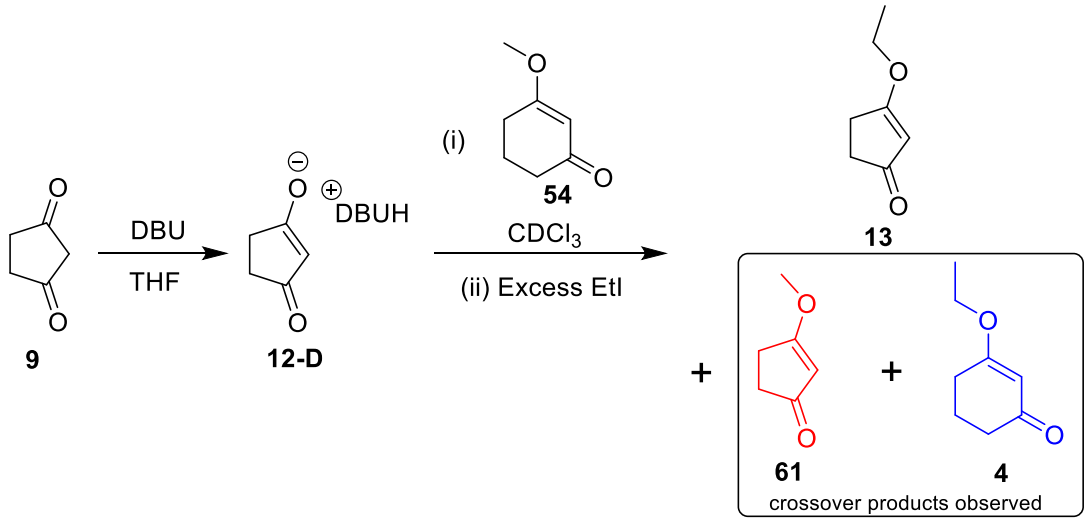
^{1}H NMR (300 MHz, $CDCl_3$) of crude mixture: [a,b]

Assigned to **54**: δ 5.36 (s, 1H, C=C<u>H</u>), 3.70 (s, 3H, OC<u>H</u>$_3$), 2.42 (t, *J* = 6.3 Hz, 2H, C<u>H</u>$_2$C=C). [18]

Assigned to **12-D**: δ 4.76 (s, <u>1.56H</u> (1H of compound **12-D**)).

No signals associated with **61** were observed. [22]

(vii) Crossover Experiment of 3-Methoxycyclohex-2-en-1-one (54) with Enolate 12-D and Excess Ethyl Iodide in $CDCl_3$



To a Schlenk flask in a glove box containing an inert atmosphere of nitrogen gas was added 1,3-cyclopentanedione (**9**) (0.018 g, 0.18 mmol). Dry $CDCl_3$ (0.7 ml) was added which dissolved the dione. DBU (**2**) (0.030 g, 0.20 mmol) was added dropwise and the mixture was stirred. After 10 minutes, enone **54** (0.027 g, 0.21 mmol) was added dropwise to the flask. EtI (0.044 g, 0.28 mmol) was added neat to the solution whilst the reaction mixture was stirred. After addition, the solution was stirred vigorously for 20 minutes. The Schlenk flask was sealed using a glass stopper and subsequently

[a] The relevant ^{1}H NMR spectra are shown in Figure B165 and Figure B166 in Appendix B.

[b] Signals of **12-D** and **54** that are overlapping with other signals: δ 2.38 – 2.31 (m, contains 4H of **12-D** and 2H of **54**), 2.07 – 1.95 (m, contains 2H of **54** and 4H of DBU (**2**) and DBU derivatives).

removed from the glove box, where the solution was allowed to stir overnight at room temperature (~ 18 hours). After stirring overnight, a fine white/grey solid had formed in the reaction flask.

An empty NMR tube was placed in a long Schlenk tube. The long Schlenk tube, containing the NMR tube, was evacuated and re-filled with nitrogen ≥ 3 times, creating an inert atmosphere inside the flask. The reaction mixture was added to the NMR tube under inert atmosphere by syringe. An additional aliquot of $CDCl_3$ (0.2 ml) was added to the NMR tube. The NMR tube was sealed with a rubber septum cap. After fitting the rubber septum to the NMR tube, the seal was secured by wrapping the external edge of the septum where it contacted the surface of the NMR tube with PTFE tape. The outside of the PTFE tape and rubber septum were then wrapped with a layer of Parafilm to further secure the nitrogen atmosphere inside the NMR tube. The NMR tube was then transferred to the NMR spectrometer and a ^{1}H NMR spectrum was recorded (see Figure 5-6 below for an image of the ^{1}H NMR spectrum).

To ensure the identity of the crossover products was correct, the reaction mixture was spiked with an authentic sample of **4** (< 0.010 g) and another spectrum was recorded. The signals which were assigned as belonging to **4** grew in size after **4** was spiked in (see Figure 5-7 below). The reaction mixture was then spiked with **61** (< 0.010 g) and another spectrum was measured. The signals which were assigned as belonging to **61** grew in size after **61** was spiked in (see Figure 5-8 below).

^{1}H NMR (300 MHz, $CDCl_3$) of crude mixture (see Figure 5-6 below for an image of the ^{1}H NMR spectrum) [a] – important signals which indicate the formation of crossover products are highlighted:

Assigned to **13**: δ 5.30 (s, 1H, C=C<u>H</u>), 4.07 (q, *J* = 7.1 Hz, 2H, OC<u>H</u>$_2$CH$_3$), 2.65 – 2.60 (m, 2H, C<u>H</u>$_2$C=O), 1.42 (t, *J* = 7.1 Hz, 3H, OCH$_2$C<u>H</u>$_3$).

Assigned to **54**: δ 5.37 (s, 1H, C=C<u>H</u>), 3.71 (s, 3H, OC<u>H</u>$_3$).

Assigned to **61**: δ 3.87 (s, 3H, OC<u>H</u>$_3$).

Assigned to **4**: δ 5.34 (s, 1H, C=C<u>H</u>), 3.91 (q, *J* = 7.0 Hz, 2H, OC<u>H</u>$_2$CH$_3$), 1.37 (t, *J* = 7.1 Hz, 3H, OCH$_2$C<u>H</u>$_3$).

[a] The full ^{1}H NMR spectra are shown in Figure B167, Figure B168, Figure B169, Figure B170, Figure B171 and Figure B172 in Appendix B.

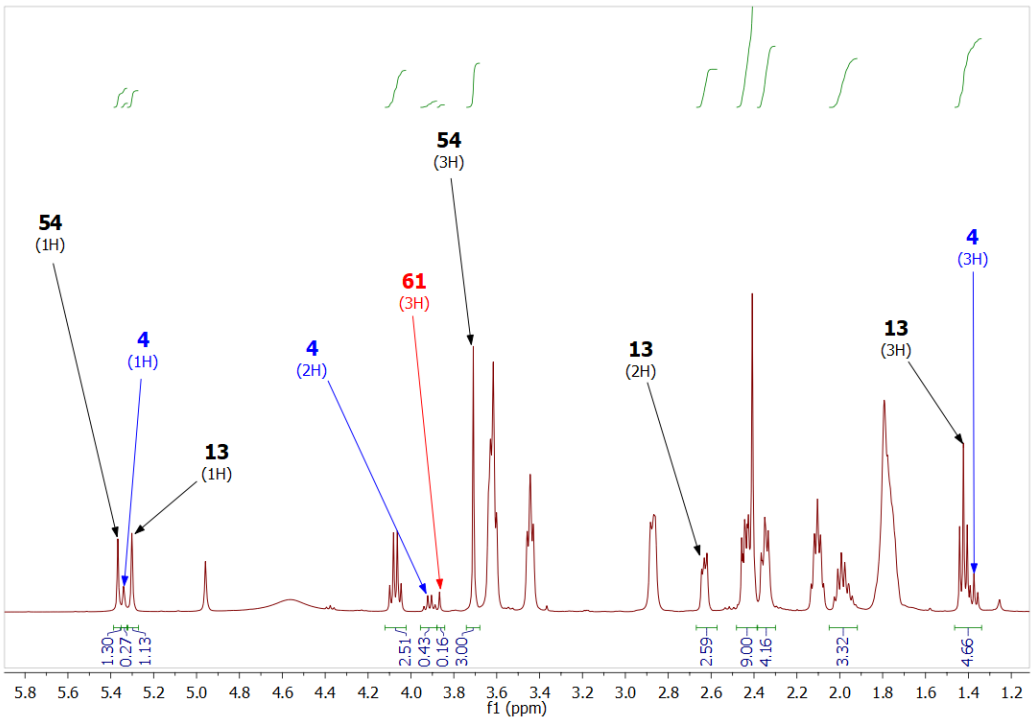


Figure 5-6: ^{1}H NMR spectrum of the crude reaction mixture after excess **EtI** was added to a solution of **12-D** and **54** in THF. The formation of 3-ethoxycyclopent-2-en-1-one (**13**) from enolate **12-D** proceeded, as expected. However, the signals of products **61** and **4** are also observed in the spectrum, indicating that crossover of products has occurred.

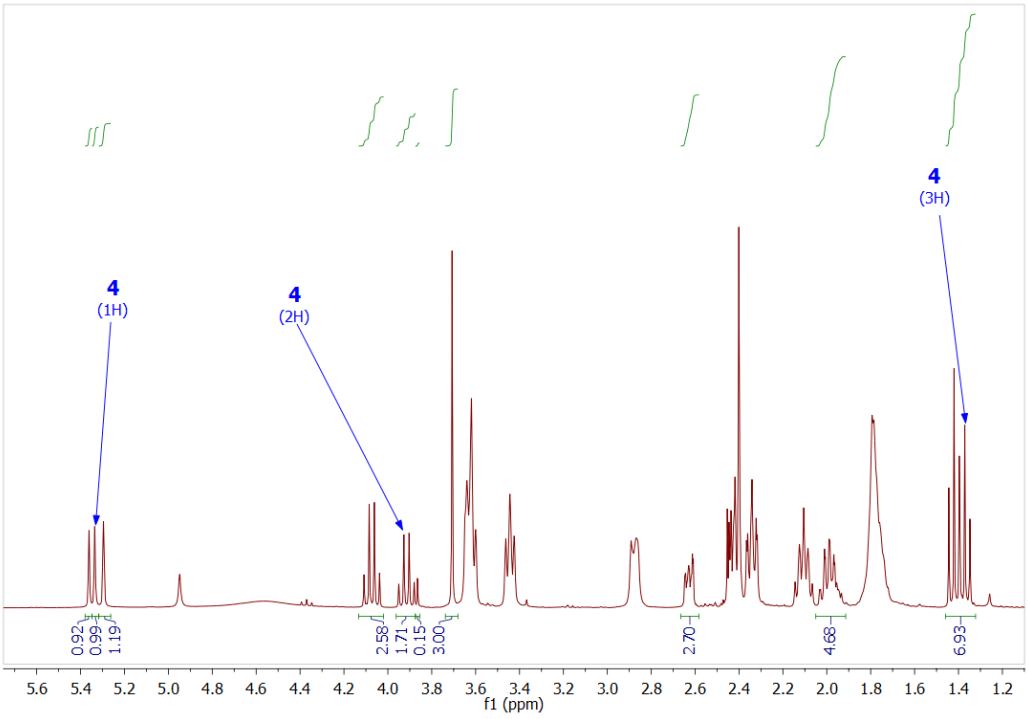


Figure 5-7: ^{1}H NMR spectrum of the crude reaction mixture shown above after an authentic sample of (**4**) was spiked in. The signals assigned to **4** (δ 5.34 (s, 1H), 3.91 (q, *J* = 7.0 Hz, 2H), 1.37 (t, *J* = 7.1 Hz, 3H)) have grown after the sample of **4** was introduced *via* spike.

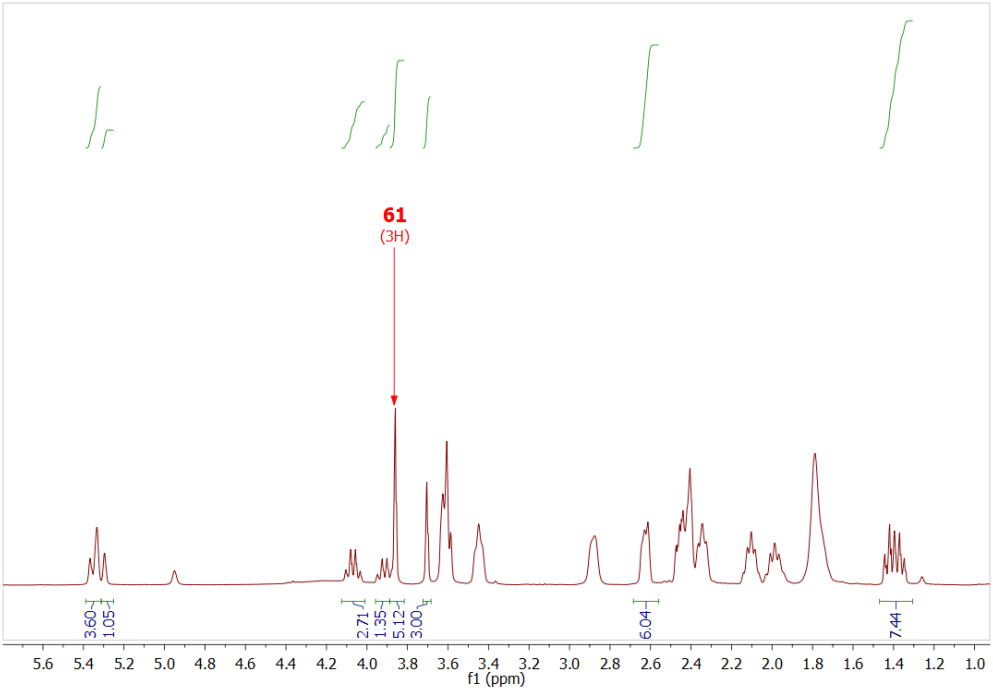
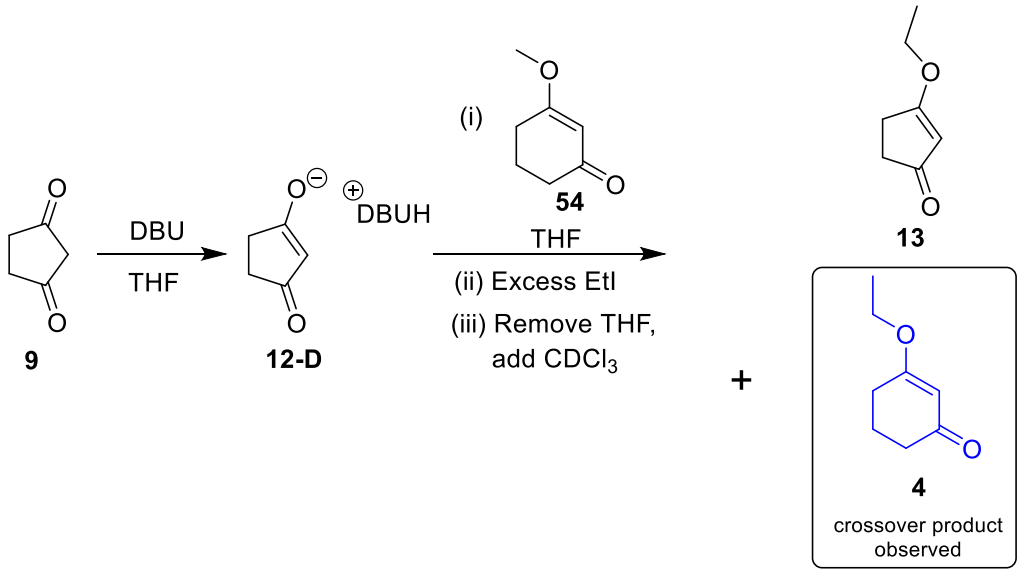


Figure 5-8: ^{1}H NMR spectrum of the crude reaction mixture shown above after an authentic sample of (**61**) was spiked in. The signal assigned to **61** (δ 3.87 (s, 3H)) has grown after a sample of **61** was introduced *via* spike.

(viii) Crossover Experiment of 3-Methoxycyclohex-2-en-1-one (54) with Enolate 12-D and Excess Ethyl Iodide in THF



To a Schlenk flask in a glove box containing an inert atmosphere of nitrogen gas was added 1,3-cyclopentanedione (**9**) (0.022 g, 0.22 mmol). Dry THF (1 ml) was added which dissolved the dione. DBU (**2**) (0.037 g, 0.24 mmol) was added dropwise and the mixture was stirred. After 10 minutes, enone **54** (0.028 g, 0.22 mmol) was added dropwise to the flask. EtI (0.052 g, 0.33 mmol) was added neat to the solution whilst the reaction mixture was stirred. After addition, the solution was stirred vigorously for 20 minutes. The Schlenk flask was sealed using a glass stopper and subsequently removed from the glove box, where the solution was allowed to stir overnight at room

temperature (~ 18 hours). After stirring overnight, a fine white/grey solid had formed in the reaction flask. The side-arm of the reaction flask was connected with rubber tubing to a vacuum trap, which was itself connected to a Schlenk manifold. The trap was placed under vacuum ($\leq 5 \times 10^{-3}$ mbar). The vacuum trap and the tubing connecting it to the reaction flask and the Schlenk manifold were then filled with nitrogen gas by the pump and fill technique.[2] The trap was then placed under vacuum and then cooled with liquid N_2. At this point the stopcock on the Schlenk flask was opened and the solvent was removed and collected in the trap. After approximately 30 minutes, the entirety of the trap and the Schlenk flask were re-filled with nitrogen gas through the Schlenk manifold and the stopcock of the Schlenk flask was closed. The trap was removed and the flask was re-attached directly to the Schlenk manifold, using the pump and fill technique to establish a nitrogen atmosphere in the tubing used for the attachment. Dry $CDCl_3$ (0.7 ml) was added to the flask by syringe to dissolve the crude reaction mixture.

An empty NMR tube was placed in a long Schlenk tube. The long Schlenk tube, containing the NMR tube, was evacuated and re-filled with nitrogen ≥ 3 times, creating an inert atmosphere inside the flask. The reaction mixture was added to the NMR tube under inert atmosphere by syringe. The NMR tube was sealed with a rubber septum cap. After fitting the rubber septum to the NMR tube, the seal was secured by wrapping the external edge of the septum where it contacted the surface of the NMR tube with PTFE tape. The outside of the PTFE tape and rubber septum were then wrapped with a layer of Parafilm to further secure the nitrogen atmosphere inside the NMR tube. The NMR tube was then transferred to the NMR spectrometer and a ^{1}H NMR spectrum was recorded (see Figure 5-9 below for an image of the ^{1}H NMR spectrum).

^{1}H NMR (300 MHz, $CDCl_3$) of crude mixture (see Figure 5-9 below for an image of the ^{1}H NMR spectrum) [a] – important signals which indicate the formation of crossover products are highlighted: [b]

Assigned to **13**: δ 4.03 (q, *J* = 7.1 Hz, 2H, $OC\underline{H}_2CH_3$), 2.63 – 2.55 (m, 2H, $C\underline{H}_2C{=}O$).

Assigned to **54**: δ 5.34 (m, 1H, $C{=}C\underline{H}$, overlaps with 1H signal of **4**), 3.71 (m, 3H, $OC\underline{H}_3$, overlaps with THF signal).

Assigned to **4**: δ 5.31 (s, 1H, $C{=}C\underline{H}$, overlaps with 1H signal of **54**), 3.87 (q, *J* = 7.0 Hz, 2H, $OC\underline{H}_2CH_3$).

To ensure the identity of the crossover product was correct, the reaction mixture was spiked with an authentic sample of **4** (< 0.010 g) and another spectrum was recorded. The signals which were assigned as belonging to **4** grew in size after **4** was spiked in (see Figure 5-10 below).

[a] The full ^{1}H NMR spectra are shown in Figure B173, Figure B174, Figure B175 and Figure B176 in Appendix B.

[b] Signals of **13, 54** and **4** that are overlapping with other signals: δ 5.36 – 5.29 (m, contains 1H of **54** and 1H of **4**), 5.28 – 5.23 (m, contains 1H of **13**), 3.76 – 3.62 (m, contains 3H of **54** and THF signal), 2.44 – 2.23 (m, contains 2H of **13**, 4H of **54** and 4H of **4**), 2.12 – 1.87 (contains 2H of **54** and signal of DBU and DBU derivatives), 1.43 – 1.29 (m, contains 3H of **13** and 3H of **4**).

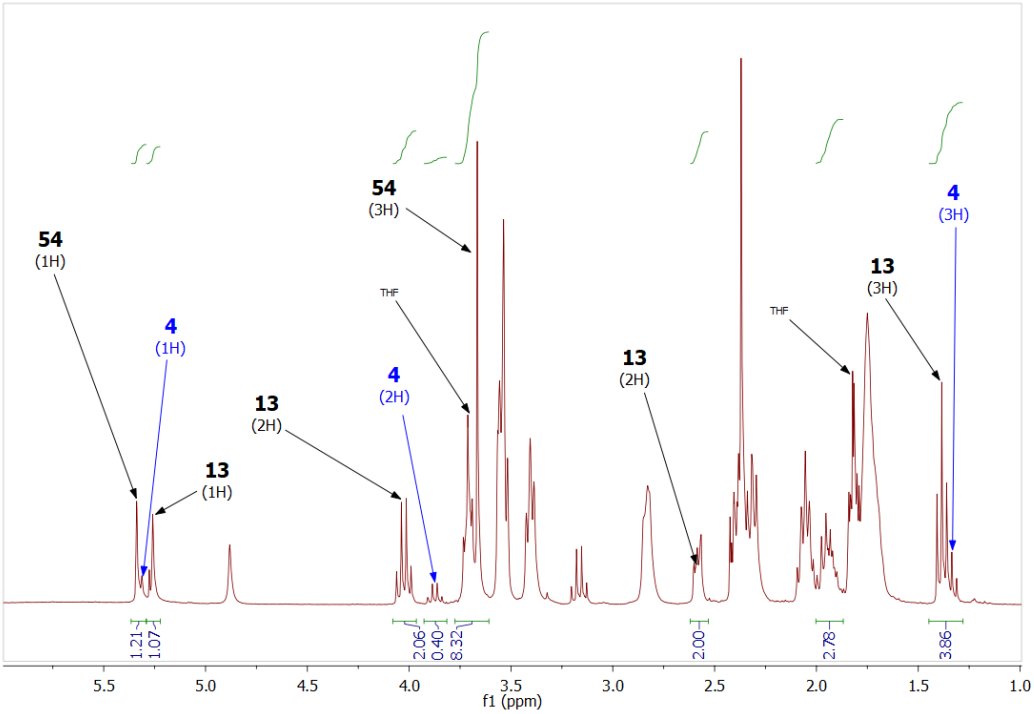


Figure 5-9: ^{1}H NMR spectrum of the crude reaction mixture after excess **EtI** was added to a solution of **12-D** and **54** in $CDCl_3$. The formation of 3-ethoxycyclopent-2-en-1-one (**13**) from enolate **12-D** proceeded, as expected. However, the signals of product **4** are also observed in the spectrum, indicating that crossover of products has occurred.

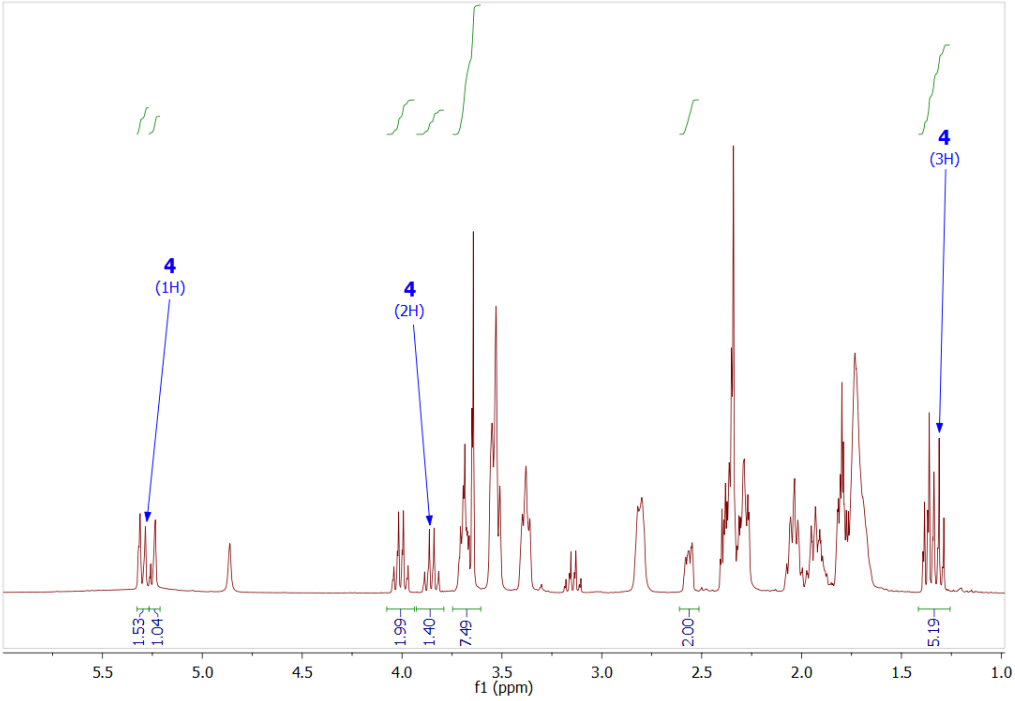
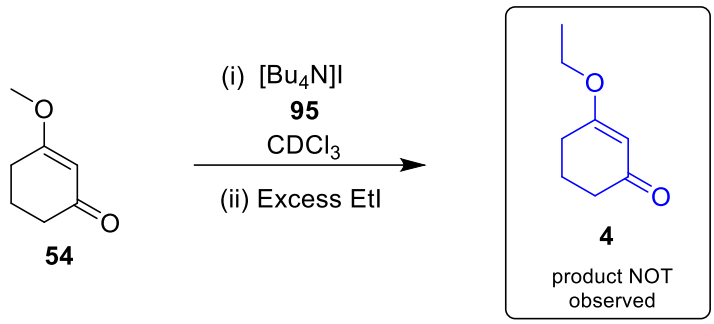


Figure 5-10: ^{1}H NMR spectrum of the crude reaction mixture shown above after an authentic sample of (**4**) was spiked in. The signals assigned to **4** (δ 5.31 (s, 1H), 3.87 (q, *J* = 7.0 Hz, 2H) have grown after the sample of **4** was introduced *via* spike.

(ix) Control Experiment of 3-Methoxycyclohex-2-en-1-one (54) with Iodide Salt 95 and Excess Ethyl Iodide in $CDCl_3$



To a Schlenk flask containing an inert atmosphere of nitrogen gas was added 0.181 g (0.490 mmol) $[Bu_4N]I$ (**95**). The solid was subsequently dissolved using dry $CDCl_3$ (0.8 ml). 3-Methoxycyclohex-2-en-1-one (**54**) (0.030 g, 0.238 mmol) was added to a separate Schlenk flask containing an inert atmosphere of nitrogen gas before being dissolved in dry $CDCl_3$ (0.5 ml). An aliquot of the $[Bu_4N]I$ in $CDCl_3$ solution (0.4 ml) was transferred into the flask containing the enone solution by syringe. After stirring for 5 minutes, EtI (0.0409 g, 0.262 mmol) was added to the flask dropwise. The flask was sealed and the mixture was stirred for 18 hours.

An empty NMR tube was placed in a long Schlenk tube. The long Schlenk tube, containing the NMR tube, was evacuated and re-filled with nitrogen ≥ 3 times, creating an inert atmosphere inside the flask. The reaction mixture was added to the NMR tube under inert atmosphere by syringe. The NMR tube was sealed with a rubber septum cap. After fitting the rubber septum to the NMR tube, the seal was secured by wrapping the external edge of the septum where it contacted the surface of the NMR tube with PTFE tape. The outside of the PTFE tape and rubber septum were then wrapped with a layer of Parafilm to further secure the nitrogen atmosphere inside the NMR tube. The NMR tube was then transferred to the NMR spectrometer and a ^1H NMR spectrum was recorded.

^1H NMR (400 MHz, $CDCl_3$) of crude mixture [a]

Assigned to **54**: δ 5.35 (s, 1H), 3.71 (s, 3H), 2.43 (t, *J* = 6.2 Hz, 2H), 2.37 – 2.31 (m, 2H), 2.04 – 1.94 (m, 2H).

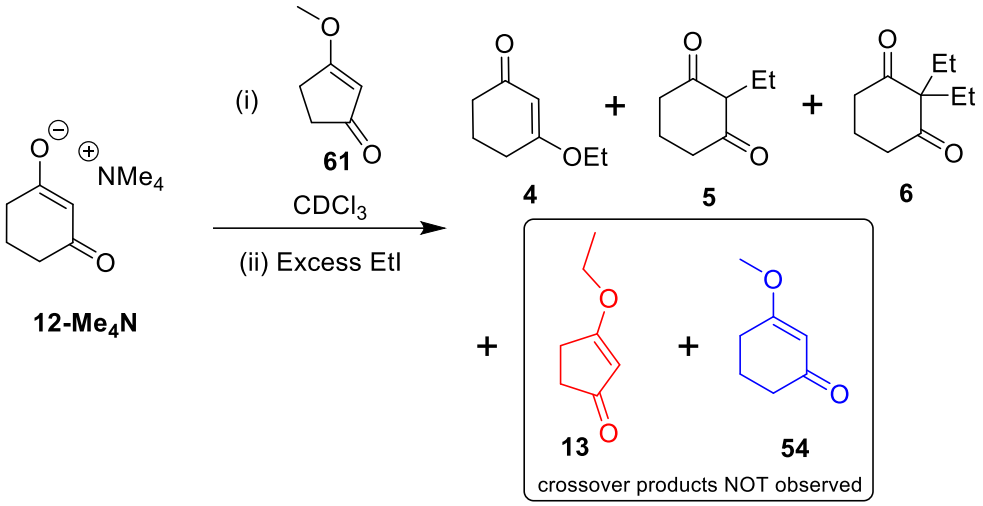
Assigned to **95**: δ 3.43 – 3.33 (m, 8H), 1.77 – 1.62 (m, 8H), 1.55 – 1.41 (m, 8H), 1.05 – 0.96 (m, 12H).

Assigned to **EtI**: δ 3.21 (q, *J* = 7.5 Hz, 1H), 1.85 (t, *J* = 7.5 Hz, 2H).

No signals associated with **4** were observed. [3]

[a] The relevant ^1H NMR spectra are shown in Figure B177 and Figure B178 in Appendix B.

(x) Crossover Experiment of 3-Methoxycyclopent-2-en-1-one (61) with Enolate 3-Me_4N and Excess Ethyl Iodide in THF



To a Schlenk flask in a glove box containing an inert atmosphere of nitrogen gas was added the tetramethylammonium enolate of cyclohexanedione (**3-Me_4N**) (0.020 g, 0.11 mmol). Dry THF (0.75 ml) was added which dissolved the enolate. Enone **61** (0.012 g, 0.11 mmol) was added dropwise to the flask, giving a homogeneous solution. EtI (0.034 g, 0.22 mmol) was added neat to the solution whilst the reaction mixture was stirred. Precipitation was observed immediately upon addition of the EtI. The Schlenk flask was sealed using a glass stopper and subsequently removed from the glove box, where the solution was allowed to stir for 3 days at room temperature. The side-arm of the reaction flask was connected with rubber tubing to a vacuum trap, which was itself connected to a Schlenk manifold. The trap was placed under vacuum ($\leq 5 \times 10^{-3}$ mbar). The vacuum trap and the tubing connecting it to the reaction flask and the Schlenk manifold were then filled with nitrogen gas by the pump and fill technique.[2] The trap was then placed under vacuum and then cooled with liquid N_2. At this point the stopcock on the Schlenk flask was opened and the solvent was removed and collected in the trap. After approximately 30 minutes, the entirety of the trap and the Schlenk flask were re-filled with nitrogen gas through the Schlenk manifold and the stopcock of the Schlenk flask was closed. The trap was removed and the flask was re-attached directly to the Schlenk manifold, using the pump and fill technique to establish a nitrogen atmosphere in the tubing used for the attachment. Dry $CDCl_3$ (0.7 ml) was added to the flask by syringe to dissolve the crude reaction mixture.

Subsequently, the reaction mixture was taken up in a syringe and passed through a cotton wool plug into an NMR tube. The residual solid was washed with $CDCl_3$ (approx. 0.2 ml) into the NMR tube. The sample was analysed by 1H NMR spectroscopy.

Only signals of the enone (**61**) and the ethylation products of a reaction between **3-Me4N** and EtI were observed in the NMR spectra recorded, i.e., no crossover products were formed.

^{1}H NMR (300 MHz, $CDCl_3$) of crude mixture: [a,b]

Assigned to **4**: δ 5.34 (s, 1H, C=C<u>H</u>), 3.91 (q, *J* = 7.0 Hz, 2H, OC<u>H</u>$_2$CH$_3$), 1.37 (t, *J* = 7.0 Hz, 3H, OCH$_2$C<u>H</u>$_3$). [3]

Assigned to **61**: δ 5.32 (t, *J* = 1.1 Hz, 1H, C=C<u>H</u>), 3.85 (s, 3H, OC<u>H</u>$_3$).

Assigned to **5**: δ 0.94 (t, *J* = 7.4 Hz, 3H, C-CH$_2$C<u>H</u>$_3$).

Assigned to **6**: δ 0.75 (t, *J* = 7.4 Hz, 6H, C-CH$_2$C<u>H</u>$_3$).

No signals associated with **13** or **54** were observed. [7,18]

[a] The relevant ^{1}H NMR spectra are shown in Figure B179 and Figure B180 in Appendix B.

[b] Signals of **61**, **4**, **5**, and **6** that are overlapping with other signals: δ 2.65 – 2.57 (m, contains 2H of **61** and 4H of **6**), 2.49 – 2.28 (m, contains 2H of **61**, 4H of **4** and 4H of **5**), 2.04 – 1.92 (m, contains 2H of **4**, 2H of **5** and 2H of **6**), 1.89 – 1.75 (m, contains 2H of **5**, 4H of **6**, EtI and THF signals),

5.10. References

1. Williams, D. B. G.; Lawton, M. *J. Org. Chem.* **2010**, *75*, 8351–8354.
2. Shriver, D. F.; Drezdon, M. A. T*he Manipulation of Air-Sensitive Compounds*, 2nd Edition.; John Wiley & Sons: New York; 1986.
3. Lin, S.; Lu, X. *Org. Lett.* **2010**, *12*, 2536–2539.
4. Wada, Y.; Murata, R.; Fujii, Y.; Asano, K.; Matsubara, S. *Org. Lett.* **2020**, *22*, 4710–4715.
5. Byrne, S. J.; Fletcher, A. J.; Hebeisen, P.; Willis, M. C. *Org. Biomol. Chem.* **2010**, *8*, 758–760.
6. Rosenbaum, L.-C.; Häfner, M.; Gaich, T. *Angew. Chem. Int. Ed.* **2021**, *60*, 2939–2942.
7. Poplata, S.; Bauer, A.; Storch, G.; Bach, T. *Chem. Eur. J.* **2019**, *25*, 8135–8148.
8. Ramachary, D. B.; Kishor, M. *Org. Biomol. Chem.* **2008**, *6*, 4176–4187.
9. Jenkins, T. J.; Burnell, D. J. *J. Org. Chem.* **1994**, *59*, 1485–1491.
10. Alward, S. J.; Fallis, A. G. *Can. J. Chem.* **1984**, *62*, 121–127.
11. Brenninger, C.; Pöthig, A.; Bach, T. *Angew. Chem. Int. Ed.* **2017**, *56*, 4337–4341.
12. Constantino, M. G.; Júnior, V. L.; da Silva, G. V. J. *Magn. Reson. Chem.* **2005**, *43*, 346–347.
13. Madhavachary, R.; Ramachary, D. B. *Eur. J. Org. Chem.* **2014**, *2014*, 7317–7323.
14. Ding, Y.-X.; Zhu, Z.-H.; Wang, H.; Yu, C.-B.; Zhou, Y.-G. *Sci. China Chem.* **2021**, *64*, 232–237.
15. Poplata, S.; Bach, T. *J. Am. Chem. Soc.* **2018**, *140*, 3228–3231.
16. Ramachary, D. B.; Kishor, M. *J. Org. Chem.* **2007**, *72*, 5056–5068.
17. Troughton, E. B.; Molter, K. E.; Arnett, E. M. *J. Am. Chem. Soc.* **1984**, *106*, 6726–6735.
18. Huang, D.; Lo, Y.-H.; Liu, Y.-H.; Peng, S.-M.; Liu, S.-T. *Organometallics* **2013**, *32*, 4009–4015.
19. Armaly, A. M.; Bar, S.; Schindler, C. S. *Org. Lett.* **2017**, *19*, 3958–3961.
20. Fukaya, K.; Tanaka, Y.; Sato, A. C.; Kodama, K.; Yamazaki, H.; Ishimoto, T.; Nozaki, Y.; Iwaki, Y. M.; Yuki, Y.; Umei, K.; Sugai, T.; Yamaguchi, Y.; Watanabe, A.; Oishi, T.; Sato, T.; Chida, N. *Org. Lett.* **2015**, *17*, 2570–2573.
21. Kraft, P.; Bruneau, A. *Eur. J. Org. Chem.* **2007**, *2007*, 2257–2267.
22. Winkler, C. K.; Stueckler, C.; Mueller, N. J.; Pressnitz, D.; Faber, K. *Eur. J. Org. Chem.* **2010**, *2010*, 6354–6358.
23. Brun, O.; Agramunt, J.; Raich, L.; Rovira, C.; Pedroso, E.; Grandas, A. *Org. Lett.* **2016**, *18*, 4836–4839.
24. Subramanyam, R.; Bartlett, P. D.; Iglesias, G. Y. M.; Watson, W. H.; Galloy, J. *J. Org. Chem.* **1982**, *47*, 4491–4498.
25. Jones, M. J.; Callejo, R.; Slawin, A. M. Z.; Bühl, M.; O'Hagan, D. *Beilstein J. Org. Chem.* **2016**, *12*, 2823–2827.
26. Ziegler, E.; Wolfbeis, O. S.; Trummer, I. *Z. Für Naturforschung B* **1982**, *37*, 105–107.
27. Brasca, M. G.; Amboldi, N.; Ballinari, D.; Cameron, A.; Casale, E.; Cervi, G.; Colombo, M.; Colotta, F.; Croci, V.; D'Alessio, R.; Fiorentini, F.; Isacchi, A.; Mercurio, C.; Moretti, W.; Panzeri, A.; Pastori, W.; Pevarello, P.; Quartieri, F.; Roletto, F.; Traquandi, G.; Vianello, P.; Vulpetti, A.; Ciomei, M. *J. Med. Chem.* **2009**, *52*, 5152–5163.
28. Qin, X.-L.; Wu, G.-J.; Han, F.-S. *J. Org. Chem.* **2022**, *87*, 3223–3233.
29. Mandai, H.; Hironaka, T.; Mitsudo, K.; Suga, S. *Chem. Lett.* **2020**.
30. Lertpibulpanya, D.; Marsden, S. P. *Org. Biomol. Chem.* **2006**, *4*, 3498–3504.

31. Parvathalu, N.; Agalave, S. G.; Mohanta, N.; Gnanaprakasam, B. *Org. Biomol. Chem.* **2019**, *17*, 3258–3266.
32. Correa, J.; Mainero, R. M. *J. Org. Chem.* **1969**, *34*, 2192–2195.
33. Slagmaat, C. A. M. R. van; Faber, T.; Chou, K. C.; Freire, A. J. S.; Hadavi, D.; Han, P.; Quaedflieg, P. J. L. M.; Verzijl, G. K. M.; Alsters, P. L.; Wildeman, S. M. A. D. *Dalton Trans.* **2021**, *50*, 10102–10112.
34. Kumamoto, T.; Katakawa, K.; Yonenaga, D.; Terada, T.; Aida, N.; Sakamoto, A.; Hoshino, K. *Heterocycles* **2014**, *88*, 817.
35. Lassalas, P.; Gay, B.; Lasfargeas, C.; James, M. J.; Tran, V.; Vijayendran, K. G.; Brunden, K. R.; Kozlowski, M. C.; Thomas, C. J.; Smith, A. B.; Huryn, D. M.; Ballatore, C. *J. Med. Chem.* **2016**, *59*, 3183–3203.
36. Mohanta, N.; Chaudhari, M. B.; Digrawal, N. K.; Gnanaprakasam, B. *Org. Process Res. Dev.* **2019**, *23*, 1034–1045.
37. Zhao, C.-L.; Yang, J.; Han, Z.-Z.; Zhang, C.-P. *J. Fluor. Chem.* **2017**, *204*, 23–30.
38. Sohail, M.; Tanaka, F. *Chem. Eur. J.* **2020**, *26*, 222–229.
39. Nguyen, T. V.; Bekensir, A. *Org. Lett.* **2014**, *16*, 1720–1723.
40. Kennedy, J. W. J.; Vietrich, S.; Weinmann, H.; Brittain, D. E. A. *J. Org. Chem.* **2008**, *73*, 5151–5154.

Chapter 6: Development of a Novel Model for Rationalising Selectivity in Reactions of Ambident Nucleophiles

6.1 Introduction 342

6.2. Basis for Development of a New General Model for Rationalisation of Selectivities in Reactions of Ambident Nucleophiles (Including Enolates) 343

6.2.1. Background for the Proposed New Rationale 343

6.2.2. Details on Experimental Investigations Used in Development of New Model 353

6.2.3. Details on Computational Investigations Used in Development of New Model 357

6.2.4. Rationalisation of High O-Selectivity in Reactions of Enolates Derived from Cyclic 1,3-Diones 360

6.3. Construction of Gibbs Energy Profile Diagrams for Reactions of Enolate 1-Me_4N with Ethylating Agents in CD_3CN 366

6.3.1. Computational Determination of $\Delta_r G°$ Values for Ethylation Reactions of **43** 366

6.3.2. Experimental Elucidation of Product Ratios (O/C Ratios) 368

6.3.3. Determination of Values of $\Delta G^‡$ for Ethylation Reactions of DMAP (as a Competitor Nucleophile) 369

6.3.4. Experiments for Determination of $\Delta G^‡$ Values for Reactions of Enolate **1-Me_4N** with Ethylating Agents in CD_3CN 378

6.3.5. Development of the Process for Modelling Gibbs Energy Surfaces Focusing on the Reactions of Enolate **1-Me_4N** + Ethylating Agents 381

6.4. Construction of Gibbs Energy Profile Diagrams for Reactions of Enolate 1-Me_4N with Methylating Agents in CD_3CN 395

6.4.1. Reactions of Enolate **1-Me_4N** with Methylating Agents in CD_3CN 395

6.4.2. Experimental Determination of Values of $\Delta G^‡$ for Methylation Reactions of **1-Me_4N** 396

6.4.3. Computational Determination of $\Delta_r G°$ Values for Methylation Reactions of **43** 398

6.4.4. Gibbs Energy Surfaces of the Reactions of Enolate **1-Me_4N** + Methylating Agents 401

6.5. Discussion of on O- vs C-Selectivity in Reactions of Enolates and Generation of Approximated Gibbs Energy Profile Diagrams 407

6.7.1. General Trends in O/C Selectivity in Reactions of the Enolate **1-Me_4N** 407

6.7.2. Generation of Approximate Gibbs Energy Profile Diagrams 408

6.6. References 419

Appendices referred to in the text are available at the following link:
https://tinyurl.com/KSheehyPhDThesisAppendices

6.1. Introduction

The outcomes of the reactions of the cyclic enolates in section 4.2, as well as the numerous literature examples outlined in section 1.3 demonstrate the inadequacies associated with the using the HSAB treatment of ambident reactivity to predict the outcomes of reactions of ambident nucleophiles. The applicability of the HSAB theory towards rationalising these reactions seems particularly unlikely when considering that every "soft" electrophile trialled (including MeI and CD_3I) failed to reliably effect predominant C-alkylation[a] in reactions of those cyclic enolates under different reaction conditions. With no functional model available to explain the reactivity of the enolates described in chapter 4 (and others),[1–5] it is desirable to explore the construction and testing of a new model to rationalise the selectivities observed in reactions of enolates in both this project and in previous literature reports.

At the outset of this project, it was envisaged that the same Marcus theory-based approach used in rationalising the selectivities of reactions of diazine *N*-oxides (see Chapters 2 and 3) would be applied in modelling the outcomes of the reactions of enolates. However, attempts to calculate $\Delta G^{\ddagger}$ values for selected alkylation reactions of enolates gave results that deviated significantly from the $\Delta G^{\ddagger}$ values determined experimentally for the reactions in question, and hence naturally led to predicted O/C ratios that that did not accord with experimental observations. There are multiple reasons that could plausibly account for the observed discrepancies between the computational and experimental results for these systems. There are well known problems associated with calculations involving ionic reactants,[6–8] including the influence of solvent effects[9–16] and entropy effects[10,13–20] and how these are incorporated into a calculation. In addition, accounting for the effects of aggregate formation in solution in reactions involving ionic species is simply not possible using existing quantum mechanical computational techniques.

Taking the above into account, and recognising that the Marcus theory-based approach would have a critical dependence on being able to derive intrinsic barrier values for reactions of ionic reactants computationally, it was decided to pursue an alternative approach, which is described below, starting in section 6.2.

[a] C-alkylation is the expected outcome for reactions of enolates with "soft" electrophiles based on the HSAB rationale, as was addressed in Chapter 1 (see section 1.2.4) and Chapter 4 (see section 4.2.5).

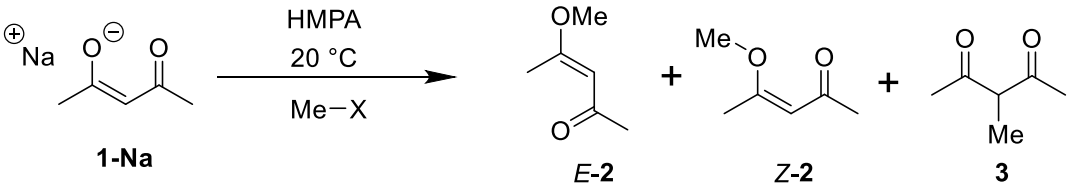
6.2. Basis for Development of a New General Model for Rationalisation of Selectivities in Reactions of Ambident Nucleophiles (Including Enolates)

6.2.1. Background for the Proposed New Rationale

Having demonstrated through a multitude of examples in Chapter 4 that neither HSAB theory, nor the related concepts of "charge control" or "orbital control" can sufficiently account for the selectivity observed in reactions of ambident nucleophiles, a new model must be generated which can account for the selectivity observed in these instances. The aim of this chapter is to generate a novel model which accounts for the experimentally observed reactivity in Chapter 4 – namely the occurrence that "soft" electrophiles such and MeI and EtI can react preferentially at the "hard" nucleophilic site of certain cyclic enolate species.

Any model attempting to account for the behaviour of ambident enolate anions must also be able to account for changes selectivity of the type exemplified in Scheme 6-1, taken from the work of Reutov and co-workers.[21] In this example, reactions of enolate **1-Na** were conducted with electrophiles MeOTs and MeI in HPMA at 20 °C. It was observed that when using MeOTs as the electrophile, almost complete O-methylation (formation of *E*-**2** and *Z*-**2**) was observed. When the reaction was performed with MeI as the electrophile, the C-alkylation product (**3**) was instead formed almost to the complete exclusion of the O-alkylation products (*E*-**2** and *Z*-**2**).

Scheme 6-1. The selectivity of the reaction of the enolate **1-Na** with two electrophiles was studied by Reutov and co-workers.[21]



The aim of the model proposed here is to construct Gibbs energy surfaces (i.e., in two dimensions, reaction co-ordinate diagrams) which describe each of the reactions of interest (O- and C-methylation in the example shown in Scheme 6-1) and use these diagrams to understand why differences in selectivity can arise between reactions of ambident nucleophiles with different electrophiles. To initiate the process of constructing the Gibbs energy surface for any given reaction, a concept taken from Marcus theory is employed: a parabola is used to represent the Gibbs energy well of the reactants and an additional parabola is used to represent the Gibbs energy well of the products (recall Chapter 1 section 1.4.1). As can be seen in Figure 6-1(a), the parabolas are positioned such that following criteria are satisfied:

(i) The Gibbs energy difference between the parabola apices (i.e., the distance along the vertical axis) is equal to the $\Delta_r G°$ value for the reaction.

(ii) The point of intersection of the parabolas occurs at a height equal to the $\Delta G^{‡}$ value for the reaction above the apex of the parabola representing the Gibbs energy of the reactants. The intersection point of the parabolas hence represents the transition state of the reaction.

This approach is essentially different means of representing a reaction co-ordinate diagram, as can be seen by comparing Figure 6-1(a) with the reaction co-ordinate diagram shown in Figure 6-1(b). As there are two possible products for reactions of an ambident nucleophile, a Gibbs energy profile diagram for such systems has two reaction co-ordinate diagrams originating from the Gibbs energy well of reactants. An example of such a system, using one of the reactions drawn in Scheme 6-1 (specifically **1-Na** with MeI) for illustrative purposes, is drawn below in Figure 6-2.

The Gibbs energy well of the reactants (i.e., **1-Na** and MeI) is represented by the parabola in the centre of the image. This Gibbs energy well may be described as the "reactant parabola" in Figure 6-2 below. As there are two possible pathways (e.g., O-methylation (*E*-**2** and *Z*-**2**) and C-methylation (**3**)), there are two reaction co-ordinates extending from the Gibbs energy well of the reactants. The parabola representing the Gibbs energy well of the C-alkylation products is drawn on the right of the image in orange, and the other "product parabola" (on the left-hand side, in blue) represents the Gibbs energy well of the O-alkylation products. The transition states for the processes are represented by the points of intersection of the central "reactant parabola" with each of the "product parabolas".

Figure 6-1. (a) A Gibbs energy profile diagram represented using elements found in Marcus theory – mainly the concept of representing the Gibbs energy wells of reactants and products as parabolas. **(b)** A standard Gibbs energy profile diagram (i.e., a section through a Gibbs energy surface). As can be seen by comparing these two representations of Gibbs energy surfaces, they are analogous to one another.

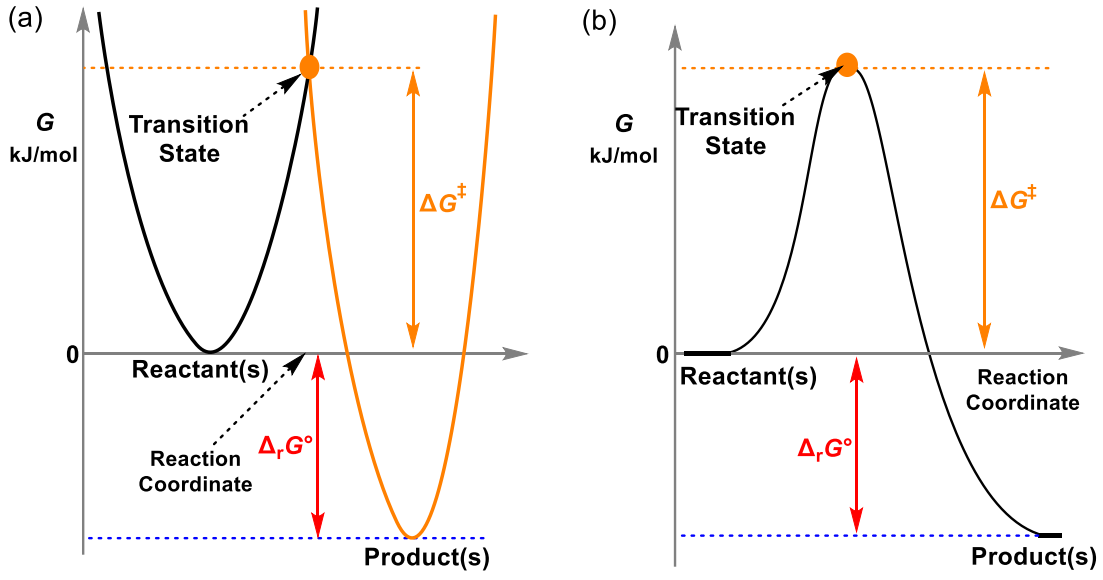
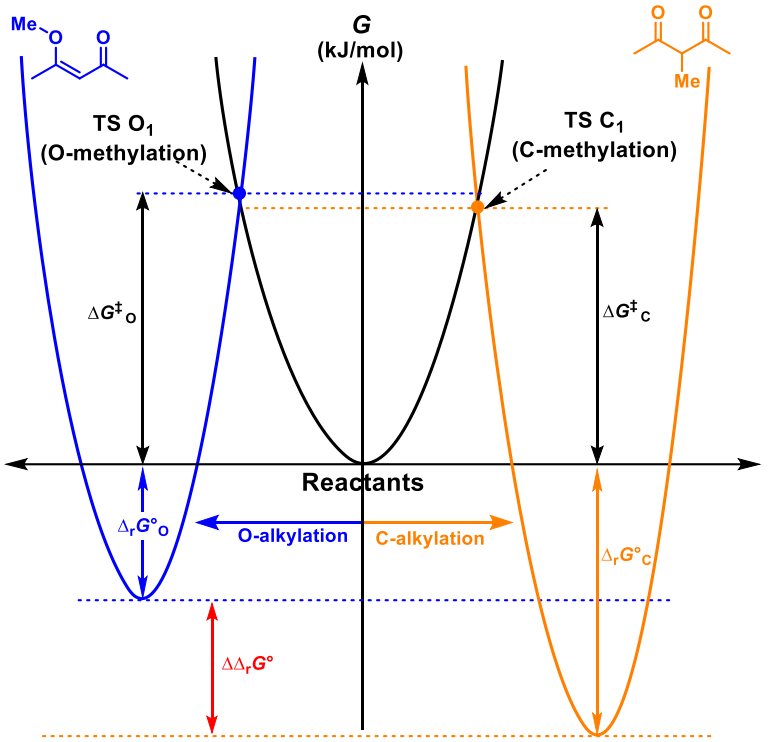


Figure 6-2. A parabolic representation of the reaction co-ordinate for a reaction of enolate **1-Na** with MeI. The intersection points of the parabolas may be approximated as the transition states for the O- and C-methylation processes. The transition state for the O-methylation process is marked "TS O_1", and the transition state for the C-methylation process is marked "TS C_1".



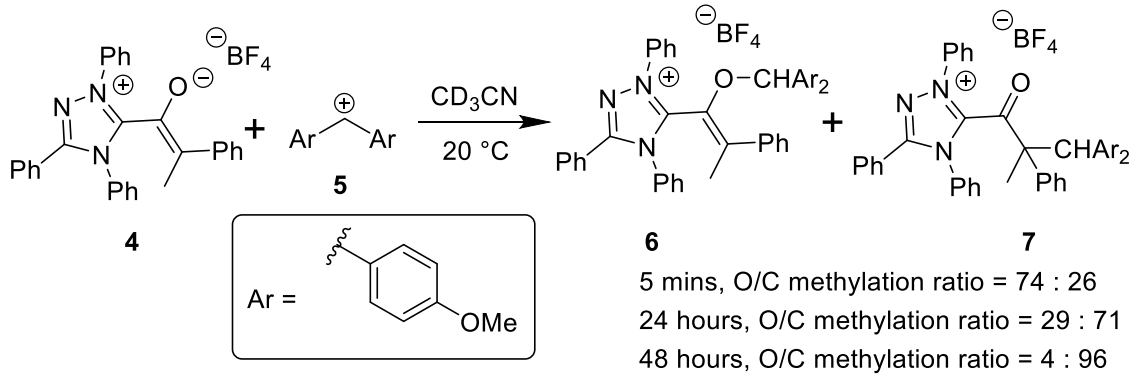
In Figure 6-2, representing the reaction of enolate **1-Na** + MeI (Scheme 6-1), there is a preference for C-alkylation for this enolate **1-Na** in a reaction with MeI (i.e., the transition state for carbon alkylation, TS C_1, is lower in energy than the transition state for O-alkylation, TS O_1, and the Gibbs energy of activation for C-methylation ($\Delta G^{\ddagger}_{C}$) is smaller than Gibbs energy of activation for O-methylation ($\Delta G^{\ddagger}_{O}$)). As a result of this difference in activation barriers for the competing processes, the formation of product **3** (the C-methylation product) is kinetically favoured over the formation of products *E*-**2** and *Z*-**2** (the O-methylation products). This reflects the O/C product ratio for this reaction seen in Scheme 6-1.

In the situation depicted in Figure 6-2, the relative magnitudes of the activation barrier ($\Delta G^{\ddagger}$) values ($\Delta G^{\ddagger}_{C}$ vs $\Delta G^{\ddagger}_{O}$; i.e., the relative heights of the intersection points) reflects the fact that C-methylation is kinetically favoured over O-methylation, i.e., $\Delta G^{\ddagger}_{C} < \Delta G^{\ddagger}_{O}$. This image also indicates that the C-methylation reaction is *thermodynamically* favoured over O-methylation (i.e., $\Delta_r G°_{C}$ is significantly more negative than $\Delta_r G°_{O}$). There is ample precedent, established both in this project and in the literature, that indicates C-alkylation of enolates to generally be thermodynamically favoured over O-alkylation (see Scheme 1-16, Tables 1-26 and 1-28 and associated discussion in Chapter 1. In computational data available in the literature in which $\Delta_r G°$ values for reactions of enolates are calculated, the calculated values show a strong thermodynamic preference for C-alkylated product formation over O-alkylated product formation. Such computational data can be found in

the work of Breugst *et al.*,[22] Jones *et al.*,[23] and Lee *et. al.*,[24] and Houk and Paddon-Row.[25] Our collaborator, Prof. Martin Breugst (TU Chemnitz, Germany) has carried out calculations on alkylation reactions of enolates. A full discussion on these calculations is included later in this chapter (in section 6.2.3 below), but it is appropriate to address one aspect of the calculations at this point. These calculations show that formation of the C-alkylation products of a reaction such as the one depicted above in Figure 6-2 is thermodynamically preferred to formation of the O-alkylation products of the same reaction (i.e., in the reactions of enolate **1-Na** with methylating agents such as MeI, MeOTs, MeOMs).

The observation of C-alkylation being thermodynamically preferred over O-alkylation in reaction of enolates has also been made experimentally, as can be seen in the work of Byrne, Karaghiosoff and Mayr,[26] and Maji and Mayr.[27] In the work of Maji and Mayr, the thermodynamic preference for C-alkylation is demonstrated in reactions of azolium enolates with various benzhydrylium ions (see Scheme 6-2 below).

Scheme 6-2. The reactions of azolium enolates (such as **4**) with benzhydrylium ions (such as **5**) in CD_3CN at 20 °C were studied by Maji and Mayr.[27] The O-alkylation (**6**) product was kinetically favoured, and formed in greater amounts than the C-alkylation product after 5 minutes. Upon re-analysis of the reaction mixture after 24 hours, the thermodynamically preferable C-alkylation adduct (**7**) was found to be the major product.



4 **5** **6** **7**

5 mins, O/C methylation ratio = 74 : 26
24 hours, O/C methylation ratio = 29 : 71
48 hours, O/C methylation ratio = 4 : 96

In the reaction shown in Scheme 6-2, the ^{1}H NMR spectrum of the reaction mixture 5 minutes into the reaction showed that the O-alkylation adduct **6** and the C-alkylation adduct **7** had formed in a ratio of 74 : 26. However, when the reaction mixture was analysed by ^{1}H NMR spectroscopy after 24 hours, the relative amount of the O-alkylation adduct present had decreased, with the product ratio now at 29 : 71 in favour of the C-alkylation product. After 48 hours, the ratio had drifted to 4 : 96 in favour of the C-alkylation product. Numerous examples which show an identical trend (i.e., where the ratio of O-alkylation adducts to C-alkylation adducts is high initially, but reduces over time) may be seen in the paper of Maji and Mayr.[27] The authors ascribe this behaviour to the fact that the benzhydrylium ions (such as **5** in Scheme 6-2 above) react with the oxygen atom of the azolium enolate (e.g., **4** in Scheme 6-2) faster than the carbon atom, but the reversible formation of the O-alkylation product eventually gives rise to the thermodynamically preferable products of C-attack.

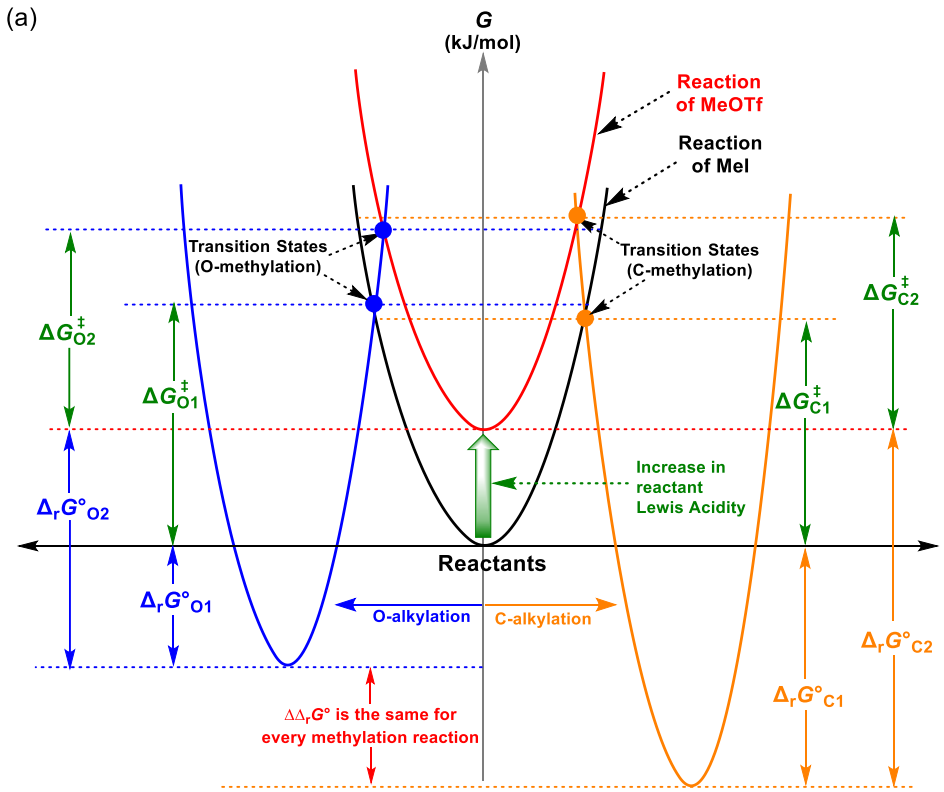
The key starting point for development of the novel rationale for ambident reactivity that is proposed here is the concept that the methylation products formed in reactions of a particular ambident nucleophile (such as **1-Na**) always have the same *relative* Gibbs energies regardless of which methylating agent is employed to methylate the ambident nucleophile. The implication of this is that the parabolas which represent the Gibbs energy wells of the products of all methylation reactions of a particular ambident nucleophile can be placed in precisely the same position in a Gibbs energy profile diagram for any reaction of that ambident nucleophile with *any* methylating agent.

Assuming this is the case in Figure 6-2, the magnitude of the $\Delta_r G°$ value for each of the reactions of **1-Na** with a particular methylating agent is dictated solely by the width and position of the central parabola representing the Gibbs energy well of the reactants. That is, the differences between the $\Delta G^{‡}$ values and the difference between the $\Delta_r G°$ values observed when two different methylating agents react with **1-Na** arise as a result of differences in the widths and positions (i.e., apex co-ordinates) of the Gibbs energy wells of the reactants. To compare the reactivities of different methylating agents (with a given ambident nucleophile) against one another using this model, only the width/curvature and position (apex co-ordinates) of the centre parabola (the parabola representing the Gibbs energy of the reactants or "reactant parabola") must change.

Suppose that it is indeed the case that the Gibbs energy profile diagrams for the reactions of an ambident nucleophile with different methylating agents (as a representative series of related electrophiles) all have identically shaped product Gibbs energy wells (product parabolas) in identical positions, and differ only in the widths and positions of the Gibbs energy wells of the reactants (reactant parabolas). If this is the case, then if one considers the Gibbs energy profile diagram for the reaction of the same ambident nucleophile with a different, more Lewis acidic methylating agent than MeI (e.g., MeOTf), it is possible that this diagram may be obtained simply by taking the reactant parabola for the reaction involving MeI (i.e., without changing its width) and pushing it upwards in the diagram (placing its apex at a higher vertical co-ordinate). As will be shown below, while this scenario is possible, it is one of three broad possibilities that may affect the relative rates of O- and C-alkylation in reactions of enolates. In many instances, all three of these possibilities that may lead to changes in the observed selectivity when comparing reactions of enolates with different alkylating agents may apply.

Consider as an example the reactions of **1-Na** with MeI and MeOTf. The Gibbs energy profile diagram for the reaction of **1-Na** + MeI is shown above in Figure 6-2. To apply the approach suggested above, the reactant parabola (i.e., the central parabola) in the diagram needs to be pushed upwards. The vertical distance the parabola is raised by is equal to the $\Delta_r G°$ values between the reactions that are being compared. An example of the result of this modification is shown below in Figure 6-3.

Figure 6-3. Overlaid Gibbs energy diagrams for reaction of an enolate (**1-Na**) with different methylating agents (**1-Na** + MeI reactant parabola in black, **1-Na** + MeOTf reactant parabola in red). The black parabola in this diagram (relating to the reaction of **1-Na** with MeI) intersects the orange parabola at a lower vertical position (i.e., there is a lower $\Delta G^{\ddagger}$ value for C-methylation). The red parabola in this example (relating to the reaction of **1-Na** with MeOTf) intersects the blue parabola at a lower vertical position (i.e., there is a lower $\Delta G^{\ddagger}$ value for O-methylation).

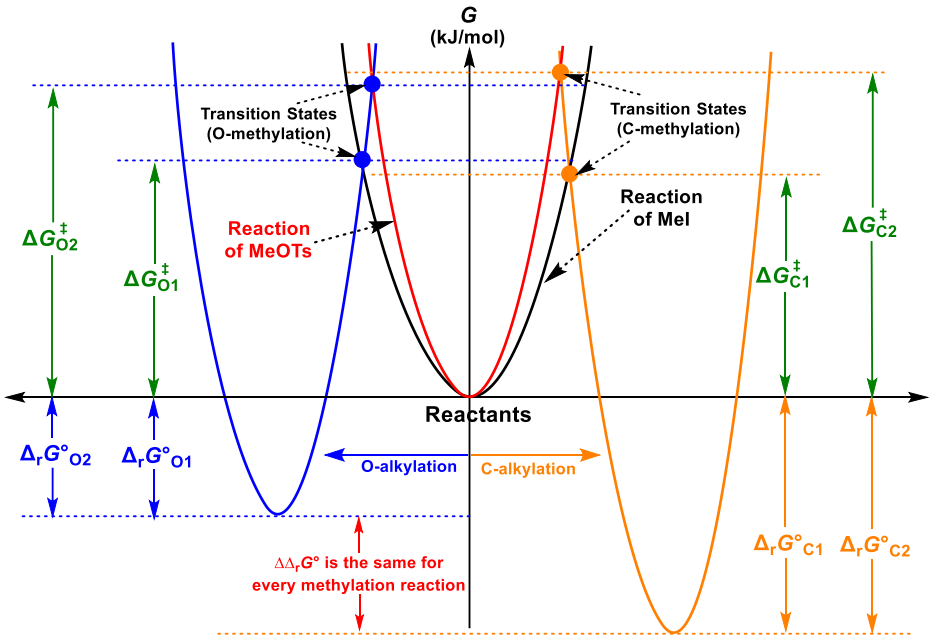


In this diagram, the product parabola for the O-methylation process (in blue) is shown to the left-hand side of the diagram. The product parabola for the C-methylation process (in orange) is shown to the right-hand side of the diagram. When the reaction considered is enolate **1-Na** with MeI (black reactant parabola in the centre of the diagram), the intersection point with the product parabola representing C-methylation is at a lower position than the intersection point with the product parabola representing O-methylation. However, if the central reactant parabola (which remains the same width and shape) is moved upwards relative to the initially drawn parabola, it may represent the reactant parabola of a reaction of enolate **1-Na** with a methylating agent of significantly higher Lewis acidity, such as MeOTf (i.e., the reactant parabola of **1-Na** with MeOTf is represented by the red reactant parabola in Figure 6-3 above). In moving this central reactant parabola upwards while keeping the shapes and positions of each of the product parabolas invariant, it is observed that the intersection point with the product parabola for the O-methylation process (in blue) now appears at a lower vertical position than the intersection point with the product parabola for the C-methylation process (in orange). The ordering of the transition states (i.e., the heights of the intersection points of the

reactant parabola with the product parabolas) has changed for the reaction of **1-Na** with MeOTf (red reactant parabola) compared to the reaction of **1-Na** with MeI (black reactant parabola). That is, just by pushing the reactant parabola upwards in the Gibbs energy profile diagram, *the ordering of the Gibbs energies of the transition states for O- and C-methylation switches*.

This example appears to account for why the selectivity for the reaction of **1-Na** with MeI results in predominant C-alkylation, but upon switching to a reagent with a significantly higher Lewis acidity (such as MeOTf), O-alkylation is the predominant process. A similar switching in the ordering of the Gibbs energies of the transition states results if, instead of pushing the reactant parabola upwards, its width is made narrower – see, for example, Figure 6-4.

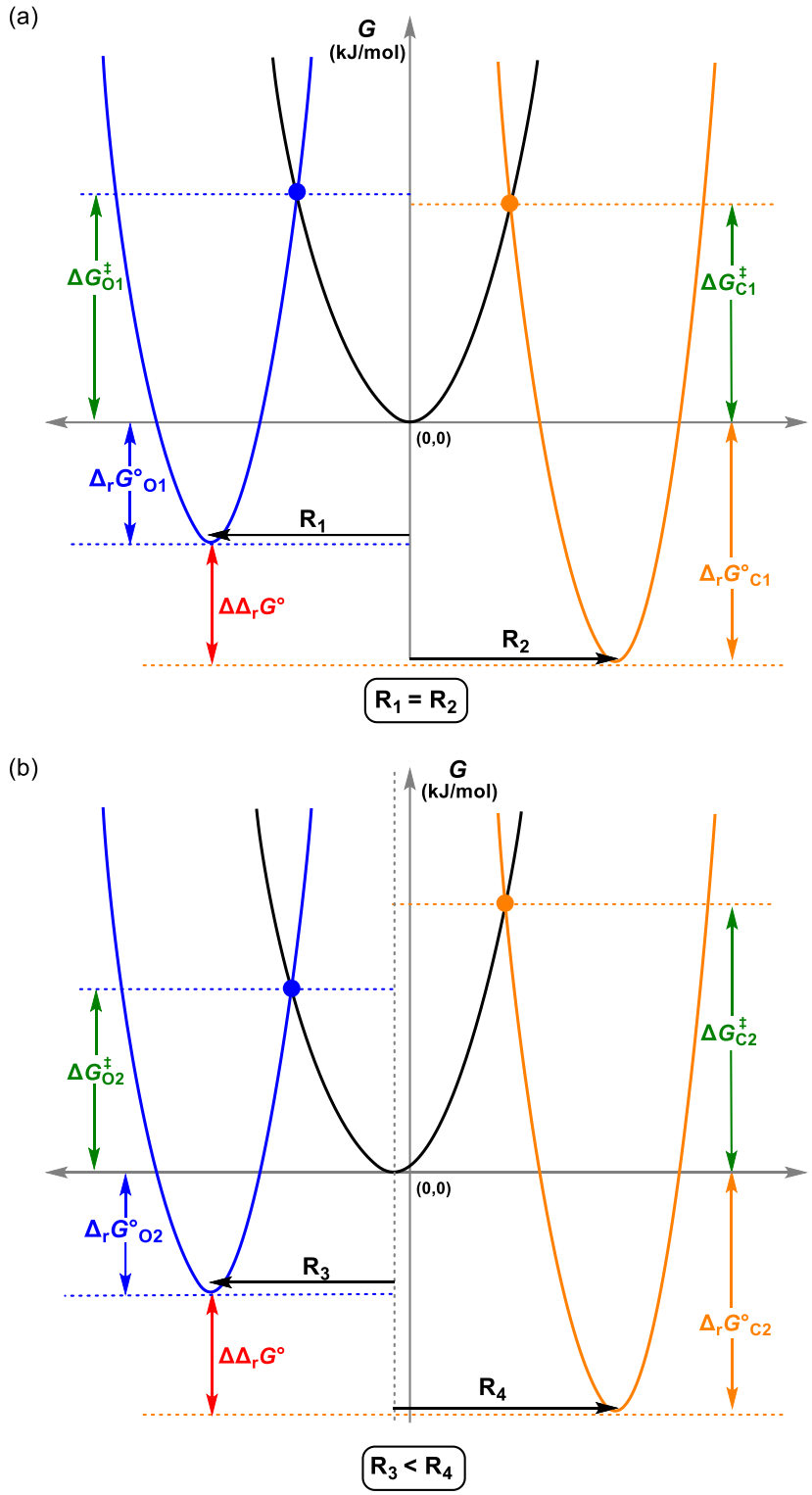
Figure 6-4. Overlaid Gibbs energy diagrams for reaction of an enolate (**1-Na**) with different methylating agents (**1-Na** + MeI reactant parabola in black, **1-Na** + MeOTs reactant parabola in red). The black parabola intersects the orange parabola at a lower vertical position (i.e., there is a lower $\Delta G^{\ddagger}$ value for C-methylation). The red parabola in each case intersects the blue parabola at a lower vertical position (i.e., there is a lower $\Delta G^{\ddagger}$ value for C-methylation). [a]



Another possible scenario is illustrated below in Figure 6-5, in which the horizontal position of the central reactant parabola is changed between the diagrams shown in Figure 6-5(a) and Figure 6-5(b). In this example, the distance between the apices of the reactant parabola and the product parabolas are identical in Figure 6-5(a) (i.e., the horizontal distance R_1 is equal to the distance R_2). In that case, the C-alkylation process is determined to be favoured, owing to the lower Gibbs energy of activation for that process (i.e., $\Delta G^{\ddagger}_{C1} < \Delta G^{\ddagger}_{O1}$).

[a] The reactant parabolas in Figure 6-5 have each been given the same apex position in this diagram for illustrative purpose. As can be seen in the data in Table 6-13 in section 6.4.3 below, the precise position of the reactant parabola for the reaction involving MeOTs should be at a slightly higher vertical co-ordinate.

Figure 6-5. By altering the horizontal position of the central reactant parabola, an inversion in selectivity may be observed. **(a)** A certain O/C selectivity may be observed when the distances between the apices of the reactant parabola with each product parabolas (i.e., $R_1 = R_2$). **(b)** If the central reactant parabola were moved to the left (i.e., such that $R_3 < R_4$) and the shapes/curvatures of each of the product parabolas remained the same, a switch in the O/C selectivity is predicted.



In Figure 6-5(b), the parabola widths and curvatures remain identical, as do the $\Delta_r G°$ values associated with the O- and C-alkylation processes, respectively (and hence the $\Delta\Delta_r G°$ values also remain the same (note that $\Delta\Delta_r G° = \Delta_r G°_O - \Delta_r G°_C$)). However, in this illustration, the central reactant parabola has been moved to the left (as drawn), thereby decreasing the distance between the apex of that parabola and the apex of the product parabola for the O-alkylation process (i.e., R_3), and simultaneously increasing the distance of the apex of the reactant parabola and the apex of the product parabola for the C-alkylation process (i.e., R_4). The effect of this horizontal shift of the reactant parabola is that the selectivity predicted by this diagram is vastly different to the selectivity predicted by Figure 6-5(a). The O-alkylation process is now predicted to be the significantly more favourable process (i.e., $\Delta G^{\ddagger}_{C2} > \Delta G^{\ddagger}_{O2}$).

This large influence of the horizontal position of the parabola could occur in combination with a change in the width of the reactant parabola (as seen in Figure 6-4), further altering the selectivity predicted by the model. It is therefore possible that a large variety of information is required to make quantitative assumptions about O/C selectivity in reactions examined by this model – the relative vertical positions of the parabola, the width of each of the parabolas and the relative horizontal position of each parabola.

If the model above is qualitatively accurate and enables the differences observed in O- vs. C-selectivity between reactions of a given ambident nucleophile with a series of alkylating agents to be accounted for, then the selectivity that is observed is dictated by the properties of the Gibbs energy wells of the reactants (i.e., the central reactant parabola). As described above, there are three properties of the reactant parabola that may change – the width of the parabola (as is illustrated in Figure 6-4), the vertical co-ordinate of the apex (see Figure 6-3) and the horizontal co-ordinate of the apex (see Figure 6-5(a) and (b). The latter two parameters serve to specify the position of a given parabola.

It may be the case that neither the horizontal co-ordinates of the parabola apices nor the parabola widths change a large amount from reaction to reaction within a series of reactions of an ambident nucleophile such as an enolate with a series of alkylating agents that all transfer the same alkyl group (e.g., methylating agents). If this is the case, it may be possible to establish the existence of relatively straightforward qualitative relationships between the Lewis acidity of the alkylating agent and the propensity towards O- or C-selectivity in reactions of that alkylating agent with ambident nucleophiles such as enolates.

It is, of course, possible that the Gibbs energy wells (parabolas) of the reactants do not retain the exact same widths or horizontal or vertical apex co-ordinates upon switching from one electrophile to another in a series of alkylating agents. There is no reason to expect that the reactant and products Gibbs energy wells should not vary in their widths (curvatures) upon going from reaction to reaction, nor that each parabola should lie along the same vertical axis. If this proves to be the case, then it is likely not to be possible to derive simple relationships such as a correlation between the Lewis acidity of the alkylating agent and the propensity towards a certain mode of selectivity.

Taking the above into consideration, the goal at the outset of this part of the project was therefore to collect data that would enable qualitative models of Gibbs energy profile diagrams for reactions of enolates with alkylating agents to be built, and to establish whether there are any obvious qualitative relationships that can be established between the Gibbs energy profile diagram models. Some of the data needed to execute such an investigation has already been mentioned above – i.e., experimental data regarding the selectivity of reactions of enolates (i.e., O/C product ratios) with various "series" of alkylating agents (e.g., methylating agents), and computationally derived values of $\Delta_r G°$ for the competing processes of O- and C-alkylation. In addition to these, experiments in which the rate constants for the competing processes of O- and C-alkylation are measured are necessary. These can be used to derive a value for the activation barrier for each process, i.e., values of $\Delta G^{\ddagger}_{O}$ and $\Delta G^{\ddagger}_{C}$).

The product ratio data (i.e., O/C ratios for the reactions of an enolate with numerous alkylating agents in a series, such as methylating agents) are necessary in order to define which mode of reaction is kinetically preferred in each reaction, which will be reflected in any model which is representing each reaction. The O/C ratios may also be used to determine the expected difference between the activation barriers for the competing processes of O- and C-alkylation, by the relationship seen below in Equation 6.1.

$$\frac{k_C}{k_O} = e^{-\left(\frac{\Delta\Delta G^{\ddagger}}{RT}\right)} = e^{-\left(\frac{\Delta G^{\ddagger}_{C} - \Delta G^{\ddagger}_{O}}{RT}\right)} \quad (6.1)$$

The rate measurement experiments are necessary to derive values of the activation barriers for each process (i.e., the values of $\Delta G^{\ddagger}_{O}$ and $\Delta G^{\ddagger}_{C}$). In the model, these values identify the co-ordinates on the vertical axis (the Gibbs energy axis) of the points at which the reactant parabola intersects each of the product parabolas (i.e., the location of each of the transition states (one for O-alkylation and one for C-alkylation)). Determining these quantities experimentally allows the positions of the transition states (i.e., intersection points) to be defined on a Gibbs energy profile diagram of the type shown in Figure 6-2.

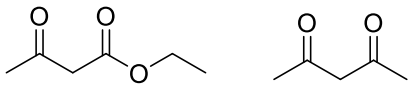
The computational data, provided by Prof. Martin Breugst of TU Chemnitz (Germany), is necessary to determine the thermodynamic preference for each of the products in a reaction of a given enolate with an alkylating agent. This data provides $\Delta_r G°$ values for the potential products of a reaction of an enolate with a given electrophile. In the context of the representation being employed here, the $\Delta_r G°$ value for a reaction corresponds to the depths of the Gibbs energy well of the products. The value of $\Delta_r G°$ is equal to the difference between the co-ordinates on the vertical axis of the apices of the reactant parabola and product parabola for the reaction in question. These thermodynamic quantities may then be combined with the experimentally derived observations regarding the kinetics of each reaction in order to build a Gibbs energy profile diagram (similar to the example in Figure 6-2) which incorporates the various features of the reaction in question.

The long-term goal of this project (i.e., beyond what is described herein) is to develop a quantitative version of the proposed method for building Gibbs energy profile diagrams. That is, it is hoped to be able to make use of the Gibbs energy profile diagram created for one reaction to be able to build the Gibbs energy profile diagrams for other reactions, and hence predict the rates of the reactions involved and the ratios of the products formed. Regardless of whether simple qualitative relationships are found to exist, or whether more complex relationships exist between one Gibbs energy profile diagram and another, if quantitative relationships between such diagrams for related reactions are to be found, a method will be required which is capable of specifying the dimensions of the horizontal axis in Gibbs energy profile diagrams. At present, there is no known method (*via* computational modelling or experimental observation) of obtaining quantitative information about the dimensions of a Gibbs energy profile diagram that can be compared between different reactions. As a result, novel methods of comparing the Gibbs energy profile diagrams of different reactions, either relatively or in an absolute sense, would need to be devised in order to develop a quantitative version of the novel model. Potential methods of accessing this information are discussed in section 6.6. As methods of defining the horizontal dimension of a Gibbs energy profile diagram do not exist at present, a qualitative model of the reactions of enolates is all that is possible for the time being. The precise method used to build these qualitative diagrams is described below, beginning in section 6.3.

6.2.2. Details on Experimental Investigations Used in Development of New Model

To develop the novel model for rationalising ambident reactivity as outlined above, new reactions employing different ambident nucleophiles to those seen in Chapters 2 and 4 were carried out. It was hoped that by using new ambident substrates, the shortcomings (summarised below) associated with the data sets discussed previously would be minimised. An appropriate investigation into the proposed model requires a data set which covers a larger range of selectivity than was observed in Chapter 4 – in which cyclic enolates produced a relatively high degree of O-selectivity with all of the electrophiles used in the study. A set of reactions in which certain electrophiles give almost exclusive O-selectivity and others give almost exclusive C-selectivity would be most suitable for the development and testing of the model proposed here. The use of enolates which were soluble in a wide range of organic solvents was also desirable, as was employing enolates with counter-cations that did not produce many signals in a ^{1}H NMR spectrum. Both of these considerations could be met satisfactorily through careful choice of the counter-cation for the enolates which were selected for study. Enolates of a set of acyclic 1,3-diketones (**8** and **9**, see Chart 6-1 below) were prepared and used in a series of methylation and ethylation reactions to further the development of the proposed model for selectivity in reactions of ambident nucleophiles.

Chart 6-1. Acyclic 1,3-diketones used in this study to probe the factors which influence the reactivity of ambident anions. The 1,3-diketones are deprotonated with a variety of organic and inorganic bases to produce ambident enolate species.



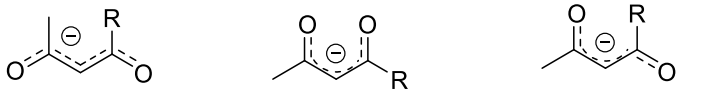
8 **9**

To ensure that the product ratios (i.e., the ratio of O- to C-alkylation products formed) of the reactions of acyclic enolates with various electrophiles was reflective of the kinetic ratio of the products (i.e., of the relative rates of formation of the products), experimental procedures involving a minimal amount of reaction mixture manipulation were necessary, similar to those described in section 4.1. The reaction of the ambident nucleophile was always carried out in a deuterated solvent and the formation of the products was directly observed by ^{1}H NMR spectroscopic monitoring of the reaction mixture. To quantify the selectivity of the reaction in question, the amount of O-alkylation products formed was directly compared to the amount of C-alkylation products formed in a given reaction – identical to the procedure described in Chapter 4.

Similar precautions to those described in section 4.1 were taken in this study in order to minimise the influence of external factors which may alter the selectivity of a reaction. Detailed descriptions of the precautions taken in these reactions may be found in Section 7.1 of Chapter 7.

Unlike in the case of the cyclic enolates described in Chapter 4, the anionic enolates form from **8** and **9** are not constrained to exist in certain conformation. The enolates derived from these compounds may exist as any of the conformations shown in Figure 6-6 below. This may result in differences in the kinetics of alkylations of each enolate conformation,[28,29] in addition to creating differences in the thermodynamic favourabilities of formation of the various isomers of a given product which may form through reactions of different enolate conformations.

Figure 6-6. The various conformations which the enolates of acyclic 1,3-diketones may assume. Depending on the conformation of the enolate when the alkylation reaction occurs, product isomers may be formed with differing thermodynamic properties.

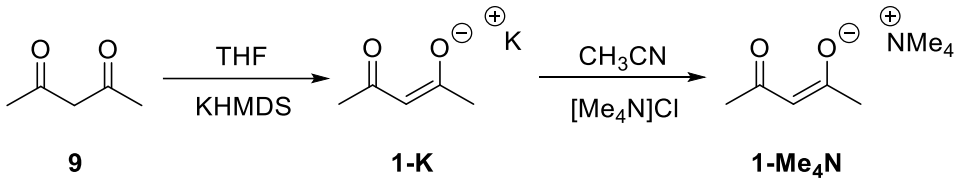


W-shaped (*E*,*E*) **U-shaped (*Z*,*Z*)** **"Sickle-shaped" (*Z*,*E*)**

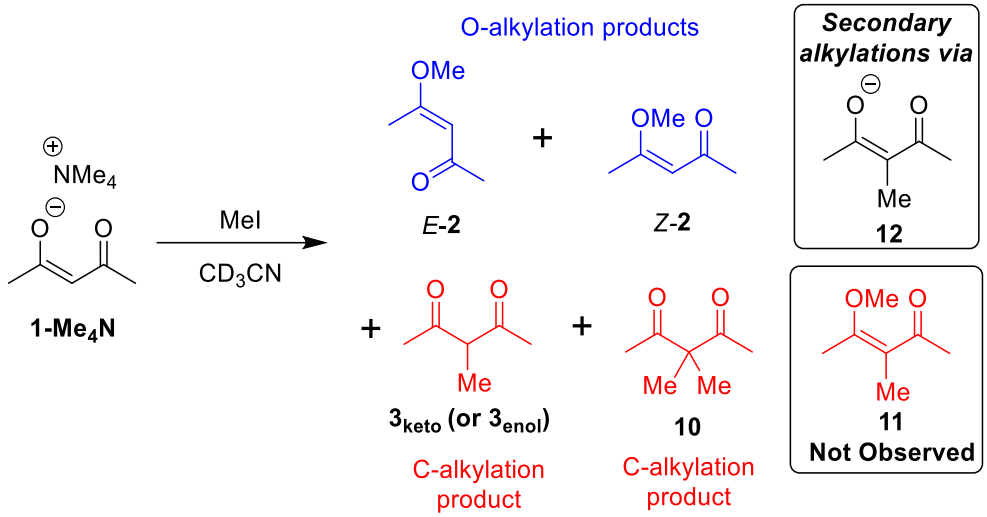
The tetramethylammonium enolate derived from **9** (i.e., **1-Me$_4$N**) was synthesised as outlined in Scheme 6-3 below. The reasons for choosing the tetramethylammonium cation (Me_4N^+) to form the enolate are identical to those mentioned in section 4.1 – this enolate was expected to be reasonably soluble in a number of organic solvents and salts of the

counter-ion would contribute only one signal to the ^{1}H NMR spectrum of a reaction mixture.

Scheme 6-3. Enolate **1-Me$_4$N** was synthesised by the initial formation of the potassium enolate of **9** (i.e., **1-K**) using KHMDS, followed by a salt metathesis reaction using [NMe$_4$]Cl in CH$_3$CN.



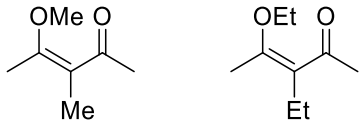
Scheme 6-4. Reaction of enolate **1-Me$_4$N** in CD$_3$CN with a limiting amount of an alkylating agent (MeI) to form products *E*-**2**, *Z*-**2**, **3$_{keto}$**, **3$_{enol}$** and **10**.



An example of a typical reaction of an acyclic enolate which is the focus of this section is shown above in Scheme 6-4. In the example reaction, the solid enolate **1-Me$_4$N** was dissolved in CD$_3$CN. A limiting amount of an electrophile (MeI in the case illustrated in Scheme 6-4) was added directly to the enolate solution and the mixture was allowed to react. The reaction mixture was maintained at a constant temperature throughout the process. The reaction mixture was then examined by ^{1}H NMR spectroscopy to observe the proportions of the various products (*E*-**2**, *Z*-**2**, **3$_{keto}$**, **3$_{enol}$** and **10**) formed. Two O-mono-methylation products were formed – the *E*- and *Z*-isomers of the vinyl ether product (see *E*-**2** and *Z*-**2** in Scheme 6-4) which result from the O-methylation of different conformations of enolate **1-Me$_4$N**. The C-mono alkylation product (**3**) may occur in two different tautomeric forms, which are denoted **3$_{keto}$** and **3$_{enol}$**. Note that in many of the schemes drawn in the sections below, only one of the tautomeric forms is drawn. However, when calculating O/C product ratios, both tautomers are accounted for in the calculations. Two secondary alkylation products (i.e., di-alkylation products) can form in this reaction *via* deprotonation of the C-mono alkylation products to give another enolate (see **12** in Scheme 6-4 above), which may undergo another alkylation reaction. The mixed di-alkylation product (**11**, see Chart 6-2 below) was never observed in any of the reactions

in this chapter. As a result, the mixed di-alkylation product is not drawn in any of the schemes below which depict alkylation reactions of **1-Me$_4$N**. The integrations of the signals of each of the reaction products (i.e., *E*-**2**, *Z*-**2**, **3$_{keto}$**, **3$_{enol}$** and **10** in Scheme 6-4) in the ^{1}H NMR spectrum of a given reaction mixture are used in the calculation of the O/C ratio. A detailed explanation of the method for obtaining the O/C ratio from a reaction mixture is given in section 7.1 of Chapter 7. Analysis and interpretation of the results of these experiments is given below, in sections 6.3 to 6.5.

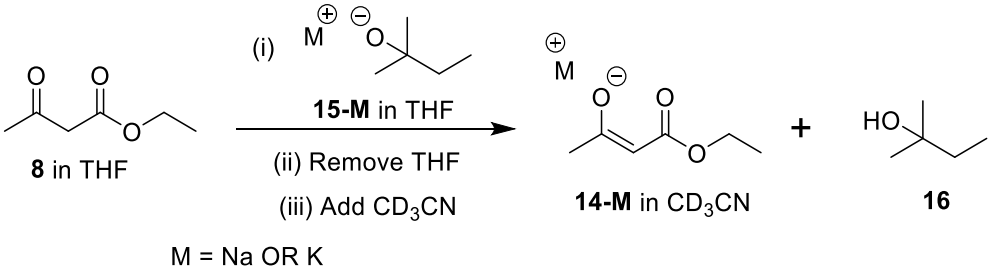
Chart 6-2. The formation of the O/C-dialkylation products **11** and **13** shown below is possible in reactions of the type outlined in Scheme 6-4. There was no spectroscopic evidence which indicated that these products formed in any of the experiments carried out below.



11 **13**

Reactions of various ethylating and methylating agents with enolate **1-Me$_4$N** in $CDCl_3$ and of enolates **14-Na** and **14-K** (synthesised from keto-ester **8** as outlined in Scheme 6-5) in CD_3CN were also carried out in this study to investigate the influence of the solvent and of the enolate counter-cation. Data regarding the O/C selectivity of these reactions was determined experimentally and values of $\Delta_r G°$ were determined for the reactions computationally. However, these results are not included in this chapter, as data pertaining to the rate constants for the O- and C-alkylation reactions of these enolates could not be accessed using the NMR spectroscopic method that was employed for reactions of **1-Me$_4$N** in CD_3CN due to issues caused by production of insoluble salts as the reactions progressed. The product ratio data and computational $\Delta_r G°$ data recorded for the reactions of **1-Me$_4$N** in $CDCl_3$ and of **14-Na** and **14-K** may be found in Appendix D. The O/C ratios and $\Delta_r G°$ values of these reactions will not be discussed further in this chapter in the context of the model proposed in section 6.2 above. A future continuation of this project will incorporate attempts using alternative means to access values of $\Delta G^{‡}_O$ and $\Delta G^{‡}_C$ for the reactions of **1-Me$_4$N** (in $CDCl_3$), **14-K** and **14-Na** with alkylating agents, and will make use of the data recorded in this project.

Scheme 6-5. Synthetic route used to generate the potassium and sodium enolates **14-Na** and **14-K**.



6.2.3. Details on Computational Investigations Used in Development of New Model

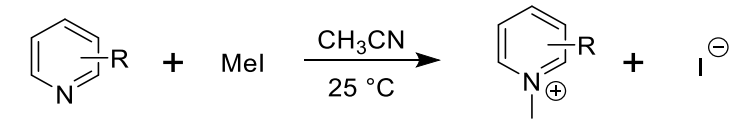
As described above, there are several key pieces of data that are required in order to be able to build Gibbs energy profile diagrams of the type shown in Figures 6-3 and 6-4. One of these, the $\Delta_r G°$ values for the reactions, can only be accessed *via* quantum chemical calculations. The requisite calculations were carried out by our computational collaborator Prof. Martin Breugst (TU Chemnitz, Germany) at the DLPNO-CCSD(T)/def2-TZVPPD/SMD(CH_3CN)//M06-2X-D3/6-311+G(d,p)/SMD(CH_3CN) level of theory, employing an SMD solvent model. This indicates that a continuum solvent model using the properties of a given solvent (in this case, CH_3CN) was employed – meaning the dielectric constant, refractive index, acidity/basicity and the surface tension at the solvent-solute boundary are accounted for.[30] Explicit solvent molecules were not included in the model, and the calculations were performed on enolates with no counter-cation. The counter-cation was omitted from the calculations as it is essentially impossible to make an unambiguous decision about how to place the counter-cation in the model, and also because nothing is currently known about the aggregation characteristics or effects for reactions of this enolate with any particular cation. However, literature precedent exists for analysing analogous reactions using a computational approach in which the counter-cation is omitted.[22] Future work in this project will include attempts to account for the influence of the enolate counter-cation, but at present, it is not evident how to approach this in a manner that produces physically meaningful, unambiguous results.

The results of these computational investigations and a discussion of their implications is found below in sections 6.2.4, 6.3.1 and 6.4.3. In the remainder of this section, details will be given of some computational investigations that were undertaken by Prof. Breugst to verify the effectiveness of the computational approach employed for calculating $\Delta_r G°$ values. This involved seeking out literature reports on reversible nucleophile alkylation reactions for which $\Delta_r G°$ values had been measured experimentally, and then using the computational method employed for the calculations on reactions of enolates to determine how closely it could reproduce the known experimental $\Delta_r G°$ value in each case. The first computational investigations conducted to test the ability of the computational method to reproduce known literature $\Delta_r G°$ values involved reactions of substituted pyridines with MeI in CH_3CN at 25 °C from a study by Arnett and Reich (see Table 6-1).[31] As can be seen by comparing the experimentally derived values listed in Table 6-1 to the calculated values, the values derived from the calculations succeed at closely replicating these quantities. The largest deviation seen above between an experimentally derived $\Delta_r G°$ value from the work of Arnett and Reich and a value of $\Delta_r G°$ which was determined computationally was 4 kJ mol $^{-1}$ (see Table 6-1, entry (iii)).

Other cases in which calculated values of $\Delta_r G°$ are reasonably close to experimentally derived values are shown below in Table 6-2. In these instances, the reactions between different Lewis bases and various benzhydrylium ions were analysed in various solvents at 20 °C by Mayr and co-workers.[32] In the reactions from the paper, the benzhydrylium ions (**5**, **30**, **33** and **36**) had $^{-}BF_4$ counter-ions, and the counter-ion of the benzoate species

(**35**) was tetra *n*-butylammonium (*n*-Bu_4N^+). No counter-ion was accounted for in the calculations of the $\Delta_rG°$ values in Table 6-2, either in the base of the benzoate species (**35**) or any of the benzhydrylium ions (**5**, **30**, **33** and **36**). In the studies in which these results were reported, equilibrium constants for these reactions were measured photometrically, from which values of $\Delta_rG°$ may be derived. For the purposes of this study, values of $\Delta_rG°$ for the same reactions were determined computationally for comparison.

Table 6-1. $\Delta_rG°$ values for the N-methylation reactions of various substituted pyridines (**17**, **19**, **21**, **23** and **25**) by MeI in CH_3CN at 25 °C were determined experimentally by Arnett and Reich.[31] The $\Delta_rG°$ value of each reaction was also computed using quantum chemical calculations employing a CH_3CN solvent model. [a]



17, 19, 21, 23, 25 → **18, 20, 22, 24, 26**

17, **18** R = H
19, **20** R = *m*-Br
21, **22** R = *m*-Cl
23, **24** R = *o*-Cl
25, **26** R = *p*-CN

Entry	Substituent	Experimental $\Delta_rG°$ (kJ mol^{-1})	Calculated $\Delta_rG°$ (kJ mol^{-1})
(i)	H	–50	–48
(ii)	*m*-Br	–26	–29
(iii)	*m*-Cl	–25 [b]	–29
(iv)	*o*-Cl	–11	–9
(v)	*p*-CN	–21	–24

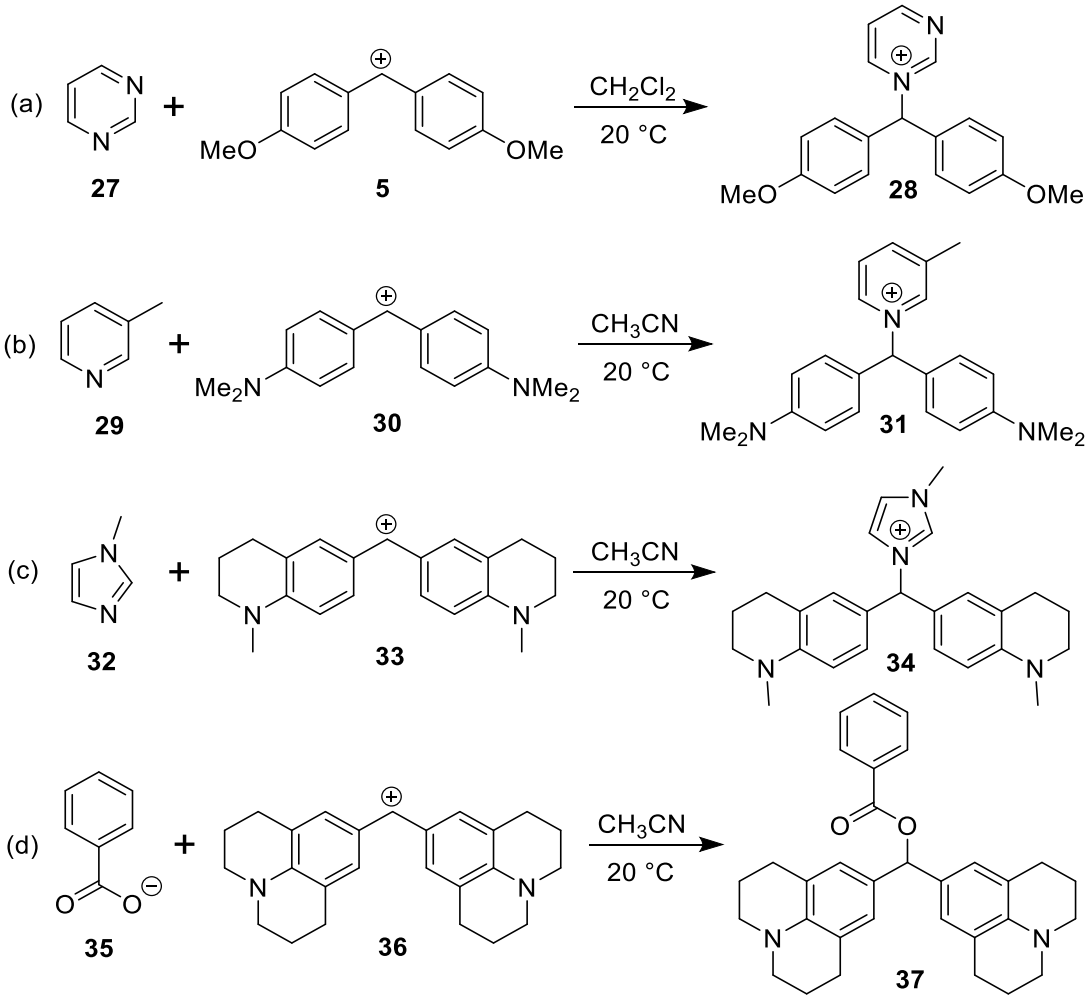
[a] The $\Delta_rG°$ values were calculated at the DLPNO-CCSD(T)/def2-TZVPPD/SMD(CH_3CN)//M06-2X-D3/6-311+G(d,p)/SMD(CH_3CN) level of theory by Prof. Martin Breugst at TU Chemnitz, Germany.

[b] The $\Delta_rG°$ value for this reaction given in a table in the original publication is –21 kJ mol^{-1}. This appears to be a mistake, however, as utilisation of the value of *K* reported in the paper leads to a value of $\Delta_rG°$ of –25 kJ mol^{-1}.

As may be seen in Table 6-2, the calculated values of $\Delta_rG°$ are reasonably accurate estimates of the experimentally determined values. Particularly in the cases of Table 6-2 entries (i) and (iii), the computational model reproduces the expected values of $\Delta_rG°$ closely. The values calculated in Table 6-2 entries (ii) and (iv) differ noticeably from the experimentally derived values, however, indicating that the accuracy of the model may fluctuate when moving from one reaction to another.

However, taking findings in Tables 6-1 and 6-2 in combination, it is apparent that the computational model employed by Prof. Martin Breugst is capable of reproducing experimentally derived values of $\Delta_rG°$ for various nucleophilic substitution reactions reasonably closely. In the context of developing the novel model for ambident reactivity, the values of $\Delta_rG°$ produced by this computational method seem sufficiently accurate for our purposes.

Table 6-2. $\Delta_rG°$ values for the reactions of various Lewis bases with benzhydrylium ions in CH_2Cl_2 and CH_3CN at 20 °C were determined experimentally by Mayr and co-workers.[32] The $\Delta_rG°$ value of each reaction was also computed using quantum chemical calculations. [a]



Entry	Reaction	Solvent	Experimental $\Delta_rG°$ (kJ mol^{-1})	Calculated $\Delta_rG°$ (kJ mol^{-1})
(i)	(a)	CH_2Cl_2	–34.3	–36.0
(ii)	(b)	CH_3CN	–13.5	–18.0
(iii)	(c)	CH_3CN	–22.1	–22.2
(iv)	(d)	CH_3CN	–26.9	–18.0

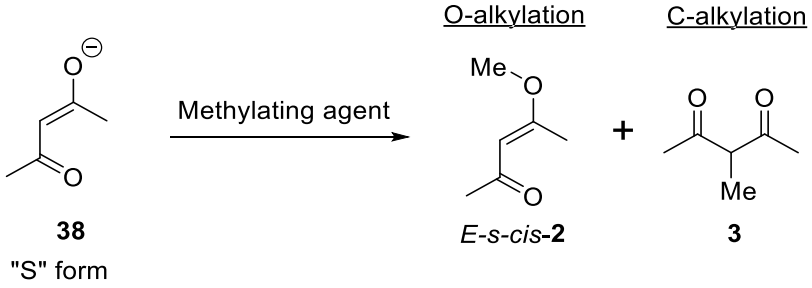
[a] The $\Delta_rG°$ values were calculated at the DLPNO-CCSD(T)/def2-TZVPPD/SMD(CH_2Cl_2)//M06-2X-D3/6-311+G(d,p)/SMD(CH_2Cl_2) and DLPNO-CCSD(T)/def2-TZVPPD/SMD(CH_3CN)//M06-2X-D3/6-311+G(d,p)/SMD(CH_3CN) level of theory by Prof. Martin Breugst at TU Chemnitz, Germany.

6.2.4. Rationalisation of High O-Selectivity in Reactions of Enolates Derived from Cyclic 1,3-Diones

Before continuing with a description of the information which is needed to develop the proposed new model for ambident reactivity, it is appropriate to re-visit the results from the investigation of reactions of enolates derived from cyclic 1,3-diones which were discussed in Chapter 4. High levels of O-selectivity were observed in reactions of those enolates with EtI in various solvents (see sections 4.2.1, 4.2.2 and 4.2.3), in reactions of those enolates with CD_3I in THF (see section 4.2.5) and in reactions of those enolates with various benzyl bromides in CD_3CN (see section 4.3). By considering these results in the context of a variation on the approach discussed above, it is possible to understand the origin of the high O-selectivity in the reactions of these enolates.

The calculated $\Delta_r G°$ values for the processes of O- and C- methylation of the enolate (**38**) derived from 2,4-pentanedione (**9**) with various methylating agents are shown below in Table 6-3.

Table 6-3. $\Delta_r G°$ values for the processes of O- and C- methylation ($\Delta_r G°_O$ and $\Delta_r G°_C$) of the enolate **38** by various methylating agents were determined using quantum chemical calculations. The calculations were conducted using a CH_3CN solvent model. [a]



38
"S" form

E-s-cis-**2**

3

Entry	Methylating agent	$\Delta_r G°_O$ [b]	$\Delta_r G°_C$	$\Delta\Delta_r G°$
(i)	MeI	–71	–154	83
(ii)	MeOMs	–74	–157	83
(iii)	MeOTs	–84	–167	83
(iv)	MeOTf	–91	–174	83
(v)	$(Me)_2SO_4$	–139	–222	83
(vi)	Me_3O^+	–139	–223	83

[a] The $\Delta_r G°$ values were calculated at the DLPNO-CCSD(T)/def2-TZVPPD/SMD(CH_3CN)//M06-2X-D3/6-311+G(d,p)/SMD(CH_3CN) level of theory by Prof. Martin Breugst at TU Chemnitz, Germany. All values given in kJ mol^{-1}.

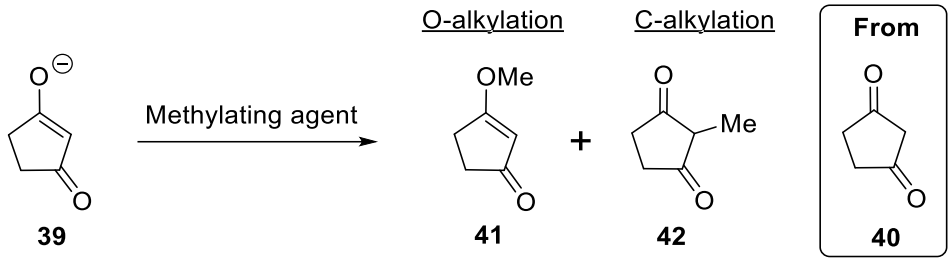
[b] The $\Delta_r G°_O$ values in this table were calculated for the *E-s-cis* form of the O-alkylation product, which is the lowest energy conformation. The calculations for the other conformations are shown in section 6.4.3. The $\Delta\Delta_r G°$ trends observed in this table are maintained regardless of the O-alkylation product conformation.

This data was calculated in an identical manner to the approach described in section 6.2.3. In this data, formation of the C-methylation products was found to be more thermodynamically preferable to formation of the O-methylation products in every

instance (as is to be expected from the literature precedents discussed above). In each case, the relative difference ($\Delta\Delta_rG°$, see Figure 6-2 above (note that $\Delta\Delta_rG° = \Delta_rG°_O - \Delta_rG°_C$)) in the Gibbs energies of reaction for the two methylation processes ($\Delta_rG°_C$ and $\Delta_rG°_O$) was found to be identical for each methylating reagent (i.e., the difference in Gibbs energy between the processes was 83 kJ mol^{-1} for each methylation reaction (see Table 6-3)). Although this relative difference ($\Delta\Delta_rG°$) was the same, the values for the standard Gibbs energy of reaction for each case were calculated to be different. For example, the C-methylation reaction of **38** by MeI was calculated to have a standard Gibbs energy of reaction of –154 kJ mol^{-1} (see Table 6-3 entry (i)), whereas the C-methylation reaction of **38** by MeOTf was calculated to have a standard Gibbs energy of reaction of –174 kJ mol^{-1} (see Table 6-3 entry (iv)).

Additional calculations which generated $\Delta_rG°$ values for the processes of O- and C-methylation of the enolate (**39**) derived from 1,3-cyclopentanedione (**40**) with various methylating agents are shown in Table 6-4. The computations in Table 6-4 reveal that for methylation reactions of enolate **39** (just as was the case with enolate **38** shown above (see results in Table 6-4)), the difference in Gibbs energy values for the products (i.e., $\Delta\Delta_rG°$) is always essentially the same, regardless of the methylating agent employed.

Table 6-4. $\Delta_rG°$ values for the processes of O- and C- methylation ($\Delta_rG°_O$ and $\Delta_rG°_C$) of the enolate **39** by various methylating agents were determined using quantum chemical calculations. The calculations were conducted using a CH_3CN solvent model. [a]



Entry	Methylating agent	$\Delta_rG°_O$	$\Delta_rG°_C$	$\Delta\Delta_rG°$
(i)	MeI	–63	–122	59
(ii)	MeOMs	–66	–125	59
(iii)	MeOTs	–76	–135	59
(iv)	MeOTf	–131	–190	59
(v)	$(MeO)_2CO$	+2	–58	60
(vi)	$(MeO)_2SO_2$	–83	–142	59

[a] The $\Delta_rG°$ values were calculated at the DLPNO-CCSD(T)/def2-TZVPPD/SMD(CH_3CN)//M06-2X-D3/6-311+G(d,p)/SMD(CH_3CN) level of theory by Prof. Martin Breugst at TU Chemnitz, Germany. All values given in kJ mol^{-1}.

Analysis of the calculated values from the reaction of **38** with MeI (Table 6-3 entry (i)) and **39** with MeI (Table 6-4 entry (i)) provides a possible explanation for why O-methylation is kinetically preferred in the reaction of enolate **39** and MeI (as was seen

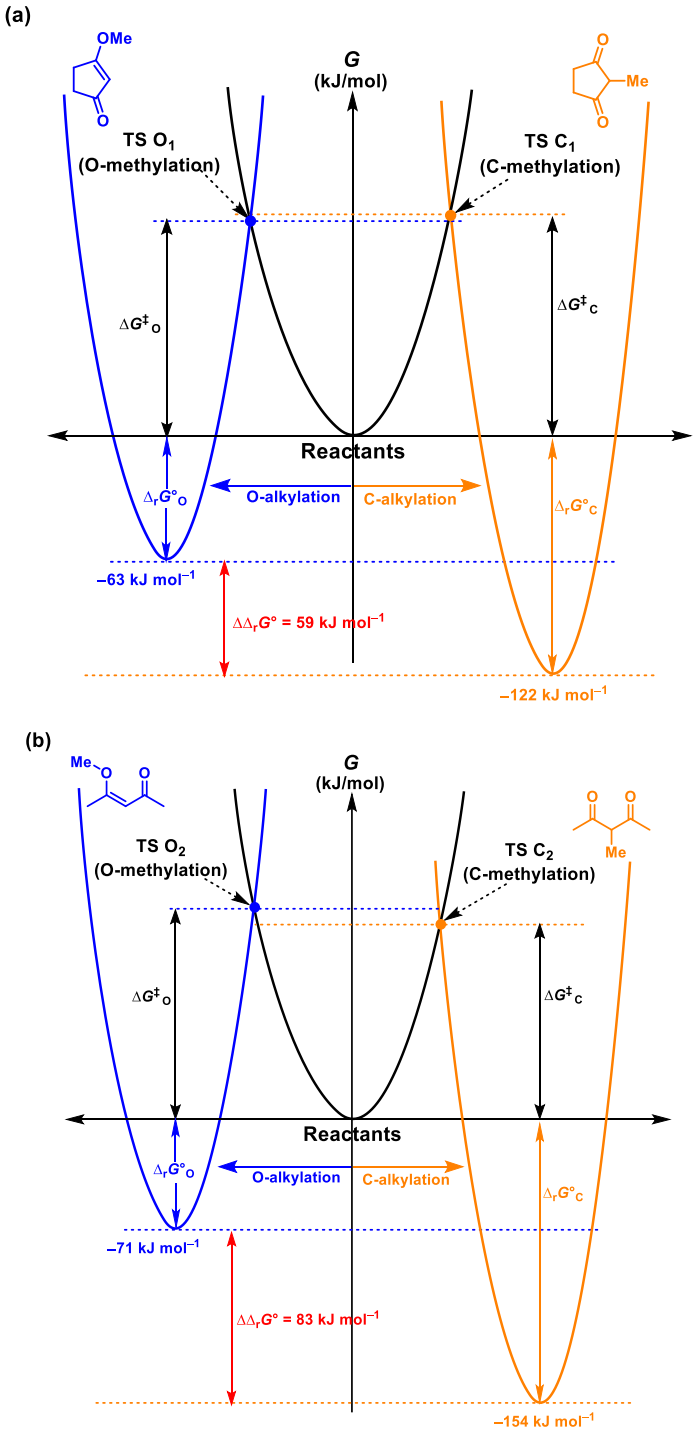
using CD_3I in reactions in Chapter 4), an occurrence which is in stark contrast to the kinetically preferred C-methylation of enolate **38** by the same electrophile (as is seen in the literature example mentioned in Scheme 6-1 and is also observed in experiments conducted as part of this project (in CD_3CN solvent)). It is apparent that some factor is responsible for causing a decrease in the activation energy of the O-alkylation reaction (i.e., $\Delta G^{\ddagger}_{O}$) of enolate **39** with MeI, or an increase in the activation energy of the C-alkylation reaction (i.e., $\Delta G^{\ddagger}_{C}$) of the same reactants.

The $\Delta_r G°$ values for the O-methylation reactions of **38** and **39** are comparatively similar (-71 kJ mol^{-1} for **38** (see Table 6-3 entry (i)), -63 kJ mol^{-1} for **39** (see Table 6-4 entry (i))). In contrast, there is a much larger difference between the $\Delta_r G°$ values for the C-methylation reactions of **38** and **39**; -154 kJ mol^{-1} for **38** (see Table 6-3 entry (i)) vs. -122 kJ mol^{-1} for **39** (see Table 6-4 entry (i)). Based on this observation, the large differences in the O/C selectivities of the reactions of enolate **38** and **39** with MeI can be accounted for (see below) using the approach outlined in section 6.2 above, wherein the Gibbs energy wells of the products and reactants are treated as parabolas.

Two Gibbs energy profile diagrams of the type initially drawn in Figure 6-2 were created which display the experimentally observed selectivities of these MeI-mediated methylation reactions as well as the computationally derived inferences about the thermodynamic preference for C-alkylation in both of the reactions studied (see Figure 6-7(a) and (b) above). Figure 6-7(a) represents the reaction of **39** + MeI, which was shown to undergo preferential O-methylation in Chapter 4. To represent this experimentally observed selectivity, the transition state (intersection point) for the O-methylation reaction of **39** (intersection of the reactant parabola with the right-hand product parabola, in blue) is shown in Figure 6-7(a) to be lower than the intersection point for the C-methylation reaction of **39** (intersection of the reactant parabola with the left hand product parabola, in orange).

Figure 6-7(b) represents the reaction of **38** + MeI, which is known to be highly selective for C-methylation. Consequently, the transition state (intersection point) for the C-methylation reaction of **38** (intersection of the reactant parabola with the right-hand product parabola, in orange) is shown in Figure 6-7(b) to be significantly lower than the intersection point for the O-methylation reaction of **38** (intersection of the reactant parabola with the left-hand product parabola, in blue). One can make use of this (and the fact that the C-methylation reaction of **39** is so much less exergonic than the C-methylation reaction of **38**) to understand the origin of the observed (kinetically favoured) O-selectivity in the reaction of **39** + MeI.

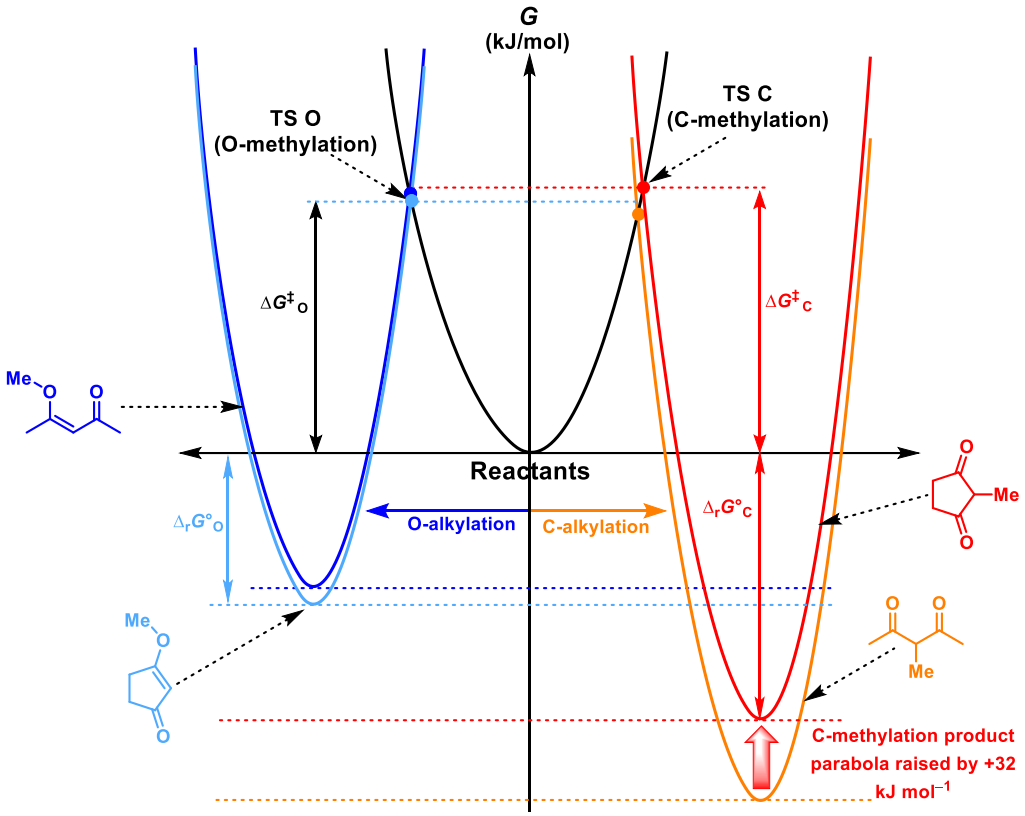
Figure 6-7. (a) A parabolic representation of the reaction co-ordinate for a reaction of enolate **39** with MeI. The O-alkylation process was observed experimentally to be kinetically favoured, and the C-alkylation process was determined computationally to be thermodynamically favoured by 59 kJ mol^{-1}. **(b)** A parabolic representation of the reaction co-ordinate for a reaction of enolate **38** with MeI. The C-alkylation process was observed experimentally to be kinetically favoured, and the C-alkylation process was determined computationally to be thermodynamically favoured by 83 kJ mol^{-1}.



The primary difference between the two models of each methylation reaction is the vertical positioning of the product parabola for the C-methylation reaction (i.e., the depth

of the Gibbs energy well for the process of C-methylation). If it is assumed that the Gibbs energy wells (which are represented by parabolas in these diagrams) in the Gibbs energy profile diagram for the reaction of **39** with MeI are similar (with regards to the width/curvature) to the corresponding parabolas in the diagram for the reaction of **38** with MeI, then the origin of the difference in selectivities can be understood by overlaying the Gibbs energy profile diagrams of Figures 6-7(a) and (b) in one diagram (see Figure 6-8). In taking this approach, it is implicitly assumed that the activation energies for the O-alkylation processes in the two reactions are similar.

Figure 6-8. A parabolic representation of the reaction co-ordinate for a reaction of enolate **38** with MeI. If the apex of the C-methylation product parabola (on the right-hand side) is raised by 32 kJ mol^{-1}, the transition state for C-methylation also moves up in Gibbs energy, such that this transition state lies at a higher Gibbs energy than the transition state for O-methylation. Hence, formation of the O-alkylation product is expected to be the kinetically preferred process.



By overlaying the two Gibbs energy profile diagrams in one image, the following observation becomes clear: if the Gibbs energy profile diagram originally found in Figure 6-7(b) is modified by raising the C-methylation product parabola (orange parabola on the right hand side) up by 32 kJ mol^{-1} (the difference between the $\Delta_rG°_C$ values for the reaction of **39** + MeI and the reaction of **38** + MeI), then the Gibbs energy profile diagram that is generated is a good approximation of the diagram in Figure 6-7(a), i.e., the Gibbs energy profile diagram for the reaction of **39** + MeI (strictly, the O-methylation product parabola on the left hand side should also be *lowered* by *ca.* 8 kJ mol^{-1}). An important consequence of raising up the C-methylation product parabola in Figure 6-8 (see the red

parabola) is that the transition state for C-methylation ($\Delta G^{\ddagger}_{C}$) (the point of intersection of this parabola with the reactant parabola) also moves up in Gibbs energy. The result is that the transition state for C-methylation in this modified Gibbs energy profile diagram lies at a higher Gibbs energy than the transition state for O-methylation, i.e., $\Delta G^{\ddagger}_{O} < \Delta G^{\ddagger}_{C}$, and O-methylation has become the kinetically favoured process.

This simple observation appears to account for the difference in selectivity between the reactions of the two enolates **38** and **39** with MeI, in which one reaction gives preferential O-methylation with MeI and the other give preferential C-methylation with MeI.

6.3. Construction of Gibbs Energy Profile Diagrams for Reactions of Enolate 1-Me_4N with Ethylating Agents in CD_3CN

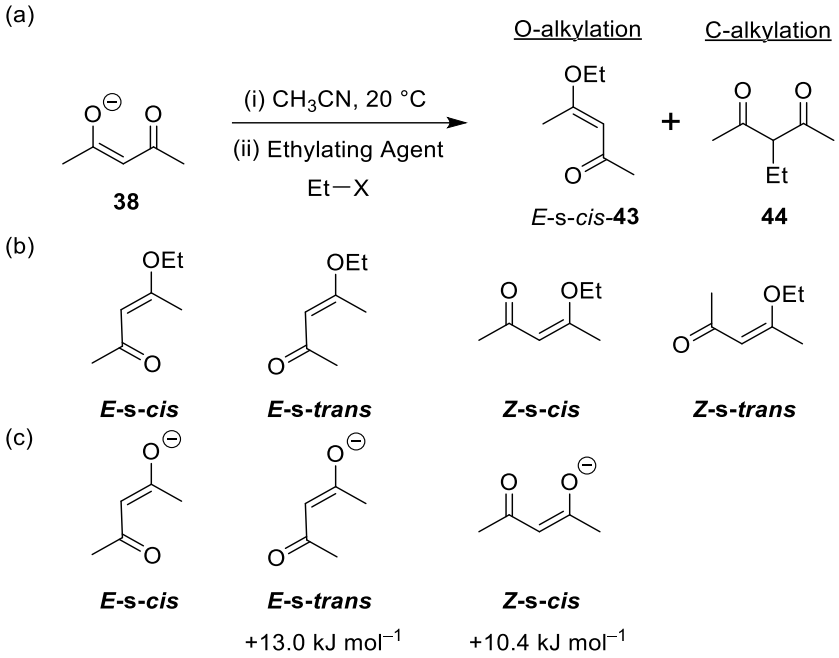
In this section, details will be given on the computational thermodynamic data and experimental Gibbs energy of activation data that were collected on the reactions of enolate **1-Me_4N** with ethylating agents. Subsequently, it will be shown how these data were used to construct Gibbs energy profile diagrams for these reactions using the principles of the novel approach described above.

6.3.1. Computational Determination of $\Delta_r G°$ Values for Ethylation Reactions of 38

To be able to construct a Gibbs energy profile diagram in the manner outlined in Figure 6-3 above that describes the reaction of an enolate with an ethylating agent, values of $\Delta_r G°$ are required for the O- and C-ethylation reactions of **38** (the enolate of 2,4-pentanedione (**9**)) and the ethylating agent in question. These values can be used to specify the differences between the vertical co-ordinates of the apices of the reactant parabola and product parabolas in the Gibbs energy profile diagram for the reaction in question.

Quantum chemical calculations were performed by Prof. Martin Breugst (a collaborator of the Byrne group in TU Chemnitz, Germany) using the approach described above in Section 6-2 to generate $\Delta_r G°$ values for the processes of O- and C-ethylation of **38**, the enolate of 2,4-pentanedione (**9**) with various ethylating agents in CH_3CN. The results of these computations are shown in Table 6-5. Note that since there exists considerable ambiguity in the literature over reliable incorporation of cation-anion interactions in quantum chemical calculations,[6–8] and since the computational approach discussed in section 6.2.3 involving calculations with counter-ions omitted was shown to reproduce $\Delta_r G°$ values of reversible reactions from the literature reasonably closely, the choice was made to conduct the calculations on the reactions of the enolate shown in Table 6-5 in the absence of the Me_4N^+ counter-cation. For reactions of enolate **38** (which is the acetylacetonate ion, i.e., **1-Me_4N** without its Me_4N^+ counter-cation), four distinct forms of the O-alkylation product may be formed (i.e., two pairs of conformers; see Table 6-5(b)). The standard Gibbs energy of reaction was calculated for the formation of each of the possible forms of the O-alkylation product. In each case, formation of the *E*-s-*cis* form of the O-alkylation product was found to be the most thermodynamically favourable of the O-alkylation processes (i.e., producing the most negative values of $\Delta_r G°$). When calculating the relative difference between the Gibbs energies of reaction (i.e., $\Delta\Delta_r G°$) between the processes of O- and C-alkylation for a given reagent, the value of the *E*-s-*cis* conformation of the O-alkylation product was used in each case for this reason. Note that in addition to different isomers of the O-alkylation product being possible (and accounted for in the calculations), different conformations of the *enolate* are also possible. The *E*-s-*cis* conformation of the enolate **38** was calculated to be the lowest Gibbs energy conformation of the enolate. The structures of each of these enolate conformations are shown in Table 6-5(c) below, along with the differences in Gibbs energy calculated for each isomer relative to the *E*-s-*cis* enolate (i.e., the isomer which is calculated to have the lowest Gibbs energy value).

Table 6-5. (a) $\Delta_rG°$ values for the processes of O- and C-alkylation ($\Delta_rG°_O$ and $\Delta_rG°_C$) of the enolate **38** by various ethylating agents using a CH_3CN solvent model were determined using quantum chemical calculations. The calculations were conducted using a CH_3CN solvent model at a calculated temperature of 20 °C. [a] **(b)** Four different conformations of O-mono-ethylation product may be formed, each with varying thermodynamic properties. **(c)** The different possible conformations of enolate **38** with differences in Gibbs energy relative to the most stable *E*-s-*cis* conformation shown.



#	Alkylating agent	$\Delta_rG°_O$ (*E*-s-*cis*)	$\Delta_rG°_O$ [b] (*E*-s-*trans*)	$\Delta_rG°_O$ [c] (*Z*-s-*cis*)	$\Delta_rG°_O$ [d] (*Z*-s-*trans*)	$\Delta_rG°_C$	$\Delta\Delta_rG°$ [e]
(i)	EtBr	–29.0	–18.8	–13.2	–19.0	–99.3	70.3
(ii)	EtOMs	–72.6	–62.4	–56.8	–62.6	–142.9	70.3
(iii)	EtOTs	–76.8	–66.6	–61.1	–66.9	–147.2	70.3
(iv)	EtI	–78.2	–68.0	–62.5	–68.2	–148.5	70.3
(v)	$(EtO)_2SO_2$	–88.9	–78.7	–73.1	–78.9	–159.2	70.3
(vi)	EtOTf	–133.8	–123.6	–118.1	–123.8	–204.1	70.3
(vii)	Et_3O^+	–139.0	–128.8	–123.3	–129.0	–209.3	70.3

[a] The $\Delta_rG°$ values (in kJ mol^{-1}) were calculated at the DLPNO-CCSD(T)/def2-TZVPPD/SMD(CH_3CN)//M06-2X-D3/6-311+G(d,p)/SMD(CH_3CN) level of theory by Prof. Martin Breugst. All values given in kJ mol^{-1}.

[b] The $\Delta_rG°_O$ values in this column were calculated for the transformation of the *E-s-trans* enolate to the *E-s-trans* vinyl ether.

[c] The $\Delta_rG°_O$ values in this column were calculated for the transformation of the *Z-s-cis* enolate to the *Z-s-cis* vinyl ether.

[d] The $\Delta_rG°_O$ values in this column were calculated for the transformation of the *E*-s-*cis* enolate (which is identical to the *Z-s-trans* enolate) to the *Z-s-trans* vinyl ether.

[e] The $\Delta\Delta_rG°$ values were calculated using the lowest value of $\Delta_rG°_O$ in each case. As the *E*-s-*cis* isomer of the O-alkylation product is the most thermodynamically favourable in each case, this results in the $\Delta\Delta_rG°$ values being the difference in standard Gibbs energy of reaction between $\Delta_rG°_{O\ (E\text{-}s\text{-}cis)}$ and $\Delta_rG°_C$.

The values seen in the "$\Delta_r G°_{O\ (E\text{-s-}cis)}$" column in Table 6-5 above relates to the Gibbs energy difference between the *E*-s-*cis* enolate and *E*-s-*cis* vinyl ether. The standard Gibbs energies of reaction for C-alkylations (in the "$\Delta_r G°_C$" column) were also calculated using the Gibbs energy level of the *E*-s-*cis* enolate. In order to calculate the $\Delta_r G°_C$ values for reactions of the other conformation of the enolate **38** with ethylating agents, the relevant energy difference between the enolate conformations may simply be subtracted from the value of $\Delta_r G°_C$ given for that reaction in Table 6-5 above. For example, the $\Delta_r G°_C$ value of the reaction of the *E*-s-*trans* enolate with EtI is –161.5 kJ mol^{-1}, which is calculated by subtracting 13.0 kJ mol^{-1} from the value of $\Delta_r G°_C$ given for the reaction of **38** with EtI in Table 6-5 entry (iv).

The O- and C-ethylation of enolate **38** was calculated to have the smallest negative values of $\Delta_r G°$ in a reaction with EtBr (see Table 6-5 entry (i)). The reaction of enolate **38** with Et_3O^+ gave the largest negative values of $\Delta_r G°$ for the O- and C-ethylation processes (see Table 6-5 entry (vii)). The values of $\Delta_r G°$ which were calculated for the reactions of **38** with EtOTf were similar to those calculated for the reactions using Et_3O^+, which were far more negative than any of the other values calculated in Table 6-5 entries (i) to (v) (compare Table 6-5 entry (vi) to entry (vii)). The O- and C-ethylation reactions of enolate **38** with EtOMs, EtOTs and EtI each produced very similar values of $\Delta_r G°$ for their respective alkylation processes (compare Table 6-5 entry (ii), entry (iii) and entry (iv)).

6.3.2. Experimental Elucidation of Product Ratios (O/C Ratios)

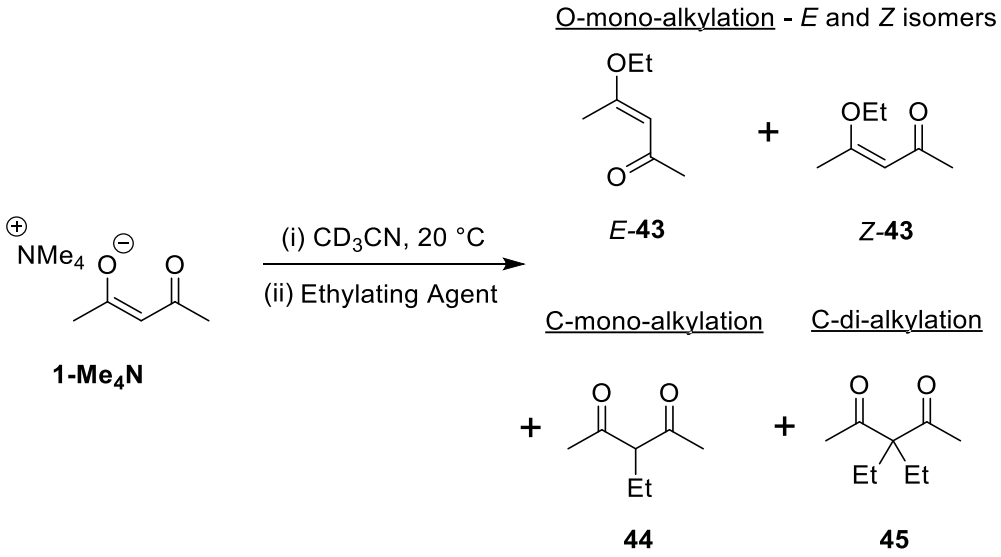
Product ratios (O/C ratios) for reactions of enolates (such as **1-Me$_4$N**) are required to indicate the differences in the heights of the Gibbs energy of activation barriers for competing O- and C-alkylation processes. The experimentally derived O/C ratio of a reaction demonstrates which process is kinetically preferred in a reaction (thereby allowing identification of which product parabola intersects the reactant parabola at a lower vertical position, see Figure 6-8 above) and indicates the difference in the relative heights of the Gibbs energy of activation barriers (see Equation 6.1 above).

Table 6-6 below shows the O/C ratios derived from the reaction of enolate **1-Me$_4$N** with numerous ethylating agents in CD_3CN. The reactions were maintained at a constant temperature of 20 °C and allowed to proceed for approximately 18 hours before being analysed by ^{1}H NMR spectroscopy.

Each ethylating agent used in Table 6-6 successfully underwent reaction with **1-Me$_4$N** in CD_3CN. The reactions of EtI and EtBr with **1-Me$_4$N** in CD_3CN (Table 6-6 entries (iv) and (i)) both resulted in a high proportion of C-alkylation products being formed, whereas use of each of the other reagents resulted in preferential O-alkylation in CD_3CN (see entries (ii), (iii) and entries (v) – (vii)). The reaction of **1-Me$_4$N** with $[Et_3O]BF_4$ showed the highest O/C ratio of the ethylating agents tested (see Table 6-6 entry (vii)) and the reaction of **1-Me$_4$N** with EtI resulted in the lowest proportion of O-alkylation products being formed (see Table 6-6 entry (iv)). This series of ethylations contains multiple O-selective and C-selective reactions, each with unique observed proportions of O- and C-alkylation products. There are no reactions for which exclusive O- or C-ethylations occur

– meaning a Gibbs energy profile diagram could theoretically be plotted as described in section 6.2 for each reaction system as a series of overlapping parabolas, using the transition states at the points of intersection between the parabolas as a guide to construct the diagrams.

Table 6-6. O/C ratios of the products of the reactions of enolate **1-Me$_4$N** with various ethylating agents in CD_3CN and $CDCl_3$. [a]



#	Solvent	Ethylating Agent	O-Ethylation Products	C-Ethylation Products	O/C Ratio [a,b]
(i)	CD_3CN	EtBr	*E*-**43**, *Z*-**43**	**44**, **45**	25:75
(ii)	CD_3CN	EtOMs	*E*-**43**, *Z*-**43**	**44**, **45**	85:15
(iii)	CD_3CN	EtOTs	*E*-**43**, *Z*-**43**	**44**, **45**	87:13
(iv)	CD_3CN	EtI	*E*-**43**, *Z*-**43**	**44**, **45**	10:90
(v)	CD_3CN	$(EtO)_2SO_2$	*E*-**43**, *Z*-**43**	**44**, **45**	80:20
(vi)	CD_3CN	EtOTf	*E*-**43**, *Z*-**43**	**44**, **45**	84:16
(vii)	CD_3CN	$[Et_3O]BF_4$	*E*-**43**, *Z*-**43**	**44**, **45**	88:12

[a] The O/C ratio was determined by direct analysis of the reaction mixture by ^{1}H NMR spectroscopy.

[b] The percentage of C-alkylation is the combined proportion of C-mono-alkylation product and C-di-alkylation product. No mixed O/C-di-alkylation products were observed in any of the reaction mixtures. See Chapter 7 section 7.2 for details on the individual reactions.

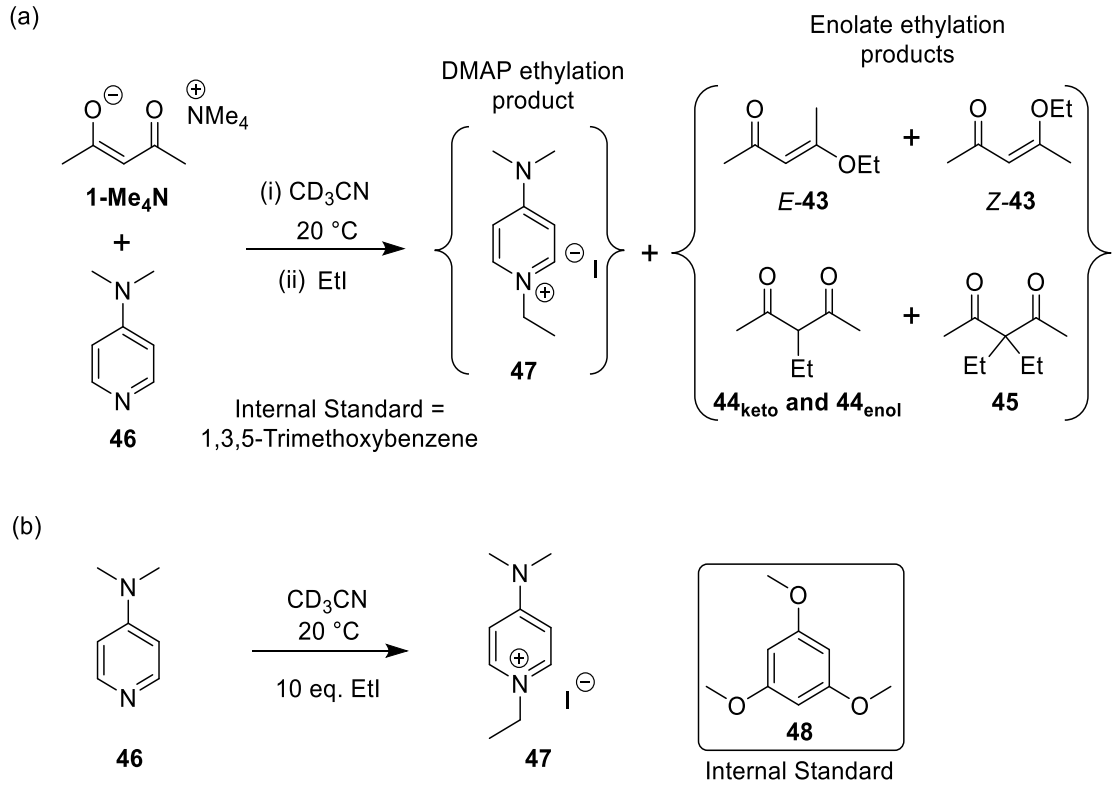
6.3.3. Experimental Determination of Values of $\Delta G^{\ddagger}$ for Ethylation Reactions of DMAP (as a Competitor Nucleophile)

In order to be able to build a model of the Gibbs energy profile diagram for the reaction of an enolate with an alkylating agent in the manner outlined in Figure 6-3 (and the associated discussion), it is necessary to identify the Gibbs energy of activation values ($\Delta G^{\ddagger}$) for the competing O- and C-alkylation processes. The value of $\Delta G^{\ddagger}$ for one of these

processes (e.g., C-alkylation) provides the vertical co-ordinate of the point at which the reactant parabola intersects with the product parabola for the reaction in question (i.e., the vertical co-ordinate of the transition state).

Gibbs energy of activation data and rate data concerning the reactions of ambident nucleophiles such as **1-Me$_4$N** are inherently difficult to access – there are two competing reactions occurring simultaneously, with an individual value and rate constant associated with each process. The reactions produce salts as by-products and are thus not conducive to potentiometric or conductometric analysis, nor are they distinct enough from one another chemically that Ultraviolet-visible spectroscopy or IR spectroscopy would be useful in monitoring the rate of formation of the various products.

Scheme 6-6. (a) In the reaction drawn below, the reaction of the nucleophile dimethylaminopyridine (**46**) and EtI occurs in concerted competition with the reaction of **1-Me$_4$N** and EtI. **(b)** An experiment measuring the rate of reaction between **46** and EtI under the same conditions employed in the competition experiment. The relative rates of the enolate ethylation processes could be estimated using the knowledge of rate data pertaining to the reaction of **46** with EtI.



In order to estimate the rate constants and the activation energies for the competing processes involved in enolate alkylation, experiments were devised in which the reaction of an enolate with a limiting amount of an electrophile occurs simultaneously and competitively with another nucleophile (see example in Scheme 6-6(a)). The rate of reaction of the enolate alkylation processes can thus be compared in relative terms to the reaction of the competing nucleophile – if a large amount of the competitor nucleophile

is found to have been alkylated by the limiting amount of the alkylating agent, then the rate of reaction of that nucleophile is known to be faster than either of the processes of enolate alkylation. By comparing the proportions of products formed in such a reaction, the *relative rates* of the alkylation processes can be determined. If the rate of the reaction between the competitor nucleophile and the alkylating agent under the same conditions is known (by an experiment similar to the one shown in Scheme 6-6(b)), then a rate constant and $\Delta G^{\ddagger}$ values for the competing enolate processes can be extrapolated from the experiment in which these nucleophiles competed for a limited amount of an alkylating agent (a competition experiment, see Scheme 6-6(a)). Thus, using this approach, two experiments are required to estimate the 2nd order rate constants for the O- and C- alkylation reactions of the enolate and a given alkylating agent – an experiment determining the rate constant for alkylation of the intended competitor nucleophile by the alkylating agent, and an experiment involving competition between the enolate and the competitor nucleophile for the alkylating agent. As the work on reactions of ambident nucleophiles in Chapters 2 and 4 proceeded effectively using ^{1}H NMR spectroscopy as the primary analytical method, a ^{1}H NMR spectroscopy procedure was utilised as the method for extracting the relevant data from both rate measurement experiments and competition experiments. Through the use of an internal standard (1,3,5-trimethoxybenzene, **48**) of known concentration in the reaction mixture, the concentration of any alkylation product could be determined by comparing the integrated ^{1}H NMR signals of those products to the ^{1}H NMR signals of the internal standard.

The competing nucleophile used for this purpose was dimethylaminopyridine (DMAP, **46**), which was chosen for its useful physical properties, and because it was found to have similar nucleophilicity towards alkylating agents as **1**-**Me$_4$N** (i.e., reactions of **46** with various electrophiles did not occur so quickly that no enolate alkylation products formed when the two nucleophiles competed for a limiting amount of an electrophile). This compound is an air-stable solid, which enables precise weighing and a high degree of accuracy when determining the concentration of **46** in a competition experiment (akin to the reaction shown in Scheme 6-6(a)) or in an experiment in which the rate of reaction between **46** and an electrophile was determined (akin to the reaction shown in Scheme 6-6(b)). Additionally, the ^{1}H NMR signals of this compound (and its methylation and ethylation products, one of which is seen in Scheme 6-6 (**47**)) do not occur in the same region of the ^{1}H NMR spectrum as any signals of products resulting from enolate alkylation (i.e., the signals of *E*-**43**, *Z*-**43**, **44** and **45** in Scheme 6-6(a)). The internal standard for these reactions was chosen to be 1,3,5-trimethoxybenzene (**48**) due to its favourable physical and ^{1}H NMR spectroscopic properties.

In an experiment in which the rate of a reaction of **46** and an alkylating agent was measured (e.g., Scheme 6-6(b)), conditions are employed which enable the reaction to proceed with pseudo-first-order kinetics. This was achieved through the "isolation method" – a set of conditions in which one of the two reactants in a 2nd order reaction is present in large excess, and hence can be treated as if its concentration were essentially constant. The expected rate law for the pseudo-first order reaction illustrated in Scheme 6-6(b) is shown below in Equation 6.2.

$$\text{Rate} = k[\mathbf{EtI}][\mathbf{46}] = (k[\mathbf{EtI}]_0)[\mathbf{46}] = k_{\text{obs}}[\mathbf{46}] \quad (6.2)$$

$$k_{\text{obs}} = k[\mathbf{EtI}]_0 \quad (6.3)$$

Using the example shown in Scheme 6-6(b), the addition of ten equivalents of EtI (in relation to **46**, the nucleophile) creates a scenario in which only 10% of the initially added EtI will have undergone reaction when all of the nucleophile has been consumed. Consequently, the initial concentration of the EtI and the final concentration can be considered constant. To obtain extremely accurate results, a very large excess of one reactant is often considered necessary in order to make this supposition. However, in this context, in which the rate of reaction was estimated by monitoring the reaction by ^{1}H NMR spectroscopy, adding a large excess of one reagent would result in a ^{1}H NMR spectrum that is uninterpretable. Ten equivalents of the electrophile was chosen as a compromise that allowed excess electrophile to be added, but ensured that the most or all of the signals in the ^{1}H NMR spectra of the reaction mixture could be readily observed and accurately integrated, though the potential error ascribed to any values derived from this method must be recognised. The use of ten equivalents of one of the reactants in a kinetic study of this nature has numerous precedents in the literature.[33]

The use of an internal standard of known concentration (**48** in Scheme 6-6(b)) in the reaction mixture allows the exact concentration of the alkylation product formed during the reaction of **46** with the ethylating agent (e.g., **47** in Scheme 6-6(b)) to be calculated at any given timepoint (i.e., any spectrum of the reaction mixture). Continuous measurement of the increasing concentration of the alkylation product over time allowed a pseudo-first-order rate constant (k_{obs}) to be calculated. Using the known initial concentration of the electrophile ([**EtI**]$_0$ in Equations 6.2 and 6.3 above), the second-order rate constant (k) for the reaction can be found using the relationship between k_{obs} and [**EtI**]$_0$ that is described in Equation 6.3.

The rate constants and Gibbs energy of activation values ($\Delta G^{\ddagger}$) for reactions of dimethylaminopyridine (DMAP, **46**) with various methylating and ethylating agents (similar to the example given in Scheme 6-6(b)) were calculated and are displayed below in Table 6-7. The exact process by which these quantities were calculated may be found in section 7.3. Each reaction proceeded in CD_3CN under an inert atmosphere of nitrogen gas inside a sealed NMR tube. The reaction mixtures were maintained at 20 °C inside the probe of the NMR spectrometer for the duration of the experiment. To observe the change in concentration of the reactants and products over time, the size of certain relevant signals were monitored in each individual ^{1}H NMR spectrum. The integration value for the DMAP alkylation product in a reaction was assigned a concentration value relative to the known concentration of the internal standard 1,3,5-trimethoxybenzene (**48**). The first-order rate constant k_{obs} at a given nucleophile concentration was obtained by least-squares fitting of the single-exponential function [**Product**]$_t$ = [**DMAP**]$_0$ $(1 - e^{-k_{\text{obs}}t})$ + C to the growth curve formed by plotting the values of ([**Product**]$_t$) versus time, where [**DMAP**]$_0$ is the concentration of the limiting reagent (**DMAP**) at time 0 and [**Product**]$_t$ is the concentration of the DMAP alkylation product in question at time t. C is a constant.

An example of a plot of the values of ([**49**]$_t$) (the concentration values associated with the alkylation product formed in a reaction of DMAP (**46**) with EtBr at various timepoints) versus time is shown in Figure 6-9(a) below.

Approximate values for the second-order rate constants k were obtained by dividing k_{obs} by the concentration of the electrophile, as can be extrapolated from Equation 6.3. The resulting value of the rate constant k was related to $\Delta G^{\ddagger}$ by a rearranged form of the Eyring equation, shown below as Equation 6.4.

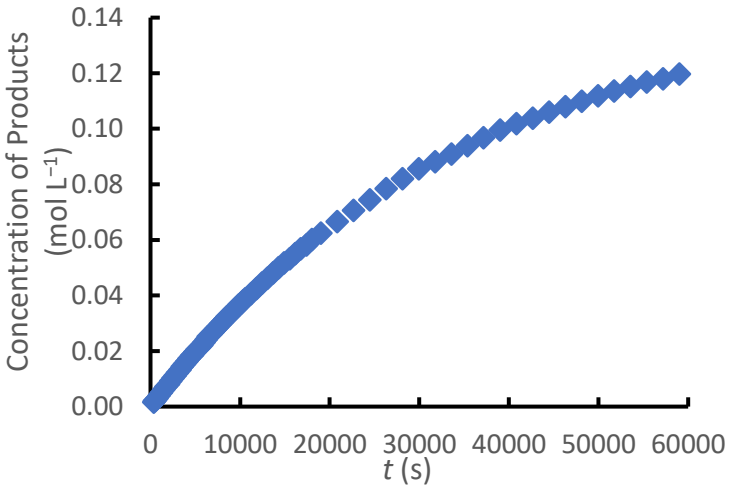
$$RT \ln\left(\left(\frac{1}{k}\right)\left(\frac{k_B T}{h}\right)\left(\frac{RT}{p^{\circ}}\right)\right) = \Delta G^{\ddagger} \qquad (6.4)$$

where:

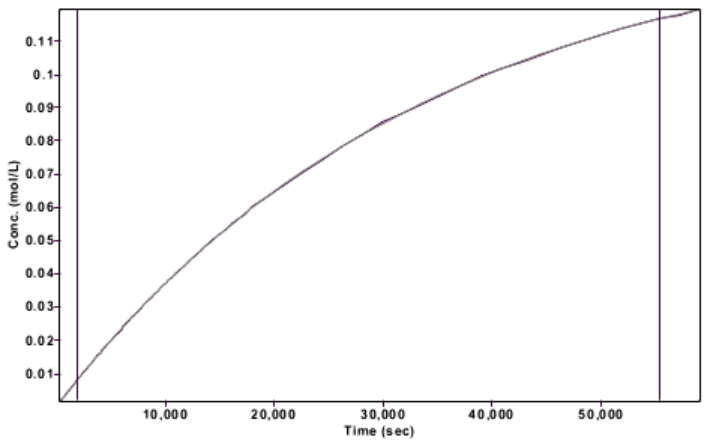
$$R = 8.314\ \text{J K}^{-1}\text{mol}^{-1} \quad T = 293.15\ \text{K}$$
$$p^{\circ} = 10^{5}\ \text{N m}^{-2} \quad k_B = 1.38 \times 10^{-23}\ \text{J K}^{-1} \quad h = 6.63 \times 10^{-34}\ \text{J s}$$

Figure 6-9. (a) The plot of ([**49**]$_t$) versus time for the reaction of 4-dimethylaminopyridine (**46**) + EtBr in CD_3CN at 20 °C. **(b)** The least-squares fitting of the single-exponential function $[\mathbf{49}]_t = [\mathbf{46}]_0 (1 - e^{-kobst} + C)$ to the growth curve obtained by plotting the values of ([**49**]$_t$) versus time.

(a)

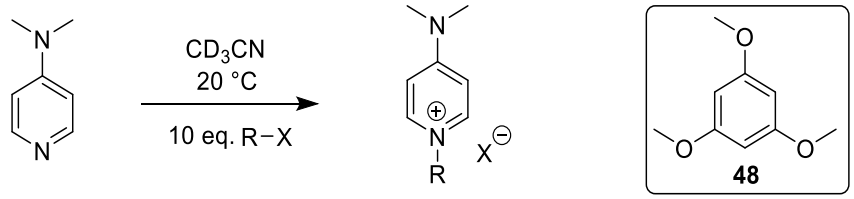


(b)



The values of k_{obs}, k and $\Delta G^{‡}$ at 20 °C which were calculated for the reactions of **46** with various methylating and ethylating agents in CD_3CN are shown below in Table 6-7. The experimentally determined activation barriers ($\Delta G^{‡}$) of reactions of DMAP (**46**) with these electrophiles, in combination with the competition experiments of the type illustrated in Scheme 6-6(a) allowed access to estimated values of the activation barriers ($\Delta G^{‡}$) for the processes of O- and C-alkylation of the enolate **1-Me$_4$N**.

Table 6-7. Values of the rate constant (k) and $\Delta G^{‡}$ for the reactions of **46** with various methylating and ethylating agents in CD_3CN at 20 °C were determined through continuous monitoring of reaction progress by ^{1}H NMR spectroscopy. [a]



47 R = Et, X = I **49** R = Et, X = Br
50 R = Et, X = OMs **53** R = Me, X = I
51 R = Et, X = OTs **54** R = Me, X = OMs
52 R = Et, X = $(EtO)SO_3$ **55** R = Me, X = OTs

Entry	R—X	$[R—X]_0$ (mol L^{-1})	k_{obs} (s^{-1})	k (L mol^{-1} s^{-1})	$\Delta G^{‡}$ (kJ mol^{-1})
(i)	EtI	0.686	9.36×10^{-5}	1.36×10^{-4}	101.2 ± 0.6 [b]
(ii)	EtOMs	1.16	1.00×10^{-5}	8.62×10^{-6}	108.1 ± 1.0
(iii)	EtOTs	1.24	2.12×10^{-5}	1.71×10^{-5}	106.3 ± 0.7
(iv)	$(EtO)_2SO_2$	0.303	1.27×10^{-4}	4.19×10^{-4}	98.5 ± 0.6
(v)	EtBr	1.70	2.96×10^{-5}	1.74×10^{-5}	106.2 ± 0.6
(vi)	MeI	N/A	N/A	N/A	83.9 ± 1.7 [c]
(vii)	MeOMs	0.257	1.13×10^{-4}	4.40×10^{-4}	98.4 ± 0.6
(viii)	MeOTs	0.148	1.54×10^{-4}	1.04×10^{-3}	96.3 ± 0.6

[a] The concentration of the alkylation product in the reaction mixture at each timepoint was determined by analysis of the ^{1}H NMR signals of that product and comparison with the ^{1}H NMR signals of an internal standard of known concentration.
[b] An error was estimated for each value of $\Delta G^{‡}$ calculated using a rate measurement experiment. Details of how the various considered sources of error were incorporated into the value are available in section 7.3.
[c] The value of $\Delta G^{‡}$ obtained for the reaction of **46** with MeI was calculated using a rate constant and activation parameters for this reaction in CH_3CN which were reported in the literature.[34] Details of these parameters may be found in section 7.3. The paper in question estimates experimental errors of *ca.* 2%, which has been used to generate an estimated error for the value of $\Delta G^{‡}$.

The rate constants and $\Delta G^{‡}$ values were successfully determined for the reactions of **46** with seven electrophiles in CD_3CN at 20 °C. A $\Delta G^{‡}$ value for the reaction of **46** with MeI was calculated using activation parameters for this reaction in CH_3CN, which had been previously reported in the literature.[34] The specific details and calculations for each

experiment may be found in section 7.3. An estimated error was calculated for each of the values of $\Delta G^{\ddagger}$ to account for the error incurred by the practicalities involved in measuring the rate constants for these reactions by this method. Specifically, the error analysis is employed in an attempt to account for discrepancies in the integration of product signals in the ^{1}H NMR spectrum (and the subsequent effect on the calculated k_{obs} value), errors in the masses and volumes of the reagents used in the experiments and potential temperature variance in the probe of the NMR spectrometer as the reactions proceeded.

The values of k and $\Delta G^{\ddagger}$ were calculated using datapoints which comprised varying levels of conversion and reaction length. Slow reactions, such as **46** + EtOMs (Table 6-7 entry (ii)), only proceeded to approximately 30% conversion after over 13 hours at 20 °C. Faster reactions, such as **46** + MeOTs (Table 6-7 entry (viii)), reached 87% conversion after approximately 3 hours and 30 minutes at 20 °C. Acquiring data concerning the rate of a reaction by this method necessitated the measurement of dozens of timepoints over a considerable range of conversion, so alteration of the concentration of the reagents was necessary in order to cause the reactions to occur at a rate that was convenient to measure using ^{1}H NMR spectroscopy. In practice, this manifested as using relatively high concentrations of reagents in reactions which were found to proceed slowly (see the high concentration of the electrophile used in the reactions of EtOMs, EtOTs and EtBr in Table 6-7 (entries (ii), (iii) and (v))). In instances where the reaction was fast, the concentration of each reagent was decreased (see Table 6-7 entries (iv), (vii) and (viii)).

The reaction between **46** and EtOMs was found to have the highest Gibbs energy of activation of the electrophiles studied (see Table 6-7 entry (ii)), while the reaction of **46** with MeI was calculated to have the lowest value of $\Delta G^{\ddagger}$ (Table 6-7 entry (vi)). For experiments involving alkyl halides, the reaction of EtI + **46** (Table 6-7 entry (i)) was calculated to be significantly more kinetically favourable than the corresponding reactions involving EtBr (entry (v)). Comparison of the reactions of EtOMs and EtOTs with **46** (Table 6-7 entries (ii) and (iii)) with the reactions of MeOMs and MeOTs with **46** (Table 6-7 entries (vii) and (viii)) provides insight on the influence of the alkyl group of the electrophile on the observed Gibbs energy of activation. The reactions of the sulfonate methylating agents (Table 6-7, entries (vii) and (viii)) were found have significantly lower Gibbs energy of activation values (of the order of ≥ 10 kJ mol^{-1} in each case) than the corresponding ethylation reactions (Table 6-7, entries (ii) and (iii)). The same was found to be true to an even greater degree when comparing the values of $\Delta G^{\ddagger}$ calculated from the rate measurement of **46** + EtI with the value calculated using literature data for the reaction of **46** + MeI. The reaction of **46** + $(EtO)_2SO_2$ (Table 6-7, entry (iv)) was found to have the lowest Gibbs energy of activation value of the ethylating agents for which rate constant determinations were possible using the NMR spectroscopic method, with a rate roughly equal to that found in the reaction of **46** with MeOMs (entry (vii)).

The necessity for the reactions to occur at a rate which was convenient to measure using NMR spectroscopy rendered the measurement of rate data for certain reactive

electrophiles impossible. Reactions of **46** with EtOTf, MeOTf, MeI and $(Me_2O)_2SO_2$ in CD_3CN occurred too quickly to be measured using the NMR spectroscopic method described above. It was not possible to reduce the concentration of the reactants sufficiently in order to slow these reactions to a point at which rate data could be measured. For example, the reaction of **46** with MeOTs described in Table 6-7 (entry (viii)) used 1.4 mg of **46** as the starting material for the reaction to be slowed to a degree which allowed measurement of the rate. Further reduction of the concentration of the starting materials would be likely to result in inaccurate signal integrations in the resulting ^{1}H NMR spectra, even when using the most powerful spectrometer that was available for the study (600 MHz). The inability to acquire data on these fast reactions highlighted the drawbacks of using ^{1}H NMR spectroscopy to estimate the rate of a reaction.

The eight calculated values of $\Delta G^{\ddagger}$ for the reactions of DMAP (**46**) with various electrophiles were used in conjunction with the competition experiments described in Scheme 6-6(a) in order to access estimated values of $\Delta G^{\ddagger}$ for the processes of O- and C-alkylation of the enolate **1-Me$_4$N** with those electrophiles.

The competition experiments were carried out in conditions as similar as possible to those in the experiments in which the rate data for reactions of DMAP (**46**) were measured – i.e., the reactions was in CD_3CN, and the reaction mixtures were maintained at 20 °C throughout the course of the reaction. As was the case with the experiments in which O/C ratios were measured (see Table 6-6), the reactions were maintained under an inert atmosphere of nitrogen gas in a Schlenk flask before being transferred to an NMR tube and analysed by ^{1}H NMR after approximately 18 hours. In each case, the two nucleophiles (**46** and **1-Me$_4$N**, see Table 6-8 below) and the internal standard 1,3,5-trimethoxybenzene (**48**) were dissolved in CD_3CN before a solution containing a limiting amount of the electrophile was added to the flask. After 18 hours of stirring at 20 °C, the reaction mixture was analysed by ^{1}H NMR spectroscopy. Using key diagnostic signals for each of the products (and starting materials), the relative amounts of each product which had formed was determined. Using the precisely known concentration of the internal standard, the relative concentration of the DMAP alkylation product could be compared to the products formed from the O- and C-alkylation of the enolate **1-Me$_4$N**. The difference in the Gibbs energy of activation between an enolate alkylation product (e.g., O-alkylation in the example shown in Equation 6.5) and the Gibbs energy of activation for a DMAP alkylation product is described by the relationship shown in Equation 6.5. Note that this is simply a rearrangement of Equation 6.1 which was discussed previously. A similar relationship exists between the rate constant associated with the rate of C-alkylation (k_C) with the rate of DMAP (**46**) alkylation (k_{DMAP}).

$$\Delta\Delta G^{\ddagger} = -RT \ln \frac{k_O}{k_{DMAP}} \qquad (6.5)$$

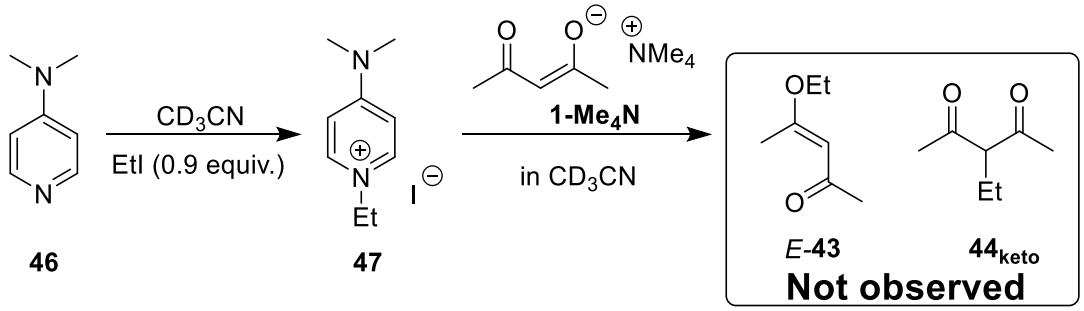
Hence, by using the ratio of DMAP alkylation products formed to the proportion of O-alkylation products formed, the ratio of the rate constants can be determined and the difference in the values of $\Delta G^{\ddagger}$ between the two alkylation processes can be determined. As the $\Delta G^{\ddagger}$ values for the reactions of DMAP with various electrophiles was known from

the results described in Table 6-7 above, values of $\Delta G^{\ddagger}$ for the enolate alkylation processes could be estimated by this method. A full description of the experimental procedure for these reactions, as well as an in-depth explanation of how values of $\Delta G^{\ddagger}$ are determined for the processes of enolate O- and C-alkylation processes using the previously established values of $\Delta G^{\ddagger}$ for the reactions between **46** and various electrophiles may be found in section 7.4.

The competition experiments described above also serve to demonstrate the irreversibility of formation of the enolate alkylation products under these conditions. At the conclusion of a given competition experiment, the products of enolate alkylation (such as *E*-**43** and **44$_{keto}$** in Scheme 6-6(a) above) are present in solution concurrently with an excess of each of the nucleophiles **1-Me$_4$N** and DMAP (**46**). If the formation of any of these products were reversible, the concentration of the reversibly formed products would be observed to decrease over time by continued ^{1}H NMR spectroscopic analysis. However, the ratios of the products (and absolute concentrations of the products) in reaction mixtures of the competition experiments were universally seen to remain constant over time, indicating that the formation of those products is irreversible under those reaction conditions.

A separate experiment, shown below in Scheme 6-7, demonstrated the irreversibility of formation of the alkylation products of DMAP (**46**) with EtI under conditions similar to those in the competition experiments.

Scheme 6-7. A control experiment to probe the reversibility of formation of (**47**) when the enolate **1-Me$_4$N** is present in CD_3CN. As no enolate ethylation products were observed, the irreversible formation of **47** is confirmed under these conditions.



Initially, DMAP (**46**) was ethylated by a limiting amount of EtI in CD_3CN. The reaction mixture was analysed by ^{1}H NMR spectroscopy to determine that the EtI was completely consumed, indicating that there was no possibility of a subsequently added nucleophile being ethylated by EtI. After confirmation of this, a solution of the enolate **1-Me$_4$N** in CD_3CN was added to the reaction mixture and the mixture was stirred. Subsequent ^{1}H NMR analysis of the ^{1}H NMR spectrum of the reaction mixture indicated that the only constituents of the mixture were unreacted DMAP (**46**), **47** and the enolate **1-Me$_4$N**. The absence of any enolate ethylation products indicated that the reaction of DMAP + EtI was irreversible, as any EtI which would form would be (at least partially) intercepted by the nucleophilic enolate species (**1-Me$_4$N**). Additionally, this experiment demonstrated that the nucleophilic attack of **1-Me$_4$N** on the ethylation product **47** was not possible under these reaction conditions.

Using Mayr's scale of nucleophilicity parameters,[35,36] the nucleophilicities towards benzhydrylium ions of the acetylacetonate ion (**38**)[37] and DMAP (**46**)[38] in DMSO may be compared. The acetylacetonate ion (**38**) in the work of Lucius, Loos and Mayr was derived from a mixture of the potassium enolate of acetylacetone (**1-K**) with 18-crown-6 in DMSO solution. It is observed in these data that the nucleophilicity of the acetylacetonate ion (*N* parameter = 17.64) is higher than the nucleophilicity of DMAP (**46**, *N* parameter = 14.80) in DMSO. This is significant, as it indicates that **46** is a good choice of competitor nucleophile for the control experiment of Scheme 6-7. In the case of the reaction illustrated in Scheme 6-7, the higher nucleophilicity of **38** confirms that in the event of a reversible reaction between **46** and EtI, enolate **38** should out-compete **46** for the newly formed EtI in the solution. However, **38** is not so strongly nucleophilic that it should directly substitute a DMAP (**46**) ethylation product (such as **47**) to form ethylation products (such as *E*-**43** or **44**$_{\mathbf{keto}}$).

6.3.4. Competition Experiments for Determination of $\Delta G^{\ddagger}$ Values for Reactions of Enolate 1-Me$_4$N with Ethylating Agents in CD$_3$CN

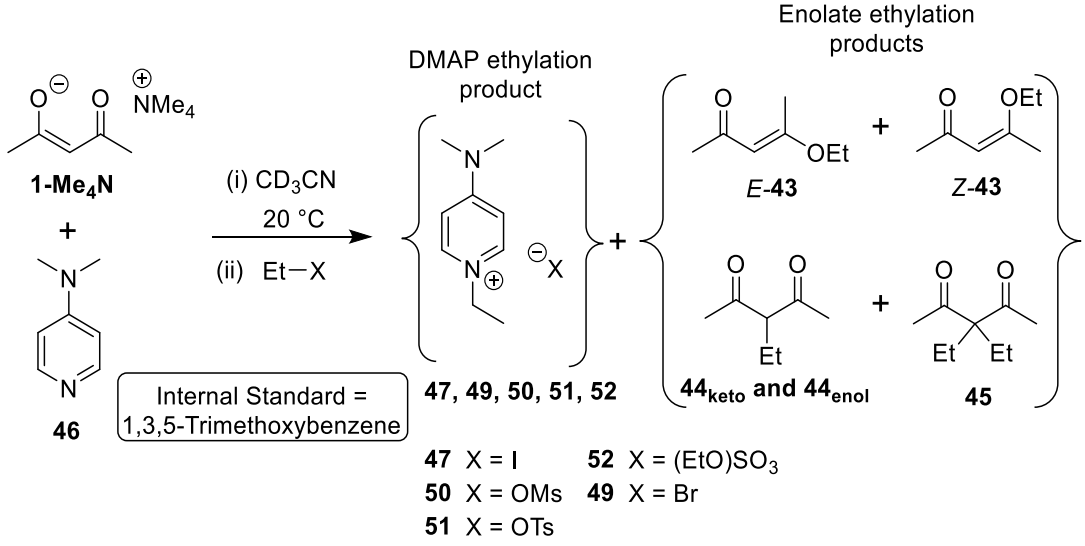
The ranges of values of $\Delta G^{\ddagger}$ which were estimated for the reactions of the enolate **1-Me$_4$N** with various ethylating agents in CD_3CN at 20 °C are reported below in Table 6-8. These values were determined using the approach described in section 6.3.3, wherein the rates of DMAP (**46**) alkylation by a certain ethylating agent was initially determined. $\Delta G^{\ddagger}$ values for enolate ethylation reactions were then estimated through the use of the known value of $\Delta G^{\ddagger}$ for the reaction of that ethylating agent and **46** and a competition experiment in which enolate **1-Me$_4$N** and **46** compete for a limiting amount of the ethylating agent in question.

As the instantaneous quantities (or concentrations) of the reactants and products in each reaction was unknown (as the reaction was not monitored as it progressed), limiting values of these quantities were used to enable estimation of the values of *k* (the rate constant) and $\Delta G^{\ddagger}$ for the processes of O- and C-alkylation as they occur relative to the values for DMAP alkylation. This results in the $\Delta G^{\ddagger}$ values being reported as a range for each of the processes. The upper bounds of the $\Delta G^{\ddagger}$ values were obtained by using the known quantities of reagents which were added to the reaction mixture initially, while the lower bounds were obtained by using the concentrations of the reactants that are observed in the ^{1}H NMR spectrum recorded at the conclusion of the reaction.

Mean values of $\Delta G^{\ddagger}$ for each O- and C-ethylation processes have been calculated and are displayed in Table 6-8. Also provided are the O/C ratios observed in the competition experiments, which may be compared to the analogous results found in Table 6-6. There are slight discrepancies between the O/C ratios obtained from the reactions of each electrophile in the competition experiments versus the values for the O/C ratio that were obtained in the experiments in which no competitor nucleophile or internal standard was present. A slightly increased proportion of O-ethylation products was observed in most competition experiments compared to the level which was observed in the experiments described in Table 6-6. For example, the reaction of **1-Me$_4$N** with $(EtO)_2SO_2$ in CD_3CN (see Table 6-6 entry (v)) produced an O/C ratio of 80:20, whereas the corresponding

competition experiment utilising $(EtO)_2SO_2$ showed an O/C ratio of 84:16 amongst the products (see Table 6-8 entry (v) below).

Table 6-8. Values of the rate constant (k) and $\Delta G^{\ddagger}$ for the processes of O- and C-alkylation of **1-Me$_4$N** with various ethylating agents in CD_3CN at 20 °C were determined through the use of competition experiments. Upon conclusion of the reaction, the proportions of enolate alkylation products formed was compared to the amount of products formed from the ethylation of **46**, for which rate data was known. [a]



#	Et–X	$\Delta G^{\ddagger}_O$ Range [b] (kJ mol^{-1})	Mean $\Delta G^{\ddagger}_O$ (kJ mol^{-1})	$\Delta G^{\ddagger}_C$ Range [b] (kJ mol^{-1})	Mean $\Delta G^{\ddagger}_C$ (kJ mol^{-1})	O/C Ratio
(i)	EtBr	98.7 – 103.6	101.2	96.4 – 101.3	98.9	28:72
(ii)	EtOMs	106.0 – 103.7	104.8	109.6 – 111.8	110.6	92:8
(iii)	EtOTs	100.8 – 103.5	102.2	106.2 – 108.9	107.6	90:10
(iv)	EtI	94.2 – 99.7	97.0	89.2 – 94.7	92.0	12:88
(v)	$(EtO)_2SO_2$	93.1 – 95.6	94.4	97.1 – 99.6	98.4	84:16

[a] The concentration of the alkylation products in the reaction mixture was determined by analysis of the ^{1}H NMR signals of each product and comparison with the ^{1}H NMR signals of an internal standard of known concentration.

[b] The Gibbs energies of activation ($\Delta G^{\ddagger}$) for the processes of O- and C-alkylation were calculated as a range of values. Details of how the ranges of values were calculated are given in section 7.4.

The differences between the previously calculated O/C ratios for alkylation reactions of **1-Me$_4$N** in CD_3CN at 20 °C (as seen in Table 6-6) and the O/C ratios observed in the competition experiments are highlighted below in Table 6-9. Also highlighted in Table 6-9 are the Gibbs energy of activation differences ($\Delta\Delta G^{\ddagger}$) between the processes of O- and C-alkylation which are expected to arise from the O/C ratio of a given experiment (see Equation 6.1, in which the Gibbs energy of activation difference can be related to the ratio of the rate constants). Whether the value of $\Delta\Delta G^{\ddagger}$ is negative or positive is related

to the preferred mode of alkylation – a negative value of $\Delta\Delta G^{\ddagger}$ indicates that O-alkylation is preferred, and a positive value of $\Delta\Delta G^{\ddagger}$ indicates that C-alkylation is preferred.

Table 6-9. O/C ratios of the products of the reactions of enolate **1-Me$_4$N** with various alkylating agents in CD_3CN and the expected Gibbs energy of activation difference ($\Delta\Delta G^{\ddagger}$) between the processes of O- and C-alkylation when using these O/C ratios are shown below. Also shown are the O/C ratios observed for the corresponding enolate alkylation in the corresponding competition experiment, as well as the difference in the mean $\Delta G^{\ddagger}$ values which were calculated for these processes in Table 6-8. [a]

Entry	Alkylating Agent	O/C Ratio	Expected $\Delta\Delta G^{\ddagger}$ (kJ mol^{-1})	Competition experiment O/C Ratio	Calculated $\Delta\Delta G^{\ddagger}$ (kJ mol^{-1})
(i)	EtBr	25:75	2.7	28:72	2.3
(ii)	EtOMs	85:15	–4.2	92:8	–5.8
(iii)	EtOTs	87:13	–4.6	90:10	–5.4
(iv)	EtI	10:90	5.4	12:88	5.0
(v)	$(EtO)_2SO_2$	80:20	–3.4	84:16	–4.0

[a] The concentration of the alkylation products in the reaction mixture was determined by analysis of the ^{1}H NMR signals of each product and comparison with the ^{1}H NMR signals of an internal standard of known concentration.

Thus, for example, in a reaction between **1-Me$_4$N** and EtI in CD_3CN at 20 °C (the reaction described in Table 6-6 entry (iv), and by entry (iv) in Table 6-8), it can be determined using the O/C ratio of 10:90 that the C-ethylation process should have a Gibbs energy of activation at 20 °C that is 5.4 kJ mol^{-1} lower than the O-ethylation process (see Table 6-9 entry (iv)). By taking the mean values of $\Delta G^{\ddagger}$ for each of the processes as described in Table 6-8 entry (iv), the difference between the O- and C-ethylation processes was calculated to be 5.0 kJ mol^{-1}. The difference between the values of $\Delta\Delta G^{\ddagger}$ which are expected for each reaction (using the O/C ratio found in Tables 6-6) versus the $\Delta\Delta G^{\ddagger}$ value which may be calculated for each reaction using the mean $\Delta G^{\ddagger}$ values seen in Table 6-8 are highlighted above. In most instances, the expected value differs from the calculated value by a small margin (< 0.8 kJ mol^{-1}). The exception to this is the reaction of EtOMs (Table 6-9 entry (ii)), which displayed variance of 1.6 kJ mol^{-1} from the expected value. This reaction also displays the largest change in O/C ratio from the previously observed value out of the series of reactions shown in Table 6-6. There are slight differences in all cases (see Table 6-9) between the O/C ratios observed in the experiments described in this section (competition experiments, in which the alkylation reactions occurred in the presence of DMAP (**46**) and pyridinium salts derived from DMAP) and the O/C ratios observed in the corresponding reactions described in section 6.3.2 above (in which no pyridinium salts were present).

It is reasonable to expect that the observed O/C ratio of a reaction of **1-Me$_4$N** could be different when DMAP (**46**) and any subsequent DMAP alkylation products (e.g., **47**) are present in the reaction mixture. Any alkylation product formed from DMAP would result

in a change in the overall polarity of the reaction medium, which would be reasonably expected to change the activation energy of all enolate alkylation processes to some extent. Additionally, the presence of a pyridinium salt derived from DMAP could potentially result in the formation of new enolate aggregates (involving *N*-alkylpyridinium ions) that cannot be formed in reactions in which DMAP (**46**) is not present. The aggregates may exhibit slightly different reactivity characteristics to the enolate aggregates present in a reaction of **1-Me$_4$N** and an ethylating agent alone. The discussion in section 1.2.3 highlights the influence that ion aggregates may have on the selectivities of reactions of ambident nucleophiles such as enolates.

In potentially changing the ionic species in the reaction, as well as changing the reaction medium itself, it seems likely that the Gibbs energies of activation of the alkylation processes in the reaction could change. As such, the competition experiments only provide approximations of the rate constants and activation energy values for the reactions in conducted in the absence of DMAP (and hence *N*-alkylpyridinium ions) (i.e., the reactions described in Table 6-6).

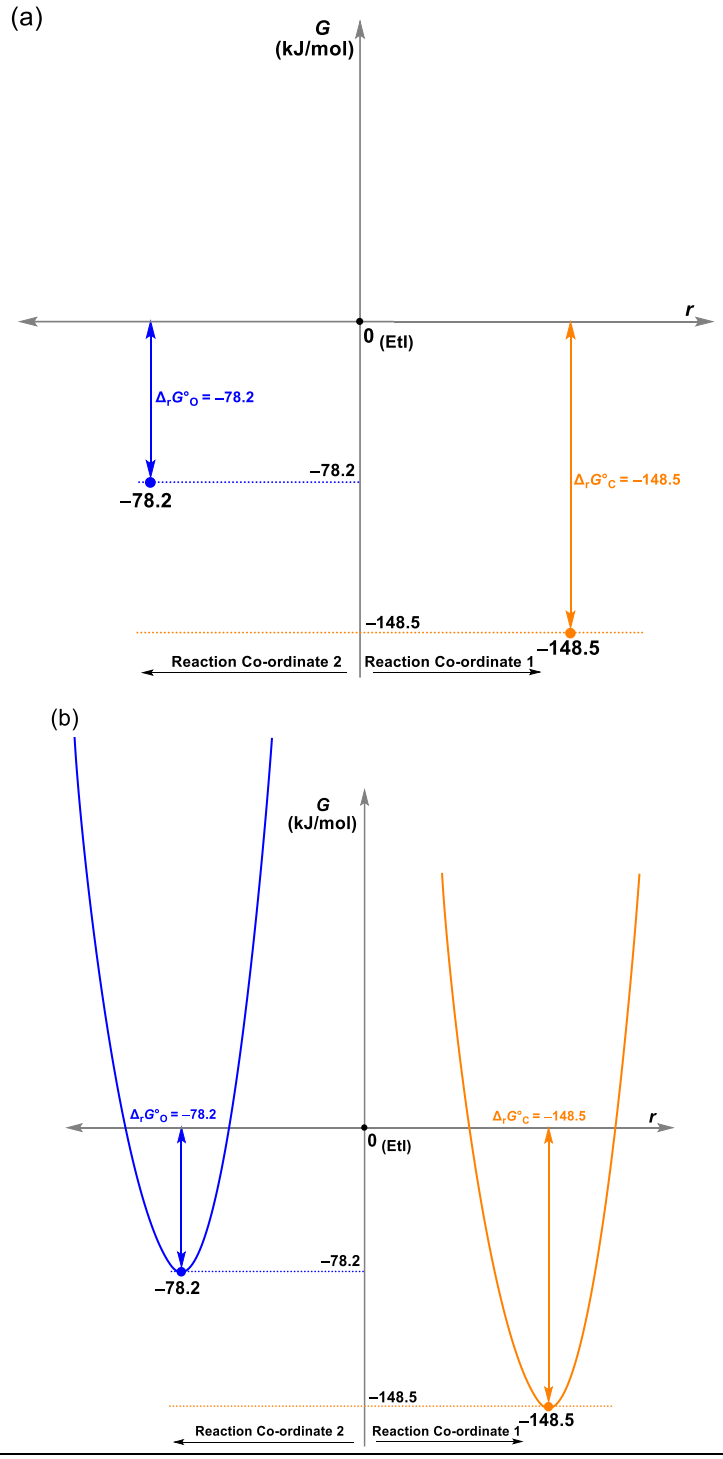
6.3.5. Development of the Process for Modelling Gibbs Energy Surfaces Focusing on the Reactions of Enolate 1-Me$_4$N + Ethylating Agents

Novel models for Gibbs energy profile diagrams can be built using the various experimentally derived and computationally derived quantities and this process (described above) is applied below, using the reactions of the enolate **1-Me$_4$N** with various ethylating agents in CD_3CN as an exemplar.

(a) Gibbs Energy Profile Diagram for Reaction of 1-Me$_4$N + EtI

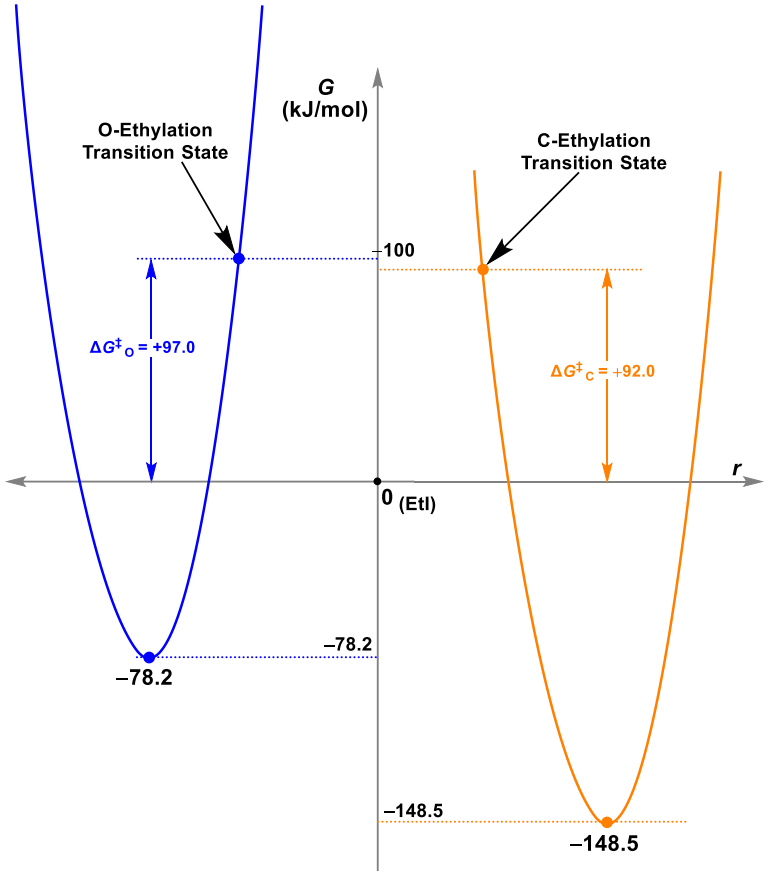
The first step involved in the development of the model is the construction of a Gibbs energy profile diagram which describes the characteristics of a randomly chosen example reaction from the set in question (in this case, a series of ethylating agents) – for instance, the reaction of the enolate **1-Me$_4$N** with EtI. The construction of the diagram begins with the placement of the vertical co-ordinates of the apices of the parabolas. For the reactant parabola for the reaction of enolate **1-Me$_4$N** with EtI, the apex is placed at zero on the y-axis. The vertical co-ordinates of the apices of the product parabolas are then specified according to the known $\Delta_r G°$ values for the O- and C-ethylation reactions of that enolate (**1-Me$_4$N**) with EtI. The known $\Delta_r G°$ values referred to here are derived from computational data, given in section 6.3.1 above. Recall that the values of $\Delta_r G°$ are calculated using the anionic enolate **38** (i.e., the Me_4N^+ counter-cation is not accounted for in the calculations). Using this data, the image shown below in Figure 6-10(a) may be constructed. The O-alkylation products (blue point in Figure 6-10) were found to have a Gibbs energy value 78.2 kJ mol^{-1} lower than that of the reactants (**1-Me$_4$N** + EtI, see black point in Figure 6-10) (see section 6.3.1, Table 6-5 entry (iv)). The C-alkylation products (orange point in Figure 6-10) were found to have a Gibbs energy value 148.5 kJ mol^{-1} lower than that of the reactants (see section 6.3.1, Table 6-5 entry (iv)).

Figure 6-10. (a) Gibbs energy profile diagrams for O- and C-ethylation reactions of enolate **1-Me$_4$N** with EtI. Using computationally derived $\Delta_rG°$ values obtained from calculations on the enolate **38** (see Table 6-5), the position of the apex of each of the parabolas may be assigned. **(b)** The product parabolas for O-ethylation (blue) and C-ethylation (orange) are inserted such that the apex of each one lies at the value of $\Delta_rG°$ which was calculated for that reaction. The blue and orange product parabolas are identical, but their width is chosen at random.



Next, two "product parabolas", which represent the Gibbs energy well associated with the O-ethylation products and the Gibbs energy well associated with the C-ethylation products (blue and orange parabolas in Figure 6-10(b) above) of identical width are inserted. The distance between the horizontal co-ordinates of the parabolas is chosen arbitrarily. This is done because there is no information regarding the horizontal axis dimensions available (at present) that can be used in constructing these diagrams. As there is no meaningful way to represent these distances, using parabolas of an arbitrary width and arbitrary distances apart allows the model to be tested without the potential for randomly chosen differences between the parabola to prejudice the results derived from the analysis conducted using the model. Each parabola is positioned such that its apex has the correct vertical co-ordinate (i.e., such that its apex occurs at the same $\Delta_r G°$ value that was determined computationally for the reaction in question). An illustration of this step is shown above in Figure 6-10(b).

Figure 6-11. Gibbs energy diagrams for reaction of enolate **1-Me$_4$N** with EtI. The intersection points of the reactant parabola (not yet shown below) and the product parabolas (which represent the transition states) for the processes of O- and C-ethylation may be determined using the experimentally derived values of the activation barrier ($\Delta G^‡$) for each process.

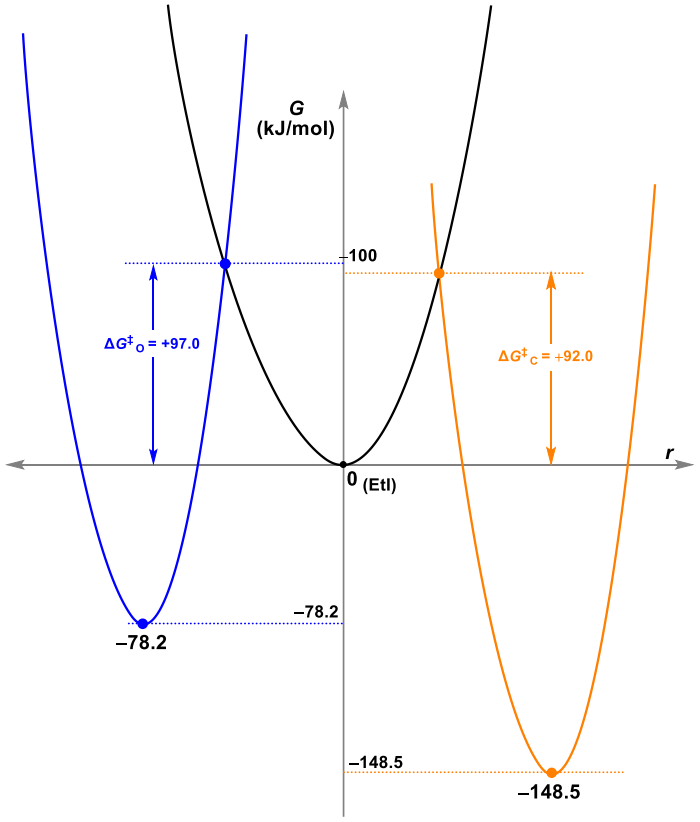


At this point, the vertical co-ordinates of the transition states for the O- and C-ethylation reactions are specified according to known $\Delta G^‡$ values for the competing processes of O- and C-ethylation of **1-Me$_4$N** in a reaction with EtI. The known values of $\Delta G^‡$ referred to here are determined experimentally, and the values themselves and the method by which

they were calculated were given in section 6.3.4 above. The value of $\Delta G^{\ddagger}$ associated with the C-ethylation of **1-Me$_4$N** with EtI (i.e., $\Delta G^{\ddagger}_{C}$) was determined to be 92.0 kJ mol^{-1}, and the value of $\Delta G^{\ddagger}$ associated with the O-ethylation of **1-Me$_4$N** with EtI (i.e., $\Delta G^{\ddagger}_{O}$) was determined to be 97.0 kJ mol^{-1} (see section 6.3.4, Table 6-8 entry (iv)). Using these values of the activation barrier ($\Delta G^{\ddagger}$) to determine the vertical barrier height, a horizontal line is projected from each of the appropriate co-ordinates of the vertical axis across in the direction of the appropriate product parabola. In the present example, a horizontal line with a vertical height of 92.0 kJ mol^{-1} is projected from the x-axis towards the orange parabola (see Figure 6-11 above), and a horizontal line with a vertical height of 97.0 kJ mol^{-1} is projected from the x-axis towards the blue parabola. The first point at which these lines intersect the product parabolas in question gives the position of the transition state (i.e., the point at which the reactant parabola should intersect the product parabola in question).

From the diagram in Figure 6-11, the Gibbs energy well of the reactants (or "reactant parabola") may then be inserted (see Figure 6-12 below). There is only one parabola that passes through the specified points (i.e., the transition states, marked in Figure 6-11) and also has its apex on the line $G = 0$. The Gibbs energy profile diagram is then completed with the addition of this unique parabola, as shown in Figure 6-12 below.

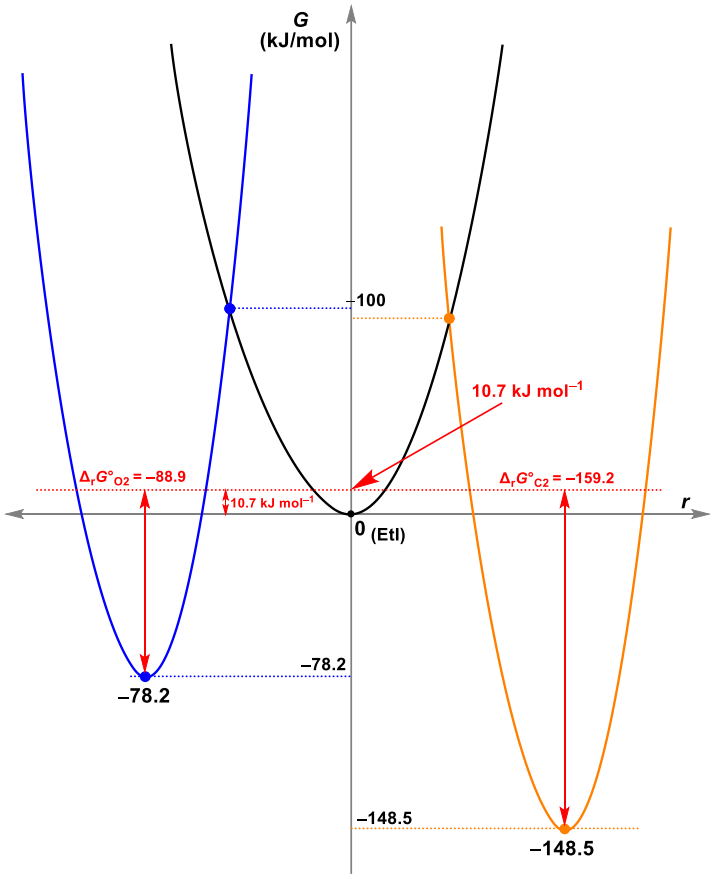
Figure 6-12. The Gibbs energy profile diagram for the reaction of enolate **1-Me$_4$N** with EtI is complete with the addition of the reactant parabola. The width and curvature of the reactant parabola is determined by the points at which it must intersect the two adjacent product parabolas – only one parabola exists that passes through the transition states specified in the diagram and also has its apex on the line $G = 0$.



(b) Gibbs Energy Profile Diagram for Reaction of 1-Me_4N + $(EtO)_2SO_2$

Having constructed one of the Gibbs energy profile diagrams (for the reaction of **1-Me_4N** with EtI in CD_3CN), it is now possible to make use of the previously made assumption that the positions of the product parabolas is essentially invariant for all ethylation reactions, no matter which ethylating agent is employed. The relative difference in the standard Gibbs energy of reaction ($\Delta\Delta_rG°$) for the competing processes of O- and C-ethylation in the reactions of enolate **1-Me_4N** with various ethylating agents remained the same (at 70.3 kJ mol^{-1}) no matter which ethylating agent was employed (see section 6.3.1, Table 6-5). As a result, the Gibbs energy profile diagram showed in Figure 6-12 above can be further built upon with the addition of another reactant parabola, which represents the Gibbs energy well of the reactants in the reaction of enolate **1-Me_4N** with a different ethylating agent. $(EtO)_2SO_2$ is used as the example ethylating agent in this case.

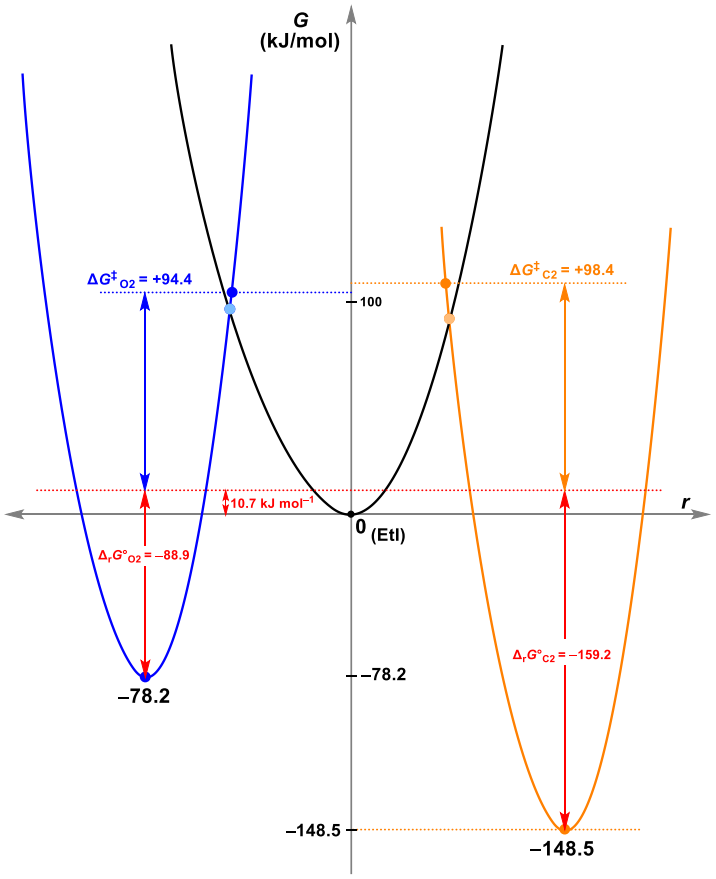
Figure 6-13. The Gibbs energy profile diagram for the reaction of enolate **1-Me_4N** with EtI is overlaid with new vertical co-ordinates (see the red dashed line) that represent the apex of the reactant parabola resulting from a reaction of **1-Me_4N** with $(EtO)_2SO_2$. Calculated values of $\Delta_rG°$ from a reaction **1-Me_4N** with $(EtO)_2SO_2$ (seen in red) can be overlaid on the existing Gibbs energy profile diagram to determine the apex height of the reactant parabola for a reaction of **1-Me_4N** with $(EtO)_2SO_2$.



The co-ordinate on the vertical axis of the new reactant parabola apex (for the reaction of **1-Me_4N** with $(EtO)_2SO_2$) is calculated using the known values of $\Delta_rG°$ for the processes of O- and C-ethylation of **38** with $(EtO)_2SO_2$ (which is shown in section 6.3.1, Table 6-5

entry (v) above). The $\Delta_rG°$ value associated with O-ethylation of **38** by $(EtO)_2SO_2$ ($\Delta_rG°_{O2}$ in Figure 6-13 above) is –88.9 kJ mol^{-1}, and the $\Delta_rG°$ value associated with C-ethylation of **38** by $(EtO)_2SO_2$ ($\Delta_rG°_{C2}$ in Figure 6-13 above) is –159.2 kJ mol^{-1}. Comparison of these values with the $\Delta_rG°$ values associated with the O- and C-ethylations of **38** by EtI in Figure 6-10(a) and (b) (–78.2 kJ mol^{-1} and –148.5 kJ mol^{-1}, respectively) shows that both ethylation processes have a value that is more negative by 10.7 kJ mol^{-1} when $(EtO)_2SO_2$ is used as the ethylating agent in place of EtI. In the diagram in Figure 6-13, this difference in $\Delta_rG°$ values between the reactions of the two ethylating agents *may be represented as an upward movement of the reactant parabola, such that the apex of the new reactant parabola will lie somewhere along a horizontal line 10.7 kJ mol^{-1} above the horizontal axis*. As the $\Delta_rG°$ values for the reaction of **38** with $(EtO)_2SO_2$ has larger negative values for the O- and C-ethylation processes than the $\Delta_rG°$ values for the reaction of **38** with EtI (O- and C-ethylation processes, respectively), this indicates that the Lewis acidity of $(EtO)_2SO_2$ towards **38** is higher than that of EtI. Since the horizontal co-ordinate of the new reactant parabola apex cannot be specified at this point, a horizontal line 10.7 kJ mol^{-1} above the line $G = 0$ is inserted into the diagram (see the red horizontal dashed line in Figure 6-13). The apex of the new reactant parabola will be somewhere along this line.

Figure 6-14. The Gibbs energy profile diagram for the reaction of enolate **1-Me$_4$N** with EtI is overlaid with new vertical co-ordinates (see the blue and orange dashed lines) that represent the vertical co-ordinates of the activation barriers ($\Delta G^‡$) from a reaction of **1-Me$_4$N** with $(EtO)_2SO_2$.



From this point, new co-ordinates are added on the vertical axis that indicate the positions of the transition states for the O- and C-ethylation reactions of **1-Me$_4$N** in a reaction with $(EtO)_2SO_2$. Again, these positions are determined using known $\Delta G^{\ddagger}$ values for the competing processes of O- and C-ethylation in a reaction of **1-Me$_4$N** by $(EtO)_2SO_2$ (94.4 kJ mol^{-1} and 98.4 kJ mol^{-1}, respectively), which were given in section 6.3.4, Table 6-8 entry (v) above. Using these values of the activation barrier ($\Delta G^{\ddagger}$) to determine the vertical barrier height, a horizontal line is projected from each of the appropriate co-ordinates on the vertical axis across in the direction of the appropriate product parabola. As previously, the first point at which each line intersects the relevant product parabola is the transition state for the reaction in question. In Figure 6-14 above, the known values of $\Delta G^{\ddagger}_{O}$ and $\Delta G^{\ddagger}_{C}$ have been assigned on the vertical axis, and lines have been projected across until the point at which they intersect the adjacent product parabola.

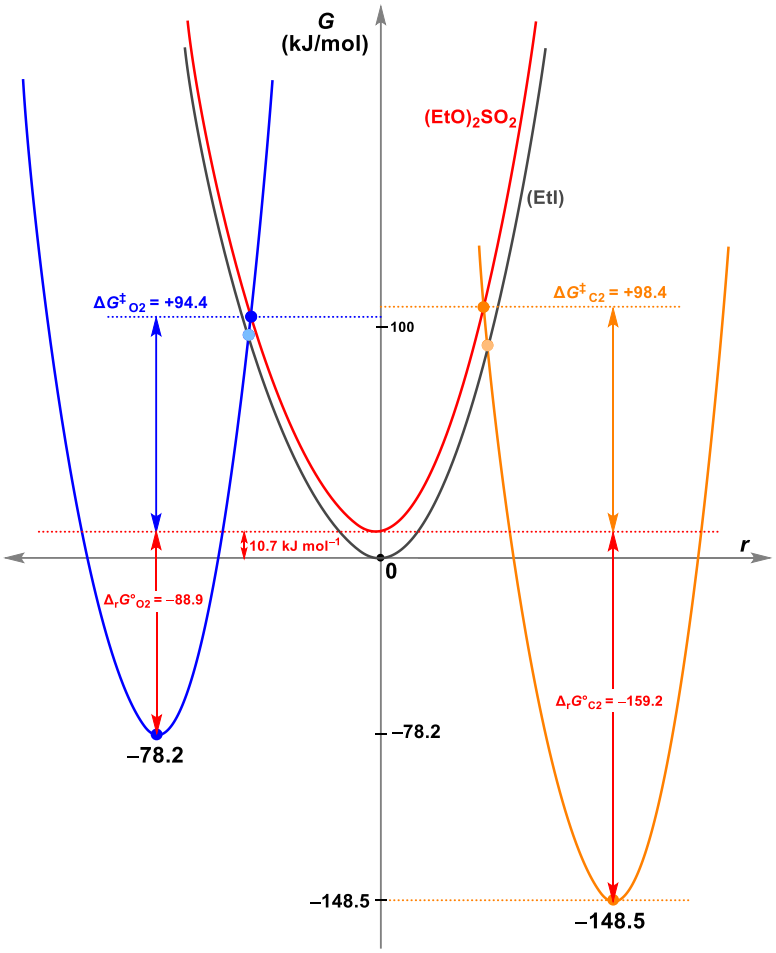
With the new intersection points added to the diagram (see Figure 6-14 above), a new reactant parabola may be drawn which passes through the specified points (i.e., the transition states, marked in Figure 6-14) and also has its apex on the line $G = 10.7$. The diagram showing the uniquely defined reactant parabola for the reaction of **1-Me$_4$N** with $(EtO)_2SO_2$ overlaid on top of the Gibbs energy profile diagram for the reaction of **1-Me$_4$N** with EtI is shown below in Figure 6-15.

The curvature of the reactant parabola inserted for the reaction of **1-Me$_4$N** with $(EtO)_2SO_2$ (see the parabola in red in Figure 6-15) is slightly different compared to the parabola representing the reaction of **1-Me$_4$N** with EtI (the parabola in black in Figure 6-15). Specifically, the red parabola in Figure 6-15 is narrower than the reactant parabola relating to the reaction of EtI with **1-Me$_4$N**. Additionally, the apex of the red parabola has moved to the left (as drawn) along the horizontal axis relative to the horizontal position of the black parabola. These manipulations were required in order to satisfy the necessary criteria for the construction of the parabola representing the reaction of **1-Me$_4$N** with $(EtO)_2SO_2$. This example relates to the scenarios which were outlined in section 6.2.1 above, regarding the effect of moving a reactant parabola up or down while keeping the product parabolas in the same place (see Figure 6-3) and the effect of moving a reactant parabola left or right horizontally relative to another reactant parabola (see Figure 6-5). The reactant parabola for the reaction of **1-Me$_4$N** with $(EtO)_2SO_2$ has an altered (i.e., narrower) width compared to the reactant parabola for the reaction of **1-Me$_4$N** with EtI. This fact, in combination with the movement (up and to the left, as drawn in Figure 6-15) of the reactant parabola for the reaction of **1-Me$_4$N** with $(EtO)_2SO_2$ results in the reaction becoming O-selective (while, in contrast, the reaction of **1-Me$_4$N** with EtI is highly selective for C-ethylation – see above). There is no way at present to understand or predict the relative positions of the reactant parabolas in the overlaid Gibbs energy profile diagrams for two different ethylation reactions of **1-Me4N** (or, more precisely, the relative co-ordinates of the reactant parabola apices along the horizontal axis). Instead, trends will be established in these reactions and subsequently analysed.

Following the construction of a diagram like the one shown below in Figure 6-15, the processes described above can be repeated using the computational and experimental data

($\Delta_rG°$ values and $\Delta G^{‡}$ values, respectively) from other ethylation reactions to construct further diagrams, or to continue overlaying further reactant parabolas on top of the originally constructed diagram to generate new Gibbs energy profile diagrams for different reactions (involving different ethylating agents).

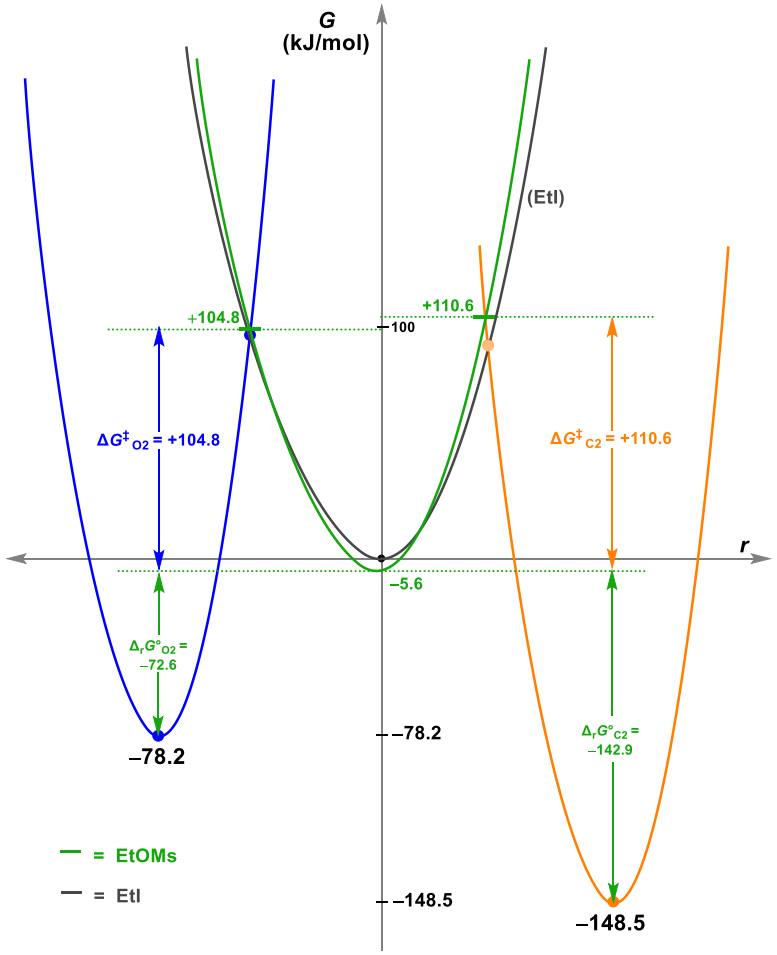
Figure 6-15. The Gibbs energy profile diagram for the reaction of enolate **1-Me$_4$N** with EtI is overlaid with new reactant parabola (in red) for the reaction of enolate **1-Me$_4$N** with $(EtO)_2SO_2$. The reactant parabola is constructed using the known height of its apex and the two transition states which it must pass through on the intersection points with the product parabolas (in blue and orange below).



(c) Gibbs Energy Profile Diagram for Reaction of 1-Me$_4$N + EtOMs

Using the relevant activation barrier values and the vertical position of the apex, new reactant parabolas may be constructed and overlaid on top of the Gibbs energy profile diagram for the purposes of comparison with the reaction of **1-Me$_4$N** with EtI in CD_3CN. In Figure 6-16 below, the values (in green) associated with the O- and C-ethylation of **1-Me$_4$N** by EtOMs were used to construct a reactant parabola for that reaction (see Table 6-5 in section 6.3.1 and Table 6-8 in section 6.3.4) in the manner described above for the reaction of **1-Me$_4$N** with $(EtO)_2SO_2$. This parabola was overlaid on top of the Gibbs energy profile diagram for the reaction of **1-Me$_4$N** with EtI, and is shown below in Figure 6-16.

Figure 6-16. The Gibbs energy profile diagram for the reaction of enolate **1-Me$_4$N** with EtI in CD_3CN is overlaid with a reactant parabola which represents the reaction of **1-Me$_4$N** with EtOMs in CD_3CN. The activation barrier positions and apex height positions are colour coded to allow each reaction to be distinguished from the other.



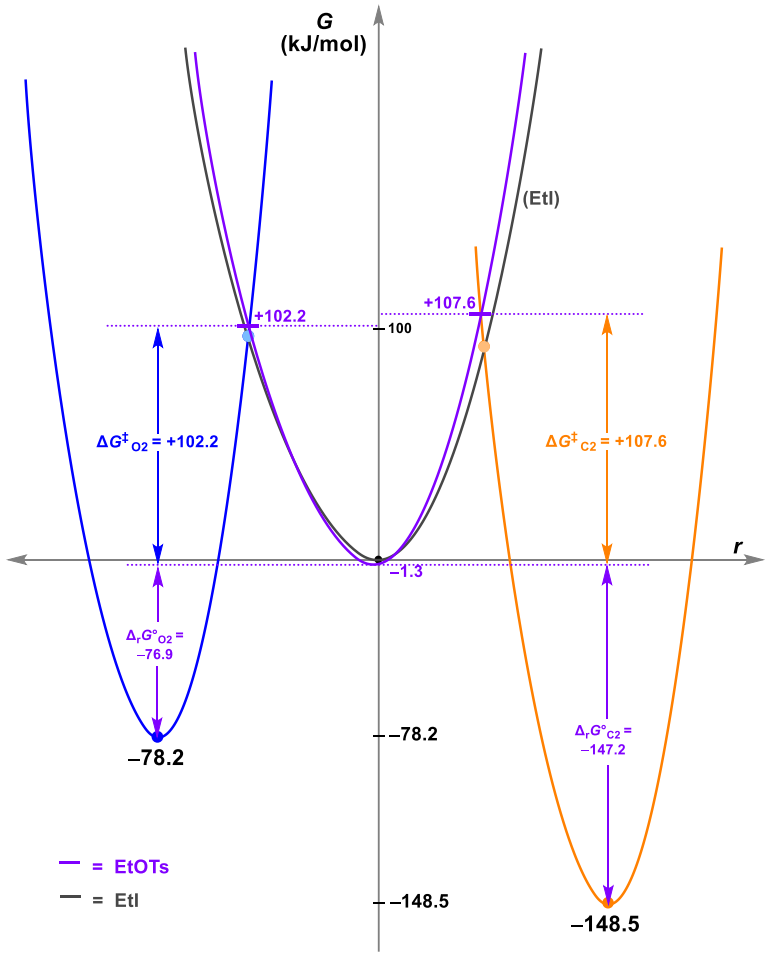
As was the case when the reactant parabola relating to the reaction of $(EtO)_2SO_2$ was compared to the reactant parabola of the EtI reaction (see Figure 6-15 and associated discussion), the reactant parabola for the reaction of EtOMs (green parabola in Figure 6-16) is narrower (i.e., greater curvature) than the parabola representing the reaction with EtI. The parabola is also shifted to the left (as drawn) on the x-axis relative to the reactant parabola for the reaction with EtI, and its apex is 5.6 kJ mol^{-1} lower than the EtI reactant parabola. This shift of the reactant parabola apex to the left of the diagram (as drawn, see Figure 6-5 in section 6.2.1 above) combined with the narrower width of the reactant parabola for this reaction results in a decrease in the width of the activation barrier for the O-ethylation process, which is likely to be significant in understanding why the reaction of **1-Me$_4$N** with EtOMs is substantially more O-selective than the corresponding reaction of **1-Me$_4$N** with EtI. As both EtOMs and EtI display a similar degree of Lewis acidity towards **1-Me$_4$N** (based on the calculated $\Delta_rG°$ values for the reactions of the two ethylating agents with **1-Me$_4$N** – see Table 6-5 in section 6.3.1), the source of the experimentally observed high degree of O-selectivity in reactions of **1-Me$_4$N** with EtOMs must relate to the relatively narrower reactant parabola and the fact that the apex of this

reactant parabola has a different horizontal co-ordinate to the apex of the reactant parabola which represents the reaction of **1-Me$_4$N** with EtI.

(d) Gibbs Energy Profile Diagram for Reaction of 1-Me$_4$N + EtOTs

In Figure 6-17 below, the values (in purple) associated with the O- and C-ethylation of **1-Me$_4$N** by EtOTs were used to construct a reactant parabola (see Table 6-5 in section 6.3.1 and Table 6-8 in section 6.3.4). This parabola was overlaid on top of the Gibbs energy profile diagram for the reaction of **1-Me$_4$N** with EtI, and is shown below in Figure 6-17. The resulting reactant parabola (in purple in Figure 6-17 below) is similar to the one constructed for the reaction of EtOMs with **1-Me$_4$N** above (see Figure 6-16). This is perhaps to be expected, considering the similar values of $\Delta_rG°_O$, $\Delta_rG°_C$, $\Delta G^‡_O$ and $\Delta G^‡_C$ between the two reactions which were determined computationally and measured experimentally.

Figure 6-17. The Gibbs energy profile diagram for the reaction of enolate **1-Me$_4$N** with EtI in CD_3CN is overlaid with a reactant parabola which represents the reaction of **1-Me$_4$N** with EtOTs in CD_3CN. The activation barrier positions and apex height positions are colour coded to allow each reaction to be distinguished from the other.



The purple reactant parabola in Figure 6-17 is shifted to the left (as drawn) on the x-axis relative to the reactant parabola for the reaction of **1-Me$_4$N** with EtI. This shift to the left

of the diagram (see Figure 6-5 in section 6.2.1 above) results in a decrease in the width of the activation barrier for the O-ethylation process. As was the case in Figure 6-16 above, the purple reactant parabola is also narrower than the reactant parabola associated with the EtI reaction. In Figure 6-4 in section 6.2.1 above, narrowing of the width of a reactant parabola is listed as another alteration to the reactant parabola which may result in an increase in the O-selectivity of the reaction in question. The combination of each of these modifications to the position and curvature of the reactant parabola for the reaction of **1-Me$_4$N** with EtOTs compared to the reaction of **1-Me$_4$N** with EtI contributes to the differences observed between the selectivities of each reaction. The similar values of $\Delta_rG°_O$, $\Delta_rG°_C$, $\Delta G^‡_O$ and $\Delta G^‡_C$ which were calculated for these reactions demonstrates that the source of the preferential O-methylation in a reaction of **1-Me$_4$N** with EtOTs is the narrower reactant parabola and the fact that the apex of this reactant parabola has moved horizontally to the left (as drawn) in comparison to the reactant parabola which represents the reaction of **1-Me$_4$N** with EtI.

(e) Gibbs Energy Profile Diagram for Reaction of 1-Me$_4$N + EtBr

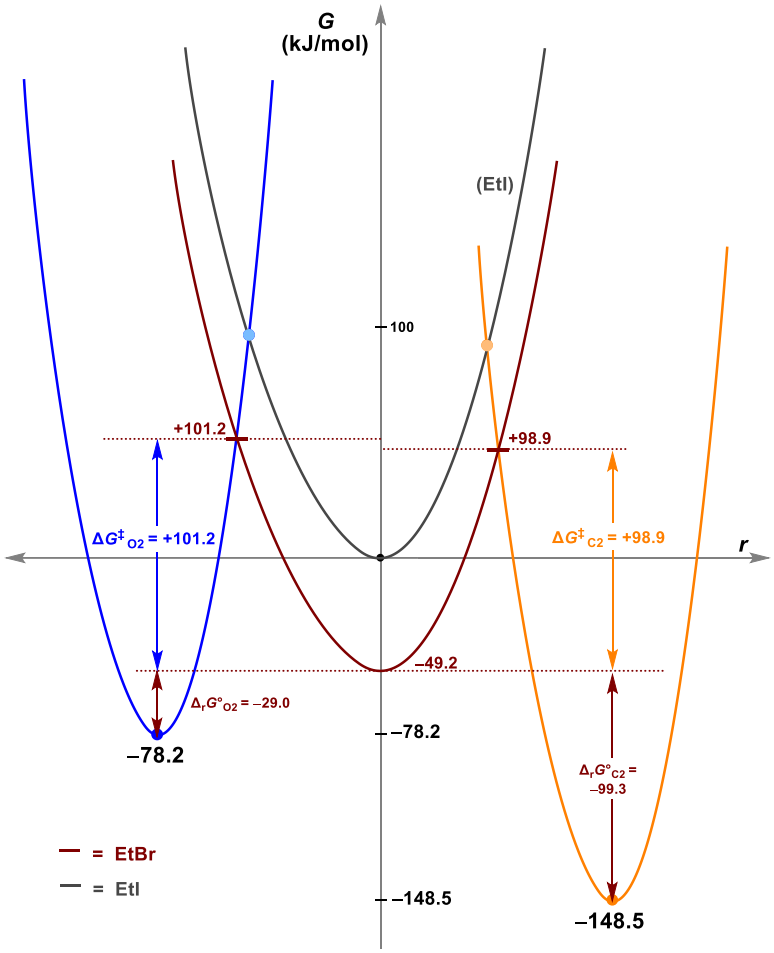
In Figure 6-18 below, the values (in dark red) associated with the O- and C-ethylation of **1-Me$_4$N** by EtBr were used to construct a reactant parabola (see Table 6-5 in section 6.3.1 and Table 6-8 in section 6.3.4). This parabola was overlaid on top of the Gibbs energy profile diagram for the reaction of **1-Me$_4$N** with EtI, and is shown below in Figure 6-18.

The apex of this reactant parabola occurs at a significantly lower vertical position than the corresponding parabola for the reaction of **1-Me$_4$N** with EtI (as a consequence of the values of $\Delta_rG°$ being significantly more negative in the case of the ethylation reactions of **1-Me$_4$N** employing EtI – compare Table 6-5 entries (ii) and (vii)). Additionally, the dark red reactant parabola is significantly wider than the reactant parabola associated with the reaction of **1-Me$_4$N** with EtI. Interestingly, the reactant parabola associated with the reaction of **1-Me$_4$N** with EtBr is the only case of the examples shown here in which it was possible to construct the reactant parabola in almost exactly the same position on the horizontal axis as the reactant parabola associated with the reaction of **1-Me$_4$N** with EtI (i.e., both the parabolas for the reaction involving EtI and that for the reaction involving EtBr have essentially the same horizontal co-ordinates for their apices). This may potentially be significant, as the reaction of **1-Me$_4$N** with EtBr is the only other reaction of those shown here which is found to have a kinetic preference for C-ethylation (see Table 6-6, compare entry (ii) to (vii)).

It is interesting to note that for the reactant parabolas which were constructed for each of the reactions which underwent preferential O-ethylation (i.e., reactions of **1-Me$_4$N** with EtOMs, EtOTs or $(EtO)_2SO_2$), the reactant parabola were narrower than the reactant parabola representing the reaction of **1-Me$_4$N** with EtI (see Figure 6-15, 6-16 and 6-17 above). However, the reactant parabola for the reaction of **1-Me$_4$N** with EtBr in CD_3CN (dark red parabola in Figure 6-18 above) is significantly wider than the reactant parabola for the reaction of **1-Me$_4$N** with EtI. Despite this, the increased width of the parabola (and the resulting increased width of the activation barriers) does not result in the reaction of **1-Me$_4$N** with EtBr being *less O-selective* that the corresponding reaction with EtI (see

Table 6-6, compare entry (ii) to (vii)). That is, there are some reactant parabolas which have been constructed here which are narrower than the one for the reaction of **1-Me$_4$N** with EtI, and others that are wider relative to the reactant parabola constructed for the reaction of **1-Me$_4$N** with EtI, but yet the reaction involving EtI is the one which produced the lowest quantity of O-ethylation products in CD_3CN.

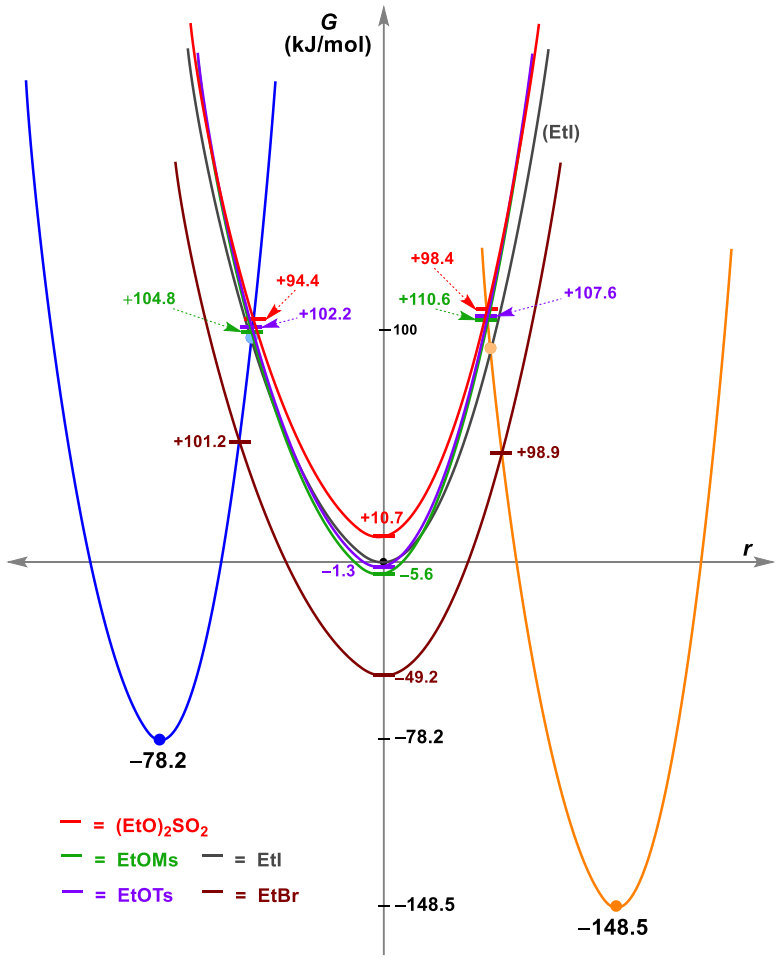
Figure 6-18. The Gibbs energy profile diagram for the reaction of enolate **1-Me$_4$N** with EtI in CD_3CN is overlaid with a reactant parabola which represents the reaction of **1-Me$_4$N** with EtBr in CD_3CN. The activation barrier positions, and apex height positions are colour coded to allow each reaction to be distinguished from the other.



(f) Overlaid Gibbs Energy Profile Diagrams for All Ethylation Reactions of 1-Me$_4$N Investigated

Shown below in Figure 6-19 is all of the reactant parabolas constructed in Figures 6-15, 6-16, 6-17, and 6-18 above overlaid together on top of the Gibbs energy profile diagram for the reaction of **1-Me$_4$N** with EtI. This representation allows the variety of parabola widths and curvatures which were constructed for each of the respective ethylation reactions to be easily compared.

Figure 6-19. The Gibbs energy profile diagram for the reaction of enolate **1-Me$_4$N** with EtI in CD_3CN is overlaid with new reactant parabolas for three additional reactions of **1-Me$_4$N** with ethylating agents in CD_3CN. The activation barrier positions, and apex height positions are colour coded to allow each unique reaction to be distinguished from one another.



Comparison of the green reactant parabola (representing the reaction of **1-Me$_4$N** with EtOMs) and purple reactant parabola (representing the reaction of **1-Me$_4$N** with EtOTs) in Figure 6-19 allows the extreme similarities between the reactions of **1-Me$_4$N** with these ethylating agents to be observed. The reactant parabolas representing the reactions of **1-Me$_4$N** with $(EtO)_2SO_2$, EtOMs and EtOTs (the red, green and purple reactant parabolas in Figure 6-19 below) are all located in a similar position on the horizontal axis – that is, they are all positioned to the left relative to the parabola representing the reaction of **1-Me$_4$N** with EtI. This results in the apex of each of the reactant parabolas being closer to the apex of the product parabola for O-ethylation, which results in a lower activation barrier for the O-ethylation process relative to the C-ethylation process (as was originally seen in Figure 6-5 above, in which the influence of the horizontal position of a central reactant parabola on the positions of the intersection points was examined).

Since Gibbs energies of activation for the reactions of **1-Me$_4$N** with EtOTf and **1-Me$_4$N** with $[Et_3O]BF_4$ were not available, no Gibbs energy profile diagrams could be created for these reactions using the approach described above. Some unsuccessful approaches

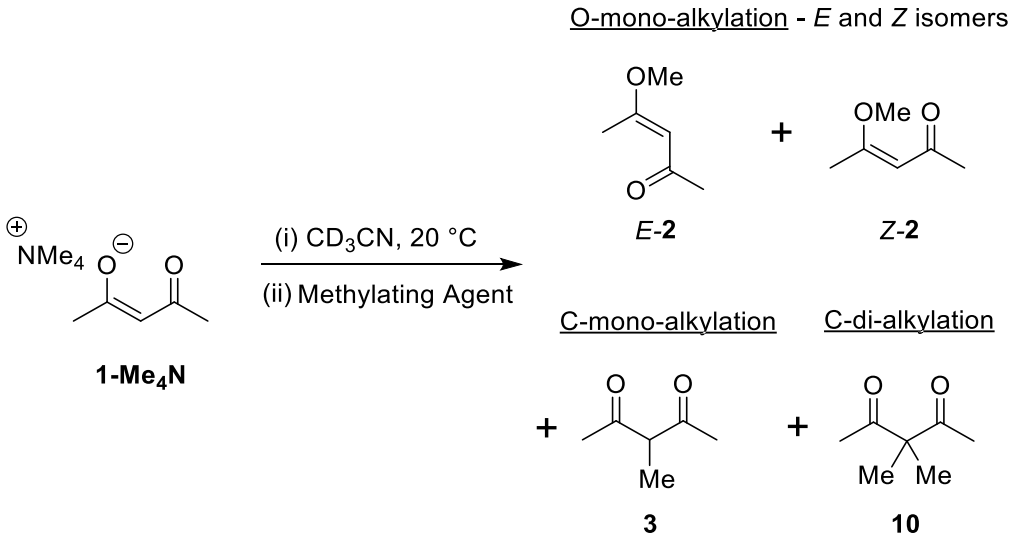
were devised to access approximate $\Delta G^{\ddagger}$ values for O- and C-ethylation reactions of **1-Me$_4$N** + EtOTf (and $[Et_3O]BF_4$) *via* competition experiments, but no definitive results were obtained from these attempts. In a later section (section 6.5), a speculative estimate of the $\Delta G^{\ddagger}$ values for O- and C-ethylation reactions of **1-Me$_4$N** with EtOTf and $[Et_3O]BF_4$ will be made, and these data will be used to make tentative approximations of the Gibbs energy profile diagrams for these reactions.

6.4. Construction of Gibbs Energy Profile Diagrams for Reactions of Enolate 1-Me_4N with Methylating Agents in CD_3CN

6.4.1. Reactions of Enolate 1-Me_4N with Methylating Agents in CD_3CN

Shown in Table 6-10 are the O/C ratios derived from the reaction of enolate **1-Me_4N** with numerous methylating agents in CD_3CN. Each reaction was maintained at a constant temperature of 20 °C and allowed to proceed for approximately 18 hours before being analysed by ^1H NMR spectroscopy.

Table 6-10. O/C ratios of the products of the reactions of enolate **1-Me_4N** with various methylating agents in CD_3CN at 20 °C. [a]



#	Solvent	Methylating Agent	O-Methylation Products	C-Methylation Products	O/C Ratio [a,b]
(i)	CD_3CN	MeI	*E*-**2**, *Z*-**2**	**3**, **10**	2:98
(ii)	CD_3CN	MeOMs	*E*-**2**, *Z*-**2**	**3**, **10**	74:26
(iii)	CD_3CN	MeOTs	*E*-**2**, *Z*-**2**	**3**, **10**	74:26
(iv)	CD_3CN	$(MeO)_2SO_2$	*E*-**2**, *Z*-**2**	**3**, **10**	75:25
(v)	CD_3CN	$[Me_3O]BF_4$	*E*-**2**, *Z*-**2**	**3**, **10**	100:0
(vi)	CD_3CN	MeOTf	*E*-**2**, *Z*-**2**	**3**, **10**	79:21

[a] The O/C ratio was determined by direct analysis of the reaction mixture by ^1H NMR spectroscopy.

[b] The percentage of C-alkylation is the combined proportion of C-mono-alkylation product and C-di-alkylation product. No mixed O/C-di-alkylation products were observed in any of the reaction mixtures. See Chapter 7 section 7.2 for details on the individual reactions.

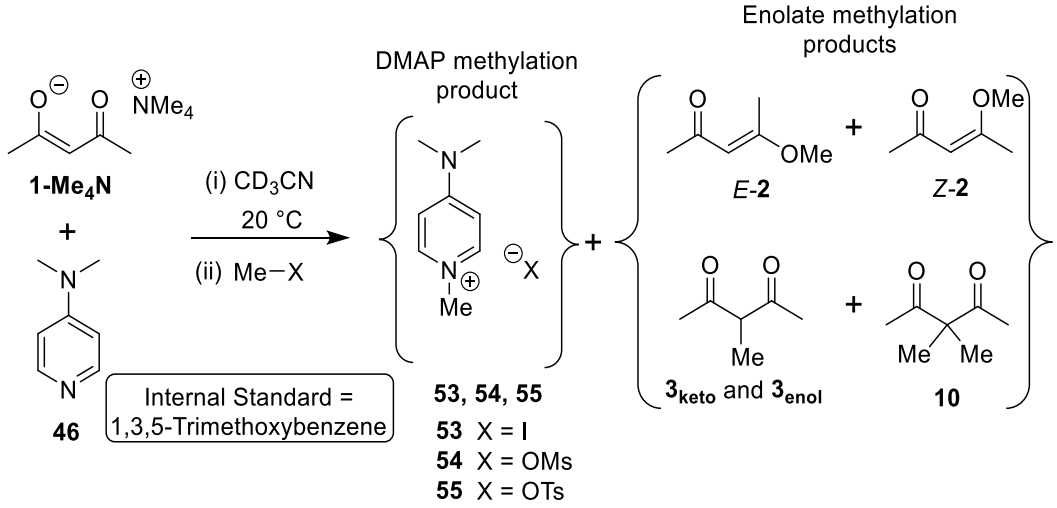
Table 6-10 above shows the O/C ratios derived from the reaction of enolate **1-Me_4N** with numerous methylating agents in CD_3CN. The reactions were maintained at a constant temperature of 20 °C and allowed to proceed for approximately 18 hours before being analysed by ^1H NMR spectroscopy. As may be seen in Table 6-10 above, **1-Me_4N** underwent reaction with each of the methylating agents used in this study in CD_3CN. A range of reactivity was displayed, with almost exclusive C-alkylation occurring in a

reaction between **1-Me$_4$N** and MeI (Table 6-10, entry (i)) and exclusive O-alkylation occurring in the reaction of **1-Me$_4$N** with $[Me_3O]BF_4$ (Table 6-10, entry (v)). Each of the reactions of MeOMs, MeOTs and $(MeO)_2SO_2$ (Table 6-10 entries (ii), (iii) and (iv)) resulted in an approximate O/C ratio of 75:25.

6.4.2. Experimental Determination of Values of $\Delta G^{\ddagger}$ for Methylation Reactions of 1-Me$_4$N

The ranges of values of $\Delta G^{\ddagger}$ which were estimated for the reactions of the enolate **1-Me$_4$N** with three methylating agents in CD_3CN at 20 °C are reported below in Table 6-11. Recall from Table 6-7 above that the Gibbs energy of activation for the reaction of DMAP (**46**) with MeI (which was used to derive the values in Table 6-11 entry (i) below) was not determined experimentally, but calculated using literature values.

Table 6-11. Values of the rate constant (k) and $\Delta G^{\ddagger}$ for the processes of O- and C-alkylation of **1-Me$_4$N** with various methylating agents in CD_3CN at 20 °C were determined through the use of competition experiments. The simultaneous reactions of DMAP (**46**) and **1-Me$_4$N** with a limiting quantity of the methylating agent resulted in a mixture of methylation products. Upon conclusion of the reaction, the proportions of enolate alkylation products formed was compared to the amount of products formed from the methylation of **46**, for which rate data was known. [a]



#	Me–X	$\Delta G^{\ddagger}_O$ Range [b] (kJ mol^{-1})	Mean $\Delta G^{\ddagger}_O$ (kJ mol^{-1})	$\Delta G^{\ddagger}_C$ Range (kJ mol^{-1})	Mean $\Delta G^{\ddagger}_C$ (kJ mol^{-1})	O/C Ratio
(i)	MeI	85.5 – 89.4	87.5	76.2 – 80.0	78.1	2:98
(ii)	MeOMs	97.7 – 98.6	98.2	100.8 – 101.6	101.2	78:22
(iii)	MeOTs	93.8 – 95.8	94.8	97.5 – 99.6	98.6	83:17

[a] The concentration of the alkylation products in the reaction mixture was determined by analysis of the ^{1}H NMR signals of each product and comparison with the ^{1}H NMR signals of an internal standard of known concentration.

[b] The Gibbs energies of activation ($\Delta G^{\ddagger}$) for the processes of O- and C-alkylation were calculated as a range of values. Details of how the ranges of values were calculated may be seen in section 7.4.

As was the case in Table 6-8 above, limiting values of the concentrations of the reactants and the products were used to enable estimation of the values of *k* (the rate constant) and $\Delta G^{\ddagger}$ for the processes of O- and C-alkylation as they occur relative to the values for DMAP (**46**) alkylation. This results in the $\Delta G^{\ddagger}$ values being reported as a range for each of the processes.

Mean values of $\Delta G^{\ddagger}$ for each O- and C-methylation processes have been calculated and are displayed in Table 6-11. Also provided are the O/C ratios observed in the competition experiments, which may be compared to the analogous results found in Table 6-10. There are slight differences between the O/C ratios obtained from the reactions of each electrophile in the competition experiments versus the values for the O/C ratio that were obtained in the experiments in which no competitor nucleophile or internal standard was present. An increased proportion of O-methylation products was observed in the competition experiments employing MeOMs (Table 6-11 entry (ii) and MeOTs (Table 6-11 entry (ii). For example, the reaction of **1-Me$_4$N** with MeOTs in CD_3CN (see Table 6-10 entry (ii)) produced an O/C ratio of 74:26, whereas the corresponding competition experiment utilising MeOTs showed an O/C ratio of 83:17 amongst the products (see Table 6-11 entry (iii) above).

Table 6-12. O/C ratios of the products of the reactions of enolate **1-Me$_4$N** with various methylating agents in CD_3CN and the expected Gibbs energy of activation difference ($\Delta\Delta G^{\ddagger}$) between the processes of O- and C-methylation when using these O/C ratios are shown below. Also shown are the O/C ratios observed for the corresponding enolate methylation in the corresponding competition experiment, as well as the difference in the mean $\Delta G^{\ddagger}$ values which were calculated for these processes in Table 6-10 and 6-11. [a]

Entry	Alkylating Agent	O/C Ratio	Expected $\Delta\Delta G^{\ddagger}$ (kJ mol^{-1})	Competition experiment O/C Ratio	Calculated $\Delta\Delta G^{\ddagger}$ (kJ mol^{-1})
(i)	MeI	2:98	9.5	2:98	9.4
(ii)	MeOMs	74:26	–2.5	78:22	–3.0
(iii)	MeOTs	74:26	–2.5	83:17	–3.8

[a] The concentration of the alkylation products in the reaction mixture was determined by analysis of the ^{1}H NMR signals of each product and comparison with the ^{1}H NMR signals of an internal standard of known concentration.

[b] The Gibbs energies of activation ($\Delta G^{\ddagger}$) for the processes of O- and C-alkylation were calculated as a range of values. Details of how the ranges of values were calculated may be seen in section 7.4.

The differences between the previously calculated O/C ratios for methylation reactions of **1-Me$_4$N** in CD_3CN at 20 °C (as seen in Table 6-10) and the O/C ratios observed in the competition experiments are highlighted above in Table 6-12. Also highlighted in Table 6-12 are the Gibbs energy of activation differences ($\Delta\Delta G^{\ddagger}$) between the processes of O- and C-alkylation which are expected to arise from the O/C ratio of a given experiment (see Equation 6.1, in which the Gibbs energy of activation difference can be related to the ratio of the rate constants). Whether the value of $\Delta\Delta G^{\ddagger}$ is negative or positive is related

to the preferred mode of alkylation – a negative value of $\Delta\Delta G^{\ddagger}$ indicates that O-alkylation is preferred, and a positive value of $\Delta\Delta G^{\ddagger}$ indicates that C-alkylation is preferred.

Thus, for example, in a reaction between **1-Me$_4$N** and MeI in CD_3CN at 20 °C (the reaction described in Table 6-10 entry (i), and by entry (i) in Table 6-12), it can be determined using the O/C ratio of 2:98 that the C-ethylation process should have a Gibbs energy of activation that is 9.4 kJ mol^{-1} lower than the O-ethylation process (see Table 6-12 entry (i)). By taking the mean values of $\Delta G^{\ddagger}$ for each of the processes as described in Table 6-11 entry (i), the difference between the O- and C-ethylation processes was calculated to be 9.5 kJ mol^{-1}. The difference between the expected values of $\Delta\Delta G^{\ddagger}$ and the calculated values of $\Delta\Delta G^{\ddagger}$ are greatest for the reactions of MeOMs (Table 6-12 entry (ii)) and MeOTs (Table 6-12 entry (iii)). As was described above in section 6.3.4, this difference arises from the different O/C ratios which were recorded in each experiment, which is to be expected given the altered reactivity of the enolate which may occur in the reaction mixture of a competition experiment compared to a reaction in which the enolate and the electrophile are the sole reactants.

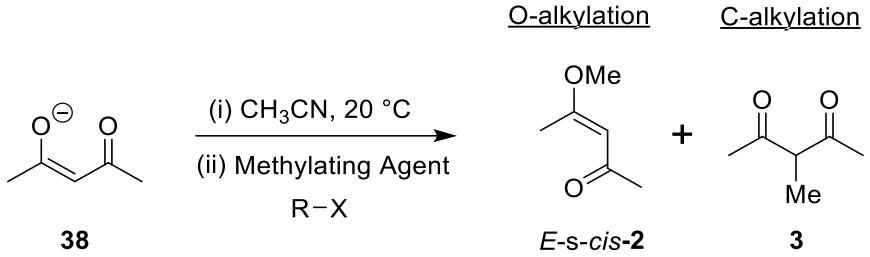
6.4.3. Computational Determination of $\Delta_r G°$ Values for Methylation Reactions of 38

The values of $\Delta_r G°$ for the processes of O- and C-methylation of **38**, the enolate of 2,4-pentanedione (**9**) were calculated to enable the construction of Gibbs energy profile diagrams of the type shown in section 6.3.5. These values enabled the determination of the relative apex heights of the product parabolas.

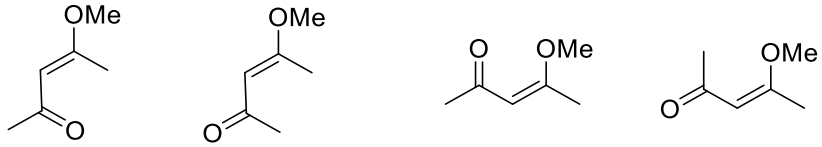
Quantum chemical calculations were performed by Prof. Martin Breugst (a collaborator of the Byrne group in TU Chemnitz, Germany) using the approach described above in section 6.2 to generate $\Delta_r G°$ values for the processes of O- and C-methylation of **38** with various methylating agents in CH_3CN. The results of these computations are shown in Table 6-13. For the reasons established in section 6.3.1 above, it was decided to conduct the calculations on the reactions of the enolate shown in Table 6-13 in the absence of the Me_4N^+ counter-cation. As was the case in Table 6-5, standard Gibbs energies of reaction values were calculated for four different conformations of O-alkylation product which could potentially form. In each case, the *E*-s-*cis* conformation of the O-alkylation product was found to be the most thermodynamically favourable of the O-alkylation products (i.e., producing the most negative values of $\Delta_r G°$). When calculating the relative difference between the Gibbs energies of reaction (i.e., $\Delta\Delta_r G°$) between the processes of O- and C-alkylation for a given reagent, the value of the *E*-s-*cis* conformation of the O-alkylation product was used in each case for this reason.

Table 6-13. **(a)** $\Delta_r G°$ values for the processes of O- and C-alkylation ($\Delta_r G°_O$ and $\Delta_r G°_C$) of the enolate **38** by various methylating agents using a CH_3CN solvent model were determined using quantum chemical calculations. The calculations were conducted using a CH_3CN solvent model at a calculated temperature of 20 °C. [a] **(b)** Structures of the four different conformations of O-mono-methylation product that may be formed.

(a)



(b)



#	Alkylating agent	$\Delta_r G°_O$ (*E*-s-*cis*)	$\Delta_r G°_O$ [b] (*E*-s-*trans*)	$\Delta_r G°_O$ [c] (*Z*-s-*cis*)	$\Delta_r G°_O$ [d] (*Z*-s-*trans*)	$\Delta_r G°_C$	$\Delta\Delta_r G°$ [e]
(i)	MeI	–71.1	–61.8	–56.5	–59.9	–154.2	83.1
(ii)	MeOMs	–74.0	–64.7	–59.4	–62.8	–157.1	83.1
(iii)	MeOTs	–83.9	–74.7	–69.3	–72.7	–167.0	83.1
(iv)	$(MeO)_2SO_2$	–91.2	–82.0	–76.6	–80.1	–174.3	83.1
(v)	$[Me_3O]BF_4$	–138.9	–129.6	–124.3	–127.7	–222.0	83.1
(vi)	MeOTf	–139.4	–130.1	–124.8	–128.2	–222.5	83.1

[a] The $\Delta_r G°$ values (in kJ mol^{-1}) were calculated at the DLPNO-CCSD(T)/def2-TZVPPD/SMD(CH_3CN)//M06-2X-D3/6-311+G(d,p)/SMD(CH_3CN) level of theory by Prof. Martin Breugst.

[b] The $\Delta_r G°_O$ values in this column were calculated for the transformation of the *E-s-trans* enolate to the *E-s-trans* vinyl ether.

[c] The $\Delta_r G°_O$ values in this column were calculated for the transformation of the *Z-s-cis* enolate to the *Z-s-cis* vinyl ether.

[d] The $\Delta_r G°_O$ values in this column were calculated for the transformation of the *E*-s-*cis* enolate (which is identical to the *Z-s-trans* enolate) to the *Z-s-trans* vinyl ether.

[e] The $\Delta\Delta_r G°$ values were calculated using the lowest value of $\Delta_r G°_O$ in each case. As the *E*-s-*cis* isomer of the O-alkylation product is the most thermodynamically favourable in each case, this results in the $\Delta\Delta_r G°$ values being the difference in Gibbs energy of reaction between $\Delta_r G°_{O\,(E\text{-}s\text{-}cis)}$ and $\Delta_r G°_C$.

The products of reactions of MeOTf and $[Me_3O]BF_4$ (Table 6-13 entries (vi) and (v)) are calculated to have the lowest Gibbs energy of reaction (i.e., the most Lewis acidity towards **38**) out of the set of methylating agents analysed. As such, they should produce the highest O/C ratios of any reactions in this series – a fact which is seen to be true when

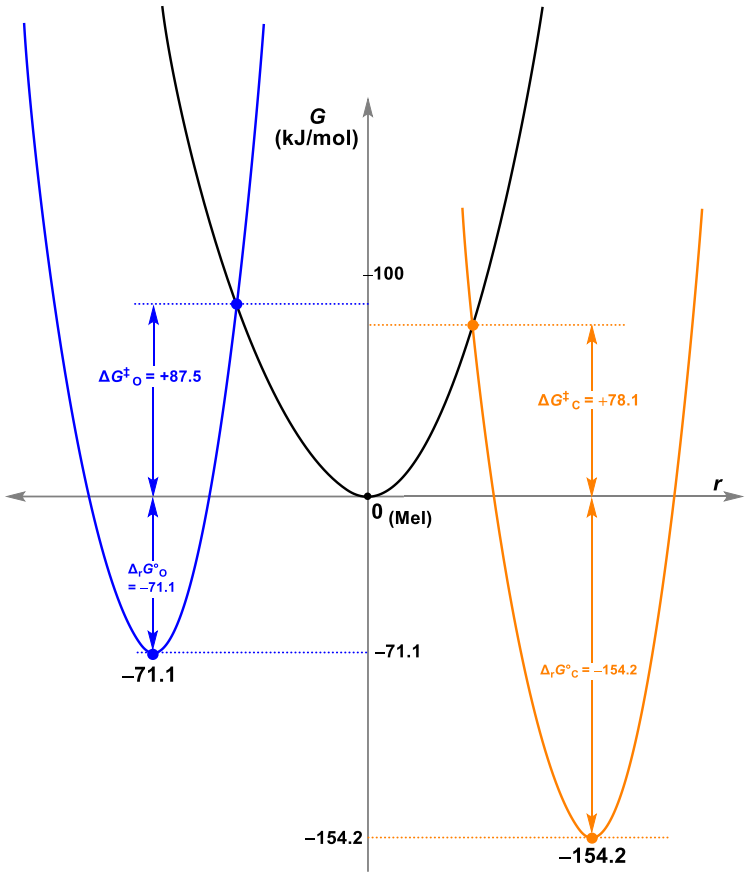
looking at the O/C ratios for the corresponding reactions of **1-Me$_4$N** (see Table 6-10 entries (v) and (vi)). However, the calculated values of $\Delta_r G°$ for the formation of O- and C-methylation products are almost identical (compare the values of $\Delta_r G°_{O\ (E\text{-s-}cis)}$ and $\Delta_r G°_C$ in Table 6-10 entry (vi) with entry (v)). If the Lewis acidity of the alkylating agent were the decisive factor influencing the observed O/C ratios of these reactions, the reactions of MeOTf and [Me$_3$O]BF$_4$ should have almost identical ratios of O- and C-methylation products. Instead, the reaction of [Me$_3$O]BF$_4$ was exclusively O-selective (see Table 6-10 entry (v)) whereas the reaction of MeOTf results in an O/C ratio of 79:21 (see Table 6-10 entry (vi)). It is worth noting that in this set of calculated $\Delta_r G°$ values, the reaction of **38** with MeI is calculated to have the least negative values of $\Delta_r G°$ (see Table 6-13 entry (i)). As such, it is less exergonic than the reaction of **38** with MeOMs (see Table 6-13 entry (ii)) and the reaction of **38** with MeOTs (see Table 6-13 entry (iii)). This is noteworthy as in the corresponding values of $\Delta_r G°$ which were calculated for reactions in which **38** was ethylated by various ethylating agents (see Table 6-5), the reaction of **38** with EtI (Table 6-5 entry (iv)) was more exergonic than the corresponding reactions of **38** with EtOMs (Table 6-5 entry (ii)) and EtOTs (Table 6-5 entry (iii)).

6.4.4. Gibbs Energy Surfaces of the Reactions of Enolate 1-Me$_4$N + Methylating Agents

(a) Gibbs energy Profile Diagram for Reaction of 1-Me$_4$N + MeI

Using the relevant data shown above (i.e., the calculated $\Delta_rG°$ values in Table 6-13, and the experimentally derived $\Delta G^‡$ values for the processes of O- and C-methylation of the enolate **1-Me$_4$N** by various methylating agents in CD_3CN from Table 6-11 above), Gibbs energy profile diagrams could be constructed for this series of reactions using the process outlined in section 6.3.5. The Gibbs energy profile diagram for the reaction of **1-Me$_4$N** with MeI in CD_3CN is shown below in Figure 6-20.

Figure 6-20. The Gibbs energy profile diagram for the reaction of enolate **1-Me$_4$N** with MeI in CD_3CN is constructed using the calculated values of $\Delta_rG°_O$ and $\Delta_rG°_C$ and the experimentally derived values of $\Delta G^‡_O$ and $\Delta G^‡_C$. The width and curvature of the reactant parabola is determined by the points at which it must intersect the two adjacent product parabolas – only one parabola exists that passes through the transition states specified in the diagram and also has its apex on the line $G = 0$.



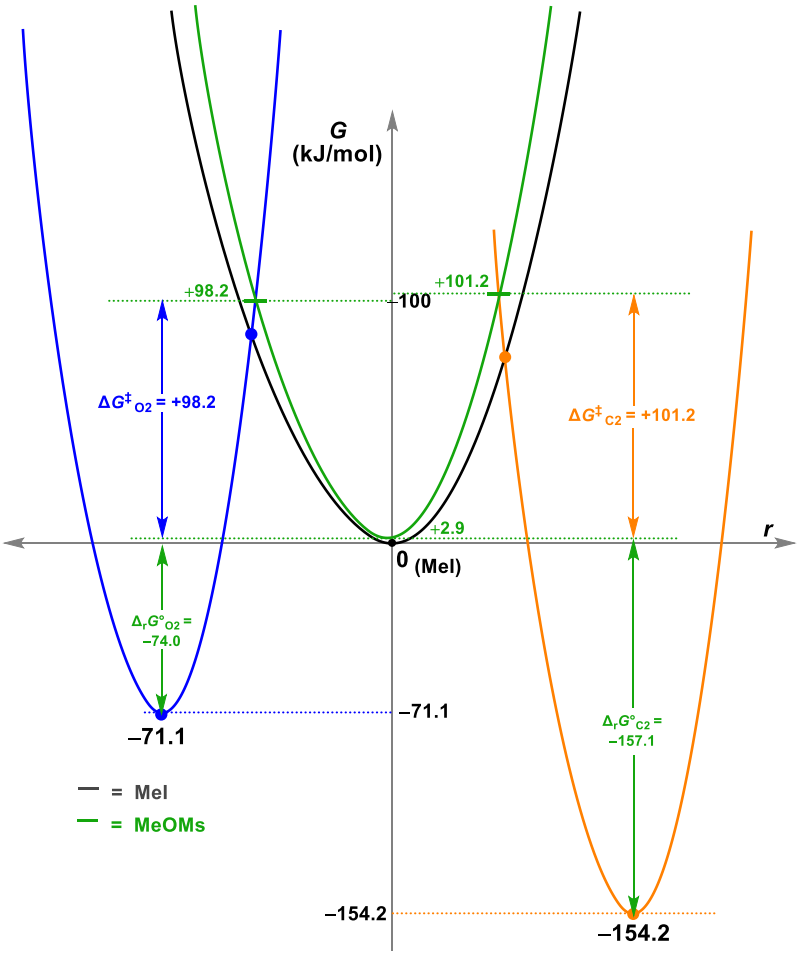
(b) Gibbs Energy Profile Diagram for Reaction of 1-Me$_4$N + MeOMs

Having constructed one of the Gibbs energy profile diagrams (for the reaction of **1-Me$_4$N** with MeI in CD_3CN), it is now possible to make use of the previously made assumption that the positions of the product parabolas is essentially invariant for all methylation reactions, no matter which ethylating agent is employed. The relative difference in the

standard Gibbs energy of reaction ($\Delta\Delta_rG°$) for the competing processes of O- and C-ethylation in the reactions of enolate **1-Me$_4$N** with various ethylating agents remained the same (at 83.1 kJ mol^{-1}) no matter which methylating agent was employed (see Table 6-13 above). As a result, the Gibbs energy profile diagram shown in Figure 6-20 above can be further built upon with the addition of another reactant parabola, which represents the Gibbs energy well of the reactants in the reaction of enolate **1-Me$_4$N** with a different ethylating agent.

Using the Gibbs energy profile diagram for the reaction of **1-Me$_4$N** with MeI in CD_3CN as the starting point, the relevant data (i.e., calculated values of $\Delta_rG°_O$ and $\Delta_rG°_C$ from Table 6-13, and values of $\Delta G^‡_O$ and $\Delta G^‡_C$ from Table 6-11) were inserted into this diagram that were necessary to construct the reactant parabola for the reaction of **1-Me$_4$N** with MeOMs in CD_3CN. The diagram showing these inserted values of $\Delta_rG°$ and $\Delta G^‡$ is shown below in Figure 6-21.

Figure 6-21. The Gibbs energy profile diagram for the reaction of enolate **1-Me$_4$N** with MeI in CD_3CN is overlaid with a reactant parabola which represents the reaction of **1-Me$_4$N** with MeOMs in CD_3CN. The activation barrier positions, and apex height positions are colour coded to allow each reaction to be distinguished from the other.



In Figure 6-21 above, the values (in green) associated with the O- and C-methylation of **1-Me$_4$N** by MeOMs were used to construct a reactant parabola. This parabola was overlaid on top of the Gibbs energy profile diagram for the reaction of **1-Me$_4$N** with MeI. The reactant parabola for the reaction of MeOMs (green parabola in Figure 6-21) is considerably narrower (i.e., it has a greater curvature) than the parabola representing the reaction with MeI. The parabola is also shifted to the left (as drawn) on the x-axis relative to the reactant parabola for the reaction with MeI, with an apex 2.9 kJ mol^{-1} higher than the MeI reactant parabola. This shift to the left of the diagram (see Figure 6-5 in section 6.2.1 above) results in a decrease in the width of the activation barrier for the O-methylation process, with the result being that the reaction of **1-Me$_4$N** with MeOMs is O-selective, while the reaction of **1-Me$_4$N** with MeI is C-selective.

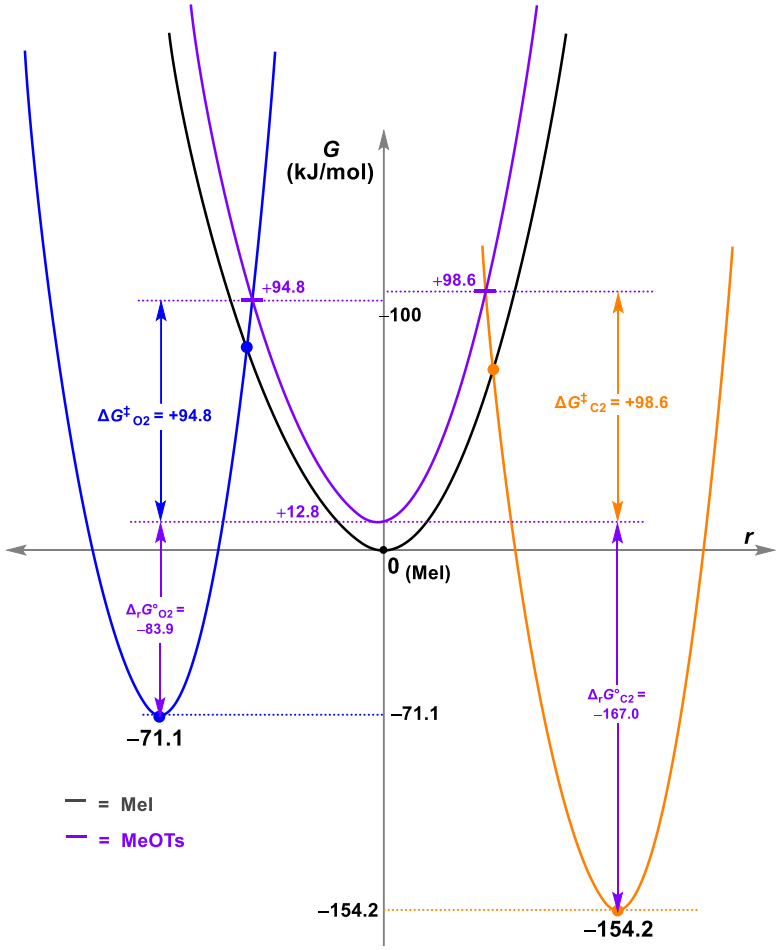
Parallels exist between this Gibbs energy profile diagram and the one constructed in section (c) of section 6.3.5 above. In that example, the reactions of **1-Me$_4$N** with EtI and **1-Me$_4$N** with EtOMs were being compared in the overlaid Gibbs energy profile diagram. In that instance (Figure 6-16) and the case shown in Figure 6-21 shown above, the reaction of the alkyl iodide (i.e., EtI or MeI) with **1-Me$_4$N** results in lower activation barriers for the O- and C-alkylation processes, and C-alkylation is kinetically preferred.

Again, in both instances, when the alkyl methanesulfonate (EtOMs or MeOMs) is used in a reaction with **1-Me$_4$N**, the reactant parabola is narrower, and moved to the left relative to the reactant parabola corresponding to the reaction of **1-Me$_4$N** with the alkyl halide (as drawn). However, in the example shown in Figure 6-21, the O- and C-alkylation reactions of EtOMs and **1-Me$_4$N** are calculated to be less exergonic than the reactions of EtI with **1-Me$_4$N** (i.e., the apex of the reactant parabola for **1-Me$_4$N** with EtOMs is slightly *below* and to the left of the apex of the reactant parabola for **1-Me$_4$N** with EtI). In the case shown in Figure 6-16, the apex of the reactant parabola for the reaction of **1-Me$_4$N** with MeOMs is *above* and to the left of the apex of the reactant parabola for **1-Me$_4$N** with MeI (due to the larger negative values of $\Delta_r G°$ associated with the O-and C-methylation reactions of MeOMs with **1-Me$_4$N**, see Table 6-13 above). The outcome in both cases is that the movement of the alkyl methanesulfonate + **1-Me$_4$N** reactant parabolas (i.e., EtOMs or MeOMs) relative to the alkyl iodide + **1-Me$_4$N** reactant parabolas (i.e., EtI or MeI) results in O-alkylation becoming the preferred process. The fact that this occurs regardless of whether or not the reactant parabola moves up or down indicates that the narrowing of the reactant parabola and the horizontal movement of the reactant parabola in each instance (Figures 6-16 and 6-21) can lead to switches from C- to O-selectivity even in instances in which the reactant parabola does not shift upwards along the Gibbs energy (vertical) axis.

(c) Gibbs Energy Profile Diagram for Reaction of 1-Me$_4$N + MeOTs

In Figure 6-22 below, the values (in purple) associated with the O- and C-methylation of **1-Me$_4$N** by MeOTs were used to construct a reactant parabola for this reaction. This parabola was overlaid on top of the Gibbs energy profile diagram for the reaction of **1-Me$_4$N** with MeI, and is shown below in Figure 6-22.

Figure 6-22. The Gibbs energy profile diagram for the reaction of enolate **1-Me$_4$N** with MeI in CD_3CN is overlaid with a reactant parabola which represents the reaction of **1-Me$_4$N** with MeOTs in CD_3CN. The activation barrier positions, and apex height positions are colour coded to allow each reaction to be distinguished from the other.



The purple reactant parabola in Figure 6-22 is shifted to the left (as drawn) on the x-axis relative to the reactant parabola for the reaction of **1-Me$_4$N** with MeI. This shift to the left of the diagram (as drawn, see Figure 6-5 in section 6.2.1 above) results in a decrease in the width of the activation barrier for the O-methylation process. As was the case in Figure 6-21 above, the purple reactant parabola is also narrower than the reactant parabola associated with the MeI reaction. In Figure 6-4 in section 6.2.1 above, this narrowing of the curvature of a reactant parabola is listed as another alteration to the reactant parabola which may result in an increase in the O-selectivity of the reaction in question. The resulting reactant parabola (in purple in Figure 6-22 above) has an extremely similar curvature to the one constructed for the reaction of MeOMs with **1-Me$_4$N** above (see Figure 6-21).

An instance in which reactant parabolas have a near-identical curvature has been noted before in sections (c) and (d) of section 6.3.5, for the reactions of **1-Me$_4$N** with EtOMs and the reaction of **1-Me$_4$N** with EtOTs. In that case, however, each reaction had extremely similar values of $\Delta_rG°_O$, $\Delta_rG°_C$, $\Delta G^‡_O$ and $\Delta G^‡_C$ which were determined computationally and measured experimentally (and subsequently used to construct the

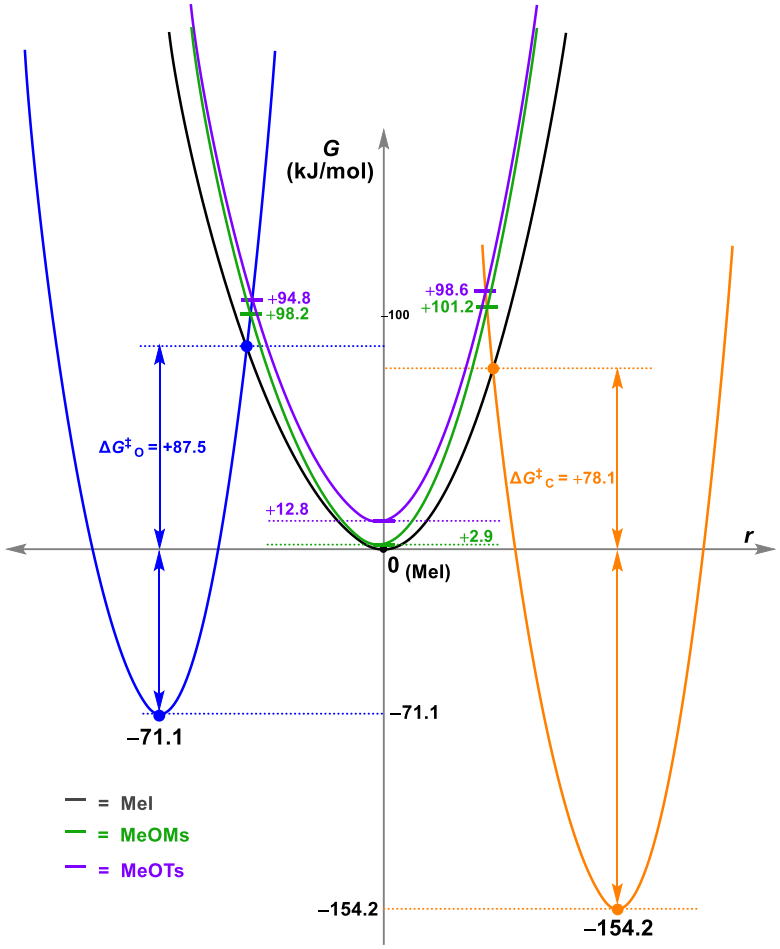
Gibbs energy profile diagrams in Figures 6-16 and 6-17). In the case of the reactions of **1-Me$_4$N** with MeOMs and MeOTs, there are larger differences between the values used to construct the Gibbs energy profile diagrams, particularly in the values of $\Delta_r G°_O$ and $\Delta_r G°_C$. It is thus interesting to note that the curvature of the reactant parabolas for the reaction of **1-Me$_4$N** with MeOMs and the reaction of **1-Me$_4$N** with MeOTs are so similar despite the fact that the quantities used to construct the parabolas were considerably different. The experimentally observed O/C ratio for the reaction of **1-Me$_4$N** with MeOTs is slightly higher than the O/C ratio recorded for the reaction of **1-Me$_4$N** with MeOMs. Given the extremely similar widths and horizontal co-ordinates of the apices of the reactant parabolas which represent each of these ethylation reactions, it is possible that the source of the greater O-selectivity observed in the reaction of **1-Me$_4$N** with MeOTs is the slightly higher degree of Lewis acidity that MeOTs is calculated to have towards **1-Me$_4$N** compared to MeOMs (based on the calculated $\Delta_r G°$ values for these reactions shown in Table 6-13 above).

(d) Overlaid Gibbs Energy Profile Diagrams for All Methylation Reactions of 1-Me$_4$N Investigated

Shown below in Figure 6-23 is each of the reactant parabolas constructed in Figures 6-21 and 6-22 above overlaid together on top of the Gibbs energy profile diagram for the reaction of **1-Me$_4$N** with MeI. Comparison of the green reactant parabola (representing the reaction of **1-Me$_4$N** with MeOMs) and purple reactant parabola (representing the reaction of **1-Me$_4$N** with MeOTs) in Figure 6-23 allows the close similarities between the reactions of **1-Me$_4$N** with these methylating agents to be observed. The reactant parabolas representing the reactions of **1-Me$_4$N** with MeOMs and MeOTs (the green and purple reactant parabolas in Figure 6-23 below) each have their apex located at a similar co-ordinate on the horizontal axis. They are both positioned to the left (as drawn) relative to the parabola representing the reaction of **1-Me$_4$N** with MeI. This results in a narrower Gibbs energy of activation barrier for the O-methylation process relative to the C-methylation process in each case.

As explained earlier, Gibbs energies of activation for the reactions of **1-Me$_4$N** with MeOTf, **1-Me$_4$N** with $(MeO)_2SO_2$ and **1-Me$_4$N** with $[Me_3O]BF_4$ could not be accessed. As was the case using ethyl triflate and triethyloxonium tetrafluoroborate in section 6.3.5, reactions of these methylating agents with DMAP (**46**) was too fast to be measured using the ^{1}H NMR spectroscopic method employed described in section 6.3.3 above. Some unsuccessful approaches were devised to access approximate $\Delta G^‡$ values for O- and C-ethylation reaction of **1-Me$_4$N** + MeOTf *via* competition experiments, but no definitive results were obtained from these attempts. In the next section (section 6.5), a speculative estimate of the $\Delta G^‡$ values for O- and C-ethylation reactions of **1-Me$_4$N** with MeOTf and $[Me_3O]BF_4$ will be made, and these data will be used to make tentative approximations of the Gibbs energy profile diagrams for these reactions.

Figure 6-23. The Gibbs energy profile diagram for the reaction of enolate **1-Me$_4$N** with MeI in CD_3CN is overlaid with new reactant parabolas for two additional reactions of **1-Me$_4$N** with methylating agents in CD_3CN. The activation barrier positions, and apex height positions are colour coded to allow each unique reaction to be distinguished from one another.



6.5. Discussion on O- vs C-Selectivity in Reactions of Enolates and Generation of Approximated Gibbs Energy Profile Diagrams

6.5.1. General Trends in O/C Selectivity in Reactions of the Enolate 1-Me_4N

This section contains a brief description of the trends in O/C selectivity which were observed in the reactions of enolates in sections 6.3 and 6.4.

An examination of data pertaining to the O/C selectivity of alkylation reactions of enolate **1-Me_4N** shows that the reactions of alkyl triflates (i.e., MeOTf, EtOTf) with this enolate (i.e., **1-Me_4N)** do not result in O/C ratios that are much larger than the O/C ratios recorded for reactions with alkyl methanesulfonates (i.e., MeOMs, EtOMs) and alkyl toluenesulfonates (i.e., MeOTs, EtOTs). This occurs despite the fact that the Lewis acidities of the alkyl triflates with enolates such as **38** are consistently calculated to be much greater (i.e., more negative values of $\Delta_r G°$) than reactions of alkyl methanesulfonates and alkyl toluenesulfonates. An example of this trend may be seen in reactions of **1-Me_4N** in CD_3CN by comparing the O/C selectivities of the reactions of **1-Me_4N** with EtOTf in CD_3CN and **1-Me_4N** with EtOMs in CD_3CN (compare Table 6-6 entries (vi) and (ii)). The O/C ratio observed in the reaction with EtOTf was 84:16, and the selectivity observed in the reaction with EtOMs was 85:15. The values of $\Delta_r G°$ calculated (using enolate **38**) for each of these reactions are shown in Table 6-5 entries (ii) and (vi). The $\Delta_r G°_O$ and $\Delta_r G°_C$ values calculated for the reactions employing EtOTf have a far greater negative value than the values calculated for the reaction of EtOMs. For example, $\Delta_r G°_O$ for the reaction of **38** with EtOTf is –133.8 kJ mol^{-1} (Table 6-5 entry (vi)), and the value of $\Delta_r G°_O$ for the reaction of **38** with EtOMs is –72.6 kJ mol^{-1} (Table 6-5 entry (ii)).

The discussion regarding the effect that the movement of the central reactant parabola will have on the selectivity of a given reaction in this model is given in section 6.2.1. Recall that in Figure 6-3, it is shown that by "raising up" the central reactant parabola relative to another reactant parabola (thereby representing the differences in $\Delta_r G°$ values between the products of two distinct reactions), the amount of O-alkylation is generally seen to be increased. The data discussed above indicate that the Gibbs energy profile diagrams associated with reactions of alkyl triflates with enolates (such as **1-Me_4N**) should result in central reactant parabolas that are "raised up" relative to the reactant parabolas of reactions of alkyl methanesulfonates (due to the greater negative values of $\Delta_r G°$ associated with the O- and C-alkylation reactions of alkyl triflates). However, despite this upward movement of the reactant parabola, the O/C selectivity of reactions of alkyl triflates is not seen to be particularly different to the selectivity observed in reactions of alkyl methanesulfonates (e.g., compare the O/C ratios in Table 6-6 entries (vi) and (ii)) across the reactions conducted with any of the enolates studied. In the context of the novel model for rationalising ambident reactivity discussed in this chapter, this observation implies that the curvature of the reactant parabola for reactions of enolates with alkyl triflates must be shallower than the reactant parabolas which represent the reactions of enolates with alkyl methanesulfonates and alkyl toluenesulfonates. Further

discussion on this point will be given below in relation to the Gibbs energy profile diagram for the reaction of EtOTf with enolate **1-Me$_4$N**.

6.5.2. Generation of Approximate Gibbs Energy Profile Diagrams

(i) Methylation Reactions of Enolate 1-Me$_4$N

As described in section 6.3.3, the values of $\Delta G^{\ddagger}$ for reactions of EtOTf, MeOTf and other electrophiles with DMAP (**46**) occurred too quickly to be measured using the NMR spectroscopic method described in section 6.3. As a result, no values of $\Delta G^{\ddagger}$ for the reactions of **1-Me$_4$N** with those electrophiles could be estimated through the use of competition experiments.

Through the use of literature data which reports the rates of reactions of different nucleophiles with multiple alkylating agents, speculative values of $\Delta G^{\ddagger}$ may be determined using the values of $\Delta G^{\ddagger}$ which were calculated for the O- and C-alkylation reactions of **1-Me$_4$N** in sections 6.3 and 6.4 above. By comparing the literature rates of reaction for reactions of a given nucleophile with MeOTf and MeI, for example, the values of $\Delta G^{\ddagger}$ calculated for the O- and C-methylation reactions of **1-Me$_4$N** in section 6.4 can be modulated to approximate the values of $\Delta G^{\ddagger}$ for the reactions of **1-Me$_4$N** with MeOTf. The approximate values of $\Delta G^{\ddagger}$ calculated by this process should not be considered to be as reliable as the values of $\Delta G^{\ddagger}$ calculated for the reactions of **1-Me$_4$N** with various electrophiles in section 6.3 and 6.4.

Literature data which enabled this endeavour was found in a publication by Lewis and Vanderpool.[39] In this study, the rates of reaction are determined for the reactions of various substituted thiolates with various electrophiles such as MeOTf, MeI, MeOMs and MeOTs. Shown in Table 6-14 are the values of *k* for reactions of potassium phenylthiolate (**56-K**) and potassium 4-nitrophenylthiolate (**57-K**) with various methylating agents. These values of *k* can be converted into values of $\Delta G^{\ddagger}$ using Equation 6.4 found in section 6.3.3 above, and these values of $\Delta G^{\ddagger}$ are listed below in Table 6-14.

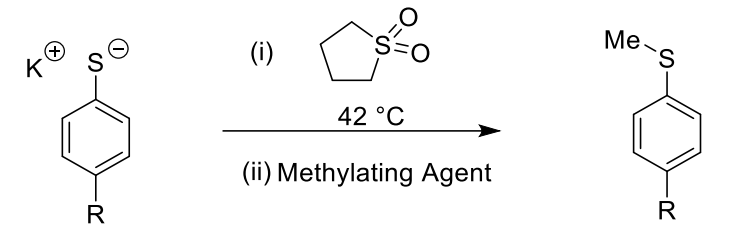
The values of $\Delta G^{\ddagger}$ calculated (at 42 °C, or 315.15 K) here offer an insight into the extent to which the $\Delta G^{\ddagger}$ values of the reactions of a given nucleophile with different methylating agents differ from each other. For example, it is observed that for the reactions of **56-K** with MeI and of **56-K** with MeOTf, the difference between the Gibbs energies of activation ($\Delta\Delta G^{\ddagger}$) is given by:

$$\Delta\Delta G^{\ddagger} = \Delta G^{\ddagger}_{\text{MeI}} - \Delta G^{\ddagger}_{\text{MeOTf}} = (57.2 - 44.8)\ \text{kJ mol}^{-1} = 12.4\ \text{kJ mol}^{-1} \qquad (6.6)$$

where $\Delta G^{\ddagger}_{\text{MeI}}$ is the Gibbs energy of activation for the reaction of **56-K** + MeI (Table 6-14 entry (iii)), and $\Delta G^{\ddagger}_{\text{MeOTf}}$ is the corresponding quantity for the reaction of **56-K** + MeOTf (Table 6-14 entry (iv)). That is, the Gibbs energy of activation barrier for the methylation reaction using MeOTf is lower by 12.4 kJ mol^{-1}. Using an identical approach for the reactions of **57-K** with MeI and **57-K** with MeOTf, the difference between the

Gibbs energies of activation ($\Delta\Delta G^{\ddagger}$) is equal to 13.8 kJ mol^{-1} (compare Table 6-14 entry (vii) with entry (viii)). [a]

Table 6-14. Values of *k* for the reactions of substituted thiophenoxides (**56-K** and **57-K**) in sulfolane at 42 °C were calculated by Lewis and Vanderpool.[39] [a]



56-K R = H
57-K R = NO_2

58 R = H
59 R = NO_2

#	Nucleophile	R	Methylating Agent	*k* (L mol^{-1} s^{-1})	$\Delta G^{\ddagger}$ (kJ mol^{-1})
(i)	**56-K**	H	MeOMs	1.04×10^{2}	73.7
(ii)	**56-K**	H	MeOTs	4.34×10^{2}	70.0
(iii)	**56-K**	H	MeI	5.67×10^{4}	57.2
(iv)	**56-K**	H	MeOTf	6.35×10^{6}	44.8
(v)	**56-K**	H	$[Me_3O]BF_4$	1.90×10^{8}	35.9
(vi)	**57-K**	NO_2	MeOMs	6.20×10^{-1}	87.1
(vii)	**57-K**	NO_2	MeOTs	1.68×10^{0}	84.3
(viii)	**57-K**	NO_2	MeI	2.79×10^{2}	71.1
(ix)	**57-K**	NO_2	MeOTf	5.47×10^{4}	57.3
(x)	**57-K**	NO_2	$[Me_3O]BF_4$	4.09×10^{6}	46.0

[a] The rates of reaction were determined using continuous potentiometric analysis of the reaction mixtures. The rate constants were calculated by dividing the pseudo-first-order rate constant, obtained from the first-order plot, by the average concentration of the reagent which was in excess.

The $\Delta\Delta G^{\ddagger}$ values determined in this way (for any pair of methylating agents) can be used in tandem with the $\Delta G^{\ddagger}$ values determined above for reactions of enolate **1-Me$_4$N** with alkylating agents to give a rough estimate of the $\Delta G^{\ddagger}$ value for the reaction of **1-Me$_4$N** + MeOTf (i.e., for the reactions that were too fast for rate constant determinations to be realised). For example, using the value of $\Delta G^{\ddagger}$ of 78.1 kJ mol^{-1} determined above for the reaction of enolate **1-Me$_4$N** + MeI (see Table 6-11 entry (i)), and an approximate $\Delta\Delta G^{\ddagger}$ value of 13 kJ mol^{-1} estimated as a rough average of the $\Delta\Delta G^{\ddagger}$ values 12.4 kJ mol^{-1} (from reactions of **56-K** + MeOTf and **56-K** + MeI) and 13.8 kJ mol^{-1} (from reactions of **57-K** + MeOTf and **57-K** + MeI), an estimate of *ca.* 65 kJ mol^{-1} for the $\Delta G^{\ddagger}$ value of the O-methylation reaction of **1-Me$_4$N** + MeOTf at 293.15 K is obtained (O-methylation being

[a] Note that $\Delta\Delta G^{\ddagger}$ values are relatively insensitive to changes in temperature over small ranges. Although the use of data for reactions conducted at 20° C would be ideal, the data employed here is obtained from reactions conducted at 42° C.

the faster reaction vs. C-methylation in this case). Similar estimates generated using data for reactions of the other methylating agents from Table 6-14 also give values below 70 kJ mol^{-1} for the $\Delta G^{\ddagger}$ value of the O-methylation reaction of **1-Me$_4$N** + MeOTf.

Below, an example is given that demonstrates that, while this approach could never be expected to give quantitatively accurate answers, in an approximate sense, values of $\Delta G^{\ddagger}$ for methylation reactions can be estimated using the known trends in values of $\Delta\Delta G^{\ddagger}$ for alkylation reactions of other nucleophiles. As established above, the preferred C-methylation of enolate **1-Me$_4$N** by MeI in CD_3CN is calculated to have a value of $\Delta G^{\ddagger}$ of 78.1 kJ mol^{-1} (see Table 6-11 entry (i)). The preferred O-methylation of enolate **1-Me$_4$N** by MeOMs in CD_3CN is calculated to have a value of $\Delta G^{\ddagger}$ of 98.2 kJ mol^{-1} (see Table 6-11 entry (ii)). This indicates that there is a difference in the values of $\Delta G^{\ddagger}$ calculated for these reactions of 20.1 kJ mol^{-1} at 293.15 K. In the reactions of **56-K** with MeOMs and MeI (see Table 6-14 entries (i) and (iii)) and the reactions of **56-K** with MeOMs and MeI (see Table 6-14 entries (v) and (vii)), the differences in the values of $\Delta G^{\ddagger}$ are calculated to be 16.5 kJ mol^{-1} and 16.0 kJ mol^{-1} at 315.15 K, respectively, i.e., within 4 kJ mol^{-1} (< 1 kcal mol^{-1}) of the experimentally observed difference. Note that as Gibbs energies are temperature dependent, the features of the diagrams constructed by this method would change if the temperature is changed.

Using this estimated value of $\Delta G^{\ddagger}$ associated with the O-methylation reaction of **1-Me$_4$N** + MeOTf (*ca.* 65 kJ mol^{-1}) established above, an estimated value of $\Delta G^{\ddagger}$ associated with the C-methylation reaction can be calculated using knowledge of the O/C selectivity that was observed in a reaction of MeOTf with enolate **1-Me$_4$N** in CD_3CN (which is 79:21, see Table 6-10 entry (vi)) and Equation 6.1.

$$\frac{k_C}{k_O} = e^{-\left(\frac{\Delta\Delta G^{\ddagger}}{RT}\right)} = e^{-\left(\frac{\Delta G^{\ddagger}_{C} - \Delta G^{\ddagger}_{O}}{RT}\right)} \quad (6.1)$$

$$\frac{21}{79} = e^{-\left(\frac{\Delta G^{\ddagger}_{C} - 65\ \text{kJ mol}^{-1}}{RT}\right)}$$

Using Equation 6.1 and the estimated value of $\Delta G^{\ddagger}_{O}$ which was calculated for the O-methylation of **1-Me$_4$N** with MeOTf, the estimated value of $\Delta G^{\ddagger}_{C}$ for the C-methylation reaction of **1-Me$_4$N** with MeOTf is 68.2 kJ mol^{-1}. Using these estimated values of $\Delta G^{\ddagger}_{O}$ and $\Delta G^{\ddagger}_{C}$, in combination with the calculated values of $\Delta_r G°$ for these reactions (see Table 6-13 entry (vi)) in section 6.4.3), an additional Gibbs energy profile diagram may be constructed which approximates the diagram which would be observed for a reaction of **1-Me$_4$N** with MeOTf. The values of $\Delta_r G°$ between the respective O- and C-methylation reactions of **1-Me$_4$N** by MeI and MeOTf differ by 68.3 kJ mol^{-1} (see Table 6-13, compare entries (i) and (vi). As was the case when reactant parabolas (which represent the Gibbs energy well of the reactants) were previously inserted into Gibbs energy profile diagrams, there is one uniquely defined parabola that passes through the transition states which are specified above and also has its apex on the line G = +68.3 kJ mol^{-1}. This speculative

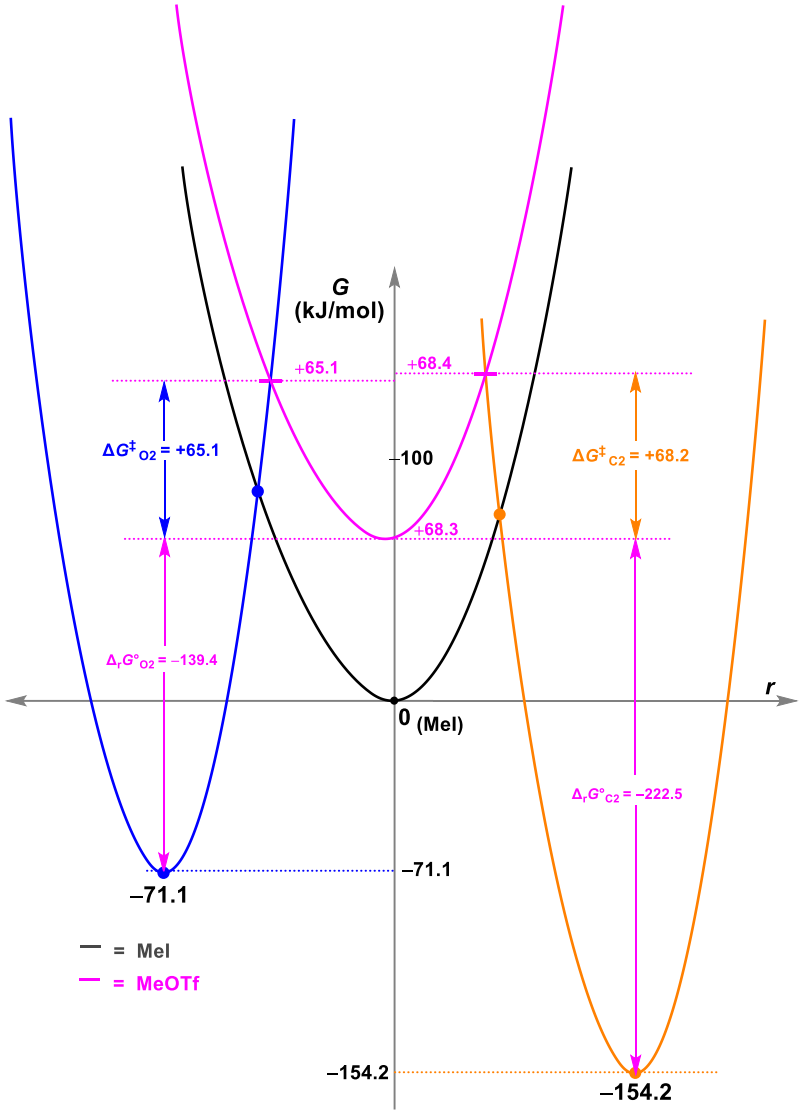
Gibbs energy profile diagram is constructed in Figure 6-24, overlaid on top of the Gibbs energy profile diagram for the reaction of **1-Me$_4$N** with MeI in CD_3CN (from Figure 6-20 in section 6.4.4 above).

The apex of this reactant parabola occurs at a significantly higher vertical position than the corresponding parabola for the reaction of **1-Me$_4$N** with MeI (as a consequence of the values of $\Delta_r G°$ being significantly more negative in the case of the methylation reactions of **1-Me$_4$N** employing MeOTf, compare Table 6-13 entries (i) and (vi)). The pink reactant parabola is only slightly narrower than the reactant parabola associated with the reaction of **1-Me$_4$N** with MeI. This is an interesting observation, as the other reactant parabola for methylation reactions which give preferential O-alkylation (i.e., the reactant parabola for the reactions of **1-Me$_4$N** with MeOMs and the reaction of **1-Me$_4$N** with MeOTs) are significantly narrower than the reactant parabola associated with the reaction of **1-Me$_4$N** with MeI. In turn, this indicates that the reactant parabola which represents the reaction of **1-Me$_4$N** with MeOTf is wider than the reactant parabola for the reactions of **1-Me$_4$N** with MeOMs and **1-Me$_4$N** with MeOTs. The reactant parabola which represents the reaction of **1-Me$_4$N** with MeOTf is also positioned to the left (as drawn) of the reactant parabola representing the reaction of **1-Me$_4$N** with MeI, similar to what was observed in each of the other two examples shown in section 6.4.4.

As the reactant parabola for the reaction of **1-Me$_4$N** with MeOTf is wider than the corresponding reactions of **1-Me$_4$N** with MeOMs and MeOTs, the similar levels of O-selectivity observed experimentally between each of these reactions may arise as a consequence of the significantly more negative values of $\Delta_r G°$ associated with the O- and C-methylation reactions of **1-Me$_4$N** in a reaction with MeOTf. As demonstrated by the scenario illustrated in Figure 6-4 in section 6.2, a wider reaction parabola should lead to a relative preference towards the more thermodynamically favoured product in instances in which the apices of each parabola lie at the same vertical co-ordinate. The fact that the reactant parabola associated with the reaction of **1-Me$_4$N** with MeOTf is the widest parabola of those constructed for methylation reactions of **1-Me$_4$N** in addition to being the most O-selective indicates that the origin of the O-selectivity in this reaction must relate to the reactant parabola being significantly higher up on the Gibbs energy axis and significantly closer to the O-alkylation product parabola (i.e., moved to the left, as drawn in the diagrams above) than the reactant parabola for the reaction of **1-Me$_4$N** + MeI.

Recall that at present, there is no method of ascribing physical significance to a change in the horizontal co-ordinates of the apex of a given reactant parabola relative to another parabola. It is not possible to predict movements of this nature upon switching from one ethylating agent to another, nor is it possible to comment on why the horizontal co-ordinates of the apex of the reactant parabola are different from one another.

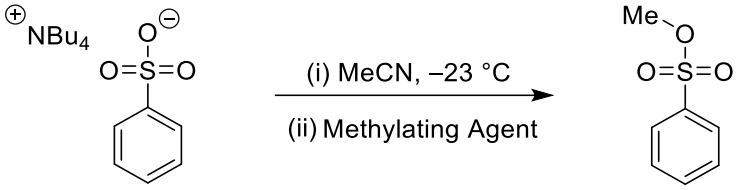
Figure 6-24. The Gibbs energy profile diagram for the reaction of enolate **1-Me$_4$N** with MeI in CD_3CN is overlaid with a reactant parabola which represents the reaction of **1-Me$_4$N** with MeOTf in CD_3CN. The activation barrier positions, and apex height positions are colour coded to allow each reaction to be distinguished from the other.



Approximate values of $\Delta G^{\ddagger}$ associated with the methylation reactions of **1-Me$_4$N** by $[Me_3O]BF_4$ in CD_3CN were calculated by the same approach as described above (i.e., through the use of literature rate data which compares the rates of reaction of various methylating agents). Reactions of $[Me_3O]BF_4$ are included in the rate measurements made by Lewis and Vanderpool in Table 6-15 below.

In the reactions of **56-K** with $[Me_3O]BF_4$ and MeI (see Table 6-14 entries (v) and (iii)) and the reactions of **57-K** with $[Me_3O]BF_4$ and MeI (see Table 6-14 entries (x) and (viii)), the differences in the values of $\Delta G^{\ddagger}$ is calculated to be 21.3 kJ mol^{-1} and 25.1 kJ mol^{-1}, respectively. The work of Kevill and Lin also provides a source of comparison for the values of $\Delta G^{\ddagger}$ associated with the O-methylation of *n*-tetrabutylammonium benzenesulfonate (**60**) with MeOTf and $[Me_3O]BF_4$ in MeCN (see Table 6-15 below).[40]

Table 6-15. Values of *k* for the reactions of *n*-tetrabutylammonium benzenesulfonate (**60**) in MeCN at –23 °C were calculated by Kevill and Lin.[40]



60 **61**

#	Methylating Agent	k (L mol^{-1} s^{-1})	$\Delta G^{\ddagger}$ (kJ mol^{-1})
(i)	MeOTf	6.81×10^{3}	48.9
(ii)	$[Me_3O]BF_4$	7.71×10^{4}	43.8

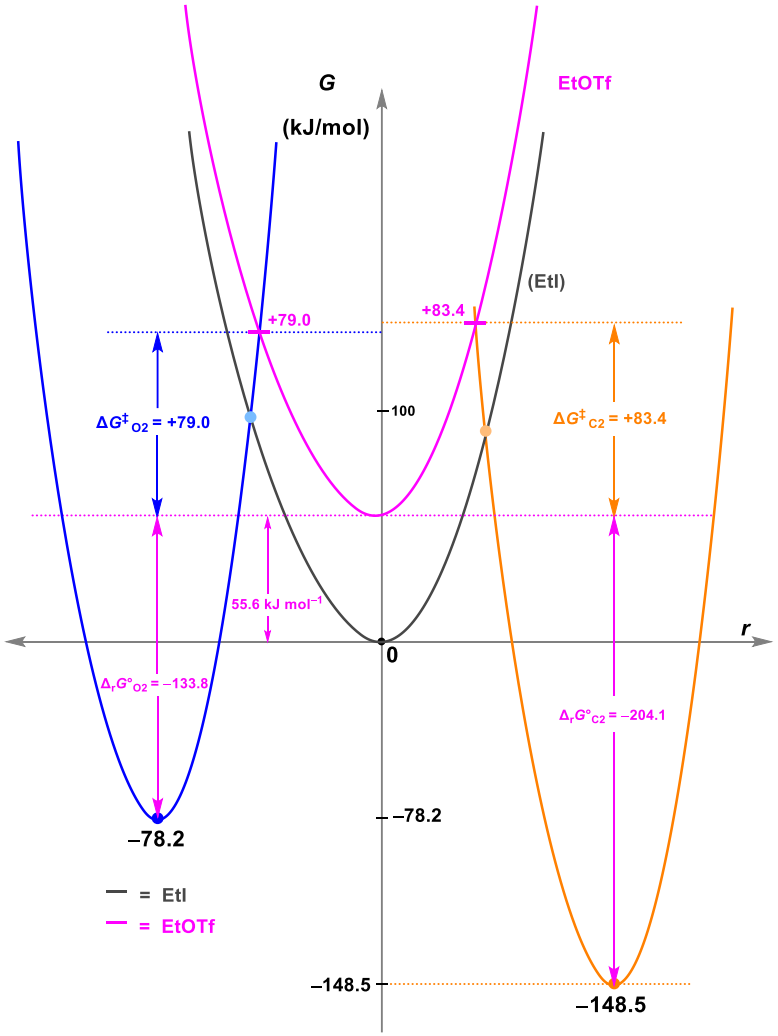
In these reactions, the value of $\Delta G^{\ddagger}$ associated with the methylation of **60** with MeOTf and $[Me_3O]BF_4$ differ by 5.1 kJ mol^{-1}. There are several instances in the literature in which the rates of methylations of nucleophiles by MeOTf and are $[Me_3O]BF_4$ compared, but the nucleophiles employed in many of these studies are uncharged.[40,41] Lewis, Kukes and Slater measure the rates of methylation reactions of an uncharged nucleophile by various methylating agents, and specifically comment on the fact that the relative rates of reaction between MeOTf and $[Me_3O]BF_4$ may change depending on whether the nucleophile is anionic or neutral.[41] The choice was made to use the relative rates of methylation of reactions of MeOTf and $[Me_3O]BF_4$ for anionic nucleophiles in informing the approximate values of $\Delta G^{\ddagger}$ associated with the methylation reactions of **1-Me$_4$N** by $[Me_3O]BF_4$, as enolates are anionic nucleophiles and thus better represented by the anionic substrates shown in Table 6-14 and 6-15.

Using the method of estimation outlined above, the Gibbs energy of activation barrier for the preferred alkylation process of the reaction of **1-Me$_4$N** with $[Me_3O]BF_4$ (i.e., the O-methylation process) may be roughly estimated to be 23 kJ mol^{-1} lower than the $\Delta G^{\ddagger}$ value calculated for the C-alkylation reaction of **1-Me$_4$N** with MeI. However, an estimated value of $\Delta G^{\ddagger}$ associated with the C-methylation reaction of enolate **1-Me$_4$N** with $[Me_3O]BF_4$ in CD_3CN could not be determined due to the exclusive O-methylation which was experimentally observed in that reaction (see Table 6-10 entry (vi)). As no C-alkylation products were formed in the reaction, the difference in Gibbs energy of activation between the processes of O- and C-alkylation cannot be determined through the use of Equation 6.1.

(ii) Ethylation Reactions of Enolate 1-Me_4N

Using the exact speculative method described above to obtain approximate values of $\Delta G^{\ddagger}_{O}$ and $\Delta G^{\ddagger}_{C}$ for reactions for which rates could not be analysed by the method described in section 6.3.3, Gibbs energy profile diagrams were constructed which approximate the reactant parabolas for reactions of EtOTf and $[Et_3O]BF_4$ in reactions with **1-Me_4N** in CD_3CN.

Figure 6-25. The Gibbs energy profile diagram for the reaction of enolate **1-Me_4N** with EtI in CD_3CN is overlaid with a reactant parabola which represents the reaction of **1-Me_4N** with EtOTf in CD_3CN. The activation barrier positions, and apex height positions are colour coded to allow each reaction to be distinguished from the other.



The Gibbs energy of activation barrier for the preferred alkylation process of the reaction of **1-Me_4N** with EtOTf (i.e., the O-methylation process) was roughly estimated to be 13 kJ mol^{-1} lower than the $\Delta G^{\ddagger}$ value calculated for the C-alkylation reaction of **1-Me_4N** with EtI. This estimate is based on the exact same data which was used to approximate the values of $\Delta G^{\ddagger}$ used to allow comparison of the methylation reactions, seen in Table 6-14 (i.e., the approximation is being made that the $\Delta\Delta G^{\ddagger}$ values that would be observed for ethylation reactions are the same as what is observed for methylation reactions). Using the calculated value of $\Delta G^{\ddagger}$ for the C-methylation of enolate **1-Me_4N** by EtI in CD_3CN

of 92.0 kJ mol^{-1} (see Table 6-8 entry (iv)), the value of $\Delta G^{\ddagger}$ associated with the O-methylation of **1-Me$_4$N** by EtOTf in CD_3CN was estimated to be 79.0 kJ mol^{-1}. Using this estimated value of $\Delta G^{\ddagger}$ and the O/C selectivity that was observed in a reaction of enolate **1-Me$_4$N** with EtOTf in CD_3CN (which is 86:14, see Table 6-6 entry (vi)) and Equation 6.1, the value of $\Delta G^{\ddagger}$ associated with the C-ethylation reaction was estimated to be 83.4 kJ mol^{-1}.

Using these estimated values of $\Delta G^{\ddagger}_{O}$ and $\Delta G^{\ddagger}_{C}$, in combination with the calculated values of $\Delta_r G°$ for the reactions of **38** with EtOTf in CD_3CN (see Table 6-5 entry (vi)) in section 6.4.3), an additional approximate Gibbs energy profile diagram may be constructed for the reaction of **1-Me$_4$N** with EtOTf. This speculative Gibbs energy profile diagram is constructed in Figure 6-25, overlaid on top of the Gibbs energy profile diagram for the reaction of **1-Me$_4$N** with EtI in CD_3CN.

The apex of this reactant parabola occurs at a significantly higher vertical position than the corresponding parabola for the reaction of **1-Me$_4$N** with EtI (as a consequence of the values of $\Delta_r G°$ being significantly more negative in the case of the ethylation reactions of **38** employing EtOTf, compare Table 6-5 entries (iv) and (vi)). Additionally, the uniquely defined pink reactant parabola has essentially the exact same curvature as the reactant parabola associated with the reaction of **1-Me$_4$N** with EtI. This is an interesting observation, as these reactions were observed to give opposing levels of selectivity for O- and C-methylation (compare Table 6-6 entries (iv) and (vi)). The approximate reactant parabola representing the reaction of **1-Me$_4$N** with EtOTf (i.e., the pink parabola) is also moved horizontally to the left (as drawn) relative to the black parabola representing the reaction of **1-Me$_4$N** with EtI.

The fact that the reaction of **1-Me$_4$N** with EtOTf gives a similar O/C ratio to the reactions of **1-Me$_4$N** with EtOMs or EtOMs despite having significantly more negative values of $\Delta_r G°$ associated with the O- and C-ethylation reactions can be rationalised by examining the width of the reactant parabola for the reaction of **1-Me$_4$N** with EtOTf. The reactant parabola representing the reaction of **1-Me$_4$N** with EtOTf is wider than the reactant parabolas associated with the reactions of **1-Me$_4$N** with EtOMs or EtOTs, although it is interesting to note that it is of an almost identical width to the reactant parabola representing the reaction of **1-Me$_4$N** with EtI. This example demonstrates the interplay between the various aspects of reactant parabola curvature and position which combine to give the overall selectivity of the reaction in question – a significant difference in the apex heights of two reactant parabola that each represent an ethylation reaction does not necessarily indicate that the expected O/C selectivity between those reactions will be considerably different. In the same vein (when comparing the reactant parabola for the reaction of **1-Me$_4$N** with EtOTf with the reactant parabola for the reaction of **1-Me$_4$N** with EtOTf), the curvature of the parabola is not uniquely determinative of the selectivity of the subsequent reaction. In this instance, the fact that the apex of the reactant parabola representing the reaction of **1-Me$_4$N** with EtOTf is at a higher vertical co-ordinate and moved to the left (as drawn in Figure 6-25) relative to the apex of the reactant parabola

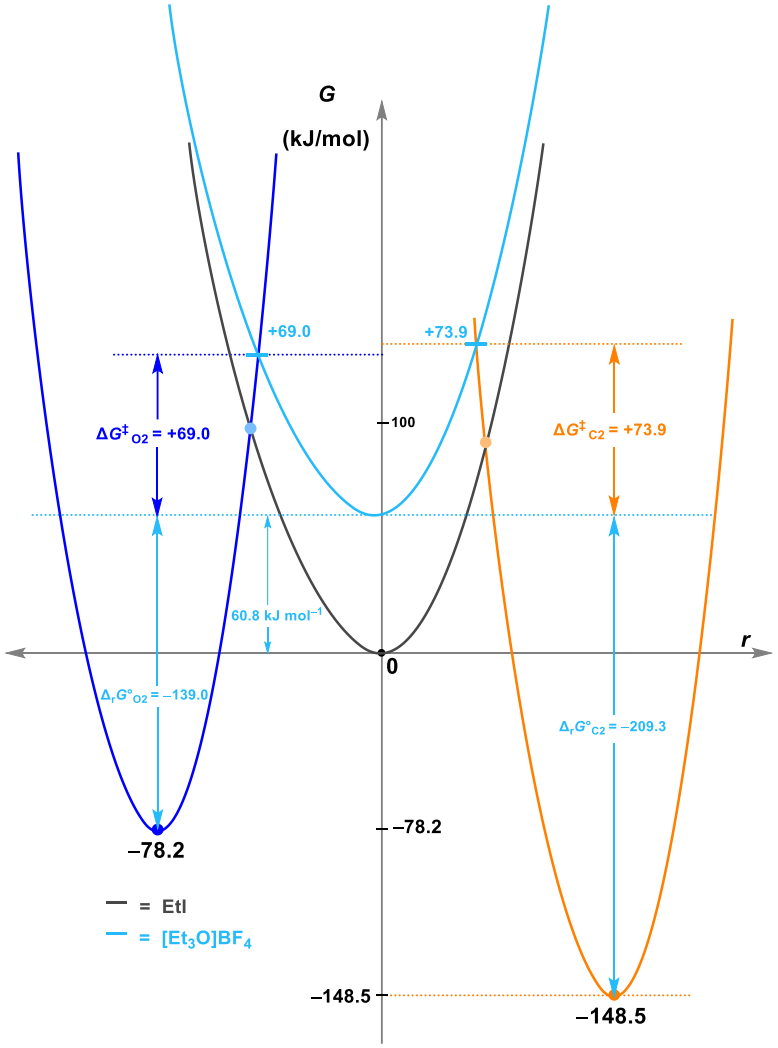
for the reaction of **1-Me$_4$N** with EtI is what leads to the preferential O-ethylation in that reaction.

The Gibbs energy of activation barrier for the preferred alkylation process of the reaction of **1-Me$_4$N** with [Et$_3$O]BF$_4$ (i.e., the O-methylation process) was estimated to be roughly 23 kJ mol^{-1} lower than the $\Delta G^{\ddagger}$ value calculated for the C-alkylation reaction of **1-Me$_4$N** with EtI. This estimate is based on the exact same data which was used to approximate the values of $\Delta G^{\ddagger}$ used to allow comparison of the methylation reactions of MeOTf and [Me$_3$O]BF$_4$, seen in Table 6-14. Using the calculated value of $\Delta G^{\ddagger}$ for the C-ethylation of enolate **1-Me$_4$N** by EtI in CD$_3$CN of 92.0 kJ mol^{-1} (see Table 6-8 entry (iv)), the value of $\Delta G^{\ddagger}$ associated with the O-methylation of **1-Me$_4$N** by [Et$_3$O]BF$_4$ in CD$_3$CN was estimated to be 69.0 kJ mol^{-1}. Using this estimated value of $\Delta G^{\ddagger}$ and the O/C selectivity that was observed in a reaction of enolate **1-Me$_4$N** with [Et$_3$O]BF$_4$ in CD$_3$CN (which is 88:12, see Table 6-6 entry (vi)) and Equation 6.1, the value of $\Delta G^{\ddagger}$ associated with the C-ethylation reaction was estimated to be 73.9 kJ mol^{-1}.

Using these estimated values of $\Delta G^{\ddagger}_{O}$ and $\Delta G^{\ddagger}_{C}$, in combination with the calculated values of $\Delta_r G°$ for the reactions of **38** with [Et$_3$O]BF$_4$ in CD$_3$CN (see Table 6-5 entry (vii)) in section 6.4.3), an additional Gibbs energy profile diagram may be constructed which approximates the diagram which would be observed for a reaction of **1-Me$_4$N** with [Et$_3$O]BF$_4$. This speculative Gibbs energy profile diagram is constructed in Figure 6-26, overlaid on top of the Gibbs energy profile diagram for the reaction of **1-Me$_4$N** with EtI in CD$_3$CN.

The apex of the light blue reactant parabola occurs at a significantly higher vertical position than the corresponding parabola for the reaction of **1-Me$_4$N** with EtI (as the values of $\Delta_r G°$ which were calculated for the reaction of **38** with [Et$_3$O]BF$_4$ were the largest negative values out of those calculated for the ethylation reactions of **38** see Table 6-5 entry (vii)). The light blue reactant parabola is also moved horizontally to the left (as drawn) relative to the black reactant parabola, thereby decreasing the width of the Gibbs energy of activation barrier for the O-methylation process. Additionally, the light blue reactant parabola is broader than the reactant parabola associated with the reaction of **1-Me$_4$N** with EtI. Along with the reactant parabola representing the reaction of **1-Me$_4$N** with EtBr (see Figure 6-18), this parabola is one of only two reactant parabolas which are determined to be broader than the reactant parabola representing the reaction of **1-Me$_4$N** with EtI amongst the Gibbs energy profile diagrams constructed for ethylation reactions of **1-Me$_4$N**. This gives rise to the interesting observation that the reactant parabola associated with the reaction that gives the highest level of C-alkylation (i.e., the black parabola in Figure 6-26) and the reactant parabola associated with the reaction that gives the highest level of O-alkylation (i.e., the light blue parabola in Figure 6-26) are amongst the widest reactant parabola of those constructed to represent the Gibbs energy profile diagrams of ethylation reactions of **1-Me$_4$N**.

Figure 6-26. The Gibbs energy profile diagram for the reaction of enolate **1-Me$_4$N** with EtI in CD_3CN is overlaid with a reactant parabola which represents the reaction of **1-Me$_4$N** with $[Et_3O]BF_4$ in CD_3CN. The activation barrier positions, and apex height positions are colour coded to allow each reaction to be distinguished from the other.



One implication of the scenario originally outlined in Figure 6-4 in section 6.2 (and associated discussion) concerning the width/curvature of the reactant parabola is that for a reactant parabola with its apex as a given value of *G*, the narrower the reactant parabola is, the higher the proportion of the *thermodynamically disfavoured* product that will be formed. Note that this does not indicate that the thermodynamically disfavoured product will be the kinetic product in such a case, only that a parabola that is narrow will predict a selectivity that consists of more of the thermodynamically disfavoured product than a wider parabola. This also indicates that the wider a reactant parabola is, the higher the proportion of thermodynamically favoured product that will be formed. In this context, it is interesting to note that the reactant parabola associated with the reaction of **1-Me$_4$N** with $[Et_3O]BF_4$ is broader than the corresponding reactant parabola representing a reaction of **1-Me$_4$N** with EtI. Hence, this effect should lessen the O-selectivity of a reaction between **1-Me$_4$N** with $[Et_3O]BF_4$. Despite this influence of the width of the parabola on the O/C selectivity, the reaction of **1-Me$_4$N** with $[Et_3O]BF_4$ was observed

experimentally to be considerably O-selective. It is apparent that this high degree of O-selectivity must be brought about as a consequence of a combination of the apex of the reaction parabola for the reaction of **1-Me_4N** with $[Et_3O]BF_4$ being placed at a higher vertical co-ordinate, and the movement of the reactant parabola to the left (as drawn in Figure 6-26) relative to the reactant parabola which represents the reaction of **1-Me_4N** with EtI.

6.6. References

1. Mayr, H.; Breugst, M.; Ofial, A. R. *Angew. Chem. Int. Ed.* **2011**, *50*, 6470–6505.
2. Breugst, M.; Mayr, H. *J. Am. Chem. Soc.* **2010**, *132*, 15380–15389.
3. Breugst, M.; Tokuyasu, T.; Mayr, H. *J. Org. Chem.* **2010**, *75*, 5250–5258.
4. Loos, R.; Kobayashi, S.; Mayr, H. *J. Am. Chem. Soc.* **2003**, *125*, 14126–14132.
5. Sheehy, K. J.; Bateman, L. M.; Flosbach, N. T.; Breugst, M.; Byrne, P. A. *Chem. Sci.* **2020**, *11*, 9630–9647.
6. Plata, R. E.; Singleton, D. A. *J. Am. Chem. Soc.* **2015**, *137*, 3811–3826.
7. Jorner, K.; Tomberg, A.; Bauer, C.; Sköld, C.; Norrby, P.-O. *Nat. Rev. Chem.* **2021**, *5*, 240–255.
8. Chin, Y. P.; See, N. W.; Jenkins, I. D.; Krenske, E. H. *Org. Biomol. Chem.* **2022**, *20*, 2028–2042.
9. Skyner, R. E.; McDonagh, J. L.; Groom, C. R.; Mourik, T. van; Mitchell, J. B. O. *Phys. Chem. Chem. Phys.* **2015**, *17*, 6174–6191.
10. Gorges, J.; Grimme, S.; Hansen, A.; Pracht, P. *Phys. Chem. Chem. Phys.* **2022**, *24*, 12249–12259.
11. Houk, K. N.; Liu, F. *Acc. Chem. Res.* **2017**, *50*, 539–543.
12. Takano, Y.; Houk, K. N. *J. Chem. Theory Comput.* **2005**, *1*, 70–77.
13. Nagaoka, M.; Okuyama-Yoshida, N.; Yamabe, T. *J. Phys. Chem. A* **1998**, *102*, 8202–8208.
14. Ho, J.; Klamt, A.; Coote, M. L. *J. Phys. Chem. A* **2010**, *114*, 13442–13444.
15. Garza, A. J. *J. Chem. Theory Comput.* **2019**, *15*, 3204–3214.
16. Conquest, O. J.; Roman, T.; Marianov, A.; Kochubei, A.; Jiang, Y.; Stampfl, C. *J. Chem. Theory Comput.* **2021**, *17*, 7753–7771.
17. Grimme, S.; Schreiner, P. R. *Angew. Chem. Int. Ed.* **2018**, *57*, 4170–4176.
18. Woodward, R. B.; Baer, H. *J. Am. Chem. Soc.* **1944**, *66*, 645–649.
19. Hare, S. R.; Tantillo, D. J. *Beilstein J. Org. Chem.* **2016**, *12*, 377–390.
20. Tantillo, D. J. *J. Am. Chem. Soc.* **2022**, *144*, 13996–14004.
21. Kurts, A. L.; Genkina, N. K.; Macias, A.; Beletskaya, L. P.; Reutov, O. A. *Tetrahedron* **1971**, *27*, 4777–4785.
22. Breugst, M.; Zipse, H.; Guthrie, J. P.; Mayr, H. *Angew. Chem. Int. Ed.* **2010**, *49*, 5165–5169.
23. Jones, M. E.; Kass, S. R.; Filley, J.; Barkley, R. M.; Ellison, G. B. *J. Am. Chem. Soc.* **1985**, *107*, 109–115.
24. Lee, I.; Park, H. Y.; Han, I.-S.; Kim, C. K.; Kim, C. K.; Lee, B.-S. *Bull. Korean Chem. Soc.* **1999**, *20*, 559–566.
25. Houk, K. N.; Paddon-Row, M. N. *J. Am. Chem. Soc.* **1986**, *108*, 2659–2662.
26. Byrne, P. A.; Karaghiosoff, K.; Mayr, H. *J. Am. Chem. Soc.* **2016**, *138*, 11272–11281.
27. Maji, B.; Mayr, H. *Angew. Chem. Int. Ed.* **2013**, *52*, 11163–11167.
28. Heiszwolf, G. J.; Kloosterziel, H. *Recl. Trav. Chim. Pays-Bas* **1970**, *89*, 1153–1169.
29. Miller, B.; Margulies, H.; Drabb, T.; Wayne, R. *Tetrahedron Lett.* **1970**, *11*, 3805–3808.
30. Marenich, A. V.; Cramer, C. J.; Truhlar, D. G. *J. Phys. Chem. B* **2009**, *113*, 6378–6396.
31. Arnett, E. M.; Reich, R. *J. Am. Chem. Soc.* **1980**, *102*, 5892–5902.
32. Mayr, H.; Ammer, J.; Baidya, M.; Maji, B.; Nigst, T. A.; Ofial, A. R.; Singer, T. *J. Am. Chem. Soc.* **2015**, *137*, 2580–2599.

33. Reddy, S. R.; Manikyamba, P. *J. Chem. Sci.* **2006**, *118*, 257–260.
34. Kondo, Y.; Uematsu, R.; Nakamura, Y.; Kusabayashi, S. *J. Chem. Soc. Perkin Trans. 2* **1988**, No. 7, 1219–1224.
35. Mayr, H.; Ofial, A. R. *J. Phys. Org. Chem.* **2008**, *21*, 584–595.
36. Mayr, H.; Ofial, A. R. *Pure Appl. Chem.* **2005**, *77*, 1807–1821.
37. Lucius, R.; Loos, R.; Mayr, H. *Angew. Chem. Int. Ed.* **2002**, *41*, 91–95.
38. Nigst, T. A.; Ammer, J.; Mayr, H. *J. Phys. Chem. A* **2012**, *116*, 8494–8499.
39. Lewis, E. S.; Vanderpool, S. H. *J. Am. Chem. Soc.* **1978**, *100*, 6421–6424.
40. Kevill, D. N.; Lin, G. M. L. *Tetrahedron Lett.* **1978**, *19*, 949–952.
41. Lewis, E. S.; Kukes, S.; Slater, C. D. *J. Am. Chem. Soc.* **1980**, *102*, 303–306.

Chapter 7: Experimental for Development of Novel Model

Table of Contents

7.1. General Experimental **422**

7.2. Reactions of 1-Me_4N with Various Alkylating Agents in CD_3CN **428**

7.2.1. Reactions of **1-Me_4N** with Various Methylating Agents in CD_3CN 428

7.2.2. Reactions of **1-Me_4N** with Various Ethylating Agents in CD_3CN 438

7.3. Determination of $\Delta G^{\ddagger}$ Values for Reactions of DMAP + Various Electrophiles in CD_3CN **447**

7.4. Competition Experiments Between Enolate 1-Me_4N and DMAP with Various Electrophiles in CD_3CN at 20 °C **475**

7.4.1. Control Experiment to Establish the Irreversibility of Formation of DMAP (**46**) Alkylation Products 475

7.4.2. Reactions Experiments Between Enolate 1-Me_4N and DMAP with Ethylating Agents in CD_3CN at 20 °C 477

7.5. References **506**

Appendices referred to in the text are available at the following link:

https://tinyurl.com/KSheehyPhDThesisAppendices

7.1. General Experimental

Commercial 1,3-diketones, bases and alkylating agents were obtained from Fluorochem, Sigma-Aldrich and Alfa Aesar.

CH_2Cl_2, $CDCl_3$, CD_3CN, $(CH_3)_2SO$, $(CD_3)_2SO$ and THF were dried over activated 3 Å molecular sieves and stored under an atmosphere of nitrogen in flasks with grease-free J. Young's valves.[1] CH_3CN was dried over activated 4 Å molecular sieves and stored in the same fashion. Molecular sieves (10 weight percent per unit volume of compound to be dried, 20 weight percent was used when drying THF) were activated by flame drying in the storage flask(s) for 5 – 10 minutes (depending on quantity of sieves to be dried).[1] After flame-drying, the storage flask was immediately connected to a Schlenk line, subjected to vacuum (between 2 and 5×10^{-3} mbar), and allowed to stand until the sieves had cooled. The flask was then subjected to several vacuum/refill cycles to establish a nitrogen atmosphere inside, and the solvent/compound to be dried was then added by cannula transfer directly from a Winchester bottle which was sealed using a rubber septum (sized for a B29 ground glass socket joint).

Solvents that were used in relative bulk (MeCN, CH_2Cl_2, THF) were stored in a specialised flask with two J. Young's valves, one of which was modified to facilitate easy access of a needle to the body of the flask through the side-arm of the valve. When accessing the dry solvent, the angled side-arm was sealed with a rubber septum, and the small volume contained between the septum and the sealed J. Young's valve was flushed with a stream of nitrogen gas for a minimum of five minutes prior to opening the valve. The solvent required several days after commencing drying to reach maximal dryness (< 10 ppm H_2O according to analysis by Karl Fischer titration), but was dry enough for most purposes after one day. MeCN and THF stored in this manner was found to retain water contents of less than 10 ppm for more than one year.

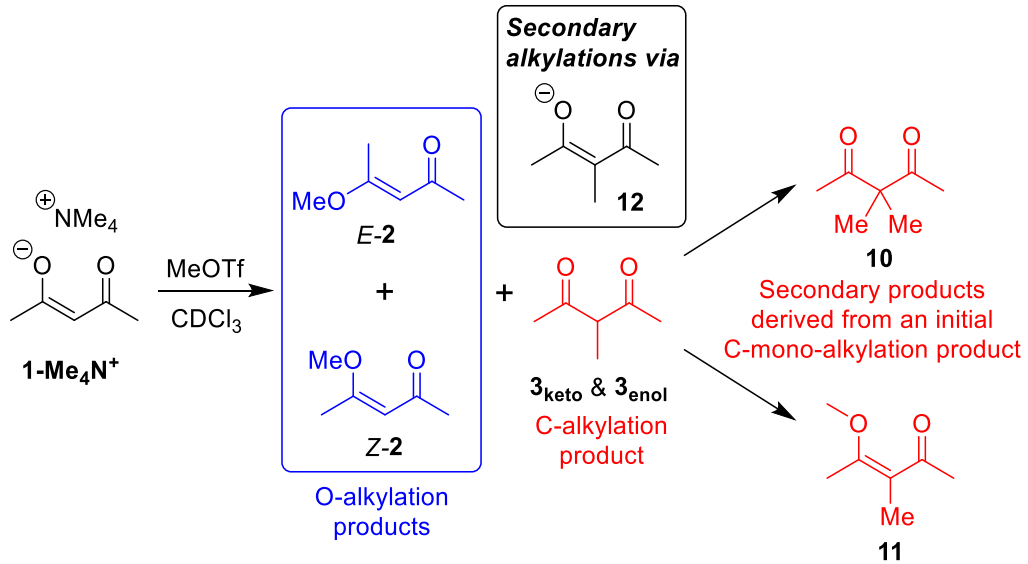
For all reactions conducted using Schlenk glassware, the Schlenk flask was dried in an oven, then attached to vacuum *via* Schlenk manifold and placed under vacuum ($\leq 5 \times 10^{-3}$ mbar). The flask was then filled with nitrogen gas by the pump and fill technique (three repeats of the following cycle: evacuation to $\leq 5 \times 10^{-3}$ mbar, re-fill with nitrogen gas).[2] Solids and reagents were then introduced to the flasks under fast nitrogen flow.

NMR spectra were recorded on Bruker Avance III 600, Bruker Avance I 400 and Bruker Avance III 300 NMR spectrometers, in proton coupled mode using tetramethysilane (TMS) as the internal chemical shift reference standard. Proton NMR spectra (proton coupled mode, 600 MHz, 400 MHz and 300 MHz respectively) and ^{13}C NMR spectra (proton decoupled mode; 150 MHz, 100 MHz and 75 MHz, respectively) were acquired at 300 K on the 300 MHz instrument and 293 K on the 400 MHz and 600 MHz instruments. All spectra were run at University College Cork. Proton spectra acquired in regular non-deuterated solvents were acquired using the Bruker NOESY presat (noesygppr) water suppression pulse sequence. Chemical shifts (δ) are expressed as parts per million (ppm), positive shift being downfield from TMS;

coupling constants (*J*) are expressed in Hertz (Hz). Splitting patterns in ^{1}H-NMR spectra are designated as: s (singlet), bs (broad singlet), d (doublet), dd (doublet of doublets), ddd (doublet of doublets of doublets), t (triplet), td (triplet of doublets), q (quartet), quin (quintet) and m (multiplet).

Assignment of O vs C Ratios

For each reaction of an enolate with an alkylating agent, the selectivity between O-alkylation and C-alkylation of the enolate (the O/C ratio) was determined by comparing the integrations of various signals seen in the ^{1}H NMR spectra of the crude product mixtures. The signals employed for comparison were required to be adequately baseline separated to ensure accurate integration values. Integrations were only used for the purpose of the ratio calculation if they were associated with signals that could be unambiguously attributed to one of the 6 possible alkylation products. Note that of the 6 possible products, there are a pair of isomers and a pair of tautomers. The O-alkylation products may form as *E*- or *Z*- isomers (compounds *E*-**2** and *Z*-**2** in Scheme 7-1 below) and the C-mono-alkylated product may exist as the keto or enol tautomer (**3**$_{keto}$ and **3**$_{enol}$ in Scheme 7-1 below). The assignments were made in conjunction with reference to literature NMR values of various alkylation products. Of the 6 possible products of each reaction, only the O-mono-methylated products (the *E*- and *Z*-enol ethers) were considered as the "O" portion of the ratio, i.e., to obtain the O/C ratio, the integrations of the signals of the O-mono-alkylation products (products *E*-**2** and *Z*-**2** in Scheme 7-1) were compared to the sum of the integrations of the 4 other products (**3**$_{keto}$, **3**$_{enol}$,**10** and **11**). This is explained by Scheme 7-1, which shows that the C-di-alkylated product **10** and the O/C mixed di-alkylation product **11** are formed from an initial C-alkylation product.



Scheme 7-1: Alkylation of **1-Me$_4$N**. O-alkylation may result in formation of the *E*-enol ether (*E*-**2**) or the *Z*-enol ether (*Z*-**2**). C-alkylation may result in the keto- and enol- tautomers of compound **3** existing in an equilibrium. Di-alkylation products **10** and **11** are derived from C-mono-alkylation product **3**.

Although the formation of **11** (the product which initially undergoes alkylation at the C-position, and then undergoes a subsequent O-alkylation) is possible in principle,

signals of this product are not observed in any of the spectra in this chapter. This phenomenon is observed in reactions of **1-Me$_4$N** with all electrophiles, and as a result, the structure of the O/C mixed dialkylation product is omitted from the schemes used to describe each reaction.

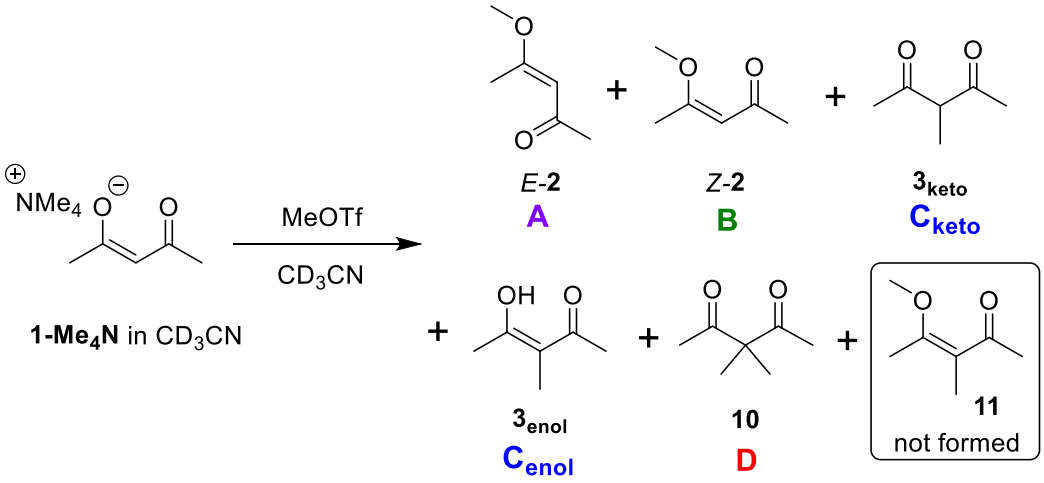
The percentages of O-alkylation and C-alkylation, respectively, are given by Equations 7-1 and 7-2 shown below:

$$\text{Percentage of O-alkylation} = \frac{[E\text{-}\mathbf{2}]+[Z\text{-}\mathbf{2}]}{[E\text{-}\mathbf{2}]+[Z\text{-}\mathbf{2}]+[\mathbf{3_{keto}}]+[\mathbf{3_{enol}}]+[\mathbf{10}]} \times 100 \qquad (7\text{-}1)$$

$$\text{Percentage of C-alkylation} = \frac{[\mathbf{3_{keto}}]+[\mathbf{3_{enol}}]+[\mathbf{10}]}{[E\text{-}\mathbf{2}]+[Z\text{-}\mathbf{2}]+[\mathbf{3_{keto}}]+[\mathbf{3_{enol}}]+[\mathbf{10}]} \times 100 \qquad (7\text{-}2)$$

where [**Y**] is the concentration in mol L^{-1} of compound **Y** (i.e., where **Y** = *E*-**2**, *Z*-**2**, **3**$_{keto}$, **3**$_{enol}$ or **10**). In the calculations of the O/C ratios, the integrations of compounds *E*-**2**, *Z*-**2**, **3**$_{keto}$, **3**$_{enol}$ or **10** are substituted directly in place of the molar concentrations in the above equations.

An example of an O vs C assignment for a crude product mixture from the reaction in Scheme 7-2 is shown in Figure 7-1. The spectrum was produced from a reaction using Procedure A below (see page 431) with the tetramethylammonium enolate of acetylacetone (**1-Me$_4$N**) and methyl triflate in CD_3CN.



Scheme 7-2: Reaction of enolate **1-Me$_4$N** (the tetramethylammonium enolate of acetylacetone) with methyl triflate in CD_3CN. Details on how the enolate **1-Me$_4$N** was synthesised may be found in section 7.2 below. The coloured labels in the diagram enable identification of each compound in Figure 7-1 and 7-2 below.

Possible products of the reaction include the O-alkylation products *E*-**2** (the *E*-enol ether) and *Z*-**2** (the *Z*-enol ether). C-alkylation products **3**$_{keto}$, **3**$_{enol}$, **10** and **11** may also form in these conditions (see Scheme 7-2 above). The section of the crude ^{1}H NMR spectrum showing the relevant signals is shown in Figure 7-1 below. Comparisons of the chemical shifts and relative integrations of the signals present with those of values reported in the literature allow the signals at 5.62 (s, 1H), 3.66 (s, 3H) and 2.23 (s, 3H) to be assigned to *E*-**2**, the *E*-enol ether isomer of the O-mono-alkylation product. Another 3H singlet signal associated with this product should be visible at

approximately 2.12 ppm, however, this signal is partially obscured by signals from other products. The signals at 5.07 (s, 1H), 2.21 (s, 3H), 2.06 (s, 3H) are assigned to *Z*-**2**, the *Z*-enol ether isomer of the O-mono-alkylation product. The signals at 2.17 (s, 6H) and 1.23 (d, J = 7.1 Hz, 3H) are assigned to the keto form of the C-mono-alkylation product, $\mathbf{3}_{\mathbf{keto}}$. The signal at 1.84 (s, 3H) is assigned to the enol form of the C-mono-alkylation product, $\mathbf{3}_{\mathbf{enol}}$. The signal at 1.32 (s, 6H) is assigned to the C-di-alkylation product, **10**. Apart from those explicitly mentioned above, no other distinctive baseline-separated signals can be observed for any of these products, as they are overlapping with the signals of other products. No distinctive NMR signals of the O/C mixed di-alkylation product **11**, which could form *via* initial C-alkylation – see above) can be seen in the spectrum of the reaction mixture. No analogous O/C mixed di-alkylation products are observed in any of the spectra in this section, and as such are not represented in the schemes used to describe these reactions.

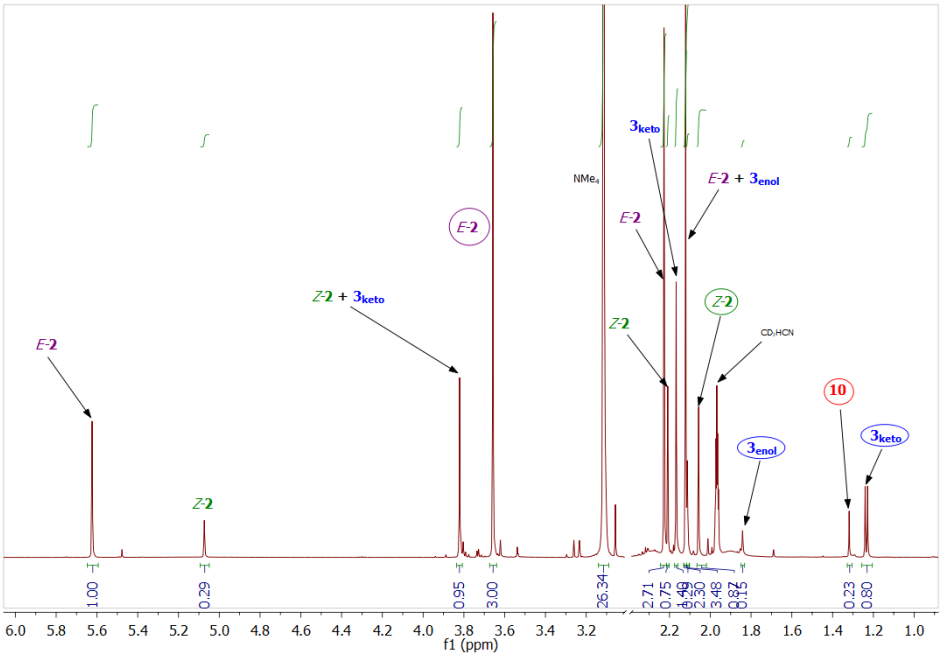


Figure 7-1: ^{1}H NMR spectrum of crude reaction mixture obtained from the reaction of **1-Me$_4$N** with methyl triflate in CD_3CN.

Based on the ^{1}H NMR spectral data given above, the integrations (relative to *E*-**2**) of 1H each of O- and C-alkylation products *E*-**2**, *Z*-**2**, $\mathbf{3}_{\mathbf{keto}}$, $\mathbf{3}_{\mathbf{enol}}$ and **10** is:

$$I_{E-\mathbf{2}} = \frac{3.00}{3} = 1.00; \quad I_{Z-\mathbf{2}} = \frac{0.87}{3} = 0.29;$$

$$I_{\mathbf{3}_{\mathbf{keto}}} = \frac{0.80}{3} = 0.26; \quad I_{\mathbf{3}_{\mathbf{enol}}} = \frac{0.15}{3} = 0.05; \quad I_{\mathbf{10}} = \frac{0.23}{6} = 0.0383$$

where $I_{\mathbf{X}}$ is the integration of 1H of compound **X** (**X** = *E*-**2**, *Z*-**2**, $\mathbf{3}_{\mathbf{keto}}$, $\mathbf{3}_{\mathbf{enol}}$ or **10**) relative to 1H of *E*-**2**.

Note that the integration values of the signals associated with compounds *E*-**2,** *Z*-**2**, $\mathbf{3}_{\mathbf{keto}}$, and $\mathbf{3}_{\mathbf{enol}}$ are divided by 3 as they represent 3H signals. The integration value of the signal associated with compound **10** is divided by 6 as it represents a 6H signal. The relative integration of each compound is proportional to its relative concentration (mol L^{-1}), i.e., $[\mathbf{X}] \propto I_{\mathbf{X}}$, and hence the relative integrations can be used to determine

the relative proportions of O- and C-alkylation products formed in the reaction. Hence the percentage of O-alkylation is given by:

$$\text{Percentage of O-alkylation} = \frac{I_{E\text{-}2} + I_{Z\text{-}2}}{I_{E\text{-}2} + I_{Z\text{-}2} + I_{3_{\text{keto}}} + I_{3_{\text{enol}}} + I_{10}} \times 100$$

$$\text{Percentage of O-alkylation} = \frac{1.00 + 0.29}{1.00 + 0.29 + 0.26 + 0.05 + 0.0383} \times 100 = 79\%$$

Integrations give an O vs C ratio of 79:21.

Note that there are baseline separated signals of the *E*-enol ether (*E*-**2**) and the *Z*-enol ether (*Z*-**2**) in Figure 7-1 at 5.62 and 5.07 ppm respectively that are not used in the calculation to determine the O/C ratio. The signals of vinyl protons of O-alkylation products are never used in these calculations as they are often affected by H/D exchange from the deuterated reaction solvent. This effect is more pronounced when $CDCl_3$ is the reaction solvent – an example of this may be seen below in the spectrum of the reaction of **1-Me$_4$N** with methyl triflate in $CDCl_3$ (Figure 7-2).

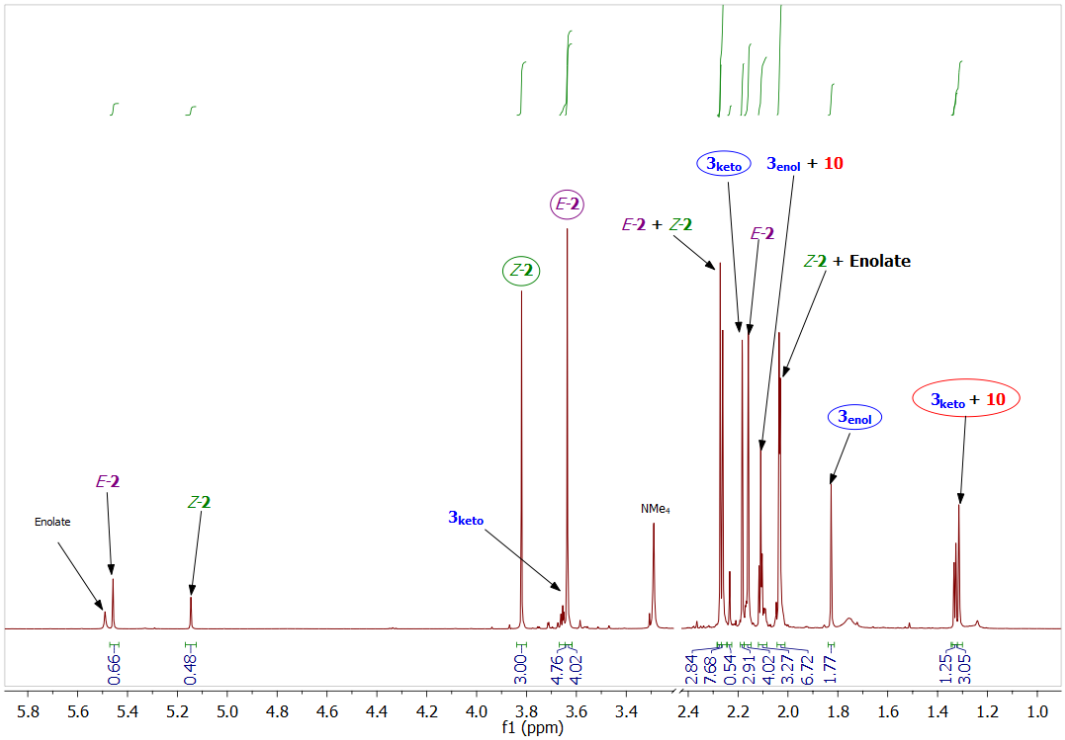


Figure 7-2: ^{1}H NMR spectrum of crude reaction mixture obtained from the reaction of **1-Me$_4$N** with methyl triflate in $CDCl_3$. The signals of the vinyl protons (at 5.46 ppm and 5.15 ppm) are undersized compared to the 3H methoxy signals of the same compounds (at 3.64 ppm and 3.82 ppm, respectively).

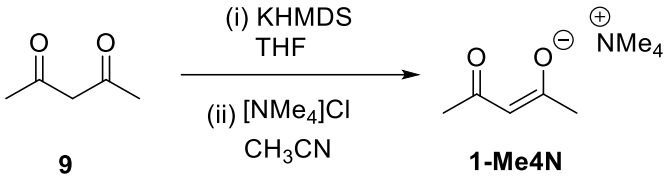
The vinyl proton signal of the *E*-enol ether (*E*-**2**) at 5.46 ppm is undersized compared to the signal of the methoxy protons at 3.64 ppm. The same is true for the vinyl proton signal of the *Z*-enol ether (*Z*-**2**) at 5.15 ppm, which is undersized compared to the signal of the methoxy protons at 3.82 ppm. If the signals at 5.46 ppm and 5.15 ppm were used in the calculation of the O/C ratio, the proportion of O-alkylation products present in the reaction mixture would be underrepresented. An identical effect is observed when

the signal associated with the α-proton of C-mono-alkylation products (e.g., see compound **3$_{keto}$** in Scheme 7-2) is integrated. This is demonstrated by the signal at 3.66 ppm (overlaps with a signal of *E*-**2**) in Figure 7-2, which is significantly undersized compared to other signals of this compound. For this reason, none of the vinyl proton signals in enol ether compounds or α-proton signals of C-mono-alkylation products are used in determining the O/C ratio. Although the example shown above is taken from a reaction of **1-Me$_4$N** in $CDCl_3$, this issue also effects the reactions of **1-Me$_4$N** with alkylating agents in CD_3CN that are shown in sections 7.2 and 7.4 below, and thus these signals are never used in the calculation of O/C ratios in this chapter.

7.2. Reactions of 1-Me_4N with Various Alkylating Agents in CD_3CN

7.2.1. Reactions of 1-Me_4N with Various Methylating Agents in CD_3CN

(i) Synthesis of the Tetramethylammonium Enolate of 2,4-Pentanedione



9 **1-Me4N**

Note: All operations in the following procedure were conducted under an atmosphere of nitrogen gas.

2,4-pentanedione (**9**) (0.662 g, 6.61 mmol) was dissolved in THF (4 ml). KHMDS (1.20 g, 6.02 mmol) was dissolved in THF (16 ml) in a Schlenk flask with a cone-shaped ground glass joint. The dione solution was added to the KHMDS solution dropwise at room temp over *ca.* 1 hr. The dione flask was washed out with separate 3 ml and 2 ml portions of THF. The washings were transferred to the reaction mixture. A white solid suspended in a pale yellow liquid resulted. This was stirred overnight, then the Schlenk flask with a cone-shaped ground glass joint was fitted with a Schlenk filtration apparatus, and mixture was filtered. The residual solid in the Schlenk flask with a cone-shaped ground glass joint was rinsed with THF into the filter stick and onto the frit. The solid was washed with three portions of THF (3 × 3 ml). The solvent was pushed through the frit the using nitrogen pressure. The flask containing the filtrate was removed, and an empty Schlenk flask (with nitrogen atmosphere *via* connection to Schlenk manifold) was fitted. The solid in the Schlenk filtration apparatus was dried under vacuum before being sealed and transferred into a glove box containing a nitrogen atmosphere. The solid potassium enolate (0.563 g, 4.07 mmol, 68%) was transferred from the Schlenk filtration apparatus into a Schlenk flask with a cone-shaped ground glass joint, and tetramethylammonium chloride (0.446 g, 4.07 mmol) was also added. The Schlenk flask with a cone-shaped ground glass joint was sealed using a ground glass socket joint fitted with a stopcock. The ground glass joint was secured with a Keck clamp. This flask was removed from the glove box and fitted to nitrogen supply *via* the second stopcock. The side arm of the Schlenk flask was fitted with a rubber septum, and the space between the septum and the closed stopcock was flushed with nitrogen, and then the stopcock was opened. Dry CH_3CN (20 ml) was added, and the mixture was stirred for a week. Neither solid appeared to dissolve, but after stirring for a week, the appearance of the mixture had changed, and the solid present was much finer (KCl). This mixture was filtered through a Schlenk filtration apparatus as above to remove undissolved KCl and unreacted potassium enolate. The solids were collected on the frit of the Schlenk filtration apparatus and washed twice with CH_3CN (2 × 3 ml). The combined filtrate was concentrated under vacuum using a 2nd trap between the reaction mixture and the Schlenk line, yielding a yellow/brown solid (0.632 g, 3.65 mmol, 90 %). The ^{1}H NMR spectrum showed the solid to be the Me_4N enolate of 2,4-pentanedione (**1-Me_4N**).

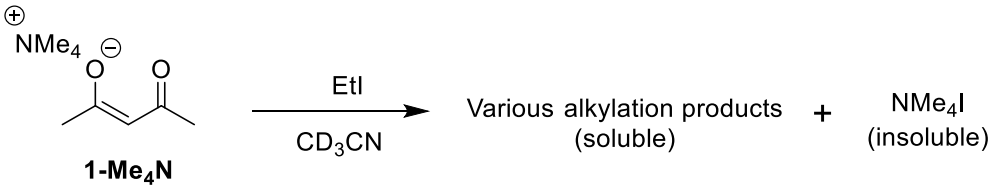
^{1}H NMR (300 MHz, $CDCl_3$) δ 3.29 (s, 12H), 2.15 (s, 1H), 1.91 (bs, 6H).

Note: The product was extremely hygroscopic and was stored in a glove box.

General Procedure A: Alkylation of the Tetramethylammonium Enolate of Acetylacetone in CD_3CN and $CDCl_3$

The following procedure (Procedure A) was used to establish the ratios of products formed by the reaction of the tetramethylammonium enolate of acetylacetone and an electrophile in CD_3CN or $CDCl_3$:

The tetramethylammonium enolate of acetylacetone (1.0 equivalent) was added to a Schlenk flask in the glovebox under nitrogen. This flask was removed from the glove box and attached to a Schlenk manifold. Dry CD_3CN or $CDCl_3$ (0.85 ml) was added to the flask. The alkylating agent (0.8 equivalents) was then introduced to the flask dropwise with stirring (solid alkylating agents were dissolved in a minimal amount of CD_3CN or $CDCl_3$ before addition). The flask was then sealed and the mixture was allowed to stir for 18 hours at 20 °C. After 18 hours, a small amount of solid generally has formed in the flask (the salt by-product created in the reaction – for example a reaction of **1-Me_4N** and ethyl iodide produces tetramethylammonium iodide as a by-product).



1-Me_4N

An empty NMR tube was placed in a long Schlenk tube. The long Schlenk tube, containing the NMR tube, was evacuated and re-filled with nitrogen ≥ 3 times, creating an inert atmosphere inside the flask. The entire reaction mixture was drawn into a syringe through a needle. A syringe filter was quickly fitted between the needle and the syringe. The reaction mixture was passed through the syringe filter into the NMR tube under nitrogen. The NMR tube was then sealed by a rubber septum cap. After fitting the rubber septum to the NMR tube, the seal was secured by wrapping the external edge of the septum where it contacted the surface of the NMR tube with PTFE tape. The outside of the PTFE tape and rubber septum were then wrapped with a layer of Parafilm to further secure the nitrogen atmosphere inside the NMR tube. The NMR tube was then transferred to the NMR spectrometer and ^{1}H NMR spectra were recorded.

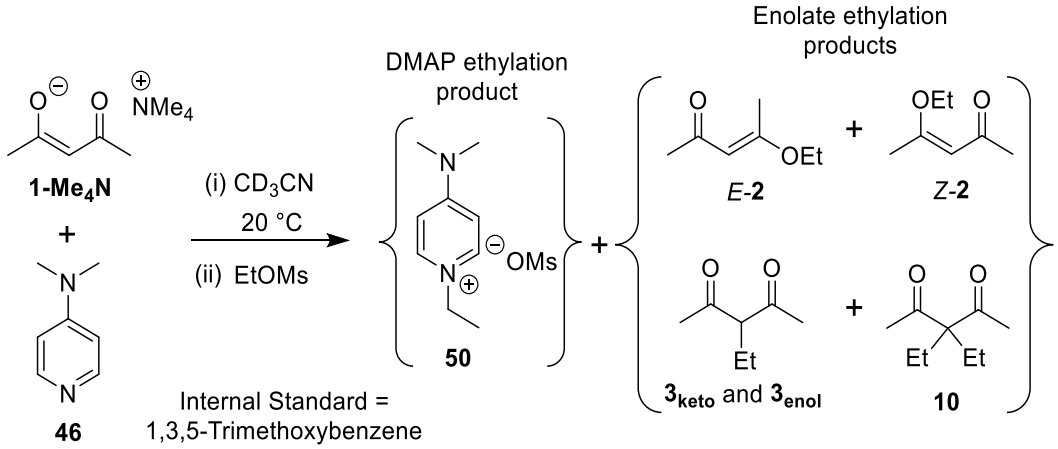
Note: All masses recorded in experiments employing this general procedure were recorded using analytical balances which were accurate to five decimal places, and hence the masses are reported as accurate to four decimal places. The exception to this standard is reagents which were weighed in a glovebox, which are reported as accurate to three decimal places. Only the tetramethylammonium enolate of acetylacetone (**1-Me_4N**) and trimethyloxonium tetrafluoroborate ($[Me_3O]BF_4$) were weighed in a glovebox in experiments using this general procedure.

Note: The solid produced in the reaction in some instances was allowed to remain in the flask without being filtered using a syringe filter. The solid was then dissolved in

DMSO-d_6 and examined by ^{1}H NMR spectroscopy to ensure that no organic material (i.e., a potential product of the enolate reaction) was contained within the solid. Certain experiments of this type utilised a stock solution of the tetramethylammonium enolate of acetylacetone in CD_3CN rather than solid enolate weighed out in a glovebox. Such experiments can be identified in the descriptions below by the inclusion of a value for the molarity of the enolate stock solution.

Note: The stock solutions of the tetramethylammonium enolate of acetylacetone in CD_3CN were always stored in a J. Young's flask under an atmosphere of nitrogen. Despite this precaution, decomposition of the enolate solution occurred over time (approximately 1 week). Decomposition of the enolate in the stock solution is believed to be the source of the ethyl acetate signals which may be seen in the spectra of some of the reactions below. The presence of ethyl acetate in the reaction mixtures was confirmed through the analysis of ^{13}C and 2D NMR spectra. Ethyl acetate formation was only observed in reactions which employed ethylating agents. It is possible that methyl acetate formation has occurred in reactions which used methylating agents. The process by which the ethyl acetate forms is as yet undetermined. It was minimised in relevant experiments by only using stock solutions in reactions immediately after the stock solution was prepared. Despite these precautions, small signals resulting from the presence of ethyl acetate are present in the ^{1}H NMR spectra of some of the reaction mixtures in which ethylating agents were employed (see below).

The presence of ethyl acetate in spectra of experiments which employed stock solutions of the tetramethylammonium enolate of acetylacetone in CD_3CN was confirmed by a "spike" experiment, where a drop of ethyl acetate was added to a reaction mixture in which ethyl acetate was deemed to have formed. An example of such a "spike" experiment is shown below.



Scheme 7-3: Competition reaction of enolate **1-Me$_4$N** (the tetramethylammonium enolate of acetylacetone) and DMAP with ethyl mesylate in CD_3CN. Formation of ethyl acetate was observed in this reaction and confirmed by an ethyl acetate "spike" experiment.

Shown below in Figure 7-3 is the ^{1}H NMR spectrum of the reaction mixture described in Scheme 7-3. All signals shown below can be accounted for when considering the starting materials and the expected products, with the exception of the ^{1}H NMR signals of EtOAc at δ 4.08 ppm and 1.23 ppm.[3]

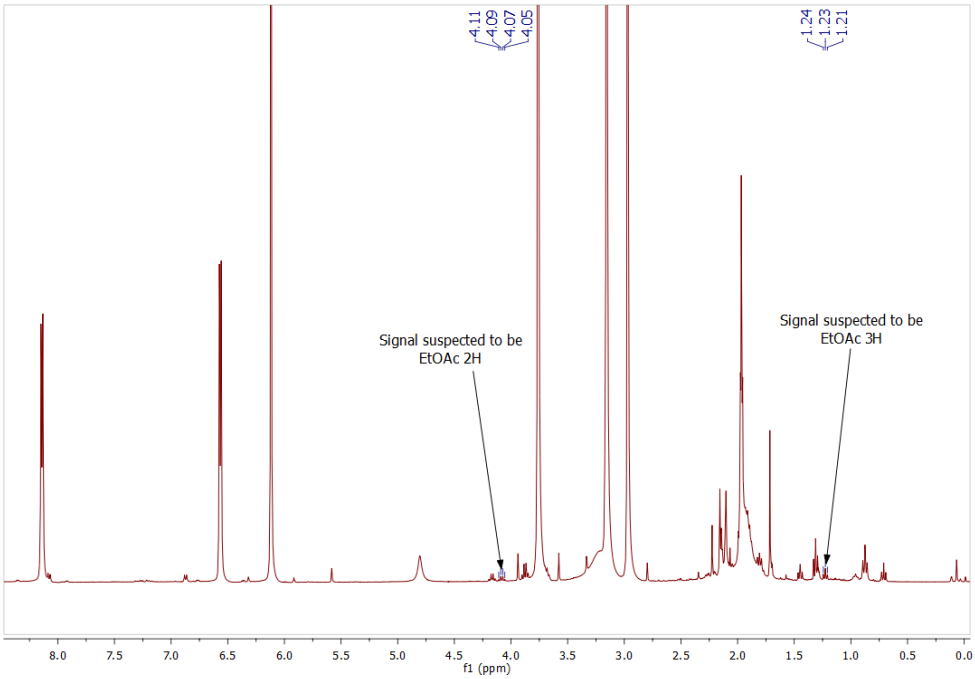


Figure 7-3: ^{1}H NMR spectrum of crude reaction mixture obtained from the reaction shown in Scheme 7-3. Unknown signals, believed to be present as a result of ethyl acetate synthesis in the reaction, are seen at δ 4.08 ppm and 1.23 ppm.

The signals in question increased in size when a drop of ethyl acetate was added, indicating that ethyl acetate had indeed formed in the reaction mixture. The ^{1}H NMR spectrum obtained after a drop of ethyl acetate was added to the reaction mixture is shown below in Figure 7-4.

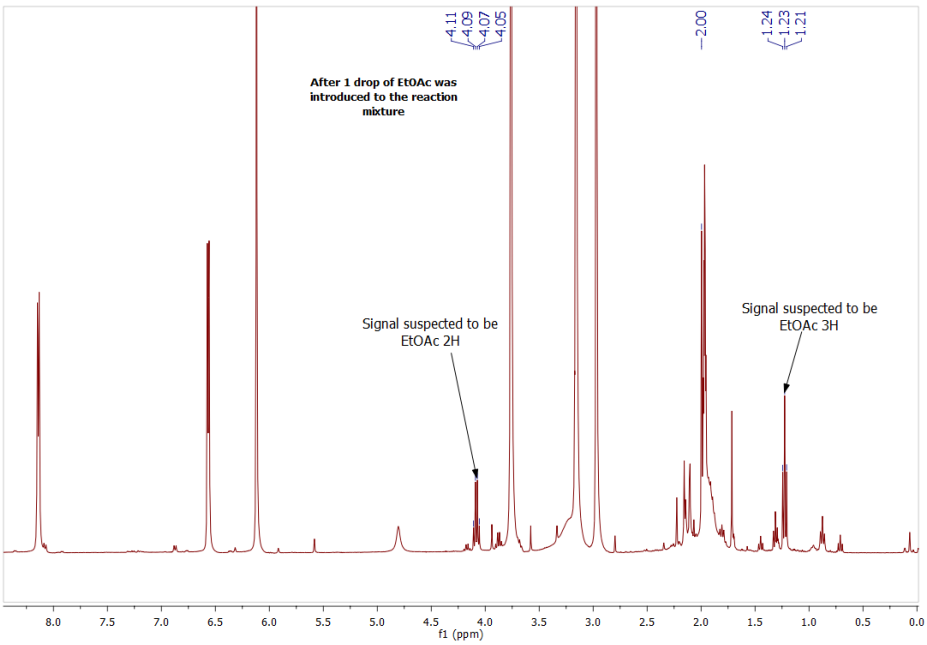
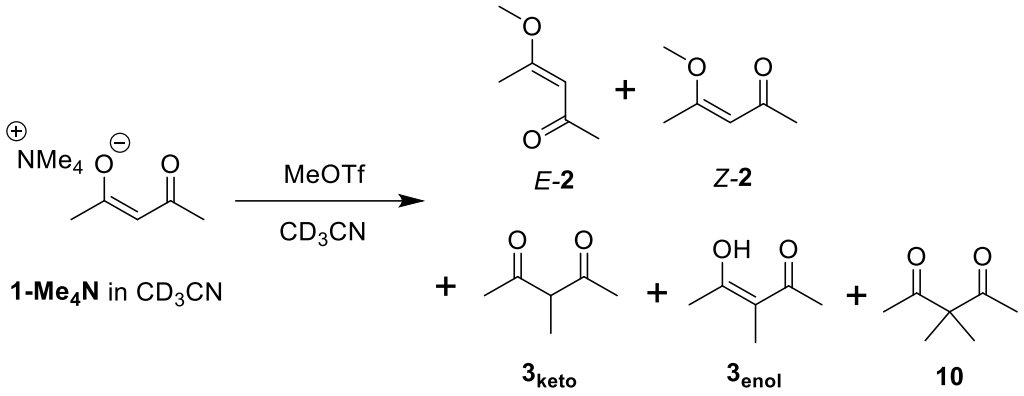


Figure 7-4: ^{1}H NMR spectrum of the same crude reaction mixture shown in Figure 7-3 after addition of a drop of EtOAc. The unknown signals have grown in size, indicating that ethyl acetate is present in the reaction mixture.

(i) Reaction of Enolate 1-Me_4N with Methyl Triflate in CD_3CN



Reaction of **1-Me_4N** (0.014 g, 0.081 mmol) and methyl triflate (0.0123 g, 0.075 mmol) in CD_3CN (0.75 ml) at 20 °C by procedure A.

^{1}H NMR (600 MHz, CD_3CN) of crude mixture of alkylation products (the underlined integrations are expressed relative to 1H of compound *E*-**2**): [a,b]

Assigned to *E*-**2**: δ 5.62 (s, 1H, C=C<u>H</u>), 3.66 (s, 3H, OC<u>H</u>$_3$), 2.23 (s, 3H, C<u>H</u>$_3$C=C). [4]

Assigned to *Z*-**2**: δ 5.07 (s, 0.29H, C=C<u>H</u> (1H of compound *Z*-**2**)), 2.21 (s, 0.75H, C<u>H</u>$_3$C=O (3H of compound *Z*-**2**)), 2.06 (s, 0.87H, C<u>H</u>$_3$C=C (3H of compound *Z*-**2**)). [4]

Assigned to **3**$_{keto}$: δ 2.17 (s, 1.40H, C<u>H</u>$_3$C=O (6H of compound **3**$_{keto}$)), 1.23 (d, *J* = 7.1 Hz, 0.80H, C(C<u>H</u>$_3$) (3H of compound **3**$_{keto}$)). [5]

Assigned to **3**$_{enol}$: δ 1.84 (s, 0.15H, C(C<u>H</u>$_3$) (3H of compound **3**$_{enol}$)). [5]

Assigned to **10**: δ 1.32 (s, 0.23H, C(C<u>H</u>$_3$)$_2$ (6H of compound **10**)). [6]

Based on the ^{1}H NMR spectral data given above, the integrations of 1H each of O- and C-alkylation products *E*-**2**, *Z*-**2**, **3**$_{keto}$, **3**$_{enol}$ and **10** relative to 1H of *E*-**2** are as follows:

$$I_{E-\mathbf{2}} = \frac{3.00}{3} = 1.00; \quad I_{Z-\mathbf{2}} = \frac{0.87}{3} = 0.29;$$

$$I_{\mathbf{3}_{keto}} = \frac{0.80}{3} = 0.26; \quad I_{\mathbf{3}_{enol}} = \frac{0.15}{3} = 0.05; \quad I_{\mathbf{10}} = \frac{0.23}{6} = 0.038$$

where $I_{\mathbf{X}}$ is the integration of 1H of compound **X** (**X** = *E*-**2**, *Z*-**2**, **3**$_{keto}$, **3**$_{enol}$ or **10**) relative to 1H of compound *E*-**2**. Since $I_{\mathbf{X}} \propto [\mathbf{X}]$ (concentration of **X** in mol L^{-1}), the percentage of O-alkylation is given by:

$$\text{Percentage of O-alkylation} = \frac{I_{E-\mathbf{2}} + I_{Z-\mathbf{2}}}{I_{E-\mathbf{2}} + I_{E-\mathbf{2}} + I_{\mathbf{3}_{keto}} + I_{\mathbf{3}_{enol}} + I_{\mathbf{10}}} \times 100$$

$$\text{Percentage of O-alkylation} = \frac{1.00 + 0.29}{1.00 + 0.29 + 0.26 + 0.05 + 0.038} \times 100 = 79\%$$

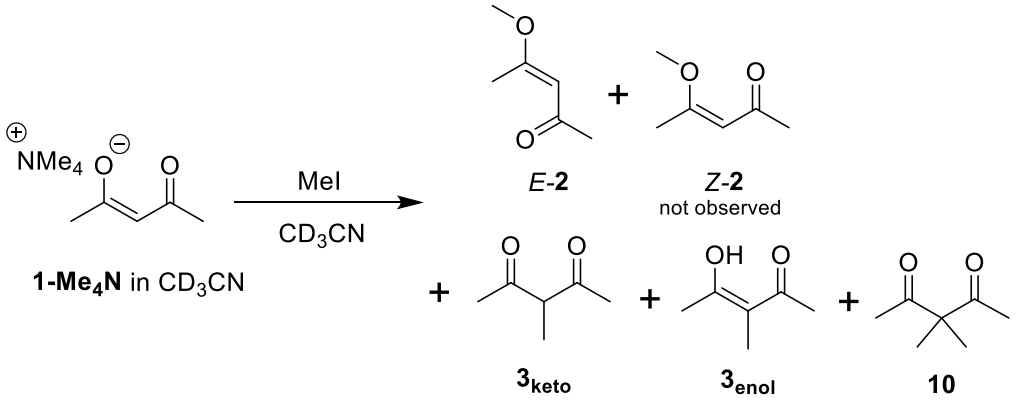
Integrations give an <u>O vs C</u> ratio of 79:21

---

[a] The relevant ^{1}H NMR spectra are shown in Figure C1 and Figure C2 in Appendix C.

[b] Signals of *E*-**2**, *Z*-**2**, **3**$_{keto}$, **3**$_{enol}$ and **10** that are overlapping with other signals: δ 3.83 – 3.79 (m, contains 3H of *Z*-**2** and 1H of **3**$_{keto}$), 2.13 – 2.10 (m, contains 3H of *E*-**2**, 6H of **3**$_{enol}$ and 6H of **10**).

(ii) Reaction of Enolate 1-Me$_4$N with Methyl Iodide in CD$_3$CN



Reaction of **1-Me$_4$N** (0.026 g, 0.15 mmol) and methyl iodide (0.0232 g, 0.163 mmol) in CD$_3$CN (0.85 ml) at 20 °C by procedure A.

^{1}H NMR (600 MHz, CD$_3$CN) of crude mixture of alkylation products (the underlined integrations are expressed relative to 1H of compound **3$_{keto}$**): [a,b,c]

Assigned to *E*-**2**: δ 5.62 (s, 0.05H, C=C<u>H</u> (1H of compound *E*-**2**)), 3.66 (s, 0.12H, OC<u>H</u>$_3$ (3H of compound *E*-**2**)), 2.19 (s, 0.10H, C<u>H</u>$_3$C=C (3H of compound *E*-**2**)). [4]

Assigned to **3$_{keto}$**: δ 3.81 (q, *J* = 7.1 Hz, 0.88H, C(O)C<u>H</u>C(O) (1H of compound **3$_{keto}$**)), 2.17 – 2.14 (m, 6H, C<u>H</u>$_3$C=O, 6H of compound **3$_{keto}$** and 6H of deuterated compound **3$_{keto}$**), 1.24 (d, *J* = 7.1 Hz, 3H, C(C<u>H</u>$_3$)). [5]

Assigned to **3$_{enol}$**: δ 1.85 (s, 0.76H, C(C<u>H</u>$_3$) (3H of compound **3$_{enol}$**)). [5]

Assigned to **10**: δ 1.32 (s, 2.35H, C(C<u>H</u>$_3$)$_2$ (6H of compound **10**)). [6]

Based on the ^{1}H NMR spectral data given above, the integrations of 1H each of O- and C-alkylation products *E*-**2**, **3$_{keto}$**, **3$_{enol}$** and **10** relative to 1H of **3$_{keto}$** are as follows:

$$I_{E-\mathbf{2}} = \frac{0.12}{3} = 0.04;\ \ I_{\mathbf{3_{keto}}} = \frac{6.00}{6} = 1.00;\ \ I_{\mathbf{3_{enol}}} = \frac{0.76}{3} = 0.25;\ \ I_{\mathbf{10}} = \frac{2.35}{6} = 0.392$$

where $I_{\mathbf{X}}$ is the integration of 1H of compound **X** (**X** = *E*-**2**, **3$_{keto}$**, **3$_{enol}$** or **10**) relative to 1H of compound **3$_{keto}$**. Since $I_{\mathbf{X}} \propto [\mathbf{X}]$ (concentration of **X** in mol L^{-1}), the percentage of O-alkylation is given by:

$$\text{Percentage of O-alkylation} = \frac{I_{E-\mathbf{2}}}{I_{E-\mathbf{2}} + I_{\mathbf{3_{keto}}} + I_{\mathbf{3_{enol}}} + I_{\mathbf{10}}} \times\ 100$$

$$\text{Percentage of O-alkylation} = \frac{0.04}{0.04 + 1.00 + 0.25 + 0.392} \times\ 100 = 2\%$$

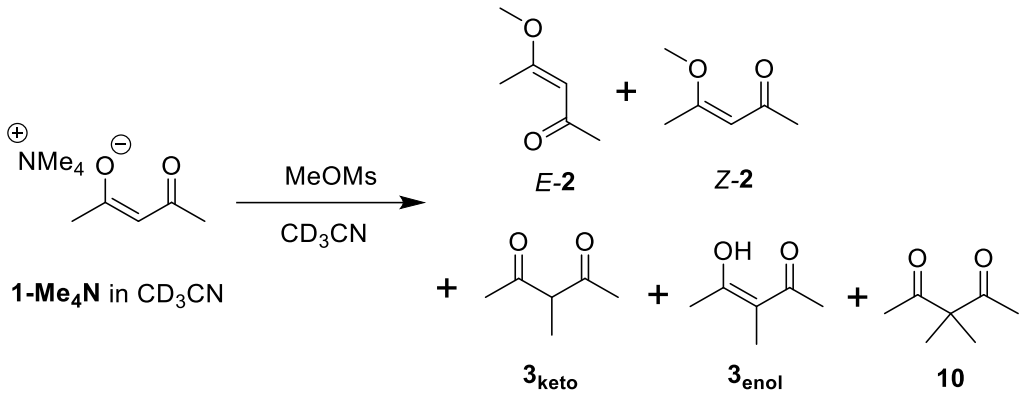
Integrations give an <u>O vs C</u> ratio of 2:98

(iii) Reaction of Enolate 1-Me$_4$N with Methyl Mesylate in CD$_3$CN

[a] The relevant ^{1}H NMR spectra are shown in Figure C3 and Figure C4 in Appendix C.

[b] Signals of *E*-**2**, **3$_{keto}$**, **3$_{enol}$** and **10** that are overlapping with other signals: δ 2.13 – 2.11 (m, contains 3H of *E*-**2**, 6H of **3$_{enol}$** and 6H of **10**).

[c] The vinyl signal of the enol ether products at δ 5.62 as well as the signal associated with the α-proton of the C-mono-alkylation product at δ 3.81 are undersized and thus not used in determining the O/C ratio. See pages 428 and 429 for details.



Reaction of **1-Me$_4$N** (0.021 g, 0.12 mmol) and methyl mesylate (0.0135 g, 0.123 mmol) in CD_3CN (0.85 ml) at 20 °C by procedure A.

^{1}H NMR (600 MHz, CD_3CN) of crude mixture of alkylation products (the underlined integrations are expressed relative to 1H of compound *E*-**2**): [a,b,c]

Assigned to *E*-**2**: δ 5.62 (s, 1H, C=C<u>H</u>), 3.66 (s, 3H, OC<u>H</u>$_3$). [4]

Assigned to *Z*-**2**: 5.08 (s, 0.10H, C=C<u>H</u> (1H of compound *Z*-**2**)), 2.06 (s, 0.32H, C<u>H</u>$_3$C=C (3H of compound *Z*-**2**)). [4]

Assigned to **3$_{keto}$**: δ 2.17 (s, 1.46H, C<u>H</u>$_3$C=O (6H of compound **3$_{keto}$**)), 1.24 (d, *J* = 7.1 Hz, 0.74H, C(C<u>H</u>$_3$) (3H of compound **3$_{keto}$**)). [5]

Assigned to **3$_{enol}$**: δ 1.85 (s, 0.20H, C(C<u>H</u>$_3$) (3H of compound **3$_{enol}$**)). [5]

Assigned to **10**: δ 1.32 (s, 0.41H, C(C<u>H</u>$_3$)$_2$ (6H of compound **10**)). [6]

Based on the ^{1}H NMR spectral data given above, the integrations of 1H each of O- and C-alkylation products *E*-**2**, *Z*-**2**, **3$_{keto}$**, **3$_{enol}$** and **10** relative to 1H of *E*-**2** are as follows:

$$I_{E-\mathbf{2}} = \frac{3.00}{3} = 1.00; \quad I_{Z-\mathbf{2}} = \frac{0.32}{3} = 0.11;$$

$$I_{\mathbf{3_{keto}}} = \frac{0.74}{3} = 0.25; \quad I_{\mathbf{3_{enol}}} = \frac{0.20}{3} = 0.067; \quad I_{\mathbf{10}} = \frac{0.41}{6} = 0.068$$

where $I_{\mathbf{X}}$ is the integration of 1H of compound **X** (**X** = *E*-**2**, *Z*-**2**, **3$_{keto}$**, **3$_{enol}$** or **10**) relative to 1H of compound *E*-**2**. Since $I_{\mathbf{X}} \propto [\mathbf{X}]$ (concentration of **X** in mol L^{-1}), the percentage of O-alkylation is given by:

$$\text{Percentage of O-alkylation} = \frac{I_{E-\mathbf{2}} + I_{Z-\mathbf{2}}}{I_{E-\mathbf{2}} + I_{E-\mathbf{2}} + I_{\mathbf{3_{keto}}} + I_{\mathbf{3_{enol}}} + I_{\mathbf{10}}} \times 100$$

$$\text{Percentage of O-alkylation} = \frac{1.00 + 0.11}{1.00 + 0.11 + 0.25 + 0.067 + 0.068} \times 100 = 74\%$$

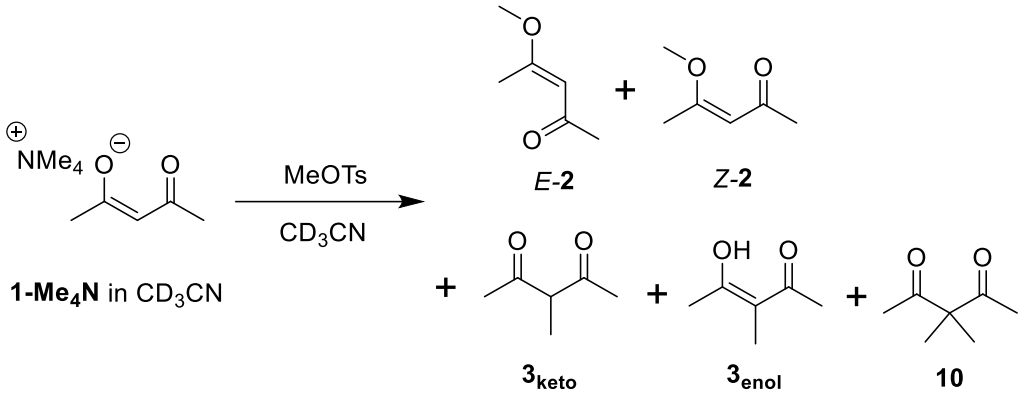
[a] The relevant ^{1}H NMR spectra are shown in Figure C5 and Figure C6 in Appendix C.

[b] Signals of *E*-**2**, *Z*-**2**, **3$_{keto}$**, **3$_{enol}$** and **10** that are overlapping with other signals: δ 3.83 – 3.78 (m, contains 3H of *Z*-**2** and 1H of **3$_{keto}$**), 2.25 – 2.20 (m, contains 3H of *E*-**2** and 3H of *Z*-**2**), 2.14 – 2.10 (m, contains 3H of *E*-**2**, 6H of **3$_{enol}$** and 6H of **10**).

[c] The vinyl signals of the enol ether products at δ 5.62 and 5.08 are undersized and thus not used in determining the O/C ratio. See pages 428 and 429 for details.

Integrations give an O vs C ratio of 74:26

(iv) Reaction of Enolate 1-Me$_4$N with Methyl Tosylate in CD$_3$CN



Reaction of **1-Me$_4$N** (0.030 g, 0.17 mmol) and methyl tosylate (0.0344 g, 0.185 mmol) in CD_3CN (0.85 ml) at 20 °C by procedure A.

^{1}H NMR (600 MHz, CD_3CN) of crude mixture of alkylation products (the underlined integrations are expressed relative to 1H of compound *E*-**2**): [a,b,c]

Assigned to *E*-**2**: δ 3.66 (s, 3H, OCH_3), 2.23 (s, 3H, CH_3C=C). [4]

Assigned to *Z*-**2**: δ 5.08 (s, 0.24H, C=CH (1H of compound *Z*-**2**)), 2.21 (s, 0.68H, CH_3C=O (3H of compound *Z*-**2**)). [4]

Assigned to **3$_{keto}$**: δ 2.17 (s, 1.72H, CH_3C=O (6H of compound **3$_{keto}$**)), 1.23 (d, J = 7.1 Hz, 0.75H, C(CH_3) (3H of compound **3$_{keto}$**)). [5]

Assigned to **3$_{enol}$**: δ 1.85 (s, 0.24H, C(CH_3) (3H of compound **3$_{enol}$**)). [5]

Assigned to **10**: δ 1.32 (s, 0.57H, C(CH_3)$_2$ (6H of compound **10**)). [6]

Based on the ^{1}H NMR spectral data given above, the integrations of 1H each of O- and C-alkylation products *E*-**2**, *Z*-**2**, **3$_{keto}$**, **3$_{enol}$** and **10** relative to 1H of *E*-**2** are as follows:

$$I_{E-\mathbf{2}} = \frac{3.00}{3} = 1.00; \quad I_{Z-\mathbf{2}} = \frac{0.68}{3} = 0.23;$$

$$I_{\mathbf{3_{keto}}} = \frac{0.75}{3} = 0.25; \quad I_{\mathbf{3_{enol}}} = \frac{0.24}{3} = 0.08; \quad I_{\mathbf{10}} = \frac{0.57}{6} = 0.095$$

where $I_{\mathbf{X}}$ is the integration of 1H of compound **X** (**X** = *E*-**2**, *Z*-**2**, **3$_{keto}$**, **3$_{enol}$** or **10**) relative to 1H of compound *E*-**2**. Since $I_{\mathbf{X}} \propto [\mathbf{X}]$ (concentration of **X** in mol L^{-1}), the percentage of O-alkylation is given by:

[a] The relevant ^{1}H NMR spectra are shown in Figure C7 and Figure C8 in Appendix C.

[b] Signals of *E*-**2**, *Z*-**2**, **3$_{keto}$**, **3$_{enol}$** and **10** that are overlapping with other signals: δ 5.64 – 5.61 (m, contains 1H of *E*-**2**), 3.83 – 3.78 (m, contains 3H of *Z*-**2** and 1H of **3$_{keto}$**), 2.13 – 2.10 (m, contains 3H of *E*-**2**, 6H of **3$_{enol}$** and 6H of **10**).

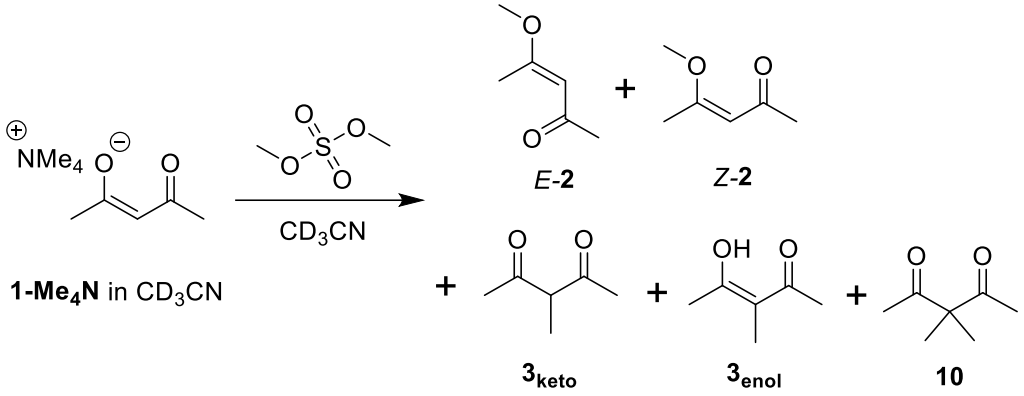
[c] The vinyl signal of the enol ether products at δ 5.08 is undersized and thus not used in determining the O/C ratio. See pages 428 and 429 for details.

$$\text{Percentage of O-alkylation} = \frac{I_{E-\mathbf{2}} + I_{Z-\mathbf{2}}}{I_{E-\mathbf{2}} + I_{E-\mathbf{2}} + I_{\mathbf{3_{keto}}} + I_{\mathbf{3_{enol}}} + I_{\mathbf{10}}} \times 100$$

$$\text{Percentage of O-alkylation} = \frac{1.00 + 0.23}{1.00 + 0.23 + 0.25 + 0.08 + 0.095} \times 100 = 74\%$$

Integrations give an O vs C ratio of 74:26

(v) Reaction of Enolate 1-Me_4N with Dimethyl Sulfate in CD_3CN



Reaction of **1-Me_4N** (0.030 g, 0.17 mmol) and dimethyl sulfate (0.0175 g, 0.139 mmol) in CD_3CN (0.85 ml) at 20 °C by procedure A.

^{1}H NMR (600 MHz, CD_3CN) of crude mixture of alkylation products (the underlined integrations are expressed relative to 1H of compound *E*-**2**): [a,b,c]

Assigned to *E*-**2**: δ 5.62 (s, 1H, C=C<u>H</u>), 3.65 (s, 3H, OC<u>H</u>$_3$). [4]

Assigned to *Z*-**2**: δ 5.07 (s, 0.28H, C=C<u>H</u> (1H of compound *Z*-**2**)), 2.06 (s, 0.83H, C<u>H</u>$_3$C=C (3H of compound *Z*-**2**)). [4]

Assigned to **3$_{keto}$**: δ 2.16 (s, 1.83H, C<u>H</u>$_3$C=O (6H of compound **3$_{keto}$**)), 1.23 (d, *J* = 7.1 Hz, 0.90H, C(C<u>H</u>$_3$) (3H of compound **3$_{keto}$**)). [5]

Assigned to **3$_{enol}$**: δ 1.84 (s, 0.16H, C(C<u>H</u>$_3$) (3H of compound **3$_{enol}$**)). [5]

Assigned to **10**: δ 1.31 (s, 0.41H, C(C<u>H</u>$_3$)$_2$ (6H of compound **10**)). [6]

Based on the ^{1}H NMR spectral data given above, the integrations of 1H each of O- and C-alkylation products *E*-**2**, *Z*-**2**, **3$_{keto}$**, **3$_{enol}$** and **10** relative to 1H of *E*-**2** are as follows:

$$I_{E-\mathbf{2}} = \frac{3.00}{3} = 1.00; \quad I_{Z-\mathbf{2}} = \frac{0.83}{3} = 0.28;$$

$$I_{\mathbf{3_{keto}}} = \frac{0.90}{3} = 0.30; \quad I_{\mathbf{3_{enol}}} = \frac{0.16}{3} = 0.053; \quad I_{\mathbf{10}} = \frac{0.41}{6} = 0.068$$

[a] The relevant ^{1}H NMR spectra are shown in Figure C9 and Figure C10 in Appendix C.

[b] Signals of *E*-**2**, *Z*-**2**, **3$_{keto}$**, **3$_{enol}$** and **10** that are overlapping with other signals: δ 3.84 – 3.79 (m, contains 3H of *Z*-**2** and 1H of **3$_{keto}$**), 2.23 – 2.18 (m, contains 3H of *E*-**2** and 3H of *Z*-**2**), 2.13 – 2.10 (m, contains 3H of *E*-**2**, 6H of **3$_{enol}$** and 6H of **10**).

[c] The vinyl signals of the enol ether products at δ 5.62 and 5.07 are undersized and thus not used in determining the O/C ratio. See pages 428 and 429 for details.

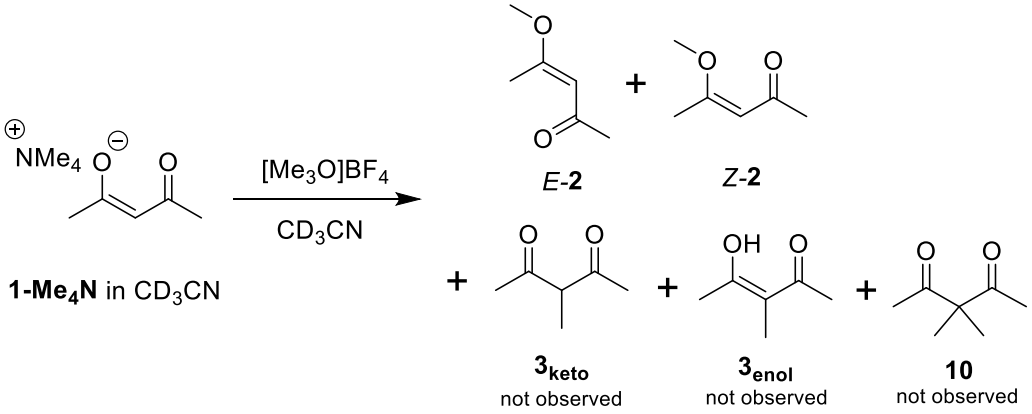
where $I_{\mathbf{X}}$ is the integration of 1H of compound **X** (**X** = *E*-**2**, *Z*-**2**, $\mathbf{3_{keto}}$, $\mathbf{3_{enol}}$ or **10**) relative to 1H of compound *E*-**2**. Since $I_{\mathbf{X}} \propto [\mathbf{X}]$ (concentration of **X** in mol L^{-1}), the percentage of O-alkylation is given by:

$$\text{Percentage of O-alkylation} = \frac{I_{E-\mathbf{2}} + I_{Z-\mathbf{2}}}{I_{E-\mathbf{2}} + I_{E-\mathbf{2}} + I_{\mathbf{3_{keto}}} + I_{\mathbf{3_{enol}}} + I_{\mathbf{10}}} \times 100$$

$$\text{Percentage of O-alkylation} = \frac{1.00 + 0.28}{1.00 + 0.28 + 0.30 + 0.053 + 0.068} \times 100 = 75\%$$

Integrations give an O vs C ratio of 75:25

(vi) Reaction of Enolate 1-Me_4N with $[Me_3O]BF_4$ in CD_3CN



Reaction of **1-Me_4N** (0.041 g, 0.24 mmol) in CD_3CN (0.45 ml) and $[Me_3O]BF_4$ (0.030 g, 0.20 mmol; added as a solution in CD_3CN (0.40 ml)) at 20 °C by procedure A.

^{1}H NMR (600 MHz, CD_3CN) of crude mixture of alkylation products (the underlined integrations are expressed relative to 1H of compound *E*-**2**): [a,b]

Assigned to *E*-**2**: δ 5.62 (s, 1H, C=C<u>H</u>), 3.65 (s, 3H, OC<u>H</u>$_3$), 2.12 (s, 3H, C<u>H</u>$_3$C=O). [4]

Assigned to *Z*-**2**: δ 5.07 (s, 0.04H, C=C<u>H</u> (1H of compound *Z*-**2**)), 3.82 (s, 0.14H, OC<u>H</u>$_3$ (3H of compound *Z*-**2**)), 2.05 (s, 0.12H, C<u>H</u>$_3$C=C (3H of compound *Z*-**2**)). [4]

No signals of C-methylation products $\mathbf{3_{keto}}$, $\mathbf{3_{enol}}$ or **10** were observed in this spectrum. Consequently, this reaction is deemed to be essentially 100% selective for O-methylation.

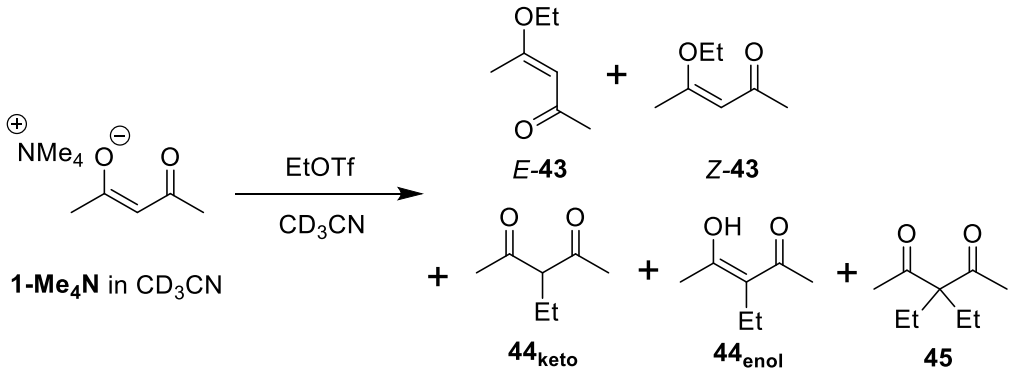
i.e., the O vs C ratio is 100:0

[a] The relevant ^{1}H NMR spectra are shown in Figure C11 and Figure C12 in Appendix C.

[b] Signals of *E*-**2** and *Z*-**2** that are overlapping with other signals: δ 2.24 – 2.19 (m, contains 3H of *E*-**2** and 3H of *Z*-**2**).

7.2.2. Reactions of 1-Me_4N with Various Ethylating Agents in CD_3CN

(i) Reaction of Enolate 1-Me_4N with Ethyl Triflate in CD_3CN



Reaction of **1-Me_4N** (0.035 g, 0.20 mmol) and ethyl triflate (0.0332 g, 0.186 mmol) in CD_3CN (0.85 ml) at 20 °C by procedure A.

^{1}H NMR (600 MHz, CD_3CN) of crude mixture of alkylation products (the underlined integrations are expressed relative to 1H of compound *E*-**43**): [a,b,c]

Assigned to *E*-**43**: δ 5.59 (s, 1H, C=C<u>H</u>), 3.88 (q, *J* = 7.0 Hz, 2H, OC<u>H</u>$_2$CH$_3$), 2.22 (s, 3H, C<u>H</u>$_3$C=C), 2.10 (s, 3H, C<u>H</u>$_3$C=O). [4]

Assigned to *Z*-**43**: δ 5.03 (s, 0.43H, C=C<u>H</u> (1H of compound *Z*-**43**)), 4.13 (q, *J* = 7.0 Hz, 0.92H, OC<u>H</u>$_2$CH$_3$ (2H of compound *Z*-**43**)), 2.25 (s, 1.33H, C<u>H</u>$_3$C=O (3H of compound *Z*-**43**)), 2.05 (s, 1.31H, C<u>H</u>$_3$C=C (3H of compound *Z*-**43**)). [4]

Assigned to **44_{keto}**: δ 3.69 (t, *J* = 7.1 Hz, 0.21H, C(O)C<u>H</u>C(O) (1H of compound **44_{keto}**)), 2.16 (s, 1.26H, C<u>H</u>$_3$C=O (6H of compound **44_{keto}**)), 1.83 – 1.77 (m, 0.50H, C(C<u>H</u>$_2$CH$_3$) (2H of compound **44_{keto}**)), 0.87 (t, *J* = 7.4 Hz, 0.68H, C(CH$_2$C<u>H</u>$_3$) (3H of compound **44_{keto}**)). [7]

Assigned to **44_{enol}**: δ 2.13 (s, 0.15H, C<u>H</u>$_3$C=O (6H of compound **44_{enol}**)), 1.03 (t, *J* = 7.1 Hz, 0.07H, C(CH$_2$C<u>H</u>$_3$) (3H of compound **44_{enol}**)). [7]

Assigned to **45**: δ 2.07 (s, 0.11H (6H of compound **45**)), 0.71 (t, *J* = 7.6 Hz, 0.14H, C(CH$_2$C<u>H</u>$_3$)$_2$ (6H of compound **45**)). [8]

Based on the ^{1}H NMR spectral data given above, the integrations of 1H each of O- and C-alkylation products *E*-**43**, *Z*-**43**, **44_{keto}**, **44_{enol}** and **45** relative to 1H of *E*-**43** are as follows:

$$I_{E-\mathbf{43}} = \frac{2.00}{2} = 1.00; \quad I_{Z-\mathbf{43}} = \frac{0.92}{2} = 0.46;$$

$$I_{\mathbf{44_{keto}}} = \frac{0.68}{3} = 0.23; \quad I_{\mathbf{44_{enol}}} = \frac{0.07}{3} = 0.023; \quad I_{\mathbf{45}} = \frac{0.14}{6} = 0.023$$

[a] The relevant ^{1}H NMR spectra are shown in Figure C13 and Figure C14 in Appendix C.

[b] Signals of *E*-**43**, *Z*-**43**, **44_{enol}** and **45** that are overlapping with other signals: δ 2.31 – 2.26 (m, contains 2H of **44_{enol}**), 1.93 – 1.87 (m, contains 4H of **45**), 1.35 – 1.29 (m, contains 3H of *E*-**43** and 3H of *Z*-**43**).

[c] The vinyl signals of the enol ether products at δ 5.59 and 5.03 as well as the signal associated with the α-proton of the C-mono-alkylation product at δ 3.69 may be undersized and thus not used in determining the O/C ratio. See pages 428 and 429 for details.

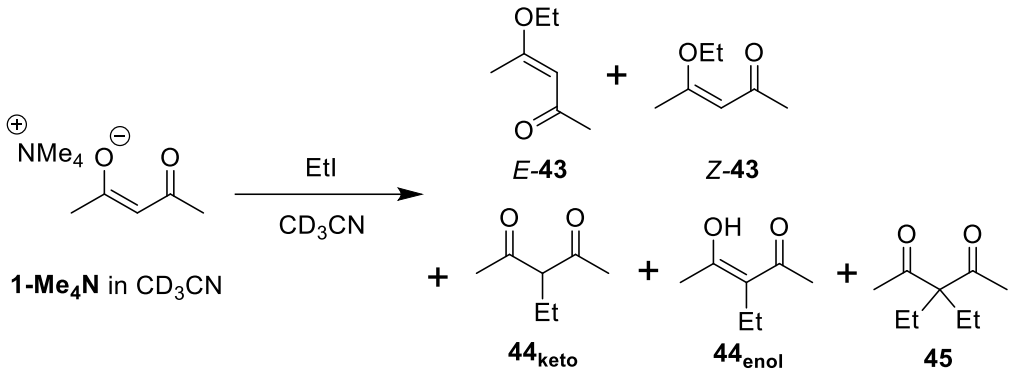
where $I_{\mathbf{X}}$ is the integration of 1H of compound **X** (**X** = *E*-**43**, *Z*-**43**, **44**$_{\mathbf{keto}}$, **44**$_{\mathbf{enol}}$ or **45**) relative to 1H of compound *E*-**43**. Since $I_{\mathbf{X}} \propto [\mathbf{X}]$ (concentration of **X** in mol L^{-1}), the percentage of O-alkylation is given by:

$$\text{Percentage of O-alkylation} = \frac{I_{E-\mathbf{43}} + I_{Z-\mathbf{43}}}{I_{E-\mathbf{43}} + I_{Z-\mathbf{43}} + I_{\mathbf{44}_{\mathbf{keto}}} + I_{\mathbf{44}_{\mathbf{enol}}} + I_{\mathbf{45}}} \times 100$$

$$\text{Percentage of O-alkylation} = \frac{1.00 + 0.46}{1.00 + 0.46 + 0.23 + 0.023 + 0.023} \times 100 = 84\%$$

Integrations give an O vs C ratio of 84:16

(ii) Reaction of Enolate 1-Me$_4$N with Ethyl Iodide in CD$_3$CN



Reaction of **1-Me$_4$N** (0.037 g, 0.21 mmol) and ethyl iodide (0.0325 g, 0.208 mmol) in CD_3CN (0.85 ml) at 20 °C by procedure A.

^{1}H NMR (600 MHz, CD_3CN) of crude mixture of alkylation products (the underlined integrations are expressed relative to 1H of compound **44**$_{\mathbf{keto}}$): [a,b,c]

Assigned to *E*-**43**: δ 5.59 (s, 0.10H, C=C<u>H</u> (1H of compound *E*-**43**)), 3.89 (q, *J* = 7.0 Hz, 0.21H, OC<u>H</u>$_2$CH$_3$ (2H of compound *E*-**43**)), 2.10 (s, 0.29H, C<u>H</u>$_3$C=O (3H of compound *E*-**43**)). [4]

Assigned to *Z*-**43**: 5.04 (s, 0.03H, C=C<u>H</u> (1H of compound *Z*-**43**)), 4.13 (q, *J* = 7.0 Hz, 0.08H, OC<u>H</u>$_2$CH$_3$ (2H of compound *Z*-**43**)). [4]

Assigned to **44**$_{\mathbf{keto}}$: δ 3.69 (t, *J* = 7.1 Hz, 0.89H, C(O)C<u>H</u>C(O)), 1.81 (quint, *J* = 7.3 Hz, 2H, C(C<u>H</u>$_2$CH$_3$)), 0.88 (t, *J* = 7.3 Hz, 3H, C(CH$_2$C<u>H</u>$_3$)). [7]

Assigned to **44**$_{\mathbf{enol}}$: δ 1.05 (t, *J* = 7.5 Hz, 0.41H, C(CH$_2$C<u>H</u>$_3$) (3H of compound **44**$_{\mathbf{enol}}$)). [7]

[a] The relevant ^{1}H NMR spectra are shown in Figure C15 and Figure C16 in Appendix C.

[b] Signals of E-**43**, Z-**43**, **44**$_{\mathbf{keto}}$, **44**$_{\mathbf{enol}}$ and **45** that are overlapping with other signals: δ 2.32 – 2.20 (m, contains 3H of E-**43**, 3H of Z-**43** and 2H of **44**$_{\mathbf{enol}}$), 2.17 – 2.12 (m, contains 6H of **44**$_{\mathbf{keto}}$ and 6H of **44**$_{\mathbf{enol}}$), 2.08 – 2.05 (m, contains 3H of Z-**43** and 6H of **45**), 1.36 – 1.30 (m, contains 3H of E-**43** and 3H of Z-**43**).

[c] The vinyl signals of the enol ether products at δ 5.59 and 5.04 as well as the signal associated with the α-proton of the C-mono-alkylation product at δ 3.69 are undersized and thus not used in determining the O/C ratio. See pages 428 and 429 for details.

Assigned to **45**: δ 1.91 (q, *J* = 7.6 Hz, 0.69H, C(C<u>H</u>$_2$CH$_3$)$_2$ (4H of compound **45**)), 0.71 (t, *J* = 7.6 Hz, 1.07H, C(CH$_2$C<u>H</u>$_3$)$_2$ (6H of compound **45**)). [8]

Based on the ^{1}H NMR spectral data given above, the integrations of 1H each of O- and C-alkylation products *E*-**43**, *Z*-**43**, **44$_{keto}$**, **44$_{enol}$** and **45** relative to 1H of **44$_{keto}$** are as follows:

$$I_{E-\mathbf{43}} = \frac{0.21}{2} = 0.105; \quad I_{Z-\mathbf{43}} = \frac{0.08}{2} = 0.04;$$

$$I_{\mathbf{44_{keto}}} = \frac{3.00}{3} = 1.00; \quad I_{\mathbf{44_{enol}}} = \frac{0.41}{3} = 0.14; \quad I_{\mathbf{45}} = \frac{1.07}{6} = 0.178$$

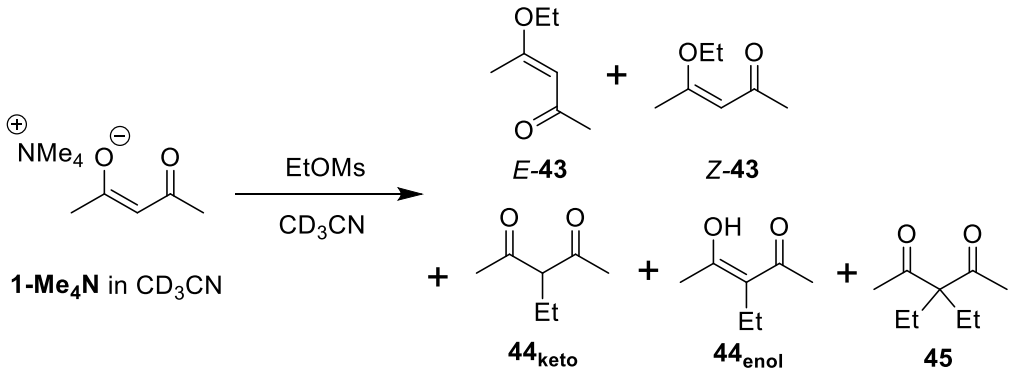
where $I_{\mathbf{X}}$ is the integration of 1H of compound **X** (**X** = *E*-**43**, *Z*-**43**, **44$_{keto}$**, **44$_{enol}$** or **45**) relative to 1H of compound **44$_{keto}$**. Since $I_{\mathbf{X}} \propto [\mathbf{X}]$ (concentration of **X** in mol L^{-1}), the percentage of O-alkylation is given by:

$$\text{Percentage of O-alkylation} = \frac{I_{E-\mathbf{43}} + I_{Z-\mathbf{43}}}{I_{E-\mathbf{43}} + I_{Z-\mathbf{43}} + I_{\mathbf{44_{keto}}} + I_{\mathbf{44_{enol}}} + I_{\mathbf{45}}} \times 100$$

$$\text{Percentage of O-alkylation} = \frac{0.105 + 0.04}{0.105 + 0.04 + 1.00 + 0.14 + 0.178} \times 100 = 10\%$$

Integrations give an O vs C ratio of 10:90

(iii) Reaction of Enolate 1-Me$_4$N with Ethyl Mesylate in CD$_3$CN



Reaction of **1-Me$_4$N** (0.033 g, 0.19 mmol) and ethyl mesylate (0.0233 g, 0.188 mmol) in CD$_3$CN (0.85 ml) at 20 °C by procedure A.

^{1}H NMR (600 MHz, CD$_3$CN) of crude mixture of alkylation products (the underlined integrations are expressed relative to 1H of compound *E*-**43**): [a,b]

Assigned to *E*-**43**: δ 5.59 (s, 1H, C=C<u>H</u>), 3.89 (q, *J* = 7.0 Hz, 2H, OC<u>H</u>$_2$CH$_3$), 2.23 (s, 3H, C<u>H</u>$_3$C=C), 2.10 (s, 3H, C<u>H</u>$_3$C=O). [4]

[a] The relevant ^{1}H NMR spectra are shown in Figure C17 and Figure C18 in Appendix C.

[b] Signals of *E*-**43**, *Z*-**43**, **44$_{keto}$**, **44$_{enol}$** and **45** that are overlapping with other signals: δ 2.34 – 2.28 (m, contains 2H of **44$_{enol}$**), 2.14 (s, contains 6H of **44$_{enol}$**), 1.94 – 1.87 (m, contains 4H of **45**), 1.39 – 1.29 (m, contains 3H of *E*-**43**, 3H of *Z*-**43** and EtOMs signal).

Assigned to *Z*-**43**: δ 5.04 (s, 0.11H, C=C<u>H</u> (1H of compound *Z*-**43**)), 4.13 (q, *J* = 7.0 Hz, 0.23H, OC<u>H</u>$_2$CH$_3$ (2H of compound *Z*-**43**)), 2.26 (s, 0.34H, CH$_3$C=O (3H of compound *Z*-**43**)), 2.05 (s, 0.34H, C<u>H</u>$_3$C=C (3H of compound *Z*-**43**)). [4]

Assigned to **44$_{keto}$**: δ 3.69 (t, *J* = 7.1 Hz, 0.16H, C(O)C<u>H</u>C(O) (1H of compound **44$_{keto}$**)), 2.16 (s, 0.93H, C<u>H</u>$_3$C=O (6H of compound **44$_{keto}$**)), 1.81 (quint, *J* = 7.4 Hz, 0.34H, C(C<u>H</u>$_2$CH$_3$) (2H of compound **44$_{keto}$**)), 0.88 (t, *J* = 7.4 Hz, 0.49H, C(CH$_2$C<u>H</u>$_3$) (3H of compound **44$_{keto}$**)). [7]

Assigned to **44$_{enol}$**: δ 1.05 (t, *J* = 7.5 Hz, 0.07H, C(CH$_2$C<u>H</u>$_3$)$_2$ (3H of compound **44$_{enol}$**)). [7]

Assigned to **45**: δ 2.07 (s, 0.07H, C<u>H</u>$_3$C=O (6H of compound **45**)), 0.71 (t, *J* = 7.6 Hz, 0.08H, C(CH$_2$C<u>H</u>$_3$)$_2$ (6H of compound **45**)). [8]

Based on the ^{1}H NMR spectral data given above, the integrations of 1H each of O- and C-alkylation products *E*-**43**, *Z*-**43**, **44$_{keto}$**, **44$_{enol}$** and **45** relative to 1H of *E*-**43** are as follows:

$$I_{E-\mathbf{43}} = \frac{2.00}{2} = 1.00; \quad I_{Z-\mathbf{43}} = \frac{0.23}{2} = 0.115;$$

$$I_{\mathbf{44}_{\mathbf{keto}}} = \frac{0.49}{3} = 0.163; \quad I_{\mathbf{44}_{\mathbf{enol}}} = \frac{0.07}{3} = 0.023; \quad I_{\mathbf{45}} = \frac{0.08}{6} = 0.013$$

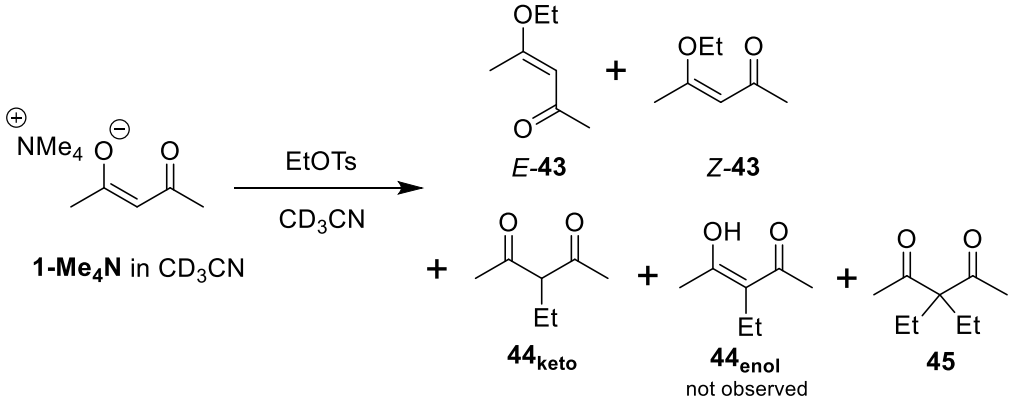
where $I_{\mathbf{X}}$ is the integration of 1H of compound **X** (**X** = *E*-**43**, *Z*-**43**, **44$_{keto}$**, **44$_{enol}$** or **45**) relative to 1H of compound *E*-**43**. Since $I_{\mathbf{X}} \propto [\mathbf{X}]$ (concentration of **X** in mol L^{-1}), the percentage of O-alkylation is given by:

$$\text{Percentage of O-alkylation} = \frac{I_{E-\mathbf{43}} + I_{Z-\mathbf{43}}}{I_{E-\mathbf{43}} + I_{Z-\mathbf{43}} + I_{\mathbf{44}_{\mathbf{keto}}} + I_{\mathbf{44}_{\mathbf{enol}}} + I_{\mathbf{45}}} \times 100$$

$$\text{Percentage of O-alkylation} = \frac{1.00 + 0.115}{1.00 + 0.115 + 0.163 + 0.023 + 0.013} \times 100 = 85\%$$

Integrations give an O vs C ratio of 85:15

(iv) Reaction of Enolate 1-Me$_4$N with Ethyl Tosylate in CD$_3$CN



Reaction of **1-Me$_4$N** (0.033 g, 0.19 mmol) in CD$_3$CN (0.45 ml) and ethyl tosylate (0.0354 g, 0.177 mmol; added as a solution in CD$_3$CN (0.40 ml)) at 20 °C by procedure A.

^{1}H NMR (600 MHz, CD_3CN) of crude mixture of alkylation products (the underlined integrations are expressed relative to 1H of compound *E*-**43**): [a,b,c]

Assigned to *E*-**43**: δ 5.59 (s, 1H, C=C<u>H</u>), 3.88 (q, *J* = 7.0 Hz, 2H, OC<u>H</u>$_2$CH$_3$), 2.22 (s, 3H, C<u>H</u>$_3$C=C), 2.10 (s, 3H, C<u>H</u>$_3$C=O). [4]

Assigned to *Z*-**43**: δ 5.04 (s, 0.03H, C=C<u>H</u> (1H of compound *Z*-**43**)), 4.13 (q, *J* = 7.0 Hz, 0.06H, OC<u>H</u>$_2$CH$_3$ (2H of compound *Z*-**43**)), 2.25 (s, 0.08H, C<u>H</u>$_3$C=O (3H of compound *Z*-**43**)), 2.04 (s, 0.10H, C<u>H</u>$_3$C=C (3H of compound *Z*-**43**)). [4]

Assigned to **44$_{keto}$**: δ 3.69 (t, *J* = 7.1 Hz, 0.11H, C(O)C<u>H</u>C(O) (1H of compound **44$_{keto}$**)), 2.16 (s, 0.61H, C<u>H</u>$_3$C=O (6H of compound **44$_{keto}$**)), 1.83 – 1.77 (m, 0.28H, C(C<u>H</u>$_2$CH$_3$) (2H of compound **44$_{keto}$**)), 0.87 (t, *J* = 7.4 Hz, 0.38H, C(CH$_2$C<u>H</u>$_3$) (3H of compound **44$_{keto}$**)). [7]

Assigned to **45**: δ 2.07 (s, 0.10H, C<u>H</u>$_3$C=O (6H of compound **45**)), 0.71 (t, *J* = 7.6 Hz, 0.14H, C(CH$_2$C<u>H</u>$_3$)$_2$ (6H of compound **45**)). [8]

Based on the ^{1}H NMR spectral data given above, the integrations of 1H each of O- and C-alkylation products *E*-**43**, *Z*-**43**, **44$_{keto}$** and **45** relative to 1H of *E*-**43** are as follows:

$$I_{E-\mathbf{43}} = \frac{2.00}{2} = 1.00;\ I_{Z-\mathbf{43}} = \frac{0.06}{2} = 0.03;\ I_{\mathbf{44_{keto}}} = \frac{0.38}{3} = 0.13;\ I_{\mathbf{45}} = \frac{0.14}{6} = 0.023$$

where $I_{\mathbf{X}}$ is the integration of 1H of compound **X** (**X** = *E*-**43**, *Z*-**43**, **44$_{keto}$** or **45**) relative to 1H of compound *E*-**43**. Since $I_{\mathbf{X}} \propto [\mathbf{X}]$ (concentration of **X** in mol L^{-1}), the percentage of O-alkylation is given by:

$$\text{Percentage of O-alkylation} = \frac{I_{E-\mathbf{43}} + I_{Z-\mathbf{43}}}{I_{E-\mathbf{43}} + I_{Z-\mathbf{43}} + I_{\mathbf{44_{keto}}} + I_{\mathbf{45}}} \times 100$$

$$\text{Percentage of O-alkylation} = \frac{1.00 + 0.03}{1.00 + 0.03 + 0.13 + 0.023} \times 100 = 87\%$$

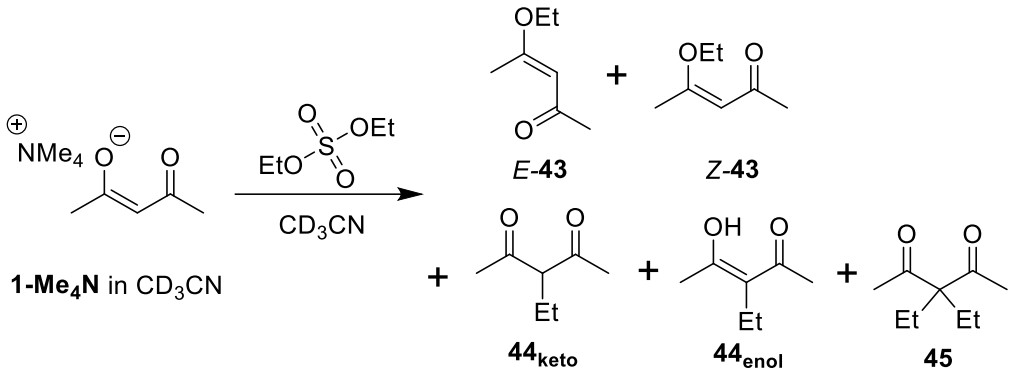
Integrations give an <u>O vs C</u> ratio of 87:13

[a] The relevant ^{1}H NMR spectra are shown in Figure C19 and Figure C20 in Appendix C.

[b] Signals of *E*-**43**, *Z*-**43** and **45** that are overlapping with other signals: δ 1.93 – 1.88 (m, contains 4H of **45**), 1.34 – 1.28 (m, contains 3H of *E*-**43** and 3H of *Z*-**43**).

[c] The vinyl signals of the enol ether products at δ 5.59 and 5.04 as well as the signal associated with the α-proton of the C-mono-alkylation product at δ 3.69 may be undersized and thus not used in determining the O/C ratio. See pages 428 and 429 for details.

(v) Reaction of Enolate 1-Me_4N with Diethyl Sulfate in CD_3CN



Reaction of a 0.44 mol L^{-1} stock solution of **1-Me_4N** (0.40 ml, 0.176 mmol) and diethyl sulfate (0.0234 g, 0.152 mmol) in CD_3CN (0.85 ml) at 20 °C by procedure A.

^{1}H NMR (600 MHz, CD_3CN) of crude mixture of alkylation products (the underlined integrations are expressed relative to 1H of compound *E*-**43**): [a,b,c]

Assigned to *E*-**43**: δ 5.59 (s, 1H, C=C<u>H</u>), 2.22 (s, 3H, C<u>H</u>$_3$C=C), 2.10 (s, 3H, C<u>H</u>$_3$C=O). [4]

Assigned to *Z*-**43**: δ 5.03 (s, 0.23H, C=C<u>H</u> (1H of compound *Z*-**43**)), 4.13 (q, *J* = 7.0 Hz, 0.50H, OC<u>H</u>$_2$CH$_3$ (2H of compound *Z*-**43**)), 2.25 (s, 0.73H, C<u>H</u>$_3$C=O (3H of compound *Z*-**43**)), 2.05 (s, 0.72H, C<u>H</u>$_3$C=C (3H of compound *Z*-**43**)). [4]

Assigned to **44_{keto}**: δ 3.69 (t, *J* = 7.1 Hz, 0.18H, C(O)C<u>H</u>C(O) (1H of compound **44_{keto}**)), 2.15 (s, 1.22H, C<u>H</u>$_3$C=O (6H of compound **44_{keto}**)), 0.87 (t, *J* = 7.4 Hz, 0.74H, C(CH$_2$C<u>H</u>$_3$) (3H of compound **44_{keto}**)).[7]

Assigned to **44_{enol}**: δ 2.13 (s, 0.13H, C<u>H</u>$_3$C=O (6H of compound **44_{enol}**)), 1.04 (t, *J* = 7.5 Hz, 0.09H, C(CH$_2$C<u>H</u>$_3$) (6H of compound **44_{enol}**)). [7]

Assigned to **45**: δ 2.06 (s, 0.13H, C<u>H</u>$_3$C=O (6H of compound **45**)), 1.90 (q, *J* = 7.6 Hz, 0.10H, C(C<u>H</u>$_2$CH$_3$)$_2$ (4H of compound **45**)), 0.70 (t, *J* = 7.6 Hz, 0.16H, C(CH$_2$C<u>H</u>$_3$)$_2$ (6H of compound **45**)). [8]

Based on the ^{1}H NMR spectral data given above, the integrations of 1H each of O- and C-alkylation products *E*-**43**, *Z*-**43**, **44_{keto}**, **44_{enol}** and **45** relative to 1H of *E*-**43** are as follows:

$$I_{E-\mathbf{43}} = \frac{3.00}{3} = 1.00; \quad I_{Z-\mathbf{43}} = \frac{0.50}{2} = 0.25;$$

[a] The relevant ^{1}H NMR spectra are shown in Figure C21 and Figure C22 in Appendix C.

[b] Signals of *E*-**43**, *Z*-**43**, **44_{keto}** and **44_{enol}** that are overlapping with other signals: δ 3.92 – 3.86 (m, contains 3H of *E*-**43** and ethyl sulfate signal), 2.31 – 2.26 (m, contains 2H of **44_{enol}**), 1.82 – 1.76 (m, contains 2H of **44_{keto}**), 1.34 – 1.29 (m, contains 3H of *E*-**43** and 3H of *Z*-**43**).

[c] The vinyl signals of the enol ether products at δ 5.59 and 5.03 as well as the signal associated with the α-proton of the C-mono-alkylation product at δ 3.69 may be undersized and thus not used in determining the O/C ratio. See pages 428 and 429 for details.

$$I_{\mathbf{44_{keto}}} = \frac{0.74}{3} = 0.25; \quad I_{\mathbf{44_{enol}}} = \frac{0.09}{3} = 0.03; \quad I_{\mathbf{45}} = \frac{0.16}{6} = 0.026$$

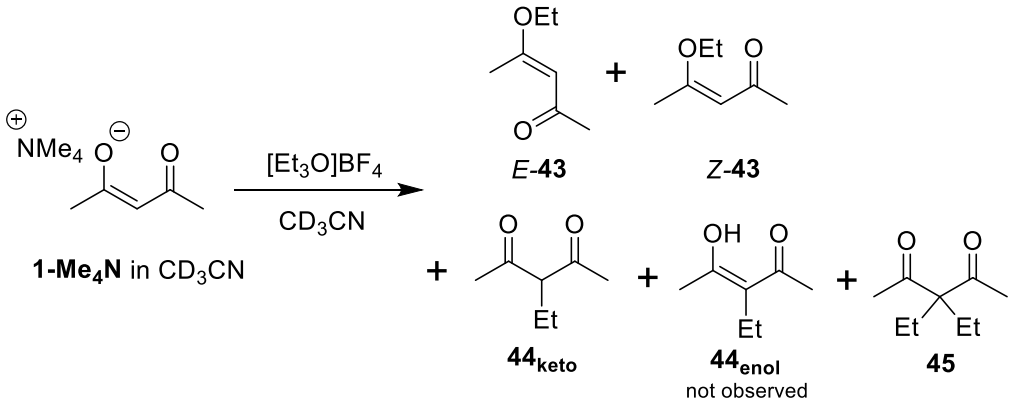
where $I_{\mathbf{X}}$ is the integration of 1H of compound **X** (**X** = *E*-**43**, *Z*-**43**, **44keto**, **44enol** or **45**) relative to 1H of compound *E*-**43**. Since $I_{\mathbf{X}} \propto [\mathbf{X}]$ (concentration of **X** in mol L^{-1}), the percentage of O-alkylation is given by:

$$\text{Percentage of O-alkylation} = \frac{I_{E-\mathbf{43}} + I_{Z-\mathbf{43}}}{I_{E-\mathbf{43}} + I_{Z-\mathbf{43}} + I_{\mathbf{44_{keto}}} + I_{\mathbf{44_{enol}}} + I_{\mathbf{45}}} \times 100$$

$$\text{Percentage of O-alkylation} = \frac{1.00 + 0.25}{1.00 + 0.25 + 0.25 + 0.03 + 0.026} \times 100 = 80\%$$

Integrations give an O vs C ratio of 80:20

(vi) Reaction of Enolate 1-Me4N with [Et3O]BF4 in CD3CN



Reaction of **1-Me4N** (0.031 g, 0.18 mmol) in CD_3CN (0.45 ml) and $[Et_3O]BF_4$ (0.0288 g, 0.152 mmol; added as a solution in CD_3CN (0.40 ml)) at 20 °C by procedure A.

^{1}H NMR (600 MHz, CD_3CN) of crude mixture of alkylation products (the underlined integrations are expressed relative to 1H of compound *E*-**43**): [a,b,c]

Assigned to *E*-**43**: δ 5.59 (s, 1H, C=C<u>H</u>), 3.88 (q, *J* = 7.0 Hz, 2H, OC<u>H</u>$_2$CH$_3$), 2.22 (s, 3H, C<u>H</u>$_3$C=C), 2.10 (s, 3H, C<u>H</u>$_3$C=O). [4]

Assigned to *Z*-**43**: δ 5.04 (s, 0.50H, C=C<u>H</u> (1H of compound *Z*-**43**)), 4.13 (q, *J* = 7.0 Hz, 0.95H, OC<u>H</u>$_2$CH$_3$ (2H of compound *Z*-**43**)), 2.25 (s, 1.43H, C<u>H</u>$_3$C=O (3H of compound *Z*-**43**)), 2.05 (s, 1.38H, C<u>H</u>$_3$C=C (3H of compound *Z*-**43**)). [4]

Assigned to **44keto**: δ 3.69 (t, *J* = 7.1 Hz, 0.18H (1H of compound **44keto**)), 2.16 (s, 1.00H, C<u>H</u>$_3$C=O (6H of compound **44keto**)), 1.84 – 1.77 (m, 0.40H, C(C<u>H</u>$_2$CH$_3$) (2H of compound **44keto**)), 0.87 (t, *J* = 7.4 Hz, 0.57H, C(CH$_2$C<u>H</u>$_3$) (3H of compound **44keto**)). [7]

---

[a] The relevant ^{1}H NMR spectra are shown in Figure C23 and Figure C24 in Appendix C.

[b] Signals of *E*-**43**, *Z*-**43** and **45** that are overlapping with other signals: δ 1.93 – 1.88 (m, contains 4H of **45**), 1.35 – 1.28 (m, contains 3H of *E*-**43** and 3H of *Z*-**43**).

[c] The vinyl signals of the enol ether products at δ 5.59 and 5.04 as well as the signal associated with the α-proton of the C-mono-alkylation product at δ 3.69 may be undersized and thus not used in determining the O/C ratio. See pages 428 and 429 for details.

Assigned to **45**: δ 2.07 (s, 0.07H, $CH_3C{=}O$ (6H of compound **45**)), 0.71 (t, *J* = 7.6 Hz, 0.11H, $C(CH_2CH_3)_2$ (6H of compound **45**)). [8]

Based on the ^{1}H NMR spectral data given above, the integrations of 1H each of O- and C-alkylation products *E*-**43**, *Z*-**43**, **44**$_{\mathbf{keto}}$ and **45** relative to 1H of *E*-**43** are as follows:

$$I_{E-\mathbf{43}} = \frac{2.00}{2} = 1.00;\ I_{Z-\mathbf{43}} = \frac{0.95}{2} = 0.48;\ I_{\mathbf{44_{keto}}} = \frac{0.57}{3} = 0.19;\ I_{\mathbf{45}} = \frac{0.11}{6} = 0.018$$

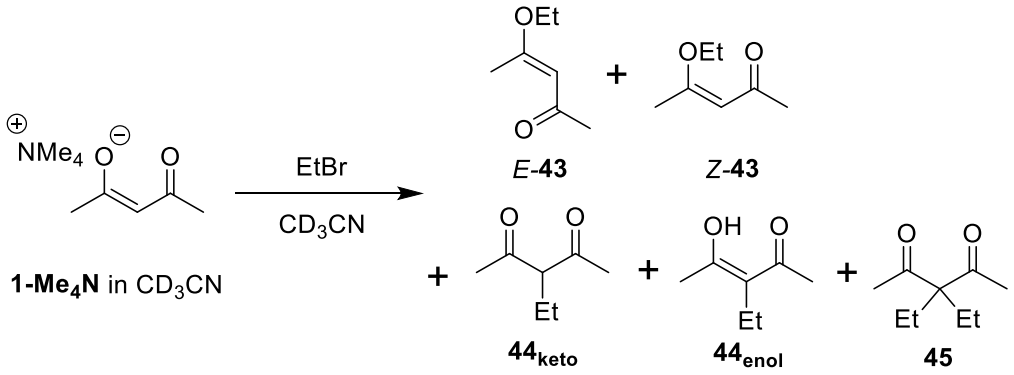
where $I_{\mathbf{X}}$ is the integration of 1H of compound **X** (**X** = *E*-**43**, *Z*-**43**, **44**$_{\mathbf{keto}}$ or **45**) relative to 1H of compound *E*-**43**. Since $I_{\mathbf{X}} \propto [\mathbf{X}]$ (concentration of **X** in mol L^{-1}), the percentage of O-alkylation is given by:

$$\text{Percentage of O-alkylation} = \frac{I_{E-\mathbf{43}} + I_{Z-\mathbf{43}}}{I_{E-\mathbf{43}} + I_{Z-\mathbf{43}} + I_{\mathbf{44_{keto}}} + I_{\mathbf{45}}} \times 100$$

$$\text{Percentage of O-alkylation} = \frac{1.00 + 0.48}{1.00 + 0.48 + 0.19 + 0.018} \times 100 = 88\%$$

Integrations give an O vs C ratio of 88:12

(vii) Reaction of Enolate 1-Me$_4$N with Ethyl Bromide in CD$_3$CN



Reaction of a 0.67 mol L^{-1} stock solution of **1-Me$_4$N** (0.30 ml, 0.201 mmol) and ethyl bromide (0.0198 g, 0.182 mmol) in CD_3CN (0.85 ml) at 20 °C by procedure A.

^{1}H NMR (600 MHz, CD_3CN) of crude mixture of alkylation products (the underlined integrations are expressed relative to 1H of compound *E*-**43**): [a,b,c]

Assigned to *E*-**43**: δ 5.59 (s, 1H, C=C<u>H</u>), 3.89 (q, *J* = 7.0 Hz, 2H, $OC\underline{H}_2CH_3$), 2.23 (s, 3H, $C\underline{H}_3C{=}C$), 2.10 (s, 3H, $C\underline{H}_3C{=}O$). [4]

[a] The relevant ^{1}H NMR spectra are shown in Figure C25 and Figure C26 in Appendix C.

[b] Signals of *E*-**43,** *Z*-**43**, **44**$_{\mathbf{keto}}$, **44**$_{\mathbf{enol}}$ and **45** that are overlapping with other signals: δ 4.17 – 4.05 (m, contains 3H of *Z*-**43** and EtOAc signal), 2.32 – 2.27 (m, contains 2H of **44**$_{\mathbf{enol}}$), 2.16 (s, contains 6H of **44**$_{\mathbf{keto}}$), 2.11 – 2.03 (m, contains 3H of *Z*-**43**, 6H of **44**$_{\mathbf{enol}}$ and 6H of **45**), 1.95 – 1.87 (m, contains 4H of **45**), 1.86 – 1.76 (m, contains 2H of **44**$_{\mathbf{keto}}$), 1.36 – 1.27 (m, contains 3H of *E*-**43** and 3H of *Z*-**43**).

[c] The vinyl signals of the enol ether products at δ 5.59 and 5.04 as well as the signal associated with the α-proton of the C-mono-alkylation product at δ 3.69 are undersized and thus not used in determining the O/C ratio. See pages 428 and 429 for details.

Assigned to *Z*-**43**: δ 5.04 (s, 0.22H, C=CH (1H of compound *Z*-**43**)), 2.25 (s, 0.62H, CH_3C=O (3H of compound *Z*-**43**)). [4]

Assigned to **44keto**: δ 3.69 (t, *J* = 7.0 Hz, 2.87H, C(O)CHC(O) (1H of compound **44keto**)), 0.88 (t, *J* = 7.4 Hz, 9.31H, $C(CH_2CH_3)$ (3H of compound **44keto**)). [7]

Assigned to **44enol**: δ 1.03 (t, *J* = 6.4 Hz, 1.28H, $C(CH_2CH_3)$ (3H of compound **44enol**)). [7]

Assigned to **45**: δ 0.72 (t, *J* = 7.6 Hz, 3.29H, $C(CH_2CH_3)_2$ (6H of compound **45**)). [8]

Although no suitable baseline-separated signal is available is available for compound *Z*-**43**, the integration of the overlapping signals of compounds *E*-**43** and *Z*-**43** in the range δ 1.36 – 1.31 (3H of each compound) allows the quantity $I_{E\text{-}43} + I_{Z\text{-}43}$ to be calculated as follows:

$$I_{E-43} + I_{Z-43} = \frac{3.98}{3} = 1.326$$

Based on the ^{1}H NMR spectral data given above, the integrations of 1H each of O- and C-alkylation products *E*-**43**, *Z*-**43**, **44keto**, **44enol** and **45** relative to 1H of *E*-**43** are as follows:

$$I_{E\text{-}43} + I_{Z-43} = 1.326$$

$$I_{44_{\text{keto}}} = \frac{9.31}{3} = 3.10; \quad I_{44_{\text{enol}}} = \frac{1.28}{3} = 0.426; \quad I_{45} = \frac{3.29}{6} = 0.548$$

where $I_{\mathbf{X}}$ is the integration of 1H of compound **X** (**X** = *E*-**43**, *Z*-**43**, **44keto**, **44enol** or **45**) relative to 1H of compound *E*-**43**. Since $I_{\mathbf{X}} \propto [\mathbf{X}]$ (concentration of **X** in mol L^{-1}), the percentage of O-alkylation is given by:

$$\text{Percentage of O-alkylation} = \frac{I_{E-43} + I_{Z-43}}{I_{E-43} + I_{Z-43} + I_{44_{\text{keto}}} + I_{44_{\text{enol}}} + I_{45}} \times 100$$

$$\text{Percentage of O-alkylation} = \frac{1.326}{1.326 + 3.10 + 0.426 + 0.548} \times 100 = 25\%$$

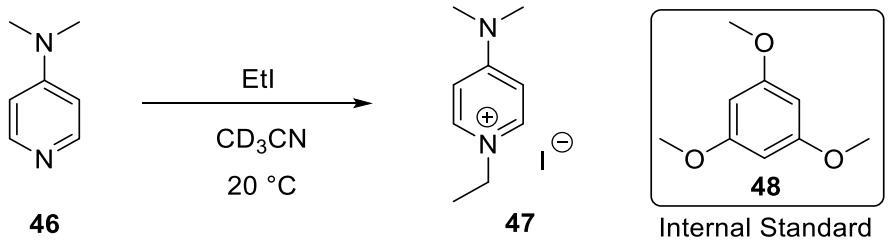
Integrations give an O vs C ratio of 25:75

7.3. Determination of $\Delta G^{\ddagger}$ Values for Reactions of DMAP + Various Electrophiles in CD_3CN

(i) Reaction of DMAP (46) + EtI in CD_3CN at 20 °C

Note: The general procedure B for measurement and determination of 2nd order rate constants is described below in full for the reaction of 4-dimethylaminopyridine with ethyl iodide in CD_3CN at 20 °C. For other reactions, only a brief summation of the reaction and the subsequent data will be supplied.

4-Dimethylaminopyridine (**46**) (0.0067 g, 0.0549 mmol) was weighed out and dissolved in dry CD_3CN (0.30 ml) in a Schlenk flask under nitrogen atmosphere. This solution was taken up in a syringe and the syringe was placed in a long Schlenk flask which was then sealed. 1,3,5-Trimethoxybenzene (**48**) (0.0092 g, 0.0549 mmol) was weighed out and added to a separate Schlenk flask. Ethyl iodide (0.0856 g, 0.549 mmol, 10 equivalents) was added to the flask containing the 1,3,5-trimethoxybenzene, followed by dry CD_3CN (0.5 ml). An empty NMR tube was placed in a long Schlenk tube. The long Schlenk tube, containing the NMR tube, was evacuated and re-filled with nitrogen ≥ 3 times, creating an inert atmosphere inside the flask. The entire reaction mixture was drawn into a syringe through a needle. The reaction mixture was added into the NMR tube under nitrogen. The NMR tube was then sealed by a rubber septum cap. After fitting the rubber septum to the NMR tube, the seal was secured by wrapping the external edge of the septum where it contacted the surface of the NMR tube with PTFE tape. The outside of the PTFE tape and rubber septum were then wrapped with a layer of Parafilm to further secure the nitrogen atmosphere inside the NMR tube. The NMR tube was retained in the large Schlenk flask under nitrogen.



The Schlenk tubes were placed in the room in which the NMR spectrometer was housed for 20 minutes to allow the solutions in the flasks to equilibrate to the controlled room temperature of 20 °C. The NMR tube containing the EtI solution was removed from the Schlenk flask and placed in the NMR spectrometer. The probe of the spectrometer was also kept at 20 °C. After obtaining the first ^1H NMR spectrum and shimming the sample, the NMR tube was ejected. The 4-dimethylaminopyridine (**46**) solution (0.30 ml, containing 0.0549 mmol 4-dimethylaminopyridine) in its syringe was removed from its Schlenk flask and added to the NMR tube by injection through the rubber septum. The septum was re-wrapped with Parafilm after removal of the syringe. The NMR tube was momentarily inverted to homogenise the solution contained therein, and was then rapidly returned to the spectrometer to obtain NMR spectra of the ongoing reaction at certain intervals.

Each spectrum was obtained on a 600 MHz instrument using 4 scans, a 5 second relaxation delay and a 30° pulse. The time ascribed to each spectrum was when the

spectrum measurement ended. In the obtained spectra, the 9H signal of 1,3,5-trimethoxybenzene (**48**) at δ 3.76 was set at a constant integral value throughout and the other signals were given relative to this value.

The following signals were observed in the spectra after the addition of 4-dimethylaminopyridine (**46**):

^{1}H NMR (600 MHz, CD_3CN)

Assigned to **46**: δ 8.18 – 8.11 (m, 2H), 6.58 – 6.55 (m, 2H), 2.98 (s, 6H). [9]

Assigned to **47**: δ 7.98 – 7.96 (m, 2H), 6.87 – 6.84 (m, 2H), 4.14 (q, *J* = 7.3 Hz, 2H), 3.18 (s, 6H), 1.45 (t, *J* = 7.3 Hz, 3H).

Assigned to **48**: δ 6.11 (s, 3H), 3.76 (s, 9H).

Assigned to **EtI**: δ 3.26 (q, *J* = 7.5 Hz, 2H), 1.82 (t, *J* = 7.5 Hz, 3H).

To observe the change in concentration of the reactants and products over time, the size of certain signals were monitored in each individual ^{1}H NMR spectrum. Each of the signals used for this purpose in this experiment can be seen below in Figure 7-5. The consumption of **46** in each spectrum was monitored by observing the decrease in the integration value of the signal at 6.57 ppm relative to the 9H signal of 1,3,5-trimethoxybenzene (**48**). The formation of **47** in each spectrum was monitored by observing the increase in the integration value of the 2H signal at 4.14 ppm relative to the 9H signal of 1,3,5-trimethoxybenzene (**48**).

Note: ^{13}C satellite peaks of the 9H signal of **48** at δ 3.76 appear at δ 3.88 and 3.64. These signals were included in the integration value for that signal. ^{13}C satellite peaks of the 2H signal of **46** at δ 6.57 appear at δ 6.71 – 6.69 and 6.44 – 6.42. These signals were included in the integration value for that signal. ^{13}C satellite peaks of the 9H signal of **47** at δ 4.14 appear at δ 4.32 – 4.28 and 4.08 – 4.04. These signals were included in the integration value for that signal.

A representative spectrum that was recorded during this experiment is seen in Figure C27 in Appendix C.

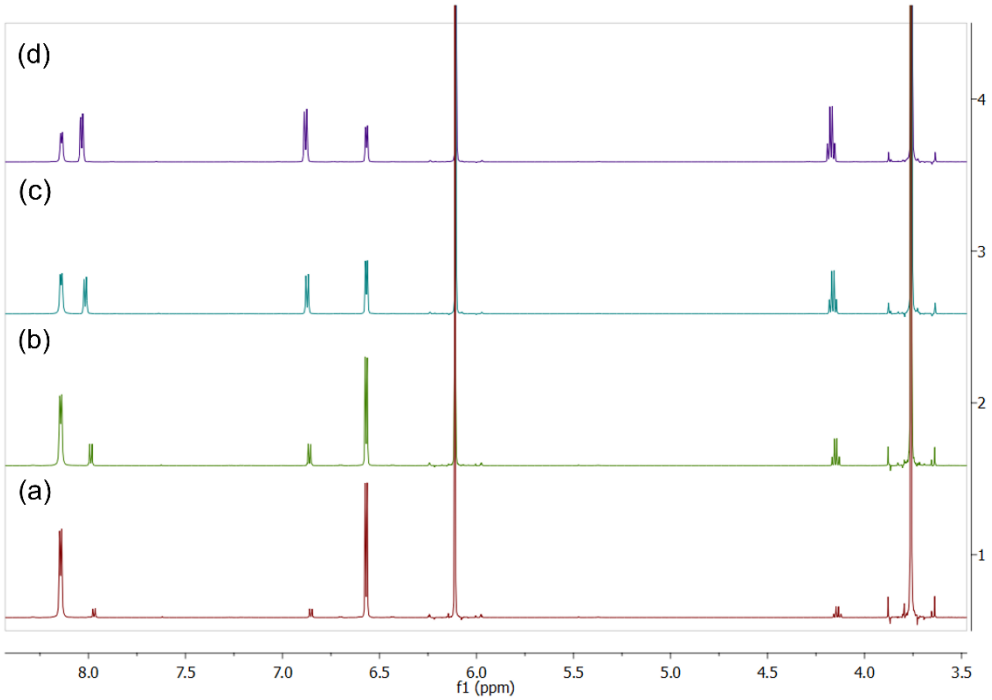


Figure 7-5: Stacked ^{1}H NMR spectra in CD_3CN of the reaction of **46** and EtI. The signals of **47** appear as the reaction progresses. The reaction progresses from the bottom of the stacked spectra (spectrum (a)) to the top (spectrum (d)).

The integration value for **47** was assigned a concentration value ($[\mathbf{47}]_t$) relative to the concentration of **48**. The concentration of **48** was 6.86 $\times 10^{-2}$ mmol mL^{-1}.

As the 9H signal of **48** was arbitrarily set to = 90.00 units, when a signal is integrated to be equal to 1H of the compound, 10.00 integration units = 0.0686 mmol mL^{-1}, or 1 integration unit = 0.00686 mmol mL^{-1}.

Thus, to assign a concentration value ($[\mathbf{47}]_t$) for **47** in a given spectrum:

$$[\mathbf{47}]_{t=x} = \left(\frac{\text{integration value}}{2}\right)(0.00686\ \text{mmol/ml})$$

at a given timepoint *x*. The integration value is divided by 2 in this case as a 2H signal of **47** (at 4.14 ppm) is being used to calculate the concentration.

At *t* = 307 seconds, the integration value of the signal at 4.14 ppm was equal to 0.58 integration units relative to **48**, giving:

$$[\mathbf{47}]_{t=307\ \text{s}} = \left(\frac{0.58}{2}\right)(0.00686\ \text{mmol/ml}) \ = \ 0.00199\ \text{mmol/ml}$$

This procedure was continued at various time points to monitor the formation of **47**. After 312 minutes, conversion was approximately 91%. An approximate value of the pseudo-1st order rate constant was derived based on data recorded for 64 timepoints of the reaction up to this level of conversion.

The integration values and calculated concentration values of **47** are shown below in Table 7-1.

The temperature of solutions during kinetic studies was kept constant (20 ± 0.1 °C). In all kinetic runs, the concentration of the electrophile was at least 10 times higher than that of the nucleophile, resulting in pseudo-first-order kinetics. The first-order rate constant k_{obs} at a given nucleophile concentration was obtained by least-squares fitting of the single-exponential function $[\mathbf{47}]_t = [\mathbf{46}]_0 (1 - e^{-k_{obs}t} + C)$ to the growth curve formed by plotting the values of ($[\mathbf{47}]_t$) versus time (see Figure 7-6 below), where $[\mathbf{46}]_0$ and $[\mathbf{47}]_t$ are the concentrations of **47** at time *t* and the concentration of **46** at time 0, respectively, and C is a constant. An approximate value for the second-order rate constant *k* were obtained by dividing k_{obs} by the concentration of the electrophile (which was in excess).

The graph of ($[\mathbf{47}]_t$) versus time is shown below in Figure 7-6.

For the 2nd order reaction of **47** with EtI (and rate constant *k*):

$$\text{Rate} = k[\mathbf{47}][\text{EtI}]$$

By including ≥ 10 equivalents of EtI, the approximation can be made that:

$$[\text{EtI}]_t = [\text{EtI}]_0$$

Thus, for this pseudo-1st order reaction:

$$\text{Rate} = k_{\text{obs}}[\mathbf{47}]$$

where $k_{\text{obs}} = k[\text{EtI}]_0$

The least squares fitting of the plot of the values of [**47**]*t* shown in Table 7-1 versus time (see plot in Figure 7-6) to the function $[\mathbf{47}]_t = [\mathbf{46}]_0 (1 - e^{-k_{obs}t} + C)$ gives a value of the pseudo-1st order rate constant of $k_{\text{obs}} = 9.36 \times 10^{-5}\ \text{s}^{-1}$. The coefficient of determination (R^2) value is 0.9999. Hence, since $[\text{EtI}]_0 = 0.686\ \text{mol L}^{-1}$,

$$k = \frac{9.36 \times 10^{-5}\ \text{s}^{-1}}{0.686\ \text{mol L}^{-1}}$$

$$= 1.36 \times 10^{-4}\ \text{L mol}^{-1}\ \text{s}^{-1}$$

Table 7-1. Recorded integration values (I_{47}) and calculated concentrations of **47** at various time points during the reaction of DMAP with ethyl iodide in CD_3CN at 20 °C.

Time (s)	I_{47}	$[\mathbf{47}]_t$ (mmol/ml)	Time (s)	I_{47}	$[\mathbf{47}]_t$ (mmol/ml)	Time (s)	I_{47}	$[\mathbf{47}]_t$ (mmol/ml)
0	0	0	**2034**	3.09	0.0106	**8106**	9.36	0.0321
307	0.58	0.0020	**2300**	3.46	0.0119	**8371**	9.60	0.0329
379	0.68	0.0023	**2566**	3.76	0.0129	**8637**	9.80	0.0336
452	0.80	0.0027	**2831**	4.14	0.0142	**8901**	9.95	0.0341
525	0.92	0.0032	**3096**	4.43	0.0152	**9167**	10.18	0.0349
598	1.03	0.0035	**3359**	4.76	0.0163	**9433**	10.48	0.0359
671	1.15	0.0039	**3625**	5.07	0.0174	**9699**	10.54	0.0362
743	1.28	0.0044	**3890**	5.37	0.0184	**9961**	10.74	0.0368
816	1.36	0.0047	**4156**	5.68	0.0195	**10596**	11.03	0.0378
888	1.51	0.0052	**4422**	5.95	0.0204	**11222**	11.39	0.0391
961	1.58	0.0054	**4685**	6.28	0.0215	**11848**	11.91	0.0409
1034	1.67	0.0057	**4950**	6.63	0.0227	**12472**	12.10	0.0415
1107	1.81	0.0062	**5215**	6.87	0.0236	**13098**	12.44	0.0427
1181	1.90	0.0065	**5480**	7.13	0.0245	**13724**	12.75	0.0437
1254	2.01	0.0069	**5986**	7.59	0.0260	**14350**	12.97	0.0445
1327	2.12	0.0073	**6250**	7.89	0.0271	**14974**	13.27	0.0455
1400	2.23	0.0076	**6515**	7.99	0.0274	**15598**	13.48	0.0462
1473	2.33	0.0080	**6781**	8.38	0.0287	**16223**	13.73	0.0471
1546	2.45	0.0084	**7047**	8.53	0.0293	**16849**	14	0.0480
1619	2.52	0.0086	**7312**	8.76	0.0300	**17475**	14.24	0.0488
1692	2.63	0.0090	**7577**	8.98	0.0308	**18719**	14.54	0.0499
1769	2.76	0.0095	**7843**	9.20	0.0316			

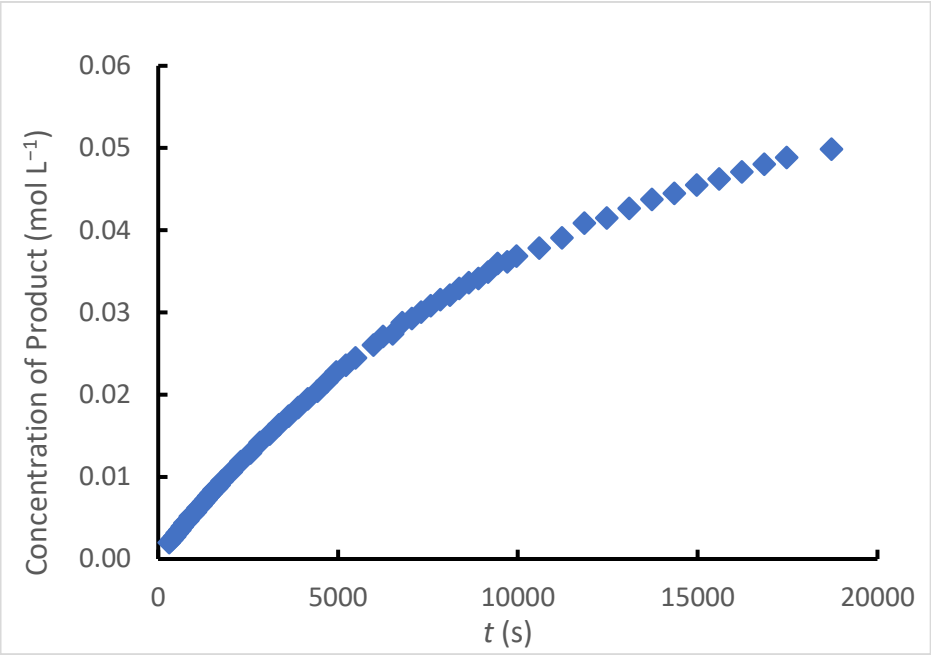


Figure 7-6: The plot of ([**47**]$_t$) versus time for the reaction of 4-dimethylaminopyridine (**46**) + EtI in CD_3CN at 20 °C.

This value of the rate constant *k* may be related to $\Delta G^{\ddagger}$ by the Eyring equation:

$$k = \boldsymbol{\kappa}\frac{k_B T}{h} \times \frac{RT}{p^{\circ}}\, e^{-\frac{\Delta G^{\ddagger}}{RT}}$$

as seen in Atkins' Physical Chemistry, 9th ed. Section 22.4 pg. 848.[10] The transmission coefficient κ is taken to equal 1.

This equation can be rearranged to:

$$RT \ln\left(\left(\frac{1}{k}\right)\left(\frac{k_B T}{h}\right)\left(\frac{RT}{p^{\circ}}\right)\right) = \Delta G^{\ddagger}$$

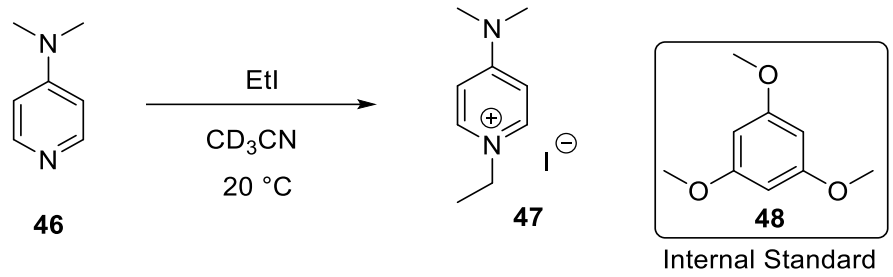
giving:

$$\Delta G^{\ddagger} = 101.2 \text{ kJ mol}^{-1}$$

where:

$$R = 8.314 \text{ J K}^{-1}\text{mol}^{-1} \quad T = 293.15 \text{ K}$$
$$p^{\circ} = 10^5 \text{ N m}^{-2} \quad k_B = 1.38 \times 10^{-23} \text{ J K}^{-1} \quad h = 6.63 \times 10^{-34} \text{ J s}$$

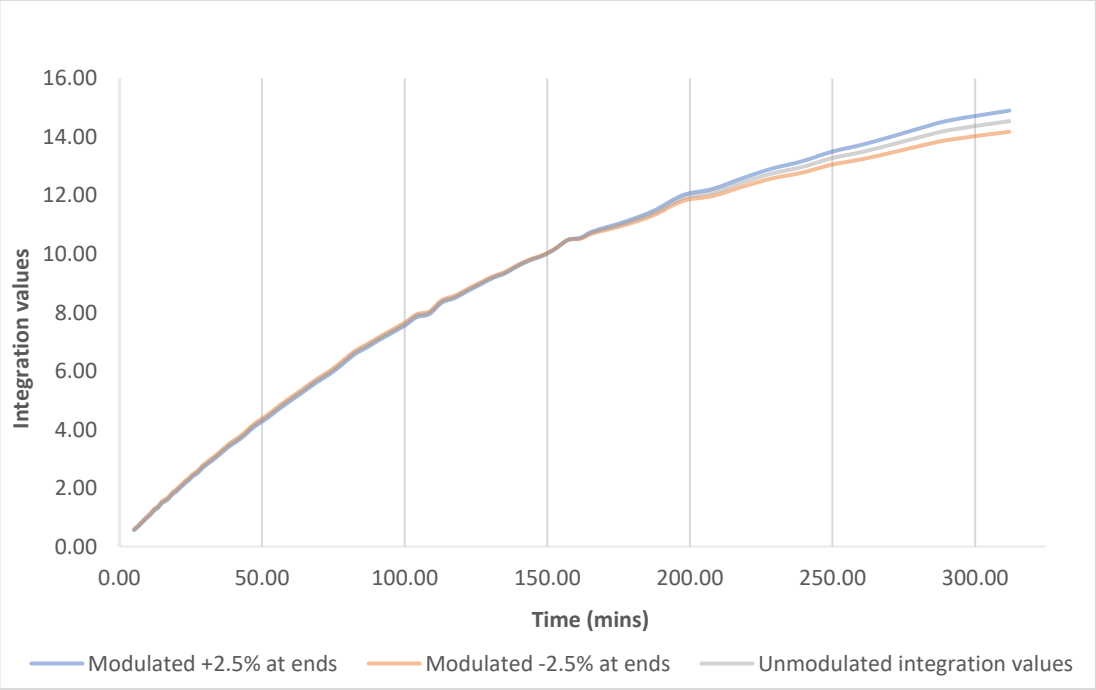
An error analysis for each of the rate measurement reactions described in section 7.3 was performed. Shown below is the error analysis for the reaction of ethyl iodide and DMAP (**46**) in CD_3CN as described in section 7.3 experiment (i). Three sources of error are individually considered, before being compiled into an overall error range.



(i) k_{obs} error

The error on the measurement of integrations of [**47**] (i.e., the integrations of signals of **47**) in this experiment is approximately 5%, or ± 2.5%. The maximum possible error that could be engendered in the value of k_{obs} (extracted as the exponent in the equation $[\mathbf{47}]_t = [\mathbf{46}]_0 (1 - e^{-k_{obs}t} + C)$ which results from potential errors in integration values from an NMR spectrum would arise if the largest over-estimation of the true integration value occurred on the first datapoint and the largest under-estimation of the true integration value occurred on the last data point (or *vice versa*), with a grading of error for the points in between such that there is no error on the datapoint which lies in the middle of the plot. This scenario would result in the largest possible change in the exponent, and hence the largest change in the curvature of the growth plot.

By this method, new values of k_{obs} may be calculated which reflect the maximum possible error engendered in k_{obs} that results from an error of ± 2.5% on the integrations values.



Modulation of the initially measured point by – 2.5% and the final measured point by + 2.5% with a variable grade of error applied to each intermediate datapoint gives a k_{obs} value of:

$$k_{\text{obs}} = 0.00008600$$

Converting to *k*, using $[\text{EtI}]_0 = 0.686$ mmol ml^{-1} gives:

$$k = k_{\text{obs}} \times [\text{EtI}]_0 = 0.0001254$$

Using this value of *k* to calculate $\Delta G^{\ddagger}$ using the Eyring equation gives:

$$\Delta G^{\ddagger} = RT \ln\left(\left(\frac{1}{k}\right)\left(\frac{k_B T}{h}\right)\left(\frac{RT}{p^{\circ}}\right)\right) = 101.43 \text{ kJ mol}^{-1}$$

Modulation of the initially measured point by + 2.5% and the final measured point by – 2.5% with a variable grade of error applied to each intermediate datapoint gives a k_{obs} value of:

$$k_{\text{obs}} = 0.00010185$$

Converting to *k*, using $[\text{EtI}]_0 = 0.686$ mmol ml^{-1} gives:

$$k = k_{\text{obs}} \times [\text{EtI}]_0 = 0.0001485$$

Using this value of *k* to calculate $\Delta G^{\ddagger}$ using the Eyring equation gives:

$$\Delta G^{\ddagger} = RT \ln\left(\left(\frac{1}{k}\right)\left(\frac{k_B T}{h}\right)\left(\frac{RT}{p^{\circ}}\right)\right) = 101.02 \text{ kJ mol}^{-1}$$

Thus an error range of ± 0.21 kJ mol^{-1} is obtained either side of 101.22 kJ mol^{-1}.

(ii) Random Error

A conservative estimate of a ± 5% error was applied on the masses recorded in this experiment.

Accounting for random error, the amount of EtI weighed in this reaction is therefore:

$$0.0856 \text{ g} \pm 0.0043 \text{ g}$$

hence upon converting to moles:

$$n_{\mathbf{EtI}} = 0.549 \text{ mmol} \pm 0.027 \text{ mmol}$$

A very conservative estimate of the error on the total volume of the reaction mixture of 5% was also applied. This estimate would readily account for any minor losses of solvent due to solvent evaporation. This estimate gives:

$$0.80 \text{ ml} \pm 0.04 \text{ ml}$$

Using these ranges of values, an upper and lower limit for the concentration of $[\text{EtI}]_0$ in the reaction mixture may be calculated. The upper bound of concentration considers the largest possible amount of electrophile in the lowest possible among of solvent:

$$= \frac{0.549 + 0.027 \text{ mmol}}{0.80 - 0.04 \text{ ml}} = 0.758 \text{ mol L}^{-1}$$

The lower bound of concentration considers the lowest possible amount of internal standard in the largest possible among of solvent:

$$= \frac{0.549 - 0.027 \text{ mmol}}{0.80 + 0.04 \text{ ml}} = 0.621 \text{ mol L}^{-1}$$

Using these values to calculate *k* in the manner shown in Section 3.1, as well as using the Eyring equation:

$$RT \ln\left(\left(\frac{1}{k}\right)\left(\frac{k_B T}{h}\right)\left(\frac{RT}{p^\circ}\right)\right) = \Delta G^\ddagger$$

An error range of ± 0.24 kJ mol^{-1} is obtained either side of 101.22 kJ mol^{-1}.

(iii) Temperature Variance

The internal temperature of the Bruker Avance III 600 MHz spectrometer was maintained at 293.15 K for the rate measurement experiment. Although the systematic error associated with this would be equal to ± 0.1 K, a conservative estimate for a maximum variance of ± 0.5 K was adopted.

Therefore, T = 293.15 ± 0.5 K

Using the previously calculated value of *k* shown on page 452, as well as the adjusted values for *T* in the Eyring equation:

$$RT \ln\left(\left(\frac{1}{k}\right)\left(\frac{k_B T}{h}\right)\left(\frac{RT}{p^\circ}\right)\right) = \Delta G^\ddagger$$

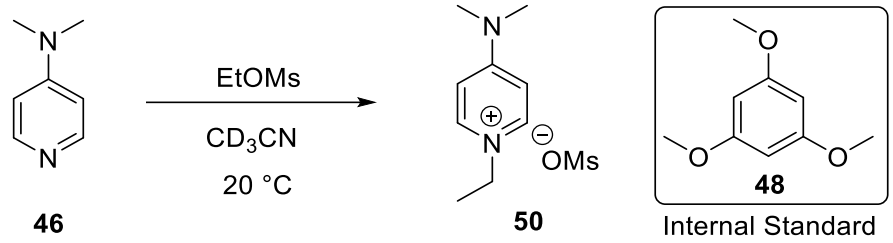
An error range of ± 0.18 kJ mol^{-1} is obtained either side of 101.22 kJ mol^{-1}.

(iv) Combined Sources of Error

Combining all of the three considered sources of error, the Gibbs energy of activation for the reaction of DMAP + EtI in CD_3CN at 20 °C was determined to be:

$$\Delta G^\ddagger = 101.2 \pm 0.6 \text{ kJ mol}^{-1}$$

(ii) Reaction of DMAP (46) + EtOMs in CD_3CN at 20 °C



From 4-dimethylaminopyridine (**46**) (0.0100 g, 0.082 mmol) and ethyl mesylate (0.1077 g, 0.867 mmol, 10 equivalents) in dry CD_3CN (0.75 ml) at 20 °C by procedure B. 1,3,5-Trimethoxybenzene (**48**) (0.0139 g, 0.083 mmol) was added as an internal standard.

The procedure followed for this experiment was identical to that described above in the representative general procedure in section 7.3 part (i), other than the points highlighted below.

The following signals were observed in the spectra after the addition of DMAP:

^{1}H NMR (600 MHz, CD_3CN)

Assigned to **46**: δ 8.16 – 8.11 (m, 2H), 6.59 – 6.56 (m, 2H), 2.98 (s, 6H). [9]

Assigned to **50**: δ 8.01 – 7.97 (m, 2H), 6.88 – 6.84 (m, 2H), 4.16 – 4.12 (m, 2H), 3.18 (s, 6H), 1.49 – 1.43 (m, 3H).

Assigned to **48**: δ 6.12 (s, 3H), 3.76 (s, 9H).

Assigned to **EtOMs**: δ 4.31 – 4.23 (m, 2H), 2.98 (s, 3H), 1.41 – 1.33 (m, 3H).

Spectra were recorded at various time points to monitor the formation of **50**. In each spectrum, the integration value of the signal of **50** at δ 6.58 relative to the integration of the signal of 1,3,5-trimethoxybenzene at δ 3.76 was used to establish the concentration of the **50** relative to that of 1,3,5-trimethoxybenzene (**48**) (0.1106 mmol ml^{-1}). The integration values and calculated concentration values of **50** are shown below in Table 7-2. After 13 hours and 20 minutes, conversion was approximately 30%. An approximate value of the pseudo-1st order rate constant was derived based on data recorded for 48 timepoints of the reaction up to this level of conversion. A representative spectrum that was recorded during this experiment is seen in Figure C28 in Appendix C.

Table 7-2. Recorded integration values (I_{50}) and calculated concentrations of **50** at various time points during the reaction of DMAP with EtOMs in CD_3CN at 20 °C.

Time (s)	I_{50}	$[\mathbf{50}]_t$ (mmol/ml)	Time (s)	I_{50}	$[\mathbf{50}]_t$ (mmol/ml)	Time (s)	I_{50}	$[\mathbf{50}]_t$ (mmol/ml)
0	0	0	**5805**	0.86	0.0048	**24597**	3.30	0.0182
380	0.07	0.0004	**6438**	0.95	0.0053	**25830**	3.45	0.0191
490	0.08	0.0004	**7071**	1.04	0.0058	**28261**	3.72	0.0206
601	0.08	0.0004	**7704**	1.13	0.0062	**28371**	4.05	0.0224
871	0.14	0.0008	**8337**	1.21	0.0067	**31404**	4.07	0.0225
1532	0.24	0.0013	**8971**	1.33	0.0074	**33237**	4.28	0.0237
1833	0.28	0.0015	**9866**	1.44	0.0080	**35070**	4.49	0.0248
2166	0.32	0.0018	**11064**	1.60	0.0088	**36901**	4.71	0.0260
2499	0.37	0.0020	**12297**	1.76	0.0097	**38734**	4.88	0.0270
2832	0.42	0.0023	**14731**	2.08	0.0115	**40567**	5.09	0.0281
3166	0.50	0.0028	**15964**	2.25	0.0124	**42400**	5.25	0.0290
3496	0.54	0.0030	**17197**	2.45	0.0135	**44234**	5.46	0.0302
3829	0.57	0.0032	**18430**	2.54	0.0140	**46067**	5.63	0.0311
4162	0.63	0.0035	**19663**	2.70	0.0149	**47900**	5.83	0.0322
4496	0.68	0.0038	**20897**	2.86	0.0158	**48010**	5.84	0.0323
4829	0.74	0.0041	**22130**	3.01	0.0166			
5172	0.77	0.0043	**23363**	3.15	0.0174			

The least squares fitting of the plot of the values of [**50**]*t* shown in Table 7-2 versus time (see plot in Figure 7-7) to the function $[\mathbf{50}]_t = [\mathbf{46}]_0 (1 - e^{-k_{obs}t} + C)$ gives a value of the pseudo-1st order rate constant of $k_{obs} = 1.00 \times 10^{-5}$ s^{-1}. The coefficient of determination (R^2) value is 0.9993. Hence, since $[\text{EtOMs}]_0 = 1.16$ mol L^{-1},

$$k = \frac{1.00 \times 10^{-5}\ \text{s}^{-1}}{1.16\ \text{mol L}^{-1}}$$

$$= 8.62 \times 10^{-6}\ \text{L mol}^{-1}\ \text{s}^{-1}$$

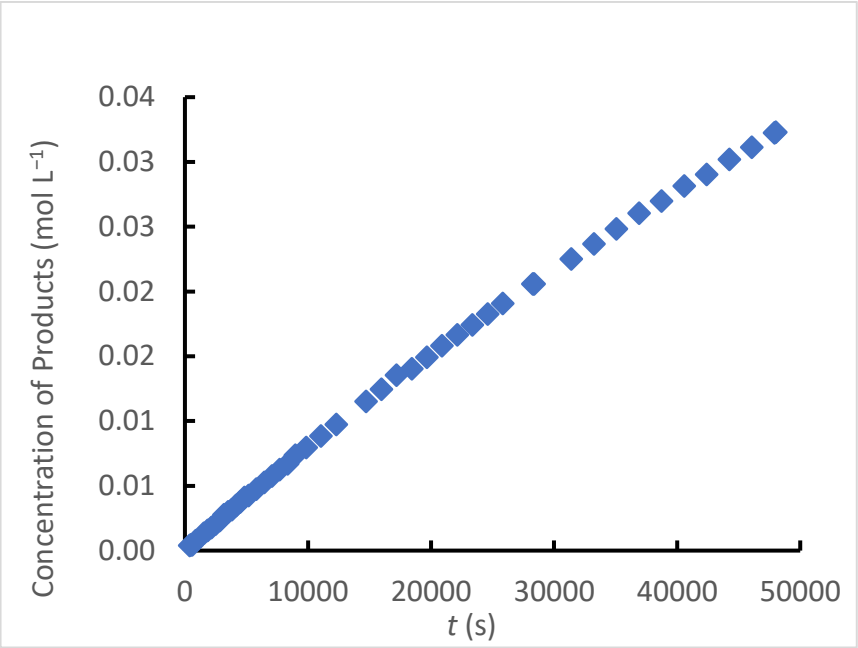


Figure 7-7: The plot of ([**50**]$_t$) versus time for the reaction of 4-dimethylaminopyridine (**46**) + EtOMs in CD_3CN at 20 °C.

The value of $\Delta G^{\ddagger}$ was determined by the following equation:

$$RT \ln\left(\left(\frac{1}{k}\right)\left(\frac{k_B T}{h}\right)\left(\frac{RT}{p^{\circ}}\right)\right) = \Delta G^{\ddagger}$$

giving:

$$\Delta G^{\ddagger} = 108.1 \text{ kJ mol}^{-1}$$

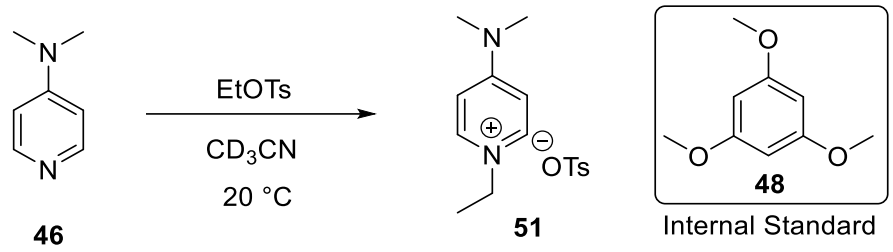
where:

$$R = 8.314 \text{ J K}^{-1}\text{mol}^{-1} \quad T = 293.15 \text{ K}$$
$$p^{\circ} = 10^5 \text{ N m}^{-2} \quad k_B = 1.38 \times 10^{-23} \text{ J K}^{-1} \quad h = 6.63 \times 10^{-34} \text{ J s}$$

An error analysis identical to the one demonstrated on pages 455 – 457 was performed for this reaction. Combining all of the three considered sources of error, the Gibbs energy of activation for the reaction of DMAP + EtOMs in CD_3CN at 20 °C was determined to be:

$$\Delta G^{\ddagger} = 108.1 \pm 1.0 \text{ kJ mol}^{-1}$$

(iii) Reaction of DMAP (46) + EtOTs in CD_3CN at 20 °C



From 4-dimethylaminopyridine (**46**) (0.0114 g, 0.0933 mmol) and ethyl tosylate (0.1868 g, 0.933 mmol, 10 equivalents) in dry CD_3CN (0.75 ml) at 20 °C by procedure B. 1,3,5-Trimethoxybenzene (**48**) (0.0159 g, 0.0945 mmol) was added as an internal standard.

The procedure followed for this experiment was identical to that described above in the representative general procedure in section 7.3 part (i), other than the points highlighted below.

The following signals were observed in the spectra after the addition of DMAP:

^{1}H NMR (600 MHz, CD_3CN)

Assigned to **46**: δ 8.17 – 8.12 (m, 2H), 6.59 – 6.52 (m, 2H), 2.96 (s, 6H). [9]

Assigned to **51**: δ 8.03 – 7.99 (m, 2H), 6.84 – 6.80 (m, 2H), 4.15 (q, *J* = 7.3 Hz, 2H), 3.14 (s, 6H), 1.43 (t, *J* = 7.3 Hz, 3H).

Assigned to **48**: δ 6.12 (s, 3H), 3.76 (s, 9H).

Assigned to **EtOTs**: δ 7.84 – 7.75 (m, 2H), 7.45 – 7.41 (m, 2H), 4.08 (q, *J* = 7.1 Hz, 2H), 2.43 (s, 3H), 1.24 (t, *J* = 7.1 Hz, 3H).

Spectra were recorded at various time points to monitor the formation of **51**. In each spectrum, the integration value of the signal of **51** at δ 1.43 relative to the integration of the signal of 1,3,5-trimethoxybenzene at δ 3.76 was used to establish the concentration of the **51** relative to that of 1,3,5-trimethoxybenzene (0.126 mmol ml^{-1}). The integration values and calculated concentration values of **51** are shown below in Table 7-3. After 15 hours and 35 minutes, conversion was approximately 68%. An approximate value of the pseudo-1st order rate constant was derived based on data recorded for 51 timepoints of the reaction up to this level of conversion. A representative spectrum that was recorded during this experiment is seen in Figure C29 in Appendix C.

Table 7-3. Recorded integration values (I_{51}) and calculated concentrations of **51** at various time points during the reaction of DMAP with EtOTs in CD_3CN at 20 °C.

Time (s)	I_{51}	$[\mathbf{51}]_t$ (mmol/ml)	Time (s)	I_{51}	$[\mathbf{51}]_t$ (mmol/ml)	Time (s)	I_{51}	$[\mathbf{51}]_t$ (mmol/ml)
0	0	0	**4931**	2.85	0.0120	**19612**	9.66	0.0406
323	0.26	0.0011	**5265**	3.03	0.0127	**21445**	10.38	0.0436
493	0.30	0.0013	**5598**	3.11	0.0131	**23279**	11.03	0.0463
605	0.40	0.0017	**5932**	3.28	0.0138	**25112**	11.62	0.0488
716	0.45	0.0019	**6266**	3.63	0.0152	**26945**	12.40	0.0521
827	0.49	0.0021	**6602**	3.77	0.0158	**28779**	13.08	0.0549
937	0.57	0.0024	**6944**	3.91	0.0164	**30613**	13.82	0.0580
1268	0.73	0.0031	**7878**	4.42	0.0186	**32446**	14.30	0.0601
1601	1.00	0.0042	**8812**	4.81	0.0202	**34280**	14.79	0.0621
1934	1.15	0.0048	**9746**	5.34	0.0224	**36114**	15.24	0.0640
2244	1.33	0.0056	**10680**	5.83	0.0245	**37947**	15.65	0.0657
2598	1.54	0.0065	**11614**	6.31	0.0265	**41581**	16.90	0.0710
2931	1.71	0.0072	**12545**	6.71	0.0282	**45215**	17.48	0.0734
3265	1.92	0.0081	**13446**	7.09	0.0298	**48849**	18.44	0.0774
3598	2.10	0.0088	**14378**	7.58	0.0318	**52482**	18.97	0.0797
3932	2.32	0.0097	**14553**	7.65	0.0321	**56116**	20	0.0840
4265	2.51	0.0105	**15944**	8.23	0.0346			
4598	2.62	0.0110	**17778**	8.92	0.0375			

The least squares fitting of the plot of the values of [**51**]*t* shown in Table 7-3 versus time (see plot in Figure 7-8) to the function $[\mathbf{51}]_t = [\mathbf{46}]_0 (1 - e^{-k_{obs}t} + C)$ gives a value of the pseudo-1st order rate constant of $k_{obs} = 2.12 \times 10^{-5}$ s^{-1}. The coefficient of determination (R^2) value is 0.9998. Hence, since $[EtOTs]_0 = 1.24$ mol L^{-1},

$$k = \frac{2.12 \times 10^{-5}\ \text{s}^{-1}}{1.24\ \text{mol L}^{-1}}$$

$$= 1.71 \times 10^{-5}\ \text{L mol}^{-1}\ \text{s}^{-1}$$

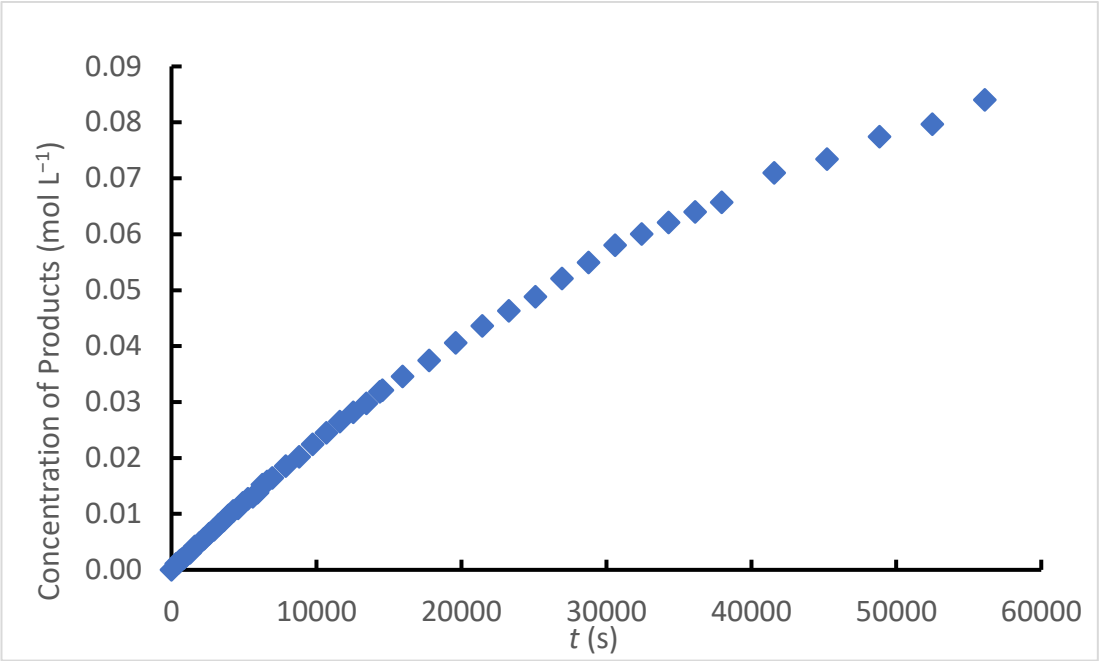


Figure 7-8: The plot of ([**51**]$_t$) versus time for the reaction of 4-dimethylaminopyridine + EtOTs in CD_3CN at 20 °C.

The value of $\Delta G^{\ddagger}$ was determined by the following equation:

$$RT \ln\left(\left(\frac{1}{k}\right)\left(\frac{k_B T}{h}\right)\left(\frac{RT}{p^{\circ}}\right)\right) = \Delta G^{\ddagger}$$

giving:

$$\Delta G^{\ddagger} = 106.3 \text{ kJ mol}^{-1}$$

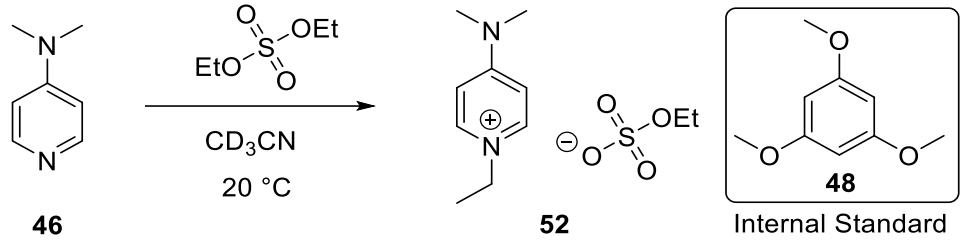
where:

$$R = 8.314 \text{ J K}^{-1}\text{mol}^{-1} \quad T = 293.15 \text{ K}$$
$$p^{\circ} = 10^5 \text{ N m}^{-2} \quad k_B = 1.38 \times 10^{-23} \text{ J K}^{-1} \quad h = 6.63 \times 10^{-34} \text{ J s}$$

An error analysis identical to the one demonstrated on pages 455 – 457 was performed for this reaction. Combining all of the three considered sources of error, the Gibbs energy of activation for the reaction of DMAP + EtOTs in CD_3CN at 20 °C was determined to be:

$$\Delta G^{\ddagger} = 106.3 \pm 0.7 \text{ kJ mol}^{-1}$$

(iv) Reaction of DMAP (46) + Diethyl Sulfate in CD_3CN at 20 °C



From 4-dimethylaminopyridine (**46**) (0.0028 g, 0.0229 mmol) and diethyl sulfate (0.0373 g, 0.242 mmol, 10 equivalents) in dry CD_3CN (0.80 ml) at 20 °C by procedure B. 1,3,5-Trimethoxybenzene (**48**) (0.0038 g, 0.0228 mmol) was added as an internal standard.

The procedure followed for this experiment was identical to that described above in the representative general procedure in section 7.3 part (i), other than the points highlighted below.

The following signals were observed in the spectra after the addition of DMAP:

^{1}H NMR (600 MHz, CD_3CN)

Assigned to **46**: δ 8.19 – 8.09 (m, 2H), 6.64 – 6.54 (m, 2H), 2.99 (s, 6H). [9]

Assigned to **52**: δ 8.00 – 7.97 (m, 2H), 6.89 – 6.84 (m, 2H), 4.15 (q, *J* = 7.3 Hz, 2H), 3.19 (s, 6H), 1.45 (t, *J* = 7.3 Hz, 3H).

Assigned to **48**: δ 6.12 (s, 3H), 3.76 (s, 9H).

Assigned to **$(EtO)_2SO_2$**: δ 4.34 (q, *J* = 7.1 Hz, 4H), 1.40 (t, *J* = 7.1 Hz, 6H).

Spectra were recorded at various time points to monitor the formation of **52**. In each spectrum, the integration value of the signal of **52** at δ 6.89 – 6.84 relative to the integration of the signal of 1,3,5-trimethoxybenzene at δ 3.76 was used to establish the concentration of the **52** relative to that of 1,3,5-trimethoxybenzene (0.0285 mmol ml^{-1}). The integration values and calculated concentration values of **52** are shown below in Table 7-4. After 3 hours and 48 minutes, conversion was approximately 98%. An approximate value of the pseudo-1st order rate constant was derived based on data recorded for 83 timepoints of the reaction up to this level of conversion. A representative spectrum that was recorded during this experiment is seen in Figure C30 in Appendix C.

Table 7-4. Recorded integration values (I_{52}) and calculated concentrations of **52** at various time points during the reaction of DMAP with diethyl sulfate in CD_3CN at 20 °C.

Time (s)	I_{52}	$[\mathbf{52}]_t$ (mmol/ml)	Time (s)	I_{52}	$[\mathbf{52}]_t$ (mmol/ml)	Time (s)	I_{52}	$[\mathbf{52}]_t$ (mmol/ml)
0	0	0	**1838**	3.80	0.0054	**5486**	8.89	0.0127
226	0.58	0.0008	**1894**	3.87	0.0055	**5622**	8.97	0.0128
283	0.74	0.0011	**1951**	4.02	0.0057	**5761**	9.18	0.0131
343	0.86	0.0012	**2013**	4.04	0.0058	**5899**	9.20	0.0131
402	0.96	0.0014	**2151**	4.26	0.0061	**6038**	9.32	0.0133
460	1.07	0.0015	**2290**	4.55	0.0065	**6102**	9.53	0.0136
519	1.17	0.0017	**2429**	4.78	0.0068	**6362**	9.74	0.0139
577	1.30	0.0019	**2568**	4.99	0.0071	**6622**	9.87	0.0141
635	1.48	0.0021	**2706**	5.12	0.0073	**6880**	10.28	0.0146
693	1.57	0.0022	**2845**	5.47	0.0078	**7139**	10.45	0.0149
751	1.68	0.0024	**2984**	5.64	0.0080	**7398**	10.71	0.0153
824	1.86	0.0027	**3122**	5.78	0.0082	**7657**	10.91	0.0155
882	1.95	0.0028	**3261**	5.98	0.0085	**7916**	11.02	0.0157
940	2.06	0.0029	**3400**	6.22	0.0089	**8178**	11.25	0.0160
1000	2.21	0.0031	**3539**	6.43	0.0092	**8433**	11.58	0.0165
1059	2.28	0.0032	**3678**	6.62	0.0094	**8692**	11.72	0.0167
1117	2.42	0.0034	**3817**	6.77	0.0096	**8951**	11.89	0.0169
1176	2.54	0.0036	**3953**	6.94	0.0099	**9207**	12.02	0.0171
1236	2.64	0.0038	**4091**	7.13	0.0102	**9466**	12.28	0.0175
1295	2.82	0.0040	**4230**	7.40	0.0105	**9725**	12.46	0.0178
1354	2.92	0.0042	**4369**	7.46	0.0106	**9984**	12.54	0.0179
1435	2.99	0.0043	**4508**	7.56	0.0108	**10068**	12.92	0.0184
1494	3.13	0.0045	**4645**	7.90	0.0113	**10688**	12.97	0.0185
1553	3.28	0.0047	**4784**	8.06	0.0115	**11307**	13.38	0.0191
1611	3.35	0.0048	**4923**	8.18	0.0117	**11926**	13.73	0.0196
1668	3.44	0.0049	**5062**	8.32	0.0119	**12545**	13.93	0.0199
1725	3.61	0.0051	**5201**	8.47	0.0121	**13164**	14.26	0.0203
1781	3.70	0.0053	**5341**	8.75	0.0125	**13670**	14.38	0.0205

The least squares fitting of the plot of the values of [**52**]*t* shown in Table 7-4 versus time (see plot in Figure 7-9) to the function $[\mathbf{52}]_t = [\mathbf{46}]_0 (1 - e^{-k_{obs}t} + C)$ gives a value of the pseudo-1st order rate constant of $k_{obs} = 1.27 \times 10^{-4}$ s^{-1}. The coefficient of determination (R^2) value is 0.9997. Hence, since $[(EtO)_2SO_2]_0 = 0.303$ mol L^{-1},

$$k = \frac{1.27 \times 10^{-4}\ \text{s}^{-1}}{0.303\ \text{mol L}^{-1}}$$

$$= 4.19 \times 10^{-4}\ \text{L mol}^{-1}\ \text{s}^{-1}$$

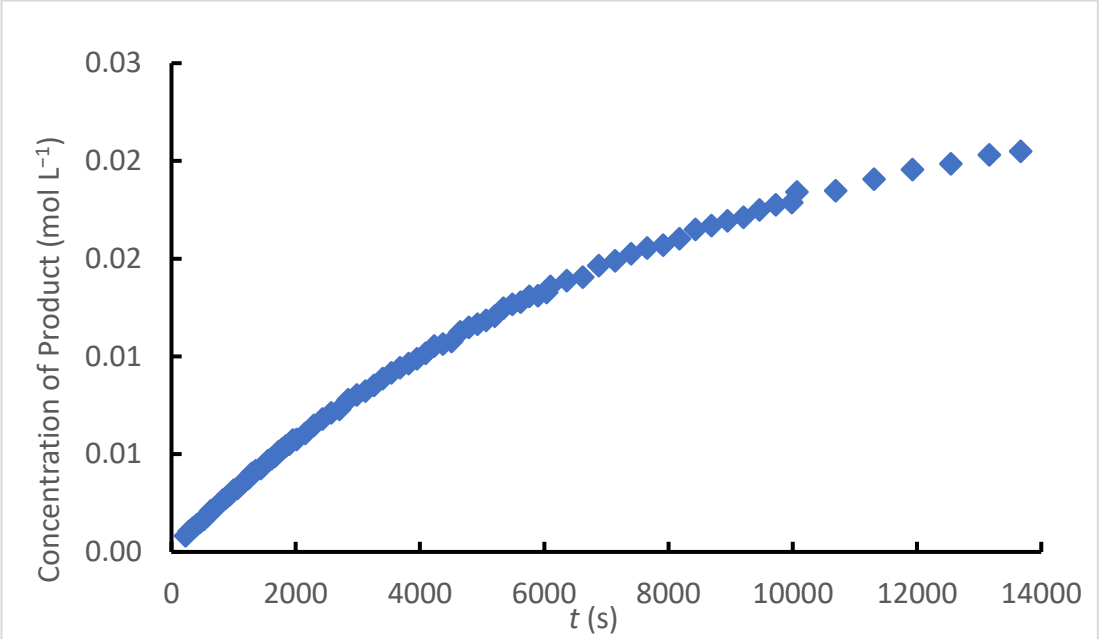


Figure 7-9: The plot of ([**52**]$_t$) versus time for the reaction of 4-dimethylaminopyridine (**46**) + diethyl sulfate in CD_3CN at 20 °C.

The value of $\Delta G^{\ddagger}$ was determined by the following equation:

$$RT \ln\left(\left(\frac{1}{k}\right)\left(\frac{k_B T}{h}\right)\left(\frac{RT}{p^{\circ}}\right)\right) = \Delta G^{\ddagger}$$

giving:

$$\Delta G^{\ddagger} = 98.5\ \text{kJ mol}^{-1}$$

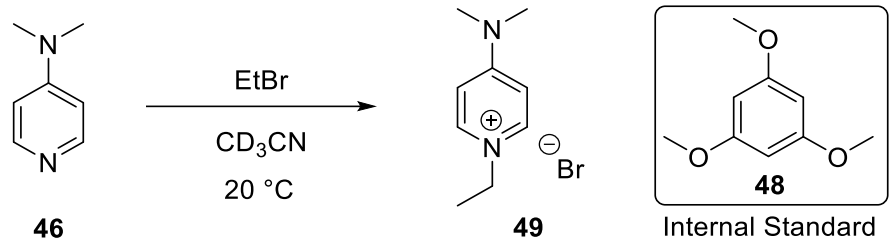
where:

$$R = 8.314\ \text{J K}^{-1}\text{mol}^{-1} \quad T = 293.15\ \text{K}$$
$$p^{\circ} = 10^5\ \text{N m}^{-2} \quad k_B = 1.38 \times 10^{-23}\ \text{J K}^{-1} \quad h = 6.63 \times 10^{-34}\ \text{J s}$$

An error analysis identical to the one demonstrated on pages 455 – 457 was performed for this reaction. Combining all of the three considered sources of error, the Gibbs energy of activation for the reaction of DMAP + diethyl sulfate in CD_3CN at 20 °C was determined to be:

$$\Delta G^{\ddagger} = 98.5 \pm 0.6\ \text{kJ mol}^{-1}$$

(v) Reaction of DMAP (46) + EtBr in CD_3CN at 20 °C



From 4-dimethylaminopyridine (**46**) (0.0155 g, 0.127 mmol) and ethyl bromide (0.1479 g, 1.357 mmol, 10 equivalents) in dry CD_3CN (0.80 ml) at 20 °C by procedure B. 1,3,5-Trimethoxybenzene (**48**) (0.0283 g, 0.127 mmol) was added as an internal standard.

The procedure followed for this experiment was identical to that described above in the representative general procedure in section 7.3 part (i), other than the points highlighted below.

The following signals were observed in the spectra after the addition of DMAP:

^{1}H NMR (600 MHz, CD_3CN)

Assigned to **46**: δ 8.16 – 8.13 (m, 2H), 6.59 – 6.54 (m, 2H), 2.98 (s, 6H). [9]

Assigned to **49**: δ 8.06 – 8.03 (m, 2H), 6.89 – 6.84 (m, 2H), 4.17 (q, *J* = 7.3 Hz, 2H), 3.18 (s, 6H), 1.45 (t, *J* = 7.3 Hz, 3H).

Assigned to **48**: δ 6.11 (s, 3H), 3.76 (s, 9H).

Assigned to **EtBr**: δ 3.50 (q, *J* = 7.3 Hz, 2H), 1.65 (t, *J* = 7.3 Hz, 3H).

Spectra were recorded at various time points to monitor the formation of **49**. In each spectrum, the integration value of the signal of **49** at δ 6.89 – 6.84 relative to the integration of the signal of 1,3,5-trimethoxybenzene at δ 6.11 was used to establish the concentration of the **49** relative to that of 1,3,5-trimethoxybenzene (0.1585 mmol ml^{-1}). The integration values and calculated concentration values of **49** are shown below in Table 7-5. After 16 hours and 23 minutes, conversion was approximately 76%. An approximate value of the pseudo-1st order rate constant was derived based on data recorded for 78 timepoints of the reaction up to this level of conversion. A representative spectrum that was recorded during this experiment is seen in Figure C31 in Appendix C.

Table 7-5. Recorded integration values (I_{49}) and calculated concentrations of **49** at various time points during the reaction of DMAP with EtBr in CD_3CN at 20 °C.

Time (s)	I_{49}	$[\mathbf{49}]_t$ (mmol/ml)	Time (s)	I_{49}	$[\mathbf{49}]_t$ (mmol/ml)	Time (s)	I_{49}	$[\mathbf{49}]_t$ (mmol/ml)
0	0	0	**6455**	3.19	0.0253	**17395**	7.35	0.0582
365	0.21	0.0017	**6753**	3.30	0.0262	**18012**	7.59	0.0602
460	0.26	0.0021	**7011**	3.41	0.0270	**19030**	7.89	0.0625
557	0.30	0.0024	**7269**	3.52	0.0279	**20849**	8.41	0.0666
713	0.39	0.0031	**7527**	3.62	0.0287	**22666**	8.92	0.0707
971	0.51	0.0040	**7785**	3.76	0.0298	**24484**	9.40	0.0745
1226	0.64	0.0051	**8042**	3.86	0.0306	**26302**	9.90	0.0785
1484	0.78	0.0062	**8299**	3.97	0.0315	**28120**	10.36	0.0821
1742	0.91	0.0072	**8556**	4.09	0.0324	**29938**	10.81	0.0857
1999	1.03	0.0082	**8814**	4.17	0.0330	**31756**	11.13	0.0882
2256	1.17	0.0093	**9072**	4.29	0.0340	**33574**	11.48	0.0910
2514	1.30	0.0103	**9329**	4.40	0.0349	**35392**	11.85	0.0939
2771	1.42	0.0113	**9587**	4.50	0.0357	**37174**	12.22	0.0968
3026	1.55	0.0123	**9845**	4.62	0.0366	**39028**	12.56	0.0995
3284	1.68	0.0133	**10103**	4.69	0.0372	**40846**	12.86	0.1019
3542	1.82	0.0144	**10361**	4.82	0.0382	**42664**	13.1	0.1038
3803	1.94	0.0154	**10600**	4.90	0.0388	**44482**	13.38	0.1060
4057	2.06	0.0163	**11217**	5.13	0.0407	**46300**	13.63	0.1080
4315	2.19	0.0174	**11835**	5.37	0.0426	**48118**	13.87	0.1099
4573	2.31	0.0183	**12452**	5.62	0.0445	**49936**	14.12	0.1119
4691	2.35	0.0186	**13070**	5.84	0.0463	**51751**	14.34	0.1136
4947	2.48	0.0197	**13688**	6.08	0.0482	**53569**	14.54	0.1152
5205	2.60	0.0206	**14303**	6.32	0.0501	**55387**	14.74	0.1168
5463	2.70	0.0214	**14921**	6.54	0.0518	**57205**	14.89	0.1180
5721	2.80	0.0222	**15542**	6.72	0.0533	**59023**	15.11	0.1197
5979	2.93	0.0232	**16159**	6.96	0.0552			
6237	3.06	0.0243	**16777**	7.17	0.0568			

The least squares fitting of the plot of the values of [**49**]*t* shown in Table 7-5 versus time (see plot in Figure 7-10) to the function $[\mathbf{49}]_t = [\mathbf{46}]_0 (1 - e^{-k_{obs}t} + C)$ gives a value of the pseudo-1st order rate constant of $k_{obs} = 2.96 \times 10^{-5}$ s^{-1}. The coefficient of determination (R^2) value is 0.9999. Hence, since $[EtBr]_0 = 1.70$ mol L^{-1},

$$k = \frac{2.96 \times 10^{-5}\ \text{s}^{-1}}{1.70\ \text{mol L}^{-1}}$$

$$= 1.74 \times 10^{-5}\ \text{L mol}^{-1}\ \text{s}^{-1}$$

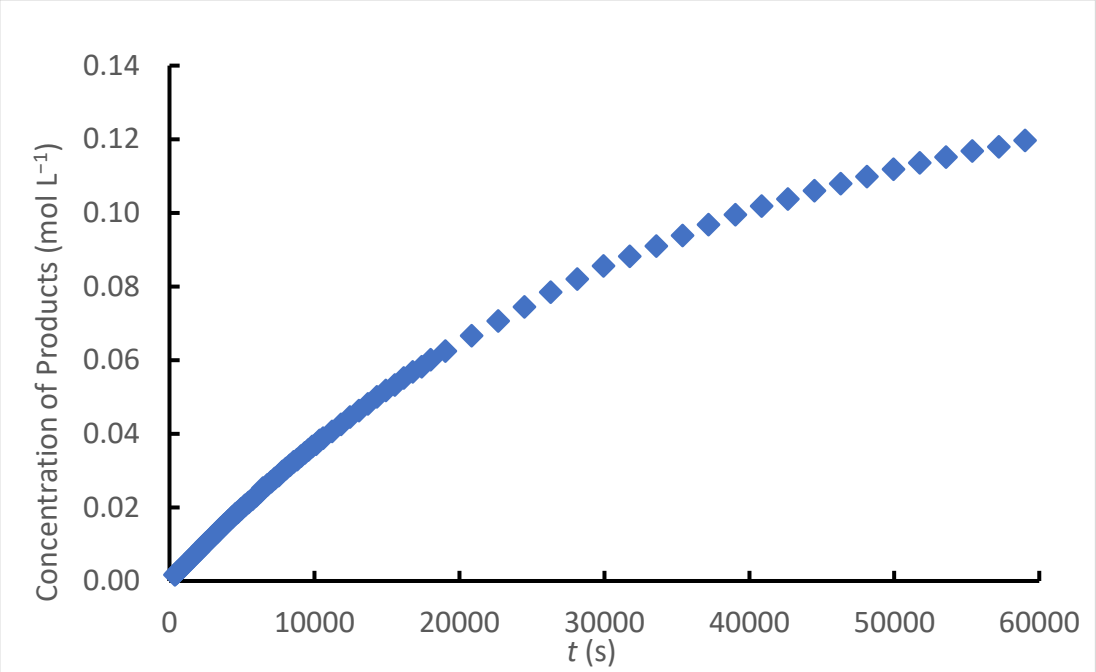


Figure 7-10: The plot of ([**49**]$_t$) versus time for the reaction of 4-dimethylaminopyridine + EtBr in CD_3CN at 20 °C.

The value of $\Delta G^{\ddagger}$ was determined by the following equation:

$$RT \ln\left(\left(\frac{1}{k}\right)\left(\frac{k_B T}{h}\right)\left(\frac{RT}{p^{\circ}}\right)\right) = \Delta G^{\ddagger}$$

giving:

$$\Delta G^{\ddagger} = 106.2\ \text{kJ mol}^{-1}$$

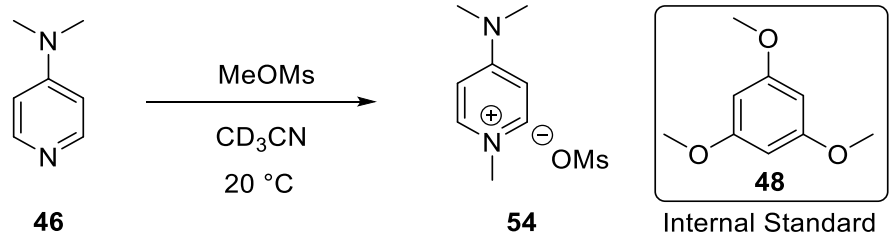
where:

$$R = 8.314\ \text{J K}^{-1}\text{mol}^{-1} \quad T = 293.15\ \text{K}$$
$$p^{\circ} = 10^5\ \text{N m}^{-2} \quad k_B = 1.38 \times 10^{-23}\ \text{J K}^{-1} \quad h = 6.63 \times 10^{-34}\ \text{J s}$$

An error analysis identical to the one demonstrated on pages 455 – 457 was performed for this reaction. Combining all of the three considered sources of error, the Gibbs energy of activation for the reaction of DMAP + EtBr in CD_3CN at 20 °C was determined to be:

$$\Delta G^{\ddagger} = 106.2 \pm 0.6\ \text{kJ mol}^{-1}$$

(vi) Reaction of DMAP (46) + MeOMs in CD_3CN at 20 °C



From 4-dimethylaminopyridine (**46**) (0.0023 g, 0.0186 mmol) and methyl mesylate (0.0226 g, 0.2052 mmol, 10 equivalents) in dry CD_3CN (0.80 ml) at 20 °C by procedure B. 1,3,5-Trimethoxybenzene (**48**) (0.0032 g, 0.0190 mmol) was added as an internal standard.

The procedure followed for this experiment was identical to that described above in the representative general procedure in section 7.3 part (i), other than the points highlighted below.

The following signals were observed in the spectra after the addition of DMAP:

^{1}H NMR (600 MHz, CD_3CN)

Assigned to **46**: δ 8.16 – 8.11 (m, 2H), 6.65 – 6.58 (m, 2H), 3.03 (s, 6H). [9]

Assigned to **54**: δ 7.94 – 7.89 (m, 2H), 6.89 – 6.82 (m, 2H), 3.18 (s, 6H).

Assigned to **48**: δ 6.12 (s, 3H), 3.76 (s, 9H).

Assigned to **MeOMs**: δ 3.89 (s, 3H), 3.03 (s, 3H).

Spectra were recorded at various time points to monitor the formation of **54**. In each spectrum, the integration value of the signal of **54** at δ 7.94 – 7.89 relative to the integration of the signal of 1,3,5-trimethoxybenzene at δ 6.12 was used to establish the concentration of the **54** relative to that of 1,3,5-trimethoxybenzene (0.02379 mmol ml^{-1}). The integration values and calculated concentration values of **54** are shown below in Table 7-6. After 4 hours and 52 minutes, conversion was approximately 80%. An approximate value of the pseudo-1st order rate constant was derived based on data recorded for 69 timepoints of the reaction up to this level of conversion. A representative spectrum that was recorded during this experiment is seen in Figure C32 in Appendix C.

Table 7-6. Recorded integration values (I_{54}) and calculated concentrations of **54** at various time points during the reaction of DMAP with MeOMs in CD_3CN at 20 °C.

Time (s)	I_{54}	$[\mathbf{54}]_t$ (mmol/ml)	Time (s)	I_{54}	$[\mathbf{54}]_t$ (mmol/ml)	Time (s)	I_{54}	$[\mathbf{54}]_t$ (mmol/ml)
0	0	0	**2193**	2.81	0.0033	**7618**	7.19	0.0086
289	0.44	0.0005	**2339**	3.00	0.0036	**7944**	7.40	0.0088
362	0.56	0.0007	**2485**	3.10	0.0037	**8268**	7.58	0.0090
435	0.65	0.0008	**2630**	3.30	0.0039	**8594**	7.79	0.0093
508	0.77	0.0009	**2775**	3.47	0.0041	**8920**	7.87	0.0094
581	0.86	0.0010	**2921**	3.57	0.0042	**9245**	8.06	0.0096
654	0.95	0.0011	**3067**	3.73	0.0044	**9570**	8.17	0.0097
726	1.04	0.0012	**3213**	3.85	0.0046	**9896**	8.45	0.0101
799	1.14	0.0014	**3355**	3.97	0.0047	**10226**	8.54	0.0102
872	1.25	0.0015	**3501**	4.18	0.0050	**10852**	8.91	0.0106
944	1.32	0.0016	**3645**	4.26	0.0051	**11477**	9.02	0.0107
1020	1.41	0.0017	**3791**	4.37	0.0052	**12102**	9.27	0.0110
1094	1.53	0.0018	**3937**	4.54	0.0054	**12728**	9.51	0.0113
1167	1.60	0.0019	**4044**	4.65	0.0055	**13354**	9.78	0.0116
1239	1.69	0.0020	**4369**	4.95	0.0059	**13979**	9.92	0.0118
1312	1.81	0.0022	**4695**	5.20	0.0062	**14225**	9.99	0.0119
1384	1.92	0.0023	**5021**	5.46	0.0065	**14426**	10.03	0.0119
1457	1.94	0.0023	**5346**	5.67	0.0067	**15052**	10.21	0.0121
1530	2.05	0.0024	**5671**	5.95	0.0071	**15678**	10.39	0.0124
1602	2.13	0.0025	**5994**	6.16	0.0073	**16304**	10.51	0.0125
1677	2.23	0.0027	**6320**	6.42	0.0076	**16930**	10.7	0.0127
1757	2.35	0.0028	**6645**	6.63	0.0079	**17556**	10.9	0.0130
1903	2.48	0.0029	**6967**	6.76	0.0080			
2047	2.62	0.0031	**7292**	7.01	0.0083			

The least squares fitting of the plot of the values of [**54**]*t* shown in Table 7-6 versus time (see plot in Figure 7-11) to the function $[\mathbf{54}]_t = [\mathbf{46}]_0 (1 - e^{-k_{obs}t} + C)$ gives a value of the pseudo-1st order rate constant of $k_{obs} = 1.13 \times 10^{-4}$ s^{-1}. The coefficient of determination (R^2) value is 0.9998. Hence, since $[\text{MeOMs}]_0 = 0.257$ mol L^{-1},

$$k = \frac{1.13 \times 10^{-4}\ \text{s}^{-1}}{0.257\ \text{mol L}^{-1}}$$

$$= 4.40 \times 10^{-4}\ \text{L mol}^{-1}\ \text{s}^{-1}$$

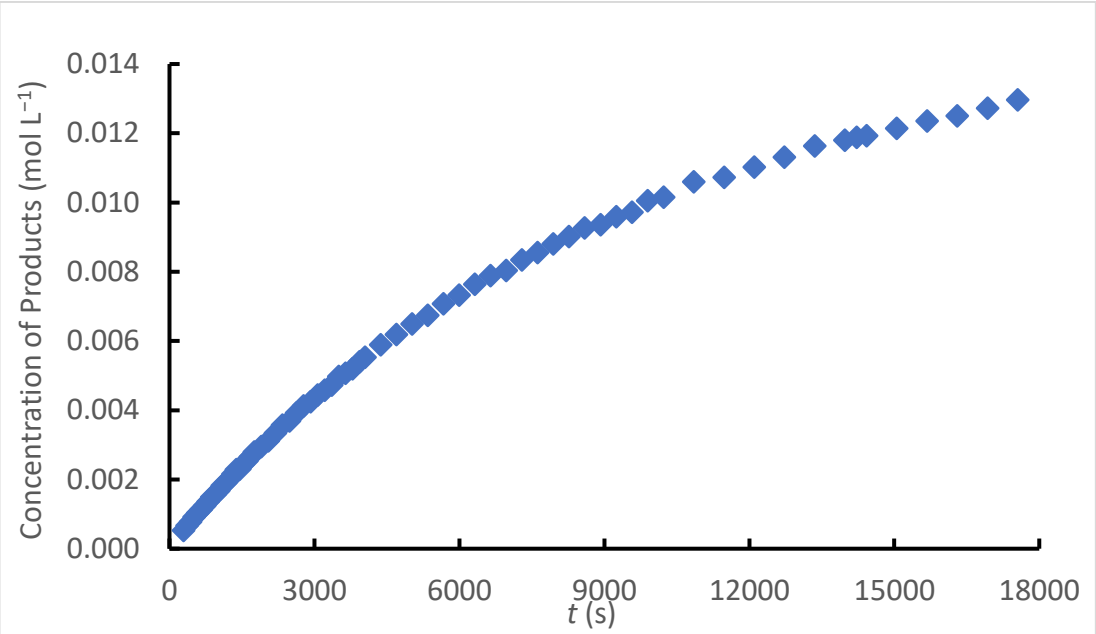


Figure 7-11: The plot of ([**54**]$_t$) versus time for the reaction of 4-dimethylaminopyridine (**46**) + MeOMs in CD_3CN at 20 °C.

The value of $\Delta G^{\ddagger}$ was determined by the following equation:

$$RT \ln\left(\left(\frac{1}{k}\right)\left(\frac{k_B T}{h}\right)\left(\frac{RT}{p^{\circ}}\right)\right) = \Delta G^{\ddagger}$$

giving:

$$\Delta G^{\ddagger} = 98.4 \text{ kJ mol}^{-1}$$

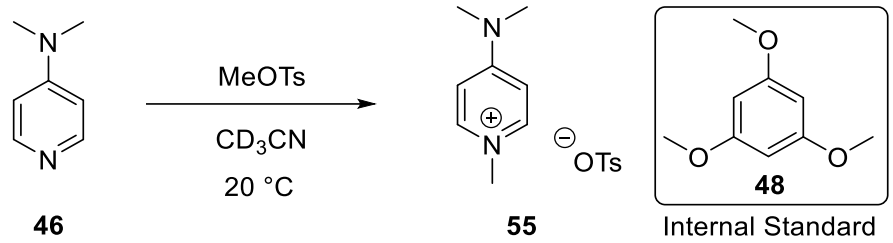
where:

$$R = 8.314 \text{ J K}^{-1}\text{mol}^{-1} \quad T = 293.15 \text{ K}$$
$$p^{\circ} = 10^5 \text{ N m}^{-2} \quad k_B = 1.38 \times 10^{-23} \text{ J K}^{-1} \quad h = 6.63 \times 10^{-34} \text{ J s}$$

An error analysis identical to the one demonstrated on pages 455 – 457 was performed for this reaction. Combining all of the three considered sources of error, the Gibbs energy of activation for the reaction of DMAP + MeOMs in CD_3CN at 20 °C was determined to be:

$$\Delta G^{\ddagger} = 98.4 \pm 0.6 \text{ kJ mol}^{-1}$$

(vii) Reaction of DMAP (46) + MeOTs in CD_3CN at 20 °C



46 **55**

From 4-dimethylaminopyridine (**46**) (0.0014 g, 0.0109 mmol) and methyl tosylate (0.0221 g, 0.1187 mmol, 10 equivalents) in dry CD_3CN (0.80 ml) at 20 °C by procedure B. 1,3,5-Trimethoxybenzene (**48**) (0.0018 g, 0.0109 mmol) was added as an internal standard.

The procedure followed for this experiment was identical to that described above in the representative general procedure in section 7.3 part (i), other than the points highlighted below.

The following signals were observed in the spectra after the addition of DMAP:

^{1}H NMR (600 MHz, CD_3CN)

Assigned to **46**: δ 8.18 – 8.09 (m, 2H), 6.63 – 6.55 (m, 2H), 2.98 (s, 6H). [9]

Assigned to **55**: δ 7.92 – 7.87 (m, 2H), 6.85 – 6.80 (m, 2H), 3.17 (s, 6H).

Assigned to **48**: δ 6.12 (s, 3H), 3.76 (s, 9H).

Assigned to **MeOTs**: δ 7.83 – 7.80 (m, 2H), 7.50 – 7.44 (m, 2H), 3.72 (s, 3H), 2.47 (s, 3H).

Spectra were recorded at various time points to monitor the formation of **55**. In each spectrum, the integration value of the signal of **55** at δ 6.85 – 6.80 relative to the integration of the signal of 1,3,5-trimethoxybenzene at δ 6.12 was used to establish the concentration of the **55** relative to that of 1,3,5-trimethoxybenzene (0.01363 mmol ml^{-1}). The integration values and calculated concentration values of **55** are shown below in Table 7-7. After 3 hours and 35 minutes, conversion was approximately 87%. An approximate value of the pseudo-1st order rate constant was derived based on data recorded for 74 timepoints of the reaction up to this level of conversion. A representative spectrum that was recorded during this experiment is seen in Figure C33 in Appendix C.

Note: An error in the NMR spectrometer automation software resulted in a 26-minute period in which no ^{1}H NMR spectra were recorded for the reaction mixture. This error is the source of the gap between measured data points which may be seen in Figure 7-12.

Table 7-7. Recorded integration values (I_{55}) and calculated concentrations of **55** at various time points during the reaction of DMAP with MeOTs in CD_3CN at 20 °C.

Time (s)	I_{55}	$[\mathbf{55}]_t$ (mmol/ml)	Time (s)	I_{55}	$[\mathbf{55}]_t$ (mmol/ml)	Time (s)	I_{55}	$[\mathbf{55}]_t$ (mmol/ml)
0	0	0	**2104**	3.68	0.0025	**4454**	6.52	0.0044
352	0.73	0.0005	**2176**	3.86	0.0026	**4659**	6.61	0.0045
425	0.94	0.0006	**2249**	3.89	0.0027	**4865**	6.93	0.0047
497	1.06	0.0007	**2321**	3.96	0.0027	**5071**	7.07	0.0048
570	1.19	0.0008	**2393**	4.14	0.0028	**5277**	7.17	0.0049
642	1.35	0.0009	**2465**	4.23	0.0029	**5480**	7.46	0.0051
714	1.47	0.0010	**2537**	4.29	0.0029	**5685**	7.55	0.0051
786	1.56	0.0011	**2609**	4.44	0.0030	**5890**	7.81	0.0053
858	1.69	0.0012	**2681**	4.48	0.0031	**6093**	7.92	0.0054
930	1.82	0.0012	**2753**	4.58	0.0031	**6299**	8.01	0.0055
1003	1.99	0.0014	**2825**	4.66	0.0032	**6505**	8.16	0.0056
1080	2.06	0.0014	**2898**	4.75	0.0032	**6710**	8.26	0.0056
1153	2.25	0.0015	**2970**	4.77	0.0032	**6915**	8.52	0.0058
1226	2.39	0.0016	**3042**	4.87	0.0033	**7121**	8.57	0.0058
1299	2.43	0.0017	**3114**	5.07	0.0035	**7327**	8.74	0.0060
1372	2.53	0.0017	**3187**	5.13	0.0035	**7530**	8.83	0.0060
1444	2.73	0.0019	**3264**	5.17	0.0035	**7736**	8.88	0.0060
1517	2.82	0.0019	**3336**	5.24	0.0036	**9301**	9.85	0.0067
1589	2.92	0.0020	**3409**	5.41	0.0037	**9817**	9.95	0.0068
1662	2.98	0.0020	**3481**	5.43	0.0037	**10443**	10.31	0.0070
1722	3.18	0.0022	**3553**	5.52	0.0038	**10716**	10.41	0.0071
1816	3.32	0.0023	**3632**	5.63	0.0038	**11269**	10.76	0.0073
1888	3.37	0.0023	**3837**	5.90	0.0040	**11794**	10.87	0.0074
1960	3.47	0.0024	**4042**	6.00	0.0041	**12345**	11.04	0.0075
2032	3.57	0.0024	**4248**	6.22	0.0042	**12898**	11.25	0.0077

The least squares fitting of the plot of the values of [**55**]*t* shown in Table 7-7 versus time (see plot in Figure 7-12) to the function $[\mathbf{55}]_t = [\mathbf{46}]_0 (1 - e^{-k_{obs}t} + C)$ gives a value of the pseudo-1st order rate constant of $k_{obs} = 1.54 \times 10^{-4}$ s^{-1}. The coefficient of determination (R^2) value is 0.9994. Hence, since $[MeOTs]_0 = 0.148$ mol L^{-1},

$$k = \frac{1.54 \times 10^{-4}\ \mathrm{s}^{-1}}{0.148\ \mathrm{mol\ L}^{-1}}$$

$$= 1.04 \times 10^{-3}\ \text{L mol}^{-1}\ \text{s}^{-1}$$

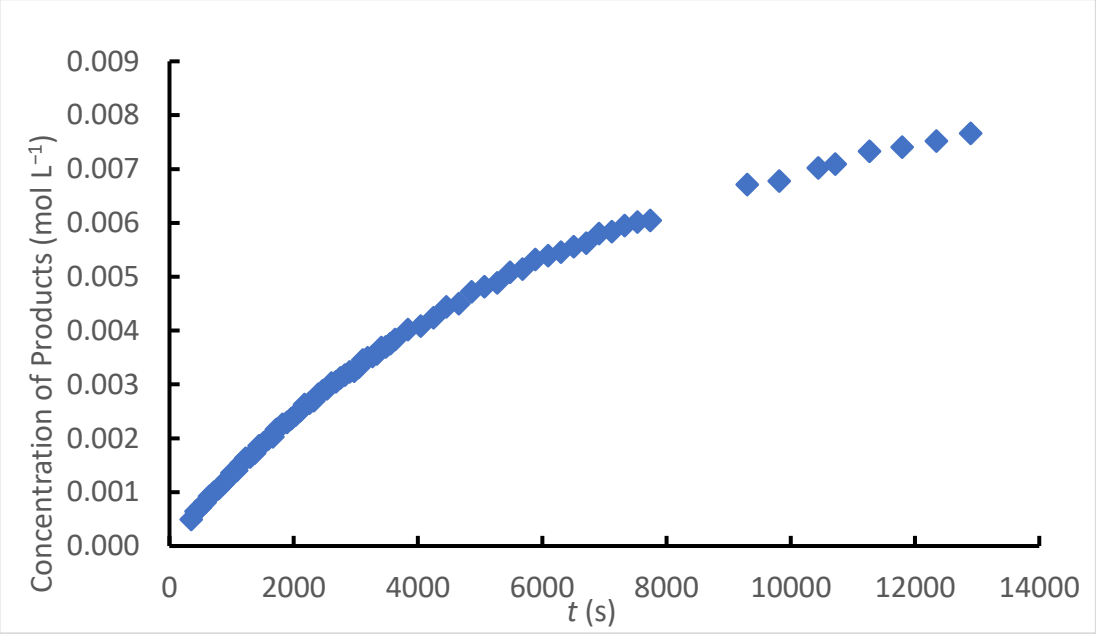


Figure 7-12: The plot of ([**55**]$_t$) versus time for the reaction of 4-dimethylaminopyridine + MeOTs in CD_3CN at 20 °C.

The value of $\Delta G^{\ddagger}$ was determined by the following equation:

$$RT \ln\left(\left(\frac{1}{k}\right)\left(\frac{k_B T}{h}\right)\left(\frac{RT}{p^{\circ}}\right)\right) = \Delta G^{\ddagger}$$

giving:

$$\Delta G^{\ddagger} = 96.3\ \text{kJ mol}^{-1}$$

where:

$$R = 8.314\ \text{J K}^{-1}\text{mol}^{-1} \quad T = 293.15\ \text{K}$$
$$p^{\circ} = 10^5\ \text{N m}^{-2} \quad k_B = 1.38 \times 10^{-23}\ \text{J K}^{-1} \quad h = 6.63 \times 10^{-34}\ \text{J s}$$

An error analysis identical to the one demonstrated on pages 455 – 457 was performed for this reaction. Combining all of the three considered sources of error, the Gibbs energy of activation for the reaction of DMAP + MeOTs in CD_3CN at 20 °C was determined to be:

$$\Delta G^{\ddagger} = 96.3 \pm 0.6\ \text{kJ mol}^{-1}$$

(viii) Reaction of DMAP (46) + MeI in CD_3CN

The rate constant and activation parameters from the reaction of 4-dimethylaminopyridine (**46**) and methyl iodide in acetonitrile have been reported by Kusabayashi and co-workers.[11]

The rate constant *k* for the reaction at 30 °C was calculated to be 1.38×10^{-2} L mol^{-1} s^{-1}.

The activation parameters for the reaction, $\Delta H^{\ddagger}$ and $\Delta S^{\ddagger}$ were reported to be 47.9 kJ mol^{-1} and −122.7 J K^{-1} mol^{-1} respectively.[11]

Using this information, the $\Delta G^{\ddagger}$ value for the reaction of 4-dimethylaminopyridine and methyl iodide in acetonitrile at 20 °C may be calculated as follows:

$$\Delta G^{\ddagger} = \Delta H^{\ddagger} - T\Delta S^{\ddagger}$$

$$\Delta G^{\ddagger} = 47.9 \text{ kJ mol}^{-1} - 293.15 \text{ K } (122.7 \text{ J K}^{-1}\text{mol}^{-1})$$

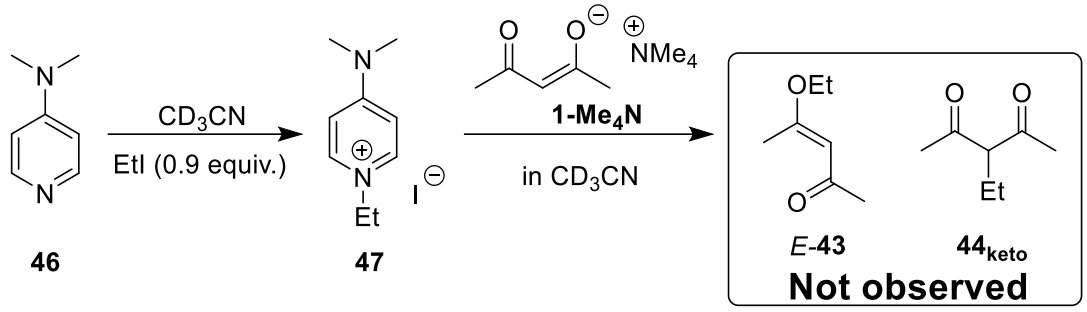
$$\Delta G^{\ddagger} = 47.9 \text{ kJ mol}^{-1} - \ (-3597 \text{ J mol}^{-1})$$

$$\Delta G^{\ddagger} = 47.9 \text{ kJ mol}^{-1} + \ 35.97 \text{ kJ mol}^{-1}$$

$$\Delta G^{\ddagger} = 83.9 \text{ kJ mol}^{-1}$$

7.4. Competition Experiments Between Enolate 1-Me_4N and DMAP with Various Electrophiles in CD_3CN at 20 °C

7.4.1. Control Experiment to Establish the Irreversibility of Formation of DMAP (46) Alkylation Products



4-Dimethylaminopyridine (**46**) (0.0152 g, 0.125 mmol) was weighed out and added to an empty Schlenk flask. The flask was fitted with a greased stopper and greased stopcock and fixed to a Schlenk manifold. The flask was placed under vacuum ($\leq 5 \times 10^{-3}$ mbar). The flask was then filled with nitrogen gas by the pump and fill technique, being refilled with nitrogen ≥ 3 times thereby creating an inert atmosphere inside the flask.[2] Dry CD_3CN (0.6 ml) was added to the flask by syringe. Ethyl iodide (0.0175 g, 0.112 mmol) was added to the flask by syringe and the mixture was stirred. The mixture was agitated to ensure complete dissolution of all solids.

An empty NMR tube was placed in a long Schlenk tube which was fitted with a greased stopper and greased stopcock and fixed to a Schlenk manifold. The long Schlenk tube, containing the NMR tube, was evacuated and re-filled with nitrogen ≥ 3 times, creating an inert atmosphere inside the flask. Rubber septa were fitted to the Schlenk flask containing the reactants and the Schlenk tube. The reaction mixture was drawn into a syringe and added to the NMR tube. The NMR tube was fitted with a rubber septum using a set of tweezers. After fitting the rubber septum to the NMR tube, the seal was secured by wrapping the external edge of the septum where it contacted the surface of the NMR tube with PTFE tape. The outside of the PTFE tape and rubber septum were then wrapped with a layer of Parafilm to further secure the nitrogen atmosphere inside the NMR tube. The NMR tube was placed in the NMR spectrometer and NMR spectra were then recorded to monitor the consumption of the EtI. After 4 days, ^{1}H NMR spectroscopy revealed complete consumption of the EtI.

^{1}H NMR (300 MHz, (CD_3CN) (Spectrum A): [a,b]

Assigned to **46**: δ 6.62 – 6.51 (m, 2H), 2.97 (s, 6H). [9]

Assigned to **47**: δ 6.97 – 6.87 (m, 2H), 4.21 (q, *J* = 7.3 Hz, 2H), 3.20 (s, 6H), 1.46 (t, *J* = 7.3 Hz, 3H).

No signals that could be assigned to EtI were present.

[a] The relevant ^{1}H NMR spectra are shown in Figure C34 and C35 in Appendix C.

[b] Signals of **46** and **47** that are overlapping with other signals: δ 8.17 – 8.05 (m, contains 2H of **46** and 2H of **47**).

A portion of a 0.79 mol L^{-1} stock solution of the tetramethylammonium enolate of acetylacetone (**1-Me$_4$N**) in CD_3CN (0.1 ml, 0.079 mmol) was injected into the NMR tube through the septum cap by syringe and the tube was agitated. Multiple NMR spectra were subsequently recorded. No signals which could be assigned to ethylation products of **1-Me$_4$N** (such as *E*-**43** or **44$_{keto}$**) could be observed in the resulting ^{1}H NMR spectra. The absence of any enolate ethylation products indicated that the reaction of **46** and EtI was irreversible, as any EtI which would form would be (at least partially) intercepted by the nucleophilic enolate species (**1-Me$_4$N**). Additionally, this experiment demonstrated that the nucleophilic attack of **1-Me$_4$N** on the ethylation product **47** was not possible under these reaction conditions.

^{1}H NMR (300 MHz, (CD_3CN) (Spectrum A): [a,b]

Assigned to **46**: δ 6.57 (app. dd, app. *J* = 4.9, 1.6 Hz, 1H), 2.97 (s, 6H). [9]

Assigned to **47**: δ 6.90 (app. d, app. *J* = 7.8 Hz, 2H), 4.18 (q, *J* = 7.3 Hz, 2H), 1.45 (t, *J* = 7.3 Hz, 3H).

Assigned to **1-Me$_4$N**: δ 4.74 (s, 1H).

No signals that could be assigned to *E*-**43** or **44$_{keto}$** were present.

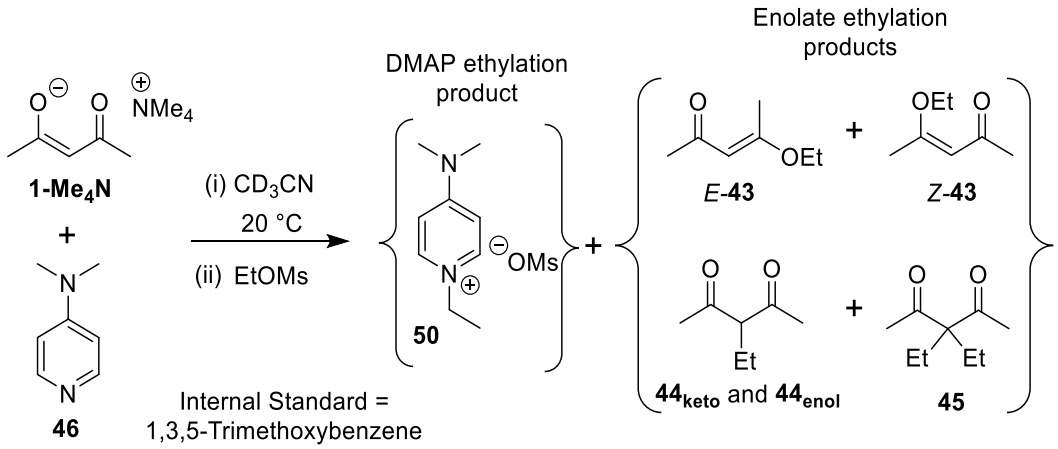
[a] The relevant ^{1}H NMR spectra is shown in Figure C36 and C37 in Appendix C.

[b] Signals of **46** and **47** that are overlapping with other signals: δ 8.22 – 8.05 (m, contains 2H of **46** and 2H of **47**), 3.24 – 3.07 (m, contains 6H of **47** and NMe_4 signal),

7.4.2. Competition Experiments Between Enolate 1-Me_4N and DMAP with Ethylating Agents in CD_3CN at 20 °C

(i) Competition Reaction of DMAP + Enolate 1-Me_4N + EtOMs in CD_3CN at 20 °C

Note: The general procedure C for a competition reaction between 4-dimethylaminopyridine (DMAP, **46**) and the tetramethylammonium enolate of acetylacetone (**1-Me_4N**) for an electrophile at 20 °C is described below in full using the reaction of 4-dimethylaminopyridine (**46**), **1-Me_4N** and EtOMs in CD_3CN as an exemplar. For other reactions, only a brief summation of the reaction and the subsequent data will be supplied. As the description on how $\Delta G^{\ddagger}$ values for each of the O- and C-alkylation processes is quite detailed, an exemplar calculation will be shown in full for this experiment only – for other experiments, the relevant data and $\Delta G^{\ddagger}$ values will be summarised in Tables.



4-Dimethylaminopyridine (**46**) (0.0145 g, 0.119 mmol) and 1,3,5-trimethoxybenzene (**48**) (0.0200 g, 0.119 mmol) were weighed out and added to an empty Schlenk flask. The flask was fitted with a greased stopper and greased stopcock and fixed to a Schlenk manifold. The flask was placed under vacuum ($\leq 5 \times 10^{-3}$ mbar). The flask was then filled with nitrogen gas by the pump and fill technique, being refilled with nitrogen ≥ 3 times thereby creating an inert atmosphere inside the flask.[2] A portion of a 0.67 mol L^{-1} stock solution of the tetramethylammonium enolate of acetylacetone (**1-Me_4N**) in CD_3CN (0.15 ml, 0.101 mmol) was added to the flask by syringe, followed by dry CD_3CN (0.4 ml). The mixture was agitated to ensure complete dissolution of all solids. The Schlenk flask was placed in an oil bath set to 20 °C for 15 minutes before proceeding.

A second Schlenk flask was prepared and attached to a Schlenk manifold. The flask was placed under vacuum ($\leq 5 \times 10^{-3}$ mbar). The flask was then filled with nitrogen gas by the pump and fill technique (≥ 3 vacuum/refill cycles),[2] thereby creating an inert atmosphere inside the flask. Ethyl mesylate (0.0106 g, 0.0854 mmol) was added to the flask by syringe, followed by dry CD_3CN (0.30 ml). Rubber septa were fitted to both Schlenk flasks containing the reactants. The entire ethyl mesylate solution was drawn into a syringe and added to the mixture of nucleophiles dropwise with stirring. The Schlenk flask was containing the reaction mixture was resealed with a greased

stopper and remained in the oil bath at 20 °C. The reaction mixture was stirred for 18 hours at this temperature.

An empty NMR tube was placed in a long Schlenk tube which was fitted with a greased stopper and greased stopcock and fixed to a Schlenk manifold. The long Schlenk tube, containing the NMR tube, was evacuated and re-filled with nitrogen ≥ 3 times, creating an inert atmosphere inside the flask. Rubber septa were fitted to the Schlenk flask containing the reactants and the Schlenk tube. The reaction mixture was drawn into a syringe and added to the NMR tube. The NMR tube was fitted with a rubber septum using a set of tweezers. After fitting the rubber septum to the NMR tube, the seal was secured by wrapping the external edge of the septum where it contacted the surface of the NMR tube with PTFE tape. The outside of the PTFE tape and rubber septum were then wrapped with a layer of Parafilm to further secure the nitrogen atmosphere inside the NMR tube. The NMR tube was placed in the NMR spectrometer and various NMR spectra were then recorded.

Note: The stock solution of the tetramethylammonium enolate of acetylacetone in CD_3CN was always stored in a J. Young's flask under an atmosphere of nitrogen. Despite this precaution, decomposition of the enolate solution may occur over time (approximately 1 week). Decomposition of the enolate in the stock solution is believed to be the source of the ethyl acetate signals which may be seen in the spectra of some of the reactions below. Further discussion of this phenomenon can be found on page 432.

Note: In each reaction of this type, a fine solid is formed as a by-product of the reaction of the enolate with the electrophile (e.g., $(Me_4N)OMs$ is produced in a reaction with ethyl mesylate). This small amount of solid was drawn into the syringe along with the reaction mixture and added to the NMR tube, where it was allowed to settle to the bottom of the tube before a ^1H NMR spectrum was taken.

Note: Due to the excess of starting nucleophiles and the large number of products produced in the reaction, exact assignment of each signal of the products in the NMR spectra is difficult (particularly in the 2.35 – 1.87 ppm range). Instead, the relative quantities of the products are determined using the integration values of key diagnostic signals belonging to those products (e.g., the 3H triplet of an attached ethyl group). These signals are listed out below and used in the various calculations to determine the relative amounts of alkylation that has occurred with each of the competing nucleophiles.

The integration value of the 3H signal of **48** at 6.12 ppm was set to equal 3.00 and all other integration values are given relative to this value.

^{1}H NMR (400 MHz, (CD_3CN) of crude mixture of alkylation products (the underlined integrations are expressed relative to 1H of internal standard **48**): [a,b,c]

Assigned to **48**: δ 6.12 (s, 3H), 3.76 (s, 9H).

Assigned to **46**: δ 8.17 – 8.11 (m, 1.44H (contains 2H of compound **46**)), 6.60 – 6.54 (m, 1.65H (contains 2H of compound **46**)), 2.97 (s, 5.06H (contains 6H of compound **46**)). [9]

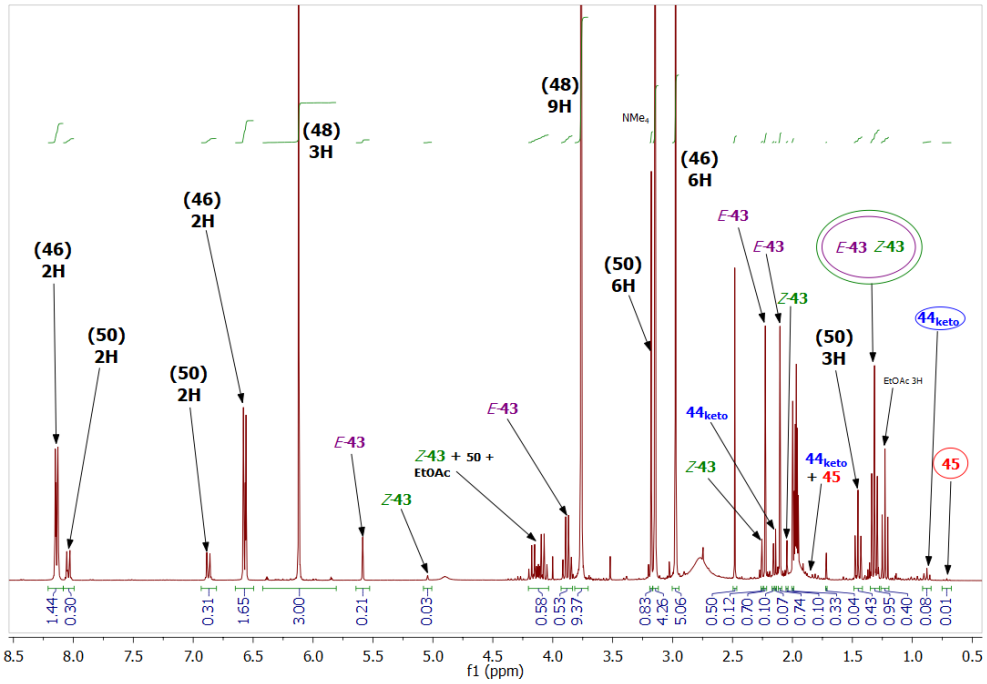
Assigned to **50**: δ 8.07 – 8.02 (m, 0.30H (contains 2H of compound **50**)), 6.91 – 6.84 (m, 0.31H (contains 2H of compound **50**)), 1.45 (t, *J* = 7.3 Hz, 0.43H (contains 3H of compound **50**)).

Assigned to *E*-**43**: δ 5.59 (s, 0.21H, C=CH (contains 1H of compound *E*-**43**)), 3.88 (q, *J* = 7.0 Hz, 0.53H, O$CH_2$$CH_3$ (contains 2H of compound *E*-**43**)), 2.23 (s, approx. 0.70H, CH_3C=C (contains 3H of compound *E*-**43**)). [4]

Assigned to *Z*-**43**: δ 5.04 (s, 0.03H, C=CH (contains 1H of compound *Z*-**43**)). [4]

Assigned to **44$_{keto}$**: δ 0.88 (t, *J* = 7.4 Hz, 0.08H, C($CH_2$$CH_3$) (contains 3H of compound **44$_{keto}$**)). [7]

Assigned to **45**: δ 0.71 (t, *J* = 7.6 Hz, 0.01H, C($CH_2$$CH_3$)$_2$ (contains 6H of compound **45**)). [8]



[a] The relevant ^{1}H NMR spectra are shown in Figure C38 and Figure C39 in Appendix C.

[b] Signals of *E*-**43**, *Z*-**43**, **44$_{keto}$**, **45** and **50** that are overlapping with other signals: δ 4.22 – 4.03 (m, contains 2H of *Z*-**43**, 2H of **50** and EtOAc signal), 3.19 – 3.13 (m, contains NMe_4 signal and 6H of **50**), 2.26 – 2.23 (m, contains 3H of *Z*-**43**), 2.16 – 2.12 (m, contains 6H of **44$_{keto}$**), 2.11 – 2.09 (m, contains 3H of *E*-**43**), 2.06 – 2.03 (m, contains 3H of *Z*-**43** and 6H of **45**), 1.92 – 1.86 (m, contains 4H of **45**), 1.85 – 1.76 (m, contains 2H of **44$_{keto}$**), 1.35 – 1.28 (m, contains 3H of *E*-**43** and 3H of *Z*-**43**).

[c] The vinyl signals of the enol ether products at δ 5.59 and 5.04 are undersized and thus not used in determining the O/C ratio. See pages 428 and 429 for details.

Figure 7-13: ^{1}H NMR spectrum of the competition reaction of DMAP and Enolate **1-Me$_4$N** with EtOMs in CD_3CN at 20 °C.

Determination of Ratio of Enolate Alkylation vs. DMAP Alkylation

In the following paragraphs, $I_{\mathbf{X}}$ is the integration of 1H of compound **X** (**X** = *E*-**43**, *Z*-**43**, **44$_{keto}$** or **45**) relative to 1H of the internal standard, **48**.

Although no suitable baseline-separated signal is available is available for compound *Z*-**43**, the integration (relative to the internal standard, **48)** of the overlapping signals of compounds *E*-**43** and *Z*-**43** at δ 1.35 – 1.28 (3H of each compound) allows the quantity $I_{E\text{-}\mathbf{43}} + I_{Z\text{-}\mathbf{43}}$ to be calculated as follows:

$$I_{E-\mathbf{43}} + I_{Z-\mathbf{43}} = \frac{0.95}{3} = 0.317$$

Based on the ^{1}H NMR spectral data given above, the integrations (relative to the internal standard, **48**) of 1H each of C-alkylation products **44$_{keto}$** and **45** are:

$$I_{\mathbf{44}_{\mathbf{keto}}} = \frac{0.08}{3} = 0.027; \quad I_{\mathbf{45}} = \frac{0.01}{6} = 0.0017$$

The integration (relative to the internal standard, **48**) of 1H of **50** is:

$$I_{\mathbf{50}} = \frac{0.31}{2} = 0.155$$

For any given compound **X**, $[\mathbf{X}] \propto I_{\mathbf{X}}$ (where [**X**] = concentration of **X** (mol L^{-1})). Hence, the relative integration values (I**X** values) determined above can be used to determine the relative amounts formed of the products in the reaction mixture.

The amount of O-alkylation product formed (from **1-Me$_4$N**) is 2.05 times the amount of DMAP alkylation product formed:

$$\frac{I_{E\text{-}\mathbf{43}} + I_{Z\text{-}\mathbf{43}}}{I_{\mathbf{50}}} = \frac{0.317}{0.155} = 2.05$$

Similarly, the amount of C-alkylation products formed (from **1-Me$_4$N**) is 0.185 times the amount of DMAP alkylation product formed:

$$\frac{I_{\mathbf{44}_{\mathbf{keto}}} + I_{\mathbf{45}}}{I_{\mathbf{50}}} = \frac{0.027 + 0.0017}{0.155} = 0.185$$

Also using the relative integration values shown above, the percentage of O-alkylation in this reaction can be determined as follows:

$$\text{Percentage of O-alkylation} = \frac{I_{E-\mathbf{43}} + I_{Z-\mathbf{43}}}{I_{E-\mathbf{43}} + I_{Z-\mathbf{43}} + I_{\mathbf{44}_{\mathbf{keto}}} + I_{\mathbf{45}}} \times 100$$

$$= \frac{0.317}{0.317 + 0.027 + 0.0017} \times 100 = 92\%$$

Hence, the O vs C ratio in this reaction was 92:8.

Determination of $\Delta G^{\ddagger}$ Values for Enolate O- and C-Alkylation

The rate of O-alkylation of **1-Me$_4$N** in this reaction is equal to $k_O[\mathbf{1-Me_4N}][\mathrm{EtOMs}]$, and the rate of alkylation of DMAP is equal to $k_{DMAP}[\mathbf{46}][\mathrm{EtOMs}]$. Hence, the ratio of enolate O-alkylation products to DMAP alkylation products in the reaction is given by:

$$\text{Enolate/DMAP alkylation ratio} = \frac{k_O[\mathbf{1-Me_4N}][\mathrm{EtOMs}]}{k_{DMAP}[\mathbf{46}][\mathrm{EtOMs}]} = \frac{k_O[\mathbf{1-Me_4N}]}{k_{DMAP}[\mathbf{46}]}$$

$$= \left(\frac{k_O}{k_{DMAP}}\right) \times \left(\frac{n_{\mathbf{1-Me_4N}}}{n_{\mathbf{46}}}\right)$$

where $n_{\mathbf{1\text{-}Me4N}}$ and $n_{\mathbf{46}}$ are respectively, the amounts present (in mmol) of **1-Me$_4$N** and **46** (and making use of the fact that the reaction mixture volume is the same for both species). Since the instantaneous values of $n_{\mathbf{1\text{-}Me4N}}$ and $n_{\mathbf{46}}$ are not generally readily available, limiting values of these quantities were determined to enable estimation of the values of k_O and k_C relative to k_{DMAP}. The amounts of the reactants at the beginning of the reaction (in mmol), $n^{\text{init}}_{\mathbf{1-Me4N}}$ and $n^{\text{init}}_{\mathbf{46}}$, are known, and using these values, an upper bound to the ratio of k_O to k_{DMAP} can be determined as shown below.

The initial amount of **1-Me$_4$N** present, $n^{\text{init}}_{\mathbf{1-Me4N}}$ was 0.101 mmol. The initial amount of **46** present, $n^{\text{init}}_{\mathbf{46}}$, was 0.119 mmol. Hence,

$$\frac{n^{\text{init}}_{\mathbf{1-Me4N}}}{n^{\text{init}}_{\mathbf{46}}} = \frac{0.101\ \text{mmol}}{0.119\ \text{mmol}} = 0.849$$

Since the ratio of O-alkylation product (**43**) to DMAP alkylation product (**50**) formed in this reaction was 2.05 (as shown above), it follows that

$$\left(\frac{k_O}{k_{DMAP}}\right) \times \left(\frac{n^{\text{init}}_{\mathbf{1-Me4N}}}{n^{\text{init}}_{\mathbf{46}}}\right) = \left(\frac{k_O}{k_{DMAP}}\right) \times 0.849 = 2.05$$

and hence [a]

$$k_O = \frac{2.05}{0.849} \times k_{DMAP} = \frac{2.05}{0.849} \times 8.62 \times 10^{-6}\ \text{L mol}^{-1}\ \text{s}^{-1}$$

$$= 2.08 \times 10^{-5}\ \text{L mol}^{-1}\ \text{s}^{-1}$$

Since

$$\Delta\Delta G^{\ddagger} = -RT \ln \frac{k_O}{k_{DMAP}}$$

[a] The values of k_{DMAP} and $\Delta G^{\ddagger}_{DMAP}$ used here were determined experimentally in section 7.3, experiment (ii).

And $\Delta G^{\ddagger}$ for the ethylation of DMAP by EtOMs in CD_3CN was calculated to be 108.1 kJ mol^{-1}, $\Delta G^{\ddagger}$ for the O-ethylation of **1-Me$_4$N** by EtOMs in CD_3CN is

$$\Delta G_{\mathrm{O}}^{\ddagger} = \Delta G_{\mathrm{DMAP}}^{\ddagger} - RT \ln\left(\frac{k_{\mathrm{O}}}{k_{\mathrm{DMAP}}}\right)$$

$$= 108.1 \text{ kJ mol}^{-1} - RT \ln\left(\frac{2.05}{0.849}\right)$$

$$= 108.1 \text{ kJ mol}^{-1} - 2.15 \text{ kJ mol}^{-1}$$

$$= 106.0 \text{ kJ mol}^{-1}$$

where:

$$R = 8.314 \text{ J K}^{-1}\text{mol}^{-1} \quad T = 293.15 \text{ K}$$

This gives an upper bound for the value of $\Delta G^{\ddagger}$ for O-ethylation of **1-Me$_4$N** of 106.0 kJ mol^{-1}.

Using a similar approach, a lower bound for $\Delta G^{\ddagger}$ for O-ethylation of **1-Me$_4$N** was estimated using the known amounts (in mmol) of the reactants and products present at the end of the reaction. In the ^{1}H NMR spectrum recorded after all of the EtOMs had been consumed, the integrations (relative to 1H of the 1,3,5-trimethoxybenzene (**48**) internal standard) of characteristic signals present of DMAP (δ 6.60 – 6.54, 2H) and **50** (δ 6.91 – 6.84, 2H), respectively, scaled to 1H per compound, were:

$$I_{\mathbf{46}} = \frac{1.65}{2} = 0.825; \quad I_{\mathbf{50}} = \frac{0.31}{2} = 0.155$$

From these integration values, the percentage of *unreacted* DMAP in this reaction was determined as follows:

$$\%\text{ DMAP remaining} = \frac{I_{\mathbf{46}}}{I_{\mathbf{46}} + I_{\mathbf{50}}} \times 100$$

$$= \frac{0.825}{0.825 + 0.155} \times 100 = 84.2\%$$

The amount of DMAP ($n_{\mathbf{46}}^{\mathrm{final}}$), that was present at the end of the reaction was then determined based off the known initial amount of DMAP added (0.119 mmol):

$$n_{\mathbf{46}}^{\mathrm{final}} = 0.119 \text{ mmol} \times 0.842 = 0.100 \text{ mmol}$$

The amount of **1-Me$_4$N** remaining at the end of the reaction ($n_{\mathbf{1-Me4N}}^{\mathrm{final}}$) was then determined as shown below. As no EtOMs remained in the solution, it was assumed that all of the EtOMs which did not react with DMAP has reacted with **1-Me$_4$N** to produce the O-alkylation and C-alkylation products (**43** – **45**) (amount = $n_{\mathbf{43-45}}^{\mathrm{final}}$ mmol). Hence:

$$n_{\mathbf{43-45}}^{\text{final}} = n_{\text{EtOMs}}^{\text{init}} - n_{\mathbf{50}}^{\text{final}}$$
$$= 0.0854 \text{ mmol} - 0.019 \text{ mmol} = 0.0664 \text{ mmol}$$

The amount of O-alkylation and C-alkylation products (**43 – 45**) formed, $n_{\mathbf{43-45}}^{\text{final}}$, can then be used to determine the amount of enolate **1-Me$_4$N** remaining at the end of the reaction ($n_{\mathbf{1-Me4N}}^{\text{final}}$) as follows, using the known initial amount of **1-Me$_4$N** present at the start of the reaction ($n_{\mathbf{1-Me4N}}^{\text{init}}$ = 0.101 mmol):

$$n_{\mathbf{1-Me4N}}^{\text{final}} = n_{\mathbf{1-Me4N}}^{\text{init}} - n_{\mathbf{43-45}}^{\text{final}}$$
$$= 0.101 \text{ mmol} - 0.0664 \text{ mmol} = 0.0346 \text{ mmol}$$

It is thus determined that 0.0346 mmol **1-Me$_4$N** remained at the end of the reaction. Consequently, the ratio of the amounts of the competing nucleophiles (enolate **1-Me$_4$N** and DMAP) at the end of the reaction was:

$$\frac{n_{\mathbf{1-Me4N}}^{\text{final}}}{n_{\mathbf{46}}^{\text{final}}} = \frac{0.0346 \text{ mmol}}{0.100 \text{ mmol}} = 0.346$$

Since the ratio of O-alkylation product to DMAP alkylation product formed in this reaction was 2.05 (as shown above), it follows that

$$\left(\frac{k_{\text{O}}}{k_{\text{DMAP}}}\right) \times \left(\frac{n_{\mathbf{1-Me4N}}^{\text{init}}}{n_{\mathbf{46}}^{\text{init}}}\right) = \left(\frac{k_{\text{O}}}{k_{\text{DMAP}}}\right) \times 0.346 \quad = 2.05$$

and hence [a]

$$k_{\text{O}} = \frac{2.05}{0.346} \times k_{\text{DMAP}} = \frac{2.05}{0.346} \times 8.62 \times 10^{-6} \text{ L mol}^{-1} \text{ s}^{-1}$$
$$= 5.11 \times 10^{-5} \text{ L mol}^{-1} \text{ s}^{-1}$$

Using this value for k_{O} and that $\Delta G^{\ddagger}$ for the ethylation of DMAP by EtOMs in CD_3CN ($\Delta G_{\text{DMAP}}^{\ddagger}$) was calculated to be 108.1 kJ mol^{-1}, a lower bound for the value of $\Delta G^{\ddagger}$ for the O-ethylation of **1-Me$_4$N** by EtOMs in CD_3CN ($\Delta G_{\text{O}}^{\ddagger}$) can be calculated as follows:

$$\Delta G_{\text{O}}^{\ddagger} = \Delta G_{\text{DMAP}}^{\ddagger} - RT \ln\left(\frac{k_{\text{O}}}{k_{\text{DMAP}}}\right) = 108.1 \text{ kJ mol}^{-1} - RT \ln\left(\frac{2.05}{0.346}\right)$$
$$= 103.8 \text{ kJ mol}^{-1}$$

Through the use of these combined approaches, the value of $\Delta G^{\ddagger}$ for O-ethylation of **1-Me$_4$N** was estimated to be within the range of **103.8 – 106.0 kJ mol^{-1}**.

An identical approach is used to estimate the value of $\Delta G^{\ddagger}$ for C-ethylation of **1-Me$_4$N**. The concentration data for **50** and **1-Me$_4$N** is identical when calculating the $\Delta G^{\ddagger}$ values for C-ethylation, as are the scaling factors. The k_{DMAP} and $\Delta G^{\ddagger}_{\text{DMAP}}$ values are also

[a] The values of k_{DMAP} and $\Delta G^{\ddagger}_{\text{DMAP}}$ used here were determined experimentally in section 7.3, experiment (ii).

identical to those used above. The amount of C-alkylation products formed (from **1-Me$_4$N**) is 0.185 times as much as the amount of DMAP alkylation product.

$$\Delta G^{\ddagger}{}_{\mathrm{C}} = \Delta G^{\ddagger}{}_{\mathrm{DMAP}} - RT \ln\left(\frac{0.185}{0.849}\right)$$

$$= 111.8 \text{ kJ mol}^{-1}$$

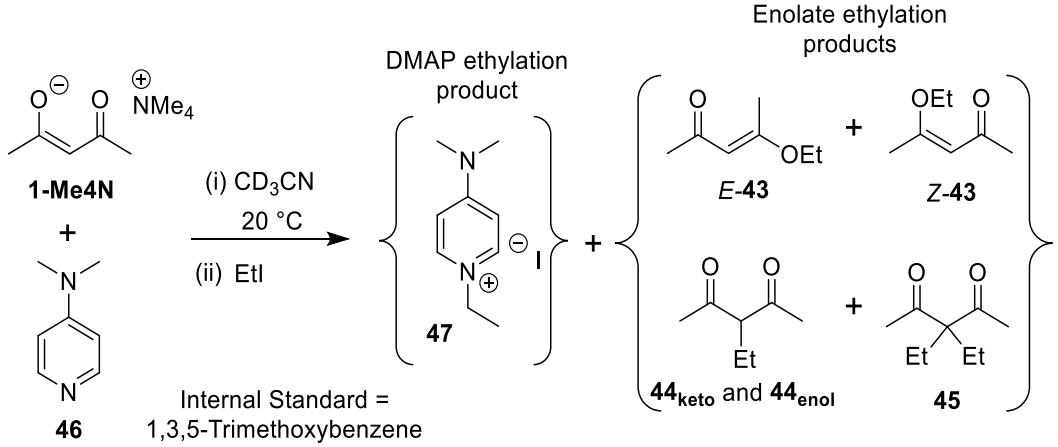
$$\Delta G^{\ddagger}{}_{\mathrm{C}} = \Delta G^{\ddagger}{}_{\mathrm{DMAP}} - RT \ln\left(\frac{0.185}{0.346}\right)$$

$$= 109.6 \text{ kJ mol}^{-1}$$

This allows the value of $\Delta G^{\ddagger}$ for C-ethylation of **1-Me$_4$N** to be estimated to be within the range of **109.6 – 111.8 kJ mol^{-1}**.

Owing to the length of discussion required to fully elaborate on how each value of $\Delta G^{\ddagger}$ is extracted for each of the O- and C-alkylation processes, only this exemplar calculation will be shown in full – for the experiments below, the relevant data and $\Delta G^{\ddagger}$ values will be summarised in Tables.

(ii) Reaction of DMAP + Enolate 1-Me$_4$N + EtI in CD$_3$CN at 20 °C



From 4-dimethylaminopyridine (**46**) (0.0146 g, 0.120 mmol), a 0.67 mol L^{-1} stock solution of **1-Me$_4$N** in CD$_3$CN (0.15 ml, 0.101 mmol) and EtI (0.0152 g, 0.0974 mmol) in CD$_3$CN (0.70 ml) at 20 °C after 5 days by Procedure C. 1,3,5-Trimethoxybenzene (**48**) (0.0200 g, 0.119 mmol) was added as an internal standard.

The procedure followed for this experiment was identical to that described above in the representative general procedure in section 7.4 part (i), other than the points highlighted below.

The integration value of the 3H signal of **48** at 6.12 ppm was set to equal 3.00 and all other integration values are given relative to this value.

^{1}H NMR (400 MHz, (CD_3CN) of crude mixture of alkylation products (the underlined integrations are expressed relative to 1H of internal standard **48**: [a,b,c]

Assigned to **48**: δ 6.12 (s, 3H), 3.77 (s, 9H).

Assigned to **46**: δ 8.17 – 8.10 (m, 1.83H (contains 2H of compound **46**)), 6.60 – 6.53 (m, 1.96H (contains 2H of compound **46**)), 2.98 (s, 5.92H (contains 6H of compound **46**)). [9]

Assigned to **47**: δ 8.01 (d, *J* = 7.7 Hz, 0.10H (contains 2H of compound **47**)), 6.86 (d, *J* = 7.7 Hz, 0.11H (contains 2H of compound **47**)), 3.18 (s, 0.28H (contains 6H of compound **47**)), 1.46 (t, *J* = 7.3 Hz, 0.16H (contains 3H of compound **47**)).

Assigned to *E*-**43**: δ 5.59 (s, 0.06H, C=C$\underline{H}$ (contains 1H of compound *E*-**43**)), 3.88 (q, *J* = 7.0 Hz, 0.11H, OC$\underline{H}_2$CH$_3$ (contains 2H of compound *E*-**43**)), 2.23 (s, approx. 0.14H, C$\underline{H}_3$C=C (contains 3H of compound *E*-**43**)). [4]

Assigned to *Z*-**43**: δ 5.05 (s, 0.02H, C=C$\underline{H}$ (contains 1H of compound *Z*-**43**)). [4]

Assigned to **44$_{keto}$**: δ 1.81 (quint, *J* = 7.4 Hz, 0.96H, C(C$\underline{H}_2$CH$_3$) (contains 2H of compound **44$_{keto}$**)), 0.88 (t, *J* = 7.4 Hz, 1.49H, C(CH$_2$C$\underline{H}_3$) (contains 3H of compound **44$_{keto}$**)). [7]

Assigned to **44$_{enol}$**: δ 1.05 (t, *J* = 7.4 Hz, 0.21H, C(CH$_2$C$\underline{H}_3$) (contains 3H of compound **44$_{enol}$**)). [7]

Assigned to **45**: δ 0.72 (t, *J* = 7.6 Hz, 0.57H, C(CH$_2$C$\underline{H}_3$)$_2$ (contains 6H of compound **45**)). [8]

In the following paragraphs, $I_{\mathbf{X}}$ is the integration of 1H of compound **X** (**X** = *E*-**43**, *Z*-**43**, **44$_{keto}$**, **44$_{enol}$**, **45** or **47**) relative to 1H of the internal standard, **48**.

Although no suitable baseline-separated signal is available is available for compound *Z*-**43**, the integration of the overlapping signals of compounds *E*-**43** and *Z*-**43** in the range δ 1.37 – 1.32 (3H of each compound) allows the quantity $I_{E\text{-}\mathbf{43}} + I_{Z\text{-}\mathbf{43}}$ to be calculated as follows:

$$I_{E-\mathbf{43}} + I_{Z-\mathbf{43}} = \frac{0.26}{3} = 0.086$$

Based on the ^{1}H NMR spectral data given above, the integrations (relative to the internal standard, **48**) of 1H each of C-alkylation products **44$_{keto}$**, **44$_{enol}$** and **45** are:

$$I_{\mathbf{44}_{\mathbf{keto}}} = \frac{1.49}{3} = 0.496; \quad I_{\mathbf{44}_{\mathbf{enol}}} = \frac{0.21}{3} = 0.07; \quad I_{\mathbf{45}} = \frac{0.57}{6} = 0.095$$

The integration (relative to the internal standard, **48**) of 1H of **47** is:

---

[a] The relevant ^{1}H NMR spectra are shown in Figure C40 and Figure C41 in Appendix C.

[b] Signals of *E*-**43**, *Z*-**43**, **44$_{keto}$**, **44$_{enol}$**, **45** and **47** that are overlapping with other signals: δ 4.20 – 4.04 (m, contains 2H of *Z*-**43** and 2H of **47**), 3.68 (t, *J* = 7.1 Hz, contains 1H of **44$_{keto}$**), 2.33 – 2.25 (m, contains 3H of *Z*-**43** and 2H of **44$_{enol}$**), 2.18 – 2.09 (m, contains 3H of *E*-**43**, 6H of **44$_{keto}$** and 6H of **44$_{enol}$**), 2.09 – 2.03 (m, contains 6H of **45**), 2.01 – 1.98 (m, contains 3H of *Z*-**43** and enolate signal), 1.94 – 1.87 (m, contains 4H of **45**), 1.37 – 1.27 (m, contains 3H of *E*-**43** and 3H of *Z*-**43**).

[c] The vinyl signals of the enol ether products at δ 5.59 and 5.05 are undersized and thus not used in determining the O/C ratio. See pages 428 and 429 for details.

$$I_{\mathbf{47}} = \frac{0.11}{2} = 0.055$$

For any given compound **X**, $[\mathbf{X}] \propto I_{\mathbf{X}}$ (where [**X**] = concentration of **X** (mol L^{-1})). Hence, the relative integration values (Ix values) determined above can be used to determine the relative amounts formed of the products in the reaction mixture.

The amount of O-alkylation product formed (from **1-Me$_4$N**) is 1.56 times the amount of DMAP alkylation product formed:

$$\frac{I_{E-\mathbf{43}} + I_{Z-\mathbf{43}}}{I_{\mathbf{47}}} = \frac{0.086}{0.055} = 1.56$$

Similarly, the amount of C-alkylation products formed (from **1-Me$_4$N**) is 12.0 times the amount of DMAP alkylation product formed:

$$\frac{I_{\mathbf{44_{keto}}} + I_{\mathbf{44_{enol}}} + I_{\mathbf{45}}}{I_{\mathbf{47}}} = \frac{0.496 + 0.07 + 0.095}{0.055} = 12.0$$

Also using the relative integration values shown above, the percentage of O-alkylation in this reaction can be determined as follows:

$$\text{Percentage of O-alkylation} = \frac{I_{E-\mathbf{43}} + I_{Z-\mathbf{43}}}{I_{E-\mathbf{43}} + I_{Z-\mathbf{43}} + I_{\mathbf{44_{keto}}} + I_{\mathbf{45}}} \times 100$$

$$\text{Percentage of O-alkylation} = \frac{0.086}{0.086 + 0.496 + 0.07 + 0.095} \times 100 = 12\%$$

Integrations give an O vs C ratio of 12:88

Using these quantities, a range of $\Delta G^{\ddagger}$ values for the processes of O- and C- alkylation of **1-Me$_4$N** by EtI in CD_3CN at 20 °C may be calculated. The relevant data is shown in Table 7-8.

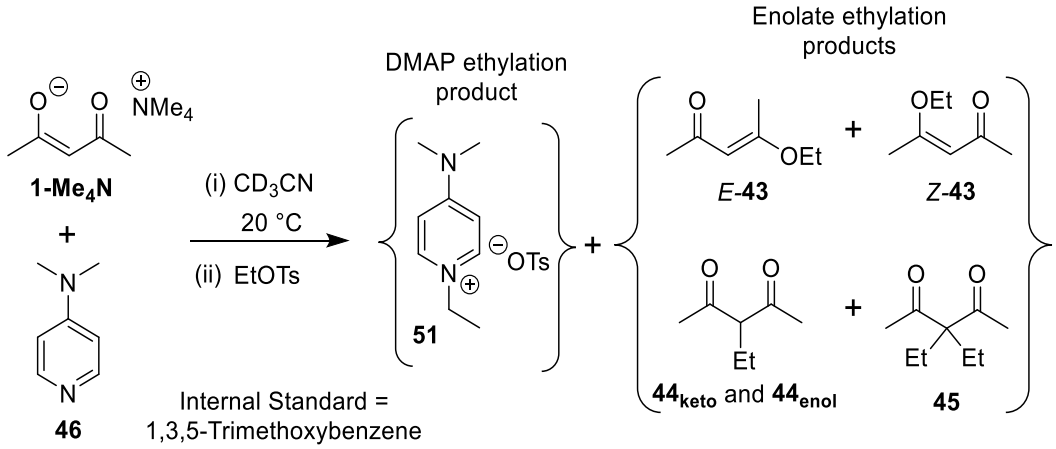
Note: The procedure used to estimate the values of $\Delta G^{\ddagger}$ for O- and C-alkylations of **1-Me$_4$N** with EtI is identical to that explained in detail in the exemplar at the start of this section (i.e., section 7.4 experiment (i)). Only the relevant figures used to calculate the values of $\Delta G^{\ddagger}$ are shown here, and not the full details of the calculations.

Table 7-8. Data used to estimate the value of $\Delta G^{\ddagger}$ for O- and C-ethylation of **1-Me$_4$N** by EtI in CD_3CN at 20 °C. R = 8.314 J K^{-1} mol^{-1} and T = 293.15 K.

O- and C-alkylation Upper Bound		**O- and C-alkylation Lower Bound**	
1.56 times as many O-alkylation products as DMAP alkylation products		1.56 times as many O-alkylation products as DMAP alkylation products	
$n^{\text{init}}_{\mathbf{1-Me4N}}$	0.101 mmol	$n^{\text{final}}_{\mathbf{1-Me4N}}$	0.01 mmol
$n^{\text{init}}_{\mathbf{46}}$	0.120 mmol	$n^{\text{final}}_{\mathbf{46}}$	0.114 mmol
Scaling factor	0.842	Scaling factor	0.088
k_{DMAP}	1.36 × 10^{-4} L mol^{-1} s^{-1}	k_{DMAP}	1.36 × 10^{-4} L mol^{-1} s^{-1}
k_{O}	2.52 × 10^{-4} L mol^{-1} s^{-1}	k_{O}	2.41 × 10^{-3} L mol^{-1} s^{-1}
$\Delta G^{\ddagger}_{\text{O}} = \Delta G^{\ddagger}_{\text{DMAP}} - RT\ln\left(\frac{k_{\text{O}}}{k_{\text{DMAP}}}\right)$		$\Delta G^{\ddagger}_{\text{O}} = \Delta G^{\ddagger}_{\text{DMAP}} - RT\ln\left(\frac{k_{\text{O}}}{k_{\text{DMAP}}}\right)$	
$\Delta G^{\ddagger}_{\text{DMAP}}$	101.2 kJ mol^{-1}	$\Delta G^{\ddagger}_{\text{DMAP}}$	101.2 kJ mol^{-1}
$\Delta G^{\ddagger}_{\text{O}}$	**99.7 kJ mol^{-1}**	$\Delta G^{\ddagger}_{\text{O}}$	**94.2 kJ mol^{-1}**
$\Delta G^{\ddagger}$ for O-ethylation of **1-Me$_4$N by EtI in CD_3CN at 20°C** is estimated to be within the range of **94.2 – 99.7 kJ mol^{-1}**			

12.0 times as many C-alkylation products as DMAP alkylation products		12.0 times as many C-alkylation products as DMAP alkylation products	
k_{C}	1.94 × 10^{-3} L mol^{-1} s^{-1}	k_{C}	1.85 × 10^{-2} L mol^{-1} s^{-1}
$\Delta G^{\ddagger}_{\text{C}} = \Delta G^{\ddagger}_{\text{DMAP}} - RT\ln\left(\frac{k_{\text{C}}}{k_{\text{DMAP}}}\right)$		$\Delta G^{\ddagger}_{\text{C}} = \Delta G^{\ddagger}_{\text{DMAP}} - RT\ln\left(\frac{k_{\text{C}}}{k_{\text{DMAP}}}\right)$	
$\Delta G^{\ddagger}_{\text{DMAP}}$	101.2 kJ mol^{-1}	$\Delta G^{\ddagger}_{\text{DMAP}}$	101.2 kJ mol^{-1}
$\Delta G^{\ddagger}_{\text{C}}$	**94.7 kJ mol^{-1}**	$\Delta G^{\ddagger}_{\text{C}}$	**89.2 kJ mol^{-1}**
$\Delta G^{\ddagger}$ for C-ethylation of **1-Me$_4$N by EtI in CD_3CN at 20°C** is estimated to be within the range of **89.2 – 94.7 kJ mol^{-1}**			

(iii) Reaction of DMAP + Enolate 1-Me_4N + EtOTs in CD_3CN at 20 °C



From 4-dimethylaminopyridine (**46**) (0.0145 g, 0.119 mmol), a 0.67 mol L^{-1} stock solution of **1-Me_4N** in CD_3CN (0.15 ml, 0.101 mmol) and EtOTs (0.0182 g, 0.0908 mmol) in CD_3CN (0.70 ml) at 20 °C after 5 days by Procedure C. 1,3,5-Trimethoxybenzene (**48**) (0.0200 g, 0.119 mmol) was added as an internal standard.

The integration value of the 3H signal of **48** at 6.12 ppm was set to equal 3.00 and all other integration values are given relative to this value.

^{1}H NMR (400 MHz, (CD_3CN) of crude mixture of alkylation products (the underlined integrations are expressed relative to 1H of internal standard **48**: [a,b,c]

Assigned to **48**: δ 6.12 (s, 3H), 3.76 (s, 9H).

Assigned to **46**: δ 8.18 – 8.10 (m, 1.58H (contains 2H of compound **46**)), 6.60 – 6.53 (m, 1.65H (contains 2H of compound **46**)), 2.97 (s, 5.06H (contains 6H of compound **46**)). [9]

Assigned to **51**: δ 8.08 – 8.01 (m, 0.30H (contains 2H of compound **51**)), 6.90 – 6.81 (m, 0.31H (contains 2H of compound **51**)), 1.44 (t, *J* = 7.3 Hz, 0.46H (contains 3H of compound **51**)).

Assigned to *E*-**43**: δ 5.59 (s, 0.23H, C=C<u>H</u> (contains 1H of compound *E*-**43**)), 3.88 (q, *J* = 7.0 Hz, 0.64H, O<u>CH</u>$_2$CH$_3$ (contains 2H of compound *E*-**43**)), 2.23 (s, approx. 0.83H, <u>CH</u>$_3$C=C (contains 3H of compound *E*-**43**)), 2.10 (s, approx. 0.86H, <u>CH</u>$_3$C=O (contains 3H of compound *E*-**43**)). [4]

Assigned to *Z*-**43**: δ 5.04 (s, 0.05H, C=C<u>H</u> (contains 1H of compound *Z*-**43**)), 2.26 (s, approx. 0.23H, <u>CH</u>$_3$C=O (contains 3H of compound *Z*-**43**)), 2.04 (s, approx. 0.23H, <u>CH</u>$_3$C=C (contains 3H of compound *Z*-**43**)). [4]

---

[a] The relevant ^{1}H NMR spectra are shown in Figure C42 and Figure C43 in Appendix C.

[b] Signals of *E*-**43**, *Z*-**43**, **44$_{keto}$**, **45** and **51** that are overlapping with other signals: δ 4.20 – 4.03 (m, contains 2H of *Z*-**43**, 2H of **51** and EtOAc signal), 3.20 – 3.08 (m, contains NMe_4 signal and 6H of **51**), 2.18 – 2.13 (m, contains 6H of **44$_{keto}$**), 2.09 – 2.06 (m, contains 6H of **45**), 1.92 – 1.75 (m, contains 2H of **44$_{keto}$** and 4H of **45**), 1.37 – 1.27 (m, contains 3H of *E*-**43** and 3H of *Z*-**43**).

[c] The vinyl signals of the enol ether products at δ 5.59 and 5.04 are undersized and thus not used in determining the O/C ratio. See pages 428 and 429 for details.

Assigned to **44$_{keto}$**: δ 0.88 (t, *J* = 7.4 Hz, <u>0.13H</u>, C($CH_2C\underline{H}_3$) (contains 3H of compound **44$_{keto}$**)). [7]

Assigned to **45**: δ 0.71 (t, *J* = 7.6 Hz, <u>0.02H</u>, $C(CH_2C\underline{H}_3)_2$ (contains 6H of compound **45**)). [8]

In the following paragraphs, $I_{\mathbf{X}}$ is the integration of 1H of compound **X** (**X** = *E*-**43**, *Z*-**43**, **44$_{keto}$**, **45** or **51**) relative to 1H of the internal standard, **48**.

Although no suitable baseline-separated signal is available is available for compound *Z*-**43**, the integration of the overlapping signals of compounds *E*-**43** and *Z*-**43** in the range δ 1.37 – 1.27 (3H of each compound) allows the quantity $I_{E\text{-}\mathbf{43}} + I_{Z\text{-}\mathbf{43}}$ to be calculated as follows:

$$I_{E-\mathbf{43}} + I_{Z\text{-}\mathbf{43}} = \frac{1.26}{3} = 0.42$$

Based on the ^{1}H NMR spectral data given above, the integrations (relative to the internal standard, **48**) of 1H each of C-alkylation products **44$_{keto}$** and **45** are:

$$I_{\mathbf{44_{keto}}} = \frac{0.13}{3} = 0.043;\ \ I_{\mathbf{45}} = \frac{0.02}{6} = 0.003$$

The integration (relative to the internal standard, **48**) of 1H of **51** is:

$$I_{\mathbf{51}} = \frac{0.31}{2} = 0.155$$

For any given compound **X**, $[\mathbf{X}] \propto I_{\mathbf{X}}$ (where [**X**] = concentration of **X** (mol L^{-1})). Hence, the relative integration values (IX values) determined above can be used to determine the relative amounts formed of the products in the reaction mixture.

The amount of O-alkylation product formed (from **1-Me$_4$N**) is 2.71 times the amount of DMAP alkylation product formed:

$$\frac{I_{E-\mathbf{43}} + I_{Z-\mathbf{43}}}{I_{\mathbf{51}}} = \frac{0.42}{0.155} = 2.71$$

Similarly, the amount of C-alkylation products formed (from **1-Me$_4$N**) is 0.297 times the amount of DMAP alkylation product formed:

$$\frac{I_{\mathbf{44_{keto}}} + I_{\mathbf{45}}}{I_{\mathbf{51}}} = \frac{0.043 + 0.003}{0.155} = 0.297$$

Also using the relative integration values shown above, the percentage of O-alkylation in this reaction can be determined as follows:

$$\text{Percentage of O-alkylation} = \frac{I_{E-\mathbf{43}} + I_{Z-\mathbf{43}}}{I_{E-\mathbf{43}} + I_{Z-\mathbf{43}} + I_{\mathbf{44_{keto}}} + I_{\mathbf{45}}} \times\ 100$$

$$= \frac{0.42}{0.42 + 0.043 + 0.003} \times 100 = 90\%$$

Hence, the <u>O vs C</u> ratio in this reaction was 90:10.

Using these quantities, a range of $\Delta G^{\ddagger}$ values for the processes of O- and C- alkylation of **1-Me$_4$N** by EtOTs in CD_3CN at 20 °C may be calculated. The relevant data is shown in Table 7-9.

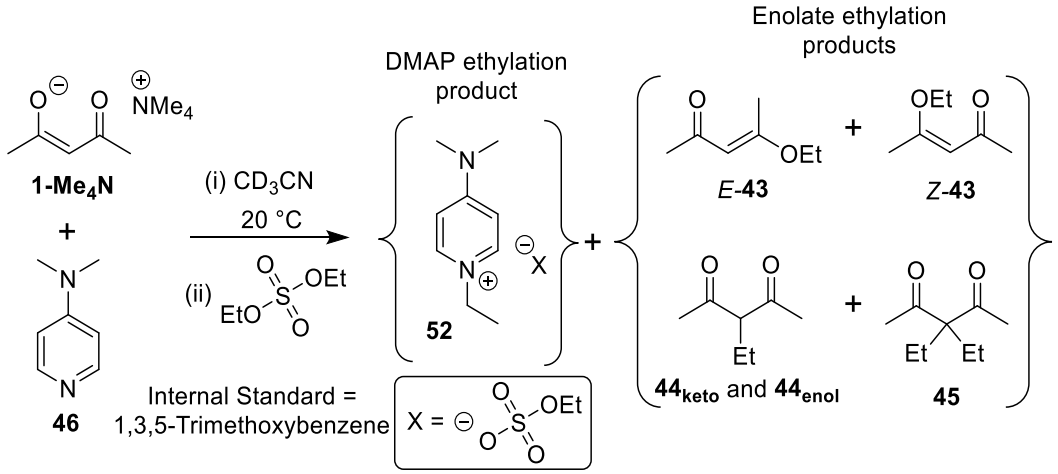
Note: The procedure used to estimate the values of $\Delta G^{\ddagger}$ for O- and C-alkylations of **1-Me$_4$N** with EtOTs is identical to that explained in detail in the exemplar at the start of this section (i.e., section 7.4 experiment (i)). Only the relevant figures used to calculate the values of $\Delta G^{\ddagger}$ are shown here, and not the full details of the calculations.

Table 7-9. Data used to estimate the value of $\Delta G^{\ddagger}$ for O- and C-ethylation of **1-Me$_4$N** by EtOTs in CD_3CN at 20 °C. R = 8.314 J K^{-1} mol^{-1} and T = 293.15 K.

O- and C-alkylation Upper Bound		**O- and C-alkylation Lower Bound**	
2.71 times as many O-alkylation products as DMAP alkylation products		2.71 times as many O-alkylation products as DMAP alkylation products	
$n^{\text{init}}_{\mathbf{1-Me4N}}$	0.101 mmol	$n^{\text{final}}_{\mathbf{1-Me4N}}$	0.029 mmol
$n^{\text{init}}_{\mathbf{46}}$	0.119 mmol	$n^{\text{final}}_{\mathbf{46}}$	0.100 mmol
Scaling factor	0.849	Scaling factor	0.29
k_{DMAP}	1.71 × 10^{-4} L mol^{-1} s^{-1}	k_{DMAP}	1.71 × 10^{-4} L mol^{-1} s^{-1}
k_{O}	5.46 × 10^{-4} L mol^{-1} s^{-1}	k_{O}	1.60 × 10^{-3} L mol^{-1} s^{-1}
$\Delta G^{\ddagger}_{\text{O}} = \Delta G^{\ddagger}_{\text{DMAP}} - RT\ln\left(\frac{k_{\text{O}}}{k_{\text{DMAP}}}\right)$		$\Delta G^{\ddagger}_{\text{O}} = \Delta G^{\ddagger}_{\text{DMAP}} - RT\ln\left(\frac{k_{\text{O}}}{k_{\text{DMAP}}}\right)$	
$\Delta G^{\ddagger}_{\text{DMAP}}$	106.3 kJ mol^{-1}	$\Delta G^{\ddagger}_{\text{DMAP}}$	106.3 kJ mol^{-1}
$\Delta G^{\ddagger}_{\text{O}}$	**103.5 kJ mol^{-1}**	$\Delta G^{\ddagger}_{\text{O}}$	**100.8 kJ mol^{-1}**
$\Delta G^{\ddagger}$ for O-ethylation of **1-Me$_4$N by EtOTs in CD_3CN at 20°C** is estimated to be within the range of **100.8 – 103.5 kJ mol^{-1}**			

0.297 times as many C-alkylation products as DMAP alkylation products		0.297 times as many C-alkylation products as DMAP alkylation products	
k_{C}	5.98 × 10^{-5} L mol^{-1} s^{-1}	k_{C}	1.75 × 10^{-4} L mol^{-1} s^{-1}
$\Delta G^{\ddagger}_{\text{C}} = \Delta G^{\ddagger}_{\text{DMAP}} - RT\ln\left(\frac{k_{\text{C}}}{k_{\text{DMAP}}}\right)$		$\Delta G^{\ddagger}_{\text{C}} = \Delta G^{\ddagger}_{\text{DMAP}} - RT\ln\left(\frac{k_{\text{C}}}{k_{\text{DMAP}}}\right)$	
$\Delta G^{\ddagger}_{\text{DMAP}}$	106.3 kJ mol^{-1}	$\Delta G^{\ddagger}_{\text{DMAP}}$	106.3 kJ mol^{-1}
$\Delta G^{\ddagger}_{\text{C}}$	**108.9 kJ mol^{-1}**	$\Delta G^{\ddagger}_{\text{C}}$	**106.2 kJ mol^{-1}**
$\Delta G^{\ddagger}$ for C-ethylation of **1-Me$_4$N by EtOTs in CD_3CN at 20°C** is estimated to be within the range of **106.2 – 108.9 kJ mol^{-1}**			

(iv) Reaction of DMAP + Enolate 1-Me_4N + diethyl sulfate in CD_3CN at 20 °C



From 4-dimethylaminopyridine (**46**) (0.0145 g, 0.119 mmol), a 0.67 mol L^{-1} stock solution of **1-Me_4N** in CD_3CN (0.15 ml, 0.101 mmol) and diethyl sulfate (0.0146 g, 0.0947 mmol) in CD_3CN (0.70 ml) at 20 °C after 23 hours by Procedure C. 1,3,5-Trimethoxybenzene (**48**) (0.0199 g, 0.119 mmol) was added as an internal standard.

The integration value of the 3H signal of **48** at 6.12 ppm was set to equal 3.00 and all other integration values are given relative to this value.

^{1}H NMR (400 MHz, (CD_3CN) of crude mixture of alkylation products (the underlined integrations are expressed relative to 1H of internal standard **48**): [a,b,c]

Assigned to **48**: δ 6.12 (s, 3H), 3.76 (s, 9H).

Assigned to **46**: δ 8.18 – 8.10 (m, 1.45H (contains 2H of compound **46**)), 6.60 – 6.53 (m, 1.60H (contains 2H of compound **46**)), 2.97 (s, 4.89H (contains 6H of compound **46**)). [9]

Assigned to **52**: δ 8.09 – 8.02 (m, 0.38H (contains 2H of compound **52**)), 6.92 – 6.85 (m, 0.38H (contains 2H of compound **52**)), 1.45 (t, *J* = 7.3 Hz, 0.46H (contains 3H of compound **52**)).

Assigned to *E*-**43**: δ 5.59 (s, 0.34H, C=C<u>H</u> (contains 1H of compound *E*-**43**)), 2.22 (s, approx. 1.07H, C<u>H</u>$_3$C=C (contains 3H of compound *E*-**43**)), 2.10 (s, approx. 1.09H, C<u>H</u>$_3$C=O (contains 3H of compound *E*-**43**)). [4]

Assigned to *Z*-**43**: δ 5.04 (s, 0.11H, C=C<u>H</u> (contains 1H of compound *Z*-**43**)), 2.25 (s, approx. 0.40H, C<u>H</u>$_3$C=O (contains 3H of compound *Z*-**43**)), 2.04 (s, approx. 0.40H, C<u>H</u>$_3$C=C (contains 3H of compound *Z*-**43**)). [4]

---

[a] The relevant ^{1}H NMR spectra are shown in Figure C44 and Figure C45 in Appendix C.

[b] Signals of *E*-**43**, *Z*-**43**, **44$_{keto}$**, **45** and **52** that are overlapping with other signals: δ 4.23 – 4.06 (m, contains 2H of *Z*-**43**, 2H of **52** and EtOAc signal), 3.95 – 3.82 (m, contains 2H of *E*-**43** and ethyl sulfate signal), 3.23 – 3.13 (m, contains NMe_4 signal and 6H of **52**), 1.94 – 1.75 (m, contains 2H of **44$_{keto}$** and 4H of **45**), 1.36 – 1.28 (m, contains 3H of *E*-**43** and 3H of *Z*-**43**).

[c] The vinyl signals of the enol ether products at δ 5.59 and 5.04 are undersized and thus not used in determining the O/C ratio. See pages 428 and 429 for details.

Assigned to **44$_{keto}$**: δ 2.16 (s, approx. 0.49H, C$\underline{H}_3$C=O (contains 6H of compound **44$_{keto}$**)), 0.88 (t, *J* = 7.4 Hz, 0.28H, C(CH$_2$C$\underline{H}_3$) (contains 3H of compound **44$_{keto}$**)). [7]

Assigned to **45**: δ 2.07 (s, approx. 0.04H, C$\underline{H}_3$C=O (contains 6H of compound **45**)), 0.71 (t, *J* = 7.6 Hz, 0.05H, C(CH$_2$C$\underline{H}_3$)$_2$ (contains 6H of compound **45**)). [8]

In the following paragraphs, $I_{\mathbf{X}}$ is the integration of 1H of compound **X** (**X** = *E*-**43**, *Z*-**43**, **44$_{keto}$**, **45** or **52**) relative to 1H of the internal standard, **48**.

Although no suitable baseline-separated signal is available is available for compound *Z*-**43**, the integration of the overlapping signals of compounds *E*-**43** and *Z*-**43** in the range δ 1.36 – 1.28 (3H of each compound) allows the quantity $I_{E\text{-}\mathbf{43}} + I_{Z\text{-}\mathbf{43}}$ to be calculated as follows:

$$I_{E-\mathbf{43}} + I_{Z-\mathbf{43}} = \frac{1.60}{3} = 0.533$$

Based on the ^{1}H NMR spectral data given above, the integrations (relative to the internal standard, **48**) of 1H each of C-alkylation products **44$_{keto}$** and **45** are:

$$I_{\mathbf{44}_{\mathbf{keto}}} = \frac{0.28}{3} = 0.093; \; I_{\mathbf{45}} = \frac{0.05}{6} = 0.0083$$

The integration (relative to the internal standard, **48**) of 1H of **52** is:

$$I_{\mathbf{52}} = \frac{0.38}{2} = 0.19$$

For any given compound **X**, $[\mathbf{X}] \propto I_{\mathbf{X}}$ (where [**X**] = concentration of **X** (mol L^{-1})). Hence, the relative integration values ($I_{\mathbf{X}}$ values) determined above can be used to determine the relative amounts formed of the products in the reaction mixture.

The amount of O-alkylation product formed (from **1-Me$_4$N**) is 2.81 times the amount of DMAP alkylation product formed:

$$\frac{I_{E-\mathbf{43}} + I_{Z-\mathbf{43}}}{I_{\mathbf{52}}} = \frac{0.533}{0.19} = 2.81$$

Similarly, the amount of C-alkylation products formed (from **1-Me$_4$N**) is 0.533 times the amount of DMAP alkylation product formed:

$$\frac{I_{\mathbf{44}_{\mathbf{keto}}} + I_{\mathbf{45}}}{I_{\mathbf{52}}} = \frac{0.093 + 0.0083}{0.19} = 0.533$$

Also using the relative integration values shown above, the percentage of O-alkylation in this reaction can be determined as follows:

$$\text{Percentage of O-alkylation} = \frac{I_{E-\mathbf{43}} + I_{Z-\mathbf{43}}}{I_{E-\mathbf{43}} + I_{Z-\mathbf{43}} + I_{\mathbf{44}_{\mathbf{keto}}} + I_{\mathbf{45}}} \times \; 100$$

$$= \frac{0.533}{0.533 + 0.093 + 0.0083} \times 100 = 84\%$$

Hence, the O vs C ratio in this reaction was 84:16.

Using these quantities, a range of $\Delta G^{\ddagger}$ values for the processes of O- and C- alkylation of **1-Me$_4$N** by diethyl sulfate in CD_3CN at 20 °C may be calculated. The relevant data is shown in Table 7-10.

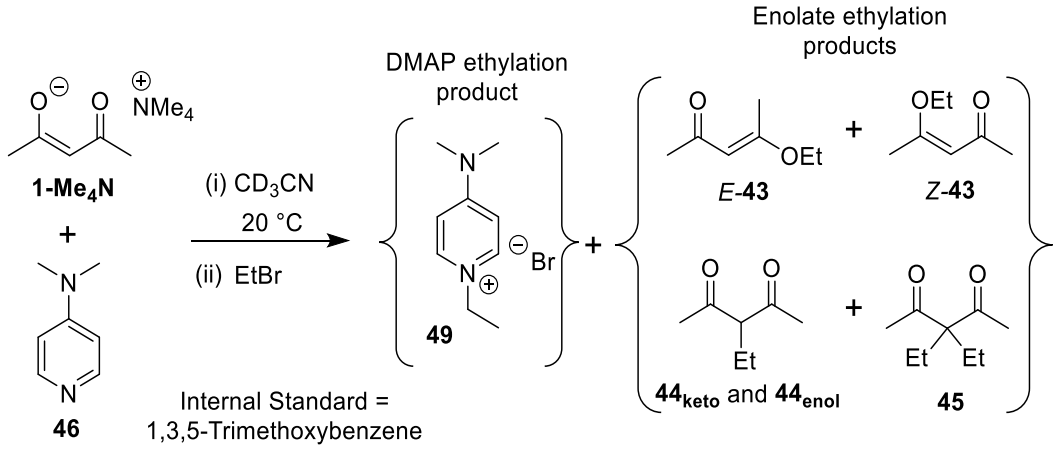
Note: The procedure used to estimate the values of $\Delta G^{\ddagger}$ for O- and C-alkylations of **1-Me$_4$N** with diethyl sulfate is identical to that explained in detail in the exemplar at the start of this section (i.e., section 7.4 experiment (i)). Only the relevant figures used to calculate the values of $\Delta G^{\ddagger}$ are shown here, and not the full calculations themselves.

Table 7-10. Data used to estimate the value of $\Delta G^{\ddagger}$ for O- and C-ethylation of **1-Me$_4$N** by diethyl sulfate in CD_3CN at 20 °C. R = 8.314 J K^{-1} mol^{-1} and T = 293.15 K.

O- and C-alkylation Upper Bound		**O- and C-alkylation Lower Bound**	
2.81 times as many O-alkylation products as DMAP alkylation products		2.81 times as many O-alkylation products as DMAP alkylation products	
$n^{\text{init}}_{\mathbf{1-Me4N}}$	0.101 mmol	$n^{\text{final}}_{\mathbf{1-Me4N}}$	0.0293 mmol
$n^{\text{init}}_{\mathbf{46}}$	0.119 mmol	$n^{\text{final}}_{\mathbf{46}}$	0.096 mmol
Scaling factor	0.849	Scaling factor	0.305
k_{DMAP}	4.19 × 10^{-4} L mol^{-1} s^{-1}	k_{DMAP}	4.19 × 10^{-4} L mol^{-1} s^{-1}
k_{O}	1.39 × 10^{-3} L mol^{-1} s^{-1}	k_{O}	3.87 × 10^{-3} L mol^{-1} s^{-1}
$\Delta G^{\ddagger}_{\text{O}} = \Delta G^{\ddagger}_{\text{DMAP}} - RT\ln\left(\frac{k_{\text{O}}}{k_{\text{DMAP}}}\right)$		$\Delta G^{\ddagger}_{\text{O}} = \Delta G^{\ddagger}_{\text{DMAP}} - RT\ln\left(\frac{k_{\text{O}}}{k_{\text{DMAP}}}\right)$	
$\Delta G^{\ddagger}_{\text{DMAP}}$	98.5 kJ mol^{-1}	$\Delta G^{\ddagger}_{\text{DMAP}}$	98.5 kJ mol^{-1}
$\Delta G^{\ddagger}_{\text{O}}$	**95.6 kJ mol^{-1}**	$\Delta G^{\ddagger}_{\text{O}}$	**93.1 kJ mol^{-1}**
$\Delta G^{\ddagger}$ for O-ethylation of **1-Me$_4$N by diethyl sulfate in CD_3CN at 20°C** is estimated to be within the range of **93.1 – 95.6 kJ mol^{-1}**			

0.533 times as many C-alkylation products as DMAP alkylation products		0.533 times as many C-alkylation products as DMAP alkylation products	
k_{C}	2.64 × 10^{-4} L mol^{-1} s^{-1}	k_{C}	7.34 × 10^{-4} L mol^{-1} s^{-1}
$\Delta G^{\ddagger}_{\text{C}} = \Delta G^{\ddagger}_{\text{DMAP}} - RT\ln\left(\frac{k_{\text{C}}}{k_{\text{DMAP}}}\right)$		$\Delta G^{\ddagger}_{\text{C}} = \Delta G^{\ddagger}_{\text{DMAP}} - RT\ln\left(\frac{k_{\text{C}}}{k_{\text{DMAP}}}\right)$	
$\Delta G^{\ddagger}_{\text{DMAP}}$	98.5 kJ mol^{-1}	$\Delta G^{\ddagger}_{\text{DMAP}}$	98.5 kJ mol^{-1}
$\Delta G^{\ddagger}_{\text{C}}$	**99.6 kJ mol^{-1}**	$\Delta G^{\ddagger}_{\text{C}}$	**97.1 kJ mol^{-1}**
$\Delta G^{\ddagger}$ for C-ethylation of **1-Me$_4$N by diethyl sulfate in CD_3CN at 20°C** is estimated to be within the range of **97.1 – 99.6 kJ mol^{-1}**			

(v) Reaction of DMAP + Enolate 1-Me_4N + EtBr in CD_3CN at 20 °C



From 4-dimethylaminopyridine (**46**) (0.0146 g, 0.120 mmol), a 0.67 mol L^{-1} stock solution of **1-Me_4N** in CD_3CN (0.15 ml, 0.101 mmol) and EtBr (0.0099 g, 0.0908 mmol) in CD_3CN (0.70 ml) at 20 °C after 5 days by Procedure C. 1,3,5-Trimethoxybenzene (**48**) (0.0199 g, 0.119 mmol) was added as an internal standard.

The integration value of the 3H signal of **48** at 6.12 ppm was set to equal 3.00 and all other integration values are given relative to this value.

^{1}H NMR (400 MHz, (CD_3CN) of crude mixture of alkylation products (the underlined integrations are expressed relative to 1H of internal standard **48**: [a,b,c]

Assigned to **48**: δ 6.12 (s, 3H), 3.76 (s, 9H).

Assigned to **46**: δ 8.18 – 8.10 (m, 1.62H (contains 2H of compound **46**)), 6.60 – 6.52 (m, 1.91H (contains 2H of compound **46**)), 2.97 (s, 5.90H (contains 6H of compound **46**)). [9]

Assigned to **49**: δ 8.11 – 8.05 (m, 0.02H (contains 2H of compound **49**)), 6.90 – 6.85 (m, 0.05H (contains 2H of compound **49**)).

Assigned to *E*-**43**: δ 5.58 (s, 0.03H, C=C<u>H</u> (contains 1H of compound *E*-**43**)), 2.23 (s, approx. 0.10H, CH_3C=C (contains 3H of compound *E*-**43**)). [4]

Assigned to *Z*-**43**: δ 5.04 (s, 0.01H, C=C<u>H</u> (contains 1H of compound *Z*-**43**)). [4]

Assigned to **44$_{keto}$**: δ All signals are overlapping with others. [7]

Assigned to **44$_{enol}$**: δ All signals are overlapping with others. [7]

---

[a] The relevant ^{1}H NMR spectra are shown in Figure C46 and Figure C47 in Appendix C.

[b] Signals of *E*-**43**, *Z*-**43**, **44$_{keto}$**, **44$_{enol}$**, **45** and **49** that are overlapping with other signals: δ 4.21 – 4.03 (m, contains 2H of *Z*-**43**, 2H of **49** and EtOAc signal), 3.91 – 3.83 (m, contains 2H of *E*-**43**), 3.72 – 3.64 (m, contains 1H of **44$_{keto}$**), 3.21 – 3.12 (m, contains NMe_4 signal and 6H of **49**), 2.30 – 2.24 (m, contains 3H of *Z*-**43** and 2H of **44$_{enol}$**), 2.17 – 2.12 (m, contains 6H of **44$_{keto}$** and 6H of **44$_{enol}$**), 2.12 – 2.08 (m, contains 3H of *E*-**43**), 2.07 (s, contains 6H of **45**), 2.04 (s, contains 3H of *Z*-**43**), 1.88 – 1.75 (m, contains 2H of **44$_{keto}$** and 4H of **45**), 1.48 – 1.41 (m, contains 3H of **49**), 1.36 – 1.27 (m, contains 3H of *E*-**43** and 3H of *Z*-**43**), 1.00 – 0.83 (m, contains 3H of **44$_{keto}$** and 3H of **44$_{enol}$**).

[c] The vinyl signals of the enol ether products at δ 5.58 and 5.04 are undersized and thus not used in determining the O/C ratio. See pages 428 and 429 for details.

Assigned to **45**: δ 0.71 (t, *J* = 7.6 Hz, 0.07H, $C(CH_2C\underline{H}_3)_2$ (contains 6H of compound **45**)). [8]

In the following paragraphs, $I_{\mathbf{X}}$ is the integration of 1H of compound **X** (**X** = *E*-**43**, *Z*-**43**, **44**$_{\mathbf{keto}}$, **44**$_{\mathbf{enol}}$, **45** or **49**) relative to 1H of the internal standard, **48**.

Although no suitable baseline-separated signal is available is available for compound *Z*-**43**, the integration of the overlapping signals of compounds *E*-**43** and *Z*-**43** in the range δ 1.36 – 1.27 (3H of each compound) allows the quantity $I_{E\text{-}\mathbf{43}} + I_{Z\text{-}\mathbf{43}}$ to be calculated as follows:

$$I_{E-\mathbf{43}} + I_{Z-\mathbf{43}} = \frac{0.19}{3} = 0.063$$

Although no suitable baseline-separated signal is available is available for compounds **44**$_{\mathbf{keto}}$ or **44**$_{\mathbf{enol}}$, the integration of the overlapping signals of compounds **44**$_{\mathbf{keto}}$ and **44**$_{\mathbf{enol}}$ at δ 1.00 – 0.83 (3H of each compound) allows the quantity $I_{\mathbf{44keto}} + I_{\mathbf{44enol}}$ to be calculated as follows:

$$I_{\mathbf{44}_{\mathbf{keto}}} + I_{\mathbf{44}_{\mathbf{enol}}} = \frac{0.45}{3} = 0.15$$

Based on the ^{1}H NMR spectral data given above, the integrations (relative to the internal standard, **48**) of 1H each of C-alkylation products **44**$_{\mathbf{keto}}$, **44**$_{\mathbf{enol}}$ and **45** are:

$$I_{\mathbf{44}_{\mathbf{keto}}} + I_{\mathbf{44}_{\mathbf{enol}}} = 0.15;\ I_{\mathbf{45}} = \frac{0.07}{6} = 0.0116$$

The integration (relative to the internal standard, **48**) of 1H of **49** is:

$$I_{\mathbf{49}} = \frac{0.05}{2} = 0.025$$

For any given compound **X**, $[\mathbf{X}] \propto I_{\mathbf{X}}$ (where [**X**] = concentration of **X** (mol L^{-1})). Hence, the relative integration values (IX values) determined above can be used to determine the relative amounts formed of the products in the reaction mixture.

The amount of O-alkylation product formed (from **1**-**Me**$_4$**N**) is 2.52 times the amount of DMAP alkylation product formed:

$$\frac{I_{E-\mathbf{43}} + I_{Z-\mathbf{43}}}{I_{\mathbf{49}}} = \frac{0.063}{0.025} = 2.52$$

Similarly, the amount of C-alkylation products formed (from **1**-**Me**$_4$**N**) is 6.46 times the amount of DMAP alkylation product formed:

$$\frac{I_{\mathbf{44}_{\mathbf{keto}}} + I_{\mathbf{44}_{\mathbf{enol}}} + I_{\mathbf{45}}}{I_{\mathbf{49}}} = \frac{0.15 + 0.0116}{0.025} = 6.46$$

Also using the relative integration values shown above, the percentage of O-alkylation in this reaction can be determined as follows:

$$\text{Percentage of O-alkylation} = \frac{I_{E-\mathbf{43}} + I_{Z-\mathbf{43}}}{I_{E-\mathbf{43}} + I_{Z-\mathbf{43}} + I_{\mathbf{44}_{\mathbf{keto}}} + I_{\mathbf{44}_{\mathbf{enol}}} + I_{\mathbf{45}}} \times 100$$

$$= \frac{0.063}{0.063 + 0.15 + 0.0116} \times 100 = 28\%$$

Hence, the O vs C ratio in this reaction was 28:72

Using these quantities, a range of $\Delta G^{\ddagger}$ values for the processes of O- and C- alkylation of **1-Me$_4$N** in CD_3CN at 20 °C may be calculated. The relevant data is shown in Table 7-11.

Note: The procedure used to estimate the values of $\Delta G^{\ddagger}$ for O- and C-alkylations of **1-Me$_4$N** with EtBr is identical to that explained in detail in the exemplar at the start of this section (i.e., section 7.4 experiment (i)). Only the relevant figures used to calculate the values of $\Delta G^{\ddagger}$ are shown here, and not the full calculations themselves.

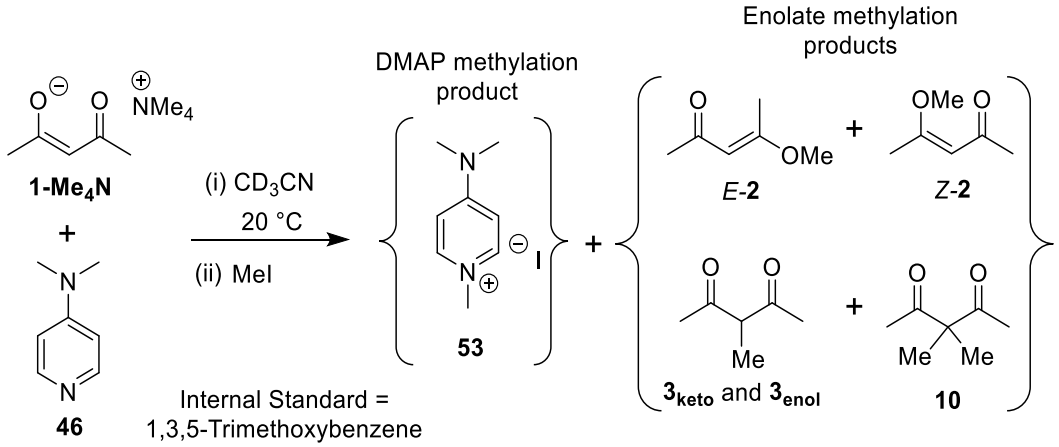
Table 7-11. Data used to estimate the value of $\Delta G^{\ddagger}$ for O- and C-ethylation of **1-Me$_4$N** by EtBr in CD_3CN at 20 °C. R = 8.314 J K^{-1} mol^{-1} and T = 293.15 K.

O- and C-alkylation Upper Bound		**O- and C-alkylation Lower Bound**	
2.52 times as many O-alkylation products as DMAP alkylation products		2.52 times as many O-alkylation products as DMAP alkylation products	
$n^{\text{init}}_{\mathbf{1-Me4N}}$	0.101 mmol	$n^{\text{final}}_{\mathbf{1-Me4N}}$	0.0132 mmol
$n^{\text{init}}_{\mathbf{46}}$	0.119 mmol	$n^{\text{final}}_{\mathbf{46}}$	0.116 mmol
Scaling factor	0.849	Scaling factor	0.114
k_{DMAP}	1.74 × 10^{-5} L mol^{-1} s^{-1}	k_{DMAP}	1.74 × 10^{-5} L mol^{-1} s^{-1}
k_{O}	5.19 × 10^{-5} L mol^{-1} s^{-1}	k_{O}	3.87 × 10^{-4} L mol^{-1} s^{-1}
$\Delta G^{\ddagger}_{\text{O}} = \Delta G^{\ddagger}_{\text{DMAP}} - RT\ln\left(\frac{k_{\text{O}}}{k_{\text{DMAP}}}\right)$		$\Delta G^{\ddagger}_{\text{O}} = \Delta G^{\ddagger}_{\text{DMAP}} - RT\ln\left(\frac{k_{\text{O}}}{k_{\text{DMAP}}}\right)$	
$\Delta G^{\ddagger}_{\text{DMAP}}$	106.2 kJ mol^{-1}	$\Delta G^{\ddagger}_{\text{DMAP}}$	106.2 kJ mol^{-1}
$\Delta G^{\ddagger}_{\text{O}}$	**103.6 kJ mol^{-1}**	$\Delta G^{\ddagger}_{\text{O}}$	**98.7 kJ mol^{-1}**
$\Delta G^{\ddagger}$ for O-ethylation of **1-Me$_4$N by EtBr in CD_3CN at 20°C** is estimated to be within the range of **98.7 – 103.6 kJ mol^{-1}**			

6.46 times as many C-alkylation products as DMAP alkylation products		6.46 times as many C-alkylation products as DMAP alkylation products	
k_{C}	1.33 × 10^{-4} L mol^{-1} s^{-1}	k_{C}	9.92 × 10^{-4} L mol^{-1} s^{-1}
$\Delta G^{\ddagger}_{\text{C}} = \Delta G^{\ddagger}_{\text{DMAP}} - RT\ln\left(\frac{k_{\text{C}}}{k_{\text{DMAP}}}\right)$		$\Delta G^{\ddagger}_{\text{C}} = \Delta G^{\ddagger}_{\text{DMAP}} - RT\ln\left(\frac{k_{\text{C}}}{k_{\text{DMAP}}}\right)$	
$\Delta G^{\ddagger}_{\text{DMAP}}$	106.2 kJ mol^{-1}	$\Delta G^{\ddagger}_{\text{DMAP}}$	106.2 kJ mol^{-1}
$\Delta G^{\ddagger}_{\text{C}}$	**101.3 kJ mol^{-1}**	$\Delta G^{\ddagger}_{\text{C}}$	**96.4 kJ mol^{-1}**
$\Delta G^{\ddagger}$ for C-ethylation of **1-Me$_4$N by EtBr in CD_3CN at 20°C** is estimated to be within the range of **96.4 – 101.3 kJ mol^{-1}**			

7.4.3. Competition Experiments Between Enolate 1-Me_4N and DMAP with Methylating Agents in CD_3CN at 20 °C

(i) Reaction of DMAP + Enolate 1-Me_4N + MeI in CD_3CN at 20 °C



From 4-dimethylaminopyridine (**46**) (0.0145 g, 0.119 mmol), a 0.67 mol L^{-1} stock solution of **1-Me_4N** in CD_3CN (0.15 ml, 0.101 mmol) and MeI (0.0129 g, 0.0909 mmol) in CD_3CN (0.70 ml) at 20 °C after 20 hours by Procedure C. 1,3,5-Trimethoxybenzene (**48**) (0.0200 g, 0.119 mmol) was added as an internal standard.

The integration value of the 3H signal of **48** at 6.12 ppm was set to equal 3.00 and all other integration values are given relative to this value.

^{1}H NMR (400 MHz, (CD_3CN) of crude mixture of alkylation products (the underlined integrations are expressed relative to 1H of internal standard **48**: [a,b,c]

Assigned to **48**: δ 6.12 (s, 3H), 3.77 (s, 9H).

Assigned to **46**: δ 8.19 – 8.10 (m, 1.57H (contains 2H of compound **46**)), 6.58 – 6.53 (m, 1.82H (contains 2H of compound **46**)), 2.98 (s, 5.72H (contains 6H of compound **46**)). [9]

Assigned to **53**: δ 7.98 – 7.91 (m, 0.14H (contains 2H of compound **53**)), 6.88 – 6.80 (m, 0.15H (contains 2H of compound **53**)), 3.88 (s, 0.21H (contains 3H of compound **53**)).

Assigned to *E*-**2**: δ 5.62 (s, 0.01H, C=C<u>H</u> (contains 1H of compound *E*-**2**)), 3.66 (s, 0.02H, O$C\underline{H}_3$ (contains 3H of compound *E*-**2**)). [4]

Assigned to **3$_{keto}$**: δ 1.27 – 1.21 (m, 0.67H, $C(C\underline{H}_3)$ (contains 3H of compound **3$_{keto}$**)). [5]

Assigned to **10**: δ 1.32 (s, 0.51H, $C(C\underline{H}_3)_2$ (contains 6H of compound **10**)). [6]

[a] The relevant ^{1}H NMR spectra are shown in Figure C48 and Figure C49 in Appendix C.

[b] Signals of *E*-**2**, **3$_{keto}$**, **10** and **53** that are overlapping with other signals: δ 3.21 – 3.12 (m, contains NMe_4 signal and 6H of **53**), 2.27 – 2.21 (m, contains 3H of *E*-**2**), 2.19 – 2.09 (m, contains 3H of *E*-**2**, 6H of **3$_{keto}$** and 6H of **10**).

[c] The vinyl signal of the enol ether product at δ 5.62 is undersized and thus not used in determining the O/C ratio. See pages 428 and 429 for details.

In the following paragraphs, $I_{\mathbf{X}}$ is the integration of 1H of compound **X** (**X** = *E*-**2**, **3**$_{\mathbf{keto}}$, **10** and **53**) relative to 1H of the internal standard, **48**.

Based on the ^{1}H NMR spectral data given above, the integrations (relative to the internal standard, **48**) of 1H each of the O-alkylation product *E*-**2** is:

$$I_{E-\mathbf{2}} = \frac{0.02}{3} = 0.0066$$

Based on the ^{1}H NMR spectral data given above, the integrations (relative to the internal standard, **48**) of 1H each of C-alkylation products **3**$_{\mathbf{keto}}$ and **10** are:

$$I_{\mathbf{3_{keto}}} = \frac{0.67}{3} = 0.223; \quad I_{\mathbf{10}} = \frac{0.51}{6} = 0.085$$

The integration (relative to the internal standard, **48**) of 1H of **53** is:

$$I_{\mathbf{53}} = \frac{0.15}{2} = 0.075$$

For any given compound **X**, $[\mathbf{X}] \propto I_{\mathbf{X}}$ (where [**X**] = concentration of **X** (mol L^{-1})). Hence, the relative integration values (IX values) determined above can be used to determine the relative amounts formed of the products in the reaction mixture.

The amount of O-alkylation product formed (from **1-Me$_4$N**) is 0.088 times the amount of DMAP alkylation product formed:

$$\frac{I_{E-\mathbf{2}}}{I_{\mathbf{53}}} = \frac{0.0066}{0.075} = 0.088$$

Similarly, the amount of C-alkylation products formed (from **1-Me$_4$N**) is 4.11 times the amount of DMAP alkylation product formed:

$$\frac{I_{\mathbf{3_{keto}}} + I_{\mathbf{10}}}{I_{\mathbf{53}}} = \frac{0.223 + 0.085}{0.075} = 4.11$$

Also using the relative integration values shown above, the percentage of O-alkylation in this reaction can be determined as follows:

$$\text{Percentage of O-alkylation} = \frac{I_{E-\mathbf{2}}}{I_{E-\mathbf{2}} + I_{\mathbf{3_{keto}}} + I_{\mathbf{10}}} \times 100$$

$$= \frac{0.0066}{0.0066 + 0.223 + 0.085} \times 100 = 2\%$$

Hence, the O vs C ratio in this reaction was 2:98.

Using these quantities, a range of $\Delta G^{\ddagger}$ values for the processes of O- and C- alkylation of **1-Me$_4$N** by MeI in CD_3CN at 20 °C may be calculated. The relevant data is shown in Table 7-12.

Note: The procedure used to estimate the values of $\Delta G^{\ddagger}$ for O- and C-alkylations of **1-Me$_4$N** with MeI is identical to that explained in detail in the exemplar at the start of

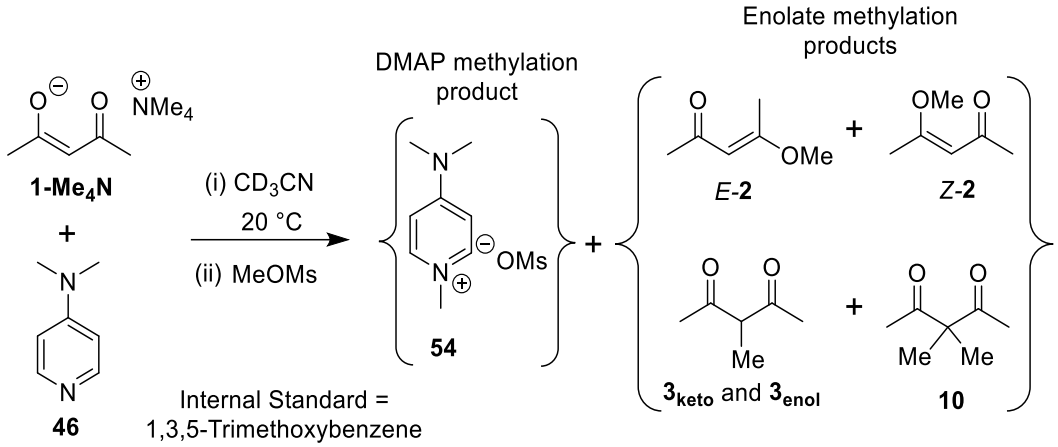
this section (i.e., section 7.4 experiment (i)). Only the relevant figures used to calculate the values of $\Delta G^{\ddagger}$ are shown here, and not the full calculations themselves.

Table 7-12. Data used to estimate the value of $\Delta G^{\ddagger}$ for O- and C-methylation of **1-Me$_4$N** by MeI in CD_3CN at 20 °C. R = 8.314 J K^{-1} mol^{-1} and T = 293.15 K.

O- and C-alkylation Upper Bound		**O- and C-alkylation Lower Bound**	
0.088 times as many O-alkylation products as DMAP alkylation products		0.088 times as many O-alkylation products as DMAP alkylation products	
$n^{\text{init}}_{\mathbf{1-Me4N}}$	0.101 mmol	$n^{\text{final}}_{\mathbf{1-Me4N}}$	0.0191 mmol
$n^{\text{init}}_{\mathbf{46}}$	0.119 mmol	$n^{\text{final}}_{\mathbf{46}}$	0.110 mmol
Scaling factor	0.849	Scaling factor	0.174
k_{DMAP}	1.38 × 10^{-2} L mol^{-1} s^{-1}	k_{DMAP}	1.38 × 10^{-2} L mol^{-1} s^{-1}
k_{O}	1.43 × 10^{-3} L mol^{-1} s^{-1}	k_{O}	6.98 × 10^{-3} L mol^{-1} s^{-1}
$\Delta G^{\ddagger}_{\text{O}} = \Delta G^{\ddagger}_{\text{DMAP}} - RT\ln\left(\frac{k_{\text{O}}}{k_{\text{DMAP}}}\right)$		$\Delta G^{\ddagger}_{\text{O}} = \Delta G^{\ddagger}_{\text{DMAP}} - RT\ln\left(\frac{k_{\text{O}}}{k_{\text{DMAP}}}\right)$	
$\Delta G^{\ddagger}_{\text{DMAP}}$	83.9 kJ mol^{-1}	$\Delta G^{\ddagger}_{\text{DMAP}}$	83.9 kJ mol^{-1}
$\Delta G^{\ddagger}_{\text{O}}$	**89.4 kJ mol^{-1}**	$\Delta G^{\ddagger}_{\text{O}}$	**85.5 kJ mol^{-1}**
$\Delta G^{\ddagger}$ for O-methylation of **1-Me$_4$N by MeI in CD_3CN at 20°C** is estimated to be within the range of **85.5 – 89.4 kJ mol^{-1}**			

4.11 times as many C-alkylation products as DMAP alkylation products		4.11 times as many C-alkylation products as DMAP alkylation products	
k_{C}	6.68 × 10^{-2} L mol^{-1} s^{-1}	k_{C}	3.26 × 10^{-1} L mol^{-1} s^{-1}
$\Delta G^{\ddagger}_{\text{C}} = \Delta G^{\ddagger}_{\text{DMAP}} - RT\ln\left(\frac{k_{\text{C}}}{k_{\text{DMAP}}}\right)$		$\Delta G^{\ddagger}_{\text{C}} = \Delta G^{\ddagger}_{\text{DMAP}} - RT\ln\left(\frac{k_{\text{C}}}{k_{\text{DMAP}}}\right)$	
$\Delta G^{\ddagger}_{\text{DMAP}}$	83.9 kJ mol^{-1}	$\Delta G^{\ddagger}_{\text{DMAP}}$	83.9 kJ mol^{-1}
$\Delta G^{\ddagger}_{\text{C}}$	**80.0 kJ mol^{-1}**	$\Delta G^{\ddagger}_{\text{C}}$	**76.2 kJ mol^{-1}**
$\Delta G^{\ddagger}$ for C-methylation of **1-Me$_4$N by MeI in CD_3CN at 20°C** is estimated to be within the range of **76.2 – 80.0 kJ mol^{-1}**			

(ii) Reaction of DMAP + Enolate 1-Me_4N + MeOMs in CD_3CN at 20 °C



From 4-dimethylaminopyridine (**46**) (0.0145 g, 0.119 mmol), a 0.67 mol L^{-1} stock solution of **1-Me_4N** in CD_3CN (0.15 ml, 0.101 mmol) and MeOMs (0.0101 g, 0.0917 mmol) in CD_3CN (0.70 ml) at 20 °C after 16 hours by Procedure C. 1,3,5-Trimethoxybenzene (**48**) (0.0200 g, 0.119 mmol) was added as an internal standard.

The integration value of the 3H signal of **48** at 6.12 ppm was set to equal 3.00 and all other integration values are given relative to this value.

^{1}H NMR (400 MHz, (CD_3CN) of crude mixture of alkylation products (the underlined integrations are expressed relative to 1H of internal standard **48**: [a,b,c]

Assigned to **48**: δ 6.12 (s, 3H), 3.76 (s, 9H).

Assigned to **46**: δ 8.18 – 8.10 (m, 1.13H (contains 2H of compound **46**)), 6.61 – 6.52 (m, 1.34H (contains 2H of compound **46**)), 2.98 (s, 4.08H (contains 6H of compound **46**)). [9]

Assigned to **54**: δ 8.02 – 7.94 (m, 0.64H (contains 2H of compound **54**)), 6.89 – 6.81 (m, 0.65H (contains 2H of compound **54**)), 3.89 (s, 0.95H (contains 3H of compound **54**)).

Assigned to *E*-**2**: δ 5.62 (s, 0.21H, C=C**H** (contains 1H of compound *E*-**2**)), 3.66 (s, 0.63H, OCH_3 (contains 3H of compound *E*-**2**)). [4]

Assigned to *Z*-**2**: δ 5.08 (s, 0.04H, C=C**H** (contains 1H of compound *Z*-**2**)), 2.05 (s, 0.14H, CH_3C=C (contains 3H of compound *Z*-**2**)). [4]

Assigned to **3$_{keto}$**: δ 1.24 (d, *J* = 7.1 Hz, 0.19H, C(CH_3) (contains 3H of compound **3$_{keto}$**)). [5]

Assigned to **10**: δ 1.32 (s, 0.06H, C(CH_3)$_2$ (contains 6H of compound **10**)). [6]

[a] The relevant ^{1}H NMR spectra are shown in Figure C50 and Figure C51 in Appendix C.

[b] Signals of *E*-**2**, *Z*-**2**, **3$_{keto}$**, **10** and **54** that are overlapping with other signals: δ 3.82 (s, contains 3H of *Z*-**2**), 3.22 – 3.13 (m, contains NMe_4 signal and 6H of **54**), 2.24 – 2.20 (m, contains 3H of *E*-**2** and 3H of *Z*-**2**), 2.19 – 2.08 (m, contains 3H of *E*-**2**, 6H of **3$_{keto}$** and 6H of **10**).

[c] The vinyl signals of the enol ether products at δ 5.58 and 5.08 are undersized and thus not used in determining the O/C ratio. See pages 428 and 429 for details.

In the following paragraphs, $I_{\mathbf{X}}$ is the integration of 1H of compound **X** (**X** = *E*-**2**, *Z*-**2**, **3**$_{\mathbf{keto}}$, **10** or **54**) relative to 1H of the internal standard, **48**.

Based on the ^{1}H NMR spectral data given above, the integrations (relative to the internal standard, **48**) of 1H each of O-alkylation products *E*-**2** and *Z*-**2** are:

$$I_{E-\mathbf{2}} = \frac{0.63}{3} = 0.21; \quad I_{Z-\mathbf{2}} = \frac{0.14}{3} = 0.046$$

Based on the ^{1}H NMR spectral data given above, the integrations (relative to the internal standard, **48**) of 1H each of C-alkylation products **3**$_{\mathbf{keto}}$ and **10** are:

$$I_{\mathbf{3_{keto}}} = \frac{0.19}{3} = 0.063; \quad I_{\mathbf{10}} = \frac{0.06}{6} = 0.01$$

The integration (relative to the internal standard, **48**) of 1H of **54** is:

$$I_{\mathbf{54}} = \frac{0.65}{2} = 0.325$$

For any given compound **X**, $[\mathbf{X}] \propto I_{\mathbf{X}}$ (where [**X**] = concentration of **X** (mol L^{-1})). Hence, the relative integration values (I**X** values) determined above can be used to determine the relative amounts formed of the products in the reaction mixture.

The amount of O-alkylation product formed (from **1-Me$_4$N**) is 0.788 times the amount of DMAP alkylation product formed:

$$\frac{I_{E-\mathbf{2}} + I_{Z-\mathbf{2}}}{I_{\mathbf{54}}} = \frac{0.21 + 0.046}{0.325} = 0.788$$

Similarly, the amount of C-alkylation products formed (from **1-Me$_4$N**) is 0.225 times the amount of DMAP alkylation product formed:

$$\frac{I_{\mathbf{3_{keto}}} + I_{\mathbf{10}}}{I_{\mathbf{54}}} = \frac{0.063 + 0.01}{0.325} = 0.225$$

Also using the relative integration values shown above, the percentage of O-alkylation in this reaction can be determined as follows:

$$\text{Percentage of O-alkylation} = \frac{I_{E-\mathbf{2}} + I_{Z-\mathbf{2}}}{I_{E-\mathbf{2}} + I_{Z-\mathbf{2}} + I_{\mathbf{3_{keto}}} + I_{\mathbf{10}}} \times 100$$

$$= \frac{0.21 + 0.046}{0.21 + 0.046 + 0.063 + 0.01} \times 100 = 78\%$$

Hence, the O vs C ratio in this reaction was 78:22.

Using these quantities, a range of $\Delta G^{\ddagger}$ values for the processes of O- and C- alkylation of **1-Me$_4$N** in CD_3CN at 20 °C may be calculated. The relevant data is shown in Table 7-13.

Note: The procedure used to estimate the values of $\Delta G^{\ddagger}$ for O- and C-alkylations of **1-Me$_4$N** with MeOMs is identical to that explained in detail in the exemplar at the start

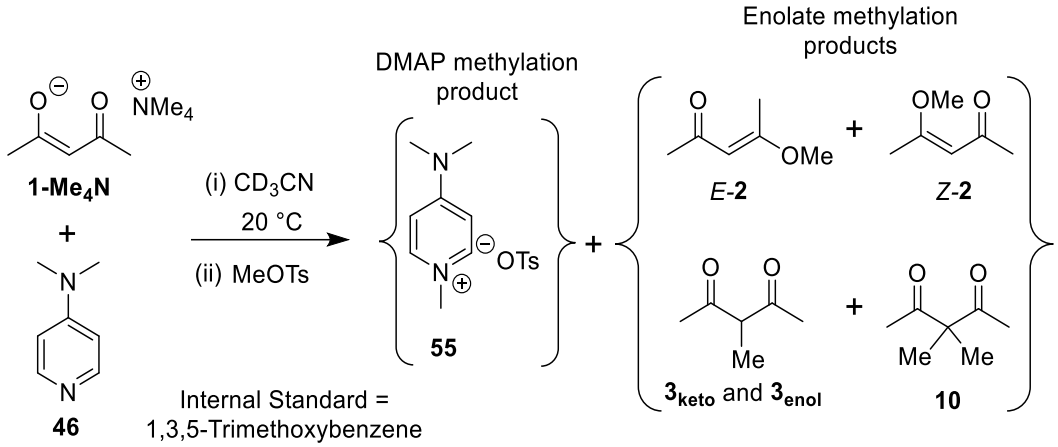
of this section (i.e., section 7.4 experiment (i)). Only the relevant figures used to calculate the values of $\Delta G^{\ddagger}$ are shown here, and not the full calculations themselves.

Table 7-13. Data used to estimate the value of $\Delta G^{\ddagger}$ for O- and C-methylation of **1-Me$_4$N** by MeOMs in CD_3CN at 20 °C. R = 8.314 J K^{-1} mol^{-1} and T = 293.15 K.

O- and C-alkylation Upper Bound		**O- and C-alkylation Lower Bound**	
0.788 times as many O-alkylation products as DMAP alkylation products		0.788 times as many O-alkylation products as DMAP alkylation products	
$n^{\text{init}}_{\mathbf{1-Me4N}}$	0.101 mmol	$n^{\text{final}}_{\mathbf{1-Me4N}}$	0.0484 mmol
$n^{\text{init}}_{\mathbf{46}}$	0.119 mmol	$n^{\text{final}}_{\mathbf{46}}$	0.0801 mmol
Scaling factor	0.849	Scaling factor	0.604
k_{DMAP}	4.40 × 10^{-4} L mol^{-1} s^{-1}	k_{DMAP}	4.40 × 10^{-4} L mol^{-1} s^{-1}
k_{O}	4.07 × 10^{-4} L mol^{-1} s^{-1}	k_{O}	5.73 × 10^{-4} L mol^{-1} s^{-1}
$\Delta G^{\ddagger}_{\text{O}} = \Delta G^{\ddagger}_{\text{DMAP}} - RT\ln\left(\frac{k_{\text{O}}}{k_{\text{DMAP}}}\right)$		$\Delta G^{\ddagger}_{\text{O}} = \Delta G^{\ddagger}_{\text{DMAP}} - RT\ln\left(\frac{k_{\text{O}}}{k_{\text{DMAP}}}\right)$	
$\Delta G^{\ddagger}_{\text{DMAP}}$	98.4 kJ mol^{-1}	$\Delta G^{\ddagger}_{\text{DMAP}}$	98.4 kJ mol^{-1}
$\Delta G^{\ddagger}_{\text{O}}$	**98.6 kJ mol^{-1}**	$\Delta G^{\ddagger}_{\text{O}}$	**97.7 kJ mol^{-1}**
$\Delta G^{\ddagger}$ for O-methylation of **1-Me$_4$N by MeOMs in CD_3CN at 20°C** is estimated to be within the range of **97.7 – 98.6 kJ mol^{-1}**			

0.225 times as many C-alkylation products as DMAP alkylation products		0.225 times as many C-alkylation products as DMAP alkylation products	
k_{C}	1.16 × 10^{-4} L mol^{-1} s^{-1}	k_{C}	1.64 × 10^{-4} L mol^{-1} s^{-1}
$\Delta G^{\ddagger}_{\text{C}} = \Delta G^{\ddagger}_{\text{DMAP}} - RT\ln\left(\frac{k_{\text{C}}}{k_{\text{DMAP}}}\right)$		$\Delta G^{\ddagger}_{\text{C}} = \Delta G^{\ddagger}_{\text{DMAP}} - RT\ln\left(\frac{k_{\text{C}}}{k_{\text{DMAP}}}\right)$	
$\Delta G^{\ddagger}_{\text{DMAP}}$	98.4 kJ mol^{-1}	$\Delta G^{\ddagger}_{\text{DMAP}}$	98.4 kJ mol^{-1}
$\Delta G^{\ddagger}_{\text{C}}$	**101.6 kJ mol^{-1}**	$\Delta G^{\ddagger}_{\text{C}}$	**100.8 kJ mol^{-1}**
$\Delta G^{\ddagger}$ for C-methylation of **1-Me$_4$N by MeOMs in CD_3CN at 20°C** is estimated to be within the range of **100.8 – 101.6 kJ mol^{-1}**			

(iii) Reaction of 4 DMAP + Enolate 1-Me$_4$N + MeOTs in CD$_3$CN at 20 °C



From 4-dimethylaminopyridine (**46**) (0.0145 g, 0.119 mmol), a 0.67 mol L^{-1} stock solution of **1-Me$_4$N** in CD$_3$CN (0.15 ml, 0.101 mmol) and MeOTs (0.0175 g, 0.0940 mmol) in CD$_3$CN (0.70 ml) at 20 °C after 18 hours by Procedure C. 1,3,5-Trimethoxybenzene (**48**) (0.0200 g, 0.119 mmol) was added as an internal standard.

The integration value of the 3H signal of **48** at 6.12 ppm was set to equal 3.00 and all other integration values are given relative to this value.

1H NMR (400 MHz, (CD$_3$CN) of crude mixture of alkylation products (the underlined integrations are expressed relative to 1H of internal standard **48**: [a,b,c]

Assigned to **48**: δ 6.12 (s, 3H), 3.76 (s, 9H).

Assigned to **46**: δ 8.18 – 8.10 (m, 1.29H (contains 2H of compound **46**)), 6.60 – 6.53 (m, 1.39H (contains 2H of compound **46**)), 2.97 (s, 4.28H (contains 6H of compound **46**)). [9]

Assigned to **55**: δ 8.02 – 7.94 (m, 0.52H (contains 2H of compound **55**)), 6.88 – 6.80 (m, 0.52H (contains 2H of compound **55**)), 3.89 (s, 0.79H (contains 3H of compound **55**)).

Assigned to *E*-**2**: δ 5.62 (s, 0.09H, C=C**H** (contains 1H of compound *E*-**2**)), 3.65 (s, 0.28H, OC**H**$_3$ (contains 3H of compound *E*-**2**)). [4]

Assigned to *Z*-**2**: δ 5.08 (s, 0.02H, C=C**H** (contains 1H of compound *Z*-**2**)), 3.81 (s, 0.09H, OC**H**$_3$ (contains 3H of compound *Z*-**2**)), 2.05 (s, 0.09H, C**H**$_3$C=C (contains 3H of compound *Z*-**2**)). [4]

Assigned to **3$_{keto}$**: δ 1.30 – 1.19 (m, 0.04H, C(C**H**$_3$) (contains 3H of compound **3$_{keto}$**)). [5]

Assigned to **10**: δ 1.32 (s, 0.03H, C(C**H**$_3$)$_2$ (contains 6H of compound **10**)). [6]

---

[a] The relevant ^{1}H NMR spectra are shown in Figure C52 and Figure C53 in Appendix C.

[b] Signals of *E*-**2**, *Z*-**2**, **3$_{keto}$**, **10** and **55** that are overlapping with other signals: δ 3.22 – 3.11 (m, contains NMe$_4$ signal and 6H of **55**), 2.25 – 2.20 (m, contains 3H of *E*-**2** and 3H of *Z*-**2**), 2.17 – 2.09 (m, contains 3H of *E*-**2**, 6H of **3$_{keto}$** and 6H of **10**).

[c] The vinyl signals of the enol ether products at δ 5.62 and 5.08 are undersized and thus not used in determining the O/C ratio. See pages 428 and 429 for details.

In the following paragraphs, $I_{\mathbf{X}}$ is the integration of 1H of compound **X** (**X** = *E*-**2**, *Z*-**2**, **3**$_{\mathbf{keto}}$, **10** or **55**) relative to 1H of the internal standard, **48**.

Based on the ^{1}H NMR spectral data given above, the integrations (relative to the internal standard, **48**) of 1H each of O-alkylation products *E*-**2** and *Z*-**2** are:

$$I_{E-\mathbf{2}} = \frac{0.61}{3} = 0.203; \quad I_{Z-\mathbf{2}} = \frac{0.09}{3} = 0.03$$

Based on the ^{1}H NMR spectral data given above, the integrations (relative to the internal standard, **48**) of 1H each of C-alkylation products **3**$_{\mathbf{keto}}$ and **10** are:

$$I_{\mathbf{3_{keto}}} = \frac{0.09}{3} = 0.03; \quad I_{\mathbf{10}} = \frac{0.12}{6} = 0.02$$

The integration (relative to the internal standard, **48**) of 1H of **55** is:

$$I_{\mathbf{55}} = \frac{0.45}{2} = 0.225$$

For any given compound **X**, $[\mathbf{X}] \propto I_{\mathbf{X}}$ (where [**X**] = concentration of **X** (mol L^{-1})). Hence, the relative integration values (Ix values) determined above can be used to determine the relative amounts formed of the products in the reaction mixture.

The amount of O-alkylation product formed (from **1-Me$_4$N**) is 1.04 times the amount of DMAP alkylation product formed:

$$\frac{I_{E-\mathbf{2}} + I_{Z-\mathbf{2}}}{I_{\mathbf{55}}} = \frac{0.203 + 0.03}{0.225} = 1.04$$

Similarly, the amount of C-alkylation products formed (from **1-Me$_4$N**) is 0.222 times the amount of DMAP alkylation product formed:

$$\frac{I_{\mathbf{3_{keto}}} + I_{\mathbf{10}}}{I_{\mathbf{55}}} = \frac{0.03 + 0.02}{0.225} = 0.222$$

Also using the relative integration values shown above, the percentage of O-alkylation in this reaction can be determined as follows:

$$\text{Percentage of O-alkylation} = \frac{I_{E-\mathbf{2}} + I_{Z-\mathbf{2}}}{I_{E-\mathbf{2}} + I_{Z-\mathbf{2}} + I_{\mathbf{3_{keto}}} + I_{\mathbf{10}}} \times 100$$

$$= \frac{0.203 + 0.03}{0.203 + 0.03 + 0.03 + 0.02} \times 100 = 82\%$$

Hence, the O vs C ratio in this reaction was 82:18.

Using these quantities, a range of $\Delta G^{\ddagger}$ values for the processes of O- and C- alkylation of **1-Me$_4$N** in CD_3CN at 20 °C may be calculated. The relevant data is shown in Table 7-14.

Note: The procedure used to estimate the values of $\Delta G^{\ddagger}$ for O- and C-alkylations of **1-Me$_4$N** with MeOTs is identical to that explained in detail in the exemplar at the start

of this section (i.e., section 7.4 experiment (i)). Only the relevant figures used to calculate the values of $\Delta G^{\ddagger}$ are shown here, and not the full calculations themselves.

Table 7-14. Data used to estimate the value of $\Delta G^{\ddagger}$ for O- and C-methylation of **1-Me$_4$N** by MeOTs in CD_3CN at 20 °C. R = 8.314 J K^{-1} mol^{-1} and T = 293.15 K.

O- and C-alkylation Upper Bound		**O- and C-alkylation Lower Bound**	
1.04 times as many O-alkylation products as DMAP alkylation products		1.04 times as many O-alkylation products as DMAP alkylation products	
$n^{\text{init}}_{\mathbf{1-Me4N}}$	0.101 mmol	$n^{\text{final}}_{\mathbf{1-Me4N}}$	0.034 mmol
$n^{\text{init}}_{\mathbf{46}}$	0.119 mmol	$n^{\text{final}}_{\mathbf{46}}$	0.092 mmol
Scaling factor	0.849	Scaling factor	0.370
k_{DMAP}	1.04 × 10^{-3} L mol^{-1} s^{-1}	k_{DMAP}	1.04 × 10^{-3} L mol^{-1} s^{-1}
k_{O}	1.27 × 10^{-3} L mol^{-1} s^{-1}	k_{O}	2.92 × 10^{-3} L mol^{-1} s^{-1}
$\Delta G^{\ddagger}_{\text{O}} = \Delta G^{\ddagger}_{\text{DMAP}} - RT\ln\left(\frac{k_{\text{O}}}{k_{\text{DMAP}}}\right)$		$\Delta G^{\ddagger}_{\text{O}} = \Delta G^{\ddagger}_{\text{DMAP}} - RT\ln\left(\frac{k_{\text{O}}}{k_{\text{DMAP}}}\right)$	
$\Delta G^{\ddagger}_{\text{DMAP}}$	96.3 kJ mol^{-1}	$\Delta G^{\ddagger}_{\text{DMAP}}$	96.3 kJ mol^{-1}
$\Delta G^{\ddagger}_{\text{O}}$	**95.8 kJ mol^{-1}**	$\Delta G^{\ddagger}_{\text{O}}$	**93.8 kJ mol^{-1}**
$\Delta G^{\ddagger}$ for O-methylation of **1-Me$_4$N by MeOTs in CD_3CN at 20°C** is estimated to be within the range of **93.8 – 95.8 kJ mol^{-1}**			

0.222 times as many C-alkylation products as DMAP alkylation products		0.222 times as many C-alkylation products as DMAP alkylation products	
k_{C}	2.72 × 10^{-4} L mol^{-1} s^{-1}	k_{C}	6.24 × 10^{-4} L mol^{-1} s^{-1}
$\Delta G^{\ddagger}_{\text{C}} = \Delta G^{\ddagger}_{\text{DMAP}} - RT\ln\left(\frac{k_{\text{C}}}{k_{\text{DMAP}}}\right)$		$\Delta G^{\ddagger}_{\text{C}} = \Delta G^{\ddagger}_{\text{DMAP}} - RT\ln\left(\frac{k_{\text{C}}}{k_{\text{DMAP}}}\right)$	
$\Delta G^{\ddagger}_{\text{DMAP}}$	96.3 kJ mol^{-1}	$\Delta G^{\ddagger}_{\text{DMAP}}$	96.3 kJ mol^{-1}
$\Delta G^{\ddagger}_{\text{C}}$	**99.6 kJ mol^{-1}**	$\Delta G^{\ddagger}_{\text{C}}$	**97.5 kJ mol^{-1}**
$\Delta G^{\ddagger}$ for C-methylation of **1-Me$_4$N by MeOTs in CD_3CN at 20°C** is estimated to be within the range of **97.5 – 99.6 kJ mol^{-1}**			

7.5. References

1. Williams, D. B. G.; Lawton, M. *J. Org. Chem.* **2010**, *75*, 8351–8354.
2. Shriver, D. F.; Drezdon, M. A. *The Manipulation of Air-Sensitive Compounds*, 2nd Edition.; John Wiley & Sons: New York; 1986.
3. Fulmer, G. R.; Miller, A. J. M.; Sherden, N. H.; Gottlieb, H. E.; Nudelman, A.; Stoltz, B. M.; Bercaw, J. E.; Goldberg, K. I. *Organometallics* **2010**, *29*, 2176–2179.
4. Dabrowski, J.; Tencer, M. *Bull. Chem. Soc. Jpn.* **1976**, *49*, 981–986.
5. Terent'ev, A. O.; Vil', V. A.; Yaremenko, I. A.; Bityukov, O. V.; Levitsky, D. O.; Chernyshev, V. V.; Nikishin, G. I.; Fleury, F. *New J. Chem.* **2014**, *38*, 1493–1502.
6. Choudhary, A.; Baumstark, A. L. *Synthesis* **1989**, *1989*, 688–690.
7. Kalaitzakis, D.; Rozzell, J. D.; Smonou, I.; Kambourakis, S. *Adv. Synth. Catal.* **2006**, *348*, 1958–1969.
8. Hooz, J.; Smith, J. *J. Org. Chem.* **1972**, *37*, 4200–4202.
9. Kleinmaier, R.; Arenz, S.; Karim, A.; Carlsson, A.-C. C.; Erdélyi, M. *Magn. Reson. Chem.* **2013**, *51*, 46–53.
10. Atkins, P. W.; De Paula, J. *Physical Chemistry*, 9th Edition.; Oxford University Press: Oxford, 2010.
11. Kondo, Y.; Uematsu, R.; Nakamura, Y.; Kusabayashi, S. *J. Chem. Soc. Perkin Trans. 2* **1988**, No. 7, 1219–1224.

Chapter 8: Conclusions & Future Work

8.1. Conclusions **508**

8.2. Future Work **511**

8.3. References **514**

8.1. Conclusions

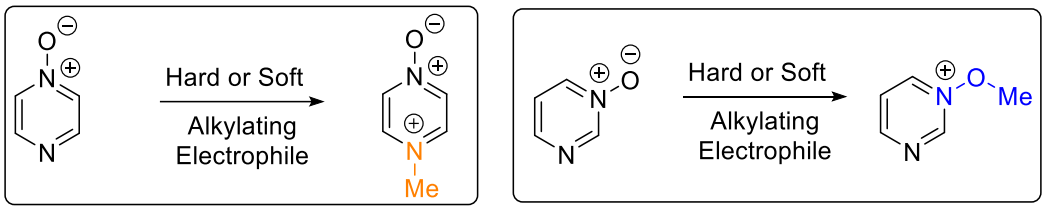
The work outlined in this thesis demonstrates the numerous difficulties encountered when attempting to scrutinise the selectivity associated with the reactions of ambident nucleophiles. As detailed in Chapter 2, even the simple act of positively identifying which of the possible products of such a reaction is favoured may prove itself a difficult task. The examples contained within this thesis, obtained through a detailed analysis of literature precedents and subsequent experimentation, agree with the previously ascertained conclusions of Mayr and co-workers that the HSAB treatment of ambident reactivity is an inadequate means of predicting or understanding the outcomes of reactions of ambident nucleophiles.[1] The nebulous descriptions of "hard" and "soft" local sites of ambident nucleophiles which characterise the so-called "local" HSAB principle do little to interrogate the underlying phenomena at play in these reactions. Notably, as was demonstrated in Chapter 2, the act of classifying a particular atom in an ambident nucleophile as "hard" or "soft" may not necessarily be a simple task, even with the aid of chemical computations.

For examples in which the designation of certain atoms as "hard" or "soft" sites is more obvious, as is the case when examining the carbon and oxygen nucleophilic centres of an enolate anion, the work in Chapter 4 demonstrates that these designations may not assist in predicting the selectivities of reactions of that enolate with representative "hard" and "soft" electrophiles. Instead, it was demonstrated that a variety of factors may influence the preferred products (i.e., O-alkylation products or C-alkylation products) in such a reaction – including the solvent chosen for a reaction and the counter-ion of the enolate in question. These findings were broadly in line with the observations and discussions found in manuscripts from the literature regarding reactions of ambident species which predate the popularisation of employing HSAB theory as a tool to analyse ambident reactivity.

The utility of the Marcus theory-based approach to ambident reactivity outlined by Mayr and co-workers was confirmed in the examination of the reactivity of diazine *N*-oxides in Chapter 2.[1] This investigation demonstrated that it is reasonable to expect that calculations based on Marcus theory can allow for semi-quantitative predictions of the preferred nucleophilic site in reactions of ambident nucleophiles. The calculation of the intrinsic barrier ($\Delta G^{\ddagger}_{int}$) associated with a given reaction thus has a demonstrated value when attempting to predict the outcome of that reaction (see Figure 8-1). However, this approach has numerous drawbacks, most obvious of which being that this quantity can only be accessed through chemical computation, and that the accuracy of the value of $\Delta G^{\ddagger}_{int}$ which is calculated depends on the compatibility of the reaction with current computational chemistry capabilities. Reactions of negatively charged ambident nucleophiles with counter-cations, which comprise vast categories of compounds such as enolates and nitrates, are not compatible with the Marcus theory-based approach because it is not possible to incorporate a counter-cation into the relevant calculations needed to determine the intrinsic barrier for a reaction. Although this may become possible in the future through advancements in computational chemistry methodologies, this

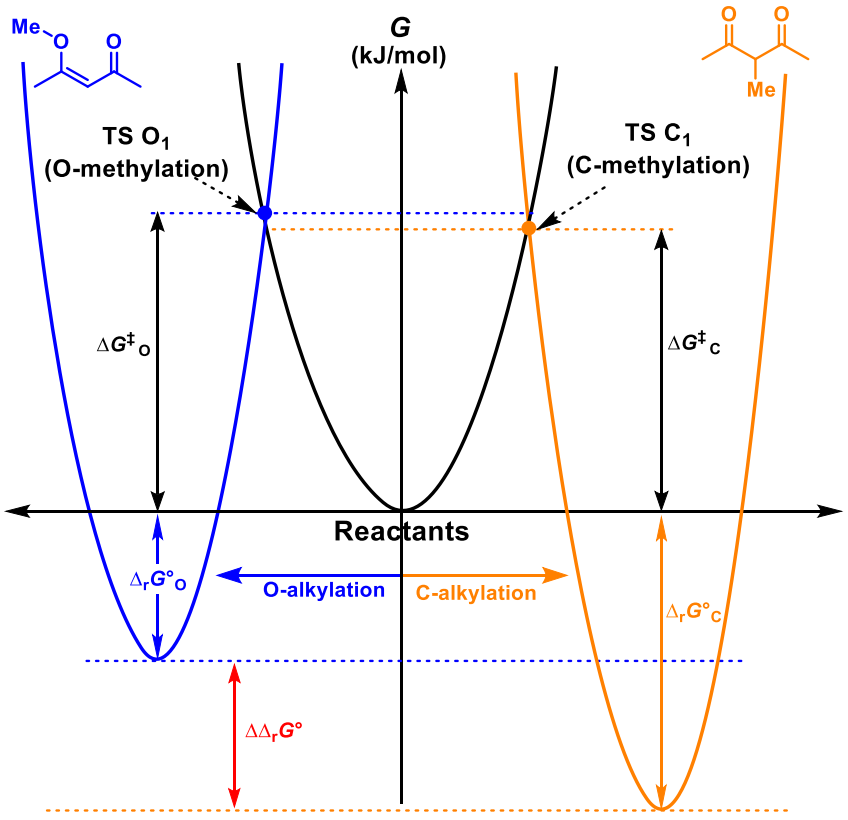
shortcoming results in an inability to analyse the reactivity of enolate anions through the lens of the Marcus theory-based approach.

Figure 8-1. The Marcus theory-based approach outlined in Chapter 2 was capable of correctly predicting the unexpected selectivity which was observed experimentally in reactions of pyrazine *N*-oxide and pyrimidine *N*-oxide with various alkylating agents.



As a result, the process of developing a novel model for ambident reactivity has been initiated in this thesis, as described in Chapter 6. This model aims to account for the observations made in experiments performed in Chapters 2 and 4, as well as the findings of the vast number of literature reactions which were presented in Chapter 1. The work presented in Chapter 6 involved construction of Gibbs energy profile diagrams using experimentally derived values of $\Delta G^{\ddagger}$ and computationally derived values of $\Delta_r G°$, using a novel method to visualise the topology of the Gibbs energy profiles for the reactions of ambident nucleophiles (see Figure 8-2).

Figure 8-2. An illustrated example of the Gibbs energy profile diagrams used in the novel model used to rationalise ambident reactivity, as described in Chapter 6.



Analysis of numerous Gibbs energy profile diagrams that were generated to describe reactions of an enolate with various alkylating agents revealed that there are three major factors that influence the relative magnitudes of the $\Delta G^{\ddagger}$ values for the O- and C-alkylation processes in any one enolate alkylation reaction: (i) The vertical position of the central reactant parabola (which depends on the Lewis acidity of the alkylating agent), (ii) the horizontal position of the apex of the central reactant parabola, and (iii) the width/curvature of the central reactant parabola. Since any or all of these factors may change from one alkylation reaction of a given enolate to another alkylation reaction of the same enolate, no one factor of these three is solely responsible for dictating the selectivity for O- vs. C-alkylation in nucleophilic substitution reactions of enolates with alkylating agents. Making further progress in understanding the factors that control O- vs. C-selectivity in these reactions (or, more generally, site-selectivity in reactions of ambident nucleophiles) will require development of an approach that enables the precise widths/curvatures of the Gibbs energy wells (and hence the extent of the reaction coordinate along the horizontal axis) to be precisely specified (see "Future Work" in Section 8.2 below for further details).

While definitive comment on the origins of the observed O- vs C-alkylation selectivity cannot be made based on the descriptive model developed herein, the development of this model has enabled establishment of instructive trends in the topologies of the Gibbs energy profile diagrams of representative enolate alkylation reactions. For example, the reactions of alkyl triflates (i.e., MeOTf, EtOTf) with a given enolate resulted in O/C ratios that were very similar to those recorded for reactions of the same enolate with alkyl methanesulfonates (i.e., MeOMs, EtOMs) and alkyl toluenesulfonates (i.e., MeOTs, EtOTs), despite the fact that the Lewis acidities of the reactions of alkyl triflates with enolates were consistently calculated to be much greater (i.e., to have more negative values of $\Delta_r G°$) than reactions of alkyl methanesulfonates and alkyl toluenesulfonates. This implies that the curvature of the reactant parabola for reactions of enolates with alkyl triflates is shallower than the reactant parabolas which represent the reactions of enolates with alkyl methanesulfonates and alkyl toluenesulfonates.

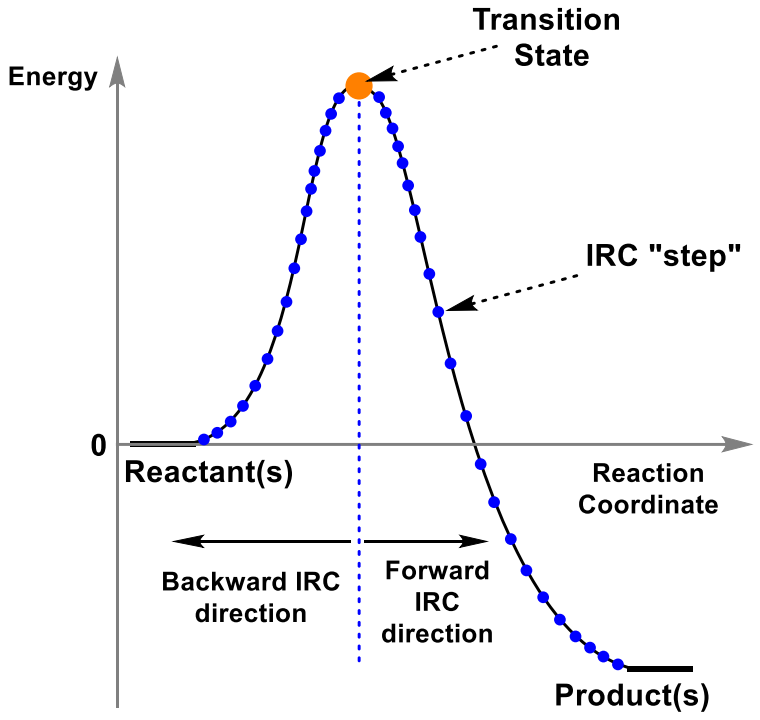
The analysis of Gibbs energy profile diagrams established that the horizontal position of the apex of the central reactant parabola in a given diagram had a large influence on the selectivity which was observed in that reaction. Using Figure 8-2 above as an example, it was seen that when the apex of the central reactant parabola (in black) was moved closer to the apex of the product parabola for O-methylation (in blue), this resulted in a lower activation barrier for the O-methylation process relative to the C-methylation process.

8.2. Future Work

The key work which needs to be pursued in order to continue the development of the novel model for ambident reactivity proposed in Chapter 6 is to identify a method of ascribing a physical basis to the dimensions of the horizontal axis of a Gibbs energy profile diagram. Methods that have been conceived for this purpose and will be investigated include the use of computational "intrinsic reaction co-ordinate" (IRC) calculations.

"Intrinsic reaction co-ordinate" (IRC) calculations[2–5] are a method of verifying that a transition state of a chemical process has been located by another computational method. This is performed by identifying the energy minima which are connected through that transition state (i.e., the energy minima of the reactants and the products). An IRC calculation attempts to identify the minimum energy reaction pathway along a potential energy surface between the transition state of a reaction and the reactants and products through the use of mass-weighted co-ordinates. A visual representation of this method is shown below in Figure 8-3.

Figure 8-3. An illustrated representation of the "intrinsic reaction co-ordinate" calculation. The lowest energy pathway between the transition state and the reactants and products is outlined by determination of the point of lowest energy of various "steps" away from the transition state in both the forward and backward direction.



Many "steps" of fixed size are constructed away from the transition state and the point of lowest energy at this distance is sought by computations. Once located, the point of lowest energy is defined to lie on the path of minimum energy, and another "step" is constructed

at the same distance away from this point as used was previously. This process is repeated (in each direction) until the local minima of the potential energy surface are reached.

Although the distance between "steps" of an IRC calculation is not determined by atomic distance or energy considerations, a calculation of this type may provide utility in determining the required information about the horizontal axis of a reaction co-ordinate which would allow the analysis of that reaction in the context of the novel model for ambident reactivity outlined in this chapter. The key issue that would be addressed using IRC calculations (or other reaction pathway tracing techniques)[6,7] would be to remove the need to set the apices of the reactant and product parabolas at an arbitrary horizontal distance away from one another. IRC plots, like the one shown in Figure 8-3 above, contain long sections either side of the transition state which represent linear decreases in the potential energy of the system. By determining the slopes of these linear pre-transition state and post-transition state sections of the IRC plot, the steepness of the barriers may be used to infer information about the curvatures (widths) and relative positions of the reactant and product parabolas in a Gibbs energy profile diagram for the same reaction. The slope of the pre-transition state barrier will assist in defining the position of the reactant parabola, and the slope of the post-transition state barrier will assist in defining the position of product parabola. Although the resulting placement of the positions of the parabolas will not be entirely unambiguous, their shapes will be specified in a non-arbitrary way, enabling the development of the model in the direction of quantitative analysis of reactions of ambident nucleophiles. Investigations into this method of obtaining information about the horizontal dimension of a reaction co-ordinate are forthcoming from our external collaborators. These data will be combined with the experimental and computational data reported herein to produce a quantitative version of the model introduced above, i.e., this will enable $\Delta G^{\ddagger}$ values and O/C ratios for reactions of enolates to be predicted.

Experimentally, the future of this project lies in the development of convenient and effective techniques for measuring the rate constants (and $\Delta G^{\ddagger}$ values) for reactions of enolates and other ambident species. Although the ^{1}H NMR spectroscopic method employed in this chapter proved capable of generating rate parameters for a number of reactions of interest, certain reactions proved to be beyond the limits of this technique. Future use of a stopped-flow NMR spectroscopy system[8,9] may enable the measurement of rate data for reactions which were inaccessible by the methods reported in this chapter.

The generation of a large amount of rate data for various nucleophiles (including non-ambident nucleophiles) would assist in accessing rate data for reactions which cannot be accessed by the methods employed in this chapter. By measuring the rates of reactions of nucleophiles that are less Lewis basic than the nucleophile of interest, a series of competition experiments may be planned that will allow indirect access to the activation parameters of reactions of stronger nucleophiles. In essence, this would simply be a further development on the work carried out in section 6.3.4, wherein the rates of reaction of **1-Me$_4$N** were accessed through competition experiments employing a weaker nucleophile (DMAP) for which the rates of reaction with various alkylating agents were

previously measured. Although the rate of reaction of DMAP with EtOTf was too fast to be measured by the ^{1}H NMR spectroscopic method employed in this chapter, it is possible that the reaction of another, weaker nucleophile with EtOTf occurs at a rate which is convenient to measure. Eventually, through careful selection of nucleophiles and competitor nucleophiles, the rates of reaction for alkylations of **1**-**Me$_4$N** could be determined through relative comparison with a series of reactions of weaker nucleophiles.

Finally, alternative methods aside from the ^{1}H NMR spectroscopic method described above could be investigated which would allow convenient determination of activation barrier data for reactions of ambident nucleophiles (such as enolates). Titration methods such as those employed by Arnett and Reich[10] and Kevill and Lin[11] represent particularly interesting avenues of inquiry. If such techniques were pursued, the substrates and methodology could be carefully selected to enable the effective measurement of rate data for nucleophiles of interest, thereby minimising common pitfalls observed in this chapter which eliminated the possibility for the measurement of the rates of certain reactions, such as solubility issues.

8.3. References

1. Mayr, H.; Breugst, M.; Ofial, A. R. *Angew. Chem. Int. Ed.* **2011**, *50*, 6470–6505.
2. Fukui, K. *J. Phys. Chem.* **1970**, *74*, 4161–4163.
3. Fukui, K. *Acc. Chem. Res.* **1981**, *14*, 363–368.
4. Deng, L.; Ziegler, T. *Int. J. Quantum Chem.* **1994**, *52*, 731–765.
5. Maeda, S.; Harabuchi, Y.; Ono, Y.; Taketsugu, T.; Morokuma, K. *Int. J. Quantum Chem.* **2015**, *115*, 258–269.
6. Iftimie, R.; Minary, P.; Tuckerman, M. E. *Proc. Natl. Acad. Sci.* **2005**, *102*, 6654–6659.
7. Sun, Q.; Lu, X.; Tantillo, D. J. *ChemPhysChem* **2021**, *22*, 649–656.
8. Grimaldi, J.; Baldo, J.; McMurray, C.; Sykes, B. D. *J. Am. Chem. Soc.* **1972**, *94*, 7641–7645.
9. Gomez-Hens, A.; Perez-Bendito, D. *Anal. Chim. Acta* **1991**, *242*, 147–177.
10. Arnett, E. M.; Reich, R. *J. Am. Chem. Soc.* **1980**, *102*, 5892–5902.
11. Kevill, D. N.; Lin, G. M. L. *Tetrahedron Lett.* **1978**, *19*, 949–952.